

2018

ANNUAL PROGRESS REPORT

DOE Hydrogen and Fuel Cells Program

U.S. Department of Energy
1000 Independence Avenue, S.W.
Washington, DC 20585-0121

FY 2018
PROGRESS REPORT FOR THE DOE
HYDROGEN AND FUEL CELLS PROGRAM

April 2019
DOE/GO-102019-5156

Approved by Sunita Satyapal, Director, Hydrogen and Fuel Cells Program

NOTICE

This work was authored in part by the National Renewable Energy Laboratory, operated by Alliance for Sustainable Energy, LLC, for the U.S. Department of Energy (DOE) under Contract No. DE-AC36-08GO28308. Funding provided by U.S. Department of Energy Office of Energy Efficiency and Renewable Energy Fuel Cell Technologies Office. The views expressed herein do not necessarily represent the views of the DOE or the U.S. Government.

This report is available at no cost from the National Renewable Energy Laboratory (NREL) at www.nrel.gov/publications.

U.S. Department of Energy (DOE) reports produced after 1991 and a growing number of pre-1991 documents are available free via www.OSTI.gov.

Outline

Introduction

Hydrogen Fuel R&D

- Hydrogen Fuel R&D Subprogram Overview
- Hydrogen Production Analysis
 - Strategic Analysis, Inc.: Analysis of Advanced Hydrogen Production Pathways
- Electrolysis Production
 - Giner, Inc.: High-Temperature Alkaline Water Electrolysis
 - Tetramer Technologies, LLC: New Approaches to Improved Proton Exchange Membrane Electrolyzer Ion Exchange Membranes
- Biological Production
 - National Renewable Energy Laboratory: Biomass to Hydrogen (B2H2)
 - Oregon State University: Novel Hybrid Microbial Electrochemical System for Efficient Hydrogen Generation from Biomass
- HydroGEN Consortium
 - National Renewable Energy Laboratory: HydroGEN Overview: A Consortium on Advanced Water Splitting Materials
 - Proton OnSite: Benchmarking Advanced Water Splitting Technologies: Best Practices in Materials Characterization
- High-Temperature Electrolysis
 - University of Connecticut: HydroGEN Seedling: Proton-Conducting Solid Oxide Electrolysis Cells for Large-Scale Hydrogen Production at Intermediate Temperatures
 - Northwestern University: HydroGEN Seedling: Degradation Characterization and Modeling of a New Solid Oxide Electrolysis Cell Utilizing Accelerated Life Testing
 - United Technologies Research Center: HydroGEN Seedling: Thin-Film, Metal-Supported, High-Performance, and Durable Proton-Solid Oxide Electrolyzer Cell
- Low-Temperature Electrolysis
 - Proton OnSite: HydroGEN Seedling: High-Efficiency Proton Exchange Membrane Water Electrolysis Enabled by Advanced Catalysts, Membranes, and Processes
 - Northeastern University: HydroGEN Seedling: Enabling Efficient Water Splitting with Advanced Materials Designed for High-pH Membrane Interface
 - Argonne National Laboratory: HydroGEN Seedling: Platinum-Group-Metal-Free Oxygen Evolution Reaction Catalysts for Proton Exchange Membrane Electrolyzers
 - Los Alamos National Laboratory: HydroGEN Seedling: High-Performance Ultralow-Cost Non-Precious-Metal Catalyst System for Anion Exchange Membrane Electrolyzer
 - Los Alamos National Laboratory: HydroGEN Seedling: Scalable Elastomeric Membranes for Alkaline Water Electrolysis
- Photoelectrochemical Production

- Rutgers University: HydroGEN Seedling: Best-in-Class Platinum-Group-Metal-Free Catalyst Integrated Tandem Junction Photoelectrochemical Water Splitting Devices
- Stanford University: HydroGEN Seedling: Protective Catalyst Systems on III-V and Si-Based Semiconductors for Efficient, Durable Photoelectrochemical Water Splitting Devices
- University of Hawaii: HydroGEN Seedling: Novel Chalcopyrites For Advanced Photoelectrochemical Water Splitting
- University of Michigan: HydroGEN Seedling: Monolithically Integrated Thin-Film/Silicon Tandem Photoelectrodes for High-Efficiency and Stable Photoelectrochemical Water Splitting
- High-Temperature Thermochemical
 - Colorado School of Mines: HydroGEN Seedling: Accelerated Discovery of Solar Thermochemical Hydrogen Production Materials via High-Throughput Computational and Experimental Methods
 - University of Colorado Boulder: HydroGEN Seedling: Computationally Accelerated Discovery and Experimental Demonstration of High-Performance Materials for Advanced Solar Thermochemical Hydrogen Production
 - Northwestern University: HydroGEN Seedling: Transformative Materials for High-Efficiency Thermochemical Production of Solar Fuels
 - Arizona State University: HydroGEN Seedling: Mixed Ionic Electronic Conducting Quaternary Perovskites: Materials by Design for Solar Thermochemical Hydrogen
 - Greenway Energy, LLC: HydroGEN Seedling: High-Temperature Reactor Catalyst Material Development for Low-Cost and Efficient Solar-Driven Sulfur-Based Processes
- Testing and Analysis – Storage
 - Argonne National Laboratory: Systems Analysis of Physical and Materials-Based Hydrogen Storage
 - Strategic Analysis, Inc.: Hydrogen Storage Cost Analysis
- Systems Engineering – Storage
 - National Renewable Energy Laboratory: Hydrogen Storage System Modeling: Public Access, Maintenance, and Enhancements
 - Savannah River National Laboratory: Investigation of Solid-State Hydrides for Autonomous Fuel Cell Vehicles
- Advanced Materials – Storage
 - California Institute of Technology: Design and Synthesis of Materials with High Capacities for Hydrogen Physisorption
 - University of Michigan: Hydrogen Adsorbents with High Volumetric Density: New Materials and System Projections
 - Sandia National Laboratories: HyMARC: A Consortium for Advancing Hydrogen Storage Materials
 - National Renewable Energy Laboratory: HySCORE: Hydrogen Storage Characterization and Optimization Research Effort
 - Argonne National Laboratory: HyMARC Seedling: “Graphene-Wrapped” Complex Hydrides as High-Capacity, Regenerable Hydrogen Storage Materials
 - Liox Power: HyMARC Seedling: Electrolyte-Assisted Hydrogen Storage Reactions

- University of Hawaii: HyMARC Seedling: Development of Magnesium Boride Etherates as Hydrogen Storage Materials
- National Renewable Energy Laboratory: HyMARC Seedling: Fluorinated Covalent Organic Frameworks: A Novel Pathway to Enhance Hydrogen Sorption and Control Isosteric Heats of Adsorption
- National Renewable Energy Laboratory: HyMARC Seedling: Atomic Layer Deposition Synthesis of Novel Nanostructured Metal Borohydrides
- University of Michigan: HyMARC Seedling: Optimized Hydrogen Adsorbents via Machine Learning and Crystal Engineering
- University of California, Berkeley: HyMARC Seedling: Super Metalated Frameworks as Hydrogen Sponges
- Advanced Tanks – Storage
 - University of Kentucky: Precursor Processing Development for Low-Cost, High-Strength Carbon Fiber for Composite Overwrapped Pressure Vessel Applications
 - Pennsylvania State University: Developing a New Polyolefin Precursor for Low-Cost, High-Strength Carbon Fiber
 - Oak Ridge National Laboratory: Novel Plasticized Melt-Spinning Process of Polyacrylonitrile Fibers Based on Task-Specific Ionic Liquids
 - Pacific Northwest National Laboratory: Material Challenges for Cryogenic Hydrogen Storage Technologies

Fuel Cell R&D

- Fuel Cell R&D Subprogram Overview
- Catalysts and Electrodes
 - Argonne National Laboratory: Tailored High-Performance Low-Platinum-Group-Metal Alloy Cathode Catalysts
 - Brookhaven National Laboratory: Platinum Monolayer Electrocatalysts
 - National Renewable Energy Laboratory: Extended Surface Electrocatalyst Development
 - 3M Company: Highly Active, Durable, and Ultra-Low-Platinum-Group-Metal Nanostructured Thin Film Oxygen Reduction Reaction Catalysts and Supports
 - General Motors: Highly Accessible Catalysts for Durable High-Power Performance
 - Washington University in St. Louis: Corrosion-Resistant Non-Carbon Electrocatalyst Supports for Proton Exchange Fuel Cells
 - Argonne National Laboratory: ElectroCat (Electrocatalysis Consortium)
 - Los Alamos National Laboratory: Advanced Electrocatalysts Through Crystallographic Enhancement
 - Ford Motor Company: Vapor Deposition Process for Engineering of Dispersed Polymer Electrolyte Membrane Fuel Cell Oxygen Reduction Reaction Pt/NbOx/C Catalysts
 - Giner, Inc.: ElectroCat: Durable Mn-Based Platinum-Group-Metal-Free Catalysts for Polymer Electrolyte Membrane Fuel Cells

- Carnegie Mellon University: ElectroCat: Advanced Platinum-Group-Metal-Free Cathode Engineering for High Power Density and Durability
- Pacific Northwest National Laboratory: ElectroCat: Highly Active and Durable Platinum-Group-Metal-Free Oxygen Reduction Reaction Electrocatalysts through the Synergy of Active Sites
- Greenway Energy, LLC: ElectroCat: Platinum-Group-Metal-Free Engineered Framework Nano-Structure Catalyst
- Argonne National Laboratory: Highly Efficient and Durable Cathode Catalyst with Ultralow Platinum Loading Through Synergetic Platinum/Platinum-Group-Metal-Free Catalytic Interaction
- Electrolytes and Membranes
 - Giner, Inc.: FY15 SBIR II Release 2: Ionomer Dispersion Impact on Fuel Cell and Electrolyzer Performance and Durability
 - Los Alamos National Laboratory: Advanced Materials for Fully Integrated Membrane Electrode Assemblies in Anion Exchange Membrane Fuel Cells
 - National Renewable Energy Laboratory: Advanced Ionomers and Membrane Electrode Assemblies for Alkaline Membrane Fuel Cells
 - Los Alamos National Laboratory: Polymer-Based Fuel Cells that Operate from 80°C to 220°C
 - NanoSonic, Inc.: FY17 SBIR II Release 1: Novel Hydrocarbon Ionomers for Durable Polymer Electrolyte Membranes
- Fuel Cell Performance and Durability
 - Los Alamos National Laboratory: FC-PAD: Fuel Cell Performance and Durability Consortium
 - 3M Company: Novel Ionomers and Electrode Structures for Improved Polymer Electrolyte Membrane Fuel Cell Electrode Performance at Low Platinum-Group-Metal Loadings
 - General Motors: Durable High-Power Membrane Electrode Assemblies with Low Platinum Loading
 - United Technologies Research Center: High-Performance Polymer Electrolyte Membrane Fuel Cell Electrode Structures
 - Vanderbilt University: Fuel Cell Membrane Electrode Assemblies with Ultra-Low-Platinum Nanofiber Electrodes
- MEAs, Cells, and Other Stack Components
 - Advent Technologies, Inc.: Facilitated Direct Liquid Fuel Cells with High-Temperature Membrane Electrode Assemblies
 - Giner, Inc.: Advanced Catalysts and Membrane Electrode Assemblies for Reversible Alkaline Membrane Fuel Cells
 - pH Matter, LLC: FY16 SBIR II Release 1: Regenerative Fuel Cell System
- Testing and Technical Assessment
 - Argonne National Laboratory: Performance of Advanced Automotive Fuel Cell Stacks and Systems with State-of-the-Art d-PtCo/C Cathode Catalyst in Membrane Electrode Assemblies
 - Strategic Analysis, Inc.: Fuel Cell Systems Analysis

Technology Acceleration and Hydrogen Infrastructure R&D

- Technology Acceleration and Hydrogen Infrastructure R&D Overview

- Technology Acceleration
 - National Renewable Energy Laboratory: Fuel Cell Membrane Electrode Assembly Manufacturing R&D
 - Ohio Fuel Cell Coalition: Clean Energy Supply Chain and Manufacturing Competitiveness Analysis for Hydrogen and Fuel Cell Technologies
 - Virginia Clean Cities at James Madison University: Hydrogen Fuel Cell Nexus Business-to-Business Website
 - Automated Dynamics: Continuous Fiber Composite Electrofusion Coupler
 - Mainstream Engineering: In-Line Quality Control of Polymer Electrolyte Membrane Materials
 - National Renewable Energy Laboratory: Manufacturing Competitiveness Analysis for Hydrogen Refueling Stations
 - Oak Ridge National Laboratory: Roll-to-Roll Advanced Materials Manufacturing Lab Consortium
 - Hawaii Natural Energy Institute: Hydrogen Energy Systems as a Grid Management Tool
 - Plug Power, Inc.: Fuel-Cell-Powered Airport Ground Support Equipment Deployment
 - Sandia National Laboratories: Maritime Fuel Cell Generator Project
 - Pacific Northwest National Laboratory: Demonstration of Fuel Cell Auxiliary Power Unit to Power Truck Refrigeration Units in Refrigerated Trucks
 - Federal Express Corporation: FedEx Express Hydrogen Fuel Cell Extended-Range Battery Electric Vehicles
 - US Hybrid: Northeast Demonstration and Deployment of FCRx200
 - National Renewable Energy Laboratory: Technology Validation: Fuel Cell Bus Evaluations
 - National Renewable Energy Laboratory: Hydrogen Station Data Collection and Analysis
 - Lawrence Livermore National Laboratory: Performance and Durability Testing of Volumetrically Efficient Cryogenic Vessels and High-Pressure Liquid Hydrogen Pump
 - Idaho National Laboratory: Grid Integration and Hydrogen Energy Generation: Modeling and Validation of Electrolyzers in Real-Time Grid Simulation
 - Center for Transportation and the Environment: Fuel Cell Hybrid Electric Delivery Van
 - Electricore, Inc.: Innovative Advanced Hydrogen Mobile Fueler
 - Idaho National Laboratory: High-Temperature Electrolysis Test Stand
 - FuelCell Energy, Inc.: Modular Solid Oxide Electrolysis Cell System for Efficient Hydrogen Production at High Current Density
 - National Renewable Energy Laboratory: Optimal Stationary Fuel Cell Integration and Control (Energy Dispatch Controller)
 - Lawrence Berkeley National Laboratory: Integrated Systems Modeling of the Interactions between Stationary Hydrogen, Vehicles, and Grid Resources
 - National Renewable Energy Laboratory: H2@Scale: Experimental Characterization of Durability of Advanced Electrolyzer Concepts in Dynamic Loading
 - Sandia National Laboratories: Hydrogen Stations for Urban Sites
 - Argonne National Laboratory: Toyota Mirai Testing

- Hydrogen Infrastructure R&D
 - Sandia National Laboratories: Fatigue Performance of High-Strength Pipeline Steels and Their Welds in Hydrogen Gas Service
 - National Renewable Energy Laboratory: 700-bar Hydrogen Dispenser Hose Reliability Improvement
 - Southwest Research Institute: Hydrogen Compression Application of the Linear Motor Reciprocating Compressor
 - Pacific Northwest National Laboratory: Magnetocaloric Hydrogen Liquefaction
 - Giner ELX, Inc.: Electrochemical Compression
 - Greenway Energy, LLC: Hybrid Electrochemical Hydrogen/Metal Hydride Compressor
 - Sandia National Laboratories: Metal Hydride Compression
 - National Renewable Energy Laboratory: Dispenser Reliability
 - Ivys Energy Solutions: Advancing Hydrogen Dispenser Technology by Using Innovative Intelligent Networks
 - NanoSonic, Inc.: Cryogenically Flexible, Low-Permeability Hydrogen Delivery Hose
 - GVD Corporation: Advanced Barrier Coatings for Harsh Environments
 - General Engineering & Research: Low-Cost Magnetocaloric Materials Discovery
 - Xergy Inc.: Novel Membranes for Electrochemical Hydrogen Compression Enabling Increased Pressure Capability and Higher Pumping Efficiency

Safety, Codes and Standards

- Safety, Codes and Standards Subprogram Overview
 - National Renewable Energy Laboratory: National Codes and Standards Development and Outreach
 - Sandia National Laboratories: R&D for Safety, Codes and Standards: Materials and Components Compatibility
 - Los Alamos National Laboratory: Fuel Quality Assurance Research and Development and Impurity Testing in Support of Codes and Standards
 - Sandia National Laboratories: R&D for Safety, Codes and Standards: Hydrogen Behavior
 - Sandia National Laboratories: Hydrogen Quantitative Risk Assessment
 - Pacific Northwest National Laboratory: Hydrogen Safety Panel, Safety Knowledge Tools, and First Responder Training Resources
 - National Renewable Energy Laboratory: NREL Hydrogen Sensor Testing Laboratory
 - Pacific Northwest National Laboratory: Compatibility of Polymeric Materials Used in the Hydrogen Infrastructure
 - City and County of San Francisco: Advancing Fuel Cell Electric Vehicles in San Francisco and Beyond

Systems Analysis

- Systems Analysis Subprogram Overview

-
- Argonne National Laboratory: Regional Water Stress Analysis with Hydrogen Production at Scale
 - Argonne National Laboratory: Analysis of Technology Improvement in Fuel Cell Vehicles
 - National Renewable Energy Laboratory: Sustainability Analysis: Hydrogen Regional Sustainability (HyReS)
 - National Renewable Energy Laboratory: Regional Supply of Hydrogen
 - National Renewable Energy Laboratory: Market Segmentation Analysis of Medium- and Heavy-Duty Trucks with a Fuel Cell Emphasis
 - Argonne National Laboratory: Analysis of Cost Impacts of Integrating Advanced Onboard Storage Systems with Hydrogen Delivery
 - National Renewable Energy Laboratory: H2@Scale Analysis

Small Business Innovation Research

H2@Scale Cooperative Research and Development Agreement Projects

Acronyms, Abbreviations, and Definitions

Primary Contacts Index

Hydrogen and Fuel Cells Program Contacts

Project Listings by State

Project Listings by Organization

Introduction

The U.S. Department of Energy’s Hydrogen and Fuel Cells Program (the Program) focuses on early stage research and development (R&D) activities and works with stakeholders to enable the widespread market acceptance of hydrogen and fuel cell technologies across diverse applications. The Program is coordinated across the U.S. Department of Energy (DOE), incorporating activities in the offices of Energy Efficiency and Renewable Energy (EERE)—led through the Fuel Cell Technologies Office (FCTO)— Fossil Energy (FE), Nuclear Energy (NE), Science (SC), and Advanced Research Projects Agency–Energy (ARPA-E). Every year, FCTO publishes an Annual Progress Report documenting progress, accomplishments, and technology status with respect to performance metrics. This report includes several hundred pages of accomplishments achieved by DOE-funded projects in the last year. The following summary includes only a few examples. More details can be found in the individual subprogram introductions, subsequent project reports, and in the corresponding 2018 Annual Merit Review and Peer Evaluation Report.

In Fiscal Year (FY) 2018, Congress appropriated approximately \$115 million for hydrogen and fuel cell activities in EERE’s FCTO and approximately \$30 million for FE’s solid oxide activities. In addition, funding within ARPA-E, NE, and SC relevant to hydrogen and fuel cell activities amounted to approximately \$20 million, \$2 million, and \$19 million, respectively. This represents a total DOE budget for FY 2018 of approximately \$185 million related to hydrogen and fuel cell technologies.¹ While FCTO is the primary office related to hydrogen and fuel cells in DOE’s congressional budget request, the Program coordinates across all relevant offices, and pertinent activities are identified during the year based on gap analyses and merit-reviewed project proposals that may be selected through competitive funding opportunities, which vary from year to year. In addition to FCTO-funded progress, this report includes examples of progress provided by managers within other DOE offices.

H2@Scale Activities

In FY 2018, the Program’s primary efforts focused on increasing its emphasis on Hydrogen at Scale (H2@Scale).² H2@Scale is a DOE initiative that brings together stakeholders to advance affordable hydrogen production, transport, storage, and utilization to increase revenue opportunities and impact in multiple energy sectors. Figure 1 depicts the H2@Scale conceptual vision with hydrogen as an energy carrier that enables new value-added applications. The premise of H2@Scale is that hydrogen can be generated and used in various industries by leveraging low-cost sources of energy that are intermittently available throughout the year (such as solar or wind) *as well as* baseload power (such as nuclear) from generators that are being economically challenged by ongoing changes in the energy sector. By optimizing the use of otherwise-curtailed energy, as well as energy sources that cannot be turned down rapidly enough to compensate for intermittent renewables, H2@Scale offers innovative ways to enable energy security, energy storage, resilience, and economic value. R&D efforts include scalable concepts for dispatchable hydrogen production, delivery, and storage, including hydrogen carriers, liquefaction, materials development, and systems integration across diverse generation sources and end uses.

¹ Historical budgets are available at <https://www.hydrogen.energy.gov/budget.html>.

² For more information, see <https://energy.gov/eere/fuelcells/h2-scale>.

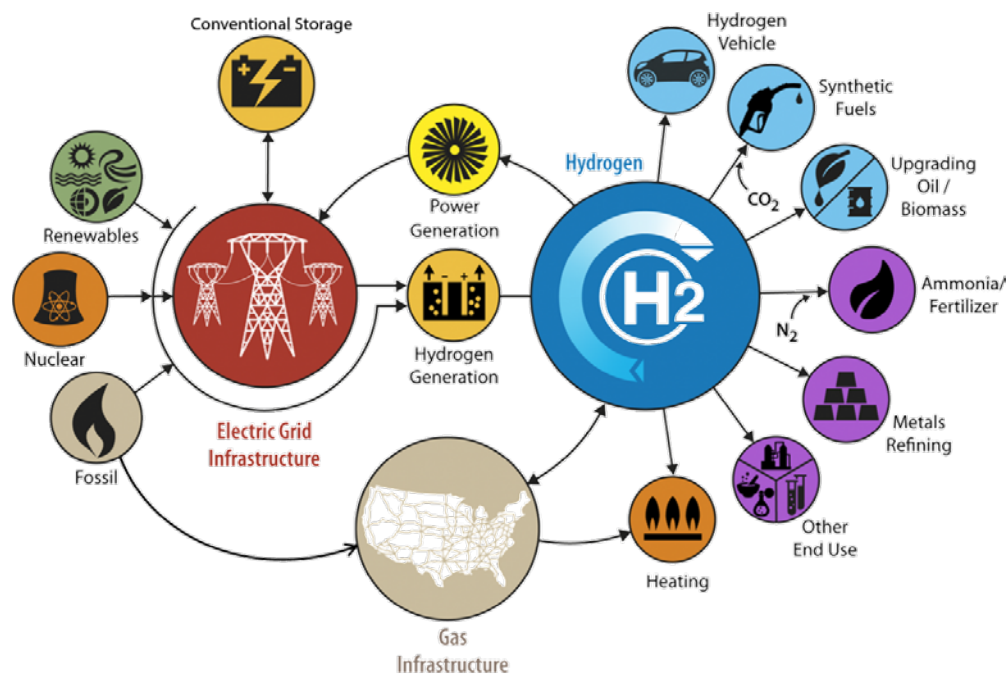


Figure 1. Schematic of H2@Scale

The H2@Scale initiative also provides a framework in which national laboratories and industry can work together through government co-funded projects to accelerate the early-stage research, development, and demonstration of applicable hydrogen technologies.

In FY 2018, the Program held a kickoff meeting for more than 20 H2@Scale cooperative research and development agreement (CRADA) projects that were selected in late FY 2017. H2@Scale CRADA projects are being funded at the national laboratories by industry and nonprofit organizations, with cost match from FCTO. Project focus areas include integrating hydrogen production with electricity generation and transmission; reducing the cost of hydrogen production technologies; and lowering the cost, reducing footprint, and improving reliability of hydrogen fueling infrastructure. The H2@Scale “consortium” refers to the group of national laboratory and private sector partners that have ongoing CRADA projects. In FY 2018, the Program revised the original structure of the thematic areas within H2@Scale from a project-oriented format into four working group themes: “Make,” “Move,” “Use,” and “Store” hydrogen. Subsequent to the August 2018 kickoff meeting, members of project teams related to hydrogen production and grid integration held the first Make working group meeting in December 2018. These working group meetings occur monthly to facilitate collaboration in specific areas.

Through a collaboration between FCTO and NE, a team of national laboratory researchers led by the National Renewable Energy Laboratory (NREL), and including Argonne National Laboratory (ANL), Idaho National Laboratory, and others, conducted a comprehensive analysis of the technical and economic potential of the H2@Scale vision in the United States. The analysis is currently under DOE review. Preliminary results characterize the maximum potential demand for hydrogen in the United States as roughly 150 million metric tonnes per year (MMTY) and the economic potential demand as 22–45 MMTY; for reference, U.S. hydrogen demand is currently approximately 10 MMTY. Analysis also indicates that ample, diverse energy resources (e.g., solar power, wind power, nuclear power, and natural gas) are available throughout the United States to satisfy the maximum potential demand for hydrogen.

Also in FY 2018, the Program competitively selected four new projects to demonstrate first-of-a-kind hydrogen-focused integrated renewable energy production, storage, and transportation fuel distribution/retailing systems. These projects will demonstrate use of electrolyzers to supply grid services at a

solar farm, autonomous hydrogen fueling technologies, electrolysis of wastewater, and synthesis of methanol and dimethyl ether from streams of hydrogen and carbon dioxide. The Program also selected four new projects to enable cost-competitive manufacturing of megawatt-scale electrolyzers. Electrolyzers at megawatt scales are expected to be required in emerging applications, such as the provision of grid services or hydrogen production at fueling stations.

Lastly, the Program released two H2@Scale-related Requests for Information (RFIs) in FY 2018 to gather information from stakeholders. In August 2018, in collaboration with eight other DOE offices, the Program released a comprehensive H2@Scale RFI. This RFI aimed to identify and quantify domestic resources compatible with large-scale hydrogen production, and to identify pathways to enable effective near- and long-term leveraging of these resources in major industries requiring affordable, secure, domestic, and scalable hydrogen supplies. Information gathered from the RFI may guide H2@Scale projects and funding opportunities in FY 2019. In June 2018, the Program released an RFI to gather feedback on regulatory barriers to the development of hydrogen infrastructure. DOE will review the information gathered to identify priority R&D to reduce regulatory barriers affecting implementation of hydrogen technologies and potential courses of action to reduce deployment time and cost; share the information with relevant agencies with regulatory authority; and explore opportunities for interagency collaboration.

The Program also continued to prioritize early-stage R&D working through four consortia: Electrocatalysis Consortium (ElectroCAT), HydroGEN Advanced Water Splitting Materials Consortium (HydroGEN), Hydrogen Materials—Advanced Research Consortium (HyMARC), and the newly formed Hydrogen Materials Compatibility Consortium (H-Mat). These consortia aim to make unique, world-class expertise and capabilities of national labs more accessible and available to university and industry partners across the country. This approach creates a collaborative foundation for an innovation ecosystem that can bring in a steady influx of competitively selected projects to tackle the most pressing technical challenges in the field. Under the umbrella of DOE's Energy Materials Network (EMN), these efforts use state-of-the-art computational, high throughput/combinatorial synthesis, and characterization tools; data management such as machine learning; and other approaches to accelerate progress in energy materials R&D through a multi-disciplinary team approach.

Patents and Commercialized Technologies

Each year, FCTO tracks U.S. patents granted specifically as a result of its funding as just one indicator of cutting-edge innovation. Cumulatively, this funding has led to more than 730 hydrogen and fuel cell patents with approximately 35% coming from the national labs.³ More than 30 technologies have been commercialized as a result of this research, including catalysts for fuel cells, high-pressure hydrogen tanks, electrolyzers for hydrogen production, and fuel cell system components. DOE-funded research has also cut the cost of automotive fuel cells by 60% in the last decade,⁴ quadrupled durability to over 120,000 miles,⁵ and cut electrolyzer stack costs by 80% since 2002.⁶

EXAMPLES OF PROGRESS AND ACCOMPLISHMENTS BY KEY ACTIVITY

Hydrogen Fuel R&D

The Hydrogen Fuel R&D subprogram focuses on early-stage R&D to reduce the cost and improve the reliability of technologies used to produce and store hydrogen from diverse domestic energy resources. The subprogram evaluates its project portfolio with respect to its potential to meet DOE's ultimate cost targets of

³ Pathways to Success: Innovations Enabled by the U.S. Department of Energy Fuel Cell Technologies Office, https://www.energy.gov/sites/prod/files/2018/11/f57/fcto_2017_pathways_commercial_success.pdf

⁴ DOE Hydrogen and Fuel Cells Program Record #16020, https://www.hydrogen.energy.gov/pdfs/16020_fuel_cell_system_cost_2016.pdf

⁵ DOE Hydrogen and Fuel Cells Program Record #16019, https://www.hydrogen.energy.gov/pdfs/16019_fuel_cell_stack_durability_2016.pdf

⁶ DOE Hydrogen and Fuel Cells Program Record #14004, https://www.hydrogen.energy.gov/pdfs/14004_h2_production_cost_pem_electrolysis.pdf

<\$2/kg for hydrogen production, and \$8/kWh for hydrogen storage system cost while achieving 2.2 kWh/kg and 1.7 kWh/L for hydrogen storage system gravimetric and volumetric energy densities, respectively.

FY 2018 activities focused primarily on early-stage R&D funded through the subprogram's two consortia:

1. HydroGEN to accelerate research, development, and deployment of advanced water splitting technologies for clean, sustainable hydrogen production.
2. HyMARC to accelerate the discovery of breakthrough hydrogen storage materials.



The Hydrogen Fuel R&D subprogram made significant progress on several fronts during FY 2018. Specific examples include the following.

- HydroGEN successfully engaged in an interagency collaboration with the National Science Foundation's (NSF) Designing Materials to Revolutionize and Engineer our Future (DMREF) program element, resulting in four NSF DMREF projects that will leverage HydroGEN's expertise and capabilities in three water splitting technologies—photoelectrochemical (PEC), low temperature electrolysis (LTE), and solar thermochemical (STCH).
- In PEC materials R&D, Rutgers achieved a solar-to-hydrogen efficiency of 11.5% with a platinum-group-metal (PGM)-free Ni₅P₄ hydrogen evolution catalyst integrated with a high-performing photoabsorber; this exceeds the target of 10% efficiency and is on par with conventional PtRu catalysts.
- In the areas of STCH materials R&D, the University of Colorado Boulder developed machine learning models for the discovery of efficient and stable STCH materials, identifying ~28,000 stable perovskite formulations from more than 1.1 million possible candidates with greater than 90% accuracy.
- Hydrogen storage R&D accomplishments included the demonstration of lower-cost polyacrylonitrile (PAN) feedstock material fiber spinning and conversion to high strength carbon fiber, resulting in 14% cost reduction compared to the current PAN. The University of Kentucky also demonstrated efficient solvent recovery and reduced fresh water use.
- A HyMARC seedling project conducted by the University of Hawaii demonstrated hydrogenation of MgB₂ to Mg(BH₄)₂ at 25% lower temperature and 22% lower pressure than prior state of the art.

Fuel Cell R&D

One of the most important metrics used to guide the Fuel Cell R&D subprogram's R&D efforts is the projected high-volume manufacturing cost for automotive fuel cells, which is tracked periodically. The subprogram is targeting an interim cost of \$40/kW and durability of 5,000 hours by 2025. Long-term competitiveness with alternative powertrains is expected to require further cost reduction to \$30/kW and 8,000 hours durability, which represent the subprogram's ultimate targets. The industry peer-reviewed cost projection for an 80-kW_{net} automotive polymer electrolyte membrane (PEM) fuel cell system based on next-generation laboratory technology and operating on direct hydrogen is \$50/kW_{net} when manufactured at 100,000 units/year and \$45/kW_{net} when manufactured at 500,000 units/year.⁷ However, this status does not quite meet the durability targets of 5,000 hours by 2025 and further analysis is underway to update the cost projections.

⁷ Hydrogen and Fuel Cells Program Record #16020, https://www.hydrogen.energy.gov/pdfs/16020_fuel_cell_system_cost_2016.pdf

In FY 2018, the ElectroCat and Fuel Cell Consortium for Performance and Durability (FC-PAD) made significant progress in R&D of PGM-free and low-PGM catalysts and electrodes, respectively. Highlights include the following.

- FC-PAD continued to conduct foundational R&D on low-PGM catalysts and electrodes that is critical to decreasing cost and improving performance and durability of PEMFCs. For example, FC-PAD researchers conducted extensive characterization and electrochemical testing of stack materials to benchmark on-road commercial fuel cell technology.
- ElectroCat made a number of breakthroughs in PGM-free catalysts. The consortium made key insights into the structure and density of active sites by counting with molecular probes, backed up by electrochemical, spectroscopic, and computational tools.
 - The core consortium improved catalyst performance in membrane electrode assemblies by more than 50% compared to the 2016 baseline. In one example, PGM-free catalysts achieved 27 mA/cm² compared to the 2016 baseline of 16 (mA/cm²), a more than 65% improvement.
 - The consortium also began working with new industry and academic partners to improve PGM-free catalysts, resulting in record performance for Co- and Mn-based catalysts.
- A project led by Los Alamos National Laboratory (LANL) has developed novel membranes and electrode ionomers to enable fuel cells operating over a temperature range of 80°– 220°C, with demonstrated power density of nearly 1.5 W/cm² at 200°C. In this project, a highly conductive phosphonated ionomer and a phosphoric-acid-doped, ion-pair-coordinated quaternary ammonium hydrocarbon-based polymer membrane increased low-temperature performance and water tolerance with significantly decreased phosphoric acid leaching. This project will be continued through a grant recently awarded by ARPA-E, demonstrating effective cross-office coordination.



Technology Acceleration and Hydrogen Infrastructure R&D

Technology Acceleration and Hydrogen Infrastructure R&D activities help accelerate the transition of early-stage hydrogen and fuel cell research to subsequent stages of development and leverage the private sector to enable deployment. This includes R&D to integrate hydrogen production technologies with the electricity grid, advance technologies that can be used in hybrid energy systems, lower the cost of manufacturing hydrogen and fuel cell technologies, reduce the cost of hydrogen transport and distribution, reduce the cost and improve reliability of hydrogen fueling stations, and support the infrastructure component supply chain. In FY 2018, hydrogen delivery R&D was moved into a new Hydrogen Infrastructure R&D budget line item in the FY 2019 budget request, emphasizing the importance of hydrogen delivery R&D in the context of hydrogen infrastructure.

In FY 2018, Technology Acceleration and Hydrogen Infrastructure R&D made significant progress to advance cost-competitive hydrogen technologies and establish the viability of hydrogen in emerging applications. R&D is aimed at achieving the Program's objective of \$5/kg for hydrogen delivery and dispensing by 2025 (\$2/kg ultimate target) and supporting the Program's H2@Scale initiative.

Examples of key accomplishments in FY 2018 include the following.

- In collaboration with the Safety, Codes and Standards subprogram and the hydrogen storage activity within the Hydrogen Fuel R&D subprogram, Technology Acceleration and Hydrogen Infrastructure R&D initiated activities to launch the Hydrogen Materials Compatibility (H-Mat)



national laboratory consortium. H-Mat will conduct materials research to reduce the costs and enhance the durability of steels and polymers in hydrogen service.

- One of the 27 fuel cell electric buses undergoing performance evaluation by NREL exceeded DOE's ultimate target for fuel cell durability of 25,000 hours. Twelve buses have exceeded 19,000 hours to date. NREL continued to collect data on bus maintenance costs and hydrogen consumption and completed its annual report on status versus targets.
- GVD Corporation determined that its novel coatings for hydrogen compressor seals can reduce seal erosion by 70%. GVD's coatings comprise polymeric and inorganic layers that enhance seal flexibility and lubricity, and they are expected to reduce hydrogen permeation by 10-fold.
- Giner ELX achieved one of the highest known efficiencies to date for 350-bar electrochemical hydrogen compression—4 kWh/kg at an inlet pressure of 100 bar and outlet pressure of 350 bar. Giner's compressor concept relies on novel aromatic membranes that achieve 30% less drag than conventional perfluorosulfonic acid membranes and 50% less back diffusion.
- Ivys Energy Solutions established that its approach to wireless communication between vehicles and fueling stations, using digital short range communication, can exceed the requirements of the SAE International J2799 standard. Ivys also established that its novel metering technology, based on Coriolis meters, can achieve an accuracy of at least 2%. The accuracy of 2% exceeds the current hydrogen meter accuracy requirement of 5% specified in the National Institute of Standards and Technology Handbook 44.
- NREL and Gore scanned rolls of fuel cell membrane material on a web-line optical research apparatus at NREL to obtain a two-dimensional thickness map (at ~1 mm spatial resolution). This map can be easily be analyzed to locate where thickness is above or below defined thresholds for quality control. In-line mapping of thickness will help enable high-volume manufacturing and cost reduction of membranes for fuel cells and electrolyzers.
- ANL completed performance evaluation of the Toyota Mirai under varying conditions, including outside temperature (-7°C to 35°C). Systems engineering solutions have enabled excellent durability.

Safety, Codes and Standards

The Safety, Codes and Standards subprogram focuses on R&D that enables safety as well as the development of codes and standards by industry, informed by FCTO's foundational research. The subprogram identifies and performs early-stage R&D that provides a fundamental understanding of the relevant physics, critical data, and safety information used to develop and revise technically sound and defensible codes and standards.

FY 2018 accomplishments include the following.

- Sandia National Laboratories (SNL) published a report documenting a "Hydrogen Fuel Cell Electric Vehicle Tunnel Safety Study" that provided a scientific basis for allowing fuel cell electric vehicles (FCEVs) in tunnels. The report is intended to enable the adoption of FCEVs in the northeast region of the United States.
- Pacific Northwest National Laboratory (PNNL) partnered with the American Institute of Chemical Engineers to establish the Center for Hydrogen Safety, enabling long-term sustainability and broader impact of the Hydrogen Safety Panel and its safety knowledge resources.
- LANL completed the planning and installation of an in-line fuel analyzer in the field (with H2Frontier) and conducted on-site baseline measurements while adding wireless capabilities for remote testing.

- SNL developed and proposed design curves for pressure-vessel steels—applicable to both Cr-Mo and Ni-Cr-Mo steels—to the ASME (the American Society of Mechanical Engineers) Pressure Vessel Committee as the basis for a code case that will allow pressure vessel design for high-pressure hydrogen without additional testing burden.

Systems Analysis

Systems Analysis activities are foundational to the Program and help identify technology gaps, impacts, and future R&D needs. Systems Analysis also supports H2@Scale activities as demonstrated by the results reported above.

Two separate projects evaluated the cost impacts of FCTO-funded R&D. A comparative total cost of ownership analysis was completed for five different truck powertrain technologies (diesel, diesel hybrid-electric, compressed natural gas, battery electric, and fuel cell electric) in three different truck applications (Class 8 long haul, Class 8 short haul, and Class 4 parcel delivery) for three time periods reflecting different technology status levels (2018, 2020, and 2040). The study found fuel cell powertrain trucks to have the lowest total cost of ownership of the various powertrains by 2020, if FCTO program cost and performance targets are met.

The second study evaluated the potential of reducing fueling station costs by integrating advanced onboard storage systems with hydrogen delivery technology. The analysis concluded that the hydrogen delivery and refueling cost is strongly impacted by the pressure and temperature requirements of an FCEV's onboard storage systems. Low-pressure and near-ambient-temperature dispensing can significantly reduce hydrogen dispensing cost to FCEV customers. These onboard storage options, including their respective boundary conditions, will be integrated with hydrogen delivery technologies to evaluate the cost impact on the hydrogen pathways. The inputs and assumptions used in these analysis efforts are the result of collaboration with EERE's Vehicle Technologies Office and Bioenergy Technologies Office.

OTHER PROGRAM ACTIVITIES AND HIGHLIGHTS FROM FY 2017–2018

ARPA-E Programs in Fuel Cells and Electrolyzers for Energy Conversion and Storage

ARPA-E's FY 2018 funding for fuel cells and electrolyzers for energy conversion and storage activities was approximately \$20 million, which was applied to focused programs as well as projects within the more general OPEN 2015 solicitation. In FY 2019, ARPA-E anticipates a budget of approximately \$15 million in related selected projects from the recent OPEN 2018 solicitation. The mission of the program is to develop new disruptive technologies for efficient, cost-effective electrical storage and generation systems using renewable energy and natural gas with applications for transportation, commercial, and industrial power customers across the economy, resulting in increased energy efficiency and security, significant fuel and energy savings, and reduced emissions. The drivers are growth of intermittent renewable energy and cheap and abundant natural gas, the need for increased energy efficiency throughout the whole economy, an increased demand for clean/electrified transportation, and the growth of microgrids and distributed energy generation.

Duration Addition to electricity Storage

The mission of the Duration Addition to electricity Storage (DAYS) program is to develop energy storage systems that provide power to the electric grid for durations of 10 hours to up to 100 hours, opening significant new opportunities to increase grid resilience and performance. The extended discharge times of DAYS projects will enable a new set of grid applications including long-lasting backup power and greater integration of domestic, renewable energy resources. Project teams will develop storage systems that are deployable in almost any location and charge and discharge electricity at a target fixed cost per cycle. The FY 2018 budget for projects related to chemical storage is approximately \$12 million with projects commencing in FY 2019.

Renewable Energy to Fuels through Utilization of Energy-dense Liquids

The Renewable Energy to Fuels through Utilization of Energy-dense Liquids (REFUEL) program mission is to reduce transportation and storage costs of energy from remote renewable intermittent sources to consumers and enable the use of existing infrastructure to deliver electricity or hydrogen at the end point. Specific program goals are to:

- Develop catalytic or electrochemical fuel cracking to deliver hydrogen at 30 bar at a cost <\$4.5/kg, enabling hydrogen fueling stations.
- Develop fuel cell technologies for conversion of fuels to electricity with source-to-use cost <\$0.30/kWh.

Reliable Electricity Based on Electrochemical Systems

The Reliable Electricity Based on Electrochemical Systems (REBELS) mission is to develop transformational electrochemical fuel cell technologies for distributed power generation to improve grid stability, increase energy security, and balance intermittent renewable technologies while reducing CO₂ emissions associated with current distributed generation systems. Specific accomplishments include the following:

- The Colorado School of Mines achieved 150 mW/cm² power density at 500°C on direct methane fuel and showed stability for thousands of hours. The project is now scaling up to larger prototypes.
- Georgia Tech achieved 200 mW/cm² power density at 500°C on 97% methane fuel.

Integration and Optimization of Novel Ion-Conducting Solids

Funded in FY 2016, the Integration and Optimization of Novel Ion-Conducting Solids (IONICS) mission is to create components for electrochemical cells using solid ion conductors to enable transformational performance and cost improvements. The FY 2018 budget was approximately \$7 million. Specific accomplishments include the following:

- Increased the energy content of lithium battery packs by >30% and reduced the cost of energy storage.
- Developed flow batteries with fully installed costs of \$150/kWh for a 5-hour duration.
- Created alkaline-conducting membranes that open a path to fuel cells and electrolyzers without expensive, rare elements like platinum.

Innovative Natural-Gas Technologies for Efficiency Gain in Reliable and Affordable Thermochemical Electricity-Generation

Funded in FY 2017 with projects commencing in FY 2018, the mission of the Innovative Natural-Gas Technologies for Efficiency Gain in Reliable and Affordable Thermochemical Electricity-Generation (INTEGRATE) program is to reduce the cost and increase the primary energy efficiency associated with the provision of electric power to commercial and industrial customers. The approach taken is to support the development of natural-gas-fueled distributed generation systems (<1 MW) with electric efficiencies of ≥70% and installed costs of ≤\$1,800/kW and focus on engine/solid oxide fuel cell (SOFC) hybrid systems to leverage available thermo-economic synergies.

Office of Science, Basic Energy Sciences

The Basic Energy Sciences program within the Office of Science had a cross-cut spending level of approximately \$20 million in FY 2018. Hydrogen and fuel cells were among the topics in the Energy Frontier Research Center solicitation in FY 2018, and two Energy Frontier Research Centers were awarded that have components focused on hydrogen production.

Specific accomplishments include the following:

- Increases in catalytic reactivity were realized by tailoring the oxide surfaces at the atomic level. Layer-by-layer synthesis of perovskite oxide catalysts was utilized to precisely locate the reactive dopant atoms and increase catalytic activity while avoiding surface poisoning reactions.
- A single-site water oxidation catalyst was designed that increased the reaction rate more than 100 times at low pH. By utilizing computational insights, a catalyst was designed to more easily accommodate the water molecule and lower the barriers to oxidation, thereby substantially increasing the rate of hydrogen production.
- New insights into hydrogen bonding in a metal-organic framework material are allowing selective diffusion of gases through the material. Hydrogen-containing molecules such as NH₃ and H₂O can displace other molecules in the metal-organic framework crystallite via a hydrogen bond and then block molecules such as CO₂, while allowing hydrocarbons to pass through.

Office of Fossil Energy, Solid Oxide Fuel Cell Program

The SOFC Program within FE had an enacted budget of \$30 million in FY 2018. The Program's mission is to enable the generation of efficient, low-cost electricity from natural gas or coal. The near-term goal is to develop natural-gas-fueled distributed generation and small-scale, modular coal-fueled systems, with a long-term goal of coal and natural gas utility-scale applications with carbon capture and sequestration. Drivers include cost and efficiency benefits to coal and natural gas power systems and the development of near-term natural gas distributed generation applications. The Program maintains a portfolio of approximately 50 projects that focus on cell and core technology and systems development. Researchers from academia, national laboratories, research institutions, and small businesses collaborate with SOFC developers to address and resolve reliability issues, improve performance, and reduce the cost of SOFC power systems. Based on progressively larger natural-gas-fueled validation tests, MWe-class distributed generation SOFC power systems that are cost competitive with existing distributed generation technologies are envisioned circa 2020.

Specific FY 2018 accomplishments include the following:

- Field tested a 250 kWe pressurized prototype system.
- Factory tested a 200 kWe prototype system.
- Awarded two projects to initiate conceptual design and conduct techno-economic evaluation of a distributed generation, natural-gas-fueled MWe-class SOFC power system.

Office of Nuclear Energy

NE is working with partners in EERE and industry to evaluate the potential demonstration of commercial-scale production of hydrogen using heat and electricity from a nuclear energy system. In addition to the emissions-free electricity currently produced by nuclear reactors, some advanced nuclear reactor designs will operate at very high temperatures, making them well suited for promising new thermally driven hydrogen production processes. These advanced reactors, now being developed by NE, could provide the low-cost heat necessary for these processes to economically produce hydrogen. Hydrogen production is also being assessed for light-water reactor technologies (currently operating and new builds), although these systems will likely be operated at somewhat lower efficiency than advanced high-temperature reactors.

In FY 2018, NE provided funding for collaborative research to analyze (via advanced modeling and simulation tools) and develop the following technologies that use nuclear reactors to produce hydrogen, in collaboration with FCTO.

- High-temperature electrolysis (HTE): HTE uses electricity to produce hydrogen from steam instead of liquid water. This method promises higher efficiencies than standard electrolysis, which is employed commercially today. The new high-temperature design involves many technical challenges, including the

development of high-temperature materials and membranes. FY 2018 research indicates the potential to use steam produced via current light-water reactor technologies, in addition to advanced reactor designs, to support HTE.

- **Reactor/hydrogen production process interface:** The interface between the nuclear reactor and the hydrogen production system involves potentially long heat transfer paths at elevated temperatures, heat exchangers that are subject to both elevated temperature and corrosive chemical environments, new safety and regulatory issues, and supporting systems for chemical processes and hydrogen and oxygen storage. FY 2018 research under NE focused on developing high-fidelity, dynamic modeling and simulation tools that can be applied to determine optimal system design and operation for use of light-water reactor technologies to support hydrogen production via HTE.

FY 2018 NE funding also supported development of a detailed engineering design for an electrically heated thermal energy distribution system that can support testing and demonstration of a thermal-energy-driven high-temperature electrolysis system. This thermal energy input can be controlled in a manner that emulates the integration with a light water reactor. It is anticipated that this thermal system will be constructed in FY 2019 to support future nuclear system demonstration.

INTERNATIONAL ACTIVITIES

International Partnership for Hydrogen and Fuel Cells in the Economy

The International Partnership for Hydrogen and Fuel Cells in the Economy (IPHE) is a forum for governments to work together to advance worldwide progress in hydrogen and fuel cell technologies. It includes 18 member countries (Australia, Austria, Brazil, Canada, China, France, Germany, Iceland, India, Italy, Japan, the Netherlands, Norway, the Republic of Korea, the Russian Federation, South Africa, the United Kingdom, and the United States) and the European Commission. Additional countries expressed interest in 2018 as well. The United States was elected as chair at the May 2018 Steering Committee meeting in Japan and subsequently chaired the Steering Committee meeting in South Africa. In October Japan hosted the first Hydrogen Energy Ministerial in more than 15 years, attended by representatives from 20 countries including Deputy Secretary of Energy Dan Brouillette. IPHE agreed to rename its Regulations, Codes and Standards (RCS) Working Group to RCSS by adding an emphasis on safety. Sharing safety information, harmonizing codes and standards, and ensuring a global market for the growing supply chain are examples of focus areas within IPHE.

International Energy Agency

The United States is involved in international collaboration on clean energy technologies through the International Energy Agency's Technology Collaboration Programme (TCP) on Advanced Fuel Cells. This TCP provides a mechanism for member countries to share the results of pre-competitive R&D and analysis activities related to innovative fuel cell and electrolyzer technologies. In FY 2018, the TCP on Advanced Fuel Cells held an outreach event at its Executive Committee meeting in cooperation with the Austrian Energy Agency. The event was targeted toward Austrian stakeholders and addressed the market readiness of fuel cells. The TCP voted to set up a subtask on heavy duty vehicles in the Polymer Electrolyte Fuel Cells Annex and it is considering a new subtask on maritime application. The focus of the topical meeting in 2020 will be on heavy-duty transportation with onboard storage opportunities. The Executive Committee will explore standardization of measurement and reporting procedures in electrolysis to help facilitate R&D of different electrolyzer technologies.

EXTERNAL COORDINATION, INPUT, AND ASSESSMENTS

Hydrogen and Fuel Cells Technical Advisory Committee

The Hydrogen and Fuel Cells Technical Advisory Committee (HTAC), a congressionally mandated committee to advise the Secretary of Energy, formally convened twice in FY 2018. In December 2018, HTAC submitted its tenth annual report to DOE, which summarizes progress in hydrogen and fuel cell technologies, domestic and international RD&D, and commercialization activities, and offers recommendations on DOE's hydrogen-

related R&D activities and initiatives. HTAC also convened two subcommittees: (1) one tasked with creating outreach modules for a general audience providing basic information on key hydrogen and fuel cell topics, and (2) one to explore the global competitiveness of the U.S. hydrogen and fuel cell industry and any steps DOE could take to help improve the U.S. position.

Federal Inter-Agency Coordination

The Hydrogen and Fuel Cell Interagency Task Force, mandated by the Energy Policy Act of 2005, includes senior representatives from federal agencies supporting hydrogen and fuel cell activities. In 2018 the Program convened, for the first time, a one-day track of presentations from other federal, state, and regional agencies at the Hydrogen and Fuel Cells Program Annual Merit Review and Peer Evaluation. These oral and poster sessions included briefings on hydrogen and fuel cells related activities being conducted by other DOE offices, the Department of Defense (DoD), NASA, Department of Transportation (DOT), United States Postal Services (USPS), National Park Service, and Environmental Protection Agency, among others. In addition, panels were held with representatives from state and regional organizations to discuss progress on regional hydrogen infrastructure and state-funded hydrogen and fuel cell activities.

This year, a new interagency collaboration was started with DOT's Federal Railroad Administration to assess hydrogen and fuel cell technologies for rail applications. In another new interagency collaboration with DoD's Army Tank Automotive Research, Development and Engineering Center (TARDEC), a joint workshop was held to evaluate hydrogen refueling infrastructure pathways for tactical vehicles. DOE convenes monthly meetings with an Interagency Working Group to share information, which in FY 2018 included webinars covering a variety of topics such as NASA's Mars Mission, the TARDEC fuel cell programs, and the USPS's fuel cell lift truck operations results.

FY 2018 Annual Merit Review and Peer Evaluation

The Program's Annual Merit Review and Peer Evaluation Meeting (AMR) took place June 13–15, 2018, in Washington, D.C., and provided an opportunity for the Program to obtain expert peer reviews of the projects it supports and to report its accomplishments and progress. More than 850 participants attended, and more than 175 experts peer reviewed almost 120 of the Program's projects. For the first time, the AMR included participation of FE's SOFC Program (which ran a full 2.5-day track of oral and poster presentations) and activities from other federal and state agencies. The 2018 AMR was also preceded by a National Hydrogen and Fuel Cell Forum, showcasing industry progress, exhibits of technologies, and opportunities for industry. The report summarizing the results and comments from the AMR reviews is available on DOE's website.⁸ The 2019 AMR is being held April 29–May 1, in Crystal City, Virginia, and will continue to involve the SOFC Program and other DOE offices and federal agencies.

Funds Saved through Active Project Management

The AMR is a key part of the Program's comprehensive approach toward active management of its projects. Termination of underperforming projects—identified through the AMR as well as through other go/no-go decisions (with criteria defined in the project scope of work)—helped the Program redirect approximately \$6.0 million in funding in FY 2018, \$3.3 million in funding in FY 2017, \$2.4 million in funding in FY 2016, and more than \$48 million since FY 2010. In addition, the Program implements EERE's robust active project management requirements to identify and resolve issues early and to mitigate risks in impactful ways, helping underperforming projects get back on track.

⁸ https://www.hydrogen.energy.gov/annual_review.html

IN CLOSING ...

The hydrogen and fuel cell market is growing rapidly in the United States and the world beyond. In fact, 70,000 fuel cell units totaling 650 megawatts of fuel cell power were shipped worldwide in 2017, with several hydrogen and fuel cell companies reporting a collective \$2 billion in revenue.

States have invested more than \$180 million in hydrogen infrastructure within the past decade and there were more than 35 retail hydrogen stations in the United States, as of the end of 2018. California has more than 30 of those stations and has planned for a total of 200 stations in the coming years.

There were more than 5,600 commercial fuel cell cars on the road (either leased or sold) at the end of 2018. Along with the Toyota Mirai and the Hyundai Tucson, the new Hyundai NEXO with autonomous capability is now available to retail consumers in select U.S. locations.

At DOE, Deputy Secretary Dan Brouillette and Undersecretary for Energy Mark Menezes drove one of the brand-new Hyundai NEXOs. On loan from Hyundai and Toyota, DOE's pair of fuel cell vehicles have been used for interagency, congressional, and community outreach across the Washington, D.C. area, in addition to getting real-world fueling data that will help guide future early stage R&D efforts.

But it's not just about fuel cell cars. The status at the end of 2018 includes: 240 MW of backup power, more than 20,000 forklifts, and more than 30 fuel cell buses in the United States. Long-range, heavy-duty vehicles are emerging as key applications, and fuel cell delivery and parcel trucks are starting deliveries in California and New York. These early-market applications pave the way for expanding hydrogen infrastructure and contribute substantially to the widespread adoption of hydrogen and fuel cells.

Additional advancements in the hydrogen technologies are expected through DOE's H2@Scale initiative by incentivizing the private sector and national laboratories to tackle key challenges together. Throughout FY 2018, hydrogen was increasingly being recognized as an energy carrier that can unite all our nation's energy resources: natural gas, coal, nuclear, and renewables. The fact that several utilities joined the initiative is a testament to the increased interest. However, there are still a number of challenges, and a major focus is achieving continued cost reductions, performance improvements and economies of scale. H2@Scale offers the opportunity for technology scale up that can enable affordability and lead to viable, sustainable industries across sectors. It is the next-generation vision for hydrogen, beyond light-duty passenger vehicles, and the Program is committed to advancing this work.

This introduction provides only a few examples of activities conducted during FY 2018. The hundreds of pages that follow provide more detail from project recipients, demonstrating the value and impact of DOE funds. The DOE Hydrogen and Fuel Cells Program will continue to work in close collaboration with key stakeholders and will continue its strong commitment to effective stewardship of taxpayer dollars, fostering R&D and innovation, and enabling the success of hydrogen and fuel cell technologies as one component of an "all of the above" energy strategy for the nation.



Dr. Sunita Satyapal

Director, Hydrogen and Fuel Cells Program
Fuel Cell Technologies Office
U.S. Department of Energy

Hydrogen Fuel R&D Subprogram Overview

INTRODUCTION

The Hydrogen Fuel R&D subprogram focuses on early-stage research and development (R&D) to reduce the cost and improve the reliability of technologies used to produce and store hydrogen from diverse domestic energy resources. The hydrogen delivery component of the subprogram was transferred into the new Hydrogen Infrastructure R&D line item in the fiscal year (FY) 2019 President's Budget Request and received appropriations under that line item. In support of R&D needs identified through the U.S. Department of Energy's (DOE's) H2@Scale efforts, the Hydrogen Fuel R&D subprogram is developing a portfolio of hydrogen production and storage technology pathways. The subprogram addresses technical challenges through a portfolio of projects in two R&D areas:

- **Hydrogen production** addresses low-cost, highly efficient hydrogen production technologies that utilize diverse domestic sources of energy. Early-stage R&D activities include advanced water splitting and innovative concepts such as biological hydrogen production. The former is predominantly coordinated through the HydroGEN Advanced Water Splitting Materials consortium (HydroGEN) to accelerate research, development, and deployment of advanced water splitting technologies for clean, sustainable hydrogen production.
- **Hydrogen storage** addresses cost-effective onboard and offboard hydrogen storage technologies with improved energy density. Early-stage R&D activities include high-pressure compressed storage, materials-based storage, and hydrogen carriers. The latter two are coordinated through the Hydrogen Materials—Advanced Research Consortium (HyMARC) to accelerate the discovery of breakthrough hydrogen storage materials.

In FY 2018, hydrogen production projects focused primarily on early-stage R&D for advanced water splitting materials and systems funded through HydroGEN, which is part of the DOE Energy Materials Network. Production pathways under investigation included advanced high- and low-temperature electrochemical water splitting (HTE, LTE), direct solar thermochemical (STCH) and photoelectrochemical (PEC) water splitting, and novel reforming processes for hydrocarbon and waste-stream feedstocks (including thermal, catalytic, and microbial-based processes). Hydrogen storage projects in FY 2018 focused on materials-based hydrogen storage R&D through HyMARC and on advanced tanks through development of precursor fibers for low-cost carbon fiber.

GOALS

The Hydrogen Fuel R&D subprogram goals are to develop:

- Low-cost, highly efficient technologies for *hydrogen production* from diverse domestic resources for both centralized and distributed production applications
- Innovative, low-cost, and energy-dense *hydrogen storage* technologies for transportation and stationary applications, including niche areas such as portable power and material handling equipment.

OBJECTIVES

The Hydrogen Fuel R&D subprogram evaluates its project portfolio with respect to its potential to meet DOE's ultimate cost targets of <\$2 per kilogram (or gasoline gallon equivalent, gge) for hydrogen production and \$8/kWh for hydrogen storage systems while achieving 2.2 kWh/kg and 1.7kWh/L for hydrogen storage system gravimetric and volumetric energy densities, respectively. Interim objectives, consistent with DOE's H2@Scale vision, include:

- Reduce the cost of *hydrogen production* from diverse domestic resources to $< \$2/\text{kg}$ (with a near-term target of $< \$7/\text{kg}$ and an ultimate target of $< \$4/\text{kg}$ for delivered and dispensed hydrogen). This cost is independent of the technology pathway and takes into consideration a range of assumptions for fuel cell electric vehicles (FCEVs) to be competitive.
- Develop *hydrogen storage* systems achieving 1.8 kWh/kg and 1.3 kWh/L for gravimetric and volumetric densities, respectively, at a cost of $\$9/\text{kWh}$ by 2025.

FY 2018 TECHNOLOGY STATUS AND ACCOMPLISHMENTS

The Hydrogen Fuel R&D subprogram actively monitors the technical progress achieved through the hydrogen production and storage project portfolios and incorporates that progress into the status of the technology with respect to performance metrics such as cost, efficiency, and energy density.

Figure 1 shows recent and current status for the high-volume projected costs of hydrogen production for several of the near- to mid-term production pathways, highlighting the cost reductions in recent years resulting from ongoing early-stage R&D. Although natural gas reforming (without carbon capture) already meets the DOE cost target of $< \$2/\text{kg}$, continued early-stage R&D is needed to enable the innovations essential for reducing cost in other large-scale hydrogen production technology pathways utilizing diverse and sustainable domestic resources.

Figure 2 shows the current status of high-pressure compressed hydrogen storage systems for various performance metrics against DOE's ultimate targets. In addition to system cost challenges, compressed hydrogen storage systems are unable to meet the ultimate goal for energy density. The density of hydrogen gas poses a theoretical limitation that prevents ambient compressed hydrogen systems from being able to meet the energy density targets. To address this challenge the subprogram portfolio includes less mature cold/cryo-compressed and materials-based hydrogen storage technologies that have the potential to satisfy all onboard hydrogen storage targets, including energy density.

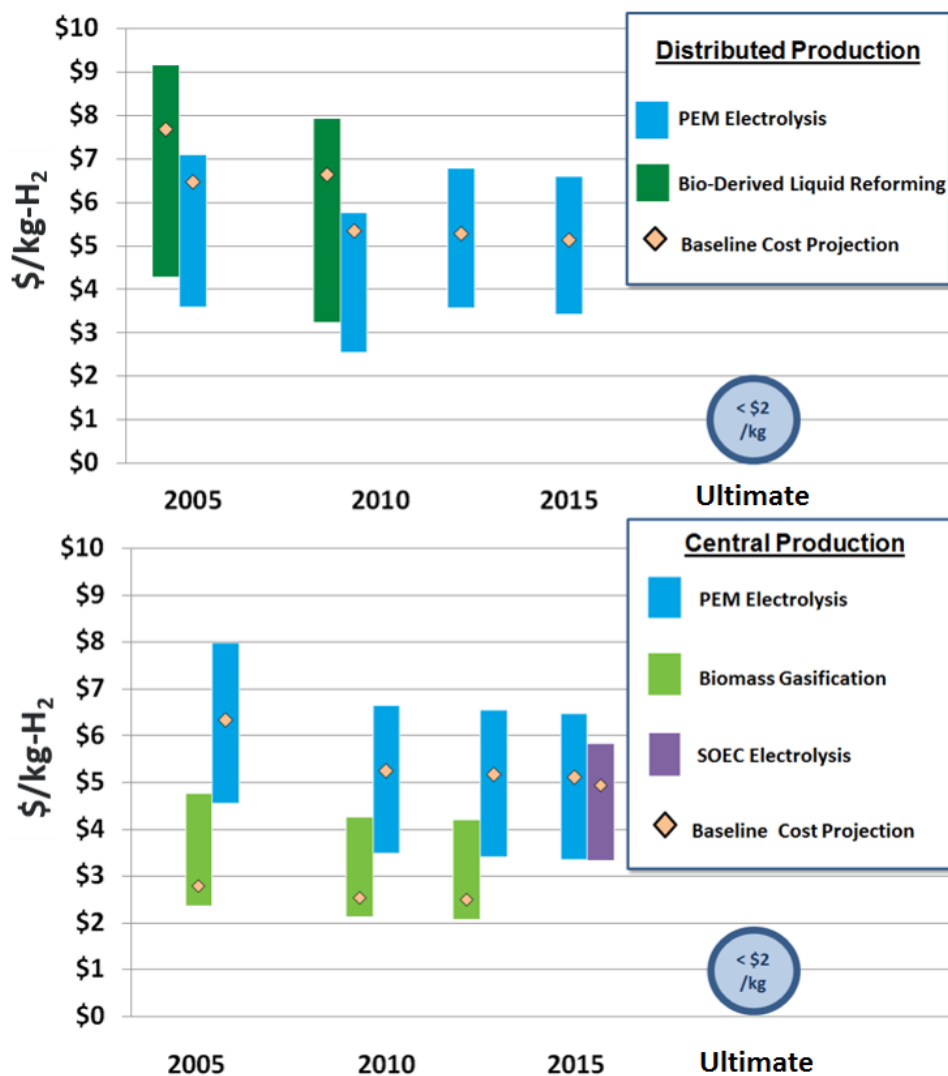


Figure 1. Status for the high-volume projected costs of hydrogen production

Range of hydrogen production costs, untaxed, for near- to mid-term distributed and centralized pathways. The high end of each bar represents a pathway-specific high feedstock cost as well as an escalation of capital cost, while the low end reflects a low feedstock cost and no capital escalation. Bars for different years in the same pathway represent improvements in the costs of the specific pathway, based on specific reference data for the appropriate year and pathway. Detailed information is included in the DOE Hydrogen and Fuel Cells Program Records 14005¹ and 16014.²

¹ *Hydrogen Production Status 2006-2013*, Program Record (Hydrogen and Fuel Cells Program) 14005, U.S. Department of Energy, 2014. https://www.hydrogen.energy.gov/pdfs/14005_hydrogen_production_status_2006-2013.pdf

² *Hydrogen Production Cost from Solid Oxide Electrolysis*, Program Record (Hydrogen and Fuel Cells Program) 16014, U.S. Department of Energy, 2016. https://www.hydrogen.energy.gov/pdfs/16014_h2_production_cost_solid_oxide_electrolysis.pdf

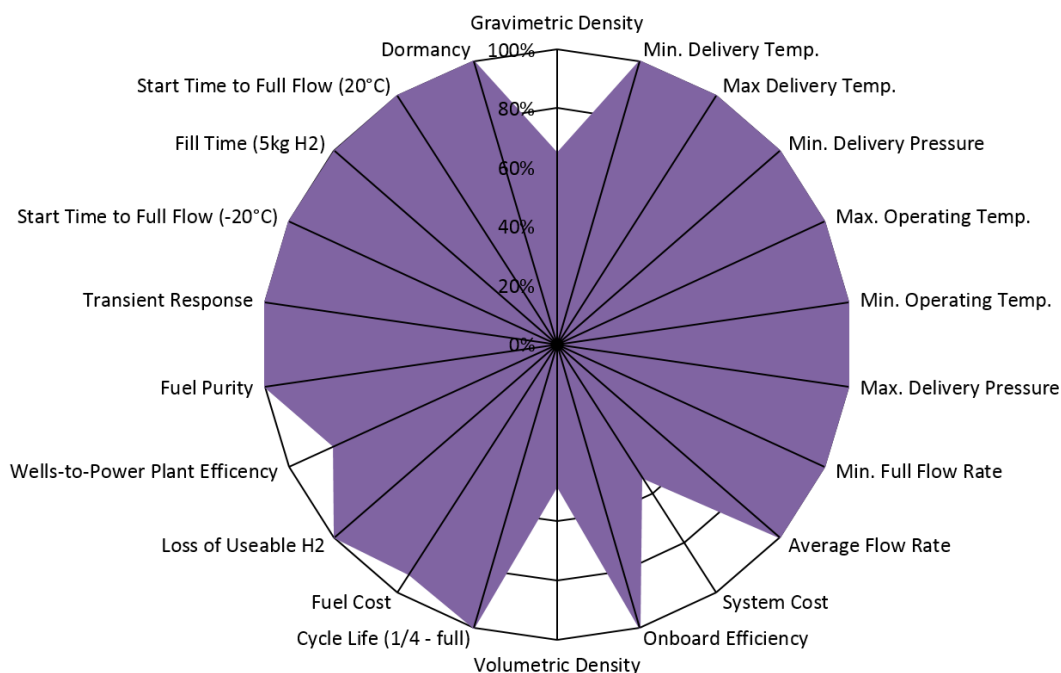


Figure 2. Current status of high-pressure compressed hydrogen storage systems

Current projected performance of a state-of-the-art 700-bar compressed hydrogen storage system with 5.6 kg usable hydrogen storage with ultimate onboard automotive targets³

Subprogram-Level Accomplishments

The Hydrogen Fuel R&D subprogram made significant progress on several fronts during FY 2018. Specific examples include the following.

Hydrogen Production

- The HydroGEN consortium incorporated 19 new funding opportunity announcement (FOA)-awarded projects working across the four advanced water splitting (AWS) technologies and leveraging the capabilities and expertise of six core national laboratories—National Renewable Energy Laboratory (NREL), Sandia National Laboratories (SNL), Lawrence Berkeley National Laboratory (LBNL), Lawrence Livermore National Laboratory (LLNL), Idaho National Laboratory (INL), and Savannah River National Laboratory (SRNL)—to accelerate materials research in order to advance the development of water splitting technologies.
- HydroGEN successfully engaged in an interagency collaboration with the National Science Foundation’s (NSF) Designing Materials to Revolutionize and Engineer our Future (DMREF) program element, resulting in four NSF DMREF projects that will leverage HydroGEN’s expertise and capabilities in three water splitting technologies (PEC, LTE, and STCH).
- The subprogram engaged stakeholders with the release of a Request for Information entitled “H2@Scale: Determining Opportunities to Facilitate Wide-Scale Hydrogen Adoption for Energy Security and

³ *Fuel Cell System Cost—2015*, Program Record (Hydrogen and Fuel Cells Program) 15015, U.S. Department of Energy, 2015. https://www.hydrogen.energy.gov/pdfs/15015_fuel_cell_system_cost_2015.pdf

Economic Growth.” This resulted in more than 70 responses from academic, national laboratory, and industry stakeholders providing their experience and expertise on expanding hydrogen production at large scale across the United States.

- R&D projects in the current hydrogen production portfolio made significant progress, including advances in early-stage materials research for advanced low- and high-temperature electrolysis (including catalyst and membrane innovations); advances in materials research foundational to the PEC and STCH pathways (including novel energy-conversion materials and catalysts); and progress in cutting-edge metabolic engineering for enabling early-stage biological approaches to the conversion of hydrocarbon feedstocks based on biomass and waste streams. The progress is described in further detail in the project-level accomplishments section below.

Hydrogen Storage

- In FY 2018, the hydrogen storage activity negotiated a four-year second phase for the HyMARC effort. For the second phase, the core national laboratory team is being expanded beyond the initial national laboratory team of SNL, LLNL, and LBNL to include NREL, Pacific Northwest National Laboratory (PNNL), the SLAC National Accelerator Laboratory, and the National Institute of Standards and Technology (NIST) Center for Neutron Research, thus fully integrating the former “HySCORE” team into HyMARC. In support of the H2@Scale initiative, second-phase HyMARC activities will include performing foundational research on hydrogen carriers for bulk hydrogen storage and transport as well as on materials for onboard vehicle storage.
- The subprogram completed Phase I go/no-go decisions on seven of the nine initial seedling projects selected through the FOAs in FY 2016 and 2017. Three projects met their go criteria and will be supported for additional research. Four projects did not meet their go criteria and the projects have been discontinued. The two remaining seedling projects are scheduled to complete their Phase I efforts in early FY 2019.
- With support from the subprogram, the HyMARC team published two significant peer-reviewed papers in FY 2018 to provide guidance to researchers developing viable hydrogen storage materials. First was a perspective article titled “An assessment of the strategies for the development of solid-state adsorbents for vehicular hydrogen storage” in the journal *Energy and Environmental Science*. The second was a review paper titled “Nanostructured Metal Hydrides for Hydrogen Storage” in the journal *Chemical Reviews*.
- The subprogram initiated a new effort to evaluate materials for use in cryogenic hydrogen applications, specifically for those applications that require a high number of pressure and temperature cycles, such as cryo-compressed and cryo-sorbents storage. This effort, which will be incorporated into the new Hydrogen Materials (H-Mat) Consortium activities, is being led by PNNL and includes participation from SNL, Oak Ridge National Laboratory (ORNL), and Argonne National Laboratory (ANL).

New Project Selections

In FY 2018, the Hydrogen Fuel R&D subprogram added three HTE projects to support early-stage R&D efforts addressing critical challenges and barriers to hydrogen production via water splitting. The three projects are listed below:

- FuelCell Energy will develop advanced high-temperature water splitting systems for production of hydrogen through efficient and durable electrolytic cells and stacks using innovative proton-conducting ceramic materials and operating at a temperature $\geq 500^{\circ}\text{C}$.
- West Virginia University, through the HydroGEN consortium, will develop new HTE materials capable of durable and efficient operation at temperatures compatible with nuclear energy heat sources. Their

innovations will focus on solving the low performance/high degradation of solid oxide electrolysis cells by developing intermediate-temperature proton-conducting solid oxide electrolysis cells with robust electrode structure and intrinsically advantageous electrode kinetics.

- Saint-Gobain, through the HydroGEN consortium, will develop durable materials for cost-effective advanced water splitting utilizing all-ceramic solid oxide electrolyzer stack technology. They will focus on adapting their novel, all-ceramic stack technology to HTE with a focus on addressing fundamental durability challenges.

Project-Level Accomplishments

During FY 2018, projects in the Hydrogen Fuel R&D portfolio made important progress in several key areas. Examples include the following.

Electrolytic Hydrogen Production

- Achieved cell performance of 1.39 V at 600 mA/cm² for over 30 hours in a high-temperature alkaline electrolyzer using molten hydroxides in porous zirconia matrix as the electrolyte demonstrating a first-of-its-kind high-temperature electrolysis system. (Giner, Inc.)

Biological Conversion of Hydrocarbon Feedstocks for Hydrogen Production

- Demonstrated hydrogen production with a yield of 8.5 mol H₂/mol glucose, just shy of the 2020 target of 9 mol H₂/mol glucose with a novel 10 L hybrid fermentation and microbial electrolysis cell reactor system. (Oregon State University)

HydroGEN Project Accomplishments

The HydroGEN consortium fosters cross-cutting materials innovation using theory-guided applied materials research and development to advance all emerging thermochemical and electrolysis AWS pathways (LTE, HTE, PEC, and STCH), including hybridized systems. Throughout FY 2018 HydroGEN has fostered collaboration between the core national laboratories and industry and academic partners resulting in the exchange of more than 100 material samples, the engagement of 150 collaborators using the web hosting site, 26 published articles, two records of inventions, 44 unique resource nodes utilized by project partners, the establishment of a literature database, and expansion of a data hub for facile sharing and dissemination of data to the scientific community with more than 100 users and nearly 4,000 data files to date. The following highlights are from the HydroGEN seedling projects that are leveraging HydroGEN capabilities to accelerate their materials R&D.

Low-Temperature Electrolysis Materials R&D

- Demonstrated advanced membrane electrode assembly with performance of 1.8 A/cm² at <1.7 V, exceeding near-term performance targets of 1.8 A/cm² at 1.85 V, using next-generation cell components and demonstrated 800 hours of durability at 2 A/cm², operating at 80°C and 30 bar. (Proton Onsite)
- Successfully fabricated novel alkaline exchange membranes via a low-cost synthesis approach based on acid-catalyzed condensation reaction. (LANL)
- Developed two series of metal organic framework-derived platinum group metal (PGM)-free oxygen evolution catalysts for polymer electrolyte membrane electrolyzers, both of which demonstrated less than 15 mV difference (<2% difference) from the state of the art. (ANL)

High-Temperature Electrolysis Materials R&D

- Developed an experimentally validated model for electrolyte degradation in solid oxide electrolysis cells to predict the conditions where electrolyte failure occurs. (Northwestern University)

- Demonstrated a proton-conducting electrochemical cell with a performance of 1.2 A/cm² at <1.4 V and ≤650°C, which meets the target of >1 A/cm² at <1.4 V. (University of Connecticut)
- Developed a metal-supported, proton-conducting electrolyte button cell using a novel process for electrolyte deposition, exceeding performance targets of 0.8 A/cm² at 1.4 V. (United Technologies Research Center)

Photoelectrochemical Materials R&D

- Achieved a solar-to-hydrogen efficiency of 11.5% with a PGM-free Ni₅P₄ hydrogen evolution catalyst integrated with a high-performing photoabsorber, exceeding the target of 10% efficiency and on par with conventional PtRu catalysts. (Rutgers)
- Demonstrated a GaN/Si photocathode with stable operation for >100 hour at high photocurrent density of ~38 mA/cm², without surface protection. (University of Michigan)
- Demonstrated >100-hour stability for a III-V photocathode with a non-precious metal hydrogen evolution catalyst at >10 mA/cm² under 1-sun, meeting the target. (Stanford)

Solar Thermochemical Materials R&D

- Developed machine learning models for the discovery of efficient and stable STCH materials, identifying ~28,000 stable perovskite formulations from more than 1.1 million possible candidates with more than 90% accuracy. (University of Colorado Boulder)
- Demonstrated >200 μmol H₂/g with three compositions of Ce_xSr_{2-x}MnO₄, significantly exceeding the target of 59 μmol H₂/g (based on the performance of ceria under similar conditions). (Colorado School of Mines)

High-Pressure Compressed Hydrogen Storage

- Demonstrated lower-cost polyacrylonitrile (PAN) feedstock material fiber spinning and conversion to high strength carbon fiber, resulting in 14% cost reduction compared to the current PAN. Also demonstrated efficient solvent recovery and reduced fresh water use. (University of Kentucky)
- Developed four new low-cost polyolefin- and polyethylene-pitch-based precursors with >80% carbon yield. (Penn State University)
- Demonstrated >10°C decrease in PAN melt temperature using ionic liquid as plasticizer. The decreased PAN melt temperature enables the melt spinning process, which indicates a potential 50% cost reduction in the production process compared to conventional wet spinning. (Oak Ridge National Laboratory)

Advanced Materials-Based Hydrogen Storage

The HyMARC lab team completed activities that established an improved understanding about scientific gaps impeding the advancement of solid-state storage materials. Some of these include:

- Determined and validated an accurate Mg-B-H phase diagram that includes high-pressure and high-temperature regimes. (LLNL/SNL/PNNL)
- Accurately determined the enthalpy and entropy of hydrogen desorption in bulk Mg(BH₄)₂, addressing a gap in the literature. (SNL)

- Computationally determined that introduction of boron into coronene, as a model system for activated carbon, provides no improvement in binding energy for several optimized, stable structures. (PNNL/NREL)
- Assessed potential of confinement stress/strain to tune thermodynamics and kinetics of hydrogen uptake and release. (LLNL/LBNL)
- Elucidated the sorption mechanisms for complex hydrides and established that titanium doesn't play a role on the material surface; however, oxides do for NaAlH₄ desorption. (SNL/LBNL/LLNL)

HyMARC Project Accomplishments

The HyMARC seedling projects are high-risk, high-reward projects that focus on material development and rely heavily on the HyMARC core national lab team for guidance to accelerate their materials development efforts through computational, synthetic, characterization, and validation capabilities. Examples of progress achieved by the HyMARC seedling projects include:

- Demonstrated hydrogenation of MgB₂ to Mg(BH₄)₂ at 25% lower temperature and 22% lower pressure than prior state of the art. (University of Hawaii)
- Demonstrated that the addition of an electrolyte facilitates a 10x improvement in dehydrogenation kinetics for Mg(BH₄)₂ compared to the bulk material. (Liox Power)
- Demonstrated the ability to form Al₂O₃ coating on Mg(BH₄)₂ nanoparticles with improved reversibility and kinetics. (NREL)
- Identified more than 69,000 real and hypothetical metal organic framework structures with the potential to outperform the current state-of-the-art material through computational machine learning techniques. (University of Michigan)

Technoeconomic Analysis

The subprogram also continued carrying out technoeconomic assessments of hydrogen production and storage technologies to ensure the overall portfolio is heading toward meeting DOE's ultimate goals. Examples of analysis activities in FY 2018 include:

- Completed the update of the H2A (Hydrogen Analysis) Production model to v3.2018. The new version has been released and is available at https://www.hydrogen.energy.gov/h2a_production.html. It includes updates to feedstock costs (Annual Energy Outlook 2017), reference dollar years (2016\$), and plant start dates for current (2015) and future (2040) scenarios. H2A v3.2108 also includes changes to the financing default from 100% percent equity to 40% equity, and the federal tax rate from 35% to 21%. A significant change is the ability to analyze cases using constant debt-to-equity ratio over the plant life, which is a new H2A default. Previously published case studies have been updated to the new version of the model.
- Performed initial analysis of three potential hydrogen carriers for bulk hydrogen transport and compared the cost and energy efficiency of compressed hydrogen delivery. This initial analysis focused on delivery to a terminal at a city gate with a hydrogen demand of 50,000 kg per day. The capital costs for the carrier production and dehydrogenation facilities were identified as key costs that need to be lowered to improve carrier competitiveness. (ANL)

BUDGET

The FY 2018 appropriation for the Hydrogen Fuel R&D subprogram totaled \$38 million. The hydrogen production and storage R&D portfolios were funded at \$22 million and \$16 million, respectively. The hydrogen delivery portion is described in the Technology Acceleration and Hydrogen Infrastructure R&D section of the Annual Progress Report. The estimated budget breakdown for the hydrogen production and hydrogen storage portfolio is shown in Figure 3 and Figure 4.

Funds going toward the hydrogen storage portfolio supported a variety of early-phase R&D efforts on advanced hydrogen storage materials, including hydrogen carriers, and allowed for their coordination through HyMARC to ensure impact was maximized and resources were effectively utilized. Hydrogen storage funding also supported innovative R&D to lower the cost of high-pressure storage systems through low-cost carbon fiber precursor processing and alternative fibers.

Funds going toward hydrogen production supported R&D projects advancing direct solar water splitting, advanced electrolysis, innovative concepts, and benchmarking and analysis.

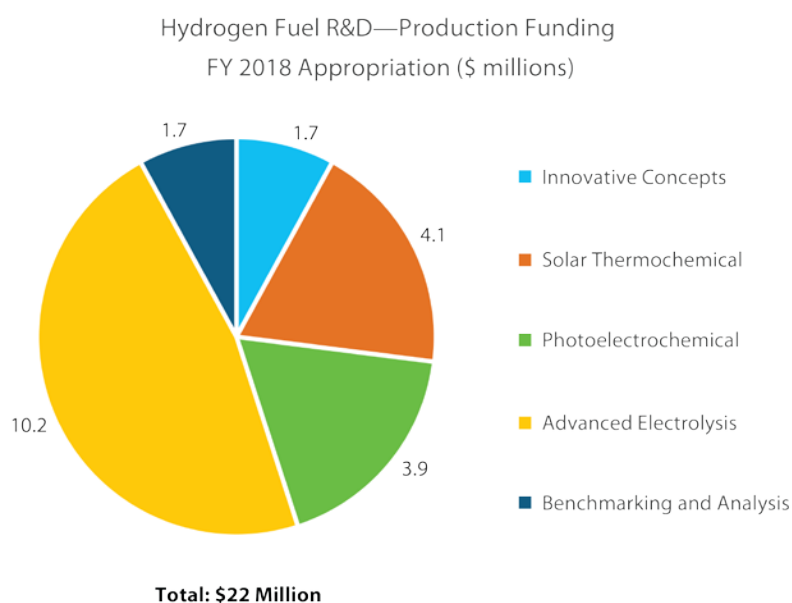


Figure 3. Hydrogen Fuel R&D subprogram FY 2018 appropriation for hydrogen production activities

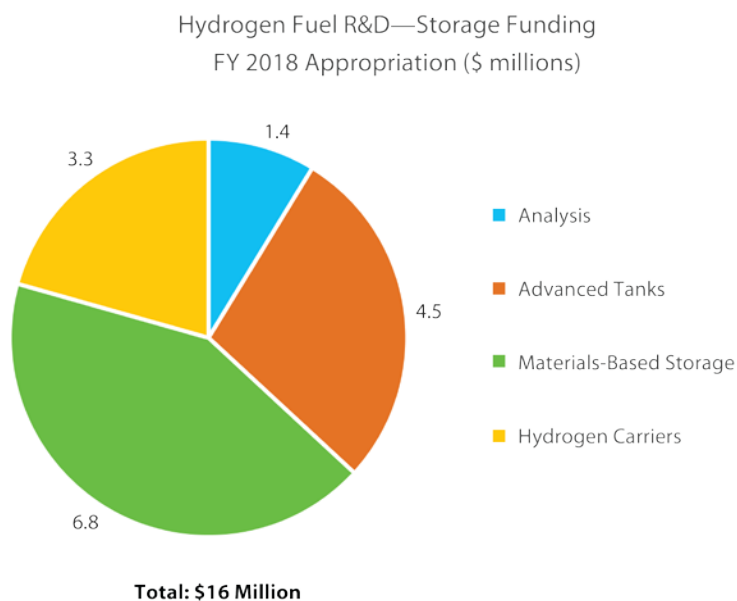


Figure 4. Hydrogen Fuel R&D subprogram FY 2018 appropriation for hydrogen storage activities

UPCOMING ACTIVITIES AND PLANS

The Hydrogen Fuel R&D subprogram will continue efforts to maximize early-stage R&D in advanced hydrogen production and storage technologies with the potential to meet DOE's ultimate targets. In addition, the subprogram will initiate the following activities in FY 2019:

- Pursue early-stage R&D in the bulk storage and transportation of hydrogen, including hydrogen carriers, to support the H2@Scale initiative
- Expand early-stage R&D in materials-based storage to identify promising materials with the potential to store hydrogen and natural gas onboard heavy-duty transportation applications
- Continue support of foundational research needs in hydrogen production identified through H2@Scale efforts, including continued emphasis on research innovations for enhancing efficiency and durability and reducing costs in materials systems for all hydrogen production pathways
- Expand early-stage R&D through the HydroGEN Advanced Water Splitting Materials consortium, including Phase II of the 19 projects and ongoing enhancement of the HydroGEN national laboratory core capabilities in advanced electrochemical, PEC, and thermochemical water splitting
- Expand emphasis on the development of robust materials-characterization protocols and performance-benchmarking standards to verify the potential of materials innovations
- Continue leveraging cross-office and cross-agency R&D opportunities and resources, including expanded collaboration with the NSF, the DOE Office of Basic Energy Sciences program in solar fuels, and the Advanced Research Projects Agency-Energy.
- Launch the BioH2 consortium aimed at addressing several technical barriers that must be overcome to realize technoeconomic feasibility of biological hydrogen production to meet the DOE hydrogen

production cost goal of <\$2/kg. By leveraging the world-class capabilities and scientific expertise of the national laboratories, the multi-lab BioH₂ consortium will deliver the multidisciplinary and synergistic expertise to address technical barriers associated with fermentation and microbial electrolysis cells.

Eric Miller

Hydrogen Production Subprogram Manager
Fuel Cell Technologies Office
Office of Energy Efficiency and Renewable
Energy
U.S. Department of Energy
1000 Independence Ave., SW
Washington, DC 20585-0121
Phone: (202) 586-5829
Email: Eric.Miller@ee.doe.gov

Ned Stetson

Hydrogen Storage Subprogram Manager
Fuel Cell Technologies Office
Office of Energy Efficiency and Renewable
Energy
U.S. Department of Energy
1000 Independence Ave., SW
Washington, DC 20585-0121
Phone: (202) 586-9995
Email: Ned.Stetson@ee.doe.gov

Analysis of Advanced Hydrogen Production Pathways

Brian James (Primary Contact), Daniel DeSantis, Genevieve Saur (NREL)
Strategic Analysis, Inc.
4075 Wilson Blvd
Arlington, VA 22203
Phone: (703) 778-7114
Email: bjames@sainc.com

DOE Manager: Eric Miller
Phone: (202) 287-5829
Email: Eric.Miller@ee.doe.gov

Contract Number: DE-EE0008084

Subcontractors:

- National Renewable Energy Laboratory (NREL), Golden, CO
- Argonne National Laboratory, Argonne, IL

Project Start Date: October 1, 2016
Project End Date: September 30, 2020

Overall Objectives

- Perform cost analysis of various hydrogen production and delivery pathways.
- Identify key cost and performance bottlenecks of the given pathways.
- Conduct deep-dive analyses and optimization studies on hydrogen delivery scenarios.
- Supply information from techno-economic studies to DOE for life cycle analysis.
- Respond to the scope and topic areas as defined by DOE.

Fiscal Year (FY) 2018 Objectives

- Completed a techno-economic analysis for a wire-wrapped steel vessel suitable for high-pressure cascade storage of hydrogen.
- Conduct a techno-economic analysis on the cost of transmitting energy: electrical transmission lines, gaseous pipelines, and liquid pipelines.

Technical Barriers

This project addresses the following technical barriers from the Hydrogen Delivery and Hydrogen Storage sections of the Fuel Cell Technologies Office Multi-Year Research, Development, and Demonstration Plan¹:

- D) High As-Installed Cost of Pipelines (Hydrogen Delivery)
- E) Gaseous Hydrogen Storage and Tube Trailer Delivery Cost (Hydrogen Storage).

Technical Targets

Techno-Economic Analysis of a Cascade Storage System:

The 2020 DOE cost target for hydrogen storage for on-site hydrogen stations is \$600/kg H₂ (uninstalled).² These storage tanks have traditionally been large-diameter, thick-walled vessels of steel construction, with a pressure rating over 12,500 psi to allow fast-fill cascade refueling to 10,000 psi automotive storage tanks. As a result of their construction, the tanks are generally significant cost drivers for on-site hydrogen stations and the cost of a tank exceeds the 2020 DOE target. To meet the DOE 2020 on-site storage target, new tanks or new manufacturing processes will be required. To that end, Strategic Analysis, Inc. (SA) completed a techno-economic analysis focused on advanced designs for a steel-wire-overwrapped, Type I stationary hydrogen storage system that may lead to significantly reduced dispensing site hydrogen storage costs compared to the high-pressure storage FY 2015 target (\$2,000/kg H₂).

Comparative Techno-Economic Analysis for the Transmission of Energy:

The 2020 DOE target for delivered hydrogen is \$4/kg H₂ and encompasses the costs of hydrogen production, transmission, and dispensing. However, the cost of transmitting energy over long

¹ <https://www.energy.gov/eere/fuelcells/downloads/fuel-cell-technologies-office-multi-year-research-development-and-22>

² The DOE target for hydrogen storage tanks/pressure vessels includes the cost of the pressure vessel, painting, cleaning, testing and a suitable mounting frame.

distances is largely unstated in the public literature yet is a crucial step in creating high-output, cost-competitive renewable energy “farms.”

Consequently, an analysis was conducted to examine the transmission costs of a variety of energy carriers. Future analysis may then combine those transmission costs with the other elements of the full energy pathway to assess the delivered cost of hydrogen for comparison to the DOE targets.

FY 2018 Accomplishments

- Completed a techno-economic analysis for a wire-wrapped steel vessel suitable for high-pressure cascade storage of hydrogen.
- Completed an analysis of the cost of transmission of energy. This work has been compiled into a report and presented to DOE.

INTRODUCTION

Two main tasks were conducted in Year 2 of the project. The first task was a techno-economic analysis of Type I wire-wrapped pressure vessels. This analysis was initiated in Year 1 and finalized in Year 2, with documentation of the costs of the WireTough Cylinders, LLC, storage tank production process and a cost comparison for hydrogen storage. The documentation was provided to DOE after completion. The cost of hydrogen cascade storage tanks such as those used at hydrogen dispensing stations is generally considered to be a significant component of station cost. Hydrogen storage tanks at a station are generally used to hold and dispense hydrogen at pressures up to 12,500 psi. Traditionally, the tanks used for these storage applications are large, thick-walled steel vessels. Due to the thickness of the steel required to hold such high pressures, these tanks are expensive and will not meet the DOE 2020 cost targets for on-site storage. New developments for manufacturing suitable high-pressure storage tanks, such as the wire-wrapping steel tanks as proposed by WireTough, could significantly reduce the cost of hydrogen storage at a dispensing station. The analysis conducted by SA focused on projecting a manufacturing process suitable for fabricating up to 3,000 tanks per year and creating a cost model to predict the cost of manufacturing the tanks.

The second Year 2 task of the project was to conduct a cost analysis of energy transmission for various transmission methods and energy carriers. Energy transmission costs are of particular interest when considering large-scale, remote renewable energy production (solar, wind, biomass) and long-distance energy transmission (1,000+ miles) to population centers. Energy transmission can be accomplished via electrical power lines, gaseous pipeline, or liquid pipeline, although depending on the ultimate end-form of the energy, conversion costs may be incurred. Until recently, little data has been published in the scientific literature regarding the cost of transmission of energy. Transmission cost has traditionally been blended with some combination of production, conversion, and/or dispensing cost, thereby making it difficult to compare transmission-only cost. Comparing transmission costs for various methods and fuels is also difficult due to the different cost units used by various data sources. To achieve a fair comparison of transmission costs, SA examined a variety of cost modeling methodologies and data for electrical transmission lines as well as oil and natural gas pipelines. These cost models were modified by SA to create a new cost model with a consistent set of physical, operating, and financial assumptions. The results of the modified SA cost model provide an equitable comparison of transmission cost, considering both construction cost (\$/MW-mile) and total transmission cost (\$/MWh).

APPROACH

Techno-Economic Analysis of a Cascade Storage System

To properly analyze the hydrogen storage vessel developed by WireTough, a ground-up Design for Manufacture and Assembly (DFMA) cost estimation methodology was used. The DFMA process breaks down each manufacturing process step into the material cost, equipment cost, labor cost, utility cost, and tooling cost. The equipment cost is the capital cost of any production equipment, amortized over the life of the production equipment, with extra cost provisions made for maintenance and repair. Key process parameter values for the DFMA analysis were provided by WireTough and further supported by material and equipment cost quotations from various manufacturers. All process parameters and assumptions were reviewed by WireTough for accuracy and appropriateness. While the DFMA analysis focused on the vessel, costs were also tabulated for the complete cascade storage system (i.e., mounting brackets, lines, valves). The finalized results were compared to the DOE cost targets for hydrogen on-site storage.

Comparative Techno-Economic Analysis for the Transmission of Energy

The energy transmission cost analysis examined six transport systems: electrical transmission line; liquid pipelines carrying oil, methanol, or ethanol; and compressed gas pipelines carrying either natural gas or hydrogen. This cost analysis focused solely on the cost of transmission and thus does not consider the method of production for any energy carrier (i.e., electricity, hydrogen, oil) or the cost of conversion (i.e., hydrogen production, natural gas combustion for electrical production). The pipeline and electrical line cost models used in this work are derived from published data sets on the construction of pipelines and electrical lines in the

United States. New construction of transmission lines or pipelines was assumed. The cost model for the electrical transmission line was developed by the Black & Veatch Corporation for use by the Western Electric Coordinating Council [1]. Two cost models for determining the capital cost for the construction of gas pipelines were considered. The first is a study by Rui et al. [2], which examines the capital cost of 412 on-shore pipeline construction projects between 1992 and 2008. The second cost model, described by Brown et al. [3], uses 30 years of on-shore natural gas pipeline cost data, ranging from 1980 to 2010. Both models are derived from data published by the Oil and Gas Journal.

A total transmission distance of 1,000 miles is assumed for all systems. This is approximately the distance between St. Louis, Missouri, and New York City, New York, and is meant to represent long-distance transport over a variety of terrains, from a large energy production site to a large energy consumption site. All calculations are completed with a utilization factor of 100%, indicating that the given transmission method is being used continuously at nominal design capacity. While 100% utilization is unlikely for real-world application, such an assumption provides the lowest levelized cost of energy transmission for all carriers and allows for accurate comparison of the cost of transmission between electrical transmission lines and fuel pipelines. Sufficient cost breakdown detail is given to allow the reader to estimate capital costs (\$/mile-MW) at other utilizations. The total cost of transmission for each transmission method includes an amortization of the capital cost, as well as annual expenses for fixed and variable operating costs, and is reported in \$/MWh. A Monte Carlo analysis was performed as a method to determine the likely cost of energy transmission by a given method. The range of values returned by the Monte Carlo analysis was taken to be the 90% confidence interval and is marked as the bounds for error in the analysis results.³

RESULTS

Techno-Economic Analysis of a Cascade Storage System

The wire-wrapping process begins with a 30-foot-long steel liner rated for approximately 6,600 psi.⁴ The liner is carried by crane to a wire-wrapping station, which combines 24 steel wires into a wire tow band that is then wrapped around the cylindrical section of the liner. The end domes of the liner are not covered in the wire wrapping process. Epoxy is applied to the wires as they are wrapped. The epoxy protects the wires from corrosion, provides added strength and rigidity, and prevents wire movement during pressure cycling. The outer layer of wires is taped with non-adhesive tape and then covered with epoxy. The assembly is next sent to an oven for partial epoxy curing, followed by a full cure at room temperature. The pressure vessel is then put through an autofrettage process to impart internal residual compressive stress. Finally, the pressure vessel is painted with an ultraviolet-resistant paint.

The vessel analysis was extended to develop a suitable storage cost for use in H2A cases. To do this, a theoretical balance of system (BOS) was developed to formulate a cost for a storage system that could be used at a hydrogen forecourt station. The theoretical station would have a bank of three sets of two tanks and feed to six dispensers (See Figure 1). When possible, the components required for the BOS (e.g., valves, pressure relief devices, thermocouples) were quoted by manufacturing companies. When price quotes were not available, SA used historical data to generate component pricing. The BOS also includes projected costs for installation, markup, and component assembly and testing. The combination of the storage vessel prices and the BOS prices can then be used as a total system cost for analysis of the delivered price of hydrogen.

³ The cost model used for electrical transmission was not well suited to Monte Carlo analysis and the error was thus marked at +/-50%. This range is in keeping with data reported in the literature [4–6].

⁴ For clarity within this report, the solid-metal-walled pressure vessel is called a liner, while the completed, wire-wrapped product is termed a pressure vessel.

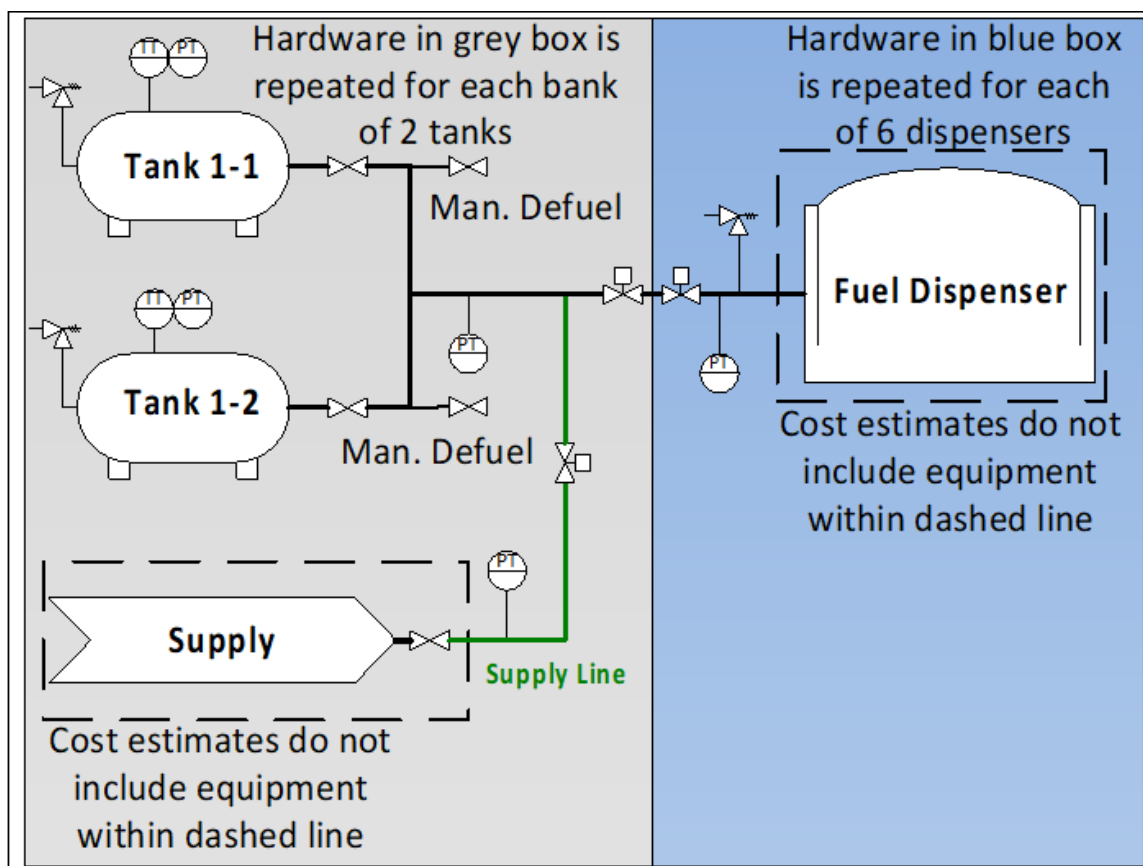


Figure 1. A section of the dispensing system modeled. Diagram shows the system and BOS for two high-pressure tanks and one dispenser. The complete modeled system is six tanks, broken into three banks of two tanks, with each bank feeding into any of six dispensers. All hardware presented in the gray box is repeated for each bank of two tanks. All hardware presented in the blue box is repeated for each of six dispensers.

The projected price (after markup)⁵ of the pressure vessel (as defined by DOE) at low production volumes, as it is currently manufactured, is approximately \$803/kg H₂ (\$28,145/unit), based on a one vessel per day production rate. At higher production rates and process adjustments to account for automation, the projected price drops to less than \$593/kg H₂ (\$21,000/unit). When compared to DOE storage cost targets, the wire-wrapped vessels show significant improvement over the FY 2015 targets and approach the FY 2020 cost target of \$600/kg (see Figure 3).⁶ The projected costs are also lower than the cascade storage tank prices used within the H2A models.

⁵ A markup rate of 25% (at all production rates) was used to translate manufacturing cost into expected sales price (inclusive of company profit, overhead, general and administrative expenses, etc.). This rate is based on information garnered from the annual report of a high-volume pressure vessel manufacturer, Hexagon, and is extrapolated from the company's publicly reported gross margin and cost of goods sold. While markup rates can vary substantially company to company, even within an industry, Hexagon is judged to be an industry standard in hydrogen and compressed natural gas storage vessels, and thus is thought to be an appropriate markup rate benchmark.

⁶ In order to make direct comparison to the DOE targets and align with the DOE terminology for stationary gaseous hydrogen storage costs, the term "tank" is used in Figure 3 to describe the WireTough pressure vessel. Further, "price" and "cost" are used interchangeably for Figure 3, as the purchase cost to a hydrogen forecourt station for a high-pressure storage tank is identical to the price WireTough would charge for its product. A table of DOE's target prices for hydrogen storage, along with descriptions of the components in question, can be found here: <https://energy.gov/eere/fuelcells/doe-technical-targets-hydrogen-delivery>.

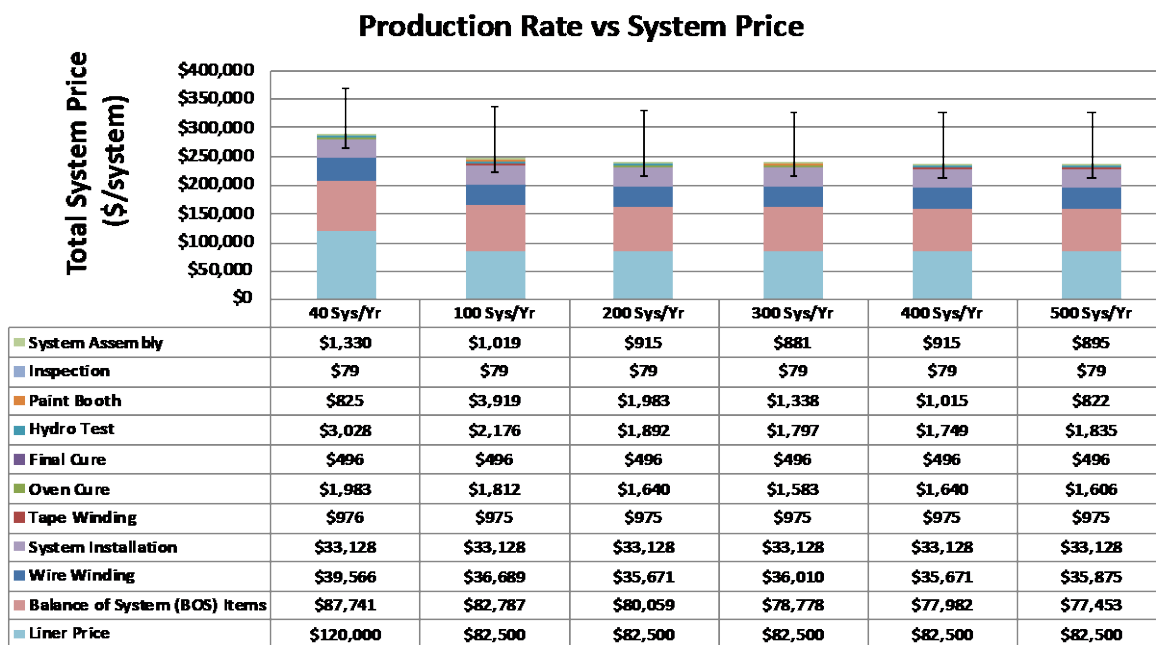


Figure 2. Predicted cost of producing Type I wire-wrapped hydrogen vessels at different annual production rates

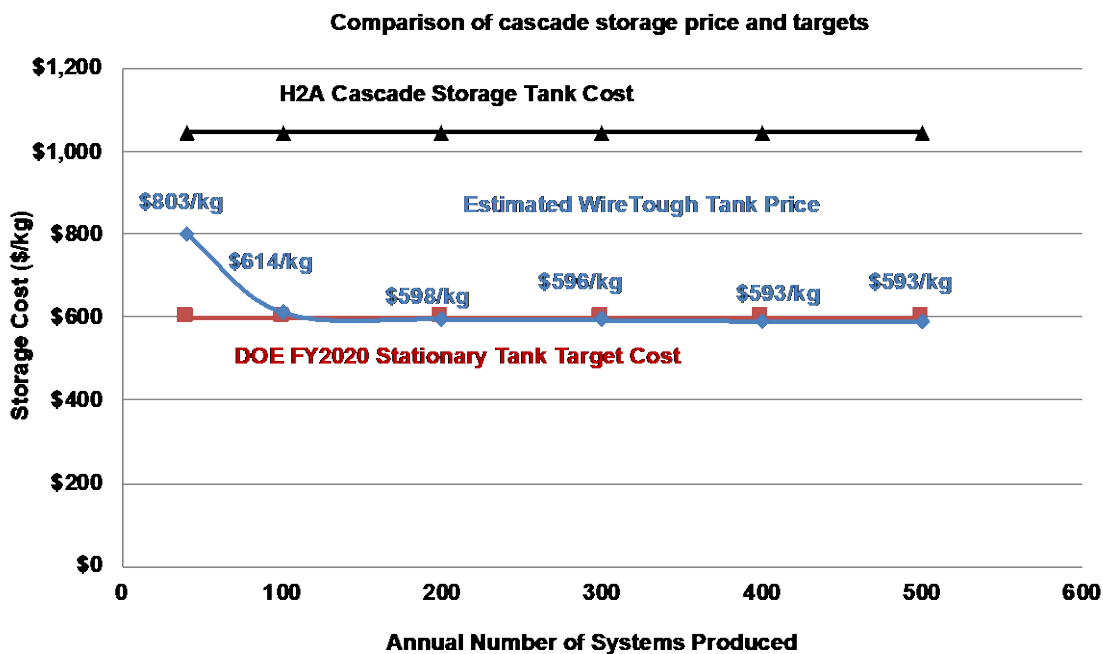


Figure 3. Comparison of wire-wrapped pressure vessel cost projections to the DOE target

Cost projections for the complete cascade storage system, including BOS, ranged from \$1,203/kg H₂ to \$958/kg H₂. The limited variation in costs at production rates between 240 and 3,000 pressure vessels/year is a result of a constant liner cost being used at each of those production rates. With such a dominant cost being held constant at different production rates, the variation in total cost with varying production rate is minimized.

Comparative Techno-Economic Analysis for the Transmission of Energy

Electrical transmission is actually the highest transmission cost among the six analyzed energy carriers and is nearly eight times greater than the cost of transmitting hydrogen via a pipeline. This is notable as hydrogen is the most expensive chemical fuel to transmit of the five fuels analyzed. The chemical fuels with the highest energy densities are the least expensive to transmit (See Figure 4). Wide error bars are present in Figure 4 for the pipeline costs and are a direct result of the wide variation of pipeline capital cost in the literature: Brown et al. costs [3] are 3.5 times greater than those of Rui et al. [2]. Further uncertainty stems from the location of construction (up to a 44% cost variation compared to the average cost).

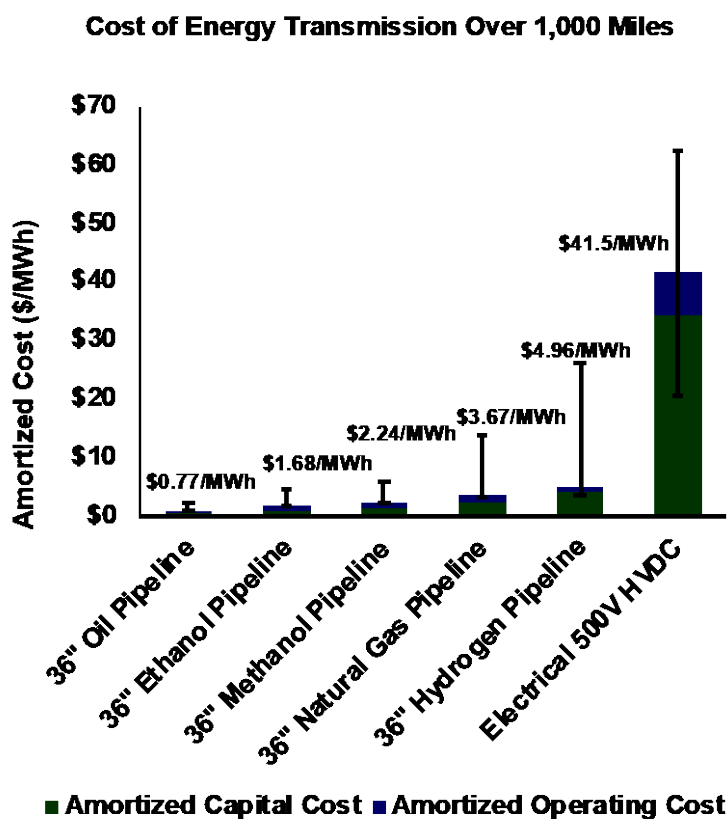


Figure 4. Amortized costs for each method of transmission analyzed

CONCLUSIONS AND UPCOMING ACTIVITIES

Techno-Economic Analysis of a Cascade Storage System

The WireTough wire-wrapped hydrogen storage system appears to be a cost-effective alternative to Type I tanks for stationary high-pressure applications. Preliminary analysis projects a pressure vessel cost of ~\$600/kg of stored hydrogen (uninstalled), achieving the 2020 DOE target of \$600/kg and surpassing the DOE 2015 status cost of \$2,000/kg (See Figure 3).

Comparative Techno-Economic Analysis for the Transmission of Energy

The energy transmission analysis offers a new perspective on the cost of transmitting energy and indicates that the cost of transmitting hydrogen through a pipeline is actually less than the cost of electrical transmission on a \$/MWh basis. Liquid fuels transmitted by pipeline are even less expensive. Future analysis should combine these transmission cost results with the cost for production and energy conversion (if needed) to assess the full cost of each production-transmission pathway.

FY 2018 PUBLICATIONS/PRESENTATIONS

1. Brian D. James, Cassidy Houchins, Genevieve Saur, Jennie M. Huya-Kouadio, and Daniel A. DeSantis, “Analysis of Advanced H₂ Production Pathways,” presented at the DOE Annual Merit Review Meeting, 14 June 2018, Washington, D.C.

REFERENCES

1. Ryan Pletka, Jagmeet Khangura, Andy Rawlins, Elizabeth Waldren, and Dan Warden. *Capital Costs for Transmission and Substations* (2014). https://www.wecc.biz/Reliability/2014_TEPPC_Transmission_CapCost_Report_B+V.pdf.
2. Zhenhua, Rui, Paul Metz, Doug B. Reynolds, Gang Chen, and Xiyu Zhou. “Historical Pipeline Construction Cost Analysis.” *Int. J. of Oil* 4 (June 2011): 244–63. <https://doi.org/10.1504/IJOGCT.2011.040838>.
3. Daryl Brown, Jim Cabe, and Tyson Stout. 2011. “National Lab Uses OGJ Data to Develop Cost Equations.” *Oil and Gas Journal* 109, no. 1 (2011). https://www.researchgate.net/publication/236421832_National_Lab_Uses_OGJ_Data_to_Develop_Cost_Equations.
4. Fadl H. Saadi, Nathan S. Lewis, and Eric W. McFarland. “Relative Costs of Transporting Electrical and Chemical Energy.” *Energy and Environmental Science* 11, no. 3 (2018): 469–75. <https://doi.org/10.1039/C7EE01987D>.
5. Kelly Eurek, Wesley Cole, David Bielen, Nate Blair, Stuart Cohen, Bethany Frew, Jonathan Ho, et al. “Regional Energy Deployment System (ReEDS) Model Documentation: Version 2016.” NREL/TP-6A20-67067 (Golden, CO: National Renewable Energy Laboratory, 2016). <https://doi.org/10.2172/1332909>.
6. Ryan Pletka, Derek Djeu, Joshua Finn, Adam Hanna, Cristin Holmgren, Kevin Joyce, Maggie Lock, Sally Maki, and Tim Mason. *Renewable Energy Transmission Initiative (RETI) Phase 2B Draft Report* (2010).

High-Temperature Alkaline Water Electrolysis

Hui Xu (Primary Contact), Kailash Patil, Andrew Sweet, Winfield Greene, Steve McCatty (Giner), Prabhakar Singh, and Heo Su (UConn)
Giner, Inc. (Giner)
89 Rumford Ave,
Newton, MA 02466
Phone: (781) 529-0573
Email: hxu@ginerinc.com

DOE Manager: David Peterson
Phone: (720) 356-1747
Email: David.Peterson@ee.doe.gov

Contract Number: DE-EE0007644

Subcontractor:
University of Connecticut (UConn), Storrs, CT

Project Start Date: January 1, 2017
Project End Date: December 31, 2019

Overall Objectives

The overall objective is to develop high-temperature alkaline water electrolysis using molten hydroxides in porous-based alumina, zirconia, or lithium aluminate. Some of our targets are below.

- Develop alumina- and zirconia-based matrices with good corrosion resistance.
- Develop anode and cathode catalysts with enhanced hydrogen evolution reaction (HER) and oxygen evolution reaction (OER) activity.
- Assemble and test single electrolyzer cells and test their performance and durability (at 0.5–1.0 A/cm² and 1,000 hours).
- Construct and test a 1.8-kW electrolyzer stack.

Fiscal Year (FY) 2018 Objectives

- Develop alumina- and zirconia-based matrices.
- Measure the OH⁻ ion conductivity of the composite electrolyte.
- Optimize slurry formulation of the catalysts using the tape casting process.

- Demonstrate single cell performance <1.5 V at 1,000 mA/cm² at temperature <550°C.

Technical Barriers

This project addresses the following technical barriers from the Hydrogen Production section of the Fuel Cell Technologies Office Multi-Year Research, Development, and Demonstration Plan¹:

- (A) Operating cost: prohibitive electricity consumption for water electrolysis
- (B) Capital cost: associated with platinum group metals or expensive high-temperature materials.

Technical Targets

This project will develop high-temperature alkaline water electrolysis.

- Composite electrolyte OH⁻ conductivity >0.1 S/cm in temperature of 350°C to 550°C.
- Per-cell area-specific resistance (ASR) of ≤0.2 Ohm-cm² at 350°C to 550°C using a membrane thickness of 200 μm.
- Single cell performance <1.5 V at 1,000 mA/cm² at temperature <550°C.
- Stack electrical efficiency >90% lower heating value (LHV) hydrogen with current density at 1.2 A/cm².

FY 2018 Accomplishments

- Achieved composite electrolyte OH⁻ conductivity >0.1 S/cm while the temperature ranged from 350°C to 550°C.
- Obtained per-cell ASR of ≤0.2 Ohm-cm² using a membrane thickness of 100–200 μm.
- Successfully developed strategies to mitigate hot corrosion of high-temperature alkaline electrolysis (HTAE) components including current collectors and end plates.

¹ <https://energy.gov/eere/fuelcells/downloads/fuel-cell-technologies-office-multi-year-research-development-and-22>

- Successfully demonstrated single cell performance <1.5 V at 1,000 mA/cm² at temperature <550°C.

Table 1. Distributed Forecourt Water Electrolysis Hydrogen Production

Characteristic	Units	2011 Status	2015 Target	2020 Target
Hydrogen levelized cost (production only)	\$/kg H ₂	4.20	3.90	2.30
Electrolyzer system capital cost	\$/kg	0.70	0.50	0.50
	\$/kW	430	300	300
System energy efficiency	% (LHV)	74	76	77
	kWh/kg	45	44	43
Stack energy efficiency	% (LHV)	74	76	77
	kWh/kg	45	44	43
Electricity price	\$/kWh	From AEO 2009	From AEO 2009	0.037

AEO – Annual Energy Outlook

INTRODUCTION

Hydrogen production for mobile and energy storage applications from water electrolysis is attractive due to its high efficiency, fast ramp rates, and high-pressure capability. However, current hydrogen production from electrolysis comprises only a small fraction of the global hydrogen market due to the high cost associated with expensive stack materials (membrane, catalyst, and bipolar plates) and electricity consumption of the commercially available electrolysis systems. This program aims to develop a high-temperature alkaline water electrolyzer that can simultaneously reduce the electrolyzer cost (by adopting low-cost material) and improve energy efficiency (due to enabling high-temperature operation). The project will use HTAE that employs single or binary hydroxide (lithium, sodium, or potassium hydroxide) impregnated into a porous oxide matrix as the electrolyte membrane.

The operating temperature of HTAE can vary from 350°C to 550°C, dependent on the category and ratio of each individual electrolyte. In this process, single or mixed alkali/alkaline earth hydroxides (LiOH, NaOH, or KOH) can be first melted and subsequently impregnated in three porous metal oxides—MO-1, MO-2, or MO-3. The meticulously designed metal oxide matrices can well retain molten hydroxides via capillary forces [1–2].

APPROACH

The approaches to achieve the technical targets are listed in Table 2. The technical targets will be validated first in a single electrolyzer cell and then in 1.8-kW electrolyzer stack tests.

Table 2. Approaches to Achieve High-Temperature Alkaline Water Electrolysis

Technical Targets	Approaches
Composite electrolyte OH ⁻ conductivity >0.1 S/cm in temperature of 350 °C to 550 °C	Explore different composite electrolytes to increase the OH ⁻ conductivity
Per-cell ASR of membranes ≤0.2 Ohm-cm ² at 350 °C to 550 °C	Develop thin alumina- or zirconia-based matrices with good mechanical strength Adopt electrolyte with high OH ⁻ conductivity
Single cell performance <1.5 V at 1,000 mA/cm ² at temperature 300 °C to 550 °C	Adopt membranes with low ASR Employ high-performance catalysts Mitigate hot-corrosion-caused component resistance increase

RESULTS

The matrix robustness (to withstand thermomechanical stress) impacts the electrolyzer’s performance and endurance. In this project, both aluminate- (MO-1) and zirconia (MO-3)-based matrix metal oxides were used as the matrix support materials. Thin aluminate- and zirconia-based matrices were fabricated using the tape casting method. The green tape fabrication of the electrolyte support matrix was optimized for a solvent based slurry formulation process. The temperatures for binder and pore-former removal and for subsequent sintering processes were determined using heating/cooling cycles. The heating rate for removing binder was 3°C/min up to 425°C and the cooling rate was 5°C/min down to room temperature. The microstructure and porosity/pore size of the sintered matrices were analyzed by scanning electron microscopy (SEM) and Hg-porosimetry (AutoPore IV, Micromeritics).

The fabrication of a green sheet tape using a doctor blade and green sheet matrix’s thickness is shown in Figure 1(a). A SEM image of sintered metal oxide matrix showed porous structure and no cracks were observed after sintering at 550°C in air atmosphere for 2 h (Figure 1(b)).

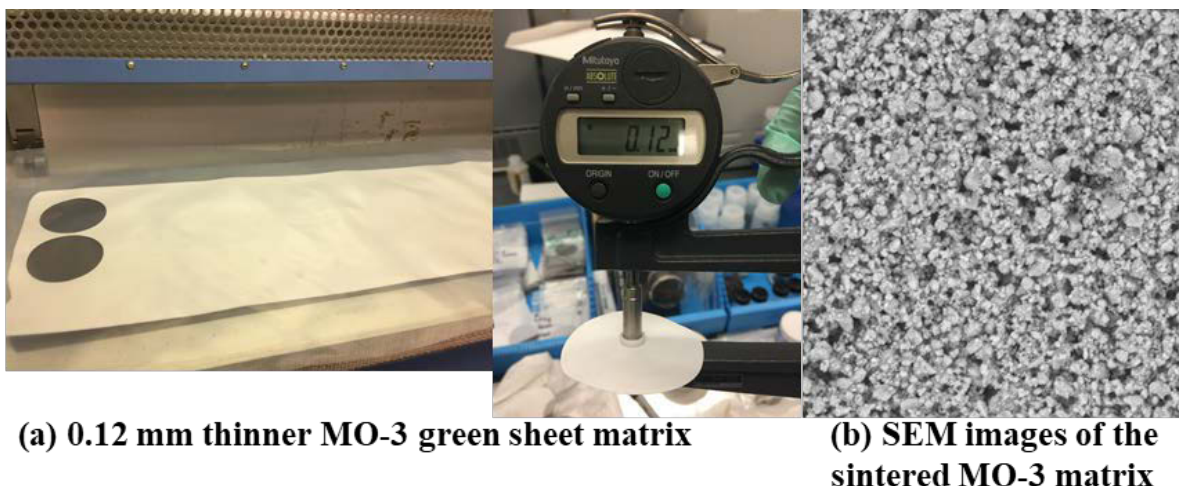


Figure 1. Fabricated metal oxide green sheet matrix: (a) 0.12 mm matrix thickness and (b) SEM image of MO-3 matrix sintered at 550°C for 2 h

The phase and microstructural changes of metal oxides in hydroxide medium were evaluated. We immersed metal oxides in molten ($\text{Li}_{0.52}/\text{Na}_{0.48}$)OH melts at 550°C for 10 h and 100 h time periods. The X-ray diffraction (XRD) patterns of MO-1 and MO-3 powders before and after their immersion tests are shown in Figure 2. The crystalline phase of $\gamma\text{-LiAlO}_2$ reveals that MO-1 phase transformation occurred in molten hydroxide for a 10 h duration (Figure 2, top panel); the minor phases of $\gamma\text{-LiAlO}_2$ and lithium aluminum hydroxide hydrate appeared after performing the immersion test for 10 h. Increasing the immersion time to 100 h caused the intensity of MO-1 peaks to increase. The XRD patterns of the MO-3 powders obtained after immersion in molten (Li/Na)OH at 550°C for different lengths of time are shown in the bottom panel of Figure 2. The MO-3 powder was more stable and no apparent reactions with molten Li/Na hydroxide melts were observed. The minor phase of lithium hydroxide hydroxyl hydrate ($\text{LiOH}(\text{OH})_2\cdot\text{H}_2\text{O}$) was not completely removed during the washing process after immersion test.

The OH^- ion conductivities of the single or binary mixture of the electrolyte samples were measured. The temperature dependence of OH^- conductivities for the hydroxide/metal oxide composites is shown in Figure 3(a). The binary LiOH/NaOH hydroxide melt demonstrated the highest OH^- ion conductivity, 0.52 S/cm at 550°C. The conductivity of the single/binary hydroxide electrolyte improved with increased temperature. The ASRs of the prepared matrices are shown in Figure 3(b). It is clearly seen that the ASR decreased as the temperature increased from 350°C to 550°C. The lowest ASR was only 0.02 Ohm-cm².

The green sheet electrodes with a variety of thicknesses (0.20 to 0.25 mm) were developed in the lab using doctor blade. The electrolyzer button cells (13 cm²) were tested to evaluate the HTAE performance. Button-cell components including anode and cathode frame and current collectors were made with high-corrosion-resistance stainless steel (S316) materials. The hydroxide electrolyte powders were stored in the cathode channel of the separator. During the cell conditioning process, the hydroxide electrolyte easily penetrated into the matrix from the cathode channels after the organic additives burned out.

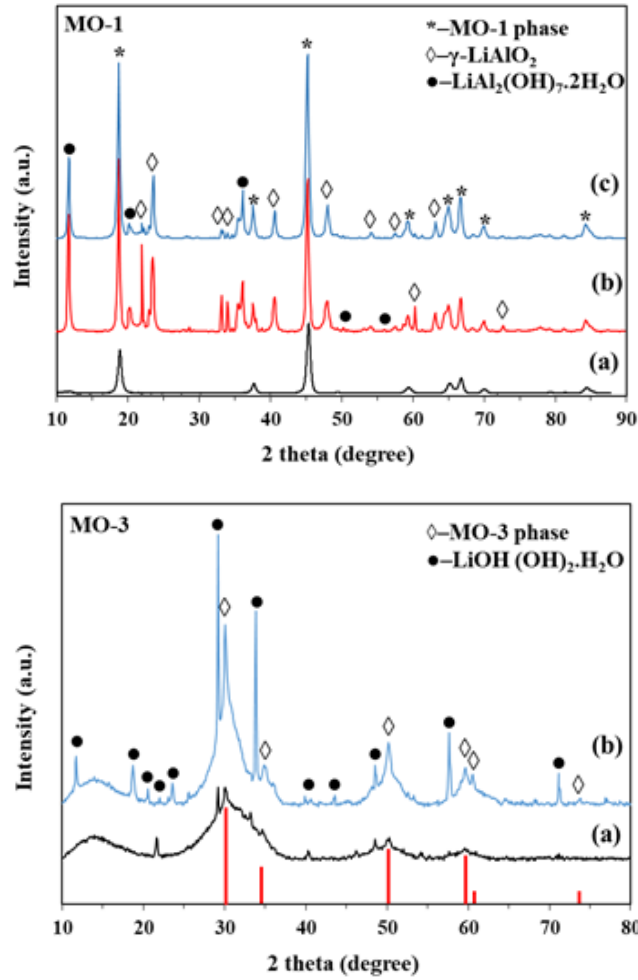


Figure 2. XRD patterns of metal oxide powder immersion in molten (Li/Na)OH at 550 °C. (Top) MO-1: (a) powder as received, (b) 10 h, and (c) 100 h duration. (Bottom) MO-3: (a) 10 h and (b) 100 h duration (red lines indicate the assigned of pure phase of MO-3 powder).

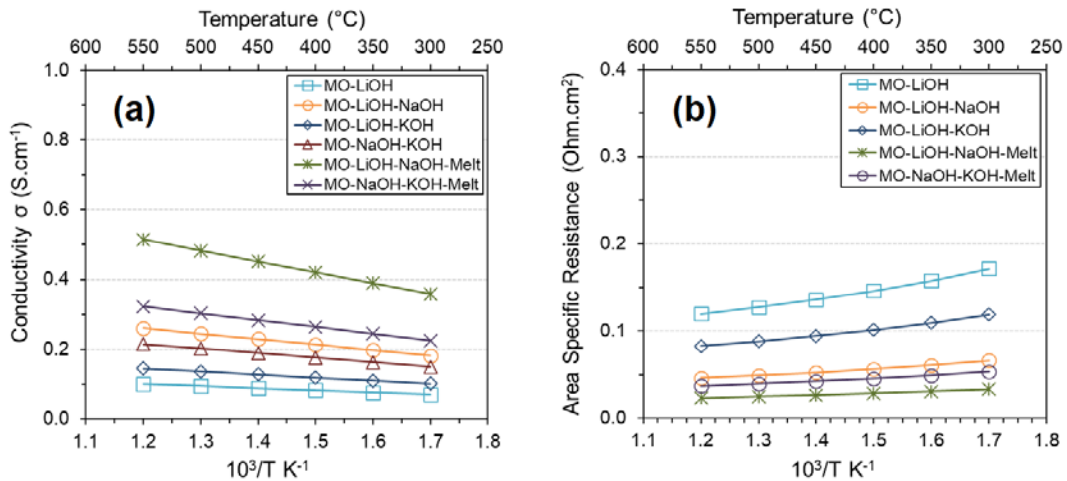


Figure 3. (a) Temperature dependence of the OH⁻ ion conductivity of single/binary hydroxides at 300°–550 °C in air atmosphere; (b) ASR at 300°–550 °C in air atmosphere and thickness of 0.12 mm

We have made tremendous progress in improving the cell performance by improving anode and cathode catalyst activity, adopting matrix with small thickness but good mechanical strength, reducing component corrosion, and optimizing operating conditions. As a result of corrosion reduction and thinner matrix, the high-frequency resistance dropped substantially, and the cell performance improved accordingly. A single cell performance of 1.5 V at 1,000 mA/cm² at 550°C was achieved as shown in Figure 4(a). The 30-hour durability at 600 mA/cm² was demonstrated in Figure 4(b) and the performance continued improving during the course of durability testing.

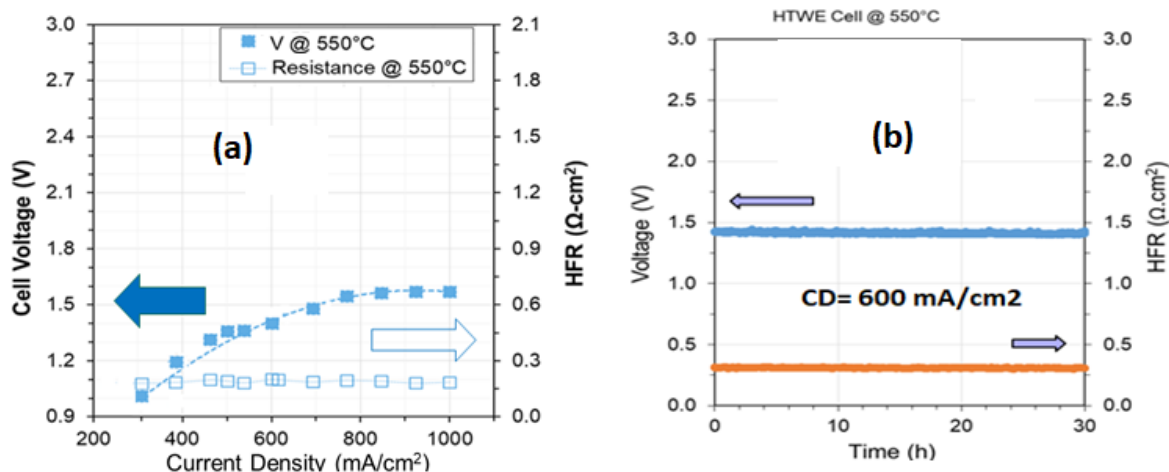


Figure 4. HTAE cell (13 cm²) performance and durability: (a) single cell performance; (b) durability test up to 30 hours

CONCLUSIONS AND UPCOMING ACTIVITIES

- Successfully developed metal oxide matrices in various materials and thickness using the tape casting process.
- Achieved superior OH⁻ ion conductivity and low ASR. High OH⁻ ion conductivity up to 0.5 S/cm of molten binary hydroxide was achieved.
- Successfully developed cathode and anode electrodes using the tape casting process.
- Designed and constructed high-performance HTAE cells. Successfully demonstrated single cell performance <1.5 V at 1,000 mA/cm².

We will strive to further improve the HTAE cell performance at lowered temperature (~450°C), reduce component corrosion, and design a 10-cell short stack that will meet targeted performance, durability, and energy efficiency.

- Evaluate the matrix solubility in hydroxide electrolyte from 400°C to 550°C.
- Further optimize component and operating conditions of the long-term single cell durability.
- Design the stack cell components to construct a 1.8-kW stack.

FY 2018 PUBLICATIONS/PRESENTATIONS

1. Hui Xu and Kailash Patil, “High Temperature Alkaline Water Electrolysis,” presented at the 2018 DOE Annual Merit Review and Peer Evaluation Meeting, Washington, DC, June 2018.
2. Kailash Patil, Andrew Sweet, Winfield Greene and Hui Xu, “High-Temperature Molten Alkaline Water Electrolysis,” 233rd ECS meeting, Seattle WA, May 2018.

3. Hui Xu and Kailash Patil, “Components for High-Temperature Alkaline Water Electrolysis,” provisional patent, filed in 2018.

REFERENCES

1. “H₂ Production and Delivery Cost Apportionment,” DOE Hydrogen and Fuel Cells Program Record #12001 (2012), http://www.hydrogen.energy.gov/pdfs/12001_h2_pd_cost_apportionment.pdf.
2. D. Anthony, J. Rand, and R. Dell, *Hydrogen Energy Challenges and Prospects* (RSC Energy Series, 2008), DOI:10.1039/9781847558022.

New Approaches to Improved Proton Exchange Membrane Electrolyzer Ion Exchange Membranes

Earl H. Wagener (Primary Contact),
Brad P. Morgan, Chris Topping
Tetramer Technologies LLC
657 S. Mechanic St.
Pendleton, SC 29670
Phone: (864) 646-6282
Email: earl.wagener@tetramer.com

DOE Manager: David Peterson
Phone: (720) 356-1747
Email: David.Peterson@ee.doe.gov

Contract Number: DE-SC0011305

Subcontractor:
Proton OnSite, Wallingford, CT

Project Start Date: April 6, 2015
Project End Date: April 5, 2019

Overall Objectives

- Optimize electrolyzer membrane performance.
- Refine polymer/membrane and cell architecture to maximize durability.
- Down-select materials for optimization of membrane composite configuration.
- Scale up and confirm cost estimates.
- Build prototype.

Fiscal Year (FY) 2018 Objectives

- Modify cell design.
- Define ionomer specifications.
- Define membrane specifications.
- Scale up synthesis and define standard operating procedures.

Technical Barriers

This project addresses the following technical barrier from the Hydrogen Production section of the Fuel Cell Technologies Office Multi-Year Research, Development, and Demonstration Plan¹:

- (F) Capital Cost
- (G) System Efficiency and Electricity Cost
- (K) Manufacturing
- (L) Operations and Maintenance.

Technical Targets

- Improved performance, reduced hydrogen permeation, and lower costs compared with commercial perfluorosulfonic acid baseline.
- Membrane polarization loss after 500 hours (200 mA/cm², 400 psi, 50°C) <10 mV.
- Reduction in crossover loss at 50°C and ≥200 psi.

FY 2018 Accomplishments

- Defined cell design for prototype.
- Close to down-selection of material configuration for prototype cell stack.
- Down-selected membrane configuration for prototype cell stack.
- Demonstrated very low hydrogen crossover after 500 hours of operation at 1.8 A/cm², 50°C, 400 psi.
- Recorded >80 mV improvement in initial performance vs. Phase II baseline.
- Developed methods to reduce performance and durability hindering swell for high-ion exchange capacity (IEC) ionomers.
- A commercial coater who is keen to initiate production trials assessed continuous roll coating approaches to down-selected membrane configuration.
- Developed inverse design model for the optimal enthalpy of reduction as a function of operating conditions, including yield.
- Developed operating design model for estimating cycle efficiency.

¹ <https://www.energy.gov/eere/fuelcells/downloads/fuel-cell-technologies-office-multi-year-research-development-and-22>

INTRODUCTION

The potential to use ion exchange membrane-based electrolyzers at much higher differential pressures than fuel cells minimizes the need for additional costly mechanical compression of the hydrogen produced. However, this high pressure differential requires a robust membrane that is able to prohibit hazardous back diffusion of hydrogen to the oxygen source. A common solution to both enhance mechanical durability and reduce hydrogen diffusion is to simply increase the thickness of the membrane; however, this increases ionic resistance and can significantly reduce the efficiency of the system. Increasing the operating temperature can improve efficiency, but this usually accelerates physical and chemical membrane degradation, especially at higher pressures. Due to the limitations of current commercial membranes, new approaches are needed to enable efficient, cost-effective proton exchange membrane-based hydrogen generation.

We previously demonstrated excellent performance and low hydrogen permeation at less than half the thickness of current commercial perfluorosulfonic acid membranes. During 2018 we have further developed our ionomer chemistry, down-selected material and membrane configurations, and demonstrated reproducibility in ionomer synthesis and membrane fabrication in preparation for prototype cell stack fabrication during FY 2019.

APPROACH

Ionomers were custom synthesized and characterized at Tetramer and membranes were supplied to Proton OnSite for electrolyzer performance evaluation under conditions to emulate current commercial units. Specific ionomer and membrane variables investigated include backbone polymer architecture and molecular weight; ion exchange capacity; membrane thickness and configuration (including the incorporation of supports and additives); and membrane casting and post-cast treatment techniques. Membranes were evaluated for physical integrity, electrochemical performance, water uptake and swell, hydrogen permeability (crossover), and durability. Cell design modifications and membrane treatments also were investigated to enhance compatibility and optimize performance.

RESULTS

During this project to date, more than 70 different membranes have been produced at Tetramer and supplied to Proton OnSite for performance evaluation. During this 2018 period specifically, we have further developed our leading ionomer structures and membrane configurations and made additional down-selections based on the assessment of 30 new membranes. As a result, specification limits have been more tightly defined for ionomer backbone molecular architecture, ion exchange capacity and molecular weight, and membrane configuration. We are approaching final down-selections for prototype fabrication.

Effective methods to mitigate performance and durability issues caused by excessive swell of high-IEC ionomers have been demonstrated (Figure 1). The two most effective techniques are currently being employed as a means of further enhancing down-selected materials to extend durability.

Scale-up and reproducibility studies have been successfully carried out, incorporating process developments to improve ionomer yields and reduce waste. Our existing standard operating procedures and production cost analyses will be updated during FY 2019 based on these developments. We remain confident in the scalability of our ionomer synthesis and our previously projected membrane production cost savings (compared with commercial perfluorosulfonic acid products such as Nafion).

An initial performance improvement of >80 mV was recorded for our recent (scaled up) material down-selection, compared with Phase II Tetramer baseline membrane (Figure 2).

Cell design modifications and membrane surface treatments have been investigated at Proton OnSite to enhance the compatibility of our novel membranes with existing cell hardware. These developments will be incorporated into a prototype multi-cell stack electrolyzer unit.

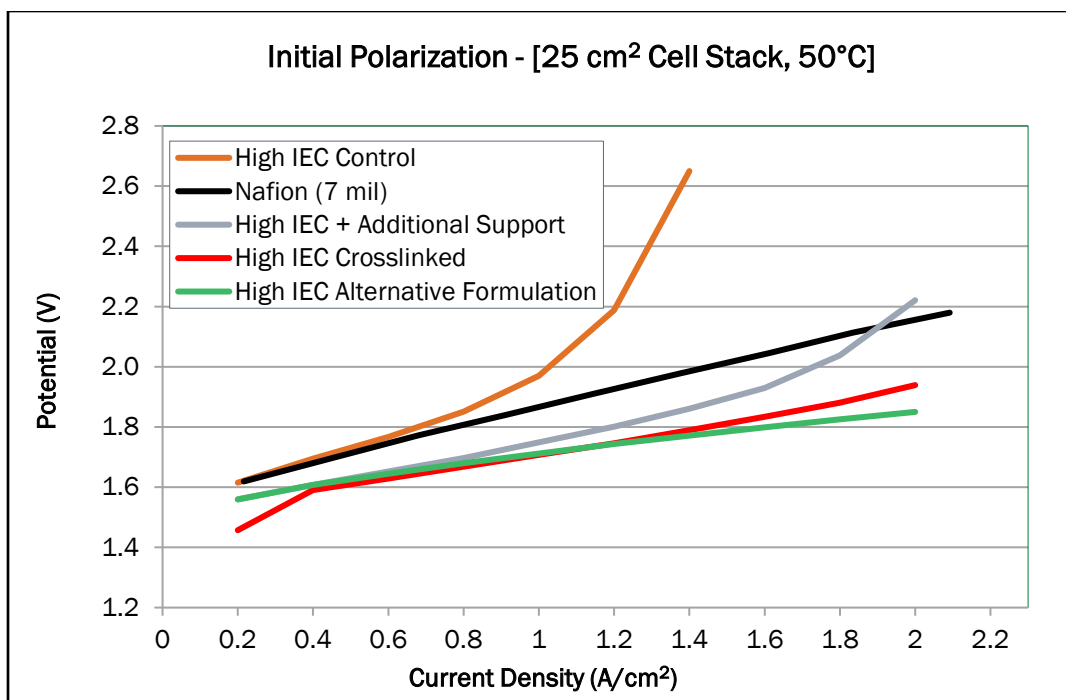


Figure 1. Performance and durability improvements of high-IEC materials by controlling swell

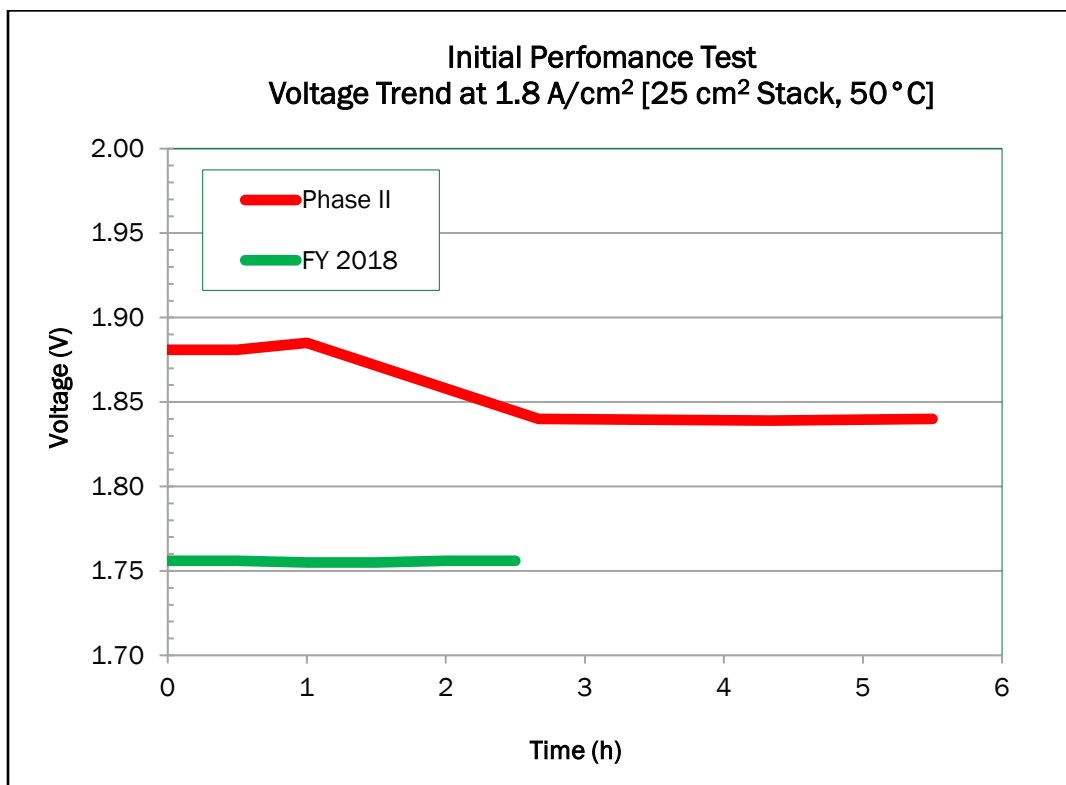


Figure 2. Initial performance screening data showing >80 mV improvement for a FY 2018 scaled-up ionomer vs. Tetramer Phase IIB baseline

CONCLUSIONS AND UPCOMING ACTIVITIES

Down-selected ionomer scale-up and reproducibility studies have been successful to date and processes have been further developed to improve efficiency and reduce material costs and waste. Standard operating procedures and production cost evaluations will be updated to incorporate these developments.

Our 2018 down-selected membranes demonstrate further improved performance and reduced hydrogen permeation compared with the commercial perfluorosulfonic acid baseline (7-mil Nafion) with a potential cost reduction of >50%. The overall advantages of this new technology project to a significant reduction in hydrogen production costs.

Following the conclusion of our currently ongoing tests to demonstrate extended durability (target = 5,000 hours, 50°C, 15 bar), a multi-cell prototype electrolyzer unit will be fabricated at Proton OnSite, incorporating Proton's cell design modifications. This unit will be assessed for performance and durability under standard operating conditions to allow direct comparison with existing Nafion-based units. If funding is available, we plan to pursue commercialization with Proton OnSite.

Biomass to Hydrogen (B2H2)

Pin-Ching Maness (Primary Contact), Katherine Chou, Lauren Magnusson, Jonathan Lo, and Wei Xiong

National Renewable Energy Laboratory
15013 Denver West Parkway
Golden, CO 80401
Phone: (303) 384-6114
Email: pinching.maness@nrel.gov

DOE Manager: Katie Randolph
Phone: (720) 356-1759
Email: Katie.Randolph@ee.doe.gov

Subcontractor:
Pennsylvania State University, State College, PA

Project Start Date: July 2015
Project End Date: Project continuation and direction determined annually by DOE

- Engineer *C. thermocellum* to co-utilize both the C6 (cellulose-derived) and C5 (hemicellulose-derived) sugars to improved biomass utilization, hence lowering feedstock cost.
- Use ¹³C-metabolic flux analysis and identify the most important pathway leading to maximal hydrogen production from cellulose-derived sugar.
- Redesign the MEC reactor by doubling cathode area (one cathode on each side of the anode chamber) to increase hydrogen production when using a platinum-free cathode catalyst.
- Improve anode performance by replacing small brushes (0.8 cm diameter) with seven larger brush anodes (1.5 cm diameter) to increase fiber density.
- Examine using a nickel catalyst (salts on activated carbon or a Ni powder) to see if hydrogen production rate can be improved compared to stainless steel.
- Investigate the performance of a more compact MEC by also looking at a flat anode.

Overall Objectives

- Optimize rates and yields of hydrogen production in a sequencing fed-batch bioreactor by varying hydraulic retention time and reactor volume replacement.
- Improve biomass utilization by engineering *C. thermocellum* to co-utilize both the six-carbon (C6) sugars (cellulose) and five-carbon (C5) sugar (hemicellulose) to lower feedstock cost.
- Optimize genetic tools to transform *C. thermocellum* and obtain mutants lacking the targeted competing pathways to improve hydrogen molar yield.
- Demonstrate hydrogen production from the National Renewable Energy Laboratory (NREL) fermentation effluent to improve overall energy efficiency in hydrogen production from cellulosic biomass using a microbial electrolysis cell (MEC) reactor.

Fiscal Year (FY) 2018 Objectives

- Optimize batch parameters and ferment corn stover lignocellulose to hydrogen with a rate of 2.5 L-H₂/L/d.

Technical Barriers

This project supports research and development on DOE Technical Task 6, subtasks “Molecular and Systems Engineering for Dark Fermentative Hydrogen Production” and “Molecular and Systems Engineering for MEC,” and it addresses barriers AX, AY, and AZ from the Hydrogen Production section of the Fuel Cell Technologies Office Multi-Year Research, Development, and Demonstration Plan¹:

(AX) H₂ Molar Yield

(AY) Feedstock Cost

(AZ) System Engineering.

Technical Targets

Progress toward meeting DOE’s dark fermentation technical targets is shown in Table 1.

¹ <https://www.energy.gov/eere/fuelcells/downloads/fuel-cell-technologies-office-multi-year-research-development-and-22>

FY 2018 Accomplishments

- We obtained a hydrogen production rate of 2.6 L/L-d in *C. thermocellum* fermenting pretreated biomass in a batch bioreactor.
- Using laboratory adaptive evolution, we improved the rate of xylose utilization by 3.5-fold in a *C. thermocellum* mutant engineered to co-utilize both C6 sugar and C5 sugar simultaneously without cross inhibition.
- By feeding *C. thermocellum* with ¹³C-labeled glucose, we constructed a high-resolution cellular carbon flux map and identified the most important glycolytic pathway leading to maximal hydrogen production.
- Using two cathode chambers (one on each side of the anode chamber) increased the hydrogen production from 1.3 ± 0.3 L-H₂/L_{reactor}-d to 2.3 ± 0.0 L-H₂/L_{reactor}-d (based on current density).
- The operation of the MEC with larger-diameter brush anodes (1.5 cm) and stainless steel wool cathodes further increased hydrogen production to 2.8 ± 0.3 L-H₂/L_{reactor}-d.
- Using a cathode made by adsorbing nickel onto activated carbon (AC) produced a higher hydrogen production rate (1.1 ± 0.1 L-H₂/L_{reactor}-d) than using a Ni foam cathode (1.0 ± 0.1 L-H₂/L_{reactor}-d), but lower than that of stainless steel wool.
- Cathodes made using nickel powder blended with AC had a hydrogen production rate 36% higher than only Ni powder (AC-NiP, 0.38 ± 0.08 L-H₂/L_{reactor}-d; pure Ni 0.28 ± 0.02 L-H₂/L_{reactor}-d) in different MEC (smaller chamber, 56 mL, no recirculation).

Table 1. Progress Toward Meeting DOE Technical Targets in Dark Fermentation

Characteristics	Units	Current Status	2015 Target	2020 Target
Yield of H ₂ from glucose	mole H ₂ /mole glucose	2–3.2	6 ^a	--
Feedstock cost	cents/lb glucose	13.5	10	8
Duration of continuous production (fermentation)	time	17 days	3 months	--
MEC cost of electrodes	\$/m ²	\$2,400	\$300	\$50
MEC production rate	L-H ₂ /L-reactor-d	2.8	1	---

^aYield of H₂ from glucose: DOE has a 2015 target of an H₂ molar yield of 6 (4 from fermentation and 2 from MEC) from each mole of glucose as the feedstock, derived from cellulose.

Feedstock cost: The DOE Bioenergy Technologies Office is conducting research to meet its 2015 target of 10 cents/lb biomass-derived glucose. NREL's approach is to use cellulolytic microbes to ferment cellulose and hemicellulose directly, which will result in lower feedstock costs.

INTRODUCTION

Biomass-derived glucose feedstock is a major operating cost driver for economic hydrogen production via fermentation. DOE's Fuel Cells Technologies Office is taking advantage of the DOE's Bioenergy Technology Office's investment in developing less expensive glucose from biomass to meet its cost target of 10 cents/lb by 2015. One alternative and viable approach to addressing the glucose feedstock technical barrier (Barrier AZ) is to use certain cellulose-degrading microbes that can ferment biomass-derived cellulose directly for hydrogen production. One such model microbe is the cellulose-degrading bacterium *Clostridium thermocellum*, which was reported to exhibit one of the highest growth rates using crystalline cellulose [1].

Another technical barrier to fermentation is the relatively low molar yield of hydrogen from glucose (mol H₂/mol sugar; Technical Barrier AX) using existing metabolic pathways in the cells. Biological pathways maximally yield 4 mol hydrogen per 1 mol glucose (the biological maximum) [2]. However, most laboratories have reported a molar yield of 2 or less [3, 4]. Molecular engineering to block competing pathways is a viable option toward improving hydrogen molar yield. This strategy has resulted in improved hydrogen molar yield in *Enterobacter aerogenes* [5].

A promising parallel approach to move past the biological fermentation limit has been developed by a team of scientists led by Bruce Logan at Pennsylvania State University (PSU). In the absence of oxygen, and by adding a slight amount of positive potential (-250 mV) to the circuit, Logan's group has produced hydrogen from acetate (a fermentation byproduct) at a molar yield of 2.9–3.8 (versus a theoretical maximum of 4) in a modified microbial fuel cell called an MEC [6]. It demonstrated for the first time a potential route for producing up to 8 moles of hydrogen per mole of acetate or potentially up to 12 moles of hydrogen per mole of glucose when coupled to a dark fermentation process. Indeed, in FY 2009 the team reported a combined molar yield of 9.95 when fermentation was coupled to an MEC in an integrated system [7]. Combining fermentation with MECs could therefore address Technical Barrier AX and improve the techno-economic feasibility of hydrogen production via fermentation.

APPROACH

NREL's approach to addressing high feedstock cost is to optimize the performance of the cellulose-degrading bacterium *C. thermocellum* using corn stover lignocellulose as the feedstock. To achieve this goal, we are optimizing the various parameters in a batch and sequencing fed-batch reactor to improve longevity, yield, and rate of hydrogen production, using corn stover biomass pretreated via a de-acetylation and mechanically refined (DMR) process. We also engineer *C. thermocellum* to utilize all the sugars in biomass (both C6 and C5) aimed to lower feedstock cost. To improve hydrogen molar yield, we are selectively blocking competing metabolic pathways in this organism via genetic methods. Through a subcontract, PSU is testing the performance of an MEC using both a synthetic effluent and the real waste stream from lignocellulosic fermentation generated at NREL.

RESULTS

Achieving High Rate of Hydrogen Production from Lignocellulose Fermentation

We conducted several batch experiments with the goal of optimizing and increasing biomass substrate loading in batch and fed-batch mode, to obtain an average hydrogen production rate of at least 2.5 L/L_{reactor}/day for a duration of minimally 24 h using DMR biomass as the substrate. We tested 30 g/L DMR (as cellulose) in batch mode and Figure 1 summarizes the hydrogen and carbon dioxide (CO₂) production of *C. thermocellum*. When calculating the rate over the most productive portion of the fermentation (25 hours in the linear portion of the fermentation), we achieved a rate of 2.6 L/L_{reactor}/day. *C. thermocellum* also exhibited a lag phase of approximately 10 hours. As we have shown in repeated fed-batch fermentation, we are able to significantly decrease, if not eliminate, the lag phase completely.

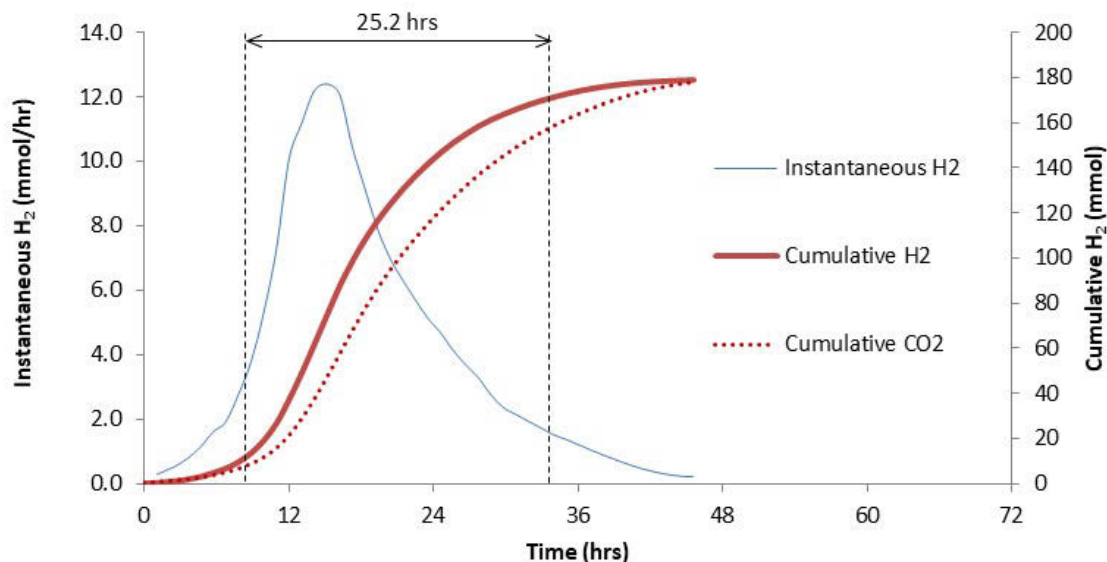


Figure 1. Hydrogen and CO₂ production by *C. thermocellum* when cultured in batch mode on 30 g/L (as cellulose) DMR substrate

Improving the Rate of Xylose Metabolism by 3.5-Fold

DMR-pretreated biomass generates a solid fraction containing both cellulosic (C6) and hemicellulosic (C5) sugars. *C. thermocellum* naturally can ferment cellulose directly to hydrogen without needing expensive cellulase enzyme cocktail, yet the wild-type strain lacks the ability to metabolize C5 sugar. Demonstrating co-metabolism of C6/C5 sugars efficiently hence is the goal in FY 2018 to improve the economic feasibility of fermentative hydrogen production. We previously have generated *C. thermocellum* mutant lines capable of co-metabolizing monomeric xylose (C5 hemicellulosic sugar) with cellobiose (cellulose-derived glucose dimer) with no cross-inhibition. Yet xylose metabolism still displays a lag phase. Via adaptive evolution (repeated sub-culture and transfer in xylose), we have evolved a variant that displays 3.5-fold improvement in the rate of xylose metabolism. The outcomes illustrate a significant improvement in biomass conversion to hydrogen with lower biomass feedstock cost.

Probing the Most Important Hydrogen Production Pathway via ¹³C-Metabolic Flux Analysis

Using isotope tracer (feeding ¹³C-glucose), gas chromatography-mass spectrometry, and metabolic flux modeling, we deciphered the metabolic network of *C. thermocellum* and uncovered that the Embden–Meyerhof–Parnas (EMP) pathway is the predominant glycolytic route supporting hydrogen production whereas the Entner–Doudoroff (ED) pathway and oxidative pentose phosphate pathway are inactive. To gain a quantitative understanding, we further formulate a fluxome map to quantify the metabolic fluxes through central metabolic pathways (Figure 2). The EMP pathway yields both NADH and reduced ferredoxins (2 moles each) compared to the ED pathway (3 NADH and 1 NADPH). Both NADH and reduced ferredoxin are the putative electron mediators toward hydrogen production based on its homologs in other related microbes. Cellulose hydrolysis via the EMP pathway therefore should yield more hydrogen compared to the ED pathway, which explains the copious amount of hydrogen produced by *C. thermocellum*. This work represents the first global *in vivo* investigation of the principal carbon metabolism of *C. thermocellum*. Further manipulations of the EMP pathway should increase hydrogen production further.

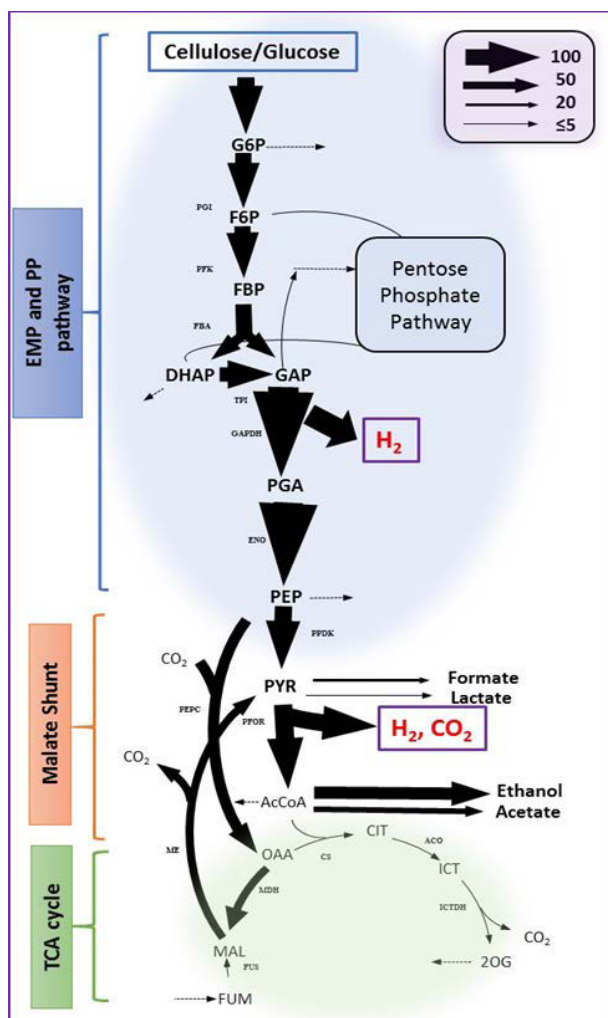


Figure 2. Carbon metabolic map of *C. thermocellum*. The growth medium was supplemented with U-13C-glucose (5.6 mM) in 22.2 mM unlabeled glucose (80%). Cells in late log phase were harvested (OD600 near 0.6) and the intracellular amino acids were extracted for gas chromatography-mass spectrometry analysis. G6P: glucose-6-phosphate; F6P: fructose-6-phosphate; FBP: fructose 1,6-bisphosphate; DHAP: dihydroxyacetone phosphate; GAP: glyceraldehyde-3-phosphate; PGA: 3-phosphoglycerate; PEP: phosphoenolpyruvate; PYR: pyruvate; AcCoA: acetyl CoA; OAA: oxaloacetate; MAL: malate; CIT: citrate; ICT: isocitrate; 2OG: 2-oxoglutarate; FUM: fumarate.

Impact of MEC Configuration and Operation on Hydrogen Production Rates

The goal of this project is to optimize the configuration of the MEC to maximize the hydrogen production rate. Electrically connecting two cathodes to the anode (Figure 3) doubled the hydrogen production from 1.3 ± 0.3 L-H₂/L_{reactor}-d to 2.3 ± 0.0 L-H₂/L_{reactor}-d (based on current production) using a stainless steel wool cathode. However, this increased current production could not be sustained, likely due to insufficient biofilm on the small (0.8 cm diameter) anodes. Therefore, thicker brushes (1.5 cm diameter, seven brushes) were used, which enabled stable current generation and a hydrogen production rate as high as 4.7 L-H₂/L_{reactor}-d over the first 7 h of recirculation of the anolyte, and 2.8 ± 0.3 L-H₂/L_{reactor}-d averaged over a 17 h cycle. The electrode potential was monitored with a reference electrode (Ag/AgCl) showing that the anode was primarily limiting performance, likely due to the low concentration of acetate in the synthetic fermentation effluent. Based on preliminary tests it is possible that performance can be further improved by replacing the seven 1.5-cm

diameter brushes with a single 4.5-cm diameter brush, pressed between the two anion exchange membranes, as this will provide for flow through the brush fibers rather than around the brushes.

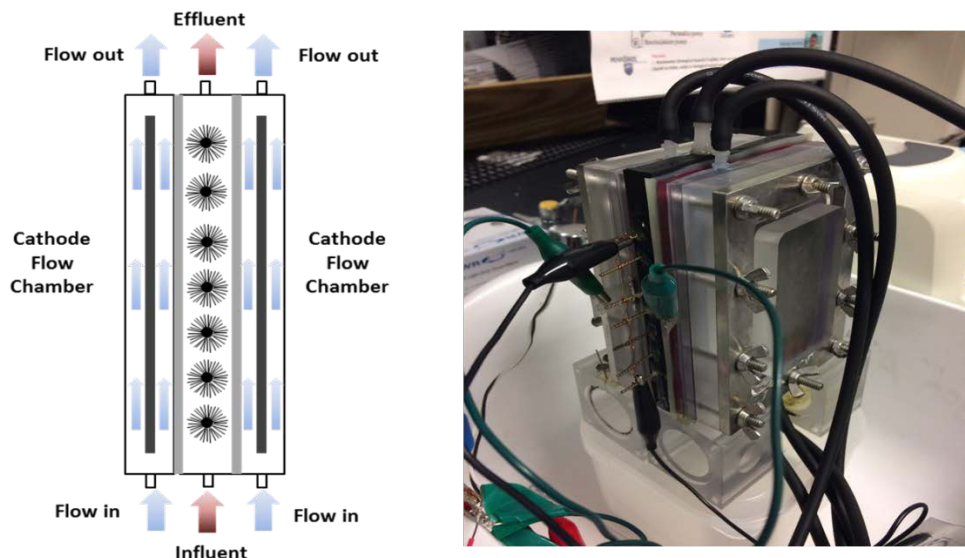


Figure 3. A new scalable MEC reactor with two cathode flow chambers: a schematic diagram (left), and a photo of the reactor (right)

Developing Non-Precious-Metal-Based Cathode Catalysts for MECs

Nickel is known to be a good, non-precious catalyst for the hydrogen evolution reaction. To examine its performance in MECs, Ni was adsorbed using a salt ($\text{NiCl}_2 \cdot 6\text{H}_2\text{O}$) onto high-surface-area AC to produce AC-Ni cathodes. The AC-Ni cathode (8.8 mg/cm^2 -electrode surface area) was tested in a 168 mL MEC (100 mL anode chamber, with 68 mL using a single cathode chamber). Synthetic fermentation effluent ($1.2 \text{ g-chemical oxygen demand/L}$) was continuously provided to the anode chamber and 50 mM phosphate buffer solution (pH 7) was recirculated through the cathode chamber at a rate of 40 mL/min. The MEC with the AC-Ni cathode produced $1.1 \pm 0.1 \text{ L-H}_2/\text{L-d}$ of hydrogen over 7 days of operation, which was significantly better ($p < 0.05$) than that obtained using Ni foam ($1.0 \pm 0.1 \text{ L-H}_2/\text{L-d}$), a material that has been used by others as an alternative to Pt. The better performance of the AC-Ni cathode was assumed to be due to the high specific surface of AC, which made more Ni available as a catalyst per projected area of cathode than the foam. Because Ni could be lost over time, we tested performance of a regenerated cathode. We removed the Ni using an acid solution and re-adsorbed additional Ni and found that the regenerated cathodes performed as well as or better than the original cathodes.

A cathode was also tested using Ni powder blended with the AC, rather than having the Ni adsorbed, in MECs fed with synthetic fermentation effluent in a different MEC (smaller chamber, 56 mL, no recirculation). The AC cathodes blended with Ni powder (4.4 mg/cm^2 loading) produced $0.38 \pm 0.08 \text{ L-H}_2/\text{L}_{\text{reactor-d}}$, which was higher than that obtained by Ni powder cathodes (no AC, $0.28 \pm 0.02 \text{ L-H}_2/\text{L}_{\text{reactor-d}}$). These current densities were lower than that of the AC-Ni cathodes, thus this catalyst was not further tested in larger MECs.

CONCLUSIONS AND UPCOMING ACTIVITIES

- We measured an average hydrogen production rate of 2.6 L/L-d in *C. thermocellum* fermenting pretreated corn stover over a period of 25 hours.
- We generated and adapted *C. thermocellum* mutant lines and improved rate of xylose consumption by 3.5-fold.

- Via ^{13}C -metabolic flux analysis, we generated a high-resolution flux map and identified the EMP pathway is important in *C. thermocellum* for cellulose conversion to hydrogen.
- We doubled the hydrogen production rate by connecting two cathode chambers to one anode to reach $2.8 \pm 0.3 \text{ L-H}_2/\text{L}_{\text{reactor}}\text{-d}$.
- Increasing the diameter of the brushes from 0.8 cm to 1.5 cm helped to stabilize reactor performance in terms of current production.

In the future, we will operate the batch and sequencing fed-batch bioreactors fermenting DMR-pretreated corn stover lignocellulose with increased solid loading, using *C. thermocellum* strains engineered and adapted to convert xylose (along with cellulose) at a faster rate. The aim is to increase rate of hydrogen production while lowering feedstock cost. We have generated a series of *C. thermocellum* mutants lacking carbon-competing pathways. We will conduct ^{13}C -metabolic flux analysis to gain insight as to how pathway redirections influence carbon and electron flux toward maximizing hydrogen production. The task using ionic liquid pretreatment was closed out in Q1, FY 2017. We will continue to examine alternative materials and catalysts for the cathode to improve reactor operation aimed at increasing hydrogen production and lowering MEC cost. A new larger brush will be tested in the two-cathode MEC to further improve the anode performance and biofilm development. The acetate concentration in the feed will be increased to stabilize the anode performance in both flat and brush anode MECs.

FY 2018 PUBLICATIONS/PRESENTATIONS

1. W. Xiong, J. Lo, K.J. Chou, C. Chao, L. Magnusson, T. Dong, and P.C. Maness, “Isotope-assisted metabolite analysis sheds light on central carbon metabolism of a model cellulolytic bacterium *Clostridium thermocellum*,” *Frontier in Microbiol.* 9 (2018): Article 1947, DOI: 10.3389/fmicb.2018.01947.
2. W. Xiong, L.H. Reyes, W.E. Michener, P.C. Maness, and K.J. Chou, “Engineering cellulolytic bacterium *Clostridium thermocellum* to co-ferment cellulose- and hemicellulose-derived sugars simultaneously,” *Biotechnol. Bioeng.* 115 (2018): 1755–1763, DOI: 10.1002/bit.26590.
3. K.J. Chou, “Metabolic Engineering of a cellulose-degrading bacterium *Clostridium thermocellum* for biofuels production,” Invited talk at Colorado State Univ., March 22, 2018.
4. P.C. Maness, Poster Presentation PD038, DOE Hydrogen and Fuel Cells Program Annual Merit Review, June 14, 2018, Washington, D.C.
5. K.-Y. Kim and B.E. Logan, “Dynamic flow and the use of inexpensive nickel-added activated carbon cathodes to achieve cost-effective hydrogen production in microbial electrolysis cells,” Abstract Proceedings of the 6th International Meeting of International Society for Microbial Electrochemistry and Technology (ISMET6), Universidade NOVA de Lisboa, Lisbon, Portugal, Oct. 3–6, 2017, poster presentation.
6. K.-Y. Kim and B.E. Logan, “Evaluation of alternative cathode materials for hydrogen production in Microbial electrolysis cells (MECs),” Abstract Proceedings of the Association of Environmental Engineering and Science Professors (AEESP) 2017 Conference, University of Michigan, Ann Arbor, June 20–22, 2017, poster presentation.
7. E. Zikmund, K.-Y. Kim, and B.E. Logan, “Hydrogen production rates with closely-spaced felt anodes and cathodes compared to brush anodes in two-chamber microbial electrolysis cells.” *International Journal of Hydrogen Energy* 43, no. 20 (2018): 9599–9606.
8. K.-Y. Kim, W. Yang, and B.E. Logan, “Regenerable nickel-functionalized activated carbon cathodes enhanced by metal adsorption to improve hydrogen production in microbial electrolysis cells.” *Environmental Science & Technology* 52, no. 12 (2018): 7131–7137.

9. K.-Y. Kim, E. Zikmund, and B.E. Logan, “Impact of catholyte recirculation on different 3-dimensional stainless steel cathodes in microbial electrolysis cells.” *International Journal of Hydrogen Energy* 42 (2017): 29708–29715.
10. B.E. Logan, E. Zikmund, W. Yang, R. Rossi, K.-Y. Kim, P.E. Saikaly, and F. Zhang, “Impact of ohmic resistance on measured electrode potentials and maximum power production in microbial fuel cells,” *Environmental Science and Technology* 52 (2018): 8977–8985.

REFERENCES

1. Y.P. Zhang and L.R. Lynd, “Cellulose utilization by *Clostridium thermocellum*: bioenergetics and hydrolysis product assimilation,” *Proc. Natl. Acad. Sci. USA* 102 (2005): 7321–7325.
2. F.R. Hawkes, R. Dinsdale, D.L. Hawkes, and I. Hussy, “Sustainable fermentative hydrogen production: Challenges for process optimization,” *Intl. J. Hydrogen Energy* 27 (2002) 1339–1347.
3. B.E. Logan, S.E. Oh, I.S. Kim, and S. Van Ginkel, “Biological hydrogen production measured in batch anaerobic respirometers,” *Environ. Sci. Technol.* 36 (2002): 2530–2535.
4. S. Van Ginkel and S. Sung, “Biohydrogen production as a function of pH and substrate concentration,” *Environ. Sci. Technol.* 35 (2001): 4726–4730.
5. M.A. Rachman, Y. Furutani, Y. Nakashimada, T. Kakizono, and N. Nishio, “Enhanced hydrogen production in altered mixed acid fermentation of glucose by *Enterobacter aerogenes*,” *J. Ferm. Eng.* 83 (1997): 358–363.
6. S. Cheng, and B.E. Logan, “Sustainable and efficient biohydrogen production via electrogenesis,” *Proc. Natl. Acad. Sci. USA.* 104 (2007): 18871–18873.
7. E. Lalaurette, S. Thammannagowda, A. Mohagheghi, P.C. Maness, and B.E. Logan, “Hydrogen production from cellulose in a two-stage process combining fermentation and electrohydrogenesis,” *Intl. J. Hydrogen Energy* 34 (2009): 6201–6210.
8. A. Guss, D.G. Olson, N.C. Caiazza, and L.R. Lynd, “Dcm methylation is detrimental to plasmid transformation in *Clostridium thermocellum*,” *Biotechnol. Biofuels* 5 (2012): 30–41.
9. M. Liszka, A. Kang, S. Konda, K. Tran, J. Gladden, S. Singh, J.D. Keasling, C.D. Scown, T.S. Lee, B. Simmons, and K.L. Sale, “Switchable Ionic Liquids Based on Di-Carboxylic Acids for One-Pot Conversion of Biomass to an Advanced Biofuel,” *Green Chemistry* (2016), DOI: 10.1039/C6GC00657D.
10. D. Argyros, S.A. Tripathi, T.F. Barrett, S.R. Rogers, L.F. Feinberg, D.G. Olson, J.M. Foden, B.B. Miller, L.R. Lynd, D.A. Hogsett, and N.C. Caiazza, “High ethanol titers from cellulose by using metabolically engineered thermophilic anaerobic microbes,” *Appl. Environ. Microbiol.* 77 (2011): 8288–8294.

Novel Hybrid Microbial Electrochemical System for Efficient Hydrogen Generation from Biomass

Hong Liu (Primary Contact), Yuyan Shao,
Vilayanur Viswanathan, Murthy Ganti
Oregon State University/Pacific Northwest National
Laboratory
116 Gilmore Hall
Oregon State University
Corvallis, OR 97331
Phone: (541) 737-6309
Email: liuh@engr.orst.edu

DOE Manager: Katie Randolph
Phone: (720) 356-1759
Email: Katie.Randolph@ee.doe.gov

Project Start Date: February 1, 2016
Project End Date: April 30, 2020

Overall Objectives

- Design and fabricate a low-cost, robust, and highly efficient fermentation and microbial electrochemical system.
- Determine the techno-economic feasibility of the system using biomass hydrolysates and wastewater.

Fiscal Year (FY) 2018 Objectives

- Continue the investigation on hydrogen production through the fermentation and microbial electrolysis cell (F-MEC) process.
- Design and fabricate a 10-liter F-MEC reactor.
- Evaluate the F-MEC reactor.
- Develop cost performance model.

Technical Barriers

This project addresses the following technical barriers from the Hydrogen Production section of the Fuel Cell Technologies Office Multi-Year Research, Development, and Demonstration Plan¹:

(AX) Hydrogen Molar Yield

(AAA) Electrode Cost

(AAB) Solution Density (Production Rate).

Technical Targets

Progress has been made in achieving the DOE targets listed in the Multi-Year Research, Development, and Demonstration Plan. Table 1 lists DOE's technical targets and where our research and development efforts stand to date.

The overall goal of this project is to develop and scale-up our novel hybrid F-MEC system that can be integrated with well-developed lignocellulose pretreatment/hydrolysis or wastewater treatment processes for efficient hydrogen production at a cost less than \$2/kg H₂.

FY 2018 Accomplishments

- Optimized fermentative hydrogen production conditions using immobilized fermentative bacteria. The hydrogen production rate reached over 20 L/L-reactor/day by fermentation alone.
- Identified the key reason causing the decrease of hydrogen production efficiency in microbial electrolysis cells (MECs) during long-term operation.
- Developed a method to effectively inhibit homoacetogenesis in MECs.
- Revealed the synthesis-structure-property relationship of molybdenum phosphide (MoP) hydrogen evolution reaction (HER) catalysts with high activity (comparable to platinum).
- Designed and fabricated a 10-liter F-MEC reactor.
- Evaluated the F-MEC with glucose. More than 20 L/L-reactor/day hydrogen production was achieved in the 10-L reactor operated under continuous-flow mode.

¹ <https://www.energy.gov/eere/fuelcells/downloads/fuel-cell-technologies-office-multi-year-research-development-and-22>

Table 1. Progress Toward Meeting Technical Targets for Dark Fermentative Hydrogen Production and MECs

Characteristic	Units	DOE 2015 Targets	DOE 2020 Targets	Project Status
Yield of hydrogen production from glucose by integrated MEC-fermentation	mol H ₂ /mol glucose	6	9	8.5
MEC cost of electrodes	\$/m ²	300	50	90

INTRODUCTION

The global interest in hydrogen production has been stimulated by the promise of the clean operation and high efficiencies of hydrogen fuel cells. Currently, almost all the hydrogen produced is from non-renewable fossil sources. Hydrogen can be produced from renewable biomass by biological dark fermentation. Unfortunately, the hydrogen yields using current fermentation techniques are low. Hydrogen can also be produced by MEC, which can overcome the fermentation barrier and achieve higher hydrogen yield. However, the key challenges for realizing the practical applications of MECs include (1) difficulty in utilizing biomass directly and in utilizing certain biomass components, such as sugars; (2) low hydrogen production rate or high energy input due to inefficient reactor designs, high cathode overpotential, and high solution resistance; and (3) high capital cost due to high electrode and membrane or separator costs. In this project, we will develop a hybrid system that integrates the dark fermentation and MEC processes and overcomes the challenges identified above.

APPROACH

The overall approach of this project is to develop an efficient F-MEC for hydrogen generation from lignocellulosic biomass hydrolysates and sugar-rich wastewater through maximizing the hydrogen production rate and yield of both processes. Because MEC cathode material is a key factor affecting both capital and operational costs of the system, robust and low-cost cathode materials with low overpotentials will also be developed. A cost-performance model will be used to supplement the H2A analysis tool throughout the project to prioritize the critical factors and demonstrate potential to meet DOE cost goals.

We identified suitable bacterial cultures for the hybrid system in FY 2016. In FY 2017, we focused on determining the optimal operational conditions using small lab reactors, developing low-cost and low-overpotential cathode catalyst, and conducting cost and performance analysis. In FY 2018, we have continued the investigation on fermentation and MEC process and designed, fabricated, and evaluated a scaled-up F-MEC reactor.

RESULTS

Continuous Hydrogen Production by Fermentation

We investigated the effect of immobilized bacterial biomass content in reactor on hydrogen production. We found that increasing the biomass content to 20%–40% can result in more than 20 L/L-reactor/day of hydrogen production through fermentation alone using simulated hydrolysate solution, which contained mixed sugars at a ratio of 58.9% glucose, 35.6% xylose, 7.4% mannose, 5.2% galactose, and 2.9% arabinose (Figure 1).

Reducing Hydrogen Uptake by Homoacetogens in MECs

We observed that hydrogen recovery decreased while the coulombic efficiency was over 100% during long-term operation. Our liquid sample analysis and microbial community characterization revealed that the growth of homoacetogens (acetobacterium) caused the low cathodic recovery (Figure 2a). We also found that the hydrogen consumption rate was more affected by hydrogen partial pressure than acetate concentration in the presence of homoacetogens. We further demonstrated that chloroform (0.02%) can be used as an effective homoacetogen inhibitor to reduce hydrogen uptake by homoacetogens (Figure 2b).

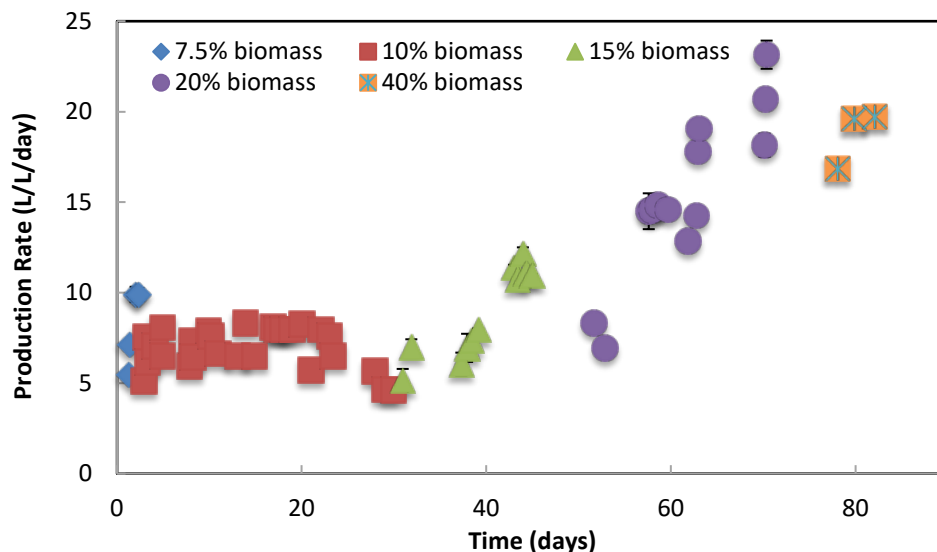


Figure 1. Continuous hydrogen production with immobilized sludge beads at 7.5%–40% (v/v) ratio of beads to media

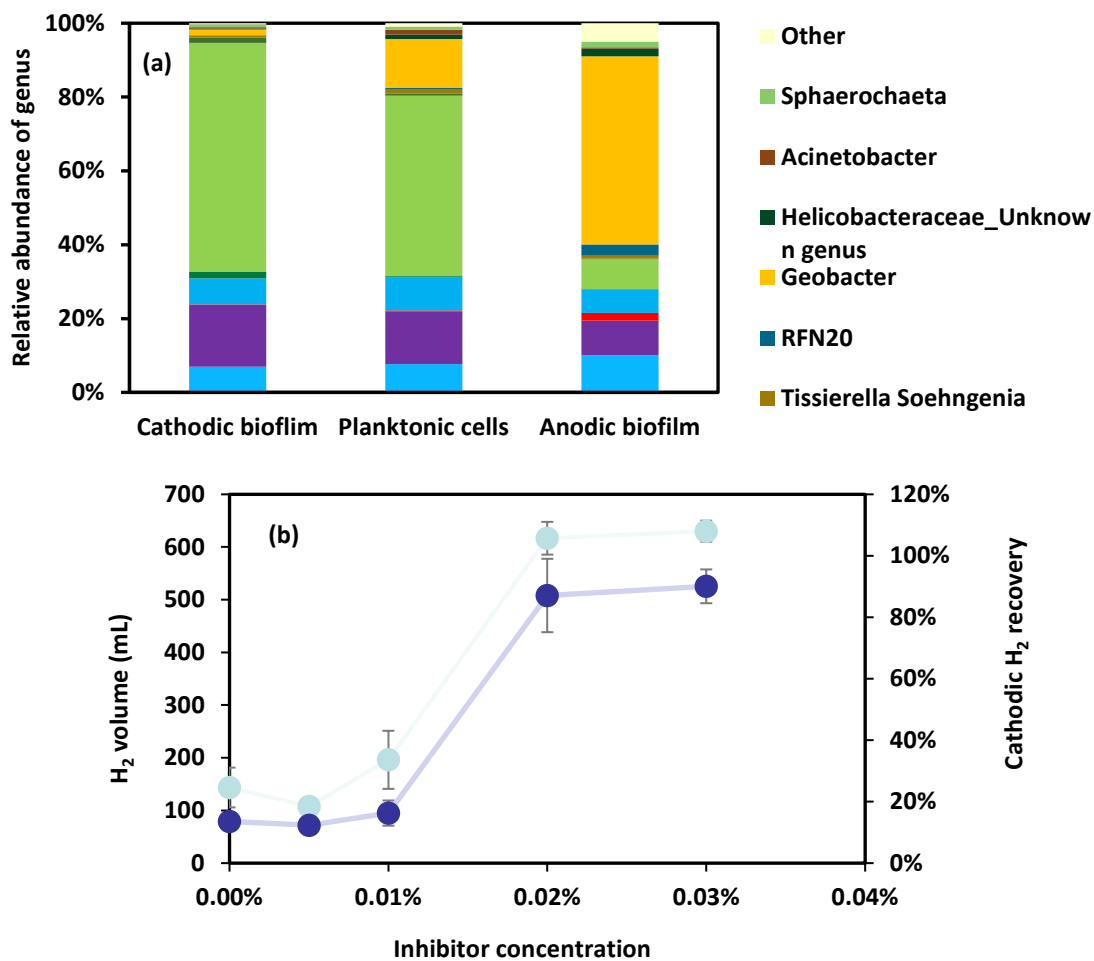


Figure 2. Relative abundance of genus in cathodic, planktonic, and anodic microbial communities. Genus with less than 1% of relative abundance were classified into others (a); and effect of chloroform concentration on hydrogen production (b).

MEC Cathode Development

We investigated the structure-property relationship of MoP electrocatalysts that demonstrate comparable performance to platinum catalyst. The higher catalytic activity for MoP-700 with P-rich surface is possible because the P-terminated surface allows Mo to be exposed, because P atom size is only half that of Mo, and there is synergy between Mo and P, which promotes HER in neutral solution (Figure 3). We also found the reversible transformation of MoP structure (i.e., heat treatment of MoP-700 at 750°C leads to its dephosphorization with the formation of MoP-750, which can be transformed back to MoP-700). This indicates a proper post-treatment of commercial MoP may achieve the desired surface structure that enables high performance—a more scalable, cost-effective method for production of this material.

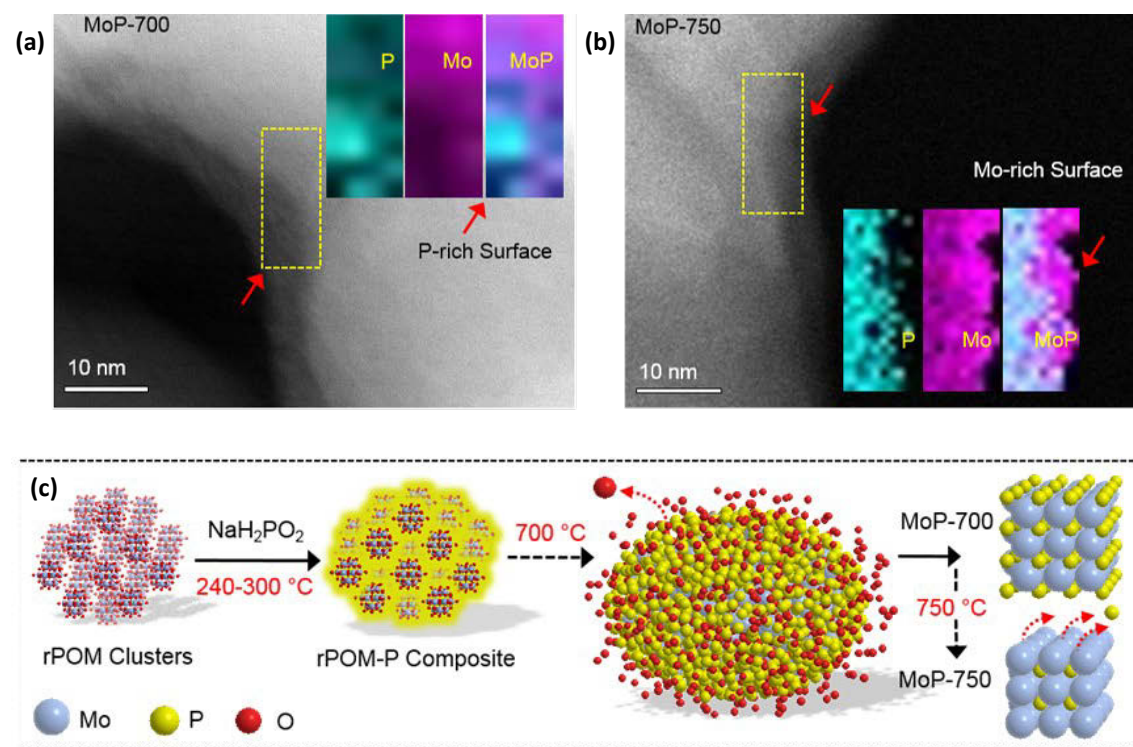


Figure 3. Micrographs of materials and schematic illustration of the synthesis of MoP. STEM images and corresponding EELS mapping of (a) MoP-700 and (b) MoP-750. (c) Schematic diagram illustrates the synthesis process of MoP-700 and MoP-750.

Scaled-Up (10-L) F-MEC Reactor Design and Fabrication

We designed the reactor based on the performance of small lab-scale fermentative reactors and MECs and developed a procedure to fabricate the cathodes. The assembled reactor has a fermentation volume of 0.8 L and an MEC portion of 9.3 L. Five pieces of cathode each with a surface area of 563 cm² and six pieces of anode each with 1,689 cm² area were installed in the MEC portion. The electrodes were arranged in the direction of the flow so that high fluid speeds could be achieved with recirculation (Figure 4).

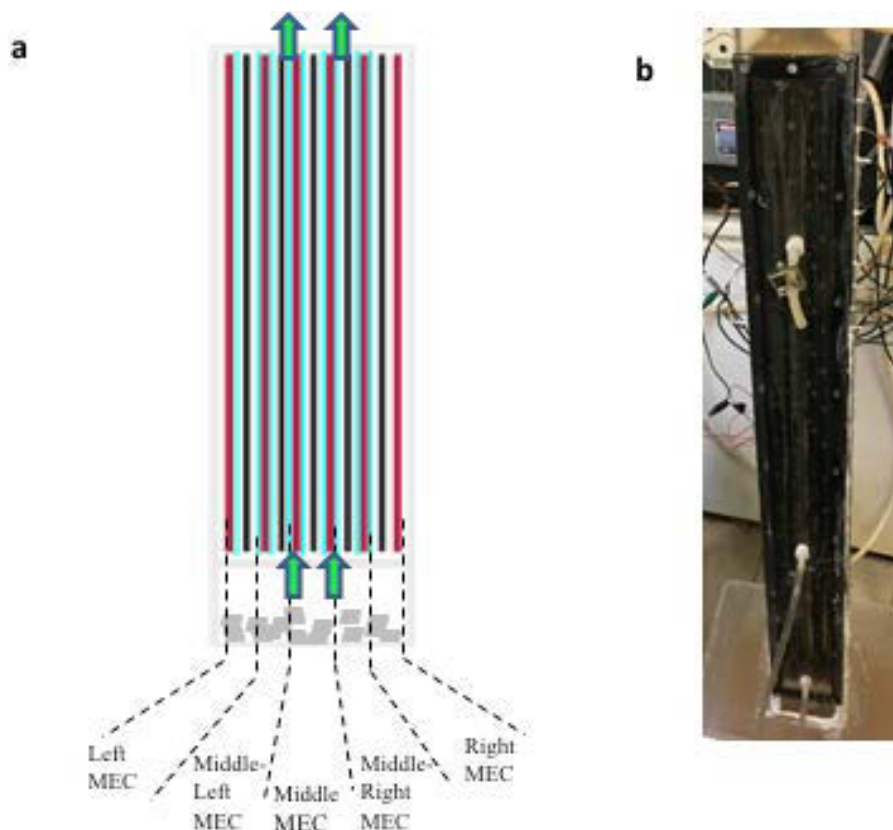


Figure 4. (a) Diagram of reactor electrode configurations with recirculation inlets and outlets—green arrows; anode set—red; cathode—black; separator—blue; and fermentative beads in bottom—gray. (b) Photo of the F-MEC reactor.

F-MEC Evaluation in Continuous Flow Mode

After about one month of startup period, the reactor was switched to continuous flow mode using acetate. We observed that the cathode can reach a current density of 35–40 A/m² at an applied voltage of 1.0 V. Fermentation beads containing immobilized fermentative bacteria were then added to the fermentation zone of the reactor and glucose was added to the feeding solution. Our preliminary testing demonstrates that a hydrogen production rate over 20 L/L-reactor/day can be achieved with glucose in the scaled-up F-MEC reactor (Figure 5).

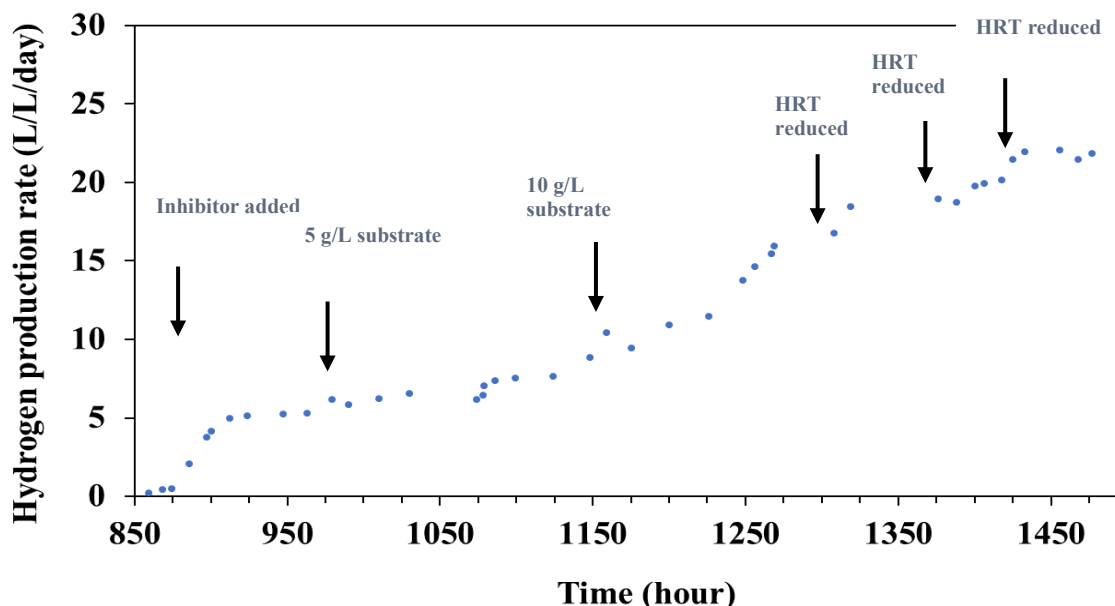


Figure 5. Continuous hydrogen production in 10-liter F-MEC

CONCLUSIONS AND UPCOMING ACTIVITIES

We have made significant progress toward reaching our project target. We have identified an issue (homoacetogenesis) associated with the MEC process for long-term operation and developed a solution. We have revealed the structure-property relationship of MoP electrocatalysts that demonstrate comparable performance to platinum catalyst. We have designed, fabricated, and preliminarily evaluated a scaled-up 10-liter F-MEC reactor.

Future work includes the following.

- Identity the reasons causing the instability of the large reactor.
- Finish the evaluation of the large reactor with wastewater and biomass hydrolysate.

SPECIAL RECOGNITIONS AND AWARDS/PATENTS ISSUED

1. Patent filed on “Modified transition metal-phosphide catalysts with enhanced catalytic activity in neutral media and process of making,” by Yuyan Shao at Pacific Northwest National Laboratory.

FY 2018 PUBLICATIONS/PRESENTATIONS

1. Luguang Wang, Lakhveer Singh, and Hong Liu. “Revealing the Hydrogen Consumption-Production Loop in Single Chamber Microbial electrolysis cells (MECs).” *International Journal of Hydrogen Energy*. 43, no. 29 (19 July 2018): 13064–13071.
2. Cheng Li, Luguang Wang, Hong Liu. “Enhanced Redox Conductivity and Enriched Geobacteraceae of Exoelectrogenic Biofilms in Response to Static Magnetic Field.” *Appl. Microbiol. Biotechnol.* (2018 Jun 20). doi: 10.1007/s00253-018-9158-3.
3. Luguang Wang, Stephanie Trujillo, and Hong Liu. “Using Acetylene as a Low-cost and Effective Methanogenesis Inhibitor in Single Chamber Microbial Electrolysis Cells.” Submitted to *Bioresource Technology*.
4. Andrew Miller, Lakhveer Singh, and Hong Liu. “Quantifying the International Resistances in Single Chamber (MECs).” Submitted to *Environment International*.

5. Luguang Wang, Lakhveer Singh, and Hong Liu. “Chloroform as an Effective Homoacetogen Inhibitor to Enhance Hydrogen Recovery in Single Chamber Microbial Electrolysis Cells (MECs).” Submitted to *Chemical Engineering Journal*.
6. Andrew Miller. Master thesis: “Microbial Electrolysis Cells for the Production of Hydrogen Gas: Evaluation of Internal Resistance and Design for Scale-Up.”
7. Hong Liu, Yuyan Shao, and Vilayanur Viswanathan. “Novel Hybrid Microbial Electrochemical System for Efficient Hydrogen Generation from Biomass,” presented at the DOE AMR meeting, Washington, D.C., June 2018.
8. Hong Liu. “Microbial Electrochemical System for Hydrogen Generation from Biomass and Waste Streams,” 22nd World Hydrogen Energy Conference, June 17–22, 2018, Rio, Brazil.
9. Hong Liu. “Energy Recovery from Waste Streams Using Microbial Electrochemical Systems,” Separation Technology Event at Lappeenranta University in Finland, August 22, 2018 (Invited talk).
10. Yuyan Shao. “Surface Atom Synergy in Electrocatalysis on Precious Metal Free Catalysts,” Nature Conference on Materials Electrochemistry: Fundamentals and Applications, January 15, 2018, Shenzhen, China (Invited talk).
11. Yuyan Shao. “Materials Electrochemistry for Energy Conversion and Storage @Scale,” UC Riverside Seminar, April 2, 2018, Riverside, CA, United States.

HydroGEN Overview: A Consortium on Advanced Water-Splitting Materials

Huyen N. Dinh (Primary Contact, National Renewable Energy Laboratory [NREL]), Richard Boardman (Idaho National Laboratory [INL]), Anthony McDaniel (Sandia National Laboratories [SNL]), Héctor Colón-Mercado (Savannah River National Laboratory [SRNL]), Tadashi Ogitsu (Lawrence Livermore National Laboratory [LLNL]), Adam Weber (Lawrence Berkeley National Laboratory [LBNL])
National Renewable Energy Laboratory
15013 Denver West Parkway
Golden, CO 80401
Phone: (303) 275-3605
Email: Huyen.Dinh@nrel.gov

DOE Manager: Katie Randolph
Phone: (720) 356-1759
Email: Katie.Randolph@ee.doe.gov

Project Start Date: June 2016
Project End Date: Project continuation and direction determined annually by DOE

- Establish cooperative research and development agreements that leverage the node capabilities of HydroGEN.
- Develop benchmarking standards and procedures to ensure consistency in reporting and proving the principles of advanced water-splitting materials (AWSM).
- Enable funding opportunity announcement (FOA) projects to meet their technical goals through joint research activities and interactions with the nodes.

Fiscal Year (FY) 2018 Objectives

- Collaborate and conduct research with the new FOA-awarded HydroGEN projects (18 seedling projects and one benchmarking project).
- Facilitate the rapid implementation of non-disclosure agreements (NDAs), material transfer agreements, intellectual property, and contract agreements to streamline access to the labs.
- Review the current palette of lab resource nodes (>80) and identify new resources that can be included in HydroGEN to keep the nodes updated and relevant.
- Enable and enhance the technical accomplishments of FOA projects and achieve project goals through node interactions.
- Further develop the HydroGEN website (e.g., update the capabilities and add publications and presentations).
- Hold workshops with partners focused on each of the four water splitting pathways to increase the collective understanding of R&D activities, needs, node capabilities, and opportunities for collaboration.

Overall Objectives

- Facilitate collaboration between the four advanced water-splitting pathways on common materials challenges and resource needs.
- Socialize and inform the general hydrogen community about the HydroGEN Energy Materials Network (EMN) consortium.
- Identify new and review current resource nodes to ensure that they are relevant, unique, and available to support HydroGEN.
- Develop the HydroGEN website to make it user friendly, easily searchable by capability node and/or laboratory, and an information-rich resource about HydroGEN activities.
- Develop and facilitate execution of a catalog of standardized technology transfer agreements (TTAs) that can provide rapid access to the labs.
- Develop an accessible, searchable, and secure HydroGEN Data Hub and SharePoint site to support collaborative science.

Technical Barriers

This project addresses the following technical barriers from the Hydrogen Production section of

the Fuel Cell Technologies Office Multi-Year Research, Development, and Demonstration Plan¹:

- (F) Capital Cost
- (G) System Efficiency
- (K) Manufacturing
- (L) Operations and Maintenance
- (S) High-Temperature Robust Materials
- (T) Coupling Concentrated Solar Energy and Thermochemical Cycles
- (W) Materials and Catalysts Development
- (X) Chemical Reactor Development and Capital Costs
- (AC) Solar Receiver and Reactor Interface Development
- (AE) Materials Efficiency—Bulk and Interface
- (AF) Materials Durability—Bulk and Interface
- (AG) Integrated Device Configurations
- (AH) Reactor Designs
- (AI) Auxiliary Materials
- (AJ) Synthesis and Manufacturing
- (AL) Operations and Maintenance.

Technical Targets

HydroGEN is an EMN consortium that is led by six national laboratories (NREL, LBNL, SNL, LLNL, INL, SRNL) and fosters cross-cutting materials innovation, using theory-guided applied materials research and development, to advance all emerging water-splitting pathways (low-temperature electrolysis [LTE], high-temperature electrolysis [HTE], photoelectrochemical [PEC] and solar thermochemical [STCH], which includes hybridized thermochemical and electrolysis approaches to water splitting) for clean and

sustainable hydrogen production that meets the following DOE targets:

- Cost of hydrogen production <\$2/kg H₂
- Efficiency and durability targets that vary for different water-splitting pathways.

FY 2018 Accomplishments

HydroGEN is an Energy Materials Network (EMN) consortia, comprising >80 unique, world-class capabilities/expertise in materials theory/computation, advanced materials synthesis, characterization, analysis, and integration. Each capability represents a resource node—a combination of a tool, technique, and expertise—that is unique to the national laboratory system, available to external stakeholders, and relevant to at least one of the HydroGEN water-splitting pathways.

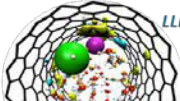
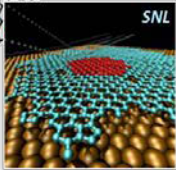
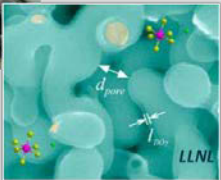
- Expanded the highly collaborative HydroGEN consortium, incorporating 19 new FOA-awarded projects working together across four water splitting technologies, and leveraging the six core labs' capabilities and expertise, to accelerate materials research in order to advance the development of water-splitting technologies.
- HydroGEN successfully engaged in an inter-agency collaboration with the National Science Foundation's (NSF) Designing Materials to Revolutionize and Engineer our Future (DMREF) program element, resulting in four NSF DMREF projects that will leverage the HydroGEN EMN experts and capabilities in three water splitting technologies (PEC, LTE, and STCH).
- Produced many high-value products:
 - Collaboration among 11 national labs, 7 companies, and 30 universities
 - Personnel exchanged for collaborative research
 - >100 material samples exchanged
 - >180 registered researchers on the HydroGEN collaboration site

¹ <https://energy.gov/eere/fuelcells/downloads/fuel-cell-technologies-office-multi-year-research-development-and-22>

- >25 papers published or submitted for publication
- Two records of inventions
- One facility proposal submitted
- One EMN-wide meeting on Machine Learning and Data Analytics organized.
- Continually updated and expanded the HydroGEN website (<https://www.h2awsm.org/>). It currently houses 14 news items, and a new publication subsite that compiles lists of HydroGEN journal articles (13) published, and presentations (21) given. The capability nodes have been reviewed and updated on the user-friendly node search engine.
- Eighteen FOA-awarded projects utilized 44 nodes.
- Established 40 new or substantially updated nodes.
- Maintained and expanded the HydroGEN Data Hub (<https://datahub.h2awsm.org/>), a secure project space for team members to store, view, and share project data and to disseminate data to the scientific community and public once the private, secure data has been reviewed and curated. The Data Hub has 128 users and 3,889 data files. Three Data Hub highlights include:
 - Developed, shared, and demonstrated new data tools for visualization, uploading large datasets, and metadata assignments.
 - Advanced metadata definitions and application program interface (API) access.
 - Established a data publication process.
- Developed multiple standard, pre-approved, mutual TTAs, including NDAs, material transfer agreements, intellectual property management plans, and cooperative research and development agreements, to streamline access to the national labs' materials capability network (<https://www.h2awsm.org/working-with-hydrogen>).
 - The standard HydroGEN NDAs were signed by all six core labs within two months.
 - The 19 new FOA project NDAs were executed within two weeks.

HydroGEN has a world-class materials capability network, comprising >80 unique, capabilities/expertise in materials theory/computation, advanced materials synthesis, characterization, analysis, and integration (Figure 2). Each capability represents a resource node—a combination of a tool, technique, and expertise—that is unique to the national laboratory system, available to external stakeholders, and relevant to one of the HydroGEN water-splitting pathways. HydroGEN capability nodes are assigned a readiness category (1, 2, or 3) to inform potential users of their development status. For example, a category 1 node is fully developed and has been used for AWSM research. A category 3 node requires significant development for use by an AWSM project partner.

HydroGEN AWSM Consortium comprise more than 80 unique, world-class capabilities/expertise in:

Materials Theory/Computation	Advanced Materials Synthesis	Characterization & Analytics
 <p>LLNL</p> <p>Bulk & interfacial models of aqueous electrolytes</p>  <p>SNL</p> <p>LAMMPS classic molecular dynamics modeling relevant to H₂O splitting</p>	 <p>NREL</p> <p>High-throughput spray system for electrode fabrication</p>  <p>LLNL</p> <p>Conformal ultrathin TiO₂ ALD coating on bulk nanoporous gold</p>	 <p>SNL</p> <p>Stagnation flow reactor to evaluate kinetics of redox material at high-T</p>  <p>INL</p> <p>TAP reactor for extracting quantitative kinetic data</p>

HydroGEN fosters cross-cutting innovation using theory-guided applied materials R&D to advance all emerging water-splitting pathways for hydrogen production

Website: <https://www.h2awsm.org/>

Figure 2. The HydroGEN AWSM consortium fosters cross-cutting innovation using the world-class, unique capabilities and expertise in materials theory and computation, advanced materials synthesis, and characterization at the national labs

APPROACH

The goal of the consortium is to advance the level of maturity of the various water-splitting pathways for hydrogen production by offering national laboratory capabilities, including leading technology experts and equipment resources relevant to materials research in these pathways, to outside stakeholders. The user-friendly node search engine (<https://www.h2awsm.org/capabilities>) allows stakeholders to quickly identify capability nodes that can be used to advance their materials research and development.

The consortium addresses the cross-cutting material challenges using synthesis and characterization methods that are guided by computational studies and fundamental materials science knowledge. While it is recognized that each pathway has unique material and/or integration challenges, one of the strategies of this consortium is to apply its core capabilities and expert knowledge across research disciplines and water-splitting technology pathways in order to develop critical materials and amplify the consortium's effectiveness.

RESULTS

The HydroGEN EMN is a large consortium comprising more than 180 individual participants, including technology and capability node experts, principal investigators (PIs), postdoctoral researchers, graduate students, data experts, TTA experts, communications specialists, and website developers. NREL created a user-friendly, secured collaboration (SharePoint) site to enhance communication, information sharing, and

collaboration among the 19 FOA-awarded project members, the steering committee members, Fuel Cell Technologies Office leadership team, the Data Team, the TTA team, and the lab node experts. NREL's Data Team has developed a secured Data Hub for all projects to share data with each other. The Data Team, which has representation from the six core national labs, has monthly teleconferences. HydroGEN's steering committee, similarly represented by the six labs, has biweekly webinars to ensure effective communication, timely progress, and transparency.

HydroGEN FY 2018 Data Team Highlights

Developed, shared, and demonstrated new data tools: The Data Team has developed several new data tools for use in the HydroGEN Data Hub, including the Multi-spectra Viz tool for visualizing multiple spectra files together in one graph; the EMN Intelligent Uploader tool written in Python for uploading large datasets of transmission electron microscopy, X-ray diffraction, and Raman spectroscopy with automated metadata; the Defect Properties Viz tool developed by LLNL for dynamic visualization of defect functional properties in allowed composition space; and the stagnation flow reactor (SFR) Data Tool, developed by SNL, for data packaging, metadata assignment, and upload of large experimental datasets from SFR experiments. The Data Team has also implemented "data tool demos" within the User Resources project so that everyone can see example of the data tools and how they work.

Developed advanced metadata definitions and API access: The Data Team continued to refine and develop metadata standards for data types common in HydroGEN. Specifically, the Data Team has made improvements to the data-set-level metadata definitions, as well as individual file-level metadata. The faceted search capability enables quick search across all data sets (across projects as security allows) based on the metadata defined. The Data Team hosted an API tutorial to educate researchers on how to programmatically upload data into the Data Hub as well as write programs to search and download data, based on metadata values.

Established a data publication process: The data publication process enabled making data sets publicly available. This process involves the following steps: PI requests a data set be made public; steering committee reviews; Data Team curates a digital object identifier from the Office of Scientific and Technical Information and assigns it to the data set; and Data Hub administrator moves the data set to public availability. The digital object identifier enables researchers to identify the related data set within the references of publications so that readers can link back to the relevant data.

HydroGEN FY 2018 R&D Highlights

The HydroGEN EMN has a balanced AWSM R&D portfolio (Figure 3) across the six core labs, 18 FOA-awarded materials projects, and one benchmarking project. Of the 80 capability nodes within HydroGEN, more than 44 are being leveraged by the FOA-awarded projects. Furthermore, >35 capabilities have been updated this year and five new capability nodes were added to HydroGEN. The HydroGEN core labs performed and supported computational, experimental, and analytical tasks, in collaboration with 18 FOA-awarded projects, and documented at least three AWSMs with improvements in efficiency, durability, and/or material cost, providing a pathway to meet the ultimate hydrogen production cost target of <\$2/kg H₂. Below are some HydroGEN project R&D highlights for each water-splitting pathway.

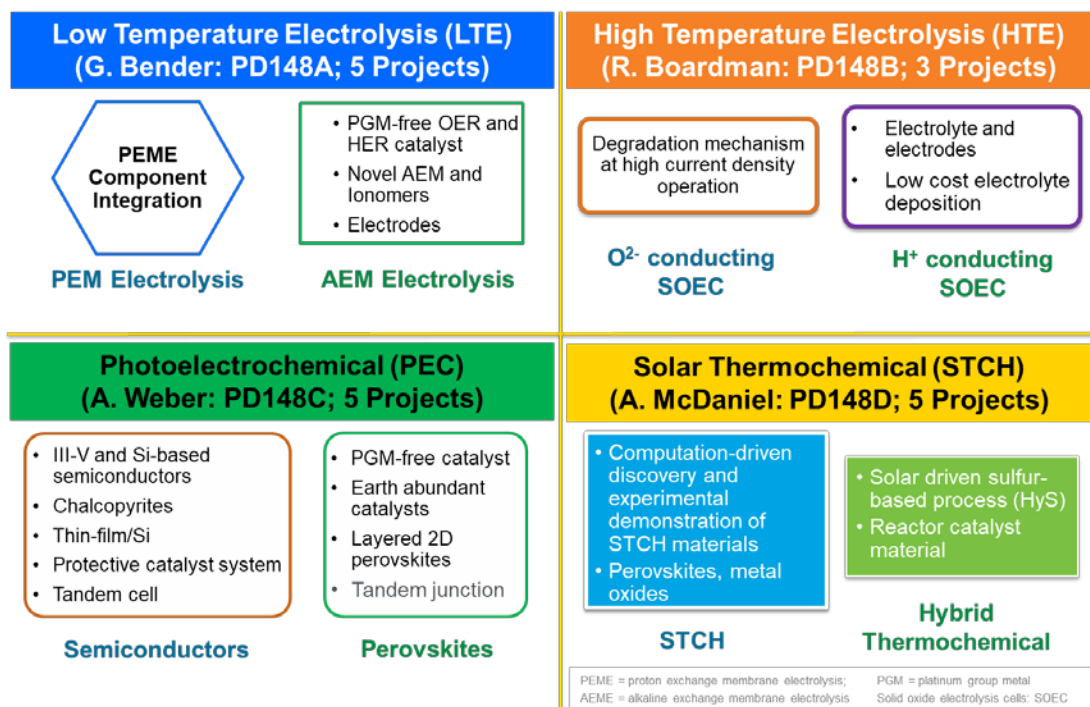


Figure 3. HydroGEN has a balanced AWSM R&D portfolio across the six core labs, 18 FOA-awarded materials projects, and one benchmarking project

PEC:

- Rutgers University, together with the NREL MOVPE III-V semiconductor synthesis and NREL PEC characterization nodes, demonstrated that Rutgers' platinum group metal (PGM)-free Ni₅P₄ hydrogen evolution reaction catalysts/TiN on p-GaInP₂ have performance on par with and stability greater than that of PGM catalysts (PtRu/p-GaInP₂). When NREL's high-performance photoabsorber (GaInP₂/GaAs) was optimized and integrated with Rutgers' PGM-free electrocatalysts (LiCoO₂ oxygen evolution reaction and Ni₅P₄ hydrogen evolution reaction catalysts) and protection layer (TiN) for unassisted water splitting, a solar-to-hydrogen efficiency of 11.5% was achieved, which is greater than the go/no-go solar-to-hydrogen efficiency metric of 10%. This was tested and verified by the NREL PEC benchmarking node.
- The performance and corrosion mechanisms of University of Michigan (UM) GaN/Si and T₃N₅ photoelectrodes were characterized and optimized by the NREL "Surface Analysis Cluster Tool," NREL "Surface Modifications for Catalysis and Corrosion Mitigation," and LBNL "Probing and Mitigating Chemical and Photochemical Corrosion of Electrochemical and Photoelectrochemical Assemblies" nodes. The UM project is focused on developing Si-based high-efficiency PEC tandem water-splitting devices, using nanowire tunnel junction to fabricate 1.7–2.0 eV top photoelectrodes on Si wafers and N-terminated GaN to protect against photocorrosion. A GaN/Si photocathode with stable operation for >100 h at a very high photocurrent density of ~38 mA/cm², without using any extra surface protection, was demonstrated. Detailed theoretical studies of the GaN surfaces and GaN/water interfaces have also been performed by the LLNL "Computational Materials Diagnostics and Optimization of Photoelectrochemical Devices" node to better understand the effect N-terminated GaN surfaces have on solar water splitting. These studies are further correlated with the stability analysis of the photoelectrodes.

- University of Hawaii, together with the LLNL “Computational Materials Diagnostics and Optimization of Photoelectrochemical Devices” node, investigated the thermodynamic stability of chalcopyrite compounds and competing phases (e.g., ordered vacancy compound) that can form during fabrication and processing of the photoabsorber chalcopyrite materials, and the impact the ordered vacancy compound phase can have on device performance. This understanding can help tune the material synthesis process conditions to achieve the desired ordered vacancy compound-type phases and enhance device performance. The NREL “I-III-VI Compound Semiconductors for Water Splitting” node successfully integrated chalcopyrite on transparent conductive substrate via deliberate alkali doping (CuGa_3Se_5 doped with NaF) and achieved the best photocurrent onset (0.4 V vs. reversible hydrogen electrode) ever observed for bare CuGa_3Se_5 , making it a promising material for tandem water splitting devices.

LTE:

- Proton Onsite met and exceeded near-term performance targets of 1.85 V at 2.0 A/cm², using Proton-synthesized high-activity IrRu oxide catalysts of different compositions. Proton’s proton exchange membrane water electrolysis cell also demonstrated 800 h of durability at 2 A/cm², operating at 80°C and 30 bar. The NREL “Electrolysis Catalyst Ex-situ Characterization and Standardization” node contributed toward a better understanding of IrRu oxide catalyst stability. Proton’s improved cell efficiency is a step toward achieving its proton exchange membrane water electrolysis cell efficiency goal of 43 kWh/kg (1.7 V at 90°C) and at a cost of \$2/kg H₂, a huge improvement from the state-of-the-art cell efficiency of 53 kWh/kg.
- Collaboratively, LANL, SNL, and NREL demonstrated promising alkaline exchange membrane water electrolysis performance, comparable to iridium oxide, using SNL’s anion exchange membrane node, LANL-developed PGM-free oxygen evolution reaction perovskite catalyst, and NREL’s expertise in membrane electrode assembly fabrication (“Multicomponent Ink Development, High-Throughput Fabrication, and Scaling Studies” node) and cell electrolysis testing (“In-Situ Testing Capabilities for Hydrogen Generation” node).
- ANL, together with the LLNL “Ab Initio Modeling of Electrochemical Interfaces” and LBNL “Density Functional Theory and Ab Initio Calculations” nodes, investigated the factors that may alter the transport property of a cobalt-based oxygen evolution reaction catalyst, developed by ANL for proton exchange membrane electrolysis. The LLNL team found the origin of the discrepancy between the reported experimental and theory-derived electronic structure of cobalt oxide. This resulted in the confidence to choose a specific theory that can provide reliable information about the electronic structure of the cobalt oxide materials family. This is crucial to reliably identify the factors that determine the transport property of this material, which affects the overall catalytic activity.

HTE:

- Using Northwestern University catalyst, YSZ electrolyte ($(\text{ZrO}_2)_{0.92}(\text{Y}_2\text{O}_3)_{0.08}$), and LBNL “Metal-Supported Solid Oxide Cell” and INL “Advanced Electrode and Solid Electrolyte Materials for Elevated Temperature Water Electrolysis” nodes, the collaboration demonstrated a metal-supported solid oxide electrolysis cell (SOEC) for the first time in electrolysis mode, with the highest performance for oxygen-conducting-type electrolysis cells to date and promising stability. The advantages of a metal-supported SOEC are low cost, high strength, and thermal cycling capability. Furthermore, the data from INL SOEC button cell tests will help Northwestern University establish a deeper understanding of cell degradation, a major barrier for SOECs.
- Three HydroGEN EMN nodes (LBNL, INL, and NREL) provided critical support to the United Technologies Research Center proton-conducting SOEC project by addressing technical barriers in metal alloy durability, electrode/electrolyte material optimization and stability, and SOEC modeling. Various

combinations of metal alloys and protective coatings were identified as acceptable for proton-SOEC conditions. High-performance proton electrolytes and steam electrodes were identified and tested by the INL “Advanced Materials for Elevated Temperature Water Electrolysis” node. The resulting button cell performance exceeded the DOE performance target. An electrochemical model and a cell model were developed by the NREL “Multi-Scale Thermochemical and Electrochemical Modeling for Material Scale-Up to Component and System Design” node for SOEC performance characterization and to simulate cell/stack operation for material scale up. In addition, INL provided critical support in cell performance testing for United Technologies Research Center and the University of Connecticut.

STCH:

- Colorado School of Mines, along with NREL’s “First Principles Materials Theory for Advanced Water Splitting Pathways” and “Thin Film Combinatorial Capabilities for Advanced Water Splitting Technologies” capability nodes, were able to validate their approach to combine theoretical and experimental materials discovery. First principles theory was used to screen for potential candidates using descriptors developed by NREL that can greatly reduce the search space and associated computational effort. The team envisions building combinatorial libraries of these theory-inspired material formulations and using optical techniques for rapid analysis of redox potential. With the candidate material formulations beginning to emerge from theory, the team produced thin films from materials with known redox behavior in order to develop and validate experimental protocols and further refine their optical analysis methods.
- Arizona State University is developing an all-density-functional-theory methodology for producing CALPHAD model results to more rapidly derive state maps of important thermodynamic relationships in redox materials; namely the dependence of defect concentration on temperature and oxygen partial pressure. SNL’s “Uncertainty Quantification in Computational Models of Physical Systems” node is using Bayesian statistical uncertainty quantification to assess the impact of imperfect knowledge (i.e., the synthetic CALPHAD model predictions) on the outcome of computational material screening. Thus far, the computations are able to reproduce experimental redox and water-splitting behavior for CeO₂ and Zr-doped CeO₂, as well as identify sufficiently robust functionals for deriving the aforementioned thermodynamic relationships.
- The University of Colorado Boulder, with help from NREL’s “First Principles Materials Theory for Advanced Water Splitting Pathways” node, was able to develop and apply machine learning models to identify ~28,000 stable perovskite formulations (both simple and complex) from over 1.1 million possible candidates. And from this pool of stable perovskites, several hundred materials have oxygen vacancy formation energies in the range of interest for STCH materials. SNL’s “Virtually Accessible Laser Heated Stagnation Flow Reactor” and “High-Temperature X-ray Diffraction” nodes are validating the results of the machine-learned thermodynamic screening by characterizing water splitting kinetics and crystal structures for a select number of these material formulations.

Hybrid:

- Greenway Energy (GWE) is developing a hybrid-sulfur system for low-cost and efficient hydrogen production. In collaboration with University of South Carolina, GWE and INL “Catalysts for Harsh Environment” node demonstrated a 30% improvement in performance and better stability for a novel catalyst that can lead to lower hydrogen costs by minimizing or replacing the use of PGM catalysts. An Invention Disclosure Record, listing both University of South Carolina and INL staff, was filed for the composition and synthesis of the catalyst. GWE and NREL “Engineering of Balance of Plant for High-Temperature Systems” node collaboratively designed a balance-of-plant system and developed a novel solar receiver/reactor integrated with the novel NREL solar-plant design that has the potential to eliminate \$60 million in cost from a particle-based baseline hybrid-sulfur system and will allow a hydrogen cost reduction of almost 50% compared to the previous baseline economic assessment (\$2.5/kg

vs. \$5.18/kg H₂). A Record of Invention for the hybrid-sulfur system and the receiver reactor was filed. SRNL “Flow Sheet Development Technoeconomic Analysis” node developed a flow sheet to allow for a direct-solar-heated high-temperature decomposition reactor. Independent operation of the two primary reaction steps with storage of water, liquid SO₂, and concentrated sulfuric acid allowed Greenway Energy to take advantage of fluctuations in cost and availability of electricity. Furthermore, optimal conditions for operation of the high-temperature decomposition reactor were identified. Possibilities for further improvements in efficiency were also identified and should help drive production cost closer to the \$2/kg H₂ target in the next phase.

HydroGEN EMN lab members collaborated and engaged extensively with the Benchmarking Team (FOA-awarded project) to develop four AWSM questionnaires, four AWSM test frameworks, two working group meetings, conference presentations, and >80 HydroGEN capability node assessments. The development of best practices in materials characterization and benchmarking is critical to accelerate AWSM discovery and development.

CONCLUSIONS AND UPCOMING ACTIVITIES

Conclusions

- The HydroGEN EMN is a national-lab-led consortium comprising six core labs and has expanded to include 18 FOA-awarded materials projects with a balanced AWSM R&D portfolio, one benchmarking project, and four NSF DMREF collaborative projects.
- The HydroGEN core labs performed and supported computational, experimental, and analytical tasks, in collaboration with 18 FOA-awarded projects, to accelerate the AWSM development with improvements in efficiency, durability, and/or material cost, providing a pathway to meet the ultimate hydrogen production cost target of <\$2/kg H₂.
- The Data Team developed a secured HydroGEN Data Hub (<https://datahub.h2awsm.org/>) for all projects to store, view, and share data with each other and to make digital data accessible to the scientific community and public. The Data Team has developed, shared, and demonstrated new data tools for visualization, uploading large datasets, and metadata assignments; advanced metadata definitions and API access; and established a data publication process.
- The HydroGEN TTA team developed multiple standard, pre-approved, mutual TTAs, including NDAs, material transfer agreements, intellectual property management plans, and cooperative research and development agreements, to streamline access to the national labs’ materials capability network (<https://www.h2awsm.org/working-with-hydrogen>).

Proposed Future Work

- Core labs will align scope of work with the relevant seedling projects’ go/no-go decision points, and the core labs’ interaction with a specific seedling project will end if that project does not achieve its go/no-go decision metric.
- Integrate the whole system (capability nodes, FOA awardees, data infrastructure, TTA) to accelerate the R&D of HydroGEN critical materials development to deployment.
- Continue to review, maintain, and develop current and identify new relevant HydroGEN capability nodes.
- Continue to develop a user-friendly, secure, and dynamic HydroGEN Data Hub that accelerates learning and information exchange among the HydroGEN EMN labs, their partners, other EMNs, and the advanced electrolysis, PEC, and STCH communities.

- Continue to work closely with the Benchmarking Team to establish benchmarking, standard protocols, and metrics for the different water-splitting technologies.
- Develop supernode concepts, one in each of the AWSM technologies, through which the core labs work collaboratively to demonstrate the power of integrating and utilizing the HydroGEN capabilities and to address a specific research gap.
- Conduct outreach via conference presentations and participation, benchmarking workshops, website updates, publications, and generally socializing the HydroGEN EMN concept to the community.

SPECIAL RECOGNITIONS AND AWARDS/PATENTS ISSUED

1. “Nanofiber Electrocatalyst,” Di-Jia Liu and Lina Chong, US patent application filed in 2018.
2. “Prussian Blue Analogue-Derived Catalysts for PEM Electrolyzer,” Di-Jia Liu and Hao Wang, US patent application filed in 2018.
3. Zetian Mi was elected Fellow of Optical Society of America in 2018.

FY 2018 PUBLICATIONS/PRESENTATIONS

Publications

1. Sheng Chu, Srinivas Vanka, Yichen Wang, Jiseok Gim, Yongjie Wang, Yong-Ho Ra, Robert Hovden, Hong Guo, Ishiang Shih, and Zetian Mi. “Solar Water Oxidation by an InGaN Nanowire Photoanode with a Bandgap of 1.7 eV.” *ACS Energy Lett.* 3, no. 2 (January 2, 2018): 307–314. <https://doi.org/10.1021/acsenergylett.7b01138>.
2. J.B. Varley, V. Lordi, T. Ogitsu, A. Deangelis, K. Horsley, and N. Gaillard. “Assessing the Role of Hydrogen in Fermi-Level Pinning in Chalcopyrite and Kesterite Solar Absorbers from First-Principles Calculations.” *Journal of Applied Physics* 123, no. 16 (March 7, 2018): 161408. <https://doi.org/10.1063/1.5006272>.
3. Sheng Chu, Srinivas Vanka, Yichen Wang, Jiseok Gim, Yongjie Wang, Yong-Ho Ra, Robert Hovden, Hong Guo, Ishiang Shih, and Zetian Mi. “Solar Water Oxidation by an InGaN Nanowire Photoanode with a Bandgap of 1.7 eV.” *ACS Energy Letters* 3, no. 2 (February 9, 2018): 307–14. <https://doi.org/10.1021/acsenergylett.7b01138>.
4. Tuan Anh Pham, Xueqiang Zhang, Brandon C. Wood, David Prendergast, Sylwia Ptasinska, and Tadashi Ogitsu. “Integrating Ab Initio Simulations and X-Ray Photoelectron Spectroscopy: Toward A Realistic Description of Oxidized Solid/Liquid Interfaces.” *The Journal of Physical Chemistry Letters* 9, no. 1 (January 4, 2018): 194–203. <https://doi.org/10.1021/acs.jpcclett.7b01382>.
5. Yuanyue Liu, Jingjie Wu, Ken P. Hackenberg, Jing Zhang, Y. Morris Wang, Yingchao Yang, Kuntal Keyshar, Jing Gu, Tadashi Ogitsu, Robert Vajtai, Jun Lou, Pulickel M. Ajayan, Brandon C. Wood & Boris I. Yakobson. “Self-optimizing, highly surface-active layered metal dichalcogenide catalysts for hydrogen evolution.” *Nature Energy* 6 (2017): 17127.
6. Y. He, D. Wang. “Toward Practical Solar Hydrogen Production.” *Chem.* 4 (2018): 405–408.
7. F.A. Chowdhury, M.L. Trudeau, H. Guo, and Z. Mi. “A Photochemical Diode Artificial Photosynthesis System for Unassisted High Efficiency Overall Pure Water Splitting.” *Nature Communications* 9 (2018): 1707. <https://doi.org/10.1038/s41467-018-04067DO>.
8. S. Chu, S. Vanka, Y. Wang, J. Gim, Y. Wang, Y.-H. Ra, R. Hovden, H. Guo, I. Shih, and Z. Mi. “Solar Water Oxidation by an InGaN Nanowire Photoanode with a Bandgap of 1.7 eV.” *ACS Energy Letters* 3 (2018): 307.
9. X. Guan, F.A. Chowdhury, N. Pant, L. Guo, L. Vayssieres, and Z. Mi. “Efficient Unassisted Overall Photocatalytic Seawater Splitting on GaN-Based Nanowire Arrays.” *J. Phys. Chem. C.* 122, no. 25 (2018): 13797–13802. <https://doi.org/10.1021/acs.jpcc.8b00875>.

10. N. Ramaswamy, S. Ghoshal, M. K. Bates, Q. Jia, J. Li, and S. Mukerjee. “Hydrogen oxidation reaction in alkaline media: Relationship between electrocatalysis and electrochemical double layer.” *Nano Energy* 41 (2017): 765–771.
11. J. Li, S. Ghoshal, M. K. Bates, T. E. Miller, V. Davies, E. Stavitski, K. Attenkofer, S. Mukerjee, Zi-Feng Ma, and Q. Jia. “Experimental Proof of the Bifunctional Mechanism for Hydrogen Oxidation.” *Angewandte Chemie Comm.* 56 (2017): 15594.
12. J.W. Vickers, H.N. Dinh, K. Randolph, A.Z., Weber, A.H. McDaniel, R. Boardman, T. Ogitsu, H. Colon-Mercado, D. Peterson, and E.L. Miller. “HydroGEN: An AWSM Energy Materials Network.” *ECS Transactions* 85, no. 11 (2018): 3–14. <https://doi.org/10.1149/08511.0003ecst>.
13. Stephan Lany. “Communication: The Electronic Entropy of Charged Defect Formation and Its Impact on Thermochemical Redox Cycles.” *The Journal of Chemical Physics* 148, no. 7 (February 16, 2018): 071101. <https://doi.org/10.1063/1.5022176>.
14. A. Singh, J. Lapp, J. Grobbel, S. Brendelberger, J.P. Reinhold, L. Olivera, I. Ermanoski, N.P. Siegel, A. McDaniel, M. Roeb, C. Sattler. “Design of a Pilot Scale Directly Irradiated, High Temperature, and Low Pressure Moving Particle Cavity Chamber for Metal Oxide Reduction.” *Solar Energy* 157 (2017): 365–376. doi:10.1016/j.solener.2017.08.040.
15. A.H. McDaniel. “Renewable Energy Carriers Derived from Concentrating Solar Power and Nonstoichiometric Oxides,” *Current Opinion in Green and Sustainable Chemistry* 4 (2017): 37–43. doi:10.1016/j.cogsc.2017.02.004.
16. Article in March 2018 issue of *Chemical Engineering* (www.chemengonline.com) titled “Solar Chemistry Heats Up” written by staff editor Gerald Ondrey.
17. Darwin Arifin and Alan W. Weimer. “Kinetics and Mechanism of Solar-thermochemical H₂ and CO Production by Oxidation of Reduced CeO₂.” *Solar Energy* 160 (2018): 178–185, doi:10.1016/j.solener.2017.11.075.
18. Harnoor Kaur, Meng Wang, Maximilian B. Gorenssek, and Chau-Chyun Chen. “Thermodynamic modeling of the hybrid sulfur (HyS) cycle for hydrogen production.” *Fluid Phase Equilibria* 460 (March 25, 2018): 175–188. <https://doi.org/10.1016/j.fluid.2017.12.025>.
19. Maximilian B. Gorenssek, Claudio Corgnale, and William A. Summers. “Development of the hybrid sulfur cycle for use with concentrated solar heat. I. Conceptual design.” *International Journal of Hydrogen Energy* 42 (2017): 20939.
20. Taylor R. Garrick, Cody H. Wilkins, Andrew T. Pingitore, Jacob Mehlhoff, Alex Gullledge, Brian C. Benicewicz, and John W. Weidner. “Characterizing Voltage Losses in an SO₂ Depolarized Electrolyzer Using Sulfonated Polybenzimidazole Membranes.” *Journal of the Electrochemical Society* 164 (2017): F1591–F1595.

Presentations

1. **(Invited)** Anthony H. McDaniel and Ivan Ermanoski, “Perovskites and Particle Reactor: A Multinational Effort to Advance Solar Hydrogen,” ASME Power Energy 2018 Conference, Orlando, FL, June 2018.
2. Z. Ma, J. Martinek, P. Davenport, and C. Corgnale, “Integrating Thermochemical and Electrochemical Processes with a Concentrating Solar Thermal System for Hydrogen Production,” ASME Power Energy 2018 Conference, Orlando, FL, June 2018.
3. **(Invited)** H.N. Dinh, J.W. Vickers, K. Randolph, A.Z., Weber, A.H. McDaniel, R. Boardman, T. Ogitsu, H. Colon-Mercado, D. Peterson, and E.L. Miller, “HydroGEN: An AWSM Energy Materials Network,” 233rd Electrochemical Society Meeting, Seattle, WA, May 2018.
4. **(Invited)** K.E. Ayers, “Low Temperature Electrolysis for Hydrogen and Oxygen Generation - a Tutorial on Catalyst and Electrode Development for Proton and Anion Exchange Membrane-Based Systems,” 233rd Electrochemical Society Meeting, Seattle, WA, May 2018.

5. **(Invited)** J. Holladay, B. S. Pivovar, K. E. Ayers, O. A. Marina, E. B. Stechel, and C. Xiang, “An Overview of H₂@Scale and Water Splitting Protocol Development,” 233rd Electrochemical Society Meeting, Seattle, WA, May 14, 2018.
6. **(Invited)** S. Mukerjee, J. Li, and Q. Jia, “Current understanding of the slow kinetics of the hydrogen evolution reaction in alkaline media,” 233rd Electrochemical Society Meeting, Seattle, WA, May 13–17, 2018.
7. Q. Jia, J. Li, and S. Mukerjee, “Understanding the improved kinetics of the hydrogen evolution/oxidation reactions of the Pt-oxophilic metal systems in alkaline medium,” 233rd Electrochemical Society Meeting, Seattle, WA, May 13–17, 2018.
8. H.T. Chung, A.S. Lee, Y.S. Kim, C. Fujimoto, L.W. Wang, G. Teeter, G. Bender, and P. Zelenay, “Carbon-Free Perovskite Oxide Oxygen Evolution Reaction Catalysts for AEM Electrolyze,” 233rd Electrochemical Society Meeting, Seattle, WA, May 2018.
9. Chengxiang (“CX”) Xiang, “Development of Best Practices and Standard Protocols in Benchmarking Photoelectrochemical (PEC) Hydrogen Production,” 233rd Electrochemical Society Meeting, Seattle, WA, May 17, 2018.
10. S. Hwang, A.B. Laursen, S.H. Porter, Y. Hongbin, M. Li, V. Manichev, K.U.D. Calvino, V. Amarasinghe, M. Greenblatt, E. Garfunkel, and G.C. Dismukes, “Titanium Nitride As a Conducting Interfacial Layer between Hydrogen Evolution Catalysts and Silicon Photocathodes for Stable Solar-to-Hydrogen Water Splitting Devices,” 233rd Electrochemical Society Meeting, Seattle, WA, May 17, 2018.
11. **(Invited)** T. Ogitsu, J. Varley, A.D. DeAngelis, K. Horsley, and N. Gaillard, “Integrating Ab-Initio Simulations and Experimental Characterization Methods: Towards Accelerated Chalcopyrite Materials Development for Hydrogen Production,” 233rd Electrochemical Society Meeting, Seattle, WA, May 15, 2018.
12. Boxun Hu, Ashish N. Aphale, Michael Reiser, Seraphim Belko, Olga A. Marina, Jeffrey Stevenson, and Prabhakar Singh, “Solid Oxide Electrolysis for Hydrogen Production: From Oxygen Ion to Proton Conducting Cells,” 233rd Electrochemical Society Meeting, Seattle, WA, May 13–17, 2018.
13. **(Invited)** Z. Mi, “Artificial Photosynthesis on III-Nitride Nanowire Arrays,” 233rd Electrochemical Society Meeting, Seattle, WA, May 13–17, 2018.
14. **(Invited)** Z. Mi, “Solar Water Splitting and CO₂ Reduction on III-Nitride Nanostructures,” MRS Spring Meeting, Phoenix, AZ, April 2–6, 2018.
15. **(Invited)** D. Wang, “Understanding the Interface between Photoelectrodes and Catalysts,” MRS Spring Meeting, Phoenix, AZ, April 2–6, 2018.
16. H. Hajibabaei and T. Hamann, “Direct Deposition of Crystalline Tantalum Nitride (Ta₃N₅) on FTO via High-Temperature Atomic Layer Deposition (ALD),” Gordon Research Conference; Renewable Energy: Solar Fuels, January 28–February 2, 2018.
17. **(Invited)** H.N. Dinh, K. Randolph, E. Miller, “An EMN Model for Early R&D,” 2018 DOE Hydrogen and Fuel Cell Technical Advisory Committee (HTAC) Meeting, Washington, DC, February 14, 2018.
18. S. Hwang, S.H. Porter, A.B. Laursen, H. Yang, M. Li, V. Manichev, K.U.D. Calvino, V. Amarasinghe, M. Greenblatt, E. Garfunkel and G.C. Dismukes, “Nickel Phosphide Catalyst and Titanium Nitride Protection Layer for High Efficient and Stable Siliconbased Photocathode,” Annual Meeting at Catalysis Society of Metropolitan New York, Lehigh University, April 2018.
19. A. Kashi, S. Hwang, A.B. Laursen, G.C. Dismukes, “Characterization of Highly Active Electrodeposited Li_xCoO₂ Thin Film Anodes in PGM-free Photoelectrochemical Cells,” Annual Meeting at Catalysis Society of Metropolitan New York, Lehigh University, April 2018.
20. **(Invited)** Dong Ding, “Application of Intermediate-Temperature Electrochemical Processes in Energy Conversion Technologies at Idaho National Laboratory (INL),” Lecture for faculty and graduate students,

Department of Chemical and Materials Engineering, New Mexico State University, Las Cruces, NM, April 27, 2018.

21. **(Invited)** Anthony McDaniel, Debora R. Barcellos, Michael Sanders, Joshua Sugar, Ryan O'Hayre, "Hydrogen Production by Solar Thermochemical Water Splitting: Searching for Optimal Nonstoichiometric Perovskite Oxides," 255th ACS National Meeting & Exposition, New Orleans, LA, March 2018.
22. Huyen N. Dinh, "An Overview of HydroGEN: A DOE Energy Materials Network, Aimed at Accelerating the R&D of Advanced Water Splitting Materials," Fuel Cell Seminar and Energy Exposition, Long Beach, CA, November 2017.
23. Zhiwen Ma, "Concentrating Solar Power Technology for Green Syngas and Hydrogen Production," 2017 Syngas Technologies Conference, Colorado Springs, CO, October 2017.
24. **(Invited)** Tadashi Ogitsu, "Computational design of novel catalyst system." Global Conference on Catalysis and Reaction Engineering 2017, Las Vegas, NV, October 19–21, 2017.
25. **(Invited)** Yanfa Yan, "New materials for photoelectrochemical water splitting," 232nd Electrochemical Society Meeting, National Harbor, MD, October 2, 2017.
26. Wei Wu, Dong Ding, and Ting He, "Development of high performance intermediate temperature proton-conducting solid oxide electrolysis cells," 232nd Electrochemical Society Meeting, National Harbor, MD, October 1–5, 2017.
27. **(Invited)** E.B. Stechel, "HydroGEN: Advanced Water Splitting Materials," International Workshop on Solar Thermochemistry, Julich, Germany, September 12–14, 2017.
28. Ting He and Dong Ding, "Perovskite Proton Conductors for Energy Conversion and Storage at Intermediate Temperatures," 20th Topical Meeting of the International Society of Electrochemistry, Buenos Aires, Argentina, March 19–22, 2017.

Collaborative Meetings Organized and Participated In

HydroGEN EMN Project Kick-Off Meeting

1. HydroGEN AWSM Project Kick-Off Meeting (>100 attendees), National Renewable Energy Laboratory, Golden, CO, November 14–15, 2018.

EMN-Wide Data Meeting

1. Application of Machine Learning and Data Analytics for Energy Materials Network Consortia 2018 (AMD4EMN 2018), organized by Y. Han, B. Wood, T. Ogitsu, HPCIC Innovation Center, Lawrence Livermore National Lab, Livermore, CA, May 2–3, 2018.

Benchmarking Meetings

1. HydroGEN AWSM Benchmarking Meeting (PEC Working Group Meeting), organized by CX Xiang, T. Deutsch, T. Ogitsu, and H. Dinh, Seattle, WA, May 13, 2018.
2. HydroGEN LTE/HTE Benchmarking Discussion, organized by K.E. Ayers, H. Dinh, and N. Danilovic, 233rd ECS Meeting, Seattle, WA, May 14, 2018.

Hydrogen Production Tech Team (HPTT) Review Meetings

1. HydroGEN Photoelectrochemical Water Splitting Project Reviews, Webinar, February 6, 2018.
2. HydroGEN Low Temperature Electrolysis Project Reviews, hosted by N. Danilovic and A. Weber, Lawrence Berkeley National Lab, Berkeley, CA, April 10, 2018.
3. HydroGEN Solar Thermochemical Water Splitting Project Reviews, Webinar, May 8, 2018.
4. HydroGEN High Temperature Electrolysis Project Reviews, planned to be at Idaho National Lab, Summer 2018.

Benchmarking Advanced Water Splitting Technologies: Best Practices in Materials Characterization

Katherine Ayers (Primary Contact),
George Roberts
Proton OnSite
10 Technology Drive
Wallingford, CT 06492
Phone: (203)-678-2190
Email: KAyers@protononsite.com

DOE Manager: Katie Randolph
Phone: (720) 356-1759
Email: Katie.Randolph@ee.doe.gov

Contract Number: DE-EE0008092

Subcontractors:

- Caltech-Joint Center for Artificial Photosynthesis, Pasadena, CA
- Pacific Northwest National Laboratory, Richland, WA
- Arizona State University, Tempe, AZ

Project Start Date: September 1, 2017
Project End Date: October 31, 2020

Overall Objectives

- Develop a framework of protocols/standards for testing performance of materials, components, devices, and systems.
- Facilitate acceptance of community-wide technology.
- Establish an annual project meeting to share learnings and develop recommendations within and across technology areas.
- Assess capabilities and identify gaps for development of advanced water splitting technologies.
- Promote acceptance of protocols and methodologies including cost and performance assessments and database comparisons.
- Assemble roadmaps to further development of each technology pathway.

Fiscal Year (FY) 2018 Objectives

- Hold a Year 1 workshop to present output of capabilities, assess gaps, and solicit input to define details of bench-scale protocol development based on initial framework.
- Prepare important questions and parameters for each technology area and surveys for dissemination.
- Complete and synthesize capabilities assessments including surveys of each node with 80% response rate.
- Complete and synthesize gap assessment including questionnaires with a goal of 50% response rate.
- Compile and publish workshop results and outcome report.

Technical Barriers

This project addresses the following technical barriers from the Systems Analysis section of the Fuel Cell Technologies Office Multi-Year Research, Development, and Demonstration (MYRDD) Plan¹:

- C. Inconsistent Data, Assumptions and Guidelines
- D. Insufficient Suite of Models and Tools.

Technical Targets

This project is focused on developing standards and test protocols that result in technologies to produce hydrogen consistent with the following DOE technical targets:

- Support DOE Hydrogen and Fuel Cells Program goals to sustainably produce hydrogen for <\$2/kg.

FY 2018 Accomplishments

- A framework and questionnaire were developed with input from node experts at

¹ <https://www.energy.gov/eere/fuelcells/downloads/fuel-cell-technologies-office-multi-year-research-development-and-22>

national labs for each technology in a common format.

- A questionnaire for each technology was distributed to the broad community for input and responses were collected.
- The framework was reviewed by questionnaire respondents that “opted in” to provide feedback.
- The assessment of node capabilities was completed and a single table to summarize capabilities and readiness was developed.
- Quarterly newsletters were sent out to the advanced water splitting technologies community.
- The fall community-wide meeting was held at Arizona State University on October 24–25, 2018.

INTRODUCTION

The high-level project goal is to create a comprehensive best-practices benchmarking framework at the materials, component, device, and systems levels for advanced water splitting technologies. All advanced water splitting pathways covered under the HydroGEN Energy Materials Network (EMN) Consortium, which include advanced high- and low-temperature electrolysis of water, photoelectrochemical water splitting, and solar thermochemical hydrogen, need these best practices to advance materials discovery. These practices will also aid the H2@Scale DOE initiative to accomplish their goals of large-scale hydrogen production.

The overall objective for this effort is to guide development of a water splitting roadmap across the different technologies, based on the varying maturity levels and challenges of each approach, to assist DOE in maintaining a balanced R&D portfolio. To support this objective, the team is working with the HydroGEN EMN Consortium and water splitting community to assess and document current best practices and material standards, assess existing capabilities and needs, and recommend next steps and priorities.

APPROACH

The overall project is divided into two major phases, Budget Period (BP) 1 and BP 2, across 3 years. In BP 1, the team will focus on development of the database framework and proposed bench-scale protocols to be introduced within the community. BP 2 will pursue validation/revision of the proposed protocol through user experience and development of a vision for the “subscale” category. Strategies for stakeholder engagement throughout the project will include annual cross-technology workshops as described below, as well as organization of conference symposia for specific technology areas for more focused, in-depth discussions and monthly virtual meetings per approach to gather stakeholder input and feedback.

RESULTS

HydroGEN Node Capabilities Assessment

A common table of node readiness levels was developed to identify capability gaps in the nodes with respect to the test frameworks developed for each water splitting technology. Updates were made to the HydroGEN advanced water splitting node capabilities website (<https://www.h2awsm.org/capabilities>) to incorporate agreed-upon changes to readiness levels from the assessment.

Each technology area principal investigator then assessed each of the test methods/protocols in their respective framework documents against the current node readiness levels. The goal of this exercise was to identify shortfalls in the node capabilities required to support the technology frameworks and make recommendations for augmenting the capabilities. Each test in the framework was reviewed and a relevant node was assigned where there was a clear match. In cases where gaps were identified, suggestions were made for labs that may be better suited for the testing (sometimes outside of the EMN). The details of this assessment were reviewed with DOE and an action plan will be developed to close the gaps.

Questionnaire

A questionnaire was created and distributed for each of the water splitting pathways. Distribution lists were developed to include EMN project leads, national lab node leads, and industry, academic, and international experts. The goal of this effort was to collect broad feedback across the water splitting community with a specific target of obtaining at least a 50% response rate from EMN Level 1 node leads and project principal investigators. These inputs are archived on the HydroGEN data hub (<https://datahub.h2awsm.org/project/about/benchmarking>). An example of feedback received is shown in Figure 1.

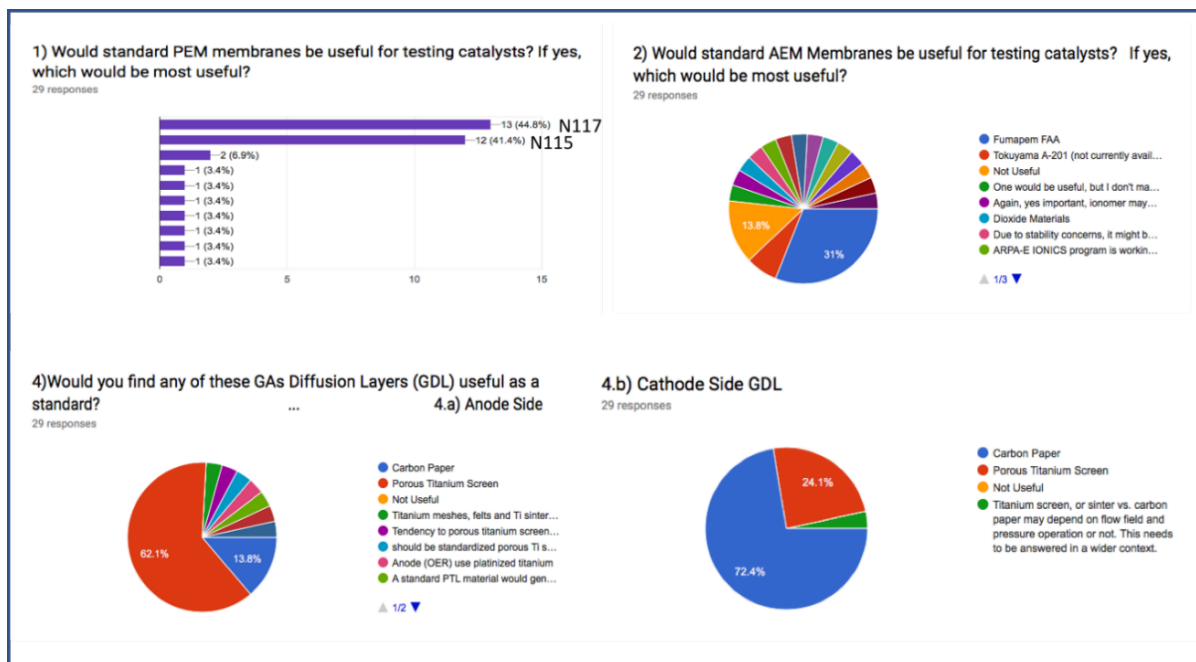


Figure 1. Example low-temperature electrolysis questionnaire results

Framework

A standardized framework was developed that could be applied across all water splitting technology pathways for developing comprehensive best practices of benchmarking methods. It was decided to focus on two primary categories: ex situ materials testing and in situ testing. The ex situ testing can be performed on individual materials using standard test methods and phased to allow for rapid evaluation. In situ testing targets the evaluation of materials in representative system operation and conditions for a given water splitting technology.

Standards for use in calibrating test equipment and test methods were identified along with minimum performance criteria for comparison based on inputs from subject matter experts and published literature. Individual frameworks have been developed for each technology and continue to be refined based on feedback from the questionnaire and workshop breakout sessions.

Workshop

A community-wide workshop was planned for October 24–25, 2018, at Arizona State University, Tempe campus.

Workshop objectives:

- Understand the needs of the community for effective comparison of results based on surveys
- Review and refine draft frameworks for standardized testing by component or configuration
- Hold face-to-face discussions about protocol development in breakout sessions
- Refine methods based on community engagement
- Leverage international efforts to increase harmony across the field
- Realize increased usage of database and Zotero capability for community benefit.

Representative intended outputs:

- Protocols Version 1.0
- Documentation on further needs/gaps in protocols and benchmarking in each technology pathway
- A perspective or viewpoint paper on crosscutting and/or overall advanced water splitting technology pathways.

The workshop comprised a plenary session and a series of breakout sessions (Figure 2) followed by a wrap up.

2018 HydroGEN Advanced Water Splitting Technology Pathways Benchmarking and Protocols Workshop - Breakout Sessions			
Breakout Session #	Session ID	Technology	Topic
1	C1-A	PEC/LTE	Membrane operating at different regimes
1	C1-B	LTE, PEC	Theory on catalytic reactions with metal oxides and other materials
1	C1-C	PEC, LTE, HTE, STCH	Standards development and crosscutting measurement issues
1	S1-A	STCH	Performance Metrics - units, system boundaries
2	H2-A	HTE	Electrolyte: oxygen and proton conductors
2	L2-A	LTE	PEM: Membrane Physical Requirements/Tests
2	L2-B	LTE	Non-PGM Catalyst: OER Stability & Activity
2	P2-A	PEC	Protocol development in a half cell vs. a full cell
2	P2-B	PEC	In situ/operando methods for PEC interfaces and devices
2	S2-A	STCH	Standard materials and form factors
2	S2-B	STCH	Detailed thermodynamics - operating conditions and methodology
3	H3-A	HTE	Electrode Activity & Stability
3	L3-A	LTE	AEM: Membrane Physical Requirements/Tests
3	L3-B	LTE	PGM Catalyst: OER Stability & Activity
3	P3-A	PEC	Protocols for PEC stability testing
3	P3-B	PEC	PEC electrolytes
3	S3-A	STCH	"Quick and dirty" thermodynamic screen
3	S3-B	STCH	Extracting thermodynamic variables from theory and experiment
4	H4-A	HTE	Cell test protocols
4	L4-A	LTE	PTL: Characteristics & Characterization Tools
4	L4-B	LTE	MEA Device Level Protocols: Criteria/Tests
4	P4-A	PEC	Prototype formats and key metrics for benchmarking.
4	P4-B	PEC	Protocol development on OER/HER activity benchmarking at intermediate/dynamic current density
4	S4-A	STCH	Detailed kinetic screening
4	S4-B	STCH	Systems analysis and TEA
5	H5-A	HTE	In situ methods for degradation studies
5	L5-A	LTE	Carbon GDL: Physical Requirements/Tests
5	L5-B	LTE	Full Stack Level Protocols: Criteria/Tests
5	P5-A	PEC	PEC Nodes capabilities and gaps assessment.
5	S5-A	STCH	"Quick and dirty" kinetics screening
5	S5-B	STCH	Durability protocols
6	H6-A	HTE	Full stack test protocols
6	C6-A	PEC/STCH, LTE/HTE	Comparative analysis on key cross-cutting metrics (definition and discussion of device efficiency, cost of hydrogen, etc)
6	L6-A	LTE	HOLD FOR AD-HOC SESSIONS
6	P6-A	PEC	HOLD FOR AD-HOC SESSIONS
6	S6-A	STCH	HOLD FOR AD-HOC SESSIONS

Figure 2. HydroGEN advanced water splitting workshop breakout sessions

The breakout sessions encompassed the majority of the workshop and were intended to dig deeper into each section of the testing frameworks for each water splitting technology. Specific emphasis was placed on

establishing test methods, standards, and performance criteria. A session leader was identified for each session who was responsible for leading the discussion and summarizing the outputs. Following the workshop, the outputs from each of the sessions are being integrated into their respective testing frameworks and will serve as the basis for test method development.

CONCLUSIONS AND UPCOMING ACTIVITIES

Upcoming activity will focus on integrating all the outputs of the workshop breakout sessions into a revised test framework. Each test will be reviewed, and assignments will be made to various stakeholders to write detailed test methods. Test protocols will be developed and validated and will include accelerated testing and the definition of degradation mechanisms. A strategy for closing the gaps in node capabilities will be developed.

There are no issues expected to affect project progress at this time.

FY 2018 PUBLICATIONS/PRESENTATIONS

1. E.B. Stechel, “HydroGEN: Advanced Water Splitting Materials,” Invited presentation at the International Workshop on Solar Thermochemistry, Julich, Germany, September 12–14, 2017.
2. HydroGEN AWSM Benchmarking Meeting (PEC Working Group Meeting), organized by CX Xiang, T. Deutsch, T. Ogitsu and H. Dinh, Seattle, WA, May 13, 2018.
3. J. Holladay (Pacific Northwest National Laboratory), B.S. Pivovar (National Renewable Energy Laboratory), K.E. Ayers (Proton OnSite), O.A. Marina (Pacific Northwest National Laboratory), E.B. Stechel (ASU-LightWorks), and C. Xiang (California Institute of Technology), “An Overview of H₂@Scale and Water Splitting Protocol Development,” Invited, 233rd ECS, Seattle, WA, May 14, 2018.
4. K.E. Ayers (Proton OnSite), “Low Temperature Electrolysis for Hydrogen and Oxygen Generation—A Tutorial on Catalyst and Electrode Development for Proton and Anion Exchange Membrane-Based Systems,” Invited, 233rd ECS, Seattle, WA, May 14, 2018.
5. HydroGEN LTE/HTE Benchmarking Discussion, organized by K. E. Ayers, H. Dinh, and N. Danilovic, 233rd ECS, Seattle, WA, May 14, 2018.
6. Chengxiang (“CX”) Xiang, “Development of Best Practices and Standard Protocols in Benchmarking Photoelectrochemical (PEC) Hydrogen Production,” 233rd ECS, Seattle, WA, May 17, 2018.
7. K.E. Ayers, “Benchmarking Advanced Water Splitting Technologies,” U.S. Department of Energy's Hydrogen and Fuel Cells Program 2018 Annual Merit Review and Peer Evaluation Meeting, Washington, DC, June 13, 2018.
8. K.E. Ayers, C. Capuano, and P. Mani, “High Efficiency PEM Electrolysis: Potential for H₂@Scale,” 234th ECS, Cancun, Mexico, October 2, 2018.

HydroGEN Seedling: Proton-Conducting Solid Oxide Electrolysis Cells for Large-Scale Hydrogen Production at Intermediate Temperatures

Prabhakar Singh¹ (Primary Contact), Boxun Hu¹, Ugur Pasaogullari¹, Olga Marina², and Jeff Stevenson²

¹ University of Connecticut (UConn), Storrs CT

² Pacific Northwest National Laboratory, Richland WA

DOE Manager: David Peterson

Phone: (720) 356-1747

Email: David.Peterson@ee.doe.gov

Contract Number: DE-EE0008078

Subcontractor:

Pacific Northwest National Laboratory, Richland, WA

Project Start Date: October 1, 2017

Project End Date: September 30, 2020

Overall Objectives

- Develop proton-conducting solid oxide electrolysis cells (SOEC) and stacks for large-scale hydrogen production at intermediate temperatures.
- Achieve an operating current density (>1 A/cm²) with the performance degradation rate not to exceed the DOE performance metric (<4 mV/1,000 h).
- Demonstrate stable intermediate-temperature (600°–800°C) operation with low area-specific resistance (ASR) through bulk, interface, and surface optimizations
- Meet hydrogen production cost goal ($<\$2$ /kg H₂) by the use of non-noble and non-strategic cell and stack component materials.

Fiscal Year (FY) 2018 Objectives

- Select structurally stable electrolyte and electrode materials by density functional theory, first principles, and thermochemical calculations under proton-conducting SOEC operating conditions.

- Develop electrolyte formulations capable of densification ($>90\%$) below 1,400°C in oxidizing atmospheres and demonstrate high conductivity (>0.01 Ω·cm⁻¹ at 650°C) and bulk structural and chemical uniformity.
- Fabricate single SOECs using tape cast and other thin-film processing to achieve thin electrolyte (<25 μm) for low ASR.
- Demonstrate electrochemical performance of at least 1 A/cm² at ≤ 1.4 V at a temperature of ≤ 700 °C and a relatively stable electrolysis performance (<10 mV/1,000 h) for 50-hour test in real-world electrolyzer operating conditions.

Technical Barriers

This project addresses the following technical barriers (for high temperature steam electrolysis) from the Hydrogen Production section of the Fuel Cell Technologies Office Multi-Year Research, Development, and Demonstration Plan¹:

- Complex processing and fabrication techniques
- High sintering temperature for proton-conducting electrolyte densification ($>1,400$ °C)
- Decrease in conductivity during processing and operation
- High-temperature gas sealing and operation with thermal cycling
- Chemical and structural instability in presence of contaminants such as Cr and Si.

Technical Targets

This project is developing proton-conducting electrolysis cells for the large-scale hydrogen production at intermediate temperature. Insights gained from these studies will be applied toward the design and synthesis of proton-conducting

¹ <https://www.energy.gov/eere/fuelcells/downloads/fuel-cell-technologies-office-multi-year-research-development-and-22>

electrolyte materials that meet the DOE hydrogen production targets shown in Table 1.

FY 2018 Accomplishments

- Proton-conducting electrolyte and electrode materials have been selected and synthesized using sol-gel and conventional solid-state ceramic processing methods. The powder synthesis process has been validated at 20-gram batch scale for BZY and BZCY-Yb proton-conducting powders.
- BZY and BZCY-Yb electrolyte discs have been prepared using reactive/fugitive sintering aids (nanosized ZnO). Sintering of BZCY-Yb at 1,350°C in oxygen shows the densification (>97% density), which is 100°C lower than the state of the art (1,450°C). The conductivity of sintered BZY and BZCY-Yb measured by four-probe technique are ~0.01 and 0.04 S/cm, respectively.
- Proton-conducting SOEC full cells with low ASR have been fabricated using thin dense electrolyte (15–20 μm) and porous electrodes using the Idaho National Laboratory (INL) node.
- Button-cell testing of steam electrolysis in the temperature range of 600°–800°C has been conducted. Electrochemical performance met the program milestones (1.4 V at 1 A/cm² and 50-hour performance stability).
- Technical progress and accomplishments met the program milestones (Milestone 1-1, 2-1, 3-1, and 4-1, and Budget Period 1 go/no-go).
- The overall program goals for Budget Period 1 and the go/no-go decision have been achieved.

Table 1. Progress Toward Meeting Technical Targets for Intermediate-Temperature Steam Electrolysis

Characteristic	Units	State of the Art	EERE Proposed Targets	Project Status
Electrolyte conductivity	S/cm @ 650 °C	~10 ⁻³	≥0.01	0.03
Sintering temperature	°C	1,450	1,350	1,350
Electrolyte densification	%		>90	~97
Electrolyte thickness	μm	>25	<25	~15-20
Current density	A/cm ² @ 1.4 V, 700 °C	0.6	>1.0	1.3
Stability	mV/50 hour		<0.2	~0

INTRODUCTION

Proton-conducting solid oxide electrolysis cells (H-SOECs) offer economic and operational advantages for hydrogen production over the state-of-the-art oxygen-ion-conducting SOECs (O-SOECs). The objective of this project is to develop, fabricate, and test SOECs consisting of proton-conducting electrolyte, high-performance electrode, and tailored gas-solid and solid-solid interfaces. Strategies for the mitigation of cell/stack/system degradation resulting from interface separation, densification, and coarsening, and Cr-assisted poisoning are being developed and incorporated. During the last year, the project team has made progress in lowering the sintering temperature of BZCY-Yb electrolyte to 1,350°C and reducing the operating temperature of H-SOECs to 650°C without compromising the hydrogen production rate. Pure hydrogen can be directly produced by H-SOECs at a current density of 1.2 A/cm² at a temperature of 650°C with an applied voltage of 1.4 V. More work is still needed to improve durability and reliability, develop degradation mechanisms by in operando experiments and materials characterization, and optimize SOEC cell component materials and design using computational tools to meet performance, life, and cost targets.

APPROACH

Our approach for H-SOEC development leading to large-scale manufacturing and commercialization will rely on utilizing the Energy Materials Network (EMN) and core experimental and computational capabilities at the National Renewable Energy Laboratory (NREL), INL, and Pacific Northwest National Laboratory (PNNL).

- **Materials and processes:** Innovation in materials and processing techniques are employed to develop electrolyte formulations capable of densification (96%–98% density) below 1,400 °C in oxidizing atmospheres, meet the electrical conductivity target (>0.01 S/cm), and demonstrate bulk structural and chemical uniformity.
- **Synthesis and fabrication processes:** Cells utilizing tape cast multi-layer laminated electrolyte (10–20 μm) and electrode (integrated backbone, infiltration, thin-film processing) have been sintered and electrically tested. The process is being optimized to achieve target ASR and current density to meet the overall project goals (1 A/cm² at 1.4 V, 700°C).
- **Computational analysis:** Electrolyte and electrode materials composition are optimized for densification, proton conductivity, and structural stability. Select electrode and electrolyte materials have been synthesized and electrochemically tested.
- **Electrode poisoning and performance degradation mitigation:** Electrode delamination and Cr-assisted poisoning mechanisms will be developed. Mitigation approaches will be identified.

The INL-UConn collaboration spanned over the topics for the development of dense electrolyte and performance improvement of the anode. UConn utilized the INL node “Advanced Materials for Water Electrolysis at Elevated Temperatures.” Technical discussions have been held with Dr. Ding (INL) with focus on materials selection, processing techniques, and electrochemical performance evaluation. UConn also utilized the NREL node “High-Throughput Experimental Thin Film Combinatorial Capabilities.” Technical discussion held with Dr. Andriy Zakutayev (NREL) has identified the scope of work for the development of electrolyte chemistry and validation through high-temperature experiments.

RESULTS

During the first year (FY 2018), proton-conducting electrolyte and electrode materials were selected, synthesized, and utilized for the fabrication of SOECs. We have validated a sol-gel process at 20-gram batch scale for BZY and BZCY-Yb proton-conducting powders.

Sintering of BZY and BZCY-Yb electrolyte discs was conducted in oxygen environment at the temperature range of 1,250°–1,450°C. The scanning electron microscopy and focused ion beam transmission electron microscopy images show that the dense electrolyte (densification >95%) was achieved using reactive sintering

aids (such as ZnO nanopowder) at 100°C lower than the state of the art (1,450°C). The conductivity of dense electrolyte discs was measured in dry air and humidified air (3% H₂O-air) using the four-probe method (Figure 1). BZCY-Yb prepared by the sol-gel method has shown higher proton conductivity than that prepared by the solid-state method.

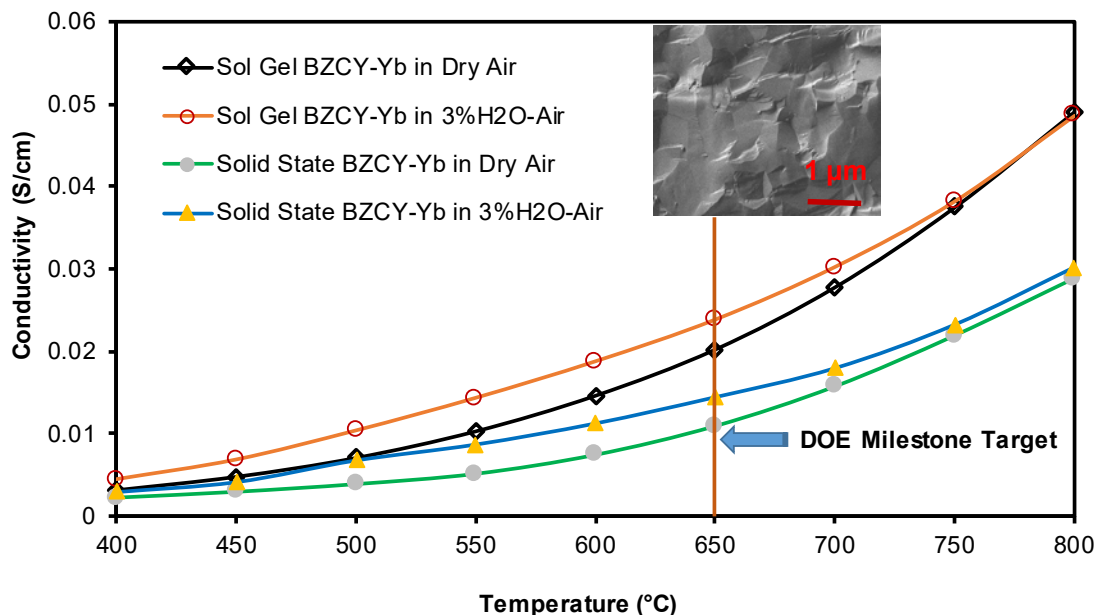


Figure 1. Conductivity of BZCY-Yb discs measured by the four-probe method at temperature range of 400°–800° C in dry and humidified air. All BZCY-Yb discs were sintered at 1,350° C in oxygen. Two types of BZCY-Yb powders were synthesized by sol-gel and solid-state methods, respectively.

H-SOEC full cells with low ASR have been fabricated using thin dense electrolyte (15–40 μm) and porous PBSCF electrodes using the INL node. Button-cell testing of steam electrolysis in the temperature range of 600°–700° C has been conducted using homemade reactors (Figure 2).

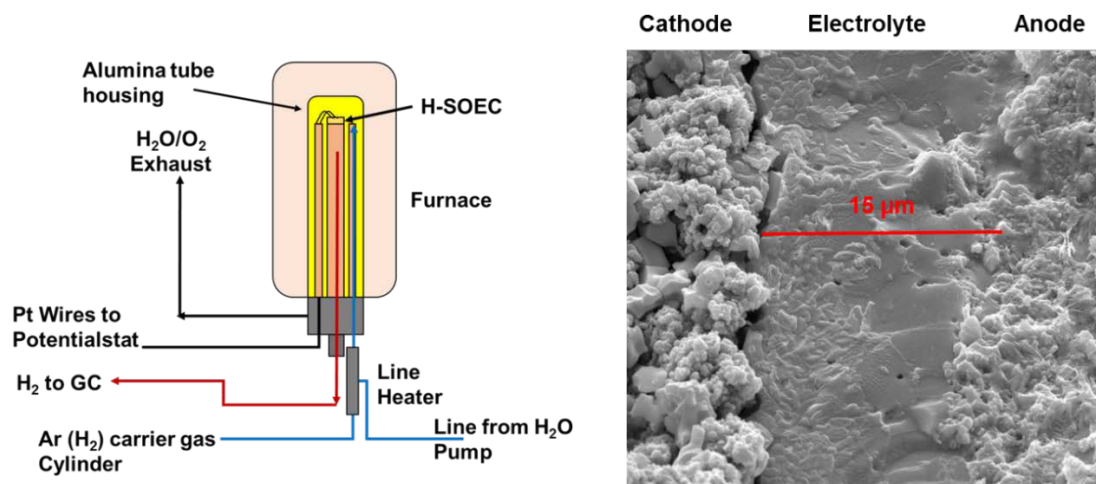


Figure 2. Steam electrolysis setup for the testing of as-fabricated H-SOEC cells with thin BZCY-Yb electrolyte. The anode and cathode were partially shown in the scanning electron microscopy image.

Selected H-SOEC electrolyte and electrode materials' electrolysis performance has been measured and been demonstrated to be relatively stable (<10 mV/1,000 h) for 50-hour tests in real-world electrolyzer operating conditions, meeting Milestone 4-1 (Figure 3). Our recent effort is to improve the current density by lowering ASR and increasing steam concentration and flow rates. Selected H-SOECs have demonstrated 1.20 and 1.32 A/cm² at ≤ 1.4 V at a temperature of 650°C and 700°C in steam electrolysis, meeting the Budget Period 1 go/no-go decision point (Figure 4).

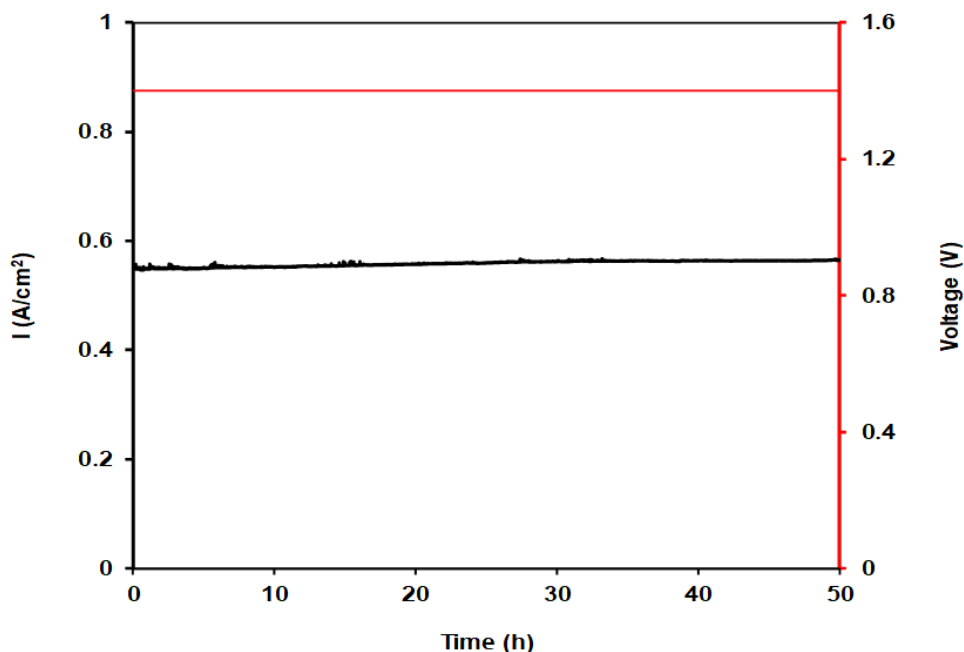


Figure 3. I-t and E-t curve of an H-SOEC cell at 700°C in 50-hour steam electrolysis test

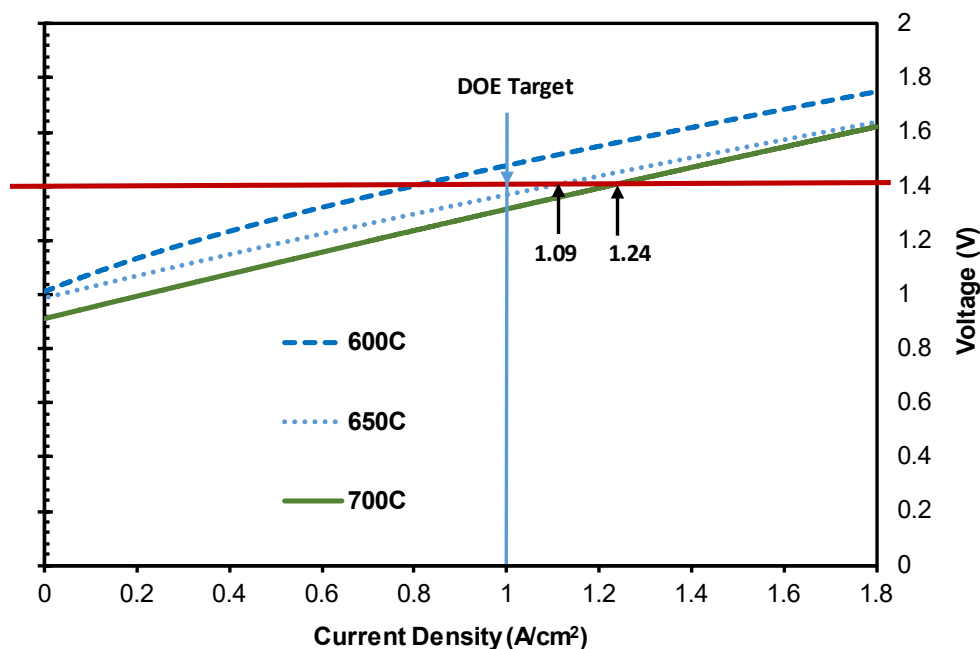


Figure 4. V-I curves of the H-SOEC in steam electrolysis at temperatures of 600°C, 650°C, and 700°C

CONCLUSIONS AND UPCOMING ACTIVITIES

Our project team has validated a sol-gel process for the synthesis of proton-conducting electrolyte materials at 20-gram scale. Dense BZCY-Yb disc (density ~97%) was obtained at a low sintering temperature (~1,350°C) for 6 hours using ZnO nanopowder as sintering aids and the BZCY-Yb's conductivity measured in 3% H₂O-air by the four-probe method reaches 0.024 S/cm at 650°C. Fabricated Ni-BZCY-Yb ||BZCY-Yb (1% ZnO)|| PBSCF cells with a thin electrolyte (<25 μm) have demonstrated stable electrolysis performance and polarization for 50 hours and the cell current density reaches 1.20 A/cm² and 1.32 A/cm² at ≤1.4 V at a temperature of and 650°C and 700°C, respectively. Our technical progress and accomplishments meet the program milestones, and the overall program goals of Budget Period 1 and the go/no-go decision have been achieved.

Large-scale manufacturing and commercialization will rely on utilizing the EMN and core experimental and computational capabilities at NREL, INL, and PNNL. This project uses INL tape-casting facilities to fabricate full cells with porous electrodes and thin electrolyte and uses NREL high-throughput experimental thin film combinatorial capabilities to optimize thin electrolyte compositions. Long-term tests at cell and SOEC stack levels will be conducted to validate the overall project target of degradation rate <4 mV/1,000 h at 1A/cm², electrical efficiency >95%, and cost of hydrogen production <\$2/gasoline gallon equivalent hydrogen.

FY 2018 PUBLICATIONS/PRESENTATIONS

1. Boxun Hu, Ashish N. Aphale, Michael Reisert, Seraphim Belko, Olga A. Marina, Jeffery Stevenson, and Prabhakar Singh, "Solid Oxide Electrolysis for Hydrogen Production: From Oxygen Ion to Proton Conducting Cells," 233rd ECS Meeting, Seattle, WA, May 13–17, 2018.
2. Boxun Hu, Michael Reisert, Ashish Aphale, Seraphim Belko, Olga Marina, Jeff Stevenson, Dong Ding, and Prabhakar Singh, "Barium Zirconate Based Electrolyte Densification Using Reactive Sintering Aids," 43rd International Conference and Exposition on Advanced Ceramics and Composites (ICACC 2019), Daytona FL, 2019, accepted.
3. Boxun Hu, Olga A. Marina, Ashish N. Aphale, Dong Ding, Hanping Ding, Andriy Zakutayev, Jeffery Stevenson, and Prabhakar Singh, "Stable Proton-Conducting Solid Oxide Electrolysis Cells for Pure Hydrogen Production at Intermediate Temperatures," 2019 Materials Research Society Spring Symposia on Advanced Water Splitting, April 22–26, 2019, Phoenix, Arizona, submitted.
4. Boxun Hu, Michael Reisert, Ashish Aphale, Seraphim Belko, Olga Marina, Jeff Stevenson, Dong Ding, and Prabhakar Singh, "Hydrogen Production by Intermediate Temperature Steam Electrolysis Using Proton-Conducting Solid Oxide Electrolysis Cells," in preparation.

REFERENCES

1. "Sintering and Stability Issues of BaZr_{0.1}Ce_{0.7}Y_{0.1}Yb_{0.1}O₃ Electrolyte for SOFCs," in *Advances in Solid Oxide Fuel Cells and Electronic Ceramics*, Ed. N.P. Bansal (John Wiley & Sons, 2015): P22–26.

HydroGEN Seedling: Degradation Characterization and Modeling of a New Solid Oxide Electrolysis Cell Utilizing Accelerated Life Testing

Scott Barnett (Primary Contact), Peter Voorhees, Beom-Kyeong Park, Qian Zhang
Northwestern University
2220 Campus Drive
Evanston, IL 60208
Phone: (847) 491-2447
Email: s-barnett@northwestern.edu

DOE Manager: David Peterson
Phone: (720) 356-1747
Email: David.Peterson@ee.doe.gov

Contract Number: DE-EE0008079

Project Start Date: September 1, 2017
Project End Date: August 31, 2020

Overall Objectives

- Develop a fundamental understanding of degradation mechanisms in solid oxide electrolysis cells (SOECs) based on accelerated testing coupled with theory.
- Develop improved SOECs that provide long lifetime at high current density in order to improve economic viability.

Fiscal Year (FY) 2018 Objectives

- Develop model for electrolyte degradation in solid oxide cells.
- Carry out experimental life tests of SOECs designed to observe electrolyte degradation processes and thereby provide input for model development and vetting.
- Develop new solid oxide cells with capability for electrolysis at high current density with low degradation rates.

Technical Barriers

This project addresses the following technical barriers from the Hydrogen Production section of the Fuel Cell Technologies Office Multi-Year

Research, Development, and Demonstration (MYRDD) Plan¹:

(F) Capital Cost

(G) System Efficiency and Electricity Cost.

Technical Targets

This project aims to study the operating characteristics and degradation mechanisms in state-of-the-art SOECs using accelerated life tests combined with modeling. SOECs are of interest because of their potential to achieve higher electricity-to-hydrogen efficiency and thereby lower the hydrogen production cost. The goal is to achieve an understanding that allows one to build SOECs that operate at high current density with good long-term stability and minimize the impact of stack cost on hydrogen production cost.

The project thereby addresses the following DOE 2020 electrolysis targets:

- Hydrogen levelized cost: \$2.30/kg
- Electrolyzer system capital cost: \$0.50/kg (\$300/kW)
- System energy efficiency: 75% lower heating value (44 kWh/kg)
- Stack energy efficiency: 77% lower heating value (43 kWh/kg).

FY 2018 Accomplishments

- Developed an electrolyte transport model that predicts the electrical and oxygen potential versus position and correctly predicts the conditions (oxygen electrode overpotential >0.2 V) where electrolyte failure occurs.
- Carried out life tests that show where failure occurs and successfully agree with the above theory. The results show that for high-quality oxygen electrodes, overpotential can become

¹ <https://www.energy.gov/eere/fuelcells/downloads/fuel-cell-technologies-office-multi-year-research-development-and-22>

large enough to cause failure only for operating temperatures $<650^{\circ}\text{C}$ or current densities $\gg 1$ A/cm^2 .

- Demonstrated high-performance SOECs that can readily meet program targets of >1 A/cm^2 at 1.3 V at operating temperature $>700^{\circ}\text{C}$.

INTRODUCTION

SOECs have the potential to produce hydrogen at lower overpotential than other methods, thereby providing energy efficiency values much higher than those of existing technologies, exceeding 90%. Because the input electrical energy is a dominant cost of electrolytically produced hydrogen, SOECs have great potential for reducing hydrogen cost. Although SOECs operate stably at relatively low current density ($\leq 0.5 \text{ A/cm}^2$), at higher current densities desired for cost-effective hydrogen production, various degradation mechanisms are observed that can severely decrease cell lifetimes.

While each of the cell components may exhibit degradation at high current density, in the first year of this project the focus has been on the electrolyte. The degradation rate increases rapidly with increasing current density because the associated increase in overpotential η yields a more extreme oxygen partial pressure at the electrode/electrolyte interface. A model was developed and used with input values from our experimental cells and testing conditions in order to calculate the oxygen partial pressure in the electrolyte. These values were compared with the pressure required for fracture based on a simple fracture model. The critical pressure and corresponding overpotential agreed well with the experimental degradation observations for multiple data sets.

APPROACH

The project aims to develop mechanistic degradation models that realistically predict long-term SOEC durability using input data from accelerated electrochemical life testing combined with quantitative microstructural and microchemical evaluation. A promising SOEC type is being further developed. The understanding achieved by combining experimental results and theory will be used to guide improvements in long-term SOEC durability and validate that this technology can reach DOE hydrogen production cost and durability targets. The approach includes (1) obtaining new experimental accelerated testing data on SOEC degradation at the oxygen electrode, fuel electrode, and electrolyte; (2) developing a predictive theory of degradation based on the accelerated test data; (3) developing and testing new electrode materials and processing methods that minimize degradation rate; (4) determining the impact of SOEC electrolyte thickness and electrode composition and microstructure on performance and degradation; (5) determining the operating conditions where degradation is minimized; and (6) validation of degradation models for extrapolating accelerated test data to predict long-term durability.

RESULTS

In the first year of this project, Northwestern University developed high-performance SOECs and carried out extensive life testing in parallel with development of a model for electrolyte degradation mechanisms. The full SOECs consist of a Ni-YSZ support, Ni-YSZ functional layer, $(\text{ZrO}_2)_{0.92}(\text{Y}_2\text{O}_3)_{0.08}$ (YSZ) electrolyte, $\text{Gd}_{0.1}\text{Ce}_{0.9}\text{O}_{1.95}$ (GDC) barrier layer, and $\text{Sr}(\text{Ti}_{0.3}\text{Fe}_{0.63}\text{Co}_{0.07})\text{O}_3$ (STFC) oxygen electrode. Performance met program targets of $>1 \text{ A/cm}^2$ current density at an operating voltage of 1.3 V for temperature $>700^\circ\text{C}$. Life tests were carried out under practical cell operating conditions: DC current density of 1 A/cm^2 at 800°C in air and 50% H_2 /50% H_2O . Although the cell voltage increased by $>150 \text{ mV}$ during the first $\sim 300 \text{ h}$, it stabilized at a value of 1,340 mV. Electrochemical impedance spectroscopy data showed that the polarization resistance gradually increased with time, before stabilizing, while the ohmic resistance remained constant. Since the STFC electrodes do not show an increase in polarization resistance under these conditions, it is suggested based on literature data [1] that this arises from the Ni-YSZ fuel electrode (note that fuel electrode degradation is outside the scope of the Year 1 work, but it will be studied in detail in the upcoming years). Cross-sectional scanning electron microscopy (SEM) analysis of the cell after life testing (Figure 1) shows a structure that appears identical to that of the as-prepared cells. That is, there was no evidence of cell degradation. This is consistent with the electrochemical impedance spectroscopy data, indicating no significant change in ohmic resistance during the life test.

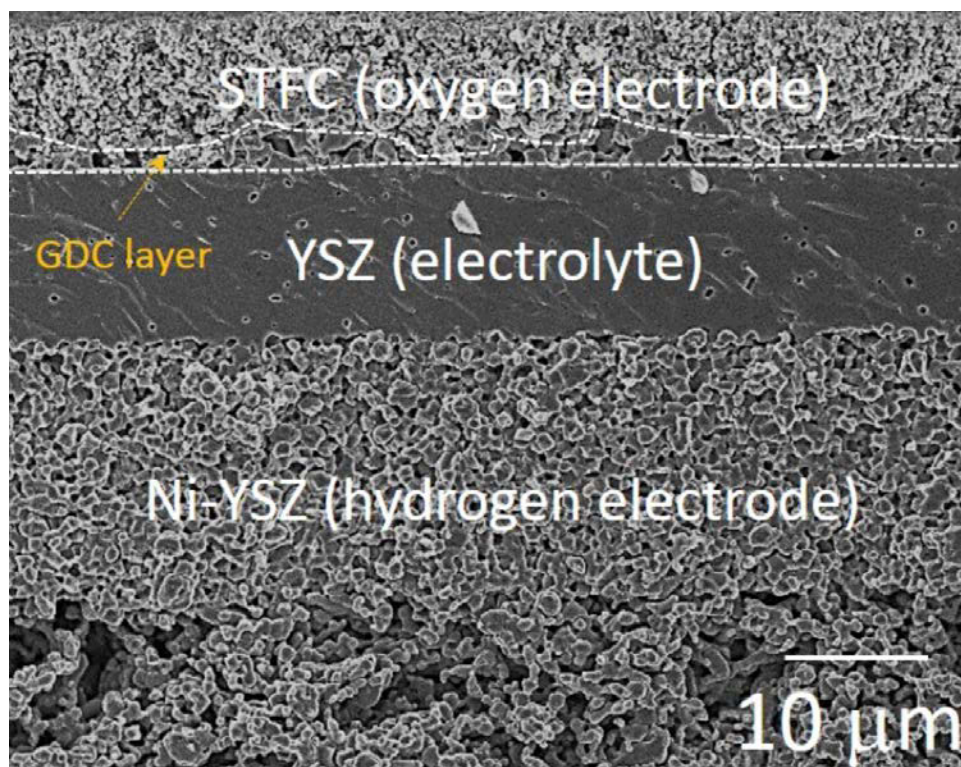


Figure 1. Cross-sectional SEM image of the SOEC after the life testing at 1 A/cm² and 800 °C

Life-test experiments were designed based on our model that predicts deleteriously high oxygen pressures in the electrolyte when the oxygen electrode overpotential is too high; this occurs when the operating temperature is too low and/or the current density is too high. The cells had YSZ electrolytes with GDC barrier layers—oxygen electrodes were Sr(Ti_{0.3}Fe_{0.7})O₃ (STF) in most cases, but (La,Sr)(Co,Fe)O₃ (LSCF) and STFC electrodes were also tested. Life tests were done with a DC electrolysis current density of 0.8–1.6 A/cm² at 600–800 °C in air. Impedance spectra were measured and used to obtain an ohmic resistance (R_{Ω}) and a polarization resistance (R_p). In order to estimate the electrode overpotential η , we used the measured R_p values together with an approximate form of the Butler-Volmer equation [2]. Different data sets were obtained by varying different aspects in the life tests:

1. Operating temperature variation to vary R_p and hence electrode overpotential
2. Varying the electrode material
3. Porous versus dense GDC barrier layer
4. Symmetric versus full cells.

Life tests were done at temperatures of 600°, 650°, 700°, and 800 °C. The R_{Ω} and R_p values were generally quite stable at the higher temperatures during the ~1,000 h tests, but at 600 °C the cell failed 144 h into the test. The dramatic decrease in cell life with decreasing temperature can be explained by a higher η , reaching 200 mV at 600 °C. Cross-sectional SEM analysis showed no sign of fracture or delamination at the higher temperatures, but the cell tested at 600 °C had an obvious fracture on the electrolysis-side electrode/electrolyte (STF/GDC) interface.

In order to prove that this effect is universal, and not just specific to STF electrodes, otherwise identical cells with LSCF and STFC electrodes were tested using the same DC current density of 0.8 A/cm² at 600 °C. Figure 2a indicates the R_{Ω} , R_p , and η values determined from the impedance data periodically collected with time for the cells with the LSCF and the STFC electrodes. These results show that LSCF, the widely used SOEC

electrode, has a higher R_p and η than STF, whereas STFC had a lower R_p and η than STF. The η values of the cell with LSCF exceeded 200 mV, and the cell failed in <200 h. The SEM image in Figure 2b shows a clear fracture at the LSCF/GDC interface. For STFC, η <200 mV, and the cell remained stable throughout the entire test. No evidence of fracture can be seen in the post-test SEM image (Figure 2c). These results suggest a critical value for fracture of \sim 200 mV.

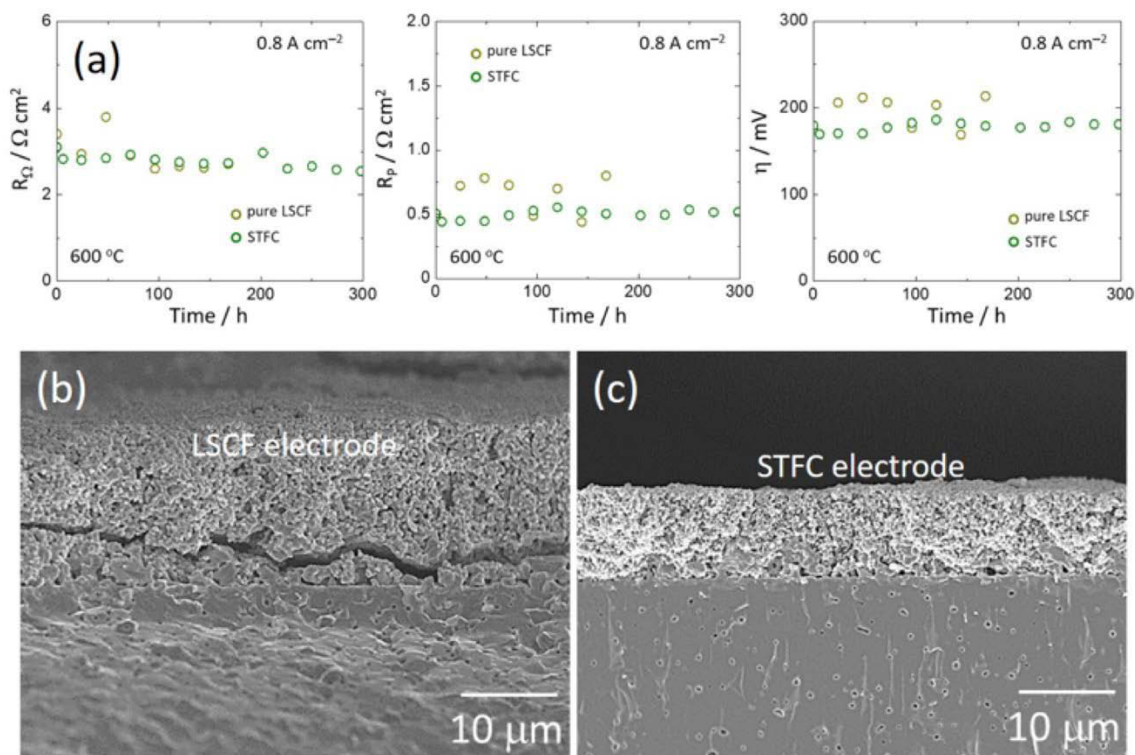


Figure 2. (a) Evolution of R_{ohm} , R_p , and η with time for the symmetric cells with the LSCF and the STFC electrodes tested at 600°C. Cross-sectional SEM images of the cells with (b) the LSCF and (c) the STFC after the life tests.

Life tests were also done on full cells—Ni-YSZ-supported SOECs with STF oxygen electrode—with the life tests carried out at 600°C and 800°C with a DC current density of 0.8 A/cm² in air and 50% H₂/50% H₂O. The cell tested at the higher temperature eventually stabilized as discussed above, whereas the cell tested at the lower temperature failed after <50 h. Cross-sectional SEM analysis showed that the higher-temperature cell had no evidence of damage whereas the 600°C-tested cell showed clear fracture at the electrode/electrolyte interface, similar to that shown in Figure 2b.

In the experiments described above, delamination was found at the SOEC side at temperature 600°C with current density 0.8 A/cm² for the cell tested in air, but not at 650°C and above. Figure 3 shows the oxygen partial pressure distribution in the electrolyte with different temperatures (600°C, 700°C, 800°C) obtained using a numerical simulation. Parameters used, including the electrolyte YSZ and GDC layer thicknesses and the electrode polarization resistances, are taken from measurements of the experimental cells. The figure shows that p_{O_2} is low at the fuel cell side of the cell but increases rapidly to values well above 1 atm and increases very slightly throughout the electrolyte with peak values at the electrolysis side of the cell. The maximum p_{O_2} value increases with decreasing temperature, reaching $\sim 10^4$ atm at 600°C.

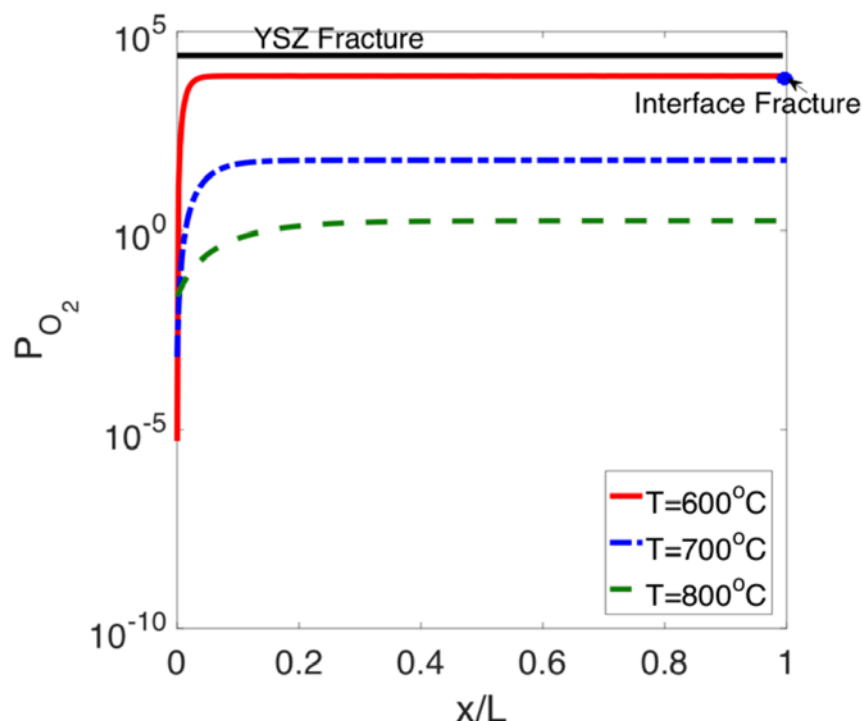


Figure 3. Distribution of oxygen partial pressure versus normalized position in a YSZ electrolyte with thickness $L = 400 \mu\text{m}$ and thin GDC barrier layers on both sides, using polarization resistance values as measured for STF electrodes in air, for different temperatures at 0.8 A/cm^2 . Also shown for comparison (in black) are calculated pressures required for YSZ fracture and for fracture of the YSZ/electrode interface. The interface fracture criterion, represented by the blue dot, is given by the fracture toughness of the perovskite.

The critical oxygen partial pressure for fracture was calculated using the expression by Virkar [3] based on the balance among surface energy at a crack surface in YSZ, strain in YSZ, and the oxygen pressure introduced electrochemically. Using the Virkar model with an initial crack radius of $\sim 1.0 \mu\text{m}$ based on the observed YSZ pore size and a YSZ fracture toughness of $3.0 \text{ MPa m}^{1/2}$ yields a critical pressure of $\sim 5 \times 10^4 \text{ atm}$. The overpotential η required to reach this pressure is 221 mV. Note that the values predicted by the electrolyte model, shown in Figure 3, are less than this value even at 600°C , indicating that fracture within the YSZ electrolyte is not expected. This prediction is correct because fracture does not occur within the electrolyte but rather at the electrolyte/electrode interface (see Figure 1). This can be explained by the lower fracture toughness of the GDC and perovskite electrode. An estimate of the fracture toughness of the perovskite electrode materials (e.g., STFC, LSCF) is $0.8 \text{ MPa m}^{1/2}$ [4], lower than that of GDC ($\sim 1.5 \text{ MPa m}^{1/2}$). Using the lower value gives rise to a critical pressure $\sim 1 \times 10^4 \text{ atm}$ achieved for $\eta = 196 \text{ mV}$ at 600°C . As shown in Figure 3, at 600°C the p_{O_2} induced by the overpotential exceeds this value, predicting the observed interfacial fracture for this condition. In addition, the calculation was carried out for full cells and compared with experimental data. Again, the predicted condition for fracture agreed well with the experimental observation.

Lawrence Berkeley National Laboratory (LBNL) adapted their metal-supported solid oxide cells, which had previously only been utilized as fuel cells, for application as SOECs. By optimizing the catalyst materials and catalyst infiltration processes, an excellent SOEC performance was obtained (i.e., current densities of -5.31 , -4.09 , -2.64 , and -1.62 A/cm^2 at 800°C , 750°C , 700°C , and 650°C , respectively, at 1.3 V and $50 \text{ vol}\%$ steam content). To the best of our knowledge, this is the highest SOEC performance for oxygen-conducting type cells. However, rapid performance degradation is observed. This has been a key challenge addressed in the first year. LBNL has carried out systematic studies to determine primary degradation modes and mechanisms. Examples include using symmetric cells operated with air on both sides to isolate the effects of oxygen ion current and

oxygen pressure, and post-life-test analysis of the cells. Results to date show promising improvements in cell stability.

Idaho National Laboratory (INL) has applied their extensive SOEC testing capabilities and expertise in this project. Specifically, they have contributed additional cell testing and data interpretation to expand the scope of the project, carrying out SOEC testing over a range of H₂/H₂O ratios.

CONCLUSIONS AND UPCOMING ACTIVITIES

The present experimental and theoretical results show stable cell operation until a specific critical value of the oxygen electrode overpotential η is exceeded, whereupon rapid electrolyte degradation and eventual cell failure results. Specifically, our experimental results indicate that fracture occurs when $\eta_{\text{exp}} > 0.19 \pm 0.015$ V. This has been shown to be valid for a few different electrode materials and both full and symmetric cells. The result applies to the YSZ electrolyte with a thin doped ceria barrier layer used in our experiments; the result has broad applicability because this design is widely used by SOEC developers. By comparison the model predicts that the overpotential at the point where fracture occurs is at $\eta_{\text{calc}} = 0.196$ V. There are no adjustable parameters used in the prediction of simulation, and thus the agreement with experiment is very good.

In the coming year, the model will be further developed to help explain degradation effects observed at the oxygen electrode and H₂/H₂O electrode. Full cell development will continue and more extensive life testing will be carried out, providing additional input to the model development. Work done at LBNL and INL will continue to provide important results, augmenting the Northwestern work with life testing of novel metal-supported cells and supporting a broader range of testing conditions. Overall, this work should lead to improved long-term stable SOECs as needed to meet hydrogen production efficiency and cost targets.

FY 2018 PUBLICATIONS/PRESENTATIONS

1. S.A. Barnett, “Degradation Characterization and Modeling of a New Solid Oxide Electrolysis Cell Utilizing Accelerated Life Testing,” Presentation at the DOE Hydrogen and Fuel Cells Program Annual Merit Review, Washington, D.C., June 2018.
2. S.A. Barnett, “Degradation Characterization and Modeling of a New Solid Oxide Electrolysis Cell Utilizing Accelerated Life Testing,” Presentation at the Hydrogen Production Technical Team review of the HydroGEN High Temperature Electrolysis projects, Idaho Falls, Idaho, September 2018.

REFERENCES

1. M. Chen, Y.L. Liu, J.J. Bentzen, W. Zhang, X. Sun, A. Hauch, Y. Tao, J.R. Bowen and P.V. Hendriksen, “Microstructural Degradation of Ni/YSZ Electrodes in Solid Oxide Electrolysis Cells under High Current,” *Journal of The Electrochemical Society* 160 (2013): F883–F891.
2. J.G. Railsback, H. Wang, Q. Liu, M.Y. Lu and S.A. Barnett, “Degradation of La_{0.6}Sr_{0.4}Fe_{0.8}Co_{0.2}O_{3- δ} Oxygen Electrodes on Ce_{0.9}Gd_{0.1}O_{3- δ} Electrolytes during Reversing Current Operation,” *Journal of The Electrochemical Society* 164 (2017): F3083–F3090.
3. A.V. Virkar, “Failure of Ion-Conducting Materials by Internal Precipitation Under Electrolytic Conditions,” in *Engineered Ceramics* (John Wiley & Sons, Inc., 2016).
4. M.D. Thouless, E. Olsson, and A. Gupta, “Cracking of Brittle Films on Elastic Substrates,” *Acta Metall. Mater.* 40 (1992): 1287–1292.

HydroGEN Seedling: Thin-Film, Metal-Supported, High-Performance, and Durable Proton-Solid Oxide Electrolyzer Cell

Tianli Zhu
United Technologies Research Center
411 Silver Lane
East Hartford, CT 06411
Phone: (860) 610-7334
Email: zhutl@utrc.utc.com

DOE Manager: David Peterson
Phone: (720) 356-1747
Email: David.Peterson@ee.doe.gov

Contract Number: DE-EE0008080

Subcontractor:
University of Connecticut (UConn), Storrs, CT

Project Start Date: October 1, 2017
Project End Date: December 31, 2018

Overall Objectives

- Demonstrate a thin-film, high-efficiency, and durable metal-supported solid oxide electrolysis cell (SOEC) based on proton-conducting electrolyte at targeted operating temperatures of 550°–650°C.
- Develop a high-temperature SOEC cell to meet the DOE performance target of 1.0 A/cm² at 1.4 V and a decay rate <0.4%/1,000 h.
- Phase 1 focuses on demonstrating the feasibility of the proposed concept via electrolysis performance demonstration of a metal-supported single cell up to 25-cm² scale.

Fiscal Year (FY) 2018 Objectives

- Develop an electrolyte deposition process based on either suspension plasma spray (SPS) or reactive spray deposition technology (RSdT).

- Fabricate metal-supported cells and demonstrate the cell performance for water electrolysis.

Technical Barriers

This project addresses the following technical barriers from the Hydrogen Production section of the Fuel Cell Technologies Office Multi-Year Research, Development, and Demonstration Plan¹:

- Capital cost of hydrogen production by water electrolysis systems
- Manufacturing
- Operation and maintenance cost for electrolysis.

Technical Targets

The objective of Phase 1 of this project is to demonstrate the feasibility of a low-cost proton-conducting metal-supported SOEC cell:

- Develop a manufacturing process for barium yttrium zirconate (BYZ)-based proton-conducting electrolyte.
- Demonstrate a proton-conducting metal-supported SOEC cell for water electrolysis for a targeted performance of >0.8 A/cm² at 1.4 V at T ≤650°C and <1%/1,000 h degradation projected from short-term durability results.

FY 2018 Accomplishments

- Demonstrated the SPS process for electrolyte deposition. A hydrogen-electrode-supported button cell with an SPS electrolyte layer exceeded the performance target of 0.8 A/cm² at 1.4 V.
- Made significant progress on half-cell fabrication (hydrogen electrode/electrolyte) on metal-supported cells.

¹ <https://www.energy.gov/eere/fuelcells/downloads/fuel-cell-technologies-office-multi-year-research-development-and-22>

INTRODUCTION

High-temperature water electrolysis can be a highly efficient and cost-competitive process for hydrogen generation when coupled with nuclear power or renewable sources such as wind or solar. The major challenge is the high degradation rate (1%–4%/1,000 h) of conventional oxygen-ion-conducting solid oxide electrolyzers due to material and interface degradation at high temperatures (typically 800°–1100°C). A stable proton-conducting electrolyte, based on doped-BaZrO₃, enables high ionic conductivity [1, 2] and the electrolysis cell can be operated at 550°–650°C. The proposed metal-supported cell design is based on mass-producible metal parts combined with low-cost thin-film cell deposition techniques (i.e., SPS or RSDT) [3]. This design should enable the electrolyzer to meet the hydrogen production cost goal of \$2/kg hydrogen.

APPROACH

This project leverages electrolyte and electrode materials developed under the Advanced Research Projects Agency–Energy’s REBELS (Reliable Electricity Based on Electrochemical Systems) project, with further advancements through process development, modeling, material discovery, and testing capabilities at United Technologies Research Center (UTRC), University of Connecticut (UConn), and national laboratories through the HydroGEN Energy Materials Network (EMN) consortium. The EMN collaborations include (1) working with Lawrence Berkeley National Laboratory (LBNL) on developing a co-sintering and catalyst infiltration technology for metal-supported cell fabrication as an alternative approach to RSDT and SPS; (2) selecting appropriate alloy materials and protective coatings through LBNL’s long-term corrosion testing; (3) optimizing electrolyte and electrode materials at Idaho National Laboratory (INL); and (4) developing an electrolyzer cell model at the National Renewable Energy Laboratory (NREL) for cell-performance optimization.

The main focus of the UTRC and UConn teams is to address a major challenge in fabricating metal-supported cells. The challenge is to develop a cell deposition process to rapidly produce fully sintered or porous ceramic coatings without high-temperature production steps such as sintering. RSDT and SPS are two promising techniques with rapid deposition rates and no high-temperature firing operations, thus enabling high throughput, simple process flow, and automation for lower fabrication cost. The SPS is a form of plasma spraying where the ceramic feedstock is dispersed in a liquid suspension before being injected into a plasma jet. It is suitable for producing finely structured or nanostructured coatings with thicknesses between 5 µm and 100 µm using suspensions of submicron or nanoscale particles. The RSDT is a flame-based deposition process, depositing films or producing nanopowders through combustion of metal-organic or metal-inorganic compounds dissolved in a solvent. These low-cost fabrication processes provide a pathway to overcome the severe limitations of a conventional, sintered ceramic SOEC with respect to (1) production cost and (2) the lack of cell mechanical robustness arising from the low mechanical strength and low fracture toughness of perovskite materials.

RESULTS

During FY 2018, UTRC and the team focused on cell fabrication, including the development of SPS for BYZ-based electrolyte deposition, as well as RSDT for electrolyte and steam electrode deposition. The performance of button cells with SPS electrolyte or RSDT layers was evaluated by INL through the HydroGEN EMN consortium.

SPS Process Development and Results

The hydrogen electrode, consisting of NiO and doped-BYZ, was mechanically pressed into a disc and fired at high temperature for sintering. The electrolyte layer was coated by Pratt & Whitney using SPS with a targeted thickness of 20–30 µm for an initial demonstration. No post heat treatment was applied to the electrolyte layer. An open circuit voltage (OCV) of 0.9 V at 500°C was obtained on a half cell with SPS electrolyte on a sintered hydrogen electrode. A similar cell, coated with INL’s steam electrode material, was tested for water electrolysis. The steam electrode is exposed to an open chamber while a ceramic tube is used to feed wet oxygen (~3% H₂O) pointing toward the active electrode area. On the hydrogen electrode side, diluted

hydrogen (~20% H₂) was used to reduce NiO and then gradually increased to pure hydrogen for fast reduction to obtain the OCV. In the test, 20% H₂/Ar was used to sweep the electrode. A current density of 0.91 A/cm² was obtained at 650°C and 1.4 V, as shown in Figure 1. This performance exceeded the project target for Phase 1 (i.e., 0.8 A/cm² at 650°C and 1.4 V). This result demonstrated that the SPS process is a promising path to produce a high-performance electrolyte at a low manufacturing cost as it eliminates the high-temperature sintering (typically >1,400°C) required to achieve a dense BYZ-based proton-conducting electrolyte. Further optimization of the SPS process is focused on improvement of the density of the electrolyte layer.

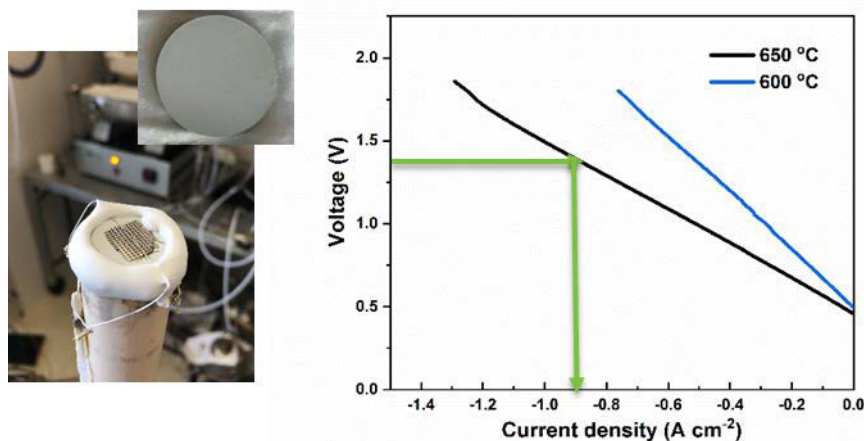


Figure 1. Left: 1-inch button cell and testing rig at INL. Right: The current-voltage curves of an anode-supported button cell with BYZ-based electrolyte (deposited by SPS) and INL's steam electrode, at 600°C and 650°C. The green arrow indicates the performance at 1.4 V and 650°C, which exceeded the performance target of Phase 1.

The same SPS process was used for electrolyte deposition on the metal-supported cells. In this case, the hydrogen electrode (NiO + electrolyte) was deposited onto a porous metal substrate (Crofer APU 22 or SS430 porous metals from GKN) using a doctor blade process. The electrode was sintered in H₂/Ar at high temperatures. The thickness of the hydrogen electrode layer was about 20–30 μm. Typically, 3x3 cm² cells were fabricated and cut into 1-inch round cells for testing at INL, as shown in Figure 2. The performance measured was much lower, achieving a current density of 0.25 A/cm² at 1.4 V. This was due to erosion of the hydrogen electrode during the SPS deposition for the electrolyte, which also caused defects in the electrolyte layer. Because the hydrogen electrode on the metal-supported cell was not as strong as the sintered pellets, the team is evaluating potential modifications to the SPS process without altering the properties of the SPS electrolyte layer. The long-term goal is to develop a plasma spray process for the electrode deposition thus enabling a low-cost manufacturing process for a complete cell.

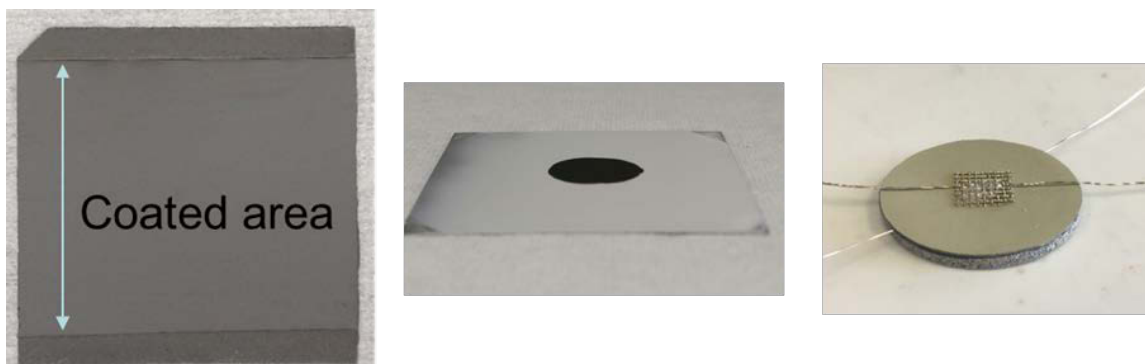


Figure 2. Left: A hydrogen-electrode coated metal cell. Middle: A 3x3 cm² cell with hydrogen electrode, SPS electrolyte, and steam electrode (3/8-inch circle). Right: 1-inch round cell assembled for testing at INL.

RSDT Process Development and Results

The team at UConn focused on developing a RSDT process for the deposition of a dense electrolyte based on doped BYZ and a porous Pr(Ba_{0.5}Sr_{0.5}Co_{1.5}Fe_{0.5})O₅ (PBSCF) steam electrode. The electrolyte deposition time was about 105 minutes, resulting in an electrolyte layer with a thickness of 1–3 μm. There was no post heat treatment. Figure 3 shows the surface image of the deposited electrolyte on a hydrogen-electrode-supported cell, confirming the formation of a dense electrolyte layer. The steam electrode layer was porous with a cauliflower structure, as shown in Figure 3. The as-deposited electrode layer showed no X-ray diffraction peaks. After annealing at 650°C for 1 hour, X-ray diffraction peaks showed that crystalline PBSCF was forming. In addition, microscopy analysis showed appropriate mixing of the elemental components of the PBSCF while energy-dispersive X-ray spectroscopy data showed that the chemical composition matched the desired composition within the error range of the equipment. The cells will be tested for steam electrolysis to demonstrate the performance of the electrolyte and steam electrode layers deposited by RSDT.

Metal-supported half cells were also fabricated using RSDT. The hydrogen electrode was deposited on a porous metal substrate by doctor blade and sintered in H₂/Ar as described earlier. The electrolyte was deposited by RSDT. The cell reached a maximum OCV of 0.55 V at 600°C and 0.82 V at 700°C. However, the OCV was not stable. Modifications of the deposition process and testing are being evaluated to improve the cell performance.

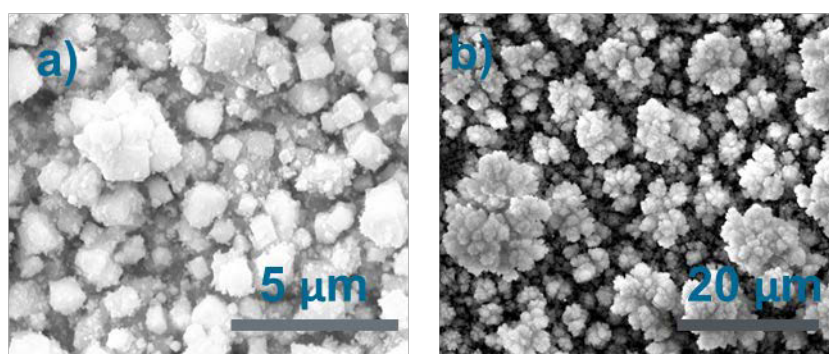


Figure 3. Scanning electron microscopy micrographs of (a) BYZ-based electrolyte deposited by RSDT and (b) PBSCF steam electrode deposited by RSDT

CONCLUSIONS AND UPCOMING ACTIVITIES

In summary, the team successfully demonstrated SPS as a feasible deposition process for the BYZ-based electrolyte. The performance of the hydrogen-electrode-supported cell, with a SPS electrolyte layer, demonstrated high electrolysis performance (with INL's steam electrode) that exceeded the project's Phase 1

target. The SPS electrolyte was applied to metal-supported cells with a doctor-bladed hydrogen electrode. The metal-supported cells showed lower performance due to a less robust anode layer on a porous metal substrate. The team also made significant progress in RSDT process development for both electrolyte and steam-electrode deposition. A hydrogen-electrode-supported cell, with RSDT electrolyte and electrode, will be tested at INL to demonstrate the performance of the RSDT electrolyte and steam electrode.

In addition, the collaboration with the HydroGEN EMN nodes (LBNL, INL, and NREL) provided critical support to address technical barriers in metal alloy durability; electrode/electrolyte material optimization and stability; and SOEC modeling. Various combinations of metal alloys and protective coatings were identified as acceptable for proton-SOEC conditions. High-performance proton electrolytes and steam electrodes were identified by INL. The button cell performance exceeded the DOE performance target. An electrochemical model and a cell model were developed by NREL for SOEC characterization and simulation and are expected to provide performance modeling of the SOEC cell/stack performance for material scale up. In addition, INL provided critical support in cell performance testing for UTRC and UConn.

The proposed effort for Phase 2 is to develop a plasma-based deposition process for the hydrogen electrode while further improving the SPS process for BYZ-based electrolytes through feedstock and process optimization. The team will also continue the collaboration with the HydroGEN EMN nodes on alternative cell deposition technology development, new material discovery, and SOEC cell/stack modeling.

FY 2018 PUBLICATIONS/PRESENTATIONS

1. T. Zhu, “Thin-Film, Metal-Supported High-Performance and Durable Proton-Solid Oxide ElectrolyzerCell,” poster at DOE Annual Merit Review, June 2018.
2. T. Zhu, “Thin-Film, Metal-Supported High-Performance and Durable Proton-Solid Oxide Electrolyzer Cell,” presented at High Temperature Electrolysis review meeting at Idaho National Laboratory, September 2018.

REFERENCES

1. K.D. Kreuer, “Proton-Conducting Oxides,” *Annu. Rev. Mater. Res.* 333 (2003): 333–359.
2. S. Choi, C.J. Kucharczyk, Y. Liang, X. Zhang, I. Takeuchi, H. Ji, and S.M. Haile, “Exceptional power density and stability at intermediate temperatures in protonic ceramic fuel cells,” *Nature Energy* 3, no. 3 (2018): 202–210.
3. R. Maric, J. Roller, and R. Neagu, *Journal of Thermal Spray Technology* 20, no. 4 (2011): 696–718.

HydroGEN Seedling: High-Efficiency Proton Exchange Membrane Water Electrolysis Enabled by Advanced Catalysts, Membranes, and Processes

Katherine Ayers (Primary Contact), Chris Capuano
Proton OnSite
10 Technology Drive
Wallingford, CT 06492
Phone: (203) 678-2190
Email: KAyers@protononsite.com

DOE Manager: David Peterson
Phone: (720) 356-1747
Email: David.Peterson@ee.doe.gov

Contract Number: DE-EE0008081

Subcontractors:

- Tufts University, Boston, MA
- Oak Ridge National Laboratory, Oak Ridge, TN

Project Start Date: September 2, 2017

Project End Date: August 30, 2020

- Complete membrane mechanical testing versus hydration condition and evaluate options for down-selection of advanced membrane.
- Demonstrate 1.8A/cm² at 1.7 V for advanced MEA.

Technical Barriers

This project addresses the following technical barriers from the Hydrogen Production section of the Fuel Cell Technologies Office Multi-Year Research, Development, and Demonstration Plan¹:

(F) Capital Cost.

Technical Targets

The current program aims to meet the targets in the table below.

Metric	State of the Art	Proposed
Membrane thickness	175 microns	50 microns
Operating temperature	58°C	80° -90°C
Cell efficiency	53 kWh/kg	43 kWh/kg

Overall Objectives

- Develop an advanced electrolysis membrane electrode assembly (MEA) that is capable of meeting the following targets:
 - Produce hydrogen at 43 kWh/kg
 - Show decay rates of less than 4 mV/1,000 h
 - Achieve costs of \$2/kg hydrogen based on \$0.02/kWh renewable energy input as estimated by the H2A (Hydrogen Analysis) model.

Fiscal Year (FY) 2018 Objectives

- Develop material tracking sheet and baseline current hydrogen costs.
- Demonstrate MEA performance of 1.85 V at 80°C with advanced catalyst and N117 baseline membrane.
- Quantify water distribution in operating cell with X-ray tomography.

FY 2018 Accomplishments

- Catalyst samples for oxygen evolution were synthesized, screened for initial performance in 25-cm² electrolysis cells, and analyzed for stability through dissolution rates.
- Several anode porous transport layers were tested and evaluated through in-operando analysis using the X-ray imaging technique.
 - Increased current density at 2 A/cm² was achieved in the test cell.
 - Data was provided to Lawrence Berkeley National Laboratory (LBNL) for incorporation into modeling activities.

¹ <https://www.energy.gov/eere/fuelcells/downloads/fuel-cell-technologies-office-multi-year-research-development-and-22>

- Oxygen evolution catalysts were deposited as electrode decals using a polytetrafluoroethylene substrate for transfer at Proton onto membrane to be formed as catalyst-coated membranes.
- Proton continued to develop the coating technique for model catalyst layers toward electrochemical and conductive imaging.
- A two-dimensional water electrolyzer model was developed; the model is able to run under differential pressure and a study was carried out to examine the effect of cathode pressure on cell performance.
- Model validation is in progress under both vapor and liquid feed conditions.

INTRODUCTION

Now that there are commercial fuel cell vehicles on the roads in the United States in regions where fueling stations are available, attention has turned to the urgent need for clean hydrogen, for fueling as well as other industrial applications. Proton exchange membrane (PEM) electrolysis is a critical near-term need that lays the groundwork for future renewable water splitting pathways. Based on cost reduction to date, PEM electrolysis systems are profitable and competitive when fielded today for hydrogen industrial gas applications and markets. However, for energy storage, hydrogen fueling, and commodity hydrogen, the price point of $> \$5.5$ /kg hydrogen and low efficiency of > 50 kWh/kg are unacceptable. The United States is also in danger of losing its competitive edge in PEM technology as European and Asian entities invest in research, development, and deployment of electrolyzer systems. However, initial feasibility work has shown that much of the materials understanding from PEM fuel cells can be applied to electrolyzers to reduce both capital and operating expense.

APPROACH

The cost and efficiency drivers for PEM electrolysis are (1) thick membranes (7–10 mm thick) to prevent excessive gas crossover and seal against 30–350 bar differential pressure, but which cause high resistive efficiency losses; (2) high catalyst loadings using conventional low-surface-area, unsupported catalysts increasing cost and decreasing efficiency; (3) manufacturing for electrode gas diffusion layers and porous transport layers (PTLs) that is not optimized for activity, durability, or cost; and (4) low-temperature operation due to membrane creep over long lifetimes at higher temperature, which again limits efficiency. This project leverages understanding of materials interactions and electrode structure to integrate thinner membranes, improved catalyst layer structures, and tailoring of catalyst-electrode interfaces to meet the targets above.

RESULTS

To increase catalyst activity, Proton synthesized high-surface-area IrOx and IrOx-RuOx blends. Because ruthenium typically dissolves at PEM electrolysis operating voltages, the approach focused on alloying the higher-activity metal in a stable matrix. Compositional ratios and synthesis techniques were evaluated through bench and performance testing. The fusion synthesis method used at Proton to fabricate catalysts was successful in increasing the surface area by $> 7x$ versus the baseline. Three candidates were focused on: 100% IrOx, 70:30 IrOx:RuOx, and 50:50 IrOx:RuOx. National Renewable Energy Laboratory (NREL) node resources were leveraged to evaluate cycling stability and demonstrated minimal metal loss in the 70:30 blend, as well as good activity in rotating disk electrode experiments. All three catalyst powders were formulated into ink suspensions and MEAs were manufactured using the deposition process used for all of Proton's commercial cell stacks to show transfer to production methods. Catalyst-coated membranes were made for the test and both polarization curves and steady-state data were collected to look for pure electrical performance and stability. Steady-state results from these tests are shown in Figure 1, confirming the rotating disk electrode evaluation.

The same catalyst compositions were incorporated into a three-cell 28-cm² cell stack for extended unattended operation with 30 bar differential pressure to best simulate what would be typical of a commercially fielded device. Polarization data was initially collected at current densities exceeding 4 A/cm², with linear response indicating no mass transfer limitations. The cell stack was allowed to run continuously under steady-state conditions in order to look for voltage decay, either indicating loss of activity through lowering of surface area or dissolution of catalyst. Under the 80°C, 30 bar differential pressure, 1.8 A/cm² operating condition, stable performance was observed up to 300 h for all three samples, with the 70:30 IrRu blend starting to show better electrical efficiency versus both the 50:50 Ir:Ru blend and the pure IrOx. The current density was then increased to 2 A/cm² and the stack was operated another 600 hours. All voltages were maintained below 1.9 V/cell, with 900 h of stable performance observed for the three high-surface-area compositions. The results from this test are shown in Figure 2, with 70:30 IrRu down-selected for integration with advanced membranes.

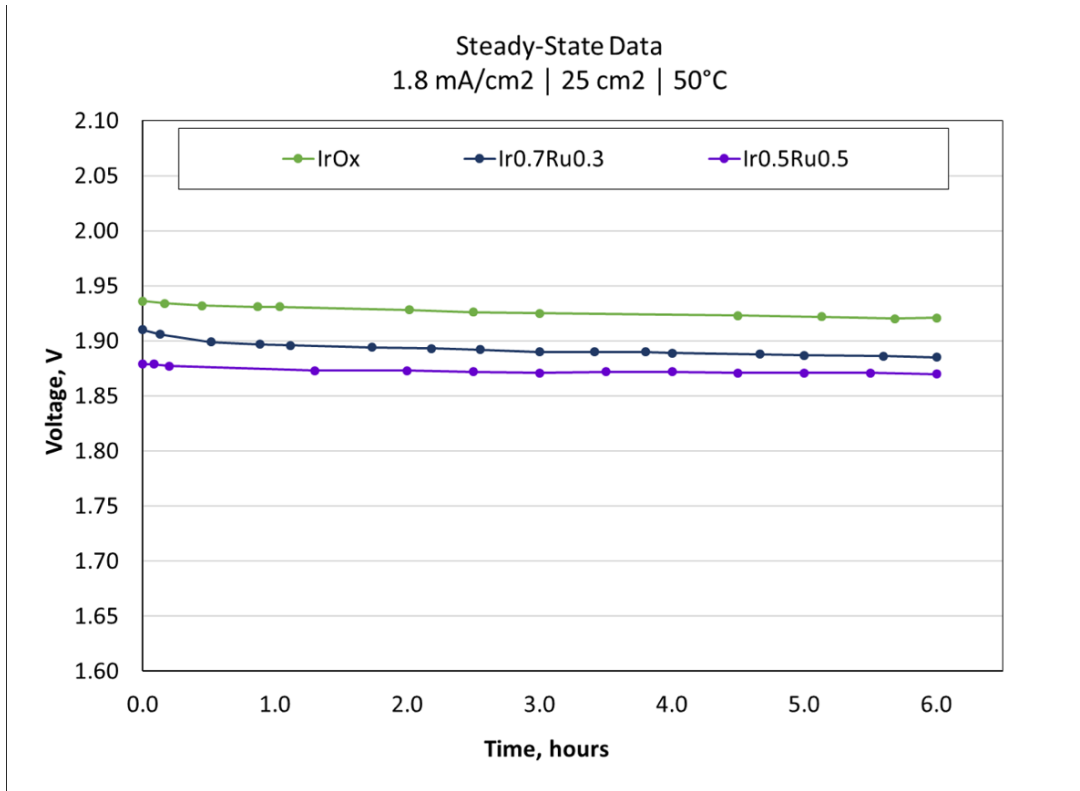


Figure 1. Short term operational data for high-surface-area IrOx, 70:30 IrRu, and 50:50 Ir:Ru

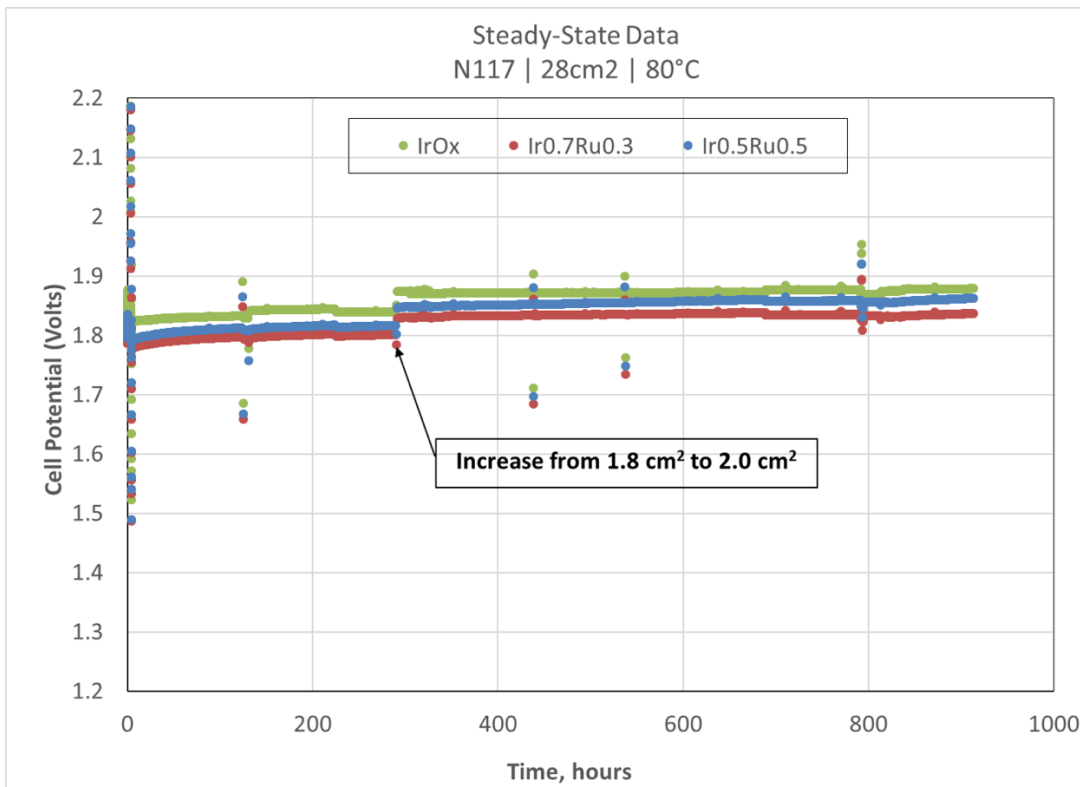


Figure 2. Steady-state operational data in Proton's 28-cm² commercial cell stack

Membrane samples were first assessed for stability and performance using Proton’s baseline catalysts to isolate performance deviations to the membranes. Membranes of 50 and 90 μm were compared to baseline N117 (175 μm). Testing was initially conducted at 30 bar, 50°C, and 1.8 A/cm² in the same 28-cm² commercial cell used to evaluate the catalysts. Over a 40-h test, voltages for both alternate membranes were stable. With successful operation of the 50 μm material, this membrane was down-selected for the final milestone based on the higher efficiency and sufficient mechanical strength.

Catalyst-coated membranes were manufactured using Proton’s production process with the down-selected membrane and catalyst. The milestone target was to achieve a <1.7 V operating cell potential at 1.8 A/cm² and 30 bar. System temperature was held at 80°C and data was collected for 7 h. As shown in Figure 3 the target of <1.7 V was achieved and held throughout the test, successfully meeting the go/no-go milestone targets. The results from this test indicate a lower-heating-value and higher-heating-value efficiency of 73% and 88%, respectively. Ongoing work is occurring through node resources at LBNL to evaluate specific creep properties as a function of hydration conditions for each membrane to predict long-term performance. Additional work was also performed with node resources at NREL to develop alternate catalyst deposition processes capable of higher loading precision and uniformity. Decals were successfully printed on polytetrafluoroethylene but transfer to membranes was incomplete. The next budget period will evaluate other deposition substrates.

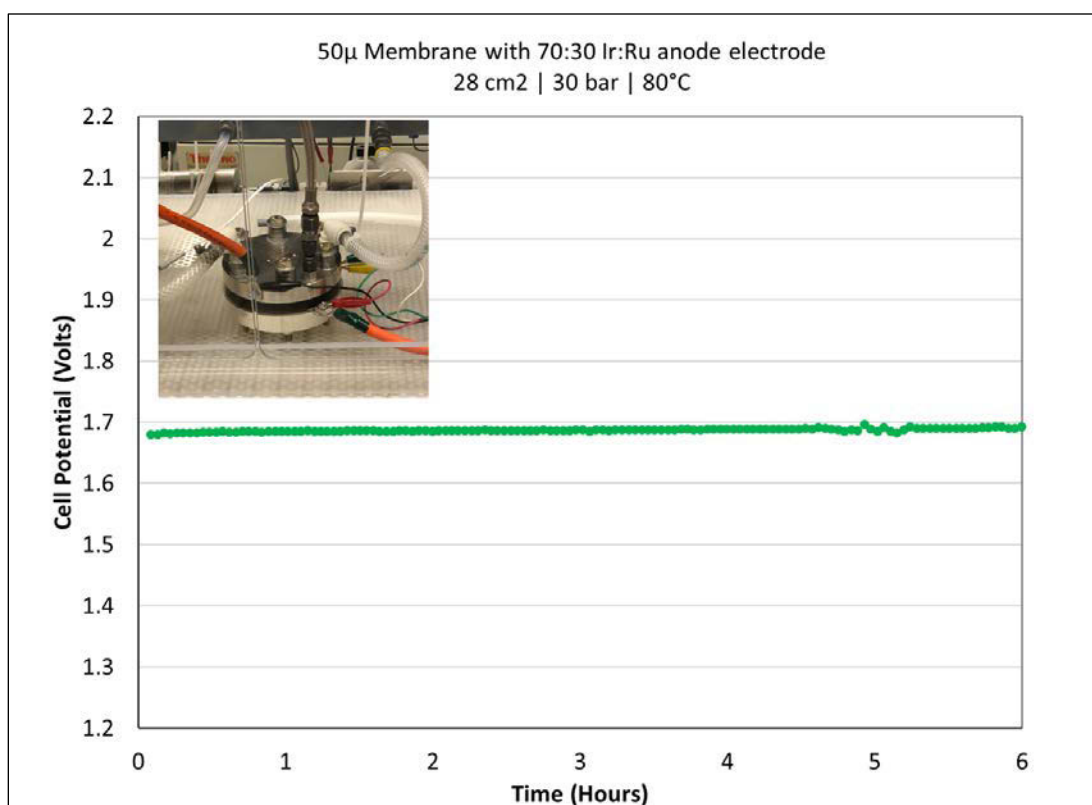


Figure 3. Steady-state data of high-efficiency MEA for go/no-go milestone

To support the next phases of development, detailed characterization of the PTL was performed. Neutron imaging of the porosity was performed, with imaging during operation at up to 2 A/cm² to attempt to determine water distribution as well. Tortuosity and porosity could be determined for different types of PTLs, but distinguishing water from air in the titanium matrix has proved challenging. The pore structure has been used to guide development of a cell-level model with node resources at LBNL to simulate PEM electrolyzer performance. Polarization curves are being simulated and parameters adjusted to better predict actual performance.

CONCLUSIONS AND UPCOMING ACTIVITIES

Advanced catalysts and membranes were separately evaluated to determine optimal materials and verify stability before integration. Proton successfully synthesized high-activity catalyst powders that have translated into measurable improvements in performance during operational tests. An improved membrane was identified that showed higher in-cell performance, supporting operating conditions of 1.8 A/cm², 80°C, and 30 bar differential pressure. The Year 1 go/no-go milestone was achieved with stable performance of the advanced integrated high-efficiency MEA at <1.7 V and 1.8 A/cm². Supporting efforts at NREL and LBNL to characterize the catalyst and membrane materials also contributed to the down-select and confidence in the materials selected. In-depth characterization and modeling of the PTL is ongoing to support testing under harsher conditions such as higher current and lower catalyst loading.

In the next phase of the project, Proton will continue to explore catalyst synthesis methods and alternative compositions to further enhance performance and identify other methods of manufacture of the electrodes for improved utilization. In addition, lower loading targets will be considered as a means of additional cost reductions. Longer-term testing and stress testing will be conducted on the materials described within this report, as well as testing of multiples to show repeatability. Specific next steps include:

- Complete time-dependent mechanical tests versus hydration condition for remaining membrane materials.
- Analyze PTL imaging data and try to understand whether there is a correlation between bubble formation and PTL type.
- Leverage reconstructed images to develop a micro-scale model that can be used study the effect of the micro-structure of porous layers.
- Validate the differential cell model at all operating conditions within 10% of experimental polarization data.
- Include the effect of hydrogen crossover in the two-dimensional model.
- Complete accelerated stress test cycling of MEAs fabricated with advanced catalysts and send to Oak Ridge National Laboratory for characterization of catalyst migration

FY 2018 PUBLICATIONS/PRESENTATIONS

1. K.E. Ayers, W.L. Gellett, and C.B. Capuano, “Electrochemical Generation of Fuels: Matching Research and Application for Advanced Water Splitting and Other Technologies,” Electrochemical Society Meeting Spring 2018.
2. K. Ayers and C. Capuano, “High Efficiency PEM Water Electrolysis Enabled by Advanced Catalysts, Membranes and Processes,” DOE Annual Merit Review and Peer Evaluation Meeting 2018.
3. K. Ayers and C. Capuano, “High Efficiency PEM Water Electrolysis Enabled by Advanced Catalysts, Membranes and Processes,” Electrochemical Society Meeting Fall 2018.

HydroGEN Seedling: Enabling Efficient Water Splitting with Advanced Materials Designed for High-pH Membrane Interface

Sanjeev Mukerjee
Northeastern University
360 Huntington Ave
Boston, MA 02115
Phone: (617) 373-2382
Email: s.mukerjee@northeastern.edu

DOE Manager: David Peterson
Phone: (720) 356-1747
Email: David.Peterson@ee.doe.gov

Subcontractors:

- University of Delaware, Newark, DE
- Advent North America, Cambridge, MA

Project Start Date: October 1, 2017
Project End Date: December 31, 2020

- Establish a requisite baseline overpotential of 150 mV at 500 mA/cm² for a supported metal/metal-oxide OER catalyst.
- Synthesize a multi-ammonium-cation side chain-based poly(aryl piperidinium) polymer (PAP-TQN) anion exchange polymer with the requisite durability (ion exchange capacity [IEC] loss of 20% or less after a 1,000-hour treatment in 1 M KOH at 95°C) and ionic conductivity (0.15 Ω-cm²).
- Initiate collaboration with Energy Materials Network (EMN) partners for subsequent determination of the physical properties of anion exchange materials and theoretical characterization of the electrode/electrolyte interface.

Overall Objectives

- Evaluate various transition metal moieties as hydrogen evolution reaction (HER) catalysts for anion exchange membrane electrolyzers (AEMELs).
- Optimize the support material for AEMEL oxygen evolution reaction (OER) catalysts.
- Develop, optimize, and characterize novel anion exchange membrane (AEM) and ionomer materials for high-temperature operation.
- Develop methods for AEMEL electrode preparation that supports high current density, efficient gas evolution, and low resistance.
- Elucidate the influence of the electrode/electrolyte interface on the kinetics of the HER and OER.

Fiscal Year (FY) 2018 Objectives

- Determine the HER activity of transition-metal catalysts. Appropriate catalysts must demonstrate an overpotential of 300 mV at 500 mA/cm².

Technical Barriers

This project addresses the following technical barriers from the Hydrogen Production section of the Fuel Cell Technologies Office Multi-Year Research, Development, and Demonstration Plan¹:

- System Efficiency and Electricity Cost.

Technical Targets

The overall project goal is cell-level performance of 1.76 V at 1 A/cm², which meets the Fuel Cell Technologies Office efficiency target of ≤\$2/kg at an efficiency of 43 kWh/kg. Component performance targets have been established using a porous electrode model to support the overall cell performance target. At the modeled scale of 50,000 kg/day and operating at 1 A/cm², the hydrogen cost is \$2.15/kg, \$1.82/kg, or \$1.76/kg, respectively, for 2, 20, or 200 plants. In the low-volume manufacturing case, it is still possible to meet the cost target by operating near 1 A/cm², sacrificing some efficiency. The overall project goals described above will be achieved by meeting the component targets outlined in Table 1.

¹ <https://www.energy.gov/eere/fuelcells/downloads/fuel-cell-technologies-office-multi-year-research-development-and-22>

FY 2018 Accomplishments

- Developed a functionalized Ni HER catalyst capable of operating at 500 mA/cm² with an overpotential of 94 mV.
- Used a NiFe/Raney Ni catalyst to achieve the requisite baseline OER overpotential of 150 mV at 500 mA/cm².
- Achieved an AEM membrane electrode assembly performance of 1.92 V at 800 mA/cm².
- Synthesized a multi-cation anion exchange polymer capable of operation at elevated temperatures (<60°C).
- Leveraged the expertise in molecular dynamics and density functional theory of our EMN collaborators to gain key insights into chemical processes at the electrode surface. The main findings from this collaboration are the following.
 - A nickel oxide surface can adsorb twice as much water as a nickel metal surface. The adsorption of water and the subsequent abstraction of a proton is the rate-determining step of hydrogen production. (Sandia National Laboratories).
 - The sequestration of carbonate anions from the electrolyte (1% potassium carbonate) causes a pH shift at the OER electrode and results in the loss in voltage (Lawrence Berkeley National Laboratory).
 - Membranes exhibit amorphous nature throughout the range of ion exchange moieties and temperatures (Lawrence Berkeley National Laboratory).
 - Durability studies independently verified the go/no-go point of less than 20% loss of IEC after 1,000-h test using 1 M KOH at 90°C (National Renewable Energy Laboratory).

Table 1. Component Targets

Target	Units	End of Project	Budget Period 1
Cell voltage	V	1.76	1.92
Current density	A/cm ²	1	0.8
Operating temperature	°C	95	85
Membrane area specific resistance	Ω·cm ²	0.08	0.15
Membrane OH ⁻ conductivity	S/cm	0.1	0.076
Cathode overpotential at design point	mV	150 mV @ 0.5 A/cm ²	300 @ 0.5 A/cm ²
Anode overpotential at design point	mV	100 mV @ 0.5 A/cm ²	150 @ 0.5 A/cm ²

INTRODUCTION

Reducing the materials cost of water electrolyzers, in particular the platinum group metal (PGM) OER and HER catalysts, is a key component for meeting DOE's goal of a \$2.00/kg levelized cost of hydrogen by 2020. The relatively recent development of AEMs allows for the use of low-cost non-PGM catalysts. In terms of OER, many studies indicate that Ni-Fe mixed oxides provide a greatly increased OER activity in comparison to pure Ni electrodes or other binary mixed oxides [1]. On the HER side, enhanced HER has been reported on Ni/MO_x by Markovic et al. [2] and Gong et al. [3]—both of whom suggested that at adjacent metal/metal-oxide sites, the metal-oxide facilitates the formation of OH_{ads}, thus weakening the H-OH bond in “activated water” and reducing activation energy for the Volmer reaction.

Operating AEMs at elevated temperatures will increase the reaction kinetics and improve performance. However, the most technologically mature anion exchange polymers cannot be used at operating temperatures >60°C for extended periods of time. Novel anion exchange materials will also be developed in the course of this project that will be thermally stable and incorporate multiple ion exchange sites.

APPROACH

This project will improve the existing NiFe OER catalyst by refining the Raney Ni support. The synthetic route involved a modified impregnation method using aniline to form an MMO as a two-dimensional film on Raney-Ni support. Despite these successes, the activity is severely limited by the relatively low surface area of Raney Ni as well as the low density of active sites. We aim to address these issues by increasing the surface area of Raney Ni support via a novel metal organic chemical vapor deposition method and increasing the active site density by developing novel polymer precursors.

Three nickel-based catalysts will be synthesized and evaluated for HER activity. NiCr/C (60% metal 1:1 Ni:Cr) provides an oxophilic metal oxide surface for the adsorption of water; chromium remains oxidized at potentials relevant to AEM operation. A functionalized monometallic nickel catalyst synthesized via heat treatment of a nickel complex chelated in the presence of a carbon support has been shown to stabilize the Ni/NO_x interface under HER conditions. Metal-organic framework (MOF)-derived electrocatalysts have already been extensively explored for various applications including oxygen reduction reaction (ORR)/OER [4] and HER [5]. The sacrificial MOF support with high nitrogen content and high microporous surface area leads to high reactivity due to the combination of inherited exceptional active site density and enhanced mass transport property. We recently demonstrated a MOF-derived Fe-N-C catalyst with ORR activity approaching that of Pt/C in both rotating disk electrode and polymer electrolyte membrane fuel cells [6]. This promising result encourages further development of metal-nitrogen-carbon catalysts for HER. As a result of initial water electrolysis testing, one or more of these catalysts will be down-selected.

The chemical stability of the poly(aryl piperidinium) (PAP) AEMs is derived from the combination of the stable piperidinium cation and the ether-bond-free aryl backbone. In addition, the rigid and hydrophobic aryl backbone enables an unprecedented combination of a high IEC and a low water uptake/swelling ratio, leading to high hydroxide conductivity and mechanical robustness. Preliminary results from one member of the PAP AEM family has already shown very high chemical stability, hydroxide conductivity and water uptake of 60 mS/cm and 25 wt% in pure water, respectively, and excellent mechanical strength (160 MPa stress). These properties translate to excellent device performance: an AEM fuel cell with a PAP membrane and the corresponding ionomer showed a peak power density of 530 mW/cm² at 95°C and demonstrated stable fuel cell performance at 90°C for 60+ h. In this project, more advanced AEMs based on the PAP polymer will be developed with multi-ammonium-cation side chain to realize superior hydroxide conductivity, chemical stability, and mechanical properties.

RESULTS

Poly(aryl piperidine) triphenyl monoquaternary ammonium (PAP-TP-MQN) was synthesized through the polymerization of 1,4-diphenyl benzene, 4-piperidinone, and 2,2,2-trifluoroacetophenone in the presence of triflic acid. Monoquaternary ammonium was synthesized through alkylation of trimethyl amine by 1,6-

iodohexane. PAP-TP was alkylated with monoquatary ammonium via the Menshutkin reaction. The resulting ionomer exhibited the high temperature and chemical stability of the baseline PAP-TP-Me ionomer with an additional anion exchange site to increase the ion conductivity. PAP-TP-MQN was subjected to 1,000-hour degradation study wherein the piece of membrane was held at 90°C while submerged in 1 M KOH. Analysis of the treated membrane with ^1H nuclear magnetic resonance (NMR) spectroscopy and titration showed a loss of IEC of 2% and 8%, respectively. Conductivity measurements conducted at 40°C and 95% relative humidity yielded a value of 30 mS/cm, which translates to an area-specific resistivity of 0.1225 $\Omega\cdot\text{cm}$. Figure 1 summarizes the ^1H NMR degradation analysis and conductivity measurements. The values for IEC loss and area-specific resistivity fall below the go/no-go values of 20% and 0.15 $\Omega\cdot\text{cm}$, respectively.

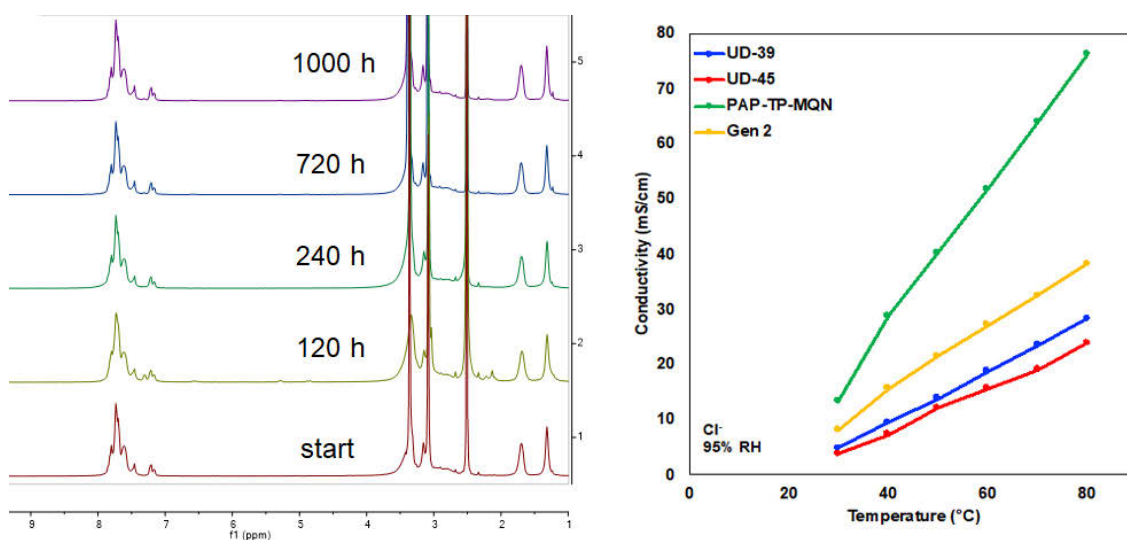


Figure 1. (Left) ^1H NMR spectra of PAP-TP-MQN after treatment in 1 M KOH at 90°C taken at various intervals. The peaks at 3.4 ppm correspond to alkyl groups bound to amines and are used to derive IEC. (Right) The conductivity of PAP-TP-MQN, PAP-TP-Me (UD-39,45), and reference data (Gen 2) taken at different temperatures at 95% relative humidity.

Three Ni-based materials were considered as possible HER catalysts for use in AEMELs for the duration of this project. Briefly, NiCr/C is a bifunctional catalyst where the chromium component remains oxidized at cathodic potentials relevant to normal AEMEL operation. The oxide moieties of this catalyst serve as favorable sites for water adsorption facilitating the breaking of the O-H bond. Preparing a functionalized nickel catalyst was another approach for HER catalysis. Here, a nickel salt was treated with an organic chelating agent, cupferron, in the presence of an appropriate carbon support and heat treated at 700°C. The heat treatment served two purposes: (1) to reduce the nickel via carbonization, and (2) form a graphitic shell around the nickel, presumably from the pyrolyzed chelating agent. The resulting catalyst, referred to as Ni-cup/C, shows high HER activity as well as anodic and cathodic stability. We hypothesize that the increased activity is a result of the graphitic shell around the Ni metal, which reduces, but does not eliminate, the formation of non-conductive metal oxide/hydroxides while retaining a certain amount of these moieties to facilitate water adsorption. Ni-MOF was synthesized via the heat treatment of ZIF-8, nickel acetate, and phenanthroline monohydrate under an ammonia atmosphere.

Of these three catalysts, NiCr/C and Ni-cup/C were tested in a hydrogen pump cell. The goal of this experiment was to assess the HER performance of these catalysts without the sluggish reaction kinetics of the OER in an AEMEL. Figure 2 (left) shows the polarization curves of these cells. Of the two, the cell equipped with a Ni-cup HER catalyst met the milestone of $\eta \leq 300$ mV at 500 mA/cm². All three catalysts were tested in an AEMEL with 1% K₂CO₃ electrolyte solution flowing over the OER catalyst and no reactant feed across the HER electrode. These cells used an iridium oxide OER catalyst and a PAP-TP-Me membrane and operated at 50°C. Based on these series of experiments (Figure 2, right), the Ni-MOF catalyst was eliminated as a viable

HER catalyst, while the NiCr/C and Ni-cup/C would be used in subsequent electrolysis studies. These activities satisfy interim milestones as well as the go/no-go milestone for HER catalysis.

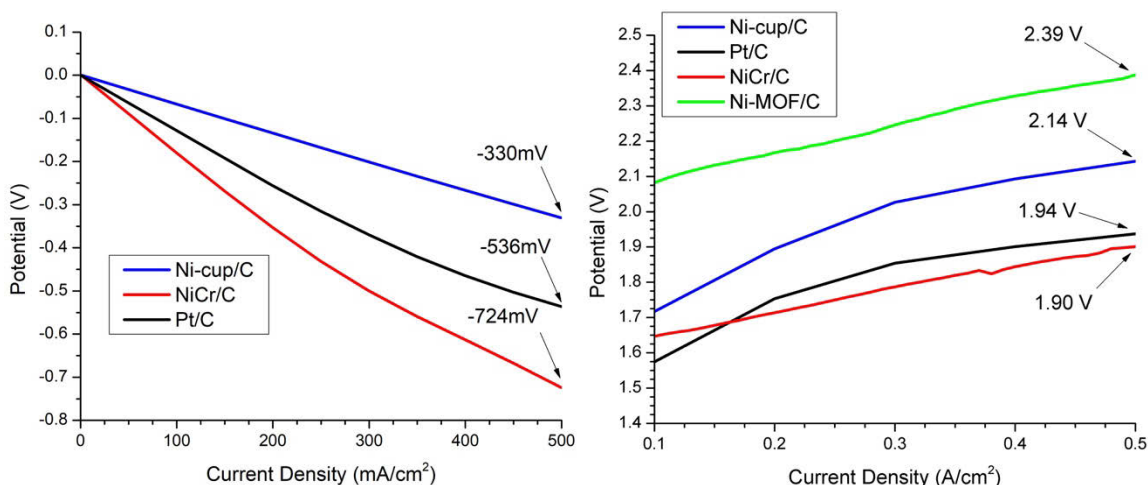


Figure 2. (Left) Polarization curves collected from hydrogen pump fuel cells each with a Pt/C OER catalyst and a Ni-cup, NiCr/C, or Pt/C HER catalysts. (Right) A comparison of polarization curves collected from AEMELs each with an iridium oxide OER catalyst and a Pt/C, Ni-cup/C, NiCr/C, or Ni-MOF HER catalyst.

The NiFe/Raney Ni was synthesized in significant quantities to satisfy the interim milestone for OER catalysis. Briefly, Ni and Fe nitrate salts were added to a slurry of Raney Ni in the presence of aniline, which served as a capping agent. A solution of NaBH₄ was added dropwise to the mixture to yield the catalyst. Figure 3 shows the polarization curve of an AEMEL cell equipped with a NiFe/Raney Ni OER electrode and Pt/C HER electrodes operating under the same conditions described in the previous paragraph. The cell required ~1.8 V to achieve a current density of 500 mA/cm². This performance is 81 mV less than that of a similar cell using IrO_x black reference OER catalysts at the same current density and satisfies the go/no-go milestone of $\eta \geq 150$ mV at 500 mA/cm². This is made on the basis of corresponding overvoltage of 450 mV on the HER electrode.

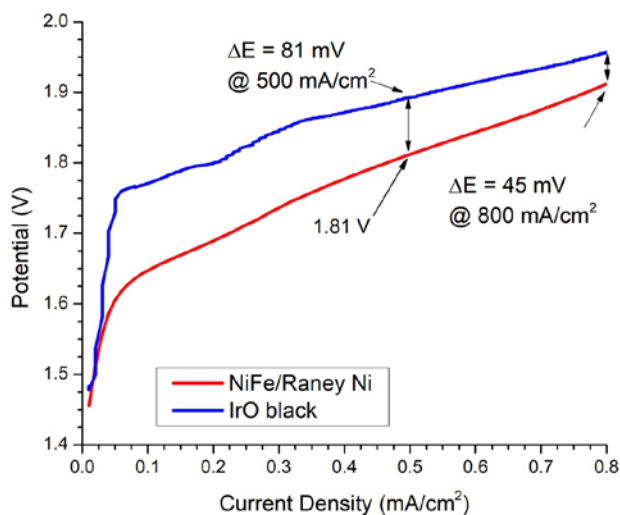


Figure 3. Polarization curves of AEMELs with NiFe/Raney and iridium oxide OER catalysts. Both cells used a Pt/C HER catalyst.

Two non-PGM membrane electrode assemblies were prepared using a NiCr/C or Ni-cup/C HER catalyst, NiFe/Raney Ni OER electrode, and PAP-TP-MQN membrane. Both were operated with 1% K₂CO₃ flowing across the OER electrode and no solution across the HER electrode. Polarization curves obtained at 50°C and 85°C are shown in Figure 4. As expected, both cells demonstrate a substantial increase in performance at higher temperatures. Sustained operation at 85°C is enabled by the ionomer materials developed for this project. At 85°C, 1.92 V and 1.95 V was required to achieve a current density of 800 mA/cm² in cells equipped with the NiCr/C and Ni-cup/C HER catalysts, respectively. This performance meets the go/no-go milestone for the non-PGM membrane electrode assembly of 1.92 at 800 mA/cm².

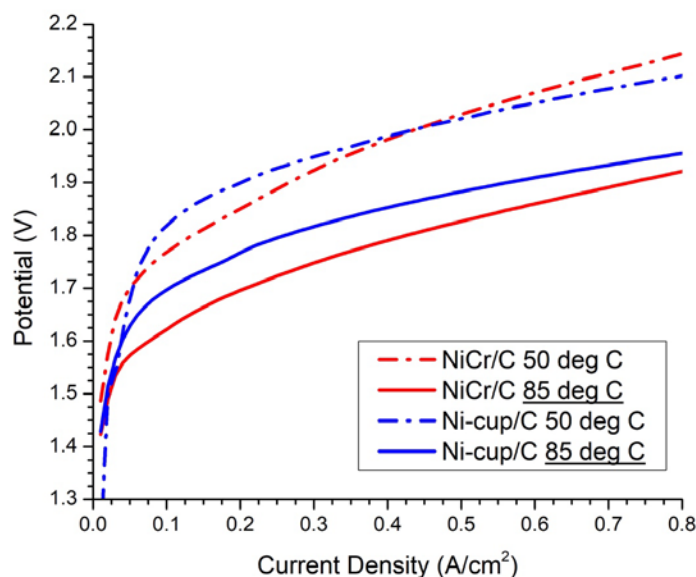


Figure 4. Polarization curves of AEMEs with NiCr/C and Ni-cup/C HER catalysts collected at 50°C and 85°C. Both cells used a NiFe/Raney Ni OER catalyst.

CONCLUSIONS AND UPCOMING ACTIVITIES

This project has met or exceeded all of the go/no-go milestones presented in Budget Period 1. In Budget Period 2 and 3, advanced electrode fabrication techniques together with further improvements in catalysts will be employed to increase the performance of the HER catalyst. Currently, commercially available Raney Ni support cannot accommodate higher loadings of NiFe. The plausibility of using chemical vapor deposition to increase NiFe loading will be investigated. The increased anion exchange sites of PAP-TP-MQN (versus baseline material) has had the unintended consequence of higher water uptake resulting in decreased mechanical stability and swelling of 22%–47%. We will seek to mitigate these negative effects by introducing various support substrates (e.g., polytetrafluoroethylene) to the membrane.

SPECIAL RECOGNITIONS AND AWARDS/PATENTS ISSUED

1. “Nitrogen Functionalized Platinum-Iridium Electrocatalyst,” U.S. patent application US180131008A1, 2018.

FY 2018 PUBLICATIONS/PRESENTATIONS

Peer-Reviewed Publications

1. Ershuhai Liu, Li Jiao, Huong Doan, Zeyan Liu, Yu Huang, Kuzhikalail M. Abraham, and Sanjeev Mukerjee, “Unifying Alkaline Hydrogen Evolution/Oxidation Reaction Kinetics by Identifying the Role of Hydroxy-Water-Cation Adducts,” Resubmitted to *JACS* (2018).

2. Qingying Jia, Ershuhai Liu, Li Jiao, and Sanjeev Mukerjee, “Current Understanding of Sluggish Kinetics of Hydrogen Evolution and Oxidation reactions in Base,” *Current Opinion in Electrochemistry* (In Press).

Presentations at National Meetings and Workshops

1. Sanjeev Mukerjee and Qingying Jia, “Fundamental aspects of regenerative hydrogen electrocatalysis in alkaline pH,” *Abstracts of Papers of the American Chemical Society* 256 (2018).
2. Sanjeev Mukerjee, Jingkun Li, and Qingying Jia, “Current Understandings of the Slow Kinetics of the Hydrogen Evolution Reaction in Alkaline Media,” *Meeting Abstracts 29* (The Electrochemical Society, 2018): 1703–1703.
3. Qingying Jia, Jingkun Li and Sanjeev Mukerjee, “Understanding the Improved Kinetics of the Hydrogen Evolution/Oxidation Reactions on Pt-Oxophilic Metal Systems in Alkaline Media,” *Meeting Abstracts 29* (The Electrochemical Society, 2018): 1710–1710.
4. Ian Kendrick, Michael Bates, Qingying Jia, Huong Doan, Wentao Liang and Sanjeev Mukerjee, “Tuning Ni Surfaces for Enhanced Oxygen Evolution Reaction,” *Meeting Abstracts 29* (The Electrochemical Society, 2018): 1702–1702.

REFERENCES

1. Lena Trotochaud et al., “Solution-Cast Metal Oxide Thin Film Electrocatalysts for Oxygen Evolution,” *Journal of the American Chemical Society* 134, no. 41 (2012): 17253–61; Mary W. Louie and Alexis T. Bell, “An Investigation of Thin-Film Ni–Fe Oxide Catalysts for the Electrochemical Evolution of Oxygen,” *Journal of the American Chemical Society* 135, no. 33 (2013): 12329–37.
2. N. Danilovic et al., “Enhancing the Alkaline Hydrogen Evolution Reaction Activity through the Bifunctionality of Ni (OH) 2/Metal Catalysts,” *Angewandte Chemie* 124, no. 50 (2012): 12663–66.
3. Ming Gong et al., “Nanoscale Nickel Oxide/Nickel Heterostructures for Active Hydrogen Evolution Electrocatalysis,” *Nature Communications* 5 (2014).
4. Jingkun Li et al., “Structural and Mechanistic Basis for the High Activity of Fe–N–C Catalysts toward Oxygen Reduction,” *Energy & Environmental Science* 9, no. 7 (2016): 2418–32; Shenlong Zhao et al., “Ultrathin Metal–organic Framework Nanosheets for Electrocatalytic Oxygen Evolution,” *Nature Energy* 1 (2016): 16184; Jun Wang et al., “Synergistic Effect between Metal–Nitrogen–Carbon Sheets and NiO Nanoparticles for Enhanced Electrochemical Water-Oxidation Performance,” *Angewandte Chemie International Edition* 54, no. 36 (2015): 10530–34.
5. Huilong Fei et al., “Atomic Cobalt on Nitrogen-Doped Graphene for Hydrogen Generation,” *Nature Communications* 6 (2015); Lili Fan et al., “Atomically Isolated Nickel Species Anchored on Graphitized Carbon for Efficient Hydrogen Evolution Electrocatalysis,” *Nature Communications* 7 (2016).
6. Jingkun Li et al., “Structural and Mechanistic Basis for the High Activity of Fe–N–C Catalysts toward Oxygen Reduction,” *Energy & Environmental Science* 9, no. 7 (2016): 2418–32.

HydroGEN Seedling: Platinum-Group-Metal-Free Oxygen Evolution Reaction Catalysts for Proton Exchange Membrane Electrolyzers

Di-Jia Liu (Primary Contact), Lina Chong,
Hao Wang

Argonne National Laboratory
9700 South Cass Avenue
Lemont, IL 60439
Phone: (630) 252-4511
Email: djliu@anl.gov

DOE Manager: David Peterson
Phone: (720) 356-1747
Email: David.Peterson@ee.doe.gov

Subcontractors:

- State University of New York at Buffalo, Buffalo, NY
- Giner, Inc., Newton, MA

Project Start Date: October 1, 2017
Project End Date: September 30, 2020

Overall Objectives

- Reduce proton exchange membrane (PEM) electrolyzer capital cost by developing transition-metal-based catalysts as the replacements for platinum-group-metal (PGM) materials for oxygen evolution reaction (OER) in the PEM electrolyzer.
- Support the low-temperature water electrolyzer system cost reduction to meet the DOE hydrogen production target of \$2/kg H₂ while maintaining the system efficiency at 43 kWh/kg H₂.

Fiscal Year (FY) 2018 Objectives

- Design and test at least 10 PGM-free OER catalysts derived from transition metal metal-organic frameworks (MOFs).
- Design and test at least four PGM-free OER catalysts with porous nano-network electrode architecture.
- Prepare at least 10 membrane electrode assemblies (MEAs) containing PGM-free

anode catalyst and evaluate them under PEM electrolyzer operating conditions.

- Demonstrate one or more PGM-free OER catalysts with potential of <15 mV higher than commercial Ir black measured at current density of 10 mA/cm² or MEA electrolyzer with current density >200 mA/cm² at 1.80 V.

Technical Barriers

This project addresses the following technical barriers from the Hydrogen Production section of the Fuel Cell Technologies Office Multi-Year Research, Development, and Demonstration Plan¹:

- Cost: low-cost PGM-free OER catalyst as the replacement for Ir in PEM electrolyzer.
- Footprint: lower hydrogen production footprint with PEM electrolyzer of high ion conductivity.
- Renewable energy integration: remove capital cost barrier of PEM electrolyzer for broadly implemented distributed renewable energy application.

Technical Targets

This project aims to develop anodic PGM-free OER catalysts for PEM electrolyzers that meet the following DOE hydrogen production targets:

- Cost: \$2/kg H₂
- System efficiency: 43 kWh/kg H₂.

FY 2018 Accomplishments

- Argonne National Laboratory (ANL) developed two series of MOF-derived PGM-free OER catalysts, ANL-Cat-A and ANL-Cat-B; both demonstrated less than 15 mV difference from Ir black (at 0.1 mg/cm² loading) when tested in acidic electrolyte.
- The University at Buffalo developed several OER catalysts derived from Fe, Co, Mn, and Ni

¹ <https://www.energy.gov/eere/fuelcells/downloads/fuel-cell-technologies-office-multi-year-research-development-and-22>

doped ZIF-8 and demonstrated improved performance.

- ANL-Cat-A and -Cat-B showed only minor activity loss (24 mV and 22 mV at 10 mA/cm²) after 10,000 voltage cycles from 1.2 to 2.0 V by rotating disk electrode (RDE) in strong acidic electrolyte. Both catalysts showed better catalyst stability than low-loading Ir black (at 0.1 mg/cm² loading) tested under the same cycling condition.
- Both ANL-Cat-A and -Cat-B were incorporated into the anode of a PEM electrolyzer and achieved 250 mA/cm² and 300 mA/cm² at 1.8 V under the operating condition at Giner, respectively, meeting go/no-go decision criteria.

INTRODUCTION

This project aims to develop next-generation, high-efficiency, and durable PGM-free OER catalysts for the PEM electrolyzer through the collaboration between ANL, University at Buffalo, and Giner, Inc. (Giner) leveraging the multiple capability nodes at the HydroGEN consortium. It is based on an initial success in demonstrating highly active PGM-free electrocatalyst in an acidic medium at Argonne National Laboratory [1–3]. The new catalysts are composed of porous yet stable transition-metal composite incorporated in a 3-D nano-network electrode architecture with potential to be inexpensive, highly active, and resistant to the oxidation corrosion during OER. The project goal is to produce one or more durable PGM-free OER catalysts with the performance approaching that of current Ir-based catalysts at <1/20 of the cost, demonstrated through the operating PEM electrolyzer.

APPROACH

This project focuses on design and synthesis of a new class of PGM-free OER catalyst for PEM electrolyzers. The new catalysts consist of highly porous yet stable transition-metal composite derived from the MOFs. The new catalysts will also be integrated into a porous nano-network electrode architecture to further improve the conductivity, mass transport, and durability against oxidative corrosion (Figure 1). The catalyst development was carried out at both ANL and University at Buffalo. The activity and durability of the new catalysts are first evaluated by the RDE method in the acidic electrolyte. The catalysts that demonstrate promising performance will then be integrated into the membrane electrode and tested under the operating PEM electrolyzer at Giner.

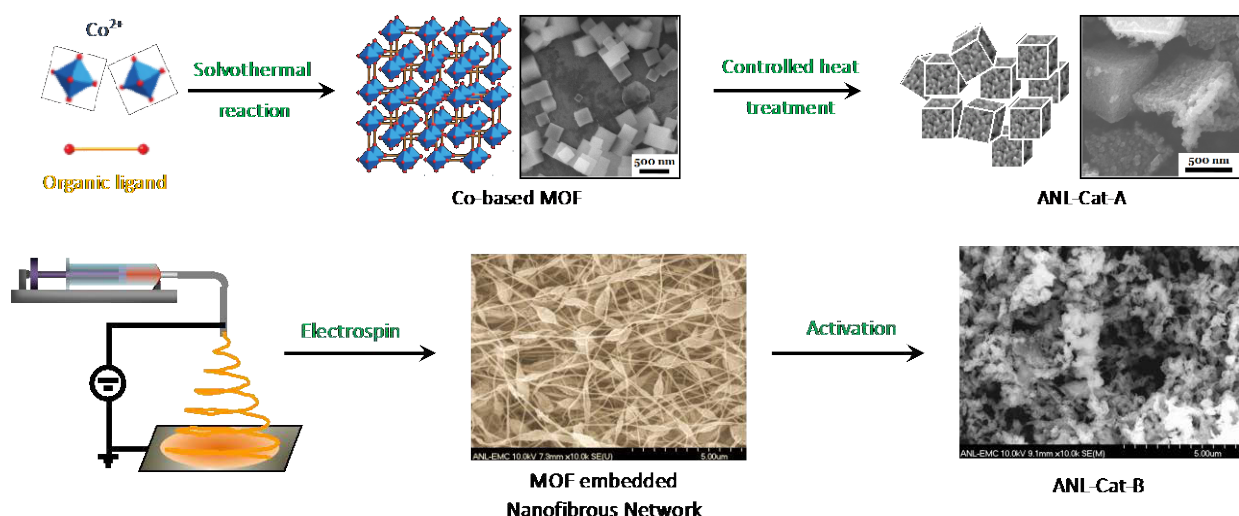


Figure 1. Synthesis scheme of ANL-Cat-A OER catalyst and ANL-Cat-B OER catalyst

As a seedling project under HydroGEN, this project leverages the expertise in the consortium in supporting the catalyst development. The specific nodes include Lawrence Berkeley National Laboratory’s (LBNL’s) “DFT and Ab Initio Calculations for Water Splitting Including Real-Time Time-Dependent Density Functional Theory,” Lawrence Livermore National Laboratory’s (LLNL’s) “Multiscale Modeling of Water-Splitting Devices,” National Renewable Energy Laboratory’s (NREL’s) “Surface Analysis Cluster Tool,” Sandia National Laboratories’ (SNL’s) “Advanced Electron Microscopy,” and NREL’s “Electrolysis Catalyst Synthesis, Ex Situ Characterization, and Standardization.”

RESULTS

This seedling project started in FY 2018. The tasks at ANL focused on developing cobalt-based OER catalysts derived from MOFs through facile solvothermal or solid-state syntheses. Two catalyst series—ANL-Cat-A and ANL-Cat-B—were developed and investigated in parallel using MOFs as sacrificial precursors through thermal activation. Meanwhile, the University at Buffalo team focused on OER catalysts derived from zeolitic

imidazolate frameworks (ZIFs) containing various combination of Fe, Co, Mn, and Ni after heat treatment. The OER catalyst activities were measured by the catalytic layer coated over rotating disk or carbon paper in strongly acidic media. Figure 2A shows the OER current density as the function of the polarization potential of a representative ANL-Cat-A with the catalyst loading of 2 mg/cm². For comparison, the same polarization was performed over Ir-black catalyst at the loading of 0.2 mg/cm². The OER potential measured at current density of 10 mA/cm² typically served as the gauge of activity. In this case, ANL-Cat-A achieved an OER potential of 1.584 V vs. reversible hydrogen electrode (RHE), which is only 29 mV higher than that of the Ir black benchmark.

The catalyst durability was measured through the multiple potential cycling from the voltage of 1.2 V to 2.0 V (vs. RHE) in the acidic electrolyte. Figure 2B shows the percentage of current density retention measured against the initial value at 1.8 V and 2.0 V during 2,000 voltage cycles. For ANL-Cat-A catalyst, the current density retentions of 90% and 80% were achieved at 1.8 V and 2.0 V, respectively. In contrast, the percentage of the current density retention for Ir black was dramatically decreased to 10% after only 1,000 voltage cycles. Both ANL catalysts demonstrated excellent activity and durability over most of the PGM-free catalysts in acidic medium reported in the literature so far.

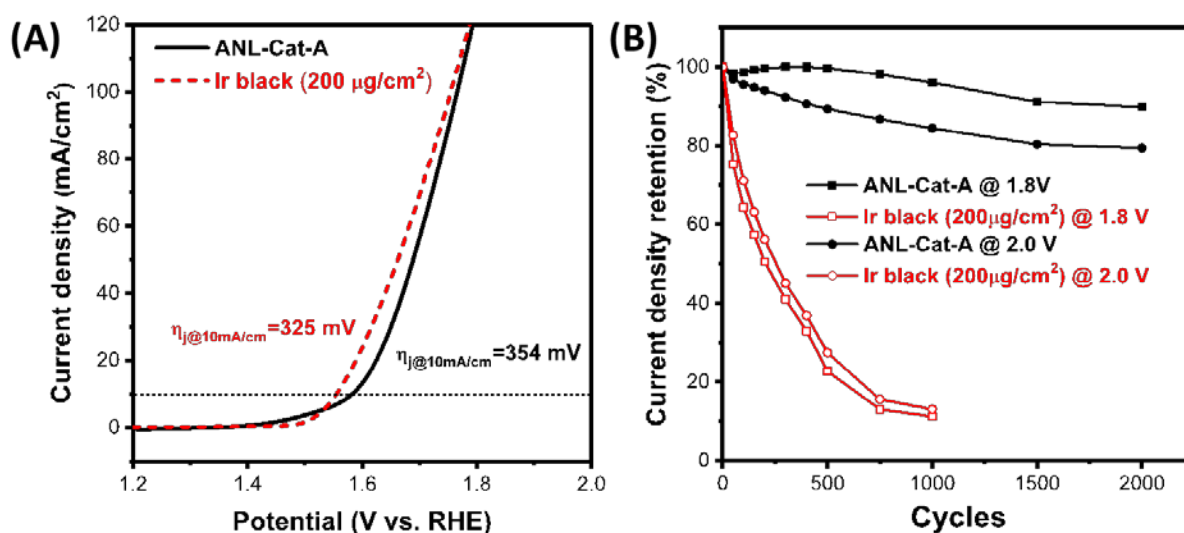


Figure 2. (A) OER current density as the function of polarization voltage measured over ANL-Cat-A catalyst and Ir black in 0.5 M H₂SO₄ electrolyte solution. (B) The retention of OER current densities measured at 1.8 V and 2.0 V for ANL-Cat-A catalyst and benchmark Ir black during 2,000 voltage cycles from 1.2 V to 2.0 V.

Several catalysts from the ANL-Cat-A and -Cat-B series were selected for evaluation in the operating PEM electrolyzer at Giner. A significant amount of effort was first devoted to the MEA optimization at ANL due to the limited knowledge in integrating the catalysts of different conductivity and morphology than the conventional electrocatalyst. Important processing parameters, such as anode catalyst loading, ionomer-to-catalyst ratio, pretreatment, and application methods, have been systematically studied. Fifteen MEAs with ANL's PGM-free OER catalysts were sent to Giner and evaluated under PEM electrolyzer operating conditions (60°C and ambient pressure). Several MEAs demonstrated OER current density >200 mA/cm² at 1.8 V. Figure 3 shows the current-voltage polarization curve of a representative MEA with anode containing ANL-Cat-B catalyst. The current density reached 300 mA/cm² at 1.8 V, exceeding the DOE Phase I go/no-go decision criteria.

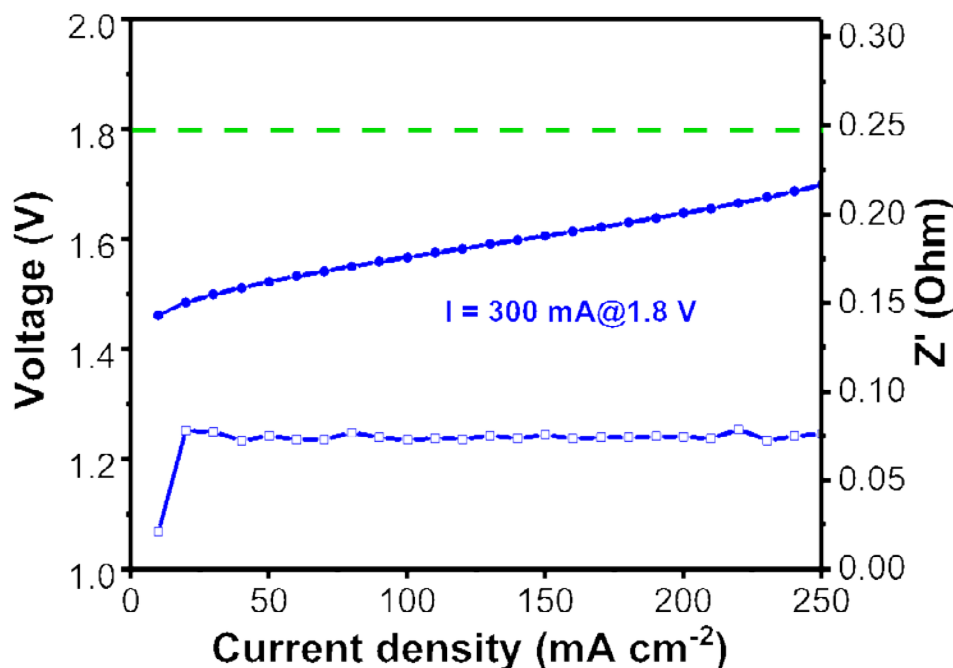


Figure 3. The current-voltage polarization of an MEA containing a representative ANL-Cat-B catalyst at anode in a PEM electrolyzer

CONCLUSIONS AND UPCOMING ACTIVITIES

ANL's PGM-free OER catalyst delivered promising performance in a PEM electrolyzer for the first time. The study clearly indicates the need to continually improve catalyst and MEA in order to compete with Ir catalyst. A PGM-free OER catalyst requires different MEA processing conditions than that in a PEM fuel cell due to the different nature of the catalyst (surface area, conductivity, operating environment, etc.) and therefore needs to be optimized accordingly. Similar to the oxygen reduction reaction catalyst, the PGM-free OER catalyst also faces stability challenges although the deactivation mechanisms are unlikely to be the same.

The project now moves to Phase II with the following research focuses:

- Improvement of OER activity through catalyst design and refinement by reprioritizing the synthesis approach and formulation, with more focus on durability and conductivity.
- MEA fabrication and testing through optimizing catalyst loading, ionomer-to-catalyst ratio, and application techniques.
- Exploration of new synthesis techniques and catalyst material with higher stability and acid resistance.
- Collaboration with HydroGEN in fundamental understanding and catalyst characterization through modeling (LLNL/Brookhaven National Laboratory), imaging (SNL), and material characterization and MEA development (NREL).

SPECIAL RECOGNITIONS AND AWARDS/PATENTS ISSUED

1. "Nanofiber Electrocatalyst," Di-Jia Liu and Lina Chong, U.S. patent application filed in 2018.
2. "Prussian Blue Analogue-Derived Catalysts for PEM Electrolyzer," Di-Jia Liu and Hao Wang, U.S. patent application filed in 2018.

FY 2018 PUBLICATIONS/PRESENTATIONS

1. Di-Jia Liu, Lina Chong, Hao Wang, Gang Wu, and Hui Xu, “PGM-free OER Catalysts for PEM Electrolyzer,” Poster presentation at the 2018 DOE Hydrogen and Fuel Cells Program Annual Merit Review and Peer Evaluation Meeting, June 13-15, 2018, Washington, D.C.

REFERENCES

1. Dan Zhao, Jiang-Lan Shui, Lauren R. Grabstanowicz, Chen Chen, Sean M. Commet, Tao Xu, Jun Lu, and Di-Jia Liu, “Highly Efficient Non-Precious Metal Electrocatalysts Prepared from One-Pot Synthesized Zeolitic Imidazolate Frameworks (ZIFs),” *Advanced Materials* 26 (2014): 1093–1097.
2. Shengqian Ma, Gabriel Goenaga, Ann Call and Di-Jia Liu, “Cobalt Imidazolate Framework as Precursor for Oxygen Reduction Reaction Electrocatalyst,” *Chemistry: A European Journal* 17 (2011): 2063–2067.
3. Jianglan Shui, Chen Chen, Lauren R. Grabstanowicz, Dan Zhao and Di-Jia Liu, “High-Efficiency Non-Precious Metal Catalyst Containing Metal-Organic Framework Precursor Inside of Carbon Nano-Network,” *Proceedings of National Academy of Sciences* 112, no. 34 (2015): 10629–10634.

HydroGEN Seedling: High-Performance Ultralow-Cost Non-Precious-Metal Catalyst System for Anion Exchange Membrane Electrolyzer

Hoon Chung (Primary Contact, LANL),
Ulises Martinez (LANL), Barr Zulevi (PPC),
Alexey Serov (PPC)
Los Alamos National Laboratory (LANL)
P.O. Box 1663; MS D429
Los Alamos, New Mexico 87544
Phone: (505) 606-0570
Email: hchung@lanl.gov

DOE Manager: David Peterson
Phone: (720) 356-1747
Email: David.Peterson@ee.doe.gov

Subcontractor:
Pajarito Powder, LLC (PPC), Albuquerque, New Mexico

Project Start Date: October 1, 2017
Project End Date: Project continuation and
direction determined annually by DOE

Overall Objectives

- Develop low-cost, active, and durable platinum-group-metal-free (PGM-free) oxygen evolution reaction (OER) and hydrogen evolution reaction (HER) catalysts to achieve high performance in a pure water-feeding anion exchange membrane (AEM) water electrolyzer.
- Demonstrate AEM electrolyzer performance of 500 mA/cm² at 2.1 V with unlimited anode or cathode.
- Produce 25 g batch of the best-performing PGM-free catalyst.

Fiscal Year (FY) 2018 Objectives

- Demonstrate OER activity of 5.1 mA/cm² at 1.65 V_{RHE} and the same degradation rate as that of IrO₂ with 5,000 cycles durability test in the potential range of 0.6 and 2.1 V_{RHE} in rotating disk electrode (RDE) measurements.
- Demonstrate HER activity of 34 mA/cm² at a 200 mV overpotential and a durability of less than 20% current density loss at a 200 mV

overpotential with 5,000 cycles in the potential range of 0.2 and -0.25 V_{RHE} in RDE measurements.

Technical Barriers

This project addresses the following technical barrier from the Hydrogen Production section of the Fuel Cell Technologies Office Multi-Year Research, Development, and Demonstration Plan¹:

- Capital Cost: develop lower-cost materials with improved efficiency and durability.

Technical Targets

This project is conducting PGM-free OER and HER catalyst development in conjunction with fundamental studies of phenomena occurring at the interface of PGM-free catalyst and ionomer. The results gained from these studies will be applied toward the design and synthesis of PGM-free catalysts that meet the DOE hydrogen production cost target:

- Cost: <\$2/kg of H₂.

FY 2018 Accomplishments

- Carbon-free perovskite oxide OER catalysts demonstrated 87% improved current density of 5.6 mA/cm² in 0.1 M KOH and 177% improved current density of 8.3 mA/cm² in 0.1 M benzyltrimethylammonium hydroxide (BTMAOH) at 1.65 V_{RHE} compared to the initial state-of-the-art (SOA) current density of 3.0 mA/cm² at 1.65 V_{RHE} in 0.1 M KOH. Cyclic and constant voltage durability tests of the carbon-free perovskite oxide catalyst exhibited comparable durability to that of IrO₂ in RDE tests.
- In pure-water-feeding AEM electrolyzer tests, carbon-free perovskite oxide OER catalysts demonstrated better performance and durability than IrO₂.

¹ <https://www.energy.gov/eere/fuelcells/downloads/fuel-cell-technologies-office-multi-year-research-development-and-22>

- $\text{Ni}_{0.95}\text{La}_{0.05}$ HER catalyst demonstrated 110% improved current density of 42 mA/cm^2 at a 200 mV overpotential in 1.0 M NaOH compared to the initial SOA current density of 20 mA/cm^2 at a 200 mV overpotential with 19% current density loss at a 200 mV overpotential in cyclic durability tests.

INTRODUCTION

Precious-metal catalysts (i.e., platinum for cathode and iridium oxide for anode) are SOA catalysts for acidic polymer electrolyte membrane (PEM) electrolyzers and contribute in a major way to the cost of the PEM electrolyzers. Alternatively, alkaline AEM electrolyzers can take advantage of utilizing low-cost PGM-free catalysts for both anode and cathode. In preliminary experiments we have developed PGM-free OER and HER catalysts exhibiting promising performance in terms of activity and durability in an electrochemical cell. We will further develop these OER and HER catalysts for AEM electrolyzer applications. If successful, this project will overcome the cost barrier of hydrogen production technology associated with electrocatalysts, required to meet the DOE-established hydrogen production target of $< \$2/\text{kg H}_2$.

APPROACH

The chosen OER catalysts are perovskite oxides for the anode and bimetallic NiLa HER catalysts for the cathode. Specifically $(\text{La}_{0.85}\text{Sr}_{0.15})\text{CoO}_{3-\delta}$ (i.e., a perovskite with higher lanthanide and lower alkaline earth metal contents) was chosen to control the valence state of the transition metals. Bimetallic NiLa and Ni(Zn)La will be synthesized via spray pyrolysis as alternatives to Pt catalysts for the AEM electrolyzer cathode. The primary responsibilities of Pajarito Powder, LLC, the partner in this project, are to make 25-cm² membrane electrode assemblies (MEA), test the electrolyzer performance, and ultimately produce a 25-g batch of the best-performing PGM-free OER and/or HER catalysts. Four nodes are involved in this project: (1) “Separator for Hydrogen Production” (Cy Fujimoto, Sandia National Laboratories) for AEM synthesis; (2) “Hydrogen in situ Testing Capabilities for Hydrogen Generation” (Guido Bender, National Renewable Energy Laboratory) for AEM electrolysis testing; (3) “Surface Analysis Cluster Tool” (Glenn Teeter, National Renewable Energy Laboratory) for composition analyses; and (4) “Density Functional Theory and Ab initio Calculations” (Lin-Wang Wang, Lawrence Berkeley National Laboratory) for theoretical understanding of electrochemical reactions.

RESULTS

Figure 1a shows the RDE HER activity of $\text{Ni}_{0.95}\text{La}_{0.05}$ catalyst. The initial current density measured at a 200 mV overpotential is 42 mA/cm². This exceeds the go/no-go decision current density of 34 mA/cm² by 8 mA/cm². The RDE 5,000 cyclic durability test was performed with a triangle sweep cycling with a sweep rate of 200 mV/s between 0.2 V and $-0.25 V_{\text{RHE}}$. The current density measured at a 200 mV overpotential after the cyclic durability test is 34 mA/cm² (i.e., the loss in current density is 19%). This loss meets the go/no-go decision criterion loss of less than 20% current density. Figure 1b is scanning electron microscopy (SEM) images of the $\text{Ni}_{0.95}\text{La}_{0.05}$ catalysts before and after the cyclic durability test. No noticeable particle growing is observed, attesting stability of the catalyst.

The current densities of carbon-free perovskite oxide-F and -G in 0.1 M KOH, the most active two catalysts among the seven developed catalysts, are 5.2 mA/cm² and 5.6 mA/cm² at 1.65 V_{RHE} , respectively (Figure 2a). Both these current densities exceed the go/no-go decision current density of 5.1 mA/cm². The RDE 1,000 cyclic durability result (the 5,000 cyclic durability test cannot be done due to catalyst detachment from the RDE electrode) with perovskite oxide-F demonstrates nearly the same durability as that of IrO_2 (Figure 2b), thus the durability target of the go/no-go decision has also been met. Figure 2b is a comparison of OER activity of perovskite oxide-F in 0.1 M KOH and 0.1 M BTMAOH. Higher OER activity is obtained in 0.1 M BTMAOH than in 0.1 M KOH. Figure 2c is a pure-water-feeding (no added electrolyte) electrolyzer test result with IrO_2 and perovskite oxide-F and -G. Perovskite oxide-F and -G demonstrate higher OER activity (higher current densities at lower voltage) and better durability (lower voltage increase during the test) compared to IrO_2 . OER activities of IrO_2 , perovskite oxide-F, and perovskite oxide-G in 0.1 M KOH are almost the same when gauged by the current density at 1.65 V_{RHE} (Figure 2a). However, in pure-water-feeding AEM electrolyzer measurements (Figure 2c), perovskite oxide-F and -G demonstrated higher OER activity than IrO_2 . This indicates that OER activity measured in 0.1 M KOH does not properly reveal the OER activity in the water electrolysis test.

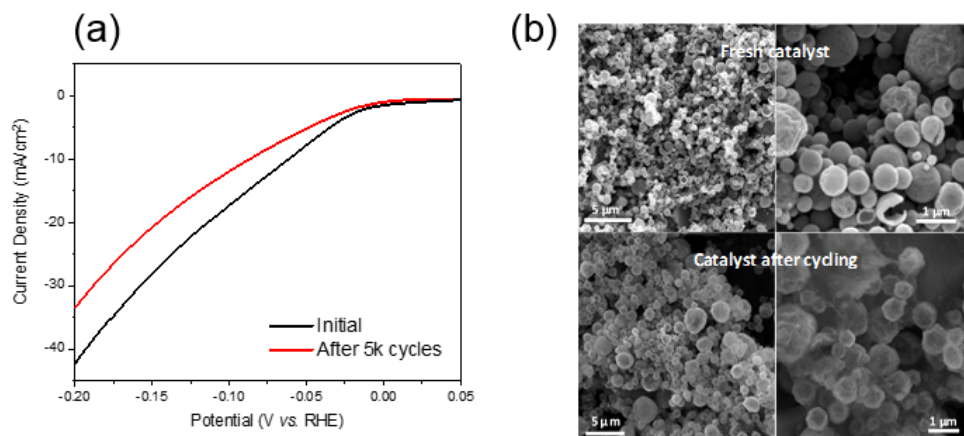


Figure 1. (a) Linear scan voltammetry plots of $\text{Ni}_{0.95}\text{La}_{0.05}$ HER catalyst. Electrolyte: N_2 -saturated 1.0 M NaOH; cell temperature: 60°C ; 1,600 rpm; scan rate: 2 mV/s. **(b)** SEM images of $\text{Ni}_{0.95}\text{La}_{0.05}$ HER catalysts before and after cyclic durability tests.

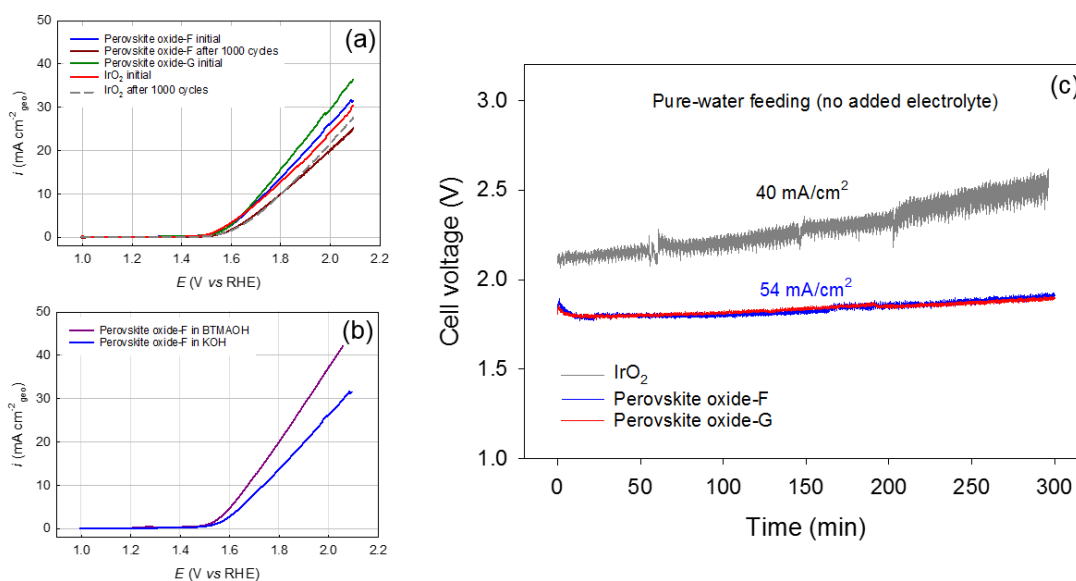


Figure 2. (a) RDE OER activities of IrO_2 , perovskite oxide-F, and perovskite oxide-G. Electrolyte: N_2 -saturated 0.1 M KOH; cell temperature: 25°C ; 1,600 rpm; scan rate: 10 mV/s. **(b)** RDE OER activity of perovskite oxide-F in 0.1 M KOH and BTMAOH. N_2 -saturated electrolytes; cell temperature: 25°C ; 1,600 rpm; scan rate: 10 mV/s. **(c)** 5-cm² electrode area MEA electrolysis test under water-feeding (no added electrolyte) condition: cell temperature 60°C ; anode catalysts: $\sim 1.0 \text{ mg/cm}^2$ for IrO_2 and perovskite oxide-F and -G; cathode: $0.35 \text{ mgPt/cm}^2 \text{ Pt/C}$.

We tested the effect of electrolyte on RDE OER activity measurements. Besides the commonly used inorganic KOH electrolyte, we also chose the organic BTMAOH electrolyte. The ammonium group in BTMA^+ is a typical functional group in AEMs and a phenyl group also is usually found in the backbone of AEMs, thus BTMAOH electrolyte contains the elements constituting the AEMs. Figure 3a shows the structure of AEM used in our AEM electrolysis tests. As shown, both an ammonium group and phenyl group exist in this AEM. Comparing the electrochemical cell OER activities measured in 0.1 M KOH (Figure 3b) and 0.1 M BTMAOH (Figure 3c) with the pure-water electrolysis results (Figure 3d), the electrochemical cell result obtained with

0.1 M BTMAOH more closely reflects the water electrolysis result. This tells us that BTMAOH solution is a more appropriate electrolyte than the KOH to gauge the activity in AEM water electrolysis.

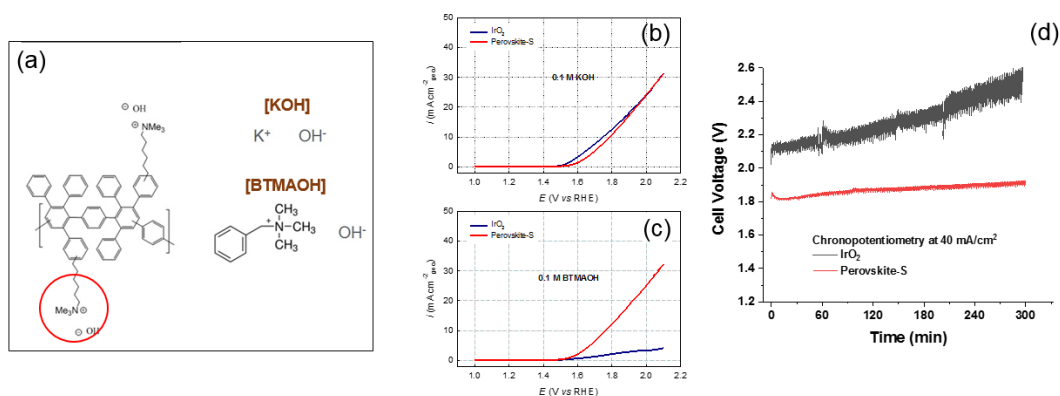


Figure 3. (a) Structures of poly(phenylene)-based anion exchange membrane with fully alkylated ammonium group cation and BTMAOH; RDE OER activity of IrO₂ and perovskite-S in (b) 0.1 M KOH and (c) 0.1 M BTMAOH. N₂-saturated 0.1 M KOH; cell temperature: 25 °C; 1,600 rpm; scan rate: 10 mV/s. (d) 5-cm² electrode area MEA electrolysis test under water-feeding (no added electrolyte) condition: cell temperature 60 °C; anode catalysts: ~1.0 mg/cm² both for IrO₂ and perovskite-S; cathode: 0.35 mg_{Pt}/cm² Pt/C.

CONCLUSIONS AND UPCOMING ACTIVITIES

We have successfully developed PGM-free OER and HER catalysts that exceeds the first year's go/no-go decision performance. In particular, carbon-free perovskite oxide OER catalysts demonstrated better activity and durability in a pure-water-feeding AEM electrolyzer test than IrO₂. In addition, BTMAOH solution is found as a more appropriate electrolyte than KOH solution in gauging AEM water electrolysis activity. Understanding the interfacial phenomena that occur at the catalyst-membrane-electrolyte in conjunction with analysis tools such as X-ray absorption spectroscopy is crucial for further improving the activity and durability of PGM-free OER and HER catalysts. Based on these findings, advanced PGM-free OER and HER catalysts will be developed in the next year. Four nodes have contributed to achieving the progress in this year; in particular, the AEM supply from Sandia National Laboratories is crucial in AEM electrolysis tests.

FY 2018 PUBLICATIONS/PRESENTATIONS

1. Hoon T. Chung, "High-Performance Ultralow-Cost Non-Precious Metal Catalyst System for AEM Electrolyzer," Poster presentation at the DOE Hydrogen and Fuel Cell Program Annual Merit Review, Washington, D.C., June 2018.
2. Hoon T. Chung et al., "Carbon-free Perovskite Oxide OER Catalysts for AEM Electrolyzer," 233rd ECS Meeting, Seattle, WA, May 2018.

HydroGEN Seedling: Scalable Elastomeric Membranes for Alkaline Water Electrolysis

Yu Seung Kim (Primary Contact), Dongguo Li,
Eun Joo Park, Sandip Maurya
Los Alamos National Laboratory
MPA-11: Materials Synthesis and Integrated Devices
Los Alamos, NM 87545
Phone: (505) 667-5782
Email: ykim@lanl.gov

DOE Manager: David Peterson
Phone: (720) 356-1747
Email: David.Peterson@ee.doe.gov

Subcontractor:
Rensselaer Polytechnic Institute, Troy, NY

Project Start Date: May 1, 2017
Project End Date: October 30, 2018

Overall Objectives

- Prepare durable and economically affordable hydroxide-conducting materials based on poly(styrene-*b*-(ethylene-co-butylene)-*b*-styrene) (SEBS) as anion exchange membranes (AEMs).
- Prepare high-performing ionomeric electrode binders for alkaline water electrolyzers.
- Demonstrate high-performance alkaline water electrolyzers.
- Demonstrate alkaline water electrolyzer durability under steady and accelerated stress conditions.

Fiscal Year (FY) 2018 Objectives

- Synthesize quaternized SEBS via acid-catalyzed Friedel-Crafts alkylation.
- Prepare soluble styrene-based ionomers for the electrode binder.
- Down-select the SEBS membrane for the membrane electrode assemblies of alkaline water electrolyzer.

Technical Barriers

This project addresses the following technical barriers from the Hydrogen Production section of the Fuel Cell Technologies Office Multi-Year Research, Development, and Demonstration Plan¹:

- Stability of polymer electrolytes
- Low cost and efficient hydrogen generation system
- Understanding the performance- and durability-limiting factors of alkaline membrane electrolyzers.

Technical Targets

Metric	Target	Status
Hydroxide conductivity (mS/cm)	40	42
% loss conductivity after 300 h, 1 M NaOH, 80 °C	<5	~0
Tensile toughness (MPa × % elongation) at 50 °C, 90% relative humidity	1,400	2,091

FY 2018 Accomplishments

- Quaternary ammonium (QA)-crosslinked SEBS AEMs were prepared and investigated.
- Semi-crystalline poly(styrene-*b*-ethylene-*b*-styrene) (SES)-based AEMs were synthesized and investigated.
- Soluble styrene-based ionomers were prepared.

¹ <https://www.energy.gov/eere/fuelcells/downloads/fuel-cell-technologies-office-multi-year-research-development-and-22>

INTRODUCTION

Our approach is to prepare a quaternized polystyrene block of SEBS by acid-catalyzed Friedel-Crafts bromoalkylation with brominated tertiary alcohol (SEBS- C_n -Br- x , where $n = 3-5$ and x is the degree of functionalization of the polystyrene block) (Figure 1). The properties of the quaternized SEBS are further optimized by incorporating di-QA groups per functionalization site for high ion exchange capacity (IEC) by the Friedel-Crafts bromoalkylation process (SEBS- C_3 -2Br- x) and the utilization of the semi-crystallinity of polyethylene block in the SES precursor polymer.

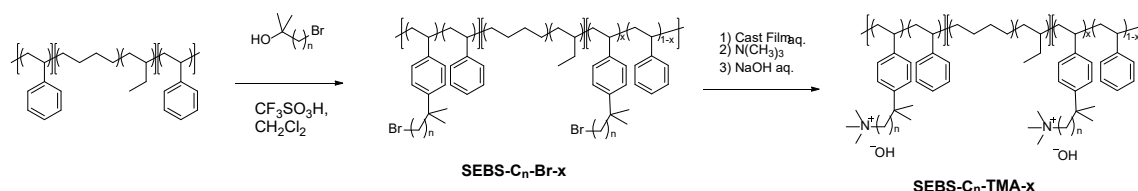


Figure 1. General synthetic procedure of acid-catalyzed SEBS

RESULTS

Preparation of Quaternized SEBS Membranes

Mono- and di-bromoalkyl side chains ($n=3$) were incorporated to the aromatic ring of the polystyrene unit of SEBS using acid-catalyzed Friedel-Crafts alkylation followed by quaternization with trimethylamine (TMA). The degree of functionalization of the polymer was 40 mol%, and the IEC of the membrane after amination of the bromoalkyl groups was 1.72 mequiv./g. Compared to a SEBS AEM with mono-QA side chain in similar IEC (i.e., SEBS- C_3 -TMA-0.8), the di-QA SEBS AEM (i.e., SEBS- C_3 -2TMA-0.4) showed slightly higher water uptake and lower hydroxide conductivities. We also found that the maximum degree of functionalization was limited around 40%, which gives an IEC of 1.72 mequiv./g. Because the di-QA SEBS AEM did not show significantly better membrane property in swelling and hydroxide conductivity, we decided to hold the direction of di-QA synthetic strategy.

Crosslinking is a representative approach to control the mechanical stability of membranes against large water uptakes [1-2]. We synthesized a crosslinked SEBS AEM using bromoalkylated SEBS and 1,6-hexanediamine. The crosslinked SEBS AEM, XL100-SEBS- C_5 -TMA-0.7 (degree of crosslinking = 100%, IEC = 1.36 mequiv./g), showed significantly lower water uptake than a non-crosslinked SEBS AEM (e.g., 30 vs. 150 wt% at room temperature in OH⁻ form, respectively).

To increase mechanical stability of the elastomeric AEMs, semi-crystalline SES precursor polymers were used as a backbone polymer. Because SESs are composed of crystalline polyethylene domains in the middle block, the tensile strength of the SES-based AEMs was higher than that of the SEBS-based AEMs in the similar IEC range. The mechanical properties of quaternized SEBS were further improved by reinforcing the membrane with polytetrafluoroethylene.

Properties of Quaternized SEBS Membranes

Table 1 shows the physical and electrochemical properties of the synthesized SEBS. The SEBS AEMs with mono-QA side chain (control) and di-QA side chain have high hydroxide conductivity, ~45 mS cm⁻¹. However, the water uptake of the membranes is over 100%. Crosslinked, semi-crystalline, and reinforced SEBS membranes have much lower water uptake, <50% with some reduction of hydroxide conductivity. The semi-crystalline SEBS meets the conductivity and water uptake milestones.

Table 1. Properties of the Synthesized SEBS

Samples	Code	IEC (mequiv./g)	Water Uptake (%)	Hydroxide Conductivity (mS cm ⁻¹)
Mono-QA-control	SEBS18-C3-TMA-0.8	1.55	150	47
Di-QA	SEBS18-C3-2TMA-0.4	1.55	173	40
Crosslinked	XL100-SEBS18-TMA-1.4	1.42	28	29
Semi-crystalline	SES25-TMA-1.7	1.71	30	42
Reinforced	RXL100-SEBS18-TMA-1.7	0.77	7	26

The chemical stability of the crosslinked (SES25-TMA-1.7) and reinforced SEBS (RXL100-SEBS18-TMA-1.7) was evaluated in 1 M NaOH at 80°C for 300 h. Table 2 shows the change of IEC and hydroxide conductivity after the test. Both AEMs showed excellent alkaline stability with less than 5% degradation. Table 2 also shows the mechanical properties of the AEMs. The crosslinked AEM showed 5.1 MPa ultimate tensile stress at 410% elongation, which is the limitation of the instrument, under 50°C and 90% relative humidity condition. Although the membrane did not break at 410% elongation, mechanical toughness (mechanical strength [MPa] × % elongation) was higher than the target value of 1,400. The mechanical properties of the reinforced AEM showed even higher mechanical toughness, ca. 4820.

Table 2. Chemical Stability and Mechanical Properties of the Synthesized SEBS

Samples	Code	Hydroxide Conductivity (mS/cm) at 80°C ^a		Tensile Properties		
		Before	After	Stress (MPa)	Elongation (%)	Toughness (stress × % elongation)
Semi-crystalline	SES25-TMA-1.7	63	64	5.1	174	4,820
Reinforced	RXL100-SEBS18-TMA-1.7	67	65	27.7	410	2,091

^a Alkaline stability test was conducted in 1 M NaOH at 80°C for 300 h.

Ionomer Synthesis

Figure 2 shows the synthetic procedure of quaternized polystyrene for the use of ionomeric binder for alkaline membrane water electrolysis. The quaternized polystyrene was synthesized using chloromethylated polystyrene and subsequent quaternization. The solubility of the ionomer was controlled by the ratio of hydrophilic and hydrophobic blocks of the ionomer. Different cationic functional groups including trimethyl ammonium, triethylammonium, and di-ammonium were incorporated into the polymer. The synthesized ionomers have the IEC range of 1.81 to 3.60 mmol/g and are soluble in alcoholic solvents including methanol, ethanol, and ethylene glycol. The ionomers are insoluble in most aprotic solvents including acetonitrile, acetone, and tetrahydrofuran but soluble in some highly polar solvents such as dimethylsulfoxide.

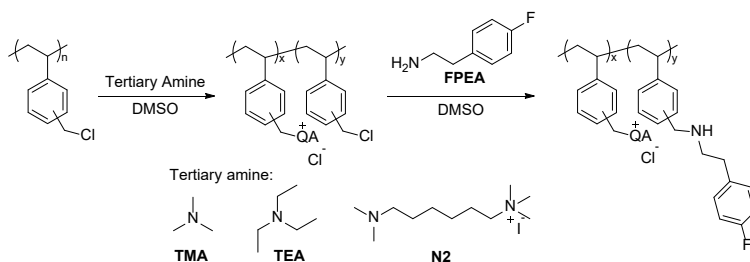


Figure 2. General synthetic procedure of quaternized polystyrene ionomer

CONCLUSIONS AND FUTURE DIRECTIONS

- Synthesized quaternized SEBS via acid-catalyzed Friedel-Craft reactions.
- Achieved the balanced hydroxide conductivity and water uptake properties through the crosslinking, semi-crystalline structure, and reinforced AEM strategies.
- Met all the project milestones (hydroxide conductivity, mechanical properties, and alkaline stability) using the semi-crystalline SEBS
- Synthesized styrene-based soluble ionomers for the electrolyzer electrode.
- Planned to conduct larger-scale synthesis of alkaline membrane and ionomers for the membrane electrode assembly testing
- Plan to investigate the performance- and durability-limiting factors for alkaline membrane-based water electrolysis.

PUBLICATIONS/PRESENTATIONS

1. Jong Yeob Jeon, Sungmin Park, Junyoung Han, Sandip Maurya, Angela D. Mohanty, Ding Tian, Nayan Saikia, Michael A. Hickner, Chang Y. Ryu, Mark E. Tuckerman, Stephen J. Paddison, Yu Seung Kim, and Chulsung Bae, “Efficient Synthesis of Aromatic Anion Exchange Membranes by Friedel-Crafts Bromoalkylation and Crosslinking of Polystyrene Block Copolymers,” *Macromolecules* (submitted 2018).

REFERENCES

1. P. Dai, Z.-H. Mo, R.-W. Xu, S. Zhang, and Y.-X. Wu, “Cross-Linked Quaternized Poly(styrene-b-(ethylene-co-butylene)-b-styrene) for Anion Exchange Membrane: Synthesis, Characterization and Properties.” *ACS Appl. Mater. Interfaces* 8 (2016): 20329–20341.
2. J. Hao, X. Gao, Y. Jiang, H. Zhang, J. Luo, Z. Shao, and B. Yi, “Crosslinked High-Performance Anion Exchange Membranes Based on poly(styrene-b-(ethylene-co-butylene)-b-styrene).” *J. Membr. Sci.* 551 (2018): 66–75.

HydroGEN Seedling: Best-in-Class Platinum-Group-Metal-Free Catalyst Integrated Tandem Junction Photoelectrochemical Water Splitting Devices

Eric Garfunkel (Co-Principal Investigator),
G. Charles Dismukes (Primary Contact,
Co-Principal Investigator), and Martha Greenblatt
Rutgers, the State University of New Jersey
610 Taylor Road
Piscataway, NJ 08854
Phone: (848) 445-1489
Email: dismukes@chem.rutgers.edu

DOE Manager: Eric Miller
Phone: (202) 287-5829
Email: Eric.Miller@ee.doe.gov

Contract Number: DE-EE0008083

Project Start Date: September 1, 2017
Project End Date: November 30, 2020

Overall Objectives

The project will engineer and compare two photoelectrochemical (PEC) cell configurations made with high-efficiency non-precious-metal catalysts for water splitting, together with two classes of photovoltaic materials chosen from proven high-performance semiconductors versus emerging low-cost semiconductors. The two configurations to be fabricated and compared are (1) high-efficiency (higher-cost) multijunction GaInP₂/GaAs photoabsorbers developed at the National Renewable Energy Laboratory (NREL) that are integrated with Rutgers-developed hydrogen evolution reaction (HER) and oxygen evolution reaction (OER) catalysts (Ni₅P₄ and LiCo₂O₄, respectively); and (2) lower-cost devices created from emerging perovskite (oxy)nitride photoabsorbers also integrated with these Rutgers catalysts. The long-term goal (Year 3) is to compare the trade-off between performance and cost for these configurations while also achieving benchmark metrics in solar-to-hydrogen (STH) efficiency and durability.

Fiscal Year (FY) 2018 Objectives

- Fabricate stable non-platinum-group-metal (non-PGM) alkali LiCoO₂ electroanode (on par with published cubic-LiCoO₂ benchmark) with stable performance.
- Develop low-temperature thin film synthesis methods for catalyst (Ni₅P₄) and protection layers that are compatible with p-GaInP₂/p⁺GaAs.
- Evaluate photoelectrochemical performance of catalyst and protection layers on a p-GaInP₂/p⁺GaAs single-junction model device
- Synthesize and evaluate photovoltaic and photoelectrochemical properties of ZnSnN₂ photoanode.

Technical Barriers

This project addresses the following technical barriers from the Hydrogen Production section of the Fuel Cell Technologies Office Multi-Year Research, Development, and Demonstration Plan¹:

- (B) System Cost
- (C) Efficiency
- (D) Durability/Operability.

Technical Targets

The goal of this project is to attain or exceed the DOE benchmark STH energy conversion efficiency of 10% (and 20% by 2020), working toward the DOE hydrogen cost goal of <\$2/kg H₂. This is being investigated in two thrusts by developing two competing monolithic PEC devices: one a high-performance device based on state-of-the-art GaAs/GaInP₂ tandem solar cells developed at NREL, and the second a high-value device based on earth-abundant photoabsorber materials. Both these devices will be paired with electrocatalysts developed for this purpose at

¹ <https://www.energy.gov/eere/fuelcells/downloads/fuel-cell-technologies-office-multi-year-research-development-and-22>

Rutgers by adapting them to thin films on the photoabsorbers. These catalysts are based on the HER catalysts (Ni_5P_4) and OER catalysts (LiCo_2O_4) previously developed at Rutgers for high-efficiency electrolyzers. Both monolithic devices will be based on a narrow and a wide bandgap material, a so-called tandem device. The aim is to meet the following DOE targets:

- STH energy conversion ratio: 20% (by 2020)
- Hydrogen cost: $< \$2/\text{kg H}_2$
- Electrode replacement lifetime: 0.5 years.

FY 2018 Accomplishments

- Synthesized and characterized activity and stability of electrochemical LiCo_2O_4 -based thin film anode. Performance achieved: >12 days sustained OER activity in 1 M NaOH.
- Successfully developed a thin film fabrication method for crystalline Ni_5P_4 at low temperature.
- Successfully fabricated TiN protection layer on p-GaInP₂/p⁺GaAs at low temperature and demonstrated it blocks atomic interdiffusion of catalyst and photoabsorber.
- Demonstrated that photoelectrochemical performance of HER catalyst and protection layers on p-GaInP₂/p⁺-GaAs exceeded the 10% goal and is on par with the PtRu benchmark catalyst. The performance was independently confirmed by the NREL Deutsch group.
- Synthesized ZnSnN_2 photoabsorber on glass and characterized by X-ray fluorescence, X-ray diffraction, Rutherford Backscattering, and conductivity measurements.
- Identified corrosion instability of ZnSnN_2 in 1 M NaOH.

INTRODUCTION

Current PEC devices suffer from low stability and efficiency; hence this project aims to address both those needs by significantly increasing the STH conversion efficiency above 10% while achieving long-term operation without corrosion.

APPROACH

The industry-accepted benchmarking standard for photoelectrochemical performance is conducted with PGM catalysts (RuO₂ and PtRu). Our approach differs by developing methods to interface two classes of photoabsorbers with the Rutgers-developed non-PGM catalysts. Our approach to increasing the STH efficiencies up to 10% has two thrusts.

Thrust 1: using GaInP₂/GaAs devices with optimizing bandgap matching to the solar spectrum coverage that provide suitable voltages for splitting water (using an NREL photovoltaic cell with solar-to-electrical power efficiencies >16%).

Thrust 2: the development of novel photoabsorbers based on earth-abundant materials that have low fabrication costs.

Thrust 2 will increase the STH efficiency by three strategies:

1. Utilization of two light absorbers with different bandgaps in a tandem configuration each tuned to achieve optimal solar spectral coverage. Corrosion-resistant metal oxides with wide bandgap are good candidates for the photoanode but inefficiently absorb red light. Spectral shifting to lower the bandgap can be achieved by N doping or substitution, which increases the absorption and ideally preserves stability.
2. (band-bending) Each absorber will have a built-in electric field gradient achieved by gradient doping to allow matching of valence and conduction band energy levels to the electrochemical potential required for the OER and HER, respectively.
3. To improve charge separation efficiency and carrier lifetime we have developed methods for the creation of thin films of both OER and HER catalysts. The OER catalyst shows significant promise in independent laboratory testing (at Proton OnSite). The photoanode/OER interface will be coupled to a silicon absorber as photocathode and Rutgers' HER catalyst to achieve the tandem PEC design.

RESULTS

Synthesis and Testing of a High-Performance Back Contact Anode

To replace the state-of-the-art PGM catalysts in our high-performance PEC device, we need to develop a highly active and stable back contact anode using our previously published cubic-LiCoO₂ material [1, 2]. This will be integrated with the illuminated GaInP₂/GaAs cathode. To achieve this, we first needed to deposit the catalyst on a conductive and anodically stable substrate. Inspiration was drawn from the dimensionally stabilized anode (DSA) design using TiO₂/Ti microporous scaffolds to increase surface area and stability under applied anodic potential [3]. We note that the DSA utilizes Ru doping of the TiO₂ to achieve reasonable conductivity and circumvent the band bending of pristine TiO₂, which would hinder anode operation in the absence of ultraviolet illumination.

Figure 1A shows long-term stability of a DSA comprising Ti-foil with a native TiO_x oxide film and top layer of electrodeposited Li_xCoO₂ film. The most active film is grown by cycling the deposition potential repeatedly until the final activity is reached. In Figure 1A the effect of O₂ bubble formation is seen as spikes in the current, but overall the electrode shows great retention of activity. Figure 1B shows the rough and particulate surface morphology of the deposited Li_xCoO₂ before the 12.8 days of stability test.

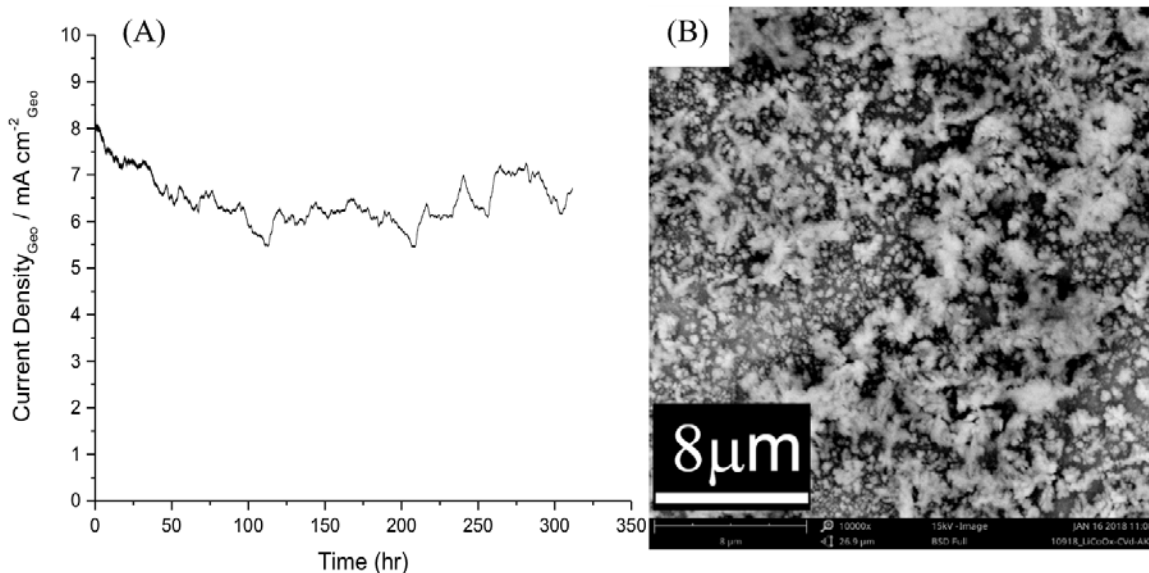


Figure 1. (A) Chronoamperometric analysis of and (B) scanning electron microscope image of the top surface of the as-synthesized electrodeposited Li_xCoO_2 thin film catalyst

Synthesis of a Protection Layer/Diffusion Barrier on High-Performance Photocathode ($\text{GaInP}_2/\text{GaAs}$ Buried-Junction Device)

For non-oxide photoelectrodes the air exposure during fabrication results in the formation of a surface oxide layer. In the case of GaInP_2 the surface oxide is a gallium indium oxide and phosphate of unknown exact composition. This oxide layer impedes the charge transfer to and capture by the catalyst layer and therefore must be removed immediately prior to deposition.

The first samples received from the NREL “III-V Semiconductor Epi-Structure and Device Design and Fabrication” node of $n\text{-GaInP}_2/p\text{-GaInP}_2/\text{GaAs}$ were therefore investigated for the best method for removal of any surface oxide from the GaInP_2 surface. X-ray photoelectron spectroscopy (XPS) studies of P, In, and Ga as a function of the etchant solution were conducted to find the optimal procedure for removing the surface oxide prior to the deposition of the protection layer. Based on three different etchants (aqueous hydrochloric acid, $\text{HF}:\text{NH}_4\text{F}$ (1:6), and aqueous ammonia solution) the indium oxide was removed most successfully by using the buffered HF etchant.

Finally, we deposited a TiN protection layer of approximately 4 nm thickness on top of a freshly cleaned GaInP_2 photocathode surface. The deposition was done using pulsed laser deposition from a TiN target at reduced temperature ($<120^\circ\text{C}$) to avoid loss of P from the GaInP_2 during deposition in high vacuum.

Development of Low-Temperature Ni_5P_4 HER Electrocatalyst Layer Synthesis and Transfer to $p\text{-GaInP}_2/p^+\text{-GaAs}$

Synthesizing phase-pure crystalline Ni_5P_4 on $\text{TiN}/\text{GaInP}_2$, without the decomposition of the photoabsorber due to interatomic diffusion into the catalyst layer and P loss, requires lowering the reaction temperature from the previous optimal conditions used for Si-photocathodes (i.e., 500°C and 3 hours). Lower temperatures can prevent atomic interdiffusion of GaInP_2 into the catalyst layer. We used a thicker Ni/TiN/Si geometry as a model system to systematically vary the temperature ($T < 400^\circ\text{C}$) and the reaction time to characterize multiple reaction conditions and probe the catalyst phase by regular X-ray diffraction, while preserving the $\text{GaInP}_2/\text{GaAs}$ samples provided by the NREL node for the final proof of concept at the optimized conditions.

Figure 2 shows the X-ray diffraction patterns for samples at various phosphidation conditions (T=temperature and t=time): T1 >400°C and t1 >1 h; T2 <400°C and t2 <1 h for a 125 nm Ni/TiN/Si sample. We note that at high temperature, over-phosphidation occurs while some Ni is still unconverted; this indicates that the surface is converted far too fast compared to the diffusion of P into the Ni. Lowering the temperature and reducing the reaction time decreases the P vapor pressure and reduces the over-phosphidation (T2). These conditions generated a catalyst layer of Ni₅P₄ with significant amount of unreacted Ni (green trace) below the converted catalyst. Because the final electrode will utilize a much thinner Ni layer (3 nm), unreacted Ni may not be the problem in this case. To confirm that a thinner Ni layer would result in increased phase purity, a 80 nm Ni/TiN/Si sample was reacted under T2_t1 conditions (purple trace). The resulting powder X-ray diffraction pattern demonstrates the peak attributed to unreacted Ni was substantially decreased without the presence of NiP₂ and confirms the above conditions are suitable for a 3 nm–10 nm Ni film. We concluded that the reaction conditions were successfully optimized for generating a phase-pure Ni₅P₄ thin film.

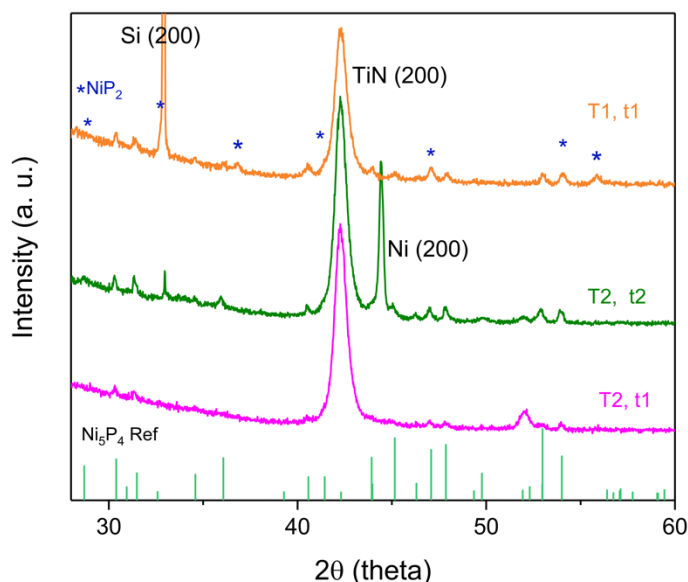


Figure 2. X-ray diffraction of different temperature and time of phosphidization on thick Ni layer with TiN protected single crystal Si model photocathode

Adapting Ni₅P₄ Synthesis on TiN/p-GaInP₂/GaAs

To transfer the above optimized reaction conditions for Ni₅P₄ synthesis on TiN/p-GaInP₂/GaAs, we evaporated a 3-nm thin layer of Ni onto the pre-cleaned GaInP₂/GaAs surface. XPS and helium ion microscope were used to confirm that only Ni and P are found at the top surface layer (~6 nm) and these uniformly cover the surface (Figure 3 and 4) seen by the absence of Ga and In. Figure 4A shows a uniform coverage of ~20 nm crystallite domains all apparently sintered together without pinholes.

To investigate the photoelectrocatalytic performance of these samples, we tested them in 0.5 M H₂SO₄ under simulated solar 1.5 AM G illumination. Figure 4B shows the current versus voltage curve (J-V curve) of Ni₅P₄/TiN on p-GaInP₂/GaAs compared to the benchmark PtRu/p-GaInP₂/GaAs tested at NREL under the same conditions. When comparing the J-V curve with the NREL benchmark, the performance of Ni₅P₄/TiN layers may be seen to be on par with the PGM-PtRu catalyst (base on V_{onset} and J_{sat}). To test the durability of Ni₅P₄/TiN/p-GaInP₂/GaAs photoelectrode, we ran chronoamperometry at 0 V vs. reversible hydrogen electrode under 1.5 AM G solar simulated illumination again in 0.5 M H₂SO₄. Figure 4C shows that less than 10% change in the photocurrent density is observed over 89 hours of testing (the duration of the test).

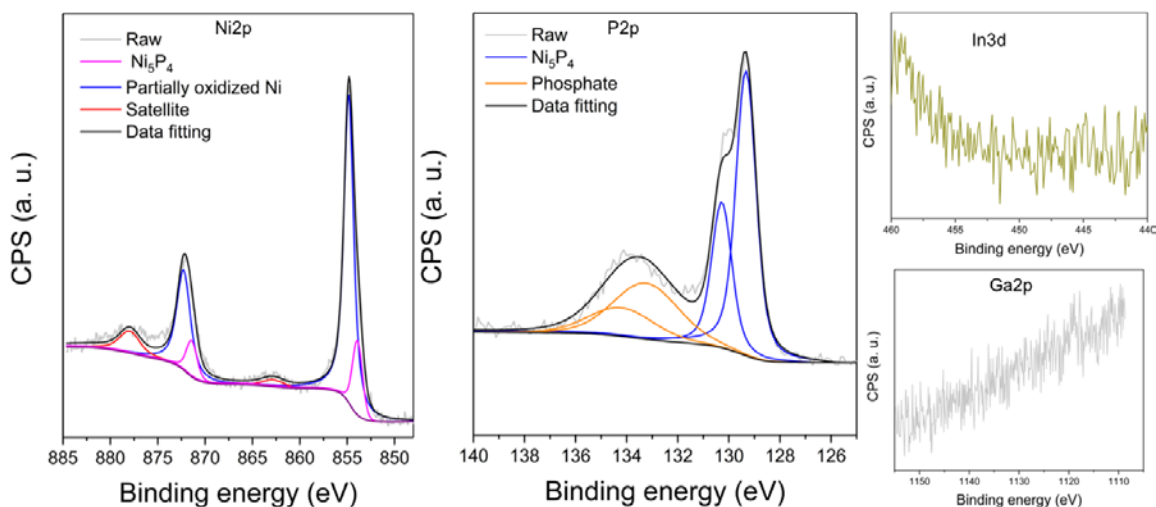


Figure 3. XPS of Ni2p, P2p, In3d, and Ga2p core levels of top layer Ni₅P₄/TiN/p-GaInP₂/GaAs

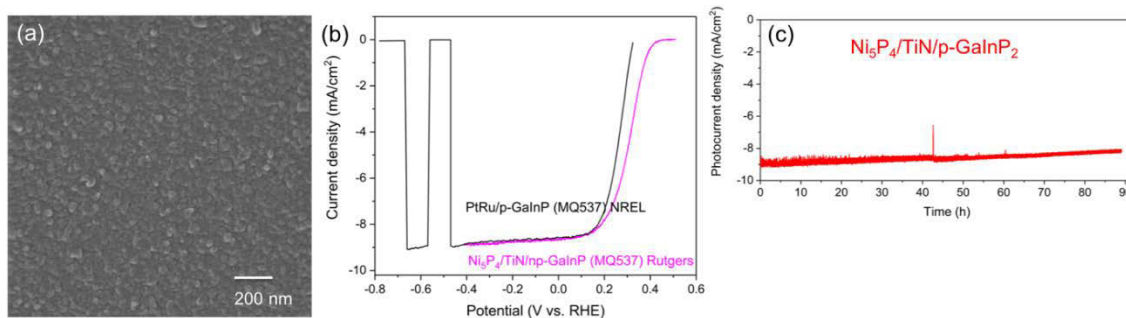


Figure 4. Helium ion microscope image of Ni₅P₄/TiN/p-GaInP₂/GaAs

CONCLUSIONS AND UPCOMING ACTIVITIES

The following conclusions are derived from the work in FY 2018:

- TiN protection layers on GaInP₂/p⁺-GaAs have demonstrated good interdiffusion protection from photoabsorber into the catalyst layer.
- Ni₅P₄ thin film synthesis was successfully adapted to lower reaction temperature on the TiN-protected p⁺-GaAs/p-GaInP₂.
- Insights gained from studying the tandem photoabsorber interface have significantly advanced progress toward a wireless, tandem PEC utilizing GaInP₂/GaAs dual junction.
- ZnSnN₂ photoabsorbers show low stability in alkali and rapid dissolution.

Future efforts toward FY 2018–2019 include the following.

Thrust 1:

- Assemble a full dual junction device of GaInP₂/GaAs with TiN and Ni₅P₄, with a RuO_x based non-illuminated anode, then characterize the photoactivity and stability.
- Test full device under on-sun conditions.

Thrust 2:

- Assemble a photoanodic device comprising OER/perovskite photoabsorber and test photoabsorbers based on either oxynitrides (with NREL Zakutayev node) or hybrid-organic/inorganic perovskite (NREL Kai node).
- Develop oxynitride photoabsorber synthesis using sputtering deposition facilities available at NREL.
- Develop hybrid-organic/inorganic perovskite photoabsorber interface with protection layers.

FY 2018 PUBLICATIONS/PRESENTATIONS

Publications

1. S. Hwang, S.H. Porter, A.B. Laursen, H. Yang, M. Li, V. Manichev, K.U.D. Calvinho, V. Amarasinghe, M. Greenblatt, E. Garfunkel, and G.C. Dismukes, “Creating stable interfaces between reactive materials: Titanium nitride protects photoabsorber-catalyst interface in water-splitting photocathodes,” (Submitted 2018).

Presentations

1. E. Garfunkel, “Photoelectrochemical Water Splitting to Form Hydrogen,” Semiconductor Surface Chemistry Meeting, Telluride, CO, 2018.
2. S. Hwang, S.H. Porter, A.B. Laursen, H. Yang, M. Li, V. Manichev, K.U.D. Calvinho, V. Amarasinghe, M. Greenblatt, E. Garfunkel, and G.C. Dismukes, “Titanium Nitride as a Conducting Interfacial Layer Between Hydrogen Evolution Catalyst and Si Photocathode for Stable Solar-to-Hydrogen Water Splitting Devices,” 233th ECS meeting in Seattle, 2018.
3. E. Garfunkel, M. Greenblatt, G.C. Dismukes, A.B. Laursen, and S. Hwang, “RU-EMN—Best-in-Class Platinum Group Metal-Free Catalyst Integrated Tandem Junction PEC Water Splitting Devices,” U.S. DRIVE Hydrogen Production Tech Team, teleconference, Feb. 6, 2018.
4. S. Hwang, S.H. Porter, A.B. Laursen, H. Yang, M. Li, V. Manichev, K.U.D. Calvinho, V. Amarasinghe, M. Greenblatt, E. Garfunkel, and G.C. Dismukes, “Nickel Phosphide Catalyst and Titanium Nitride Protection Layer for High Efficient and Stable Silicon-based Photocathode,” Annual Meeting at Catalysis Society of Metropolitan New York at Lehigh University, 2018.
5. A. Kashi, S. Hwang, A.B. Laursen, and G.C. Dismukes, “Characterization of Highly Active Electrodeposited Li_xCoO_2 Thin Film Anodes in PGM-free Photoelectrochemical Cells,” Annual Meeting at Catalysis Society of Metropolitan New York at Lehigh University, 2018.

REFERENCES

1. G.P. Gardner, Y.B. Go, D.M. Robinson, P.F. Smith, J. Hadermann, A. Abakumov, M. Greenblatt, G.C. Dismukes, *Angew. Chem. Int. Ed.* 51 (2012): 1616.
2. G. Gardner, J. Al-Sharab, N. Danilovic, Y. B. Go, K. Ayers, M. Greenblatt, G.C. Dismukes, *Energy Environ. Sci.* 9 (2016): 184.
3. S.M. Hoseinieh, F. Ashrafzadeh, M.H. Maddahi, *J. Electrochem. Soc.* 157 (2010): E50.

HydroGEN Seedling: Protective Catalyst Systems on III-V and Si-based Semiconductors for Efficient, Durable Photoelectrochemical Water Splitting Devices

Thomas Jaramillo (Primary Contact), James Harris
Stanford University
443 Via Ortega, Room #305
Stanford, CA 94305
Phone: (650) 353-1984
Email: jaramillo@stanford.edu

DOE Manager: Eric Miller
Phone: (202) 287-5829
Email: Eric.Miller@ee.doe.gov

Contract Number: DE-EE0008084

Project Start Date: September 1, 2017
Project End Date: December 31, 2018 (Phase I)

Overall Objectives

- Develop unassisted water splitting devices based on III-V materials, creating pathways to improve performance in terms of efficiency, durability, and cost.
- Develop translatable, thin-film catalyst and protection layers for the hydrogen evolution reaction (HER) and/or oxygen evolution reaction (OER) onto III-V materials (Task 1), including samples provided by the National Renewable Energy Laboratory (NREL) III-V fabrication Energy Materials Network (EMN) node.
- Develop methods to fabricate a tandem InGaN/Si photoelectrochemical (PEC) water splitting device (Task 2).
- Integrate HER and/or OER catalysts with InGaN/Si system and tandem III-V structures.
- Study degradation mechanisms of PEC devices by developing an *in operando* electrochemical flow cell to inform strategies to improve catalysts and protection layers.
- Test highly active and durable unassisted water splitting devices in an on-sun setup for

extended periods of time and study effects such as light and temperature fluctuations.

- The end of project goal is demonstration of unassisted device with >20% average solar-to-hydrogen (STH) efficiency and successful on-sun testing of unassisted water splitting devices for >2 weeks.

Fiscal Year (FY) 2018 Objectives

- Demonstrate a PEC photoelectrode that achieves >10 mA/cm² under 1-sun illumination for longer than 100 h while utilizing a non-precious-metal HER catalyst.
- Demonstrate >100 h stability of OER catalysts with III-V-based PEC devices.
- Demonstrate InGaN growth by metal organic chemical vapor deposition (MOCVD) on Si (111) substrates.
- Demonstrate high-quality undoped InGaN and p-doped InGaN by MOCVD.
- Demonstrate repeatable Si p-n junctions suitable for InGaN/Si tandem devices.
- Demonstrate effectiveness of the *in operando* microscopy and spectroscopy flow cell measurement technique on a benchmark photoelectrode system such as previously developed MoS₂/III-V photocathodes.
- Fabricate an unassisted PEC water splitting device with a non-precious-metal HER catalyst that achieves STH efficiencies >5% under 1 sun to create a pathway for >20% STH.

Technical Barriers

This project addresses the following technical barriers from the Hydrogen Production section of the Fuel Cell Technologies Office Multi-Year Research, Development, and Demonstration Plan¹:

- Materials Efficiency—Bulk and Interface

¹ <https://www.energy.gov/eere/fuelcells/downloads/fuel-cell-technologies-office-multi-year-research-development-and-22>

- Materials Durability—Bulk and Interface
- Integrated Device Configurations
- Auxiliary Materials—For Catalysis and Durability
- Synthesis and Manufacturing—Technique Development.
- Demonstrated for the first time InGaN growth on Si (111) by MOCVD, providing a lower-cost route to fabrication of high-performance tandem absorber layers.

Technical Targets

This project is conducting research into catalyst and protection layer development in photoelectrochemical devices as well as development of InGaN/Si tandem absorbers in addition to fundamental studies of degradation in photoelectrochemical systems. Insights gained from these studies will be applied toward the design and fabrication of hydrogen production devices that meet the following DOE hydrogen production targets for photoelectrochemical water splitting systems with solar concentration:

- Photoelectrochemical hydrogen cost: \$5.70/kg (2020); \$2.10/kg (ultimate)
- Capital costs (concentrator and PEC receiver): \$124/m² (2020); \$63/m² (ultimate)
- Annual electrode cost per metric tons per day (TPD) hydrogen: \$225K/yr-TPD H₂ (2020); \$14K/yr-TPD H₂ (ultimate)
- STH energy conversion ratio: 20% (2020); 25% (ultimate)
- 1-sun hydrogen production rate 1.6e-6 kg/s per m² (2020); 2.0e-6 kg/s per m² (ultimate).

FY 2018 Accomplishments

- Demonstrated 100-hour stability for a PEC photoelectrode with >10 mA/cm² under 1 sun.
- Fabricated an unassisted PEC water splitting device with a non-precious-metal HER catalyst that achieves 1-sun STH efficiency >5%, providing a viable pathway for achieving 20% STH efficiency through improved integration of the materials and interfaces.
- Under ~1.3 suns, an MoS₂-protected GaInAsP/GaAs IMM device maintained a >10% STH for the first 2 hours, operating for an additional 10 hours while decreasing to ~60% of light-limited photocurrent before failure.

INTRODUCTION

The overall goal of this project is to develop unassisted water splitting devices based on III-V materials, creating pathways to improve efficiency, durability, and cost toward DOE targets for hydrogen production via photoelectrochemistry. One major objective is to develop systems that can achieve >20% STH efficiency. Another objective is to develop high-efficiency systems that can operate on-sun for at least 2 weeks by understanding and mitigating degradation mechanisms. This research will provide new approaches to tandem photoelectrode design and fabrication that can lead to cost reduction to <\$200/m². We propose two distinct schemes. Scheme 1 aims to develop high-efficiency tandem III-V photoabsorbers (e.g., GaInP₂/GaInAs) with Scheme 2 targeting cost reduction while maintaining high efficiency by growing InGaN on crystalline Si. Both schemes will be coupled with thin-film, semi-transparent catalytic/protection layers containing reduced or zero precious metal content that can enhance durability with low cost.

APPROACH

To date, the PEC water splitting devices with the highest STH efficiencies (~10%–19%) use tandem III-V structures, generally consisting of a GaInP₂ (~1.8 eV) top absorber paired with either a GaInAs (~1.2 eV) or GaAs (1.4 eV) bottom absorber. However, these devices exhibit instability in acidic electrolyte. To mitigate this, our approach is to develop thin-film, semi-transparent catalytic/protection layers with suitable interface energetics. Our work utilizes earth-abundant transition metal sulfides and transition metal phosphides that are highly active and acid-stable. To complement this, we are also developing solution processable Ir-containing OER catalysts. While the tandem III-V/III-V approach in Scheme 1 allows for high efficiency, current methods of fabrication are costly. In parallel, we are pursuing tandem InGaN/Si absorber devices (Scheme 2) that offer potential for reduced cost by eliminating the III-V growth substrate. Collaboration with Dr. Friedman's EMN node enables the fabrication of III-V tandem absorbers with tuned bandgaps to optimize current matching in the device. Moreover, continued collaboration with EMN nodes on PEC characterization, corrosion analysis, and on-sun testing will provide the key insights needed to continue developing PEC technology.

RESULTS

We demonstrated that a thin coating of molybdenum disulfide, a non-precious-metal HER catalyst, can impart both long-term stability as well as high catalytic activity to a pn⁺-GaInP₂ photocathode. After 110 hours of testing, the MoS₂-protected device showed no loss of photocurrent density with respect to the initial photocurrent value (Figure 1), which was a main deliverable of Phase 1. The MoS₂ film was deposited by an initial ~3 nm Mo sputter followed by a sulfidation in an H₂S atmosphere. Furthermore, the Ir OER catalyst remained active and intact during these stability tests. Publication #1 noted below describes related work involving 100-h stability of a similar fabricated photocathode that provides photocurrent densities >10 mA/cm².

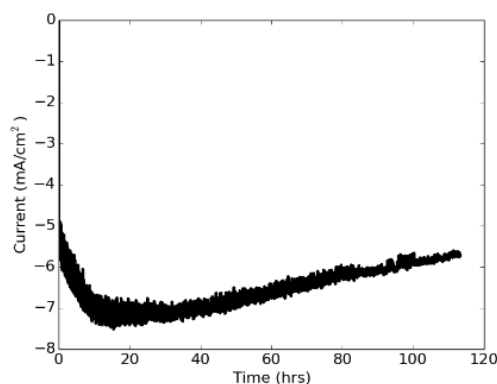


Figure 1. Electrochemical chronoamperometric characterization of pn⁺-GaInP₂/MoS₂ photocathodes in 0.5 M sulfuric acid at a constant potential of +0.1 V versus normal hydrogen electrode

We translated the MoS₂ protection scheme to inverted metamorphic multijunction (IMM) unassisted water splitting devices. These devices consist of a large bandgap III-V (e.g., GaInP₂) and small bandgap III-V (e.g.,

GaAs) grown inverted in order to minimize defect propagation in the top absorber. A compositionally graded buffer layer is also used to allow non-lattice matched III-V absorbers, such as GaInAs and GaInP₂, to be paired in order to take advantage of better bandgap matching. Under ~1.3 suns, an MoS₂-protected GaInAsP/GaAs IMM device maintained >10% STH for the first 2 hours, operating for an additional 10 hours while decreasing to about 60% of its light-limited photocurrent before failure. This is a significant improvement over the control sample, a sibling IMM sample prepared with the champion NREL PtRu catalyst that catastrophically failed within only 3 hours of testing (Figure 2). Preliminary investigation of the surfaces indicate that micron-sized defects and pinholes are present before electrochemical testing of these devices and are most likely due to the complex IMM fabrication process. We believe our MoS₂-protected IMM devices fail earlier than the III-V systems fabricated using more conventional processes (non-IMM, see Figure 1) because our protection layers are not designed to handle the larger defects that emerge from IMM fabrication. During Phase 2, we will work with the NREL fabrication node to address this issue. This will enable on-sun testing for weeks, which is a primary deliverable of Phase 2.

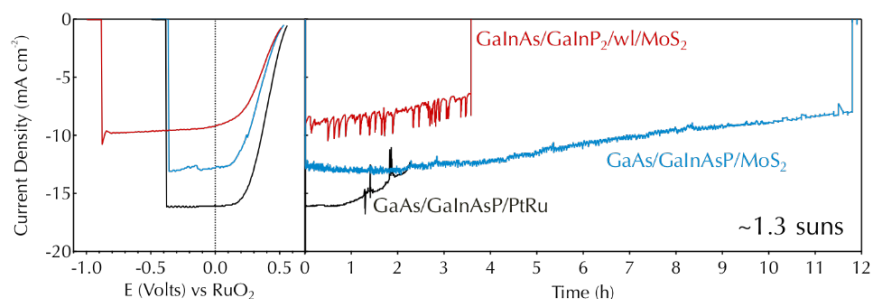


Figure 2. PEC characterization of GaInAs/GaInP₂/wl(window layer)/MoS₂, GaAs/GaInAsP/MoS₂, and GaAs/GaInAsP/PtRu unassisted water splitting devices in 0.5 M sulfuric acid

In terms of finding a suitable OER catalysis for PEC systems, we tested an Ir wire for >100 hours in 0.5 M H₂SO₄ with an applied current of 4.2 mA, since that is the approximate anode current when 20 mA/cm² is passing through a photocathode with an area of ~0.2 cm². We also are investigating the properties of our new solution-processed strontium iridium oxide (SrIrO_x) thin-film OER catalyst, which is compatible with planar photoanodes. Iridium oxide (IrO_x) and strontium iridium oxide (SrIrO_x) films were synthesized on p⁺ silicon substrates via spin coating to use as OER catalysts. Stability of 3.3 cm² anodes was measured by performing chronoamperometry at 1.6 V versus reversible hydrogen electrode for 24 hours. Initially, the IrO_x anode showed better stability performance than SrIrO_x. Stability is likely limited by the initial defects and heterogeneity in the films as well as by film delamination from the silicon substrate, which occurred at 19.5 and 18 hours, respectively. Current efforts are aimed at improving film adhesion by employing sticking layers and testing other substrates.

Toward the development of tandem InGaN/Si devices, we utilized MOCVD for nucleation and growth of InGaN films of good crystalline quality for the first time. Figure 3a is an X-ray diffraction symmetric (2theta-omega) scan of our InGaN films with various indium compositions. From the (002) diffraction peaks on this figure, it is evident that the MOCVD-grown InGaN films have excellent out-of-plane orientation. For the In_{0.55}Ga_{0.45}N film, we see the appearance of a secondary diffraction peak corresponding to that of InN, indicating that some degree of phase separation has occurred at such high indium compositions. Figure 3b is an X-ray diffraction phi scan of the (101) peak of InGaN, showing clear six-fold in-plane rotational symmetry, characteristic of good in-plane orientation for hexagonal wurtzite crystal structures. The InGaN films have smooth, densely packed film morphologies suitable as photovoltaic absorbers.

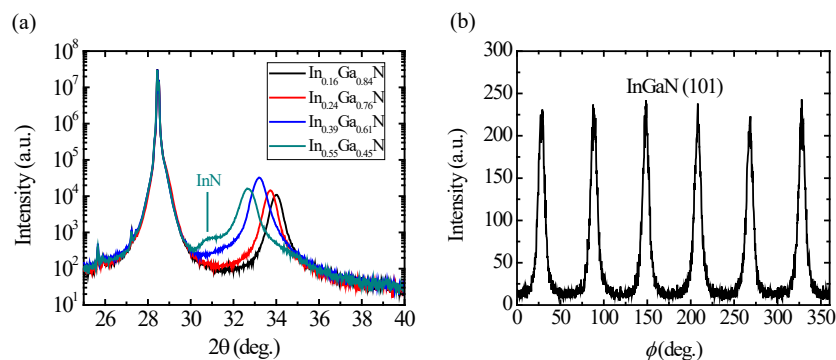


Figure 3. (a) X-ray diffraction symmetric (2theta-omega) scans of the (002) reflection for MOCVD-grown InGaN films with varying indium compositions, and (b) X-ray diffraction phi scans of the InGaN (101) reflection for a typical MOCVD-grown InGaN film

We conducted Hall effect measurements of our MOCVD-grown InGaN films. For the $\text{In}_{0.16}\text{Ga}_{0.84}\text{N}$ film, the background electron density is around $2.5 \times 10^{17} \text{ cm}^{-3}$, rendering it suitable as a photovoltaic absorber with a relatively wide depletion region width of $\sim 90 \text{ nm}$. For the $\text{In}_{0.55}\text{Ga}_{0.45}\text{N}$ film, the background electron density increases to $1.8 \times 10^{20} \text{ cm}^{-3}$, which is typical of InGaN films with high indium content but is unsuitable for photovoltaic applications.

To develop the growth of p-type InGaN through MOCVD, we added Cp_2Mg as the Mg precursor for p-type doping. We developed a two-step process first with growth at 550°C for the undoped InGaN absorber layer to achieve uniform wetting of the substrate, followed by growth of the Mg-doped InGaN layer at 750°C . Following MOCVD growth of the device stack, secondary ion mass spectroscopy analysis confirmed Mg incorporation. We observe Mg concentrations above 10^{19} cm^{-3} in the Mg-doped InGaN layer, which closely matches the Mg atomic concentrations of p-GaN reported in literature. The same InGaN device stack was further processed into solar cell devices. We observe no current rectification when sweeping between -1 V and 1 V . This lack of rectification could be because of the presence of compensating defects like nitrogen vacancies V_{N}^+ , which have lower formation energies when higher amounts of Mg doping is introduced. We are now investigating the root cause of the compensating defects, and experiments to demonstrate p-type InGaN are underway.

As a first step toward a tandem InGaN/Si device, a 125-nm-thick $\text{p}^{++}\text{-Si}$ layer ($1 \times 10^{20} \text{ cm}^{-3}$) was epitaxially grown on a (111) n-Si substrate. A 50-nm *intrinsic* InGaN layer was also grown by MOCVD on top of the Si p^{++} layer, although we have not yet fully developed p-InGaN growth on Si. The intrinsic InGaN is unlikely to be contributing photogenerated carriers, but we incorporated it in the growth process to demonstrate that we can fabricate a full tandem device once p-InGaN growth is developed. The photovoltaic device showed rectifying behavior characteristic of a p-n junction. Current-voltage data was taken in the dark and under 1 sun (not shown) with an unoptimized efficiency of 2.2%.

To demonstrate an *in operando* flow cell for photoelectrodes, we designed, machined, and tested a flow cell for use as an *in operando* microscopy and spectroscopy tool for our PEC devices. The flow cell operates with a thin quartz window $< 1 \text{ cm}$ above the sample allowing the surface to be within the working distance of a Raman or optical microscope. This flow cell contains slots for reference and counter electrodes. During validation, the current-voltage curve of a MoS_2 -protected p-GaInP photocathode matched the onset of a sibling sample tested in a typical H-cell indicating the viability of this cell for electrochemical characterization.

Furthermore, we successfully acquired *ex situ* Raman spectroscopic data of the MoS_2 protective catalyst deposited on a Si photoabsorber. The next step is to take Raman spectra of the samples *in situ*. This requires immersion of the objective lens of a Raman spectrometer in order to achieve this and we have established a dialogue with Jason Cooper of Lawrence Berkeley National Laboratory to develop that capability. This

motivates the possible inclusion of the “Photophysical Characterization of Photoelectrochemical Materials and Assemblies” node at Lawrence Berkeley National Laboratory during Phase 2 of work.

CONCLUSIONS AND UPCOMING ACTIVITIES

In summary, we demonstrated 100-hour stability for high-performance PEC photoelectrodes with >10 mA/cm² under 1 sun, and we fabricated an unassisted PEC water splitting device with a non-precious-metal HER catalyst with STH efficiencies $>5\%$ under 1 sun. This strategy provides a viable pathway for $>20\%$ STH efficiency through improved integration of materials and interfaces. Under ~ 1.3 suns, an MoS₂-protected GaInAsP/GaAs IMM device achieved $>10\%$ STH for 2 hours. In pursuit of low-cost, high-performance tandem PEC absorber layers, we also demonstrated the first InGaN growth on Si (111) by MOCVD.

Work in Phase 2 will focus on the development of working InGaN/Si tandem devices as well as on-sun testing of unassisted water splitting devices for longer than 2 weeks. We will also pursue unassisted water splitting devices with $>20\%$ average STH efficiency. Our collaborations with the EMN nodes have been fruitful for creating and understanding high-quality PEC systems. We believe that continued work with PEC characterization, corrosion analysis, on-sun testing, and III-V fabrication EMN nodes will be invaluable for the success of this project in Phase 2.

FY 2018 PUBLICATIONS/PRESENTATIONS

1. R.J. Britto, J.L. Young, Y. Yang, M.A. Steiner, D.T. LaFehr, M. Beard, T.G. Deutsch, T.F. Jaramillo, “Interfacial Engineering of Gallium Indium Phosphide Photoelectrodes for Hydrogen Evolution with Precious Metal and Non-Precious Metal Based Catalysts,” *Submitted*.
2. J.A. Gauthier, L.A. King, F. Tucker Stults, R.A. Flores, J. Kibsgaard, Y.N. Regmi, K. Chan, T.F. Jaramillo, “Transition Metal Arsenide Catalysts for the Hydrogen Evolution Reaction,” *Submitted*.
3. T.F. Jaramillo, “New Catalysts and New Routes for the Sustainable Production of Fuels and Chemicals,” Invited Presentation at Uppsala University, Department of Chemistry, Uppsala, Sweden, December 2018.
4. T.F. Jaramillo, “Developing Catalysts and Processes for the Sustainable Production of Fuels and Chemicals,” Invited Presentation at Massachusetts Institute of Technology, Department of Chemistry, Inorganic Chemistry Seminar, Cambridge, MA, December 2018.
5. T.F. Jaramillo, “Integrating non-Precious Metal H₂ Evolution Catalysts into Water Electrolyzers and Photoelectrochemical Water Splitting Devices,” Presentation at Annual Meeting of the American Institute of Chemical Engineers (AIChE), Pittsburgh, PA, October 2018.
6. T.F. Jaramillo, “Electrocatalyst Development for the Production and Consumption of Chemical Fuels,” Invited Presentation at the Bosch Energy Research Network (BERN) Symposium 2018, Sunnyvale, CA, September 2018.
7. T.F. Jaramillo, “Design and Development of Catalytic Interfaces for Electrochemical and Photoelectrochemical Processes,” Invited Presentation at the 69th Annual Meeting of the International Society of Electrochemistry, Bologna, Italy, September 2018.
8. T.F. Jaramillo, “The Past, Present, and Future of Photoanodes for Photoelectrochemical (PEC) Water-Splitting,” Invited Presentation at the Center for Chemical Innovation (CCI) Solar Fuels Capstone Meeting, Ventura, CA, July 2018.
9. T.F. Jaramillo, “Catalyzing Electrochemical Processes for Sustainable Energy,” Invited Presentation at the Gordon Research Conference (GRC): Catalysis, Accelerating Catalytic Solutions to Global Grand Challenges, Colby-Sawyer College, New London, New Hampshire, June 2018.
10. T.F. Jaramillo, “Protective Catalyst Systems on III-V and Si-based Semiconductors for Efficient, Durable Photoelectrochemical Water Splitting Devices,” Invited Poster Presentation at the DOE Hydrogen and Fuel Cells Program Annual Merit Review, Washington, D.C., June 2018.

11. T.F. Jaramillo, “Design and Development of Catalyst Materials for the Production of Fuels and Chemicals in a Sustainable Manner,” Invited Presentation at the 4th International Conference on Electrochemistry, Rome, Italy, June 2018.
12. T.F. Jaramillo, “Towards Unassisted Water-Splitting Systems: Development of Catalysts, Semiconductors, and Interfaces,” Invited Presentation at the 233rd Electrochemical Society Meeting, Seattle, WA, May 2018.
13. T.F. Jaramillo, “Catalyst Development for Sustainable Processes Involving Electrochemical Transformations,” Invited Presentation at the École Polytechnique Fédérale de Lausanne (EPFL) Winter School: Challenges and Opportunities in Energy Research, Crans-Montana, Valais, Switzerland, March 2018.
14. T.F. Jaramillo, “Developing New Materials and Processes for the Sustainable Production of Fuels and Chemicals,” Invited Presentation at the University of Texas–El Paso, Department of Chemistry, El Paso, TX, February 2018.
15. T.F. Jaramillo, “Protective Catalyst Systems on III-V and Si-Based Semiconductors for Efficient, Durable Photoelectrochemical Water Splitting Devices,” Invited Presentation at the Hydrogen Production Tech Team (HPTT) Meeting, WebEx, February 2018.
16. T.F. Jaramillo, “Carbon-free Production of H₂, NH₃, and Carbon-based Fuels and Chemicals,” Invited Presentation at The Future of Renewable Transportation, Stanford Energy 3.0 Workshop, Stanford University, Stanford, CA, February 2018.
17. T.F. Jaramillo, “Electrocatalyst Design and Development for Key Reactions in Solar Fuels,” Invited Presentation at the Renewable Energy: Solar Fuels Gordon Research Conference, Ventura, CA, January 2018.

HydroGEN Seedling: Novel Chalcopyrites for Advanced Photoelectrochemical Water Splitting

Nicolas Gaillard
University of Hawaii / Hawaii Natural Energy Institute
2440 Campus Road, Box 368
Honolulu, HI 96822
Phone: (808)-956-2342
Email: ngaillard@hawaii.edu

DOE Manager: Eric Miller
Phone: (202) 287-5829
Email: Eric.Miller@ee.doe.gov

Contract Number: DE-EE0008083

Subcontractors:

- University of Nevada, Las Vegas, Las Vegas, NV
- Stanford University, Stanford, CA

HydroGEN Energy Materials Network nodes:

- Lawrence Livermore National Laboratory, Livermore, CA
- National Renewable Energy Laboratory, Golden, CO

Project Start Date: October 1, 2017

Project End Date: September 30, 2020 (subject to annual go/no-go decision)

Overall Objectives

The overarching goal of this project is to create a chalcopyrite-based, semi-monolithic, tandem hybrid photoelectrode device prototype that can operate for at least 1,000 hours with solar-to-hydrogen (STH) efficiency >10%. This effort is supported by advanced characterization and theoretical modeling to accelerate the development of materials and interfaces. Specifically, our program aims to:

- Develop high-throughput synthesis techniques to create efficient copper chalcopyrite-based materials with ideal optoelectronic properties for photoelectrochemical (PEC) water splitting,
- Identify appropriate surface treatments to prevent photocorrosion, improve surface energetics, and facilitate the hydrogen evolution reaction.

- Create a new method to integrate temperature-incompatible materials into a semi-monolithic PEC device structure.

Fiscal Year (FY) 2018 Objectives

- Identify the appropriate doping chemical element to passivate defects in chalcopyrite materials integrated on transparent conductive substrates.
- Improve chalcopyrite stability in aqueous electrolytes using ultra-thin protection layers, with a durability goal of 500 h continuous operation at a current density >5 mA/cm²,
- Develop a transparent/conductive adhesive to serve as binding material in the semi-monolithic integration scheme.

Technical Barriers

This project addresses the following technical barriers from the Hydrogen Production section of the Fuel Cell Technologies Office Multi-Year Research, Development, and Demonstration Plan¹:

- Materials efficiency (AE)
- Materials durability (AF)
- Integrated device configuration (AG)
- Synthesis and manufacturing (AJ).

Technical Targets

In Task 1, we evaluated the effect of alkali doping on point defects in CuGa₃Se₅ and developed a baseline “printing” process that will serve as a platform for future synthesis of Ga-free, wide-bandgap chalcopyrite candidates. In Task 2, we integrated non-precious catalytic-protecting layers and Cd-free buffers to enhance chalcopyrites’ durability and charge separation efficiency, respectively. Finally in Task 3, we developed transparent conductive epoxy/nanowire composites for semi-monolithic PEC device integration, aiming for optoelectronic properties comparable to that of vacuum-processed indium-doped tin oxide.

¹ <https://www.energy.gov/eere/fuelcells/downloads/fuel-cell-technologies-office-multi-year-research-development-and-22>

The status of this project's technical targets is documented in Table 1.

FY 2018 Accomplishments

Accomplishments during the current project period include:

- Modeling of copper-deficient chalcopyrite surfaces and their impact on energetics.
- Successful integration of CuGa₃Se₅ on F:SnO₂ (FTO) substrate via deliberate alkali doping.
- Chemical analysis of printed chalcopyrites via advanced spectroscopy techniques.
- Open-circuit voltage of 920 mV achieved with 1.8 eV CuGa₃Se₅/MgZnO heterojunctions.
- Extended durability of CuGa₃Se₅ with WO₃ protective coating (400 hours so far tested).

Table 1. Progress Toward this Project's Technical Targets for FY 2018

Task #	Milestone Type	Milestone Description (Go/No-Go Decision Criteria)	Quarter	Status
1	Milestone	A printed polycrystalline chalcopyrite thin film material made of grains at least 500 nm across and with impurity concentration less than 15%.	Q1	100%
3	Milestone	Produce a nanowire and epoxy based composite demonstrating a sheet resistance below 200 Ω/sq and transparency > 70%.	Q2	100%
2	Milestone	Stabilized chalcopyrite photocathode that retains 90% of its copper content after 100 hrs of continuous operation to achieve an initial photocurrent density of 8 mA/cm ² under simulated AM1.5G illumination.	Q3	100%
1	Go/No-Go (1/2)	A solution-processed CuIn(S,Se) ₂ -based PV device with a short-circuit photocurrent density corresponding to at least 70% of the absorber's theoretical limit and free-electron losses (E _g – Voc.q) less than 600 mV .	Q4	95%, on track
2	Go/No-Go (2/2)	Demonstrate 500 hrs stability in a photoelectrode operating under simulated AM1.5G illumination at a fixed potential that achieves an initial photocurrent of 8 mA/cm ² and does not drop below 5 mA/cm ² over the duration of the test.	Q4	85%, on track

INTRODUCTION

Our multidisciplinary program combines advanced synthesis techniques, unique characterization, and theoretical approaches to improve the efficiency and durability of chalcopyrite-based hybrid photoelectrode devices, with the final goal of producing a chalcopyrite-based, semi-monolithic device with at least 10% STH efficiency.

APPROACH

We aim to advance the performance of previously identified wide-bandgap chalcopyrite materials through alkali doping, as well as develop and test the water-splitting viability of the next generation of chalcopyrites. We also see unrealized potential to improve the PEC/electrolyte interface energetics and stability, which is addressed by investigating alternative buffer materials and protective layers. Finally, to avoid the heat-stress issues facing all-chalcopyrite monolithic tandem devices, we investigate a semi-monolithic structure, which will utilize a transparent conductive bonding polymer and exfoliation technique to avoid exposing the bottom photovoltaic (PV) driver in these devices to the high temperatures required for wide-bandgap chalcopyrite synthesis.

RESULTS

Task 1: Modeling and Synthesis of Chalcopyrite Photocathodes

This first year, we investigated the thermodynamic stability of chalcopyrite-derived compounds and competing phases that can form during fabrication and processing of larger-bandgap chalcopyrites. Specifically, we focused on the properties of Cu-deficient (ordered-vacancy compound, or OVC) phases and alkali-derived phases and how they may influence device performance. For example, the existence of OVC-type phases such as CuIn_5Se_8 has long been believed to form in certain processing conditions and influence the resulting device performance via changing the nature of the various heterostructure interfaces formed. Understanding the role of these compounds and under what regimes they are expected to form is key to tuning process conditions that lead to expected performance. This knowledge is additionally helpful in identifying whether the formation of such phases should be explicitly targeted in synthesis processes. In Figure 1 we show the calculated phase diagrams for the larger-bandgap CuGaS_2 absorbers that exhibit a large sensitivity of the qualitative features of OVC-phase formation depending on details of the calculations. This illustrates the complexity in identifying under which conditions these phases are expected to be present.

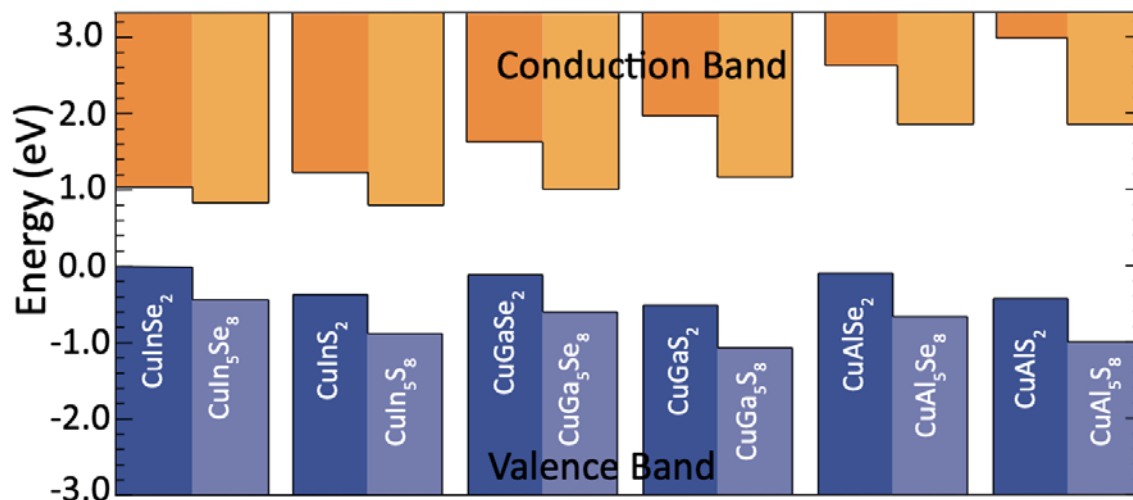


Figure 1. Effect of ordered vacancy compounds on chalcopyrites band offsets

Following these modeling efforts, we studied the effects of alkali metal doping in CuGa_3Se_5 OVC materials grown on glass substrates containing various amount of alkali and coated with Mo back contact. This study

revealed that best PEC performances are obtained on CuGa_3Se_5 absorbers grown on Na-containing SLG substrates. To test the PEC performance of CuGa_3Se_5 photocathodes in a transparent top cell configuration, absorbers were grown directly on FTO back contacts (Pilkington), which include a Na-diffusion barrier between the soda-lime glass and FTO layer. Introducing 15 nm of NaF post-deposition greatly improved the saturated photocurrent density (Figure 2). Moving to thicker pre-deposited NaF appeared also to increase the saturated photocurrent density and photocurrent onset further (up to 0.4 V versus reversible hydrogen electrode, which is the best value ever observed for NREL's bare CuGa_3Se_5). No buffers or catalyst layers were applied to these films yet, and these PEC characteristics are approaching those of the best baseline CuGa_3Se_5 films grown on Mo. These are promising results for the development of tandem water-splitting devices.

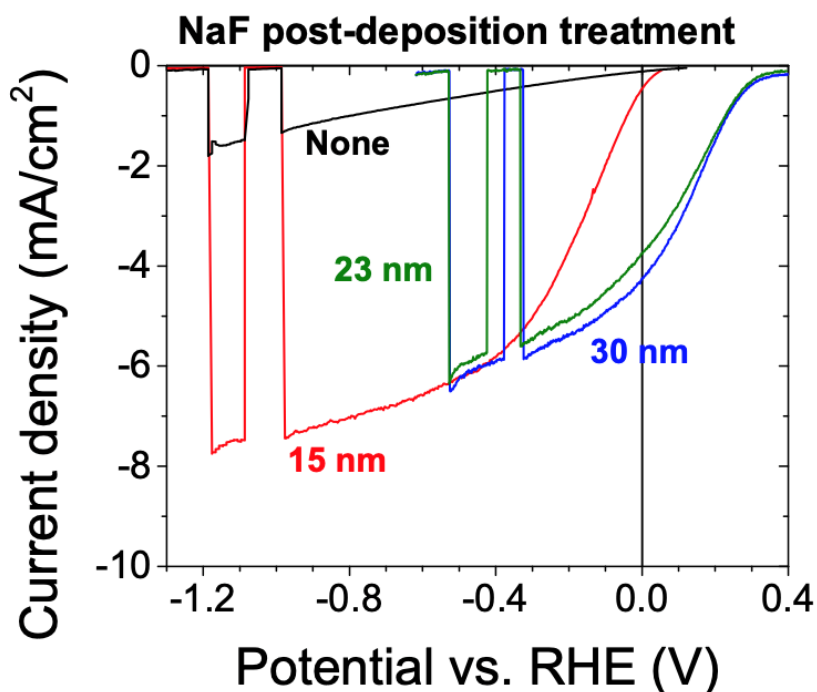


Figure 2. Linear sweep voltammetry characteristics of transparent photocathodes (glass/FTO/ CuGa_3Se_5) with different thicknesses of NaF

Task 2: Interface Engineering for Enhanced Efficiency and Durability

In the first year of this project, we focused on characterizing the electronic and chemical properties of samples produced using liquid processing (printable inks) using X-ray emission spectroscopy at Lawrence Berkeley National Laboratory. Two sample sets were analyzed: two CuInS_2 as-deposited samples and two $\text{CuIn}(\text{S},\text{Se})_2$ selenized samples. The former samples were taken at an intermediate step of the production process—in the full process, they serve as precursors to the latter sample. One sample set was made fully in air (ink formulation and coating), while the other sample set was synthesized with ink formulated in a glovebox using high-performance liquid chromatography (HPLC)-grade methanol and spin-coated in air. The results of the sulfur $L_{2,3}$ X-ray emission spectroscopy study revealed that both CuInS_2 “HPLC” and CuInS_2 “in-air” exhibited dominant transitions typical of sulfur in a sulfide environment. Also, spectral features of S-In, S-Cu, and S-O bonding were observed in these samples. The S-In and S-Cu peaks also appear in the $\text{CuIn}(\text{S},\text{Se})_2$ “HPLC” and $\text{CuIn}(\text{S},\text{Se})_2$ “in-air” spectra, which is expected because CuInS_2 is a precursor of the $\text{CuIn}(\text{S},\text{Se})_2$ samples. Nevertheless, we ruled out the presence of S-O bonds in these selenized samples. Overall, at the near-bulk surface, all four samples have similar chemical environments of sulfur, representing a high-quality $\text{CuIn}(\text{S},\text{Se})_2$ environment. Furthermore, X-ray photoelectron spectroscopy data has been taken at University of Nevada, Las Vegas to analyze the chemical surface structure of these samples. Over the course of the project

year, we find a significant reduction of carbon- and oxygen-containing adsorbates and impurities, especially when comparing sample sets processed in the glovebox to those synthesized in air.

During FY 2018 we also studied alternative buffer materials via combinatorial RF sputtering. Specifically, we integrated Ga-doped $Zn_{1-x}Mg_xO$ buffers on $CuGa_3Se_5$ -based PV devices with different configurations. Devices integrated without CdS (replaced with $Zn_{1-x}Mg_xO$) didn't exhibit any quantifiable current generation, whereas those combining both $Zn_{1-x}Mg_xO$ and CdS exhibited higher device voltage and higher current output compared to the baseline device, indicating favorable conduction band offset. Overall quantum efficiency of the devices was improved, and the long wavelength carrier collection increased with increasing Mg concentration, indicating reduction in carrier recombination. Promising results were achieved by combining Cd^{2+} partial electrolyte (PE) treatment with ZnMgO. The $CuGa_3Se_5$ device performances were found to be dependent on the temperature and the duration of the Cd^{2+} PE treatments. Comparative quantum efficiency of different device configurations (Figure 3) show that replacing CdS with Cd^{2+} PE/ $Zn_{1-x}Mg_xO$ as the window layer improves the carrier collection in the short wavelengths due to the higher bandgap of ZnMgO. Open circuit voltage up to 920 mV was measured, which can be significant for PEC water splitting applications.

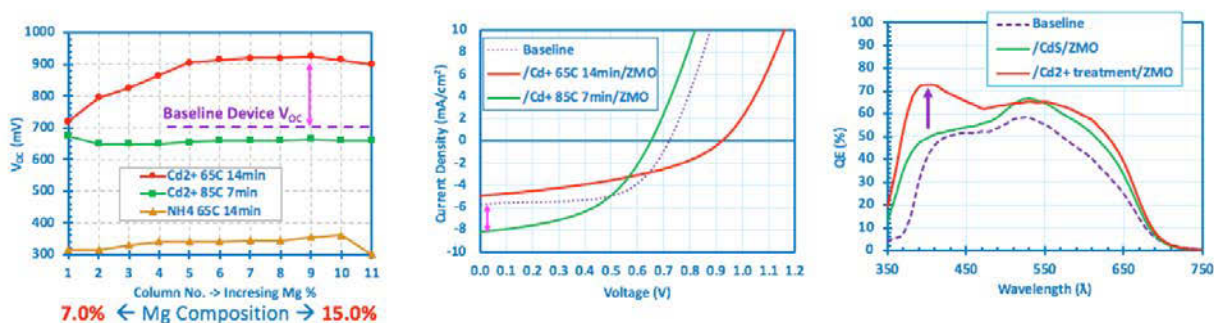


Figure 3. Solid-state performance for CdS-free $CuGa_3Se_5/Zn_{1-x}Mg_xO$ devices with different surface treatments

Finally, we developed protective and catalytic coatings for chalcopyrite photocathode operation in acidic electrolyte conditions and quantified the degradation of these protected devices. Linear sweep voltammograms measured on three $CuGa_3Se_5$ photocathodes coated with 3-nm-thick WO_3 protective layer and nanoparticulate Pt catalyst demonstrated good photocurrent onset at +0.1 V versus reversible hydrogen electrode or greater and reached a saturation photocurrent density (j_{ph}) of at least -6 mA cm^{-2} under 1 Sun illumination. Subsequent chronoamperometric (CA) durability tests were performed on these same devices with the potential being held in the light-limited region under constant illumination. Notably, two devices have reached 85% of Phase 1 go/no-go durability target (see Table 1 for details). Additionally, we measured the degradation of a $CuGa_3Se_5$ absorber film protected with a 3-nm atomic layer deposition film of WO_3 using inductively coupled plasma mass spectrometry analysis. Our study shows that the dissolved quantity of copper in solution is less than 5.6% over 100 h of testing, satisfying the Q3 milestone.

Task 3: Hybrid Photoelectrode Device Integration

During FY 2018, we focused on the development of a transparent conductive binder for semi-monolithic hybrid device integration. With this approach, we propose to solve process compatibility issues between material classes by bonding a chalcopyrite photoelectrode onto a fully processed PV driver. Excellent results were achieved with composites made of silver nanowires (AgNWs). In this experiment, AgNWs (L: $27 \pm 23 \mu\text{m}$, diam: $72 \pm 21 \text{ nm}$) suspended in isopropanol (2.55 wt%) were first dispersed in cellulose (0.96 wt%). Then, roughly 100 μL of the AgNWs/cellulose solution was spin coated onto a SLG substrate for 45 seconds at 800 rpm and subsequently annealed on a hot plate in air at 100°C . Figure 4 presents a picture of the resulting SLG/AgNWs transparent sample as well as a top view scanning electron micrograph. One can see that the AgNWs are well dispersed and form an interconnected network with enough separation in between to allow light transmission. The latter was confirmed by ultraviolet-visible analysis, showing transmission over 92% in

the 350–1,200 nm range. The sheet resistance of this sample, measured by 4-point probe technique, was 22 ohm/square, exceeding the Q2 milestone.

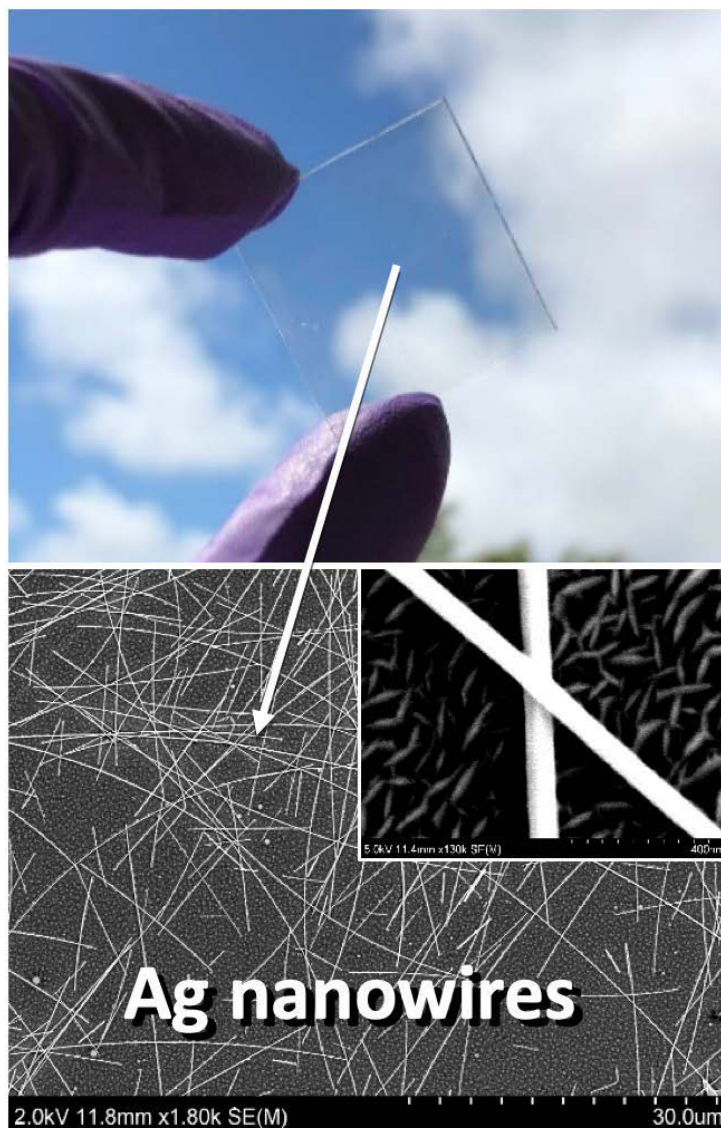


Figure 4. Optical image and scanning electron micrograph of a conductive transparent adhesive made with silver nanowires

CONCLUSIONS AND UPCOMING ACTIVITIES

- Further validate protection with WO_3 film, targeting 500 h of continuous operation.
- With help from advanced spectroscopy, improve chalcopyrites solution processing, aiming for high-efficiency solid-state CuInSe_2 devices.
- Continue the development of ZnMgO buffers, targeting over 1 V open circuit voltage.
- With help from theory, further develop chalcopyrites alkali doping to create highly efficient photocathodes on transparent substrates.

HydroGEN Seedling: Monolithically Integrated Thin-Film/Silicon Tandem Photoelectrodes for High-Efficiency and Stable Photoelectrochemical Water Splitting

Zetian Mi
University of Michigan
1301 Beal Ave
Ann Arbor, MI 48109
Phone: (734) 764-3963
Email: ztmi@umich.edu

DOE Manager: Eric Miller
Phone: (202) 287-5829
Email: Eric.Miller@ee.doe.gov

Contract Number: DE-EE0008086

Subcontractors:

- Michigan State University, East Lansing, MI
- Boston College, Boston, MA
- University of Toledo, Toledo, OH

Project Start Date: October 1, 2017

Project End Date: Project continuation and direction determined annually by DOE

Overall Objectives

- Develop monolithically integrated Si-based tandem photoelectrodes to achieve both high solar-to-hydrogen (STH) efficiency (>15%) and long-term stability (>1,000 hours) in spontaneous water splitting systems.

Fiscal Year (FY) 2018 Objectives

- Demonstrate top photoelectrodes with energy bandgap ~1.7–2.0 eV on Si that can deliver photocurrent density >10 mA/cm² and open circuit potential >0.7 V under standard one-sun illumination.
- Demonstrate proof-of-concept double-junction photoelectrode on Si, with open circuit potential further enhanced by at least 0.5 V compared to the standalone top photoelectrode.

Technical Barriers

This project addresses the following technical barriers from the Hydrogen Production section of

the Fuel Cell Technologies Office Multi-Year Research, Development, and Demonstration Plan¹:

- **Materials Durability—Bulk and Interface:** Identify intrinsically durable and efficient materials for photoelectrochemical (PEC) hydrogen generation.
- **Integrated Device Configurations:** Develop efficient, stable integrated devices to meet the ultimate targets in PEC hydrogen generation.
- **Synthesis and Manufacturing:** Scalable manufacturing of PEC materials and devices.

Technical Targets

This project is developing monolithically integrated tandem photoelectrodes on low-cost, large-area Si wafer. Success of this project will provide the materials platform for PEC water splitting devices that help meet the following DOE PEC hydrogen production targets:

- STH energy conversion ratio: 20%
- PEC electrode cost: \$200/m².

FY 2018 Accomplishments

- Demonstrated top photoelectrode with photocurrent density >12 mA/cm² at 0 V vs. normal hydrogen electrode (NHE) and open circuit potential >0.75 V.
- Demonstrated InGaN/Si double-junction photocathode that can exhibit an onset potential ~2 V vs. reversible hydrogen electrode (RHE), representing an enhancement of the photovoltage by 1.5 V compared to the Si photocathode. Such a device can perform unassisted solar water splitting.
- Demonstrated that GaN/Si photocathode can exhibit stable (>100 h) and efficient operation (photocurrent density >38 mA/cm² under one-sun illumination) without using any extra surface protection.

¹ <https://www.energy.gov/eere/fuelcells/downloads/fuel-cell-technologies-office-multi-year-research-development-and-22>

INTRODUCTION

The DOE STH conversion efficiency and cost targets for purified, 300 psi compressed hydrogen gas are 20% STH and \$5.70/kg hydrogen by 2020. The tandem PEC device concept of stacking wide-bandgap and narrow-bandgap semiconductors is a proven method that can achieve the targeted STH efficiency. To date, all efficient tandem PEC devices are based on the state-of-the-art III-V semiconductor tandem photoelectrodes. However, the expensive GaAs substrates and photocorrosion severely limited their ability to achieve the cost goal. We aim to tackle the challenges of achieving efficient, cost-effective PEC water splitting devices by developing tandem photoelectrodes, which consist of a bottom Si light absorber and a 1.7–2.0 eV top light absorber. High-performance top photoelectrode will be fabricated on large-area Si wafer using nanowire tunnel junction and will be passivated by an ultrathin N-rich GaN to protect against photocorrosion and oxidation.

The outcome of this project is to develop monolithically integrated Si-based tandem photoelectrodes, with the objective to achieve high efficiency (up to 20%) and long-term stability (>1,000 hours) in STH conversion through PEC water splitting. This project will be instrumental to establish an Si-based platform for high-efficiency PEC tandem water splitting devices and systems, which, to date, can only be achieved using prohibitively expensive GaAs-based materials. The stability of PEC water splitting devices will be fundamentally improved by utilizing N-terminated GaN protection layer. The semiconductor photoelectrodes are synthesized using industry-ready materials (e.g., Si and GaN based on standard semiconductor processing), and therefore the manufacture is controllable and scalable. The success of this project will help meet the DOE technical target for hydrogen production from PEC water splitting.

APPROACH

In this project, we aim to address the challenges of achieving efficient, cost-effective, PEC water splitting systems by combining the following unique approaches.

1. **We use Si as the bottom light absorber** to reduce the cost of the tandem water splitting devices, given its narrow energy bandgap and prevalence in industry.
2. **We use wide-bandgap GaN nanowire tunnel junction** to fabricate the top photoelectrodes on the Si platform. The GaN nanowire tunnel junction not only exhibits remarkably low resistivity but also further reduces the formation of defects and dislocations in the top light absorber because of the effective lateral surface stress relaxation.
3. **We use Ta₃N₅, BCTSSe, and In_{0.5}Ga_{0.5}N semiconductors** as the top light absorber of the double-junction photoelectrodes. These materials have bandgaps in the range of 1.7–2.0 eV, can be controllably doped n or p-type and exhibit large light absorption coefficients and superior charge carrier transport properties. Recent studies have further shown that the conduction and valence band edge positions of Ta₃N₅ and In_{0.5}Ga_{0.5}N straddle the water splitting potentials, promising photovoltages larger than 1.23 V.
4. **We use surface treatment and catalyst loading** to protect electrodes from corrosion and optimize water oxidation efficiency. We will incorporate a non-oxide coating (e.g., GaN) to eliminate this detrimental effect. We also have developed the chemistry and expertise at integrating a variety of water oxidation co-catalysts with photoanodes, which we have shown to improve the V_{on} by several hundred millivolts, which will be employed to optimize the performance of the proposed systems.

The research team consists of four investigators, including Profs. Z. Mi at University of Michigan, T. Hamann at Michigan State University, D. Wang at Boston College, and Y. Yan at University of Toledo. During the course of this project, we have established effective collaborations with the following nodes at the HydroGEN Energy Materials Network (EMN) to advance the proposed project.

1. “Surface Analysis Cluster Tool,” Glenn Teeter, National Renewable Energy Laboratory (NREL). Surface characterization and in operando X-ray photoelectron spectroscopy (XPS) measurements are being performed on the various top photoelectrodes.

2. “Probing and Mitigating Chemical and Photochemical Corrosion of Electrochemical and Photoelectrochemical Assemblies,” Francesca Toma, Lawrence Berkeley National Laboratory (LBNL). With the unique in situ techniques, including photoelectrochemical atomic force microscopy and scanning tunneling microscopy, Toma has provided services to understand the behaviors of our top electrode materials, and this information proves invaluable to our optimization efforts.
3. “Surface Modifications for Catalysis and Corrosion Mitigation,” Todd Deutsch, NREL. This collaboration helps to identify the best strategy to protect the surface against photocorrosion and oxidation.
4. “Ab Initio Modeling of Electrochemical Interfaces,” Tadashi Ogitsu, Lawrence Livermore National Laboratory (LLNL). This collaboration provides important insights of electrochemical interface and PEC device optimization through ab initio modeling and computational materials diagnostics.
5. “Computational Materials Diagnostics and Optimization of Photoelectrochemical Devices,” Tadashi Ogitsu, LLNL. Dr. Ogitsu and his team members have performed first principles studies of N-terminated GaN surfaces and the effect on solar water splitting. These studies are further correlated with the stability analysis of the photoelectrodes.

RESULTS

Controlled Synthesis of Top Photoelectrode with $E_g \sim 1.7\text{--}2.0$ eV

Critical for achieving a high-efficiency double-junction photoelectrode is a top photoelectrode that has an energy bandgap $\sim 1.7\text{--}2.0$ eV, is stable in acidic solution, and can be controllably doped n- or p-type. In this project, we have demonstrated controlled synthesis of $\text{In}_{0.5}\text{Ga}_{0.5}\text{N}$, Ta_3N_5 , and BCTSSe photoelectrodes, which have a direct bandgap of $1.7\text{--}2.0$ eV. We have further demonstrated that the surface can be covered by an atomically thin N-rich protection layer, which can protect the top photoelectrode against photocorrosion and oxidation without compromising charge carrier extraction and STH conversion efficiency.

GaN and InGaN nanowires were grown on Si wafer using a molecular beam epitaxy (MBE) system equipped with a radio frequency plasma-assisted nitrogen source. The growth was conducted in N-rich conditions to promote the formation of N-terminated surfaces to protect against photocorrosion and oxidation.

Photoluminescence (PL) spectra measured at room temperature for InGaN nanowires are shown in Figure 1. By changing the growth conditions, the PL emission wavelengths can be varied from ~ 500 nm to ~ 750 nm, corresponding to indium compositions of $\sim 24\%$ to $\sim 51\%$, respectively. For indium compositions of 45% , the energy bandgap is ~ 1.8 eV, which can serve as the top electrode for an efficient double-junction photoelectrochemical device. Significantly, the band edges of such InGaN can straddle the water redox potentials, which is essentially required for unassisted solar water splitting. InGaN is doped p-type with Mg.

In parallel, extensive studies also have been performed on the synthesis of Ta_3N_5 and BCTSSe photoelectrodes. Ta_3N_5 was directly deposited on fluorine-doped tin oxide (FTO) substrates using a custom-built and fully automated atomic layer deposition system capable of operating at elevated temperatures with a maximum temperature of 640°C . For BCTSSe, we used mixed precursor films made by co-sputtering Cu, BaS, and SnS targets. The composition and thickness of the mixed precursor film were controlled by controlling the radio frequency powers and time applied to the targets. Detailed structural characterization has also been performed on these materials, which demonstrate a high level of crystallinity.

Critical for the operation of the monolithically integrated GaN/Si photocathode is the conduction band alignment between GaN and Si. To date, however, a direct measurement of the band alignment between Si and N-polar GaN was not available to our knowledge. Dr. G. Teeter’s group at NREL performed XPS measurements on GaN/Si samples in a Physical Electronics 5600 instrument using monochromatic Al- α illumination ($h\nu = 1486.6$ eV) at a pass energy of 11.75 eV. Samples tested for XPS were bare n^+ -Si(100), thin ($\sim 2\text{--}3$ nm) n^+ -GaN/Si(100), and relatively thick (~ 30 nm) n^+ -GaN/Si(001). The samples were transferred under Ar and ultra-high vacuum into the XPS system. XPS survey spectra and high-resolution core-level spectra revealed acceptably low levels of surface contamination, enabling subsequent band-offset

measurements. A band diagram (Figure 1(b)) is constructed from the measured valence band maximums (VBMs) and the observed core-level shifts between these samples. The measured position of the VBM (1.16 ± 0.05 eV) on the bare Si surface indicates that, within uncertainty, E_F is pinned above the CBM. Deposition of 2–3 nm of GaN evidently passivates the Si surface and induces a small amount of upward band bending. Assuming the GaN band gap = 3.39 eV, for this surface E_F is ~ 0.1 eV above the GaN CBM, indicating that this thin layer is degenerately doped n -type. The interfacial valence-band offset calculated from measured VBMs and core-level shifts was 2.44 ± 0.1 eV. This value, in combination with the individual band gaps of Si and GaN, leads to a conduction band offset of -0.16 ± 0.1 eV. Our measurements confirm for the first time that the CBM between n -polar GaN and Si is approximately aligned, thereby enabling efficient charge carrier (electron) transfer from Si to GaN.

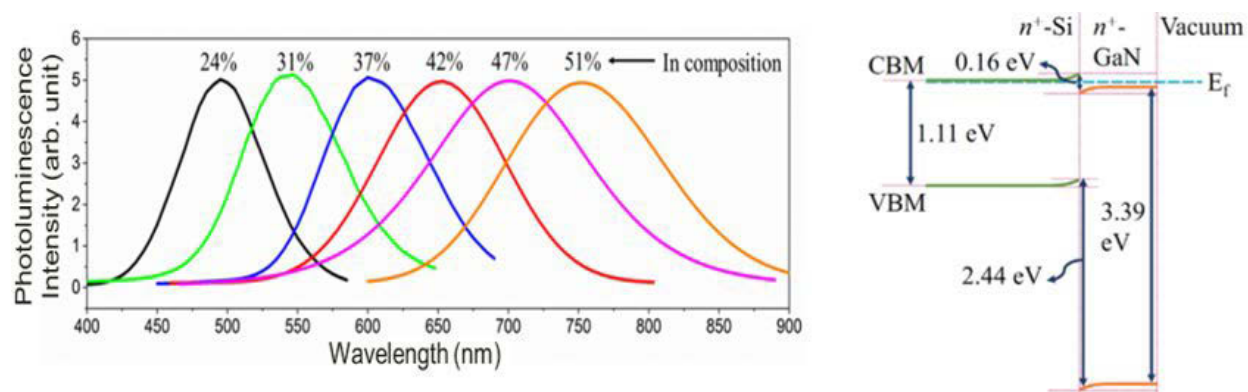


Figure 1. (a, left) Room-temperature photoluminescence spectra of different InGaN nanowires, showing that the photoluminescence emission peak can be controllably varied from 500 to 750 nm, corresponding to indium compositions of 24% to 51%. (b, right) Band diagram constructed for samples examined in XPS study for ~ 30 nm n^+ -GaN/ n^+ -Si. The bulk E_F position in the n^+ -Si wafer is positioned just below the conduction band minimum (CBM), and the extents of band bending in each layer at the interface are assumed to be approximately equal.

Performance of Top Photoelectrode

Photoelectrochemical measurements of p-InGaN nanowire photocathodes were performed in 0.5 M H_2SO_4 solution (pH ~ 0) under the illumination of 100 mW/cm² simulated AM 1.5 G solar spectrum. Shown in Figure 2(a) is the linear sweep voltammetry measurement of p-In_{0.42}Ga_{0.58}N tunnel junction photocathode. The onset potential is 0.79 V vs. NHE, and a relatively high photocurrent density of 12.3 mA cm⁻² is measured at 0 V vs. NHE. The dark current density is negligible compared to the photocurrent, confirming the measured photocurrent comes from solar energy conversion. The improved onset potential and photocurrent density of p-InGaN tunnel junction nanowire photocathode is directly related to the efficient charge separation, hole collection, and electron extraction enabled by the integration with GaN tunnel junction. We have further performed continuous solar water splitting measurements on p-InGaN tunnel junction nanowire photocathode. Shown in Figure 2(b), the hydrogen evolution in 0.5 M H_2SO_4 solution was measured as a function of time at a constant photocurrent density of ~ 12 mA/cm² under AM 1.5 G one-sun illumination. The applied bias stays nearly constant at ~ 0 V vs. NHE, illustrated in Figure 2(b). It is seen that the measured and calculated hydrogen evolution agrees well, confirming a nearly unity faradaic efficiency.

Additionally, 230-nm-thick Ta₃N₅ films on FTO substrates and control FTO electrodes were coated with the CoPi water oxidation catalyst via electrodeposition in the light and dark, respectively, at a constant current of 10 $\mu A/cm^2$ for 8 minutes. The J - E curves of these electrodes under water oxidation condition at the neutral pH are shown in Figure 2(c). The shift in the potential required to sustain a given rate of water oxidation (i.e., current density) is a good measure of the photovoltage produced by the underlying semiconductor. From this plot, comparing the potentials needed to produce 1 mA/cm² indicates the Ta₃N₅ produces a photovoltage of

0.85 V, with a photocurrent onset potential of 0.5 V vs. RHE. This exceeds the milestone of a 0.5 V photovoltage.

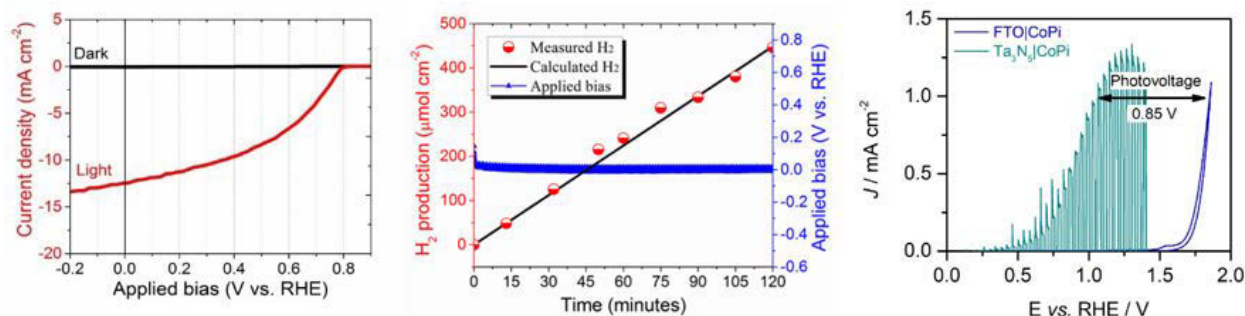


Figure 2. (a, left) Linear sweep voltammetry measurements of *p*-InGaN tunnel junction nanowire (*p*-InGaN/TJ/Si) in H₂SO₄ electrolyte (0.5 M, pH ~0) under simulated AM 1.5 G solar illumination of 100 mW/cm². (b, center) Hydrogen gas evolution under a constant photocurrent density of 12 mA/cm². The calculated hydrogen production from photocurrent is also shown (solid black curve). (c, right) Plots of *J-E* curves of CoPi-coated Ta₃N₅ and CoPi-coated FTO electrodes in chopped-light (1 sun) and dark conditions, respectively, in contact with 0.1 M potassium phosphate buffer solution at pH=7.

The performance of GaN/Si and T₃N₅ photoelectrodes has also been studied by Dr. T. Deutsch at NREL and Dr. F. Toma at LBNL. When a bias light was used, the incident photon-to-electron conversion efficiency improved dramatically, suggesting the photoelectrodeposition procedure is introducing electron trap states at the surface. NREL used atomic layer deposition to apply Pt to the GaN nanowires, which showed improved onset potential, likely due to the reduced trap states. PEC testing, XPS, inductively coupled plasma mass spectrometry, and in situ atomic force microscopy studies were carried out to systematically investigate the corrosion mechanism of Ta₃N₅ thin films. The results showed that the PEC performance of Ta₃N₅ degraded very fast when a constant bias was applied. This degradation of Ta₃N₅ was attributed to the formation of a few-nanometers-thick oxide layer at the surface during the first few minutes of PEC testing. Further analysis, such as in situ transmission electron microscopy and XPS beamline, will be conducive to qualitatively and quantitatively characterize this oxide layer, and provide insight into the corrosion mechanism of Ta₃N₅.

We also have focused on optimizing catalyst deposition with a balance between performance and cost by developing a non-aqueous method for catalyst deposition to reduce complications caused by catalyst growth in aqueous systems. It was found that Pt can be deposited on the Si photocathodes coated with GaN nanowires (GaN/Si) when the PEC water reduction occurred on the photocathodes at the same time, using a Pt mesh as the counter electrode in a one-chamber cell with a three-electrode configuration. Hydrogen evolution reaction performance of GaN/Si photocathode is improved by optimizing the non-aqueous PEC Pt deposition.

Performance of Si-Based Double-Junction Photoelectrode

Illustrated in Figure 3(a), the double junction photocathode consists of a *p*-InGaN top light absorber (In composition ~ 30%) and a Si bottom junction. The InGaN and Si segments are connected by an InGaN tunnel junction. Photogenerated electrons in the Si bottom light absorber recombine with photogenerated holes of the *p*-InGaN top light absorber. The PEC reaction was conducted in 0.5 M H₂SO₄ solution with Pt co-catalyst, silver chloride electrode (Ag/AgCl), and Pt wire as the working, reference, and counter electrode, respectively. A solar simulator (Newport Oriel) with an AM 1.5 G filter was used as the light source, and the light intensity was calibrated to be 100 mW/cm² for all experiments. Figure 3(b) shows the linear sweep voltammetry of platinumized InGaN/TJ/Si double-junction photocathode (red curve) and platinumized single-junction GaN/*n*⁺-*p* Si photocathode (GaN/Si) (blue curve) under AM 1.5 G one-sun illumination and dark condition (black curve). The GaN/Si photocathode has *V*_{on} of ~0.5 V vs. RHE whereas the double-junction InGaN/TJ/Si has *V*_{on} of ~2.3 V vs. RHE, representing an enhancement of the photovoltage by ~1.8 V compared to the Si photocathode.

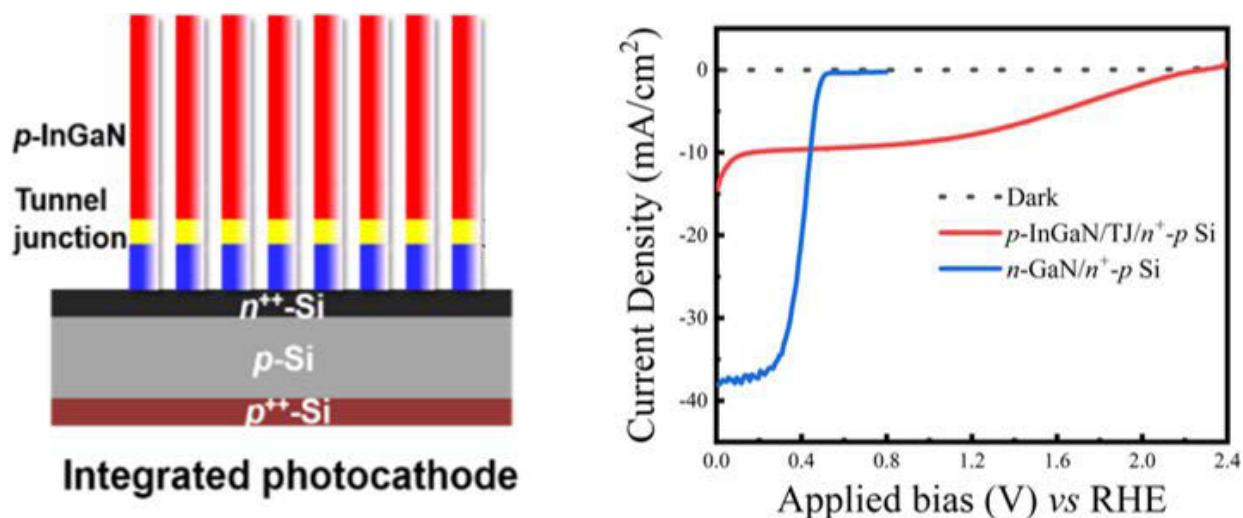


Figure 3. (a, left) Schematic illustration of a double-junction photocathode consisting of p-InGaN top junction and a Si bottom junction. The InGaN and Si are connected through a tunnel junction. (b, right) Linear sweep voltammetry measurements of the single-junction Si photocathode (blue curve) and InGaN/Si double-junction photocathode (red curve) in 0.5 M H₂SO₄ electrolyte under stimulated AM 1.5 G solar illumination of 100 mW/cm².

Long-Term Stability

We subsequently conducted a long-duration stability test for platinized n^+ -GaN nanowire/ n^+ -p Si photocathode at 0 V vs. RHE in 0.5 M H₂SO₄ under AM 1.5 G one-sun illumination. Illustrated in Figure 4(a), the photocurrent density showed no degradation for a duration of 113 h. The observed fluctuation in current is due to the accumulation and release of hydrogen bubbles from the sample surface. To maintain the same experimental conditions, the electrolyte was changed after every 24 h. To our knowledge, this high stability measured at ~ 38 mA/cm² is the best for any semiconductor photocathodes tested at a photocurrent density of 30 mA/cm², or higher, when compared with 10 h for Pt (2 nm)/SiHJ [1], 24 h for Pt/TiO₂/F:SnO₂/Ti/ n^+ -p Si [2], and 4 h for Ru/TiO₂/ p -InP [3]. We conducted detailed structural characterization of these samples through stability tests using scanning electron microscopy and transmission electron microscopy. The nanowire dimensions remained virtually the same compared to those before the experiments, suggesting that the nanowires were not etched during the long-term stability experiments. It is noticed, however, that the surface coverage of Pt nanoparticles was significantly reduced compared to that prior to the experiments. The underlying mechanisms for the long-term stability of GaN/Si photocathode are further discussed. Compared to conventional III-V semiconductors, III-nitrides have strong ionic bonds, which leads to the bunching of surface states near the band edge, rather than the forbidden bandgaps [4–5]. Therefore, the surface states of III-nitrides do not serve as nonradiative recombination centers, which is instrumental for achieving long-term stability against corrosion. Moreover, the nanowires grown by MBE have nearly perfect single-crystal wurtzite structure and are free of dislocations. Recent theoretical and experimental studies of the actual atomic structure of GaN nanowires grown by MBE further revealed that they exhibited a unique N-termination, not only for the (000 $\bar{1}$) top faces but also for their nonpolar side faces [6]. Such N-terminated surfaces can further protect against corrosion during harsh PEC reaction.

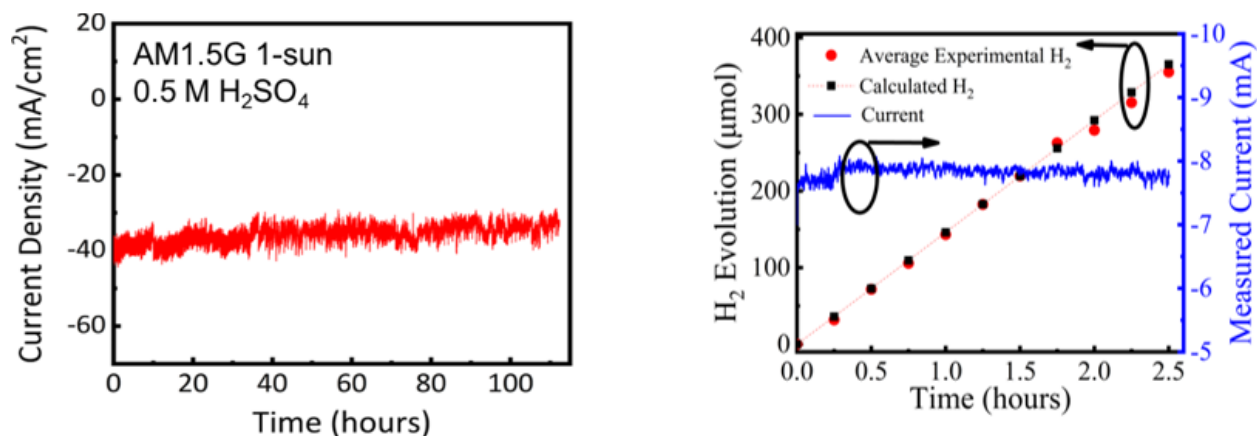


Figure 4. (a, left) PEC long-term stability measurement for platinized n^+ -GaN nanowires/ n^+ - p Si photocathode at 0 V vs. RHE in 0.5 M H_2SO_4 under AM 1.5 G one-sun illumination. The photocurrent density of photocathode showed no degradation for >100 h duration (113 h). (b, right) Hydrogen generation for platinized n^+ -GaN nanowires/ n^+ - p Si photocathode at 0.02 V vs. RHE under AM 1.5 G one-sun illumination in 0.5 M H_2SO_4 for 2.5 h. Blue curve represents the photocurrent, red dots represent the average amount of hydrogen generated at various times, and black dotted line is the theoretical amount of H_2 produced against time based on photocurrent. The Faraday efficiency is nearly 100%. The electrode area for the sample is 0.2 cm^2 , which corresponds to a photocurrent density of $\sim 39 \text{ mA}/\text{cm}^2$.

Blue curve represents the photocurrent, red dots represent the average amount of hydrogen generated at various times, and black dotted line is the theoretical amount of H_2 produced against time based on photocurrent. The Faraday efficiency is nearly 100%. The electrode area for the sample is 0.2 cm^2 , which corresponds to a photocurrent density of $\sim 39 \text{ mA}/\text{cm}^2$.

Investigation of Structural and Electronic Properties of Ga(In)N Surfaces

Dr. T. Ogitsu's group at LLNL has developed various structural models of GaN surfaces and GaN/water interfaces and has performed ab initio molecular dynamics simulations of these systems. It was found that N-rich and Ga-rich surfaces exhibited significant differences in the structural properties. The water molecules at the N-rich surface show a tendency of pointing their hydrogen atoms toward the surface N atoms, while the oxygen atoms are strongly attracted by the surface Ga atoms of the Ga-rich surface. In addition, the LLNL team has investigated the electronic structures of Ga(In)N alloys and the band bending of GaN for different surface terminations (Ga/N). Experimentally, it is known that In incorporation to GaN leads to significantly lower open circuit voltage (V_{OC}) than the theoretical value estimated from the bandgap, presumably due to imperfection in the system such as development of detrimental defects near the interface. These studies are to establish the reference points for further theoretical works with more realistic models (liquid-solid interface, incorporation of defects) as well as experimental calibration of our simulation.

CONCLUSIONS AND UPCOMING ACTIVITIES

In conclusion, this project is focused on the development of Si-based high-efficiency PEC tandem water splitting devices, with major innovations including the use of nanowire tunnel junction to fabricate 1.7–2.0 eV top photoelectrodes on Si wafers, and the discovery of N-terminated GaN to protect against photocorrosion. In this project, we have demonstrated 1.7–2.0 eV top photoelectrodes with improved performance. We have achieved photocurrent $>12 \text{ mA}/\text{cm}^2$ at 0 V vs. NHE under one-sun illumination. We have further demonstrated InGaN/Si double-junction photoelectrodes. The photovoltage is enhanced by $\sim 1.5 \text{ V}$ compared to the Si photocathode. We have also demonstrated GaN/Si photocathodes with stable operation for $>100 \text{ h}$ at a very high photocurrent density of $\sim 38 \text{ mA}/\text{cm}^2$ without using any extra surface protection. Detailed theoretical studies of the GaN surfaces and GaN/water interfaces have also been performed.

No additional work is currently funded, and there are no open issues remaining.

SPECIAL RECOGNITIONS AND AWARDS/PATENTS ISSUED

1. Zetian Mi was elected Fellow of Optical Society of America in 2018.

FY 2018 PUBLICATIONS/PRESENTATIONS

Journal Publications

1. F.A. Chowdhury, M.L. Trudeau, H. Guo and Z. Mi, “A Photochemical Diode Artificial Photosynthesis System for Unassisted High Efficiency Overall Pure Water Splitting,” *Nature Communications* 9 (2018): 1707.
2. B. Zhou, X. Kong, S. Vanka, S. Chu, P. Ghamari, Y. Wang, N. Pant, I. Shih, H. Guo, and Z. Mi, “GaN nanowire as an outstanding linker of MoS_x and planar silicon for photoelectrocatalytic water splitting,” *Nature Communications* 9 (2018): 3856.
3. S. Vanka, E. Arca, S. Cheng, K. Sun, G.A. Botton, G. Teeter, and Z. Mi, “A High Efficiency Si Photocathode Protected by Multi-Functional GaN Nanostructures,” *Nano Lett.* 18 (2018): 6530.
4. X. Guan, F.A. Chowdhury, Y. Wang, N. Pant, S. Vanka, M.L. Trudeau, L. Guo, L. Vayssieres, and Z. Mi, “Making of an industry-friendly artificial photosynthesis device,” *ACS Energy Lett.* 3 (2018): 2230.
5. S. Chu, S. Vanka, Y. Wang, J. Gim, Y. Wang, Y.-H. Ra, R. Hovden, H. Guo, I. Shih, and Z. Mi, “Solar Water Oxidation by an InGaN Nanowire Photoanode with a Bandgap of 1.7 eV,” *ACS Energy Lett.* 3 (2018): 307.
6. X. Guan, F.A. Chowdhury, N. Pant, L. Guo, L. Vayssieres, and Z. Mi, “Efficient Unassisted Overall Photocatalytic Seawater Splitting on GaN-Based Nanowire Arrays,” *J. Phys. Chem. C* 122 (2018): 13797.
7. Y. He and D. Wang, “Toward Practical Solar Hydrogen Production,” *Chem.* 4 (2018): 405–408.

Conference Presentations

1. H. Hajibabaei and T. Hamann, “Direct Deposition of Crystalline Tantalum Nitride (Ta₃N₅) on FTO via High-Temperature Atomic Layer Deposition (ALD),” Gordon Research Conference; Renewable Energy: Solar Fuels, January 28–February 2, 2018
2. (Invited talk) D. Wang, “Understanding the Interface between Photoelectrodes and Catalysts,” MRS Spring 2018, Phoenix, AZ, April 2–6, 2018.
3. (Invited talk) Yanfa Yan, “New materials for photoelectrochemical water splitting,” 232nd Electrochemical Society Meeting, National Harbor, MD, October 2, 2017.
4. (Invited talk) Z. Mi, “Solar Water Splitting and CO₂ Reduction on III-Nitride Nanostructures,” MRS Spring Meeting, Phoenix, AZ, April 2–6, 2018.
5. (Invited talk) Z. Mi, “Artificial Photosynthesis on III-Nitride Nanowire Arrays,” 233rd Electrochemical Society (ECS) Meeting, Seattle, WA, May 13–17, 2018.
6. T.A. Pham, X. Zhang, B.C. Wood, S. Ptasinska, and T. Ogitsu, “Integrating Ab-Initio Simulations and Experimental Characterization Methods for Understanding Chemistry at Complex Photoelectrochemical Interfaces,” MRS Spring 2018, Phoenix, AZ, April 2–6, 2018.
7. T.A. Pham, X. Zhang, B.C. Wood, S. Ptasinska, and T. Ogitsu, “Integrating Ab-Initio Simulations and Experimental Characterization Methods for Understanding Chemistry at Complex Photoelectrochemical Interfaces,” ECS Meeting 2018, Seattle, WA, May 13–17, 2018.

REFERENCES

1. H.P. Wang, K. Sun, S.Y. Noh, A. Kargar, M.L. Tsai, M.Y. Huang, D.L. Wang, and J.H. He, “High-Performance a-Si/c-Si Heterojunction Photoelectrodes for Photoelectrochemical Oxygen and Hydrogen Evolution,” *Nano Letters* 15, no. 5 (2015): 2817–2824.
2. M.G. Kast, L.J. Enman, N.J. Gurnon, A. Nadarajah, and S.W. Boettcher, “Solution-deposited F:SnO(2)/TiO(2) as a base-stable protective layer and antireflective coating for microtextured buried-junction H(2)-evolving Si photocathodes.” *ACS Appl Mater Interfaces* 6, no. 24 (2014): 22830–7.

3. M.H. Lee, K. Takei, J. Zhang, R. Kapadia, M. Zheng, Y.Z. Chen, J. Nah, T.S. Matthews, Y.L. Chueh, J.W. Ager, and A. Javey, “p-Type InP nanopillar photocathodes for efficient solar-driven hydrogen production.” *Angew. Chem. Int. Ed. Engl.* 51, no. 43 (2012): 10760–4.
4. T.D. Moustakas, “The role of extended defects on the performance of optoelectronic devices in nitride semiconductors.” *Phys. Status Solidi. A* 210, no. 1 (2013): 169–174.
5. M.G. Kibria, F.A. Chowdhury, S. Zhao, B. AlOtaibi, M.L. Trudeau, H. Guo, and Z. Mi, “Visible light-driven efficient overall water splitting using p-type metal-nitride nanowire arrays.” *Nature Communications* 6 (2015).
6. M.G. Kibria, R. Qiao, W. Yang, I. Boukahil, X. Kong, F.A. Chowdhury, M.L. Trudeau, W. Ji, H. Guo, F.J. Himpsel, L. Vayssieres, and Z. Mi, “Atomic-Scale Origin of Long-Term Stability and High Performance of p-GaN Nanowire Arrays for Photocatalytic Overall Pure Water Splitting.” *Adv. Mater.* 28, no. 38 (2016): 8388–8397.

HydroGEN Seedling: Accelerated Discovery of Solar Thermochemical Hydrogen Production Materials via High-Throughput Computational and Experimental Methods

Ryan O'Hayre (Primary Contact), Michael Sanders
Colorado School of Mines
1500 Illinois St.
Golden, CO 80401
Phone: (303) 273-3952
Email: rohayre@mines.edu

DOE Manager: Katie Randolph
Phone: (240) 562-1759
Email: Katie.Randolph@ee.doe.gov

Contract Number: DE-EE0008087

Project Start Date: October 1, 2017
Project End Date: September 30, 2020

Overall Objectives

- Theoretical stability analysis of at least 8,500 “potential” compounds, based on a combination of existing data located in material databases and new density functional theory (DFT) calculations.
- Determination of oxide formation enthalpy, bandgap, and atomic electronegativity for at least 500 theoretically stable compounds, based on a combination of existing data located in material databases and new DFT calculations.
- Determination of material properties that can be used as identifiers for water-splitting performance and verification of predictive capability experimentally.
- Production of combinatorial thin-film “libraries” for at least 20 material families that have been identified by the theoretical screening as candidate materials.
- Demonstration that thin-film compositions of candidate material families can be evaluated for solar thermochemical hydrogen production (STCH) potential using simple experimental techniques.
- Identification of at least three new materials that split water under any steam-to-hydrogen ratio with a hydrogen capacity at least equal to

that of cerium oxide (ceria) under the reduction conditions of 1,350°C and oxidation temperatures of 850°–1,000°C.

- Identification of one or more new materials that split water under steam-to-hydrogen ratios lower than 10:1 and with a hydrogen capacity under the reduction conditions of 1,350°C and oxidation temperatures of 850°–1,000°C at least equal to that of ceria under the reduction conditions of 1,450°C and oxidation temperatures of 850°–1,000°C.
- Characterization of final materials including cycling, durability, thermodynamic and kinetic property investigations, and performance verification at both Colorado School of Mines and Sandia National Laboratory’s Stagnation Flow Reactor facility.

Fiscal Year (FY) 2018 Objectives

- Theoretical stability analysis of at least 4,250 “potential” compounds, based on a combination of existing data located in material databases and new DFT calculations.
- Determination of oxide formation enthalpy, bandgap, and atomic electronegativity for at least 250 theoretically stable compounds, based on a combination of existing data located in material databases and new DFT calculations.
- Determination of material properties that can be used as identifiers for water-splitting performance and verification of predictive capability experimentally.
- Production of combinatorial thin-film “libraries” for at least 10 material families that have been identified by the theoretical screening as candidate materials.
- Demonstration that thin-film compositions of candidate material families can be evaluated for STCH potential using simple experimental techniques.
- Identification of at least one new material that splits water under any steam-to-hydrogen ratio

with a hydrogen capacity at least equal to that of ceria under the reduction conditions of 1,350°C and oxidation temperatures of 850°–1,000°C.

Technical Barriers

This project addresses the following technical barrier from the Hydrogen Production section of the Fuel Cell Technologies Office Multi-Year Research, Development, and Demonstration Plan¹:

(S) High-Temperature Robust Materials.

Technical Targets

The objective of this project is to discover new STCH materials. Those materials are necessary to meet the following DOE 2020 STCH targets:

- Cost: \$2/kg H₂
- Steam-to-hydrogen efficiency: 20%

FY 2018 Accomplishments

- Performed high-throughput DFT screening of 400 potential compounds and detailed DFT calculations, involving charged and neutral defects, for 15 potential compounds.
- Our National Renewable Energy Laboratory theory node partners (S. Lany et al.) identified that the propensity of an oxide to form charged oxygen vacancies (as opposed to charge-neutral vacancies) is a key (and previously overlooked) metric for STCH potential.
- Produced 15 combinatorial library films across six material families
- Successfully developed a proof-of-concept protocol for rapid optical screening of combinatorial films for thermochemical activity.
- The hydrogen production of three compositions within the Ce_xSr_{2-x}MnO₄ compositional family, x = 0.1, 0.2, and 0.3, exceeded the Milestone 3.2 target of 59 μmol H₂/g sample (based on the performance of ceria under similar conditions) with production of 218, 247, and 166 μmol H₂/g sample, respectively.

¹ <https://www.energy.gov/eere/fuelcells/downloads/fuel-cell-technologies-office-multi-year-research-development-and-22>

INTRODUCTION

Two-step metal oxide cycles for solar thermochemical hydrogen production have the potential to produce industrial-scale quantities of hydrogen. In step one, a suitable oxide is defected by driving oxygen from the lattice at high temperatures derived from concentrated solar energy. In step two, and upon exposure to steam at a lower temperature, oxygen is stripped from steam and transferred back into the oxide. This completes the cycle and results in the net production of hydrogen.

While ceria has shown itself to be the best-performing and most cycle-tolerant STCH oxide, it requires very high reduction temperatures ($>1,500^{\circ}\text{C}$) to attain sufficient per-cycle hydrogen yield. This leads to severe efficiency penalties that make the 2020 target of 20% steam-to-hydrogen efficiency unattainable. Ultimately, this work looks to culminate in the discovery and characterization of new STCH materials that can produce hydrogen at quantities that will attain the 20% steam-to-hydrogen efficiency target and facilitate the production cost target of $<\$2/\text{kg H}_2$. This requires finding a material that reduces significantly at the target reduction temperature of $1,350^{\circ}\text{C}$ under moderate oxygen partial pressures of 10–100 ppm and can split water while in the presence of hydrogen at a steam-to-hydrogen ratio of 10:1.

APPROACH

Because STCH utilizes the full solar spectrum, it has the potential to achieve high theoretic efficiency. Despite its promise, however, surprisingly few candidate STCH materials have been uncovered that can compete with ceria, which remains the state of the art. Our objective is to merge combinatorial synthesis methods with combinatorial theoretical calculations to discover new potential materials for use in two-step metal oxide cycles for STCH. This project will make significant inroads to replacing ceria by obtaining outcomes along several distinct fronts: combinatorial DFT screening; combinatorial thin-film production and testing; bulk powder synthesis and characterization; and the integration of experimental results into the refinement of DFT methodologies and screening criteria. By combining these capabilities with the high-throughput nature of combinatorial synthesis and testing, our goal is to not only efficiently and methodically uncover new potential materials that can meet DOE's 2020 targets, but to better understand fundamental links between oxide structure, chemical composition, and STCH performance.

As a HydroGEN Energy Materials Network (EMN) seedling project, we are afforded the opportunity to leverage the national labs' world-class capability and expertise. This collaboration is critical to our project, with interactions occurring with three different nodes across all three of our tasking fronts. The "First Principles Materials Theory for Advanced Water Splitting Pathways" node, led by Stephan Lany, is assisting with all DFT work, and Andriy Zakutayev's "High-Throughput Experimental Thin Film Combinatorial Capabilities" node is supplying thin films and characterization for the rapid screening effort. Finally, actual water-splitting testing is being performed using Sandia's "Virtually Accessible Laser Heated Stagnation Flow Reactor for Characterizing Redox Chemistry of Materials Under Extreme Conditions" node, overseen by Anthony McDaniel.

RESULTS

Task 1: Computation Effort

The computational effort comprises two distinct thrust areas: (1) searching for promising transition-metal-doped perovskites among known compounds, and (2) discovery of new materials using advanced structure search modeling techniques.

In the first thrust area, a detailed protocol for determining good STCH compounds was established. The workflow consisted of evaluating the formation enthalpy followed by calculating its stability against competing phases. The temperature-pressure requirements for ideal STCH material translates to a unique oxygen chemical potential window [1] that can be used as a first descriptor in determining the suitability of a given composition. This is followed by a second descriptor that relates to charged defect formation energies

(E_f). It was recently shown by the National Renewable Energy Laboratory's Stephan Lany that an additional electronic entropy contribution is obtained when the O vacancies form in a charged V_O^{2+} state [1].

Figure 1 shows the E_f relative to the valence band maximum for charged and neutral V_O for ternaries and quaternaries. A closer inspection reveals important trends such as (1) the addition of Y, La, and Ta increases the E_f ; (2) replacing Ba with Sr increases the E_f ; and (3) Ce and V additions result in E_f that is in the desired range (2.5–3.5 eV). These trends lay out a guiding principle that is critical in *informing* the selection of elements for the structure search in the second thrust area. In addition to sampling the defects for various crystallographic positions, a detailed configurational defect sampling was performed for BaMnO₃ (BMO) and BaCe_{0.25}Mn_{0.75}O₃ (BCM). It was found that the oxygen E_f can be promoted if the vacancy sits near a Ce in BCM. The magnetic configuration sampling was found to have smaller impact on E_f as demonstrated by anti-parallel and parallel states of Mn neighboring the V_O in BCM.

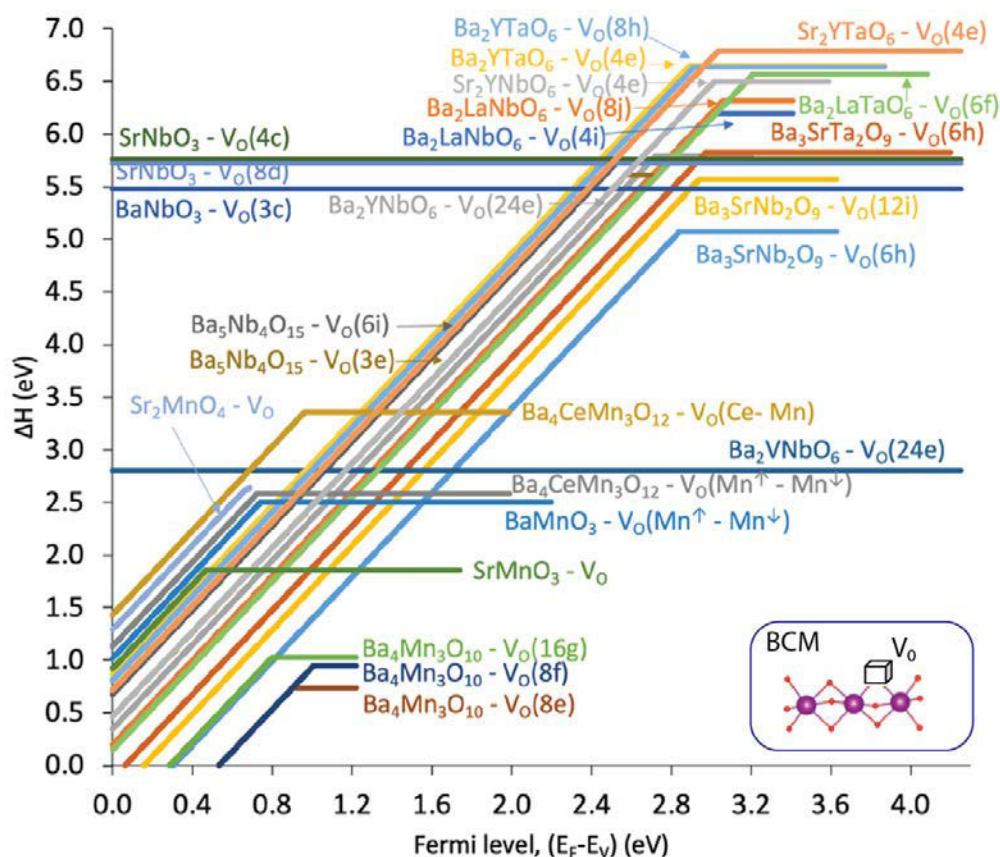


Figure 1. Calculated oxygen vacancy (V_O), charged and neutral, formation energies for several ternaries and quaternaries studied in this work. The defect calculation involved studying various Wyckoff positions (as shown by Wyckoff labels next to compositions) and magnetic configuration specifically for BaCe_{0.25}Mn_{0.75}O₃ (inset shows V_O with different Mn neighbors that can take varying spin arrangements). Compositions in the range of 2.5–3.5 eV are of greatest interest.

The second thrust area focused on discovering novel quaternary oxides using random and prototype structure search methodologies. The cation search space constituted combinations of Ba, Sr, La, Ce, and Mn, with the constraint that the unit cell had no more than 20 atoms. This limit was placed to enable proper sampling of random structures in a realistic timeline and given computational resources. Figure 2 shows predicted oxide formation enthalpy for all possible stoichiometries where the Ce and Mn oxidation states were kept fixed at +4. A cross-validation of this approach involved searching for known composition, such as BaCeO₃. The ΔH_f of BaCeO₃ was found to be in close agreement to that of the known structure (~ 0.03 eV/atom). This procedure resulted in the discovery of an La containing compound, La₂CeMn₃O₁₁, that has not been previously reported

in literature. The ΔH_f of this material is slightly higher than that of BCM, suggesting that it may be well suited to STCH application. Additional calculations are in process to further understand its potential as a STCH material.

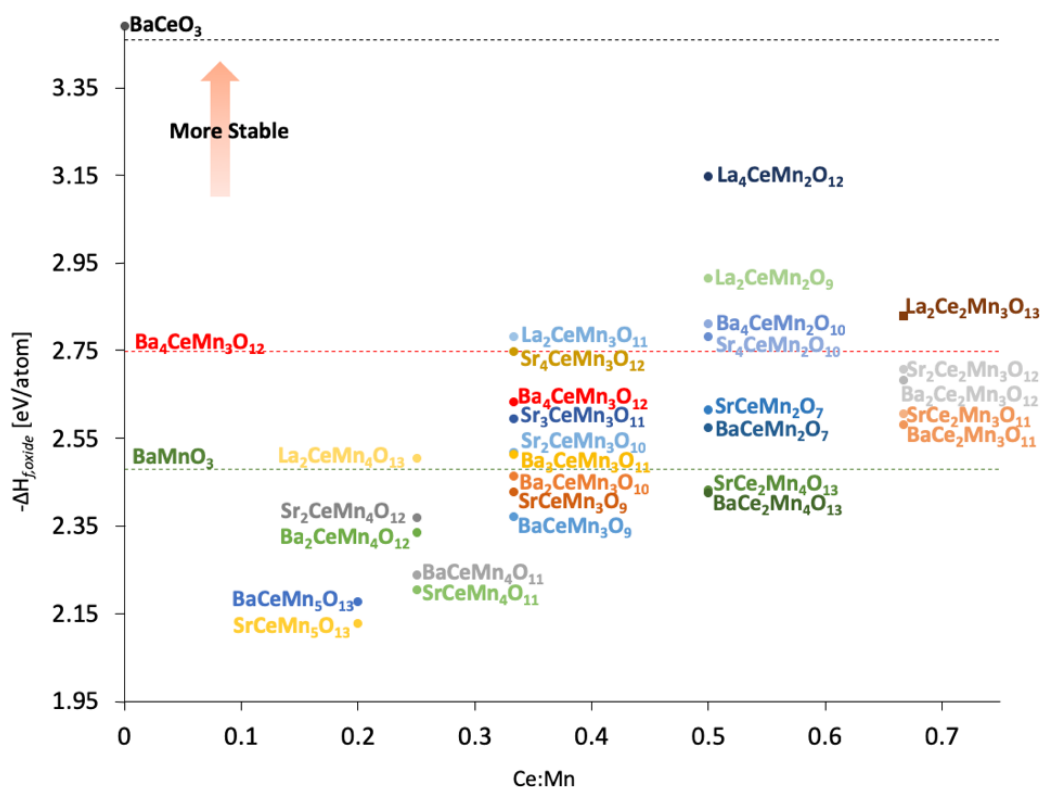


Figure 2. Predicted oxide formation enthalpy (ΔH_f) for quaternary compounds identified in the structure search procedure for [(Ba,Sr,La),Ce,Mn,O] chemical space. The horizontal dashed line corresponds to ΔH_f of known compositions. ΔH_f is a rough predictor of oxygen vacancy formation energy.

The direct tie between DFT-estimated oxygen vacancy formation energy and thermal-gravimetric-analysis-measured extent of reduction was validated across several compositional families. While previously suspected, the confirmation allows for more rapid “down-selection” of DFT-screened STCH candidates to only those that have stability and vacancy formation energies that fall within well-defined bounds. While the energy values listed in Table 1 do not all come from the same computational methodology, the general trends hold across many families and strongly correlate within a family.

Table 1. Comparison of Calculated Oxygen Vacancy Formation Energy and Experimental Extent of Reduction Results. Formation Energies Were Not All Calculated Using Same Methods.

Composition	V_o (DFT) [eV]	Extent of Reduction (Exp) [δ]
CSM1	1.8	0.175
CSM2	2.2	0.12
CSM3	2.7	0.075
BCM	3.0	0.175
BMO	2.5	0.45
BCO	10	0.02
CeO ₂	4	0.04
SLMA6464	1.5	0.20

Task 2: Combinatorial Effort

The collaboration with the thin film combinatorial node resulted in well over 20 films being produced in the first year. Some of these were single compositions used for evaluation of the optical screening method; however, 15 films had compositional variations.

Table 2. Thin-Film Compositions Produced in Year 1

Single Composition	Combinatorial Families
WO ₃	BaMnO ₃ : BaCeO ₃
Fe ₂ O ₃	BaCe _{0.25} Mn _{0.75} O ₃ : SrCeMnO ₃
BaCe _{0.25} Mn _{0.75} O ₃	BaCe _{0.25} Mn _{0.75} O ₃ : LaSrCoMnO ₃
SrCeMnO ₃	BaCe _{0.25} Mn _{0.75} O ₃ : LaSrCoO ₃
LaSrCoO ₃	BaMnO ₃ : LaSrCoO ₃
BaMnO ₃	SrMnO ₃ : LaSrCoO ₃
BaCeO ₃	
CeO ₂	

The optical-screening method showed promise in the proof-of-concept trials. Figure 3 shows images of two post-oxidized films, one BCM and the other a gradient of BCM and BMO, with the analysis overlaid. Black boxes highlight regions where there is significant color change (at this point, set to a 2% difference in any color channel [i.e., hue, saturation, or brightness]). BCM changed on both films, while the BMO, not a water splitter, did not (depending on the threshold setting). Later testing has not been as successful, and further validation is necessary to determine the long-term viability of the optical technique.

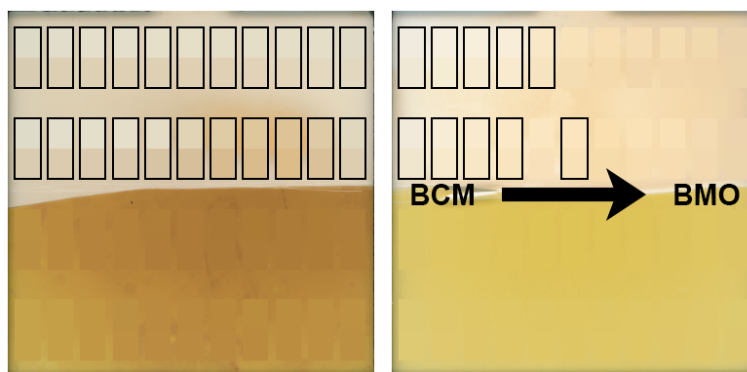


Figure 3. The reduced and then reoxidized test films, BCM on zirconia (left) and a gradient of BCM to BMO on alumina (right). Inside the overlaid rectangles is the reduced film color on top and the oxidized color on bottom. If the color change meets the threshold (currently 2%, which may be difficult to see by eye) the rectangle is highlighted with a black border. In both films, the lower half is the as-received film, while the upper half is the post-processed film (after undergoing the simulated water splitting cycle).

Task 3: Bulk Testing

Motivated by the development of BCM and the insights from our theory effort, we expanded our search for new Ce- and Mn-containing perovskites. We replaced Ba with Sr on the A-site to permit greater structural and compositional flexibility because BCM is a line-compound material that lacks this compositional tunability. In the process, we instead encountered the unexpected formation of a layered perovskite Ce_xSr_{2-x}MnO₄ (CSM), previously unreported in the literature for this compositional family. DFT calculations played a key role in the iterative process of identifying and corroborating the stability of the new phase. The hydrogen production of three compositions within the Ce_xSr_{2-x}MnO₄ compositional family, x = 0.1, 0.2, and 0.3, exceeded the Milestone 3.2 target of 59 μmol H₂/g sample (based on the performance of ceria under similar conditions) with production of 218, 247, and 166 μmol H₂/g sample, respectively. Results from Sandia's stagnation flow reactor showing the oxygen peak, during reduction, and hydrogen peak, during oxidation, are shown in Figure 4.

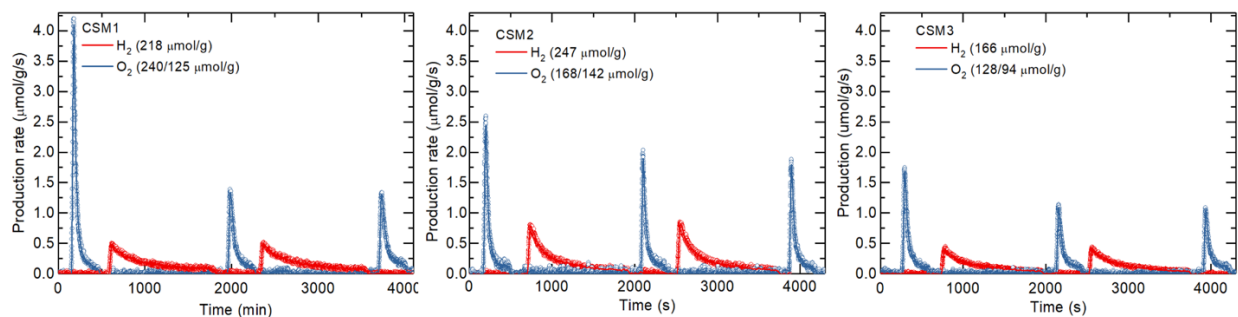


Figure 4. Water-splitting results for two complete cycles at $T_{RE} = 1,400^{\circ}\text{C}$ for 330 s and $T_{OX} = 1,000^{\circ}\text{C}$ for 1,200 s. Blue lines are oxygen peaks evolved during reduction and red lines are hydrogen peaks recorded during the reoxidation (water splitting) step. The peaks were integrated to calculate the total amount of hydrogen and oxygen produced, with the results listed in the legend. For the oxygen values, the first value indicates the oxygen produced by the initial reduction and the second value corresponds to the subsequent cycles average. The hydrogen value refers to the average hydrogen production.

CONCLUSIONS AND UPCOMING ACTIVITIES

Great progress was made in the first year of this project. The computational results not only have identified a few new compositional combinations but have helped to clarify both the target stability and defect formation energy bounds for materials screening. Furthermore, the results from our combined theory and experiment approach have helped establish how certain elements (e.g., Ba vs. Sr on the A site; Ce, Mn, V, Nb, and Y on the B-site) can be combined to favorably tune those parameters. Our development of $\text{Ce}_x\text{Sr}_{2-x}\text{MnO}_4$ is a tangible example of the payoff from this approach, and its promising performance further motivates the search for additional perovskite-related compounds with unique and potentially valuable STCH properties.

Going forward, our efforts will follow a similar track for the next year, including the continued collaboration with all three EMN nodes. Year 2 will see further refinement of the computational effort to take advantage of the lessons learned in the first year. There will also be a reversal of roles as portions of the combinatorial film effort will be used to inform the computational work, rather than vice-versa. This information will mainly consist of stable structure/phase identification and to delineate the limits of element solubility in complex, multi-cation compositional regions of interest. These are both tasks that are difficult for DFT theory but that the combinatorial thin-film experiment process is exceptionally well equipped to handle.

The optical screening technique will also be further investigated in the first part of the year. Additional testing is necessary to unequivocally determine the feasibility of such a technique. Other characterization techniques or a revamped in situ screening process may turn out to be more viable.

Finally, an in-depth thermodynamic study of the CSM system will be performed to feed valuable experimental information back to the computational team. This work dovetails nicely with the EMN's new "super-node" work on the BCM system.

FY 2018 PUBLICATIONS/PRESENTATIONS

1. Debora R. Barcellos, Michael Sanders, Jianhua Tong, Anthony H. McDaniel, and Ryan O'Hayre, "BaCe_{0.25}Mn_{0.75}O_{3-δ}—A Promising Perovskite-Type Oxide for Solar Thermochemical Hydrogen Production," *Energy Environ. Sci.* 11 (2018): 3256–3265, DOI: 10.1039/C8EE01989D.

REFERENCES

1. Stephan Lany, "Communication: The electronic entropy of charged defect formation and its impact on thermochemical redox cycles," *The Journal of Chemical Physics* 148, no. 7 (2018): 071101.

HydroGEN Seedling: Computationally Accelerated Discovery and Experimental Demonstration of High-Performance Materials for Advanced Solar Thermochemical Hydrogen Production

Charles Musgrave (Primary Contact), Alan Weimer, Aaron Holder, Zachary Bare, Christopher Bartel, Samantha Millican, Ryan Trottier
University of Colorado Boulder
Department of Chemical and Biological Engineering
Campus Box 596
3145 Colorado Blvd, JSCBB Office D121
Boulder, CO 80309
Phone: (303) 735-0411
Email: charles.musgrave@colorado.edu

DOE Manager: Katie Randolph
Phone: (240) 562-1759
Email: Katie.Randolph@ee.doe.gov

Project Start Date: October 1, 2017
Project End Date: September 30, 2020

Overall Objectives

- Utilize materials informatics and machine learning to predict materials for solar thermochemical water splitting (STWS) and demonstrate the effectiveness of our materials-by-design approach by experimentally demonstrating materials with computationally predicted thermodynamic and kinetic properties.
- Utilize materials-by-design approach to rapidly computationally prototype new STWS materials and demonstrate materials with improved performance.
- Computationally prototype doped metal oxides for thermodynamic and kinetic viability and experimentally demonstrate materials with improved hydrogen productivity, reaction kinetics, and durability.

Fiscal Year (FY) 2018 Objectives

- Utilize advanced machine-learning techniques to enable the prediction of the perovskite

crystal structures (polymorphs) relevant to STWS conditions.

- Screen materials for thermodynamic viability based on stability, oxygen vacancy formation energy (E_v), and extent of reduction (δ).
- Develop and utilize an accelerated pseudo transition state approach and machine-learned models to rapidly computationally screen materials for kinetic viability.
- Experimentally demonstrate the durability and thermodynamic and kinetic water splitting behavior of new materials predicted from our computational screening using the thermogravimetric analyzer with differential scanning calorimeter (TGA/DSC) and stagnation flow reactor (SFR).
- Complete an annual status report comparing results from the different demonstrations.

Technical Barriers

This project addresses the following technical barriers from the Hydrogen Production section of the Fuel Cell Technologies Office Multi-Year Research, Development, and Demonstration Plan¹:

(S) High-Temperature Robust Materials.

Technical Targets

This project has contributed toward progress in meeting the target for “Annual Reaction Material Cost per TBD H₂” from the Fuel Cell Technologies Office Multi-Year Research, Development, and Demonstration Plan for solar-driven high-temperature thermochemical hydrogen production. This metric incorporates active material improvements through “decreased material usage, improved cycle time, and increased material lifetime.” Specifically, this project is

¹ <https://www.energy.gov/eere/fuelcells/downloads/fuel-cell-technologies-office-multi-year-research-development-and-22>

working toward the following goals to hit this target:

- Hydrogen productivity: $>350 \mu\text{mol/g/cycle}$
- Operating temperature: $T_{\text{red}} \leq 1,450^\circ\text{C}$ and $\Delta T \leq 400^\circ\text{C}$
- Cycle times: <10 minutes
- Stability: $<10\%$ decrease in reactivity between cycles 100 and 200.

FY 2018 Accomplishments

- Developed two machine-learned descriptors that significantly narrow the search space for candidate materials to accelerate the screening of more than 1,000,000 perovskite structures.
- Advanced the capability of materials screening for kinetic properties by developing a pseudo transition state identification approach and predicted rate-limiting step in hydrogen evolution reaction.
- Identified an important thermodynamic screening parameter necessary for determining a material's water-splitting ability.

INTRODUCTION

STWS provides a promising route for efficient conversion of solar energy to hydrogen fuel; however, despite the significant number of materials that have been examined, an optimal material to drive this process has yet to be developed. This research focuses on developing a powerful new approach for materials discovery that combines quantum mechanical and machine-learned models with experimental feedback to accelerate the development of new, durable redox materials. During this year, the team has developed a machine-learned descriptor that improves the prediction of single and double perovskite stability, eliminating the need to use expensive first-principles density functional theory (DFT) quantum mechanical calculations, significantly reducing the number of potential candidate materials and reducing the computational expense of stability predictions from hours to milliseconds per material. The team has also developed a second machine-learned descriptor that predicts thermodynamic stability at relevant high-temperature conditions ($>1,300^{\circ}\text{C}$), which further reduces the computational expense of accurately prototyping new materials and considerably narrows the pool of candidate materials requiring experimental testing. In addition to reducing the materials space by machine-learned descriptors, the team has also made significant advancements in high-throughput screening of materials for kinetic and thermodynamic water-splitting viability.

APPROACH

This project will focus on the design and demonstration of mixed metal oxides for STWS with a predominant emphasis on perovskites and spinels. The redox stability of these materials at conditions at which they undergo an oxygen-vacancy-mediated STWS mechanism will be evaluated, and their thermodynamic and kinetic properties will be tuned through compositional (doping) control. We will ensure properties are evaluated with the correct topology (structure and coordination) at STWS conditions. To achieve DOE targets, materials will be designed with low thermal reduction temperatures ($<1,450^{\circ}\text{C}$), high hydrogen production capacity ($>350\ \mu\text{mol H}_2/\text{g}/\text{cycle}$), material stability and reactivity over many cycles ($<10\%$ loss in hydrogen production from cycles 100 to 200), and rapid reduction and oxidation kinetics (cycle times <10 minutes). This work will consist of four tasks to develop novel water splitting materials.

We will:

1. Develop machine-learned models for predicting phase transitions in perovskites.
2. Screen active materials for thermodynamic viability.
3. Screen active materials for kinetic viability.
4. Experimentally test promising materials for redox cycling durability and thermodynamic and kinetic performance.

RESULTS

During FY 2018, the team developed a machine-learned descriptor that improves the prediction of single- and double-perovskite stability from 74% to 92% accuracy (Figure 1), eliminating the need to use first-principles DFT calculations for $>1,000,000$ perovskite structures. This descriptor significantly focuses the material space and reduces the computational expense of stability predictions.

A decision tree classifier determines that the optimal bounds for perovskite formability using the Goldschmidt tolerance factor, t , are $0.825 < t < 1.059$, which yields a classification accuracy of 74% for 576 experimentally characterized ABX_3 solids (Figure 1a). The new tolerance factor (τ) achieves 92% classification accuracy on the set of 576 ABX_3 solids based on perovskite classification for $\tau < 4.18$, with this decision boundary identified using a one-node decision tree (Figure 1b). This result indicates that this model is truly predictive and allows for significant generalizability to predicting experimental realization for single and double perovskites that are yet to be discovered.

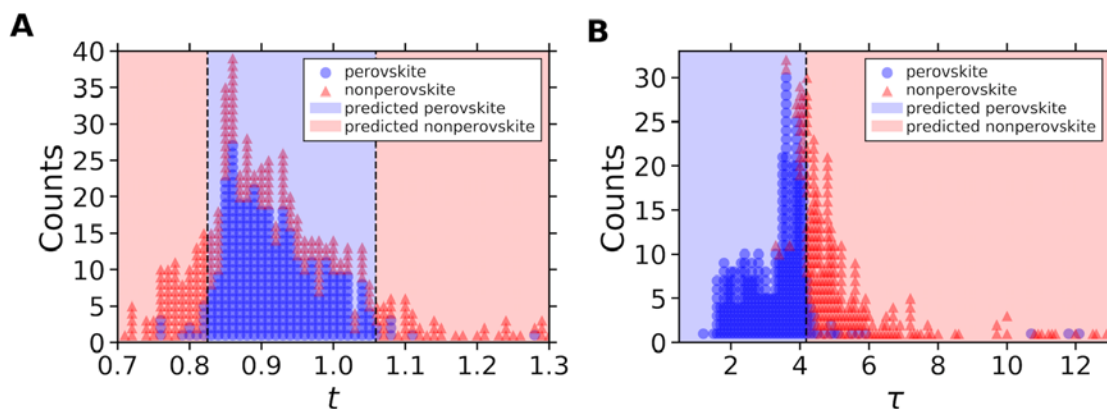


Figure 1. Assessing the performance of the improved tolerance factor. (A) A decision tree classifier determines that the optimal bounds for perovskite formability using the Goldschmidt tolerance factor, t , are $0.825 < t < 1.059$, which yields a classification accuracy of 74% for 576 experimentally characterized ABX_3 solids. (B) τ achieves 92% classification accuracy on the set of 576 ABX_3 solids based on perovskite classification for $\tau < 4.18$, with this decision boundary identified using a one-node decision tree. The largest value of τ in the experimental set of 576 compounds is 181.5; however, all points with $\tau > 13$ are correctly labeled as nonperovskite and not shown to highlight the decision boundary. The outlying compounds at $\tau > 10$ that are labeled perovskite yet have large τ are PuVO_3 , AmVO_3 , and PuCrO_3 , which may indicate poorly defined radii or incorrect experimental characterization.

During this year, a second machine-learned descriptor was developed that predicts thermodynamic stability at relevant high-temperature conditions ($>1,300^\circ\text{C}$). The sure independence screening and sparsifying operator (SISSO) approach was used to identify a simple and highly accurate descriptor for $G(T)$. The current descriptor for the $G(T)$ requires only temperature, chemical formula, and DFT-calculated density to reproduce experimental $G(T)$ with errors of ~ 40 meV/atom (Figure 2).

Figure 2a shows the performance of the SISSO-learned descriptor on the training set and Figure 2b shows distribution of residuals between the SISSO-learned descriptor and experiment on the training set. Combining this high-throughput model for the prediction of $G(T)$ with tabulated and readily available DFT-calculated ΔH_f and experimental Gibbs energies for the elements enables the rapid prediction of $\Delta G_f(T)$ from a single DFT total energy calculation. Thus, reaction energetics, thermochemical equilibrium product distributions, and temperature-dependent compound stability can be assessed for the millions of structures currently compiled in materials databases. This unprecedented ability to rapidly predict reaction equilibria for reactions involving solid compounds is illustrated in Figure 3 for a small set of example reactions.

Figure 3a shows comparison of experimental reaction energetics (labels) to those predicted using the machine-learned descriptor for $G(T)$ (dashed curves) and Figure 3b shows reaction product distributions between MoO_2 , Mo_2N , N_2 , H_2 , H_2O , and NH_3 based on Gibbs energy minimization subject to molar conservation and fixed pressure of 1 atm. In both figures, “pred” applies the SISSO-learned descriptor to $G(T)$ of the solid phases and experimental data for all other components. This model can be trivially applied to all perovskite oxides under consideration to assess the stability (or metastability) as a function of temperature, and further reduce the space of compounds that require more sophisticated (e.g., defect) calculations.

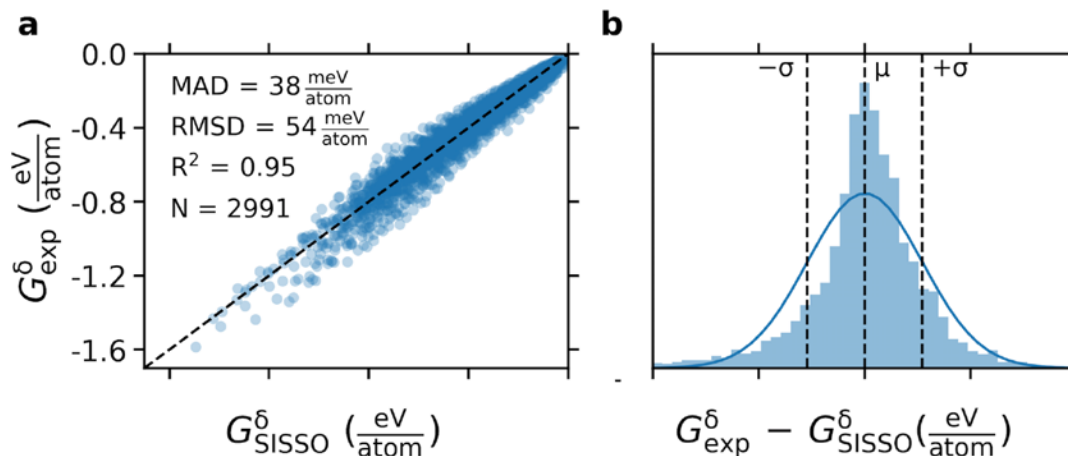


Figure 2. Descriptor performance. Performance of the SISSO-learned descriptor on the training set. MAD is the mean absolute deviation, RMSD the root mean square deviation, N the number of points shown, μ the mean deviation and σ the standard deviation. The curved lines are normal distributions constructed from μ and σ .

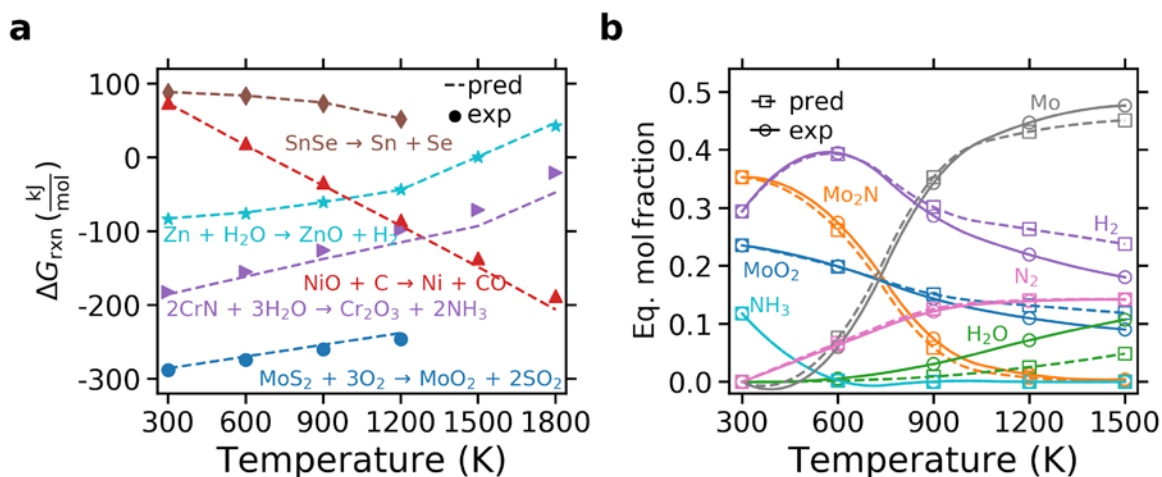


Figure 3. High-throughput reaction engineering. (a) A comparison of experimental reaction energetics (labels) to those predicted using the machine-learned descriptor for $G(T)$ (dashed curves). (b) Reaction product distribution between MoO_2 , Mo_2N , N_2 , H_2 , H_2O , and NH_3 based on Gibbs energy minimization subject to molar conservation and fixed pressure of 1 atm. In both figures, “pred” applies the SISSO-learned descriptor to $G(T)$ of the solid phases and experimental data for all other components.

In addition to focusing the chemical space by machine-learned descriptors, the team has made significant advancements in high-throughput screening of materials for kinetic and thermodynamic viability. For the thermodynamic screening, the team utilized the machine-learned model developed for perovskite stability to screen >1,000,000 potential perovskite materials down to ~27,000 stable materials to be further evaluated using DFT. All of the 328 stable ternary (ABO_3) perovskites and 425 stable double ($\text{A}_2\text{BB}'\text{O}_6$) perovskites were evaluated for STWS based on the oxygen vacancy formation energy. Further work is now being conducted to evaluate these materials based on their stability at elevated temperatures using the machine-learned model for free energy $G(T)$ described above. The team also evaluated the effect of charged defects on the predicted thermodynamic behavior of STWS materials. This study was completed in conjunction with Dr. Stephan Lany at the National Renewable Energy Laboratory utilizing the HydroGEN consortium computational node “First Principles Materials Theory for Advanced Water Splitting Pathways.” Through this work the team has demonstrated that charged antisite-vacancy defect pairs are critical for understanding the water splitting ability in hercynite. Future work will involve utilizing these charged and antisite defect

calculations to complete a full thermodynamic model for the equilibrium defect concentration at relevant temperatures in hercynite and hercynite alloys. For the kinetic screening, the team has identified the rate-limiting step in the hydrogen evolution reaction and developed accelerated pseudo transition state identification approaches. The rate-limiting step was identified from an initial screening of 23 perovskite/spinel materials. The full reaction pathway for the hydrogen and oxygen evolution surface reactions was evaluated in addition to the bulk kinetics for all 23 materials. The pseudo transition state identification approaches we developed significantly accelerate the kinetic screening of materials. These approaches involve estimating an upper/lower bound on transition state energies, utilizing atomic potentials to estimate transition state geometries, and recent developments allow the use of machine-learned models for rapid materials screening. These advancements not only limit the number of calculations needed to screen for kinetic viability but also significantly reduce the computation expense attributed to costly ab initio transition state calculations. Experimentally, the activity of four transition metal–hercynite alloys was measured in a stagnation flow reactor. These alloys produced $>200 \mu\text{mol H}_2/\text{g}$ at reduction temperatures of $1,450^\circ\text{C}$. The Mn–hercynite alloy shows the highest hydrogen production as well as an improved peak rate over pure hercynite. The experimentally measured peak rates were accurately matched against computational predictions.

CONCLUSIONS AND UPCOMING ACTIVITIES

The materials-by-design approach has thus far been developed to (1) significantly narrow the candidate materials space, (2) predict energetics at relevant high-temperature conditions, (3) increase the capabilities of state-of-the-art high-throughput kinetic screening, and (4) identify relevant thermodynamic screening parameters. The initial success of this approach has been demonstrated for transition metal–hercynite alloys by correctly rank ordering the experimental peak hydrogen production rate of four materials by the computational kinetic results. Additionally, four materials producing $>200 \mu\text{mol H}_2/\text{g}$ at reduction temperatures $\leq 1,450^\circ\text{C}$ and temperature swings $\leq 400^\circ\text{C}$ were demonstrated.

Future work by the University of Colorado team includes:

- Utilizing the charged and antisite defect calculation in a thermodynamic model to compute the equilibrium defect concentrations at relevant temperatures and pressures.
- Screening candidate perovskite materials using free energy model for stability at elevated temperatures.
- Continuing deployment of pseudo transition state approaches for rapid kinetic screening that will feed into the development of machine-learned models.

FY 2018 PUBLICATIONS/PRESENTATIONS

Publications

1. C.J. Bartel, C. Sutton, B.R. Goldsmith, R. Ouyang, C.B. Musgrave, L.M. Ghiringhelli, and M. Scheffler, “New tolerance factor to predict the stability of perovskite oxides and halides,” *Science Advances* (Accepted), <https://arxiv.org/abs/1801.07700>.
2. C.J. Bartel, S.L. Millican, A.M. Deml, J.R. Rumpitz, W. Tumas, A.W. Weimer, S. Lany, V. Stevanovic, C.B. Musgrave, and A.M. Holder, “Physical descriptor for the Gibbs energy of inorganic crystalline solids and temperature-dependent materials chemistry,” *Nature Communications* 9, no. 1: 4168.

Presentations

1. C.J. Bartel, C. Sutton, B.R. Goldsmith, R. Ouyang, C.B. Musgrave, L.M. Ghiringhelli, and M. Scheffler, “New tolerance factor to predict the stability of perovskite oxides and halides,” European Materials Research Society, September 2018.
2. R. Trottier, S.L. Millican, Z.J. Bare, and C.B. Musgrave, “Rapid Kinetic Profiling of Bulk Diffusion Barriers for Solar Thermal Water Splitting Materials,” 21st International Conference on Ternary and Multinary Compounds, September 2018.

3. C.J. Bartel, C. Sutton, B.R. Goldsmith, R. Ouyang, C.B. Musgrave, L.M. Ghiringhelli, and M. Scheffler, “New tolerance factor to predict the stability of perovskite oxides and halides,” 21st International Conference on Ternary and Multinary Compounds, September 2018.
4. S.L. Millican, A.M. Deml, A.M. Holder, V. Stevanovic, and C.B. Musgrave, “Modeling Point Defect Concentrations in Complex Materials Beyond Dilute Defects,” International Conference on Ternary and Multinary Compounds, September 2018.
5. C.J. Bartel, C. Sutton, B.R. Goldsmith, R. Ouyang, C.B. Musgrave, L.M. Ghiringhelli, and M. Scheffler, “New tolerance factor to predict the stability of perovskite oxides and halides,” Application of Machine Learning and Data Analytics for Energy Materials Network Consortia 2018, May 2018.
6. S.L. Millican, I. Androschuk, A.W. Weimer, and C.B. Musgrave, “Ab-initio Modeling and Experimental Demonstration of Metal Oxides for Solar Thermochemical Water Splitting,” American Chemical Society Spring Meeting, March 2018.
7. C.J. Bartel, C. Sutton, B.R. Goldsmith, R. Ouyang, C.B. Musgrave, L.M. Ghiringhelli, and M. Scheffler, “Improved tolerance factor for classifying the formability of perovskite oxides and halides,” American Physical Society Annual Meeting, March 2018.
8. C.J. Bartel, S.L. Millican, A.M. Deml, J.R. Rumpitz, W. Tumas, A.W. Weimer, S. Lany, V. Stevanovic, C.B. Musgrave, and A.M. Holder, “Machine learning the Gibbs energies of inorganic crystalline solids,” American Physical Society Annual Meeting, March 2018.
9. S.L. Millican, I. Androschuk, A.W. Weimer, and C.B. Musgrave, “Design and Discovery of Mixed Metal Oxides for Solar Thermochemical Water Splitting,” International Conference and Exposition on Advanced Ceramics and Composites, January 2018.
10. S.L. Millican, I. Androschuk, A.W. Weimer, and C.B. Musgrave, “Screening Metal Oxides for Solar Thermochemical H₂/CO Production,” American Institute of Chemical Engineers Annual Meeting, October, 2017.
11. S.L. Millican, I. Androschuk, A.W. Weimer, and C.B. Musgrave, “Assessing the Thermodynamic Viability of Mixed Metal Oxides for Solar Thermochemical Water Splitting,” American Institute of Chemical Engineers Annual Meeting, October 2017.
12. S.L. Millican, A.L. Hoskins, C.E. Czernik, I. Alshankiti, J.C. Netter, C.B. Musgrave, and A.W. Weimer, “Complete Approach to Hydrogen Production via Solar Thermochemical Water Splitting,” American Institute of Chemical Engineers Annual Meeting, October 2017.
13. C.J. Bartel, S.L. Millican, A.M. Deml, J.R. Rumpitz, W. Tumas, A.W. Weimer, S. Lany, V. Stevanovic, C.B. Musgrave, and A.M. Holder, “Machine learning the thermochemistry of inorganic crystalline solids,” American Institute of Chemical Engineers Annual Meeting, October 2017.

HydroGEN Seedling: Transformative Materials for High-Efficiency Thermochemical Production of Solar Fuels

Chris Wolverton (Primary Contact), Sossina Haile
Northwestern University
Dept. of Materials Science and Engineering
2220 Campus Dr.
Evanston, IL 60208
Phone: 847-467-0593
Email: c-wolverton@northwestern.edu

DOE Manager: Katie Randolph
Phone: (720) 356-1759
Email: Katie.Randolph@ee.doe.gov

Contract Number: DE-EE0008089

Project Start Date: October 1, 2017
Project End Date: September 30, 2020

Overall Objectives

- Develop a combined high-throughput computation + experimental approach to greatly accelerate materials discovery efforts for solar thermochemical hydrogen production (STCH) materials.
- Identify promising compounds that show (a) ground state stability/synthesizeability of compound, (b) thermodynamics favorable for <1,400°C reduction, and (c) thermodynamics favorable for facile water splitting. State-of-the-art currently is CeO₂ and SLMA perovskite.
- Discovery of new, higher-efficiency materials is critical toward the practical use of STCH for hydrogen production (and solar fuels, more generally).

Fiscal Year (FY) 2018 Objectives

- Experimentally measure redox thermodynamics of computationally predicted perovskites by thermal gravimetric analysis (TGA) to validate enthalpy calculations as well as obtain high-quality entropy data.
- Experimentally measure the reduction enthalpy and entropy of nine predicted perovskites.

- Validate computational predictions of oxygen vacancy formation energy by comparing with measured reduction enthalpy for perovskite materials.
- Validate high-throughput methodology for measuring thermodynamic property using thin film through electrochemical impedance.
- Initiate high-throughput computational search for promising double-perovskite compounds.

Technical Barriers

This project addresses the following technical barriers associated with solar thermochemical production of hydrogen from the Hydrogen Production section of the Fuel Cell Technologies Office Multi-Year Research, Development, and Demonstration Plan¹:

- High-Temperature Robust Materials
- Materials and Catalyst Development.

Specifically, this project is focused on the identification of promising compounds that show (a) ground state stability/synthesizeability of compound, (b) thermodynamics favorable for <1,400°C reduction, and (c) thermodynamics favorable for facile water splitting. State-of-the-art currently is CeO₂ and SLMA perovskite.

Technical Targets

In Year 1 of this project, we successfully validated our combined experimental/computational strategy for accelerated discovery of novel STCH materials. This methodology will be exploited in a high-throughput fashion in the future period of the project to address the technical barriers above.

Insights gained from these studies will be applied toward the design and synthesis of hydrogen storage materials that meet the following DOE hydrogen production targets:

- Solar-to-hydrogen conversion efficiency

¹ <https://www.energy.gov/eere/fuelcells/downloads/fuel-cell-technologies-office-multi-year-research-development-and-22>

- Reaction material cost.

FY 2018 Accomplishments

- Synthesized >10 ABO_3 compounds and characterized structural information using X-ray diffraction.
- Characterized materials using mass loss in TGA studies to obtain enthalpies and entropies of reduction of materials.
- Determined that density functional theory (DFT) calculations of oxygen vacancy formation energy accurately predict measured enthalpies, provided the correct, experimentally observed structure is used in computation. Previous high-throughput computational surveys typically performed calculations for a single structure type and hence are not sufficiently accurate for screening purposes.
- Successfully validated the computational approach for predicting enthalpies of reduction by comparison with TGA measurements. Good agreement between computation and experiment allows us to use high-throughput approaches in future project periods to accelerate discovery of STCH materials.

INTRODUCTION

Metal-oxide-based two-step solar thermochemical (STC) H₂O- and CO₂-splitting cycles are a promising route to convert solar thermal energy into fuels. The metal-oxide materials are reduced at high temperatures (Step 1), and then at low (but still elevated) temperatures, the reduced oxide is used to split H₂O or CO₂ (Step 2). However, current applications of these cycles are limited by the efficiency of the metal-oxide materials. A lower temperature for reduction is desirable, but that brings a concomitant reduction in the driving force for gas splitting. So, designing novel, high-efficiency materials is challenging. Here, we propose a joint computational-experimental project, combined with materials design strategies and high-throughput approaches, with the goal to quickly discover and demonstrate novel thermochemical materials with superior properties.

APPROACH

Background: In the first year of this project, we will use our previously developed materials design map, combined with results from (already existing) high-throughput first-principles computation to experimentally study the properties of novel, predicted materials. In particular, we will experimentally explore a set of recently predicted high-throughput perovskites. Study of these compositionally simple materials (which encompass only single elements on the A and B sites) will focus on obtaining high-quality thermodynamic properties for validation of computational prediction of enthalpy and entropy of reduction. These thermodynamic quantities play a major role in designing materials with reduced temperatures of reduction but sufficient gas-splitting rates.

The most promising of the ABO₃ materials will be modified by A and B site substitutions, both computationally and experimentally, opening an enormous combinatorial space of materials, with the promise of being able to chemically “tune in” desired STC properties. This vast composition space can only be reasonably explored using the high-throughput approaches, both computational and experimental, of this proposal. Computational screening will narrow the list of promising compounds, and experimental synthesis, stability, and redox measurements will further refine the set of materials with optimal STC properties.

RESULTS

In Year 1, we performed experimental measurements of redox thermodynamics of computationally predicted ABO₃ compounds by TGA. The aims of the experimental studies were to validate the computational determination of reduction enthalpies and to obtain high-quality entropy data. We have experimentally synthesized >10 ABO₃ compounds and determined crystal structure information by characterization via X-ray diffraction. These materials were further characterized using mass loss in TGA studies to obtain enthalpies and entropies of reduction of materials. The complete list of materials considered in Year 1 is given in Figure 1.

In parallel, DFT calculations of oxygen vacancy formation energy were performed and compared with experimental enthalpies. We determined that DFT is able to accurately predict measured enthalpies, *provided the correct, experimentally observed structure is used in computation*. The caveat is significant because previous high-throughput studies have typically assumed a single, undistorted cubic perovskite for all ABO₃ structures in calculations of oxygen vacancy formation. We find that this assumption is not accurate enough for precise materials screening, but when the experimentally observed structure type is used, the oxygen vacancy formation energies agree well with experimental measurements. Also, we have found that DFT calculations of the ground-state stability agree with the experimentally observed structure type in most cases, and the DFT ground-state structure provides a good estimate of oxygen vacancy formation energies. Thus, the prediction of these enthalpies of reduction from DFT is suitable for materials screening in high-throughput surveys, provided care is taken to determine the correct ground-state structure (or structural distortion, in the case of perovskites). The overall comparison between DFT-calculated and experimentally measured enthalpies of reduction is shown in Figure 2.

Material	Structure Type	Crystal System	Space Group
LuFeO_3	Perovskite	Orthorhombic	Pbnm
HoFeO_3	Perovskite	Orthorhombic	Pbnm
YFeO_3	Perovskite	Orthorhombic	Pnma
LuCrO_3	Perovskite	Orthorhombic	Pbnm
ErCrO_3	Perovskite	Orthorhombic	Pbnm
HoCrO_3	Perovskite	Orthorhombic	Pbnm
PrCoO_3	Perovskite	Orthorhombic	Pbnm
SmCoO_3	Perovskite	Orthorhombic	Pbnm
LaCoO_3	Perovskite	Rhombohedral	R-3c
LaNiO_3	Perovskite	Rhombohedral	R-3c
YMnO_3	" LuMnO_3 "	Hexagonal	$\text{P6}_3\text{mc}$
LuMnO_3	" LuMnO_3 "	Hexagonal	$\text{P6}_3\text{mc}$
HoMnO_3	" LuMnO_3 "	Hexagonal	$\text{P6}_3\text{mc}$
SrMnO_3	" BaMnO_3 "	Hexagonal	$\text{P6}_3/\text{mmc}$
BaMnO_3	" BaNiO_3 "	Hexagonal	$\text{P6}_3/\text{mmc}$
CaMnO_3	Perovskite	Cubic/Ortho	$\text{Pm}3\text{m}/\text{Pnma}$
LaMnO_3	Perovskite	Orthorhombic	Pnma

Figure 1. ABO_3 compounds considered in Year 1 of this project

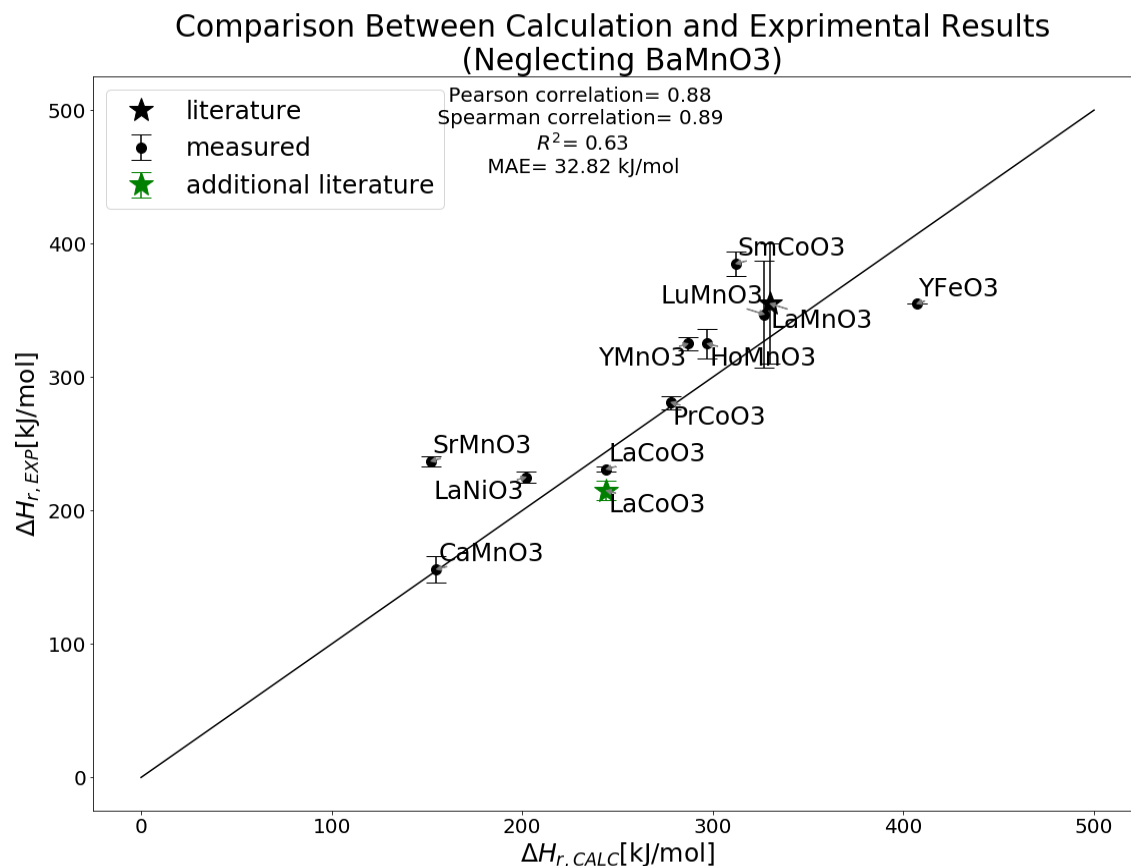


Figure 2. Comparison between calculated and experimentally measured results for reduction enthalpy of ABO₃ compounds considered. Good correlation between computation and experiment validates methodology for further high-throughput exploration to be considered in future plans.

In addition, we have begun high-throughput computational investigation of mixed A₂BB'O₆ double perovskite materials, and we have predicted several materials that satisfy screens for phase stability as well as reduction enthalpy suitable for STCH production of hydrogen. These promising materials will form the basis of some of the future experimental work in the next project period.

CONCLUSIONS AND UPCOMING ACTIVITIES

Experimental synthesis and TGA measurement of ~12 perovskite or other ABO₃ materials has been performed in Year 1. Computational prediction of these materials shows good agreement with experimental results, validating the computational strategy, provided that the correct (experimentally observed) structure is used in the calculations. Based on this successful validation, we propose the following future plans.

Experimental:

- Test site-substituted versions of the most promising materials found in Year 1
- Synthesize and test double-perovskite compounds predicted by computation in Year 1.
- Synthesize combinatorial samples for electrochemical testing.
- Continue testing of electrochemical method and comparison to TGA (e.g., thicker samples).

Computational:

- Significantly expand range of chemistries consider for potential double perovskites and use experimental data from Year 1 to validate more refined thermodynamic models.
- Begin computational search for phase-transformation reactions involving non-stoichiometry for both phases. Start with double perovskites predicted, and examine possible reduced phases involved in reactions.
- Refine models (e.g., examining outlier case of BaMnO_3 more closely):
 - Polymorphs—vacancy formation energies
 - More accurate DFT calculations.
- Obtain entropy calculations (vibrational, configurational, electronic) of reduction entropy—to compare with TGA experiments.
- Conduct high-throughput DFT screening of oxygen vacancy formation energy of double perovskites.
- Tailor oxygen vacancy formation energy by A- and B-site doping: alloying B-site metals with different reduction energies (e.g., $\text{BaMn}_x\text{Ce}_{1-x}\text{O}_3$); alloying A-site metals to control octahedral rotation, which also has large influence on oxygen vacancy formation energy.
- Expand beyond perovskites (e.g., brownmillerite $\text{A}_2\text{B}_2\text{O}_5$, Pyrochlore $\text{A}_2\text{B}_2\text{O}_7$).

HydroGEN Seedling: Mixed Ionic Electronic Conducting Quaternary Perovskites: Materials by Design for Solar Thermochemical Hydrogen

Ellen B. Stechel
Arizona State University LightWorks
800 S Cady Mall
Tempe, AZ 85281-5402
Phone: (480)-965-1657
Email: Ellen.Stechel@ASU.edu

DOE Manager: Katie Randolph
Phone: (240) 562-1759
Email: Katie.Randolph@ee.doe.gov

Contract Number: DE-EE0008090

Subcontractor:
Princeton University, Princeton, NJ

Project Start Date: October 1, 2017
Project End Date: September 30, 2020 (project continuation after Apr 1, 2019 will be determined with a go/no-go review by DOE)

Overall Objectives

The project objective is four-fold.

- Adapt and apply first-principles computational materials design capability, to calculate and validate chemical potentials for complex off-stoichiometric redox-active mixed ionic electronic conducting perovskite metal oxides.
- Relate the calculated solid-state chemical potentials to material's thermodynamics, enthalpy and entropy of reduction, and the equilibrium off-stoichiometry.
- Relate the thermodynamics of materials to theoretical and expected water-splitting performance, noting that performance is a function of operating variables and a key driver of cost.
- Identify promising material candidates that should perform better than ceria, meet the target efficiency (solar-to-hydrogen thermal efficiency >30%), and have the potential to

approach the ultimate production cost goal of <\$2/kg H₂.

Fiscal Year (FY) 2018 Objectives

The primary objective is to develop materials' design criteria and candidate materials to co-optimize materials and the operating conditions as dictated by solar thermochemical hydrogen (STCH) reactors and system designs. The expected outcomes are to achieve the following:

- A capability for materials discovery *in silico*, based on being able to calculate solid-state chemical potentials at relevant operating conditions
- A computational capability that experiments can readily validate
- Design principles for optimal and discoverable materials
- Materials' predictions tuned to the operating conditions and/or the operating conditions tuned to a material's calculated thermodynamics.

Technical Barriers

This project addresses the following technical barrier from the Hydrogen Production section of the Fuel Cell Technologies Office Multi-Year Research, Development, and Demonstration Plan¹:

(S) High-Temperature Robust Materials.

Technical Targets

This project is focused on developing materials for solar thermochemical hydrogen production that result in technologies to produce hydrogen consistent with the following DOE technical targets:

¹ <https://www.energy.gov/eere/fuelcells/downloads/fuel-cell-technologies-office-multi-year-research-development-and-22>

- Support DOE Hydrogen and Fuel Cells
Program goals to sustainably produce hydrogen for <\$2/kg.
- Support DOE Hydrogen and Fuel Cells
Program goals to achieve 2.1×10^{-6} kg/s/m² at 1 sun (252 W/m²).
- Support DOE Hydrogen and Fuel Cells
Program goals to achieve \$1.1 million for a 1-metric-ton-per-day plant (\$790/kW).
- Support DOE Hydrogen and Fuel Cells
Program goals to achieve \$11,000 materials cost for a 1-metric-ton-per-day plant.

FY 2018 Accomplishments

- Completed benchmarking for the behavior of the strongly constrained appropriately normed (SCAN) exchange-correlation functional within the framework of density functional theory (DFT).
- Identified a U value to describe redox energetics of CeO₂-Ce₂O₃ and MnO-Mn₂O₃-MnO₂.
- Developed a novel DFT-based sub-lattice formalism for estimating theoretical Gibbs energies.
- Set up and validated thermodynamic framework with experimental data for Ce-O binary, Ce-Zr-O ternary, La-Mn-O ternary, and La-Sr-Mn-O quaternary.
- Established that the framework is extendable to other quaternaries with little modification, a major step toward representing quinary (A,A')(B,B')O perovskites.
- Developed an inverse design model for the optimal enthalpy of reduction as a function of operating conditions, including yield.
- Developed an operating design model for estimating cycle efficiency.

INTRODUCTION

The current project aims to contribute to materials discovery for improved STCH materials through fundamental quantum mechanics investigations into an exciting class of redox active, mixed ionic electronic conducting metal oxides, which can stably exist over a range of oxygen stoichiometries. By characterizing key thermodynamic properties and stability, we aim to offer strategies to boost solar-to-hydrogen thermal efficiency as well as to provide experimentalists with crucial input to synthesize, validate, and perform further testing and evaluation of promising candidates. We choose off-stoichiometric materials over phase change materials for two principal reasons. First, materials undergoing major reorganization of heavy atoms will challenge the durability criteria and will typically have kinetic limitations during reduction and/or reoxidation, whereas materials that only undergo minor ordering-disordering, structural rocking, or distortion transitions should have acceptable thermomechanical stresses and fast kinetics of reduction and reoxidation. Vacancies in the anion lattice contribute to oxygen transport moving oxygen to and from the bulk and the surface. Second, going off-stoichiometry and having disorder on the anion and cation lattices generates solid-state entropy of configurational disorder, typically absent in materials undergoing a phase transition to another crystallographic structure. High entropy structural rearrangements may exist but may not simultaneously have sufficient kinetics and/or sufficient hydrogen yield.

APPROACH

Sub-Lattice Formalism

To calculate the oxygen chemical potential within the solid phase, it is important to describe accurately the Gibbs energies of the oxidized and the reduced solid. The sub-lattice formalism, which forms the backbone of thermodynamic assessments across chemistries (i.e., CALPHAD-style calculation of phase diagrams), can be used to model the Gibbs energies.

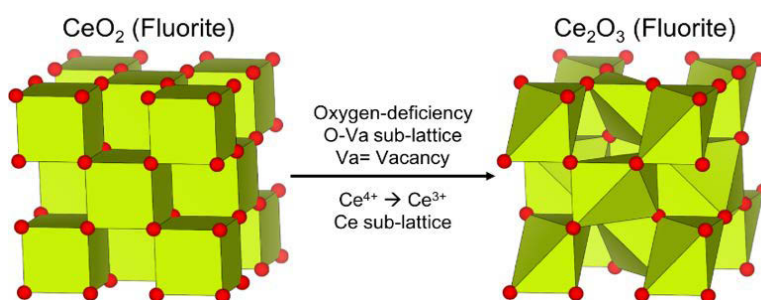


Figure 1. Illustration of the sub-lattice formalism for the fluorite phase in Ce-O binary. The structure on the left indicates stoichiometric CeO₂ while the one on the right refers to a fluorite structure with a Ce₂O₃ stoichiometry.

As an example of applying the sub-lattice formalism, consider the case of the fluorite phase of CeO₂, which undergoes thermal reduction leading to the formation of oxygen vacancies and Ce³⁺ ions. The sub-lattice formalism described here was employed by Zinkevich et al. [1] in their thermodynamic assessment of the Ce-O binary system. Nominally, the fluorite structure has two distinct sub-lattices, Ce and O, respectively. Both sub-lattices can have two species occupying those sites, namely Ce³⁺ and Ce⁴⁺ in Ce sites, and oxygen (nominally O²⁻) and vacancies in O sites. The Gibbs energy for this fluorite phase ($G_{CeO_{2-\delta}}^F$) can be written in the following functional form:

$$G_{CeO_{2-\delta}}^F = y_{Ce^{4+}}y_O G_{Ce^{4+}:O}^0 + y_{Ce^{3+}}y_O G_{Ce^{3+}:O}^0 + y_{Ce^{4+}}y_{Va} G_{Ce^{4+}:Va}^0 + y_{Ce^{3+}}y_{Va} G_{Ce^{3+}:Va}^0 + RT (y_{Ce^{4+}} \ln y_{Ce^{4+}} + y_{Ce^{3+}} \ln y_{Ce^{3+}}) + 2RT (y_O \ln y_O + y_{Va} \ln y_{Va}) + G_{excess}^F \quad (1)$$

In Equation 1, $G_{Ce^{4+}:O}^0$, $G_{Ce^{3+}:O}^0$, $G_{Ce^{4+}:Va}^0$, and $G_{Ce^{3+}:Va}^0$ are referred to as “end member” Gibbs energies with y_X corresponding to the site fraction of species X within the relevant sub-lattice. Each end member energy

corresponds to a distinct species occupancy within the fluorite structure with (i) Ce^{4+} and O occupying Ce and O sites (see left structure in Figure 1), (ii) Ce^{3+} and O occupancies (right panel in Figure 1), (iii) Ce^{4+} and oxygen vacancies within the fluorite structure, and (iv) Ce^{3+} and oxygen vacancies, respectively. Note that the Gibbs energies of non-charge-neutral structures, such as $(\text{Ce}^{4+}:\text{Va})$ and $(\text{Ce}^{3+}:\text{Va})$, are typically obtained by setting a reference state and/or using reciprocal relationships. For example, the Gibbs energy of the $(\text{Ce}^{4+}:\text{Va})$ end member is referenced to:

$$G_{\text{Ce}^{4+}:\text{Va}}^0 = G_{\text{CeO}_2} - G_{\text{O}_2}(g) \quad (2)$$

Typically, only ideal solution configurational entropy (and no other entropic contributions) is accounted for within the sub-lattice formalism. Indeed, Equation 1 has ideal-solution configurational entropy on both Ce and O sub-lattices. Finally, G_{excess}^F indicates any contributions to the Gibbs energy of the fluorite phase not captured by the end-member energies and entropy terms. Numerically, G_{excess}^F is significantly smaller as compared to the end-member and entropy contributions.

In thermodynamic assessments, experimental data (such as specific heat, enthalpy measurements, and phase transition temperatures) are used as input parameters to obtain values for the end-member and excess Gibbs energies, while the entropy term has a simpler analytical form. Here, we are calculating the relevant end-member and excess Gibbs energies entirely through DFT-based calculations, without any experimental input, and benchmark predictions that arise from a DFT-predicted model with experimental data. Specifically, we validate theoretical predictions with experimental measurements on perovskite- LaMnO_3 and SrMnO_3 .

RESULTS

Benchmarking Ternary $(\text{La,Sr})\text{MnO}_3$, 1,673K

Figure 2 displays the oxygen chemical potential profiles in $(\text{La,Sr})\text{MnO}_3$, an important candidate material for thermochemical applications, predicted by DFT+U (solid green) and from experimental data (solid red [2]). Panels a, b, c, and d of Figure 2 correspond to 10%, 20%, 30%, and 40% Sr-doping in the La sub-lattice, respectively, with all data plotted at 1,673 K (reducing conditions). Dashed green and dash-dot brown lines signify oxygen chemical potential variation in La_2O_3 and binary Mn-oxides (MnO , Mn_3O_4 , Mn_2O_3 , and MnO_2) from experimental data. Solid yellow line indicates 10 Pa oxygen partial pressure at 1,673 K. All DFT+U calculations in $(\text{La,Sr})\text{MnO}_x$ employ a SCAN+U functional with $U=2.7$ eV applied on Mn atoms only.

Importantly, the strong overlap between the solid red and solid green curves in all panels of Figure 2 indicates excellent agreement between theoretical predictions and experiments in quaternary- $(\text{La,Sr})\text{MnO}_3$, across Sr concentrations. Under oxygen partial pressures relevant for thermal reduction (solid yellow line), the measured stable compositions are $\text{Sr}_{0.1}\text{La}_{0.9}\text{MnO}_{2.988}$ (panel a), $\text{Sr}_{0.2}\text{La}_{0.8}\text{MnO}_{2.982}$ (b), $\text{Sr}_{0.3}\text{La}_{0.7}\text{MnO}_{2.978}$ (c), and $\text{Sr}_{0.4}\text{La}_{0.6}\text{MnO}_{2.974}$ (d), while theoretical predictions under identical conditions yield stable compositions of $\text{Sr}_{0.1}\text{La}_{0.9}\text{MnO}_{2.992}$, $\text{Sr}_{0.2}\text{La}_{0.8}\text{MnO}_{2.987}$, $\text{Sr}_{0.3}\text{La}_{0.7}\text{MnO}_{2.982}$, and $\text{Sr}_{0.4}\text{La}_{0.6}\text{MnO}_{2.975}$, respectively. Thus, theoretical predictions consistently slightly underestimate the experimental oxygen off-stoichiometries under Sr-substitution, with a maximum deviation of ~ 0.005 at 20% Sr-addition. Theory correctly predicts the qualitative trend of increasing O deficiency with increasing Sr content, in agreement with experiments.

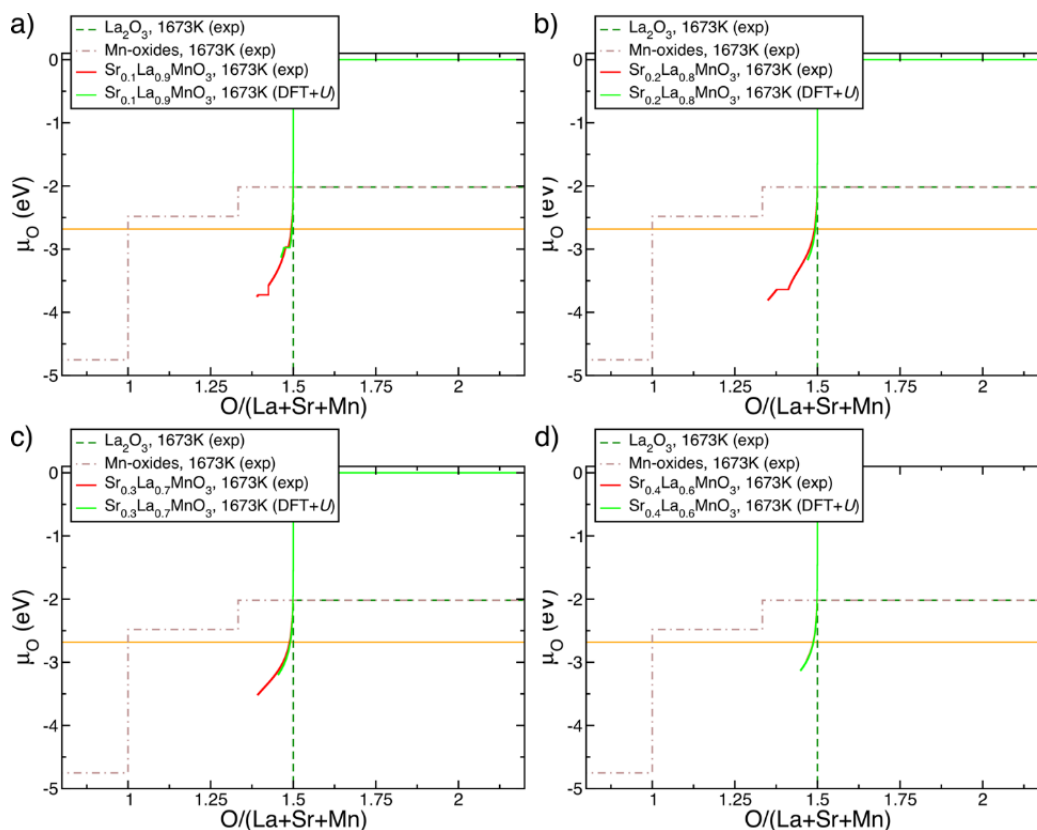


Figure 2. Comparison between experimental (red) and DFT+U-predicted (solid green) oxygen chemical potentials in perovskite-(La,Sr)MnO_x, as a function of oxygen off-stoichiometry. Dashed green and dash-dot brown lines correspond to experimental data for binary La₂O₃ and binary Mn-oxides, respectively. $U = 2.7$ eV is applied on Mn atoms during DFT+U calculations of (La,Sr)MnO_x. All data displayed here correspond to 1,673 K (temperature of thermal reduction).

Benchmarking Ternary (La,Sr)MnO₃, 873K

Figure 3 shows the oxygen chemical potential profiles in (La,Sr)MnO₃ at (a) 10%, (b) 20%, (c) 30%, and (d) 40% Sr-addition, as predicted by DFT+U (solid green) and from experimental data (solid red [2]). The solid indigo line indicates $p_{\text{H}_2\text{O}}/p_{\text{H}_2} = 9$ at 873 K, corresponding to water-splitting conditions. All DFT+U calculations add $U = 2.7$ eV on Mn atoms within a SCAN+ U framework.

Under water-splitting conditions, the theoretical calculations accurately capture the qualitative trends in oxygen off-stoichiometry, across all Sr-additions, as indicated by the strong overlap between the solid red and solid green lines in all panels of Figure 3. However, there are subtle variations between theoretical predictions and experimental observations. For example, at 10% Sr (panel a), theory predicts a significantly lower oxygen deficiency ($\text{Sr}_{0.1}\text{La}_{0.9}\text{MnO}_{2.999}$) compared to experiments ($\text{Sr}_{0.1}\text{La}_{0.9}\text{MnO}_{2.983}$). Similarly, under higher Sr additions (panels b–d, Figure 3), the perovskite phase is not expected to be thermodynamically stable under the water-splitting conditions, whereas theory predicts the perovskite to be stable with negligible oxygen deficiency. The discrepancy between theory and experiment may be due to several factors, such as La-deficiencies altering the stability of the perovskite, errors in the experimental fits to the thermodynamic Gibbs energy functions, and inaccuracies in measuring oxygen off-stoichiometry under water-splitting conditions. Note that although experimental Gibbs-energy fits indicate that the (La,Sr)MnO₃ should not be stable at >10% Sr addition under water-splitting conditions, the perovskite phase may be kinetically stable. Nevertheless, our conclusion is that our theoretical framework is robust enough, as it has been validated against ternary- and

quaternary-perovskite phases in the La-Sr-Mn-O system, and it can be further extended to quinary systems where the B-site (Mn sub-lattice) of the perovskite phase also contains substitutions.

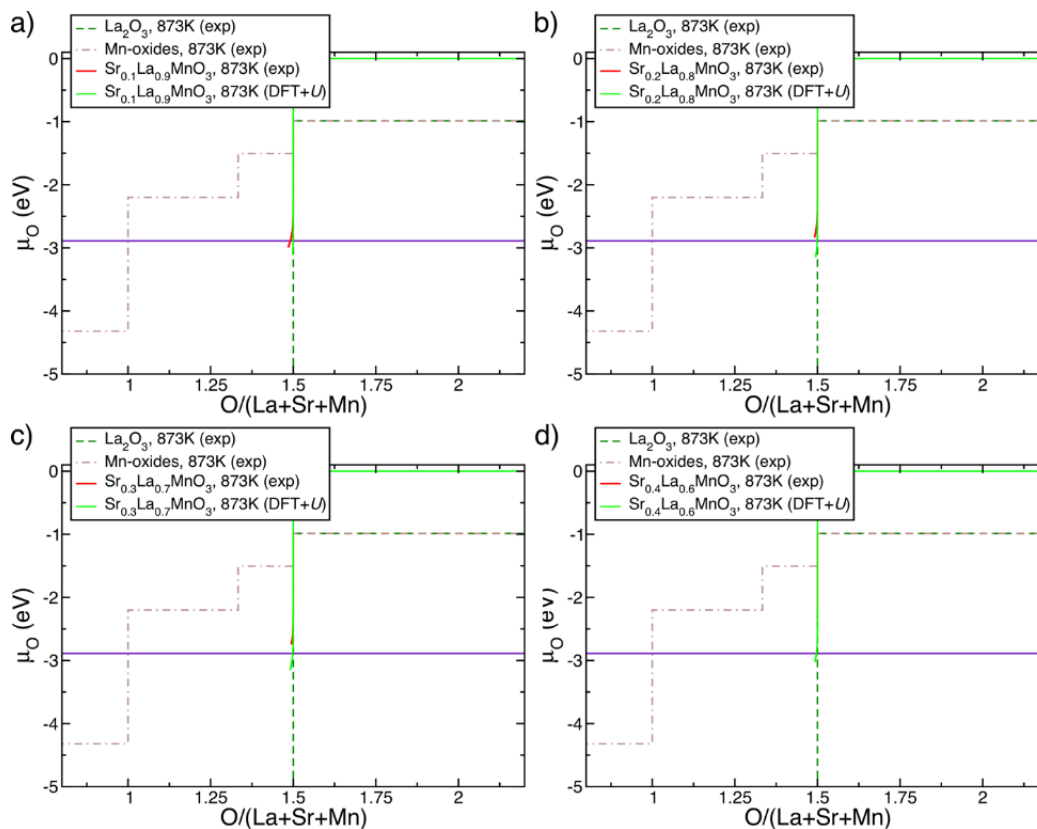


Figure 3. Comparison between experimental (red) and DFT+U-predicted (solid green) oxygen chemical potential in perovskite-(La,Sr)MnO_x, as a function of oxygen off-stoichiometry. Dashed dark green and dash-dot brown lines correspond to experimental data for binary La- and Mn-oxides, respectively. DFT+U calculations are done with $U = 2.7$ eV applied on Mn atoms. All data displayed here correspond to 873 K (temperature of water splitting).

Inverse Design

Desirable Chemical Potential Map

The benchmarking of theoretical predictions against experimental data in binary (CeO₂), ternary (La-Mn-O, Sr-Mn-O, Zr-Ce-O), and quaternary (La-Sr-Mn-O) oxides gives us confidence that the DFT-based sub-lattice formalism can act as an effective model to determine an approximate redox capacity for a given candidate material. Hence, our theoretical framework can be a refined second filter, after a high-throughput first filter based on simpler parameters such as the oxygen vacancy formation energy, to identify promising candidates for solar thermochemical applications. However, we expect to be able to identify other thermodynamic factor(s) that contribute to the oxygen off-stoichiometry of a given material, beyond the oxygen vacancy formation energy, based on the trends we observe using the sub-lattice framework, which can in turn be used to quickly screen for potential candidates.

Bayesian Inference of Thermodynamic Model Parameters

In support of this project, the principal investigator has been working closely with the Sandia National Laboratories “Uncertainty Quantification in Computational Models of Physical Systems” node principal investigator Bert Debusschere. One of the goals of the project is to predict the thermodynamic efficiency of water splitting with specified uncertainty for newly developed materials as a function of the operating

conditions. This Sandia National Laboratories node contributes to this goal by determining the confidence needed in the components that feed into that efficiency computation in order to meet the desired accuracy. The principal investigator developed the models and thermodynamic formulism.

Bayes' rule updates prior belief in parameter values (λ) with data (δ), to obtain posterior belief in the parameter values:

$$p(\lambda|d, \mathcal{M}) = \frac{p(d|\lambda, \mathcal{M})p(\lambda, \mathcal{M})}{p(d|\mathcal{M})} \quad (3)$$

We have developed four defect-free model fits of increasing complexity that allow for a relatively simple extraction of the enthalpy as well as quantifying the error in the enthalpy. The data (data can come from experiment or from computation or a combination) is assembled as a “measurement” triplet at equilibrium conditions, $\{\delta, T, pO_2\}$. We found it convenient to first convert the triplet to three transformed and unitless variables:

$$\beta = \left(\frac{T_{ref}}{T}\right) \quad (\text{temperature transform}) \quad (4a)$$

$$u \equiv \frac{1}{2} \ln \left(\frac{pO_{2,ref}}{pO_2}\right) \quad (\text{oxygen partial pressure transform}) \quad (4b)$$

$$z \equiv -\ln(\delta) \quad (\text{reduction extent transform}) \quad (4c)$$

For a defect-free model independent fit of the material relationship between $\{\delta, T, \text{ and } pO_2\}$ we use the following convenient functional form, convenient because it is easily inverted in terms of Z or in terms of u , also making it easy to determine the following:

$$z = \frac{z_{ref} + f_{10}(1-\beta) + f_{20}u + f_{30}u(1-\beta)}{1 + f_{11}(1-\beta) + f_{21}u + f_{31}u(1-\beta)} \quad (5a)$$

$$u = \frac{(z - z_{ref}) - f_{10}(1-\beta) + f_{11}z(1-\beta)}{f_{20} - f_{21}z - (f_{30} - f_{31}z)(1-\beta)} \quad (5b)$$

Model A: $f_{11} = f_{21} = f_{30} = f_{31} = 0$; Model B1: $f_{11} = f_{30} = f_{31} = 0$; Model B2: $f_{30} = f_{31} = 0$; and Model C: all parameters are active.

We infer the distribution of those parameters such that when model realizations are sampled from those random variables, they span the range of predictions due to model error [3].

In Figure 4, the shaded areas represent the mean prediction plus or minus one standard deviation, plotted in a cumulative way (i.e., the extent of the model error bars covers the cumulative effect of surrogate error, posterior uncertainty, and model error).

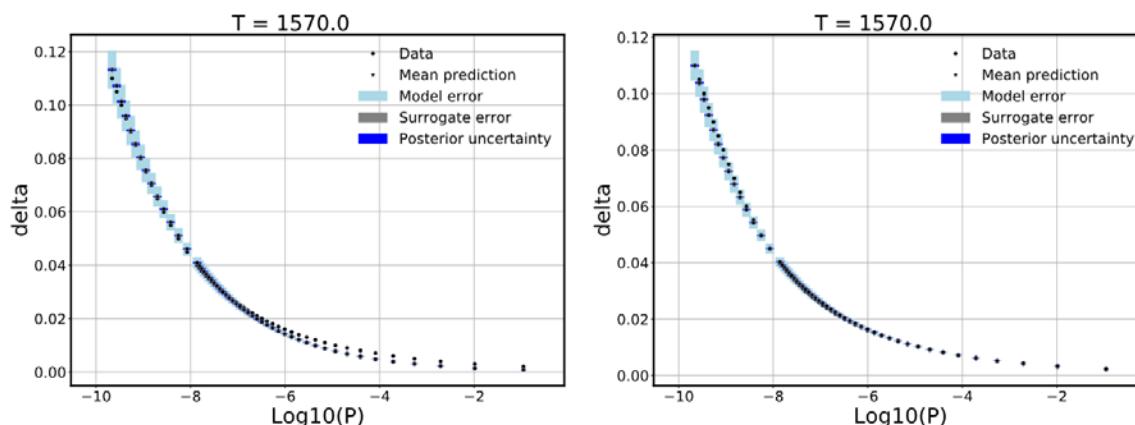


Figure 4. Model error captures the difference between data and predictions. Model error embedded in f_{10} and f_{20} for models A (left) and B1 (right). Model error is the largest contribution to predictive uncertainty. Model A: Mean parameter set is $\{z_{\text{ref}}: 14.82, f_{10}: -23.78, F_{20}: -0.4919\}$ and Model B2: Mean parameter set is $\{z_{\text{ref}}: 11.67, f_{10}: -17.37, f_{20}: -0.4384, F_{21}: -0.02567\}$.

CONCLUSIONS AND UPCOMING ACTIVITIES

The benchmarking of theoretical predictions against experimental data in binary (CeO_2), ternary (La-Mn-O , Sr-Mn-O , Zr-Ce-O), and quaternary (La-Sr-Mn-O) oxides gives us confidence that the DFT-based sub-lattice formalism can act as an effective theory and simulation model to determine an approximate redox capacity for a given candidate material. Hence, our theoretical framework can be a refined second filter, after a high-throughput first filter based on simpler parameters (e.g., the oxygen vacancy formation energy), to identify promising candidates. Moreover, we expect to be able to identify other thermodynamic factor(s) that contribute to the oxygen off-stoichiometry of a given material, beyond the oxygen vacancy formation energy, based on the trends we observe using the sub-lattice framework.

We find that the sub-lattice formalism is powerful and with quinary extensions of $(\text{La,Sr})\text{MnO}_3$ will allow for an extensive exploration of the perovskite family for candidate materials. It also permits the identification of the governing thermodynamic variables that control the oxygen deficiency of any given material, at a given temperature and oxygen partial pressure. Further characterization of uncertainty with propagation of chosen model error into thermodynamic properties will allow propagation of uncertainties into our cycle efficiency model, tying all the pieces together.

FY 2018 PUBLICATIONS/PRESENTATIONS

1. E. B. Stechel, "HydroGEN: Advanced Water Splitting Materials," Invited presentation at the International Workshop on Solar Thermochemistry, Julich, Germany, September 12–14, 2017.
2. Gopalakrishnan Sai Gautam and Emily A. Carter, "Evaluating Transition-Metal Oxides within DFT-SCAN and SCAN+U Frameworks for Solar Thermochemical Applications," *Phys. Rev. Mater.* 2 (2018): 095401.

REFERENCES

1. Matvei Zinkevich, Dejan Djurovic, and Fritz Aldinger, "Thermodynamic Modelling of the Cerium–Oxygen System," *Solid State Ionics* 177 (2006): 989.
2. A. Nicholas Grundy, Bengt Hallstedt, and Ludwig J. Gauckler, "Assessment of the La–Sr–Mn–O System," *Computer Coupling of Phase Diagrams and Thermochemistry* 28 (2004): 191–201.
3. K. Sargsyan, H.N. Najm, and R. Ghanem, R. "On the Statistical Calibration of Physical Models," *International Journal of Chemical Kinetics* 47, no. 4 (2015): 246–276.

HydroGEN Seedling: High-Temperature Reactor Catalyst Material Development for Low-Cost and Efficient Solar-Driven Sulfur-Based Processes

Claudio Corgnale (Primary Contact),
William Summers
Greenway Energy, LLC
301 Gateway Drive
Aiken, SC 29803
Phone: (803) 617-9689
Email: claudio.corgnale@greenway-energy.com

DOE Manager: Katie Randolph
Phone: (720) 356-1759
Email: Katie.Randolph@ee.doe.gov

Contract Number: DE-EE0008091

Subcontractor:
University of South Carolina, Columbia, SC

HydroGEN node laboratories:

- Idaho National Laboratory, Idaho Falls, ID
- Savannah River National Laboratory, Aiken, SC
- National Renewable Energy Laboratory, Golden, CO

Project Start Date: October 1, 2017
Project End Date: September 30, 2020

Overall Objectives

- Develop a new catalyst for the sulfuric acid decomposition, achieving nominal reaction yields about 30% higher than the current state of the art.
- Demonstrate reduced catalyst performance degradation for >400 h, achieving a 50% improvement compared to the current state of the art.
- Develop a novel solar-driven hybrid sulfur (HyS) process flowsheet, demonstrating solar-to-hydrogen overall efficiency $\geq 20\%$.
- Develop a novel direct solar receiver-reactor concept, allowing for a direct solar-driven sulfuric acid decomposition, with experimental demonstration of an electrically heated laboratory-scale system.

- Identify a solar thermochemical plant configuration demonstrating reduced overall hydrogen production costs, showing a viable path to \$2/kg H₂.

Fiscal Year (FY) 2018 Objectives

- Develop a novel baseline catalytic formulation for the sulfuric acid decomposition occurring at $T \approx 800^\circ\text{C}$ and achieve nominal reaction yields approximately 20% higher than the current state of the art (i.e., 0.28 mol SO₂/g_{Cat}/h).
- Demonstrate reduced catalyst performance degradation for about 70–100 h, achieving a degradation $\leq 0.015\%/h$.
- Develop a novel solar-driven HyS process flowsheet, demonstrating solar to hydrogen efficiency >18%.

Technical Barriers

This project addresses the following technical barriers from the Hydrogen Production section of the Fuel Cell Technologies Office Multi-Year Research, Development, and Demonstration Plan,¹ with particular reference to the thermochemical hydrogen production technologies:

- High-temperature catalyst activity and degradation
- Plant construction materials, being able to stand harsh environment with sulfur-based compounds at temperatures on the order of 800°C
- Efficient and low-cost integration of the thermochemical plant with the solar plant
- Efficient and cost-effective solar HyS plant configuration.

Technical Targets

This project is conducting both fundamental development of novel catalytic formulations for

¹ <https://www.energy.gov/eere/fuelcells/downloads/fuel-cell-technologies-office-multi-year-research-development-and-22>

sulfuric acid high-temperature decomposition reactions and engineering and system design and analysis of the solar-driven HyS cycle. Insights gained from this work will be applied to develop novel solar-driven hydrogen production systems that meet the following targets:

- H_2SO_4 decomposition catalyst nominal yield: 0.3 mol $\text{SO}_2/\text{g}_{\text{Cat}}/\text{h}$
- H_2SO_4 decomposition catalyst degradation: 0.0125%/h
- Solar-to-hydrogen efficiency: 20% (DOE target).
- Hydrogen production cost: \$2/kg H_2 (DOE target).

FY 2018 Accomplishments

- Identified and tested a novel catalytic formulation (referred to as CAT2), showing increased activity (1.8 mol $\text{SO}_2/\text{g}_{\text{Cat}}/\text{h}$) and reduced degradation, with essentially no degradation for the 72-hour test.
- Identified and simulated a novel direct receiver reactor configuration, demonstrating the feasibility of a direct solar-driven H_2SO_4 decomposition reactor with enhanced performance compared to the previous bayonet-based baseline reactor.
- Developed a novel solar HyS integrated flowsheet based on optimized solar tower plant configuration and on vapor-fed SO_2 depolarized electrolyzer (SDE) section, showing preliminary thermochemical efficiencies $\approx 37.8\%$ and solar-to-hydrogen efficiencies exceeding the target ($\approx 20.5\%$).

INTRODUCTION

The HyS process, driven by solar power, has great potential to reach high-efficiency and low-cost hydrogen production without greenhouse gas emissions. The high-temperature section of the HyS cycle, which operates the catalytic decomposition of sulfuric acid into sulfur dioxide, oxygen, and water, is a fundamental part of the cycle affecting the overall plant efficiency and cost [1, 2]. Therefore, a high-performance catalyst (i.e., low cost, high catalytic activity, and low degradation catalyst) is of critical importance to achieve high efficiency and low hydrogen cost. Research and development has highlighted that a Pt-based monometallic catalyst had unacceptable catalytic activity and performance degradation for a high-efficiency and low-cost hydrogen production process [3]. A high-efficiency solar receiver-reactor system, which incorporates the new catalyst, also needs to be developed to achieve the required plant efficiency and cost. Greenway Energy (GWE) and the University of South Carolina (USC), partnering with HydroGEN node laboratories Idaho National Laboratory (INL), Savannah River National Laboratory (SRNL), and National Renewable Energy Laboratory (NREL), propose the development of a new catalyst formulation, included in a novel solar receiver-reactor concept, to be tested experimentally in the last part of the project.

APPROACH

The work is carried out based on a three-level approach: (1) the first level analyzes the fundamental mechanisms of the H_2SO_4 catalytic decomposition, aiming to synthesize and produce a novel catalyst; (2) the second level analyzes the engineering and system aspects of the solar reactor for the sulfuric acid decomposition, proposing an innovative direct solar receiver-reactor; and (3) the third level focuses on high-level solar thermochemical process analysis, proposing new HyS flowsheets and novel solar plant integration layout. A novel catalyst preparation technique, developed by USC, uses a combination of strong electrostatic adsorption, which permits formation of very small metal particles with a narrow distribution of sizes, and electroless deposition (ED) to produce controlled bimetallic catalysts. This will result in limiting the catalyst deactivation by using very small particles of a high-surface free energy core metal with a catalytically active outer metal shell deposited by ED. A new laboratory-scale decomposition reactor will also be designed and tested (during Phase 3 of the project) to assess the nominal performance and the long-term degradation. The solar-driven HyS cycle will also be modeled, integrating the down-selected reactor concept with the other HyS interfaced equipment. A large-scale solar-driven process configuration will be identified, modeled, and optimized to achieve solar efficiencies $\geq 20\%$ and hydrogen costs $\leq \$2/\text{kg H}_2$.

GWE and USC are partnering with three HydroGEN node laboratories: INL to perform the catalyst testing, SRNL to develop the HyS flowsheet, and NREL to design and assess the performance of the interfaced solar plant and the solar balance-of-plant equipment.

RESULTS

Catalyst Material Development and Testing

Several materials were examined and tested, including both monometallic and bimetallic formulations. Table 1 shows a list of the selected materials, including the novel formulations developed at USC (currently being patented) referred to as CAT0 (monometallic formulation), CAT1 (bimetallic initial formulation), and CAT2 (bimetallic enhanced formulation). Each material was tested with sulfuric acid at approximately 90 wt% in water, $T = 800^\circ\text{C}$, and $P = 1$ bar.

Monometallic formulations, based on 1% Pt/TiO₂, were able to achieve the nominal activity target but could not maintain the same level of performance over time, failing to achieve the performance duration target. Therefore, work moved forward with the bimetallic catalysts, identified by comparing the surface free energy of the two elements and synthesized using the ED approach.

Table 1. List of Catalyst Formulations Tested at INL

Catalyst	Classification	Source
1% Pt/TiO ₂	Monometallic	USC
1% Pt/TiO ₂	Monometallic	Johnson-Matthey
5% Ir/TiO ₂	Monometallic	USC
5% Ru/TiO ₂	Monometallic	USC
1% Pt/5% Ir/TiO ₂	Bimetallic	USC
1% Pt/10% Ir/TiO ₂	Bimetallic	USC
CAT0	Monometallic	USC (novel formulation)
CAT1	Bimetallic	USC (novel formulation)
CAT2	Bimetallic	USC (novel formulation)

The main results achieved during the first year of the project for novel bimetallic formulations are shown in Figure 1, highlighting the performance of the down-selected catalytic materials.

A 1% Pt–10% Ir/TiO₂ support has been identified as a possible enhanced material for the Pt bimetallic catalyst on TiO₂ support. This formulation can exceed the nominal conversion target (0.28 mol SO₂/g_{Cat}/h) but cannot meet the degradation performance target (0.015%/h). A novel bimetallic catalyst formulation has been identified, developed, and tested, referred to as CAT2. This material was able to exceed both the nominal activity target (measured nominal activity of about 1.8 mol SO₂/g_{Cat}/h) and the degradation performance target for 72-hour tests (essentially absence of degradation observed for 72-hour tests) as shown in Figure 1. The use of co-ED, depositing Pt and Ir contemporarily, is also being examined with different Pt and Ir concentrations and different deposition conditions. Results will be available as part of the next phases of the project. A mixed Rh-Pt catalyst was also examined, with results showing poor performance in comparison with pure Pt-based formulations.

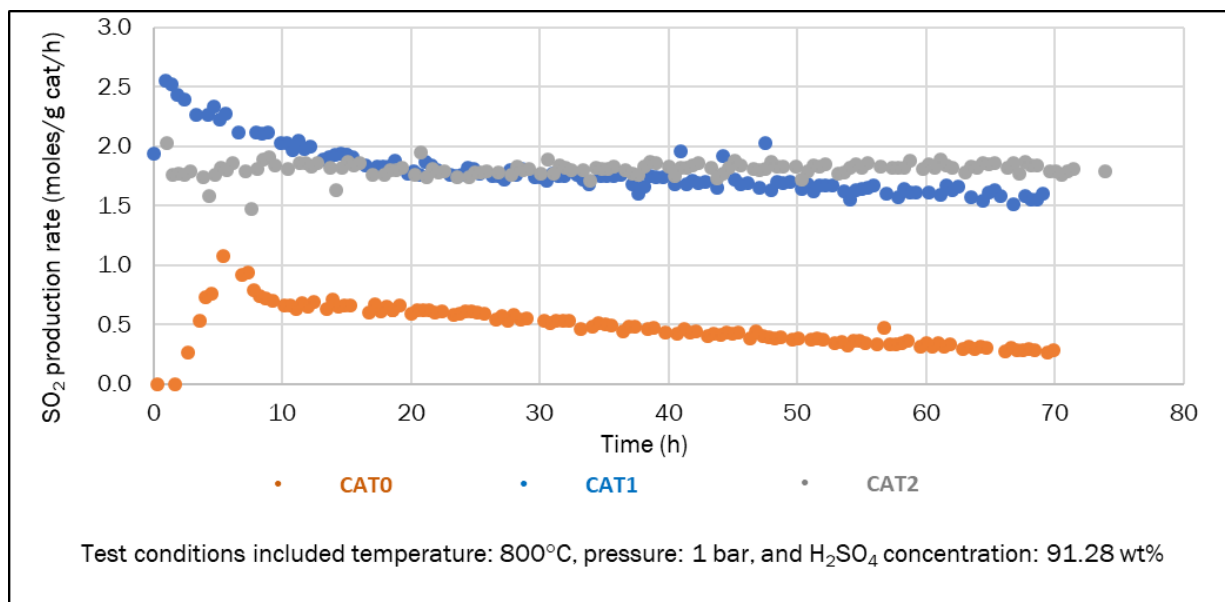


Figure 1. Novel catalyst formulation tests

Novel Direct Solar Reactor/Receiver Concept

A novel sulfuric acid decomposition reactor concept has been developed by GWE and NREL. The concept is based on a suitable modification of an NREL solar receiver, adopted for concentrated solar power plants to produce electricity, as shown in Figure 2.

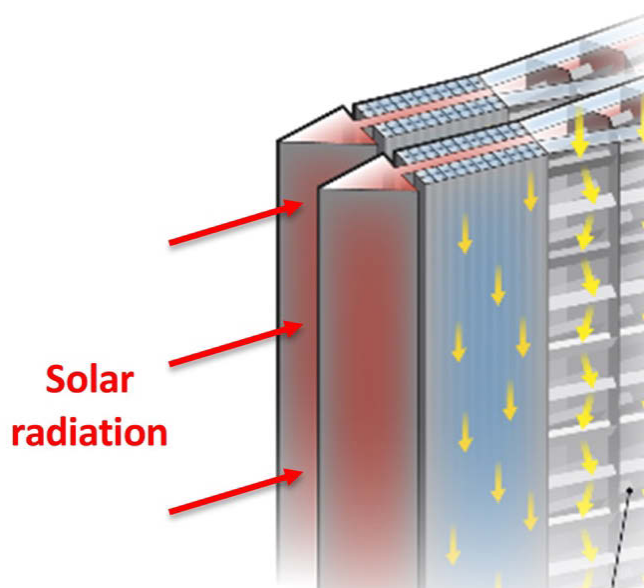


Figure 2. Novel integrated solar receiver-reactor for sulfuric acid decomposition

The concentrated sulfuric acid mixture flows in the external parallelepipedal region, in direct contact with the external wall heated by the concentrated solar radiation. The decomposed mixture flows in a counter-current arrangement in the internal parallelepipedal region, allowing internal heat recovery and exchange with the inlet sulfuric acid mixture. The proposed reactor concept allows (1) effective external solar heat transfer and internal heat recovery to be accomplished in a single highly intensified unit, (2) removal of solar intermediate heat exchangers, with the solar power transferred directly from the receiver to the HyS working fluid, and (3) high exergetic efficiency and potential cost reduction. A detailed transport phenomena computational fluid dynamics (CFD) reactive model has been developed in finite volume environment (STAR-CCM+), including mass, energy, and momentum balance equations integrated with suitable kinetics expressions [4]. Different operating conditions, including temperatures, pressures, and H_2SO_4 concentrations, were examined. Temperature and SO_2 concentration profiles obtained in the catalytic decomposition region (decomposition of SO_3 into SO_2 and O_2) of a single unit reactor are shown in Figure 3. Results demonstrate the feasibility of the proposed concept, highlighting (1) excellent internal heat recovery between the reacting mixture and the reacted mixture, (2) absence of temperature decrease during the endothermic decomposition of the SO_3 into SO_2 , and (3) linear decomposition of SO_3 into SO_2 throughout the catalytic decomposition region.

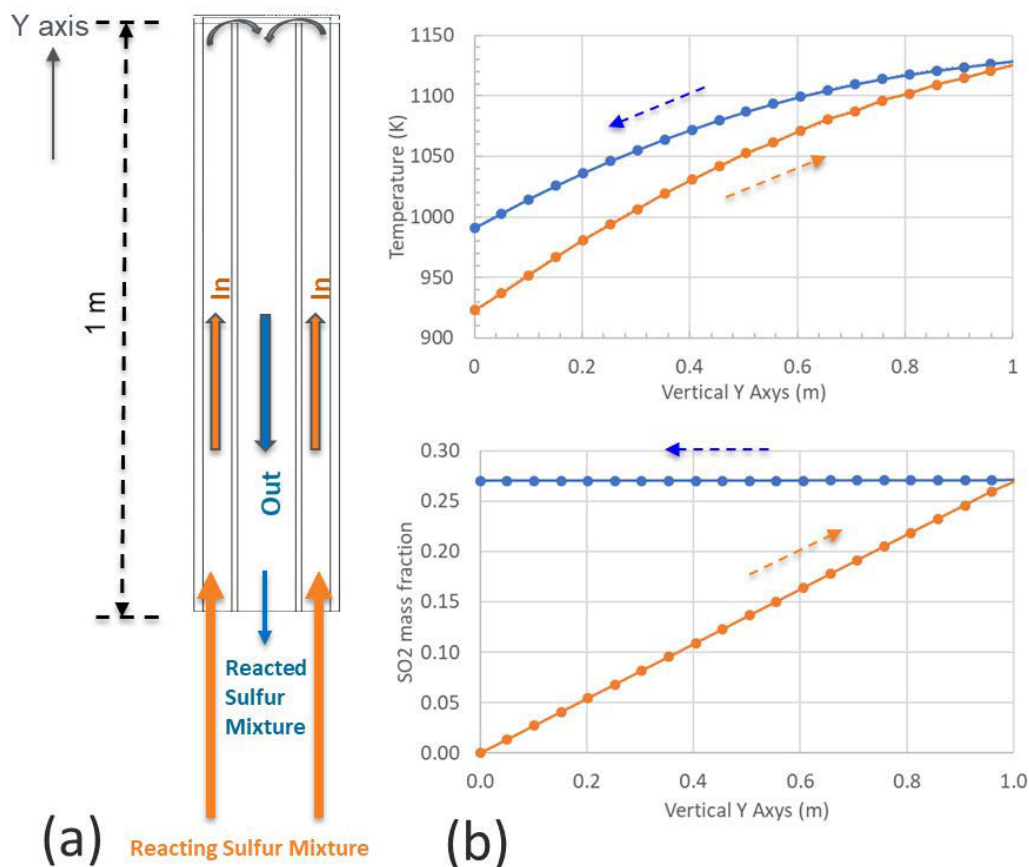


Figure 3. CFD simulation results of the novel reactor: (a) back view of the reactor, (b) temperature and SO₂ concentration profiles

Solar HyS Plant Flowsheet and Integration

A novel solar-driven HyS thermochemical flowsheet has been developed, introducing (1) a vapor-fed SDE section approach for the low-temperature section, and (2) chemical sulfur-based storage (H₂SO₄ and SO₂), replacing expensive and less-efficient thermal energy storage. By this approach the low-temperature electrochemical section will be designed to work continuously, while the high-temperature section will be designed to work on-sun based on the availability of the solar radiation. The novel HyS flowsheet has been initially developed and simulated using ASPEN Plus, resulting in the following preliminary results: (1) high-temperature section thermal duty: 345.3 kJ_{th}/mol H₂, (2) high-temperature section electric duty, mainly required for the SO₂ separation and recirculation: 10.5 kJ/mol H₂, and (3) low-temperature section electric duty: 112.4 kJ/mol H₂ with 110.2 kJ/mol H₂ required for the SDE. This results in a thermochemical efficiency (assuming an electric efficiency of 41.6%) of 37.8% (based on the low heating value of the hydrogen). The solar plant, to be coupled with the thermochemical plant, has been designed using SolarPILOT software examining different power conditions. An optimum solar power condition of 200 MW was assessed based on the cost of the heliostat field and of the solar tower (Figure 4). The 200-MW plant heliostat efficiency was calculated using Solar PILOT, resulting in 63.9%, and the novel receiver efficiency was projected to be on the order of 85%. Therefore, the overall solar-to-hydrogen efficiency has been preliminarily estimated to be equal to 20.5%. More refined calculations will be carried out during the first quarter of FY 2019 as part of one of the milestones of the project.

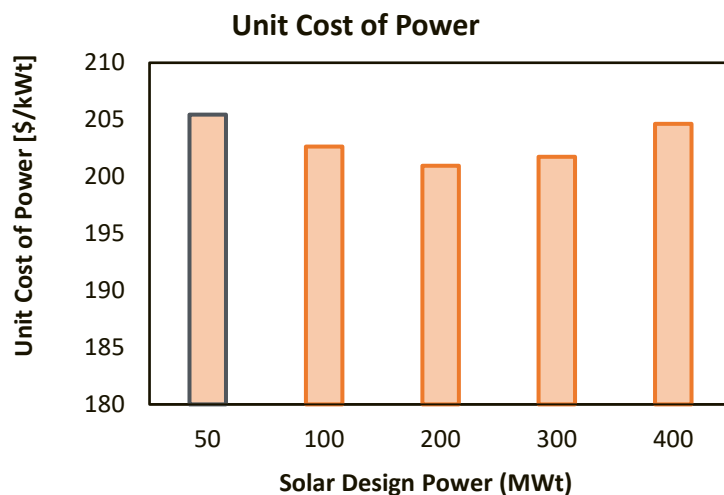


Figure 4. Techno-economic analysis results of the solar plant for different solar powers

CONCLUSIONS AND UPCOMING ACTIVITIES

The project has identified a novel catalytic formulation, currently being patented, for the decomposition of sulfuric acid at temperatures on the order of 800°C. Compared to the current state of the art, the new catalyst showed higher nominal activity and essentially absence of degradation during 72-hour tests. A novel efficient and potentially low-cost solar-driven receiver-reactor concept has also been developed and simulated to carry out the H₂SO₄ decomposition. CFD simulation results demonstrated excellent technical performance of the proposed concept in terms of temperature and concentration results. A preliminary solar thermochemical process analysis showed the potential of the integrated solar plant to achieve solar-to-hydrogen efficiencies on the order of 20%, thus meeting the DOE target.

Future work will be carried out on (1) optimization of the novel catalytic formulation, with duration tests up to 400–500 hours, (2) fabrication of the novel reactor at laboratory scale, with electrically heated experimental tests, and (3) detailed assessment of the techno-economic performance of the integrated solar thermochemical plant, including equipment design, cost assessment, and additional sensitivity analyses and process optimization.

The collaboration with the HydroGEN node laboratories involved in the project (i.e., INL, SRNL, and NREL) was instrumental to achieve the project targets and objectives. In particular, INL is world-renowned laboratory to perform sulfuric acid decomposition tests at high temperatures and at various operating conditions. USC has been working in strict conjunction with INL to develop and test the new catalysts. SRNL knowledge on HyS process flowsheeting and development was fundamental to set up a novel flowsheet and assess the thermochemical process efficiency under different operating conditions. GWE and SRNL have been working together to perform the HyS equipment design and cost evaluation. The presence of NREL in the project was also of primary importance to identify the solar plant techno-economic performance and to integrate the solar plant with the thermochemical process. GWE and NREL identified the novel reactor concept with involvement of USC in the CFD simulation of the proposed concept.

SPECIAL RECOGNITIONS AND AWARDS/PATENTS ISSUED

1. Record of Invention by NREL and GWE: Ma, Z., et al., NREL Record of Invention ROI-18-62, 2018.
2. Invention disclosure by USC and INL: Monnier, J., et al., USC ID no. 1372, 2018.

FY 2018 PUBLICATIONS/PRESENTATIONS

1. C. Corgnale et al., “Solar Driven Thermo-Electrochemical Hybrid Sulfur Process for Hydrogen Production,” ECS AiMES Meeting 2018, Cancun (Mexico), October 2018.
<https://ecs.confex.com/ecs/aimes2018/meetingapp.cgi/Paper/112622>.
2. C. Corgnale et al., “Numerical Modeling of a Novel Solar Driven Sulfuric Acid Decomposition Reactor,” ECS AiMES Meeting 2018, Cancun (Mexico), October 2018.
<https://ecs.confex.com/ecs/aimes2018/meetingapp.cgi/Paper/112623>.

REFERENCES

1. C. Corgnale et al., *Int. J. Hydrogen Energy* 36 (2011): 11604–11619.
2. C. Corgnale et al., *Solar Hybrid Sulfur Cycle Water-Splitting Process*, SRNL-STI-2015- 00546, Revision 0 (2015).
3. L.M. Petkovic et al., *Applied Catalysis A: General* 338 (2008): 27
4. C. Corgnale et al., *Int. J. Hydrogen Energy* 42 (2017): 20463–20472.

System Analysis of Physical and Materials-Based Hydrogen Storage

Rajesh K. Ahluwalia (Primary Contact), J-K Peng, Hee Seok Roh, and D. Papadias
Argonne National Laboratory
9700 South Cass Avenue
Argonne, IL 60439
Phone: (630) 252-5979
Email: walia@anl.gov

DOE Manager: Katie Randolph
Phone: (720) 356-1759
Email: Katie.Randolph@ee.doe.gov

Project Start Date: October 1, 2004
Project End Date: Project continuation and direction determined annually by DOE

Overall Objectives

- Model various developmental hydrogen storage systems.
- Provide results to DOE for assessment of performance targets and goals.
- Develop models to “reverse-engineer” particular approaches.
- Identify interface issues, opportunities, and data needs for technology development.

Fiscal Year (FY) 2018 Objectives

- Conduct system analysis of cryo-compressed hydrogen (CcH₂) storage for fuel cell buses with the constraint of 7-d dormancy for 95% full tanks.
- Investigate alternate configurations of compressed hydrogen (cH₂) storage tanks for light-duty and heavy-duty vehicles.
- Support Hydrogen Materials Advanced Research Consortium (HyMARC) activities by performing reverse engineering analysis of room-temperature hydrogen storage in sorbents.

- Support H2@Scale initiative by analyzing one-way and two-way liquid hydrogen carrier pathways.

Technical Barriers

This project addresses the following technical barriers from the Hydrogen Storage section of the Fuel Cell Technologies Office Multi-Year Research, Development, and Demonstration Plan¹:

- (A) System Weight and Volume
- (B) System Cost
- (C) Efficiency
- (E) Charging/Discharging Rates
- (J) Thermal Management
- (K) System Life Cycle Assessments.

Technical Targets

This project is conducting system-level analyses to address the DOE 2020 technical targets for onboard hydrogen storage systems:

- System gravimetric capacity: 1.5 kWh/kg
- System volumetric capacity: 1.0 kWh/L
- Minimum hydrogen delivery pressure: 5 bar
- Refueling rate: 1.5 kg/min
- Minimum full flow rate of hydrogen: 0.02 g/s/kW.

FY 2018 Accomplishments

- Showed 500-bar CcH₂ can achieve 215% increase in storage density, 90% improvement in gravimetric capacity, 170% higher volumetric capacity, and 47% savings in carbon fiber (CF) composite as compared to the Type 3 350-bar cH₂ tanks currently in use in fuel cell buses.

¹ <https://www.energy.gov/eere/fuelcells/downloads/fuel-cell-technologies-office-multi-year-research-development-and-22>

- Established targets for room-temperature sorbents: 106 ± 8 g H₂/kg excess uptake at 100 bar when compacted to 500 ± 35 kg/m³ bulk density.
- Proposed and demonstrated a concept of reinforcing the dome section with an elongated boss to realize >10% saving in CF composite for Type 4 tanks.
- Performed preliminary analysis on the cost of producing/hydrogenating hydrogen carriers, transmitting them to and dehydrogenating them at the city gate, and storing the hydrogen on site (\$5.43–\$6.02).

INTRODUCTION

Several different approaches are being pursued to develop onboard hydrogen storage systems with the goal of meeting the DOE targets for light-duty vehicle applications. Each approach has unique characteristics, such as pressure and temperature, the thermal energy and temperature of charge and discharge, and kinetics of the physical and chemical process steps involved. The approaches take into account the requirements for the materials and energy interfaces between the storage system, the fuel supply system, and the fuel user. Other storage system design and operating parameters influence the projected system costs as well. Models are being developed to understand the characteristics of storage systems based on the various approaches and to evaluate their potential to meet the DOE targets for onboard applications—including the offboard targets for energy efficiency.

APPROACH

The approach is to develop thermodynamic, kinetic, and engineering models of the various hydrogen storage systems being developed under DOE sponsorship. These models are then used to identify significant component and performance issues and to assist DOE and its contractors in evaluating alternative system configurations and design and operating parameters. Performance criteria are established that may be used, for example, in developing storage system cost models. Data is refined and validated as the models become available from the various developers. An important aspect of this work is to develop overall systems models that include the interfaces between hydrogen production and delivery, hydrogen storage, and the fuel cell.

RESULTS

Cryo-Compressed Hydrogen Storage

We revised our previous analysis of cryo-compressed hydrogen (CcH_2) storage for buses with the additional constraint of 7-d dormancy for 95% full tank [1]. We determined the required thickness of multi-layer vacuum superinsulation (MLVSI) with 0.1 mW/m.K thermal conductivity at 3-mTorr vacuum. Table 1 highlights the following advantages of liquid hydrogen refueled, supercritical CcH_2 storage at 500 bar over the baseline ambient temperature, and 350-bar compressed hydrogen storage (cH_2) in Type 3 vessels:

- >215% increase in storage density
- >90% higher gravimetric capacity
- 170% higher volumetric capacity
- 47% saving in carbon fiber (CF) composite
- >25% lower cost at 5,000 systems/year annual production.

Table 1. Supercritical CcH₂ Storage for Fuel Cell Buses

Storage Method	CcH ₂	CcH ₂	cH ₂
Storage Pressure	350 bar	500 bar	350 bar
Usable H ₂	4 x 10 kg	4 x 10 kg	8 x 5 kg
Liner	2-mm SS	2-mm SS	7.1 mm Al
Storage Temperature	64 K	70 K	288 K
Storage Density	70.3 g/L	75.5 g/L	24 g/L
Gravimetric Capacity	9.6%	8.4%	4.4%
Volumetric Capacity	46.1 g/L	50.1 g/L	18.5 g/L
CF Composite	4 x 36 kg	4 x 53.1 kg	8 x 50 kg
Insulation Thickness	18.2 mm	10.3 mm	NA
Heat Gain	3.8 W	5.7 W	NA
Dormancy: 95% Full	7.0 d	7.0 d	NA
Cost	\$10/kWh	\$11/kWh	\$15/kWh

Compressed Hydrogen Storage

As part of a larger study on alternate Type 4 tank configurations for 700-bar cH₂ storage, we conducted ABAQUS/WCM simulations to investigate the possible reduction in the number of helical layers by reinforcing the entire dome section with an aluminum boss in a 147-L tank with 391-mm inner diameter and 5-mm high-density polyethylene (HDPE) liner. A previous Mirai study on extended boss showed 5% reduction in helical winding with smaller diameter and longer flange [2], but our simulations showed no significant reduction. Figure 1a compares our boss-reinforced dome concept with the baseline boss and the elongated boss in the Mirai study. Figure 1b shows the modeled stress distribution in the boss-reinforced dome indicating small regions undergoing plastic deformation at refueling pressure. A future study will investigate the fatigue performance of the boss covering the whole dome section and the possible advantages of autofrettage in meeting any fatigue criteria that may apply. Our finite element simulations indicate that boss reinforcement reduces the thickness of CF composite helical layers by ~5.0 mm, or 13% of 37.1 mm in baseline boss configuration. This 15% reduction in total weight of CF composite is offset by a 23.2 kg increase in the weight of boss. Figure 1c compares the strains along fiber direction and indicates slight reduction in the level of strain in the composite material in the dome section but higher strain in the helical layers in the cylinder section. The reduction in CF composite may be greater in tanks with an aspect ratio higher than 5, as in these simulations, and will be investigated in future work.

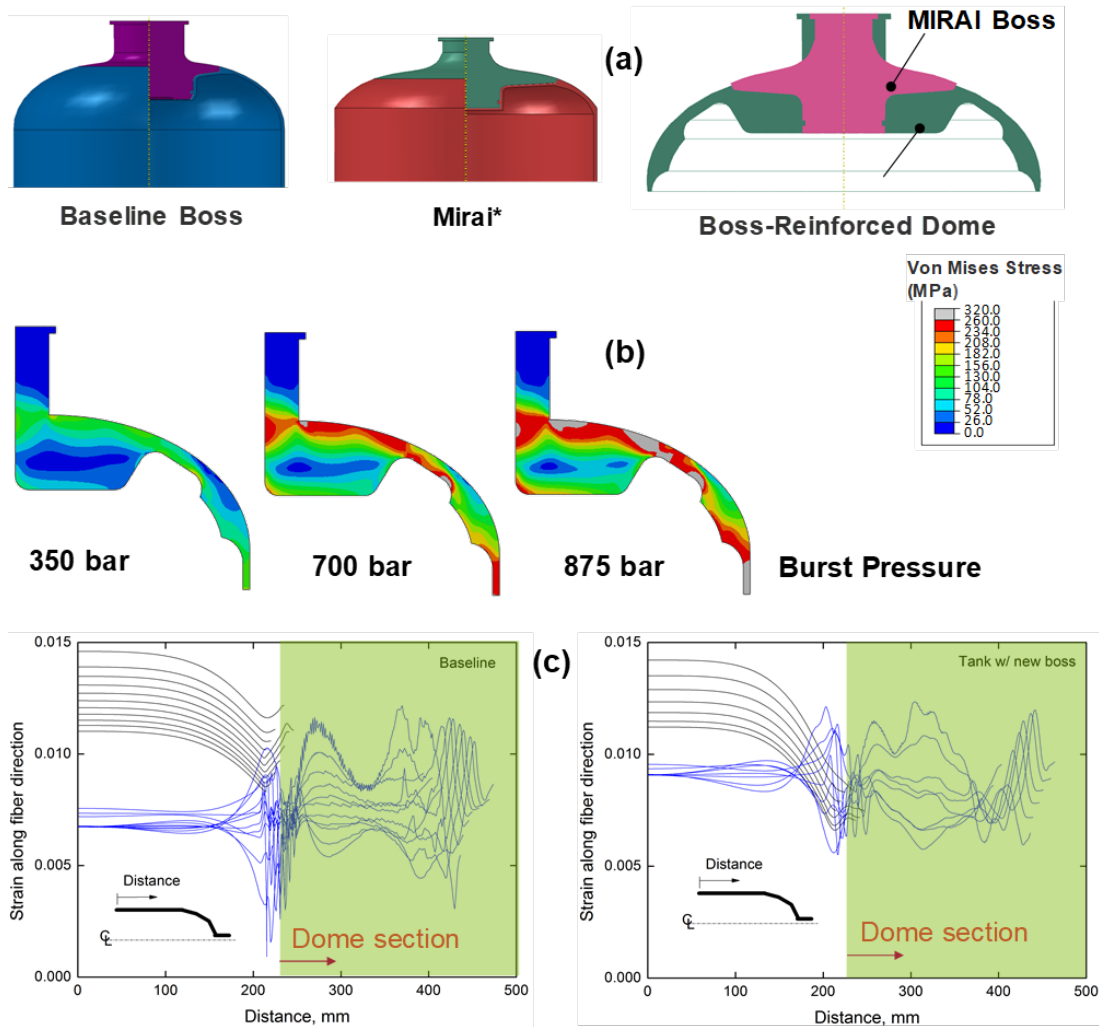


Figure 1 Boss-reinforced dome section for 700-bar Type IV tank: a) dome section; b) stress distribution in boss-reinforced dome; c) strain along fiber direction

Room-Temperature Hydrogen Storage in Sorbents

We conducted a reverse engineering analysis to determine the attributes required to meet the system targets with room-temperature sorbents in the onboard hydrogen system (Figure 2a). Table 2 lists the material attributes of interest and the system operating conditions. As in our earlier work [3], the key system requirements are 5.6 kg recoverable hydrogen and 5-bar minimum delivery pressure for the storage medium; 2.25 safety factor for the Type 4 containment vessel with 5-mm HDPE liner and 2,550-MPa strength Toray carbon fiber; and heat transfer system for 1.5 kg/min hydrogen refueling rate and 1.6 g/s hydrogen minimum full flow rate. We used a single Langmuir isotherm to represent hydrogen uptake in a sorbent.

$$N_{ex} = N_{ex}^{max} (1 - \rho_g v_a) \frac{KP}{1 + KP}$$

$$\ln(K) = \frac{\Delta S}{R} - \frac{\Delta H}{RT}$$

$$\Delta H = \Delta H^0 + \frac{R}{2} (T_0 - T)$$

$$\Delta S = \Delta S^0 + \frac{R}{2} \ln\left(\frac{T_0}{T}\right)$$

Table 2. List of Material Properties and Operating Conditions in Reverse Engineering Analysis

		Units	Target Value	Reference Value	Constraint / Variable	Comments
Sorbent	Excess Uptake at 308 K	g-H ₂ /kg	101.2	30-72	5.5 wt% gravimetric capacity	ST133
	Enthalpy of Adsorption (-ΔH°)	kJ/mol	13.2	5-20	Study variable	17-18.5 Catecholate-Ca ²⁺
	Adsorption Volume	m ³ /kg	0.012	TBD		MOF-5
	Entropy of Adsorption (-ΔS°)	J/mol/K	66.5	30-100		MOF-5, SLI
	Bulk Density of Compact	kg/m ³	513	310 - 610	40 g/L volumetric capacity	IJHE 37 (2012) 2723-2727
	Permeability	m ²	TBD	TBD		IJHE 38 (2013) 3268-3274
Operating	Off-board Coolant Temperature	K	298			T _c
Temperatures	Storage Temperature	K	308			T _c + 10°C
	Discharge Temperature	K	333			60°C on-board coolant T
Operating	Storage Pressure	bar	100	50 - 250	Study variable	
Pressures	Minimum Delivery Pressure	bar	5			DOE target
H₂ Flow Rates	Refueling Rate	kg/min	1.5			DOE target
	Minimum Full Flow Rate	g/s	1.6			DOE target
Heat Transfer	ENG/Sorbent Mass Ratio		0.05	0.05		Layered ENG & sorbent
	Bed Thermal Conductivity	W/m/K	6.3		Model value for layered ENG	IJHE 41 (2016) 4690-4702
	Number of HX Tubes		79		1.5 kg/min H ₂ refueling rate	

The main conclusion from the analysis is that reaching system targets of 5.5 wt% gravimetric capacity and 40 g/L volumetric capacity requires a sorbent with 101 g H₂/kg excess (112 g H₂/kg absolute) uptake at 100 bar and 35°C when layered with 5 wt% ENG and compacted to 513 kg/m³ bulk density. The required uptake is also a function of ΔH° and ΔS°. Figure 2b shows hydrogen uptake in a hypothetical material that has the required sorption capacity with -ΔH° = 13.2 kJ/mol and -ΔS° = 66.5 J/mol.K. For such a material, Figure 2c shows that the uptake requirement is slightly less stringent (smaller N_{ex}^{max}) at 150–175 bar storage pressure. Here, N_{ex}^{max} refers to peak excess uptake that occurs at a pressure (P_{max}), which is a function of ΔH° and temperature. For a given -ΔH°, N_{ex}^{max} is a measure of the required adsorption site density. Along with ΔH°, N_{ex}^{max} may be regarded as a material property. A material with higher N_{ex}^{max} is likely more difficult to discover meaning that it is preferable to select a storage pressure that requires the smallest N_{ex}^{max} .

Figure 2d indicates that 13.2 kJ/mol enthalpy of adsorption (-ΔH°) is about the optimum value for -ΔS° = 66.5 J/mol.K, 100–5 bar pressure swing, and 35°–60°C temperature swing. Figure 2e shows the general relationship between optimum -ΔH° and -ΔS° for specified operating pressures and temperatures.

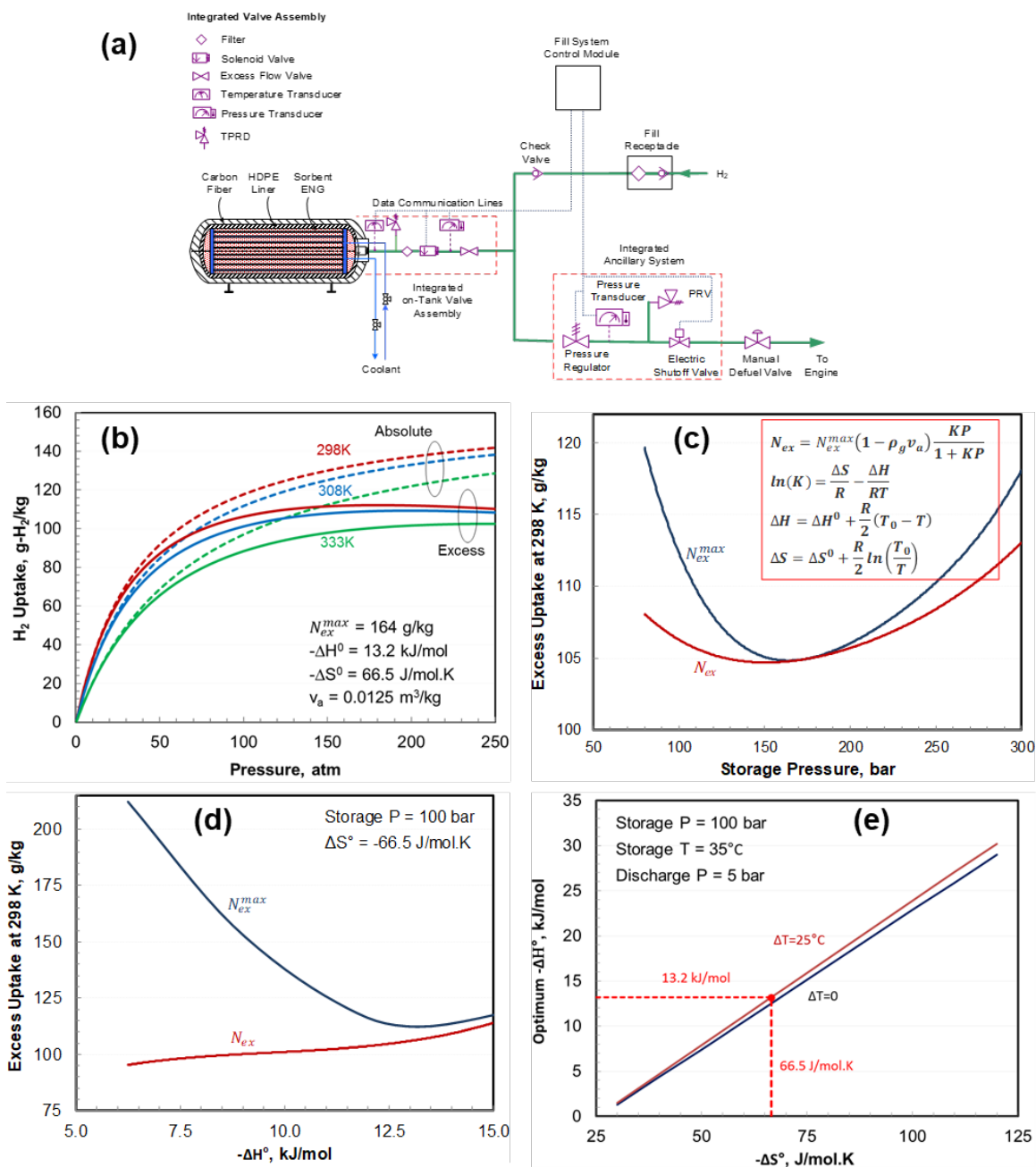


Figure 2. Hydrogen storage in room-temperature sorbents: a) schematic of the onboard storage system; b) hydrogen uptake in a hypothetical room-temperature sorbent with attributes necessary to meet the system targets; c) optimum storage pressure; d) optimum ΔH^0 for $-\Delta S^0 = 66.5$ J/mol.K; e) relationship between optimum ΔH^0 and ΔS^0

Table 3 summarizes the results for three materials with low, medium, and high ΔS^0 . It includes the optimum ΔH^0 , required uptake, refueling heat load, and CF composite for 100-bar storage pressure. The required uptakes are nearly double the maximum theoretical uptakes in metalated catachols calculated assuming four H_2 molecules absorbed per Ca^{2+} cation [4].

Table 3. Summary of Results for Low, Medium, and High ΔS° Sorbents

	Unit	Low ΔS°	Medium ΔS°	Medium ΔS°	High ΔS°
Entropy of Adsorption ($-\Delta S^\circ$)	J/mol.K	30	50	66.5	100
Enthapy of Adsorption ($-\Delta H^\circ$)	kJ/mol	1.5	7.9	13.2	23.9
Excess Uptake at 100 bar, 308 K	g-H ₂ /kg	93.6	97.2	101.2	114.1
H ₂ Stored in Sorbent	%	91.2	91.1	91.0	90.7
H ₂ Stored in Pores and Voids	%	8.8	8.9	9.0	9.3
Bulk Density of Sorbent-ENG Compact	kg/m ³	551	532	513	465
Refueling Heat Load	MJ/kg-H ₂	1.2	4.3	7.0	12.2
Carbon Fiber Composite	kg	7.6	7.6	7.6	7.6
Storage Temperature	K	308	308	308	308
Discharge Temperature	K	333	333	333	333
Storage Pressure	bar	100	100	100	100
Minimum Delivery Pressure	bar	5	5	5	5

Liquid Hydrogen Carriers

In support of H2@Scale activities, we initiated a new task to analyze liquid hydrogen carrier (LHC) pathways. As shown in Figure 3, the initial study includes three pathways that were selected to cover different classes of carriers. Liquid ammonia and liquid methyl cyclohexane (MCH)/toluene represent a class of carriers that require a steam methane reforming (SMR) plant for hydrogen production. Liquid methanol represents a class of carriers that do not require a hydrogen production step. Liquid methanol and ammonia are one-way carriers, while MCH/toluene is a two-way carrier. Liquid ammonia and MCH are easier to produce using renewable hydrogen than methanol that would also require a source for CO₂.

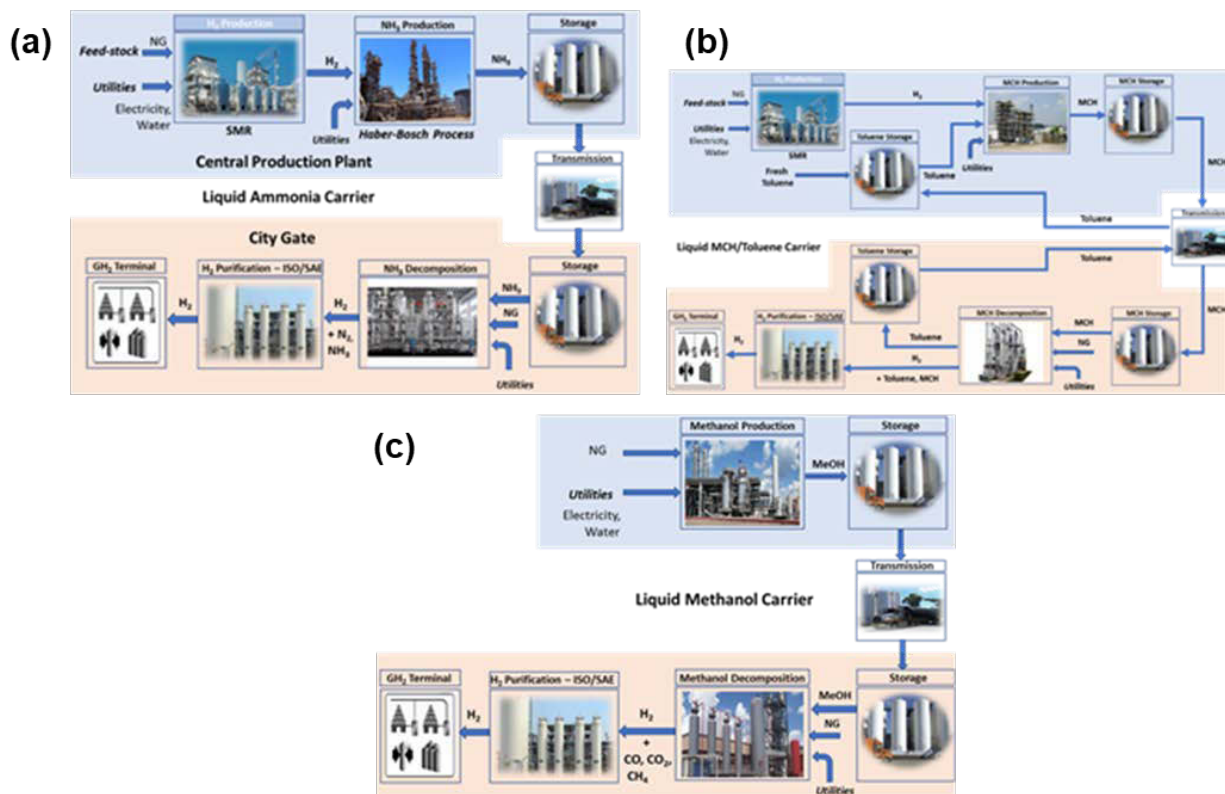


Figure 3. Hydrogen carrier pathways: a) liquid ammonia; b) liquid MCH/toluene; c) liquid methanol

Table 4 summarizes the physical properties of the carriers along with their hydrogen capacity and methods of production and decomposition. It also includes information on various modeling tools, financial assumptions, and performance parameters used to analyze the production, transmission, decomposition, and storage steps for the carrier pathways shown in Figure 3.

Table 4. Hydrogen Carrier Study: Tools and Parameters

Financial Assumptions	City H ₂ annual average daily use = 50,000 kg-H ₂ /day; Operating capacity factor = 90%; Internal rate of return (IRR) = 10%; Depreciation (MACRS)=15 yrs; Plant life=30 yrs; Construction period=3 yrs			
	NG	Electricity	Water	Toluene
Feedstock and Utilities	6.00 \$/MBtu	5.74 ¢/kWh	0.54 ¢/gal	0.768 \$/kg
H₂ Production by SMR, /kg-H₂	0.156 MBtu	0.569 kWh	3.35 gal	
Hydrogenation				
Ammonia	Haber-Bosch process and cryogenic air separation unit; 350 tpd;			
Methanol	Steam reforming of CH ₄ /CO ₂ to synthesis gas (H ₂ -CO)/(CO+CO ₂)=2.05; Conversion to methanol; methanol purification; 320 tpd;			
Toluene	99% conversion of toluene to MCH over non-PGM catalyst			
Dehydrogenation				
Ammonia	Catalytic decomposition of ammonia at high temperatures; H ₂ purification by PSA at 20 atm (85% recovery)			
Methanol	Catalytic steam reforming, H ₂ purification by PSA at 20 atm (85% recovery)			
MCH	90% conversion of MCH to toluene; 4.1% make-up toluene H ₂ purification by PSA at 20 atm (90% recovery)			
Transmission	HDSAM v 3.1, Truck Liquid Delivery			
	Ammonia	Methanol	MCH	GH₂
Payload (kg)	22,500	22,500	22,500	1,042
Volume (m³)	37	28	29	36
H₂ (kg)	3398	3465	1112	1042
GH₂ Terminal	HDSAM v 3.1, Compressed Gas H ₂ Terminal			

We obtained initial results for a scenario in which the LHC production plant is located 150 km from the city gate and the annual average daily use for the city is 50,000 kg H₂/day. The scenario may be applicable to a mid-size city like Sacramento, California, with limited market in an early transition stage. As a reference, we also analyzed a baseline gaseous hydrogen (GH₂) pathway with central SMR and truck transmission to gas terminal.

Figure 4a presents the levelized hydrogen cost at city gate broken down in terms of the costs for the various steps in the LHC pathway: hydrogen production, LHC production, LHC transmission, LHC decomposition, and hydrogen terminal. The hydrogen carrier options analyzed in this initial study incur incremental costs of 0.84–1.43 \$/kg H₂. To be competitive with the baseline GH₂ scenario, the combined cost of LHC production, decomposition and make-up, and hydrogen purification must be <0.77–1.10 \$/kg H₂. The LHC-related costs as analyzed are 2.52 \$/kg H₂ for ammonia, 1.95 \$/kg H₂ for methanol, and 2.15 \$/kg H₂ for MCH.

Figure 4b presents the breakdown of levelized hydrogen cost at city gate in terms of the costs for initial capital investment, operating and maintenance (O&M), fuel, and utilities. The following is a brief summary of the sources of the increases in levelized costs compared to the GH₂ scenario:

- Ammonia: 54% capital; comparable O&M and fuel; ~10% utilities
- Methanol: 54% capital; 41% O&M and fuel; small for utilities
- MCH: 43% capital; comparable O&M, fuel, and utilities

Figure 4c compares the energy efficiency of the different pathways. The endothermic dehydrogenation step including hydrogen purification by pressure swing adsorption (PSA) at city gate is the largest contributor to the 38%–50% increase in energy consumption for hydrogen carriers. The total energy consumption in Figure 4c includes fuel plus electrical energy, assuming 33% efficiency in generating electrical power.

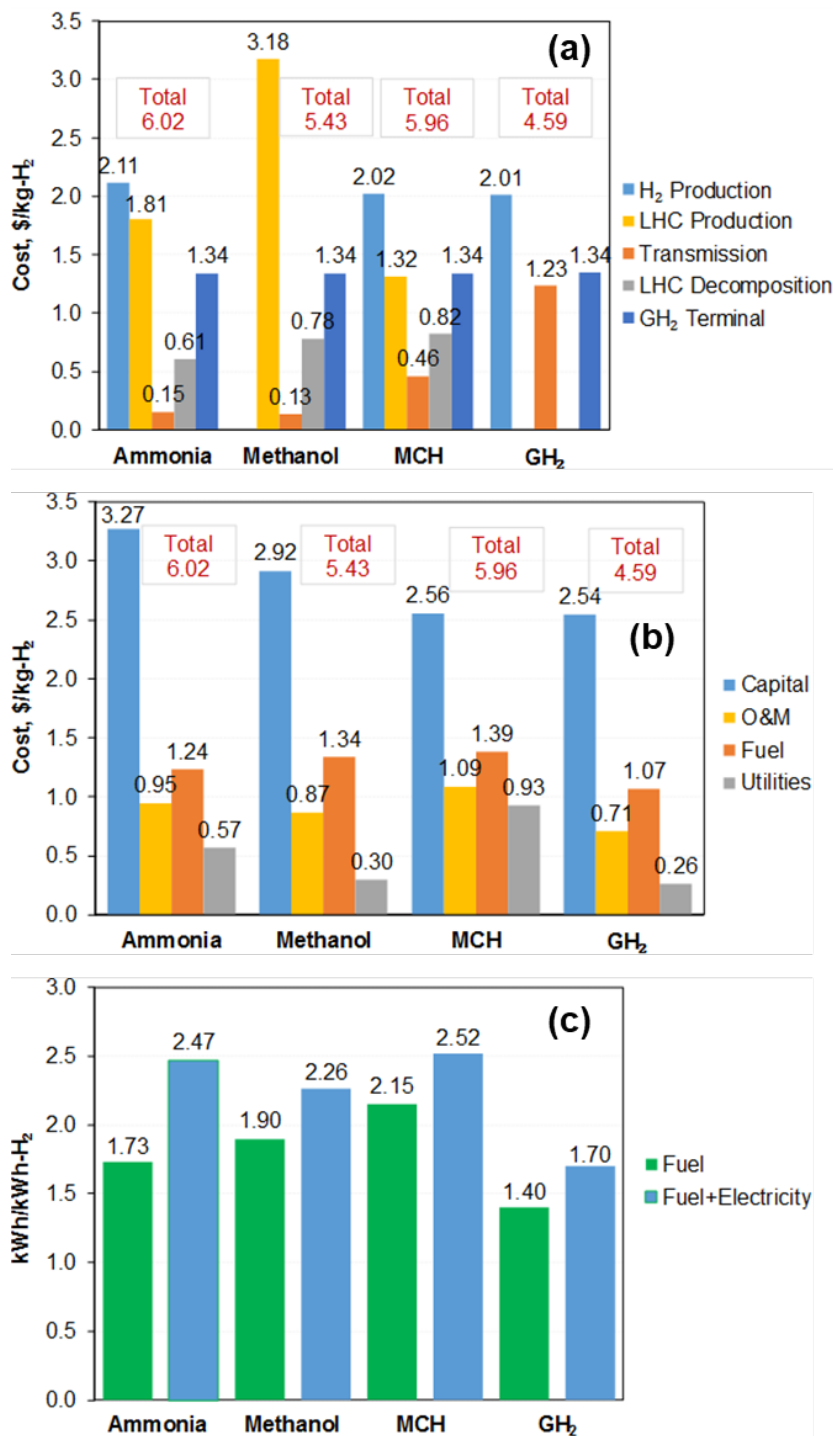


Figure 4. Analysis of hydrogen carrier pathways: a) levelized hydrogen cost at city gate (50,000 kg H₂/day); b) breakdown of levelized hydrogen cost at city gate; (c) energy efficiency

CONCLUSIONS AND UPCOMING ACTIVITIES

- Compared to Type 3 350-bar cH_2 tanks currently in use in fuel cell buses, 500-bar CcH_2 can achieve 215% increase in storage density, 90% improvement in gravimetric capacity, 170% higher volumetric capacity, and 47% saving in CF composite while satisfying the constraint of 7-d dormancy for 95% full tanks.
- A reverse-engineering analysis shows that meeting the system targets of 5.5 wt% gravimetric capacity and 40 g/L volumetric capacity requires room temperature sorbents with 106 ± 8 g H_2 /kg excess uptake at 100 bar when compacted to 500 ± 35 kg/m³ bulk density.
- Reinforcing the dome section with an elongated metal boss has the potential to realize >10% savings in CF composite for Type 4 tanks. Greater savings may be possible in tanks with a higher aspect ratio.
- We have determined the baseline cost of producing/hydrogenating one-way and two-way liquid hydrogen carriers (ammonia, methanol, and MCH/toluene), transmitting them to and dehydrogenating them at the city gate, and storing hydrogen. For the baseline scenario in which the LHC production plant is located 150 km from the city gate, 50,000 kg H_2 /day average daily use, and other assumptions listed in Table 4, the levelized cost at the city gate is 4.59–6.02 \$/kWh H_2 .
- In FY 2019, we will work with DOE, Lawrence Livermore National Laboratory, and Pacific Northwest National Laboratory to develop a material property database and tools for certification.
- In FY 2019, we will identify and analyze scenarios that favor hydrogen carriers.
- In FY 2019, we will analyze physical hydrogen storage systems for medium- and heavy-duty vehicles.

FY 2018 PUBLICATIONS/PRESENTATIONS

1. T.Q. Hua, H.S. Roh, and R.K. Ahluwalia, “Performance Assessment of 700-bar Compressed Hydrogen Storage for Light Duty Vehicles,” *International Journal of Hydrogen Energy* 42 (2017): 25121-25129.
2. R.K. Ahluwalia, J.K. Peng, H.S. Roh, T.Q. Hua, C. Houchins, and B.D. James, “Supercritical Cryo-compressed Hydrogen Storage for Fuel Cell Electric Buses,” *International Journal of Hydrogen Energy* 43 (2018): 10215-10231.
3. R.K. Ahluwalia, J.K. Peng, and T.Q. Hua, “Chemical Hydrogen Storage Material Requirements for Automotive Fuel Cell Systems,” In preparation for submission to *International Journal of Hydrogen Energy*, 2018.
4. R.K. Ahluwalia, J.K. Peng, and N. T. Stetson, “Characteristics of Low-Enthalpy Metal Hydrides for On-Board High-Pressure Hydrogen Storage Applications,” In preparation for submission to *International Journal of Hydrogen Energy*, 2018.
5. R.K. Ahluwalia, T.Q. Hua, J.K. Peng, and H.S. Roh, “System Level Analysis of Hydrogen Storage Options,” Hydrogen Storage Tech Team Meeting, Southfield, MI, January 18, 2018.

REFERENCES

1. R.K. Ahluwalia, J.K. Peng, H.S. Roh, T.Q. Hua, C. Houchins, and B.D. James, “Supercritical Cryo-compressed Hydrogen Storage for Fuel Cell Electric Buses,” *International Journal of Hydrogen Energy* 43 (2018): 10215-10231.
2. A. Yamashita, M. Kondo, S. Goto, and N. Ogami, “Development of High-Pressure Hydrogen Storage System for the Toyota Mirai,” SAE Technical Paper 2015-01-1169 (2015), doi:10.4271/2015-01-1169.
3. R.K. Ahluwalia, J-K Peng, and T. Q. Hua, “Sorbent Material Property Requirements for On-board Hydrogen Storage for Automotive Fuel Cell Systems,” *International Journal of Hydrogen Energy* 40 (2015): 6373-6390.

4. E. Tsvion, S.P. Veccham, and M. Head-Gordon, “High Temperature Hydrogen Storage of Multiple Molecules: Theoretical Insights from Metalated Catechols,” *ChemPhysChem* 18 (2017): 184-188.

Hydrogen Storage Cost Analysis

Brian D. James (Primary Contact),
Cassidy Houchins, Jennie Huya-Kouadio,
Daniel DeSantis
Strategic Analysis, Inc
4075 Wilson Blvd, Ste. 200
Arlington, VA 22203
Phone: (703)527-5410
Email: bjames@sainc.com

DOE Manager: Katie Randolph
Phone: (720) 356-1759
Email: Katie.Randolph@ee.doc.gov

Contract Number: DE-EE0007601

Subcontractors:

- Argonne National Laboratory, Lemont, IL
- Pacific Northwest National Laboratory, Richland, WA

Project Start Date: October 1, 2016

Project End Date: September 30, 2020

Overall Objectives

- Identify and/or update the configuration and performance of a variety of hydrogen storage systems for both vehicular and stationary applications.
- Conduct rigorous cost estimates of multiple hydrogen storage systems to reflect optimized components for the specific application and manufacturing processes at various rates of production.
- Explore cost parameter sensitivity to gain understanding of system cost drivers and pathways to lowering system cost.

Fiscal Year (FY) 2018 Objectives

- Examine hydrogen storage options for buses utilizing 350–700 bar cryo-compressed hydrogen (CcH₂) and 350 bar compressed hydrogen (cH₂).
- Examine the system cost of a hybrid metal hydride storage system.
- Explore the cost impacts of recent, novel ideas for improving the performance or reducing the

cost of hydrogen storage systems, such as replacing wet winding carbon fiber with advanced fiber placement of a carbon fiber tape.

Technical Barriers

This project addresses the following technical barriers from the Hydrogen Storage section of the Fuel Cell Technologies Office Multi-Year Research, Development, and Demonstration Plan¹:

(B) System Cost

(H) Balance of Plant (BOP) Components

(K) System Life-Cycle Assessments.

FY 2018 Accomplishments

- Completed analysis comparing thermoplastic carbon fiber tape with advanced fiber placement against wet fiber layup.
- Completed an analysis of several fuel cell electric bus hydrogen storage options: 350, 500, and 700 bar CcH₂ and 350 bar cH₂.
- Performed a cost tradeoff analysis between light-duty vehicle regulators and fuel cell system cost for different pressures delivered to the stack.
- Completed a first-step baseline system cost analysis of a hypothetical hybrid 350 bar metal hydride hydrogen storage system.

¹ <https://www.energy.gov/eere/fuelcells/downloads/fuel-cell-technologies-office-multi-year-research-development-and-22>

INTRODUCTION

The Fuel Cell Technologies Office (FCTO) has identified hydrogen storage as a key enabling technology for advancing hydrogen and fuel cell technologies and has established goals of developing and demonstrating viable hydrogen storage technologies for transportation and stationary applications. The cost assessment described in this report supports the overall FCTO goals by identifying the impact of components, performance levels, and manufacturing/assembly techniques on storage system cost at a variety of annual manufacturing rates. The results of this analysis enable DOE to compare the cost impact of new components, etc., to the overall 2018 and ultimate DOE cost targets. The cost breakdown of the system components and manufacturing steps can then be used to guide future R&D decisions.

APPROACH

A Design for Manufacture and Assembly (DFMA)-style cost analysis methodology was used to assess the materials and manufacturing cost of hydrogen storage systems and components. Key system design parameters and engineering system diagrams describing system functionality and postulated manufacturing process flows were obtained from a combination of industry partners, Argonne National Laboratory (ANL), Pacific Northwest National Laboratory (PNNL), and internal analysis. This data was used to develop a mechanical design of each component, including materials, dimensions, and physical construction. Based on this design, the manufacturing process train was modeled to project the cost to manufacture each part. Cost was based on the capital cost of the manufacturing equipment, operating cost of the machinery, equipment tooling amortization, material costs, and financial assumptions. Once the cost model was complete for the system design, sensitivity data for the modeled technology was obtained by varying key parameters. Results were shared with ANL, PNNL, and industry partners to obtain feedback and further refine the model.

RESULTS

Type 4 Compressed Natural Gas Analysis

In support of the Institute for Advanced Manufacturing Composites Innovation (IACMI), our 700 bar Type 4 hydrogen storage system model was adapted to provide a cost estimate for two commercially available compressed natural gas (CNG) pressure vessels. In consultation with DOE, two Hexagon TUFFSHELL tanks—a 64.4 L light-duty vehicle tank and a 537.5 L heavy-duty tank—were selected as model systems. Baseline results were discussed in the 2017 Annual Progress Report. The total composite mass for the CNG tanks was estimated from a derived performance factor for 700 bar tanks modeled by ANL and calibrated to Hexagon tanks that were burst tested at PNNL [1]. The modeled 2017 baseline tank mass (boss, liner, and composite) was within $\pm 5\%$ of a commercial comparison system, inspiring confidence that our model adequately represents realistic composite mass for mass-produced tanks.

In 2018, the model was modified to compare system costs using a novel thermoplastic tape applied using Advanced Fiber Placement (AFP), a process developed by DuPont and Steelhead Composites. In the modified manufacturing process, a tape of Panex-35 carbon fiber in a polyamide (PA-6) thermoplastic matrix is applied to the vessel by AFP. The thermoplastic tape is cured² in place, which eliminates the need for the two oven curing steps used in conventional wet-composite layup systems. The AFP capital cost was estimated from a buildup of component costs, and the composite tape price is estimated to have a similar cost per kilogram as T-700S/epoxy in the preliminary analysis. The estimated cost of the AFP system (\$1.5 million) is substantially higher than the ~\$350,000 for conventional wet composite layup. However, AFP eliminates the need for down-process curing ovens by curing in place. The fiber lay-down speed of AFP is assumed to be comparable to that of wet winding, although faster speeds may be possible with optimization according to discussions with some component suppliers. While spooled fibers and resin are used as inputs to the wet winding process, the AFP requires the fibers and thermoplastic matrix to be pre-processed together into a tape prior to use

² This process is commonly referred to as “cure in place” although technically it is not curing, as a thermoplastic matrix is used rather than a thermoset matrix.

(analogous to a pre-preg tape). The DuPont material is based on a Panex-35 (600 ksi) fiber in a polyamide (PA-6) matrix. Tape cost at high volume manufacture is estimated to be \$22.83/kg and is, coincidentally, very close to the \$23/kg estimate of the much higher strength T-700S (711 ksi) carbon fiber used in the baseline tank system. Interestingly, the relatively high price of the thermoplastic tape is not due to processing but rather to the 50% markup assumption suggested by vendor input. Should the tape become a commodity material with multiple comparable vendors, the markup is expected to go down. The higher AFP capital cost and the lower strength at comparable material cost Panex-35 led to an overall increase in the tank cost as shown in Figure 1.

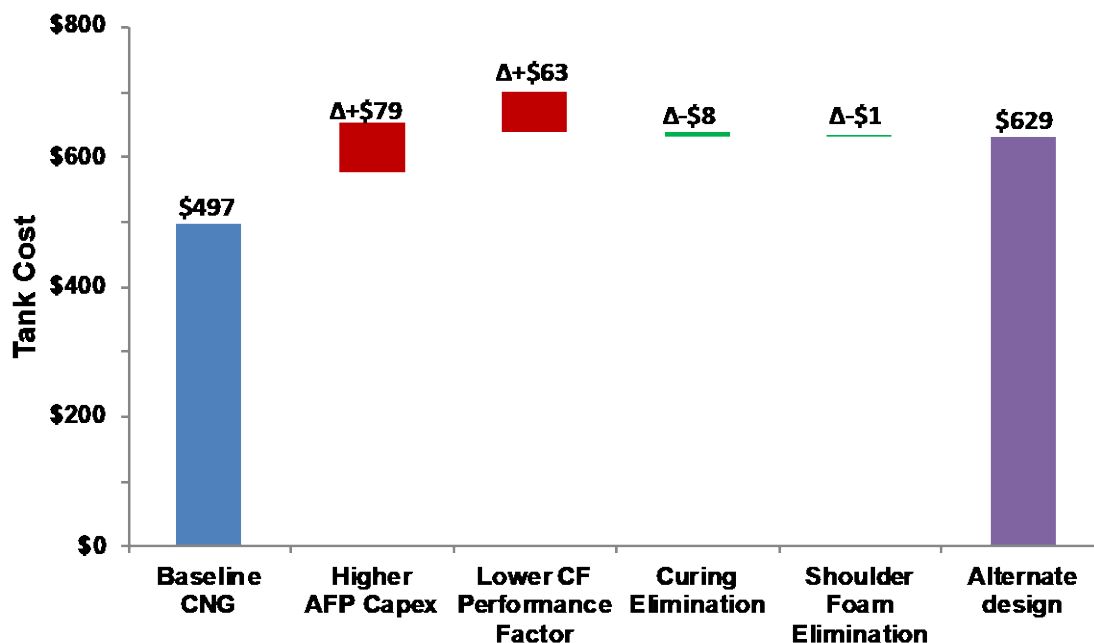


Figure 1. Waterfall chart comparing baseline wet fiber layup CNG tank cost with an alternate design using Panex-35/PA-6 thermoplastic tape applied by advanced fiber placement. Costs are for a 65 L tank and annual production of 500,000 tanks per year.

Fuel Cell Electric Bus Hydrogen Storage Options

Three different storage systems were analyzed this year for fuel cell electric bus applications: (1) 350–700 bar, <100 K CcH₂, (2) 500 bar 200 K cold compressed hydrogen (Cold-cH₂), and (3) 350 bar ambient temperature compressed hydrogen. Cryo-compressed systems are characterized by hydrogen storage in insulated Type 3 pressure vessels at cryogenic temperatures (typically 70–200 K) and elevated pressure (typically 100–500 bar). The benefits of CcH₂ storage include higher effective storage density of hydrogen (and reduced system size) without incurring the energy and cost of a full hydrogen liquefaction, and a long driving range after a full boil-off event. Hydrogen density at 700 bar and 288 K is the same as hydrogen at 500 bar and 200 K. However, the carbon fiber required for the lower-pressure cold compressed tank is approximately 71% of the carbon fiber required for the tank at 700 bar, and yet the gas temperature of the cold compressed tank is not so low to require a metal liner. For comparison, a conventional 350 bar Type 3 compressed gas storage system was analyzed. The cost results of the fuel cell electric bus analysis shown in Table 1 demonstrate that cryo-compressed storage has the potential to significantly reduce the storage cost for fuel cell electric bus applications compared to 350 bar compressed storage. The anticipated savings in carbon fiber from the higher-density cold-compressed system, however, is offset by the higher cost of insulation and the containment vessel, leading to a higher overall cost system compared to the baseline.

Table 1. System Cost Comparison

	350 bar CcH ₂	500 bar CcH ₂	700 bar CcH ₂	350 bar cH ₂	Cold-cH ₂
Liner	\$1.03	\$1.01	\$0.99	\$0.21	\$1.58
Composite	\$3.25	\$4.70	\$7.12	\$9.79	\$8.86
Insulation and Containment Vessel	\$3.48	\$3.21	\$2.92	\$0.00	\$3.05
BOP	\$3.84	\$3.85	\$3.85	\$3.25	\$3.45
Assembly and Other	\$0.04	\$0.04	\$0.04	\$0.12	\$0.04
System Cost (2007\$/kWh)	\$11.65 [-2.32, +2.90]	\$12.82 [-2.32, +2.90]	\$14.92 [-2.78, +3.61]	\$13.38 [-3.44, +5.73]	\$16.97 [-0.81, +1.59]

700 bar System Update

The baseline 700 bar Type 4 storage system design implicitly assumes a 15 bar pressure differential between the regulator inlet and outlet is required to deliver 5.6 kg hydrogen at flow (0.02 g/s/kW) for peak power fuel cell stack operations (80 kW). This assumption led to an effective empty tank pressure of 20 bar in the 2015 baseline system [1] to deliver 5 bar to the fuel cell system at full flow. However, higher fuel cell system delivery pressure allows lower-cost hydrogen recirculation components, which leads to an overall lower system cost. Cost tradeoffs comparing the combined storage system composite cost plus the fuel cell system recirculation cost are shown in Figure 2. The bottom green curve shows how composite cost scales with the storage vessel minimum empty pressure, and the two top curves sum the composite and recirculation costs (blower vs. pulsed-ejector with bypass), which determines the lowest minimum empty tank pressure. A recirculation system with a blower can function with only 5 bar to the fuel cell system and thus requires at least a 15 bar minimum tank pressure (assuming a pressure regulator drop of 10 bar). Alternately, the pulsed-ejector with bypass system requires 10 bar pressure to the fuel cell system and thus requires a minimum empty pressure of 20 bar. While the pulsed-ejector system results in a higher storage system cost of \$18 (\$0.10/kWh), the vehicle cost is actually \$322 less per system.

An alternate pathway to lower minimum empty tank pressure was recently suggested by ANL [2]: switching from a single-stage regulator to a two-stage regulator to reduce regulator pressure drop while maintaining peak flow rates. Analysis of one- and two-stage regulators suggests two-stage regulators can be as much as 50% higher cost; this added cost may not be justified merely to maintain full flow at near-empty tank conditions [3] when the gas density is low as it represents only a few percent of the total full fill mass. In 2019, balance of plant components will be updated with a goal of further consolidation and cost reduction.

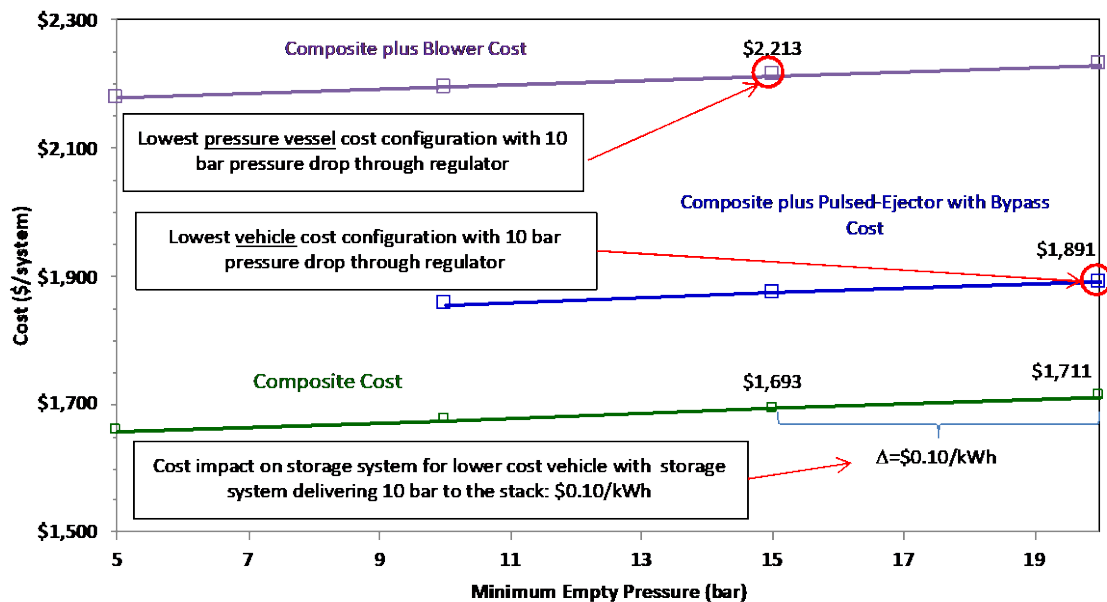


Figure 2. Cost tradeoffs between storage system minimum empty pressure and fuel cell system hydrogen recirculation cost

Metal Hydride Reverse Engineering

Strategic Analysis completed a baseline 350 bar Type 4 hybrid metal hydride storage system cost analysis based on a system proposed by ANL [4]. The system modeled is based on ANL's proposed storage system using onboard fuel cell stack coolant to heat the metal hydride bed and offboard station coolant to cool the bed during refueling. The projected system cost is \$13/kWh at 500,000 systems per year as summarized in Table 2. While the system enables a significant reduction of composite weight compared with the 700 bar compressed gas system, the additional materials and internal heat exchanger present significant cost and technical challenges. Additionally, the feasibility of a high density polyethylene (HDPE) liner for this system is questionable. The next step for this analysis is to investigate which further material and system constraints are needed to achieve the DOE cost and performance targets and to evaluate a Type 3 tank. We anticipate that the total tank volume and pressure need to be reduced to achieve the cost targets.

Table 2. Hybrid 350 bar Type 4 Metal Hydride Storage System Cost Breakdown. System Costs are Reported in 2007\$.

	Est. @500,000/yr	Notes
Type 4 pressure vessel (boss, liner, composite)	\$6/kWh	51 kg carbon fiber composite Aluminum bosses HDPE liner (blow mold only; cost for friction welding not included)
Fill receptacle	\$0.30/kWh	Based on high volume quote for 350 bar compressed gas receptacle. Cost for offboard heat transfer fluid not yet included.
Integrated regulator block	\$1.75/kWh	Analysis complete
In-tank valve	\$0.89/kWh	Analysis complete
In-tank HX	>\$1/kWh	Based on high volume tube quotes with a single bend, but does not yet include assembly or the coolant manifolds
MH/EG	\$2.70/kWh	ANL assumes 5.6% MH hydrogen capacity and 45.9 kg MH with 4.6 kg EG. Goal of this analysis is to set cost-driven targets on this parameter. Current cost assumption is \$10/kg for the MH/EG.
Other BOP	To be determined	Additional costs for storage-side coolant pump, valve, and plumbing
Total	~\$13/kWh	Compared to DOE 2020 target of \$10/kWh (\$8/kWh ultimate)

HX – heat exchanger

MH – metal hydride

EG – expanded graphite

CONCLUSIONS AND UPCOMING ACTIVITIES

- Completed analysis comparing thermoplastic carbon fiber tape with advanced fiber placement against wet fiber layup.
- Completed an analysis of several fuel cell electric bus storage options: 350, 500, and 700 bar CcH₂ and 350 bar cH₂.
- Performed a cost tradeoff analysis between light-duty vehicle regulators and fuel cell system cost for different fuel cell system delivery pressures.
- Completed a first-step baseline system cost analysis of a hypothetical hybrid 350 bar metal hydride system.

Type 4 CNG Analysis

- Completed an analysis of thermoplastic tape applied by advanced fiber placement. These results show that the higher capital cost of advanced fiber placement and the lower tensile strength of the Panex-35 based thermoplastic tape lead to a higher storage system cost. Reductions in the carbon fiber mass and capital equipment cost are needed for this technology to be cost competitive with wet fiber layup.
- This analysis task was completed at the end of FY 2018.

Fuel Cell Electric Bus Hydrogen Storage Options

- We evaluated several storage options for fuel cell electric buses, including four cryogenic systems and a conventional compressed gas system. Results of the analysis suggest that 350 bar cryo-compressed

storage leads to a 13% cost reduction compared with conventional 350 bar ambient temperature compressed gas storage.

700 bar Hydrogen Storage System Update

- A holistic analysis of 700 bar regulators, the minimum tank pressure, and fuel cell system hydrogen recirculation suggests that higher regulator output pressures, while disadvantageous for storage system cost, leads to a combined storage plus fuel cell system cost reduction.

Metal Hydride Reverse Engineering

- Baseline cost analysis of a 350 bar Type 4 hybrid metal hydride storage system based on material and system properties proposed by ANL led to a system cost of \$13/kWh. Further analysis is planned to identify a set of material and system assumptions needed to meet the DOE cost targets of \$8/kWh.

Future work by Strategic Analysis includes the following:

- Reevaluate BOP components to identify additional opportunities for consolidation and cost reductions for 700 bar Type 4 storage.
- Perform cost analysis for medium- and heavy-duty vehicle hydrogen storage requirements.
- Continue reverse engineering analysis of metal hydride and sorbent storage systems to identify a set of material and system parameters needed to meet DOE targets.

FY 2018 PUBLICATIONS/PRESENTATIONS

1. C. Houchins, B.D. James, D. DeSantis, and J. Huya-Kouadio, “Cost Trade-Offs in H₂ Storage Design Space: Cryogenic, Cold, and Ambient 40 kg H₂ On-Board Cost Analysis for Fuel Cell Electric Buses (FCEB),” presented at the Fuel Cell Seminar, Long Beach, CA, November 9, 2017.
2. R.K. Ahluwalia, J.K. Peng, H.S. Roh, T.Q. Hua, C. Houchins, and B.D. James, “Supercritical Cryo-compressed Hydrogen Storage for Fuel Cell Electric Buses,” submitted to the *International Journal of Hydrogen Energy*.
3. B.D. James and C. Houchins, “Milestone #5 Report: System Configuration and Bill of Materials,” submitted to DOE, March 30, 2018.
4. B.D. James and C. Houchins, “Hydrogen Storage Cost Analysis,” presented to the Hydrogen Storage Tech Team, January 18, 2018.

REFERENCES

1. G. Ordaz, C. Houchins, and T. Hua, “Onboard Type IV Compressed Hydrogen Storage Systems-Cost and Performance Status 2015,” DOE Hydrogen and Fuel Cells Program Record #15013, U.S. Department of Energy (2015). https://www.hydrogen.energy.gov/pdfs/15013_onboard_storage_performance_cost.pdf.
2. T.Q. Hua, H.-S. Roh, and R.K. Ahluwalia, “Performance Assessment of 700-Bar Compressed Hydrogen Storage for Light Duty Fuel Cell Vehicles,” *International Journal of Hydrogen Energy* 42, no. 40 (2017): 25121–25129. <https://doi.org/10.1016/j.ijhydene.2017.08.123>.
3. B.D. James and C. Houchins, “Hydrogen Storage Cost Analysis,” presented at the 2018 DOE Hydrogen and Fuel Cells Program Annual Merit Review and Peer Evaluation Meeting, Washington, DC, June 14, 2018.
4. R.K. Ahluwalia, J.-K. Peng, and T.Q. Hua, “Bounding Material Properties for Automotive Storage of Hydrogen in Metal Hydrides for Low-Temperature Fuel Cells.” *International Journal of Hydrogen Energy* 39, no. 27 (2014): 14874–14886. <https://doi.org/10.1016/j.ijhydene.2014.07.052>.

Hydrogen Storage System Modeling: Public Access, Maintenance, and Enhancements

Matthew Thornton (Primary Contact),¹
David Tamburello,² Kriston Brooks,³ Sam Sprik¹

¹National Renewable Energy Laboratory (NREL)

15013 Denver West Parkway

Golden, CO 80401

Phone: (303) 275-4273

Email: Matthew.Thornton@nrel.gov

²Savannah River National Laboratory (SRNL)

Savannah River Site, Bldg 999-2W

Aiken, SC 29808

Phone (803) 507-4449

Email: david.tamburello@srnl.doe.gov

³Pacific Northwest National Laboratory (PNNL)

P.O. Box 999

Richland, WA 99352

Phone (509) 372-4343

Email: kriston.brooks@pnnl.gov

DOE Managers:

Ned Stetson

Phone: (202) 586-9995

Email: Ned.Stetson@ee.doe.gov

Jesse Adams

Phone: (720) 356-1421

Email: Jesse.Adams@ee.doe.gov

Project Start Date: October 1, 2015

Project End Date: Project continuation and direction determined annually by DOE

Overall Objectives

- Coordinate the public access of select models developed under the Hydrogen Storage Engineering Center of Excellence (HSECoE) activity, including web posting of documentation and tracking downloads and web activity.
- Maintain performance of existing storage system models and update and validate as new experimental data becomes available.
- Enhance and expand existing models to improve simulation speed and application to other uses. This will focus on expanding the parameterization of the models and their flexibility in evaluating new material

candidates. This will initially include the development of preprocessor sizing routines for the adsorbent and chemical hydrogen systems followed by the metal hydride and cryo-compressed systems.

Fiscal Year (FY) 2018 Objectives

- Work with HSECoE partners to continue to update and improve models developed by the center. Make these models available and accessible to the broader research and academic community through a controlled web-based access portal and track downloads and website activity.
- Create stand-alone executable versions of the HSECoE-developed material storage models to provide first-order storage system estimates based on material property information.
- Update the hydrogen storage equations with additional, alternative theoretical storage system formulations to allow users to choose the most appropriate theory for their material.
- Develop tools to size/design storage systems based on available volume or desired hydrogen storage mass.

Technical Barriers

This project addresses the following technical barriers from the Hydrogen Storage section of the Fuel Cell Technologies Office Multi-Year Research, Development, and Demonstration Plan¹:

- System Weight and Volume
- System Cost
- Efficiency
- Charging/Discharging Rates
- Dispensing Technology
- Systems Life-Cycle Assessments.

¹ <https://www.energy.gov/eere/fuelcells/downloads/fuel-cell-technologies-office-multi-year-research-development-and-22>

Technical Targets

This project is conducting simulation and modeling studies of advanced onboard materials-based hydrogen storage technologies. Insights gleaned from these studies are being applied toward the hydrogen storage vessel design and materials synthesis that meet the following DOE 2020 hydrogen storage targets for light-duty vehicles:

- Storage system cost: \$333/kg H₂ Stored
- System gravimetric capacity: 0.045 kg H₂/kg system
- System volumetric capacity: 0.030 kg H₂/L system
- Charging/discharging rates: 3–5 min
- Well to power plant efficiency: 60%.

FY 2018 Accomplishments

- Developed a metal hydride (MH) design tool that predicts system mass and volume based on thermodynamic and kinetic properties and developed it into an executable file; uploaded the model to the hsecoe.org website.
- Used the metal hydride design tool to predict the system mass for a recently developed metal hydride and compare it to sodium alanate.
- Developed a volume-based chemical hydrogen storage design tool that predicts the mass of hydrogen available based on the volume of the hydrogen storage system.
- Used the chemical hydrogen storage design tool to predict the system mass for an ammonia borane/boric acid mixture and compare it to ammonia borane alone.
- Developed an adsorbent design tool based on the UNILAN adsorption theory to give users the option of using either Dubinin-Astakov (D-A) or UNILAN as the basis for their hydrogen storage system formulation.
- Developed a volume-based adsorbent hydrogen storage design tool that predicts the mass of hydrogen available based on the total system storage volume available.

- Updated the adsorbent system design tools to include room temperature, cold, and cryogenic temperature system design capabilities.
- Tracked and monitored web activity and downloads.
- Developed and sent out a survey to users who had downloaded models from the website to find out how the models are being used and gather suggestions.

INTRODUCTION

Overcoming challenges associated with onboard hydrogen storage is critical to the widespread adoption of hydrogen-fueled vehicles. The overarching challenge is identifying a means to store enough hydrogen onboard to enable a driving range greater than 300 miles within vehicle-related packaging, cost, safety, and performance constraints. As new hydrogen storage materials are discovered and created, material developers must predict their full-scale vehicle performance and compare their performance with pure hydrogen storage (700 bar, cryo-compressed, and liquid hydrogen storage). The goal of this work is to provide material developers with the modeling tools necessary to make these predictions based on the work done by the HSECoE.

APPROACH

The approach for FY 2018 is to complete updates, validate, enhance, troubleshoot, de-bug, and document these models developed by the HSECoE so that they can be made accessible to and useful for other researchers within the hydrogen storage community. During subsequent years, these models will be updated with alternative storage system formulations, such as different isotherm models for adsorbents and alternative chemical reaction kinetic expressions for chemical hydrogen storage (CH) materials. In addition, stand-alone system design tools that do not require special software will be developed to serve as scoping tools for the new hydrogen storage materials that may be developed.

RESULTS

The following provides results from work completed this year by the multi-lab team with a focus on implementing volume-based storage system design tools while updating their counterparts that were based on a required mass of hydrogen. The team maintained public access of select HSECoE models, documented activities in several publications, and exercised the tools with other material data sets. The team also monitored and tracked web activity and model downloads. To date there have been 225 downloads of the tank volume/cost model, 158 downloads of the framework model, 101 downloads of the MH finite element model, 65 downloads of the MH acceptability envelope, 26 downloads of the CH system design standalone, and 24 downloads of the adsorbent system design standalone.

Metal Hydride Design Tool

As with the previously developed adsorbent and CH system design tools, the newly developed MH design tool uses the thermodynamic and transport properties of a MH to estimate the storage system mass and volume. Like the previous models, the input data for the MH comes from an Excel spreadsheet and the model results are returned to another spreadsheet. This will help materials researchers understand how their materials compare to the DOE technical targets.

The first step of this process is to calculate the equilibrium pressure of the hydride based on the van't Hoff equation:

$$P_{H_2} = \exp[(\Delta H - T\Delta S)/RT]$$

If the equilibrium pressure is greater than the required 5 bar at the temperature of the fuel cell waste heat (approximately 85°C), the additional complexity of a hydrogen burner to release the hydrogen is not required. If the burner is needed, it is added to the balance of plant and the hydrogen needed to overcome the reaction enthalpy will be added to the assumed usable hydrogen. The model then estimates the cooling tube spacing during refueling based on the HSECoE's Metal Hydride Acceptability Envelope. After calculating the mass of MH needed to supply the hydrogen, the total volume and mass of the material interior to the tank can be estimated. The model then uses a MATLAB version of the tank volume/cost model (or Tankinator model) to design the tank that would be used to enclose the MH. These calculations, along with the balance of plant components, are then used to estimate the overall system mass and volume that can be compared to the DOE technical targets.

The MH stand-alone design tool was evaluated by comparing the predicted system mass of a nano-confined lithium nitride storage material that has been developed by Dr. Vitalie Stavila at Sandia National Laboratories with the more conventional MH sodium borohydride. The model was also used to determine what material parameters should be modified to improve nano- Li_3N system-level gravimetric capacity, with the analysis results shown in Table 1. The initial nano- Li_3N properties predicted a much larger system mass than NaAlH_4 despite having a higher hydrogen capacity and similar thermal conductivity and density. The model also demonstrated that small changes in entropy result in higher temperatures needed to drive off the hydrogen, thus requiring a thicker and heavier aluminum tank. As a result, the overall system mass and volume are higher despite the lower hydride mass. By increasing the entropy from -104 to -109.7 kJ/mol/K while leaving all other inputs the same, the model predicts that the system mass of both materials will be the same. Dr. Stavila also developed a KH-doped nano- Li_3N with a higher capacity, thermal conductivity, entropy, and enthalpy. The system mass predicted by this new material was nearly identical to the baseline NaAlH_4 . These results were shared with Dr. Stavila to provide direction to his material development. This modeling effort demonstrates the utility of the stand-alone metal hydride model in providing a quick screening process for developing metal hydrides.

Volume-Based CH Storage Stand-Alone Design Tool

The stand-alone CH storage system design tool was originally developed to estimate the total system volume and mass based on the desired usable hydrogen. Rather than building a vehicle around the hydrogen storage system, many designers have a limited volume and need to know the resulting capacity and range. Thus, the stand-alone CH storage design tool was modified to provide this capability, for both mass-based and volume-based design. The design parameters can then be used in the framework and a total range estimated for a particular system volume. This design tool was used in conjunction with the CH model in the framework to estimate the vehicle range as a function of storage system volume for both ammonia borane and alane, as shown in Figure 1.

CH Modeling with Newly Available Data

Purdue University had demonstrated that 20 wt% boric acid added to ammonia borane is a promising additive to decrease onset temperature as well as enhance the hydrogen release kinetics for thermolysis of ammonia borane. Working with researcher Hyan Tae Hwang, the data from this study performed in 2013 were evaluated with the CH models. The AB/BA hydrogen generation data, measured in a batch reactor up to 85°C at a rise of 1°C/minute, were simulated using Avrami kinetics with an overall reaction enthalpy based on boric acid dehydrating to metaboric acid combined with the decomposition of ammonia borane to produce hydrogen. The ammonia borane/boric acid mixture was assumed to be slurried with mineral oil as a 50/50 mixture to produce a flowable fluid that could be used in the exothermic AB model. Using the previously developed design tool coupled with the framework model, the system components and the total system mass and volume were estimated and then the framework was run using the US06 drive cycle.

The model predicted improved reaction kinetics resulting in a very small reactor required to achieve full conversion. However, it also demonstrated that the material has a lower hydrogen capacity once it is mixed with mineral oil to create a slurry. As a result, the larger volume of CH required produces a larger system mass and volume than with ammonia borane alone despite the faster kinetics and smaller reactor.

Table 1. Comparison of System Mass and Volume for nano-Li₃N to NaAlH₄

Inputs	NaAlH ₄	nano-Li ₃ N system			KH doped nano-Li ₃ N
Hydride Carrying capacity	0.056	0.062	0.086	0.062	0.065
Thermal Conductivity of Hydride Bed (with ENG)	9	8.9	8.9	8.9	10.3
Density of Hydride Bed (bulk)	720	675	675	675	720
Enthalpy per mole H ₂	-42000	-43100	-43100	-43100	-43900
Entropy	-124	-104	-104	-109.7	-115
Outputs					
System mass (kg)	331	432	331	330	339
System volume (m ³)	0.38	0.42	0.32	0.29	0.35
Total Hydride Mass (kg)	125	113	82	113	108
Percentage of DOE 2020 Gravimetric Target (%)	38	29	38	38	37
Percentage of DOE 2020 Volumetric Target (%)	49	45	59	64	53
Notes		baseline case	H ₂ capacity predicting same system mass as NaAlH ₄	entropy predicting same system mass as NaAlH ₄	KH doped nano-Li ₃ N predicting same system mass as NaAlH ₄

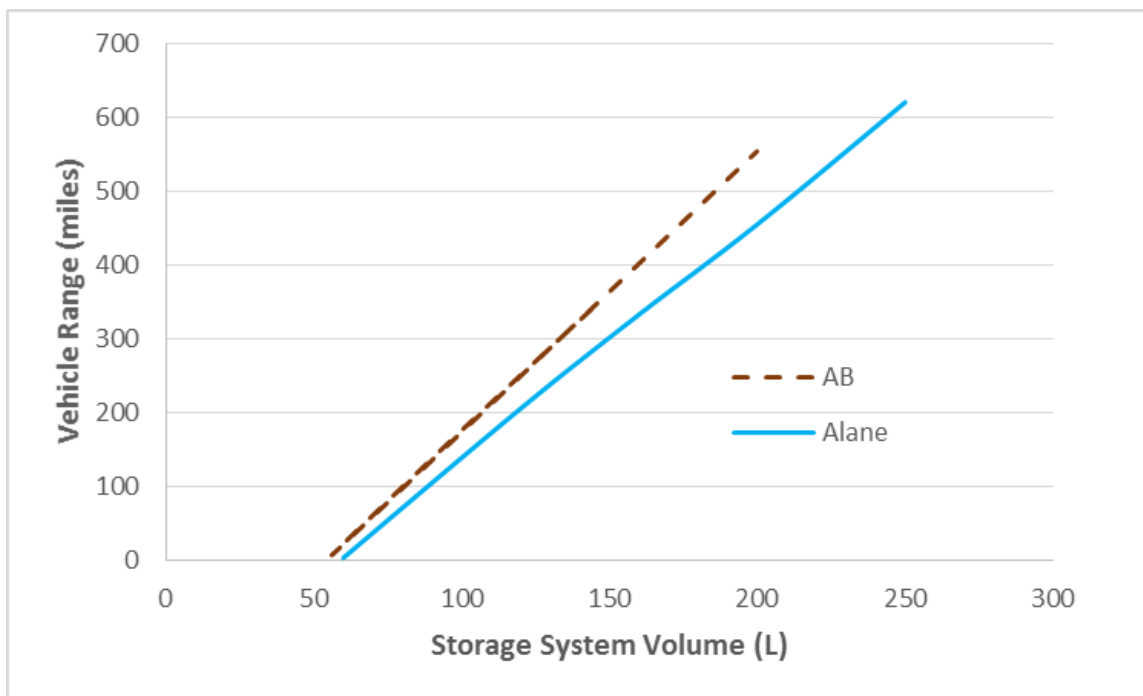


Figure 1. Vehicle range achievable for varying storage system volumes—AB and alane

Stand-Alone Adsorbent Design Tool with UNILAN Adsorption Theory

The existing stand-alone adsorption hydrogen storage system design tool is based on the D-A adsorption theory. However, not all adsorbents can be modeled well using D-A. For this reason, the stand-alone adsorption system design tool was augmented to use the UNILAN adsorption theory as an alternative basis, which describes the excess adsorption based on the following equation:

$$n_{ex} = \frac{n_{max}RT}{E_{max} - E_{min}} \ln \left[\frac{\exp(-\Delta S_0/R) + \frac{P}{P_0} \exp(E_{max}/RT)}{\exp(-\Delta S_0/R) + \frac{P}{P_0} \exp(E_{min}/RT)} \right] - cV_a$$

where: E_{max} and E_{min} = the maximum and minimum values of $-\Delta H_0$ ($|\Delta H_0|$ is the isosteric heat) [J/mol]. $-\Delta H_0$ is uniformly distributed between E_{min} and E_{max} .

P_0 = Standard pressure [10^5 Pa] = 1 bar

R = Gas constant [8.314 J/mol-K]

ΔS_0 = Entropy change relative to a standard pressure of P_0 [J/mol-K]

$\approx -8R$ for hydrogen

$\approx -9.5R$ for methane

n_{max} = Maximum coverage [mol_gas/kg_ads]

T = Temperature [K]

MOF-5 hydrogen adsorption data was used to compare the two formulations, which showed agreement within 2% of the experimental data and within 0.1% of each other.

Additional Stand-Alone Adsorbent Design Tool Updates

Several updates have been completed for the existing stand-alone adsorption hydrogen storage system design tool. One such addition is to offer volume-based storage system design. Specifically, the original adsorbent design tool used the usable hydrogen storage as the basis for designing the entire hydrogen storage system. Similar to the CH model described above, this updated version uses the maximum total volume available for the hydrogen storage system as the basis for design. Starting with the maximum total storage volume available and the operating conditions, the storage system is designed inward by accounting for the balance of plant, pressure vessel, internal heat exchanger, and the remaining volume available for the adsorbent. The results from this design method are the total hydrogen capacity and range based on the initial volume constraint.

The final adsorption storage system design tool update is the balance of plant, which has now been augmented to account for room temperature (25°C), cold gas (200 K), and cryogenic temperature (77 K) operation. While many components perform the same tasks, their mass, volume, and cost are very different when designed to operate at different temperatures. Also, cryogenic operations require much more heat transfer capabilities and more stringent insulation requirements than the room temperature operations do. By comparison, cold gas operations are a mixture of the two extreme cases and, as such, can take advantage of some of the benefits of each. The stand-alone adsorption hydrogen storage system design tool now has all three operation condition choices for each of the adsorption theory formulations (D-A and UNILAN) and each of the design bases (target hydrogen mass or maximum total available volume).

User Survey

The team was tasked with obtaining a better understanding of who is using the models developed by the HSECoE, how they can be improved, and who may be willing to collaborate with us to provide experimental data. To this end, we reviewed and finalized a SurveyMonkey questionnaire and in December sent it to the user list obtained from those downloading models from the hsecoc.org website. The user list contained 229

unique emails; 11 of those emails were not functional. We received 24 responses (about 10%), with 5 answering yes to being open to work with us to evaluate the performance of their material. Figure 2 is an example result showing that most are using the models in an academic setting followed by industrial use.

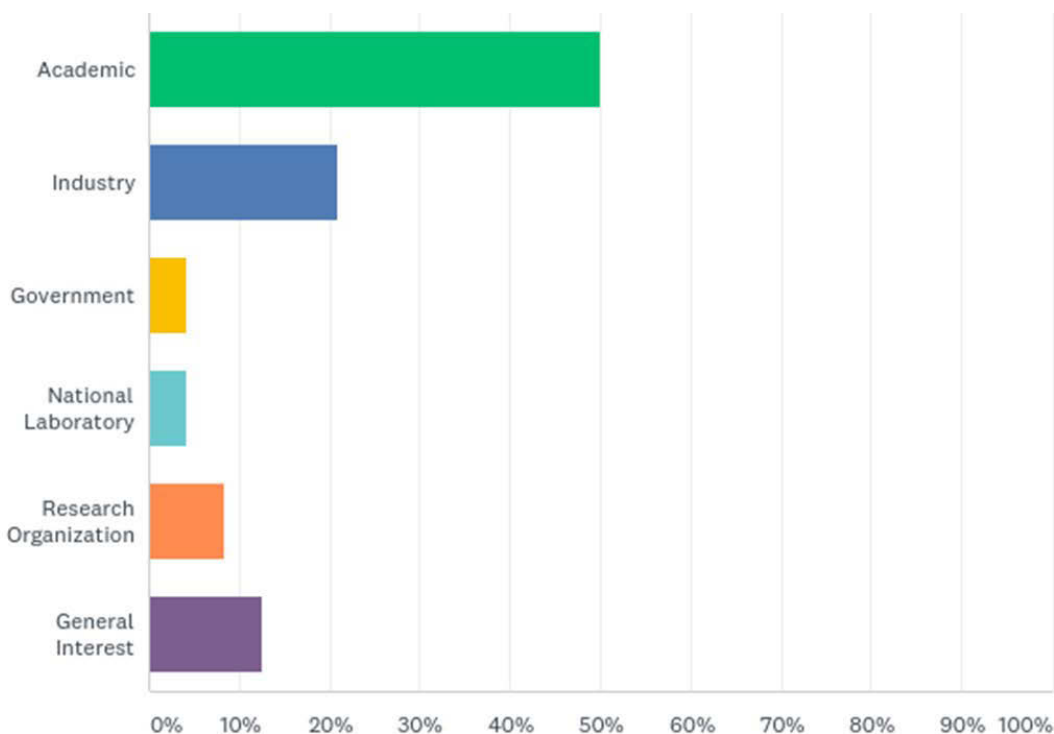


Figure 2. Survey results showing institutional setting for those using the models

The models currently developed and maintained by the team are listed in Table 2. These are either available on the website already or are in the process of being added for public download.

Table 2. HSECoE Models Available on Web Portal and Model Posting Status

Model Name	Lead	Status
MH Acceptability Envelope	SRNL	Complete
MH Finite Element Model	SRNL	Complete
Tank Volume/Cost Model	PNNL	Complete
MH Framework Model	SRNL	Complete
CH Framework Model	PNNL	Complete
Adsorption Data (AD) Framework Model	SRNL	Complete
AD Finite Element Model	SRNL	Model Complete ^a
Adsorption Data Fitting Routine	SRNL	Model Complete ^a
AD Stand-Alone System Design Tool	SRNL	Complete
CH Stand-Alone System Design Tool	PNNL	Complete

^a Awaiting user’s manual completion before the model is released to the public.

The models are made available publicly through the HSECoE web page, where website activity and model downloads are tracked. Figure 3 shows the latest website activity over the three-month period from July through September of 2018. The site received 139 visitors during this time, 85% of which were new visitors. Visitor sessions lasted an average of 4 minutes and 18 seconds and averaged 4.5 pages per visit. Figures 4 and 5 provide the user flows for the site and user origin cities, respectively.

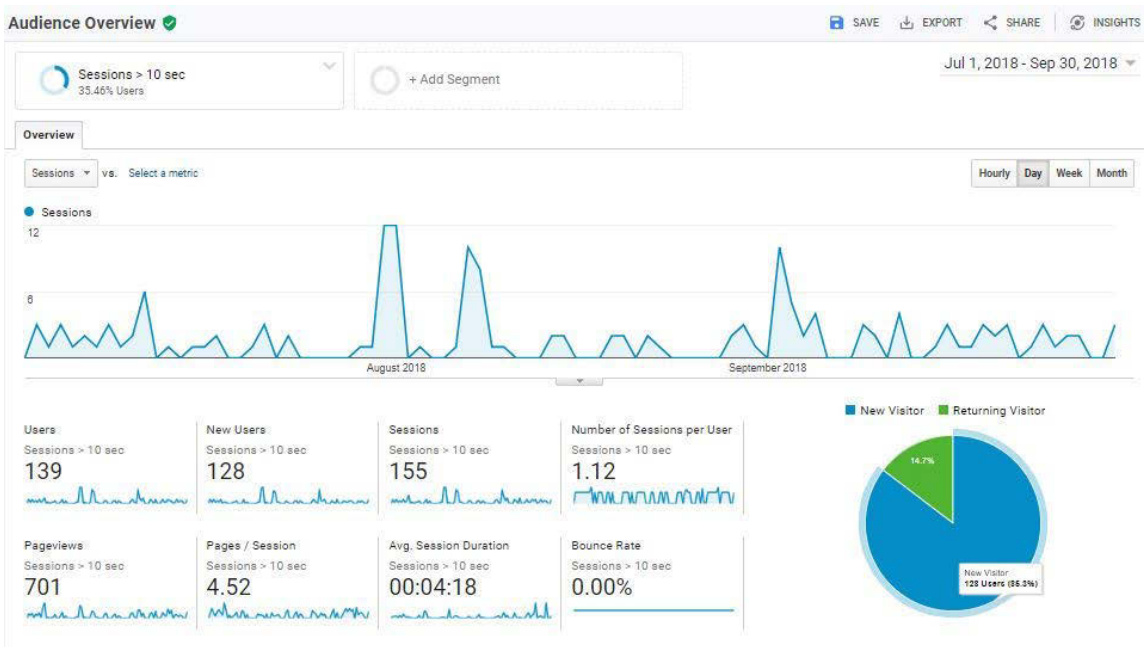


Figure 3. HSECoE web analytics: three-month site activity metrics

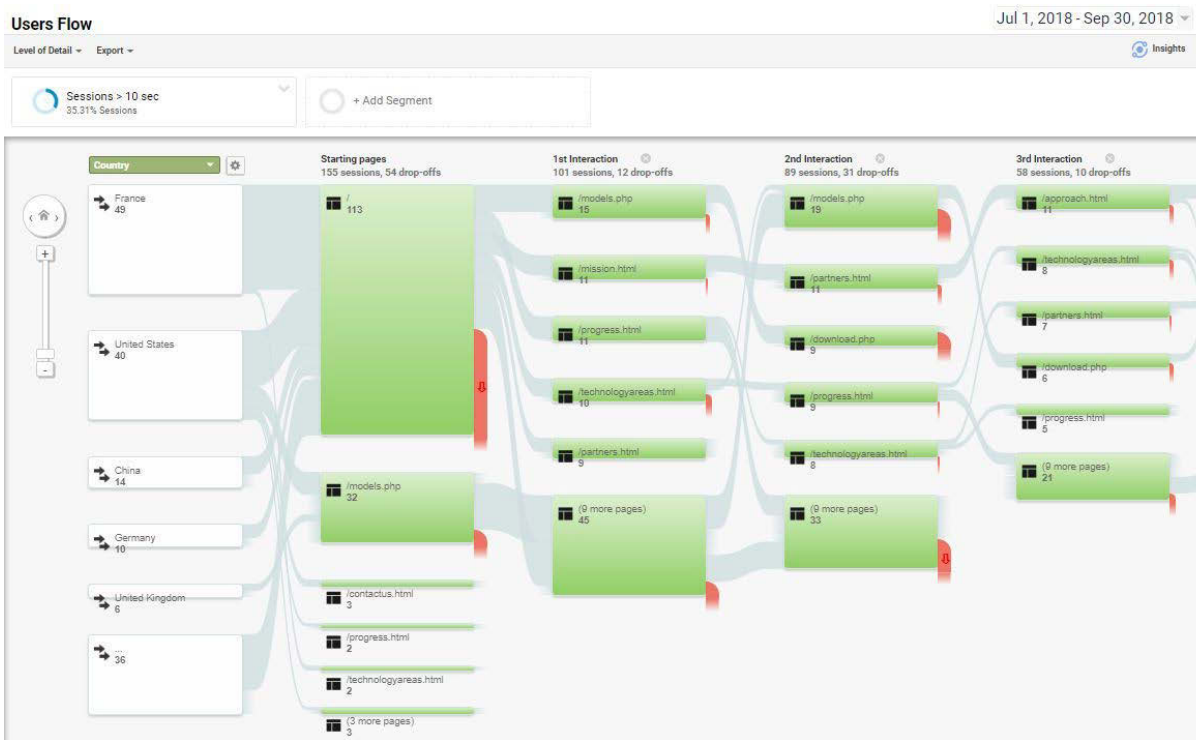


Figure 4. HSECoE web analytics: user flows

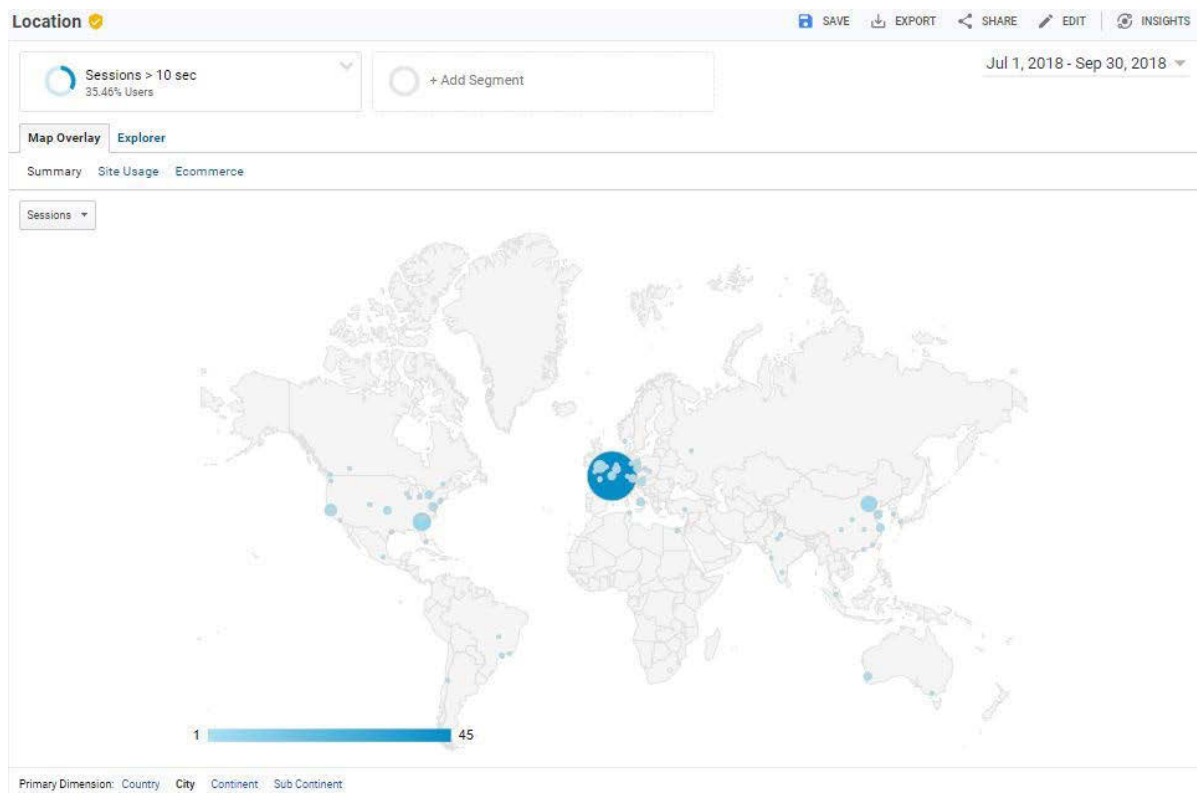


Figure 5. HSECoE web analytics: user origin countries

CONCLUSIONS AND UPCOMING ACTIVITIES

- Work with HSECoE partners to continue to update and improve models developed by the center; make these models available and accessible to the broader research and academic community through a controlled web-based access portal; and track downloads and website activity.
- Create stand-alone executable versions of the HSECoE-developed material storage models to provide first-order storage system estimates based on material property information.
- Update the hydrogen storage equations with additional, alternative theoretical storage system formulations to allow users to choose the most appropriate theory for their material.

SPECIAL RECOGNITIONS AND AWARDS/PATENTS ISSUED

1. David A. Tamburello, Matthew R. Kesterson, and Bruce J. Hardy. “Heat Transfer Unit and Method for Prefabricated Vessel.” US patent 9,809,380 B2 (November 7, 2017).

FY 2018 PUBLICATIONS/PRESENTATIONS

1. D. Tamburello, M. Thornton, S. Sprik, and K. Brooks, “Hydrogen Storage System Modeling: Public Access, Maintenance, and Enhancements,” U.S. Department of Energy Hydrogen and Fuel Cells Program Annual Merit Review and Peer Evaluation Meeting, June 15, 2018.
2. D. Tamburello, M. Thornton, S. Sprik, and K. Brooks, “Hydrogen Storage System Modeling Support: HSECoE System Modeling Update,” Hydrogen Storage Technical Team Review, January 18, 2018.
3. Bruce Hardy, David Tamburello, and Claudio Corgnale, “Hydrogen Storage Adsorbent Systems Acceptability Envelope,” International Journal of Hydrogen Energy 43, no. 42 (October 18, 2018): 19528–39, <https://doi.org/10.1016/j.ijhydene.2018.08.140>.

4. David Tamburello, Bruce Hardy, Martin Sulic, Matthew Kesterson, Claudio Corgnale, and Donald Anton, “Compact Cryo-Adsorbent Hydrogen Storage Systems for Fuel Cell Vehicles,” Proceedings of the ASME 2018 Power Conference, Paper no. 51395 (2018): V001T06A025, <https://doi.org/10.1115/POWER2018-7474>.
5. Kriston P. Brooks, Samuel J. Sprik, David A. Tamburello, and Matthew J. Thornton, “Design Tool for Estimating Chemical Hydrogen Storage System Characteristics for Light-Duty Fuel Cell Vehicles.” *International Journal of Hydrogen Energy* 43 (2018): 8846–8858, <https://doi.org/10.1016/j.ijhydene.2018.03.090>.

Investigation of Solid-State Hydrides for Autonomous Fuel Cell Vehicles

Patrick A. Ward (Primary Contact), Ragaiy Zidan, Scott McWhorter, David Tamburello
Savannah River National Laboratory
301 Gateway Dr.
Aiken, SC 29803
Phone: (803) 646-6358
Email: Patrick.Ward@srnl.doe.gov

DOE Manager: Ned Stetson
Phone: (202) 586-9995
Email: Ned.Stetson@ee.doe.gov

Project Start Date: October 1, 2016
Project End Date: Project continuation and direction determined annually by DOE

Overall Objectives

- Develop a methodology that incorporates engineering modeling and analysis tools to screen and down-select storage materials and material systems against cost and performance targets (initially developed and applied by Savannah River National Laboratory [SRNL] to light-duty vehicles in the Hydrogen Storage Engineering Center of Excellence [HSECoE]).
- Apply this methodology to an initial system design for an unmanned underwater vehicle (UUV) application for the Navy to reduce design time and lead to a more cost-effective and better-performing final product.
- Maintain hydrogen storage system capabilities and expertise at DOE and SRNL to support a variety of hydrogen and energy initiatives.
- Extend the long-term partnership between DOE and the Department of Defense in hydrogen and renewable energy systems.

Fiscal Year (FY) 2018 Objectives

- Obtain kinetic data describing the hydrogen release from α -alane produced by the newly developed SRNL method.
- Design, construct, and evaluate a prototype alane storage system incorporating enhanced

thermal transport strategies and simulated heat transfer fluid capabilities.

- Demonstrate a hydrogen storage heat exchanger system capable of heating the alane storage system to operational temperatures within 10 minutes.
- Provide experimental confirmation that available heat transfer fluid will be sufficient for complete hydrogen removal from the storage bed.
- Evaluate and mitigate any material contraction issues that may occur during hydrogen desorption and reduce thermal contact with heat exchanger surfaces.

Technical Barriers

This project addresses the following technical barriers from the Hydrogen Storage section of the Fuel Cell Technologies Office Multi-Year Research, Development, and Demonstration Plan¹:

- System Weight and Volume
- System Cost
- Efficiency
- Durability
- Charging/Discharging Rates
- Materials of Construction
- Balance-of-Plant (BOP) Components
- Thermal Management.

Technical Targets

SRNL has worked with the Navy to develop hydrogen storage targets for Navy UUV requirements, based initially on the DOE hydrogen storage targets for light-duty vehicles [1]. The proposed hydrogen storage and performance targets for Navy UUV systems include both near-term and longer-term requirements. The main difference between near- and long-term UUV targets are higher hydrogen storage densities and

¹ <https://www.energy.gov/eere/fuelcells/downloads/fuel-cell-technologies-office-multi-year-research-development-and-22>

capacities and higher associated fuel cell average and peak power requirements. While many of the proposed Navy UUV targets are similar to DOE hydrogen storage targets, some areas where they differ substantially are in initial material cost and material durability because most Department of Defense applications can withstand higher costs and shorter operating lifetimes than consumer passenger vehicles.

FY 2018 Accomplishments

- Designed, constructed, and evaluated a demonstration alane storage system at a scale of 232 g alane produced by the SRNL process intensified method.
- Acquired kinetic data on newly developed alane from the SRNL process.
- Developed enhanced thermal transport strategies for the alane hydrogen storage system.
- Evaluated contraction possibilities in the alane storage bed and determined that no significant contraction was observed.
- Exceeded UUV system startup time target of 10 minutes in shell and tube configuration alane storage bed demonstration vessel.
- Demonstrated that volumetric targets could be met for storage of alane to achieve 2x operational time versus lithium ion batteries.

INTRODUCTION

This project builds upon the core capabilities of DOE and SRNL and leverages their collective experiences to support new roles in other hydrogen applications, which includes the rapidly growing fuel cell areas for portable power and material handling equipment. Current battery technology is not able to meet the growing gravimetric and volumetric energy density demand for small portable power applications. One solution that is actively being evaluated is to use fuel cells. Fuel cells offer efficient and high-quality power but require safe, efficient, and cost-effective hydrogen storage systems to make them practical. An attractive means for storing hydrogen is to use solid-state materials that have demonstrated the ability to increase the volumetric density of hydrogen. The volumetric hydrogen density of alane (~140 g/L assuming crystal density) is more than twice that of liquid hydrogen (71 g/L) and more than three times that of compressed gas at 700 bar (40 g/L) [2]. Several materials exist that appear to be suitable for hydrogen storage for Department of Defense UUV applications, which have less stringent targets for material costs and reversibility. However, the viability of storage systems based on these materials for UUV operating conditions has never been demonstrated.

APPROACH

The overall approach of this research is to develop a methodology that incorporates engineering modeling and analyses to efficiently screen, design, and select storage materials and material systems against cost and performance targets leading to an initial system design for a UUV application. This methodology, which was initially developed by SRNL and applied to light-duty vehicles in the HSECoE, requires updates and modifications for it to be useful for other hydrogen and fuel cell applications. More specifically in this research, this methodology will be applied to UUVs to reduce design time and lead to a more cost-effective and better-performing final product. The modeling analysis applied to this project integrates various hydrogen storage system options with other system components, including fuel cell and balance of plant models, to evaluate and compare the overall performance of the onboard hydrogen storage system.

RESULTS

Previous research activities performed engineering screening analyses on a variety of metal hydrides and chemical hydrogen storage candidate materials using a modified version of the acceptability envelope tool developed for light-duty vehicles in the HSECoE [3]. Aluminum hydride (alane) was selected as the ideal candidate due to desirable volumetric and gravimetric hydrogen storage capacity and suitable desorption temperatures. Following the material selection, a demonstration reactor was developed to evaluate the release kinetics and operational feasibility of the material. For these experiments, alane from ATK, produced under different and more costly conditions, was utilized. Decomposition kinetics data was collected for ATK alane and a kinetics expression was derived to provide experimental input for system models. Recently SRNL has developed a process intensified method to produce large batch quantities of pure α -alane. This method has gained significant interest and is believed to be the lowest-cost method of alane production demonstrated on a reasonable scale (>200 grams). While the only differences between ATK alane and SRNL alane lie in the particle shape, size, and passivation layer, these differences affect the kinetics of hydrogen desorption and the long-term stability of the material. The effect of α -alane particle size is clearly illustrated by the difference in onset desorption temperatures observed by thermal gravimetric analysis. In order to appropriately evaluate the use of SRNL alane in the UUV system, desorption isotherms were carried out (Figure 1) to provide a kinetics expression for this material.

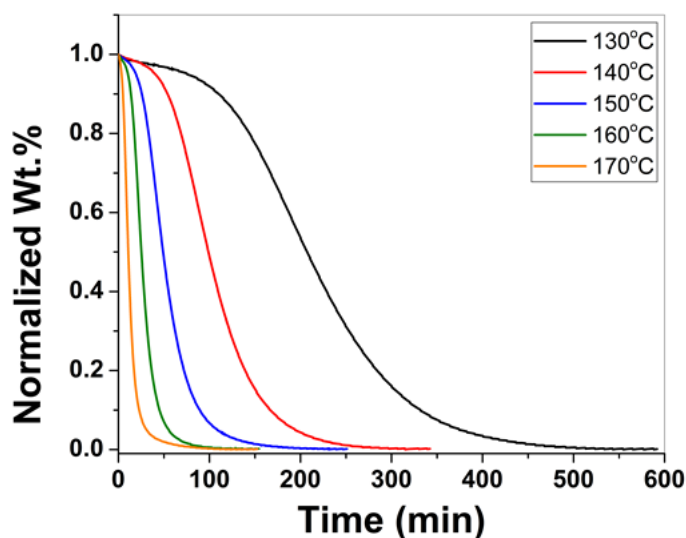


Figure 1. Isothermal desorption curves of α -alane produced by the SRNL method

To simplify the operation and design of the alane storage bed and heat exchanger design, a simple tube and shell design was selected to demonstrate the feasibility of utilizing alane in a UUV. To ensure adequate heat transfer rates within the storage bed, various methods of enhancing thermal transport were explored. It was found that the addition of expanded natural graphite (ENG) not only enhanced the thermal conductivity of the material, as shown in Figure 2, but also assisted in the compression of alane to achieve a higher packing density. Additionally, aluminum foil was used during alane pellet compression to enhance thermal conductivity and structural stability of the pellets. Another critical factor to consider in a metal hydride storage bed is the expansion or contraction of the material during hydrogen uptake and release. Because the equilibrium pressure of alane is far too great for the material to be considered reversible, only the contraction of the material needs to be considered for this application. Material contraction would hinder thermal transport by reducing material contact with the heat exchanger walls. The desorption of various alane pellets demonstrated no measurable change in the dimensions of the pellet after desorption. Although aluminum (decomposition product of alane) is denser than aluminum hydride, the particles tend to retain their initial shape after desorption and are composed of agglomerates of nanoparticles of aluminum as shown in Figure 3.

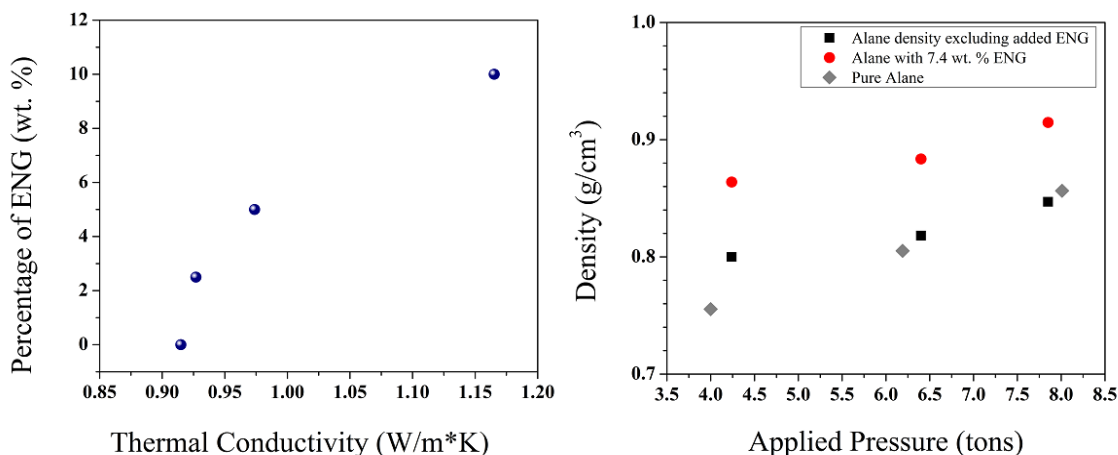


Figure 2. Thermal conductivity of SRNL alane with the addition of ENG at different weight % loadings (left) and density of alane at different applied pressures (right)

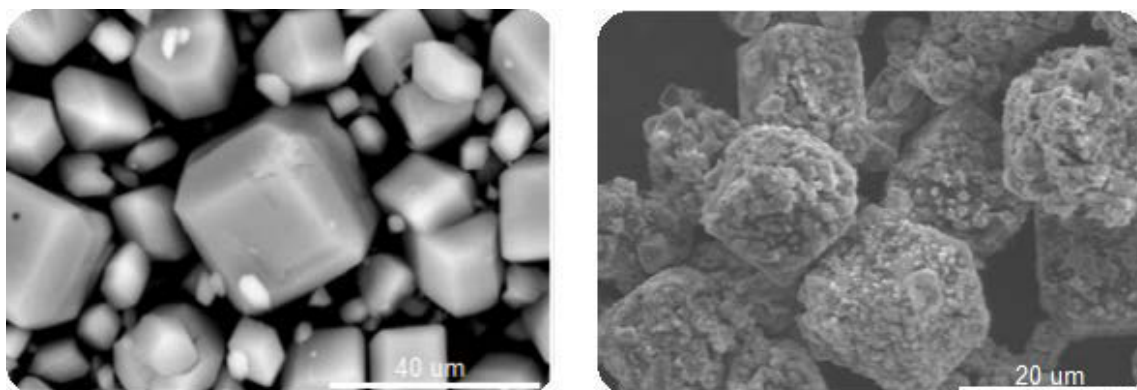


Figure 3. Scanning electron microscopy image of alane before and after desorption

To more accurately demonstrate the feasibility of the alane in the UUV system, a demonstration vessel was constructed that mimics the heat transfer fluid availability, wall thicknesses, and material volume to heat transfer fluid volume ratios that would be found in the UUV system. The demonstration vessel experiments were carried out with 232 g of SRNL alane and demonstrated that the target time of 10 minutes to preheat the storage vessel and alane to the target operational temperatures could easily be exceeded, as shown in Figure 4. These experiments also verified that the amount of heat available to desorb hydrogen from alane was sufficient (although insulation would play a significant role in extended operation). It was also demonstrated that enough alane could be stored in the given volume to extend the operational time of the UUV by a factor of 2, but modifications in the heat exchanger design would be necessary to reduce the system weight to maintain neutral buoyancy and provide adequate pressure ratings for the storage vessel.

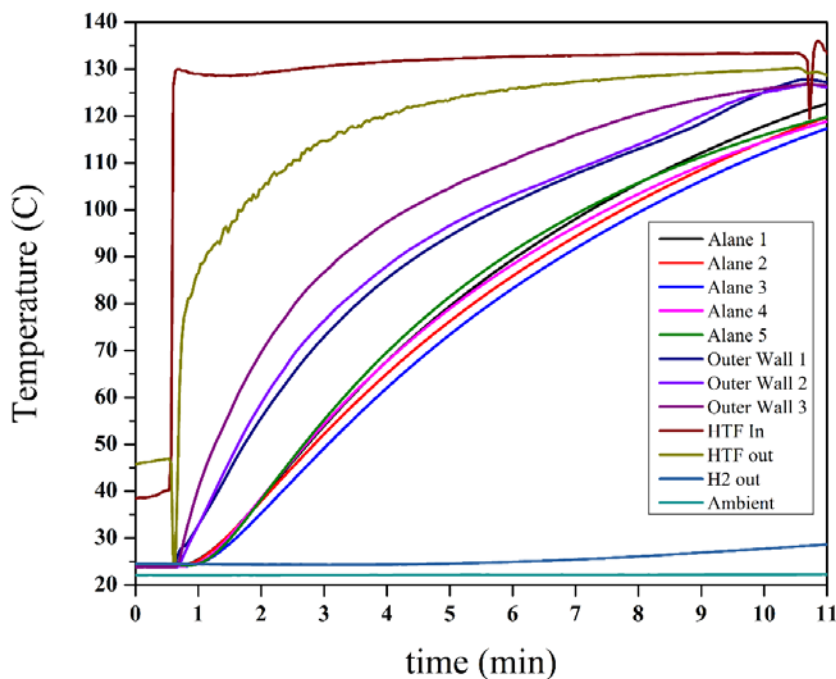


Figure 4. Temperature profile for alane demonstration vessel during initial heating to simulate on-ship preheating

CONCLUSIONS AND UPCOMING ACTIVITIES

While significant progress on the development of a hydrogen storage system for extended operation of UUVs has been accomplished, the cost and commercial availability of alane still prohibits its near-term use in this application. Due to the relatively low hydrogen release temperature of alane and its exceptional volumetric and gravimetric hydrogen capacity, aluminum hydride is still the favorable material for extending the operational time in portable power applications. Full-scale modeling of the hydrogen storage system using experimental data acquired for the alane produced by a process intensified method developed by SRNL is needed to give a higher confidence in overall system performance and provide information for optimizing operational conditions. Additionally, optimization of the heat exchanger design and construction materials needs to be evaluated to achieve system weight targets. Future work will focus on system modeling using experimental data acquired previously and the development of reduced-cost methods to produce alane at an industrial scale.

SPECIAL RECOGNITIONS AND AWARDS/PATENTS ISSUED

1. R. Zidan and P. Ward. “Mechanochemical Solid/Liquid Reaction in Formation of Alane.” Patent Application Number 15/482,913 (issued November 27, 2018).

FY 2018 PUBLICATIONS/PRESENTATIONS

1. P. Ward et al., “Investigation of Solid State Hydrides for Autonomous Fuel Cell Vehicles,” Presentation at the DOE Hydrogen and Fuel Cells Program Annual Merit Review and Peer Evaluation Meeting, Washington, D.C., June 13–15, 2018.

REFERENCES

1. U.S. Department of Energy Targets for Onboard Hydrogen Storage Systems for Light-Duty Vehicles, <https://www.energy.gov/eere/fuelcells/doe-technical-targets-onboard-hydrogen-storage-light-duty-vehicles>.
2. L. Klebanoff and J. Keller, “5-Year Review of Metal Hydride Center of Excellence,” *Int. J. Hydrogen Energy* 38 (2013) 4533–4576. In *Proceedings of the 2010 U.S. DOE Hydrogen Program Annual Merit Review*, Washington, DC, 7–11 June 2010, https://www.hydrogen.energy.gov/pdfs/review10/st029_klebanoff_2010_o_web.pdf.
3. C. Corgnale, B.J. Hardy, D.A. Tamburello, S.L. Garrison, and D.L. Anton, “Acceptability Envelope for Metal Hydride-Based Hydrogen Storage Systems,” *Int. J. Hydrogen Energy* 37 (2012): 2812e24, <http://dx.doi.org/10.1016/j.ijhydene.2011.07.037>.

Design and Synthesis of Materials with High Capacities for Hydrogen Physisorption

Brent Fultz (Primary Contact), Channing Ahn, David Boyd, Hillary Smith, Nick Weadock
California Institute of Technology (Caltech)
1200 E. California Blvd
Pasadena, CA 91125
Phone: (626) 395-2170
Email: btf@caltech.edu

DOE Manager: Jesse Adams
Phone: (720) 356-1421
Email: Jesse.Adams@ee.doe.gov

Contract Number: DE-EE0007048

Project Start Date: August 1, 2015
Project End Date: January 31, 2019

Overall Objectives

- Develop a carbon-based, functionalized material prepared by new methods (graphene) or old (exfoliated graphite) with a capacity for hydrogen storage by physisorption of 11 wt% excess and 40 g/L total (near 77 K and <100 bar), a near-constant isosteric heat of adsorption, excellent kinetics, and long cycle life.
- Understand how far hydrogen physisorption capacity can be extended beyond the present rules of thumb for carbon materials (e.g., 1 wt% excess per every 500 m²/gram). The goal is achieving >1.5 wt% excess per every 500 m²/gram.
- Demonstrate a near-constant isosteric heat of adsorption, excellent kinetics, and long cycle life.

Fiscal Year (FY) 2018 Objectives

- Identify the role of low dimensional structure and validate >40 g/L total adsorption using multi-temperature analysis over 77 to 160 K for isosteric heat validation >10 kJ/mole.

- Achieve ≥ 1.5 wt% excess hydrogen per 500 m²/g in material with >3,000 m²/g specific surface area at pressures <100 bar.
- Perform high gravimetric and volumetric density analysis to demonstrate gravimetric density meeting or exceeding 11 wt% hydrogen at 77 K and 40 bar pressure. Assess in light of Hydrogen Storage Engineering Center of Excellence tank requirements.

Technical Barriers

This project addresses the following technical barriers from the Hydrogen Storage section of the Fuel Cell Technologies Office Multi-Year Research, Development, and Demonstration Plan¹:

- (A) System Weight and Volume
- (O) Lack of Understanding of Hydrogen Physisorption and Chemisorption.

Technical Targets

This project is developing functionalized graphene materials to maximize hydrogen uptake and increase temperatures of operation. These materials are intended to meet the 2020 DOE hydrogen storage targets for high hydrogen gravimetric and volumetric capacity:

- System gravimetric capacity: 1.5 kWh/kg (4.5 wt% hydrogen)
- System volumetric capacity: 1.0 kWh/L (30 g hydrogen/L).

FY 2018 Accomplishments

- Incorporated transition metals toward enthalpy modification at nanoscale dimensions.
- Determined metal incorporation concentration via thermogravimetric analysis (TGA) and transmission electron microscopy (TEM).
- Sieverts measurements using Brunauer-Emmett-Teller (BET) apparatus showed

¹ <https://www.energy.gov/eere/fuelcells/downloads/fuel-cell-technologies-office-multi-year-research-development-and-22>

enhanced uptake with transition metal incorporation.

- Demonstrated isosteric heat enhancement from transition metal incorporation (10.8 to 14.4 kJ/mol).
- Thermally programmed desorption (TPD) analyses showed low temperature (140 K) and higher temperature (240 to 400 K) hydrogen release.

INTRODUCTION

One of the advantages of adsorbents as a storage medium is that dihydrogen retains its molecular form throughout the adsorption/desorption cycle, and the cycle requires minimal activation energy. The primary disadvantage of sorbents is that typical adsorption enthalpies are relatively weak compared to bond formation with chemical hydrogen or to interstitial atomic hydrogen in metal hydrides. Additionally, the van der Waals dimension of molecular hydrogen is large in comparison to atomic hydrogen, putting limits on the overall volumetric density that systems based on dihydrogen can achieve.

Graphene-based materials offer an excellent starting platform for hydrogen sorption owing to their high surface area for dihydrogen adsorption. The key step is to optimize functional groups on the graphene to maximize the volumetric density of dihydrogen adsorption. Part of the effort at Caltech is directed toward this optimization. While prior work on physisorbents has illustrated the importance of high surface area in achieving gravimetric uptakes of relevance to the program, volumetric densities have recently been recognized as a critical metric. Under many conditions, the nature of the adsorption process can still offer volumetric density advantages over the use of compressed gas storage, although not as high as intermetallic hydride densities. For dihydrogen that adsorbs onto a substrate, the London dispersion forces that can be regarded as transient dipoles in polarizable substances are a major contributor to physisorption processes. We are designing metal functionalizations for carbon surfaces that should optimize these attractive forces, enabling higher heats of adsorption, higher temperatures of operation, and higher capacities per surface area of material.

APPROACH

Previous work at Caltech has shown that alkali metal-intercalated graphites, which have pore dimensions similar to the graphene geometries we seek, can result in constant isosteric enthalpies of adsorption. These specialized structures have the advantage of electron back donation from the alkali metal to the graphitic planes, but these observations motivate the addition of metal atoms substitutionally in the graphene or on graphene surfaces. These local centers could increase both the isosteric heat of adsorption and the number of active sites for dihydrogen adsorption. We also note that for hydrogen on metal surfaces, adsorption and desorption typically occur above room temperature.

This project aims to promote high surface-packing density of hydrogen and high constant isosteric enthalpy in graphene and graphene-based materials. Specific key goals are to attain a high volumetric density of hydrogen, a near-constant heat of adsorption, rapid kinetics for adsorption and desorption, and long cycle life. We have altered the carbon surfaces by incorporating metal centers to increase the strength of the dispersion forces. We will continue to optimize the incorporation of these metal centers to gain better understanding of hydrogen physisorption and to reach technical targets for system gravimetric and volumetric capacity.

RESULTS

Efforts for the third phase of this project occurred in three primary areas: (1) down-selection of graphene synthesis approaches, (2) modification of graphene via metal functionalization demonstrating enhanced isosteric enthalpies and uptakes, and (3) hydrogen adsorption and desorption measurements demonstrating higher-temperature hydrogen release over a 240 to 400 K temperature range via TPD/residual gas analysis (RGA), consistent with the higher enthalpy evaluation.

This effort required down-selection of a number of graphene synthetic approaches given the discrepancies in the scientific literature, where high surface area graphene syntheses were purported to yield specific surface areas that were comparable to activated carbons. Unfortunately, the typical processing routes employed yielded material that was no different morphologically than activated carbon, as we could discern through optical and TEM studies. While problematic from the standpoint of fulfilling the metrics proposed for our third-year objectives, we directed our efforts to determining the efficacy of metal modification and hydrogen uptake enhancement.

A subset of metal-modified materials was described at the 2018 Annual Merit Review (ST120) including twelve Cu, eight Ni, three Co, three Zn, two Au, and three Ag metals that had been incorporated into carbon using metal salt solutions. Figure 1 shows TEM micrographs of some of these materials where, given the lapse of time between synthesis and analysis, the metal nanoparticles had oxidized but had retained their nanoscale dimensions. Experiments performed on the Cu-containing samples were subjected to static or flowing hydrogen gas as a reduction treatment before hydrogenation/dehydrogenation experiments were performed.

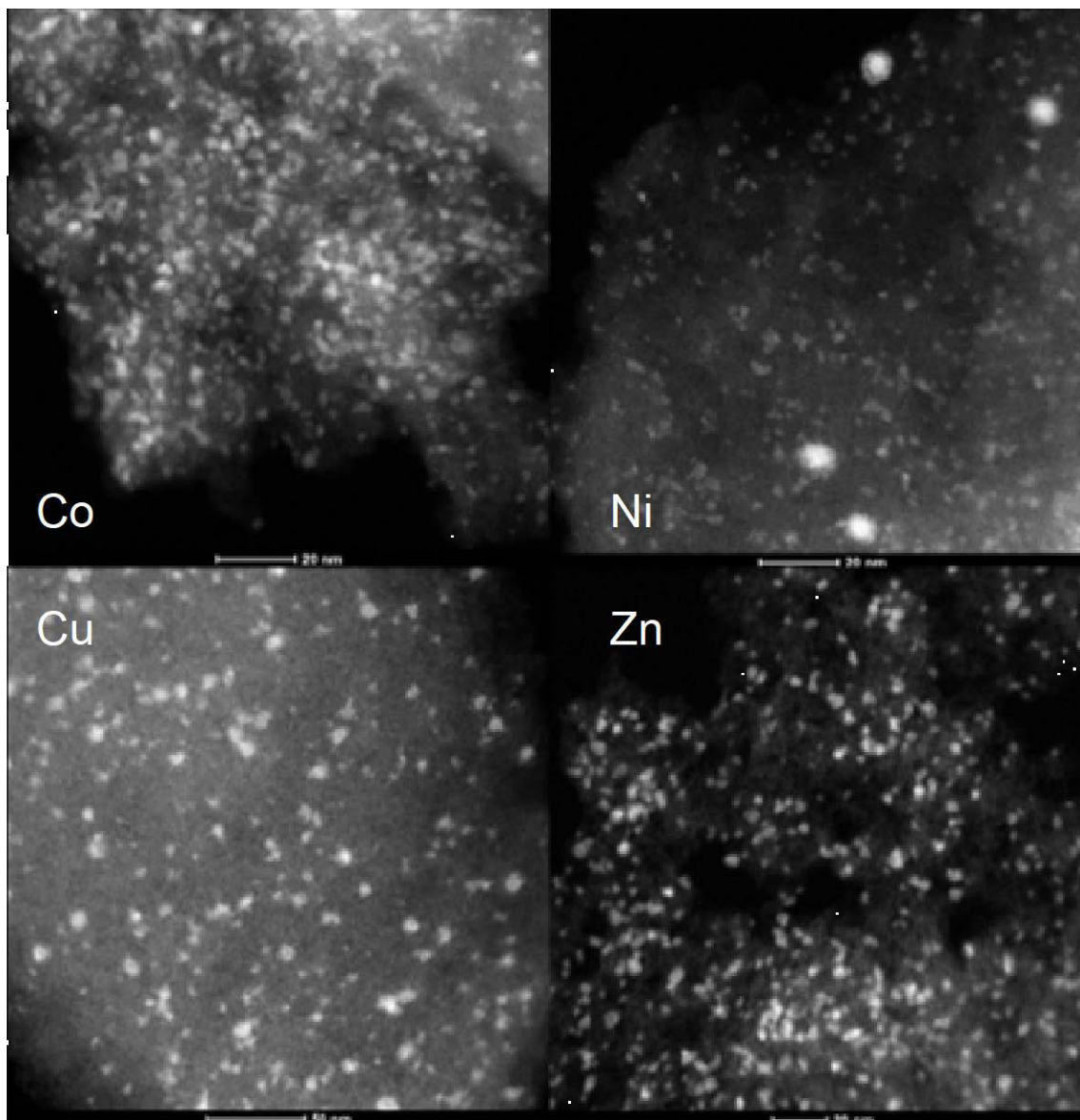


Figure 1. Transition metal incorporation showing nanoscale dimensions of the metal (oxidized during sample handling and transport to Pacific Northwest National Laboratory [PNNL]). Images courtesy of M. Bowden at PNNL.

X-ray fluorescence experiments were performed on these materials to establish the extent of metal loading; however, a baseline had to be established as the fluorescence unit had no capability for establishing direct carbon quantity comparison. An alternative technique was employed using TGA to quantify the initial metal mass fraction after the carbon has burned, leaving metal oxide. Several of these analyses are shown in Figure 2, comparing complete carbon mass loss for pure carbon samples to samples of metal-incorporated carbons.

The stability of the mass measurement at high temperatures provides a high level of confidence in the stability of this approach. Also of note is the small initial mass of material necessary for this type of analysis.

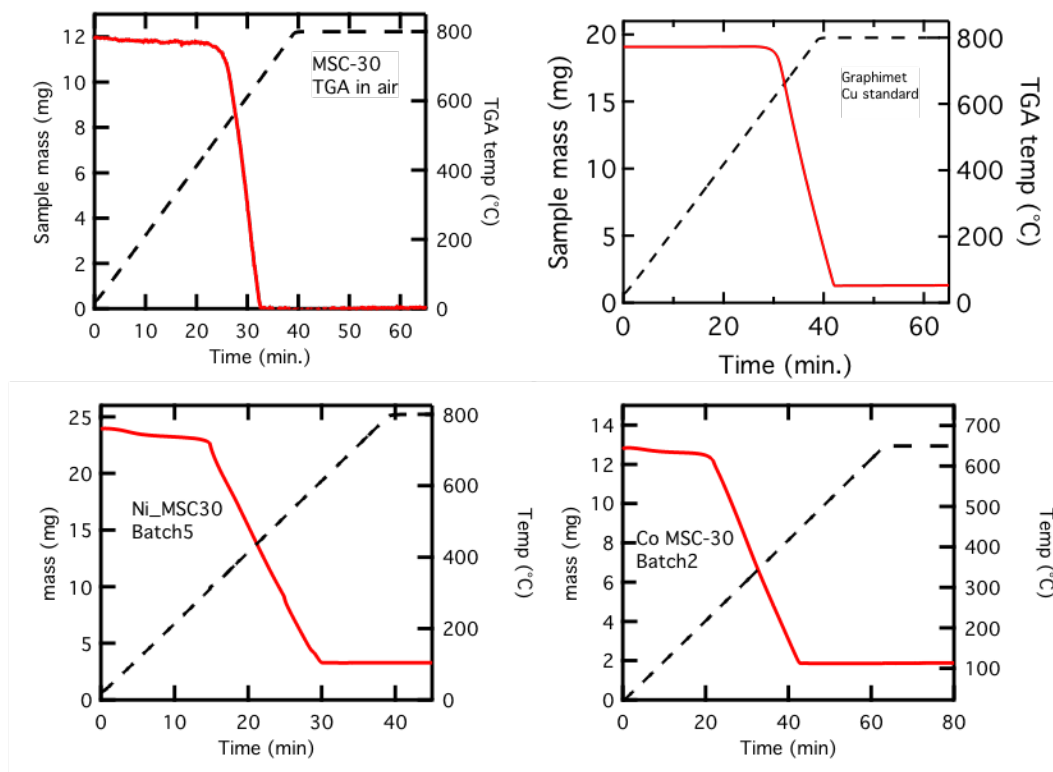


Figure 2. TGA results for the heating of pristine carbon (upper left) and metal-functionalized materials in air. Continuous heating of the samples to at least 650 °C in air causes complete loss of the carbon matrix, leaving behind fully oxidized metals. Metal-functionalized quantities were 1.1 wt% (2.5 at%) for the Ni-containing sample (lower left), 5.4 wt% Cu in a commercial “graphimet” test sample (manufacturer specified 4.53%) (upper right), and 11 wt% (2.2 at%) Co in the lower right. Results can be normalized for quicker X-ray fluorescence analysis.

Our initial evaluation of the improvement to the Henry’s law “differential enthalpy of adsorption at zero coverage” follows that of Cole et al. [1]. By plotting k_H as a function of inverse temperature, for which k_H is defined as:

$$k_H H = \lim_{p \rightarrow 0} (n/p)$$

we can determine a -10.8 kJ value for the temperature range of 240 and 296 K and -14.4 kJ at the somewhat higher 319 K temperature. All of our previous work does indicate that higher temperatures have a higher enthalpy.

We initiated TPD measurements in collaboration with the National Renewable Energy Laboratory. Once it became clear that this would be a fruitful direction, we modified an RGA setup in the lab of David Boyd at Caltech in order to obtain higher throughput and minimize sample handling complications. This allowed us to take the reactor containing sample at 77 K directly from our Sieverts apparatus to the RGA setup in Boyd’s lab. Figure 3 shows baseline data for an unmodified carbon and nanoparticles of Cu only. A gas mixture of deuterium and hydrogen in the volume ratios noted in the figures was used to probe for isotope mixing. In the carbon-only sample, we observe physisorbed gas release only peaking at 140 K, and in the Cu nanoparticle-only sample we observe chemisorbed peaks only.

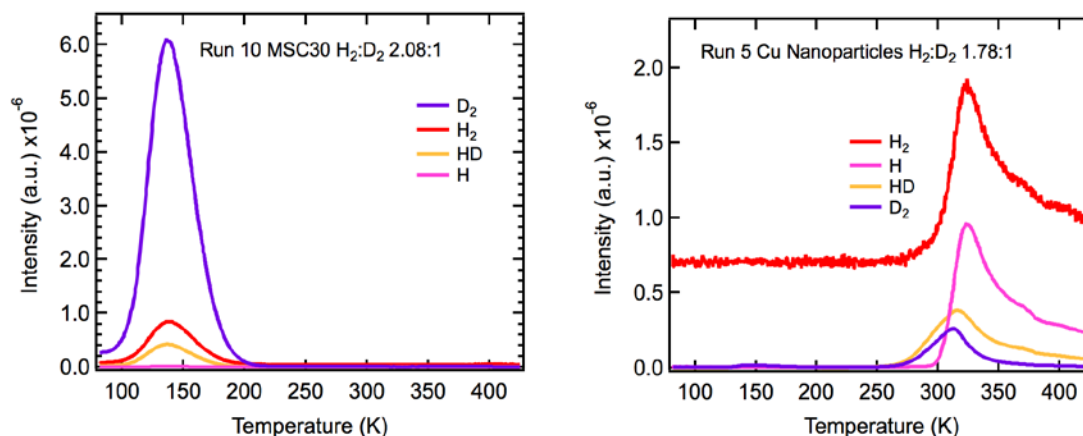


Figure 3. On left, pure MSC30-RGA traces of H₂, D₂, HD, and atomic H released ~140 K. On right, pure Cu nanoparticle-RGA traces of H₂, D₂, HD, and atomic H. Chemisorbed gas release is below 400 K. Ratio of H₂ to D₂ is slightly lower than that used in left figure data. A relatively large atomic H quantity is detected and HD formation is also evidenced → H₂ and D₂ dissociation.

Figure 4 shows a hydrogen BET isotherm from a Cu-modified sample, and the TPD RGA traces show a relatively larger quantity of chemisorbed hydrogen being released. There is also clear evidence of isotope mixing as the HD signal dominates the chemisorbed portion of the TPD data.

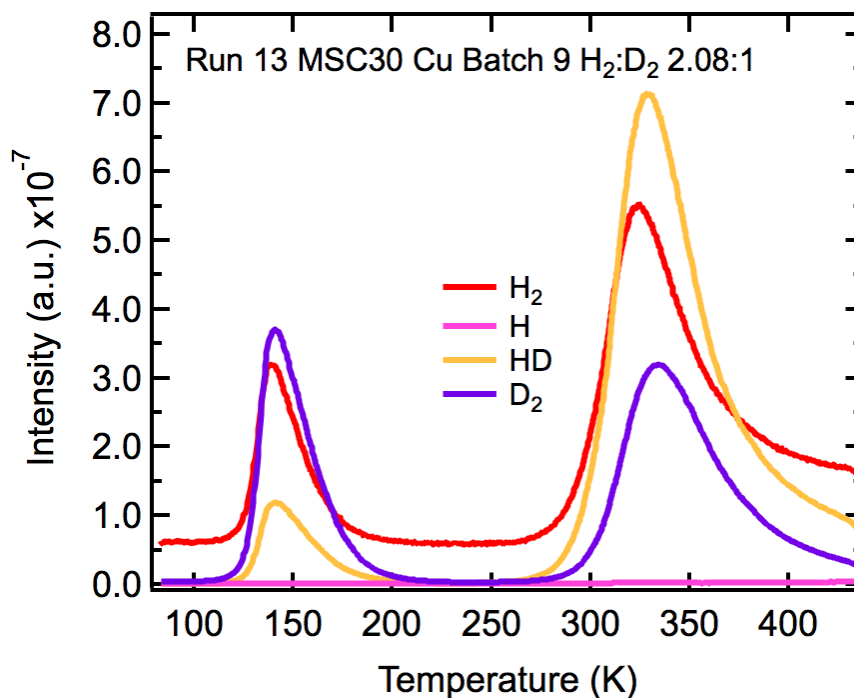


Figure 4. Cu on MSC30-RGA traces from the Batch 9 sample. The measurements used a 2:1 ratio of H₂ to D₂.

The results presented in Figure 4 show the desorption of hydrogen as a function of temperature for a Cu-modified sample. By inspection of the two temperature ranges over which hydrogen is released, it is clear that a large portion of the hydrogen is released in the higher temperature range, which is in fact the more technologically relevant regime. There are several phenomena that could be taking place to account for these

results. Some charge transfer from the metal to the carbon substrate could be taking place in addition to weak surface chemisorption of hydrogen onto the Cu surface, the latter as evidenced by isotope mixing. Given the enthalpy values we noted earlier, these observations give clear guidance for pursuing a combination of adsorbent/weak chemisorption studies.

CONCLUSIONS AND UPCOMING ACTIVITIES

As this project reaches the end of its third phase, several conclusions can be drawn:

- Relatively large quantities of graphene-based materials can be produced and functionalized with metals.
- Chemical functionalization of materials with metal salts can produce varying sizes and concentrations of metal clusters.
- TPD/RGA data between 77 K to above ambient temperature show an enhancement of hydrogen adsorption with Cu modification, indicating an increased enthalpy of adsorption in metal-functionalized materials and showing two distinct desorption regimes that we attribute to both physisorption and weak chemisorption. Enthalpy values of the higher temperature regime at 10 to >14 kJ/mole have been achieved and are in accordance with values required for technological applications.

Continuing goals for work over the no-cost extension phase of this project are to:

- Identify and quantify >40 g/L total adsorption, using multi-temperature analyses over 77 K to 400 K for isosteric heat validation >10 kJ/mole.
- Continue to pursue ≥ 1.5 wt% excess hydrogen per 500 m²/g in material with >3,000 m²/g specific surface area at pressures <100 bar and 77 K.
- Achieve net adsorption of ≥ 6 wt% hydrogen at any temperature or pressure, and achieve net adsorption of ≥ 1 wt% hydrogen at 30 bar and 300 K.
- Perform high gravimetric and volumetric density analysis to demonstrate gravimetric density meeting or exceeding 11 wt% hydrogen and volumetric capacities exceeding 40 g/L total at 77 K and 40 bar pressure.

REFERENCES

1. J.H. Cole, D.H. Everett, C.T. Marshall, A.R. Paniego, J.C. Powl and F. Rodriguez-Reinoso, "Thermodynamics of the High Temperature Adsorption of some Permanent Gases by Porous Carbons," *J. Chem. Soc. Faraday Trans. 1* 70 (1974): 2154.

Hydrogen Adsorbents with High Volumetric Density: New Materials and System Projections

Donald J. Siegel (Primary Contact, UM),
Alauddin Ahmed (UM), Yiyang Liu (UM),
Adam Matzger (UM), Justin Purewal (Ford),
Saona Seth (UM), Mike Veenstra (Ford), and
Antek Wong-Foy (UM)
University of Michigan (UM)
Ann Arbor, MI 48109
Phone: (734) 764-4808
Email: djsiegel@umich.edu

DOE Manager: Jesse Adams
Phone: (720) 356-1421
Email: Jesse.Adams@ee.doe.gov

Contract Number: DE-EE0007046

Subcontractor:
Ford Motor Company, Dearborn, MI

Project Start Date: August 1, 2015
Project End Date: July 31, 2018

Overall Objectives

- Demonstrate metal-organic frameworks (MOFs) that exhibit high volumetric and gravimetric hydrogen densities simultaneously and that exceed the performance of the benchmark adsorbent, MOF-5, at cryogenic conditions.
- Project the performance of the most promising compounds to the system level by parameterizing models developed by the Hydrogen Storage Engineering Center of Excellence (HSECoE).

Fiscal Year (FY) 2018 Objectives

- Estimate system-level performance of selected high-capacity MOFs using HSECoE system models parameterized from isotherm measurements.
- Computationally screen approximately 500,000 MOFs from the principal investigator's MOF meta-database for their usable capacities under pressure swing and temperature + pressure

swing conditions; synthesize the most promising materials predicted by computation and characterize their hydrogen uptake.

Technical Barriers

This project addresses the following technical barriers from the Hydrogen Storage section of the Fuel Cell Technologies Office Multi-Year Research, Development, and Demonstration Plan¹:

(A) System Weight and Volume

(B) System Cost

(C) Efficiency.

Technical Targets

The outcomes of this project contribute to the optimization and assessment of hydrogen storage materials and also provide input to models that project the performance of these materials at the system level. Insights gained from this study can be applied toward the development of materials that attempt to meet the DOE 2020 hydrogen storage targets, which are summarized in Table 1. The ultimate success of this project rests upon developing MOFs that outperform the baseline MOF-5 adsorbent. Therefore, Table 1 also summarizes the materials-level hydrogen capacity of MOF-5 and compares against the best adsorbents identified and demonstrated by this project to-date: IRMOF-20, SNU-70, UMCM-9, and PCN-610/NU-100.

FY 2018 Accomplishments

- Identified and experimentally demonstrated several MOFs whose usable capacities exceed that of MOF-5. Nearly 500,000 MOFs were assessed computationally under pressure swing and temperature + pressure swing conditions.
- Determined that PCN-610/NU-100 exhibits the best combination of usable (pressure swing) volumetric and gravimetric hydrogen capacity

¹ <https://www.energy.gov/eere/fuelcells/downloads/fuel-cell-technologies-office-multi-year-research-development-and-22>

of any MOF reported to date. These capacities set a new high-water mark for physisorptive hydrogen storage.

- Provided system-level projections for several of the highest-performing MOFs; these projections quantify how materials-level improvements translate to the system level.

Table 1. System-Level Technical Targets Compared to Materials-Level Performance of the Baseline MOF-5 Adsorbent and That Measured for Several MOFs Identified and Demonstrated by This Project

Storage Parameter	Units	DOE 2020 Target (System Level)	MOF-5 Baseline	Project Status: IRMOF-20	Project Status: SNU-70	Project Status: UMCM-9	Project Status: PCN-610/NU-100
Gravimetric Capacity	wt%	4.5	7.8/4.5	9.1/5.7	10.6/7.3	11.3/7.8	13.9/10.1
Volumetric Capacity	g H ₂ /L	30	51.9/31.1	51/33.4	47.9/34.3	47.4/34.1	47.6/35.5

Capacities are reported for two usable conditions: the first number refers to a temperature + pressure swing from 77 K, 100 bar to 160 K, 5 bar; the second value refers to an isothermal pressure swing at 77 K between 100 bar and 5 bar. All reported MOF capacities are reported at the materials level and are based on single-crystal densities.

INTRODUCTION

A high-capacity, low-cost method for storing hydrogen remains one of the primary barriers to the widespread commercialization of fuel cell vehicles. Although many storage technologies have been proposed, storage via adsorption remains one of the more promising approaches due to its fast kinetics, facile reversibility, and high gravimetric densities. Adsorbents struggle, however, in two key measures: volumetric density and operating temperature. For example, it is well known that high-surface-area adsorbents such as MOFs can achieve high gravimetric densities. Nevertheless, high volumetric densities are uncommon in these materials, and it has recently been suggested that total volumetric density and gravimetric density are inversely related beyond a threshold surface area. In the case of operating temperatures, the relatively weak enthalpy of hydrogen adsorption implies that high hydrogen densities are possible only at cryogenic temperatures.

Although an ideal adsorbent would overcome both of these shortcomings, it is important to recognize that volumetric density and operating temperature are controlled by different factors: the former depends upon the adsorbent's structure, whereas the latter depends on the chemistry of the hydrogen-adsorbent interaction. Therefore, distinct approaches are needed to address these independent issues. While some effort has previously been devoted to increasing ΔH (e.g., MOFs with open metal sites), attempts to increase volumetric densities have received much less attention. This is unfortunate, as analysis by the HSECoE has indicated that vehicle range is highly sensitive to volumetric density. Consequently, the development of adsorbents that simultaneously achieve high volumetric and gravimetric hydrogen densities—while maintaining reversibility and fast kinetics—would constitute a significant advance. Moreover, these materials would serve as logical starting points for follow-on efforts aimed at increasing the operating temperature.

APPROACH

This project aims to circumvent the tradeoff between total volumetric and gravimetric hydrogen densities typical of most hydrogen adsorbents. This will be accomplished by combining computational screening for promising compounds with experimental synthesis and measurement of hydrogen storage densities within those compounds. The ultimate goal is to demonstrate materials having balanced gravimetric and volumetric performance that can surpass the storage density of the benchmark compound, MOF-5. The performance of the most promising compounds will be projected to the system level by parameterizing system models developed by the HSECoE.

RESULTS

As described above, the focus of this effort is to demonstrate MOFs with a hydrogen density that surpasses that of MOF-5 in its optimal or “pristine” form (i.e., MOF-5 that has not been exposed to air and from which all solvent/reactants have been removed). Toward this goal, in FY 2016 we demonstrated IRMOF-20, a MOF whose capacities slightly surpassed that of MOF-5 (see Table 1). Subsequently, in FY 2017 we aimed to improve performance further by identifying and demonstrating MOFs that surpass the usable capacity of MOF-5 by 15%. This was accomplished by screening 469,741 MOFs (5,109 known and 464,600 hypothetical) from seven databases [1-7] for their usable capacities, assuming pressure swing operation between 5 and 100 bar. These calculations and experimental measurements demonstrated that SNU-70 can outperform both MOF-5 and IRMOF-20, as also shown in Table 1.

In FY 2018 we expanded our catalogue of screened compounds to include 10,126 known MOFs and 8,482 hypothetical compounds from four additional databases: Cambridge Structural Database curated MOFs, in-silico surface MOFs, MOF-74 analogs, and the ToBaCCo database [8-11]. A summary of the resulting meta-database of MOFs is shown in Table 2. In addition, our screening protocol was extended to temperature + pressure swing conditions: ($T_{\min}= 77$ K, $P_{\max}= 100$ bar) to ($T_{\max}= 160$ K, $P_{\min}= 5$ bar). In total, usable capacities of 43,227 MOFs under both operating conditions were calculated using Grand Canonical Monte Carlo (GCMC) analysis. Under pressure swing conditions, 12,986 and 6,059 MOFs were identified whose capacities can theoretically surpass those of MOF-5 and IRMOF-20, respectively. For temperature + pressure

swing conditions, only 186 MOFs were identified whose capacities can theoretically surpass that of MOF-5, the best-performing MOF reported to date under these conditions.

Table 2. Details of the MOF Databases and Their Subsequent Screening Based on Surface Area, Chahine Rule, and GCMC Calculated Usable Capacities of MOF-5 and IRMOF-20 at 77 K

Database	No. of MOFs	No. with Zero Surface Area	Capacity Evaluated Empirically	Capacity Evaluated with GCMC	Capacity Exceeds MOF-5 (PS/TPS)	Capacity Exceeds IRMOF-20 (PS only)
Real MOFs [1,2,11]: UM+CoRE+CSD	15,235	2,950	12,285	12,285	405/27	102
Mail-order [3]	112	4	108	112	30/0	19
In-silico deliverable [5]	2,816	154	2,662	466	27/0	6
In-silico surface [8]	8,885	283	8,602	1,058	236/0	77
MOF-74 analogs [9]	61	0	61	61	0/0	0
ToBaCCo [10]	13,512	214	13,298	290	135/2	72
Zr-MOFs [6]	204	0	204	204	126/0	35
Northwestern [4]	137,000	30,160	106,840	12,374	4,397/153	2,154
Univ. of Ottawa [7]	324,500	32,993	291,507	16,372	7,612/4	3,581
In-house	18	0	18	5	18/0	13
Total	493,458	66,758	435,585	43,227	12,986/186	6,059

Assuming a pressure swing (PS) between 5 and 100 bar or temperature + pressure swing (TPS) from (T_{\min} = 77 K, P_{\max} = 100 bar) to (T_{\max} = 160 K, P_{\min} = 5 bar). To date, MOF-5 is the highest capacity MOF under TPS conditions, thus TPS performance was compared only to MOF-5.

Figure 1 shows the calculated usable volumetric capacities of 43,227 real and hypothetical MOFs as a function of their usable gravimetric capacities. Large dots indicate the measured capacities for some of the most promising MOFs identified; these MOFs were synthesized and characterized based on the computational predictions. For comparison, MOFs demonstrated as part of prior work in this or other projects (MOF-5, IRMOF-20) are also shown. In the case of the pressure swing data, Figure 1 shows this project has successfully identified and demonstrated a series of MOFs that outperform MOF-5 both gravimetrically and volumetrically. In the case of temperature + pressure swing operation, MOF-5 remains the MOF with the greatest usable volumetric capacity; nevertheless, IRMOF-20, SNU-70, and NU-100 all exceed the performance of MOF-5 on a gravimetric basis.

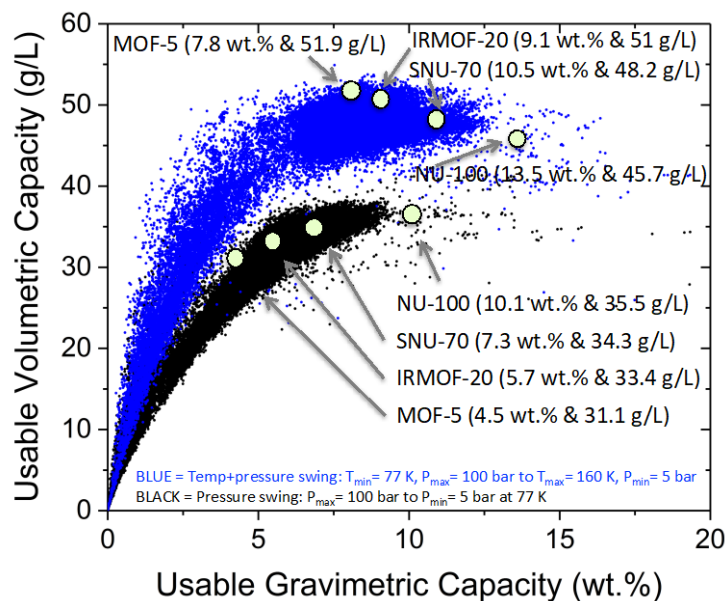


Figure 1. Calculated usable hydrogen storage capacities of 43,227 real and hypothetical MOFs assuming both pressure swing (black data points) and temperature + pressure swing operation (blue data points). Filled circles indicate measured hydrogen storage capacities of MOFs that were identified as promising compounds from computational screening.

Figure 2 illustrates how improvements in volumetric capacity at the materials level (assuming single-crystal density) translate to the system level. These projections were made using the Hex-Cell version of the adsorption system model developed by the HSECoE and adopt a realistic powder packing density. The data show that improvements in capacity achieved at the materials level are carried over to the system: a 14% increase in materials-level capacity achieved by substituting NU-100 for MOF-5 results in a similar 12% increase at the system level. Nevertheless, the absolute value of the hydrogen density is approximately 40% smaller at the system level for all MOFs considered. This is due to the large volumes associated with the insulation of the storage tank and to the volumes of other balance-of-plant components. In a similar manner, the improvement between gravimetric density on a materials level to that on the system level also was evaluated. For NU-100, a gravimetric density improvement of 124% on the materials level equated to only a 7% improvement on a system level. On an absolute basis, system gravimetric values are 40% to 70% smaller than materials-level gravimetric capacities.

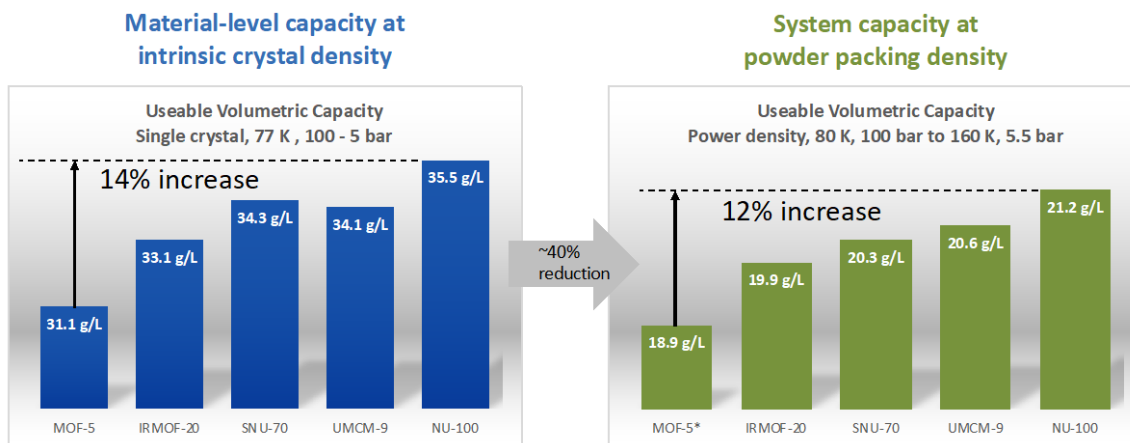


Figure 2. Demonstration of how improvements to materials-level volumetric capacity impact system-level volumetric capacity across a series of five MOFs examined in this project

CONCLUSIONS AND UPCOMING ACTIVITIES

This work has demonstrated that computational screening can successfully identify MOFs with enhanced volumetric and gravimetric hydrogen capacities. Several of the MOFs predicted by computation were synthesized, and their experimentally measured hydrogen uptake was shown to be in good agreement with the computational predictions. Based on these measurements, the HSECoE system model was used to extrapolate gains in capacity achieved at the materials level to performance at the system level.

Although this project ended in July 2018, several areas of R&D remain ripe for exploration. One obvious area is the experimental evaluation of the many other MOFs predicted by computation to have high hydrogen capacities (Table 2). The present project did not have the experimental throughput to explore more than a few dozen of these possibilities. A second area involves the efficient packing of MOF storage media. At present, gains in the single-crystal storage density predicted by the present project can be a challenge to realize at the system level due to low packing densities of the MOF powder. Strategies for increasing these densities should be explored.

FY 2018 PUBLICATIONS/PRESENTATIONS

1. M.D. Allendorf, Z. Hulvey, T. Gennett, A. Ahmed, T. Autrey, J. Camp, H. Furukawa, M. Haranczyk, M. Head-Gordon, A. Karkamkar, D.-J. Liu, J.R. Long, K.R. Meihaus, I.H. Nayyar, R. Nazarov, D.J. Siegel, V. Stavila, J.J. Urban, S.P. Veccham, and B. C. Wood, “An Assessment of Strategies for the Development of Solid-State Adsorbents for Vehicular Hydrogen Storage,” *Energy & Environmental Science* 11 (2018): 2784–2812. DOI: 10.1039/c8ee01085d.
2. Alauddin Ahmed, Yiyang Liu, Justin Purewal, Ly D. Tran, Antek G. Wong-Foy, Mike Veenstra, Adam J. Matzger, and D. J. Siegel, “Balancing Gravimetric and Volumetric Hydrogen Density in MOFs,” *Energy & Environmental Science* 10 (2017): 2459–2471. DOI: 10.1039/C7EE02477K.
3. D.J. Siegel (invited presentation), 2nd Bosch Energy Research Network (BERN) Symposium on Innovative Energy Research, Sunnyvale, CA, September 6–7, 2018.
4. D.J. Siegel (invited presentation), American Chemical Society’s 256th National Meeting, symposium on Nanoscience of Energy Storage, Boston, MA, August 19–23, 2018.
5. D.J. Siegel (invited presentation), Indian Institute of Science Education and Research (IISER-BPR), Berhampur, India, September 4, 2017.
6. D.J. Siegel (invited presentation), Telluride Science Research Center, Computational Materials Chemistry Workshop, Telluride, CO, August 7–11, 2017.

REFERENCES

1. J. Goldsmith, A.G. Wong-Foy, M.J. Cafarella, and D.J. Siegel. “Theoretical Limits of Hydrogen Storage in Metal-Organic Frameworks: Opportunities and Trade-Offs.” *Chem. Mater.* 25, no. 16 (2013): 3373–3382.
2. Y.G. Chung, J. Camp, M. Haranczyk, B.J. Sikora, W. Bury, V. Krungleviciute, T. Yildirim, O.K. Farha, D.S. Sholl, and R.Q. Snurr. “Computation-Ready, Experimental Metal-Organic Frameworks: A Tool To Enable High-Throughput Screening of Nanoporous Crystals.” *Chem. Mater.* 26 (2014): 6185–6192.
3. R.L. Martin, L.-C. Lin, K. Jariwala, B. Smit, and M. Haranczyk. “Mail-Order Metal-Organic Frameworks (MOFs): Designing Isoreticular MOF-5 Analogues Comprising Commercially Available Organic Molecules.” *J. Phys. Chem. C* 117, no. 23 (2013): 12159–12167.
4. C.E. Wilmer, M. Leaf, C.Y. Lee, O.K. Farha, B.G. Hauser, J.T. Hupp, and R.Q. Snurr. “Large-Scale Screening of Hypothetical Metal-Organic Frameworks.” *Nat. Chem.* 4, no. 2 (2011): 83–89.
5. Y. Bao, R.L. Martin, C.M. Simon, M. Haranczyk, B. Smit, and M.W. Deem. “In Silico Discovery of High Deliverable Capacity Metal-Organic Frameworks.” *J. Phys. Chem. C* 119, no. 1 (2015): 186–195.

6. D.A. Gomez-Gualdrón, O.V. Gutov, V. Krungleviciute, B. Borah, J.E. Mondloch, J.T. Hupp, T. Yildirim, O.K. Farha, and R.Q. Snurr. “Computational Design of Metal-Organic Frameworks Based on Stable Zirconium Building Units for Storage and Delivery of Methane.” *Chem. Mater.* 26, no. 19 (2014): 5632–5639.
7. M.Z. Aghaji, M. Fernandez, P.G. Boyd, T.D. Daff, and T.K. Woo. “Quantitative Structure-Property Relationship Models for Recognizing Metal Organic Frameworks (MOFs) with High CO₂ Working Capacity and CO₂/CH₄ Selectivity for Methane Purification.” *Eur. J. Inorg. Chem.* (2016).
8. Y. Bao, R.L. Martin, M. Haranczyk, and M.W. Deem. “In Silico Prediction of MOFs with High Deliverable Capacity or Internal Surface Area.” *Phys. Chem. Chem. Phys.* 17, no. 18 (2015): 11962–11973.
9. M. Witman, S. Ling, A. Gladysiak, K.C. Stylianou, B. Smit, B. Slater, and M. Haranczyk. “Rational Design of a Low-Cost, High-Performance Metal-Organic Framework for Hydrogen Storage and Carbon Capture.” *J. Phys. Chem. C* 121, no. 2 (2017): 1171–1181.
10. Y.J. Colón, D.A. Gómez-Gualdrón, and R.Q. Snurr. “Topologically Guided, Automated Construction of Metal-Organic Frameworks and Their Evaluation for Energy-Related Applications.” *Cryst. Growth Des.* 17, no. 11 (2017): 5801–5810.
11. P.Z. Moghadam, A. Li, S.B. Wiggin, A. Tao, A.G.P. Maloney, P.A. Wood, S.C. Ward, and D. Fairen-Jimenez. “Development of a Cambridge Structural Database Subset: A Collection of Metal-Organic Frameworks for Past, Present, and Future.” *Chem. Mater.* 29, no. 7 (2017): 2618–2625.

HyMARC: A Consortium for Advancing Hydrogen Storage Materials

Mark D. Allendorf (Primary Contact),
Vitalie Stavila, Lennie Klebanoff, Rob Kolasinski,
Farid El Gabaly, Xiaowang Zhao, James White
Sandia National Laboratories
7011 East Avenue
Livermore, CA 94551
Phone: (925) 294-3059
Email: mdallen@sandia.gov

DOE Manager: Ned Stetson
Phone: (202) 586-9995
Email: Ned.Stetson@ee.doe.gov

Project Start Date: September 17, 2015
Project End Date: September 30, 2018

Overall Objectives

- Accelerate discovery of breakthrough storage materials by developing foundational understanding of phenomena governing thermodynamics and kinetics.
- Develop community tools and capabilities to enable materials discovery, including computational models and databases, new characterization tools and methods, and tailorable synthetic platforms.
- Provide technical direction to the Hydrogen Materials Advanced Research Consortium (HyMARC) via leadership of Task 1 (Thermodynamics), Task 3 (Gas Surface Interactions), and Task 5 (Additives).
- Provide gas sorption and other property data needed to develop thermodynamic models of sorbents and metal hydrides, including the effects of ultrahigh hydrogen pressure.
- Identify the structure, composition, and reactivity of gas-surface and solid-solid hydride surfaces contributing to rate-limiting desorption and uptake.
- Synthesize metal hydrides and sorbents in a variety of formats (e.g., bulk powders, thin

films, nanostructures) and develop in situ techniques for their characterization.

- Apply Sandia National Laboratories (SNL) multiscale codes to discover new materials and new mechanisms of storing hydrogen, and provide input for database development.
- Elucidate the role of additives in improving hydrogen uptake and release from materials.

Fiscal Year (FY) 2018 Objectives

- Perform sensitivity analysis of local binding and second-sphere effects.
- Rank improvement strategies for sorbents and metal hydrides.
- Develop a modeling formalism for amorphous phases and defects.
- Parameterize integrated kinetic model for representative B-N-Al hydrides.
- Compute sorbent isotherms from quantum Monte Carlo data for metal-organic frameworks (MOFs).
- Publicly release codes, databases, synthetic protocols, and characterization methodologies optimized for storage materials.

Technical Barriers

This project addresses the following technical barriers from the Hydrogen Storage section of the Fuel Cell Technologies Office Multi-Year Research, Development, and Demonstration Plan¹:

- (O) Lack of Understanding of Hydrogen Physisorption and Chemisorption
- (A) System Weight and Volume
- (E) Charging/Discharging Rates
- (F) Cost, Efficiency, Durability.

¹ <https://www.energy.gov/eere/fuelcells/downloads/fuel-cell-technologies-office-multi-year-research-development-and-22>

Technical Targets

The goal of this project is to develop foundational understanding of phenomena governing thermodynamics and kinetics of hydrogen release and uptake in all classes of hydrogen storage materials. Insights gained from these studies will be applied toward the design and synthesis of hydrogen storage materials that meet the following DOE 2020 hydrogen storage targets:

- Cost: \$10/kWh net
- Specific energy: 1.8 kWh/kg
- Energy density: 1.3 kWh/L.

FY 2018 Accomplishments

- Predicted and measured thermodynamic data for $\text{Mg}(\text{BH}_4)_2$ needed to establish a validated phase diagram for this storage material.
- Determined that B-B bond activation, not H_2 bond breaking, is the rate-limiting step in the hydrogenation of MgB_2 .
- Determined the enthalpy and entropy of hydrogen desorption from bulk $\text{Mg}(\text{BH}_4)_2$, crucial data for which accurate values were lacking in the literature.
- Created a new melt-infiltration method for $\text{Mg}(\text{BH}_4)_2$ incorporation into porous hosts for synthesizing nanoscale hydrogen storage materials.
- Discovered that some MOF sorbents are not completely stable under high hydrogen pressure or upon repeated high-pressure hydrogen cycling.
- Performed the first in situ characterization of the surface chemistry of $\text{Mg}(\text{BH}_4)_2$ using synchrotron methods and low-energy ion scattering (a unique HyMARC capability), showing that the surface composition evolves in time.
- Determined the melting temperature of $\text{Mg}(\text{BH}_4)_2$ under 1,000-bar hydrogen pressure using a unique high-pressure reactor system at SNL.
- Measured low- and high-pressure hydrogen isotherms for validating computational models of hydrogen uptake by nanoporous sorbents.

- Initiated a comprehensive force-field development effort for Mg-B-H intermediates.
- Developed validated molecular dynamics models of hydrogen diffusion in magnesium hydride (MgH_2).
- Developed a new methodology for simulating nucleation kinetics of complex metal hydrides.
- Published a major review on nanoscale metal hydrides and a perspective article concerning strategies for developing new sorbent materials.

INTRODUCTION

Storage of hydrogen onboard vehicles is one of the critical technologies needed to create hydrogen-fueled transportation systems that can improve energy efficiency and resiliency, reduce oil dependency, and promote energy independence. Stakeholders in developing hydrogen infrastructure (e.g., state governments, automotive original equipment manufacturers, station providers, and industrial gas suppliers) are currently focused on high-pressure storage at 350 bar and 700 bar, in part because no viable solid-phase storage material has emerged. Early-stage research to develop foundational understanding of solid-state storage materials, including novel sorbents and high-density hydrides, is of high importance because of their unique potential to meet all DOE Fuel Cell Technologies Office targets and deliver hydrogen at lower storage pressures and higher onboard densities. However, existing materials suffer from thermodynamic and kinetic limitations that prevent their application as practical hydrogen storage media.

SNL's overall objectives and responsibilities within HyMARC are to (1) provide technical leadership to the consortium at the director level, as well as through leadership of Task 1 (Thermodynamics), Task 3 (Gas Surface Interactions), and Task 5 (Additives); (2) provide gas sorption and other property data required to develop and validate thermodynamic models of sorbents and metal hydride storage materials, including the effects of 350 bar and 700 bar hydrogen delivery pressures, serving as a resource for the consortium; (3) identify the structure, composition, and reactivity of gas surface and solid-solid hydride surfaces contributing to rate-limiting desorption and uptake; (4) provide metal hydrides and MOF sorbents in a variety of formats tailored for specific consortium tasks; (5) develop sample preparation methods and experimental protocols to enable facile use of the new characterization probes employed by HyMARC; (6) apply SNL multiscale codes to discover diffusion pathways and mechanisms of storage materials; and (7) elucidate the role of additives in promoting hydrogen storage reactions.

APPROACH

HyMARC seeks to address critical gaps in the science of hydrogen storage by leveraging recent advances in predictive multiscale modeling, high-resolution in situ characterization, and novel material synthesis techniques. By focusing on the underlying thermodynamic and kinetic limitations of storage materials, we will generate foundational understanding that will accelerate the development of all types of advanced storage materials, including sorbents, metal hydrides, and liquid carriers.

RESULTS

Substantial progress was made on each of the five tasks being performed at SNL, with all of the quarterly goals met on time. SNL principal investigators led the organization of task groups, helping to guide the science in collaboration with our partners, and scheduling and coordinating task team meetings involving all three HyMARC laboratory partners. Technical results include the following.

Task 1: Thermodynamics

SNL's effort to elucidate the factors contributing to the thermodynamics of hydrogen uptake and release by sorbents and metal hydrides provided new data and contributed to the foundational understanding of these materials.

Key results for metal hydrides: The thermodynamics of metal hydrides are a major focus of HyMARC, as these determine the conditions required to release hydrogen and recharge the storage material. Magnesium borohydride ($\text{Mg}(\text{BH}_4)_2$) stands out among the many known metal hydrides as a material with the gravimetric and volumetric capacity required to meet the DOE technical targets. However, its thermodynamic properties, including enthalpy and entropy of hydrogen desorption and the stability of its decomposition products, are poorly understood. Through experimental measurements in SNL's ultrahigh-pressure reactor, we determined for the first time that $\text{Mg}(\text{BH}_4)_2$ melts at 365°C under 1,000 bar hydrogen. We also determined that the hydrogen desorption enthalpy for the bulk material is 48 kJ/mol H_2 , indicating that its thermodynamic properties are far from optimum. These new data allowed us to develop a method to melt-infiltrate porous

materials with the hydride to create nanoparticles. Moreover, these nanoparticles begin to release hydrogen at temperatures 100°–150°C lower than the bulk, suggesting a new strategy for increasing the kinetics of hydrogen release from borohydrides. Our measurements were also used to calibrate the Mg-B-H phase diagram theoretically predicted by Lawrence Livermore National Laboratory (LLNL) (Figure 1). In this phase diagram prediction, *ab initio* molecular dynamics (AIMD) simulations were used to account for anharmonic vibrations of $B_xH_y^{n-}$ molecules. The predicted temperature-pressure conditions for phase coexistence were calibrated using the SNL pressure-composition-temperature (PCT) data. Our efforts to achieve more accurate predictions enabled us to greatly reduce the errors in the predicted reaction entropies and enthalpies. Compared with errors in these quantities of 11% and 50%, respectively, we achieved errors <3% and 12%. The validated phase diagram was used to distinguish thermodynamic products from those resulting from slow chemical kinetics.

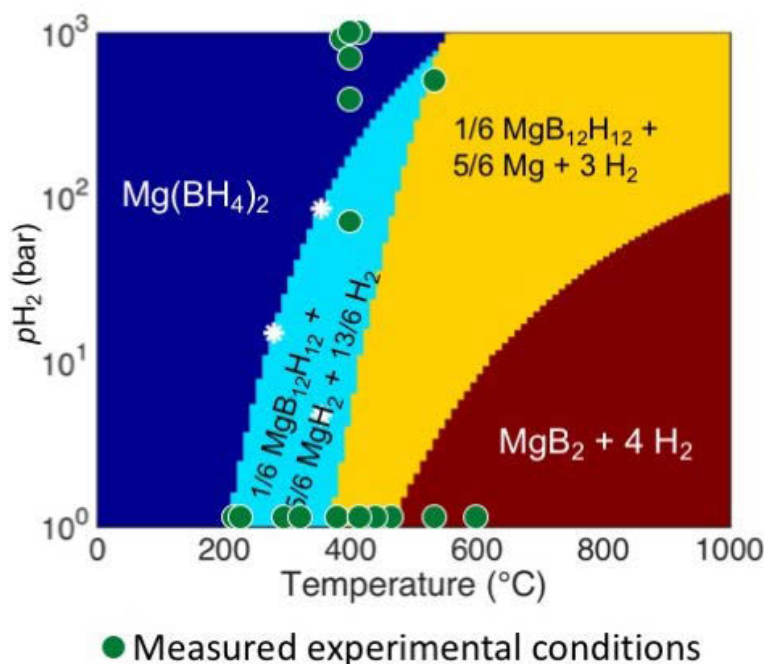


Figure 1. Comparison of Mg-B-H phase diagram, computed using density functional theory, with experimentally measured equilibrium hydrogen pressures

We also applied our computational method for calculating hydride entropies to all experimentally observed or theoretically predicted intermediate compositions and polymorphs of the Li-N-H, Na-Al-H, Li-B-H, Na-B-H, and Mg-B-H systems. An advantage of our approach is that it can separate the anharmonic and harmonic contributions to the entropy. We estimate that the former contributes up to 10 kJ/mol H_2 at 700 K, or 50% of the harmonic contributions. Consequently, we developed a new hypothesis that a “freezing” confining medium that interacts strongly with the metal hydride may suppress these anharmonic phonon modes, which could help to decouple entropic and enthalpic thermodynamic contributions.

Key results for sorbents: MOFs are a promising class of tailorable nanoporous sorbent materials that are being intensively investigated for hydrogen storage. Understanding their long-term stability under repeated cycles of low- to high-pressure hydrogen is essential for determining their long-term potential. We selected a suite of eight MOFs to compare the effects of metal ion redox activity, pore volume, and chemical structure of the organic linker groups on stability toward hydrogen cycling. The MOFs were subjected to two different

tests under the hydrogen environment: (1) extensive cycling (1,000 cycles) between 5 bar and 100 bar in hydrogen at room temperature, and (2) ultrahigh pressure (700 bar) of hydrogen at room temperature. Characterization of the MOF materials following these tests showed that most of the MOFs are stable under these conditions, with the exception of IRMOF-74-II(Mg) and IRMOF-74(Ni). IRMOF-74-II(Mg) showed ~10% loss in porosity after extensive cycling between 5 and 100 bar, and MOF-74(Ni) showed 10%–20% loss in porosity under both conditions. A detailed transmission electron microscopy study of the MOF-74(Ni) sample clearly indicates the formation of 3–5 nm nickel nanoparticles in the MOF structure. The reasons for this instability are currently under investigation.

Task 2: Kinetics of Mass Transport

We developed an automated software tool for accelerating the development and optimization of force fields for simulating the mass transport kinetics of hydrogen and other elements through storage materials. Mass transport is one of the primary phenomena affecting rates of hydrogen release and uptake by metal hydrides. Molecular dynamics methods, which assume that Newton's laws govern mass transport, are a powerful approach to simulating these processes, but they require a comprehensive force field to describe correctly the potential energy surfaces within a material. For complex molecular systems, intermolecular interactions depend on molecular species and both the spacing and relative orientation between molecules. As a result, force field development is very time consuming, as multiple parameters must be fit to thousands of target values obtained from density functional theory calculations. The parameterization tool we developed is highly automated: the only inputs required from the user are the chemical formulae of all molecules included in the simulation and files containing intermolecular interaction energies obtained from density functional theory. Each iteration of force field optimization can be completed within a matter of a few days rather than months. Using this approach, we developed a validated model for hydrogen diffusion through magnesium that accurately captures the crystalline growth of MgH₂.

Task 3: Surface Science

Using a suite of cutting-edge characterization tools that probe the surface, near-surface, and bulk regions of a hydrogen storage material, we showed for the first time that the surface of complex metal hydrides evolves dynamically as hydrogen is desorbed. Of particular significance is our observation that oxygen-containing surface species are actively involved in the release of hydrogen from titanium-doped NaAlH₄. Titanium is a well-known additive that enables the reversible release and uptake of hydrogen by this hydride, but despite extensive study (>2,000 papers published) the mechanism is still not firmly established. We employed two *in operando* diagnostics: low-energy ion scattering (LEIS) at SNL, which is uniquely sensitive to hydrogen on the monolayer atomic surface of a material, and the synchrotron-based ambient-pressure X-ray photoelectron spectroscopy (AP-XPS) facility at the Advanced Light Source (at Lawrence Berkeley National Laboratory [LBNL]), which probes the surface and subsurface (0–10 nm). In addition, we used scanning transmission X-ray microscopy (STXM) to probe the distribution of chemical species within bulk particles. Data interpretation from the two X-ray tools was facilitated by computational spectroscopy at the Molecular Foundry, located at LBNL, and at LLNL. XPS chemical shifts were computed for active species involved in dehydrogenation, based on local configurations derived from AIMD simulations. Dehydrogenation kinetics were also studied using direct barrier calculations. The results demonstrate that titanium-containing surface species play no direct role in the surface desorption chemistry. Rather, they suggest that surface hydroxides may actually facilitate surface hydrogen formation and release. This represents a paradigm shift concerning the role of surface oxygen, which is unavoidable for these highly reactive materials, and is consequently influencing the way we conceive of new hydride-based storage materials.

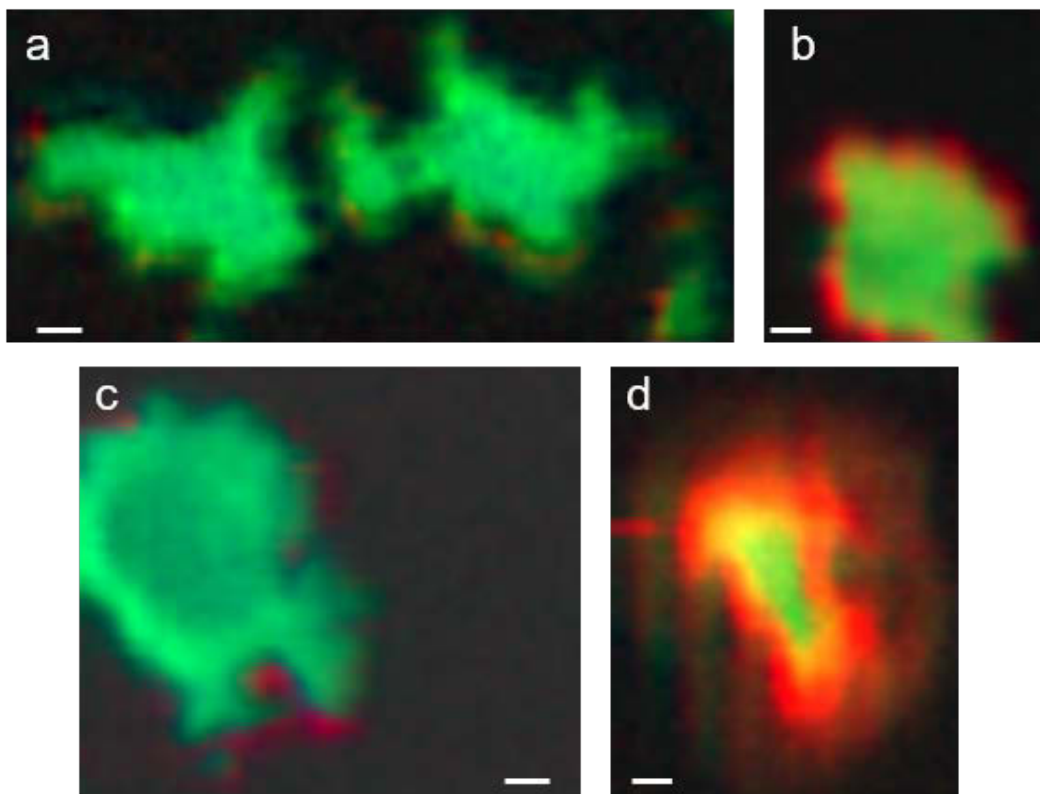


Figure 3. STXM images of samples treated at 400 °C for 72 h: (a) MgB_2 under 202 bar H_2 , (b) $\text{Mg}(\text{BH}_4)_2$ under 202 bar H_2 , (c) MgB_2 under 700 bar H_2 , (d) $\text{Mg}(\text{BH}_4)_2$ under 360 bar H_2 . Red regions correspond to $\text{Mg}(\text{BH}_4)_2$; green regions represent $\text{MgB}_{12}\text{H}_{12}$.

To understand the observed phase behavior during (de/re)hydrogenation, we formulated a computational model for complex hydrides based on advanced phase nucleation theory and involving multiple intermediates. As an initial test case, the model was parameterized by our *ab initio* thermodynamics calculations for the Mg-B-H system. We conducted a preliminary investigation of possible kinetic pathways that may lead to different types of phase microstructures. For hydrogenation of a MgB_2 particle through the $\text{MgB}_{12}\text{H}_{12}$ intermediate, we identified multiple possible phase transformation pathways by examining the phase nucleation barriers as a function of particle size and surface/interfacial energies. This modeling framework is now being extended to include more relevant intermediates, and the analyzed phase microstructures are being compared with the characterized phase morphologies by STXM measurements.

Task 5: Additives

The number of additives (e.g., transition metal halides and carbides) known to accelerate the kinetics of hydrogen desorption and uptake is large, but the mechanisms by which the rate increases are effected are largely unknown. Consequently, HyMARC investigations in this and prior years have focused on the most effective additives, in particular titanium halides (see Task 3), and on using additives as a tool to probe hydride chemistry. In the latter, we probed the mechanism of hydrogen uptake by MgB_2 . The rate-limiting step in the process to regenerate $\text{Mg}(\text{BH}_4)_2$ from this material was initially unclear but likely involved either B-B or H-H bond breaking. To probe this, we prepared samples of MgB_2 mixed with catalysts known to dissociate H_2 to form H atoms, including Fe, Pd, and WC. These additives did not significantly improve how fast MgB_2 reacted with H_2 indicating that H-H bond breaking is not the rate-limiting step. In a complementary experiment, the ability of these materials to break H-H bonds was directly measured with H-D isotopic exchange studies. These investigations showed that these additives, when combined with MgB_2 , break H-H bonds on a time scale that is fast compared to the slow hydrogenation of MgB_2 . Our results indicate that it is not H-H bond breaking

that is rate limiting, but disruption of the hexagonal B-B rings in MgB_2 or the formation of hydride (H^-) anions that limit the uptake of H_2 . Future investigations will focus on developing additive strategies addressing these possibilities.

Interactions with Seedling Projects and Collaborations

The SNL HyMARC team performed extensive measurements and testing in support of five seedling projects. More than 50 samples were exposed to hydrogen pressures ≥ 700 bar in SNL's ultrahigh-pressure reactor for two projects. In addition, XPS and porosimetry measurements were performed for two other projects, one of which resulted in a joint paper. Finally, SNL performed the go/no-go validation for two projects. Extensive collaborations with both U.S. and international organizations occurred, involving government and DOE national laboratories as well as universities.

CONCLUSIONS AND UPCOMING ACTIVITIES

Our research this year, in collaboration with LLNL and LBNL, enabled us to rank a number of material development strategies for sorbents and metal hydrides for their potential to meet DOE targets. The results of these studies were published [1, 2] and form the basis for the second phase of HyMARC, which commences in FY 2019. HyMARC will be reorganized in Phase 2 to incorporate three additional national laboratories (National Renewable Energy Laboratory, Pacific Northwest National Laboratory, and SLAC National Accelerator Laboratory), plus the National Institute of Standards and Technology Center for Neutron Research, with new research concentrated within specific “focus areas” that are the outgrowth of the research conducted in Phase 1. SNL will lead the overall effort on metal hydrides, including focus areas concentrating on atomistic simulations, experimental measurements of metal hydride thermodynamics, surfaces and solid-solid interfaces, additives, nanoscaling, and machine learning.

SPECIAL RECOGNITIONS AND AWARDS/PATENTS ISSUED

1. V. Stavila and L.E. Klebanoff, “Ternary borides and borohydrides for hydrogen storage and method of synthesis,” U.S. Patent Application 15/812,254, filed on November 14, 2017.
2. V.N. Stavila and L.E. Klebanoff, “Nanostructured Metal Amides and Nitrides for Hydrogen Storage,” U.S. Patent No 10,000, 377 B1, issued June 19, 2018.
3. J.J. Urban, A.M. Ruminski, E.S. Cho, R. Bardhan, A. Brand, B.C. Wood, T.W. Heo, P.T. Shea, S. Kang, and X. Zhou, “Hierarchically Controlled Inside-Out Doping of Mg Nanocomposites for Moderate Temperature Hydrogen Storage,” U.S. Patent #15/870,272, 2018.

FY 2018 PUBLICATIONS/PRESENTATIONS

Publications

1. X. Zhou, T.W. Heo, B.C. Wood, V. Stavila, S. Kang, M.D. Allendorf, “Temperature- and composition-dependent hydrogen diffusivity in palladium from statistically-averaged molecular dynamics,” *Scripta Mater.* 149 (2018): 103.
2. M. Dimitrievska, P. Shea, K.E. Kweon, M. Bercx, J.B. Varley, W.S. Tang, A.V. Skripov, V. Stavila, T.J. Udovic, and B.C. Wood, “Carbon incorporation and anion dynamics as synergistic drivers of ultrafast diffusion in superionic $\text{LiCB}_{11}\text{H}_{12}$ and $\text{NaCB}_{11}\text{H}_{12}$,” *Adv. Energy Mater.* 2018, 8 (2018): 1703422. DOI:10.1002/aenm.201703422.
3. W.S. Tang, M. Dimitrievska, V. Stavila, W. Zhou. H. Wu, A.A. Talin, T.J. Udovic, “Order–Disorder Transitions and Superionic Conductivity in the Sodium nido-Undeca(carba)borates,” *Chem. Mater* 29 (2017): 10496. DOI:10.1021/acs.chemmater.7b04332.
4. X.W. Zhou, T.W. Heo, B.C. Wood, V. Stavila, S. Kang, and M.D. Allendorf, “Finite-temperature behavior of PdH_x elastic constants computed by direct molecular dynamics,” *MRS Advances* 55 (2017): 3341. DOI:10.1557/adv.201.387.

5. K.G. Ray, L.E. Klebanoff, J.R.I. Lee, V. Stavila, T. W. Heo, P. Shea, A.A. Baker, S. Kang, M. Bagge-Hansen, Y.-S. Liu, J.L. White, and B.C. Wood, “Elucidating the mechanisms of MgB_2 initial hydrogenation via a combined experiment-theory study,” *Phys. Chem. Chem. Phys.* 19 (2017): 22646. DOI:10.1039/c7cp03709k.
6. M.D. Allendorf, Z. Hulvey, T. Gennett, A. Ahmed, T. Autrey, J. Camp, E.S. Cho, H. Furukawa, M. Haranczyk, M. Head-Gordon, S. Jeong, A. Karkamkar, R. Nazarov, D.J. Siegel, V. Stavila, J.J. Urban, S. P. Veccham, B.C. Wood, “An assessment of strategies for the development of solid-state adsorbents for vehicular hydrogen storage,” *Energy Environ. Sci.* 11 (2018): 2784. DOI:10.1039/C8EE01085D.
7. A. Schneemann, J.L. White, S.Y. Kang, S. Jeong, L.F. Wan, E.S. Cho, T.W. Heo, D. Prendergast, J.J. Urban, B.C. Wood, M.D. Allendorf, V. Stavila, “Nanostructured Metal Hydrides for Hydrogen Storage,” *Chem. Rev.* DOI:10.1021/acs.chemrev.8b00313.
8. C.L. Carr, W. Jayawardana, H. Zou, J.L. White, F. El Gabaly, M.S. Conradi, V. Stavila, M.D. Allendorf, E.H. Majzoub, “Anomalous H_2 Desorption Rate of NaAlH_4 Confined in Nitrogen-Doped Nanoporous Carbon Frameworks,” *Chem. Mater.* 30 (2018): 2930. DOI: 10.1021/acs.chemmater.8b00305.
9. S.R.H. Jensen, M. Paskevicius, B.R.S. Hanse, A.S. Jakobsen, K.T. Moller, J.L. White, M.D. Allendorf, V. Stavila, J. Skibsted, T.R. Jensen, “Hydrogenation properties of lithium and sodium hydride – *closo*-borate, $[\text{B}_{10}\text{H}_{10}]^{2-}$ and $[\text{B}_{12}\text{H}_{12}]^{2-}$, composites,” *Phys. Chem. Chem. Phys.* 20 (2018): 16266. DOI:10.1039/C7CP07776A.
10. S. Kang, L.E. Klebanoff, A.A. Baker, D.F. Cowgill, V. Stavila, J.R.I. Lee, M.H. Nielsen, K.G. Ray, Y.-S. Liu and B.C. Wood, “Assessing the Reactivity of TiCl_3 and TiF_3 with Hydrogen,” *Int. J. Hydrogen Energy* 43 (2018): 14507.
11. C.L. Carr, W. Jayawardana, H.Y. Zou, J.L. White, F. El Gabaly, M.S. Conradi, V. Stavila, M.D. Allendorf, E.H. Majzoub, “Anomalous H_2 Desorption Rate of NaAlH_4 Confined in Nitrogen-Doped Nanoporous Carbon Frameworks,” *Chem. Mater.* 3 (2018): 2930.
12. J. Camp, V. Stavila, M.D. Allendorf, D. Prendergast, M. Haranczyk, “Critical Factors in Computational Characterization of Hydrogen Storage in Metal-Organic Frameworks,” *J. Phys. Chem. C* 122 (2018): 18957.
13. M. Dimitrievska, V. Stavila, A.V. Soloninin, R.V. Skoryunov, O.A. Babanova, H. Wu, W. Zhou, W.S. Tang, A. Faraone, J.D. Tarver, B.A. Trump, A.V. Skripov, T.J. Udovic, “Nature of Decahydro-*closo*-decaborate Anion Reorientations in an Ordered Alkali-Metal Salt: $\text{Rb}_2\text{B}_{10}\text{H}_{10}$,” *J. Phys. Chem. C* 122 (2018): 15198.
14. G. Melaet, V. Stavila, L. Klebanoff, G.A. Somorjai, “The effect of aluminum and platinum additives on hydrogen adsorption on mesoporous silicates,” *Phys. Chem. Chem. Phys.* 20 (2018): 12075.
15. E.S. Cho, A.M. Ruminski, Y.-S. Liu, P.T. Shea, S. Kang, E.W. Zaia, J.Y. Park, Y.-D. Chuang, X. Zhou, T.W. Heo, J. Guo, B.C. Wood, and J.J. Urban, “Hierarchically controlled inside-out doping of Mg nanocomposites for moderate temperature hydrogen storage,” *Adv. Funct. Mater.* 27 (2017): 1704316.
16. W.A. Braunecker, K.E. Hurst, K.G. Ray, Z.R. Owczarczyk, M. Martinez, N. Leick, A. Kuehlen, A. Sellinger, and J.C. Johnson, “Phenyl/Perfluorophenyl Stacking Interactions Enhance Structural Order in Two-Dimensional Covalent Organic Frameworks,” *Crystal Growth & Design* 18 (2018): 4160.

Presentations

32 presentations (1 keynote and 20 invited) at national and international conferences and symposia were presented over the past 12 months.

REFERENCES

1. M.D. Allendorf, Z. Hulvey, T. Gennett, A. Ahmed, T. Autrey, J. Camp, E.S. Cho, H. Furukawa, M. Haranczyk, M. Head-Gordon, S. Jeong, A. Karkamkar, R. Nazarov, D.J. Siegel, V. Stavila, J.J. Urban,

- S.P. Veccham, B.C. Wood, “An assessment of strategies for the development of solid-state adsorbents for vehicular hydrogen storage,” *Energy Environ. Sci.* 11 (2018): 2784. DOI:10.1039/C8EE01085D.
2. A. Schneemann, J.L. White, S.Y. Kang, S. Jeong, L.F. Wan, E.S. Cho, T.W. Heo, D. Prendergast, J.J. Urban, B.C. Wood, M.D. Allendorf, V. Stavila, “Nanostructured Metal Hydrides for Hydrogen Storage,” *Chem. Rev.* DOI:10.1021/acs.chemrev.8b00313.

HySCORE: Hydrogen Storage Characterization and Optimization Research Effort

Thomas Gennett (Primary Contact), Philip Parilla, Katherine Hurst, Madison Martinez; postdocs: Noemi Leick, Sarah Shulda, Jacob Tarver (NIST), Robert Bell, Mirjana Dimitrievska (NIST), Craig Brown (NIST)
National Renewable Energy Laboratory
15013 Denver West Parkway
Golden, CO 80401
Phone: (303) 384-6628
Email: thomas.gennett@nrel.gov

Jeffrey R. Long, Martin Head-Gordon
Lawrence Berkeley National Laboratory
1 Cyclotron Rd
Berkeley, CA 94720
Phone: (510) 642-0860
Email: jrlong@lbl.gov

Tom Autrey, Mark Bowden, Abhi Karkamkar, Bojana Ginovska, Iffat Nayyar; graduate students: Phuong Nguyen, Sunil Shrestha
Pacific Northwest National Laboratory
902 Battelle Blvd
Richland, WA 99354
Phone: 509-375-3792
Email: tom.autrey@pnnl.gov

DOE Manager: Jesse Adams
Phone: (720) 356-1421
Email: Jesse.Adams@ee.doe.gov

Project Start Date: October 1, 2015
Project End Date: Project continuation and direction determined annually by DOE

- Unravel complex phenomena, guide experimental work, and accelerate progress.
- Develop *in situ* infrared spectroscopy as a tool for characterizing emerging hydrogen storage materials that may allow for a driving range greater than 300 miles.
- Seek materials with the potential for meeting the DOE targets of reversible uptake.
- Validate new concepts for hydrogen storage mechanisms in adsorbents.
- Provide accurate computational modeling for hydrogen adsorbed in porous materials.
- Develop a series of advanced characterization tools that allows for rapid advancement and in-depth understanding of next-generation hydrogen storage materials.
- Develop a hydrogen storage material with a total materials-based capacity of >45 g/L above 150 K, that is possible with hydrogen overpressures <100 bar and reversible for multiple cycles.
- Optimize thermal management in hydrogen storage systems by the incorporation of unique phase-change materials.
- Demonstrate the importance of computational methods in developing and understanding of next-generation hydrogen storage materials.

Overall Objectives

- Advance the core competencies of the DOE Fuel Cell Technologies Office (FCTO) program as related to the characterization, evaluation, qualification, and validation of next-generation and current hydrogen storage materials.
- Benchmarking theory:
 - Couple theory with experiment to benchmark and validate the computational predictions (Hydrogen Materials Advanced Research Consortium [HyMARC] collaboration).

Fiscal Year (FY) 2018 Objectives

- Integrate the HySCORE and HyMARC programs to a cohesive, synergistic collaborative group.
- Develop and validate a cryo-PCT (pressure, composition, temperature) system for hydrogen sorption measurements from 40–303 K and up to 150 bar.
- Devise a methodology for the diffuse reflectance infrared Fourier transform spectroscopy (DRIFTS) measurements, allowing us to extract the thermodynamic parameters of hydrogen binding in complicated systems.

- Assist seedling projects with PCT, thermal conductivity, thermally programmed desorption (TPD), thermogravimetric analysis, and DRIFTS, and help them meet their go/no-go metrics.
- Develop international accepted protocol for determination of volumetric capacities.
- Validate samples for hydrogen storage capabilities as determined by DOE.
- Develop and characterize materials with validated coordinately unsaturated metal centers, and/or advanced hydrides and/or framework and/or templated materials within the hydrogen storage matrix that result in volumetric capacities in excess of 45 g/L, targeted enthalpies in the ideal range of 15–20 kJ/mol, acceptable gravimetric capacities, and the ability to deliver on-demand hydrogen at an appropriate rate and pressure for hydrogen fuel cell vehicles at temperatures from 150–225 K and initial overpressure <100 bar.
- Research and development of metal-organic framework (MOF) materials with high volumetric and gravimetric hydrogen capacities.

Technical Barriers

This project addresses the following technical barriers from the Hydrogen Storage section of the Fuel Cell Technologies Office Multi-Year Research, Development, and Demonstration Plan¹:

- (A) System weight and volume
- (B) System cost
- (E) Charging/discharging rates
- (O) Lack of understanding of hydrogen physisorption and chemisorption
- (P) Reproducibility of performance.

Technical Targets

This project is conducting validation studies of various framework materials, sorbents, hydrides, and model compounds. Concurrently, the team

also is developing new characterization tools for the rapid enhancement of materials development. Insights gained from these studies will be applied toward the design and synthesis of hydrogen storage materials that meet the following DOE onboard 2020 automotive hydrogen storage targets.

- 1.5 kWh/kg system (4.5 wt% hydrogen)
- 1.0 kWh/L system (0.030 kg hydrogen/L)
- Cost of \$10/kWh (\$333/kg H₂ stored)
- An onboard efficiency of 90% and minimum delivery pressure of 5 bar
- Total refuel time of 3–5 min.

FY 2018 Accomplishments

National Renewable Energy Laboratory (NREL)

- Installed and validated performance of the variable-temperature PCT apparatus (Performance Evaluation and Measurement Plan [PEMP] Milestone). NREL completed the aforementioned milestone for isosteric heat determination and, in the process, discovered several issues that need addressing to inform the interpretation of such determinations and to do so accurately and without bias.
- Determined the ability to utilize vibrational phonons to kinetically control the release of hydrogen from a series of C2N framework materials.
- Established/validated multiple samples from seedling projects, with two “go” decisions on projects moving forward.
- Established that in volumetric determination of hydrogen sorption, the major systematic errors lie in the determination of void volumes and packing densities—achieved through a 15-lab interlaboratory collaboration.
- Established a new collaborative partner, Michael Toney at SLAC National Accelerator Laboratory, and placed an NREL postdoc on-site at SLAC in August 2018.

¹ <https://www.energy.gov/eere/fuelcells/downloads/fuel-cell-technologies-office-multi-year-research-development-and-22>

- Added capability: Supercritical CO₂ Extraction for Purification of Porous Materials.
 - Many of the highly porous sorbents have suffered from solvents clogging pores. NREL installed a supercritical CO₂ extractor that assists in the removal of solvent molecules prior to any treatment (degassing) for TPD, Brunauer-Emmett-Teller, or PCT measurements.
 - The procedure still needs to be optimized for different materials and different solvents to ensure that the cleaning process successfully removes the impurities.
- Coordinated with Sandia National Laboratories and DOE to author and publish a perspective on the use of hydrogen storage sorbents for transportation applications.

Lawrence Berkeley National Laboratory (LBNL)

- Installed *in situ* infrared spectrometer and validated the performance of the instrument at 15–373 K and 0–100 bar.
 - Installed variable temperature capability on the DRIFTS instrument.
 - Validated the variable-temperature infrared (VTIR) method for determining

thermodynamics of adsorption by comparison with published materials.

- Extensively studied the thermodynamics of H₂ binding in Cu^I-MFU-4l using *in situ* DRIFTS.
- Targeted the synthesis of a room-temperature physisorption hydrogen storage material with a high density of unsaturated metal sites.
 - Synthesized a pyridinyl phenol-containing variant of UiO-67 and metalated with Cu(I) and Li(I).
 - Synthesized two new frameworks of the M₂(dotpdc) (MOF-374) structure type containing *N,N*-chelating groups for metalation.
 - Synthesized a new V(II) framework that binds hydrogen with an optimal adsorption enthalpy for ambient-temperature storage.
- Determined a computational protocol for binding energy computation and analysis, infrared spectra, and enthalpy-entropy relationship for sorbent materials.
- Benchmarked a dataset tailored for hydrogen storage to identify cheap, high-performance density functionals.

INTRODUCTION

NREL

This collaboration is predicated on a synergistic approach to further validate hydrogen storage concepts and develop the key core capabilities necessary for accurate evaluation of hydrogen storage materials capacity, kinetics, and sorption/desorption physio-chemical processes. The overall approach involves collaborative experimental and modeling efforts. We are validating concepts and utilizing core capabilities to rapidly define, model, synthesize, and characterize the appropriate materials necessary for achieving the vehicular hydrogen storage goals set forth by DOE. The approach is multifaceted to mitigate risk and ensure success as we bridge the gap between physisorption and chemisorption to provide the basis for a new generation of hydrogen storage materials technologies.

LBNL

Porous framework materials, such as MOFs, represent several possible paths forward toward a hydrogen storage adsorbent that can, at minimum, exceed the capabilities of current high-pressure onboard storage tanks and ultimately meet the system storage targets set by the DOE. However, the binding energies and volumetric capacities for hydrogen uptake are still not within the required range. Therefore, the critical objective with adsorbents is to design and synthesize porous framework materials replete with strong hydrogen binding sites that are suitable for the room-temperature hydrogen adsorption and desorption.

Our work to develop hydrogen storage adsorbent materials is performed in collaboration with NREL, Pacific Northwest National Laboratory (PNNL), and the National Institute of Standards and Technology (NIST). Key activities at LBNL include synthesis of frameworks that adsorb hydrogen with an enthalpy (isosteric heat of adsorption Q_{st}) in the optimal range of -15 to -25 kJ/mol, preparation of frameworks with open metal sites that adsorb more than two hydrogen molecules, and variable-temperature DRIFTS analysis to collect thermodynamic parameters for hydrogen adsorption, as well as benchmarking density functional theory functionals for hydrogen storage in MOFs.

PNNL

The Hydrogen Storage subprogram supports research and development of technologies to lower the cost of near-term physical storage options and longer-term material-based hydrogen storage approaches. The program conducts R&D of low-pressure, materials-based technologies and innovative approaches to increase storage potential and broaden the range of commercial applications for hydrogen. These advanced-materials activities focus on development of core capabilities designed to enable the development of novel materials with the potential to store hydrogen near room temperature, at low-to-moderate pressures, and at energy densities greater than either liquid or compressed hydrogen on a systems basis. Key activities include improving the energetics, temperature, and rates of hydrogen release. Advanced concepts include high-capacity metal hydrides, chemical hydrogen storage materials, and hydrogen sorbent materials, as well as novel material synthesis processes. The overarching goal of the FCTO Hydrogen Storage subprogram is to develop and demonstrate viable hydrogen storage technologies for transportation, stationary, portable power, and specialty vehicle applications (e.g., material handling equipment, airport ground support equipment), with a key goal of enabling >300-mile driving range across all light-duty vehicle platforms, without reducing vehicle performance or passenger cargo space.

APPROACH

NREL

Our approach in FY 2018 included efforts to develop state-of-the-art characterization techniques for hydrogen storage materials including advanced thermal conductivity, PCT, cyclotron X-ray techniques, and neutron-based spectroscopic techniques. Through theoretical-experimental iterations, we focused on addressing questions and validating recent concepts and mechanisms related to the materials-based hydrogen storage community including:

- How do multiple hydrogen molecules adsorb on an unsaturated metal center within a sorbent?
- Is it possible to enhance the kinetics of hydride formation with additives?
- Can we control the desorption temperature through the manipulation of dynamic materials?
- How can one alter/increase the hydrogen binding energies for physisorption in non-crystalline and crystalline sorbents?

Our team directly interacts with and supports the entire HyMARC core team, as well as the HyMARC seedling projects.

LBNL

To enhance hydrogen storage capacity, MOFs with a greater density of strong binding sites on the pore surface need to be developed. Our approach incorporates organic linkers with coordinating functionalities into framework materials, which will be used to append extra-framework cations to the pore wall. Taking advantage of the framework structure to immobilize these cations in the void volume of the material, low-coordinate metals capable of binding multiple H₂ molecules at each site were targeted. Our work in FY 2018 includes optimizing routes for metalation and activation to achieve a high density of metal cations bearing multiple coordination sites for H₂ binding. In parallel with synthetic efforts, *in situ* VTIR measurements are carried out to evaluate the thermodynamic properties of framework materials. Indeed, infrared spectroscopy is a powerful technique that can be used to gain site-specific adsorption information through the spectroscopic observation of vibrational modes associated with adsorbed hydrogen. In the theory work, we began benchmarking of density functionals for hydrogen storage in porous materials in order to identify inexpensive, high-performance density functionals.

PNNL

PNNL is developing advanced characterization capabilities to provide critical approaches to validate theories and test concepts proposed in the development of new details into the chemical and physical properties of hydrogen storage materials.

- Variable-pressure magic angle spinning (MAS) nuclear magnetic resonance (NMR): Variable-pressure (1–200 bar), variable temperature (298–473 K), *in situ* multi-nuclear solid state MAS NMR is being developed to identify key intermediates in the release and uptake of hydrogen in complex metal hydrides to validate claims that additives control selectivity and enhance reversibility.
- Low-temperature solid-state NMR: Low temperature (to 5 K) solid-state ¹H NMR is being developed to measure the enthalpy of adsorption of H₂ to high-surface-area storage materials and provide the ability to validate the concept that more than one H₂ molecule can bind to a metal site on a high surface amorphous material.
- Variable-pressure liquid NMR: Variable-pressure (1–100 bar), variable-temperature (250–350 K), multi-nuclear liquid NMR is available to measure key intermediates, kinetics, and thermodynamics of hydrogen release and uptake in liquid carriers.
- Variable-pressure calorimetry: Variable-pressure (1–20 bar), variable-temperature (298–353 K) reaction calorimetry is being developed to measure kinetics and enthalpies of H₂ uptake in liquid and solid stores to benchmark and validate computational predictions of binding enthalpies in liquid carriers.

In FY 2018 our work focused on efforts to develop advanced characterization techniques for hydrogen storage materials with special emphasis on calorimetry and *in situ* NMR spectroscopy. We worked toward developing new capabilities to validate theories and novel concepts proposed by the research community; a parallel research effort on materials evaluation complements the characterization capability development. Through a

theoretical/experimental interaction, our research focus was (1) determination of the thermodynamics of H₂ uptake and release from liquid carriers (i.e., phenol, formic acid) as part of a collaboration with Dr. Karsten Mueller (Erlangen University) and Dr. Teng He (DICP), (2) binding energies of H₂ to B-doped carbon when B is located on the edge of the coronene, and (3) thermodynamics of the recycling of solvent-free Mg(B₃H₈)₂ and Mg(BH₄)₂ as part of a collaboration with Prof. Hans Hagemann (University of Geneva). In addition, we were able to assist a number of HyMARC seedling projects in their characterization efforts using NMR, X-ray diffraction, and transmission electron microscopy spectroscopies.

RESULTS

NREL

This report describes the major accomplishment of meeting the DOE-PEMP milestone using the variable-temperature PCT apparatus at NREL. The sorbent material chosen was a commercially available activated carbon known as Norit ROW 0.8, which is in a pelletized form and has been used by NREL as a standard material for testing PCT instrumentation and for interlaboratory comparisons of hydrogen capacity [1–2]. After degassing, the final mass for the sample was 1.404 g, which provided excellent signal to noise even at the higher temperatures. A series of six different temperatures were chosen at which to measure the isotherms up to pressures of ~100 bar. All isotherms consist of at least one full cycle (adsorption and desorption), and several had more. The six temperatures were grouped into three pairs so that different methods of determining the isosteric heats (Q_{st}) could be tested; the three pairs are (77 K, 87 K), (100 K, 110 K), and (273 K, 303 K). The resulting isotherms are shown in Figure 1.

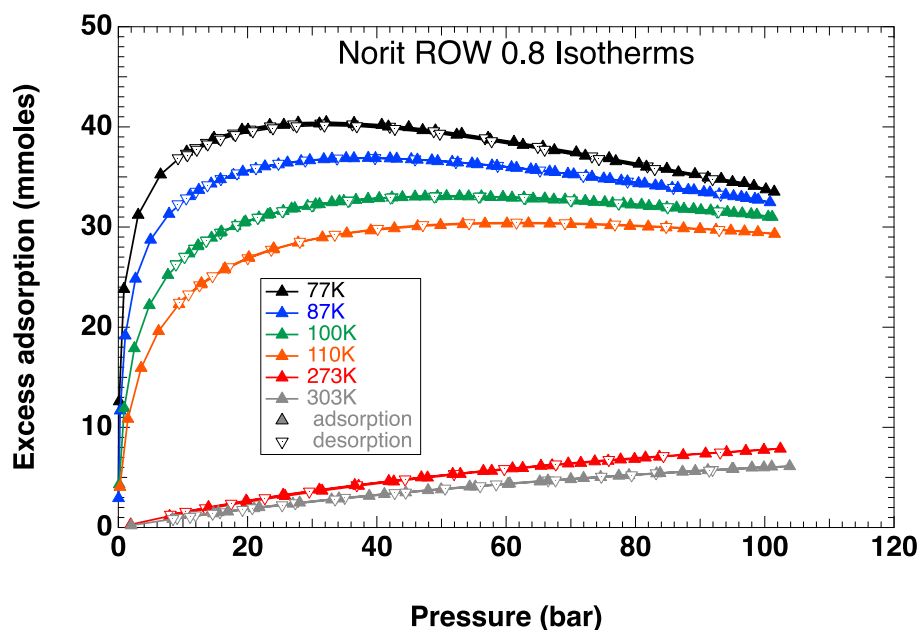


Figure 1. The isotherms obtained and used for the isosteric heat calculations on the new variable-temperature PCT apparatus

Isosteric heats can be calculated in various ways. The main definition often found in the literature is:

$$q_{st} = RT^2 \left(\frac{\partial \ln(P)}{\partial T} \right)_n = -R \left(\frac{\partial \ln(P)}{\partial \left(\frac{1}{T} \right)} \right)_n \quad (1)$$

Where q_{st} is the isosteric heat, R is the universal gas constant, T is the temperature, and P is the pressure. The n subscript indicates the adsorbed moles is held constant. A discretized version for two isotherms taken at similar temperatures, T_1 and T_2 , is:

$$q_{st} = RT_1T_2 \left(\frac{\ln(P_2/P_1)}{T_2 - T_1} \right)_n \quad (2)$$

Where again the n indicates that the pressures are at the same mole loading. Probably the most robust technique is to plot $\ln(P)$ versus $1/T$ for several temperatures to check for linearity and to measure the slope of the line, which is equal to $-q_{st}/R$ [3–4].

Because any isosteric calculations must be performed at equal mole loading, keeping the isotherms in moles is desirable. (By convention, with the PCTPro reporting standards, moles are reported as *atomic* hydrogen, not *molecular* hydrogen.) For the 77 K data, this is maximum near 30 bar and corresponds to approximately 2.82 wt% and is consistent with previous NREL measurements and the recently completed interlaboratory comparison. Also, because of the requirement for equal mole loading for the calculation, a robust method is needed to interpolate between the actual data points of the isotherm. For the very steep rise at low pressures and low temperatures, this is non-trivial. A linear interpolation method was tried and proved to be inadequately accurate. Instead, the data was fit with a Sips isotherm (Equation 3; also known as a Langmuir-Freundlich) [5–6].

$$n_{ad} = \frac{n_0(bP)^{\frac{1}{m}}}{1 + (bP)^{\frac{1}{m}}} \quad (3)$$

Where n_{ad} is the amount adsorbed as a function of pressure, P , n_0 is the saturation adsorption amount, m is the exponent factor, and b is a parameter that depends on the temperature and other factors corresponding to the physical processes of the adsorption sites. Because this is a strictly monotonically increasing function, only the initial part of isotherms was fit for those isotherms that were not monotonically increasing (i.e., the low-temperature data). An example of that fit is given in Figure 2 for the 110 K data.

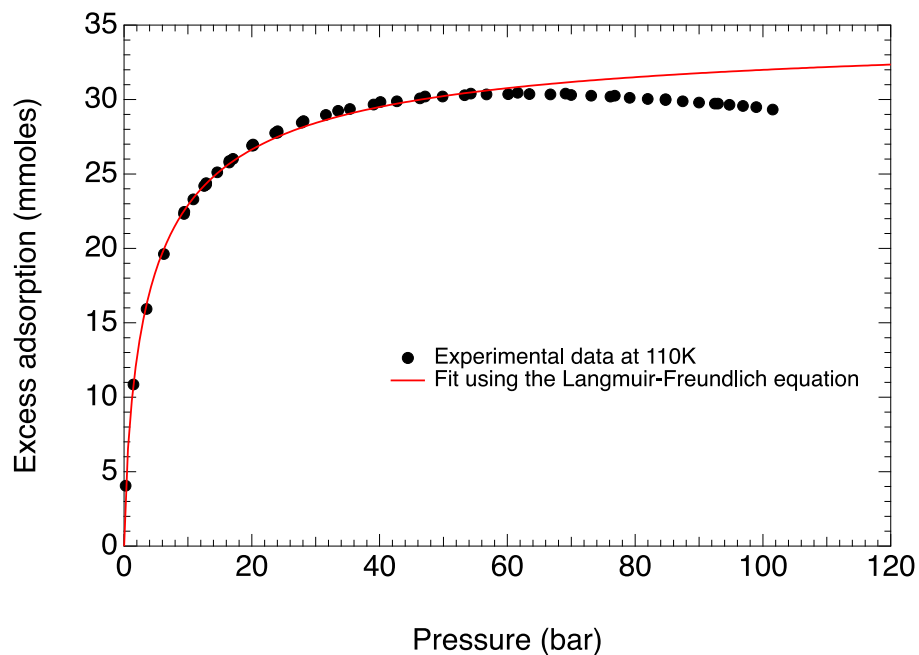


Figure 2. An example of how the isotherms were fit using the Langmuir-Freundlich isotherm function model

These fits can be inverted (i.e., solved for the pressure, P), which then becomes pressure as a function of moles adsorbed at a given temperature.

$$P = \frac{1}{b} \left(\frac{n}{n_0 - n} \right)^m \quad (4)$$

Using these inverted fit functions, the $\ln(P)$ versus $1/T$ plot at various loadings can then be made and linear fits can be performed to get the slopes yielding the isosteric heats. Figure 3 shows the result of this plot and fits for a subset of the data.

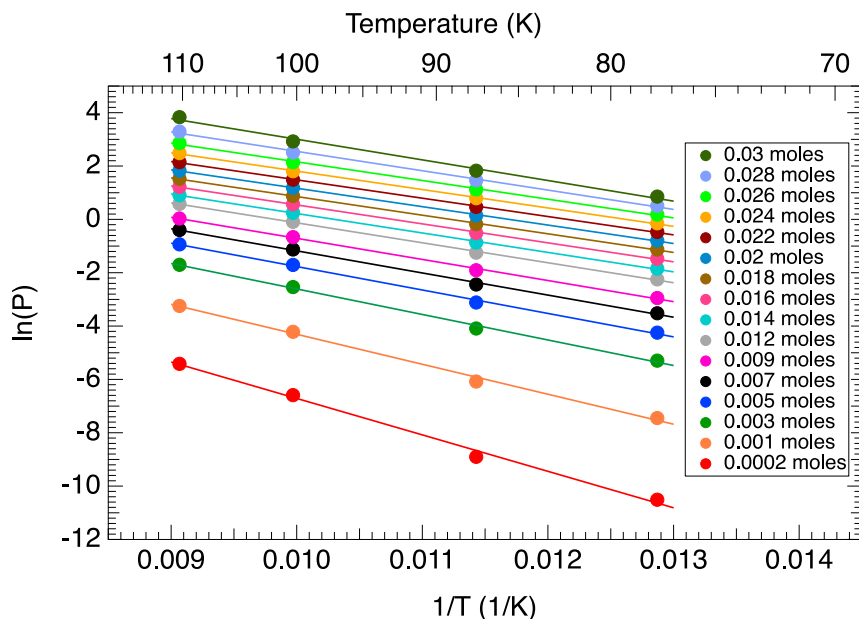


Figure 3. An example of how the isosteric heats at various mole loadings were determined from the slope of lines fitted with the $\ln(P)$ versus $1/T$ data

It can be seen from the data that a linear fit is a reasonable model at these low temperatures. While most of the linear fits are roughly parallel, and thus indicate similar Q_{st} , at the lower mole loadings the slopes are increasingly negative and indicate higher Q_{st} . This is all summarized in Figure 4, which shows the Q_{st} derived from the linear fits as a function of mole loadings again from the low-temperature data. There is a relatively constant region near 6 kJ/mole, and this agrees reasonably well with a measurement on Norit ROW 0.8 that found an average of 5 kJ/mole over surface coverages between 36% to 82% [3]. For the NREL data at low-mole loadings, the Q_{st} approaches 11 kJ/mole. There are two possible reasons for this. *First*, in the low-mole region, the isotherms at low temperature are very steep and difficult to model, and small errors in this modeling can lead to large errors in the calculation. In fact, the aforementioned literature reference deliberately avoided reporting their data in this region precisely because of this issue [3]. What is needed to get accurate low-mole estimates of the Q_{st} is to obtain a larger number of data points in the fast-rising part of the isotherm. *Second*, it is not unreasonable to expect that, for a heterogeneous adsorption surface, the stronger adsorption sites will be occupied first and so could truly represent the higher energy sites. There is also an upturn in calculated energy at high loadings. This is a well-known effect that results from the fact that the measured isotherms actually are excess capacity isotherms, not the absolute isotherms that are required for the true isosteric determination [4, 7]. Because only excess isotherms can be measured in the real world, additional modeling is needed to attempt to compensate for this; this modeling is outside the scope of this report.

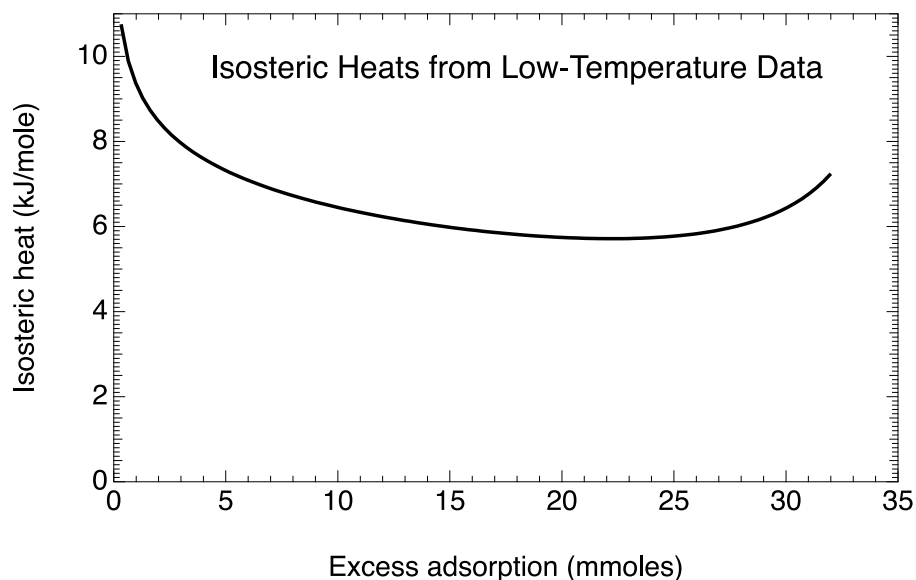


Figure 4. The isosteric data versus mole loadings from all the fitted lines of the $\ln(P)$ versus $1/T$ data. See text for detailed discussion.

To briefly summarize, NREL has successfully completed the milestone to measure the isosteric heats and has achieved good agreement with a previous measurement from the literature. During the effort to complete this milestone, NREL has discovered several issues in both measuring the data and analyzing the data, which is work continuing into FY 2019.

NIST (as part of NREL)

Structural and Dynamical Trends in the Alkali-Metal Silanides ($MSiH_3$, $M = K, Rb, Cs$) and the Potential Effect on their Hydrogen Storage Properties

We worked on elucidating the dynamical details of both the α - and β -phases of alkali-metal silanides ($MSiH_3$, $M = K, Rb, Cs$) to investigate their potential use for hydrogen storage applications. Characterization of the structures and possible SiH_3^- reorientational dynamics of these compounds was performed using various neutron scattering techniques, including neutron powder diffraction, neutron vibrational spectroscopy, neutron scattering fixed window scans, and quasielastic neutron scattering measurements (QENS). The results show that the phase transition leads to dynamical changes corresponding to the onset of rapid reorientational motions of the pyramidal SiH_3^- ions. An unusual nature of the anion dynamical transformation was observed upon transitioning between the α -phase and β -phase. Based on the dynamical measurements and calculations from QENS spectra, a phase diagram was constructed for $CsSiH_3$ presenting an evolution of different phases with the temperature. Besides being of considerable fundamental interest, these results provide better understanding of the nature of the SiH_3^- orientational mobility in the disordered and ordered phases, as well as give more detailed insights into the origin of these materials' favorable hydrogen storage properties. This work was submitted and recently published in: M. Dimitrievska, "Tracking the Progression of Anion Reorientational Behavior between α -phase and β -phase Alkali-Metal Silanides by Quasielastic Neutron Scattering," *J. Phys. Chem. C* 122, no. 42 (2018): 23985–23997.

LBNL

Materials Synthesis

Synthetic efforts at LBNL focused on the continued research into and synthesis of compounds that have the potential to bind multiple hydrogen molecules to a single metal center. One of the typical examples is synthesis of a pyridinyl phenol-containing variant of UiO-67, followed by the metalation with various metal cations.

Specifically, a derivative of UiO-67 [$\text{Zr}_6\text{O}_4(\text{OH})_4(\text{PhOHpydc})_6$; $\text{H}_2\text{PhOHpydc} = 6\text{-(4-carboxy-2-hydroxyphenyl)nicotinic acid}$] that contains free pyridine and phenol groups on the linker capable of acting as a chelating binding site was successfully synthesized (Figure 5). The material shows high crystallinity after desolvation of the framework with a high Langmuir surface area of $2,750 \text{ m}^2/\text{g}$. A variety of solvents containing mesitylcopper(I) or *n*-butyllithium were utilized for framework metalation. From inductively coupled plasma–optical emission spectrometry analysis, maximum Cu and Li loadings are estimated to be 0.1 and 4.2 per formula unit, respectively. Although the Cu-loaded framework showed a slight increase in low-pressure hydrogen uptake, Li samples showed decreased H_2 uptakes compared to the pristine framework, which is likely due to incomplete desolvation of the metalated framework even after thermal treatment *in vacuo*. Investigation of the optimal activation condition to prepare metalated frameworks with reasonable porosity is now in progress.

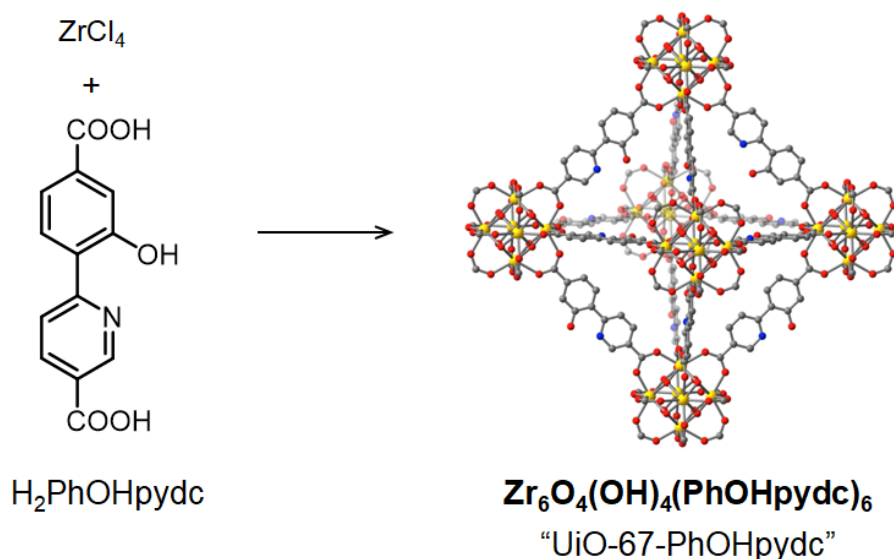


Figure 5. Synthesis and structure of UiO-67-PhOHpydc. Atom colors: C, gray; O, red; N, blue; Zr yellow; all hydrogen atoms are omitted to clarify.

Correlation Between Adsorption Enthalpy and Entropy

A target of -22 to -25 kJ/mol for the H_2 binding enthalpies has often been cited as optimal for physisorption materials [8]. However, this target assumes a strict enthalpy-entropy relation in order to arrive at the final ΔG° of adsorption. Theoretically, all enthalpy-entropy combinations giving rise to the same ΔG° will yield the same usable capacity under a set of storage conditions. In other words, synthesizing a material with a smaller $-\Delta H^\circ$ and a smaller $-\Delta S^\circ$ for the same ΔG° will lead to easier heat management at no cost to capacity. It is therefore imperative that ΔS° is considered when assessing materials alongside other thermodynamic parameters, and steps should be undertaken to understand and rationally tune ΔS° in physisorption materials. In FY 2018, Cu^{I} -MFU-4l [$\text{Cu}_2\text{Zn}_3\text{Cl}_2(\text{btdd})_3$] [9] was chosen to study the correlation between adsorption enthalpy and entropy. Measurement of VTIR spectra of the framework Cu^{I} -MFU-4l under H_2 and D_2 has allowed extraction of thermodynamic parameters of H_2 binding (Figure 6). It is remarkable that while the ΔH° of adsorption is around twice that of $\text{Ni}_2(m\text{-dobdc})$, the ΔS° is lower (Table 1). This breaks the trend of enthalpy-entropy correlations observed in most physisorption materials [10], due to the unique back-bonding interaction observed in this framework between Cu^+ and H_2 , similar to those in Kubas-type molecular complexes (Figure 7).

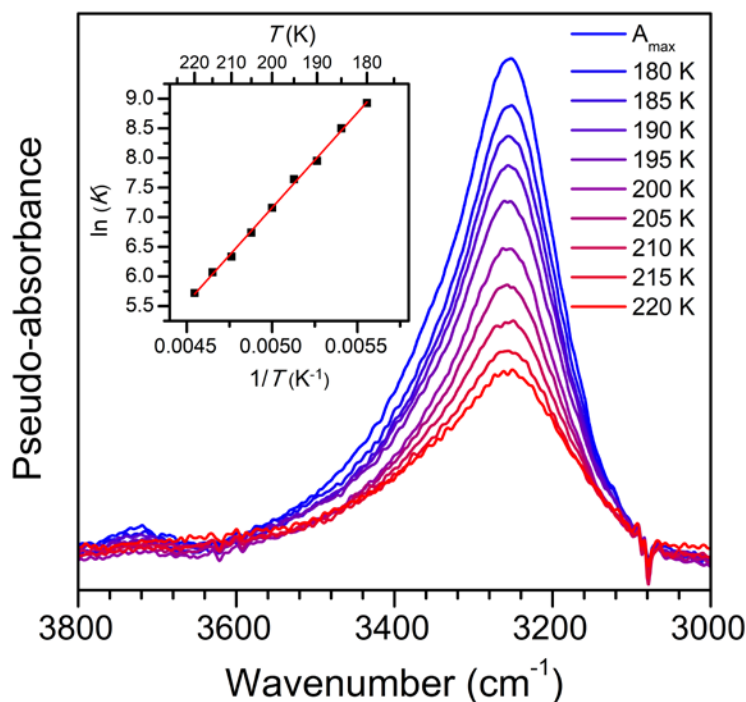


Figure 6. VTIR spectroscopy of H₂ adsorbed in Cu^I-MFU-4l. Spectra were generated by subtraction from corresponding D₂ dosed samples. Van't Hoff analysis yields a ΔH° of -26.7 kJ/mol and a ΔS° of -74 J/mol K. Cf. Ni₂(*m*-dobdc) $\Delta H^\circ = -13.6$ kJ/mol, $\Delta S^\circ = -85$ J/mol K.

Table 1. Summary of Metal Ion, Low-Pressure Excess Hydrogen Uptake, Initial Q_{st} Data, and Adsorption Enthalpy and Entropy Estimated from DRIFTS for Framework Materials Containing Open Metal Sites

MOF	Metal ion	H ₂ uptake at 77 K, 1 bar (mmol/g)	Q_{st} from isotherms (kJ/mol)	ΔH° from DRIFTS (kJ/mol)	ΔS° from DRIFTS (J/mol K)
Ni ₂ (<i>m</i> -dobdc)	Ni ²⁺	11.1	-12.3	-13.6	-85
V-MOF	V ²⁺	9.2	-21.0	-21.0	-84
Cu ^I -MFU-4l	Cu ⁺	8.1	-26.7	-33.6	-74

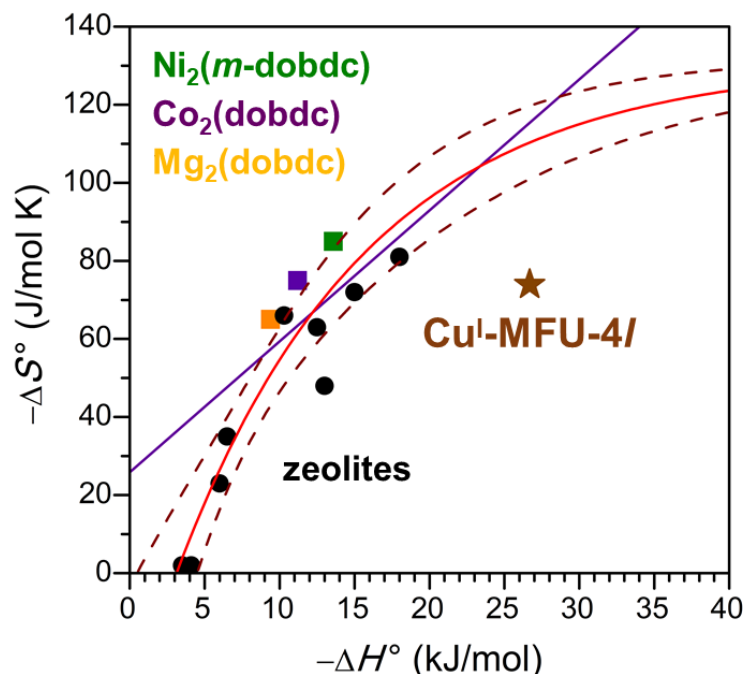


Figure 7. Thermodynamic parameters of H₂ adsorption in various sorbents. The approximate fit of enthalpy-entropy correlation for zeolites and M₂(dobdc) variants (red, 95% confidence intervals given by dark red dashed line) and optimal combinations of ΔH° and ΔS° for adsorption at 100 bar and desorption at 5 bar at 298 K (purple). Cu^I-MFU-4l represents a new class of physisorptive hydrogen adsorbents due to its unique mechanism of adsorption.

Electronic Structure Computations on Sorbents

For sorbent materials Cu^I-MFU-4l and V-MOF we have put in place a computational protocol to determine first the binding energy for small molecule adsorption, and we found significant covalent (chemi-sorbitive) character in hydrogen binding. Infrared spectra were computed to corroborate DRIFTS measurements both in terms of spectral frequencies and to validate enthalpy/entropy relationships for the hydrogen binding event in sorbent materials. The substantial expertise in energy decomposition analysis has allowed us to study quantitatively the arrested oxidative addition of hydrogen to sorbents Cu^I-MFU-4l and V-MOF, which keeps binding enthalpy in the range (20–30 kJ/mol) ideal for hydrogen storage. Possible extensions to this protocol involve incorporating periodic corrections to electronic structure, and development of sorbent-specific force-fields.

Benchmarking Density Functionals for Hydrogen Storage

We began to compile a database for benchmarking the performance of density functional binding energies of hydrogen to a binding motif against high-quality reference data. The database currently consists of metal ions, salts, and organic linkers, which serve to mimic the environment of hydrogen binding in porous sorbent frameworks like MOFs. The benchmark data was generated using coupled cluster theory extrapolated to the complete basis set limit. Around 50 density functionals were studied and their errors were characterized in terms of basis set and density functional theory quadrature grid. While the density functional ω B97M-V provides the least root mean square error (RMSE) of 1.5 kJ/mol, we recommend the significantly cheaper B97-D3(BJ), which provides a slightly increased RMSE of 1.85 kJ/mol.

PNNL

Determination of the Thermodynamics of Hydrogen Uptake and Release from Liquid Carriers (i.e., phenol, formic acid)

Hydrogen storage in formic acid: a comparison of process options. Formic acid (53 g H₂/liter) is a promising liquid storage and delivery option for hydrogen for fuel cell power applications. In this work we compare and evaluate several process options using formic acid for energy storage. Each process requires different steps, which contribute to the overall energy demand. The first step (i.e. production of formic acid) is thermodynamically unfavorable. However, the energy demand can be reduced if a formate salt is produced via a bicarbonate route instead of forming the free acid from hydrogen and carbon dioxide. This *bicarbonate/formate* approach also turns out to be comparatively more efficient in terms of hydrogen release than the formic acid route. Even though less energy efficient, catalytic decomposition of formic acid has the advantage of reaching higher volumetric power densities during hydrogen release. Efficiencies of all process options involve aqueous media and are dependent on concentration. Heating water leads to additional energy demand for hydrogen release and thus lowers the overall efficiency. Separation and purification of hydrogen contributes a minor impact to the overall energy demand. However, its effect on efficiency is not negligible. Other process options like thermal decomposition of formic acid or direct formic acid fuel cells thus far do not appear competitive. For further details, please see *Energy & Fuels* (2017), DOI:10.1021/acs.energyfuels.7b02997.

Releasing hydrogen at high pressures from ambient condition carriers: aspects for the hydrogen delivery to fueling stations. Hydrogen fueling stations require multiple stages of compression to achieve the ca. 875 bar needed to refuel hydrogen fuel cell electric vehicles to 700 bar. The physical compression equipment constitutes a large share of the total investment cost of hydrogen fueling stations. Hydrogen carriers (i.e., materials that carry either physisorbed or chemisorbed H₂) provide an opportunity to simplify hydrogen delivery because they can transport higher densities of hydrogen to the fueling station at lower pressures. We introduce the term liquid phase hydrogen carriers (LPHCs) to be inclusive of liquid carriers that may not fall under purely organic (i.e., carbon based). Some LPHCs are defined by thermodynamic properties that allow hydrogen release at elevated pressure, thus providing an opportunity to reduce the number of compressors at the fueling station. This study compares a series of LPHCs and evaluates the approach of using aqueous solutions of formic acid as an alternate approach to deliver high volumetric densities of hydrogen to fueling stations and provide a first step of compression. Formic acid can be decomposed in a reactor to hydrogen and carbon dioxide at moderate temperatures and high pressure in the presence of a suitable catalyst. While hydrogen release from most liquid carriers will provide hydrogen slightly above ambient pressure at high temperatures, hydrogen release from the decomposition of formic acid will provide hydrogen at pressures of several hundred bar. A challenge of formic acid is that the high-pressure hydrogen is accompanied by an equivalent of carbon dioxide and thus requires subsequent separation and purification operations. Nevertheless, formic acid has the advantage of being liquid, which simplifies its handling and provides a continuous supply to a release unit. Furthermore, the energy demand for hydrogen release from formic acid is lower than for most alternative hydrogen carrier materials.

Thermodynamic modification of phenol-cyclohexanol couple (ca. 6 wt%, 57 g/liter). Addition or substitution of electron-rich heteroatoms (e.g., N) for C in cycloalkanes and arenes has been shown to favorably reduce the enthalpy difference between the hydrogenated and dehydrogenated hydrogen carrier with N-ethyl carbazole as a well-studied example. Clot, Eisenstein, and Crabtree published a computational study that provided the thermodynamic parameters (ΔH , ΔS and ΔG) for H₂ release from a series of N-containing arenes. They suggested that the addition of an electron-rich N may destabilize the cycloalkane, thus reducing the reaction enthalpy for H₂ release. Teng He in Ping Chen's group at DICP has been interested in modifying the thermodynamics of hydrogen storage material by substituting an H atom with an alkaline metal atom in compounds such as phenol and aniline. Figure 8 shows the calorimetric traces for heat of hydrogenation of (a) sodium phenoxide and (b) phenol respectively to cyclohexanol in water. ΔH for hydrogenation of sodium phenoxide was measured to be -182 kJ/mol (ΔH_{exp} 60.6 kJ/mol H₂ and ΔH_{calc} 60.9 kJ/mol H₂) while ΔH for

phenol was -206 kJ/mol (ΔH_{exp} 68.7 kJ/mol H_2 and ΔH_{calc} 64.5 kJ/mol H_2). The hypothesis was that the addition of an electronegative O onto the arene would provide an electron donating group comparable to N substitution. Furthermore, substitution of an Na for the H on the HO group could increase the electron density on the carbon framework further and decrease the enthalpy of H_2 release even further.

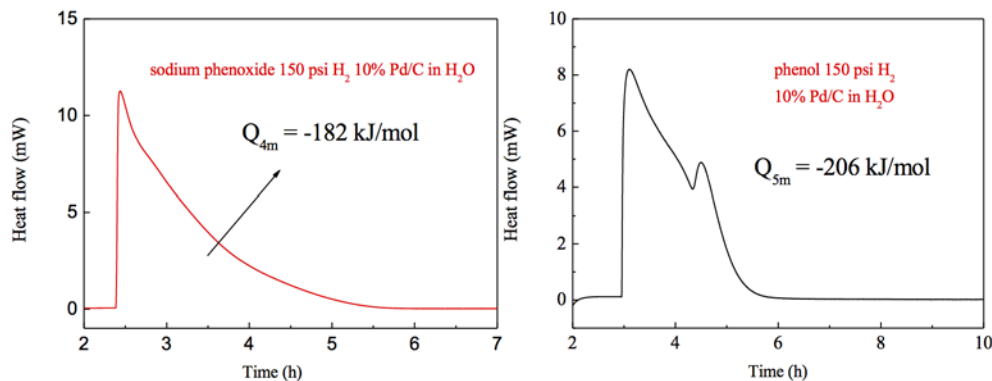


Figure 8. Calorimetric traces for heat of hydrogenation of (a) sodium phenoxide and (b) phenol respectively to cyclohexanol in water

In a related paper, Jessop and coworkers argued that there is a linear correlation between the Hammett σ (para) parameter and the enthalpy for H_2 release for a series of substituted N-substituted arenes. The more negative the Hammett σ (para) parameter, the lower the enthalpy for H_2 release. We used this hypothesis as a starting point to make predictions about the properties of phenol versus phenoxide as LPHCs in aqueous media. The results are promising and summarized below.

Binding energies of H_2 to B-doped carbon when B is located on the edge of the coronene. In addition to the previously reported binding energies of H_2 to B- and N-doped coronene model, where the doping was introduced in the central ring of the model system, we also explored possibilities of H_2 binding in cases where B is introduced at the edge (Figure 9).

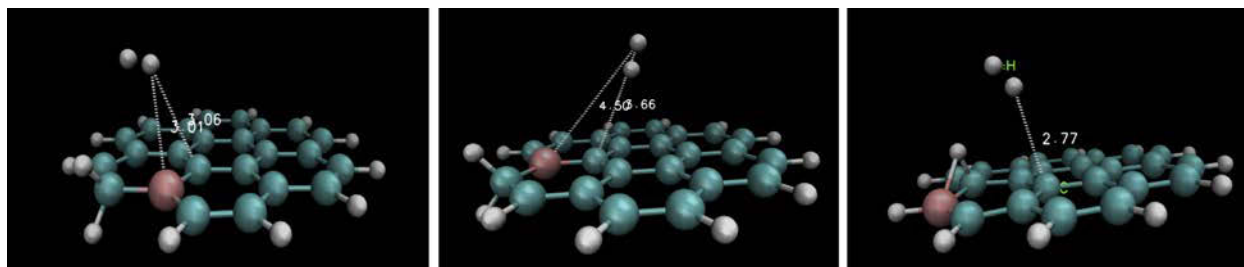


Figure 9. Image that illustrates H_2 binding in cases where B is introduced at the edge sites

As before, we used dispersion-corrected density functional theory (B3LYP+D3) level of theory, with 6-311G** basis set, using the NWChem computational package. All calculations were done in gas phase. We found that there is no improvement of the binding energy for the three different optimized stable structures, where the binding energies are in the range of 5.3 to 6.4 kJ/mol. Interestingly, when a single B atom is doped at the edge, where it is not H-terminated, the binding energy is lower than the binding of H_2 to undoped coronene, when the H_2 atom is in the vicinity of the B defect, but it is slightly stronger than coronene, when the interaction is predominantly with the carbon atoms in the center. Table 2 summarizes the binding energy of terminal B-doped coronene in comparison with previous values calculated for B inside central ring. When the B atom is H-terminated, it interacts with the H-terminal atoms on the neighboring carbon, forming an H-

bridged structure. In this case, the largest distortion from planarity is observed, and slightly enhanced binding energy.

Table 2. Binding Energies for Terminal B-Doped Coronene Compared with Previous Values Calculated for B Inside Central Ring

New values are displaced in bold italics and show no enhancement compared to non-terminal B-doped structures

System	Nomenclature	Binding Energy (kJ/mol H ₂)
C ₂₄ H ₁₂	C	6.2
B C ₂₃ H ₁₃	B	7.6
B C ₂₃ H ₁₃	<i>Bterm 1-1</i>	5.3
B C ₂₃ H ₁₃	<i>Bterm 1-2</i>	6.4
B C ₂₃ H ₁₃	<i>Bterm 2</i>	6.8
N C ₂₃ H ₁₃	N	6.7
B ₂ C ₂₂ H ₁₂	BB ortho	6.6
	BB meta	5.9
	BB para	5.6
B ₂ C ₂₂ H ₁₂	BN ortho	6.8
	BN meta	7.4
	BN para	6.9
B ₃ N ₃ C ₁₆ H ₁₂	BN cyclic	5.5

Thermodynamics of the recycling of solvent-free Mg(B₃H₈)₂ and Mg(BH₄)₂. Given the experimental challenge to make solvent-free Mg(B₃H₈)₂, we proceeded to perform experiments with the tetrahydrofuran (THF) adduct in collaboration with the University of Hawaii. We found that the THF adduct could be “reduced” to regenerate the corresponding Mg(BH₄)₂—a promising result that suggests calorimetry experiments could provide insight into the thermodynamics. We reported the result in previous quarterlies that provided an estimate of 70(10) kJ/mol H₂ for the difference between the THF adduct of B₃H₈ and the corresponding BH₄. This value was “high,” but far below the computational result suggesting 150 kJ/mol (for the solvent-free reaction). The result suggested that THF substantially stabilized the B₃H₈ intermediate, or the calculations were highly inaccurate, a troubling result.

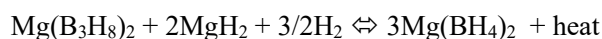
We considered two further options to help resolve the discrepancy. The calculations were performed on a “calculated” structure as no experimental structural insight is available for the Mg triborane—but an offset of 80 kJ/mol H₂ is unsatisfactory. Alternatively, the THF (i.e., a Lewis base) provided substantial stabilization compared to the solvent-free polyhedral boranes.

The results from the calorimetry experiments were not unambiguous. We were able to determine a lower limit for the hydrogenation reaction of -100 kJ/mol H₂. Notably this is greater than the hydrogenation of the THF adduct we reported previously, ca. -70 kJ/mol of H₂, but still far lower than the enthalpy predicted by theory, ca. -150 kJ/mol. We were able to provide a lower limit due to the observation that the solvent-free Mg(B₃H₈)₂ compound melts at ~80°C. In the presence of MgH₂ and H₂, the major product is the expected Mg(BH₄)₂. In the absence of MgH₂ and H₂, the major product is the closoborane, B₁₂H₁₂. We can only assign a lower limit given that the melting should generate an endotherm that reduces the magnitude of the exothermic for hydrogenation. However, several key takeaways were obtained:

- The solvent-free Mg(B₃H₈)₂ melts at a lower temperature than the THF adduct.
- The solvent-free Mg(B₃H₈)₂ decomposes upon melting whereas the THF adduct is meta-stable (i.e., it decomposes at a slightly higher temperature).
- The solvent-free Mg(B₃H₈)₂ decomposes to B₁₂H₁₂ and H₂ upon melting.

- The intermediates formed from decomposition of solvent-free $\text{Mg}(\text{B}_3\text{H}_8)_2$ can be trapped by the presence of MgH_2 and H_2 to form >95% corresponding BH_4^- , determined by *in situ* solid-state ^{11}B NMR and *ex situ* ^{11}B solution-phase NMR.
- The solvent-free $\text{Mg}(\text{B}_3\text{H}_8)_2$ reduction to $\text{Mg}(\text{BH}_4)_2$ is exothermic, ca. <-100 kJ/mol H_2 . This is more exothermic than reduction of the THF adduct, ca. -70 kJ/mol H_2 .

Figure 10 shows the *in situ* solid-state ^{11}B NMR comparing before and after heating solvent-free B_3H_8 to 100°C . The top panel shows $\text{Mg}(\text{B}_3\text{H}_8)_2$ neat resulting in formation of $\text{B}_{12}\text{H}_{12}$ and BH_4^- . The bottom panel is B_3H_8 decomposition in the presence of MgH_2 and H_2 , showing conversion of a broad B_3H_8 peak at -33 ppm to a sharp peak at -40 ppm, the BH_4^- . The middle panel compares decomposition of B_3H_8 in the presence of MgH_2 and no H_2 (red line) to decomposition with H_2 .



The enthalpy of hydrogenation is determined from the heat measured by calorimetry. Changing the sign provides the heat for making $\text{Mg}(\text{B}_3\text{H}_8)_2$ from $\text{Mg}(\text{BH}_4)_2$. An experimental value of 100 kJ/mol H_2 to compare with theory, ca. 150 kJ/mol H_2 . Experimental conditions use an excess of MgH_2 (4 equivalents) and H_2 (10 bar) to trap intermediates and push the reaction to BH_4^- .

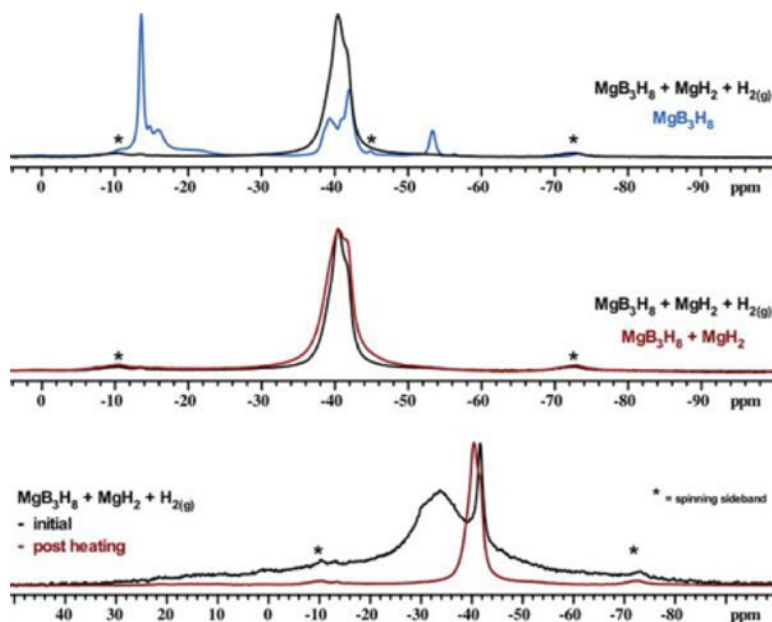


Figure 10. *In situ* solid-state ^{11}B NMR spectra comparing before and after heating solvent-free B_3H_8 to 100°C

CONCLUSIONS AND UPCOMING ACTIVITIES

NREL

In FY 2018 we made a considerable number of no-go decisions on various carbon-based sorbent materials, including B-doped carbon systems, biomass pyrolyzed products, and C2N materials with considerable purification issues. We also showed considerable success, as the diameter of a pore approaches the kinetic diameter of hydrogen, vibrational phonon modes, and not van der Waals interactions, can dominate the sorption kinetics and temperature of the sorption/desorption cycle. With respect to characterization the new variable-temperature PCT and thermal conductivity apparatus have proven to be a boon for the understanding of materials sorption processes.

In FY 2019 we have a considerable number of new initiatives that include sorbents, hydrides, and new characterization techniques for transportation, carriers, and long-term storage applications. Furthermore, the new variable-temperature PCT has also put forth a limitation of current theory/models toward the characterization of isosteric heats of adsorption. This is especially true as the sorption processes approach room temperature and the excess and absolute capacity of materials diverge. Specifically, the following are issues that need to be examined more carefully.

Experimental:

- Adequate isotherm data collection (especially steep part of curve)
- Sensitivity analysis to calibration errors (similar to excess versus absolute).

Analysis:

- Very accurate fitting/interpolation of data is required.
- Excess versus absolute capacity—absolute is required but hard to determine
- Appropriate Q_{st} equation model: $dP/dT = (S_1 - S_2) / (V_1 - V_2) = q_{st} / T(V_1 - V_2)$
- High-pressure effects—most common equation assumes ideal gas
- Q_{st} calculation protocol—most accurate way to calculate
- Temperature effects: understanding why Q_{st} estimates vary with temperature
- Temperature-dependence assumptions: this can affect Q_{st} results
- Heterogenous adsorption sites: how does this affect Q_{st} ?
- Best isotherm data fitting: which isotherms best capture the material physics?
- Determining equilibrium $K(T)$ accurately is needed for van't Hoff analysis
- Validity of van't Hoff: does it accurately apply to sorption processes?

LBNL

We have demonstrated frameworks with π -basic metals (Cu^I-MFU-4l and V^{II}-MOF) exhibit high adsorption enthalpy, which can be optimal for the room-temperature hydrogen storage. We will investigate to what degree the adsorption enthalpy of these frameworks can be tuned. Smaller pore analogues of Cu^I-MFU-4l and V^{II}-MOF will also be synthesized to increase volumetric hydrogen uptake capacities. During the evaluation of thermodynamic parameters of these materials, a very large temperature dependence of ΔH° and ΔS° upon H₂ adsorption has been observed in these frameworks by *in situ* DRIFTS measurements. The finding implies that thermodynamic parameters obtained at low temperatures may not describe behavior under conditions stipulated by DOE's ultimate storage targets. With *in situ* DRIFTS analysis we will "re-establish" some of the key parameters and physiochemical properties necessary for materials at the higher temperatures. Another approach to increase volumetric storage capacities is developing frameworks with low-coordinate metal sites. We have prepared a series of metalated frameworks; however, optimization for metalation and activation remains unsolved. We will continue metalation of frameworks with functionalized linkers to access low-coordinate metal sites. Thermodynamic properties of framework materials will be compared to the values predicted by computation. To this end, continuous efforts will be devoted to the development of a benchmark database, tailored for hydrogen binding with a variety of adsorption motifs, with the goal of providing inexpensive predictive analytics.

FY 2018 PUBLICATIONS/PRESENTATIONS

Publications

1. D. DeSantis, J.A. Mason, B.D. James, C. Houchins, J.R. Long, and M. Veenstra, “Techno-Economic Analysis of Metal–Organic Frameworks for Hydrogen and Natural Gas Storage,” *Energy Fuels* 31 (2017): 2024–2032.
2. E. Tsvion, S.P. Veccham, and M. Head-Gordon, “High Temperature Hydrogen Storage of Multiple molecules: Theoretical Insights from Metalated Catechols,” *ChemPhysChem* 18 (2017): 184–188.
3. E. Tsvion and M. Head-Gordon, “Methane Storage: Molecular Mechanisms Underlying Room-Temperature Adsorption in $Zn_4O(BDC)_3$ (MOF-5),” *J. Phys. Chem. C* 121 (2017): 12091–12100.
4. M.D. Allendorf, Z. Hulvey, T. Gennett, A. Ahmed, T. Autrey, J. Camp, E.S. Cho, H. Furukawa, M. Haranczyk, M. Head-Gordon, S. Jeong, A. Karkamkar, D. Liu, J.R. Long, K.R. Meihaus, I. Nayyar, R. Nazarov, D.J. Siegel, V. Stavila, J.J. Urban, S.P. Veccham, and B.C. Wood, “An Assessment of Strategies for the Development of Solid-State Adsorbents for Vehicular Hydrogen Storage,” *Energy Environ. Sci.* 11 (2018): 2784–2812.
5. M.T. Kapelewski, T. Runčevski, J.D. Tarver, H.Z.H. Jiang, A. Ayala, T. Gennett, S.A. FitzGerald, C.M. Brown, and J.R. Long, “Evaluating Metal–Organic Frameworks for High-Pressure H_2 Storage: Record High Volumetric Capacity in $Ni_2(m-dobdc)$,” *Chem. Mater.* In press.
6. H. Furukawa, “Synthesis and Characterization of Metal–Organic Frameworks,” in *Gas Adsorption in Metal-Organic Frameworks: Fundamentals and Applications*. (CRC Press, 2018). ISBN: 9780429469770 (ebook).
7. Mirjana Dimitrievska, Patrick Shea, Kyoung Kweon, Marnik Bercx, Joel B. Varley, Wan Si Tang, Alexander V. Skripov, Terrence J. Udovic, Vitalie Stavila, and Brandon C. Wood, “The Effects of Carbon and Anion Reorientational Dynamics in $LiCB_{11}H_{12}$ and $NaCB_{11}H_{12}$ Superionic Conductors,” *Adv. Energy Mater.* 8, no. 15 (2018): 1703422.
8. Wan Si Tang, Mirjana Dimitrievska, Vitalie Stavila, Wei Zhou, Hui Wu, A. Alec Talin, and Terrence J. Udovic, “Order-Disorder Transitions and Superionic Conductivity in the Sodium Nido-Undeca(car)borates,” *Chem. Mat.* 29, no. 24 (2017): 10496–10509.
9. Mirjana Dimitrievska, Vitalie Stavila, Alexei V. Soloninin, Roman V. Skoryunov, Olga A. Babanova, Hui Wu, Wei Zhou, Wan Si Tang, Antonio Faraone, Jacob D. Tarver, Benjamin A. Trump, Alexander V. Skripov, Terrence J. Udovic, “Nature of Decahydro-closo-decaborate Anion Reorientations in an Ordered Alkali-Metal Salt: $Rb_2B_{10}H_{10}$,” *J. Phys. Chem. C* 122, no. 27 (2018): 15198–15207.
10. Mirjana Dimitrievska, Jean-Noël Chotard, Raphaël Janot, Antonio Faraone, Wan Si Tang, Alexander V. Skripov, and Terrence J. Udovic, “Tracking the Progression of Anion Reorientational Behavior between α -phase and β -phase Alkali-Metal Silanides by Quasielastic Neutron Scattering,” *J. Phys. Chem. C* 122, no. 42 (2018): 23985–23997.
11. Marina Chong, Tom Autrey, and Craig Jensen, “Lewis Base Complexes of Magnesium Borohydride: Enhanced Kinetics and Product Selectivity upon Hydrogen Release,” *Inorganics* (2017), DOI:10.3390/inorganics5040089. Invited Special Issue: Functional Materials Based on Metal Hydrides, Inorganic Solid-State Chemistry.
12. Karsten Müller, Kriston Brooks, and Tom Autrey, “Hydrogen Storage in Formic Acid: A Comparison of Process Options,” *Energy and Fuels* (2017), DOI:10.1021/acs.energyfuels.7b02997.
13. Qi-Long Zhu, Fu-Zhan Song, Qiu-Ju Wang, Nobuko Tsumori, Yuichiro Himeda, Tom Autrey, and Qiang Xu, “Solvent-Switched In Situ Confinement Approach for Immobilizing Highly-Active Ultrafine Palladium Nanoparticles: Boosting Catalytic Hydrogen Evolution,” *J. Materials Chemistry A* (2018), DOI:10.1039/c8ta01093e.

14. Karsten Müller, Kriston Brooks, and Tom Autrey, “Releasing Hydrogen at High Pressures from Ambient Condition Carriers: Aspects for the H₂ Delivery to Fueling Stations,” *Energy and Fuels* (2018), DOI:10.1021/acs.energyfuels.8b0172.

Presentations

1. R. Chakraborty and M. Head-Gordon, “Multiscale Simulations in Chemistry with the Lattice Boltzmann Method,” Voth group at the University of Chicago, IL, February 8, 2018.
2. H. Furukawa, M.T. Kapelewski, H.Z.H. Jiang, T. Runčevski, Y.-Y. Lin, B.R. Barnett, K. Hou, G. Thiele, and J.R. Long, “Hydrogen Storage in Metal–Organic Frameworks,” 255th ACS National Meeting & Exposition, New Orleans, LA, March 21, 2018.
3. H.Z.H. Jiang and J.R. Long, “*In Situ* Characterization of Adsorbates in Nanoporous Materials with IR Spectroscopy,” 255th ACS National Meeting & Exposition, New Orleans, LA, March 22, 2018.
4. R. Chakraborty and M. Head-Gordon, “Modeling Adsorption with the Lattice Boltzmann Method,” West-Coast Theoretical Chemistry Symposium, Stanford University, CA, March 28, 2018.
5. J.R. Long, “HySCORE: LBNL Technical Activities–Hydrogen Storage in Metal–Organic Frameworks,” DOE H₂ Tech Team Meeting, Denver, CO, April 18, 2018.
6. B.R. Barnett, H.Z.H. Jiang, and J.R. Long, “Augmenting Hydrogen Sorption Enthalpies via Pi-Backdonation: Thermodynamic Ramifications for Optimizing Adsorptive Hydrogen Storage,” Organometallic Chemistry Gordon Research Conference, Newport, RI, July 10, 2018.
7. Philip Parilla, “Hydrogen Sorbent Measurement Qualification and Characterization,” 2017 AMR, Washington, DC, June 2017.
8. Philip Parilla and Thomas Gennett, “Hydrogen Storage Characterization and Optimization Research Effort within HyMARC,” ACS Meeting, New Orleans, LA, March 2018.
9. Katherine Hurst, “Results from a Multi-Laboratory Comparison of Hydrogen Volumetric Capacity Measurements,” ACS Meeting, New Orleans, LA, March 2018.
10. Katherine Hurst, “Update on NREL’s Validation Efforts: Inter-Laboratory Comparison,” Hydrogen Storage Tech Team Meeting, NREL, Golden, CO, April 2018.
11. Philip Parilla, “Update on NREL’s Characterization Efforts,” Hydrogen Storage Tech Team Meeting, NREL, Golden, CO, April 2018.
12. Thomas Gennett, “Update of Hydrogen Storage Initiatives,” McMinnville, Oregon, August 2017.
13. Thomas Gennett, “HySCORE Capabilities,” DOE FCTO Hydrogen Storage Kickoff Meeting, September 2017.
14. Thomas Gennett, “HySCORE Efforts and Capabilities,” HyMARC Consolidation Meeting, November 2017.
15. Katherine Hurst, Thomas Gennett, and Phil Parilla, Hydrogen Storage Tech Team Meeting, Detroit MI, September 2017.
16. Thomas Gennett, “Update on HySCORE Materials Efforts,” Hydrogen Storage Tech Team Meeting, NREL, Golden, CO, April 2018.
17. Thomas Gennett, “HySCORE: NREL Technical Activities,” 2017 AMR, Washington, DC, June 2017.
18. Thomas Gennett, “HySCORE: NREL Technical Activities,” H2@Scale Workshop, September 2017.
19. Thomas Gennett, “HySCORE,” ECS National Meeting, May 2017.
20. K. Hurst, S. Christensen, P. Parilla, and T. Gennett, “Modification of Borohydride Materials for Hydrogen Storage by ALD,” ALD 2017.

21. M. Dimitrievska, “Neutron Scattering Studies of Hydrogenous Materials for Next-Generation Energy Storage,” ACS National Meeting & Exposition, New Orleans, LA, 2018.
22. M. Dimitrievska, “Role of Solvent Adducts in Hydrogen Dynamics of Metal Borohydrides: Neutron-Scattering Characterization,” ACS National Meeting & Exposition, New Orleans, LA, 2018.
23. M. Dimitrievska, “Carbon Incorporation and Anion Dynamics as Synergistic Drivers for Ultrafast Diffusion in Superionic LiCB₁₁H₁₂ and NaCB₁₁H₁₂,” MRS Spring meeting, Phoenix, AZ, 2018.
24. M. Dimitrievska, “Neutron backscattering studies of hydrogenous materials for next-generation energy storage,” National Science Foundation Site Visit Review of Center for High Resolution Neutron Scattering (CHRNS), Washington, DC, 2018.
25. M. Dimitrievska, “Role of Solvent Adducts in Hydrogen Dynamics of Metal Borohydrides—Neutron-Scattering Characterization,” American Conference on Neutron Scattering, College Park, MD, June 2018.
26. T. Autrey, Boron Chemistry in the Americas (BORAM XVI), Boston College, June 26–30, 2018.
27. T. Autrey, Integration of Sustainable Energy Conference, Nuremberg, Germany, July 17–18, 2018.
28. T. Autrey, Department Seminar, Max Planck Institute, Stuttgart, July 20, 2018.
29. T. Autrey, Department Seminar, Montana State University, Oct 12, 2018.
30. T. Autrey, International Symposium on Metal-Hydrogen Systems, Guangzhou, China, October 2018.

REFERENCES

1. K. Hurst, T. Gennett, S. Shulda, and P. Parilla, “Results from a Multi-Laboratory Comparison of Hydrogen Volumetric Capacity Measurements,” In preparation 2018.
2. K.E. Hurst, P.A. Parilla, K.J. O'Neill, and T. Gennett, “An International Multi-Laboratory Investigation of Carbon-Based Hydrogen Sorbent Materials,” *Appl. Phys. A: Mater. Sci. Process.* 122, no. 1 (2016): 1–9.
3. S. Barbara, M. Ulrich, T. Natalia, S. Markus, F. Gérard, and H. Michael, “Heat of Adsorption for Hydrogen in Microporous High-Surface-Area Materials,” *ChemPhysChem* 9, no. 15 (2008): 2181–2184.
4. K.J. Gross, K.R. Carrington, S. Barcelo, A. Karkamkar, J. Purewal, S. Ma, H.-C. Zhou, P. Dantzer, K. Ott, T. Burrell, T. Semeslberger, Y. Pivak, B. Dam, D. Chandra, and P. Parilla, *Recommended Best Practices for the Characterization of Storage Properties of Hydrogen Storage Materials*, V3.34 (H2 Technology Consulting LLC, 2012), http://www1.eere.energy.gov/hydrogenandfuelcells/pdfs/best_practices_hydrogen_storage.pdf.
5. D.P. Broom, *Hydrogen Storage Materials: The Characterisation of Their Storage Properties*, (Springer: London; New York, 2011).
6. K.S.W. Sing, F. Rouquerol, and J. Rouquerol, “5-Classical Interpretation of Physisorption Isotherms at the Gas–Solid Interface,” In *Adsorption by Powders and Porous Solids* (Second Edition), Rouquerol, F.; Rouquerol, J.; Sing, K.S.W.; Llewellyn, P.; Maurin, G., Eds. (Academic Press: Oxford, 2014): 159–189.
7. F.O. Mertens, “Determination of Absolute Adsorption in Highly Ordered Porous Media,” *Surface Science* 603, no. 10 (2009): 1979–1984.
8. C.O. Areán, S. Chavan, C.P. Cabello, E. Garrone, and G.T. Palomino, “Thermodynamics of Hydrogen Adsorption on Metal–Organic Frameworks,” *ChemPhysChem* 11 (2010): 3237–3242.
9. D. Denysenko, M. Grzywa, J. Jelic, K. Reuter, and D. Volkmer, *Angew. Chem. Int. Ed.* 53 (2014): 5832–5836.
10. E. Garrone, B. Bonelli, and C. Otero Areán, “Enthalpy–Entropy Correlation for Hydrogen Adsorption on Zeolites,” *Chem. Phys. Lett.* 456 (2008): 68–70.

HyMARC Seedling: “Graphene-Wrapped” Complex Hydrides as High-Capacity, Regenerable Hydrogen Storage Materials

Di-Jia Liu (Primary Contact), Lina Chong
Argonne National Laboratory
9700 South Cass Avenue
Lemont, IL 60439
Phone: (630) 252-4511
Email: djliu@anl.gov

DOE Manager: Jesse Adams
Phone: (720) 356-1421
Email: Jesse.Adams@ee.doe.gov

Subcontractor:
Southern Illinois University, Carbondale, IL

Project Start Date: October 1, 2016
Project End Date: September 30, 2018

Fuel Cell Technologies Office Multi-Year Research, Development, and Demonstration Plan¹:

- (A) System Weight and Volume
- (B) System Cost
- (C) Efficiency
- (D) Durability/Operability
- (E) Charging/Discharging Rates
- (O) Lack of Understanding of Hydrogen Physisorption and Chemisorption.

Technical Targets

This project is to design and synthesize “graphene-wrapped” complex hydride composites as the next-generation hydrogen storage materials that meet the following DOE hydrogen storage targets.

- Excess gravimetric hydrogen storage capacity:
 - DOE 2025 target: 5.5 wt% system basis
 - Project target: 10 wt% on material basis.
- Volumetric hydrogen storage capacity:
 - DOE 2025 target: 0.040 kg H₂/L of system
 - Project target: 0.055 kg H₂/L of material total.

Overall Objectives

- To produce one or more hydride@graphene composites with regenerable hydrogen storage gravimetric density >10 wt% and volumetric density >0.055 kg H₂/L.
- To develop a scale-up plan of manufacturing the new composite at a cost of <\$333/kg H₂.
- To establish fundamental understanding on the improved dehydrogenation (DH) and rehydrogenation (RH) kinetics promoted by graphene.

Fiscal Year (FY) 2018 Objectives

- To deliver a hydride@graphene system with reversible >8 wt% total gravimetric and >0.03 kg H₂/L total volumetric hydrogen storage capacities at temperatures of <400°C over at least five DH–RH cycles.
- To reduce NaBH₄@graphene dehydrogenation temperature by exploring catalyst and structural approaches.

Technical Barriers

This project addresses the following technical barriers from the Hydrogen Storage section of the

FY 2018 Accomplishments

- Successfully synthesized catalyst-doped NaBH₄@graphene composite and demonstrated five DH and RH cycles with measured gravimetric capacity >7.4 wt% at 406°C.
- Successfully demonstrated the improvement in hydrogen release kinetics by lowering the DH temperature by 320°C over bulk NaBH₄ or 138°C over NaBH₄@graphene at the beginning of the project.

¹ <https://www.energy.gov/eere/fuelcells/downloads/fuel-cell-technologies-office-multi-year-research-development-and-22>

INTRODUCTION

This project focuses on developing a new class of hydrogen storage material, hydride@graphene or hydride@G, for next-generation hydrogen-powered fuel cell vehicles. The approach is based on a recent collaboration between Shanghai Jiao Tong University and Argonne National Laboratory [1]. Using a simple solvent-based method, we successfully synthesized a “nanoencapsulated” sodium borohydride-graphene composite, NaBH₄@G, in which NaBH₄ nanocrystallites are individually wrapped by single-layer graphenes. The new composite demonstrates regenerable and high hydrogen storage capacity in multiple DH and RH cycles. The graphene sheet tightly envelops the hydride nanoparticles like a candy wrapper and restricts the solid hydride phase from segregation and agglomeration. It also prevents the leakage of any harmful byproduct other than hydrogen, which is the only molecule permeable through the graphene layer. The hydride crystallites are encapsulated at nanometer size by graphene and can release/recharge hydrogen more readily than the bulk phase hydride.

Under this project, we planned to prepare a broader range of hydride@G composites using the complex hydrides of higher intrinsic gravimetric and volumetric densities. We also planned to explore various morphological and chemical approaches to improve the DH–RH kinetics, guided by computational modeling and collaboration with the Hydrogen Materials Advanced Research Consortium (HyMARC).

APPROACH

The approach we applied focused on improving the hydrogen storage capacity of the hydride–graphene composites by reducing the amount of graphene while maintaining the nanoencapsulation. We also focused on improving DH and RH kinetics of the NaBH₄@graphene system by incorporating catalytic additives within the graphene-wrapped solid mixture. The improved NaBH₄@graphene was evaluated by a DOE-designated lab. Throughout the project, the new hydride composites were characterized by various characterization tools. Computational modeling and simulation were carried out simultaneously to provide insights for DH–RH kinetics.

RESULTS

During FY 2018, we accomplished the following tasks.

To improve DH–RH kinetics, we prepared and evaluated a number of NaBH₄@G composites containing low concentrations of transition metals (typically around one percent) synthesized by wet chemistry. The transition metals explored were magnesium, vanadium, and nickel. These metals are known to form hydrides with lower DH temperatures. By incorporating them with NaBH₄, we anticipated that they could serve as catalysts to facilitate DH–RH reactions through solid-state interaction with NaBH₄ confined by graphene. Figure 1 shows hydrogen release as a function of temperature for a representative composite, NaBH₄+MgNiV@G, obtained from thermogravimetric analysis (TGA). For comparison, the hydrogen release from NaBH₄@G and bulk NaBH₄ are also included. The DH onset temperature for NaBH₄+MgNiV@G was lowered by 138°C compared to NaBH₄@G and 320°C compared to bulk NaBH₄, indicating significant improvement in DH kinetics by the catalysts. The challenge at this point is that a significant fraction of hydride still decomposes at temperatures above 400°C as shown by the second peak in Figure 1 for NaBH₄+MgNiV@G, which suggests that the catalyst has not interacted with the entire phase of the hydride. Better dispersion and mixing are needed to further improve the DH kinetics.

The catalyst-promoted DH kinetics are also reflected in the temperature-programmed hydrogen desorption in the hydrogen discharge capacity measurement. Figure 2 shows a side-by-side comparison between catalyst-added hydride (NaBH₄+MgNiV@G) and NaBH₄@G during step-wise hydrogen release from room temperature to 430°C at 100-degree intervals. Clearly, with the improved DH kinetics, the NaBH₄+MgNiV@G composite discharged more hydrogen than NaBH₄@G did at low temperature steps. For example, ~4 wt% hydrogen was already discharged at 300°C for NaBH₄+MgNiV@G, compared to ~1 wt% for NaBH₄@G under the same temperature. The total discharged hydrogen reached 8.2 wt% at 430°C for NaBH₄+MgNiV@G; in comparison, NaBH₄@G released a similar amount of hydrogen at 475°C.

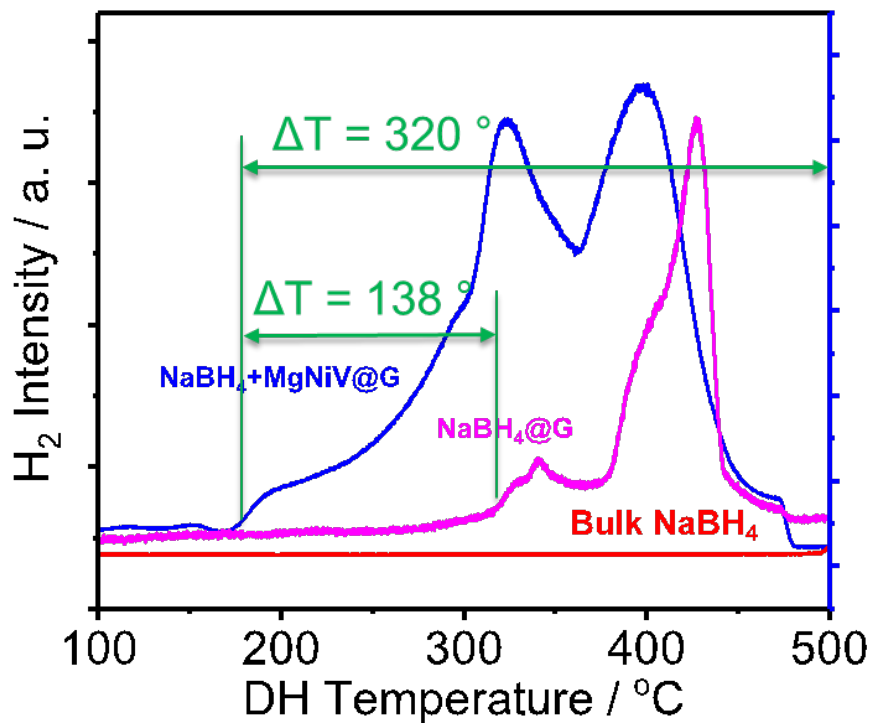


Figure 1. The hydrogen desorption as the function of temperature during TGA analysis on NaBH₄+MgNiV@G, NaBH₄@G, and bulk NaBH₄.

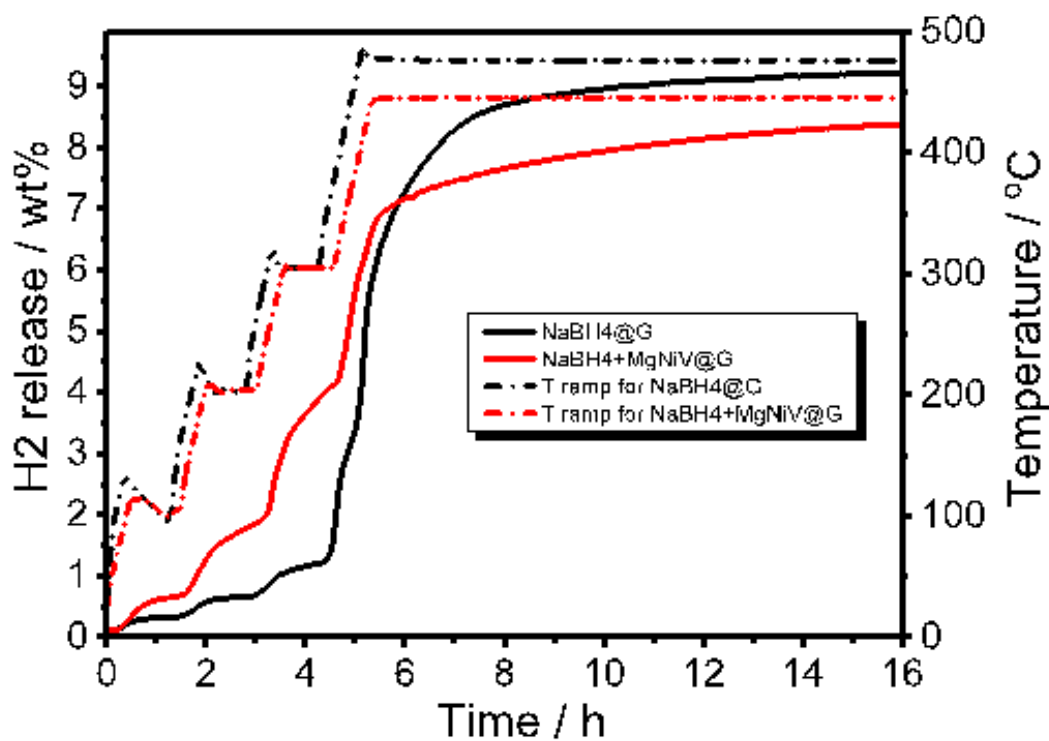


Figure 2. Comparison of hydrogen releases from NaBH₄+MgNiV@G and NaBH₄@G during step-wise temperature-programmed discharge

We also performed five DH–RH cycles for the NaBH₄+MgNiV@G composite. The DH temperature was controlled at 407°C with background hydrogen pressure less than one bar while the RH temperature was set at 350°C under charging pressure of 40 bar. Figure 3 shows the gravimetric and volumetric hydrogen storage capacities obtained during the five cycles. The very high capacity achieved during the first cycle represents an artifact from the contribution of vapor pressure of the residual organic solvent trapped during the composite synthesis. The capacities of the remaining cycles were all from pure hydrogen released from the composite, which were proved from purity analysis. At the end of the fifth cycle, the net gravimetric capacity was 7.3 wt% and the volumetric capacity was 0.042 kg/L.

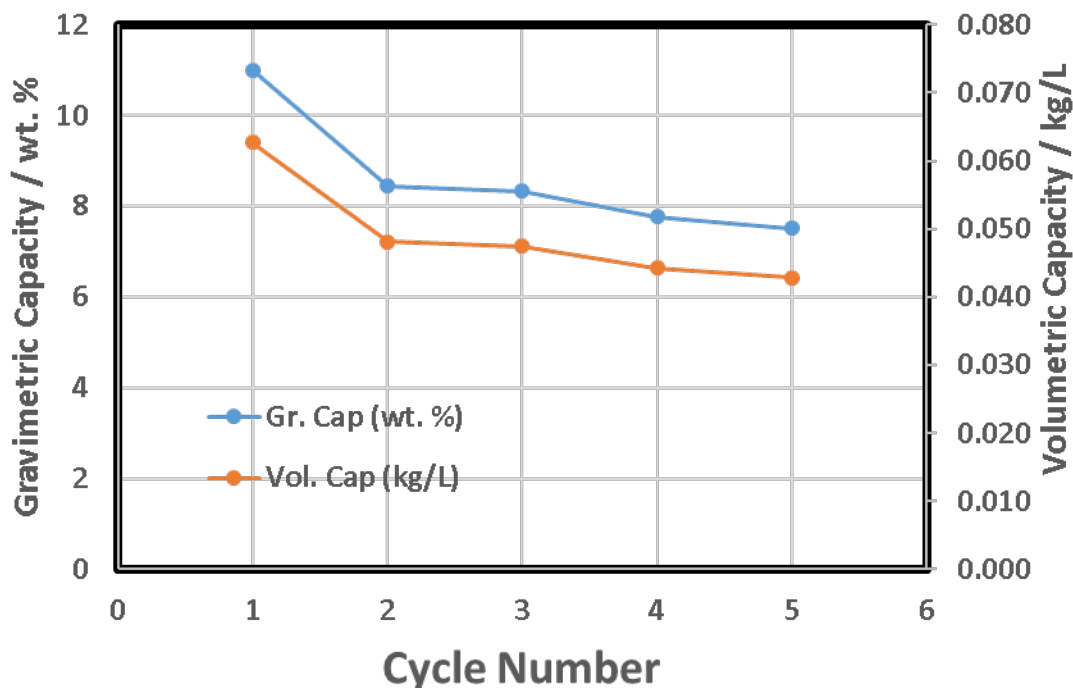


Figure 3. The hydrogen gravimetric and volumetric storage capacities as the function of cycle number over NaBH₄+MgNiV@G measured during a five-cycle DH–RH test

CONCLUSIONS AND UPCOMING ACTIVITIES

A significant improvement in DH kinetics was demonstrated in a catalyst-added NaBH₄@graphene composite. The new catalyst additive lowered initial the hydrogen discharge temperature from >500°C in bulk NaBH₄ to 180°C in NaBH₄+MgNiV@G, representing a 320°C reduction. Hydrogen release under a fixed-temperature DH cycle was achieved for NaBH₄+MgNiV@G through a five-cycle DH–RH test. The gravimetric capacity was retained at 7.5 wt% at the end of the fifth cycle.

FY 2018 PUBLICATIONS/PRESENTATIONS

1. Lina Chong and Di-Jia Liu, “Hydride@graphene Composites for Hydrogen Storage with Improved Kinetics and Cyclability,” Oral presentation at the 255th ACS National Meeting, New Orleans, LA, March 18–22, 2018.

REFERENCES

1. L. Chong, X. Zeng, W. Ding, D.-J. Liu and J. Zou, “NaBH₄ in ‘Graphene Wrapper’: Significantly Enhanced Hydrogen Storage Capacity and Regenerability through Nano-encapsulation,” *Advanced Materials* 27 (2015): 5070–5074.

HyMARC Seedling: Electrolyte-Assisted Hydrogen Storage Reactions

Channing Ahn (Primary Contact), Dan Addison, John Vajo, and Jason Graetz (HRL)
Liox Power, Inc.
129 N. Hill Ave.
Pasadena, CA 91106
Phone: (626) 395-2174
Email: cca@caltech.edu

DOE Manager: Katie Randolph
Phone: (240) 562-1759
Email: Katie.Randolph@ee.doe.gov

Contract Number: DE-EE0007849

Subcontractor:
HRL Laboratories, LLC, Malibu, CA

Project Start Date: January 20, 2017
Project End Date: June 19, 2018 (Phase 1)

Overall Objectives

- Address critical deficiencies of hydrogen storage systems design based on hydride materials, as determined by the Hydrogen Storage Engineering Center of Excellence (HSECoE).
- Obviate the need for high-temperature release of hydrogen in complex hydride and destabilization reactions through electrolyte use.
- Demonstrate a 10× improvement in dehydrogenation kinetics.

Fiscal Year (FY) 2018 Objectives

- Survey electrolytes to determine thermal and electrochemical stability, ionic conductivity, solubility (salt and hydrogen), and vapor pressure.
- Demonstrate electrolyte-assisted hydrogen evolution based on Li^+ and/or Mg^{2+} cations (or other) storage materials.

- Demonstrate electrolyte-assisted reversible hydrogen uptake based on Li^+ and/or Mg^{2+} cations with endothermic hydrogen evolution.

Technical Barriers

This project addresses the following technical barriers from the Hydrogen Storage section of the Fuel Cell Technologies Office Multi-Year Research, Development, and Demonstration Plan,¹ with sub-listings from Technical Task Description Table 3.3.8:

- (O) Lack of Understanding of Hydrogen Physisorption and Chemisorption
 - Determine the decomposition pathways and products of materials to better understand their mechanisms and kinetics.
 - Determine the hydrogen storage capacity of potential storage materials and demonstrate reproducibility of their synthesis and capacity measurements.
 - Develop reversible metal hydrides that improve kinetics while maintaining high gravimetric capacity at relevant release temperatures and pressures.

Technical Targets

While we note the system targets from the Hydrogen Storage section of the Fuel Cell Technologies Office Multi-Year Research, Development, and Demonstration Plan in Table 1, this project is conducting fundamental studies on the role of enhanced kinetics through the use of electrolyte-assisted hydrogenation/dehydrogenation on complex hydride and destabilization hydride reactions. While the systems being studied, at least on a materials basis, show capacities in excess of system targets for volumetric and gravimetric densities, the kinetics required for hydrogenation/dehydrogenation are too slow under technologically relevant temperatures. Our effort explores the improvement in kinetics with the aim

¹ <https://www.energy.gov/eere/fuelcells/downloads/fuel-cell-technologies-office-multi-year-research-development-and-22>

of nearing thermodynamic temperatures for relevant materials systems.

FY 2018 Accomplishments

- Demonstrated 10× dehydrogenation kinetic improvement using electrolyte over non-electrolyte-containing samples: MgH₂/Sn with Li/K-BH₄ eutectic, Mg(BH₄)₂ with Li/K-BH₄ eutectic, MgH₂/Si with Li/K/Cs-I ternary.
- Demonstrated rehydrogenation (at Sandia National Laboratories) of ≈2% in dehydrogenated MgH₂/Sn in Li/K-BH₄
- Demonstrated significant hydrogenation (6.3 wt%) of MgB₂ with electrolyte after Sandia hydrogenation and negligible hydrogenation (0.22 wt%) without eutectic (25× improvement).

electrolyte-containing sample as compared to likely no (or very little) rehydrogenation of dehydrogenated MgH₂/Sn containing no electrolyte under the same rehydrogenation conditions (1,000 bar).

Table 1. Technical System Targets: Onboard Hydrogen Storage for Light-Duty Fuel Cell Vehicles

Storage Parameter	Units	DOE 2020	Project Status
System Gravimetric Capacity Usable, specific energy from hydrogen (net useful energy/max system mass)	kWh/kg (kg H ₂ /kg system)	1.8 0.055	TBD
System Volumetric Capacity Usable energy density from hydrogen (net useful energy/max system volume)	kWh/L (kg H ₂ /L) system	1.3 (0.040)	TBD
Charging/Discharging Rates System fill time (5 kg)	min	3.3	TBD

TBD – to be determined

INTRODUCTION

State-of-the-art hydrogen storage material studies supported by DOE-funded projects have included complex hydrides and destabilized systems, both of which typically involve multiple solid phases [1]. While these materials can exhibit high hydrogen densities and tunable thermodynamic properties, the rates of hydrogen exchange (i.e., the rates of dehydrogenation and rehydrogenation) are too kinetically limited for relevant applications. These limitations occur in part because multiple component materials are typically formulated as solid-state powder mixtures where reaction between the phases can only take place across solid-solid interfaces where particles are in direct atomic-scale contact. Nanoscale engineering, using mechanical milling or templates, and additives or catalysts have been employed to increase reaction rates by decreasing diffusion distances and increasing interfacial contact area and mobility. While significant kinetic improvements have been achieved and are still undergoing refinement, they have thus far been insufficient for practical applications.

APPROACH

Given the interface-controlled processes of solid-state destabilization reactions that normally require thermal activation, we have defined a free energy difference that needs to be overcome before any relevant transformation or reaction can take place. Noting the difference between the effective empirically determined temperature required to promote a reaction in comparison to what might be expected on a purely thermodynamic basis, we note that the free energy barrier is typically >20 kJ. However, in so-called electrochemical conversion battery reactions that involve diffusing species in an electrolyte, the activation barrier has been observed to be as low as 4 kJ. Given the similarity of compounds used in both electrochemical and hydrogen storage reactions, the expectation is that the use of electrolytes will help lower the free energy barrier height by promoting solubilization of the diffusing species so that reactions are no longer controlled by limited interfacial areas.

Electrolytes under consideration for this effort will ultimately require redox stability, low vapor pressure, high hydrogen permeability, and relatively low mass and volume with respect to the reacting species. Our effort is aimed at evaluating and testing electrolyte suitability to enhance hydrogen storage material reaction kinetics.

RESULTS

10× Desorption Kinetic Improvement in the Mg/Si System

In fulfillment of the Phase 1 go/no-go requirements of this effort, we have demonstrated a 10× improvement in desorption kinetics in the Mg/Si destabilization system through the use of a ternary iodide salt, using an identical temperature ramp (setpoint). Data for this system is shown in Figure 1. The arrows in the plot indicate the point at which an identical 3.5 wt% desorption is achieved. In the case of the “neat” reaction in the absence of our electrolyte salt, the time required is 70 h, whereas when the electrolyte is added, the same desorption yield is achieved in 7 h.

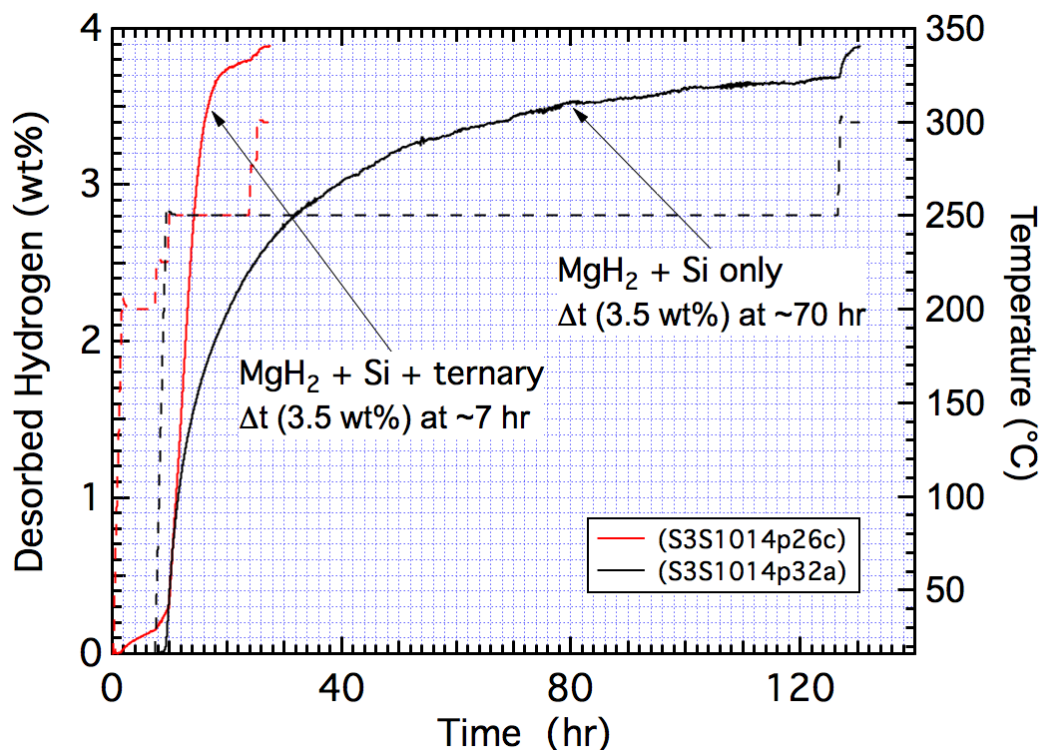


Figure 1. Hydrogen desorption as a function of time for the temperature ramps as indicated by the dotted traces. The use of an iodide ternary salt improves desorption kinetics by 10x.

10× Desorption Kinetic Improvement in the Mg/Sn System

Similar desorption kinetic improvement is seen in the Mg/Sn system at 150°C, in this case using a borohydride eutectic electrolyte. The plots demonstrating this improvement are shown in Figure 2. While higher temperatures with a somewhat lower improvement are required for more complete dehydrogenation of this destabilization system, clear kinetic improvements can be discerned. In addition, complete rehydrogenation of this system in the presence of an electrolyte was achieved, we believe for the first time, in the MgH₂/(Si or Sn) destabilization system as reported at the 2018 Storage Tech Team Meeting (Southfield, Michigan, Sept. 12, 2018).

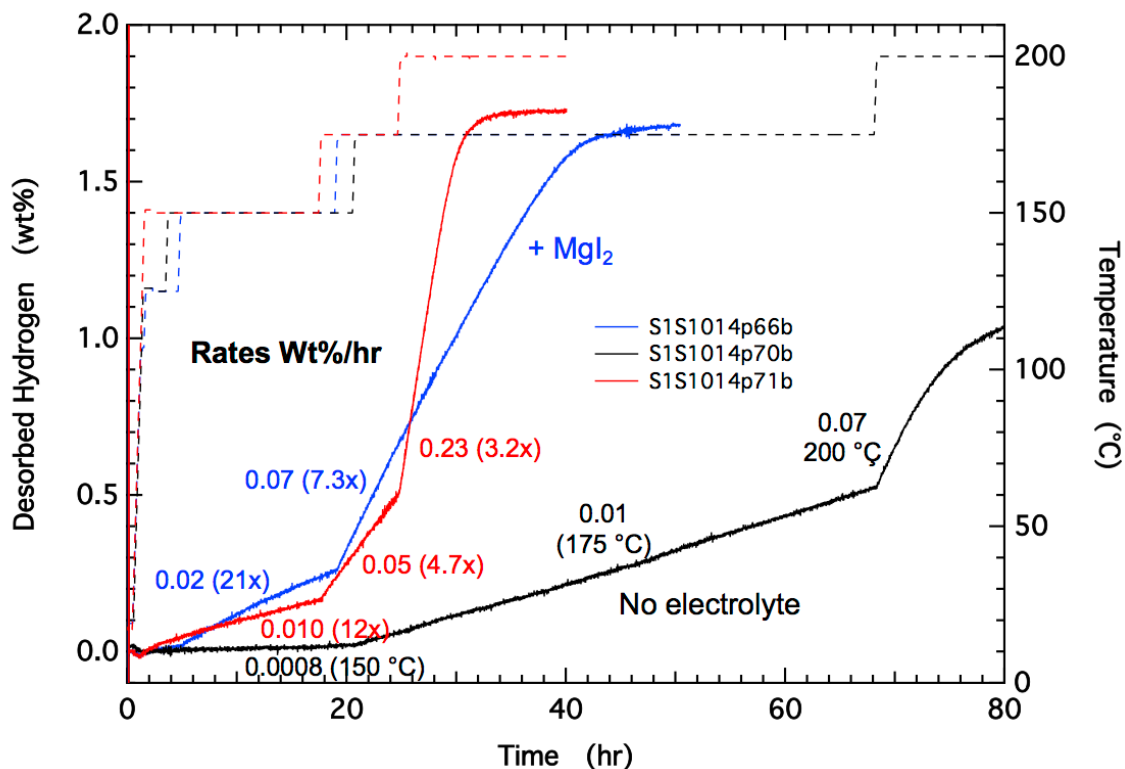


Figure 2. Hydrogen desorption in the Mg/Sn system in the presence of a borohydride electrolyte showing improved kinetics over the range of desorption temperatures. For this effort the addition of MgI_2 appeared to further improve desorption kinetics.

10× Desorption Kinetic Improvement in the $Mg(BH_4)_2$ System

The use of a borohydride electrolyte also improved the kinetics of desorption in the $Mg(BH_4)_2$ system as shown in Figure 3. The temperature maximum used in this case is $225^\circ C$ (we note that $>350^\circ C$ is required to fully dehydrogenate this compound). This particular system will be studied further as the borohydride electrolyte might also be a source of desorbed hydrogen. Nonetheless, clear differences between the “neat” compound and the use of borohydride additives greatly improve the yield in this system. We note also that from prior differential scanning calorimetry work performed in 2017, no obvious dehydrogenation of the eutectic could be seen, and the eutectic was stable to three cycles.

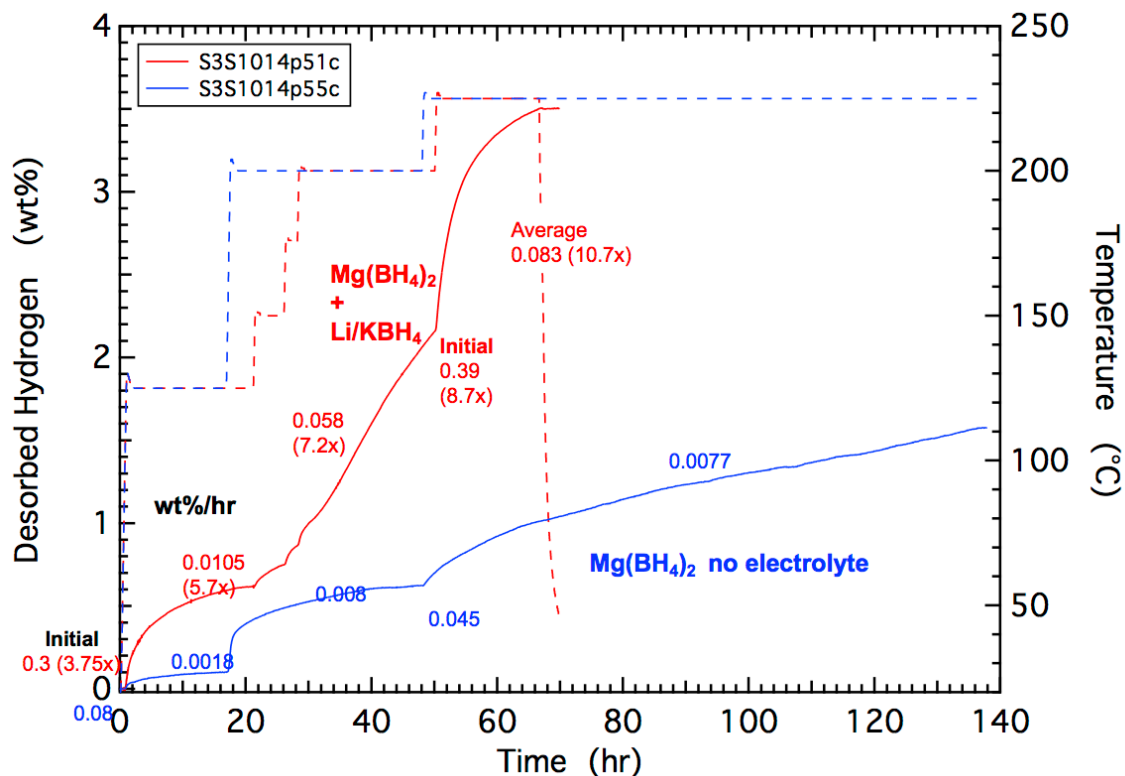


Figure 3. Desorbed hydrogen from the $\text{Mg}(\text{BH}_4)_2$ compound with (red) and without (blue) a borohydride electrolyte. The final temperature for these traces of 225 °C is below the >350 °C temperature necessary for complete dehydrogenation.

Confirmation of the Conversion of $\text{MgB}_2 \rightarrow \text{Mg}(\text{BH}_4)_2$ System Using an Iodide Electrolyte

With the help of Vitalie Stavila at Sandia National Laboratories, hydrogenation of MgB_2 both with and without an iodide electrolyte was performed using 1,000 bar pressure at 320 °C over 50 h. Subsequent dehydrogenation of these samples showed significant hydrogenation (6.3 wt%) using the electrolyte, whereas negligible (0.22 wt%) hydrogenation occurred in the absence of an electrolyte. Nuclear magnetic resonance spectroscopy was used to confirm the Sieverts results, and traces of the eutectic-containing sample before and after hydrogenation treatment are shown in Figure 4.

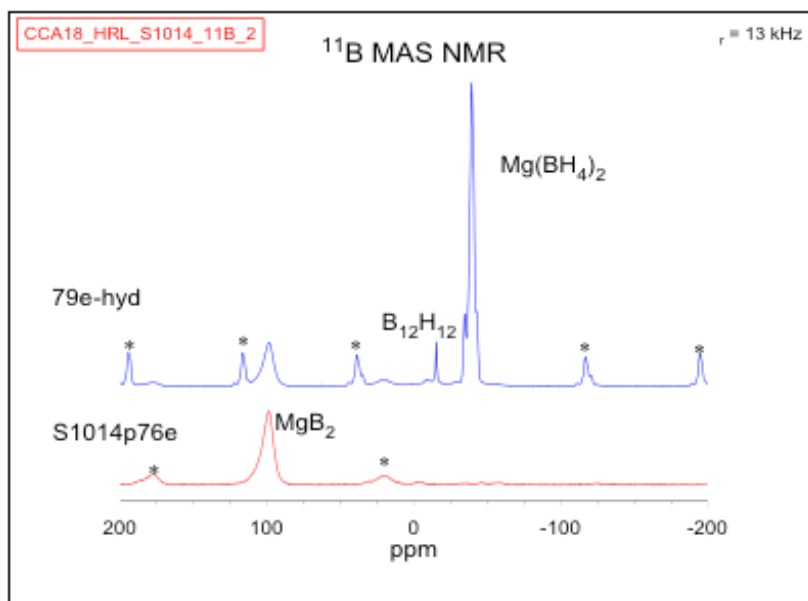


Figure 4. ^{11}B NMR confirmation of $\text{MgB}_2 \rightarrow \text{Mg}(\text{BH}_4)_2$ conversion comparing MgB_2 before hydrogenation (red trace) and after hydrogenation (blue trace) in the presence of an iodide eutectic. We note that there was little uptake without the eutectic.

PHASE 1 CONCLUSIONS AND UPCOMING ACTIVITIES FOR PHASE 2

Given our success in achieving a $10\times$ kinetic improvement with the $\text{MgH}_2/(\text{Si}$ and $\text{Sn})$ destabilization reaction and kinetic improvement of the $\text{Mg}(\text{BH}_4)_2$ compound through the use of electrolytes, solubilization of the reactant phases has enabled fulfillment of the go/no-go requirements for Phase 1 of this effort, which ended in June 2018.

Immediate tasks for Budget Period 2 of the Phase 2 effort will consist of:

- Lowering the temperature and pressure required for hydrogenation of MgB_2 and the dehydrogenation of $\text{Mg}(\text{BH}_4)_2$ or other systems (capable of ≥ 8 wt% hydrogen on a full material basis).
- Application of electrolyte assist to practical systems (capable of ≥ 4 wt% hydrogen on a full material basis).
- Demonstration of electrochemically promoted hydrogen cycling.

SPECIAL RECOGNITIONS & AWARDS/PATENTS ISSUED

1. Patent Invention Disclosure: “Hydrogen storage material formulations containing electrolytes,” filed June 1, 2017.

FY 2018 PUBLICATIONS/PRESENTATIONS

1. Channing Ahn, “HyMARC Seedling: Electrolyte Assisted Hydrogen Storage Reactions,” ST137, presented at the 2018 DOE Hydrogen and Fuel Cells Annual Merit Review, Washington DC, June 14, 2018.
2. Channing Ahn, “HyMARC Seedling: Electrolyte Assisted Hydrogen Storage Reactions,” presented to the Storage Tech Team, Southfield, MI, September 12, 2018.

REFERENCES

1. Lennie E. Klebanoff and Jay O. Keller, “5 Years of Hydrogen Storage Research in the U.S. DOE Metal Hydride Center of Excellence (MHCoe),” *International Journal of Hydrogen Energy* 38 (2013): 4533–76.

HyMARC Seedling: Development of Magnesium Boride Etherates as Hydrogen Storage Materials

Godwin Severa (Primary Contact), Cody Sugai, Stephen Kim and Craig Jensen
University of Hawaii at Manoa
1680 East West Rd, POST 109
Honolulu, HI 96822
Phone: (808) 956-3723
Email: severa@hawaii.edu

DOE Manager: Katie Randolph
Phone: (720) 356-1759
Email: Katie.Randolph@ee.doe.gov

Contract Number: DE-EE0007654

Project Start Date: October 1, 2016
Project End Date: February 28, 2019

Overall Objectives

- Improve the hydrogen cycling kinetics and cycling capacity of a magnesium boride/magnesium borohydride system to meet DOE hydrogen storage targets.
- Synthesize and characterize novel modified magnesium boride (MgB_2) materials with improved hydrogen cycling kinetics and hydrogen storage capacities.
- Determine if the reversible hydrogenation of novel modified borides show vastly improved hydrogen cycling kinetics and cycling capacities to levels that are practically viable.
- Demonstrate capability of modified MgB_2 materials to meet the DOE 2020 hydrogen storage targets.

Fiscal Year (FY) 2018 Objectives

- Continue to synthesize and characterize novel modified magnesium borides.
- Demonstrate reversible hydrogenation of ≥ 7.0 wt% at ≤ 700 bar and $\leq 300^\circ\text{C}$ by a modified MgB_2 .
- Determine the factors that limit hydrogen cycling kinetics.

Technical Barriers

This project addresses the following technical barriers from the Hydrogen Storage section of the Fuel Cell Technologies Office Multi-Year Research, Development, and Demonstration Plan¹:

- (A) System Weight and Volume
- (D) Durability/Operability
- (E) Charging/Discharging Rates
- (O) Lack of Understanding of Hydrogen Physisorption and Chemisorption.

Technical Targets

This project is determining whether the reversible hydrogenation of modified magnesium borides shows vastly improved hydrogen cycling kinetics while extending the cycling capacities to levels that are practically viable. Current improvements in kinetics have been demonstrated by the decrease in both hydrogenation pressure and temperature—to 700 bar and 300°C —of a modified magnesium boride material with at least 6 wt% hydrogen uptake. Insights gained from this project will be applied toward the development of modified boride hydrogen storage materials that meet the following DOE hydrogen storage targets:

- System gravimetric capacity: 0.055 kg H_2 /kg system
- System volumetric capacity: 0.040 Kg H_2 / L system
- Durability/operability (max hydrogen delivery temperature): 85°C
- Charging/discharging rates (system fill times for 5 kg hydrogen): 1.5 kg H_2 / min.

FY 2018 Accomplishments

- The effect of modifiers/additives on enhancing MgB_2 hydrogenation to $\text{Mg}(\text{BH}_4)_2$ was proved beyond ethers, and the presence of metals and

¹ <https://www.energy.gov/eere/fuelcells/downloads/fuel-cell-technologies-office-multi-year-research-development-and-22>

metal hydrides was observed to improve MgB_2 hydriding at 300°C and 700 bar.

- Infrared vibrational spectroscopy (FT-ATR-IR) and ^{11}B nuclear magnetic resonance (NMR) studies of hydrogenated modified MgB_2 directly confirmed $\text{Mg}(\text{BH}_4)_2$ formation.
- Temperature-programmed desorption (TPD) analyses at the National Renewable Energy Laboratory (NREL) confirmed that the 300°C and 700 bar hydrogenated MgB_2 -THF-40 mol% Mg and MgB_2 -THF-5 mol% Mg had a hydrogen uptake of about 6 wt% and 4 wt% hydrogen, respectively, after adjusting for the hydrogen released by the MgH_2 formed by the hydrogenation of added excess Mg.
- Mass spectroscopy analyses showed that the evolved hydrogen from the hydrogenated modified MgB_2 samples contained only negligible, trace amounts of impurities.

INTRODUCTION

Magnesium borohydride, $\text{Mg}(\text{BH}_4)_2$, is one of the few materials with a gravimetric hydrogen density (14.7 wt% H_2) that is sufficient to meet the requirements of DOE hydrogen storage targets and also possesses thermodynamics ($\Delta H^\circ = 39 \text{ kJ/mol H}_2$, $\Delta S = 112 \text{ J/K mol H}_2$) that permit reversible hydrogen release under moderate pressure and temperature. However, due to extremely slow kinetics, cycling between $\text{Mg}(\text{BH}_4)_2$ and MgB_2 has been accomplished only at high temperature ($\sim 400^\circ\text{C}$) and under high charging pressure ($\sim 900 \text{ bar}$). More recently, tetrahydrofuran (THF) complexed to magnesium borohydride has been shown to vastly improve the kinetics of dehydrogenation, enabling the rapid release of hydrogen at $<200^\circ\text{C}$ to give $\text{Mg}(\text{B}_{10}\text{H}_{10})$ with high selectivity. However, these types of materials have much lower hydrogen cycling capacities because of the weight contribution of the coordinated ethers. However, extending the dehydrogenation to $\text{MgB}_2\cdot(\text{ether})_x$ type materials would result in a system hydrogen density that would potentially meet DOE targets. If successful, the solid-state modified MgB_2 materials would be safer and cheaper than the high-pressure compressed hydrogen (700 bar) or liquid hydrogen alternative onboard storage systems on the market.

APPROACH

The project explores the effect of modifiers or additives such as ethers on the hydrogenation properties of MgB_2 to $\text{Mg}(\text{BH}_4)_2$. In addition to the electronic perturbation caused by the interaction of the modifiers with the magnesium or boron, which may alter the thermodynamics of the reversible hydrogenation of MgB_2 , the presence of the modifiers can also result in kinetic enhancement of phase changes in the $\text{Mg}(\text{BH}_4)_2/\text{MgB}_2$ system. Because significant hydrogenation of magnesium boride to magnesium borohydride has only been achieved at very high pressure ($\sim 900 \text{ bar}$), a high-pressure system will be utilized initially for hydrogenation of the modified borides to magnesium borohydride. We therefore intend to team with the Hydrogen Materials Advanced Research Consortium (HyMARC) to utilize their high-pressure capabilities in the hydrogenation of the modified magnesium boride as well as their surface characterization equipment. We will determine if the modifier- MgB_2 bonding remains intact during the reversible hydrogenation of boride to borohydride and, if so, what influence it has on the reaction kinetics and thermodynamics. Of foremost interest will be the reduction of the temperatures and pressures required for the hydrogenation and subsequent dehydrogenation of the boride materials. The ratio of modifier to the MgB_2 will be optimized to allow for the maximum attainable gravimetric and volumetric density without sacrificing hydrogen cycling kinetics at moderate conditions. We will determine whether the modified MgB_2 materials can access new polyborane reaction pathways that prevent formation of $\text{MgB}_{12}\text{H}_{12}$ during hydrogen cycling. An inherent endeavor of the project will be to understand the mechanisms of kinetic enhancement and intermediates formed during the hydrogenation and dehydrogenation process to optimize the hydrogen storage performance of the modified $\text{MgB}_2/\text{Mg}(\text{BH}_4)_2$ materials. A thorough correlation of experiments with theory will be utilized in this effort using HyMARC's multiscale modeling approaches (kinetic Monte Carlo simulation and phase field modeling) to help elucidate the kinetic constraints on hydrogen cycling resulting at both particle surface interfaces and within the bulk of the materials. The results of these studies will provide us with adequate insight to conceivably identify a magnesium boride species whose hydrogen cycling kinetics are adequate to meet the DOE target.

RESULTS

In the second fiscal year of the project we built upon the first fiscal year's successful validation of the project's core hypotheses: ether or ether-derived species perturb the MgB_2 material, resulting in improved hydrogenation of a modified MgB_2 ($\text{MgB}_2\text{-THF}$) to $\text{Mg}(\text{BH}_4)_2$ compared to the pure MgB_2 . The major effort in the second fiscal year was on finding approaches to further perturb the MgB_2 structure in the $\text{MgB}_2\text{-THF}$ system to enhance hydrogen uptake kinetics to meet project objectives. A major effort was placed on demonstrating that the project meets the go/no-go criteria of Budget Period 1—hydrogen uptake target of 7 wt% and hydrogen release target of 2 wt%—while still maintaining the 300°C and 700 bar hydrogenation targets achieved in the first fiscal year. Since we had observed hydrogen release in TPD-mass spectroscopy experiments we performed on $\text{MgB}_2\text{-THF}$ samples in collaboration with Dr. Gennett's group at NREL, we concluded that a hydride or metal species such as MgH_2 or Mg could be playing a role in the hydrogenation of the MgB_2 under milder conditions. Furthermore, the improved hydrogenation of the $\text{MgB}_2\text{-THF}$ doped with 5

mol% LiH prepared under milder conditions (9 h BM vs. 20 h for MgB₂-THF) supported the plausibility of hydride species playing a significant role in the MgB₂ hydrogenation process. As a result, we sought to enhance the species potentially formed during the mechanochemical reactions of MgB₂ and THF that could also be aiding hydrogen uptake kinetics in the MgB₂-THF samples. We envisioned that such a holistic consideration of the factors impacting the MgB₂ structure could help provide in-depth fundamental understanding on how the THF and/or THF-derived species are perturbing the MgB₂ structure and causing vast improvements in hydrogenation kinetics.

Modified MgB₂ synthesis procedures developed in the first fiscal year at University of Hawaii were utilized, with emphasis on a mechanochemical approach as it was observed to result in better modified MgB₂ materials. Hence, we performed mechanochemical synthesis experiments on improving hydrogen uptake kinetics of a MgB₂-THF system through use of metal hydride-based modifiers (e.g., ≤40 mol% MgH₂ and ≤40 mol% Mg). Furthermore, due to the envisioned plausibility of the metal hydride or metal modifiers improving the hydrogenation of MgB₂ without ethers, mechanical mixing of these modifiers with MgB₂ were also performed under similar reaction conditions. Following the syntheses of the modified MgB₂ materials at University of Hawaii, hydrogenation experiments of the modified MgB₂ materials were performed at 300°C, 700 bar for ≤72 hours at HyMARC's Sandia National Laboratories facility in collaboration with Dr. White, Dr. Stavila, and Dr. Allendorf. The hydrogenation of ether-modified MgB₂ samples was performed separately from that of the non-ether-modified samples.

Following hydrogenation, the products of hydrogenation were characterized at University of Hawaii by a variety of techniques including solid-state and solution ¹¹B and ¹H nuclear magnetic resonance (NMR), X-ray diffraction (XRD), infrared vibrational spectroscopy (FT-ATR-IR), thermogravimetric analysis (TGA), and differential scanning calorimetry (DSC). TGA of the hydrogenated products was performed at 5°C/min under argon flow of 100 mL/min up to 500°–600°C to determine the extent of hydrogen uptake by the samples. Much higher levels of hydrogen uptake were observed with samples of MgB₂ or MgB₂-THF materials that were ball milled with the Mg or MgH₂ (Figure 1). However, the amount of hydrogen uptake (after adjusting for the hydrogen released by the MgH₂ added to the reaction mixture or the MgH₂ formed by the hydrogenation of added excess Mg) was highly variable: 1–5 wt% depending upon the level of oxidation to MgO and Mg₃(BO₃)₂ that occurred. The extent of hydrogenation was greater than that obtained from the hydrogenation of MgB₂ modified with THF only, at 700 bar and 300°C, which released less than 1 wt% hydrogen. Thus, our results suggest that the hydrogenation of MgB₂-THF without added MgH₂ or Mg at the milder conditions results in mostly surface hydrogenation. TPD studies coupled with mass spectroscopy analyses were performed at NREL in the range of 1–50 amu on the samples of the reaction mixtures that were found to have undergone high levels of hydrogen uptake (Figure 2). These analyses verified that the evolved hydrogen contained only negligible, trace amounts of impurities. Comparison of these results with those obtained from a TiH₂ standard indicated that the hydrogenation of the MgB₂-THF-40 mol% Mg, MgB₂-THF-5 mol% Mg, and MgB₂-40 mol% MgH₂ resulted in the uptake of 6.0, 4.0, and 3.7 wt% hydrogen, respectively, after adjusting for the hydrogen released by the MgH₂ added to the reaction mixture or the MgH₂ formed by the hydrogenation of added excess Mg. As the high-pressure reactor system did not have the capability to directly measure hydrogen uptake during the high-pressure hydrogenation process, the amount of hydrogen released from the hydrogenated sample using TPD-mass spectroscopy at NREL was used as an indicator of the least amount of hydrogen uptake by the sample. The direct observation of about 8 wt% hydrogen release from TPD-mass spectroscopy analyses of hydrogenated MgB₂-THF-40 mol% Mg materials confirmed that these materials met the go/no-go hydrogen uptake target of 7 wt% and the go/no-go hydrogen release target of 2 wt%.

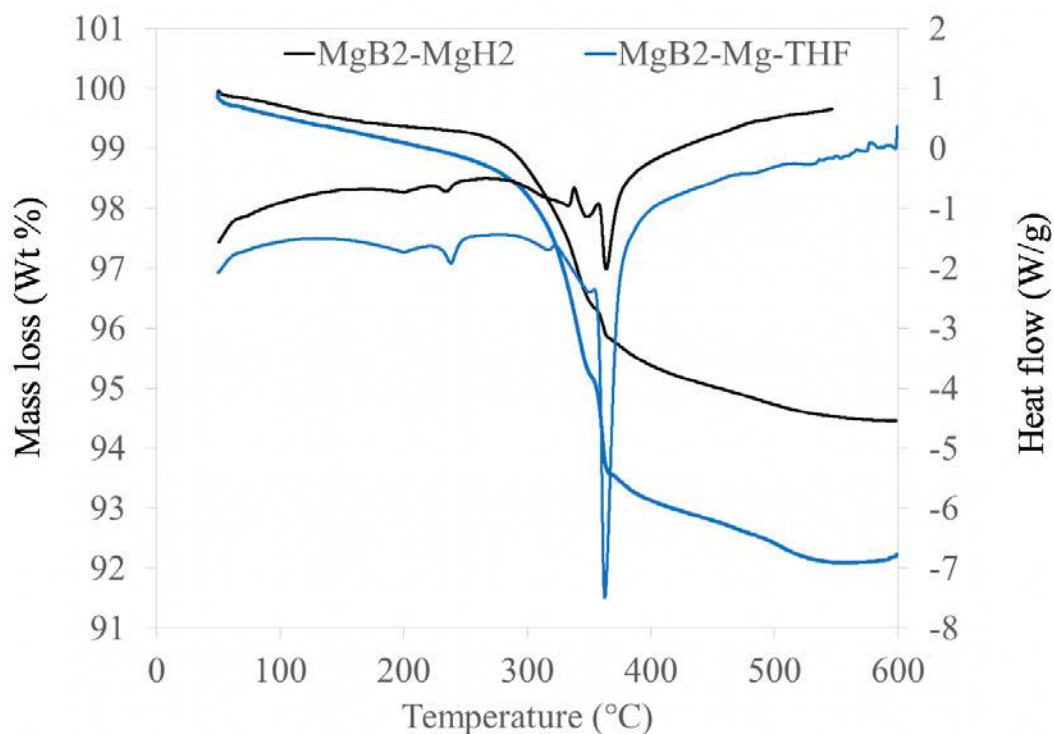


Figure 1. Typical TGA/DSC of $\text{MgB}_2\text{-THF-40 mol\% Mg}$ and $\text{MgB}_2\text{-40 mol\% MgH}_2$ hydrogenated at 700 bar and 300°C undergoing dehydrogenation

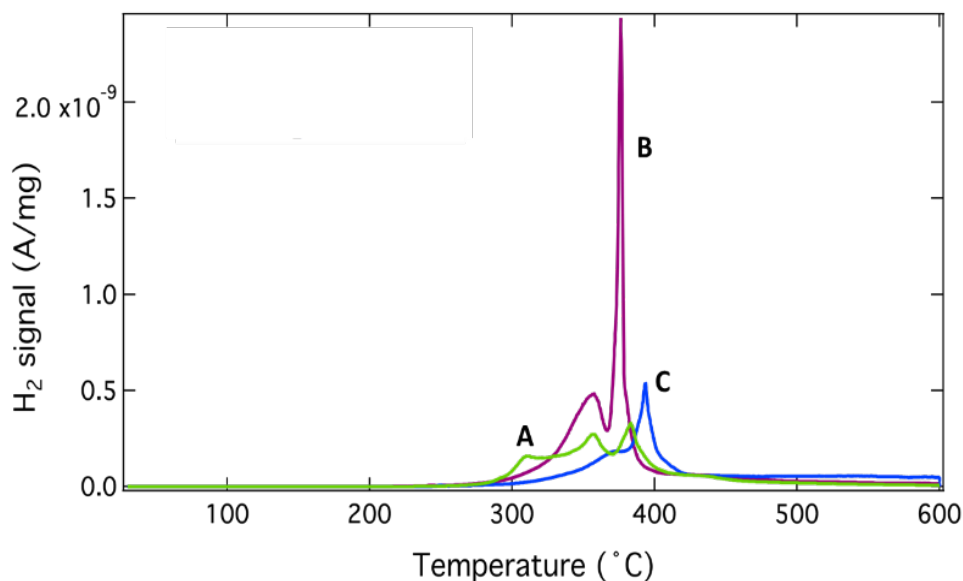


Figure 2. Typical TPD-mass spectroscopy analyses of materials hydrogenated at 700 bar and 300°C. (A) $\text{MgB}_2\text{-THF-5 mol\% Mg}$, (B) $\text{MgB}_2\text{-THF-40 mol\% Mg}$, and (C) $\text{MgB}_2\text{-40 mol\% MgH}_2$ products.

Following thermal analyses, solid and solution ^{11}B and ^1H NMR spectroscopy was performed. The presence of $\text{Mg}(\text{BH}_4)_2$ in the hydrogenated samples was confirmed by observance of peaks at about -41 ppm in the ^{11}B solid-state or solution NMR spectra (Figure 3). The products from the hydrogenation reactions were also analyzed by infrared vibration spectroscopy. The spectra were obtained using a Nicolet iS10 spectrometer with

an attached diamond crystal accessory that allowed the spectra to be collected in an attenuated total reflectance (ATR) mode. As seen in Figure 4, the spectra of the products obtained from the hydrogenation of MgB_2 -40 mol% MgH_2 and MgB_2 -THF-40 mol% Mg verify the formation of $\text{Mg}(\text{BH}_4)_2$, as the characteristic absorptions of borohydride are clearly present, the B–H stretches $2,400\text{ cm}^{-1}$ – $2,200\text{ cm}^{-1}$, and B–H bends at $1,100\text{ cm}^{-1}$ – $1,300\text{ cm}^{-1}$. The NMR and FT-ATR-IR analyses confirmed for the first time MgB_2 to $\text{Mg}(\text{BH}_4)_2$ formation from a non-ether-modified MgB_2 material at 300°C and 700 bar. These results indicate it is plausible that other modifiers besides ethers, metals, and metal hydrides may be capable of assisting in destabilizing the MgB_2 structure, enabling hydrogenation of MgB_2 to $\text{Mg}(\text{BH}_4)_2$ at much milder reaction conditions. Theoretical modeling work on the project continues to be led and performed by Dr. Wood's group at Lawrence Livermore National Laboratory, including Dr. Shinyoung Kang and Sabrina Wan. The molecular dynamic simulations of the interaction of MgB_2 layers with THF show strong interaction between THF and MgB_2 . The THF or THF-derived species are observed to interact with the Mg and B atoms. These interactions are seen to consequently induce defect formation in the MgB_2 structure, which may facilitate hydrogenation.

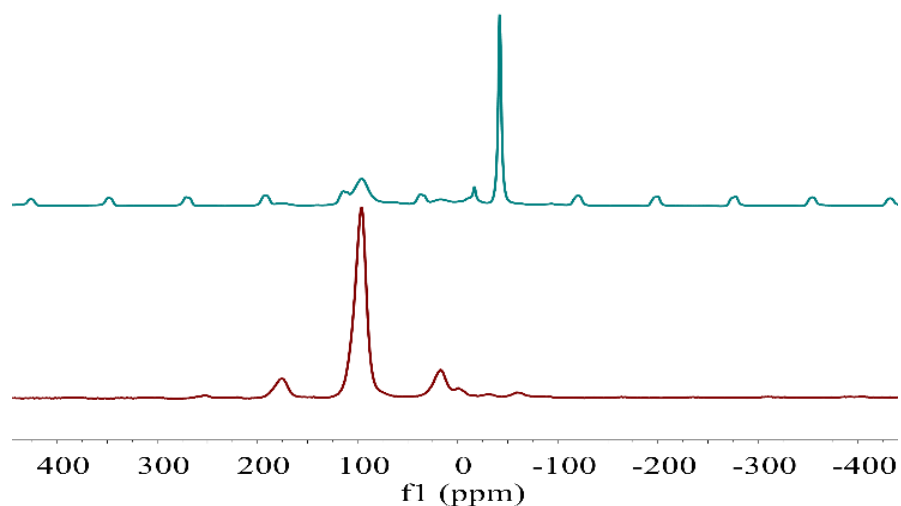


Figure 3. Solid-state ^{14}B MAS-NMR of product of MgB_2 -THF-Mg hydrogenation at 700 bar and 300°C , showing formation of $\text{Mg}(\text{BH}_4)_2$ at -41 ppm, $\text{MgB}_{12}\text{H}_{12}$ at -15 ppm, and MgB_2 at 97 ppm. The boron frequency is 128.3 MHz. All remaining peaks are spinning side bands.

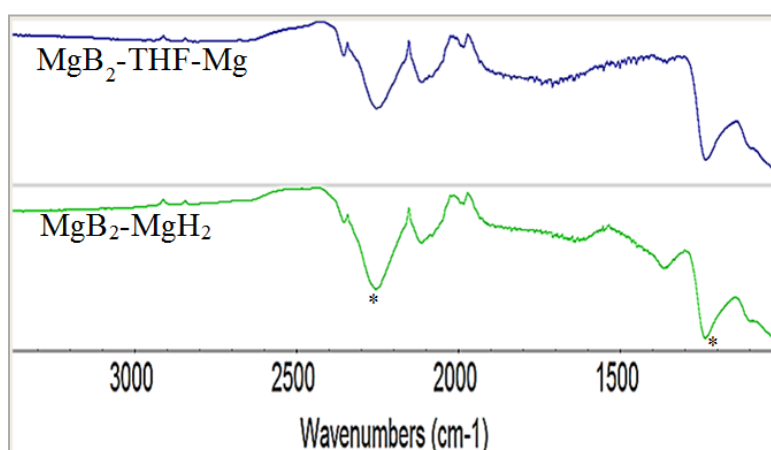


Figure 4. Typical FT-ATR-IR of hydrogenated materials, showing new intense vibrations (asterisked) at $2,200$ – $2,400\text{ cm}^{-1}$ and $1,200$ – $1,300\text{ cm}^{-1}$ due to borohydride. Peaks at $\sim 2,100\text{ cm}^{-1}$ are characteristic of the unreacted MgB_2 .

CONCLUSIONS AND UPCOMING ACTIVITIES

In the second fiscal year of the project we have managed to expand our initial hypotheses of MgB_2 perturbation beyond ether interaction, hence potentially offering new pathways for improving the kinetics of MgB_2 hydrogenation to $\text{Mg}(\text{BH}_4)_2$. We have developed modified MgB_2 materials from direct mechanochemical reactions of MgB_2 with metals and metal hydrides in the presence or absence of THF. Improved hydrogenation of MgB_2 to $\text{Mg}(\text{BH}_4)_2$ at 300°C and 700 bar was observed from the modified MgB_2 materials compared to the MgB_2 -THF only or pure MgB_2 . FT-ATR-IR and ^{11}B NMR analyses of hydrogenated modified MgB_2 directly confirmed $\text{Mg}(\text{BH}_4)_2$ formation at 300°C and 700 bar. TPD studies performed in collaboration with NREL verified that the evolved hydrogen from hydrogenated products contained only negligible, trace amounts of impurities. The TPD analyses confirmed that the hydrogenation of the MgB_2 -THF-40 mol% Mg, MgB_2 -THF-5 mol% Mg, and MgB_2 -40 mol% MgH_2 at 300°C and 700 bar results in the uptake of 6.0, 4.0, and 3.7 wt% hydrogen, respectively, after adjusting for the hydrogen released by the MgH_2 added to the reaction mixture or the MgH_2 formed by the hydrogenation of added excess Mg. Theoretical studies indicated THF interaction with MgB_2 with subsequent defect formation in MgB_2 .

Future work guided by the need to attain DOE onboard targets includes:

- Synthesize novel modified magnesium boride materials.
- Continue to lower hydrogenation temperature and pressure of modified magnesium borides to DOE 2020 target-relevant conditions.
- Perform multiple hydrogen cycling studies of the modified MgB_2 materials.
- Demonstrate reversible hydrogen uptake of ≥ 8 wt% at 400 bar and 300°C.
- Demonstrate 50% cycling stability through three cycles of an optimal formulation of a modified MgB_2 to $\text{Mg}(\text{BH}_4)_2$.
- Perform in situ NMR studies of dehydrogenation of modified Mg boranes.
- Understand mechanisms of hydrogenation enhancement by modifiers.
- Study size-dependent stability and morphology of MgB_2 clusters + particles.

FY 2018 PUBLICATIONS/PRESENTATIONS

1. G. Severa and C. Jensen, “Development of Magnesium Boride Etherates as Hydrogen Storage Materials,” Presentation at the 2018 DOE Annual Merit Review and Peer Evaluation Meeting, Washington, D.C., June 2018.
2. G. Severa, C. Jensen, C. Sugai, S. Kim, S. Kang, J. White, V. Stavila, M. Allendorf, and B. Wood, “Activated Magnesium Boride Based Materials for Hydrogen Storage,” Presentation at the 255th ACS National Meeting, New Orleans, LA, March 15–22, 2018.
3. G. Severa, C.M. Jensen, C. Sugai, and S. Kim, “Activated Magnesium Boride Materials for Hydrogen Storage,” PCT International patent, pending (2018).

HyMARC Seedling: Fluorinated Covalent Organic Frameworks: A Novel Pathway to Enhance Hydrogen Sorption and Control Isothermic Heats of Adsorption

Justin C. Johnson (Primary Contact),
Wade A. Braunecker, Katherine Hurst,
Alan Sellinger (Colorado School of Mines)
National Renewable Energy Laboratory (NREL)
15013 Denver West Parkway
Golden, Colorado 80401
Phone: (303) 384-6109
Email: justin.johnson@nrel.gov

DOE Manager: Jesse Adams
Phone: (720) 356-1421
Email: Jesse.Adams@ee.doe.gov

Subcontractor:
Colorado School of Mines, Golden, CO

Project Start Date: October 1, 2017
Project End Date: November 30, 2019

Overall Objectives

- Synthesize and characterize a series of partially fluorinated covalent organic frameworks (COFs) that are intended to exhibit improved long-range ordering and assist in tuning hydrogen binding enthalpy.
- Substitute metal-chelating moieties in the framework structure to enhance hydrogen binding enthalpy and demonstrate a pathway to values between 10 and 15 kJ/mol.
- Tune adsorption isotherms using a target mixture of binding sites, assisted by theoretical predictions.
- Produce a COF with at least 4 wt% of excess hydrogen capacity and 40 g/L total volumetric capacity. Isothermic heat of adsorption will be >10 kJ/mol for a non-metallated COF or >12 kJ/mol for a metallated COF.

Fiscal Year (FY) 2018 Objectives

- Produce 100 mg of pure COF-0, COF-OH, COF-F50, and COF-F100.

- Synthesize 100 mg of COF series (1 and 2) with linker sites for metal chelation.
- Determine relative degrees of enhanced long-range ordering between H-bonding and fluorination strategies.
- Metallate COFs and determine influence of fluorine on enhanced binding of hydrogen at metal sites.
- Determine influence of strategic fluorination on hydrogen adsorption enthalpy through solvent and modified linker adaptations.

Technical Barriers

This project addresses the following technical barriers from the Hydrogen Storage section of the Fuel Cell Technologies Office Multi-Year Research, Development, and Demonstration Plan¹:

- (A) Durability/Operability
- (D) Charging/Discharging Rates
- (O) Lack of Understanding of Hydrogen Physisorption and Chemisorption.

Technical Targets

Technical targets are shown in Table 1.

The operating ambient temperature target is recast in terms of isothermic heats of adsorption for hydrogen for this project as >12 kJ/mol.

FY 2018 Accomplishments

- Discovered that partial fluorination of COF structures can increase crystallinity and improve Brunauer-Emmet-Teller (BET) surface areas by nearly a factor of two compared with the non-fluorinated COFs.
- Measured an enhanced hydrogen gravimetric capacity for the partially fluorinated COF (~2.8 wt%) vs. the nonfluorinated COF (~1.9 wt%).

¹ <https://www.energy.gov/eere/fuelcells/downloads/fuel-cell-technologies-office-multi-year-research-development-and-22>

- Measured an enhanced hydrogen isosteric heat of adsorption for the fluorinated COF (~7 kJ/mol at low coverage) compared with the partially fluorinated COF (~6 kJ/mol at low coverage).
- Performed metalation of COF structures and discovered high binding enthalpy sites for hydrogen that can be tuned through strategic fluorination (quantitative estimates are forthcoming).
- Performed COF densification and achieved pelleted COFs with densities of 0.5–0.8 g/cm³.

Table 1. Progress Toward Meeting Technical Targets for Materials-Based Automotive Hydrogen Storage Systems

Characteristic	Units	DOE 2025 Storage System Targets	Project Status (unoptimized) – Material Performance
Excess gravimetric capacity	wt% H ₂	≥5.5	2.8
Total volumetric	g/L H ₂	40	~20

INTRODUCTION

Organic framework materials, as a unique subclass of carbon-based sorbents, have gained increasing attention for promising attributes toward gas storage. Calculations of the hydrogen capacity of optimized frameworks show potential to achieve greater than 60 g/L storage of hydrogen, placing metal-organic frameworks and COFs near the top of the class of porous materials. However, at the ensemble level, poor stacking creates a quasi-amorphous material with low structural integrity and low effective surface area. The chemical versatility of COFs allows for additional methods for producing long-range order that specifically target the inter-layer interactions in COFs but leave key pore-accessible linker sites open. These modifications (either during synthesis or post-synthetic) enable a host of strategies to improve crystalline order for better stability and higher surface area as well as to add metals with open coordination sites for enhanced hydrogen binding enthalpy.

APPROACH

Synthesis of the COF structures was performed using a condensation reaction involving aldehyde and amine precursors (Figure 1). The different COFs 1–4 were functionalized through substitution of the precursors. Reaction conditions were optimized to produce a high yield and the highest crystalline material possible as a powder. Metals were introduced into the COF structures post-synthetically using metal salts and thermal treatments. Subsequent characterization included X-ray diffraction studies for crystallinity determination, BET surface area analysis, transmission electron microscopy, and thermogravimetric analysis for COF thermal stability. Hydrogen sorption studies involved diffuse-reflectance infrared spectroscopy, temperature-programmed desorption, and pressure-composition-temperature (PCT) analysis. The PCT technique provided gravimetric capacities and isosteric heats of adsorption, which are compared for different COF structures and metalation techniques. Computational modeling was also employed to predict and understand the locations of high binding enthalpy sites for hydrogen.

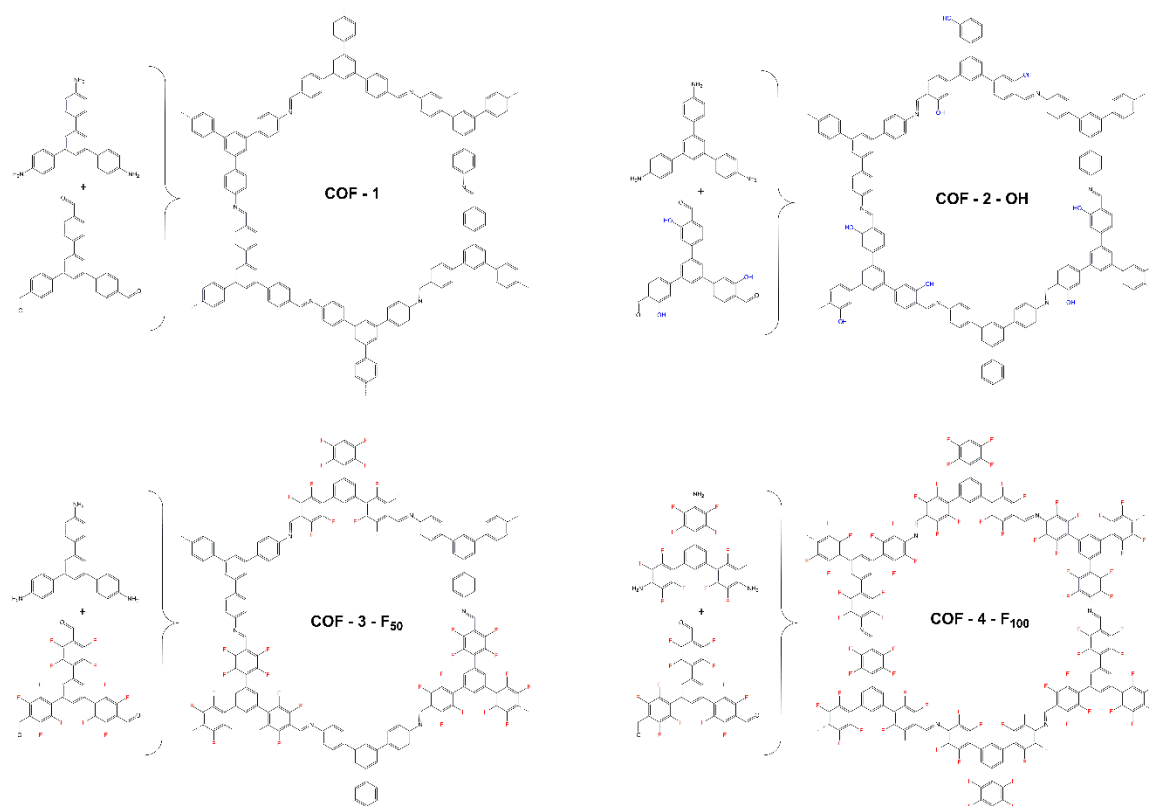


Figure 1. Structures of synthesized non-metallated COFs and the condensation reaction precursors

RESULTS

The first series of COFs synthesized to test the notion of fluorination on crystallinity and surface area is shown in Figure 1. COF-1 contains standard functionalization, COF-2 contains hydroxyl functionalization, COF-3 has roughly 50% fluorination, and COF-4 is 100% fluorinated. The respective powder X-ray diffraction patterns and BET surface areas can be found in Figure 2. The partially fluorinated COF-3 was clearly superior in terms of crystallinity and in terms of BET surface area, which reached about 95% of the predicted (Connolly) surface area. An alternating stacking motif was shown by calculations to be the most likely COF crystallization configuration; this takes advantage of perfluorophenyl and phenyl interactions that other COFs do not possess.

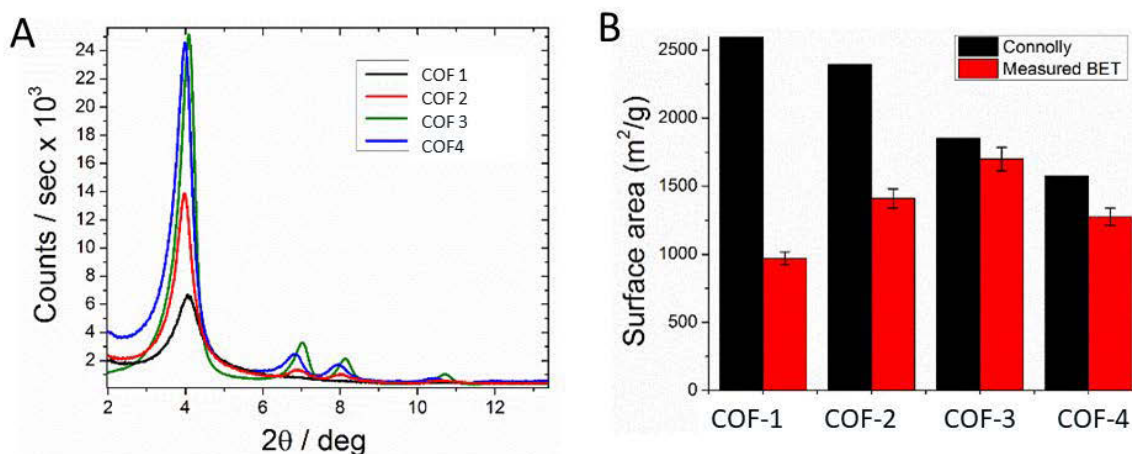


Figure 2. Powder X-ray diffraction (A) and BET surface area measurements (B) for the series of non-metallated COFs

Hydrogen sorption measurements were undertaken for all COFs, but in particular a comprehensive comparison was made between COF-1 and COF-3. The PCT sorption curves are shown in Figure 3, which reveal stronger hydrogen sorption for COF-3 than for COF-1 at 77 K. The capacity was collected at several temperatures to determine the isosteric heat of adsorption. The overall values were determined to be about 5.5 kJ/mol and about 5.0 kJ/mol for COF-3 and COF-1 respectively. However, at low coverages, the value turned up significantly for COF-3 toward 7 kJ/mol. The binding enthalpy for some preferred hydrogen sorption sites may be causing this upturn, and diffuse-reflectance infrared measurements are now being performed to confirm the result. Calculations predict a value of about 10 kJ/mol for hydrogen binding enthalpy for preferred sites in COF-3.

Metallation of COF-2 and two other related series of partially fluorinated COFs (COF-9 and COF-10) was undertaken (Figure 4). Copper salts were intercalated into the structures, and bound copper was identified using various X-ray spectroscopies as well as electron dispersive spectroscopy. Temperature-programmed desorption experiments have revealed larger binding enthalpies in the range of 9–12 kJ/mol, as well as a very strong binding site in thermally treated copper COFs, which likely have been reduced to Cu(I). Fluorination appears to affect the binding enthalpy of hydrogen in a logical fashion. Completing measurements on this series of COFs and determining an isosteric heat of adsorption is a near-term goal.

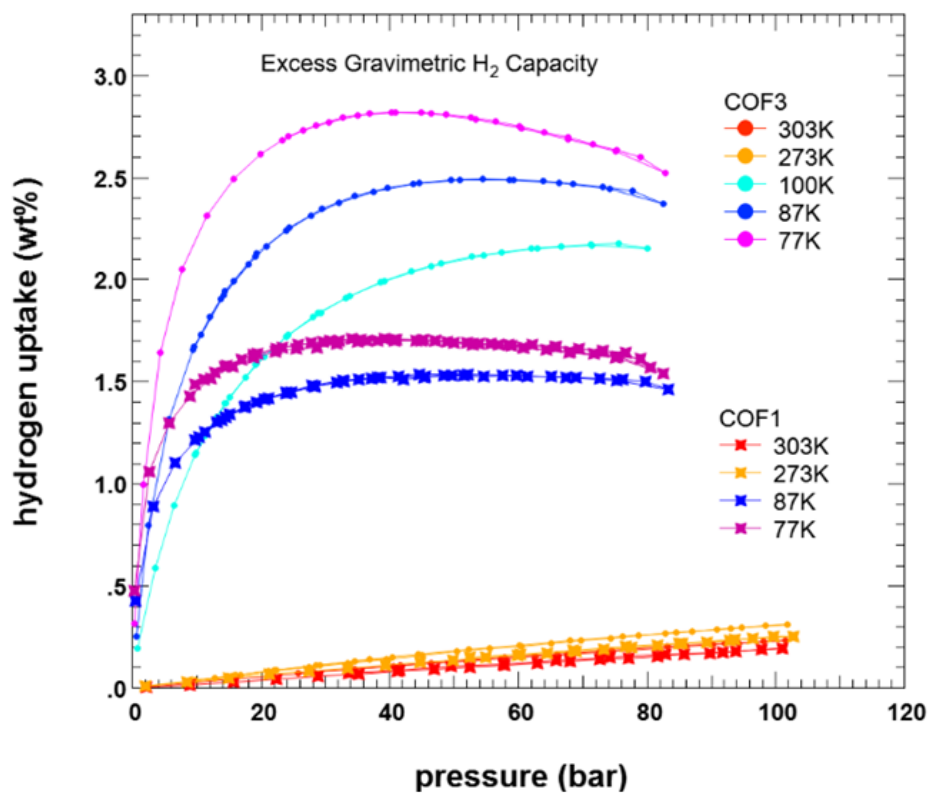


Figure 3. Hydrogen uptake vs. pressure curves measured with PCT for COF-1 and COF-3 at various temperatures

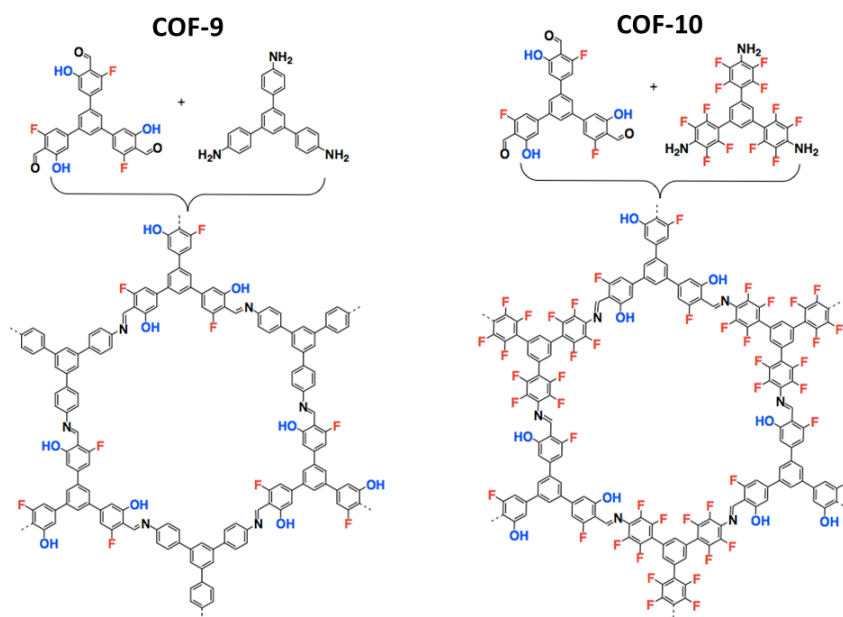


Figure 4. Structures of partially fluorinated COFs with metal binding sites between the nitrogen from the imide group and the oxygen of the hydroxyl group

CONCLUSIONS AND UPCOMING ACTIVITIES

We conclude that partially fluorinated COFs have better thermal stability, crystallinity, and gas sorption properties compared with nonfluorinated COFs. COFs with sites for binding of metal species show larger hydrogen binding enthalpies compared with non-metallated COFs, and we can tune the binding energy using fluorination. With the remaining funding for about one month of work, we will finalize the isosteric heat values using PCT for metallated COFs with differing degrees of fluorination. We will also optimize gravimetric and volumetric capacities using crystallization techniques and powder densification.

FY 2018 PUBLICATIONS/PRESENTATIONS

1. Wade A. Braunecker, Katherine E. Hurst, Zbyslaw R. Owczarczyk, Keith Ray, Madison Martinez, Noemi Leick, Amy Keuhlen, Alan Sellinger, Justin C. Johnson, “Phenyl/Perfluorophenyl Stacking Interactions Enhance Structural Order in Two-Dimensional Covalent Organic Frameworks,” *Crystal Growth and Design* 18 (2018): 4160.
2. HyMARC Kickoff Meeting, Livermore, CA, September 29, 2017.
3. Fall ACS Meeting, Boston, MA, August 20, 2018.

HyMARC Seedling: Atomic Layer Deposition Synthesis of Novel Nanostructured Metal Borohydrides

Steven Christensen (Primary Contact),
Noemi Leick, Karl Gross (subcontractor)
National Renewable Energy Laboratory (NREL)
15013 Denver West Parkway
Golden, Colorado 80401
Phone: (720) 938-8022
Email: steven.christensen@nrel.gov

DOE Manager: Jesse Adams
Phone: (720) 356-1421
Email: Jesse.Adams@ee.doe.gov

Subcontractor:
H2 Technology Consulting, Alamo, CA

Project Start Date: October 1, 2017
Project End Date: December 31, 2020

Overall Objectives / Fiscal Year (FY) 2018 Objectives*

- Demonstrate an atomic layer deposition (ALD) encapsulation matrix of magnesium borohydride that meets DOE targets for onboard hydrogen storage in light-duty vehicles by achieving a majority of the following (go/no-go):
 - Dehydrogenation/hydrogenation cyclability over three cycles
 - 3 wt% hydrogen delivery at 200°C
 - 3 wt% hydrogen uptake at 280°C, 120 bar hydrogen
 - 5x improvement on hydrogen absorption/desorption kinetics over neat $\text{Mg}(\text{BH}_4)_2$.
- Gain new insight to control hydrogen reaction pathways and kinetics (Barriers D, E, O).
- Develop ALD and vapor-phase processes that, if successful, can be scaled for manufacturing.

* This project is a 1-year seedling with potential to be expanded in a Phase 2 pending meeting the

above objectives, available funding, and DOE mission.

Technical Barriers

This project addresses the following technical barriers from the Hydrogen Storage section of the Fuel Cell Technologies Office Multi-Year Research, Development, and Demonstration Plan¹:

- (D) Durability/Operability
- (E) Charging/Discharging Rates
- (L) Lack of Understanding of Hydrogen Chemisorption.

Technical Targets

This project is developing magnesium borohydride composites that will have improved reversibility (durability/operability) and kinetics (charging/discharging rates) of hydrogen reactions. The new materials will show a path to achieving or meet the following DOE 2020 hydrogen storage targets:

- System gravimetric and volumetric capacity: 0.045 kg H_2 /kg system, 0.030 kg H_2 /L system
- Charging time (5.6 kg): 3–5 min
- Minimum full flow rate: 0.004 (g/s)/kW
- Min./max. delivery temperature: -40/85°C
- Cycle life: 1,500.

FY 2018 Accomplishments

- Developed a progression of coatings with ALD that met, surpassed, or showed a pathway to meeting individual components of the go/no-go criteria listed in overall objectives.
- Showed hydrogen cyclability over five cycles at low cycled capacity (0.5 wt%).
- Reduced hydrogen desorption temperature for $\text{Mg}(\text{BH}_4)_2$ to 107°C from 220°C.

¹ <https://www.energy.gov/eere/fuelcells/downloads/fuel-cell-technologies-office-multi-year-research-development-and-22>

- Achieved a desorbed hydrogen capacity of 6.6 wt%, which exceeded the target of 3 wt%.
- Demonstrated a ~5x improvement on hydrogen absorption and desorption kinetics.

INTRODUCTION

Domestic energy sources must be developed in order to reduce U.S. dependence on foreign fossil fuels and meet the growing demand for updated energy infrastructure with increased storage capacity. Over the past 15 years U.S. energy policy has pursued research and development of hydrogen as a viable renewable fuel for light-duty transportation and energy storage applications. Efforts from DOE along with several automakers have led to significant advancement in hydrogen-based fuel cells for light-duty vehicles. While early market adoption of hydrogen vehicles has resulted from these advances, all systems rely on storage tanks of hydrogen pressurized to 700 bar. The pressure requirements present challenges in infrastructure and delivery that could limit widespread deployment of hydrogen vehicles. Hydride materials, specifically metal borohydrides, offer a strategy to significantly reduce the pressure while still achieving the needed storage capacity-to-weight ratios. The DOE 2020 hydrogen storage system capacity targets are 30 g/L and 4.5 wt%, and the ultimate goals are 50 g/L and 6.5 wt% hydrogen. Magnesium borohydride, $\text{Mg}(\text{BH}_4)_2$, offers a hydrogen storage *material* capacity of 113 g/L and 14.9 wt%. Both the volumetric and gravimetric capacity of $\text{Mg}(\text{BH}_4)_2$ offer the potential to meet the *system* requirements DOE has identified. Development of metal borohydride technology has stalled due to the kinetics, cyclability, reaction pathways, and operating temperatures for hydrogen absorption and desorption. Prior DOE-sponsored research has shown that nanostructuring metal hydrides and the use of chemical additives can promote the necessary kinetics, control reaction pathways, and control the material phases. This project aims to incorporate these benefits into a materials hierarchy that can advance metal borohydride technology.

APPROACH

The goal of this project is to develop a completely new reversible hydrogen storage materials matrix based on encapsulation via ALD of nanostructured metal borohydrides. ALD is a vapor-phase method to grow thin films layer by layer. The metal borohydride-encapsulation architecture will include layers that will protect against loss of the nanostructure hydride and impart chemical additives to enhance kinetics and reversibility. The concept was motivated by substantial research where ALD coatings provided protective and catalytic properties to heterogeneous catalysts. ALD offers:

- Conformal coatings of materials like aluminum oxide that are inert to hydrogenation/dehydrogenation conditions
- A wide variety of chemical additives previously shown to enhance metal borohydride reversibility and kinetics like palladium or cerium oxide
- A facile means to combine these materials to tailor properties to performance.

Recent developments in ALD manufacturing have demonstrated >100 kg per day throughput on powders and other granular materials. Thus, ALD solutions to the challenges with metal borohydrides will bring to front new scientific knowledge with the potential to be scaled.

RESULTS

The project first investigated the thickness of the aluminum oxide coatings on $\text{Mg}(\text{BH}_4)_2$. Hydrogen desorption measured by temperature-programmed desorption gave the first unexpected and compelling results: hydrogen desorption improves with increasing coating thickness. Figure 1 (a) shows temperature-programmed desorption of Al_2O_3 coatings for 0, 3, 10, 50, and 100 ALD cycles. An ALD cycle is a sequence of two ALD precursor exposures (A, B) that are repeated to grow a film layer by layer. ALD of Al_2O_3 is performed by alternating exposures of trimethylaluminum and water and has a growth rate of 0.11 nanometers per cycle on flat substrates. The results from Figure 1 (a) are based on total sample mass basis, which means that the 100-cycle Al_2O_3 coating has the most inactive material (Al_2O_3) but also desorbs the most hydrogen. Furthermore, the ALD coating promotes hydrogen desorption at a lower temperature, where again the 100-cycle case performs the best. Control experiments were performed to ensure that ALD of Al_2O_3 alone does not desorb hydrogen under similar conditions. Figure 1 (b) shows an image from a transmission electron microscope of

the 100-cycle $\text{Al}_2\text{O}_3/\text{Mg}(\text{BH}_4)_2$. The image suggests that a core shell has formed, which is consistent with an encapsulated nanostructured phase. The thickness of the coating is on the order of 10–15 nanometers, which could be expected for the number of cycles performed on a granular material.

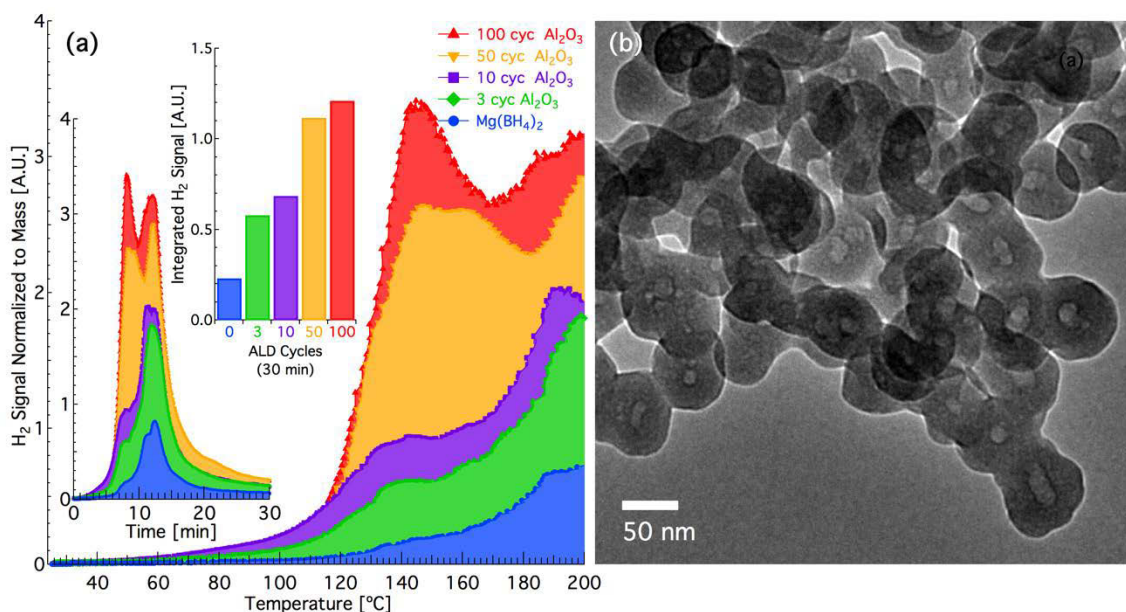


Figure 1. (a) Temperature-programmed desorption of $\text{Mg}(\text{BH}_4)_2$ coated with 3, 10, 50, and 100 cycles of Al_2O_3 . The hydrogen signal, derived from mass spectrometry, is plotted as function of temperature and time (inset). Also included as an inset is the time integration of the hydrogen signal over 30 minutes. (b) Transmission electron micrograph of $\text{Mg}(\text{BH}_4)_2$ coated with 100 cycles of Al_2O_3 .

These initial results confirm several important elements of our approach:

1. ALD coatings can produce a conformal core-shell structure
2. The coating does not inhibit hydrogen mass transport
3. Thicker coatings promote hydrogen desorption and reduce desorption onset temperature.

The latter of these addresses project and DOE goals for operability and discharge rates. This also provides the basis for the design of the materials later in the project.

Chemical additives to enhance kinetics and reversibility were next explored. Figure 2 shows the hydrogen cycling of an ALD coating on $\text{Mg}(\text{BH}_4)_2$ consisting of $\text{Al}_2\text{O}_3\text{-TiO}_2\text{-CeO}_2$. The cycling was performed with a pressure-composition-temperature (PCT) manometric apparatus. Figure 2 contains a series of hydrogen absorptions (A1, ...) and desorptions (D1, ...) measured under the criteria listed above in the overall objectives. The figure includes the hydrogen concentration (blue), system pressure (black), and sample temperature (red). The text boxes in the figure give the desorbed (blue) and absorbed (green) hydrogen quantity. Desorption is negative on the concentration scale whereas absorption is positive. The gray shaded regions on the pressure curves indicate the sample is absorbing hydrogen whereas the yellow shaded regions are transients where absorption does not occur. Absorption 1 (A1) was performed after ALD and shows little to no hydrogen uptake. Thereafter, the cycled hydrogen capacity is roughly proportional to the desorption steps. While the cycled capacity is low (0.5 wt%), the five cycles surpassed the go/no-go criteria of three cycles. The data also illustrate the aggressive goal to desorb 3 wt% hydrogen at 200°C: without the significant progress in desorption kinetics, this will not be possible. Indeed, neat $\text{Mg}(\text{BH}_4)_2$ does not desorb hydrogen until 220°C. The data from Figure 2 compared to other absorption/desorption cycles for $\text{Al}_2\text{O}_3/\text{Mg}(\text{BH}_4)_2$ and other materials indicate the Ce-based additives were important in improving cyclability and absorption.

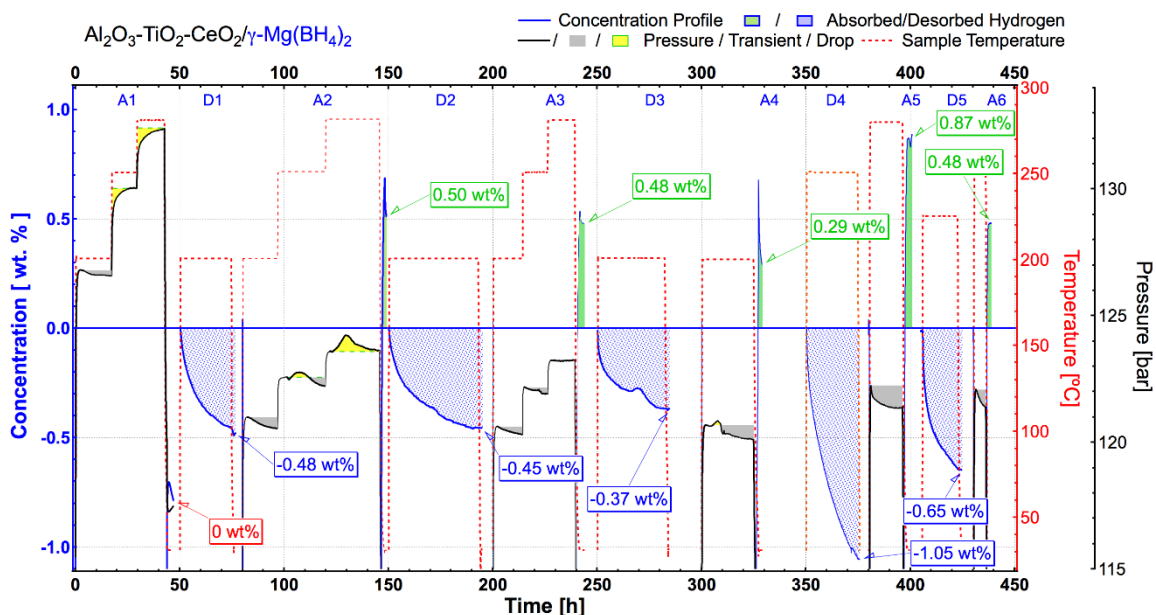


Figure 2. Hydrogen absorption (A1, A2, ...) and desorption (D1, D2, ...) cycling measured with pressure-composition-temperature manometry for $\text{Mg}(\text{BH}_4)_2$ coated with $\text{Al}_2\text{O}_3\text{-TiO}_2\text{-CeO}_2$. Represented here are hydrogen concentration (blue), sample temperature (red), and system pressure (black) where gray shaded regions indicate active hydrogen absorption. The text boxes give the hydrogen concentration after each absorption or desorption step. Absorbed hydrogen is positive on the concentration profile and desorbed hydrogen is negative.

Progress was made to increase the desorption kinetics for $\text{Mg}(\text{BH}_4)_2$ by chemical additives and new ALD processes. Screening a series of additives—including CeO_2 , TiO_2 , Pd, Ru, Al_2O_3 , and combinations of these—identified Pd/ Al_2O_3 as the leading candidate for improving desorption kinetics. The result is plotted in Figure 3, which shows 0.71 wt% hydrogen was desorbed in 24 hours, which was the best desorption result to that point but well short of the 3 wt% goal. In efforts to accelerate toward the project goals, new ALD processes were developed. The details of the ALD process and the nature of the coating are not yet ready for public disclosure. Figure 3 does show one of the results, coating X, which showed significant progress by desorbing 1.9 wt% at 200°C in 15 hours and ultimately 3 wt% after the sample temperature was raised to 220°C. Coating X/ $\text{Mg}(\text{BH}_4)_2$ also showed significant progress in absorption: 1.1 wt% was absorbed in 24 hours, making it the best so far. Figure 4 shows the progress in desorption kinetics for these new materials. The kinetic models are based on power law fits to the desorption data. A second new ALD process and coating produced even better desorption results: 6.6 wt% hydrogen, ~10 s, at 126°C. The current understanding for these new and exciting materials is unfolding and will be explored in the next phase.

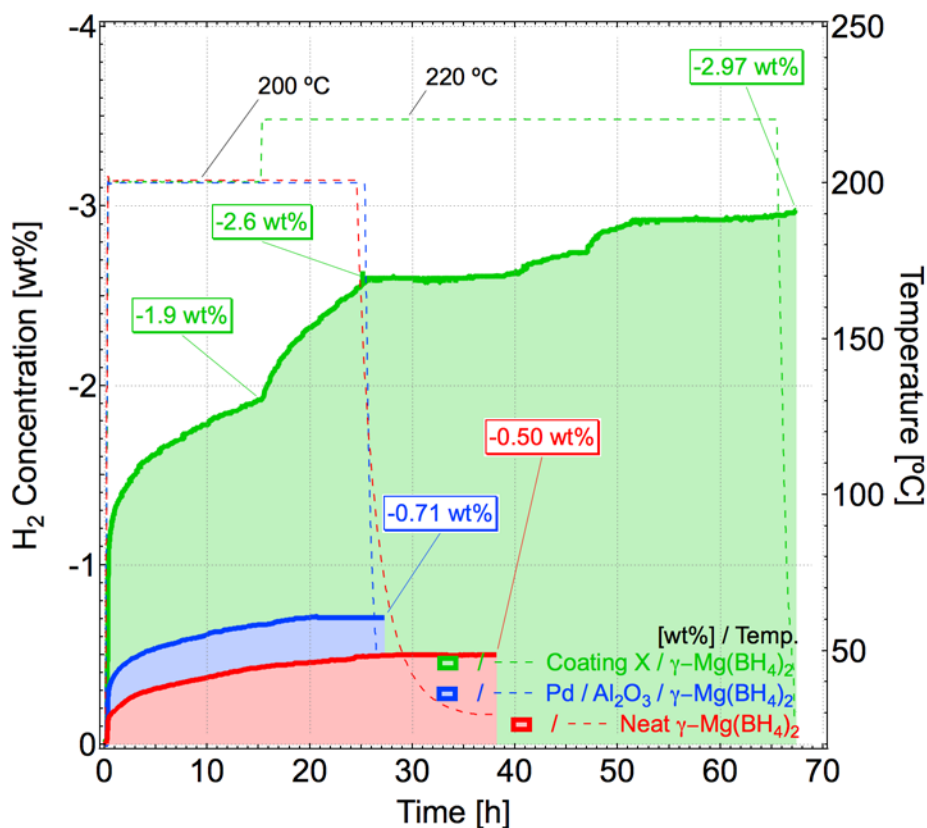


Figure 3. Hydrogen desorption progress for ALD coatings with chemical additives

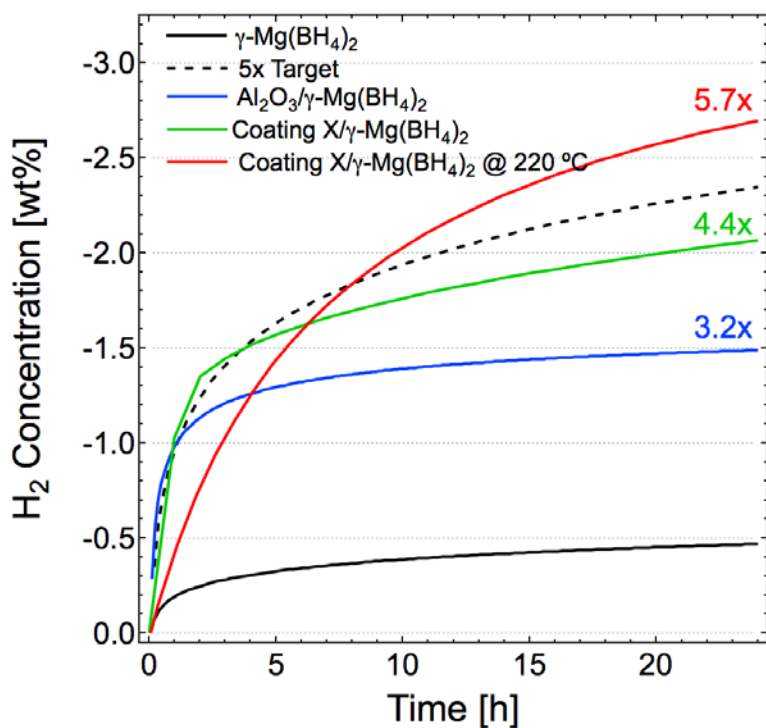


Figure 4. Hydrogen desorption kinetics for the ALD materials compared to neat Mg(BH4)2

CONCLUSIONS AND UPCOMING ACTIVITIES

The project has successfully demonstrated a new pathway to meet DOE targets for hydrogen storage. Recent developments in ALD processes and materials were key to this progress. With these progress indicators, new scientific knowledge, and synergistic activities with the Hydrogen Materials Advanced Research Consortium Energy Materials Network node, the project has been selected to Phase 2, which will focus on the using the new ALD results to improve hydrogen absorption and cyclability.

SPECIAL RECOGNITIONS AND AWARDS/PATENTS ISSUED

1. Provisional patent, “Nanostructured Composite Metal Hydrides,” USPTO Application No. 62/507,354, was converted to a non-provisional patent USPTO Application No. 15/982,232.

FY 2018 PUBLICATIONS/PRESENTATIONS

1. Presented a poster at the DOE Hydrogen and Fuel Cells Program Annual Merit Review and Peer Evaluation Meeting, Washington, DC, June 2018, ST143.
2. Presented a progress report to the DOE Hydrogen Storage Tech Team, Southfield, Michigan.

HyMARC Seedling: Optimized Hydrogen Adsorbents via Machine Learning and Crystal Engineering

Donald J. Siegel (Primary Contact, UM),
Alauddin Ahmed (UM), Suresh Kuthuru (UM)
Adam Matzger (UM), Justin Purewal (Ford), and
Mike Veenstra (Ford)
University of Michigan (UM)
Ann Arbor, MI 48109
Phone: (734) 764-4808
Email: djsiege@umich.edu

DOE Manager: Jesse Adams
Phone: (720) 356-1421
Email: Jesse.Adams@ee.doe.gov

Contract Number: DE-EE0008093

Subcontractor:
Ford Motor Company, Dearborn, MI

Project Start Date: September 1, 2017
Project End Date: August 31, 2020

Overall Objectives

- Apply machine learning (ML) techniques to design and experimentally demonstrate new metal-organic frameworks (MOFs) having usable volumetric capacities exceeding 50 g H₂/L (single-crystal/pressure swing) without compromising gravimetric capacity, kinetic performance, or reversibility.
- Control MOF crystal morphology and crystallite size distribution to increase packing density of target high-capacity MOF by at least 30% (compared to its powder tap density) with less than 15% decrease in gravimetric performance.

Fiscal Year (FY) 2018 Objectives

- Identify ranges for four MOF crystallographic properties (surface area, density, pore volume, and porosity) consistent with usable volumetric capacity of at least 40 g H₂/L and usable gravimetric capacity of at least 7 wt% (assuming an isothermal pressure swing

between 100 and 5 bar at 77 K) based on single-crystal density.

- Demonstrate that the identified ranges are within the realm of possibility for the development of new MOFs, and thus provide a pathway for meeting the DOE storage targets.
- Demonstrate the ability to predict usable capacity of an arbitrary MOF to within 85% of grand canonical Monte Carlo (GCMC) capacity using only crystal structure as input.
- Identify at least two additives to be employed during MOF synthesis that are capable of altering crystallite morphology from cubes to octahedra.

Technical Barriers

This project addresses the following technical barriers from the Hydrogen Storage section of the Fuel Cell Technologies Office Multi-Year Research, Development, and Demonstration Plan¹:

- (A) System Weight and Volume
- (B) System Cost
- (C) Efficiency.

Technical Targets

Insights gained from this study can be applied toward the development of materials that aim to meet the following DOE 2020 hydrogen storage targets:

- Cost: \$333/kg H₂
- Gravimetric capacity: 4.5 wt%
- Volumetric capacity: 30 g H₂/L

The outcomes of this project contribute to the optimization and assessment of hydrogen storage materials by identifying higher-capacity hydrogen adsorbents, in particular adsorbents that maximize volumetric hydrogen density. This project also provides input to models that project the

¹ <https://www.energy.gov/eere/fuelcells/downloads/fuel-cell-technologies-office-multi-year-research-development-and-22>

performance of these materials at the system level by quantifying and optimizing the hydrogen storage media packing density.

FY 2018 Accomplishments

- Demonstrated the ability to predict four crystallographic properties of an arbitrary MOF that correspond to specified usable gravimetric and volumetric hydrogen capacities.
- Demonstrated that the ranges of predicted crystallographic properties are within the realm of possibility for the development of new MOFs.
- Identified three additives capable of controlling morphology of MOF-5 from cubes to octahedra.
- Demonstrated control over MOF particle size from a few microns to 2 mm by varying the metal:ligand ratio. The effect of temperature and time on MOF particle size distributions was also quantified.

INTRODUCTION

A high-capacity, low-cost method for storing hydrogen remains one of the primary barriers to the widespread commercialization of fuel cell vehicles. Although many storage technologies have been proposed, storage via adsorption remains one of the more promising approaches due to its fast kinetics, facile reversibility, and high gravimetric densities. Adsorbents struggle, however, in two key measures: volumetric density and operating temperature. For example, it is well known that high-surface-area adsorbents such as MOFs can achieve high gravimetric densities. Nevertheless, high volumetric densities are uncommon in these materials, and it has recently been suggested that total volumetric density and gravimetric density are inversely related beyond a threshold surface area. In the case of operating temperatures, the relatively weak enthalpy of hydrogen adsorption implies that high hydrogen densities are possible only at cryogenic temperatures.

Although an ideal adsorbent would overcome both of these shortcomings, it is important to recognize that volumetric density and operating temperature are controlled by different factors: the former depends upon the adsorbent's structure whereas the latter depends on the chemistry of the hydrogen-adsorbent interaction. Therefore, distinct approaches are needed to address these independent issues. While some effort has previously been devoted to increasing ΔH (e.g., MOFs with open metal sites), attempts to increase volumetric densities have received much less attention. This is unfortunate, as analysis by the HSECoE has indicated that vehicle range is highly sensitive to volumetric density. Consequently, the development of adsorbents that simultaneously achieve high volumetric and gravimetric hydrogen densities—while maintaining reversibility and fast kinetics—would constitute a significant advance. Moreover, these materials would serve as logical starting points for follow-on efforts aimed at increasing the operating temperature.

APPROACH

This project aims to overcome volumetric limitations associated with physisorptive hydrogen storage at both the materials and system level. This goal will be achieved using a combination of computational techniques and experimental synthesis and testing. Our efforts will target storage media based on metal-organic frameworks (MOFs), a class of hydrogen adsorbents with highly tunable properties.

At the materials level, machine learning (ML) methods will be applied to our database of 476,007 real and hypothetical MOFs. This analysis will guide the discovery of new compounds that can break through the so-called “volumetric ceiling”. This performance ceiling was identified in our prior screening studies; it reveals that no known MOFs can surpass a usable volumetric capacity of 40 g H₂/L (assuming an isothermal pressure swing between 100 and 5 bar at 77 K). In contrast to the conventional approach to MOF discovery, where capacity is predicted from a known crystal structure, this project aims to invert this process and “reverse engineer” optimal MOFs with the aid of machine learning. The most promising compounds will be synthesized and assessed experimentally with respect to their usable hydrogen capacities.

At the system level, we will develop crystal growth and processing techniques that result in MOF-based adsorbent beds with low void fractions. Packing inefficiencies have the potential to negate improvements in volumetric performance achieved at the materials level. This project aims to close this performance gap by developing synthetic procedures that optimize particle morphology and size distribution.

RESULTS

Table 1 summarizes the inputs and outputs used in developing ML models for predicting the range of crystallographic properties that correlate with specified usable hydrogen capacities. Usable gravimetric and volumetric capacities (at 77 K assuming a pressure swing between 5 and 100 bar) determined from grand canonical Monte Carlo (GCMC) calculations were used as ML input descriptors, while the crystallographic properties were the target outputs.

In total, data from 96,402 MOFs were used for training and testing the ML models. The extremely randomized trees (ERT) [2] supervised ML algorithm was trained and tested on GCMC-calculated capacities using the Scikit-learn [3] python package. The ERT model was identified as being the most accurate ML algorithm. ERT

models were trained using data from 72,300 randomly selected MOFs from the GCMC data set. The remaining GCMC data for 24,102 MOFs were used to assess the performance of the ML model. The tunable parameters of the ERT model were optimized via a randomized grid search over plausible parameter values with 10-fold cross validation using the RandomizedSearchCV and GridSearchCV functions as implemented in Scikit-learn [3]. Table 2 summarizes the accuracy of ML predictions of crystallographic properties of MOFs using four different metrics: R^2 (correlation coefficient), AUE (average unsigned error), RMSE (root-mean-square error), and Kendall τ .

Table 1. ML Input Descriptors and Target Output Properties

ML Input Descriptor: Hydrogen storage capacity calculated via GCMC	ML Target Output: Crystallographic properties calculated via the zeo++ code [1]
Usable gravimetric (in wt%) and volumetric (in g H ₂ /L) capacities at 77 K for a pressure swing between 5 and 100 bar	(1) Single crystal density (in g/cm ³) (2) Pore volume (in cm ³ /g) (3) Void fraction (unit free) (4) Gravimetric surface area (in m ² /g) (5) Volumetric surface area (in m ² /cm ³) (6) Largest cavity diameter (in Å) (7) Pore limiting diameter (in Å)

ML models are trained using inputs to reproduce outputs.

Table 2. Accuracy of ML Predictions of MOF Crystallographic Properties

ML Predicted MOF Crystallographic Properties	R^2	AUE	RMSE	Kendall τ
Single crystal density (g/cm ³)	0.980	0.010 (g/cm ³)	0.056 (g/cm ³)	0.984
Pore volume (cm ³ /g)	0.998	0.026 (cm ³ /g)	0.035 (cm ³ /g)	0.966
Void fraction	0.947	0.017	0.029	0.904
Gravimetric surface area (m ² /g)	0.920	402 (m ² /g)	539 (m ² /g)	0.906

Correlations between ML predictions and zeo++ calculations for four crystallographic properties of MOFs are shown in Figure 1. These properties include single-crystal density, pore volume, void fraction, and gravimetric surface area. These data demonstrate the ability to predict these properties to within 92% to 99% accuracy.

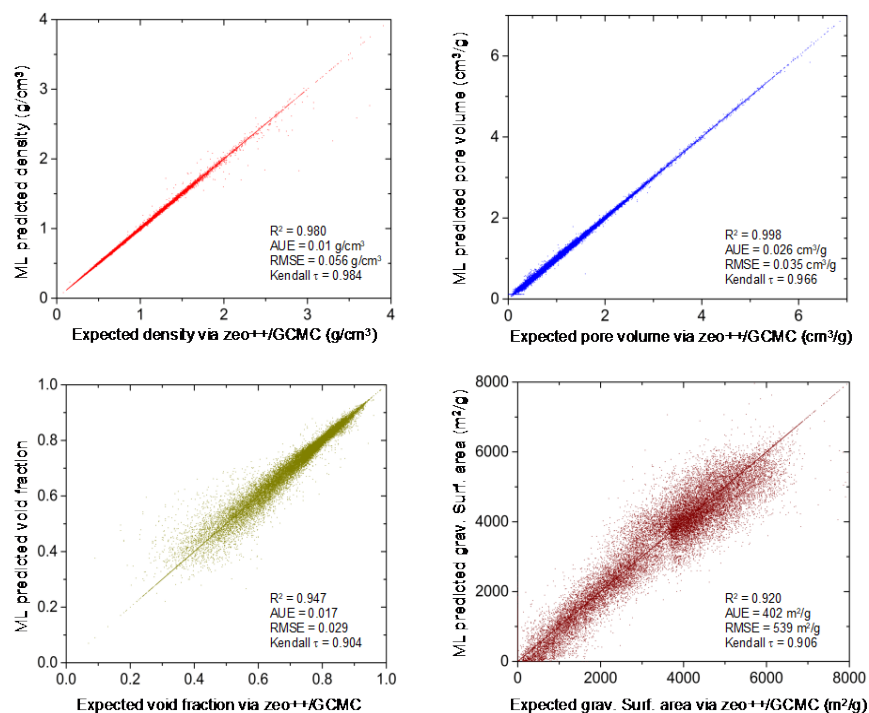


Figure 1. Comparison between ML predictions and zeo++/GCMC calculations of four crystallographic properties of 24,102 MOFs. ML models were trained using GCMC-calculated usable capacities of 72,300 MOFs as input descriptors.

Figure 2 illustrates ML predictions for four crystallographic descriptors as functions of usable gravimetric and volumetric capacities. The left y-axis represents input usable volumetric capacity while the right y-axis indicates values for a given crystallographic property. Input capacities (7 wt% and 40 g H₂/L) are indicated by white-filled black circles in each of the plots; their corresponding ML-predicted crystallographic properties are shown by filled red circles. Green dots represent the ML-predicted crystallographic properties of MOFs corresponding to the input capacities represented by the pink region. Table 3 summarizes the ML predictions of four MOF crystallographic properties corresponding to usable gravimetric and volumetric capacities of 7 wt% and 40 g H₂/L, respectively.

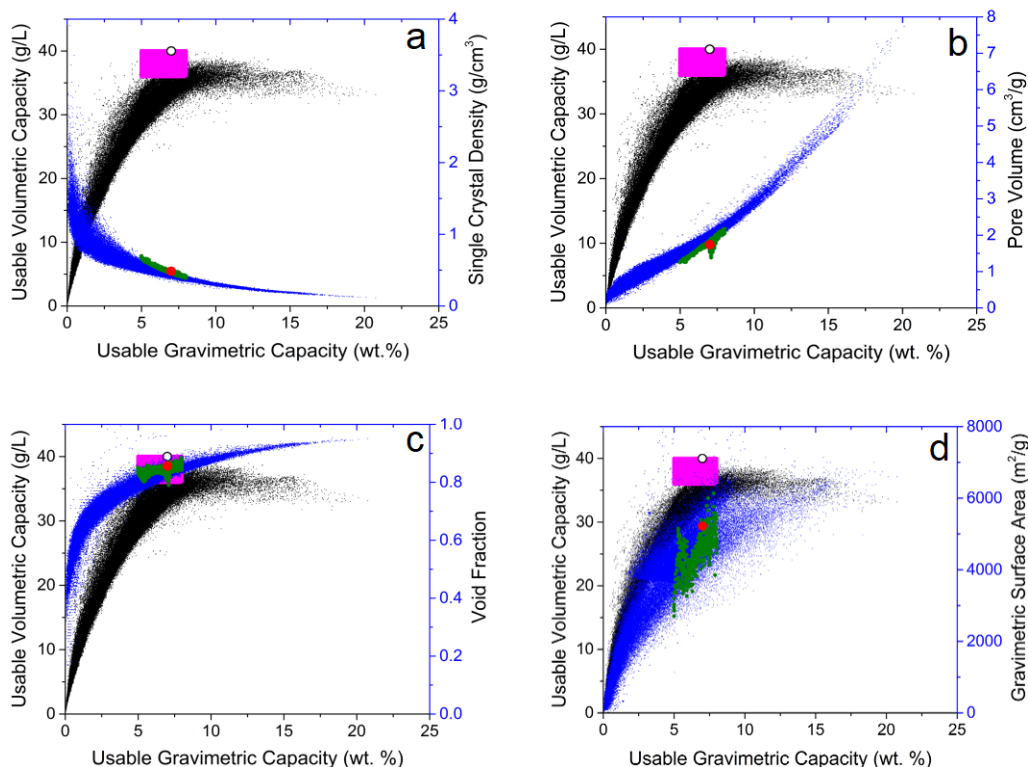


Figure 2. ML-predicted (a) single-crystal density, (b) pore volume, (c) void fraction, and (d) gravimetric surface area as a function of usable capacities. Each point in the pink rectangular region represents a usable gravimetric and volumetric capacity. Each point on the green region represents an ML-predicted crystallographic property corresponding to a specified usable gravimetric and volumetric capacity shown in the pink rectangular region. The filled red circles represent the predicted crystallographic properties corresponding to the input capacities of 7 wt% and 40 g H₂/L (indicated by white empty circles).

Table 3. MOF Crystallographic Properties Predicted by Machine Learning that Correspond to Usable Gravimetric and Volumetric Capacities of 7 wt% and 40 g H₂/L

Crystallographic Property	Range of Crystallographic Property
Single-crystal density (g/cm ³)	0.49 ± 0.01
Pore volume (cm ³ /g)	1.74 ± 0.03
Void fraction (dimensionless)	0.86 ± 0.02
Gravimetric surface area (m ² /g)	5,222 ± 402

An important aspect of MOF synthesis is the control of particle morphology, which allows properties to be tuned without changing the material composition. The morphology can be controlled via a proper choice of synthetic conditions. Usually, temperature, solvent, and the molar ratio of reagents allow for the shaping of crystal morphology. However, in the case of MOFs these effects are typically too subtle to cause gross morphological changes. In contrast, using additives in the reaction mixture strongly affects the crystal morphology, as illustrated here.

As shown in Figure 3, different morphologies of MOF-5 were synthesized by mixing a constant concentration of initial reagents (H₂BDC and Zn(NO₃)₂·6H₂O) and using different concentrations of polycarboxylates, including H₃L (a tricarboxylic linker) and H₄L (a tetracarboxylic linker). It was found that introducing ~3.7 mol% H₃L (H₃BTB, L1) to the reaction mixture generates octahedral-shaped crystals in 24 hours; introducing

the same polycarboxylate at ~1.9 mol% to the reaction mixture generates cuboctahedra-shaped crystals (24 h). Additionally, another H₃L (amine group functionalized H₃BTB, L2) polycarboxylate was identified for morphology control. Introducing ~2.8 mol% of this molecule to the reaction mixture generates cuboctahedra-shaped crystals (24 h). Finally, introducing H₄L (L3) polycarboxylate in concentrations of ~1.6 and ~6.6 mol% generates cuboctahedral- and spherical-shaped MOF-5 crystals, respectively, over the same 24-hour timeframe.

In total, the H₃L/ H₄L polycarboxylate concentration was found to be effective in controlling the crystal morphology. We succeeded in identifying three polycarboxylates that can control octahedra and cuboctahedra morphologies of MOF-5. The phase purity of obtained morphologies was confirmed through powder X-ray diffraction. The powder patterns of all morphologies were found to agree with the expected pattern of MOF-5.

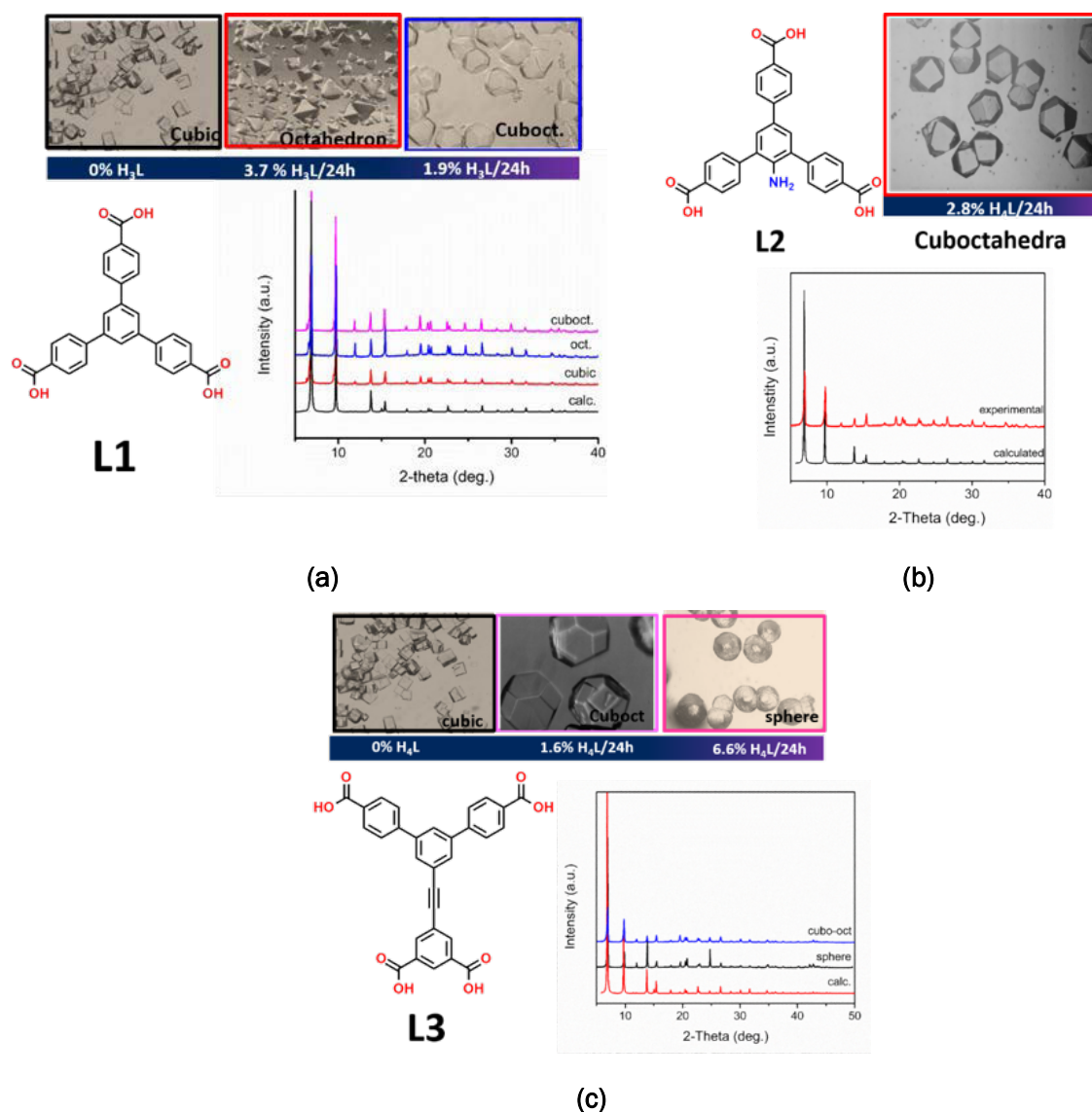


Figure 3. Optical images of different morphologies of MOF-5 crystals obtained by the addition of L1 (a), L2 (b), and L3 (c) polycarboxylates to the reaction mixture of H₂BDC and Zn(NO₃)₂·6H₂O. The respective powder X-ray diffraction patterns are also shown.

CONCLUSIONS AND UPCOMING ACTIVITIES

Using machine learning and a database of previously-calculated MOF properties, this project has demonstrated the ability to predict or “reverse-engineer” the crystallographic properties of an arbitrary MOF that correspond to a specified usable gravimetric and volumetric hydrogen capacity. Furthermore, it was demonstrated that the ranges of the predicted crystallographic properties are within the realm of possibility for the development of new MOFs. In addition to these computational accomplishments, experimental activities identified three additives capable of controlling the morphology of MOF-5 from cubes to octahedra. This development is a prerequisite for more efficient packing of MOF powders.

FY 2018 PUBLICATIONS/PRESENTATIONS

1. M.D. Allendorf, Z. Hulvey, T. Gennett, A. Ahmed, T. Autrey, J. Camp, H. Furukawa, M. Haranczyk, M. Head-Gordon, A. Karkamkar, D.-J. Liu, J.R. Long, K.R. Meihaus, I.H. Nayyar, R. Nazarov, D.J. Siegel, V. Stavila, J.J. Urban, S.P. Veccham, and B.C. Wood, “An Assessment of Strategies for the Development of Solid-State Adsorbents for Vehicular Hydrogen Storage,” *Energy & Environmental Science* 11 (2018): 2784-2812, DOI: 10.1039/c8ee01085d.
2. D.J. Siegel (invited presentation), 2nd Bosch Energy Research Network (BERN) Symposium on Innovative Energy Research, Sunnyvale, CA, September 6–7, 2018.
3. D.J. Siegel (invited presentation), American Chemical Society’s 256th National Meeting, symposium on Nanoscience of Energy Storage, Boston, MA, August 19–23, 2018.
4. D.J. Siegel (invited presentation), Indian Institute of Science Education and Research (IISER-BPR), Berhampur, India, September 4, 2017.
5. D.J. Siegel (invited presentation), Telluride Science Research Center, Computational Materials Chemistry Workshop, Telluride, CO, August 7–11, 2017.

REFERENCES

1. T.F. Willems, C.H. Rycroft, M. Kazi, J.C. Meza, and M. Haranczyk, “Algorithms and Tools for High-Throughput Geometry- Based Analysis of Crystalline Porous Materials,” *Microporous and Mesoporous Materials* 149 (2012): 134-141.
2. P. Geurts, D. Ernst and L. Wehenkel, “Extremely Randomized Trees,” *Mach. Learn.* 63 (2006): 3–42.
3. F. Pedregosa, G. Varoquaux, A. Gramfort, V. Michel, B. Thirion, O. Grisel, M. Blondel, P. Prettenhofer, R. Weiss, V. Dubourg, J. Vanderplas, A. Passos, D. Cournapeau, M. Brucher, M. Perrot and É. Duchesnay, “Scikit-learn: Machine Learning in Python,” *J. Mach. Learn. Res.* 12 (2011): 2825–2830.
4. Jonas Mockus, *Bayesian Approach to Global Optimization: Theory and Applications* (Kluwer Academic 2013).

HyMARC Seedling: Super Metalated Frameworks as Hydrogen Sponges

Omar M. Yaghi (Primary Contact),
Bunyarat Rungtaweivoranit, Roc Matheu,
Robinson W. Flaig, Nikita Hanikel, Sophia Steffens
University of California, Berkeley
Department of Chemistry
419 Latimer Hall
Berkeley, California 94720
Phone: (510) 643-5507
Email: yaghi@berkeley.edu

DOE Manager: Jesse Adams
Phone: (720) 356-1421
Email: Jesse.Adams@ee.doe.gov

Contract Number: DE-EE0008094

Project Start Date: September 1, 2017
Project End Date: August 31, 2018

Overall Objectives

- Introduce a large number of open metal sites into metal-organic frameworks (MOFs) to achieve improved hydrogen storage under ambient conditions.
- Install metal complexes in the pores of MOFs by post-synthetic modification (PSM) to produce super metalated MOFs that contain a high density of open metal sites with enhanced affinity for hydrogen molecules.
- At least double the state-of-the-art open metal site density in MOFs and thus produce hydrogen adsorbents with capacity exceeding the 2025 DOE system targets of 40 g/L and 5.5 wt% under ambient conditions.

Fiscal Year (FY) 2018 Objectives

- Synthesize crystalline functionalized IRMOF-74 series.
- Characterize IRMOF-74 backbones after PSM to quantify pore volumes and amount of metal binding sites.
- Characterize the as-synthesized super metalated frameworks to quantify metal incorporation.

- Develop a MOF with (1) double the amount of open metal sites compared to the unfunctionalized IRMOF-74 backbone before PSM and (2) total volumetric capacity of 18 g/L H₂ at 20°C and less than 100 bar based on single-crystal density.

Technical Barriers

This project addresses the following technical barriers from the Hydrogen Storage section of the Fuel Cell Technologies Office Multi-Year Research, Development, and Demonstration Plan¹:

- (C) Efficiency
- (D) Durability/Operability
- (E) Charging/Discharging Rates.

Technical Targets

The objective of this project is to introduce a large number of open metal sites into MOFs to achieve improved hydrogen storage under ambient conditions. Insights gained from these studies will be applied toward the design and synthesis of hydrogen storage materials that meet the following 2025 DOE hydrogen storage targets:

- Gravimetric capacity: 0.055 kg H₂/kg system
- Volumetric capacity: 0.040 kg H₂/L system
- Operating ambient temperature: -40°/60°C
- Operational cycle life (1/4 tank to full): 1,500 cycles
- Onboard efficiency: 90%
- System fill time (5 kg): 3–5 mins
- Minimum full flow rate: 0.02 (g/s)/kW

FY 2018 Accomplishments

- Crystalline, porous (BET SA: ~1800 m² g⁻¹) Mg-IRMOF-74-III-(CH₂NH₂)₂ was synthesized.

¹ <https://www.energy.gov/eere/fuelcells/downloads/fuel-cell-technologies-office-multi-year-research-development-and-22>

- The primary amines of the MOF were reacted with 2-hydroxybenzaldehyde to produce Mg-IRMOF-74-2OHBAL and with 3,4-dihydroxybenzaldehyde to give Mg-IRMOF-74-34OHBAL. Both reactions proceeded with quantitative yields.
- Post-synthetically modified MOFs were decorated with Ni complexes with approximately 45% yield.
- Attempts were made to activate the framework materials to liberate open metal sites.
- At 77 K, these materials exhibited gravimetric hydrogen uptake capacities of 0.923 wt%.

INTRODUCTION

MOFs possess many desirable attributes allowing for enhanced hydrogen storage. They are highly porous and systematically tunable or functionalizable [1]. Extensive studies regarding the hydrogen adsorption properties of MOFs have shown that MOFs are promising candidates as sorbent materials. There is the potential for MOFs to reach the DOE target for gravimetric hydrogen uptake, albeit at 77 K [2]. A linear correlation between gravimetric uptake and surface area at this temperature and high pressure (1–26 bar) has been observed and noted [3]. However, at typical operating temperatures (e.g., 298 K), MOFs' gravimetric hydrogen uptakes decrease dramatically due to the characteristically weak interactions between hydrogen adsorbate molecules and the frameworks [4]. To augment the strength of such interactions, several strategies have been developed including catenation and adsorption on open metal sites [5]. Of these parameters, an increase in the density of cationic open metal sites effectively enhances frameworks' interactions with hydrogen adsorbate molecules. After solvothermal MOF synthesis, solvent molecules remain and serve as capping ligands on the metal clusters. These can be removed upon evacuation to create coordinatively unsaturated open metal sites [6]. Open metal sites interact with hydrogen through charge-induced dipole interaction, greatly increasing isosteric heats of adsorption [7]. Among MOFs that apply this interaction, Ni₂(*m*-dobdc), a MOF-74 analogue, exhibits the highest observed volumetric hydrogen uptake (12.1 g L⁻¹ at 25°C and 100 bar) with adsorption enthalpy of up to 13.7 kJ mol⁻¹ at zero coverage [8]. However, these values remain below the DOE 2025 targets for hydrogen storage (40 g L⁻¹), prompting further investigation.

APPROACH

In this work, Mg-IRMOF-74-III was chosen as a platform for introducing additional open metal sites due to its high surface area, chemical tunability, stability, and availability of open metal sites that can interact with hydrogen molecules [9,10]. The organic linker of this MOF was functionalized with primary amines that were post-synthetically modified (PSM) to install metal-binding ligands for subsequent metalations [11] (Figure 1). The resultant materials were investigated for hydrogen adsorption properties and capacities.

Imine condensation was selected as a method of post-synthetic ligand installation in the MOF. This class of reactions can proceed under mild conditions with high yield. Additionally, no sterically bulky leaving group is involved in the process, allowing the reactions to occur without negative impacts from poor reactant and product diffusion [12]. In this work, the primary amines of the MOF were reacted with 2-hydroxybenzaldehyde to produce Mg-IRMOF-74-2OHBAL and with 3,4-dihydroxybenzaldehyde to give Mg-IRMOF-74-34OHBAL. These two ligands were selected based on their ability to bind to a wide variety of metals, including nickel [13,14]. Additionally, the catecholate functionality in Mg-IRMOF-74-34OHBAL can benefit hydrogen storage based on the fact that this ligand is capable of polarizing molecules such as hydrogen [15]. These MOFs were subsequently metalated with Ni(II) salts. Open metal sites of Ni(II) have the highest hydrogen adsorption enthalpies among many divalent metals [7]. Activation conditions for the resultant metalated frameworks were screened and hydrogen sorption isotherms were measured at 77 K to assess the frameworks' storage capacities.

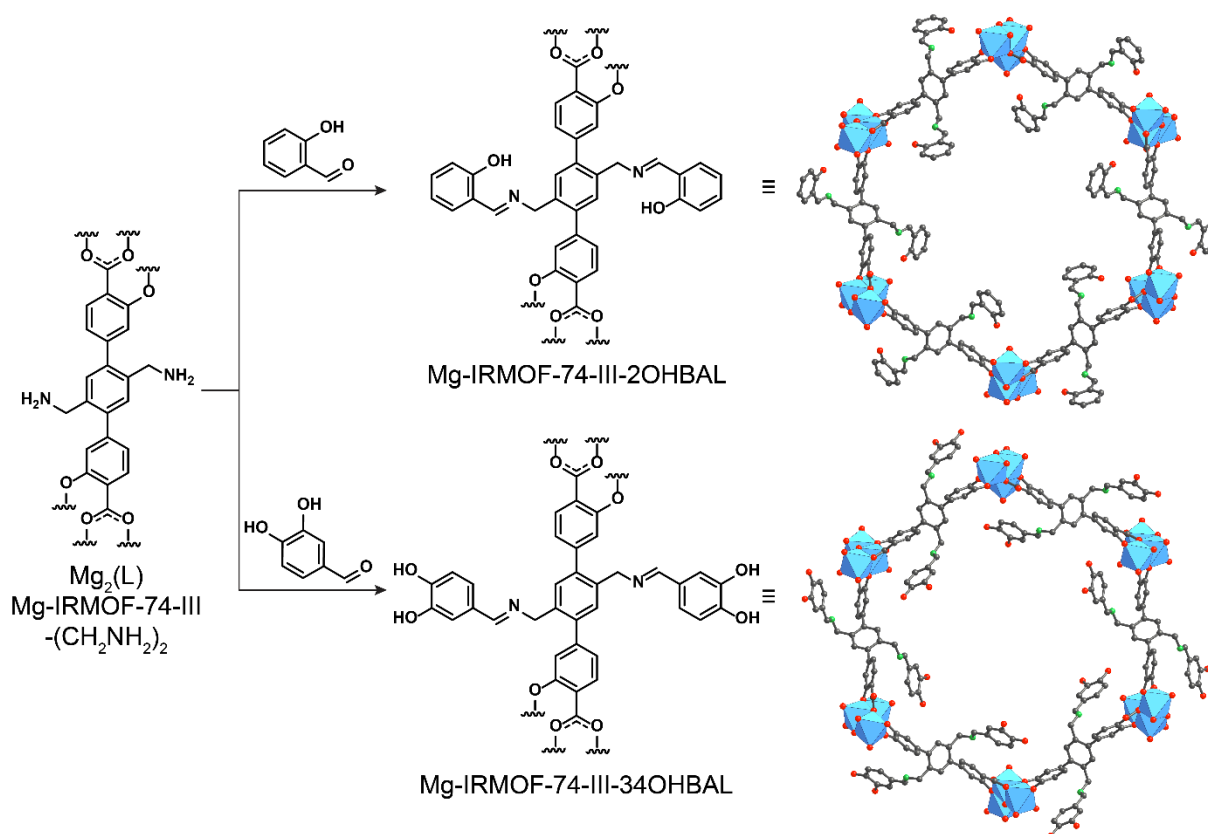


Figure 1. Post-synthetic modifications of Mg-IRMOF-74-III-(CH₂NH₂)₂ with 2-hydroxybenzaldehyde and 3,4-dihydroxybenzaldehyde to produce Mg-IRMOF-74-III-2OHBAL and Mg-IRMOF-74-III-34OHBAL, respectively

RESULTS

Mg-MOF-74 was synthesized with slight modifications from the reported procedure [16] in a 20-mL scintillation vial with Mg(NO₃)₂·6H₂O (116 mg, 0.450 mmol) and 2,5-dihydroxy-1,4-benzenedicarboxylic acid (30 mg, 0.151 mmol). The reaction was heated in a 120°C isothermal oven for a day. Yellow microcrystalline powder was washed with DMF five times (10 mL × 5) over a 48-h period and with anhydrous methanol five times (10 mL × 5) over a 48-h period.

Mg-IRMOF-74-III-(CH₂NH₂)₂ was synthesized according to the reported procedure [11]. The resulting pale-yellow powder (~100 mg) was washed with DMF three times (10 mL × 3) over a 24-h period and with ethyl acetate three times (10 mL × 3) over a 24-h period.

Mg-IRMOF-74-III-(CH₂NH₂)₂-2OHBAL was synthesized by PSM of Mg-IRMOF-74-III-(CH₂NH₂)₂. In a 20-mL scintillation vial, Mg-IRMOF-74-III-(CH₂NH₂)₂ was added to a solution of 2-hydroxybenzaldehyde (537 mg) dissolved in ethyl acetate (5 mL). The suspension was allowed to react at room temperature for 18 h. The resultant orange powder was washed with ethyl acetate five times (20 mL × 5) over a 48-h period. In preparation for material characterization, the sample was dried under vacuum at 120°C for 6 h.

Mg-IRMOF-74-III-(CH₂NH₂)₂-34OHBAL was synthesized by post-synthetic modification of Mg-IRMOF-74-III-(CH₂NH₂)₂. In a 20-mL scintillation vial, Mg-IRMOF-74-III-(CH₂NH₂)₂ was added to a solution of 3,4-dihydroxybenzaldehyde (607 mg) dissolved in ethyl acetate (20 mL). The suspension was allowed to react at room temperature for 18 h. The resultant red powder was washed with ethyl acetate five times (20 mL × 5) over a 48-h period. In preparation for material characterization, the sample was dried under vacuum at 120°C for 6 h.

To metalate Mg-IRMOF-74-III-(CH₂NH₂)₂-2OHBAL, yielding Mg-IRMOF-74-III-(CH₂NH₂)₂-2OHBAL-Ni, Mg-IRMOF-74-III-(CH₂NH₂)₂-2OHBAL (~30 mg) was washed with anhydrous MeOH three times (20 mL × 3). The MOF was added to a solution of Ni(OAc)₂·4H₂O (197 mg) dissolved in anhydrous MeOH (6 mL). The suspension was allowed to react at room temperature for 7 days. The resultant yellow powder was washed with anhydrous MeOH five times (10 mL × 5) over a 48-h period.

To metalate Mg-IRMOF-74-III-(CH₂NH₂)₂-34OHBAL, yielding Mg-IRMOF-74-III-(CH₂NH₂)₂-34OHBAL-Ni, Mg-IRMOF-74-III-(CH₂NH₂)₂-34OHBAL (~30 mg) was washed with anhydrous MeOH three times (20 mL × 3). The MOF was added to a solution of Ni(OAc)₂·4H₂O (197 mg) dissolved in anhydrous MeOH (6 mL). The suspension was allowed to react at room temperature for 7 days. The resultant red powder was washed with anhydrous MeOH five times (10 mL × 5) over a 48-h period.

Powder X-ray diffraction (PXRD) analysis indicates that the materials retain crystallinity and phase purity after PSM (Figure 2a). Nitrogen adsorption isotherms performed at 77 K indicate that these materials remain porous after these processes as well (Brunauer-Emmett-Teller surface area of Mg-IRMOF-74-III-(CH₂NH₂)₂ = 1,840 m² g⁻¹, Mg-IRMOF-74-2OHBAL = 840 m² g⁻¹, and Mg-IRMOF-74-34OHBAL = 905 m² g⁻¹) (Figure 2b). MOF powders were digested in DCI/DMSO-*d*₆ to determine the yield of the imine condensation reactions in these MOFs, demonstrating quantitative yields in reactions between the linker-based primary amines with both aldehyde derivatives. Due to imine bonds' sensitivities to acid, only hydrolyzed products were observed from ¹H-NMR analysis of digested MOF samples. To confirm the presence of imine bonds in both materials, Fourier transform infrared spectroscopy (FT-IR) was performed. The results indicated the presence of imine stretches at 1,629 and 1,639 cm⁻¹ for -2OHBAL and -34OHBAL adducts, respectively (Figure 3). These characteristic imine stretches were corroborated by the spectra obtained from molecular model compounds.

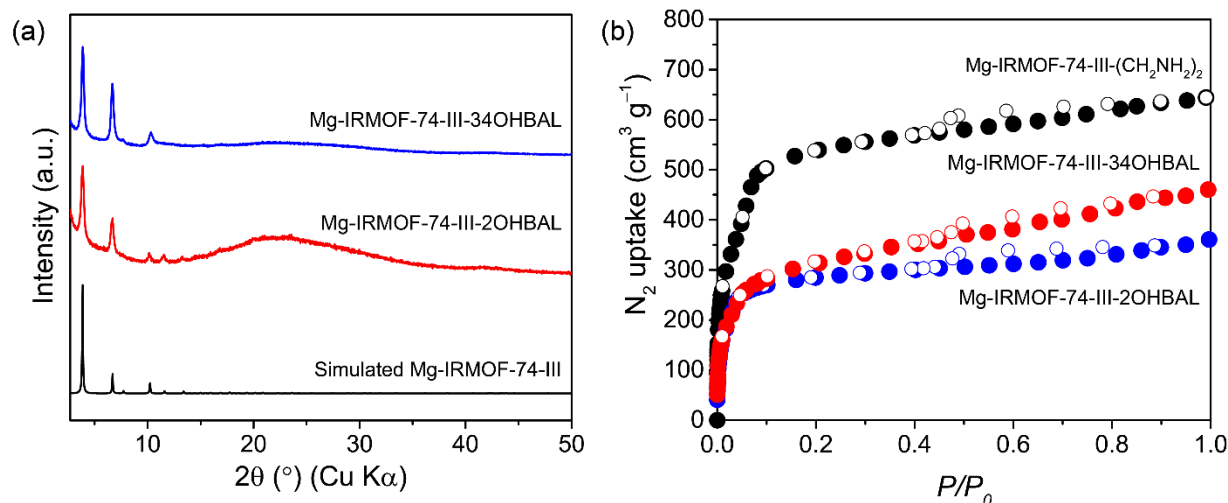


Figure 2. (a) Experimental PXRD patterns of functionalized Mg-IRMOF-74-III-(CH₂NH₂)₂ in comparison with simulated patterns of Mg-IRMOF-74-III-(CH₂NH₂)₂ and (b) nitrogen adsorption-desorption isotherms at 77 K with adsorption and desorption points represented by closed circles and open circles, respectively (P/P_0 , relative pressure)

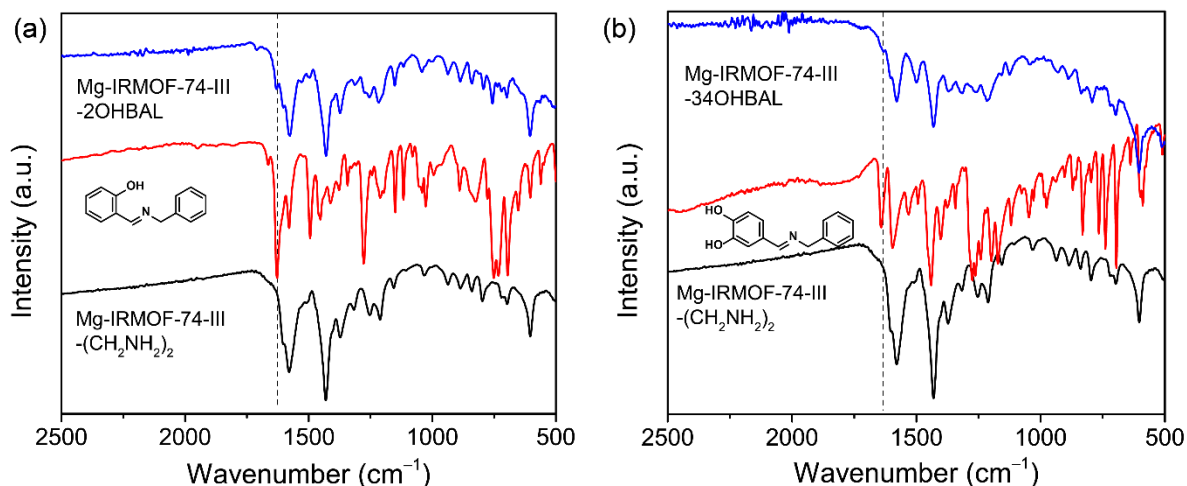


Figure 3. FT-IR spectra of Mg-IRMOF-74-III-2OHBAL and Mg-IRMOF-74-III-34OHBAL in comparison with their respective model compounds

In the metalation process, reaction conditions were optimized via screening of reaction times between 1 and 7 days and Ni salts including $\text{Ni}(\text{OAc})_2 \cdot 4\text{H}_2\text{O}$, $\text{NiCl}_2 \cdot \text{glyme}$ and $\text{Ni}(\text{NO}_3)_2 \cdot 6\text{H}_2\text{O}$. For Mg-IRMOF-74-2OHBAL, only Ni(II) from $\text{Ni}(\text{OAc})_2 \cdot 4\text{H}_2\text{O}$ successfully incorporated into the MOF structure as indicated by inductively coupled plasma analysis. This analysis indicated that the Ni/Mg molar ratio was 0.43, or a 43% metalation yield of the available ligands. Interestingly, Mg-IRMOF-74-III-34OHBAL can be metalated with all Ni(II) salts tested including $\text{Ni}(\text{OAc})_2 \cdot 4\text{H}_2\text{O}$, $\text{NiCl}_2 \cdot \text{glyme}$ and $\text{Ni}(\text{NO}_3)_2 \cdot 6\text{H}_2\text{O}$ to give Ni/Mg molar ratios of 0.44, 0.22, and 0.33, respectively. As a control experiment, Mg-MOF-74, which is a Mg-IRMOF-74-III analog with 2,5-dioxido-1,4-benzenedicarboxylate as organic linker, was synthesized and tested for metalation under similar conditions. Negligible incorporation of Ni(II) was found confirming that Ni(II) was bound to the ligands in Mg-IRMOF-74-2OHBAL and Mg-IRMOF-74-34OHBAL. Additionally, we performed X-ray photoelectron spectroscopy (XPS) of metalated samples to probe the change in the electronic properties of Ni(II) after metalation. High-resolution Ni 2p XPS spectra of these samples show two regions assigned as Ni(II) $2p_{3/2}$ and satellites (Figure 4) [17]. $\text{Ni}(\text{OAc})_2 \cdot 4\text{H}_2\text{O}$, Mg-IRMOF-74-2OHBAL-Ni and Mg-IRMOF-74-34OHBAL-Ni (metalated with $\text{Ni}(\text{OAc})_2 \cdot 4\text{H}_2\text{O}$) exhibit binding energies of 856.2, 855.8, and 855.9 eV, respectively. The decreased binding energies after metalation indicate the increase in the electron donor ability of the ligands appended to the MOF [18]. PXRD analysis indicates that these materials remain crystalline and FT-IR spectra shows that imine bonds remain intact.

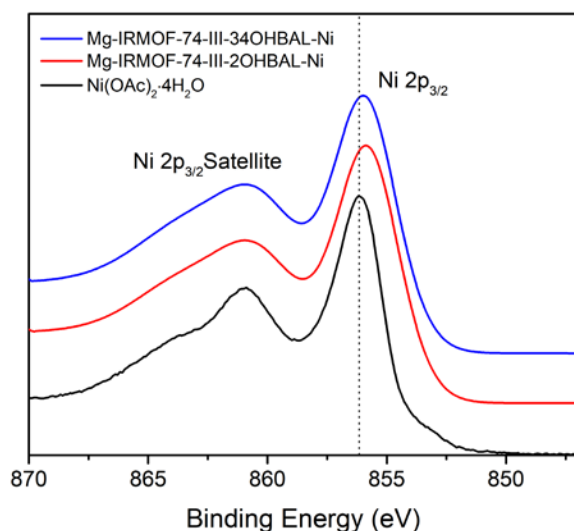


Figure 4. XPS Ni $2p_{3/2}$ spectra of Mg-IRMOF-74-III-(CH_2NH_2) $_2$ -2OHBAL-Ni and Mg-IRMOF-74-III-(CH_2NH_2) $_2$ -34OHBAL-Ni in comparison with the Ni(II) precursor, which is Ni(OAc) $_2$ ·4H $_2$ O

Low-pressure hydrogen adsorption isotherms of Mg-IRMOF-74-III-(CH_2NH_2) $_2$ -2OHBAL-Ni and Mg-IRMOF-74-III-(CH_2NH_2) $_2$ -34OHBAL-Ni were measured at 77 K. The results of these measurements (Figure 5) were compared with those for Mg-MOF-74, which is the isostructural series of Mg-IRMOF-74-III-(CH_2NH_2) $_2$ except 2,5-dioxido-1,4-benzenedicarboxylate was used as an organic linker. Mg-MOF-74 shows a steep hydrogen uptake at low pressure (isotherm slope as $P \rightarrow 0$) indicating strong interactions between H $_2$ molecules and the framework.¹¹ In contrast, Mg-IRMOF-74-III-(CH_2NH_2) $_2$ -2OHBAL-Ni and Mg-IRMOF-74-III-(CH_2NH_2) $_2$ -34OHBAL-Ni do not show such steep hydrogen uptake at low pressures. We hypothesize that the post-synthetically-installed ligands interact strongly with the frameworks' open metal sites, deactivating their interactions with hydrogen. This is evidenced by the dramatic decrease in CO $_2$ uptake capacities measured for the materials at 298 K, where no steep uptake is also observed, as is typical for such materials [11].

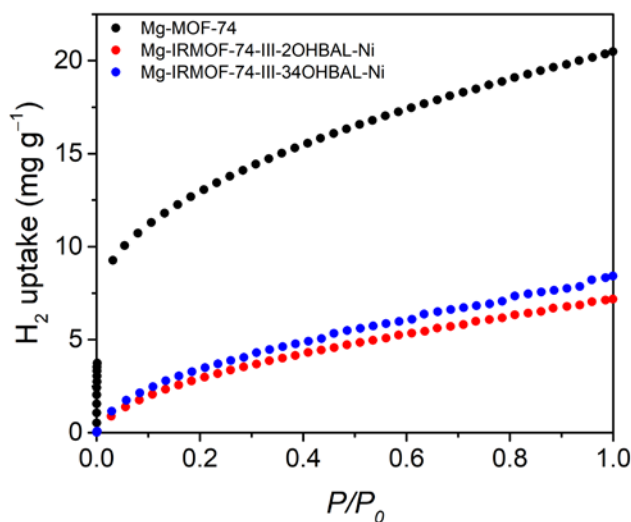


Figure 5. Comparison of low-pressure hydrogen adsorption isotherms at 77 K of Mg-MOF-74, Mg-IRMOF-74-III-2OHBAL-Ni, and Mg-IRMOF-74-III-34OHBAL-Ni

CONCLUSIONS AND UPCOMING ACTIVITIES

As was previously discussed, Mg-IRMOF-74-III analogs were synthesized, characterized, and post-synthetically modified to incorporate Ni(II) complexes. These materials did not meet the targeted goals of the project with respect to gravimetric and volumetric hydrogen adsorption capacity. Therefore, experiments designed to evaluate the materials' lifetimes, onboard efficiencies, fill times, and minimum full flow rates were not conducted. At this time, no additional work is currently funded. However, the remaining open issues could be addressed via the synthesis of and subsequent analogous experimentation on an expanded framework such as Mg-IRMOF-74-V. In this material, it is likely that the distances between the post-synthetically-installed ligands and the framework-based open metal sites will be sufficiently large as to prevent strong interactions. Should this be the case, the Mg-IRMOF-74-V analogue would exhibit higher hydrogen adsorption capacities than either Mg-IRMOF-74-III-(CH₂NH₂)₂-2OHBAL-Ni or Mg-IRMOF-74-III-(CH₂NH₂)₂-34OHBAL-Ni and would warrant additional study and potential implementation.

REFERENCES

1. H. Furukawa, K.E. Cordova, M. O'Keeffe, and O.M. Yaghi, "The Chemistry and Applications of Metal-Organic Frameworks," *Science* 341 (2013): 1230444.
2. J.L. Rowsell, A.R. Millward, K.S. Park, and O.M. Yaghi, "Hydrogen Sorption in Functionalized Metal-Organic Frameworks," *Journal of the American Chemical Society* 126 (2004): 5666-5667.
3. A.G. Wong-Foy, A.J. Matzger, and O.M. Yaghi, "Exceptional H₂ Saturation Uptake in Microporous Metal-Organic Frameworks," *Journal of the American Chemical Society* 128 (2006): 3494-3495.
4. S.S. Kaye, A. Dailly, O.M. Yaghi, and J.R. Long, "Impact of Preparation and Handling on the Hydrogen Storage Properties of Zn₄O(1,4-benzenedicarboxylate)₃ (MOF-5)," *Journal of the American Chemical Society* 129 (2007): 14176-14177.
5. J.L. Rowsell and O.M. Yaghi, "Effects of Functionalization, Catenation, and Variation of the Metal Oxide and Organic Linking Units on the Low-Pressure Hydrogen Adsorption Properties of Metal-Organic Frameworks," *Journal of the American Chemical Society* 128 (2006): 1304-1315.
6. B. Chen, M. Eddaoudi, T. Reineke, J. Kampf, M. O'Keeffe, and O. Yaghi, "Cu₂(ATC)·6H₂O: Design of Open Metal Sites in Porous Metal-Organic Crystals (ATC: 1,3,5,7-Adamantane Tetracarboxylate)," *Journal of the American Chemical Society* 122 (2000): 11559-11560.
7. W. Zhou, H. Wu, and T. Yildirim, 2008. "Enhanced H₂ Adsorption in Isostructural Metal-Organic Frameworks with Open Metal Sites: Strong Dependence of the Binding Strength on Metal Ions," *Journal of the American Chemical Society* 130 (2008): 15268-15269.
8. M.T. Kapelewski, S.J. Geier, M.R. Hudson, D. Stück, J.A. Mason, J.N. Nelson, D.J. Xiao, Z. Hulvey, E. Gilmour, and S.A. FitzGerald, "M₂(m-dobdc) (M = Mg, Mn, Fe, Co, Ni) Metal-Organic Frameworks Exhibiting Increased Charge Density and Enhanced H₂ Binding at the Open Metal Sites," *Journal of the American Chemical Society* 136 (2014): 12119-12129.
9. H. Deng, S. Grunder, K.E. Cordova, C. Valente, H. Furukawa, M. Hmadeh, F. Gándara, A.C. Whalley, Z. Liu, S. Asahina, H. Kazumori, M. O'Keeffe, O. Terasaki, J.F. Stoddart, and O.M. Yaghi, "Large Pore Apertures in a Series of Metal Organic Frameworks," *Science* 336 (2012): 1018-1023.
10. A.M. Fracaroli, P. Siman, D.A. Nagib, M. Suzuki, H. Furukawa, F.D. Toste, and O.M. Yaghi, "Seven Post-synthetic Covalent Reactions in Tandem Leading to Enzyme-like Complexity within Metal-Organic Framework Crystals," *Journal of the American Chemical Society* 138 (2016): 8352-8355.
11. R.W. Flaig, T.M. Osborn Popp, A.M. Fracaroli, E.A. Kapustin, M.J. Kalmutzki, R.M. Altamimi, F. Fathieh, J.A. Reimer, and O.M. Yaghi, "The Chemistry of CO₂ Capture in an Amine-Functionalized Metal-Organic Framework under Dry and Humid Conditions," *Journal of the American Chemical Society* 139 (2017): 12125-12128.

12. S.M. Cohen, “Postsynthetic Methods for the Functionalization of Metal–Organic Frameworks,” *Chemical Reviews* 112 (2011): 970-1000.
13. A.D. Garnovskii, A.L. Nivorozhkin, and V.I. Minkin, “Ligand Environment and the Structure of Schiff Base Adducts and Tetracoordinated Metal-Chelates,” *Coordination Chemistry Reviews* 126 (1993): 1-69.
14. P.G. Cozzi, “Metal–Salen Schiff base complexes in catalysis: practical aspects,” *Chemical Society Reviews* 33 (2004): 410-421.
15. E. Tsivion, J.R. Long, and M. Head-Gordon, “Hydrogen Physisorption on Metal–Organic Framework Linkers and Metalated Linkers: A Computational Study of the Factors That Control Binding Strength,” *Journal of the American Chemical Society* 136 (2014): 17827-17835.
16. L.J. Wang, H. Deng, H. Furukawa, F. Gándara, K.E. Cordova, D. Peri, and O.M. Yaghi, 2014. “Synthesis and Characterization of Metal–Organic Framework-74 Containing 2, 4, 6, 8, and 10 Different Metals,” *Inorganic Chemistry* 53 (2014): 5881-5883.
17. NIST X-ray Photoelectron Spectroscopy Database, NIST Standard Reference Database Number 20, National Institute of Standards and Technology, Gaithersburg MD, 20899 (2000), doi:10.18434/T4T88K, (retrieved April 2018).
18. J. Matienzo, L.I. Yin, S.O. Grim, and W.E. Swartz Jr., “X-Ray Photoelectron Spectroscopy of Nickel Compounds,” *Inorganic Chemistry* 12 (1973): 2762-2769.

Precursor Processing Development for Low-Cost, High-Strength Carbon Fiber for Composite Overwrapped Pressure Vessel Applications

Matthew C. Weisenberger (Primary Contact),
E. Ashley Morris
University of Kentucky Center for Applied Energy Research
2540 Research Park Drive
Lexington, KY 40511
Phone: (859) 257-0322
Email: Matt.Weisenberger@uky.edu

DOE Manager: Bahman Habibzadeh
Phone: (202) 287-1657
Email: Bahman.Habibzadeh@ee.doe.gov

Contract No: DE-EE0008095

Project Start Date: September 1, 2017
Project End Date: Project continuation and
direction determined annually by DOE

Overall Objectives

- Demonstrate ≥ 100 -filament, air-gap spinning of the small-diameter TechPAN precursor polymer, followed by oxidization, carbonization, and characterization of the resultant carbon fiber.
- Demonstrate single-filament carbon fiber properties approaching 4.9 GPa strength and 230 GPa modulus (similar to T700S).
- Achieve < 1 wt% residual solvent in fiber with minimal residence time for the water-minimization strategy.
- Demonstrate ≥ 10 -filament, air-gap, *hollow-fiber* spinning of TechPAN precursor polymer with outer diameter < 100 μm and inner diameter < 50 μm with specific strength and modulus approaching 635 MPa/g/cc and 8.5 GPa/g/cc.
- Demonstrate lower-energy solvent recovery through sorption in activated carbon modules with capability to capture $> 50\%$ of the solvent effluent and their thermal regeneration with $< 15\%$ loss in specific surface area.

- Demonstrate hollow carbon fiber tensile properties approaching 4.9 GPa strength and 230 GPa modulus (similar to T700S), with an analysis of specific strength pertaining to part-weight consideration.
- Deliver a cost analysis of the precursor and carbon fibers with a targeted cost potential of \$12.60/kg.

Fiscal Year (FY) 2018 Objectives

- Demonstrate ≥ 100 -filament, air-gap spinning of the small-diameter TechPAN precursor polymer, followed by oxidization, carbonization, and characterization of the resultant carbon fiber.
- Demonstrate single-filament carbon fiber properties approaching 4.9 GPa strength and 230 GPa modulus (similar to T700S).
- Achieve < 1 wt% residual solvent in fiber with minimal residence time for the water-minimization strategy.
- Deliver cost analysis showing that a reduction of $\geq 10\%$, from \$29.40/kg to \$26.46/kg, is possible via the low-cost TechPAN polymer.

Technical Barriers

This project addresses the following technical barriers from the Hydrogen Storage section of the Fuel Cell Technologies Office Multi-Year Research, Development, and Demonstration Plan¹:

- System Weight and Volume
- System Cost
- Materials of Construction.

Technical Targets

This project is focused on developing novel precursors for low-cost, high-strength carbon fiber (CF). Insights gained from these studies will be applied to composite overwrapped pressure

¹ <https://www.energy.gov/eere/fuelcells/downloads/fuel-cell-technologies-office-multi-year-research-development-and-22>

vessels. The carbon fibers developed here seek to fulfill the following DOE 2020 hydrogen storage targets:

- CF cost [1]: \$12.60/kg CF
 - Project status (given starting CF cost of \$29.40/kg): \$25.35/kg CF
- Tensile strength: 4.9 GPa (711 ksi)
- Tensile modulus: 230 GPa (33.4 Msi)
- Minimization of water is critical to reducing the cost of solvent recovery, which costs \$1.39 per 1 kg of precursor fiber.
- Delivered a cost analysis showing that a reduction of $\geq 10\%$, from \$29.40/kg to \$25.35/kg, is possible via low-cost TechPAN polymer.
- Demonstrated a coagulated fiber with hollow core, coalesced shell, and circular cross section from the 2C-shaped spinneret.

FY 2018 Accomplishments

- Demonstrated ≥ 100 -filament, air-gap spinning of the small-diameter TechPAN precursor polymer, followed by oxidization, carbonization, and characterization of the resultant carbon fiber using the custom-built, strain-controlled thermal conversion device.
 - TechPAN is a low-cost, non-exclusive, special acrylic fiber-grade terpolymer that can be supplied to the fiber industry at the tens of kilotonne scale at an anticipated cost of \$3/kg (typical exclusive, aerospace-grade polyacrylonitrile [PAN] polymer costs \$7.05/kg [2]).
 - Here, we have proven the capability of this low-cost PAN polymer to be spun and to produce high-quality carbon fibers. This represents a path to lower the polymer-precursor cost by 57%, which lowers the final carbon fiber cost by **13.8%**.
- Demonstrated single-filament carbon fiber properties approaching 4.9 GPa strength and 230 GPa modulus (similar to T700S) using TechPAN precursor.
 - During Phase 1 of the project, it is shown that TechPAN precursor can result in T700-quality properties, well exceeding the modulus metric and clearly showing 700 ksi strength at 10-mm gauge length. This demonstration proves that low-cost TechPAN-derived CF can offer a lower-cost and brand-independent path to T700 properties in CF.
- Achieved a < 1 wt% residual solvent in fiber with minimal residence time for the water-minimization strategy.

INTRODUCTION

Carbon fiber (CF) is central to produce lightweight, high-pressure, composite overwrapped pressure vessels (COPVs), which are used for onboard storage of hydrogen for fuel cell vehicles. In 2015, CF cost accounted for 62% of the cost of a hydrogen storage system, as COPVs were manufactured with T700S CF at \$29.40/kg CF [3]. The high cost of hydrogen storage, largely attributed to the carbon fiber cost, limits the application of fuel cells in vehicles. Therefore, we proposed to develop fiber processing to demonstrate carbon fiber tensile properties similar to T700S with a production cost potential of \$12.60/kg or less.

We are investigating solutions to **critical issues stemming from the precursor** that significantly contribute to the cost of CF—namely, high polymer cost, inefficient water use and solvent recovery, low fiber throughput, energy-intensive conversion, and high coefficient of variation between fibers. We anticipate hollow precursor fibers to significantly increase the throughput rate of thermal processing and to offer very high specific tensile properties.

APPROACH

We proposed a three-front approach, leveraging our unique precursor fiber processing capabilities and skillsets. To address the issues described above, we proposed the following three approaches:

1. Use and prove out a *new, low-cost, high-volume, high-quality* PAN-based precursor terpolymer, exclusively under investigation at the University of Kentucky Center for Applied Energy Research (UK CAER), known as TechPAN.
2. Develop *air-gap* solution spinning of small-diameter and *hollow* precursor filaments in multifilament continuous tows.
3. Drastically increase water and energy-use *efficiency* incurred in wash-water/solvent separations using a specially designed wash bath and activated-carbon recovery system.

RESULTS

The first milestone for the project required the demonstration of air-gap stability of nascent TechPAN polymer jets during air-gap spinning. Indeed, using our unique fiber-processing capabilities and skills sets, TechPAN precursor filaments were successfully air-gap spun in multifilament continuous tows, typically collecting 1 km in length on each spool. A typical spool of TechPAN precursor fiber is shown in Figure 1. Further work was successful in producing round cross-section filaments (as opposed to undesirable non-round or bean-shaped cross sections), shown in the inset of Figure 1, with targeted diameters of about 10 μm . These high-quality precursors from low-cost TechPAN are vital to producing high-quality carbon fibers for the replacement of costly T700 CF in COPVs.



Figure 1. Typical spool of multifilament continuous TechPAN precursor fibers with round, 10- μm fiber cross sections shown in the inset. A typical spool contained 1 km of multifilament tow length.

An efficient strain-controlled thermal conversion apparatus was designed and fabricated to enable batch conversion of TechPAN precursor fibers to CF without the need for large amounts of fiber, as is required for typical continuous thermal conversion ovens. The creation of this apparatus allowed for small-scale, batch conversion of precursor fiber with minimal fiber, while still providing strain control necessary during stabilization and carbonization to produce high-quality CF. Using this system, UK CAER successfully produced CF with tensile properties very close to those of T700 CF. This accomplishment successfully proved that low-cost TechPAN was capable of producing CF with properties amenable for COPV production.

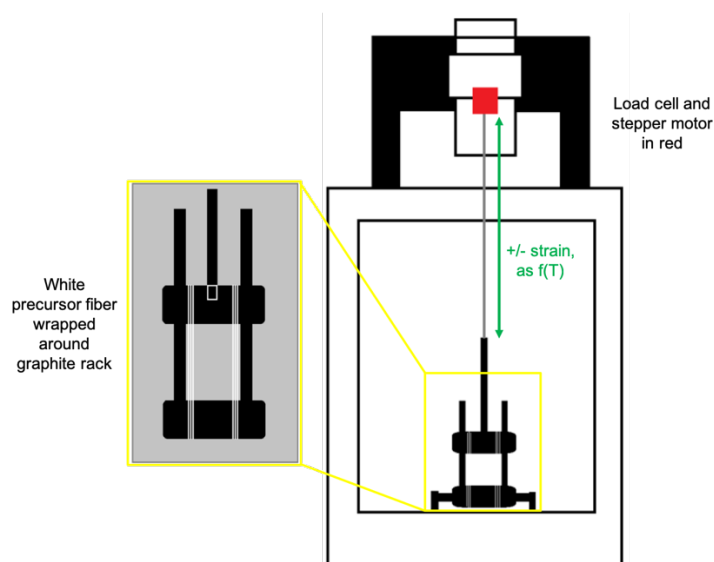


Figure 2. Efficient strain-controlled thermal conversion apparatus capable of applying programmed strain as a function of time (oven temperature) for the small-scale conversion of TechPAN precursors to CF

To reduce the high costs associated with solvent recovery (typically performed with energy-intensive distillation), UK CAER is in the process of minimizing water use during spinning, as well as performing active solvent recovery via an activated-carbon recovery system, as shown in Figure 3. Analyses of commercially

available activated carbons (ACs) were made to determine adsorption efficiency for the spinning solvent (dimethylsulfoxide, or DMSO). Breakthrough curves were generated as a function of activated-carbon mass, and studies were completed on DMSO concentration at the beginning and end of the wash bath to determine the increase in DMSO content over time. It was determined that the selected commercially available activated carbon is capable of adsorbing 1 g of DMSO for every 3 g of AC. This performance is indeed much better than expected. Additionally, using the data thus far, it is estimated that the use of AC will reduce freshwater usage by up to 86%. Our goal is to achieve at least a 50% reduction in freshwater use. Work is continuing in this area.

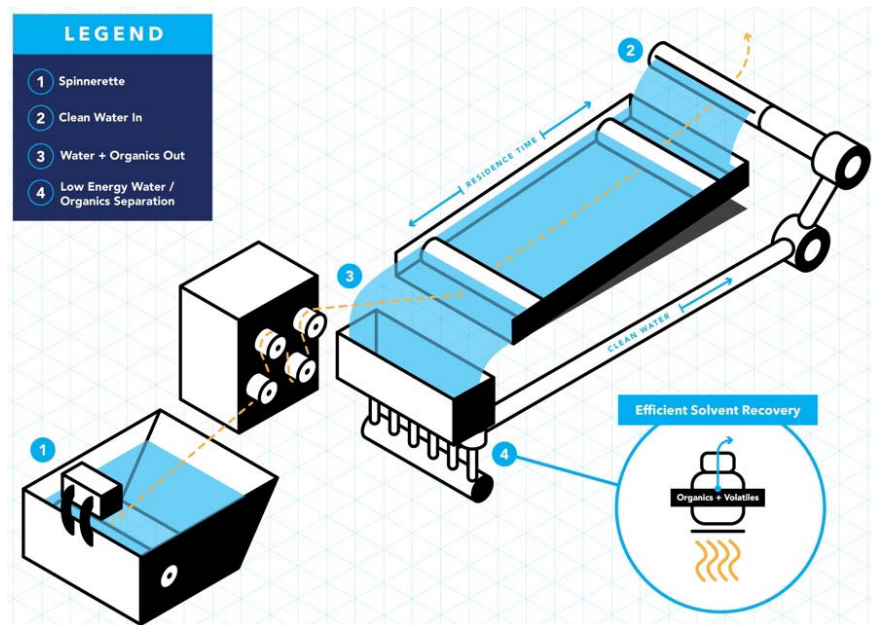


Figure 3. Efficient wash-water-solvent recovery processing concept, where low-energy separation is envisioned using activated-carbon module technology

Finally, the team is ahead of schedule with regard to producing hollow filaments from TechPAN and has already demonstrated coagulated fiber with hollow-core, coalesced-shell, and circular cross section using a 2C-shaped capillary spinneret (a non-bore-fluid approach), shown in Figure 4. The further development of these hollow filaments is the major focus of Budget Period 2.

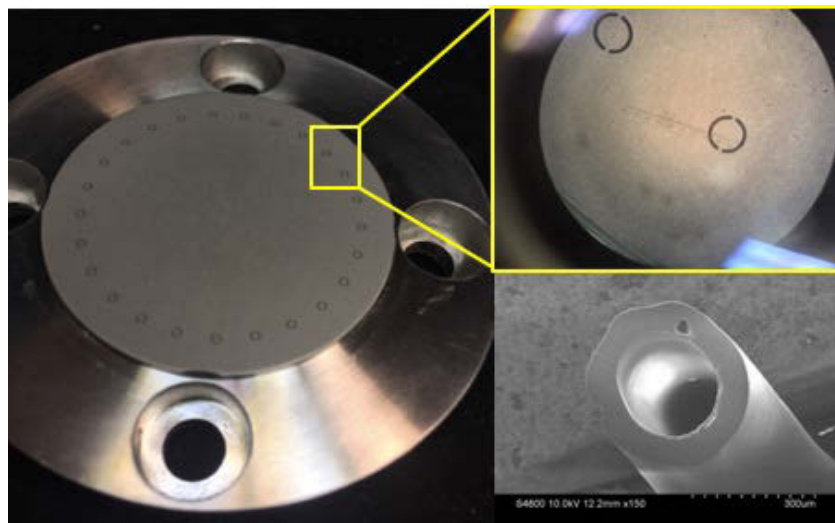


Figure 4. (Left) The 25-hole shaped spinneret “2C” is shown, with a close-up of the capillary design on the top right. The outer radius is 500 microns and the inner radius is 400 microns, with an annulus of 100 microns. Finally, on the bottom right is an image of a TechPAN hollow, circular fiber spun using this spinneret.

CONCLUSIONS AND UPCOMING ACTIVITIES

The work completed in Year 1 (Budget Period 1) has successfully proven the viability of the low-cost TechPAN as a viable precursor to achieve T700 CF properties. Additionally, the work on water minimization and solvent adsorption via activated carbon is proving very promising. Finally, we are ahead of schedule with regard to hollow-fiber spinning, having already produced a hollow-core, coalesced-shell, and circular cross-section fiber.

Future work and accomplishments by UK CAER include:

- Demonstrating ≥ 10 -filament, air-gap, hollow-fiber spinning of TechPAN precursor polymer with outer diameter $< 100 \mu\text{m}$ and inner diameter $< 50 \mu\text{m}$ with specific strength and modulus approaching 635 MPa/g/cc and 8.5 GPa/g/cc.
- Demonstrating lower-energy solvent recovery through sorption in activated-carbon modules with the capability to capture $> 50\%$ of the solvent effluent and demonstrating their thermal regeneration with $< 15\%$ loss in specific surface area.
- Demonstrating hollow carbon fiber tensile properties approaching 4.9 GPa strength and 230 GPa modulus (similar to T700S), with an analysis of specific strength pertaining to part-weight consideration.
- Delivering a cost analysis of the precursor and carbon fibers with a cost potential of \$12.60/kg.

FY 2018 PUBLICATIONS/PRESENTATIONS

1. R. Sarabia-Riquelme, N. Hochstrasser, A. Morris, and M. Weisenberger. “Insights into The Relation between Yield Point, Plastic Modulus and Degree of Crystallinity of PAN Precursor Fiber,” presented at CARBON 2018, the International Carbon Conference in Madrid, July 1–6, 2018.
2. DOE Fuel Cell Tech Team meeting, Detroit/WebEx, May 16–17, 2018.
3. DOE Annual Merit Review and Peer Evaluation Meeting, Washington, DC, June 13–15, 2018.

REFERENCES

1. DOE Fuel Cell Technologies Office Annual FOA: DE-FOA-0001647, Office of Energy Efficiency and Renewable Energy (2016), <https://eere-exchange.energy.gov/>.
2. David C. Warren, “Development of Low Cost, High Strength Commercial Textile Precursor (PAN-MA),” DOE Hydrogen and Fuel Cells Program 2014 Annual Merit Review and Peer Evaluation Meeting Proceedings (2014), https://www.hydrogen.energy.gov/pdfs/review14/st099_warren_2014_o.pdf.
3. G. Ordaz, C. Houchins, and T. Hua, “Onboard Type IV Compressed Hydrogen Storage System – Cost and Performance Status 2015,” DOE Hydrogen and Fuel Cells Program Record (2015), https://www.hydrogen.energy.gov/pdfs/15013_onboard_storage_performance_cost.pdf.

Developing a New Polyolefin Precursor for Low-Cost, High-Strength Carbon Fiber

T.C. Mike Chung
Pennsylvania State University
302 Steidle Building
University Park, PA 16802
Phone: (814) 863-1394
Email: tcc3@psu.edu

DOE Manager: Bahman Habibzadeh
Phone: (202) 287-1657
Email: Bahman.Habibzadeh@ee.doe.gov

Project Start Date: September 1, 2017
Project End Date: August 30, 2020

Overall Objectives

- Reducing the cost of composite overwrapped pressure vessels (COPVs) by the combination of low-cost precursor, melt-spinning fiber process, low carbonization temperature, high mass yield while maintaining high tensile strength.
- Developing a new polyolefin precursor that is melt-processible in forming fibers with good mechanical strength and high carbonization yield during the subsequent thermal conversion process to produce carbon fiber (CF).
- Preparing boron (B)-doped CF by co-carbonization with B-containing precursor, which can offer low carbonization temperature, high carbon (C) yield, and CF products with high tensile strength.

Fiscal Year (FY) 2018 Objectives

- Investigate the chemical routes to prepare several newly designed polymer precursors.
- Confirm the resulting monomer and polymer structures by gel permeation chromatography curves and nuclear magnetic resonance spectra.
- Evaluate the thermal conversion of new polymer precursors to C materials and identify the suitable precursors that are melt-processible and can achieve high carbonization mass yield

>80%, compared with 50% yield in current polyacrylonitrile (PAN) precursor.

Technical Barriers

This project addresses the following technical barriers from the Hydrogen Storage section of the Fuel Cell Technologies Office Multi-Year Research, Development, and Demonstration Plan¹:

- High cost of COPVs
- High cost for high-strength carbon fiber (62% of the COPV cost)
- Lack of technology in low-cost and melt-processible CF precursor that can form high-strength carbon fiber required in fabricating COPVs.

Technical Targets

This project is conducting fundamental studies of developing new CF precursors and a production process to reduce the cost of COPVs that meet the following DOE hydrogen storage targets:

- DOE 2020 cost target of \$10/kWh (~\$1,900/system)
- 5.6 kg of usable stored hydrogen in the 700-bar COPV.

FY 2018 Accomplishments

- Conducted a systematic study (design, synthesis, and evaluation) of various hydrocarbon polymers to understand the most suitable polymer structure that can generate high carbonization mass yield (>80%).
- Discovered four new polymer precursors with high C yield >80% (more than 60% higher than that of the current PAN precursor, which exhibits C yield ~50%).
- Synthesized B-containing Pitch precursor that enhances the carbonization process.
- Studied melt viscosity and viscoelastic properties of polyethylene-Pitch precursor and

¹ <https://www.energy.gov/eere/fuelcells/downloads/fuel-cell-technologies-office-multi-year-research-development-and-22>

identified the suitable melt fiber-spinning condition to form fibers.

- Collaborated with Oak Ridge National Laboratory through the LightMAT consortium in thermal conversion study.

INTRODUCTION

The current 700-bar compressed hydrogen onboard storage vessels for fuel cell electric vehicles are based on CF reinforced polymer (epoxy resin) composites. The cost of this system is estimated at above \$15/kWh, which is significantly higher than the DOE cost target. About 62% of the system cost comes from the cost of CF alone. The high cost of CF is associated with the deficiency in the current PAN fiber precursor that requires a fiber solution-spinning process and has a low carbon-conversion yield (<50%). Some interesting experimental results and economic benefits of using sulfonated polyethylene precursors have been reported, but there is still a considerable technological gap in considering them for practical CF production. The required solid-state sulfonation reaction of highly crystalline polyethylene (PE) fiber is problematic. This is because it results in an inhomogeneous distribution of functional groups that significantly impairs the effectiveness of stabilization and the subsequent carbonization reaction.

Thus, we suggested this research project to focus on developing new polyolefin-based CF precursors that can be prepared effectively and converted to high-quality CF with high tensile strength and low cost. The cost savings can be achieved through the combination of lower-cost precursor, melt-spinning fiber process, lower carbonization temperature, higher mass yield, and higher tensile strength in the resulting CF products. Our goal is to achieve the DOE cost target of \$10/kWh (about \$1,900 per vehicle with 5.6 kg of usable hydrogen), while also enhancing the CF mechanical property to higher than those of Toray T700S fiber (4,900 MPa tensile strength and 230 GPa tensile modulus).

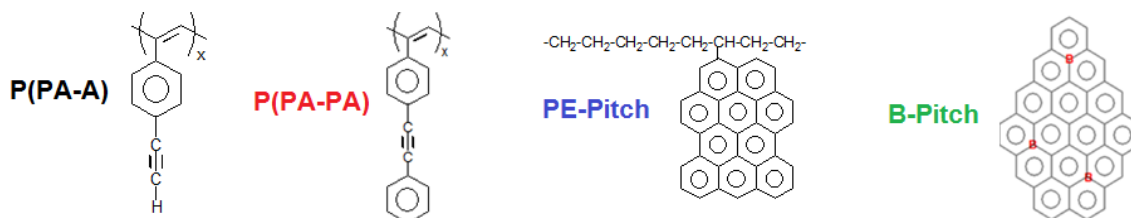
APPROACH

The research approach is based on several newly designed hydrocarbon polymers containing some reactive side groups that can effectively engage in cyclo-addition and hyper-crosslinking reactions under a mild stabilization condition. The polymers are also melt-processible for spinning into fibers. With strong bonding energy along the polymer chain and a network structure, the resulting polymer fiber under tension (similar to PAN fiber) can be heated (pyrolyzed) to drive off hydrogen atoms and induce ring fusion (carbonization) to produce a strong CF with high mass yield, high crystallinity, graphitic layer planes oriented along the fiber direction, and low defects.

In addition, another aspect of this research is to further increase the tensile strength of carbon fiber. The research approach is based on our previous findings in several B-containing precursors that produce BC_x materials with high yield, large crystallite size, and small d-spacing between C interlayers. Clearly, the in situ boron is catalyzing carbonization and graphitization of the BC_x material, and the substitutional B elements induce the dipole-dipole interaction between interlayers and reduce the d-spacing. The combination of large crystallite size, small d-spacing, and strong interlayer interaction will increase mechanical strength, especially for carbon fiber with graphene sheets aligned along the fiber direction.

RESULTS

In FY 2018, we have systematically investigated (i.e., design, synthesis, and evaluation) a series of hydrocarbon precursors. Our experimental results show four new precursors (illustrated below in Scheme 1) that achieve our first year (Phase 1) goal, with the C yield >80% (more than 60% higher than that of the current PAN precursor that exhibits a C yield ~50%). The detailed preparation procedures and evaluation for each precursor were reported in our DOE quarterly reports.



Scheme 1. Four new C precursor structures, including poly(acetylphenylacetylene) P(PA-A), poly(phenylacetylphenylacetylene) P(PA-PA), poly(ethylene-co-pitch) (PE-Pitch), and boron-containing pitch (B-Pitch)

Figure 1 shows the thermogravimetric analysis (TGA) curves of these new precursors, which were conducted in both Oak Ridge National Laboratory and Pennsylvania State laboratories with consistent results. All four samples show more than 80% C yields after heating to 1,500°C; three of them are near or above 90% yields. They are almost reaching the theoretical values for the precursor that only engages in the cyclo-addition and ring-fusion reactions with the removal of hydrogen atoms. It is interesting to note a slight dip (weight loss) at >1,250°C for the B-Pitch precursor, which may be associated with the limited B content (~2%) in the large graphene planal sheet during the carbonization at high temperatures. This phenomenon was well-documented in our previous papers (*Carbon* 34, 1181–1190, 1996; *Carbon* 48, 2526–2537, 2010). Overall, they are all potentially good precursors for our second year (Phase 2) research that will focus on preparing and evaluating CFs.

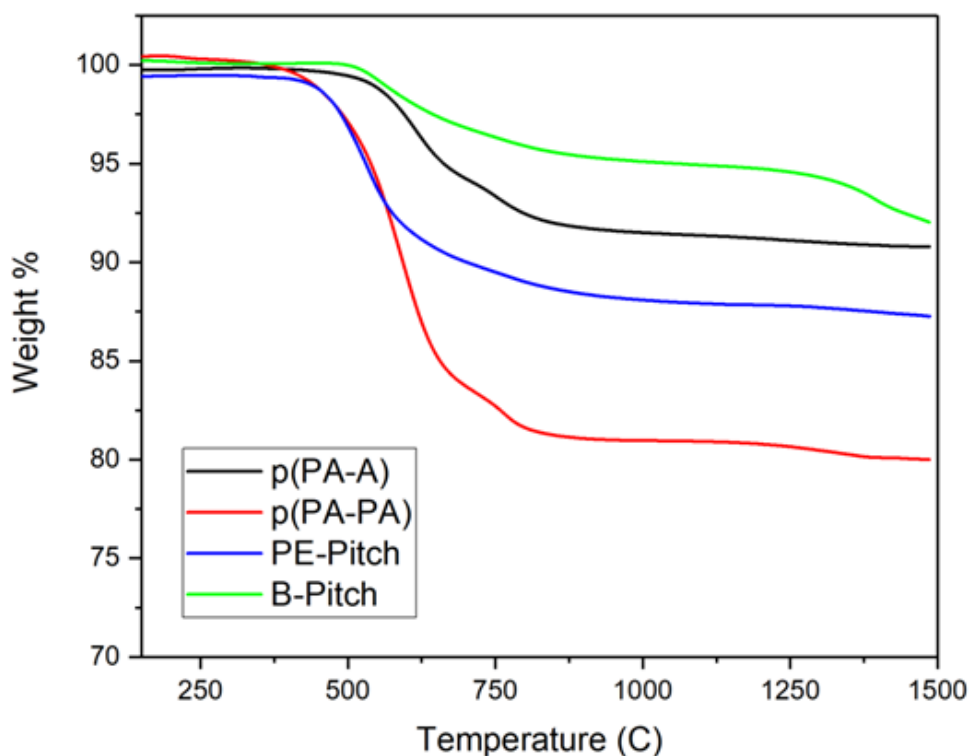
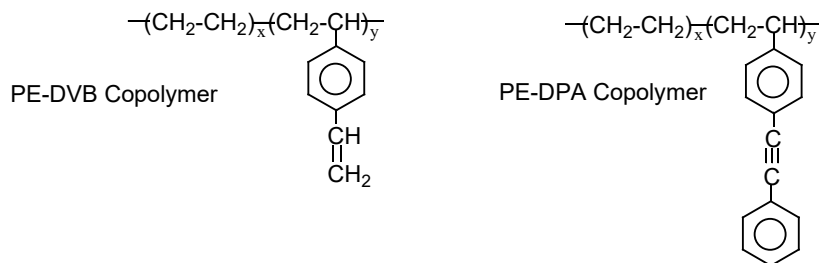


Figure 1. TGA curves of four new C precursors, including poly(PA-A), poly(PA-PA), PE-Pitch, and B-Pitch, measured at the heating rate of 10°C/min under N₂ atmosphere

Four new high-C-yield precursors represent four different processing conditions in forming fibers. We decided to focus on the PE-Pitch precursor, which is most unique in the field and has good potential to achieve our Phase 2 goal: showing a new CF production method with a combination of low-cost (scalable) precursor, efficient fiber melt-spinning process to form strong fibers, high C conversion, and high-quality CF end products. The preparation of PE-Pitch precursors involves two types of PE copolymers (illustrated below in

Scheme 2) with reactive side groups that can engage cyclo-addition and ring fusion with Pitch (polyaromatic) molecules.



Scheme 2. Two reactive PE copolymers, including poly(ethylene-co-divinylbenzene) (PE-DVB) and poly(ethylene-co-vinylidiphenylacetylene) (PE-DPA)

Two reactive PE copolymers—including PE-DVB copolymer containing styrene ($-\phi-C=C$) side groups and PE-DPA copolymer containing diphenylacetylene ($-\phi-C\equiv C-\phi$) side groups—were synthesized by metallocene-mediated copolymerization reactions using various metallocene catalysts. The detailed experimental results were discussed in our previous DOE quarterly report. The chemistry affords random copolymers with high molecular weight and narrow molecular weight and composition distributions. Table 1 summarizes several resulting PE copolymers with a broad range of copolymer compositions. The availability of a broad range of reactive PE copolymers helped us to identify the suitable thermal/reaction conditions (with scope and limitations) for carrying out the coupling reaction between reactive PE copolymers and Pitch molecules to form PE-Pitch precursors. Ideally, the resulting PE-Pitch precursors in a molten state can subsequently be melt-processed (melt fiber-spinning) into PE-Pitch fibers.

Table 1. Summary of Reaction Condition and Result of PE-DVB and PE-DPA Copolymers

PE copolymer ^a	Polymerization Condition					Polymerization Results	
	Metallocene Catalyst ^b	[Cat] (umol/L)	Ethylene pressure (psi)	[Co-Monomer] (M)	Temp/Time (°C/min)	Cat. efficiency (kg/mol*hr)	Functional group (mol%)
PE-DPA-1	$[(C_5Me_4)SiMe_2N(t-Bu)]TiCl_2$	100	50	0.33	40/60	268	8.4
PE-DPA-2	$[(C_5Me_4)SiMe_2N(t-Bu)]TiCl_2$	100	50	0.16	40/60	310	4.5
PE-DVB-1	$rac-Et(Ind)_2ZrCl_2$	25	20	0.95	50/60	2000	3.8
PE-DVB-2	$rac-Et(Ind)_2ZrCl_2$	25	20	0.32	50/60	1888	1.8
PE-DVB-3	$rac-Et(Ind)_2ZrCl_2$	25	20	0.16	50/60	2363	1.1

^a Autoclave reactor (500 ml) with toluene solvent (230 ml) in all reactions.

^b MAO/Cat. Ratio= 1500.

Several experimental results (reported in our quarterly reports) had shown the successful coupling reactions between the resulting PE-DVB or PE-DPA copolymers and Pitch molecules to form PE-Pitch precursors. Both reactive side groups exhibit a facile cyclo-addition reaction with Pitch molecules under a specific thermal condition (relatively low temperature) during the stabilization step. It is essential to identify the processing window that also allows the in situ melt fiber-spinning into PE-Pitch precursor fibers.

Rheology of the polymer melt, such as complex viscosity (η) and viscoelastic properties (i.e., storage modulus $G'(\omega)$, loss modulus $G''(\omega)$, and $\tan(\delta)$), provides a great deal of information about polymer melt that is associated with polymer structure (solid-like or liquid-like) and its melt-processability at a specific thermal condition. An ARES-G2 oscillatory rheometer with 8-mm parallel plates was used in this investigation. The 8-mm sample disc was prepared by molding the mixture of PE copolymer and Pitch material under a specific temperature, in which a homogeneous mixture was achieved without any significant reaction between two materials. Figure 2 compares the profiles of melt viscosity and viscoelastic properties between a mixture of PE-DPA copolymer (9 mol% DPA units) with Pitch 118M (1/10 wt. ratio) and a pure Pitch 118M sample (reference) during the heating process.

The solid material (polymer) will decrease its melt viscosity with the increase of temperature if the material is completely stable throughout the whole thermal process. However, in our cases, possible thermal-induced coupling reactions occur that increase the material mass and break the decreasing trend of melt viscosity. The specific breaking point will provide very important information on the structure change. As shown in Figure 2, the raw Pitch reference sample shows that all the G' , G'' viscosity values systematically decreased with heating temperature until reaching 325°C. In further increasing the temperature (>325°C), all three values turn sharply higher. Evidently, the chemical reaction among raw Pitch molecules in Pitch is initiated at a heating temperature beyond 325°C, and Pitch molecular weight increases with heating temperature. As discussed in our quarterly report, the same Pitch 118M material exhibits a liquid-crystalline mesophase at ~400°C with large polyaromatic sheet structures. On the other hand, the mixture of PE-DPA/Pitch 118M (1/10 wt. ratio) shows the breaking point at a much lower temperature (~200°C). With only 10% PE-DPA copolymer, the mixture exhibits about one order higher melt viscosity and G' and G'' values before the turning point (200°C). After reaching >200°C, all three η , G' , and G'' values increase to two orders of magnitude higher than those of the reference Pitch 118M sample at the same heating temperatures. The results clearly indicate that the coupling reaction between PE-DPA copolymer and Pitch 118 molecules is initiated at ~200°C; the coupling reaction continues in the mixture beyond this temperature (>200°C) to rapidly increase the material melt viscosity and viscoelastic properties.

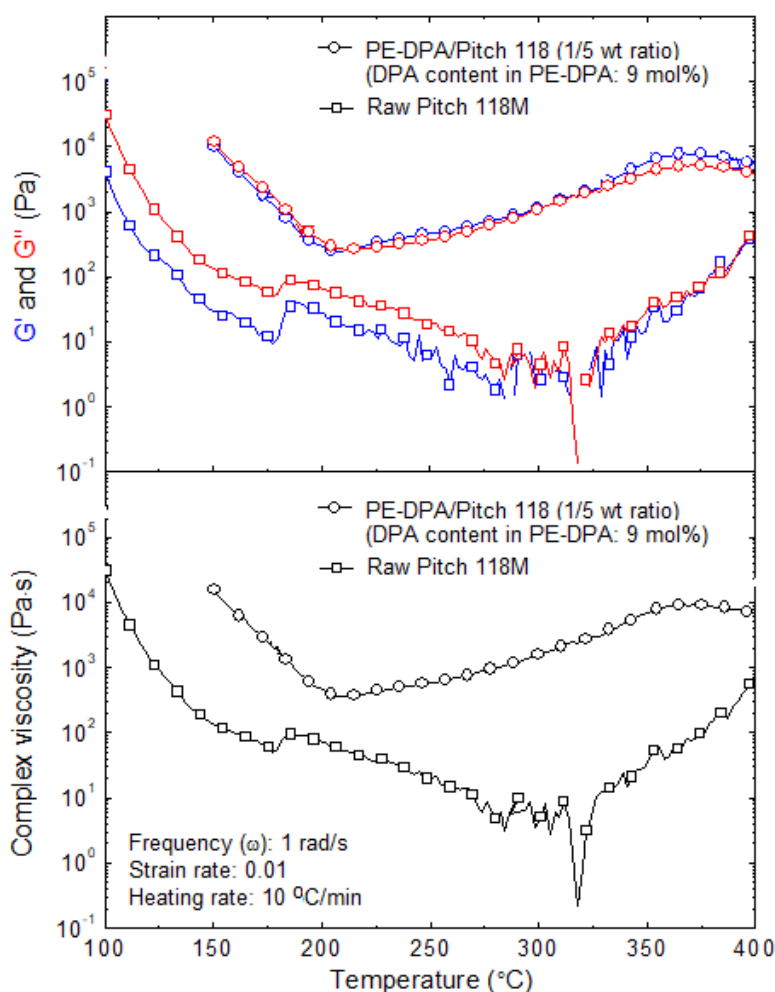


Figure 2. Comparison of (top) G' and G'' values and (bottom) complex viscosity during the thermal heating process between reference Pitch 118M and a mixture of PE-DPA copolymer (9 mol% DPA content) and Pitch 118M molecules with 1/10 wt ratio

The profiles of melt viscosity (η) and viscoelastic properties (i.e., storage modulus $G'(\omega)$, loss modulus $G''(\omega)$, and $\tan(\delta)$) for each specific mixture offer us very important information in the subsequent melt fiber-spinning process. Because of the continuous evolution of chemical structure during the thermal heating (stabilization step), the consideration of suitable spinning temperature will be based not only on the processability of fiber-spinning but also on the quality of the resulting PE-Pitch precursor fibers. In other words, based on the rheological properties at processing temperatures in Figure 2, we will also know the extent of the coupling reaction between the reactive PE copolymer and Pitch molecules at the specific temperature. As discussed, the extent of the coupling reaction determines the quality of the PE-Pitch precursor. It is highly desirable to have a melt-processible PE-Pitch precursor that also contains more than 50% volume fraction of PE-Pitch structure because the resulting PE-Pitch fiber will exhibit good mechanical properties that allow in situ stretching during the subsequent carbonization process. It also offers high carbonization yield. The ideal processing temperature is essential in realizing our goal, with a new low-cost and high-quality CF production method, through the lower-cost precursor, melt-spinning fiber process, higher mass yield, and higher tensile strength in the resulting CF products.

A Filabot desktop filament extruder equipped with a spooler, shown in Figure 3 (top), was applied in the melt fiber-spinning process. Based on the preliminary experimental results, this simple equipment is capable of melt-processing PE-Pitch precursors. Typically, the reactive PE copolymer (either PE-DVB or PE-DPA) was melt-mixed with Pitch 118M (with a specific weight ratio) in a reactor equipped with a mechanical stirrer at a specific temperature for a specific time. After achieving a homogeneous PE copolymer/Pitch mixture (containing some PE-Pitch and many free Pitch molecules), this homogeneous mixture was fed into the extruder with a controlled temperature and screw rotation speed. The PE-Pitch melt was extruded from the nozzle, and the extruded filament was then connected to a spooler with a constant rotating speed to reach the tight tolerance. The puller wheels draw the filament from the extruder, and its speed controls the extruded filament diameter. Figure 3 (bottom) shows several resulting PE-Pitch filaments that are relatively uniform in diameter and show good mechanical strength.



Figure 3. (top) Melt fiber-spinning of a PE-Pitch precursor using a Filabot desktop filament extruder and a spooler with the rotating puller wheels; (bottom) several PE-Pitch fibers prepared by the melt fiber-spinning process

CONCLUSIONS AND UPCOMING ACTIVITIES

In FY 2018 (Phase 1), we developed four new C precursors—including P(PA-A), P(PA-PA), PE-Pitch, and B-Pitch—that exhibit very high C yields (higher than the Phase 1 project objective of 80%) after heating to high carbonization temperatures. The experimental results were confirmed by Oak Ridge National Laboratory. In addition, we also investigated the fabrication of PE-Pitch precursor fibers. In a systematic study to understand the preparation of PE-Pitch precursor and its melt-processing condition, we expanded the chemistry to synthesize two reactive copolymers (PE-DVB and PE-DPA) that can engage in coupling reactions with Pitch molecules to form PE-Pitch precursors under elevated temperatures. This thermal-induced coupling reaction was monitored by melt rheology measurement. The same rheological results on PE-Pitch precursors also helped us identify the suitable melt-processing temperature for fiber spinning. Following this useful rheology

information, we successfully prepared several PE-Pitch fibers with various filament diameters. The preliminary results are very encouraging in this PE-Pitch approach. However, it is still a long way to achieve high-quality PE-Pitch precursor fibers. The immediate research activities in the coming year are to understand the effects of structure and composition in both reactive PE copolymer and Pitch material, the extent of the coupling (cyclo-addition) reaction, and the suitable fiber melt-spinning condition to obtain high-quality PE-Pitch fibers. The resulting PE-Pitch fibers will be carbonized to form the final CF products. We will certainly study the resulting CF quality, mechanical strength, and carbonization yield.

FY 2018 PUBLICATIONS/PRESENTATIONS

1. Mike Chung, Gang Zhang, and Joseph Sengeh, “Developing a New Polyolefin Precursor for Low-Cost, High-Strength Carbon Fiber,” presented at the Tech Team Meeting, Detroit, June 2018.
2. Mike Chung, “Developing a New Polyolefin Precursor for Low-Cost, High-Strength Carbon Fiber,” presented at the 2018 DOE Annual Merit Review and Peer Evaluation Meeting, Washington, D.C., June 2018.

REFERENCES

1. R. Hu and T.C. Chung. *Carbon* 34 (1996): 595.
2. R. Hu and T.C. Chung. *Carbon* 34 (1996): 1181.
3. R. Hu and T.C. Chung. *Carbon* 35 (1997): 1101.
4. Youmi Jeong, Alfred Kleinhammes, Yue Wu, and T.C. Mike Chung. *J. Am. Chem. Soc.* 130 (2008): 6668.
5. Youmi Jeong and T.C. Mike Chung. *Carbon* 49 (2011): 140.

Novel Plasticized Melt-Spinning Process of Polyacrylonitrile Fibers Based on Task-Specific Ionic Liquids

Sheng Dai (Primary Contact), Halie Martin, Huimin Luo, Richard Mayes, and Amit Naskar
Oak Ridge National Laboratory
1 Bethel Valley Road
Oak Ridge, TN 37830
Phone: (865) 576-7307
Email: dais@ornl.gov

DOE Manager: Bahman Habibzadeh
Phone: (202) 287-1657
Email: Bahman.Habibzadeh@ee.doe.gov

Subcontractor:
525 Solutions, Inc., Tuscaloosa, Alabama

Project Start Date: July 1, 2017
Project End Date: June 30, 2020

Overall Objectives

- Investigate how the molecular structures of ionic liquids (ILs) dictate plasticizing interactions with polyacrylonitrile (PAN) for controlling glass transition temperatures and rheological properties of PAN-IL composites.
- Study how the chemical interactions of ILs with PAN can be used to control the cyclization degree in intermediate ladder structures.
- Integrate the information gained from the above two tasks to develop IL-assisted melt-spinning systems that demonstrate considerably enhanced production efficiencies and improved structural properties of PAN fibers.

Fiscal Year (FY) 2018 Objectives

- Identify and synthesize task-specific ionic liquids with enhanced nitrile interactions between the PAN and that of the IL.
- Characterize the miscibility of the IL in PAN polymer spectroscopically and demonstrate >30 wt% PAN solubility in IL.

- Demonstrate the preparation of PAN-IL melts with carbon yield >50%.
- Demonstrate a >15°C decrease in PAN-IL melt temperature through differential scanning calorimetry.

Technical Barriers

This project addresses the following technical barriers from the Hydrogen Storage section of the Fuel Cell Technologies Office Multi-Year Research, Development, and Demonstration Plan¹:

- System Weight and Volume
- System Cost
- Durability/Operability.

Contribution to Achievement of DOE Hydrogen Storage Milestones

This project has contributed to achievement of the following DOE milestone from the Hydrogen Storage section of the Fuel Cell Technologies Office Multi-Year Research, Development and Demonstration Plan:

Milestone 2.7: Crosscutting: Reduce the high-volume cost of high-strength carbon fiber by 25% from \$13 per pound to ~\$9 per pound. (4Q, 2020)

Synthesizing nitrile-rich ionic liquids that will interact with PAN, decreasing the melt temperature of PAN, and allowing for melt-spinning fibers as well as the recyclability of the IL will result in a decrease in production cost of carbon fiber. Increased interactions between nitriles on IL and PAN will increase carbonization, increasing the strength of the carbon fiber.

FY 2018 Accomplishments

- Synthesized PAN-IL melts with up to 50 wt% PAN, focusing on two cation imidazolium-based targets of 1-alkyl-methylimidazolium

¹ <https://www.energy.gov/eere/fuelcells/downloads/fuel-cell-technologies-office-multi-year-research-development-and-22>

(C_n mim]) and 1-(3-cyanopropyl)-3-methylimidazolium ([MPCNIm]).

- Characterized the carbon yield of PAN-IL composites based on carbon chain length on ionic liquid, counter anion, and PAN concentration. Preliminary results indicated that after removing the IL from the composite, the carbon yield increased by about 20% compared to the original melt composite.
- PAN-IL composites suppressed the melting temperature of PAN by 20°C when compared to neat PAN. Composites with 30 wt% PAN showed the greatest melting point depression of $\geq 35^\circ\text{C}$.

INTRODUCTION

The production of high-strength carbon fibers is an energy-intensive process, and thus, it is costly. One significant cost yet to be mitigated involves the production of polyacrylonitrile (PAN) fibers prior to carbon fiber production. The current technology for PAN fiber production involves wet spinning [1]. In this process, the fibers are dissolved and fed through coagulation and rinse baths to remove the solvent and to produce fibers. This intensive process is inherently inefficient [2], which has a direct correlation to the costs of hydrogen storage systems, where the carbon fiber cost is nearly 75% of the total system cost [3]. Melt spinning the PAN into fibers would allow for significant reductions of production cost, estimated at a nearly 50% reduction of overall cost per pound [3]. This cost would be reduced through decreased capital investments, utilities, and labor, while exhibiting a 3-times-faster spinning speed [2]. However, melt-spinning virgin PAN and many PAN copolymers used to produce high-strength carbon fibers is impossible due to polymer degradation.

It is well known that the strong dipole-dipole interaction between nitrile groups in PAN leads to its degradation before melting, which makes cost-efficient melt processing impossible. There have been exciting developments in a new class of chemicals called ionic liquids, which consist of an anion associated with an organic cation, and these materials have enormous potential to act as nonvolatile “green chemistry” solvents for a broad range of chemical processes [4,5]. The ability to synthesize highly nitrile-rich ionic liquids—which have negligible vapor pressure, exhibit low toxicity, and are carbon generators upon carbonization—makes using ionic liquids in the melt-spinning production of high-strength carbon fibers an attractive alternative production route. If both the cation and anion of the IL can be functionalized with nitriles, then the interactions with PAN increase and will decrease the melting temperature. Thus, this allows the melt-spinning of PAN, which results in decreased production costs vital to the necessary decrease in hydrogen storage costs.

APPROACH

We capitalize on the vast knowledge of carbon-fiber processing at Oak Ridge National Laboratory (ORNL) including the ORNL Carbon Fiber Technology Facility (CFTF), which is equipped with both small- and large-scale fiber-spinning and carbon-fiber conversion capabilities. This will be coupled with our multi-functional IL synthesis experience and capabilities that are well-known worldwide. Our emergent plasticized melt-spinning process has the potential to dramatically cut the cost and energy associated with producing PAN-based carbon fibers. Developing the new generation of PAN-fiber melt-spinning systems represents a vital step toward the efficient precursor development for low-cost, high-strength carbon fibers used in composite overwrapped pressure vessel applications. And it will ensure that the United States will maintain a technological lead in developing and deploying advanced energy technologies.

RESULTS

During FY 2018, we focused on synthesizing and characterizing new imidazolium-based ionic liquids for the formation of PAN melt composites:

- The two main cations for the ionic liquids under investigation were 1-alkyl-methylimidazolium ([C_nmim]) and 1-(3-cyanopropyl)-3-methylimidazolium ([MPCNIm]) (Figure 1). The ability to adjust the carbon alkyl chain length and nitrile group on the cation allows for further investigation into a structure-property relationship between the polymer and the IL. Ionic liquids containing a variety of counter anions were used including bromide (Br⁻), chloride (Cl⁻), acetate (OAc⁻), and dicyanamide (DCA⁻). However, the acetate and dicyanamide anions did not form melts.
- The effect of carbon alkyl chain length and nitrile groups on cations were monitored in our PAN-IL melt investigation. Increasing the carbon alkyl chain length of the IL increased the time and energy needed to form a continuous melt with PAN.

- Melts were formed with different percentages of PAN in ILs, with PAN weight percentages ranging from 20 wt% to 50 wt%. Incorporating a lower weight percentage of IL plasticizer is an important achievement because ILs have the potential to be a cost driver while also potentially resulting in deleterious effects in the mechanical properties.

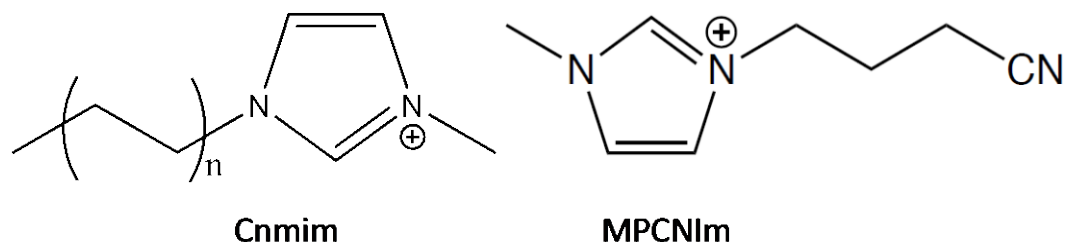


Figure 1. Chemical structure of two ionic liquid cations

The second achieved milestone in FY 2018 was synthesizing PAN-IL composites with carbon yields greater than 50%. The results are listed in Table 1.

Table 1. Thermophysical Characterization of PAN-IL Composites

Ionic Liquid	PAN (%)	Physical Appearance	Carbon Yield (%)		Melting Temperature T_m (°C)
			Original	After Washing	
----	100	white powder	33.4	---	325
[C ₂ mim]Br	20.3	light yellow gel	23.9		292.02
	30.0	light yellow gel	20.6	61.5	311.47
	46.8	light yellow gel	36.2		306.83
	50.7	black melt	30.1		298.05
[C ₄ mim]Br	19.9	yellow gel	15.7		308.82
	30.0	dark brown gel	24.4	59.4	303.20
	46.5	dark brown melt	35.0		302.94
	50.4	black melt	39.2		297.29
[C ₈ mim]Br	20.0	brown gel	13.0		313.18
	25.0	brown gel	15.7		310.62
	30.0	brown gel	19.0		309.34
[C ₁₀ mim]Br	20.0	yellow gel	10.4		307.38
	30.0	yellow gel	18.7		306.66
[C ₄ mim]Cl	20.5	brown gel	8.33		303.79
	29.9	yellow gel	13.1	56.1	305.60
	45.6	dark brown melts	26.1		298.68
	50.5	black melt	28.8		309.63
[MPCNIm]Br	20.0	light yellow gel	15.3		312.13
	27.4	yellow melt	23.9		310.09
	30.0	yellow melt	26.3	61.4	
	33.4	brown melts	26.5		308.35
	49.0	brown powder	41.7		295.14
[MPCNIm]Cl	30.0	yellow melt	21.1	52.3	270.24

- Using thermal gravimetric analysis (TGA), we found that the carbon yield for PAN-IL composites was higher from IL with shorter carbon alkyl chain lengths on the substituents. The carbon yield was generally higher for composites where the IL contained a nitrile substituent.

- The carbon yield was higher for ILs containing a bromide counter anion instead of a chloride when containing the same carbon alkyl chain lengths. A higher carbon yield is correlated to a high-strength carbon fiber.
- The recyclability of the ionic liquids was also monitored. The PAN carbon yield after washing the composite increases by 20% compared to the PAN-IL melt, as shown in Figure 2. The recycling of IL through sample washing of the composites increases the economical prospect of using ILs in a plasticized melt-spinning process for PAN fiber production.

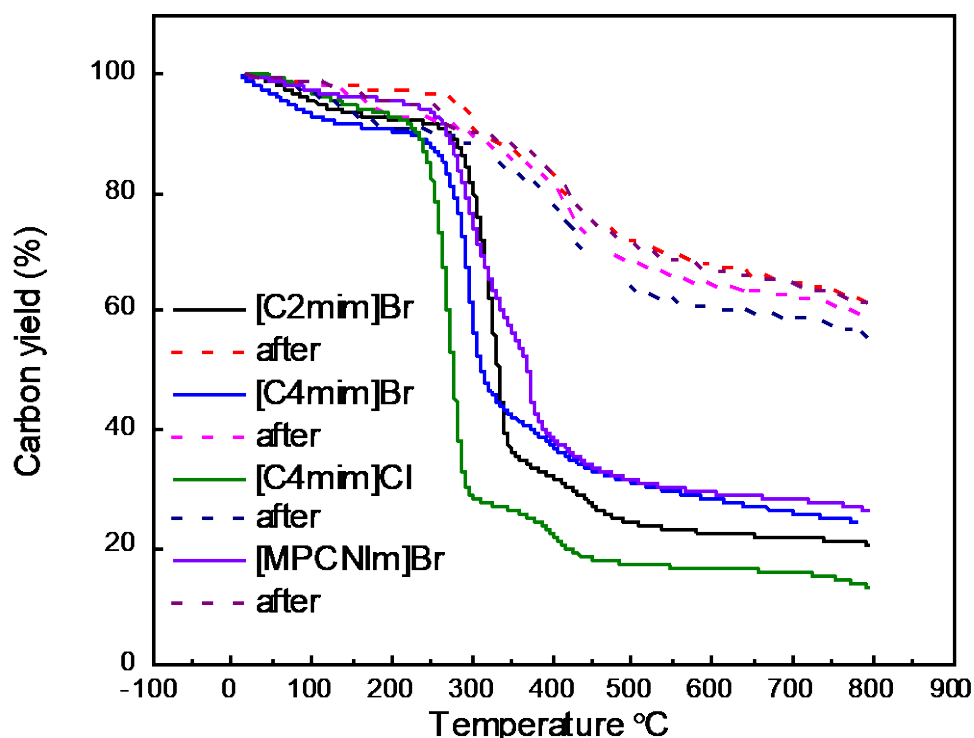


Figure 2. TGA plots of ~30 wt% PAN in IL melts before (solid lines) and after contact with water (broken lines)

Ionic liquids act as a plasticizer to suppress the melting temperature of PAN. During FY 2018, we monitored these transitions through differential scanning calorimetry (DSC), as shown in Table 1 and Figure 3.

- The melting temperature of pure PAN is at about 325°C [6]. However, this results in pure PAN being unprocessable in the melt because the polymer chains crosslink at a temperature lower than melting.
- Ionic liquids suppress the reactions between PAN nitriles at elevated temperatures. This is observed in the melting temperatures for PAN-IL composites, which are $\geq 20^\circ\text{C}$ lower than pure PAN. The decrease in the melting temperature should allow PAN fibers to be melt-spun.
- In general, as the concentration of PAN increases in the composite, the melting temperature decreases, as shown in Figure 4 for composites containing [C₄mim]Cl.
- The lower melting temperatures will lower the amount of energy necessary to process these materials into fibers.

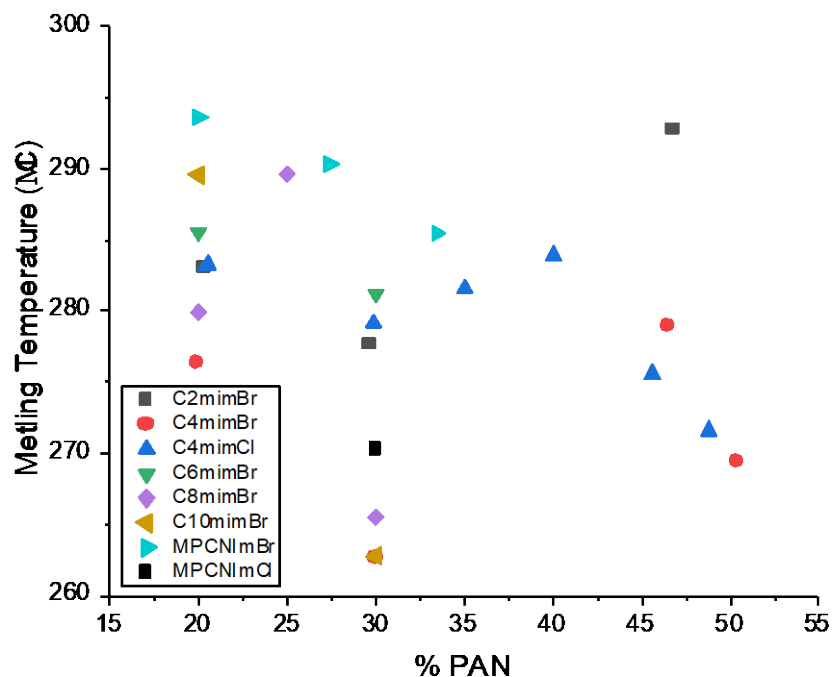


Figure 3. Melting temperature of PAN-IL composites

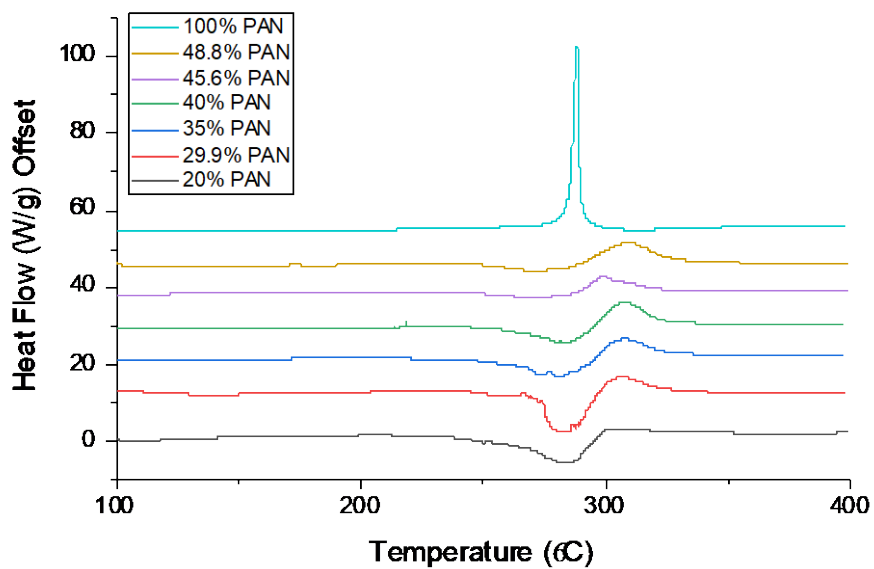


Figure 4. DSC characterization of PAN and PAN-[C4mim]Cl composites

CONCLUSIONS AND UPCOMING ACTIVITIES

In FY 2018, this project began with the synthesis and thermophysical characterization of the targeted task-specific ionic liquids, focusing on two imidazolium cations including 1-alkyl-methylimidazolium ([C_nmim]) and 1-(3-cyanopropyl)-3-methylimidazolium ([MPCNIm]). We focused on the miscibility of PAN with various ionic liquids and determined that we can produce composites with up to 50 wt% PAN and form uniform composite melts. We recorded the IL decomposition temperatures, carbon-yield productions, and melting temperatures of the PAN-IL composites. We observed that the carbon yield increased after the composite had been washed, similar to the process that the PAN fiber will go through after spinning; furthermore, the melting temperatures of the composites were lower than that of the pure PAN powder.

Studies for FY 2019 will include the following:

- Work with a subcontractor to identify the IL for scale-up and optimization synthesis based on melting temperature and rheology studies of the composite.
- Demonstrate the ability to melt-spin PAN fibers based on IL and characterize the fibers using DSC, TGA, and scanning electron microscopy.
- Perform a techno-economic analysis for scale-up of the IL production.
- Demonstrate the tensile modulus and tensile strength of melt-spun PAN fibers before and after washing.

FY 2018 PUBLICATIONS/PRESENTATIONS

1. S. Dai, “Novel Plasticized Melt Spinning Process of PAN Fibers Based on Task-Specific Ionic Liquids,” presented at 2018 DOE Hydrogen and Fuel Cells Program Annual Merit Review and Peer Evaluation Meeting, Washington, D.C., June 14, 2018.

REFERENCES

1. T.-Y. Wang, H.-C. Chang, Y.-T. Chiu, and J.-L. Tsai, “The Index of Dry-Jet Wet Spinning for Polyacrylonitrile Precursor Fibers,” *Journal of Applied Polymer Science* 132 (2015): 41265.
2. B.A. Newcomb, “Processing, Structure, and Properties of Carbon Fibers,” *Compos. Part A* 91 (2016): 262–282.
3. C.D. Warren and F.L. Paulauskas, “Development of Low-Cost, High-Strength Commercial Textile Precursor (PAN-MA),” In *DOE FCTO Annual Progress Report* (2014).
4. Z. Ma, J.H. Yu, and S. Dai, “Preparation of Inorganic Materials Using Ionic Liquids,” *Advanced Materials* 22 (2010): 261–285.
5. H. Wang, G. Gurau, and R.D. Rogers, “Ionic Liquid Processing of Cellulose,” *Chemical Society Reviews* 41 (2012): 1519–1537.
6. A.K. Gupta, D.K. Paliwal, and P. Bajaj, “Melting Behavior of Acrylonitrile Polymers,” *J. Appl. Polym. Sci.* 70, no. 13 (1998): 2703–2709.

Material Challenges for Cryogenic Hydrogen Storage Technologies

Kevin L Simmons (Primary Contact), Ken Johnson,
David Gotthold, Ngheip Nguyen
Pacific Northwest National Laboratory
PO Box 999
Richland, WA 99352
Phone: (509) 375-3651
Email: kl.simmons@pnnl.gov

DOE Manager: Bahman Habibzadeh
Phone: (202) 287-1657
Email: Bahman.Habibzadeh@ee.doe.gov

Project Start Date: January 1, 2018
Project End Date: September 30, 2020

Overall Objectives

- Provide the scientific and technical basis to enable full deployment of hydrogen and fuel cell technologies by filling the critical knowledge gap for polymer performance in hydrogen environments.
- Develop an understanding of material interaction with hydrogen to mitigate impacts on reliability and durability.
- Develop experimental test methodologies that provide material performance under hydrogen infrastructure environments.
- Disseminate material characteristics to the community to begin discussions on how to improve materials in the hydrogen infrastructure environment.
- Develop a material acceptance process that will provide detailed information to evaluate specialty resins and carbon fiber composite materials through thermomechanical testing by combining cryogenic temperature, thermal cycling from cryogenic to elevated temperatures (-253°C + 120°C), off-gassing under vacuum (10⁻⁶ torr), and fatigue cycling at non-ambient conditions equivalent to the stress states in the composite at the maximum allowable working pressure and standard test cycles.

Fiscal Year (FY) 2018 Objectives

- Complete the lab meeting report on the material properties that were identified for the thermal and mechanical models to more accurately predict pressure vessel performance through thermal cycling from cryogenic to ambient temperatures.
- Provide DOE a roadmap for the cryocompressed and cold gas storage pressure vessel materials and containment qualifications.
- Establish cryogenic testing capability requirements and procure equipment.
- Develop material models for predicting pressure vessel material performance at cryogenic temperatures under different pressure fill scenarios.

Technical Barriers

This project addresses the following technical barriers from the Hydrogen Storage section of the Fuel Cell Technologies Office Multi-Year Research, Development, and Demonstration Plan¹:

- System Weight and Volume
- System Cost
- Efficiency
- Durability/Operability
- Codes and Standards
- Materials of Construction
- Thermal Management
- Lack of Tank Performance Data and Understanding of Failure Mechanisms.

FY 2018 Accomplishments

- Held a federal lab meeting at Pacific Northwest National Laboratory (PNNL) and developed a roadmap for materials testing and qualifications.

¹ <https://www.energy.gov/eere/fuelcells/downloads/fuel-cell-technologies-office-multi-year-research-development-and-22>

- Completed a final report on results of the federal lab meeting at PNNL and submitted the report to DOE.
- Identified and procured a liquid helium cryogenic dewar with mechanical testing capability and thermal control of temperatures from 1.2 K to 300 K.
- Completed thermoelastic stress analysis to assess the magnitude of thermal stresses in the composite overwrap of a Type 4 hydrogen storage vessel model.
- Identified a composite material resin system for sub-ambient and cryogenic testing.

INTRODUCTION

The H2@Scale vision is to increase U.S. energy security, resiliency, economic growth, and jobs via high-scale hydrogen production. Hydrogen storage is a key part of H2@Scale, but new materials will be required for low-cost, lightweight storage vessels. The objective of this project is to develop a material acceptance process that will provide detailed information to evaluate specialty resins and carbon fiber composite materials through thermomechanical testing by combining cryogenic temperature, thermal cycling from cryogenic to elevated temperatures (-253°C + 120°C), off-gassing under vacuum (10^{-6} torr), and fatigue cycling at non-ambient conditions equivalent to the stress states in the composite at the maximum allowable working pressure and standard test cycles. The production of full-scale pressure vessels to validate tank materials and designs is expensive and time consuming. The ability to screen new pressure vessel materials (alternative resins, fibers, and liner materials) at the coupon level before transitioning to full-scale tank testing would significantly reduce cost and allow for more innovation through prescreening new concepts and materials. Experimental data will feed tank-level numerical modeling to predict temperature-dependent burst pressures. This process will develop and establish test methods to evaluate resins, fibers, composites, and liner materials prior to full-scale tank construction. This will either verify or disprove the hypothesis that new alternative resin, fiber, and liner systems designed for sub-ambient and cryogenic conditions will perform within acceptable limits at elevated temperatures.

APPROACH

PNNL's approach to developing the materials qualification strategy for cryogenic materials evaluation was to:

- Develop a comprehensive roadmap with input from federal lab and industrial subject matter experts
- Develop test methodologies for cryogenic materials testing
- Establish a cryogenic material properties database
- Provide material properties to performance models that predict pressure vessel performance
- Provide material testing guidelines for cryogenic materials qualifications.

The material testing data will provide input into pressure vessel models for performance analysis. The analysis will provide technical feedback loops, supporting safety factor performance and long-term pressure vessel performance.

RESULTS

On April 24, PNNL hosted a meeting of more than 20 subject matter experts from federally funded national laboratories and other government research agencies to discuss methods and technologies to test, evaluate, and rapidly screen materials for use in pressurized cryogenic storage applications and accelerate the pathway to tank qualification.

Based on the presentations, breakout sessions, and general discussions, several barriers were identified that must be addressed for the thermal and mechanical models to more accurately predict pressure vessel performance through thermal cycling from cryogenic to room temperatures. These include needing a better understanding of target operating conditions, improved testing methodology, and general lack of material performance data at low temperatures. The key materials properties that were identified are summarized in Table 1 with critical material-test combinations highlighted.

Table 1. Material Property Test Data Needed to More Accurately Simulate Hydrogen Pressure Vessel Performance throughout the Pressure and Temperature Range

Test Method/Properties	Material
Uniaxial tension providing the stress-strain curve to failure at selected temperatures throughout the entire temperature range Resulting properties: Elastic modulus, yield strength, ultimate strength, and ultimate elongation as a function of temperature	Metal liner Polymer liner Composite overwrap: resin, fibers, lamina, and laminate
Short beam shear: Interlaminar shear strength	Composite laminate
Coefficient of thermal expansion (CTE) and thermal conductivity: The CTE and thermal conductivity of composite lamina and laminates changes when matrix cracking occurs	Metal liner Polymer liner Composite overwrap: resin, fibers, lamina, laminate
Glass transition temperature	Polymer liner Composite resin
Fracture toughness Charpy impact test: Nil-ductility transition temperature as a function of combined hydrogen exposure and temperature	Metal liner Metal welds and joints
Fatigue testing: Thermomechanical cyclic loading for laminates; thermal and pressure induced for composite overwrap	Metal liner Polymer liner Composite overwrap: resin, fibers, lamina, laminate Joints (welds, etc.)
Thermal properties: Conductivity, specific heat, and thermal expansion of many solid materials at cryogenic temperatures are available from the NIST Cryogenic Materials website: https://trc.nist.gov/cryogenics/materials/materialproperties.htm The conductivity and specific heat of cryogenic liquids and gases are available at the NIST Chemistry WebBook website: https://webbook.nist.gov/chemistry/fluid/	Metal liner Polymer liner Composite overwrap: resin, fibers, lamina, laminate Hydrogen

A comprehensive survey of the literature revealed limited knowledge of mechanical properties at cryogenic temperatures and insufficient data to support modeling efforts. The available data is largely limited to tensile properties at those temperatures that are readily achievable by submersion in liquid cryogenics (i.e., 4 K [liquid helium] and 77 K [liquid nitrogen]). Additionally, information on material strain, which is critical to developing a mechanical model, is largely absent from the literature. To address these shortcomings, PNNL has purchased a cryogenic dewar for use with a mechanical load frame capable of operating throughout the range between 2 K and 300 K. Strain data will be gathered continuously with an MTS extensometer rated to 4 K.

Once validated by experimental testing, a second dewar will be specifically designed to accommodate digital image correlation (DIC) for more in-depth strain analysis, along with fatigue testing capability. This unique experimental setup will allow for comprehensive characterization of mechanical properties of pure epoxies and fiber-epoxy composites along with valuable thermal contraction information.

Previous efforts by the National Institute of Standards and Technology (NIST) demonstrated a strong influence of specimen flaws on mechanical properties at cryogenic temperatures. To mitigate this issue, a mold was specially designed to limit the presence of flaws in epoxy tensile specimens. These unique specimens require custom gripping fixtures, which have been designed and machined at PNNL.

The literature survey also identified two base resins and several curing agents as candidates for development of an epoxy system designed for use in cryogenic composite tanks. Resins diglycidyl ether of bisphenol A

(DGEBA) and diglycidyl ether of bisphenol F (DGEBF) were selected based on frequency of use in research and commercial settings, material availability, and performance at cryogenic conditions. Several common aliphatic amine curing agents, such as diethylene triamine (DETA) and triethylene tetramine (TETA), were used frequently in the literature. However, other curing agents known to increase ductility in the cured products, such as amino ethyl piperazine (AEP) and dodecyl succinic anhydride (DDSA), have not previously been studied at cryogenic temperatures. The influence of additives including reactive diluents and resin modifiers will be studied along with other modifiable factors such as cure procedure. A design of experiments has been developed to account for which factors influence cryogenic material performance.

The modeling effort has applied PNNL's EMTA-NLA (Eshelby-Mori-Tanaka Approach to Nonlinear Analysis) tool for composite materials (e.g., [1-6]) implemented in the ABAQUS finite element (FE) code to analyze an existing Type 4 hydrogen storage vessel model to predict the composite and constituent thermal stresses in the helical and hoop layers (plies) of the composite vessel. This vessel model involves six layers, which have the following stacking sequence: $90^\circ/+10^\circ/-10^\circ/90^\circ/+15^\circ/-15^\circ$ with respect to the axial direction, and thicknesses (in mm): 5 / 1 / 1 / 2.5 / 1 / 1. The fiber volume fraction of each layer is 0.6. The cylindrical part of the vessel was discretized using the composite layered shell elements of ABAQUS while the vessel's dome contribution was replaced by a distributed load at one end totalizing a force equal to $P \pi r^2$ (with r , internal radius, and P , internal pressure). Figure 1 shows the FE model of the vessel cylindrical part. The length of this part is 1.338 m and its internal radius is 0.167 m.

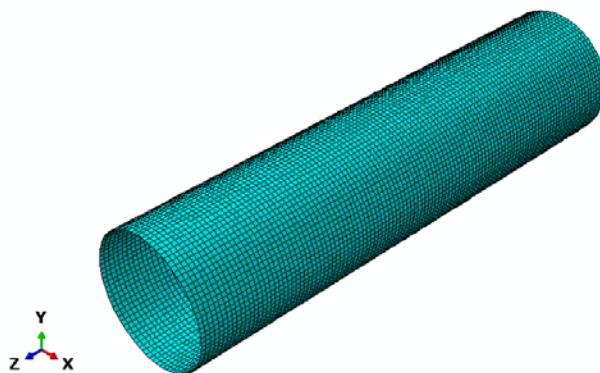


Figure 1. The simplified FE model of a Type 4 hydrogen storage vessel

The FE analyses were performed accounting for the variations of constituent thermoelastic properties with temperature according to three thermomechanical loading scenarios shown in Figure 2. In Scenario 1, the vessel is first cooled from room temperature (RT) to 77 K and then an internal pressure is applied incrementally to achieve 35 MPa at 77K. In Scenario 2, the vessel is also cooled from RT to 77 K but the internal pressure is applied concurrently until attaining 35 MPa. In Scenario 3, the vessel is cooled from RT to 150 K and during the same time, the internal pressure is applied incrementally to 35 MPa, and finally it is cooled down to 77 K at 35 MPa.

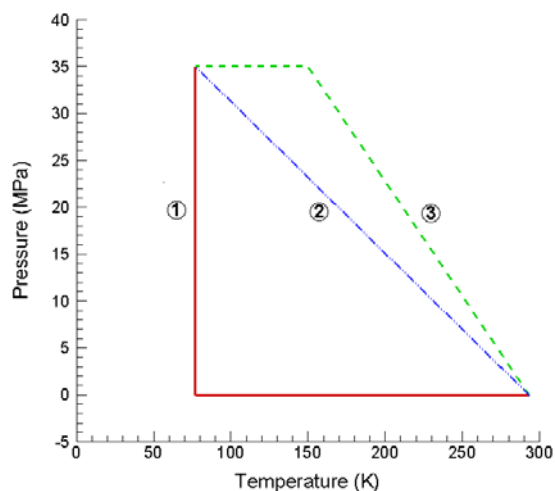


Figure 2. The three thermomechanical loading scenarios considered in the FE analysis of the hydrogen storage vessel

The analyses used existing thermoelastic properties of CF from [6] and TORAYCA’s datasheet for T700S assuming that CF’s elastic properties and longitudinal CTE were constant in the 77 K–293 K range. However, the variations of CF’s transverse CTE with temperature were accounted for in the analyses using the data in [7]. The epoxy elastic modulus was assumed to linearly vary from the value at RT (4,000 MPa) to the one at 77 K (6,000 MPa). The epoxy CTE as a function of temperature was from [8]. Figures 3(a) and 3(b) illustrate the CTEs of CF and of epoxy in the 77 K–293 K range, respectively. The longitudinal and transverse CTEs of the CF/epoxy lamina predicted as a function of temperature by EMTA-NLA during the analyses are given in Figures 4(a) and 4(b), respectively.

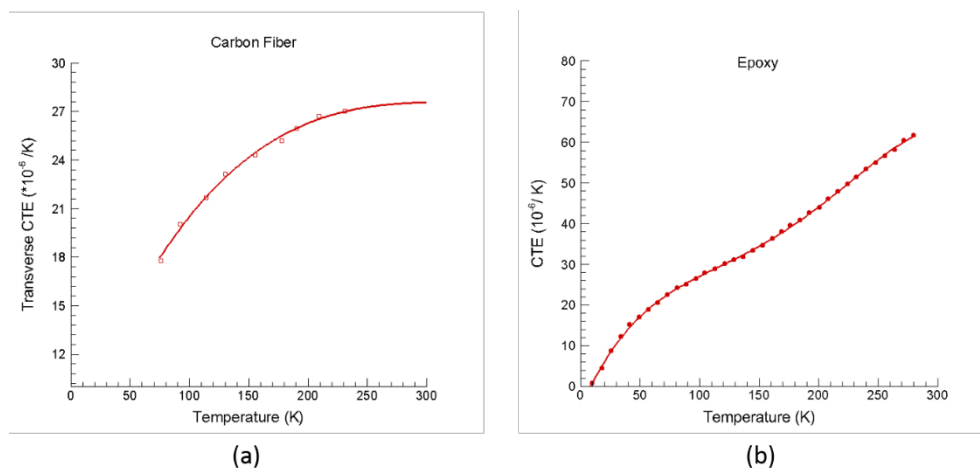


Figure 3. (a) Transverse CTE of CF based on [7] and (b) CTE of epoxy based on [8]

The analyses predicted not only composite stresses in different plies but also stresses in the fiber and matrix. As elevated thermal stresses in the epoxy matrix can induce cracking if the epoxy does not exhibit sufficient strength at low temperatures, we examine the fiber-direction and transverse-to-fiber-direction *matrix stresses* given in Figures 5 and 6 according to three thermomechanical loading scenarios. In Scenario 1, the cooling from RT to 77 K without the internal pressure application resulted in purely thermal effects that have caused matrix stresses to build up in all the plies. The application of internal pressure has then further increased matrix stresses to the highest levels at the end of loading. The evolutions of matrix stresses with temperature and pressure according to Scenarios 2 and 3 have reached the highest levels at the end of loading lower than the

levels attained in Scenario 1. If the analyses had used constant thermoelastic properties, the levels of matrix stresses at the end of loading would have been identical for all the loading scenarios. Tables 2 and 3 provide the values of matrix stresses at the end of loading according to all the loading scenarios. Compared to the other scenarios, Scenario 3 has led to the lowest matrix stresses in both fiber- and transverse-to-fiber directions.

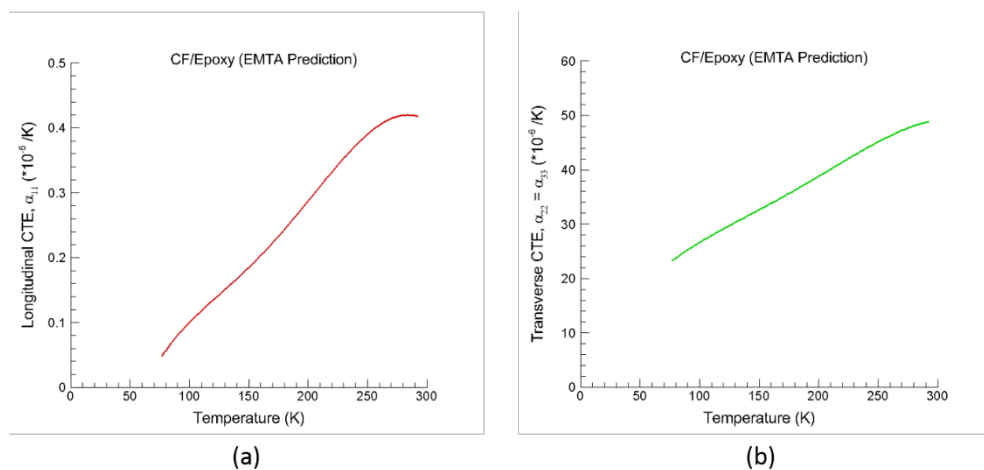


Figure 4. (a) Longitudinal and (b) transverse CTEs predicted for CF/epoxy

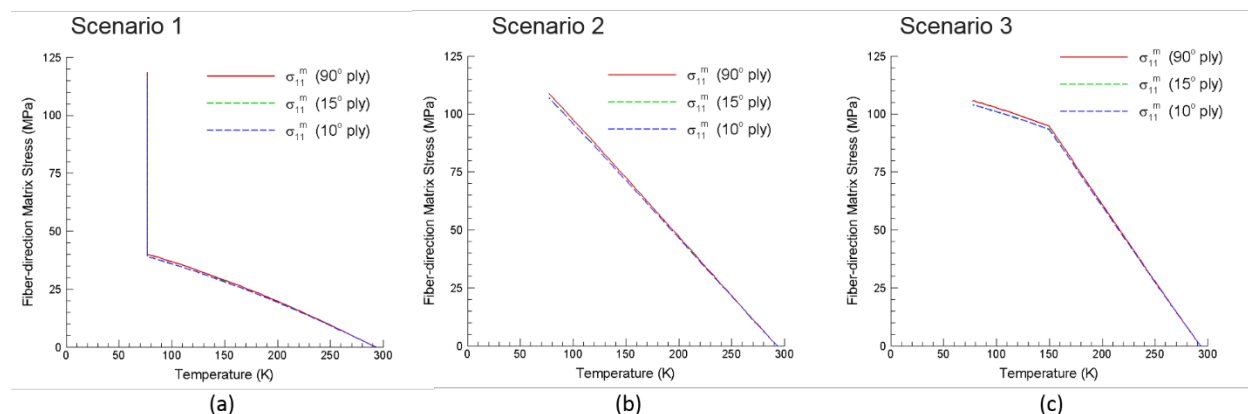


Figure 5. Predicted fiber-direction matrix stress in the helical (10° and 15°) and hoop (90°) plies according to (a) Scenario 1, (b) Scenario 2, and (c) Scenario 3

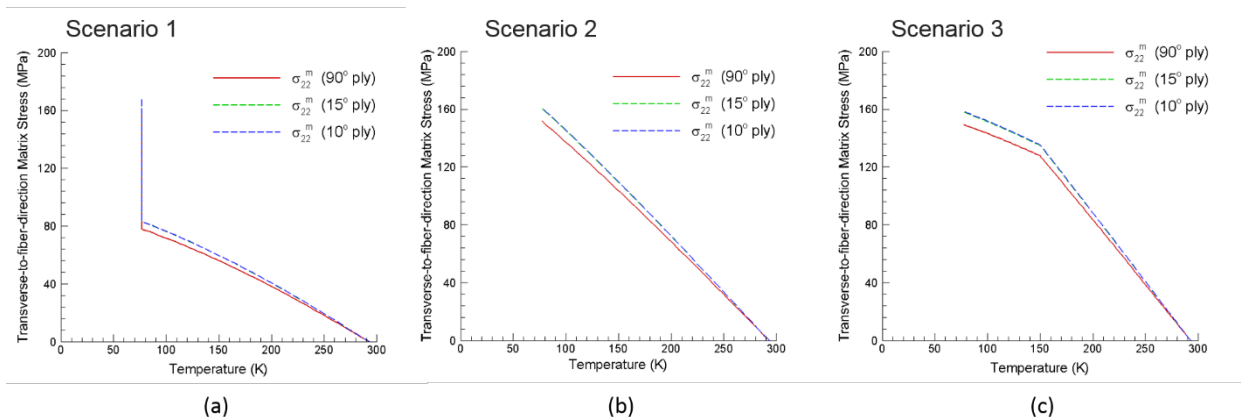


Figure 6. Predicted transverse-to-fiber-direction matrix stress in the helical (10° and 15°) and hoop (90°) plies according to (a) Scenario 1, (b) Scenario 2, and (c) Scenario 3

Table 2. Fiber-Direction Matrix Stress at the End of Loading

	90° Ply	15° Ply	10° Ply
Scenario 1	118.7	116.3	116.2
Scenario 2	109.1	107.2	107.1
Scenario 3	105.8	104.1	104.0

Table 3. Transverse-to-Fiber-Direction Matrix Stress at the End of Loading

	90° Ply	15° Ply	10° Ply
Scenario 1	159.2	168.9	169.4
Scenario 2	152.0	160.9	161.3
Scenario 3	149.3	158.0	158.4

CONCLUSIONS AND UPCOMING ACTIVITIES

Upon installation of the cryogenic mechanical properties test system, a series of tests will be conducted to identify the most influential constituents of epoxy systems. Epoxies will then be optimized for mechanical performance in fiber composite tanks. With validation of the cryogenic test system, a second system designed for fatigue testing and DIC capabilities will be procured. Data gathered during this process will be incorporated into a finite-element model that is currently in development.

Preliminary analyses of a Type 4 pressure vessel model were performed assuming the thermoelastic behavior of the constituents (i.e., CF and epoxy) and of the as-formed CF/epoxy composite overwrap. The analyses accounting for variations of thermoelastic properties with temperature have provided estimates of constituent and composite stresses resulting from three prescribed thermomechanical loading scenarios. Although these analyses were preliminary and based on simplified vessel geometry and loading conditions, they have indicated significant matrix stress levels at the end of loading that would need to be mitigated through improved material and vessel design in order to avoid failure of the composite overwrap due to transverse matrix cracking when the vessel operates in the cryogenic temperature range. Another important finding from this work is that the thermomechanical loading scenario has a significant impact on thermal stresses in the composite. Optimizing the loading scenario could help reduce the constituent stresses—in particular, matrix stresses—during the cycle, and this would help mitigate thermal stresses.

Future research activities include performing analyses for a Type 3 vessel, assessing thermal conductivity and CTE predictions, and modeling the damage and failure mechanisms observed in testing representative CF/epoxy specimens at selected temperatures from RT to a given cryogenic temperature.

FY 2018 PUBLICATIONS/PRESENTATIONS

1. K. Simmons, N. Menon, D. Smith, A. Naskar, and M. Veenstra, “Hydrogen Compatibility of Polymers,” presented at the 2018 Annual Merit Review, Washington DC, June 14, 2018.
2. K. Simmons, D. Gotthold, and K. Johnson, 2018 Material Challenges for Cryogenic Hydrogen Storage Technologies, Summary Report from the Material Qualification Lab Meeting.
3. Proceedings from the Material Challenges for Cryogenic Hydrogen Storage Technologies: Summary Report from the Material Qualification Lab Meeting, August 2018, PNNL-27830.

REFERENCES

1. J.D. Eshelby, “The Elastic Field Outside an Ellipsoidal Inclusion.” *Proceeding of the Royal Society London, Series A: Mathematical and Physical Sciences* 252 (1959): 561-569.
2. T. Mori and K. Tanaka, “Average Stress in Matrix and Average Elastic Energy of Materials with Misfitting Inclusions,” *Acta Metallurgica* 21 (1973): 571-574.
3. B.N. Nguyen, *EMTA User's Guide* (Richland, WA: Pacific Northwest National Laboratory, 2010), PNNL-19997.
4. B.N. Nguyen, *EMTA-NLA User's Guide* (Richland, WA: Pacific Northwest National Laboratory, 2010), PNNL-20013.
5. B.N. Nguyen, S.K. Bapanapalli, V. Kunc, J.H. Phelps, and C.L. Tucker III, “Prediction of the Elastic-Plastic Stress/Strain Response for Injection-Molded Long-Fiber Thermoplastics,” *Journal of Composite Materials* 43 (2009): 217-246.
6. B.N. Nguyen and K.L. Simmons, “A Multiscale Modeling Approach to Analyze Filament-Wound Composite Pressure Vessels,” *Journal of Composite Materials* 47 (2013): 2113-2123.
7. M.G. Huson, “High-Performance Pitch-Based Carbon Fiber,” In: *Structure and Properties of High-Performance Fibers*, Woodhead Publishing Series in Textiles (2017): 31-78.
8. U. Escher, “Thermal Expansion of Epoxy Resins with Different Cross-Link Densities at Low Temperatures,” *Cryogenics* 35 (1995): 775-778.

Fuel Cell R&D Subprogram Overview

INTRODUCTION

The Fuel Cell R&D subprogram supports applied, early-stage research and development (R&D) of fuel cell technologies for transportation applications, as well as stationary and cross-cutting applications, with a primary focus on reducing cost and improving durability. Early-stage research areas include catalysts, membranes, and fuel cell performance and durability. The subprogram seeks a balanced, comprehensive approach to fuel cells for near-, mid-, and longer-term applications. The development of fuel cells for transportation applications is a primary focus due to the nation's goal of significantly reducing its energy and petroleum needs and the benefits inherent in fuel cell electric vehicles (FCEVs) (e.g., high efficiency, long driving range, zero emissions). Transportation applications also include medium- and heavy-duty trucks, rail, and marine fuel cell propulsion. Stationary applications include the development of fuel cells for distributed power generation, including combined heat and power (CHP) for residential and commercial applications. Existing early markets and near-term markets generating market traction for adoption of FCEVs include primary/backup power for critical infrastructure such as data centers, auxiliary power units, and specialty applications such as material handling equipment. The subprogram's R&D portfolio is primarily focused on polymer electrolyte membrane (PEM) fuel cells, but it also includes longer-term technologies, such as alkaline membrane fuel cells, reversible fuel cells, and higher-temperature fuel cells like molten carbonate fuel cells for stationary applications.

Durability and cost are the primary challenges to fuel cell commercialization. Improvements in multiple components are required to concurrently meet these challenges. The subprogram's fuel cell tasks are delineated in the Fuel Cell Technologies Office Multi-Year Research, Development, and Demonstration Plan, with R&D focused in the key areas of fuel cell components and materials, as well as fuel cell performance and durability.

GOAL

The subprogram's goal is to advance fuel cell technologies for transportation, stationary, and cross-cutting applications.

OBJECTIVES

The subprogram's key objectives include:

- Developing a 65% peak-efficient, direct hydrogen fuel cell power system for transportation that can achieve 5,000-hour durability (ultimate 8,000 hours) and be mass produced at a cost of \$40/kW by 2025 (ultimate \$30/kW).
- Developing distributed generation and micro-CHP fuel cell systems (5 kW) operating on natural gas that achieve 45% electrical efficiency and 60,000-hour durability at an equipment cost of \$1,500/kW by 2025.
- Developing medium-scale CHP systems (100 kW–3 MW) by 2025 that achieve 50% electrical efficiency, 90% CHP efficiency and 80,000-hour durability at a cost of \$1,500/kW for operation on natural gas and \$2,100/kW when configured for operation on biogas.

FISCAL YEAR (FY) 2018 TECHNOLOGY STATUS AND ACCOMPLISHMENTS

Reducing cost and improving durability while maintaining performance continues to be the key challenge facing fuel cell technology. For platinum group metal (PGM)-based catalysts, both a reduction in PGM loading and an increase in membrane electrode assembly (MEA) areal power density are required to reduce material costs. Current state-of-the-art MEAs with very low cathode PGM loadings experience a higher than expected reduction in performance when operating at high power (i.e., close to rated power), but FY 2018 saw continued progress toward addressing this performance loss. Commercial fuel cells are expected to use PGM-based catalysts in the near term; however, reaching cost competitiveness with conventional automobiles in the long

term favors a transition from PGM-based catalysts to PGM-free catalysts. The subprogram's consortia—Fuel Cell Performance and Durability (FC-PAD) and the Electrocatalysis Consortium (ElectroCat)—made great strides in materials innovation and phenomenological understanding of fuel cell catalysts and electrode components through increased cooperation between the national laboratories and industry and academic partners.

One of the most important metrics used to guide the subprogram's R&D efforts is the projected high-volume manufacturing cost for automotive fuel cells, which is tracked on an annual basis. The subprogram is targeting a cost reduction to \$40/kW by 2025. Long-term competitiveness with alternative powertrains is expected to require further cost reduction to \$30/kW, which represents the subprogram's ultimate cost target. This year, the preliminary cost projection for an 80-kW_{net} automotive PEM fuel cell system based on next-generation laboratory technology and operating on direct hydrogen is \$50/kW_{net} (2016 U.S. dollars) when manufactured at 100,000 units/year, and \$45/kW_{net} when manufactured at a volume of 500,000 units/year.¹ For comparison, the estimated cost of automotive PEM fuel cell systems that are based on currently deployed commercial technology in 2018 is approximately \$210/kW_{net} when manufactured at a volume of 1,000 units/year, which is a closer reflection of current manufacturing rates. The expected cost for an analogous system based on state-of-the-art materials is \$181/kW_{net}.

Power system cost projections are based on beginning-of-life stack performance using MEAs made with de-alloyed PtCo on a high-surface-area carbon (PtCo/HSC) cathode catalyst developed by General Motors (GM), Pt/C anode catalyst, and a 14-micron reinforced perfluorosulfonic acid membrane. The total PGM loading is 0.125 mg_{PGM}/cm². Experiments and modeling of the PtCo/HSC cathode catalyst were consistent with an increase of power density at rated power from 1,095 to 1,183 mW/cm². The estimated system cost is shown in Figure 1.

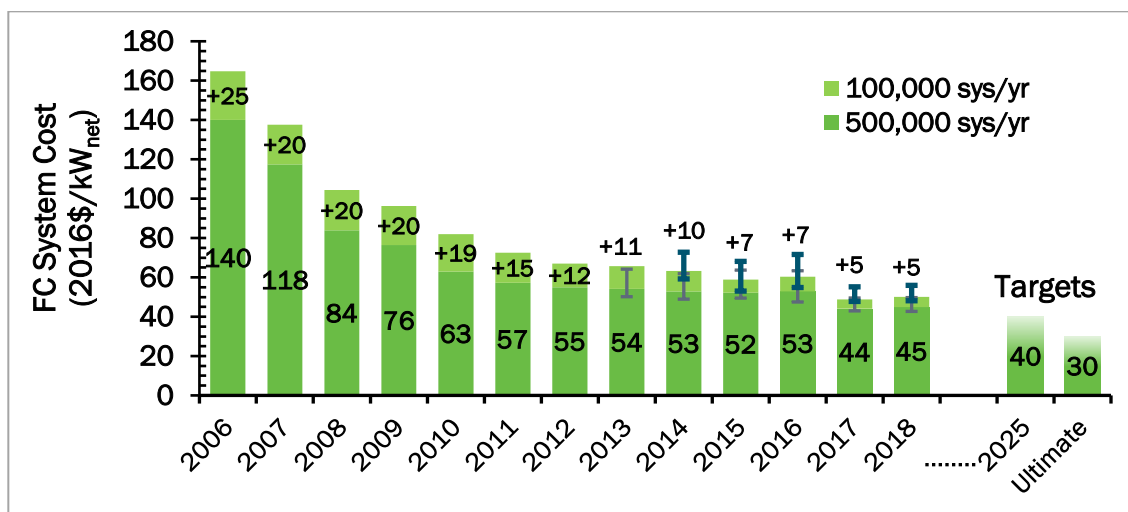


Figure 1. Modeled cost of an 80-kW_{net} PEM fuel cell system based on projection to high-volume manufacturing (2016 U.S. dollars)

The system cost analysis also includes the system description and state-of-the-art component materials and manufacturing cost for a 160-kW_{net} fuel cell system suitable for medium-duty vehicles. This system power output is equivalent to fuel cell systems for buses, and the analysis shares many common assumptions with previous analyses conducted for fuel cell buses, most recently in 2016. The system assumes a higher Pt

¹ Based on 2018 draft Fuel Cell System Cost record, to be published at https://www.hydrogen.energy.gov/program_records.html.

loading, $0.35 \text{ mg}_{\text{PGM}}/\text{cm}^2$, for increased durability. The current high-volume manufacturing system cost is estimated to be $\$80/\text{kW}_{\text{net}}$ at 100,000 systems/yr ($\$87/\text{kW}_{\text{net}}$ at 50,000 systems/yr).

To enable vehicle commercialization, fuel cell systems must also meet the subprogram's durability targets. These targets vary by application; for automotive systems, DOE has set a 2025 target of 8,000 hours, which is meant to represent the durability requirement in terms of miles driven (150,000 miles) for a larger range of drivers.

The durability of fuel cell electric buses has been evaluated since 2000 in transit agency demonstrations and has continued to increase after having surpassed the 2016 interim target of 18,000 hours in 2015. There are 12 buses that have now been on the road for more than 18,000 hours. The current bus maximum lifetime is more than 29,000 hours and was set by a bus that continues to operate, surpassing the ultimate target of 25,000 hours.² Furthermore, four other fuel cell systems have surpassed the 25,000-hour interim target. These are encouraging demonstrations of durability by several buses.

Consortia

ElectroCat (Electrocatalysis Consortium)

The subprogram established ElectroCat in FY 2016 under the umbrella of DOE's Energy Materials Network to address the materials problem of developing high-performance, low-cost, PGM-free catalysts for automotive fuel cells. ElectroCat aims to accelerate PGM-free catalyst and electrode development by coordinating relevant expertise and tools at the national labs to facilitate access to external researchers. In FY 2018, the core group of national laboratories continued to make progress in areas of catalyst and electrode development and optimization, understanding the structure-function relationship of catalytic active sites through advanced characterization, electrochemical and simulation techniques, and high-throughput modeling and synthesis of PGM-free catalysts.

- The core consortium team began working with the four awardees of the 2017 ElectroCat funding opportunity announcement (FOA): Carnegie-Mellon University, Giner, Inc., GreenWay Energy, LLC, and Pacific Northwest National Laboratory.
- **Improved catalyst synthesis and electrode optimization:** Cyanamide and polyaniline, (CM+PANI)-Fe-C, was improved to $27 \text{ mA}/\text{cm}^2$ at $0.9 \text{ V}_{\text{IR-free}}$ in H_2/O_2 on its second polarization, exceeding the 2018 milestone of $25 \text{ mA}/\text{cm}^2$ (Figure 2). This was achieved by modifying the catalyst break-in procedure and optimizing the ionomer to carbon ratio and catalyst loading in MEA testing.
- **Catalyst performance from FOA projects:** Carnegie Mellon University demonstrated $113 \text{ mA}/\text{cm}^2$ at 0.8 V and $268 \text{ mW}/\text{cm}^2$ at 0.7 V in H_2/air using a University of Buffalo-developed Fe-N-C catalyst. Giner demonstrated $16.5 \text{ mA}/\text{cm}^2$ at $0.9 \text{ V}_{\text{IR-free}}$ using a University of Buffalo-developed Mn-N-C catalyst, which is exceptional performance for a Mn-based PGM-free catalyst (Fe-free).
- **High-throughput, combinatorial methods for PGM-free catalyst R&D:** Continued work to optimize (AD)-Fe-N-C catalyst synthesis using a high-throughput robotic system, and tested samples via high-throughput oxygen reduction reaction (ORR) activity-testing using a 25-electrode combinatorial fuel cell hardware. The local atomic structure, phase composition, and near-surface composition were also characterized using X-ray diffraction, X-ray absorption spectroscopy, electron energy loss spectroscopy, and X-ray photoelectron spectroscopy.
- **Spectroscopic and electrochemical experiments with probe molecules to count active sites:** (AD)Fe-N-C catalysts exposed to nitrite solution (as a source of the nitric oxide probe molecule) showed that the

² Eudy, L. and Post, M., "Fuel Cell Buses in U.S. Transit Fleets: Current Status 2018," <https://www.nrel.gov/docs/fy19osti/72208.pdf>.

active site density is *ca.* 3×10^{12} sites cm^{-2} (*ca.* 0.5/Fe atom) and that the turnover frequency for ORR on these sites at 0.80 V is $1.7 \text{ e}^- \text{ site}^{-1} \text{ s}^{-1}$. Complementary density functional theory study has identified that probe molecules bind to Fe and to the graphene only in the presence of defects or epoxides local to the FeN_x sites, as evidenced by calculated binding energies of potential probes/poisons to various active site structures.

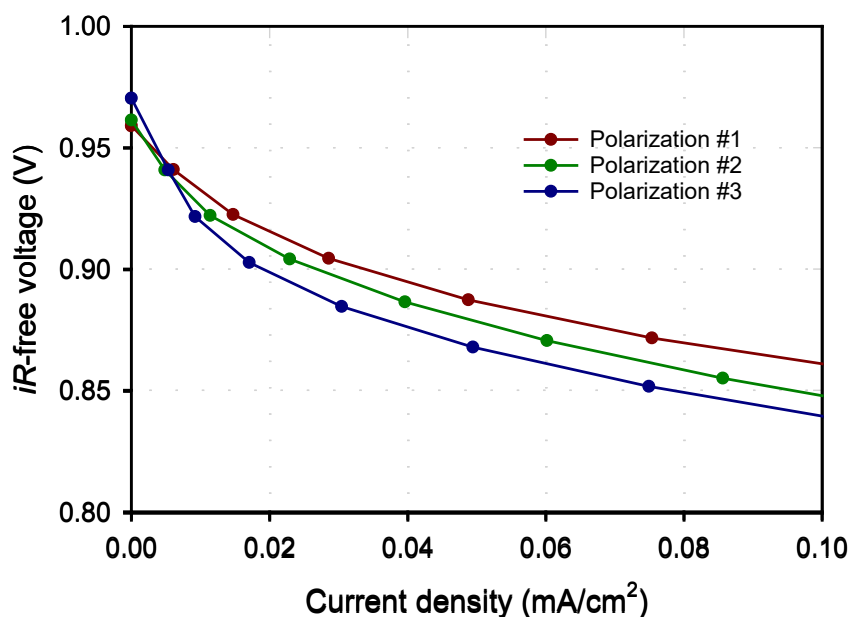


Figure 2. First three polarization curves of (AD)Fe-N-C catalyst in H_2/O_2 , 1.5 bar pressure

Late in FY 2018, a second group of FOA projects were announced, and their goals address the key challenges in PGM-free catalyst development mentioned above. Northeastern University is leading a project developing $\text{M}_x\text{-N-C}$ catalysts with a high density of multiple-metal-center sites. Indiana University-Purdue University Indianapolis is leading a project focusing on mesoporous PGM-free catalysts based on hierarchically porous carbon sphere and ionomer/catalyst interface controls within the cathode layer. Vanderbilt University is leading a project focusing on incorporation of PGM-free catalyst powders into sub-micron-diameter electrospun particle/polymer fiber catalyst layers. Pajarito Powder, LLC is leading an industry partner-led project with EWII Fuel Cells, LLC focusing on improved scalable catalyst synthesis and MEA integration. United Technologies Research Center is leading a project focusing on transition-metal oxide PGM-free catalysts based on high-throughput computational methods to identify corrosion-resistant oxides and a guided-design approach to optimization of oxygen reduction activity.

FC-PAD (Fuel Cell Performance and Durability)

The FC-PAD consortium continues to advance performance and durability of PEM fuel cells (PEMFCs) working in three main areas: (1) improving high-current-density performance at low PGM loadings, (2) developing the knowledge base for high-performance, highly durable PEMFC components, and (3) developing new diagnostics, characterization tools, and models. FC-PAD works to develop MEAs meeting the 2025 technical targets in cost, PGM loading ($\leq 0.125 \text{ mg}_{\text{PGM}}/\text{cm}^2$), performance, and durability concurrently. National laboratory members also work to support four DOE-funded FOA projects led by 3M, GM, United Technologies Research Center, and Vanderbilt University, facilitating the access of industry and academic partners to national laboratory expertise and capabilities.

- **Novel array electrodes:** FC-PAD results have indicated that state-of-the-art electrode structures are hindered by severe mass-transport limitations during high-power operation, in part due to transport resistance induced by the ionomer, particularly as the Pt loading decreases. FC-PAD is pioneering free-standing arrays of vertically oriented ionomer channels to serve as non-tortuous pathways for proton conduction with catalyst filling between the pillars, thereby improving performance with decreased ionomer needed in catalyst ink formulation.
- **Catalyst conditioning protocols:** Several commercial Pt and PtCo catalysts supported on high- and low-surface-area carbons at loadings of 0.05–0.15 mg_{Pt}/cm² were subjected to an FC-PAD-developed conditioning protocol, and the mass activity was measured to determine optimal conditioning. The number of conditioning cycles needed was unique to each catalyst. The Pt particle size distribution did not change substantially for Pt/C, whereas the average particle size in PtCo/C catalysts increased significantly. With proper conditioning it was possible to increase the mass activity by as much as a factor of 3, indicating the importance of catalyst conditioning in MEA testing.
- **On-road PEMFC technology benchmarking:** To guide future R&D needs, the consortium analyzed two PEMFC components from the Toyota Mirai (as approved by Toyota): one MEA from a Mirai stack operated for 300 hours and one MEA from a Mirai stack operated for 3,000 hours. An initial analysis of the two MEAs showed no readily evident differences between them, demonstrating excellent durability. When the individual MEA components were subjected to the DOE-US DRIVE Fuel Cell Tech Team's accelerated stress test, the materials failed tests for catalyst and support lifetime, and there was significant growth in Pt particle size and preferential Co leaching from the PtCo/C cathode catalyst. The stability of the MEA materials in a real-world drive cycle suggests that the mitigation strategies implemented in the complete Mirai fuel cell system successfully prevent MEA degradation to a great extent, albeit it at higher catalyst loadings than the DOE target.

Low-PGM Catalysts

A project led by GM has continued to make progress on the results of their accessible porous carbon-supported PtCo catalysts from 2017, which exceeded the activity target of 8 kW/g_{PGM}. The benefit of the accessible porous carbon, particularly at high current densities, is evidenced by the polarization curves in Figure 3. Remarkably, the PtCo/HSC-f catalyst matches or surpasses the performance of a catalyst used in commercial FCEVs despite having less than one-fifth the platinum loading. The PtCo/HSC-e catalyst is the same catalyst on which the state-of-the-art system cost estimate is based. Although these catalysts demonstrate exceptional performance, both need further improvement to meet performance and durability targets concurrently.

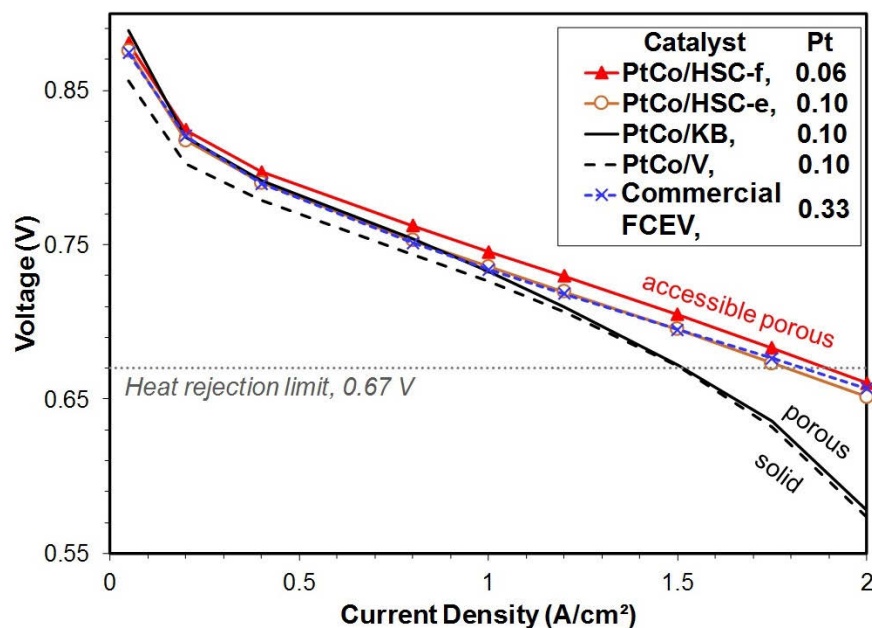


Figure 3. Fuel cell polarization curves of low-PGM-content PtCo/HSC catalysts with improved high-current-density performance compared to PtCo alloy catalysts supported on high- and low-surface-area carbons and on-the-road fuel cell technology

A project led by 3M demonstrated further progress on ultrathin-film catalysts, building on the understanding that a thin underlayer of Ir or Ta can stabilize Pt and the increased activity and stability resulting from surface additives such as Ru, Ir, Ta, and Cr. The electrocatalysts are based on a stabilized, layered catalyst structure consisting of a surface Pt layer and an underlayer of Ir between the Pt surface layer and the nanostructured thin film (NSTF) perylene red 149 whisker support. Both MEAs contain $<0.1 \text{ mg}_{\text{PGM}}$ and exceed the PGM utilization target of $8 \text{ kW/g}_{\text{PGM}}$: the 31Pt/26Ir/NSTF catalyst achieved $9.1 \text{ kW/g}_{\text{PGM}}$ and the 50Pt/11Ir/NSTF catalyst achieved $9.4 \text{ kW/g}_{\text{PGM}}$.

Innovative Fuel Cell Concepts

Intermediate-Temperature Membranes

Intermediate-temperature fuel cells have the potential to reap the benefits of favorable kinetics and decreased sensitivity to fuel impurities (e.g., CO), both of which enable reduced PGM catalyst usage as well as higher efficiency due to the production of useful waste heat and/or the elimination of balance-of-plant components. Los Alamos National Laboratory is leading a project to enable fuel cells operating over a temperature range of $80^{\circ}\text{--}220^{\circ}\text{C}$ by implementing a highly conductive, non-leachable solid phosphonated ionomer into the electrodes with a phosphoric acid-doped, ion-pair-coordinated quaternary ammonium polymer membrane. Performance testing of these MEAs in H_2/O_2 results in peak power densities of $1,130 \text{ mW/cm}^2$ and $1,480 \text{ mW/cm}^2$ at 160°C and 200°C , and significant improvement over current state-of-the-art polybenzimidazole (PBI)-based membranes across all temperature ranges (Figure 4). The improved performance of the membrane coupled with the fluorinated electrode ionomer was attributed to a combination of lower phosphoric acid poisoning, exceptional water tolerance, and higher anhydrous proton conductivity at elevated temperatures.

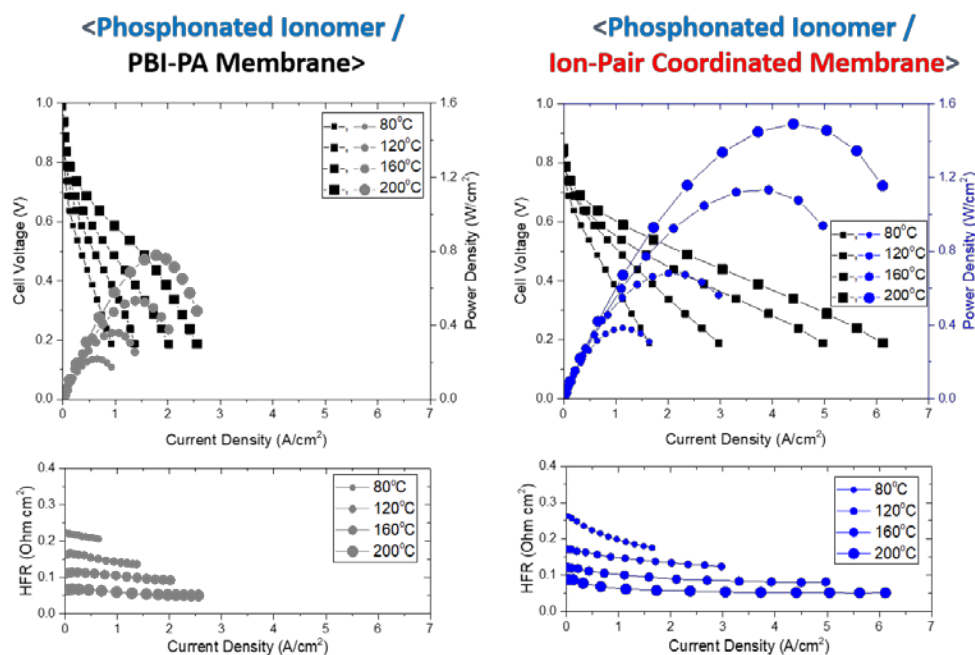


Figure 4. Polarization and power density curves (top) comparing the performance of conventional PBI-PA membranes and Los Alamos National Laboratory-developed ion-pair-coordinated membranes across operating temperatures 80°–200 °C and corresponding high-frequency resistance measurements (bottom)

Reversible Fuel Cells

Reversible fuel cells (RFCs) are able to provide easily dispatchable power and are sufficiently flexible to address grid and microgrid reliability, resiliency, and other needs. RFCs contain both fuel cell and electrolyzer functions in a single device, and they are of interest for several stationary applications, including their ability to address intermittency issues with solar and wind power with a minimal footprint.

The viability and cost-competitiveness of RFC technologies requires continued foundational R&D in materials compatibility, enhanced durability, and optimized bidirectionality to improve roundtrip efficiency and meet long-term targets of less than \$1,250/kW capital cost and a 5,000-cycle lifetime. Maintaining performance during repeated cycling between fuel cell and electrolysis modes as well as maximizing performance and efficiency in both modes are key challenges across the full range of potential RFC types.

Giner, Inc. led a project ending in FY 2018 that focused on an improved PGM-free bifunctional oxygen electrode capable of high activity for the ORR and the oxygen evolution reaction (OER) for use in reversible fuel cells. Giner and SUNY Buffalo have developed transition-metal-based oxide nanocomposites and heteroatom-doped graphene tube (carbon nanotube) catalysts with high ORR/OER activities and limited durability. These catalysts were integrated with selected anion-exchange ionomers and membranes. The MEAs were tested under both fuel cell and electrolyzer operating modes. Supporting electrolyte (KOH) decreased overpotential in electrolyzer mode and enabled demonstration of 600 h durability. The low oxidative stability of the membrane and ionomer was cited as a key barrier to cycling of the cell between electrolyzer and fuel cell modes and operation without KOH solution.

In 2018, FCTO awarded four new RFC-based projects covering all the technologies:

1. Lawrence Berkeley National Laboratory: Novel Bifunctional Electrocatalysts, Supports and Membranes for High-Performing and Durable Unitized Regenerative Fuel Cells, focusing on low-temperature reversible PEMFCs
2. Giner, Inc: High-Efficiency Reversible Alkaline Membrane Fuel Cells
3. Northwestern University: Efficient Reversible Operation and Stability of Novel Solid Oxide Fuel Cells
4. Georgia Tech: Durable, High-Performance Unitized Reversible Fuel Cells Based on Proton Conductors, focusing on ceramic-based high-temperature proton conducting electrolyte fuel cells.

BUDGET

The FY 2018 appropriation was \$32.0 million for the Fuel Cell R&D subprogram. In FY 2018 the subprogram funded early-stage R&D efforts in key areas focusing on fuel cell stack components to increase performance and durability while reducing cost, broken down into the five areas represented in Figure 5. Funding was primarily directed toward improving catalysts and electrodes to increase performance and reduce catalyst cost by developing ultra-low-PGM or PGM-free catalysts for oxygen reduction. The ElectroCat consortium, four existing FOA projects, and five new FOA projects are included in the Catalysts and Electrodes funding area. Nearly an eighth of the total funding was dedicated to the FC-PAD consortium, including the core national lab membership and its four associated industry-/university-led projects. The remaining funding was provided to award and forward-fund 16 projects from the Fuel Cell Technologies Office FY 2018 FOA covering testing, lower-cost membranes, PGM-free catalysts, and RFCs.

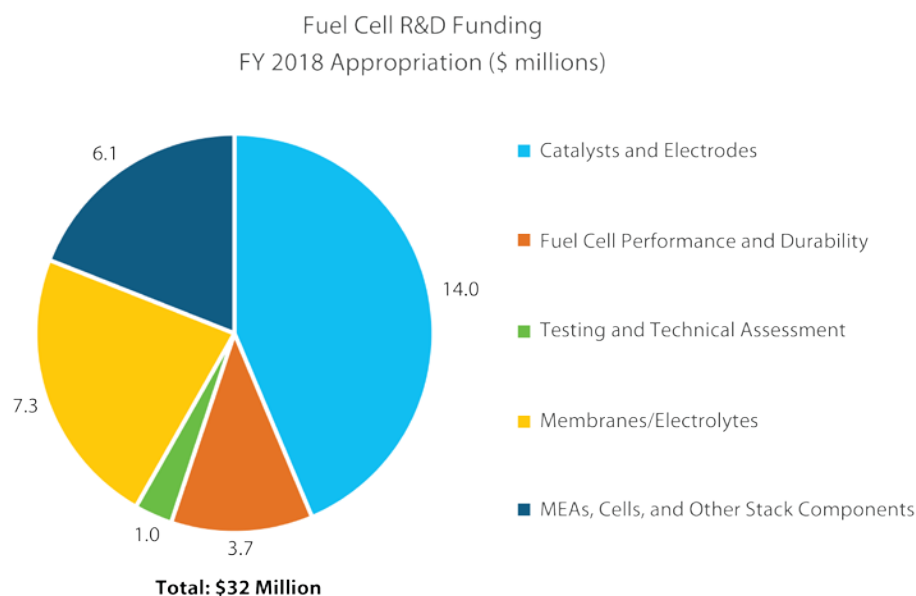


Figure 5. Fuel Cell R&D subprogram FY 2018 appropriation

FY 2019 PLANS

In FY 2019, the Fuel Cell R&D subprogram will continue early-stage applied fuel cell R&D for diverse applications that employ a variety of technologies (including PEM and alkaline membrane fuel cells). R&D will focus in the key areas of fuel cell components and materials, such as catalysts, alkaline and non-water-

dependent membranes, electrodes, and component innovations (such as components for reversible fuel cells), with an emphasis on cost reduction and durability improvement.

The subprogram's consortia will continue fostering national lab capabilities and collaborations with stakeholders and the research community. The subprogram will place particular emphasis on expediting the development of PGM-free catalysts and electrodes through ElectroCat. The Fuel Cell R&D subprogram will also continue efforts to advance fuel cell performance and durability through FC-PAD. Both consortia are now working with FOA projects, which will further increase the cooperativity and effectiveness of the respective communities. Ongoing support of modeling will guide component R&D, enabling exploration of alternate system components and configurations. Efforts to advance fuel cell performance and durability will increase emphasis on the challenging efficiency and durability requirements of medium- and heavy-duty applications, including trucks, rail, and marine.

The subprogram will further pursue early-stage R&D on components such as membranes, catalysts, and electrodes to optimize them for unitized RFCs that store energy and generate power as required in support of DOE's Beyond Batteries initiative. The subprogram will also explore the potential of stationary fuel cells to supply primary/backup power to data centers.

Dimitrios Papageorgopoulos

Fuel Cell R&D Subprogram Manager

Fuel Cell Technologies Office

Office of Energy Efficiency and Renewable Energy

U.S. Department of Energy

1000 Independence Ave., SW

Washington, DC 20585-0121

Phone: (202) 586-5463

Email: Dimitrios.Papageorgopoulos@ee.doe.gov

Tailored High-Performance Low-Platinum-Group-Metal Alloy Cathode Catalysts

Vojislav R. Stamenkovic (Primary Contact) and
Nenad M. Markovic
Argonne National Laboratory
9700 S. Cass Ave.
Lemont, IL 60439
Phone: (630) 252-8946
Email: vrstamenkovic@anl.gov

DOE Manager: Nancy Garland
Phone: (202) 586-5673
Email: Nancy.Garland@ee.doe.gov

Subcontractors:

- Oak Ridge National Laboratory, Oak Ridge, TN
- National Renewable Energy Laboratory, Golden, CO

Project Start Date: October 1, 2015
Project End Date: September 30, 2018

Overall Objectives

- Develop and deliver advanced low-PGM (platinum group metal) cathode catalysts for use in polymer electrolyte membrane fuel cells (PEMFCs) with increased mass activity at high electrode potentials and enhanced performance at high current density.
- Improve durability while reducing the total loading of PGM and cost.
- Reduce PGM loading in the catalyst through alloying of Pt with other transition metals.
- Synthesize low-PGM materials in the form of nanomaterials deployed on high surface area supports.
- Develop and evaluate durable high surface area supports for tailored nanomaterials.
- Implement scalable chemistry that would allow synthesis of tailored nanomaterials at the gram scale.
- Provide insight into the differences and similarities between rotating disk electrode (RDE) and membrane electrode assembly (MEA) performance.

- Optimize catalyst layers by studying ionomer-catalyst interaction.
- Fabricate MEAs with a total PGM loading of $<0.125 \text{ mg}_{\text{PGM}}/\text{cm}^2$ and $0.125 \text{ g}_{\text{PGM}}/\text{kW}$ with mass activity greater than $0.44 \text{ A}/\text{mg}_{\text{PGM}}$.
- Demonstrate total loss of electrochemical mass activity that is less than 40% after 30,000 voltage cycles.

Fiscal Year (FY) 2018 Objectives

- Develop active and durable catalysts for fuel cell cathodic reaction.
- Synthesize and evaluate structural and electrochemical properties of Pt-alloy nanoparticles with controlled physical parameters such as size, compositional profile, and topmost surface.
- Develop scalable process to produce larger quantities of catalysts.
- Integrate and evaluate novel carbon supports with tailored Pt-alloy nanoparticles.
- Reproducibly measure MEA performance for tailored Pt-alloy catalysts with total PGM loading of $<0.125 \text{ mg}_{\text{PGM}}/\text{cm}^2$ and mass activity $>0.44 \text{ A}/\text{mg}_{\text{PGM}}$.

Technical Barriers

This project addresses the following technical barriers from the Fuel Cells section of the Fuel Cell Technologies Office Multi-Year Research, Development, and Demonstration (MYRDD) Plan¹:

- Durability
- Cost
- Performance.

Technical Targets

The project aims to develop nanoparticles with tailored architectures and composition based on Pt-alloys with transition metals PtM (M = Ni, Co, Cr,

¹ <https://energy.gov/eere/fuelcells/downloads/fuel-cell-technologies-office-multi-year-research-development-and-22>

V, Ti), including alloys with Au, to improve performance for the fuel cell cathodic oxygen reduction reaction (ORR). The design principles focus on producing systems that have low PGM content and exhibit highly active and durable electrochemical properties evaluated in MEAs that will meet or exceed the DOE 2020 targets (Table 1).

FY 2018 Accomplishments

- Utilized unique RDE-inductively coupled plasma mass spectrometry (RDE-ICP-MS) capabilities to establish stability-structure relationships of two-dimensional and nanoparticle Pt catalysts.
- Synthesized PtCo and Pt₃Co intermetallic nanoparticles that show improved Pt and Co stability over the disordered alloy phase.
- Tested activity and durability of intermetallic PtCo nanoparticles in 50 cm² MEA.
- Synthesized Au@Pt core-shell nanoparticles with Pt₃Au composition and monodisperse size distribution
- Demonstrated effect of Au core on Pt shell in complete mitigation of Pt dissolution for 3 nm and 5 nm nanoparticles up to 1 V with RDE-ICP-MS.
- Scaled up synthesis of advanced architecture nanocage, nanoframe, and nanopinwheel catalysts to more than 0.4 grams catalyst per batch.

Table 1. Hydrogen Dispenser Targets Compared to Corresponding MYRDD Plan Targets

Characteristic	Units	DOE 2020 Electrolyte Targets	Project Status
Mass activity	A/mg _{PGM} @ 0.9 mV _{iR-free}	≥0.44	0.70
PGM total loading	mg _{PGM} /cm ² _{geo}	≤0.125	0.120
Mass activity loss	%	<40	<20

INTRODUCTION

To establish fuel cell vehicles as a major portion of the U.S. automotive market, the platinum-catalyst content in PEMFCs must be significantly reduced [1]. This requires improving the activity of the platinum catalyst such that low loadings can be used, reducing the cost of the PEMFC [2]. Additionally, the PEMFC must be able to perform up to standard for the lifetime of the vehicle, requiring an improvement in durability of the platinum catalyst [3]. These requirements necessitate development of new nanostructures to provide materials solutions to the challenges facing platinum catalyst performance. The composition, size, and architecture of Pt-alloy nanocatalysts are variables with great influence on their activity and durability. The research strategy is guided by fundamental studies on well-defined surfaces and in situ electrochemical ICP-MS for detection of instability trends [4]. New nanostructured catalysts are tested in MEAs to determine their performance standards. The goals of the project are to develop catalysts that demonstrate greater than 0.44 A/mg_{Pt} activity at 0.9 V and less than 40% loss in mass activity after standard accelerated stress tests at less than 0.125 mg_{Pt}/cm² loading in MEAs. The catalysts should also be synthesized in gram-scale batches to demonstrate promise towards scalability and commercialization.

APPROACH

This is a multi-performer project led by Argonne National Laboratory and supported by inter-lab collaborations with the National Renewable Energy Laboratory and Oak Ridge National Laboratory. Argonne leads and coordinates this applied research effort with other national laboratories; defines project scope, topics, milestones; and is responsible for deliverables as well as quarterly and annual reports to the Fuel Cell Technologies Office. The National Renewable Energy Laboratory fabricates and tests the MEAs. Oak Ridge National Laboratory characterizes synthesized materials and catalysts deployed in an MEA before and after testing protocols by electron microscopy. The approach of this project is based on the knowledge obtained from well-defined systems that will be used to tailor functional properties of corresponding nanoscale materials, with the desired shape, size, structure, and compositional profile. Integration of engineered nanomaterials in electrochemical systems requires integration of a broad range of scientific disciplines such as solid-state physics, surface science, physical chemistry, and electrochemistry. This effort also includes a combination of highly diverse experimental tools supported by state-of-the-art synthesis and characterization strategies, together with the fabrication and testing capabilities. The project is executed simultaneously in five tasks throughout the duration of the project: Task 1—Well-Defined Systems, Task 2—Synthesis of Nanoscale Materials, Task 3—Electrochemical and Structural Characterization of Catalyst, Task 4—Advanced Supports for Novel Catalysts, and Task 5—Scaling Up of Catalysts.

RESULTS

In the case of the Pt-Co system, the formation of intermetallic phases at compositions of Pt₃Co or PtCo can be utilized to induce stability in the bimetallic nanoparticle. This research has combined Task 1, Task 2, and Task 3 to develop catalysts with enhanced durability. Both PtCo and Pt₃Co compositions were studied in thin-film and nanoparticle geometry as sputtered or as synthesized, and after annealing at 700°C to induce intermetallic formation. Formation of the intermetallic phase creates an ordered structure with Pt and Co existing on specific lattice points, as opposed to randomly in a solid solution. The formation of the intermetallic phase was proven by X-ray diffraction, in which extra diffraction peaks, such as (100) and (110), are observed for intermetallic phases (Figure 1a).

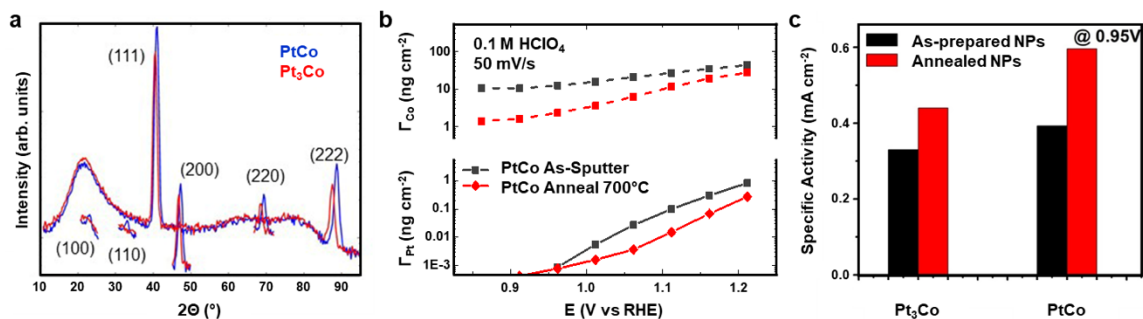


Figure 1. X-ray diffraction of intermetallic PtCo and Pt₃Co thin film catalysts (a) and their electrochemical corrosion behavior studied by RDE-ICP-MS (b). The identical compositions are synthesized as nanoparticles and demonstrate higher specific activity after forming the intermetallic structure (c).

In situ RDE-ICP-MS was used for the first time to probe the stability of Pt and Co within a given composition and phase under specific electrochemical conditions. The intermetallic phase demonstrated approximately an order-of-magnitude decrease in the dissolution rate of Co versus that of the solid solution alloy (Figure 1b). Pt was also stabilized by formation of the intermetallic, and the intermetallic nanoparticles demonstrated consistently higher specific activity than the random alloy nanoparticles (Figure 1c). By stabilizing Co against electrochemical dissolution from PtCo and Pt₃Co nanoparticles, the ORR catalyst is expected to maintain higher specific and mass activity throughout operation of a PEMFC by sustaining the beneficial effects of Co to the performance of the catalyst. The process of scaling up the synthesis of the intermetallic nanoparticles is underway and will lead to thorough evaluation in MEAs to determine this catalyst's ability to overcome the technical barriers of performance, durability, and cost.

Scale Up of Catalyst Synthesis

Task 2 within the project focused on applying advanced strategies to synthesis of electrocatalysts with enhanced properties due to their precise composition, architecture, or surface control. This type of exploratory synthesis typically occurs on the scale of producing milligrams of catalyst powder for electrochemical evaluation in Task 3. This scale is suitable for evaluation by RDE and in situ ICP-MS, and in some cases 5-cm² MEA testing. To demonstrate commercial potential, however, the synthesis of the catalyst must be scaled up and the catalyst must be tested in at least 50 cm² MEAs. Therefore, significant effort was devoted through Task 5 to scale up of the advanced catalysts developed in Task 2. The proof-of-concept was performed on 5-nm PtNi nanoparticles with multilayered Pt-skin [5]. Through a multiphase scale up strategy and fine-tuning of various synthetic variables, this rather “simple” catalyst was scaled to be produced in a five-gram batch. More recently, scale up of more “complex” catalysts such as PtNi nanoframes, nanopinwheels, and nanocages is underway [6, 7]. These architectures are more complex than spherical nanoparticles because the location of Pt and Ni within the nanomaterial must be controlled to maintain the structure. They rely on creating Ni-rich and Pt-rich regions so that the Ni-rich regions can be removed by a corrosion process to expose certain Pt-rich surfaces. This type of non-uniform Pt and Ni growth typically requires careful control of metal precursor reduction rates and reaction temperature, which are very difficult variables to tune as batch size increases. However, the synthesis of these advanced architectures is currently progressing towards the scale of hundreds of milligrams (Figure 2a–c). This will enable a broader range of MEA evaluations to be performed on these architectures, which so far rarely has been explored within the catalyst development field.

Simultaneously, a second strategy for nanoparticle scale up is being developed. A continuous process for nanoparticle synthesis will use a flow reactor (Figure 2d) to produce small quantities of nanoparticles nonstop. There are many benefits to developing nanoparticle synthesis in a flow reactor. The continuous nature allows for the product quality to be monitored online, with reaction variables such as precursor concentration and reaction temperature tuned in real time. Additionally, the difficulties of batch scale up are avoided because each “individual” reaction is maintained on a small scale similar to how the synthesis originally was

discovered. As the flow reactor is further characterized, the speed of nanoparticle scale up increases rapidly due to the continuous information feedback inherent to the process. The PtNi nanoparticles with multilayer Pt-skin already have demonstrated proof-of-concept of this nanoparticle flow reactor (Figure 2e).

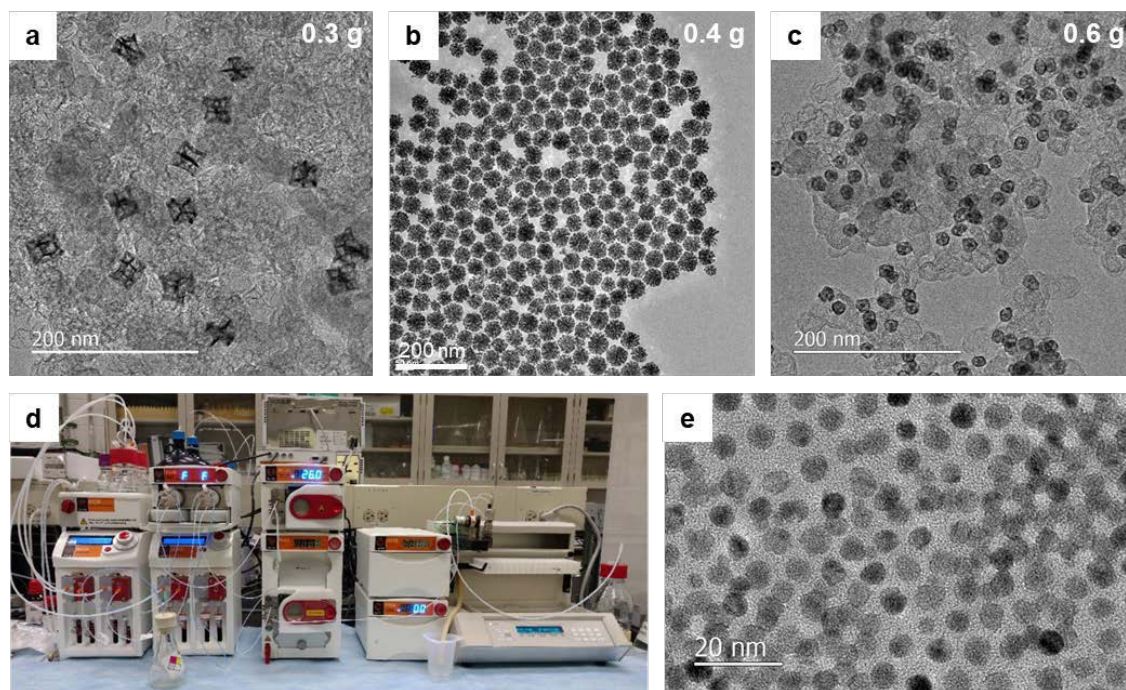


Figure 2. Scale up is now possible to the hundreds of milligram batches of (a) nanoframes, (b) nanopinwheels, and (c) nanocages. A flow reactor also is being established to study continuous flow synthesis (d), and PtNi nanoparticles have been synthesized by this process (e).

MEA Testing of Pt-Based Catalysts

To overcome the technical barriers of performance, durability, and cost, ORR catalysts must be evaluated in MEAs. Advanced architectures such as PtNi nanopinwheels are being tested in 5 cm² MEAs at Argonne National Laboratory to optimize catalyst and MEA preparation strategies (Figure 3a). Previously, PtNi nanoparticles—which was the first catalyst to be scaled up—also had been evaluated in 5 cm² MEAs. Now, the same catalyst has been evaluated in 50 cm² MEAs in collaboration with National Renewable Energy Laboratory. The tests were performed with a Nafion 211 membrane with anode and cathode catalyst deposited by ultrasonic spray coating. The ionomer-to-carbon ratio used was 0.9 with a cathode loading of 0.046 mg_{Pt} cm⁻², well below the DOE 2020 target of 0.125 mg_{Pt} cm⁻². The MEA was tested at 150 kPa, 100% relative humidity, and 80°C, with hydrogen flowing through the anode and oxygen flowing through the cathode. At 0.9 V operating potential, the PtNi nanoparticles with multilayer Pt-skin demonstrated 0.5 A/mg_{Pt}, above the DOE 2020 target of 0.44 A/mg_{Pt} (Figure 3b). This success demonstrated the tremendous power of the fundamental strategies employed in this project, starting from well-defined surfaces on which careful study yields insight that influences design of nanoparticles that can be similarly characterized by precise RDE techniques before transitioning to scale up and MEA testing.

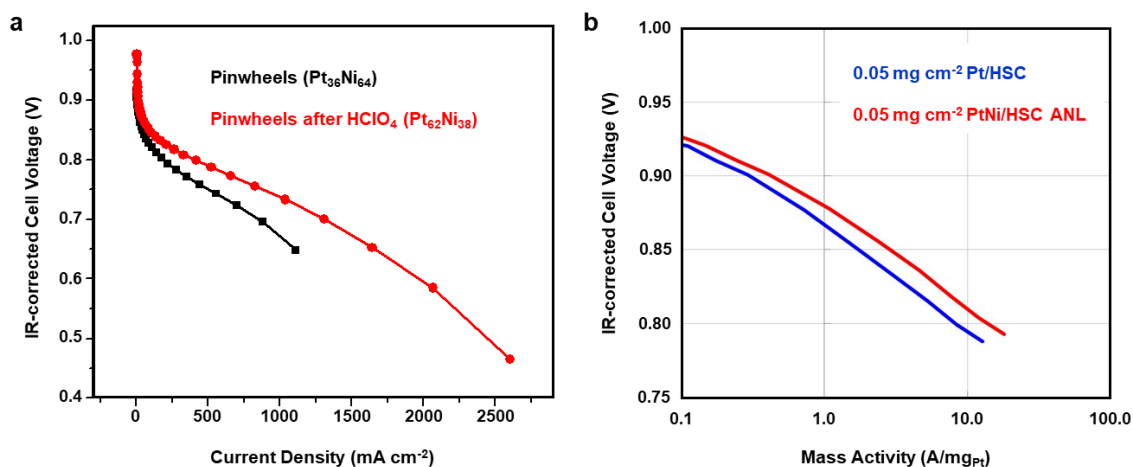


Figure 3. The performance of PtNi nanopinwheels was evaluated in a 5-cm² MEA (a) while that of PtNi multilayer skin nanoparticles was evaluated in a 50-cm² MEA (b).

CONCLUSIONS AND UPCOMING ACTIVITIES

The RDE-ICP-MS technique developed within this project continued to yield critical information about electrochemical degradation of ORR catalyst materials. Intermetallic Pt-Co phases were shown to dramatically protect against the dissolution of Co, a critical feature to maintaining the specific activity of the Pt surface. Insights from well-defined surfaces studied under high-purity electrochemical conditions guided nanomaterial synthesis of novel PtNi, PtCo, and other promising advanced architectures of ORR catalysts. These highly tuned and complex architectures—such as nanoframes and nanopinwheels—demonstrated initial promise in scale up towards gram-scale batches to enable widespread testing in MEAs. MEA evaluation was performed on PtNi nanoparticles that provided the major success of eclipsing the DOE 2020 target for mass activity at very low Pt loading, reducing cost of the catalyst layer within the PEMFC. This work is ongoing to further scale up and MEA testing of intermetallic and advanced architecture catalysts and demonstrate durability of these catalysts in 50-cm² MEAs. The effort will generate new publications and patent applications in the upcoming year, and drive the field of ORR catalyst development forward in overcoming the performance, durability, and cost technical barriers.

SPECIAL RECOGNITIONS & AWARDS/PATENTS ISSUED

1. V. Stamenkovic, N. Markovic, Y. Kang. “Multimetallic Core/Interlayer/Shell Nanoparticles,” U.S. 10,099,207 B2, United States Patent & Trademark Office (2018).

FY 2018 PUBLICATIONS/PRESENTATIONS

1. N. Becknell, P.P. Lopes, H. Lv, E. Coleman, D. Li, R. Wang, D. Strmcnik, N.M. Markovic, and V. Stamenkovic, “Tailored ORR Electrocatalysts,” 233rd Electrochemical Society Meeting, May 2018, Seattle, WA.
2. N. Becknell, P.P. Lopes, H. Lv, E. Coleman, D. Strmcnik, N. Markovic, and V. Stamenkovic. “Advanced Architectures of Nanostructured Electrocatalysts Guided by Well-Defined Surface Studies,” 256th American Chemical Society National Meeting, August 2018, Boston, MA.
3. N. Becknell, Y. Son, D. Kim, D. Li, Y. Yu, Z. Niu, T. Lei, B.T. Sneed, K.L. More, N.M. Markovic, V.R. Stamenkovic, and P. Yang. “Control of Architecture in Rhombic Dodecahedral Pt–Ni Nanoframe Electrocatalysts,” *J. Am. Chem. Soc.* 139 (2017): 11678–11681.
4. P.P. Lopes, D. Strmcnik, N.M. Markovic, and V. Stamenkovic, “Correlating Fundamental Properties of Materials to Fuel Cell Catalysts,” 233rd Electrochemical Society Meeting, May 2018, Seattle, WA.

5. P.P. Lopes, D. Tripkovic, P.F.B.D. Martins, D. Strmcnik, E.A. Ticianelli, V.R. Stamenkovic, and N.M. Markovic. “Dynamics of Electrochemical Pt Dissolution at Atomic and Molecular Levels,” *J. Electroanal. Chem.* 819 (2018): 123–129.
6. V. Stamenkovic, “Challenges in the Development of Fuel Cells Catalysts,” Fuel Cells Workshop, Bar Ilan University, November 2017, Tel Aviv, Israel.
7. V. Stamenkovic, “Design of Materials for Electrochemical Conversion and Storage,” American Chemical Society Symposia and Forum on Catalysis 31st Conference of the Chinese Chemical Society, Hangzhou, China US–Germany Energy Storage Workshop, March 2018, Washington, D.C.
8. V. Stamenkovic and N. Markovic. “Tailored High-Performance Low-Platinum-Group-Metal Alloy Cathode Catalysts,” 2018 Annual Merit Review Meeting, June 2018, Washington, D.C.

REFERENCES

1. M.K. Debe, *Nature* 486 (2012): 43.
2. V.R. Stamenkovic, B. Fowler, B.S. Mun, G.F. Wang, P.N. Ross, C.A. Lucas, and N.M. Markovic, *Science* 315 (2007): 493.
3. D. Li, C. Wang, D.S. Strmcnik, D.V. Tripkovic, X. Sun, Y. Kang, M. Chi, J.D. Snyder, D. van der Vliet, Y. Tsai, V.R. Stamenkovic, S.H. Sun, and N.M. Marković, *Energy & Environ. Sci.* 7 (2014): 4061.
4. P.P. Lopes, D. Strmcnik, D. Tripkovic, J.G. Connell, V. Stamenkovic, and N.M. Markovic, *Catal.* 6 (2016): 2536.
5. C. Wang, M.F. Chi, D.G. Li, D. Strmcnik, D. van der Vliet, G.F. Wang, V. Komanicky, K.C. Chang, A.P. Paulikas, D. Tripkovic, J. Pearson, K.L. More, N.M. Markovic, and V.R. Stamenkovic, *J. Am. Chem. Soc.* 133 (2011): 14396.
6. C. Chen, Y. Kang, Z. Huo, Z. Zhu, W. Huang, H.L. Xin, J.D. Snyder, D. Li, J.A. Herron, M. Mavrikakis, M. Chi, K.L. More, Y. Li, N.M. Marković, G.A. Somorjai, P. Yang, and V.R. Stamenkovic, *Science* 343 (2014): 1339.
7. N. Becknell, Y. Son, D. Kim, D. Li, Y. Yu, Z. Niu, T. Lei, B.T. Sneed, K.L. More, and N.M. Markovic, *J. Am. Chem. Soc.* 139 (2017): 11678.

Platinum Monolayer Electrocatalysts

Jia Wang (Primary Contact), Miomir Vukmirovic,
Kotaro Sasaki
Brookhaven National Laboratory
Upton, NY 11973-5000
Phone: (631) 344-2515
Email: jia@bnl.gov

DOE Manager: Nancy Garland
Phone: (202) 586-5673
Email: Nancy.Garland@ee.doe.gov

Subcontractor:
Los Alamos National Laboratory, Los Alamos, NM

Project Start Date: July 1, 2015
Project End Date: September 30, 2018

Overall Objectives

- Synthesize high-performance electrocatalysts for the oxygen reduction reaction (ORR) consisting of about one-monolayer (ML) Pt shell on cores made of stable, inexpensive metal, metal alloy, nitride, phosphide, or carbide nanoparticle cores.
- Increase activity and stability of Pt ML core-shell catalysts and stability of carbon supports while reducing noble metal contents.

Fiscal Year (FY) 2018 Objectives

- Design and synthesize new types of core-shell catalysts.
- Screen metal alloy, nitride, and phosphate as inexpensive core materials for high stability and promoting effect for ORR to improve Pt ML catalysts.
- Scale up syntheses of selected catalysts.
- Evaluate synthesized catalysts by membrane electrode assembly (MEA) tests.

Technical Barriers

This project addresses the following technical barriers from the Fuel Cells section of the Fuel

Cell Technologies Office Multi-Year Research, Development, and Demonstration Plan¹:

- Durability
- Cost
- Performance.

Technical Targets

This project focuses on improving durability and enhancing platinum group metal (PGM) mass activity while simplifying the synthetic processes for meeting/exceeding the DOE 2020 targets listed in Table 1.

FY 2018 Accomplishments

- Designed and synthesized dozens of non-noble-metal nanostructures in the form of alloys, nitrides, phosphides, carbides, and oxides. Four of them showed promise as suitable core material for enhancing PGM activity and durability of Pt ML catalysts.
- Demonstrated that both catalyst and support stability targets can be met using novel nanostructures.
- Delivered gram-scale synthesized catalyst samples for MEA tests.
- Exceeded 2020 DOE targets for catalyst durability (19% versus <40% loss) with PGM activity (0.37 A mg^{-1}) close to the target of 0.44 A mg^{-1} in MEA tests.
- Gained new insight in structural advantages of Pt ML skin catalysts with Ni-rich nitride cores.

¹ <https://energy.gov/eere/fuelcells/downloads/fuel-cell-technologies-office-multi-year-research-development-and-22>

Table 1. Progress Toward Meeting DOE 2020 Technical Targets for Electrocatalysts and Supports

Characteristic	Units	Target	PtNiN/C	Pt _{ML} /Pd _{NS} ^a /WNi/C	Pt-NbO _x C
Mass activity	A mg ⁻¹ PGM at 0.9 V	0.44	0.91 RDE ^b 0.37 MEA	0.22 RDE 0.07 MEA	0.56 RDE
Catalyst stability (0.6–0.95 V)	Activity loss after 30K cycles	<40%	18% RDE 19% MEA	0% RDE	4% RDE
Loss at 0.8 A/cm ² (0.6–0.95 V)	mV, cell voltage after 30,000 cycles	<30	0 MEA	4 MEA ^c	
Support stability (1–1.5 V)	Activity loss after 5,000 cycles	<40%		0% RDE	0% RDE

^a NS – nanosheet^b RDE – rotating disk electrode^c Test result after 3,000 cycles

INTRODUCTION

Further enhancing activity and durability of fuel cell catalysts while reducing the PGM content is necessary for accelerating polymer electrolyte membrane fuel cell application in the automotive industry. While Pt ML catalyst maximizes Pt utilization, the core material and structure are critically important for high performance and durability of the core-shell catalysts. Our research aims at meeting the DOE target for electrocatalysts by reducing or eliminating PGM content in core materials and enhancing core durability. Inexpensive and stable materials are synthesized into various nanostructured materials and used as cores with or without a PGM interlayer for improved activity and durability of Pt ML catalysts.

APPROACH

Our approaches to improving Pt ML catalysts in FY 2018 include (1) using metal alloy, nitride, and phosphide to stabilize Ni or Co in cores; (2) promoting formation of favorable (111) facet on Pd nanosheet that acts as the interlayer with WNi or NbN particles; and (3) embedding NbO into the surface pores of carbon support with Pt covering on top. These approaches were supported by studies for gaining insight and understanding of the effect of crystalline facets on chemical and structural properties of metal compounds. Scale-up syntheses were carried out by developing new or simplified procedures and optimized protocols.

RESULTS

Enhanced Durability by PGM-Free Cores of Metal Alloy, Phosphide, and Oxide

We used various synthesis methods to explore suitable core materials and structures for improving Pt ML catalysts—for example, ternary PdNiMo nanoparticles made by sonolysis, Pd₂Ir mixed interlayers covering Ni cores, and small particles of nitrides and carbides of Ti, V, Cr, Nb, Mo, Ta, and W. Among non-PGM metals, Ni, Co, and Fe are ORR-activity promoters, and others are studied mainly for enhancing durability. Below we discuss one example of metal alloy (WNi), one example of phosphide (Co₂P), and one example of metal oxide (NbO_x). In all three cases, distinct nanostructures play important roles in enhancing durability and activity.

WNi nanoparticles on Vulcan-XC72R (VC) carbon support were synthesized by ammonolysis, followed by thermal annealing in hydrogen gas. Pd was deposited on WNi/C in the form of a nanosheet (NS) by using CO gas as a facet-shape control agent. The strong and preferential chemisorption of CO on Pd (111) leads to the formation of Pd NS by preventing growth on the (111) basal plane. Pt ML was deposited via galvanic replacement of an underpotentially deposited Cu monolayer on the Pd nanosheets. The layered structure of Pt_{ML}/Pd_{NS}/WNi/C catalyst is schematically illustrated in Figure 1a. Measured on RDE, the mass activity of the Pt_{ML}/Pd_{NS}/WNi/C catalyst is 0.24 A mg⁻¹ PGM. After 30,000 potential cycles between 0.6 and 1.0 V, the ORR measurements showed no loss in activity. There is also no activity loss after 5,000 potential cycles between 1.0 V and 1.5 V at 500 mV/s (Figure 1b). Replacing WNi by NbN resulted in similar durability enhancement for the Pt_{ML}/Pd_{NS} catalysts. In contrast, Pt_{ML}/Pd_{NS}/C is unstable. These results indicate that WNi and NbN are highly effective in enhancing durability.

Pt-Co₂P nanorod catalyst was studied in collaboration with Prof. Zen Zhang at University of Virginia; the catalyst was made by facet-controlled syntheses to promote the formation of Pt(111) facet on Co₂P(010)-rich nanorods. Density functional theory calculations found this interface is the most favorable for ORR. Nanorods having (010) at the sides and (001) at the ends provide a large portion of the surface area with the desirable (010) facet (Figure 1c). A thin Pt layer was uniformly coated on Co₂P nanorods in the presence of Fe(CO)₅. Released CO stabilizes Co₂P against surface oxidation and facilitates the growth of close-packed Pt(111) thin layer (Figure 1d). On RDE, Pt mass activity of 0.96 A mg⁻¹ is more than twice that of PtCo/C. After 10,000 potential cycles, the mass activity decreased to 0.70 A mg⁻¹ but was still higher than 0.44 A mg⁻¹. Because the shape and morphology were retained, the durability may be further improved by higher Pt coverage on Co₂P nanorods.

Nb oxides are acid stable but electrical conductivity decreases with higher oxidation states. We verified the formation of small NbO_x (x ≤ 1) particles by X-ray diffraction (Figure 1e) for samples made with Ketjenblack

600 JD (KB) that differs from VC in having many ~ 4 nm pores on the carbon surface. These pores were used to contain the particle size and uniform coverage on carbon support. Without surface pores, it is difficult to reduce Nb(5+) precursor to low oxidation state because higher temperature is needed, causing particles to grow in size and to retain higher oxidation state. Thus, the sharp X-ray diffraction peaks at low angles corresponding to highly oxidized large Nb₂O₅ and NbO₂ particles on the sample made with VC are not seen for the sample made with KB. This indicates the formation of largely amorphous small particles on KB. The weak and broad peaks in Figure 1e correspond to NbC. Thus, the average number of O per Nb is ≤ 1 . Nearly complete reduction of Nb made these embedded particles a reducing agent for Pt spontaneous deposition on top of NbO_x. As shown by the structural model in Figure 1f, embedded NbO_x anchors down Pt particles on the carbon surface and minimizes Pt-carbon contact, which can reduce carbon corrosion and agglomeration of Pt particles. Excellent durability was achieved. A Pt-NbO_xC catalyst with Pt:Nb molar ratio 1:2 showed a PGM activity of 0.52 A mg⁻¹ after 50,000 potential cycles between 0.6 V and 1 V and no loss after 5,000 cycles between 1 V and 1.5 V.

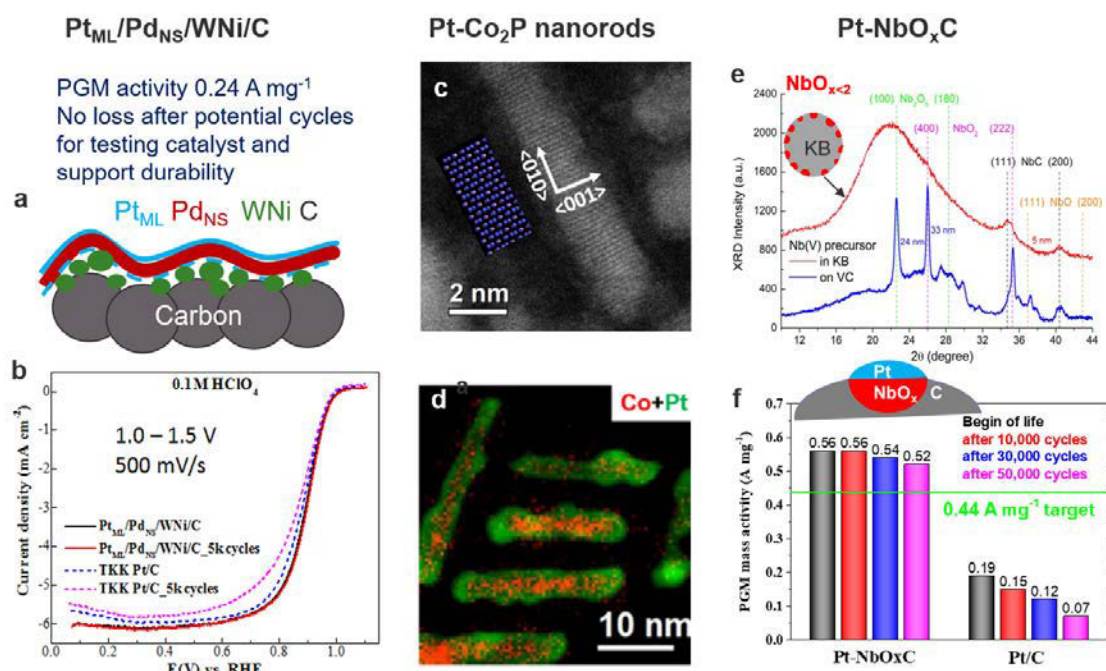


Figure 1. (a) Structural model of Pt_{ML}/Pd_{NS}/WNi/C, (b) ORR polarization curves measured on RDE for Pt_{ML}/Pd_{NS}/WNi/C compared with Pt/C before and after 5,000 cycles for testing support durability, (c) transmission electron microscopy image of Co₂P nanorods, (d) scanning transmission electron microscopy–electron energy loss spectroscopy elemental mapping of Pt-coated Co₂P nanorods, (e) XRD diffraction of NbO_xC made using KB compared to Nb₂O₅ and NbO₂ particles made using VC as supports, and (f) Pt mass activities of Pt-NbO_xC compared to Pt/C

PtNiN/C—Simplified Synthesis Procedure and Promising MEA Test Results

For scale-up synthesis of PtNiN/C catalysts, we developed a facile synthesis procedure that combines reduction and nitriding steps into one thermal treatment of Ni and Pt precursors with ammonia gas. Tested on RDE, the PtNiN/C catalyst exhibited the Pt mass activity of 0.91 A mg⁻¹, higher than that (0.86 A mg⁻¹) obtained previously. After 30,000 potential cycles between 0.6 V and 1.0 V at 50 mV/s, the losses measured were small: mass activity (-18%), electrochemical surface area (-13 %), and E_{1/2} (-13 mV). MEA test of the PtNiN/C catalyst was performed at General Motors. Figure 2a shows H₂/O₂ polarization curves at 80°C before and after 10,000 and 30,000 potential cycles. The Pt mass activity (0.37 A mg⁻¹) is higher than that of Pt/C (0.17 A mg⁻¹) but slightly lower than the target. After 30,000 potential cycles, the losses in activity (-19%) and

electrochemical surface area (-21%) were only $\sim 1/3$ those of Pt/C (-66% and -76%, respectively), and the DOE targets of <40% loss were met (Figure 2b and 2c).

Another MEA test of PtNiN/C sample was performed with H_2 /air at Los Alamos National Laboratory. Figure 2d shows no loss of cell voltage at $1 A cm^{-2}$ after 30,000 potential cycles, and the current at 0.6 V is more than twice that of Pt/C (Figure 2e). More MEA tests are planned to optimize MEA fabrication for reducing the gap between the PGM activities measured in MEA and on RDE and maximizing high-current-density performance with H_2 /air.

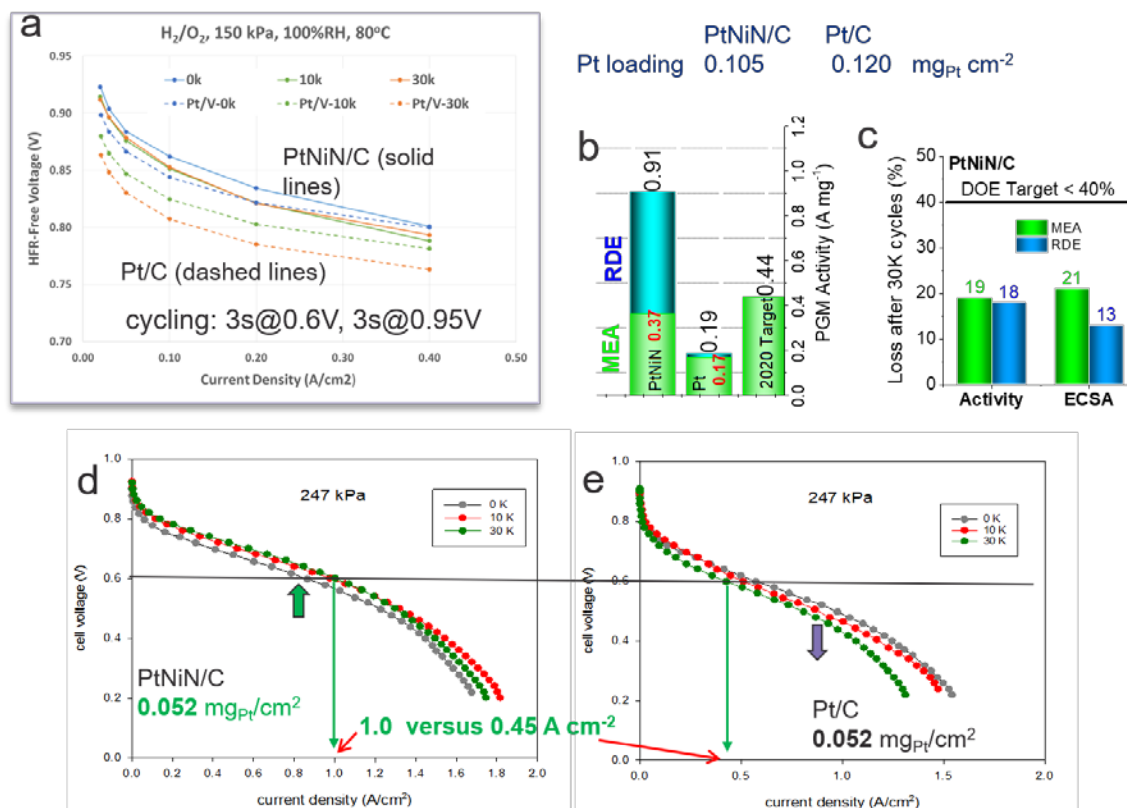


Figure 2. (a) H_2/O_2 polarization curves for cathode catalyst PtNiN/C in comparison with Pt/C before and after 10,000 and 30,000 potential cycles, (b) PGM activities for PtNiN/C catalyst measured by MEA and RDE compared to the DOE target for PGM activity, (c) durability test results for PtNiN/C after 30,000 potential cycles on RDE and in MEA, and (d, e) H_2 /air polarization curves measured before and after 10,000 and 30,000 potential cycles for PtNiN/C and Pt/C

More recent MEA tests for Pt_{ML}/Pd_{NS}/WNi/C and Pt-NbO_xC showed considerable gaps between the activities measured in MEA and on RDE. Some improvement is expected by optimizing MEA fabrication. For the Pt-NbO_xC catalyst, the high NbO_x-to-C content ratio likely resulted in significant reduction of electronic conductivity. The ultrathin catalyst layer on RDE is not as sensitive as in MEA to such an effect. New carbon material with the same ~ 4 nm pore size but lower density may help in improving MEA performance.

PtNiN/C—Structural Advantages of Pt Monolayer Skin Catalyst with Nitride Cores

As the MEA results showed the promise of PtNiN/C in meeting activity and durability targets concurrently, we further studied the intrinsic advantage of nitriding. We found that fcc-structured Ni₄N phase is particularly suitable as the core for PGM skin catalysts. For example, Figures 3a and 3b show the X-ray diffraction of Pt-Ni samples prepared in hydrogen and ammonia, respectively. The alloy particles formed in hydrogen exhibited two sets of diffraction peaks corresponding to a Pt-rich phase (sharper peaks at lower angles) and a Ni-rich

phase (smaller peaks at larger angles). In contrast, single-phase particles were formed by nitriding Pt-Ni with ammonia. The latter is preferred for making uniform catalysts. The distinct structural behavior can be attributed to the smaller lattice mismatch between Pt and Ni₄N (4.56%) than that between Pt and Ni (10.2%).

When Pt segregates to the surface, a Pt_x-(Pt_{1-x}Ni_{1/4})_{core} structure forms. For a 4 nm particle with 1:1 Pt:Ni molar ratio, $x = 0.7$ corresponds to about 1-ML-thick Pt skin as illustrated by the schematic model in Figure 3. In comparison, acid-treated PtNi skin catalysts form multilayer skin on smaller Ni-rich cores because a large portion of Ni is leached out. A thinner Pt skin yields a higher surface area per Pt mass, which is important for high-current-density-performance where kinetic barrier is less a limiting factor. Thus, it is very significant that good durability of as-synthesized PtNiN/C catalysts is demonstrated by MEA tests, which indicates that Ni-rich nitride core is quite stable and effective in enhancing the surface area of Pt and specific activity for ORR via moderate strain effect.

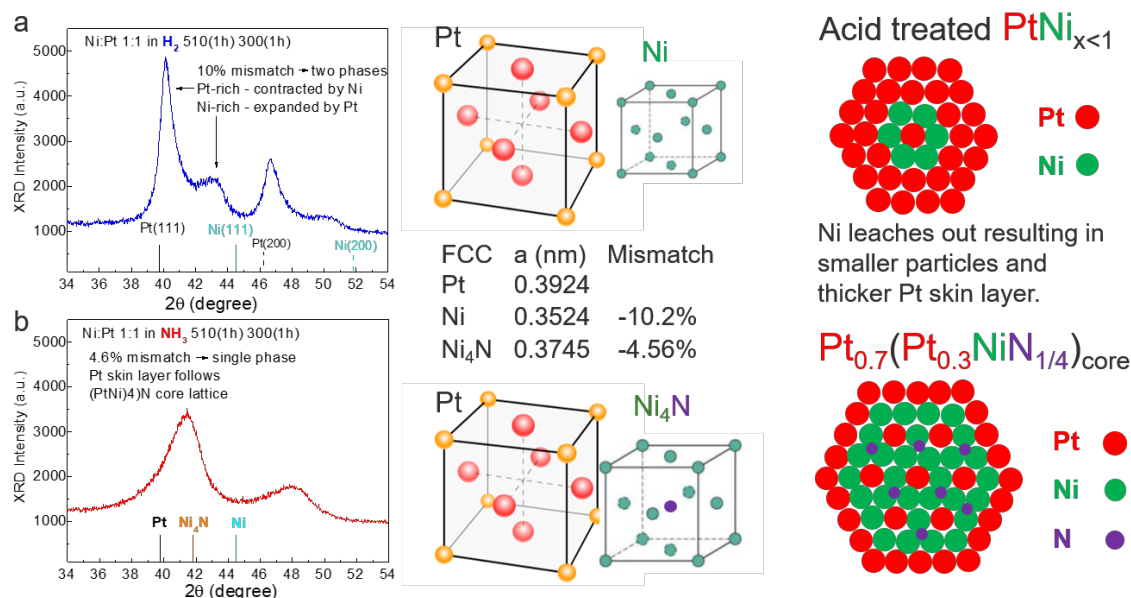


Figure 3. X-ray diffraction profiles of NiPt/C and PtNiN/C samples made by reducing metal precursors in hydrogen (a) and ammonia gas (b). Middle panel: lattice mismatch. Right panel: Structural models of Pt skin catalysts with Ni and NiN cores.

CONCLUSIONS AND UPCOMING ACTIVITIES

New results show that inexpensive metal alloy (WNi), nitride (NbN), and oxide (NbO_xC) are effective in enhancing durability and that PtNiN/C is currently more promising than Pt-Co₂P/C for meeting the targets of PGM activity and catalyst durability concurrently. We developed a facile procedure to synthesize grams-per-batch PtNiN/C catalyst. In MEA tests, PtNiN/C samples exceeded 2020 DOE targets for catalyst durability (20% versus <40% loss, no voltage loss at 0.8 A cm⁻² versus <30 mV loss) with PGM activity (0.37 A mg⁻¹) close to the target of 0.44 A mg⁻¹. In-depth structural analysis explained the advantages of nitride core for Pt ML skin catalysts.

Future work will improve PtNiN/C catalysts by optimizing synthesis parameters and looking into possible benefits of high-pressure nitriding and intermetallic ordered phases. New types of carbon supports will be studied for controlling particle size and distribution during synthesis and for beneficial effects on MEA performance. The feedback from ongoing MEA tests will be analyzed for optimization of catalysts and guiding exploration of new opportunities and approaches.

FY 2018 PUBLICATIONS/PRESENTATIONS

Publications

1. C. Liu, Z. Ma, M. Cui, Z. Zhang, X. Zhang, D. Su, C.B. Murray, J.X. Wang, and S. Zhang, “Favorable core/shell interface within Co₂P/Pt nanorods for oxygen reduction electrocatalysis,” *Nano Letters* 18 (2018): 7870–7875.
2. N.S. Marinkovic, K. Sasaki, and R. R. Adzic, “Determination of Single- and Multi- Component Nanoparticle Sizes by X-ray Absorption Spectroscopy,” *J. Electrochem. Soc.* 165 (2018): J3222–J3230.
3. G. Chen, K.A. Kuttiyiel, M. Li, D. Su, L. Du, C. Du, Y. Gao, W. Fei, G. Yin, K. Sasaki, and R.R. Adzic, “Correlating the Electrocatalytic Stability of Platinum Monolayer Catalysts to Their Structural Evolution in the Oxygen Reduction Reaction,” *J. Materials Chemistry A* 6 (2018): 20725.
4. K.A. Kuttiyiel, S. Kattel, S. Cheng, J.H. Lee, L. Wu, Y. Zhu, G.-G. Park, P. Liu, K. Sasaki, J.G. Chen, R.R. Adzic, “Au-doped Stable L10 Structured Platinum Cobalt Ordered Intermetallic Nanoparticle Catalysts for Enhanced Electrocatalysis,” *ACS Applied Energy Materials* 1 (2018): 3771–3777.
5. L. Song, Z. Liang, Z. Ma, Y. Zhang, J. Chen, R. R. Adzic, and J. X. Wang, 2018. “Temperature-dependent kinetics and reaction mechanism of ammonia oxidation on Pt, Ir, and PtIr alloy catalysts,” *J. Electrochem. Soc.* 165 (2018): J3095–J3100.
6. Z. Ma, Y. Zhang, S. Liu, W. Xu, L. Wu, Y.-C. Hsieh, P. Liu, Y. Zhu, K. Sasaki, R.R. Adzic, J.N. Renner, K.E. Ayers, and J.X. Wang, “Reaction Mechanism for Oxygen Evolution on RuO₂, IrO₂, and RuO₂@IrO₂ Core-Shell Nanocatalysts,” *J. Electroana. Chem.* 819 (2018): 296–305.
7. B. Cai, R. Hübner, K. Sasaki, D. Su, C. Ziegler, M. Vukmirovic, B. Rellinghaus, R. Adzic, A. Eychmüller, “Core-shell structuring of pure metallic aerogels towards highly efficient Pt utilization for the oxygen reduction reaction,” *Angewandte Chemie International Edition* 57 (2018): 1–5.
8. C. Okoli, K.A. Kuttiyiel, K. Sasaki, D. Su, D. Kuila, D. Mahajan, and R.R. Adzic, “Highly Dispersed Carbon Supported PdNiMo Core with Pt Monolayer Shell Electrocatalysts for Oxygen Reduction Reaction,” *ECS Transactions* 85, no. 12 (2018): 67–89.
9. Y. Zhang, F. Liu, S. Liu, D. Lu, D. Su, M. Liu, Y. Zhang, P. Liu, J.X. Wang, R.R. Adzic, and O. Gang, “Oxygen Reduction on Gold Nanocrystal Surfaces in Alkaline Electrolyte: Evidence for Surface Proton Transfer Effects,” *ECS Transactions* 85 (2018): 93–110.
10. L. Song, M.B. Vukmirovic, and R.R. Adzic, “Enhanced Oxygen Reduction Reaction Activity on Pt-Monolayer-Shell PdIr/Ni-core Catalysts,” *ECS Transactions* 85, no. 12 (2018): 57–65.
11. N.S. Marinkovic, K. Sasaki, and R.R. Adzic, “Design of efficient Pt-based electrocatalysts through characterization by X-ray absorption spectroscopy,” *Frontiers in Energy* 11 (2017): 236–244.
12. F. Lu, Y. Zhang, S. Liu, D. Lu, D. Su, M. Liu, Y. Zhang, P. Liu, J.X. Wang, R.R. Adzic, and O. Gang, “Surface-Proton-Transfer-Promoted-Four-Electron Oxygen Reduction on Gold Nanocrystal Surfaces in Alkaline Solution,” *J. Am. Chem. Soc.* 139 (2017): 7310–7317.
13. K.A. Kuttiyiel, K. Sasaki, G.-G. Park, M.B. Vukmirovic, L. Wu, Y. Zhu, J.G. Chen, and R.R. Adzic, “Janus Structured Pt–FeNC Nanoparticles as a Catalyst for the Oxygen Reduction Reaction,” *Chemical Communications* 53 (2017): 1660–1663.

Presentations

1. K. Sasaki, “Recent Advances in Platinum Core-Shell Electrocatalysts for the Oxygen Reduction Reaction,” The 8th International Fuel Cell Workshop Yamanashi University, Koku, Japan, August 23, 2018.
2. K. Sasaki, N. Marinkovic, H.S. Isaacs, and R.R. Adzic, “Synchrotron-based *In Situ* Characterization of Nanostructured Electrocatalysts for Fuel Cell Applications,” ACS National Meeting, New Orleans, March 19, 2018.

3. N. Marinkovic, K. Sasaki, and R.R. Adzic, "Insights in measuring particle size of multiatomic nanoparticles by XAS," 233rd ECS Meeting, Seattle, WA, May 14, 2018.
4. K. Sasaki, K.A. Kuttiyiel, Dong Su, Zhixiu Liang, Liang Song, and R.R. Adzic, "Nitride-Stabilized Platinum Monolayer & Core-Shell Electrocatalysts for the Oxygen Reduction Reaction," 232nd ECS Meeting, National Harbor, Maryland, October 3, 2017.
5. Y. Cai, K. Sasaki, L. Song, A. Kongkanand, and R.R. Adzic, "MEA Studies of Transition Metal Nitride Core-Pt Shell Catalysts for Fuel Cell Applications," 233rd ECS Meeting, Seattle, WA, May 14, 2018.
6. J.X. Wang, L. Song, Z. Liang, Y. Zhang, and R.R. Adzic, "Reaction Mechanism of Ammonia Oxidation Reactions," Electrochemical Society Meeting, Seattle, May 17, 2018.
7. H.L. Xin, W. Xia, Z. Liang, K. Sasaki, D. Wang, and Radoslav Adzic, "Resolving noble metal redistribution and delocalized dealloying effect at the sub-nanometer scale in low-platinum fuel cell nanocatalysts by statistically significant 4D electron microscopy and Visualizing electrochemical reactions at the nanoscale by in-situ TEM," 233rd ECS Meeting, Seattle, WA, May 14, 2018.
8. Z. Liang, J. Fu, M.B. Vukmirovic, and R.R. Adzic, "Electrochemical CO₂ Reduction on Oxide-Derived Cu Surface with Various Oxide Thicknesses," 233rd ECS Meeting, Seattle, WA, May 17, 2018.
9. Y. Zhang, F. Lu, S. Liu, D. Lu, D. Su, M. Liu, Y. Zhang, P. Liu, J.X. Wang, R.R. Adzic, and O. Gang, "Oxygen Reduction on Gold Nanocrystal Surfaces in Alkaline Electrolyte: Effects of Surface Proton Transfer," 233rd ECS Meeting, Seattle, WA, May 15, 2018.
10. J. Chen, R. Manso, L. Song, Z. Liang, and J.X. Wang, "Synthesis of Nanostructured Bimetallic Catalysts for Oxidation Reactions in Alkaline Solution," 233rd ECS Meeting, Seattle, WA, May 17, 2018.
11. H. Yu, A. Poozhikunnath, M.B. Vukmirovic, J. Roller, L.J. Bonville, R.R. Adzic, and R. Maric, "Ternary Pt-Rh-SnO₂ Catalyst Synthesized from Vapor Phase for Ethanol Oxidation," 233rd ECS Meeting, Seattle, Washington, May 14, 2018.
12. L. Song, M.B. Vukmirovic, and R.R. Adzic, "Enhanced Oxygen Reduction Reaction Activity on Pt-Monolayer-Shell PdIr/Ni-core Catalysts," 233rd ECS Meeting, Seattle, Washington, May 14, 2018.
13. Z. Liang, J. Fu, M.B. Vukmirovic, N. Marinkovic, and R.R. Adzic, "Insights into Cu₂O-Based Catalysts for Electrochemical CO₂ Reduction via in-situ ATR-IR and Raman," 255th ACS National Meeting & Exposition, New Orleans, LA, March 20, 2018.

Extended Surface Electrocatalyst Development

Bryan Pivovar and Shaun Alia (Primary Contacts), KC Neyerlin, Katie Hurst, Jason Zack, Scott Mauger, and Ahmad Mayyas
National Renewable Energy Laboratory
15013 Denver West Parkway
Golden, CO 80401
Phone: (303) 275-3748
Email: Shaun.Alia@nrel.gov

DOE Manager: David Peterson
Phone: (720) 356-1747
Email: David.Peterson@ee.doe.gov

Contract Number: DE-EE0007273

Subcontractors:

- Colorado School of Mines, Golden, CO
- University of Colorado, Boulder, CO
- ALD Nanosolutions, Broomfield, CO

Project Start Date: December 10, 2015
Project End Date: March 30, 2019

- Synthesis of >5 g of ALD-deposited Pt nanowires (PtNWs) of acceptable quality (>500 mA/mg Pt) for MEA testing.
- Quantify the non-Fickian oxygen transport resistance of at least three unique electrodes containing platinum-nickel nanowire (PtNiNW) electrocatalysts, a key metric for achieving high performance at low loading.
- In alignment with the DOE 2020 target for rated power (1,000 mW/cm²), demonstrate 600 mW/cm² at rated power (cathode 3x improvement for electrodes based on PtNiNWs).

Technical Barriers

This project addresses the following technical barriers from the Fuel Cells section of the Fuel Cell Technologies Office Multi-Year Research, Development, and Demonstration Plan¹:

- (A) Durability (of catalysts and membrane electrode assemblies)
- (B) Cost (of catalysts and membrane electrode assemblies)
- (C) Performance (of catalysts and membrane electrode assemblies)
- (D) Start-up and shut-down time and energy/transient operation.

Technical Targets

This project synthesizes novel extended thin film electrocatalyst structures (ETFECS) and incorporates these catalysts into electrodes for further study. The project has targets outlined in the Multi-Year Research, Development, and Demonstration Plan for both electrocatalysts for transportation applications and MEAs. The specific targets and status of highest relevance are presented in Table 1.

Overall Objectives

- Increasing mass activity and durability of platinum (Pt)-based electrocatalysts through the synthesis and implementation of high surface area extended surface electrocatalysts.
- Optimize fuel cell performance of extended surface electrocatalysts.
- Demonstrate DOE 2020 target performance and durability in fuel cell tests.

Fiscal Year 2018 Objectives

- Demonstrate a mass activity of >440 mA/mgPt at 0.9 V (DOE 2020 target) in fuel cell tests while also meeting at least one of the Fuel Cell Technologies Office's membrane electrode assembly (MEA) durability targets.
- Demonstrate atomic layer deposition (ALD) batch synthesis at >10 g per batch scale.

¹ <https://energy.gov/eere/fuelcells/downloads/fuel-cell-technologies-office-multi-year-research-development-and-22>

Table 1. Technical Targets for Electrocatalysts for Transportation Applications

Characteristic	Units	2020 Target	Status
Mass activity (150 kPa H ₂ /O ₂ , 80 °C, 100% relative humidity)	A/mg-Pt @ 900 mV	0.44	>0.5
Electrocatalyst support stability	% mass activity loss	<40	41
Loss in initial catalytic activity	% mass activity loss	<40	66

FY 2018 Accomplishments

- Demonstrated the ability to produce large quantities of PtNiNWs using ALD with reasonable performance.
- Repeatedly demonstrated MEA performance, in excess of DOE 2020 targets, with PtNiNWs through inter- and intra-batch testing.
- Exceeded the DOE 2020 durability target for support stability (5,000 cycles, 1–1.5 V)
- Developed Pt-Ni co-deposition technique onto cobalt (Co) nanowires for improved control of alloying and composition following acid leaching.
- Improved high-current-density performance with carbon integration and optimization in the catalyst layer.

INTRODUCTION

Conventional nanoparticle Pt/C electrocatalysts (2–5 nm) used in automotive fuel cells appear to have plateaued in terms of electrochemical area and catalytic activity. ETFECS offers the possibility of higher specific activities—comparable to that of bulk polycrystalline Pt. The ETFECS materials formed by galvanic displacement have shown promising performance and durability in rotating disk electrode tests, but have shown limitations in compositional control, reproducibility, and batch size (scale up) [1]. We are focusing on Pt and Ni ALD to address these limitations from galvanic displacement. The materials are then explored for optimum electrode structures through cell diagnostics that isolate and target mitigation strategies for loss mechanisms.

APPROACH

Our overall approach is towards developing extended surface Pt catalysts synthesized by ALD with high mass activity and durability, and incorporating these structures into robust, high-efficiency MEAs. This approach focuses on the synthesis of novel ETFECS formed by ALD, specifically with the co-deposition of Pt and Ni. We are targeting high surface areas, as this has been a specific challenge for extended surface Pt catalysts (3M [2], others [3]). Our multitiered approach involves the synthesis of novel template nanostructures, the synthesis and characterization of ALD-synthesized ETFECS, and the optimization of these materials in fuel cells.

RESULTS

In the ALD synthesis of ETFECS materials, we have taken two approaches: (1) Pt deposition onto Ni nanowires—improving batch consistency and increasing batch size while maintaining high levels of activity; and (2) Pt and Ni co-deposition onto Co nanowires to improve control of lattice integration and composition. Within Pt ALD, oxygen concentration in the packed bed reactor was found to significantly impact the performance of resulting materials. At too high of a concentration, synthesized materials oxidized and hardened into aggregates. Lower oxygen concentrations resulted in improved consistency in material composition and oxygen reduction activity. The University of Colorado Boulder synthesized catalysts at 0.5 g and 2 g batch sizes to supply the National Renewable Energy Laboratory (NREL) with material for MEA testing. For larger quantities, ALD Nanosolutions used a research fluidized bed reactor to produce 5 g batches, although further scaling could be used to produce 3 mt per day (Figure 1). Testing of the 5 g batches has shown target composition and reasonable performances when screened with rotating disk electrode tests. Microscopy of the 5 g batches further demonstrates that these materials are similar in structure to the smaller ALD batches or materials previously formed by galvanic displacement.



10-200 g
Research FBR

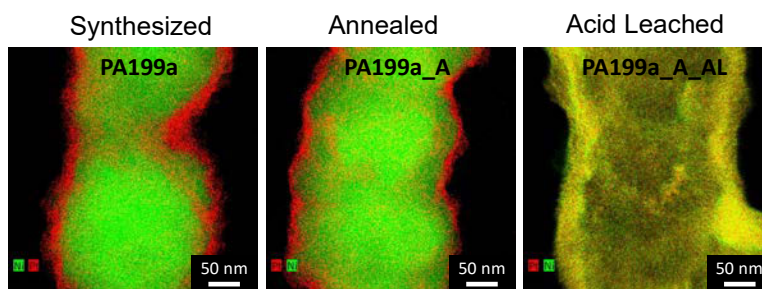
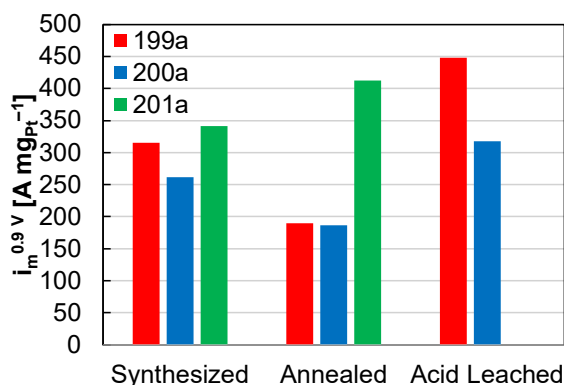


Figure 1. The 5-g batch synthesis of PtNiNWs. Mass activities in rotating disk electrode tests, as-synthesized and following hydrogen annealing and acid leaching steps. Microscopy of PtNiNWs, as-synthesized and following hydrogen annealing and acid leaching steps.

Additionally, the University of Colorado Boulder has used ALD to co-deposit Pt and Ni onto Co nanowires (Figure 2). By using co-deposition, we intend to better control Pt- and Ni-lattice integration and isolate the Pt-Ni alloy from the nanowire core to produce more active materials while maintaining high Pt composition. Through synthesis, Pt/Ni deposition cycles and temperatures were varied, where it was found that Pt and Ni deposit to different extents and at different rates. Current efforts are aimed at increasing the amount of Ni deposition so that acid leaching does not remove most of the Ni, and that the Co core is not contributing during alloying/annealing.

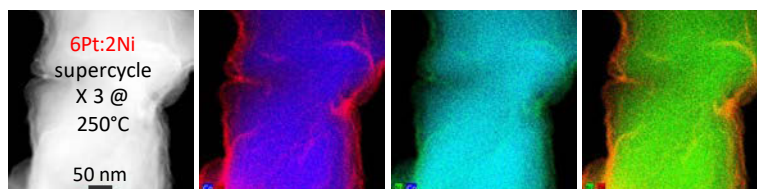


Figure 2. Schematic of Pt-Ni co-deposition onto cobalt nanowires. Microscopy and energy dispersive X-ray spectroscopy of the resulting nanowires, shown with Pt (red), Ni (green), and Co (blue).

MEA testing has been completed at NREL on a number of Pt-Ni materials. Testing of PtNiNWs formed by ALD-oxygen chemistry has shown performances in excess of the DOE 2020 target. Reducing the oxygen concentration during ALD synthesis was found to be a significant contributor, and MEA trends matched those observed from rotating disk electrode tests. Subsequent MEAs from the same batch and from different PtNiNW batches were evaluated and produced performances consistently in excess of this target (Figure 3). Additionally, the ETFECS materials surpassed the DOE target for support durability.

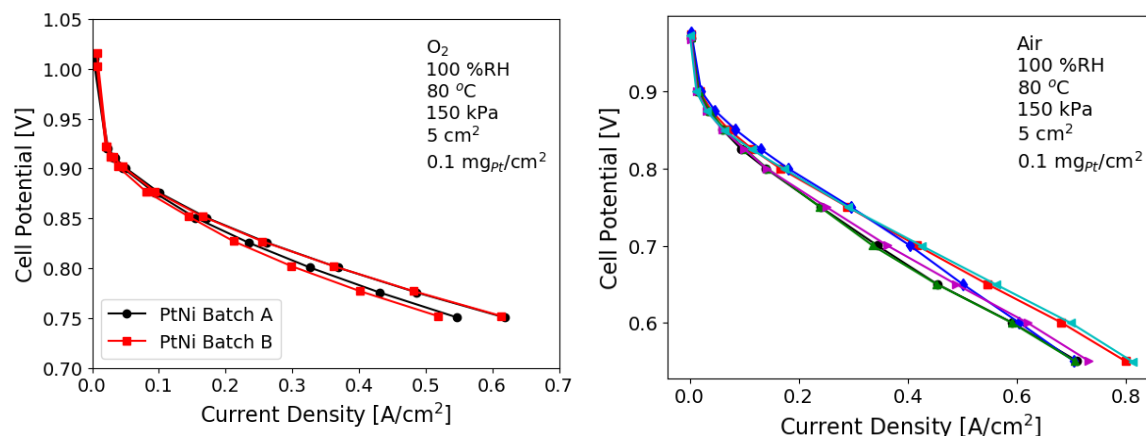


Figure 3. MEA testing of PtNiNWs to evaluate intra- and inter-batch consistency.

The MEA diagnostics and optimization were completed to evaluate and improve ETFECS performance at high current density. Studies of the non-Fickian oxygen transport resistance showed that ETFECS materials were more similar to Pt supported on Vulcan as opposed to Pt (or Pt-Co) supported on high-surface-area carbon. Analysis of local oxygen transport resistance, however, showed high resistances overall. Although the local mass transport resistance may not limit ETFECS materials, the electrode structure may be limiting, and microscopy after MEA operation showed morphological loss within the catalyst layer. Carbon was incorporated into the catalyst layer using different carbon types and at different carbon-to-catalyst ratios. The addition of Ketjenblack to the PtNiNWs was found to result in the greatest improvement at high current density (Figure 4). Although performance in the kinetic region remained relatively unchanged, a Pt-Ni to carbon ratio of 2:1 resulted in a 30% improvement at 0.6 V. Microscopy also has been used to study catalyst layer morphology and ionomer integration.

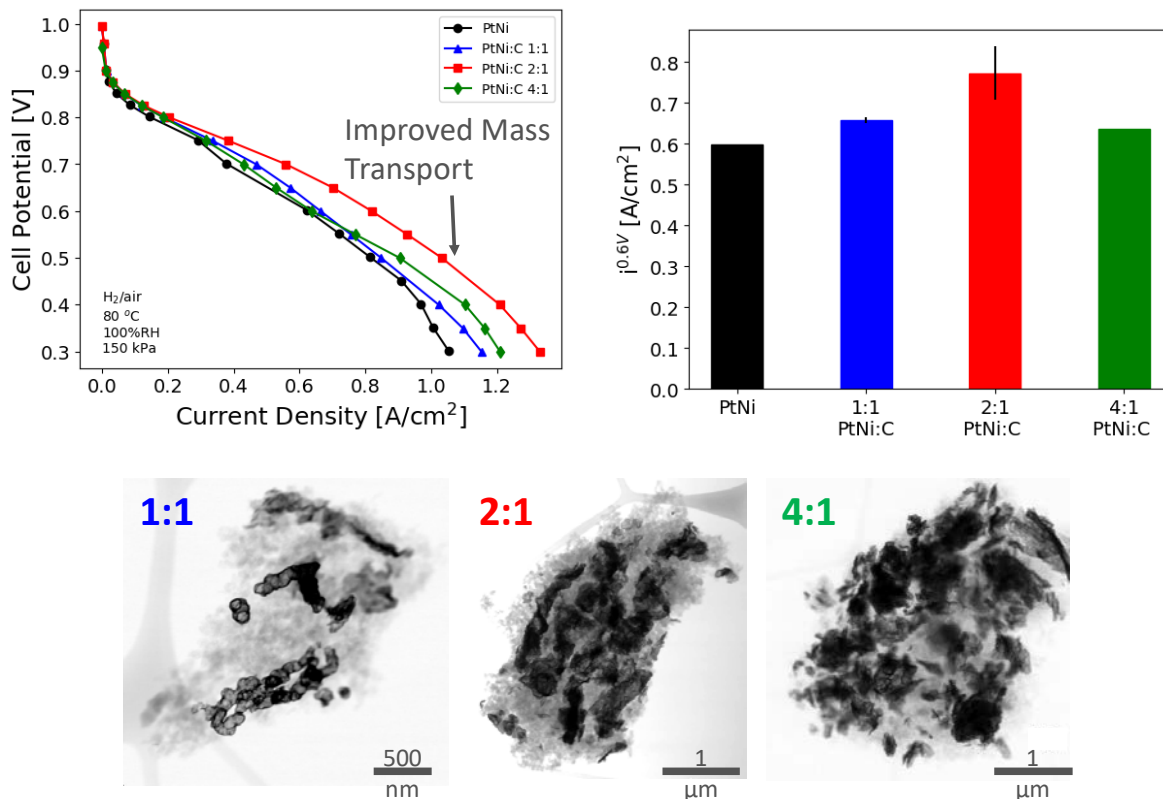


Figure 4. Polarization curves, current densities at 0.6 V, and microscopy of Pt-Ni catalyst layers with carbon (Ketjenblack) incorporated at a Pt-Ni to carbon ratio of 1:1 (blue), 2:1 (red), and 4:1 (green).

CONCLUSIONS AND UPCOMING ACTIVITIES

The project has demonstrated the ability to achieve high-performance MEAs with ALD-synthesized PtNiNWs. ALD synthesis has further demonstrated reproducibility and materials produced at a reasonable scale. Performance and durability have been significantly improved with annealing and pre-leaching. MEAs with ETFECS materials have demonstrated mass activities beyond the DOE 2020 performance target and with durability greater than the support stability target. Future work includes the following.

- Electrocatalysts
 - ALD—scale up to 10 g batch size. Further increase of electrochemical surface area and specific activity. Co-deposition of Pt and Ni/Co.
 - Post-processing optimization of resultant catalysts (annealing and acid leaching).
 - Characterization and optimization (electrochemical and structural studies).
- Fuel cell testing
 - Optimization of electrode structure/performance using ALD materials.
 - Isolation and minimization of overpotential losses in MEA electrodes (separation of mass transfer, ohmic, and kinetic losses).
 - Durability studies to quantify and minimize performance losses.

FY 2018 PUBLICATIONS/PRESENTATIONS

1. S.M. Alia, C. Ngo, S. Shulda, M.-A. Ha, A.A. Dameron, J. Nelson Weker, K.C. Neyerlin, S.S. Kocha, S. Pylypenko, B.S. Pivovar, “Exceptional Oxygen Reduction Reaction Activity and Durability of Platinum-Nickel Nanowires Through Synthesis and Post-Treatment Optimization,” *ACS Omega* 2, no. 4 (2017): 1408–1418. doi: 10.1021/acsomega.7b00054.
2. S.A. Mauger, K.C. Neyerlin, S.M. Alia, C. Ngo, S.K. Babu, K.E. Hurst, S. Pylypenko, S. Lister, B.S. Pivovar, “Fuel Cell Performance Implications of Membrane Electrode Assembly Fabrication with Platinum-Nickel Nanowire Catalysts,” *J. Electrochem. Soc.* 165, no. 3 (2018): F238–F245. doi:10.1149/2.1061803jes.
3. C. Ngo, M.J. Dzara, S. Shulda, S. Pylypenko, “Spectroscopy and Microscopy for Characterization of Fuel Cell Catalysts,” Chapter 15, *Electrocatalysts for Low Temperature Fuel Cells: Fundamentals and Recent Trends* (Wiley, 2017): 443.
4. S. Pylypenko, “Characterization of Electrocatalytic Materials: Challenges and Novel Approaches,” New Mexico Chapter AVS symposium, Albuquerque, NM, May 16, 2017.
5. S. Pylypenko, “Challenges and Novel Approaches in Multiscale Characterization of Active Materials,” Forschungszentrum Juelich, Germany, July 12, 2017.
6. S.M. Shulda, J.N. Weker, C. Ngo, S.A. Mauger, S.M. Alia, K.C. Neyerlin, B.S. Pivovar, S. Pylypenko, “Chemical and Structural Investigation of Pt-Ni Extended Surface Catalyst Electrodes,” 232nd ECS Meeting, National Harbor, MD, October 4, 2017.
7. S.M. Alia, K.C. Neyerlin, K. Hurst, J.W. Zack, S.A. Mauger, W.W. McNeary, A. Weimer, W. Medlin, S.M. Shulda, C. Ngo, S. Pylypenko, B.S. Pivovar, “Development and Implementation of Catalysts and Membrane Electrode Assemblies Based on Extended Thin Film Electrocatalysts,” 232nd ECS Meeting, National Harbor, MD, October 4, 2017.
8. S. Pylypenko, “Multi-scale characterization of nanowire-based electrocatalysts,” Rocky Mountain ACS regional meeting, Loveland, CO, October 25–28, 2017.
9. W. McNeary, K. Hurst, S.M. Alia, S.A. Mauger, K.C. Neyerlin, C. Ngo, J.W. Medlin, A.W. Weimer, S. Pylypenko, K.J. Buechler, B.S. Pivovar, “Atomic Layer Deposition for Extended Surface Electrocatalyst Development,” 2017 AIChE Annual Meeting, Minneapolis, MN, November 2, 2017.
10. W. McNeary, K. Hurst, S.M. Alia, S.A. Mauger, K.C. Neyerlin, C. Ngo, J.W. Medlin, A.W. Weimer, S. Pylypenko, K.J. Buechler, B.S. Pivovar, “Extended Thin Film Electrocatalyst Structures Via Pt Atomic Layer Deposition,” 2017 AIChE Annual Meeting, Minneapolis, MN, November 2, 2017.
11. S. Zaccarine, C. Ngo, S. Shulda, S. Pylypenko, S. Mauger, S. Alia, K.C. Neyerlin, B. Pivovar, S. Pylypenko, “Characterization of extended surface catalysts for optimization of performance in polymer electrolyte membrane fuel cells,” GRADS, CSM, April 2018.

REFERENCES

1. Shaun M. Alia, Chilan Ngo, Sarah Shulda, Mai-Anh Ha, Arrelaine A. Dameron, Johanna Nelson Weker, Kenneth C. Neyerlin, Shyam S. Kocha, Svitlana Pylypenko, and Bryan S. Pivovar, “Exceptional Oxygen Reduction Reaction Activity and Durability of Platinum–Nickel Nanowires Through Synthesis and Post-Treatment Optimization,” *ACS Omega* 2, no. 4 (2017): 1408–1418.
2. Mark K. Debe, “Advanced Cathode Catalysts and Supports for PEM Fuel Cells,” 2008 DOE Hydrogen Program Review, http://www.hydrogen.energy.gov/pdfs/review08/fc_1_debe.pdf.
3. Z. Chen, W. Li, M. Waje, Y. S. Yan, *Angew. Chem. Int. Ed.* 46 (2007): 4060–4063.

Highly Active, Durable, and Ultra-Low-Platinum-Group-Metal Nanostructured Thin Film Oxygen Reduction Reaction Catalysts and Supports

Andrew Steinbach (Primary Contact), Cemal Duru, Andrew Haug, Monika Kuznia, Krzysztof Lewinski, Jason Petrin, Grant Thoma, David Rowe, Cedric Bedoya, Jim Phipps, Michael Stephens, and Jason Bender

3M Company, Corporate Research Laboratory
3M Center, Building 201-1W-28
St. Paul, MN 55144-1000
Phone: (651) 737-0103
Email: ajsteinbach2@mmm.com

DOE Manager: David Peterson
Phone: (720) 356-1747
Email: David.Peterson@ee.doe.gov

Technical Advisor: John Kopasz
Argonne National Laboratory
Phone: (630) 252-7531
Email: kopasz@anl.gov

Contract Number: DE-EE0007270

Subcontractors:

- Johns Hopkins University, Baltimore, MD
- Purdue University, West LaFayette, IN
- Oak Ridge National Laboratory, Oak Ridge, TN
- Argonne National Laboratory, Lemont, IL

Project Start Date: January 1, 2016
Project End Date: June 30, 2019

Overall Objectives

The overall objective is development of improved thin film oxygen reduction reaction (ORR) catalysts on nanostructured thin film (NSTF) supports that achieve:

- Mass activity of 0.50 A/mg_{PGM} or more
- Platinum-group metal (PGM) total content (both electrodes) of ≤ 0.1 g/kW
- PGM total loading (both electrodes) < 0.1 mg_{PGM}/cm²

- Mass activity durability of $< 20\%$ loss
- Loss of performance < 20 mV @ 0.8 and 1.5 A/cm².

Fiscal Year (FY) 2018 Objectives

- Develop new ultra-thin film (UTF) toward achievement of activity, durability, and cost objectives.
- Employ advanced composition and structural analysis to guide electrocatalyst development, including transmission electron microscopy, energy dispersive X-ray spectroscopy (EDS), and X-ray adsorption fine structure spectroscopy (XAFS).
- Utilize density functional theory (DFT) and kinetic Monte Carlo (KMC) models to predict novel electrocatalyst concepts with improved activity and durability.

Technical Barriers

This project addresses the following technical barriers from the Fuel Cells section of the Fuel Cell Technologies Office Multi-Year Research, Development, and Demonstration Plan¹:

(A) Durability

(B) Cost

(C) Performance.

Technical Targets

Table 1 summarizes 2018 project status against the relevant 2020 DOE targets and project targets. All reported status values are measurements made in membrane electrode assembly (MEA) format.

This year, two individual project electrocatalysts were demonstrated. They exceed five of the six 2020 targets that this project addresses and have met three of six of the more stringent project targets. The electrocatalysts are based on a

¹ <https://energy.gov/eere/fuelcells/downloads/fuel-cell-technologies-office-multi-year-research-development-and-22>

stabilized, layered catalyst structure consisting of a surface Pt layer and an “underlayer” of Ir between the Pt surface layer and the NSTF perylene red 149 whisker support. The first catalyst, which comprised $50 \mu\text{g}_{\text{Pt}}/\text{cm}^2$ and $11 \mu\text{g}_{\text{Ir}}/\text{cm}^2$, demonstrated a PGM total content of $0.110 \text{ g}_{\text{PGM}}/\text{kW}$, a PGM total loading of $0.098 \text{ mg}/\text{cm}^2$, loss in catalytic (mass) activity of 20%, loss in performance at $0.8 \text{ A}/\text{cm}^2$ of 22 mV, and loss in performance at $1.5 \text{ A}/\text{cm}^2$ of less than 5 mV. The mass activity of this catalyst was $0.29 \text{ A}/\text{mg}_{\text{PGM}}$, below the DOE target of $0.44 \text{ A}/\text{mg}$. The second catalyst, which comprised $31 \mu\text{g}_{\text{Pt}}/\text{cm}^2$ and $26 \mu\text{g}_{\text{Ir}}/\text{cm}^2$, demonstrated a PGM total content of $0.106 \text{ g}_{\text{PGM}}/\text{kW}$, a PGM total loading of $0.094 \text{ mg}/\text{cm}^2$, loss in catalytic (mass) activity of 16%, loss in performance at $0.8 \text{ A}/\text{cm}^2$ of 25 mV, and loss in performance at $1.5 \text{ A}/\text{cm}^2$ of less than 5 mV. The mass activity of this catalyst was $0.27 \text{ A}/\text{mg}_{\text{PGM}}$, below the DOE target of $0.44 \text{ A}/\text{mg}_{\text{PGM}}$.

Project status values for mass activity are provided by three catalysts. Two layered catalysts—one with an Ir underlayer and the second with a Ta underlayer—yielded PGM mass activities of $0.41 \text{ A}/\text{mg}_{\text{PGM}}$ and $0.42 \text{ A}/\text{mg}_{\text{PGM}}$, respectively, approaching the DOE target. A third catalyst, consisting of a UTF PtNi alloy with a chromium surface additive, achieved $0.57 \text{ A}/\text{mg}_{\text{PGM}}$ —exceeding DOE and project targets.

FY 2018 Accomplishments

- Identified four surface additives—Ir, Ta, Ru, and Cr—that enhance the mass and specific activities of UTF PtNi catalysts within narrow composition ranges. Each of these catalysts met or exceeded the DOE activity target.
- Developed new class of UTF layered Pt/Ir catalysts that resulted in the achievement of five of six DOE targets and three of six project targets. Of note, several Pt/Ir catalysts were demonstrated to have durability that exceeded the DOE 2020 targets by 50% or more, and two Pt/Ir layered catalysts yielded specific power densities that exceeded the DOE target by about 15% to 20%, with ultra-low-PGM areal loadings below the DOE target.
- Developed a new class of UTF layered catalysts that replace Ir with lower-cost, non-precious metals, including Ta. Layered Pt/Ta catalysts with improved process parameters have resulted in up to a 4-fold gain in mass activity relative to the baseline process parameters, achieving $0.42 \text{ A}/\text{mg}_{\text{PGM}}$.
- Tracked subnanometer morphological and compositional changes in literally dozens of Pt-based UTF catalysts using high-throughput, combinatorial electron microscopy methods.
- DFT simulations were utilized to clarify the mechanism of the enhanced stability and activity of Pt/Ir in comparison with Pt. Additionally, DFT simulations provided insights for the choice of underlayer materials with improved adhesion and wetting to enable increased specific area and durability of the catalysts.
- A KMC model of Pt oxidation, reduction, and surface diffusion has been developed, providing insight into several of the surface processes occurring during an accelerated durability cycle.

Table 1. Status Compared with Technical Targets

Characteristic	2020 Target and Units	Project Target	2018 Status
PGM total content (both electrodes)	0.125 g/kW ($Q/\Delta T \leq 1.45$)	0.10	0.110 ^a 0.106 ^b
PGM total loading (both electrodes)	0.125 mg/cm ²	0.10	0.098 ^a 0.094 ^b
Loss in catalytic (mass) activity	40%	20	20 ^c 16 ^d
Loss in performance at 0.8 A/cm ²	30 mV	20	22 ^c 25 ^d
Loss in performance at 1.5 A/cm ²	30 mV	20	<5 ^{c,d}
Mass activity @ 900 mV _{IR-free}	0.44 A/mg	0.50 (in MEA)	0.41 ^e 0.42 ^f 0.57 ^g

^a 2018 UTF best of class (BOC) MEA with UTF 50Pt/11Ir/NSTF cathode.

^b 2018 UTF BOC MEA with UTF 31Pt/26Ir/NSTF cathode. BOC MEAs include low-PGM anode (UTF 9Pt/11Ir/NSTF), 14- μ m-thick supported perfluorosulfonic acid membrane, and robustness-optimized diffusion media with a cathode interlayer (16 μ g_{Pt}/cm²).

^c UTF 50Pt/11Ir.

^d UTF 31Pt/26Ir.

^e UTF 28Pt/12Ir; UTF 10Pt/Ta.

^f UTF 28PtNi+Cr.

^g PGM content values at 95 °C cell, 150 kPa hydrogen/air, 2.0 and 2.5 hydrogen and air stoichiometry, and $Q/\Delta T = 1.45$ kW/°C (0.663 V).

INTRODUCTION

State-of-the-art proton exchange membrane fuel cell (PEMFC) membrane electrode assemblies utilized in today's prototype automotive traction fuel cell systems continue to suffer from key technical and economical limitations, including high cost, insufficient durability, and low robustness to off-nominal operating conditions. Many state-of-the-art MEAs based on conventional carbon-supported Pt nanoparticle catalysts currently incorporate precious metal loadings that are significantly greater than those needed to achieve MEA cost targets; however, performance, durability, and robustness decrease significantly as loadings are reduced.

This project focuses on development of novel thin-film electrocatalysts based on 3M's NSTF catalyst technology platform. NSTF electrocatalysts and electrodes provide a unique approach toward addressing key technical challenges toward commercialization. The thin film–electrocatalyst structure imparts substantially high ORR specific activities and high resistance to electrocatalyst dissolution and sintering induced by electrochemical cycling [2]. The NSTF support is based on an oriented, submicron-scale crystalline organic pigment whisker—not carbon nanoparticles—which enables exceptional resistance to corrosion in fuel cell and water electrolysis applications [3]. NSTF electrodes are a single layer of NSTF electrocatalyst particles partially embedded into an ion-conducting membrane. They are ultrathin ($<1\ \mu\text{m}$) and do not require ionomer for proton conduction [4]. When integrated into state-of-the-art operationally robust MEAs, the NSTF electrode structure enables high absolute and specific power densities [1].

APPROACH

The project approach is to establish relationships between electrocatalyst functional response (activity, durability), physical properties (bulk and surface structure and composition), and fabrication processes (deposition, annealing, dealloying) via systematic investigation. Additionally, the project utilizes electrocatalyst modeling and advanced physical characterization to guide and accelerate development.

RESULTS

Previously, we reported results from several series of experiments with the objective of assessing the impacts of composition and structure—induced by processing—on the resultant activity and durability for a range of binary alloy electrocatalysts on NSTF supports. These catalysts comprised one of two morphologies, nanoporous thin film or ultrathin film [5]. Additionally, we reported that addition of Ir to the surface of Pt and PtNi catalysts resulted in both increased mass activity and improved electrocatalyst durability, especially stabilization of specific surface area. Such work resulted in demonstration of several catalysts, which met or substantially approached the DOE mass activity and activity durability targets. This year, electrocatalyst development has focused on furthering the activity, durability, and MEA performance of ultrathin film catalysts.

In one area of work, several additional surface additive candidates were assessed for impact on the activity and durability of UTF PtNi. For each surface additive candidate, a short rollgood of UTF PtNi catalyst with areal Pt loadings of approximately $28\text{--}30\ \mu\text{g}/\text{cm}^2$ was fabricated and sectioned. A different amount of additive was deposited onto the surface of each section. All catalysts were integrated into MEAs and tested at least in duplicate. Figure 1 (left and middle) summarizes the dependence of PGM mass activity of UTF PtNi with surface additive levels of Ir, Au, Ta, and Ru and surface additives Cr, β , δ , and π , respectively. Near 1 at% additive, Ir, Au, Ta, and Ru yielded increased mass activities relative to the 0 additive controls. In contrast, Cr surface additive did not enhance activity near 1 at%, but a large and sharp peak in mass activity—reaching $0.57\ \text{A}/\text{mg}_{\text{PGM}}$ —was obtained near 6 at%. Surface additives β , δ , and π generally decreased mass activity monotonically as additive level was increased from 0.5 up to approximately 10 at%.

Figure 1 (right) summarizes the influence of either Ir or Ta surface additive level on H_2/air performance loss after the DOE electrocatalyst accelerated stress test (AST) at $0.32\ \text{A}/\text{cm}^2$. Both surface additives were effective at increasing H_2/air performance durability, but less Ta additive was required than Ir to achieve similar durability.

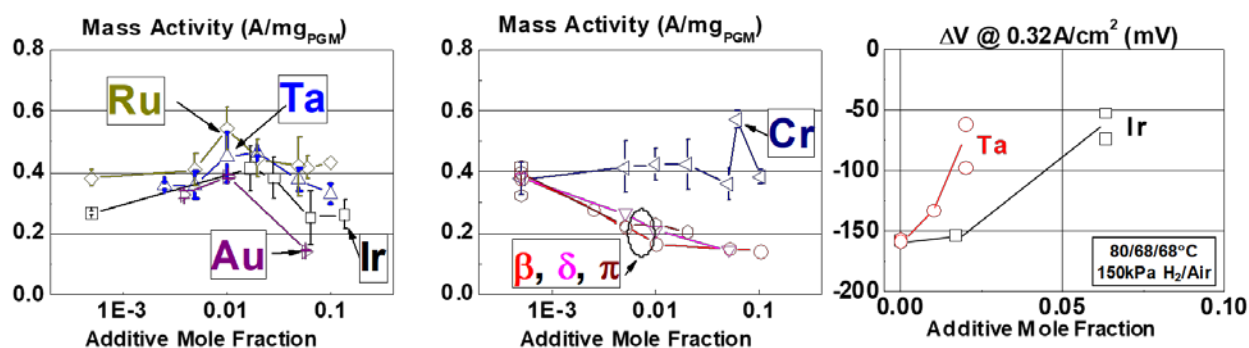


Figure 1. (Left, Middle): Influence of surface additive type and content on PGM mass activity. (Right): Dependence of Ir or Ta surface additive content on H₂/air performance change after the electrocatalyst AST.

In a second major focus area, UTF catalysts were integrated with “underlayers”—layers between the surface ORR catalyst and NSTF perylene red 149 whisker support. Key objectives of the underlayer development included improving the adhesion and wetting of the surface ORR catalyst (relative to direct adhesion to PR149) to enable increased specific area and durability at nanometer-scale catalyst thickness, and to enable increased “support” surface area to allow generation of ultrathin ORR catalyst coatings at reasonable areal electrode loadings near 50 $\mu\text{g}_{\text{PGM}}/\text{cm}^2$. Underlayer development has included assessment and optimization of precious metals, including Ir, and non-precious metal layers comprising Ta.

Figure 2 summarizes the results of several experiments assessing the impact of Ir underlayers with a range of areal loadings (equivalent to thickness on NSTF support) with fixed surface Pt catalyst layer loadings of 5 $\mu\text{g}_{\text{Pt}}/\text{cm}^2$, 10 $\mu\text{g}_{\text{Pt}}/\text{cm}^2$, 28 $\mu\text{g}_{\text{Pt}}/\text{cm}^2$, and 47 $\mu\text{g}_{\text{Pt}}/\text{cm}^2$. For reference, data for pure Pt UTF catalysts at a comparable range of Pt loadings also is shown. Integration of Ir underlayers generally resulted in significantly increased PGM mass activity and specific surface area versus pure Pt, and in some cases enhanced specific activity also was observed (top row). PGM mass activity as high as 0.41 A/mg_{PGM} was obtained at to-date optimal Pt and Ir contents of 28 $\mu\text{g}/\text{cm}^2$ and 12 $\mu\text{g}/\text{cm}^2$, respectively. The Ir underlayers also generally increased H₂/air performance, as summarized in Figure 2 (bottom). Depending upon the specific composition, Pt/Ir layered catalysts resulted in increased performance by 10s of millivolts relative to pure Pt at similar PGM areal loadings. At 20 mA/cm², 28 Pt/12 Ir (40 $\mu\text{g}_{\text{PGM}}/\text{cm}^2$) yielded a 30 mV gain over Pt with 98 $\mu\text{g}_{\text{PGM}}/\text{cm}^2$.

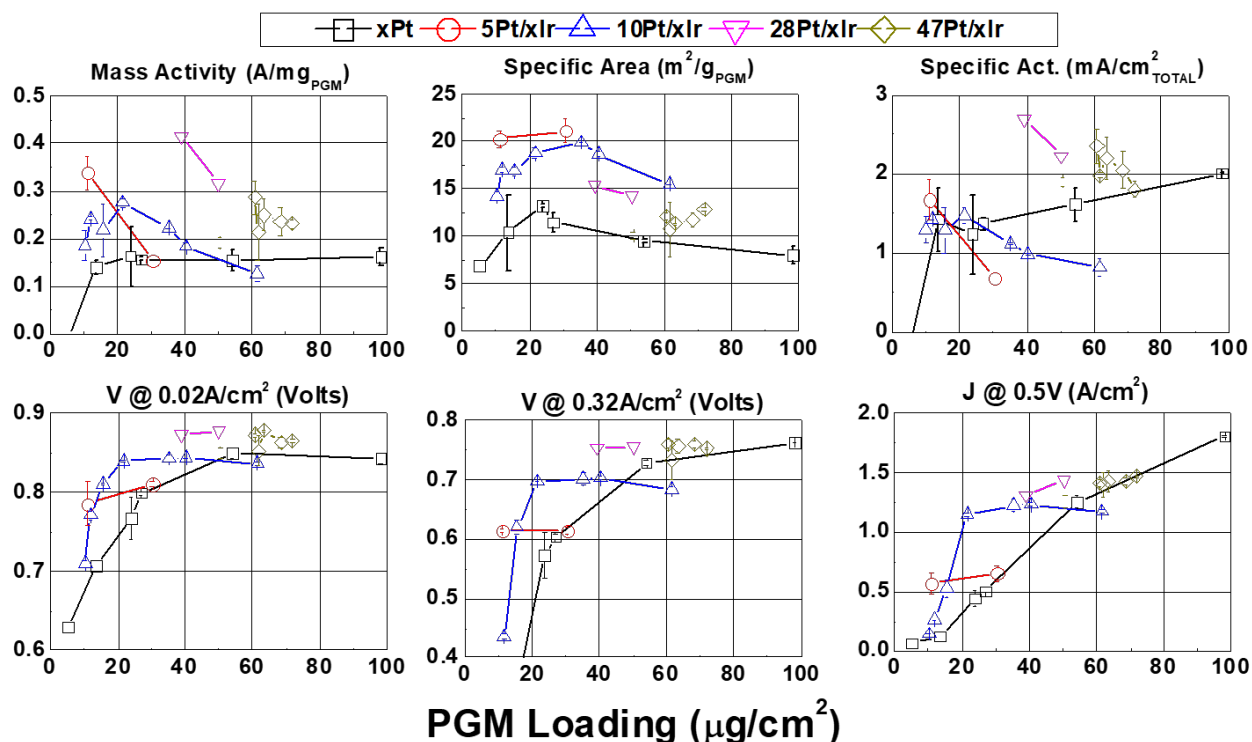


Figure 2. Layered Pt/Ir/NSTF summary. (Top): Mass activity, specific area, and specific activity. (Bottom): H_2/air performances at 0.02 A/cm^2 , 0.32 A/cm^2 , and 0.5 V.

In another series, Pt/Ir/NSTF layered catalysts were prepared with fixed Ir underlayer content and varying surface Pt layer loadings. The top row of Figure 3 summarizes the Pt mass activity and specific activity of xPt/26Ir/NSTF catalysts, revealing extremely high Pt utilization at low Pt contents. This is evidenced by Pt mass activity exceeding 1 $\text{A}/\text{mg}_{\text{Pt}}$ with Pt areal loadings of between 1.1 $\mu\text{g}/\text{cm}^2$ and 4.2 $\mu\text{g}/\text{cm}^2$. A subset of Pt/Ir/NSTF layered catalysts were evaluated by X-ray absorption spectroscopy (Figure 3, bottom). Pt-Pt bond lengths of 9Pt/26Ir/NSTF and 19Pt/26Ir/NSTF were relatively stable throughout fabrication and fuel cell testing and were slightly compressed relative to bulk Pt (2.77Å, not shown). Ir-Ir bond lengths did not depend on surface Pt loading and were similar to bulk Ir.

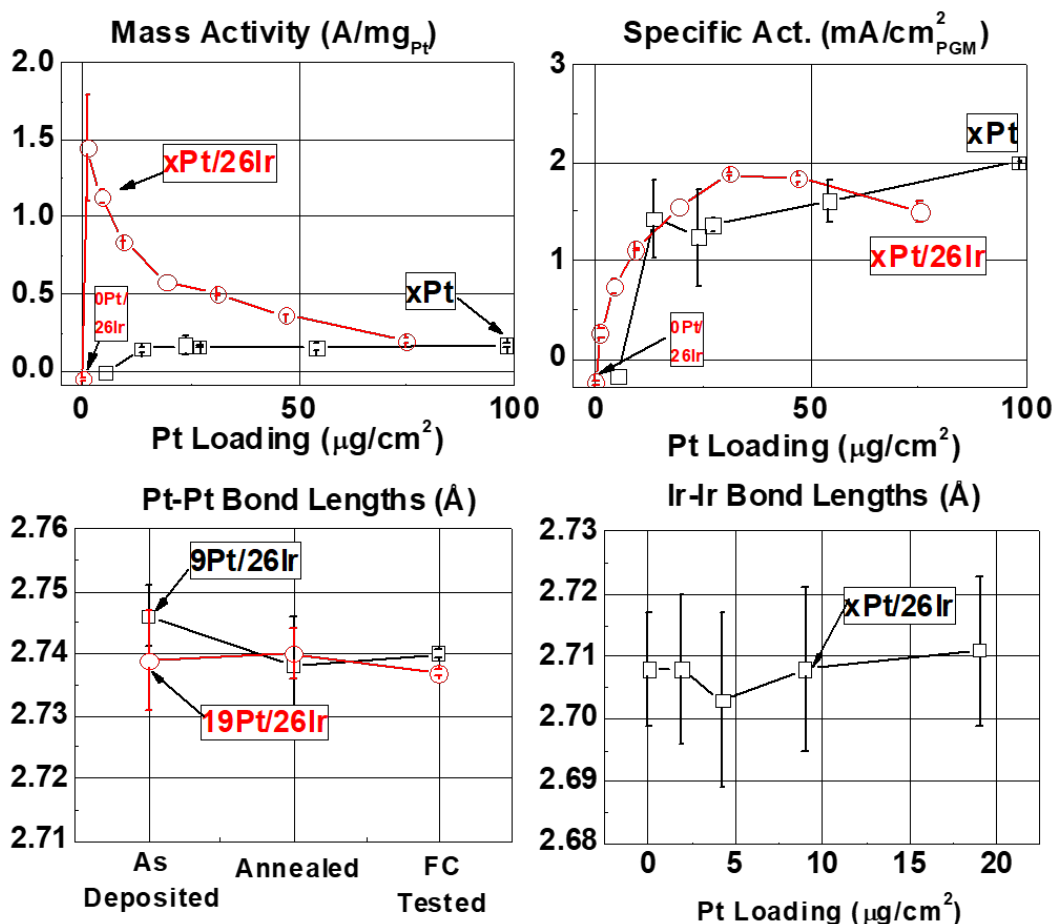


Figure 3. Characterization of Pt and Pt/Ir catalysts with varying surface Pt content. (Top): Mass and specific activities. (Bottom): XAFS-determined bond lengths.

Pt/Ir layered catalysts were assessed for electrocatalyst AST durability. Figure 4 compares H₂/air performance before and after the electrocatalyst AST for three different Pt/Ir/NSTF catalysts with a range of PGM loadings between 35 µg_{PGM}/cm² and 61 µg_{PGM}/cm² (top row) to the performances of Pt alloy nanoparticles on carbon support with 90 µg_{PGM}/cm² electrode loading (bottom left), Pt/NSTF with 54 µg_{PGM}/cm² (bottom center), and PtCoMn/NSTF with 150 µg_{PGM}/cm² (bottom right). The insets in each panel also list the average mass activity and specific area losses. In general, the Pt/Ir/NSTF layered catalysts were significantly more durable than the Pt-alloy nanoparticle catalysts and Pt/NSTF, as evidenced by relatively small downward shifts in the polarization curves (reflective of mass activity losses ranging from 4% to 21% versus the 40% DOE target) and essentially no change in the current density at low cell voltages (reflective of the low specific-area losses, ranging from 3% to 6%). In comparison, the Pt alloy nanoparticle catalyst's mass activity and specific area losses were 66% and 74%, respectively, and the Pt/NSTF losses were 52% and 27%. The performance durability of the Pt/Ir catalyst was qualitatively similar to the relatively high loaded PtCoMn/NSTF catalyst.

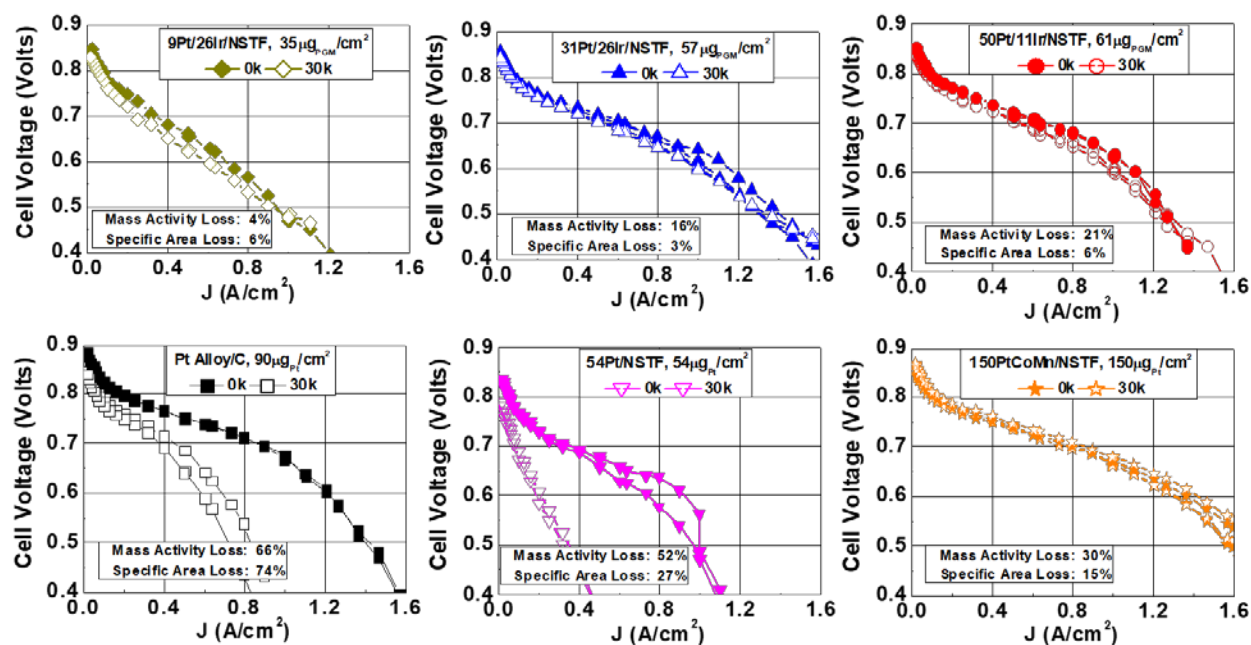


Figure 4. H_2 /air polarization curves taken before and after the electrocatalyst AST with Pt/Ir/NSTF catalysts (top), Pt-alloy nanoparticle catalyst on carbon (bottom left), Pt/NSTF catalyst without an Ir underlayer (bottom center), and high loaded PtCoMn/NSTF (bottom right).

In addition to providing stable electrochemical performance, limited studies indicate that the Pt/Ir/NSTF catalysts are compositionally and structurally stable. Figure 5 summarizes complementary high-angle annular dark-field scanning transmission electron microscopy and electron dispersive X-ray spectrum (EDS) images of 10Pt/12Ir/NSTF catalysts before and after the electrocatalyst AST. Prior to the AST, the catalyst consists of a conformal and continuous ~ 2 nm-thick coating of Pt on a ~ 2 nm layer of Ir. After testing the catalyst layers remained conformal and continuous on the PR149 whisker support, although some Ir did migrate into and through the surface Pt layer. The EDS-determined Pt and Ir mole fractions remained unchanged within measurement uncertainty.

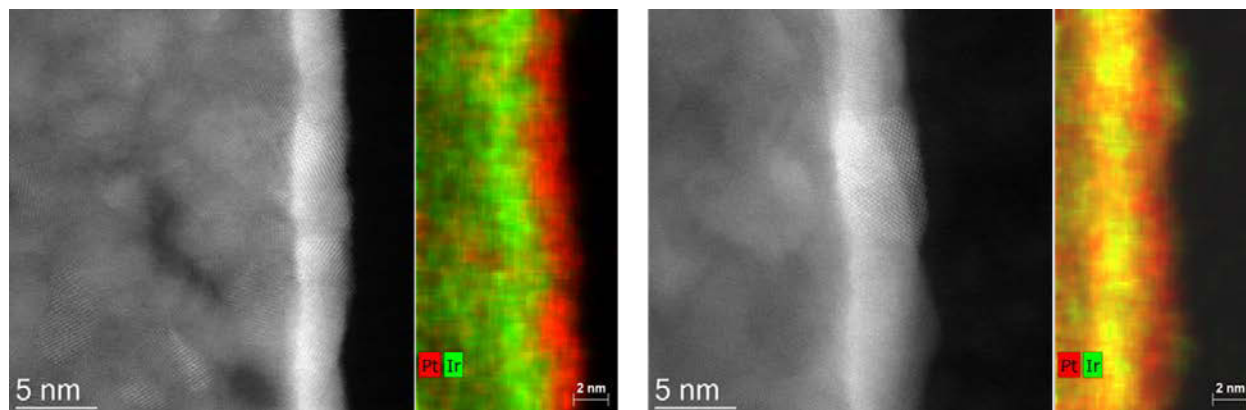


Figure 5. High-angle annular dark-field STEM-EDS of 10Pt/12Ir before electrocatalyst AST (left) and after electrocatalyst AST (right)

Pt/Ir/NSTF catalysts also were assessed for support durability using the DOE Support AST protocol, consisting of 5,000 cycles between 1 V and 1.5 V versus reversible hydrogen electrode, and at 80°C cell temperature. Figure 6 (left) summarizes H_2 /air polarization curves taken with 31Pt/26Ir/NSTF before the AST, after 5,000 cycles (target), and after 10,000 cycles. After 5,000 cycles, performance was found to increase by

approximately 100 mV at 1.2 A/cm², and an additional 5,000 cycles resulted in a modest further performance increase at higher current densities. Figure 6 (right) shows that the cyclic voltammogram of the cycled cathode essentially is identical to the uncycled cathode, consistent with the estimated <5% loss of specific area. Similar results were obtained with 50Pt/11Ir/NSTF catalyst.

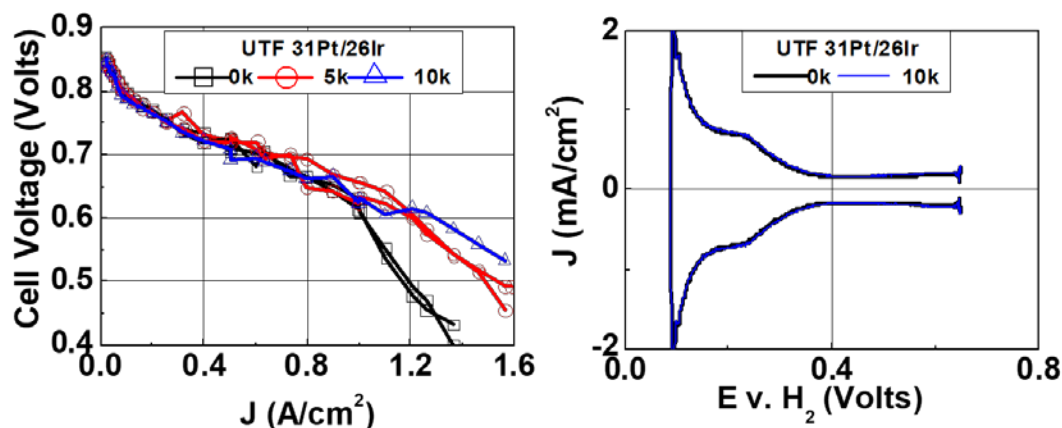


Figure 6. Support AST durability assessment of UTF 31Pt/26Ir; H₂/air polarization curves before and after 5,000 or 10,000 cycles (left); cyclic voltammograms before and after 10,000 cycles (right)

DFT was used to calculate the stability and activity trends of the Pt/Ir catalysts. Figure 7 (left) summarizes the calculated differential formation energy for a range of sub-monolayer Pt coverages on Ir(332) surfaces. Pt sub-monolayers are predicted to be thermodynamically stable on Ir(332) surfaces, as indicated by the negative differential formation energies. Additionally, KMC simulations suggest that Ir could help stabilize Pt via a mechanism in which the less-mobile Ir “pins” Pt in place, slowing structural degradation. Ir therefore is believed to stabilize Pt through a combination of thermodynamic and kinetic effects. In terms of activity, Figure 7 (right) summarizes the predicted oxygen reduction overpotentials and hydroxide binding energies for Pt(111) and a range of Pt overlayers on Ir(111). At Pt layer thicknesses between 3 and 8 monolayers, pseudomorphic Pt on Ir(111) is predicted to have enhanced activity on the order of 20x relative to Pt(111).

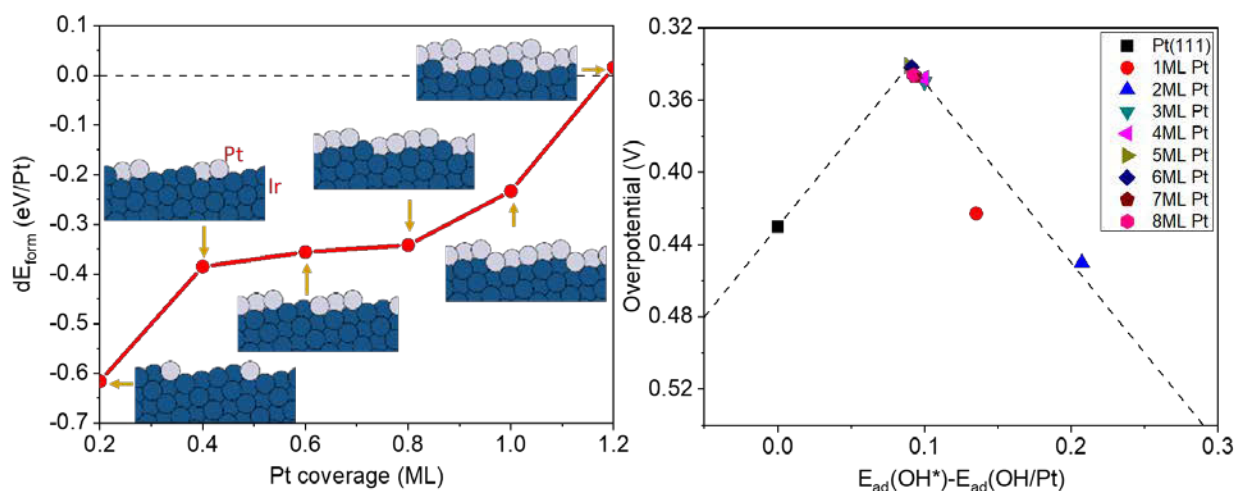


Figure 7. DFT simulations of Pt/Ir. (Left): Differential formation energy for different sub-monolayer coverages of Pt on Ir(332). (Right): Predicted activity of stabilized Pt on Ir(111) as a function of number of Pt monolayers.

Two durable Pt/Ir/NSTF layered catalysts (50Pt/11Ir/NSTF and 31Pt/26Ir/NSTF) were assessed for PGM content and operational robustness in MEAs with “best of class” (BOC) components. Pt/Ir/NSTF layered cathode catalysts were integrated with a high-performance supported 3M 725EW PFSA membrane, a 20

$\mu\text{g}_{\text{PGM}}/\text{cm}^2$ Pt/Ir/NSTF anode catalyst, and a water-permeable anode gas diffusion layer and a cathode gas diffusion layer with a low loaded ($16 \mu\text{g}_{\text{PGM}}/\text{cm}^2$) Pt/C interlayer that improved operational robustness of NSTF MEAs [1]. Total MEA PGM loadings were $0.098 \text{ mg}/\text{cm}^2$ and $0.094 \text{ mg}/\text{cm}^2$ with the 50Pt/11Ir/NSTF and 31Pt/26Ir/NSTF cathode catalysts, respectively. Figure 8 (left) summarizes the resultant H_2/air performance for replicate MEAs of each type at 95°C cell temperature, 40% relative humidity, and 150 kPa (absolute) pressure. Figure 8 (middle) summarizes performance with 250 kPa (absolute) pressure. At 150 kPa, both Pt/Ir/NSTF layered catalysts achieved similar PGM contents between $0.106 \text{ g}_{\text{PGM}}/\text{kW}$ and $0.110 \text{ g}_{\text{PGM}}/\text{kW}$ at an MEA heat rejection of $Q/\Delta T = 1.45 \text{ kW}/^\circ\text{C}$, exceeding the DOE target of $\leq 0.125 \text{ g}/\text{kW}$. At 250 kPa, both Pt/Ir/NSTF catalysts enabled MEA PGM contents of $0.086 \text{ g}_{\text{PGM}}/\text{kW}$ to $0.087 \text{ g}_{\text{PGM}}/\text{kW}$.

Figure 8 (right) compares steady-state operational robustness of the 2018 NSTF MEAs with total cathode PGM loadings of $73 \mu\text{g}_{\text{PGM}}/\text{cm}^2$ to $77 \mu\text{g}_{\text{PGM}}/\text{cm}^2$ to a reference dispersed Pt-alloy nanoparticle on carbon dispersed electrode with $250 \mu\text{g}_{\text{PGM}}/\text{cm}^2$ cathode loading and to a baseline NSTF MEA ($150 \mu\text{g}_{\text{PGM}}/\text{cm}^2$ cathode) that did not contain the robustness-enhancing anode gas diffusion layer and cathode interlayer. The 2018 BOC MEAs with the Pt/Ir/NSTF cathodes yielded dramatically improved robustness compared to the baseline NSTF MEAs. Under steady-state operation, the 2018 BOC MEAs yield current densities of ca. $0.85 \text{ A}/\text{cm}^2$ at 33°C , increasing to ca. $1.5 \text{ A}/\text{cm}^2$ at about 50°C , vs. the 0.20 to $0.55 \text{ A}/\text{cm}^2$ achieved by the baseline NSTF MEA over a similar temperature range. The 2018 BOC MEAs yielded modestly lower performance than the reference Pt-alloy nanoparticle electrode at cell temperature of less than about 45°C .

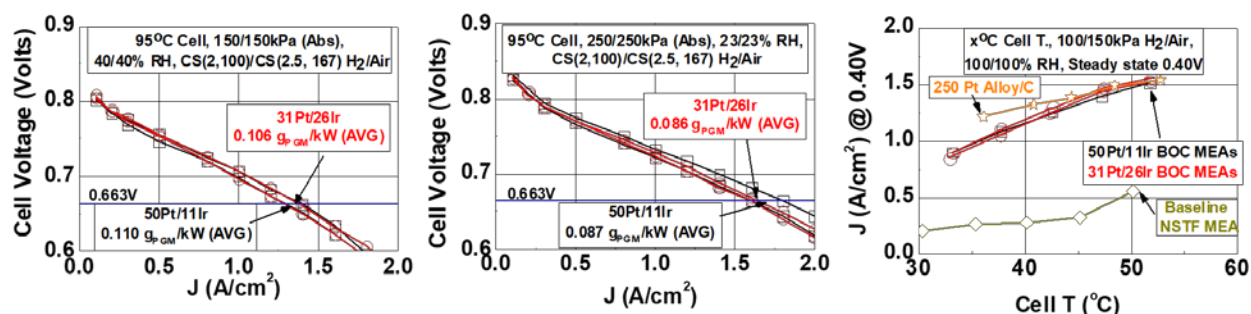


Figure 8. Performance and robustness of 2018 BOC MEAs with either 50Pt/11Ir/NSTF or 31Pt/26Ir/NSTF cathodes. (Left): H_2/air performance at 95°C , 150 kPa. (Center): H_2/air performance at 95°C , 250 kPa. (Right): Operational robustness comparisons to baseline NSTF MEA and reference Pt-alloy/C MEA.

In addition to development of catalysts with Ir underlayers, significant research has been conducted toward development of underlayers that have reduced or no precious-metal content. DFT simulations were conducted to assess the adhesion of a variety of underlayers to the PR149 whisker support. Figure 9 summarizes the predicted adhesion of Pt and Ta to a perylene red 149 molecule. Pt is predicted to adhere relatively weakly to PR149, consistent with experimental observations of dewetting. In contrast, Ta is predicted to adhere strongly to PR149, although the impact of Ta oxidation on the adhesion energy remains to be determined. Figure 10 summarizes one set of experiments, where the impact of surface Pt loading was assessed with a fixed Ta underlayer. Pt/NSTF and Pt/Ir/NSTF data is included for reference. As Pt loading on the Ta or Ir underlayers decreased from approximately $80 \mu\text{g}/\text{cm}^2$, the PGM mass activity increased, reaching a maximum activity at an intermediate Pt loading of $30 \mu\text{g}/\text{cm}^2$ to $40 \mu\text{g}/\text{cm}^2$, then decreased toward 0 as the Pt loading decreased below $20 \mu\text{g}/\text{cm}^2$. Although the PGM mass activity trends were similar with either underlayer, different trends in specific area and specific activity were observed. With the Ir underlayer, the PGM mass activity decrease below $30 \mu\text{g}/\text{cm}^2$ predominantly was because of the loss of specific activity, likely due to a significant contribution of ORR-inactive Ir to the measured surface area and resultant reduction in relative Pt surface area. Additionally, the total measured PGM-specific area increased as the Pt content on Ir was reduced toward zero, likely reflecting the specific area of Ir/NSTF. In contrast, with Ta, the specific area decreased toward 0 as the Pt loading decreased, similar to that observed with Pt directly on the NSTF support.

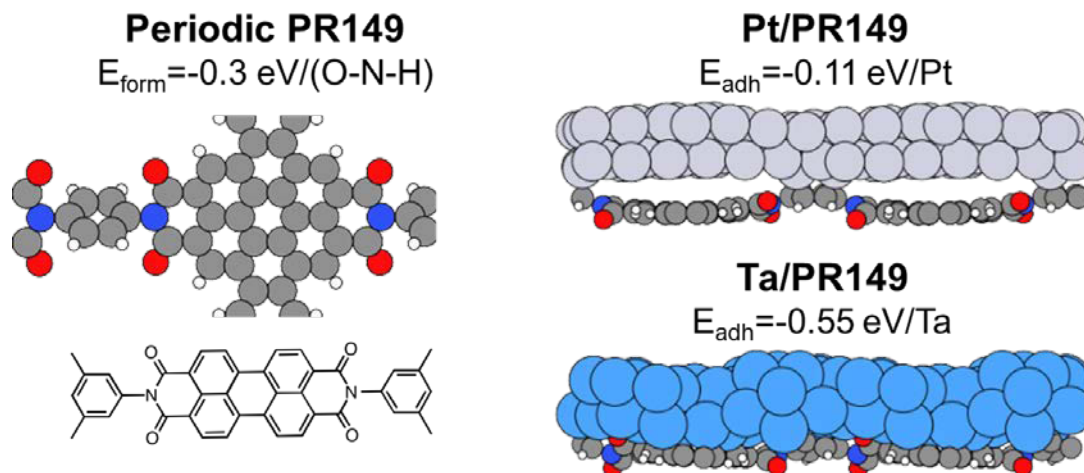


Figure 9. DFT simulations of Pt and Ta adhesion to Perylene Red 149

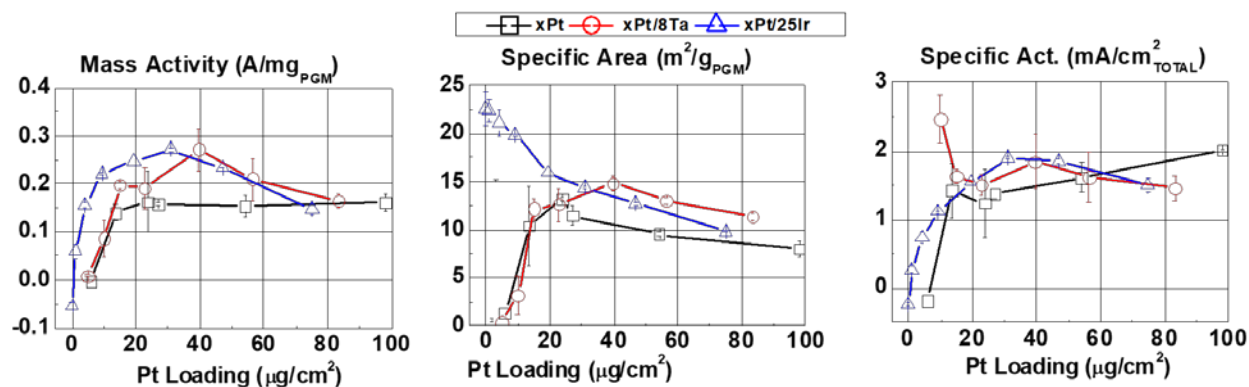


Figure 10. Comparison of PGM mass activity, specific area, and specific activity for xPt/NSTF, xPt/8Ta/NSTF, and xPt/26Ir/NSTF as a function of surface Pt loading

A subset of Pt/Ta/NSTF catalysts was analyzed for composition and structure by STEM, EDS, and XAFS. Figure 11 (left) and (center) compare STEM micrographs for 10Pt/8Ta/NSTF and 20Pt/8Ta/NSTF after fuel cell testing. The 10Pt/8Ta/NSTF consists of discontinuous Pt fibrils on the Ta underlayer, whereas with 20Pt/8Ta/NSTF the Pt layer appeared to be continuous. EDS analysis indicated that the Ta was oxidized, with O:Ta ratios of approximately 1:1. XAFS indicated that the Pt-Pt bond lengths changed only modestly as the surface Pt content on Ta increased from 10 $\mu\text{g}/\text{cm}^2$ to 78 $\mu\text{g}/\text{cm}^2$ (Figure 11, right), suggesting that the variation of specific area observed over this range was not due to significant changes in Pt.

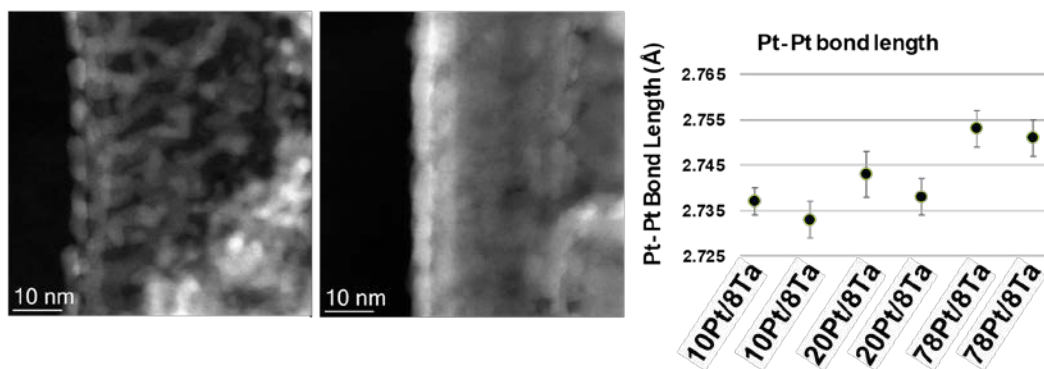


Figure 11. (Left and Center): STEM of 10Pt/8Ta/NSTF and 20Pt/8Ta/NSTF. (Right): XAFS-determined Pt-Pt bond lengths for 10Pt/8Ta, 20Pt/8Ta, and 78Pt/8Ta.

The primary hypothesis developed during the Pt/Ta/NSTF studies discussed above was that the loss of specific area and mass activity as the Pt loading on Ta decreased was due to low Pt utilization, imparted by insufficient electronic conductivity of the oxidized Ta layer and the discontinuous Pt surface coating. Experiments were conducted toward increasing the conductivity of the Ta underlayer, through modification of the Ta layer composition and changes to the catalyst processing. Figure 12 summarizes the impact of underlayer catalyst processing (“Previous” or “New”) on catalyst activity and area. The “New” processing method resulted in significantly increased specific surface area relative to the “Previous” method, especially at low Pt areal loadings and concomitant thickness on Ta. With $10 \mu\text{g}_{\text{Pt}}/\text{cm}^2$, the “New” processing method resulted in an approximate 4-fold gain in specific area, resulting in mass activity of $0.42 \text{ A}/\text{mg}_{\text{PGM}}$.

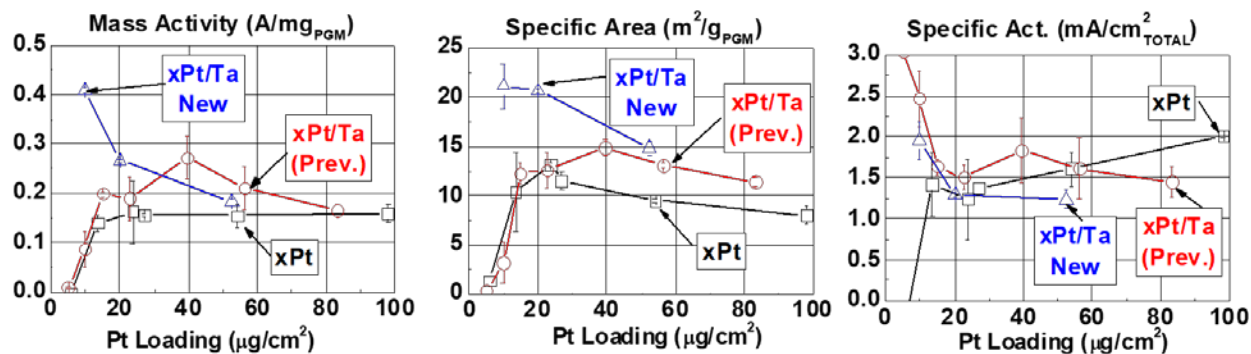


Figure 12. Mass activity, specific area, and specific activity of xPt/8Ta/NSTF with “Previous” and “New” processes

This year, work has been initiated toward development of an electrocatalyst durability model. DFT calculations were conducted to determine diffusion barriers for surface Pt atoms with different coordination levels and in the presence of oxide and hydroxide with a range of surface oxygen coverages. Additionally, interaction energies for Pt, Ni, and Ir over a range of compositions were calculated. The calculated diffusion barriers and interactions energies were integrated into a KMC model, which has been adapted to also include repeated oxidation and reduction cycles toward simulating the DOE electrocatalyst AST. Figure 13 compares a simulated defective Pt(111) surface to experiment in KOH electrolyte. Two-step oxidation is assumed, with formation of a “Pt-OH” species followed by formation of “Pt-O” species at higher potentials. The first peak (at $\sim 0.75 \text{ V}$) is assumed to be associated with hydroxylation of Pt(111) terrace sites with coordination $n = 9$. Good agreement with experiment is seen when the second peak (at $\sim 1.0 \text{ V}$) is found to be associated with step-edge and terrace vacancy edge oxidation to Pt-O. Upon reduction, reduced Pt-O species “pop out” of the terrace, simulating experimentally observed place exchange at higher potentials.

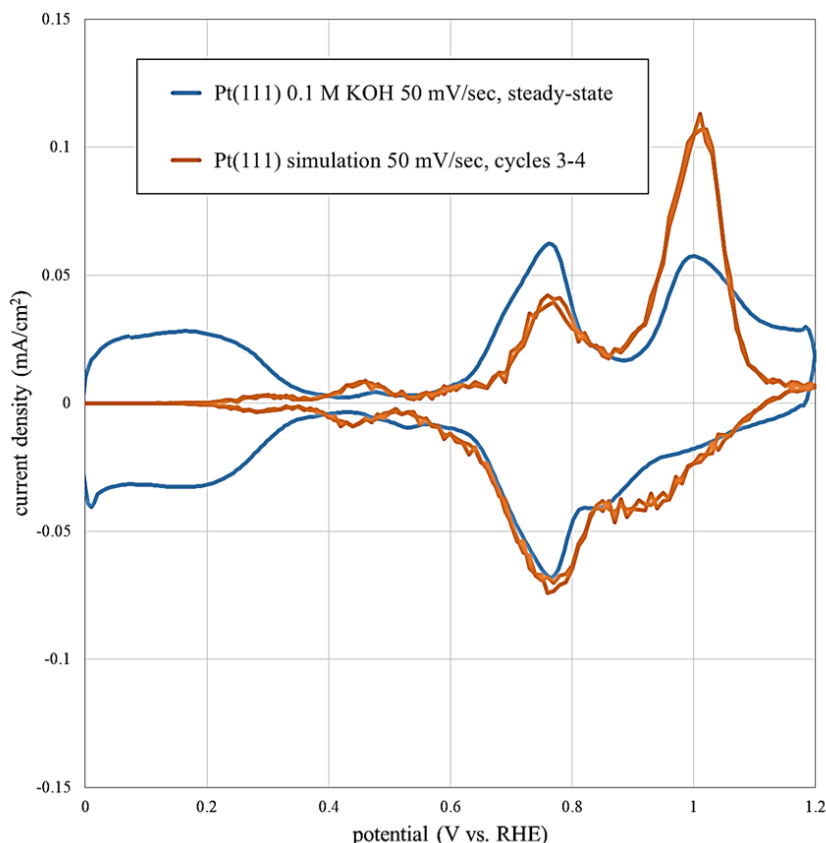


Figure 13. KMC simulation of Pt(111) oxidation and reduction as compared to experiment (0.1 M KOH)

Finally, development recently has been initiated toward implementation of NSTF catalysts and MEAs with improved break-in conditioning. STEM EDS and XAFS analysis of NSTF catalyst-coated membranes as a function of conditioning state reveal only subtle changes in composition and structure during this process. Studies also have identified that the break-in conditioning may be impacted by the slow removal of potential catalyst contaminants from the MEA during the conditioning process. Work is in progress to identify the sources of these potential contaminants and to confirm their impacts.

CONCLUSIONS AND UPCOMING ACTIVITIES

Over the past year, two UTF Pt/Ir/NSTF catalysts with ultra-low PGM content have been demonstrated that exceed five of the six DOE targets that this project addresses, and that achieve three of six of the more stringent project targets. Integration of an Ir layer between the surface Pt layer and the PR149 support has translated into significant gains in mass activity relative to pure Pt, due to increased specific area and, with some compositions, due to increased specific activity approaching values observed with highly active UTF PtNi alloys.

The Pt/Ir/NSTF catalysts are exceedingly durable toward electrocatalyst cycling, with several catalysts demonstrating mass activity losses of 20% or less and specific area losses of less than 10% after 30,000 potential cycles between 0.60 V and 1.0 V. The experimental activity and durability results are consistent with DFT simulations, which indicate high thermodynamic stability of Pt on Ir and the potential for increased specific activity, and KMC simulations, which indicate enhanced kinetic stability versus Ir-free systems. Integration of the durable Pt/Ir/NSTF catalysts with BOC components has resulted in demonstration of PGM contents of 0.106 g/kW to 0.110 g/kW at $Q/\Delta T=1.45$ kW/°C. Additionally, two surface-modified PtNi catalysts at optimal composition have produced PGM mass activities of 0.56 A/mg_{PGM} to 0.57 A/mg_{PGM}, via enhancement of specific activity as high as 3.0 mA/cm².

In future work, the project will continue the efforts toward development of one or more electrocatalysts that meet all DOE and project targets. This will be accomplished through further optimization of Pt and/or Pt-alloy surface catalysts on reduced-PGM content underlayers. Processing optimization of UTF catalysts on PGM-free underlayers also will continue, moving toward achieving entitlement of absolute and specific areas and mass activities with the underlayer approach. Simulation development will continue, with the objective of simulating a project Pt/Ir layered electrocatalyst through repeated potential cycling akin to the DOE AST and of additional screening of non-PGM underlayers. Lastly, work will continue to elucidate the factors responsible for break-in conditioning requirements with NSTF MEAs, and to identify and implement material solutions.

FY 2018 PUBLICATIONS/PRESENTATIONS

1. J. Greeley, “First principles studies of heterogeneous (electro)catalysis: incorporating structural complexity into catalyst reactivity and screening studies,” Department of Physics, Central Michigan University, October 2017, Mount Pleasant, MI.
2. A.J. Steinbach, K.A. Lewinski, A.T. Haug, C. Duru, S.M. Luopa, G.M. Thoma, J. Park, F. Sun, A.E. Hester, J.T. Petrin, M.E. Kuznia, D.J. Myers, A.J. Kropf, D.A. Cullen, J. Greeley, Z. Zeng, and J. Erlebacher, “3M NSTF Electrocatalysts for PEM Fuel Cells and Water Electrolyzers,” 232nd Meeting of The Electrochemical Society, Oct. 1, 2017, National Harbor, MD (Invited Plenary).
3. A.J. Steinbach, C. Duru, A.T. Haug, A.E. Hester, M.E. Kuznia, K.A. Lewinski, S.M. Luopa, J.T. Petrin, G.M. Thoma, A.J. Kropf, D.J. Myers, D. Yang, D.A. Cullen, J. Greeley, and Z. Zeng, “Ultrathin Film NSTF ORR Electrocatalysts for PEM Fuel Cells,” *ECS Trans.* 80, no. 8 (2017): 659–676.
4. A.J. Steinbach, “Highly Active, Durable, and Ultra-low PGM NSTF Thin Film ORR Catalysts and Supports,” USCAR Fuel Cell Tech Team, April 18, 2018, Detroit, MI.
5. A.J. Steinbach, Presentation FC143, 2018 Annual Merit Review, DOE Hydrogen and Fuel Cells Program, June 2018, Washington DC.
6. D.A. Cullen, D. Myers, J. Greeley, J. Erlebacher, G. Thoma, and A.J. Steinbach, “Exploring the Activity and Stability of Pt-based Catalysts through Analytical Electron Microscopy,” Microscopy and Microanalysis, Baltimore, MD, August 5–9, 2018.
7. Z. Zeng, J. Kubal, A. Steinbach, and J. Greeley, “First principles electrocatalysis: perspectives on computational design of fuel cell electrocatalysts,” Gordon Conference on Fuel Cells, August 2018, Smithfield, RI.
8. Z. Zeng, J. Kubal, A. Steinbach, and J. Greeley, “DFT studies of fuel cell electrochemistry,” ECS Spring Meeting, October 2018, Cancun, Mexico.

REFERENCES

1. A.J. Steinbach, Presentation FC104, 2016 Annual Merit Review, DOE Hydrogen and Fuel Cell Vehicles Technology Programs, Washington DC, June 2016.
2. M.K. Debe et al., “Stop-Start and High-Current Durability Testing of Nanostructured Thin Film Catalysts for PEM Fuel Cells,” *ECS Trans.* 3, no. 1 (2006): 835–853.
3. M.K. Debe et al., “Initial Performance and Durability of Ultra-Low Loaded NSTF Electrodes for PEM Electrolyzers,” *J. Electrochem. Soc.* 159, no. 6 (2012): K165–K176.
4. M.K. Debe, “Tutorial on the Fundamental Characteristics and Practical Properties of Nanostructured Thin Film (NSTF) Catalysts,” *J. Electrochem. Soc.* 160, no. 6 (2013): F522–F534.
5. A.J. Steinbach et al., “Highly Active, Durable, and Ultra-Low PGM NSTF Thin Film ORR Catalysts and Supports,” 2017 Annual Project Progress Report to U.S. Department of Energy, Office of Energy Efficiency and Renewable Energy, Fuel Cell Technologies Office.

Highly Accessible Catalysts for Durable High-Power Performance

Anusorn Kongkanand (Primary Contact), Venkata Yarlagadda, Michael K. Carpenter, Yun Cai, Thomas E. Moylan, Joseph M. Ziegelbauer, and Wenbin Gu
General Motors Company (GM)
850 Glenwood Ave
Pontiac, MI 48340-2920
Phone: (585) 953-5538
Email: anusorn.kongkanand@gm.com

DOE Manager: Gregory Kleen
Phone: (240) 562-1672
Email: Gregory.Kleen@ee.doe.gov

Contract Number: DE-EE0007271

Subcontractors:

- 3M Company, St. Paul, MN
- Carnegie Mellon University, Pittsburgh, PA
- Cornell University, Ithaca, NY
- Drexel University, Philadelphia, PA
- National Renewable Energy Laboratory, Golden, CO

Project Start Date: April 1, 2016
Project End Date: June 30, 2019

Overall Objectives

- Reduce overall stack cost by improving high-current-density (HCD) performance in H₂/air fuel cells appropriate to meet DOE heat rejection and Pt-loading targets.
- Maintain long-term high electrocatalytic mass activities.
- Mitigate catalyst HCD degradation.

Fiscal Year (FY) 2018 Objectives

- Optimize PtCo catalyst on accessible carbon supports for durable kinetic activity.
- Evaluate effects of electrolyte on electrode kinetics and transport.

- Quantify performance loss terms and degradation mechanism on low-platinum-group-metal (low-PGM) catalysts.

Technical Barriers

This project addresses the following technical barriers from the Fuel Cells section of the Fuel Cell Technologies Office Multi-Year Research, Development, and Demonstration Plan¹:

- (B) Cost
- (C) Performance
- (A) Durability.

Technical Targets

Table 1 shows the DOE technical targets and current project status.

FY 2018 Accomplishments

- Improved overall fuel cell performance by 10%–20% over last year's PtCo on accessible carbon catalysts by optimizing the catalyst preparation process.
- Demonstrated HCD fuel cell performance on porous carbon catalysts with ionic liquid and new ionomer.
- Reduced catalyst degradation nearly 50% by optimizing PtCo nanocrystal ordered intermetallic structure.

¹ <https://energy.gov/eere/fuelcells/downloads/fuel-cell-technologies-office-multi-year-research-development-and-22>

Table 1. Progress Toward Meeting Technical Targets for Electrocatalysts and MEAs for Transportation Applications

Metric	Units	PtCo/HSC-en	PtCo/HSC-f	Ordered-PtCo/KB	DOE 2025 Target
		2018-1	2018-2	2018-3	
PGM total loading [cathode/anode]	mg/cm ²	0.125 [0.10/0.025]	0.088 [0.063/0.025]	0.125 [0.10/0.025]	<0.125
Mass activity @ 900 mV _{IR-free}	A/mg _{PGM}	0.6 ^a	0.7 ^a	0.53 ^a	>0.44
Loss in catalytic (mass) activity	% loss	42 ^b	54 ^b	15	<40
Performance at 0.8 V (150 kPa, 80 °C)	A/cm ²	0.363	0.382	0.301	>0.3
Power at rated power (150 kPa, 94 °C)	W/cm ²	tbd	0.93	tbd	>1.0
Power at rated power (250 kPa, 94 °C)	W/cm ²	1.31	1.26	1.15	-
PGM utilization (150 kPa, 94 °C)	kW/g _{PGM}	tbd	10.6	tbd	>8
PGM utilization (250 kPa, 94 °C)	kW/g _{PGM}	10.5	14.3	9.2	-
Catalyst AST (0.6–0.95 V)	mV loss at 0.8 A/cm ²	34	47	8	<30
Support AST (1.0–1.5 V)	mV loss at 1.5 A/cm ²	>500	>500	tbd	<30

MEA – membrane electrode assembly

HSC – high-surface-area carbon

KB – Ketjen Black

AST – accelerated stability testing

Green: meets target; Red: did not meet target

^a Mass activity at 0.9 V_{RHE} in cathodic direction

^b Meets target in absolute term (i.e., >0.26 A/mg_{PGM})

INTRODUCTION

The amount of platinum used in the oxygen reduction reaction (ORR) catalyst in fuel cells must be lowered by at least 4-fold to enable proton exchange membrane fuel cells cost-competitiveness with other vehicular propulsion power sources. In our previous DOE-funded project, we demonstrated that carbon-supported Pt-alloy catalysts (PtNi/HSC and PtCo/HSC) exhibited very high ORR electrocatalytic activity and impressive durability, exceeding DOE targets [1]. However, their high-power performance fell short of the target.

As the Pt content is lowered in the cathode, approaching $<0.1 \text{ mg}_\text{Pt}/\text{cm}^2$, large oxygen and proton fluxes must be supplied to the Pt surface, causing a performance loss due to a relatively high local transport resistance in the state-of-the-art electrodes. The local resistance was associated with the electrolyte-Pt interface and Pt location/distribution [2]. In addition, the non-precious transition metal in the catalyst, such as Ni or Co, could dissolve and migrate into the ionomer phase, replacing protons and consequently lowering the ionomer proton conductivity and causing hydrodynamic performance loss. Although these Pt-alloy catalysts exhibit excellent durable high catalytic activity, the target performance at high power has not been realized, limiting its cost reduction benefit.

APPROACH

The general approach for this project is to develop and select carbon supports and electrolytes that have favorable transport properties, and subsequently develop a high-performance Pt-alloy electrode using these subcomponents. The efforts can be divided into four thrusts: (1) development of carbon support, (2) selection of electrolyte (ionomer or ionic liquid), (3) development of stable highly dispersed Pt alloy nanoparticles, and (4) understanding the effects of the transition metal on performance.

RESULTS

It was shown that the carbon support morphology has a pronounced effect on how electrocatalysts perform. Catalysts made from compact, solid carbon have most of their Pt particles on the carbon surface in contact with ionomer. The adsorption of ionomer onto Pt was shown to decrease its ORR activity and increase the local transport resistance. On the other hand, a majority of the deposited Pt particles on catalysts made with porous carbon are embedded inside the carbon pores. While this mitigates ionomer adsorption, thus increasing the ORR activity, it also can make it difficult for protons and O_2 to access the electrocatalyst sites. Last year, we showed that with the proper carbon internal pore morphology, one could obtain high ORR activity with acceptable proton and O_2 resistance in carbon's internal pores. These accessible, porous carbon catalysts have shown fuel cell performance metrics that meet DOE targets at both low and high current densities.

This year, we continued our efforts to further understand proton and O_2 transport within carbon's internal pores. Cornell University (Cornell) used high-resolution transmission electron microscope (TEM) tomography to identify the location of Pt and to measure the carbon internal pore morphology. General Motors (GM) and the National Renewable Energy Laboratory (NREL) used MEA diagnostics to distinguish the relative resistances between proton and O_2 transport in the pores. Carnegie Mellon University (CMU) performed ex situ proton and O_2 conductivity measurements on carbon black and thin ionomer films, respectively. CMU also continued to develop a mesoscale particle-pore model to delineate the fuel cell performance sensitivity, using a catalyst layer morphology consistent with the microscopy results from Cornell. From our experimental and modeling results, a preliminary guideline for an ideal catalyst morphology for optimal performance is shown in Figure 1. It is preferable to have all Pt particles within the carbon shielded away from the ionomer layer to optimize ORR activity and local transport. The primary particle size and internal pore morphology of carbon particles are also important to provide sufficient/appropriate proton and O_2 conduction.

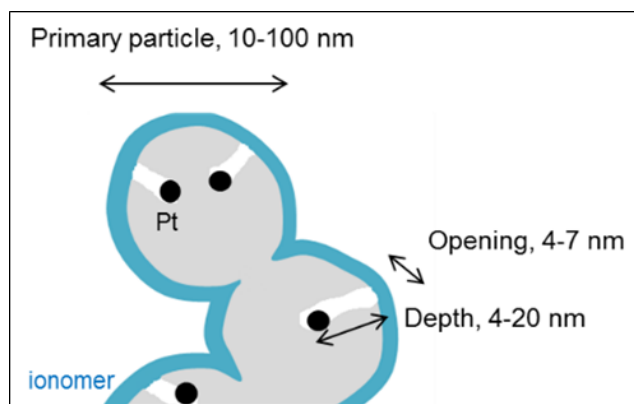


Figure 1. Illustration of cathode catalyst layer morphology to achieve optimal fuel cell performance

Voltage-cycling AST was employed on PtCo catalysts made from different carbon support types. As shown in Figure 2, PtCo on solid carbon (Vulcan) not only showed lower initial ORR activity and ECSA, but also a higher degradation rate compared to porous carbons (HSC or KB). Unsurprisingly, catalysts made with accessible carbons, having more open pore structures, showed higher degradation rates than inaccessible porous carbon. Still, the HCD benefit from better local transport could be realized on accessible carbon catalysts even after the stability test.

Cornell investigated the mechanisms of electrochemical active surface area (ECSA) loss underlying this trend using TEM of post-mortem MEA cross-sections (Figure 2b). Energy-dispersive X-ray spectroscopy quantification of the Pt mass loss through the formation of a Pt band found similar losses of around 15% for all catalysts. The degree of catalyst coarsening, however, varied significantly among the different catalysts. Vulcan-supported catalysts showed more severe surface area loss through coarsening, especially through the formation of large, irregularly shaped particles, as seen in the heavy tail in the size distributions. Such irregular particles and a distribution tail of larger particles were generally absent for HSC-supported catalysts. Electron energy loss spectroscopy (EELS) composition mapping confirmed that the large, irregular particles in aged PtCo/Vulcan frequently contained multiple PtCo cores, a signature of particle coalescence (Figure 2c). Multi-core PtCo particles were rarely observed in aged PtCo/HSC MEAs. Both catalysts also showed growth of smaller, more spherical particles, exhibiting an increase in Pt shell thickness in EELS measurements of PtCo samples, suggesting that these particles grew via Ostwald ripening. The electrochemically observed ECSA loss was quantitatively consistent with the combined expected loss due to Pt mass loss to the Pt band and catalyst coarsening, measured with scanning transmission electron microscopy techniques, indicating that these are likely the dominant ECSA degradation mechanisms under these test conditions. Together, these results indicate that Ostwald ripening is a significant coarsening mechanism for all catalysts, regardless of the support morphology, while particle coalescence only contributes significantly for catalysts with solid carbon supports. Thus, porous carbon supports suppress coalescence, likely by restricting the migration of particles embedded in carbon pores. This is an encouraging result, as it demonstrates that design of the catalyst support morphology can provide an effective strategy for mitigating catalyst degradation through particle coalescence.

Pre-project results by Cornell and other groups suggested that increase in atomic level ordering of a Pt binary alloy, a so-called ordered intermetallic, could improve both ORR activity and stability of the catalyst, yet realization of the effect in an MEA has not been obtained. Further, the heat treatment required for the high level of ordering generally results in particle sintering and loss of Pt surface area, reducing fuel cell performance. This year, Cornell used in situ techniques including heating synchrotron X-ray diffraction and heating TEM to maximize the formation of ordered intermetallic without excessive particle sintering (Figure 3a). Using this, GM was able to further improve the stability of its best catalyst. Figure 3b shows that the annealing conditions mitigate the losses in ORR activity and Pt surface area by a factor of two. The differences in catalyst decay are being studied by microscopy. The ordered intermetallics are being prepared on other accessible porous carbons in order to achieve both good fuel cell HCD performance and durability.

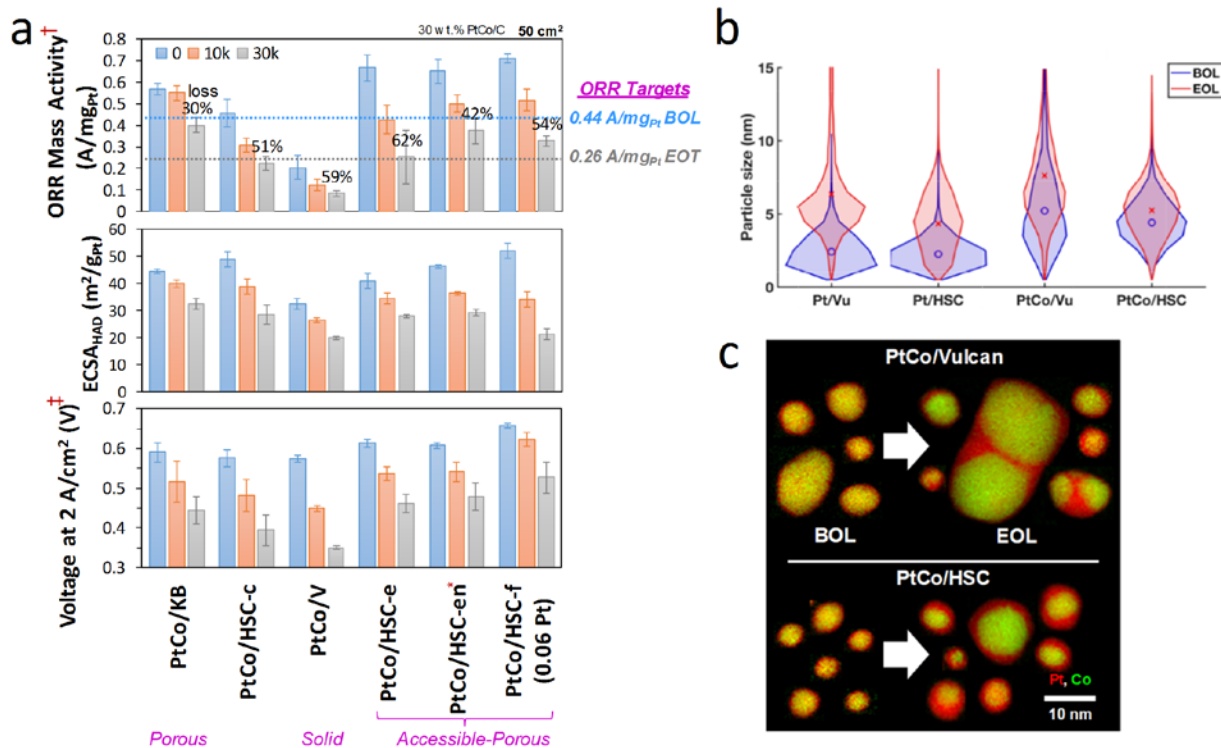


Figure 2. (a) ORR activity, Pt surface area, and voltage at 2 A/cm² of PtCo catalysts with different carbon supports during AST. (b) Particle size distribution of Pt and PtCo before and after AST. (c) TEM-EELS showing changes in Pt and Co distribution during AST.

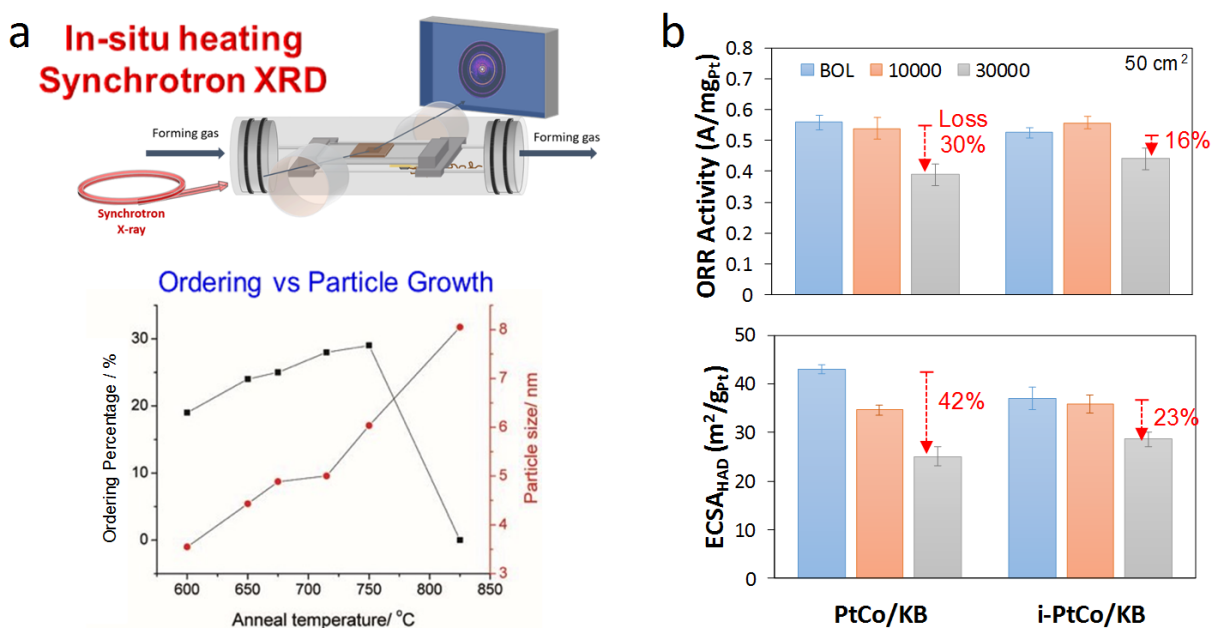


Figure 3. (a) In situ heating synchrotron X-ray diffraction experiment to study the degree of ordering and particle sintering as a function of heat-treatment conditions. (b) Improved retention of ORR activity and Pt surface area after AST by the heat treatment.

Although ionic liquids have been shown in rotating disk electrode to enhance ORR activity of Pt alloy catalyst, enhancement in a fuel cell has not been reproducibly demonstrated. This year, we established a procedure by adding the ionic liquid to the cathode after the layer was formed to prevent ionic liquid loss during application. A Pt/V cathode doped with ionic liquid showed improved fuel cell performance. Interestingly, the enhancement increases with current density, up to ~ 50 mV at 2.5 A/cm² (Figure 4a). Sub-ambient MEA diagnostics at NREL reveal that the increase is predominantly due to a potential-dependent kinetic enhancement, hypothetically as a result of competitive adsorption between the perfluorosulfonic acid ionomer and the ionic liquid. Similar, but somewhat smaller, improvement was observed with PtCo/KB. When measuring the proton accessibility of Pt on the porous carbon using CO stripping, it was found that the anion in the ionic liquid (beti) facilitates proton conduction into the carbon internal pores at low relative humidity (Figure 4b). This opens up a way to improve fuel cell performance of porous carbon catalysts under relatively dry conditions.

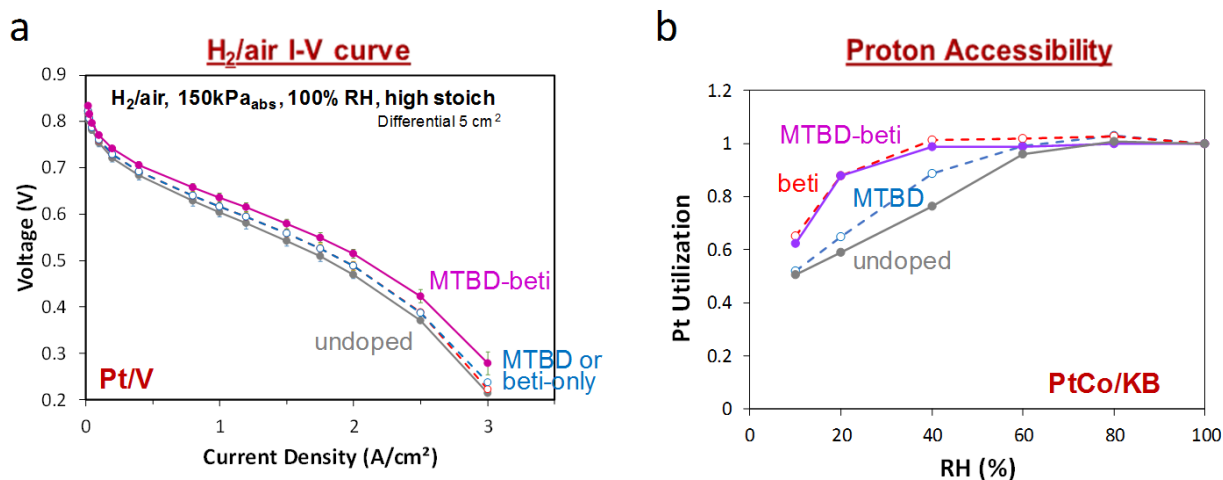


Figure 4. (a) Improved fuel cell performance by ionic liquid doping on Pt/V cathode. (b) Effect of ionic liquid ions on the proton accessibility as a function of relative humidity on PtCo/KB cathode.

CONCLUSIONS AND UPCOMING ACTIVITIES

- Promising new materials provide paths to better activity and durability:
 - Ordered intermetallic PtCo showed exceptional stability.
 - Improved ORR activity can be obtained with ionic liquid in MEAs.
 - Continual improvement in durability of accessible carbons.
- Improved understanding of low-PGM electrodes:
 - Identified that proton transport in internal pores is sufficient and that local-O₂ transport is the primary focus area to improve performance.
 - Internal pore size (opening) is the key factor for good ORR activity and transport properties.
- Upcoming activities include:
 - Implement with accessible carbons, the intermetallic alloy for better stability, and ionomer and ionic liquid for better activity.
 - Optimize intermetallic PtCo catalysts for HCD performance and durability.

- Develop and validate fundamental performance model including dissolved transitional metal cations.
- Provide MEAs for DOE validation.

SPECIAL RECOGNITIONS AND AWARDS/PATENTS ISSUED

1. “Editors’ Choice” recognition by the *Journal of The Electrochemical Society* for excellent publication.
2. Selected as “Energy Focus” article by *ACS Energy Letters* for excellent publication.
3. Two patent applications submitted.
4. Prof. Héctor D. Abruña was elected to the National Academy of Sciences.
5. Prof. Héctor D. Abruña received the A. J. Bard Award for 2019 from The Electrochemical Society.

FY 2018 PUBLICATIONS/PRESENTATIONS

Publications

1. Yin Xiong, Li Xiao, Yao Yang, Francis J. DiSalvo, and Héctor D. Abruña, “High-Loading Intermetallic Pt₃Co/C Core-shell Nanoparticles as an Enhanced Activity Catalyst towards the Oxygen Reduction Reaction (ORR),” *Chem. Mater.* 30, no. 5 (2018): 1532–1539
2. J. Braaten, A. Kongkanand, and S. Litster, “Oxygen Transport Effects of Cobalt Cation Contamination of Ionomer Thin Films in Proton Exchange Membrane Fuel Cells,” *ECS Transactions* 80 (2017): 283.
3. S. Ogawa, V. Yarlagadda, A. Kongkanand, and S. Litster, “Nano-scale simulation of platinum particle dissolution, re-deposition, and transport,” *ECS Transactions* 80, no. 8 (2017): 231–239.
4. [Invited Encyclopedia Entry] Anusorn Kongkanand, Wenbin Gu, and Mark F. Mathias, “Proton-Exchange Membrane Fuel Cells with Low-Pt Content,” In *Encyclopedia of Sustainability Science and Technology*, R.A. Meyers, Ed. (Springer, 2018), https://doi.org/10.1007/978-1-4939-2493-6_1022-1.
5. [Energy Focus] Venkata Yarlagadda, Michael K. Carpenter, Thomas E. Moylan, Ratandeep Singh Kukreja, Roland Koestner, Wenbin Gu, Levi Thompson, and Anusorn Kongkanand, “Boosting Fuel Cell Performance with Accessible Carbon Mesopores,” *ACS Energy Lett.* 3 (2018): 618.
6. [Editors’ Choice] Elliot Padgett, Nina Andrejevic, Zhongyi Liu, Anusorn Kongkanand, Wenbin Gu, Koji Moriyama, Swami Kumaraguru, Thomas E. Moylan, Ratandeep Kukreja, Yi Jiang, and David A. Muller, “Connecting nanostructure with utilization of hydrogen fuel cell catalysts using quantitative cryo-STEM tomography,” *J. Electrochem. Soc.* 165 (2018): F173.
7. Yun Cai, Joseph M. Ziegelbauer, Andrew M. Baker, Wenbin Gu, Ratandeep S. Kukreja, Anusorn Kongkanand, Mark F. Mathias, Rangachary Mukundan, and Rod L. Borup, “Electrode Edge Cobalt Cation Migration in an Operating Fuel Cell: An In Situ Micro-X-Ray Fluorescence Study,” *J. Electrochem. Soc.* 165 (2018): F3132.

Presentations

1. A. Kongkanand, “Highly-Accessible Catalysts for Durable High-Power Performance,” US Drive Fuel Cell Tech Team, Southfield, MI, April 2017.
2. H. Abruña, “Compositional and Structural Effects on ORR Electrocatalysis,” DOE CWG workshop, Argonne National Laboratory, Lemont, IL, May 3, 2017.
3. A. Kongkanand and V.R. Yarlagadda, “Recent Capabilities for Developing Low-PGM Electrodes,” DOE CWG workshop, Argonne National Laboratory, Lemont, IL, May 3, 2017.
4. C. Gittleman, A. Kongkanand, and S. Kumaraguru, “Ionomer in Catalyst Layer and Unresolved Issues,” DOE DWG workshop, Argonne National Laboratory, Lemont, IL, May 4, 2017.

5. H.D. Abruña, “Compositional and Structural Effects on ORR Electrocatalysis,” Nankai University, May 8, 2017.
6. H.D. Abruña, “Operando Methods for the Study of Energy Materials,” Huazhong University of Science and Technology, Wuhan, May 12, 2017.
7. H.D. Abruña, “Compositional and Structural Effects on ORR Electrocatalysis,” Wuhan University, May 12, 2017.
8. “Operando Methods for the Study of Energy Materials,” Dept. Chem., Univ. Buenos Aires, May 18, 2017.
9. H.D. Abruña, “Compositional and Structural Effects on ORR Electrocatalysis,” INQUIMAE, Univ. Buenos Aires, May 19, 2017.
10. H.D. Abruña, “Operando Methods for the Study of Energy Materials,” XVII Encuentro de Superficies y Materiales Nanoestructurados, Bariloche, Argentina, May 24, 2017.
11. [Invited] W. Gu, A. Kongkanand, V.R. Yarlagadda, P.T. Yu, and M.F. Mathias, “The Importance of the Cathode Catalyst Support in the Pursuit of Low-Cost PEM Fuel Cells,” ECS 231st Meeting, New Orleans, LA, May 28–June 1, 2017.
12. Venkata Yarlagadda, Samuel E. McKinney, Cristin L. Keary, Levi Thompson, Barr Halevi, and Anusorn Kongkanand, “Preparation of PEMFC Electrodes from Milligram-Amount Catalysts,” ECS 231st Meeting, New Orleans, LA, May 28–June 1, 2017.
13. Venkata Yarlagadda, Elliot Padgett, Ratandeeep Kukreja, Joseph M. Ziegelbauer, Jonathan Braaten, Shohei Ogawa, Siddharth Komini Babu, Srikanth Arisetty, Wenbin Gu, Levi Thompson, Shawn Litster, David A. Muller, and Anusorn Kongkanand, “Effects of Carbon Supports on the Stability of Pt and PtCo Nanoparticles in PEMFC Cathodes,” ECS 231st Meeting, New Orleans, LA, May 28–June 1, 2017.
14. [Invited] S. Arisetty, S. Alia, J. Zack, J.M. Ziegelbauer, N.N. Kariuki, V.R. Yarlagadda, D.J. Myers, K.C. Neyerlin, and A. Kongkanand, “Dealloying of Binary Catalysts in Hydrogen Fuel Cell,” ISE 68th Meeting, Providence, RI, August 27–September 1, 2017.
15. [Invited] S. Ogawa, S. Komini Babu, H. T. Chung, P. Zelenay, E. Padgett, D.A. Muller, A. Kongkanand, and S. Litster, “Microstructural Modeling of PEFC Catalyst Layer Performance and Durability,” ECS 232nd Meeting, National Harbor, MD, October 1–5, 2017.
16. [Invited] K.C. Neyerlin, L. Anderson, A. Chuang, K.L. More, R. Ahluwalia, S.A. Mauger, G. Bender, B.S. Pivovar, W. Gu, S. Kumaraguru, A. Kongkanand, and S.S. Kocha, “Methods for Understanding and Mitigating High Current Density Performance Losses in Low Loaded Pt-Based PEMFCs,” ECS 232nd Meeting, National Harbor, MD, October 1–5, 2017.
17. S. Ogawa, V. Yarlagadda, A. Kongkanand, and S. Litster, “Nano-Scale Simulation of Platinum Particle Dissolution, Re-Deposition, and Transport,” ECS 232nd Meeting, National Harbor, MD, October 1–5, 2017.
18. J. Braaten, A. Kongkanand, and S. Litster, “Oxygen Transport Effects of Cobalt Cation Contamination of Ionomer Thin Films in Proton Exchange Membrane Fuel Cells,” ECS 232nd Meeting, National Harbor, MD, October 1–5, 2017.
19. S. Arisetty, S.M. Alia, J.W. Zack, A. Kongkanand, V. Yarlagadda, R.S. Kukreja, J.M. Ziegelbauer, K.C. Neyerlin, N. Kariuki, D.J. Myers, B. Lakshmanan, “Catalyst Dissolution Rates during PEM Fuel Cell Operation,” ECS 232nd Meeting, National Harbor, MD, October 1–5, 2017.
20. Y. Li and J. Snyder, “Improved Activity and Durability of Ionic Liquid Composite Nanoporous Nanoparticle Electrocatalysts for Oxygen Reduction Reaction,” AIChE Fall Meeting, Minneapolis, MN, October 31, 2017.
21. Y. Li and J. Snyder, “Mitigation of Structural and Compositional Instability in 3-Dimensional, Nanoporous Electrocatalysts,” ECS Fall Meeting, Washington, DC, October 3, 2017.

22. J. Snyder and Y. Li, “Electrocatalytic Interface Engineering with Ionic Liquids,” ECS Fall Meeting, Washington, DC, October 3, 2017.
23. [Invited] J. Ziegelbauer, Y. Cai, and A. Kongkanand, “Synchrotron-based Research for Zero-emission Transportation Applications at General Motors,” CHESS/CLASSe Seminar, Cornell University, October 2017.
24. [Invited] A. Kongkanand, “Catalysts for Sustainable Fuel Cell Electric Vehicles,” Technology Collaboration Programme on Advanced Fuel Cells by the International Energy Agency (IEA), Berlin, Germany, November 15, 2017.

REFERENCES

1. B. Han et al., “Record Activity and Stability of Dealloyed Bimetallic Catalysts for Proton Exchange Membrane Fuel Cells,” *Energy Environ. Sci.* 8, no. 1 (2015): 258-266.
2. Anusorn Kongkanand, Wenbin Gu, and Mark F. Mathias, “Proton-Exchange Membrane Fuel Cells with Low-Pt Content,” In *Encyclopedia of Sustainability Science and Technology*, R.A. Meyers, Ed. (Springer, 2018), https://doi.org/10.1007/978-1-4939-2493-6_1022-1.

Corrosion-Resistant Non-Carbon Electrocatalyst Supports for Proton Exchange Fuel Cells

Vijay K. Ramani
Washington University in St. Louis
One Brooking Drive
St. Louis, MO 63130
Phone: (312) 259-0801
Email: ramani@wustl.edu

DOE Manager: Gregory Kleen
Phone: (240) 562-1672
Email: Gregory.Kleen@ee.doe.gov

Contract Number: DE-EE0007272

Subcontractors:

- Nissan Technical Center, North America, Farmington Hills, MI
- University of New Mexico, Albuquerque, NM

Project Start Date: March 1, 2016
Project End Date: August 31, 2019

Overall Objectives

- Design, develop, and demonstrate high-surface-area (>70 m²/g), high-conductivity (>0.2 S/cm) and corrosion-resistant (as per funding opportunity announcement requirements) non-carbon supports based on doped/mixed metal oxides (that do not contain platinum group metals).
- Derivatize said supports to yield functional supported platinum (Pt) electrocatalysts that leverage strong metal-support interactions (SMSI).
- Demonstrate stability, activity, and performance approaching the DOE 2020 targets, using DOE-prescribed accelerated protocols in rotating disk electrode (RDE) and membrane electrode assembly (MEA) proton exchange fuel cell (PEFC) experiments, by optimizing the structure of the support and the structure of the electrode.
- Provide DOE with at least six 50-cm² MEAs prepared using the best down-selected formulations that (a) meet all the stability

metrics, and (b) provide a clear pathway to meeting DOE 2020 targets for Pt loading and mass activity metrics.

Fiscal Year (FY) 2018 Objectives

- Density functional theory (DFT) calculations to evaluate conductivity and Pt-SMSI of relevant doped metal oxides (MOs).
- Synthesis and characterization of niobium (Nb)-doped-TiO₂ (NTO) and antimony (Sb)-doped-SnO₂ (ATO).
- Characterization of the doped metal oxides and the derived Pt catalysts.
- Electrochemical evaluation of the stability of supports and Pt/MO electrocatalysts.
- Investigation of SMSI in Pt/doped-MO systems using X-ray photoelectron spectroscopy (XPS) and DFT
- Measurement of beginning-of-life (BoL) oxygen reduction reaction (ORR) activity and electrochemically active surface area (ECSA) of selected catalysts in RDE experiments.
- Electrode optimization: RDE and MEA.
- Evaluation of selected catalysts in a PEFC: BoL ORR activity, ECSA, and fuel cell performance.

Technical Barriers

Fuel cell catalyst and catalyst support durability, catalyst performance, and catalyst cost need to be improved, in line with DOE 2020 targets from the Fuel Cells section of the Fuel Cell Technologies Office Multi-Year Research, Development, and Demonstration Plan.¹

Technical Targets

Table 1 shows the current status (with commercial Pt/C and with the Pt/RTO [ruthenium dioxide-titanium dioxide] catalyst developed in our previous DOE Fuel Cell Technologies Office

¹ <https://energy.gov/eere/fuelcells/downloads/fuel-cell-technologies-office-multi-year-research-development-and-22>

project) and the proposed targets for the current project. The preliminary data obtained with our proposed approach (see Table 1—Pt/TiO₂-Ta) was obtained without any optimization of the support, the catalyst deposition process, or the electrode preparation process. Clearly, there is much room for improvement in performance and baseline mass activity, which is precisely our goal in this project. These improvements, in conjunction with the enhancement in durability, will allow us to advance toward the DOE 2020 targets. The advantages of our approach over the incumbent technology and any alternate approach (and to even our prior success with RTO) are that we eliminate the noble metal in the support (cost reduction), we ensure 100% tolerance toward start-stop cycling, and we promote SMSI between the support and Pt, providing a pathway to enhance BoL mass activity and stability under load cycling conditions. Hence, the proposed approach addresses the remaining challenges/technical issues and provides a pathway to advance the state of the art and meet the DOE 2020 targets.

FY 2018 Accomplishments

- DFT was used to study the electronic structure of platinum supported on rutile TiO₂ surface doped with Ta and Nb. Decreased overpotential for ORR was predicted on Pt supported on Ta and Nb-doped TiO₂ surfaces relative to unsupported Pt.
- Nb-doped-TiO₂ was synthesized by aerogel method that exhibited a unique combination of high surface area (140 m²/g), high electrical

conductivity (0.3 S/cm), and high porosity. This catalyst retained 78% of its initial ECSA against the 57.6% retained by Pt/C following DOE/Fuel Cell Commercialization Conference of Japan protocol accelerated stability tests and displayed 21% higher ORR mass activity (at 0.9 V vs. reversible hydrogen electrode [RHE]) compared to commercial Pt/C. This marked improvement resulted from engineered SMSIs, which were confirmed by XPS and RDE measurement.

- ATO was synthesized and characterized at Washington University in St. Louis using a xerogel method and Pt-seeded aerogel method. Colloidal Pt deposition method was used to synthesize the catalyst with small Pt particle size. For both catalysts, no obvious decrease in the ECSA was observed during start/stop cycling tests performed in an RDE. In the fuel cell test, after 1,000 and 5,000 cycles, the iV performance for xerogel or aerogel ATO-supported catalyst was indistinguishable from the BoL iV performance (80°C, 90% relative humidity, 200 kPa_{abs}). However, the aerogel ATO-supported catalyst had much better performance than the xerogel ATO-supported catalyst did.

Table 1. Technical Targets

Metric	Units	SoA (Pt/C)	SoA (Pt/RTO)	Approach Status (Pt/Pt-aerogel-ATO)	End Target	DOE 2020 Target
Total PGM content	g/kW	0.55	0.55	0.25	0.25	<0.125
Total PGM loading	mg/cm ²	0.4	0.4	0.2	0.25	<0.125
Voltage at 1.5 A/cm ² (air)	mV	0.45	0.48	0.49	0.55	N/A
Loss in mass activity	% loss	32	33	<10%	<5%	<40
Voltage loss at 0.8 A/cm ²	mV	81	9	<5	<10	30
Voltage loss at 1.5 A/cm ²	mV	182 ⁺	20	24	<20	30
Mass activity @ 900 mV _{IR-free}	A/mg _{PGM}	0.07	0.07	ca. 0.057	0.3	0.44

SoA – state of the art

PGM – platinum group metal

INTRODUCTION

Carbon black is the commonly used catalyst support for PEFC electrocatalysts due to its high surface area and high conductivity. However, under certain automotive fuel cell operation conditions (start-stop), carbon can corrode rapidly [1], resulting in significant and irrecoverable loss in performance. To address this issue, it is desirable to explore non-carbon supports with high conductivity, high surface area, and high corrosion resistance under fuel cell operating conditions. In this project, we will design, develop, and evaluate electrochemically stable, high-surface-area, MO and doped-MO supports and supported Pt electrocatalysts therein. The Pt/MO catalysts should meet the DOE 2020 targets for stability and approach DOE 2020 targets for the BoL mass activity and Pt loading (as per DOE testing protocols).

APPROACH

DFT simulations will be performed to understand the electronic structure of the oxide upon doping and to examine SMSIs between Pt clusters and the support. The DFT results will guide dopant choice and doping levels. Once suitable combinations are identified and evaluated, we will employ the sacrificial support method pioneered by the University of New Mexico, as well as other methods suitable for the purpose, to prepare the supports with high surface area.

The evaluation of the electrochemical stability will be performed following the start-stop DOE protocol, by sweeping (linear ramp) the working electrode potential from 1 to 1.5 V (vs. RHE). The experiment will be performed for 10,000 cycles (at 500 mV/s). Cyclic voltammograms will be recorded at periodic intervals (at a scan rate of 20 mV/s) to investigate any changes in the pseudo-capacitance or the appearance of any new oxidation or reduction peaks (sign of changes in the oxide surface). The Pt catalysts (Pt deposited onto the MO) will be evaluated by using the start-stop and the load-cycling stability protocols. During the load-cycling protocol the electrode containing the Pt/MO catalyst will be cycled between 0.6 and 0.95 V (vs. RHE) for 10,000 cycles employing a square wave. Cyclic voltammograms will be performed periodically to estimate the ECSA. Linear polarization experiments will be performed to estimate mass- and area-specific activities.

RESULTS

DFT with PBEsol+ U method (Hubbard term $U=5$ set for Ti) was used to study the electronic structure of Pt supported on β -Ti₃O₅(001) and β -Ti₃O₅(010) surfaces. Calculations of the interaction energy between Pt(111) and (001) and (010) surfaces of the Magneli phase showed that there is a weaker but favorable interaction between the catalyst and the β -Ti₃O₅(001) support due to the mismatch of the cell parameters of Pt(111) surface and β -Ti₃O₅(001). Namely, the energy of interaction between Pt and β -Ti₃O₅(001) was calculated as -0.03 eV per atom. Based on the optimized structures, DFT predicts that due to the mismatch in the cell symmetry/lattice parameters between Pt(111) and β -Ti₃O₅(001), grain boundaries are expected to exist in Pt that grows on β -Ti₃O₅(001) surface. In the case of the β -Ti₃O₅(010) support, a strong interaction between the Pt(111) and the support was calculated (-0.07 eV per atom), similar to the value calculated between Pt(111) and doped rutile TiO₂ surfaces. We further calculated density of d -states of Pt(111) supported on β -Ti₃O₅(001) or β -Ti₃O₅(010) surfaces to predict the interaction energies between ORR intermediates and Pt supported on Magneli phase surfaces. The results (Figure 1, left) show that depositing Pt on either β -Ti₃O₅(001) or β -Ti₃O₅(010) surfaces lowers the d -band center of platinum by altering its electronic structure, and Pt on Magneli phase titanium oxide is expected to bind oxygen more weakly than supportless Pt does. Thus, *decreased overpotential for ORR is expected on Pt supported on Magneli phase relative to supportless Pt* (Figure 1, right). Based on DFT calculations, the ORR overpotential potential is expected to follow this relation: Pt on Ta/Nb:TiO₂(110) < Ta/Nb:TiO₂(100) \approx Pt on β -Ti₃O₅(001) < Pt on β -Ti₃O₅(010) < Pt.

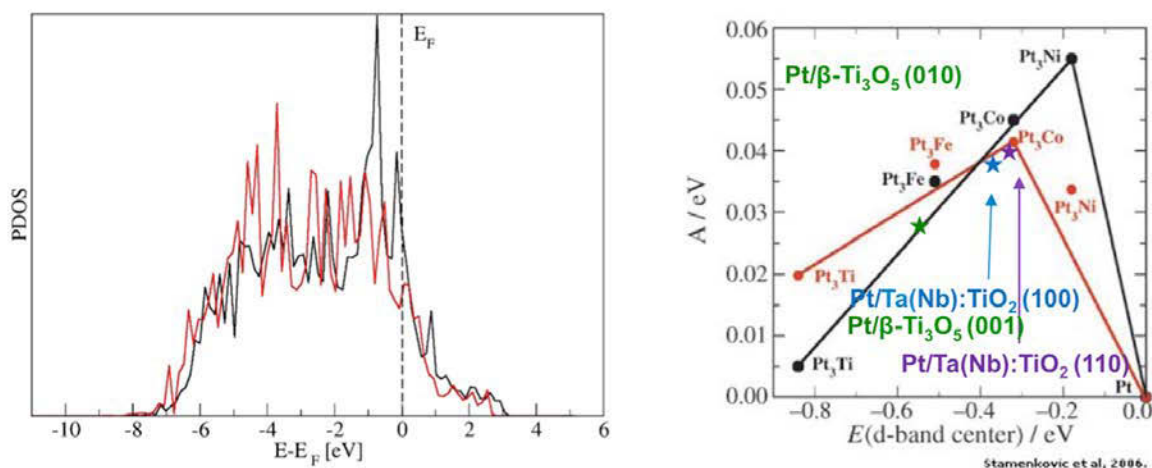
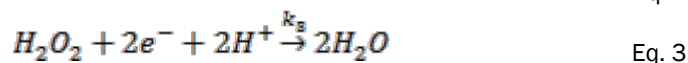


Figure 1. Left: DFT calculated d -projected density of states of Pt(111) and Pt(111) supported on β -Ti₃O₅(001) (black) and β -Ti₃O₅(010) (red). Right: Correlation of d -band center for various bulk alloys with the ORR activity (taken from [2]) and comparison with d -band center of Pt supported on TiO₂(110) and TiO₂(100) surfaces doped with 4% Ta and Nb.

Nb_{0.3}Ti_{0.7}O₂ was synthesized by the aerogel method and obtained with high surface area and high conductivity. Pt was deposited on NTO by the formic acid reduction method. The mass activity and half-wave potential of Pt/NTO showed significant improvement compared to commercial Pt/C, suggesting a 20% improvement induced by SMSI. Based on the XPS data, the peak of the Pt 4f for Pt/NTO exhibited a 625 meV switch toward lower binding energy (Figure 2a), suggesting SMSI. Using the RDE technique, the different reaction rate constants for the oxygen reduction reaction (Equations 1–3) were obtained. The result (Figure 2b) shows that in contrast to the carbon support, NTO can significantly increase the reaction rate constant (k_1) via the four-electron-transfer pathway. This can be ascribed to the SMSI between the support and the Pt cluster. The Pt cluster can secure electron donation from the NTO leading to higher electron density around the Pt atom and a decrease in the Pt d-band vacancy. The changes in the electronic structure of Pt/NTO facilitate the transition of adsorbed OH to water by modification of the binding energy of the oxygen-containing species. From Figure 2b, it is also shown that the k_2 of the Pt/C was higher than that of the Pt/NTO. This is because very weak oxygen binding energies impede O–O bond cleavage, while very strong binding energies inhibit the formation of O–H bonds and instead facilitate H₂O₂ formation. The electron structure change of the Pt/NTO should have an intermediate oxygen binding energy.



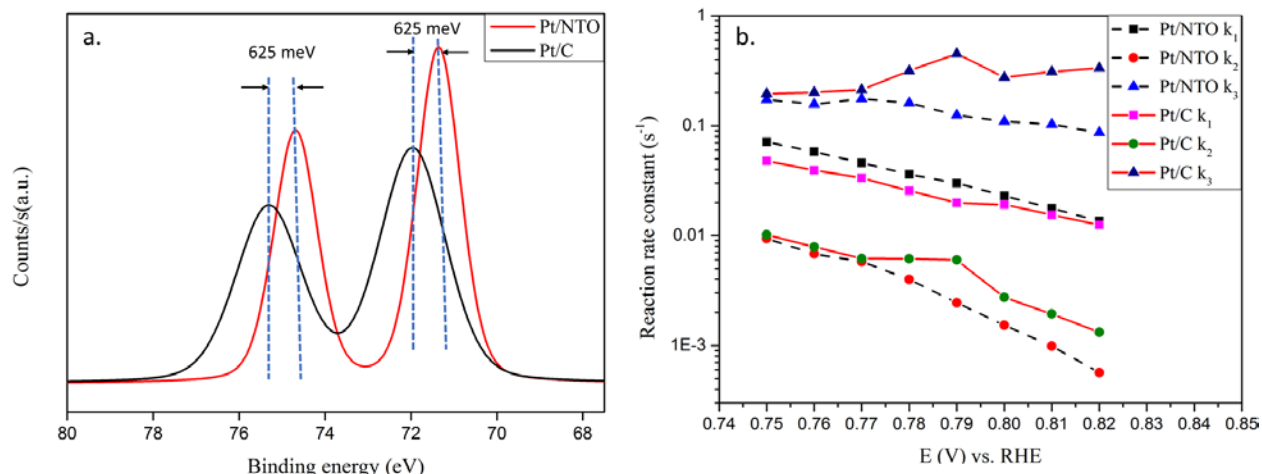


Figure 2. (a) XPS of Pt 4f region of Pt/C and Pt/NTO. (b) The rate constants k_1 k_2 k_3 as a function of potential.

In parallel, $Sb_{0.05}Sn_{0.95}O_2$ (ATO, Sb-doped-SnO₂) was synthesized by the xerogel and Pt-seeded aerogel methods. The Colloidal Pt deposition method was used to deposit Pt on the support. Both catalysts showed good electrochemical stability in RDE under start-stop cycling protocol with less than 10% of ECSA loss after 10,000 cycles (start-stop potential cycles). For the fuel cell test, Pt/Pt-aerogel-ATO displayed similar iV performance with commercial catalyst (Pt on Vulcan carbon); however, Pt/xerogel-ATO displayed poor fuel cell performance (Figure 3). After 1,000 and 5,000 cycles the iV performance for Pt/Pt-aerogel-ATO and Pt/xerogel-ATO were indistinguishable from the BoL iV performance (Figure 4). Dramatic performance losses were indeed observed for Pt/C even after 1,000 cycles.

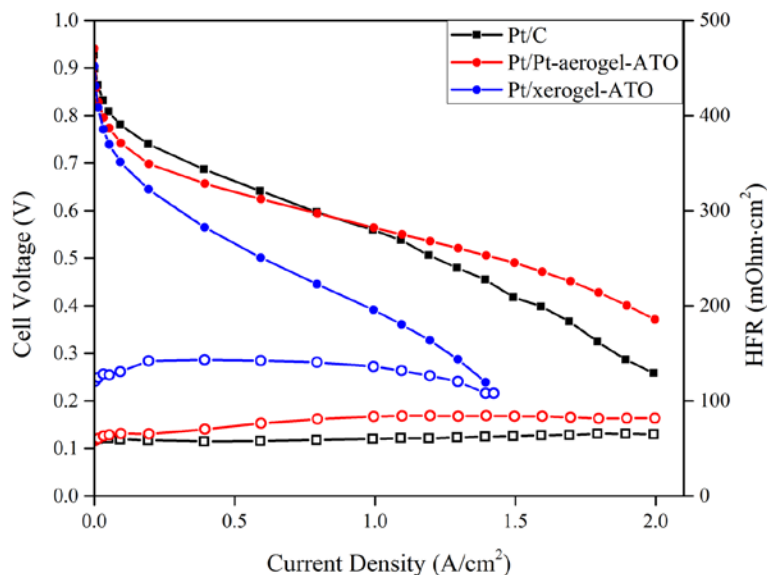


Figure 3. Comparison of fuel cell performance (H₂/air) obtained for Pt/xerogel-ATO, Pt/Pt-aerogel-ATO, and Pt/Vulcan Carbon at 80 °C, 90% relative humidity, and 200 kPa_{abs}. Pt loading at the cathode: 0.10 mg_{Pt}/cm². Pt loading at the anode: 0.10 mg_{Pt}/cm².

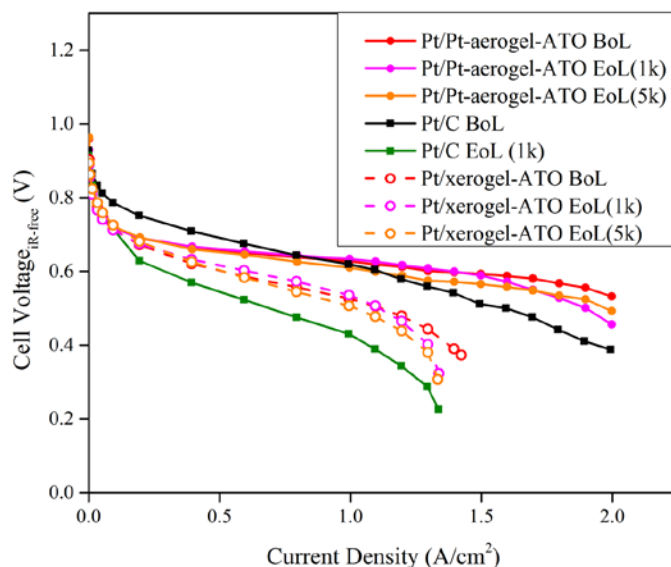


Figure 4. Comparison of fuel cell performance (H_2/air , iR -free) obtained for Pt/xerogel-ATO, Pt/Pt-aerogel-ATO, and Pt/Vulcan Carbon before (BoL) and after (end of life) start-stop protocol for 1,000 and 5,000 cycles at 80°C , 90% relative humidity, and $200\text{ kPa}_{\text{abs}}$. Pt loading at the cathode: $0.10\text{ mg}_{\text{Pt}}/\text{cm}^2$. Pt loading at the anode: $0.10\text{ mg}_{\text{Pt}}/\text{cm}^2$.

CONCLUSIONS AND FUTURE DIRECTIONS

We have used DFT to identify different doped oxides that facilitate SMSI and decrease the overpotential for ORR. In parallel, we have synthesized high-surface-area and high-conductivity NTO and successfully deposited Pt on this support yielding higher activity than the Pt/C. The improvement of activity can be ascribed to SMSI, which was confirmed by XPS. ATO was synthesized by the xerogel and Pt-seeded aerogel methods and Pt was deposited using the colloidal method. Both catalysts showed significant stability in the fuel cell accelerated test, and Pt/Pt-aerogel-ATO displayed a better fuel cell performance that was close to that of the commercial Pt/C. For the improvement of BoL performance (to reach the levels of the commercial Pt/C catalysts in terms of iV performance and ORR activity as required by DOE), catalyst and support optimization and/or catalyst layer optimization (catalyst layer thickness, ionomer loadings, and electrode porosity) will be performed. We plan to prepare more homogeneous ATO supports and to deposit Pt using atomic layer deposition (ALD). It is expected that ALD-deposited Pt catalyst would result in better BoL performance and mass activities.

FY 2018 PUBLICATIONS/PRESENTATIONS

1. Cheng He, Shrihari Sankarasubramanian, Vijay K Ramani, "Pt Supported on Nb-Doped-TiO₂ as a Highly Selective and Durable Electrocatalyst for PEFC Applications," Meeting Abstracts, *The Electrochemical Society*.

REFERENCES

1. N. Takeuchi and T.F. Fuller, *J. Electrochemical Society* 155 (2008): B770–B775.
2. V. Stamenkovic, B.S. Mun, K.J. Mayrhofer, P.N. Ross, N.M. Markovic, J. Rossmeisl, J. Greeley, and J.K. Nørskov, "Changing the activity of electrocatalysts for oxygen reduction by tuning the surface electronic structure," *Angew. Chem. Int. Ed.* 45 (2006): 2897–2901.

ElectroCat (Electrocatalysis Consortium)

Steering Committee Members:

Deborah J. Myers¹ (Argonne National Laboratory, Primary Contact), Piotr Zelenay² (Los Alamos National Laboratory), Kenneth C. Neyerlin (National Renewable Energy Laboratory), Karren L. More (Oak Ridge National Laboratory)

¹Argonne National Laboratory

Lemont, IL 60439

Phone: +1-630-252-4261

Email: dmyers@anl.gov

²Los Alamos National Laboratory

Los Alamos, NM 87545

Phone: +1-505-667-0197

Email: zelenay@lanl.gov

DOE Manager: Dimitrios Papageorgopoulos

Phone: (202) 586-5463

Email: Dimitrios.Papageorgopoulos@ee.doe.gov

Project Start Date: February 1, 2016

Project End Date: September 30, 2020

Consortium Objectives

- Expedite the development of platinum group metal-free (PGM-free) catalysts, electrodes, and membrane-electrode assemblies (MEAs) for fuel cell applications by facilitating collaboration between national laboratories.
- Foster the development of necessary capabilities.
- Create an interface for making capabilities available to industry and academic partners.

Fiscal Year (FY) 2018 Objectives

Argonne National Laboratory (ANL)

- Identity of X-ray absorption near-edge structure (XANES) spectroscopy and extended region features that are correlated with oxygen reduction reaction (ORR) activity for the atomically dispersed iron-nitrogen-carbon ((AD)Fe-N-C) catalysts using X-ray absorption fine structure (XAFS) spectroscopy data acquired from ex situ samples, in situ electrochemical experiments, and in situ pyrolysis experiments. Select and prepare six PGM-free electrode specimens and obtain 3-D micro-structures using synchrotron X-ray computed tomography (XCT).

- Automated deposition of catalyst-ionomer inks on multichannel flow double electrode (m-CFDE) glassy carbon electrodes demonstrated to result in ORR half-wave potentials within 10 mV of those measured using rotating disk electrode (RDE).
- Hydrogen-oxygen and hydrogen-air polarization curves measured for 25 electrodes simultaneously with different catalyst and ionomer-to-carbon ratios in the 25 cathode catalyst layers. Catalysts will include catalysts in the (AD)Fe-N-C class arising from high-throughput synthesis task.

Los Alamos National Laboratory (LANL)

- Demonstrate five-fold (400%) improvement in fuel cell performance of (AD)Fe-N-C catalysts at 0.80 V (measured) at 0.2 bar partial pressure of O₂ and cell temperature of 80°C.
- Evaluate active-site specificity of molecular probe methodology for PGM-free catalysts; compare binding motifs (structures and energies) of three different probe molecules adsorbed at no less than three sites local for selected Fe-based sites in activity/durability library via density functional theory.
- Identify possible degradation mechanisms via experiment and theory. Validation and publication on durability descriptor calculation automation (DDCA)-based modeling approach and calculation of activity descriptor for locally degraded structures (addition to calculated active-site library); qualification and comparison of empirical activity-loss reaction kinetic model to DDCA atomic-scale model; corroboration from active-site probe methodology and CO₂/F⁻/transition-metal emission measurements.

National Renewable Energy Laboratory (NREL)

- Demonstrate that the powder sputter and implant system (PSIS)-prepared PGM-free catalyst (e.g., deposited Fe_xN_y on black pearl) is capable of achieving a half-wave potential 0.70 V versus reversible hydrogen electrode (RHE) for the ORR with 85% selectivity.
- Demonstrate homogeneous current distribution in a subset of 6 to 7 segments located between

the bend regions and along a straight channel section in segmented cell. The current densities of all segments in this subset must be within 10% of those in a standard 5 cm² test cell while using identical PGM-free electrode compositions in both cells.

- Demonstrate the capability to fabricate PGM-free electrodes with ionomer or electrocatalyst gradients in x, y, and z dimensions.
- Separate the pressure dependent (Fickian) and independent (non-Fickian) transport resistances for at least two types of PGM-free electrocatalyst/electrode combinations.

Oak Ridge National Laboratory (ORNL)

- Conduct high-resolution scanning transmission electron microscopy (TEM) imaging and spectroscopy on at least three new (AD)-Fe-N-C catalysts and at least three metal organic framework/zeolitic imidazolate framework (ZIF)-derived catalysts in coordination with synthesis efforts at LANL and high-throughput methods at ANL. These studies will focus on understanding morphological aspects of catalysts in addition to identification of potential active sites.
- Characterize at least four PGM-free MEAs before and after degradation testing using analytical electron microscopy and tomography. This effort will be highly coordinated with efforts at LANL to develop protocols to assess performance and durability of PGM-free catalysts and with XCT and XAFS efforts at ANL.
- Complete evaluation of ORNL's new "pixel array detector" combined with cryo-electron microscopy (imaging and spectroscopy) to image/analyze thin ionomer layers in optimized PGM-free electrode morphologies.

ElectroCat Annual Milestone

- Achieve PGM-free cathode MEA performance in an H₂-O₂ fuel cell of 25 mA cm⁻² at 0.90 V (*iR*-corrected) at 1.0 bar partial pressure of O₂ and cell temperature 80°C; define performance-limiting catalyst and electrode

properties to guide the synthesis of PGM-free catalysts and fabrication of electrodes/MEAs.

Technical Barriers

This project addresses the following technical barriers from the Fuel Cells section of the Fuel Cell Technologies Office Multi-Year Research, Development, and Demonstration Plan¹:

- (A) Durability (catalyst, MEA)
- (B) Cost (catalyst)
- (C) Performance (catalyst, MEA).

Technical Targets

This project focuses on the development and implementation of high-performing and durable PGM-free cathode catalysts for polymer electrolyte fuel cells (PEFCs), following DOE technical targets outlined in the Fuel Cells section of the Multi-Year Research, Development, and Demonstration Plan.¹ The overall goal is durable PGM-free ORR catalysts that achieve an activity of 0.044 A/cm² at 0.90 V in a PEFC MEA by 2020.

FY 2018 Accomplishments

ElectroCat Development and Communication

- National laboratories are supporting four federal funding opportunity announcement (FOA) projects with 10 capabilities.
- New national laboratory capabilities were submitted, reviewed, and selected by DOE and the Steering Committee in April 2018.
- A publicly accessible data-management hub for national laboratory and FOA project datasets was developed and launched (<https://datahub.electrocat.org>).
- Nine papers were published, including one in *Science*, and 28 presentations were given (11 invited).

Performance Improvement

- Accomplished and exceeded ElectroCat FY 2017 annual milestones of 20 mA cm⁻² at 0.90

¹ <https://energy.gov/eere/fuelcells/downloads/fuel-cell-technologies-office-multi-year-research-development-and-22>

V (H₂/O₂, *i*_{R-free}) and 100 mA cm⁻² at 0.80 V (H₂/air).

- Achieved four-fold improvement of the H₂-air fuel cell performance at 0.80 V of the (AD)Fe-N-C catalyst, from 9 mA cm⁻² to 36 mA cm⁻² since the 2017 report.
- Reached half-wave potential (*E*_{1/2}) of 0.85 V with (AD)Fe-N-C in RDE testing, an increase of 0.02 V over the 2017 status.
- Improved PGM-free catalyst activity in an MEA: 21 mA/cm² at 0.90 V_{*i*_{R-free}} and 0.044 A/cm² at 0.88 V (H₂-O₂ fuel cell).

Characterization and Capability Development

- Correlated ORR activity with FeN₄ content; identified spectroscopic signatures of FeN₄ content.
- Determined that FeN_x site is formed and zinc is removed from Fe-Zn-ZIF at temperatures as low as 900°C.
- Successfully used NO and NO₂⁻ as molecular probes for ORR-active surface sites.
- Obtained further direct evidence of a majority of Fe sites being atomically dispersed and on the (AD)Fe-N-C catalyst surface using TEM, a molecular probe, and X-ray spectroscopy.
- Used TEM and XAFS to characterize Fe species and structure evolution during heat treatment, obtaining guidance for improved catalyst synthesis.

- Characterized the atomic structure and ORR activity of 40 combinatorial (Zn_{1-x}Fe_x)ZIF-F catalysts using XAFS and m-CFDE cell, identifying materials with potentially >5x ORR activity of baseline composition.
- Developed system for automated deposition of multiple inks resulting in *E*_{1/2} agreement between m-CFDE and RDE of 5 mV for PGM-free catalysts.
- Further refined the capability to characterize by XAFS the atomic structure of catalysts during heat treatment, determining the evolution of Fe species.
- Acquired MEA kinetic data for (AD)Fe-N-C cathode and applied the distributed ORR model to determine reaction order, activation energy, and the potential dependence of active site availability.

ORR Active-Site Activity and Durability Modeling

- Calculated binding energies of potential probes/poisons to various active-site structures.
- Utilized model descriptors to determine that N loss is likely responsible for PGM-free catalyst activity decrease.
- Developed and utilized logistic decay model to describe autocatalytic degradation mechanism of PGM-free catalysts.

Table 1. Progress Toward Meeting Technical Targets for PGM-Free Electrocatalysts and MEAs for Transportation Applications

Characteristic	Units	DOE 2025 Electrocatalyst and MEA Targets	ElectroCat Status
H ₂ -air fuel cell performance	mA/cm ² @ 800 mV (measured)	300	105
PGM-free catalyst activity	mA/cm ² @ 900 mV _{<i>i</i>_{R-free}}	≥44	21

INTRODUCTION AND APPROACH

ElectroCat, a DOE Energy Materials Network (EMN) consortium, uses the EMN approach to accelerate the development and implementation of PGM-free fuel cell materials. The EMN consortia leverage the existing relevant capabilities of the DOE national laboratories and develop missing strategic capabilities to accelerate core research toward discovery, development, and scale-up of materials. The EMN consortia also aid competitively selected projects led by industry, academia, and other national laboratories. Critical aspects of the EMN approach are the use of predictive simulation across all scales; high-throughput materials synthesis, screening, and characterization; and rapid data mining, correlation, and publication. In the materials discovery and development arena, ElectroCat is focused on developing and implementing PGM-free catalysts and electrodes for PEFCs. In addition to the development of PGM-free catalysts, ElectroCat focuses on creating the tools and catalyst information database critical to industrial deployment of PGM-free catalyst fuel cells.

RESULTS

Consortium Development

ElectroCat is comprised of four core national laboratories contributing their expertise in characterization, materials, and electrode synthesis/fabrication testing and diagnostics, modeling, and fabrication. These existing and demonstrated capabilities were utilized in 2018 to support the R&D efforts in the four ElectroCat 2017 FOA projects. Critical aspects of the EMN consortia are the evaluation of the utility of existing capabilities and the influx of new capabilities. This year, two capabilities were discontinued and four capabilities were added. These new capabilities—currently under evaluation—are in the areas of temperature-programmed desorption of probe molecules, wetting properties of catalysts, refined calculation of reaction energetics, and electrospinning of electrodes.

PGM-Free Catalyst Development and Characterization

Catalysts with improved microporosity: Highly porous PGM-free catalysts developed from a simple synthesis process using Zn salts (zinc chloride) and cyanamide and polyaniline as the sources of carbon and nitrogen, were further improved by using magnetic separation to decrease the content of undesired iron species prior to a final heat treatment in an inert atmosphere. Catalyst performance in the fuel cell also was improved by tuning the ionomer content and ionomer type utilized in the cathode catalyst layer. A hydrogen-oxygen fuel cell performance of 21 mA cm⁻² at 0.90 V (*iR*-free) and a hydrogen-air fuel cell performance of 105 mA cm⁻² were achieved using this approach. The hydrogen-oxygen performance exceeded the ElectroCat annual milestone of 20 mA cm⁻² and the hydrogen-air performance represents an increase of 28% over that reported in the 2017 ElectroCat Annual Progress Report (Figure 1).

Catalysts with atomically dispersed transition-metal sites: Nitrogen-doped PGM-free catalysts containing atomically-dispersed Fe, (AD)Fe-N-C, were synthesized using Zn-derived ZIFs as the parent structures. The synthesis of the catalyst precursor has been tuned to achieve a fibrous structure with the goal of enhancing the porosity of the resulting catalyst. By tuning the catalyst synthesis procedure and the electrode composition, the hydrogen-air fuel cell performance of the (AD)Fe-N-C catalyst was improved four-fold (9 mA cm⁻² to 36 mA cm⁻² at 0.80 V) since publication of the ElectroCat 2017 Annual Progress Report (Figure 2). The ORR activity of these catalysts has been correlated with their FeN_x content using linear combination fitting of the XANES spectra. XAFS analyses of these materials during the heat-treatment synthetic step shows that the proposed FeN_x active sites are formed between 650°C and 885°C (Figure 3), concurrent with Zn evaporation. The XAFS analyses also showed that FeN_x can be converted to iron carbide and metal during the heat treatment step of holding at 1,000°C. The purpose of these studies is to guide the synthetic effort in maximizing the volumetric density of FeN_x sites to enhance the ORR activity of this class of catalysts.

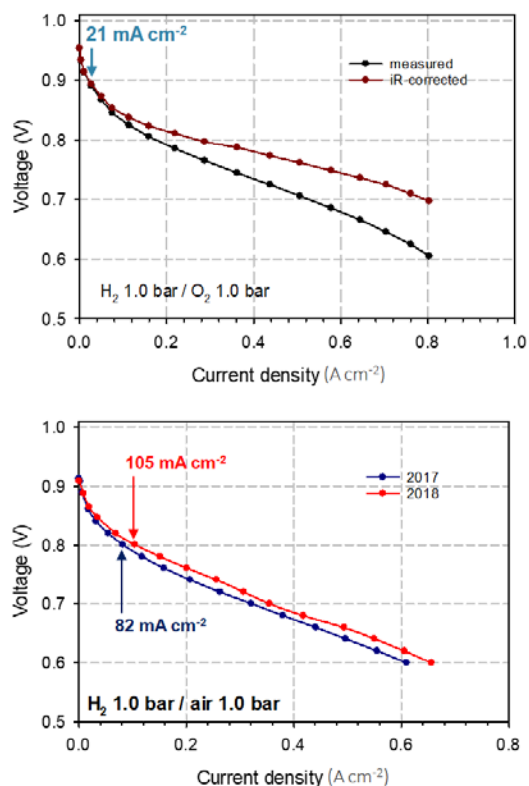


Figure 1. Hydrogen-oxygen performance and improvement in hydrogen-air fuel cell performance of (CM+PANI)-Fe-C(Zn) PGM-free catalyst compared to 2017 performance reported at the DOE 2017 Annual Merit Review

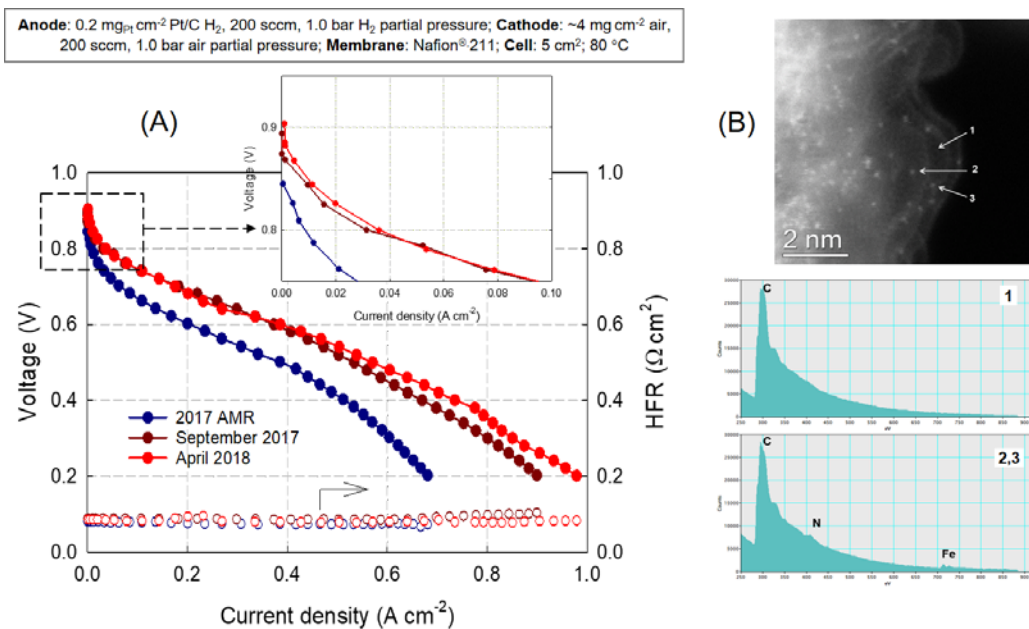


Figure 2. (A) Improvement of hydrogen-air fuel cell performance of (AD)Fe-N-C catalyst (red curve) compared to September 2017 and performance reported at DOE 2017 Annual Merit Review. (B) High-resolution TEM image and electron energy loss spectra of the (AD)Fe-N-C catalyst.

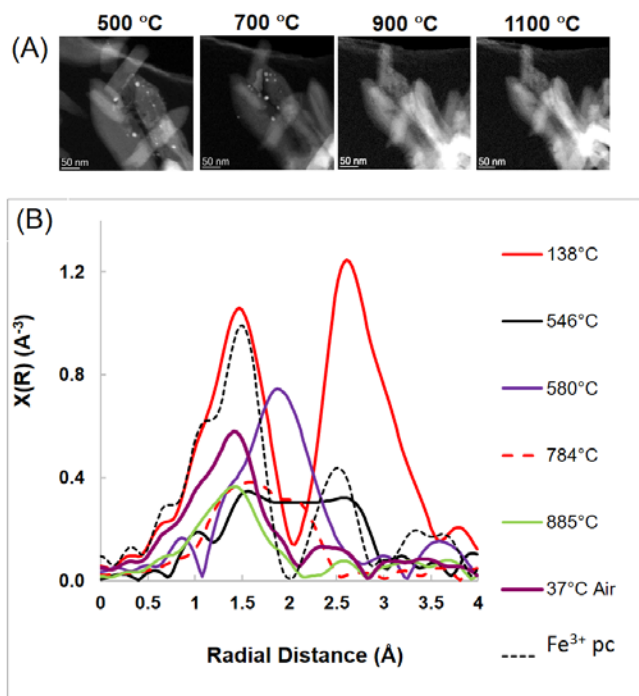


Figure 3. (A) TEM micrographs of (AD)Fe-N-C precursor during heat treatment. (B) Fourier transforms of iron K-edge XAFS showing evolution of iron speciation in the (AD)Fe-N-C catalyst precursor during high temperature heat treatment. The Fourier transform of an FeN_4 standard (Fe^{3+} phthalocyanine, Fe^{3+} pc) is shown for comparison (dotted line).

Direct detection of active sites: Spectroscopic and electrochemical experiments with probe molecules were utilized to determine the density of active sites in the (AD)Fe-N-C class of catalysts (Figure 4). These experiments—utilizing nitrite as a source of the nitric oxide probe molecule—showed that the active site density is approximately 3×10^{12} sites cm^{-2} (approximately 0.5/Fe atom) and that the turnover frequency for ORR on these sites at 0.80 V is $1.7 \text{ e}^- \text{ site}^{-1} \text{ s}^{-1}$. The accompanying potential-dependent XAFS data indicate that poisoning of the ORR occurs both with and without coordination of nitric oxide to the Fe center, pointing to a complex multi-atom active site or multiple active sites, beyond FeN_x alone. Accompanying density functional theory calculations have identified that probe molecules bind to Fe and to the graphene only in the presence of defects or epoxides local to the FeN_x sites.

ORR kinetics: Multiple MEAs with (AD)Fe-N-C cathode catalysts were tested under a variety of oxygen partial pressures and temperatures and the results were utilized as input to a distributed ORR kinetic model to derive the ORR reaction order and activation energy. These data also were fit to a potential-dependent active site availability model, based on a reduced form of the Fe center being the active site. This fit showed that near the open circuit less than 10% of the active sites are available; 100% availability is achieved at approximately 0.65 V; and the redox potential for the Fe center is 0.79 V, agreeing well with voltammetric results (Figure 5). The effective number of electrons transferred in this redox transition was calculated to be 0.7, which agrees with that calculated from linear combination fitting of potential-dependent XAFS data.

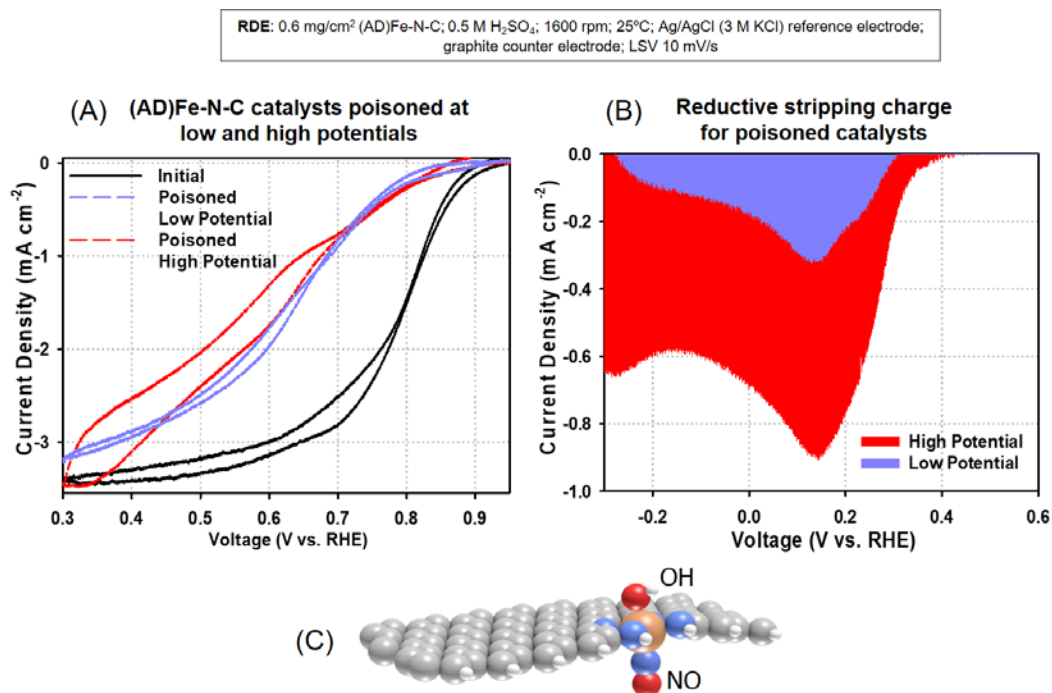


Figure 4. (A) Rotating disk electrode ORR traces of the (AD)Fe-N-C catalyst before and after exposure to nitrite probe at low and high potentials. (B) Voltammetric stripping charge for NO adsorbed from a nitrite solution at high and low potentials. (C) Depiction of active site poisoned by NO probe molecule.

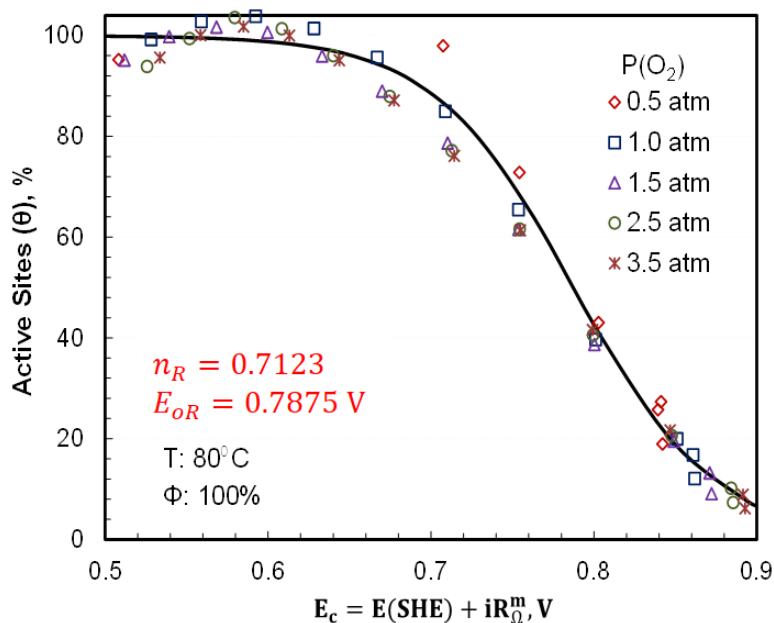


Figure 5. Fitting of the performance data for cells with (AD)Fe-N-C cathode catalyst taken with different cathode gas oxygen partial pressures to extract the availability of active sites as a function of iR -corrected cathode potential

Catalyst durability: A system was implemented for the parallel studies of F⁻, CO₂, and transition metal emissions from the cathode of an MEA at various operating conditions to gain better understanding of the possible degradation mechanisms of PGM-free catalysts. Degradation studies of the (CM+PANI)-Fe(Zn)-C catalyst operating on air showed low CO₂ and F⁻ emissions over all cell voltages. Carbon dioxide generation

increased when operating on oxygen instead of air, with the accompanying low fluoride emission rate pointing to the catalyst rather than the membrane being the source of the detected CO₂. Post-test characterization by scanning electron microscopy, EDX, and X-ray photoelectron spectroscopy (XPS) suggest that demetallation—likely following the loss of nitrogen coordination—is the main mechanism for activity loss of (CM+PANI)-Fe-C(Zn) catalysts (Figure 6). Kinetic models for MEA performance degradation suggest a two-step autocatalytic degradation mechanism where a deactivation agent, such as peroxide, is produced from the reactants.

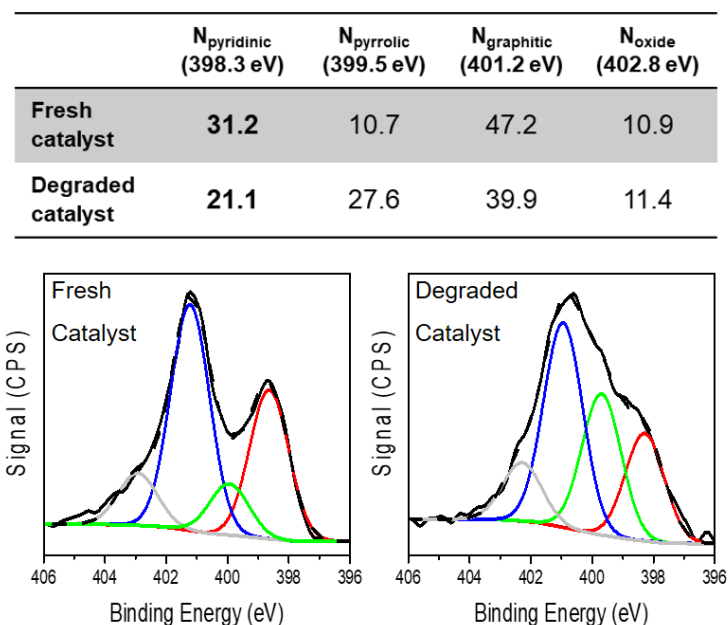


Figure 6. XPS spectra and XPS fitting results of a fresh (CM+PANI)-Fe-C(Zn) catalyst and of the same catalyst that has been degraded in an MEA

High-throughput synthesis, characterization, and performance evaluation of PGM-free catalysts and electrodes: A high-throughput and, where possible, combinatorial approach to synthesis, characterization, ORR-activity measurement, electrode fabrication, and fuel cell performance testing has been utilized to expedite progress toward achieving the ElectroCat goals. A robotic system was used to synthesis the (Zn_xFe_{1-x})ZIF-F catalyst precursors with five different iron contents and three different iron salts, and these precursors were heat-treated in a multi-sample tube furnace at three different temperatures to produce 40 unique samples. The ORR activities of the resulting catalysts were screened using a combinatorial hydrodynamic cell. The fuel cell performance was evaluated using 25-electrode combinatorial fuel cell hardware. The atomic structure, phase composition, and near-surface composition were characterized using X-ray diffraction, X-ray spectroscopy, electron energy loss spectroscopy, and XPS, respectively. The characterization showed that the fraction of Fe present as an FeN_x species was highest at the lowest heat-treatment temperature and with a Fe-to-Zn atomic ratio in the precursor of 2.5:97.5 (Figure 7). Higher heat-treatment temperatures and Fe contents favored formation of graphite-encased iron carbide species at the expense of FeN_x sites, and a reduction of near-surface Fe, pyridinic N, C/N, and clustering of atomically dispersed Fe and an increase in the degree of graphitization of the carbon matrix. The highest ORR activities were achieved using the iron nitrate and sulfate precursors, pyrolysis temperatures of 900°C and 1,000°C, and intermediate Fe-to-Zn atomic ratios (2.5:97.5 and 5:95).

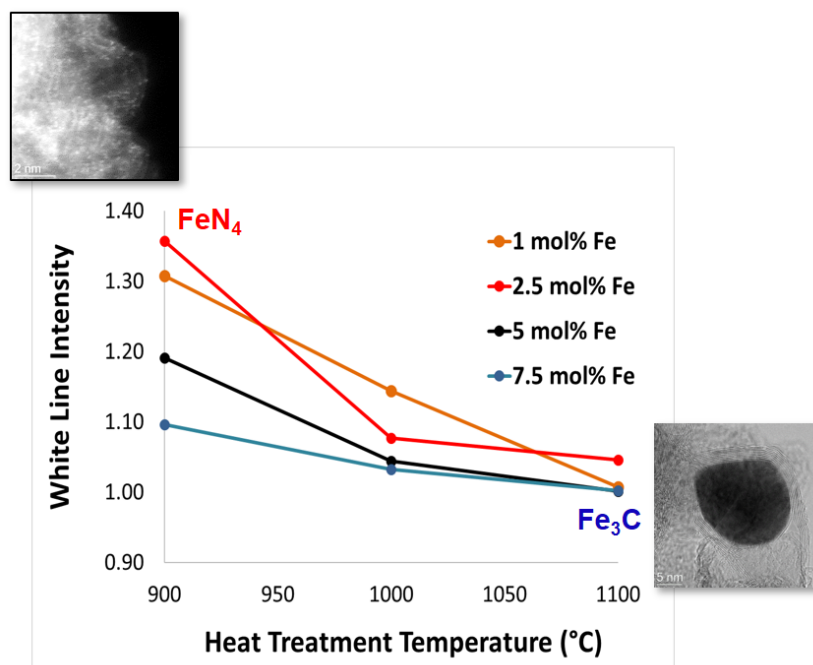


Figure 7. White line intensity in the Fe K-edge XAFS of (AD)Fe-N-C catalysts as a function of initial Fe content in the ZIF precursor and the heat-treatment temperature. The white line intensity has been shown to be proportional to the fraction of Fe in the FeN_4 coordination environment. Insets: atomic dispersion of Fe-N sites in catalyst (upper left) and graphite encased iron carbide particle (lower right).

Capability Development

ElectroCat is developing several capabilities that show potential to impact PGM-free electrocatalyst development. Examples of these capabilities are the combinatorial screening of catalyst activity using an m-CFDE cell and combinatorial fuel cell testing using segmented cell hardware. These capabilities were further developed and demonstrated this year. An automated deposition system using a programmable XY stage and a nanoliter injector was developed to deposit catalyst-ionomer inks on the 1-mm by 3-mm glassy carbon electrodes of the m-CFDE. An ORR half-wave potential agreement with RDE results of 5 mV was achieved using this deposition, versus the 30 mV agreement achieved last year with non-automated deposition. A system was developed for fabrication of electrodes with a gradient of catalyst/ionomer ratio and demonstrated for an 8-cm-long deposition. A Kelvin probe was validated as a quick screening tool to quantify ionomer gradients in electrodes. This deposition system is being used in concert with a segmented cell to accelerate the optimization of catalyst/ionomer ratio for improved performance of PGM-free electrodes and to evaluate the effects of electrode composition on durability.

CONCLUSIONS AND UPCOMING ACTIVITIES

The following are highlighted conclusions from the ElectroCat activities thus far.

- An Fe-N-C catalyst, (AD)Fe-N-C, was further developed and characterized this year resulting in a 20 mV increase in ORR half-wave potential in RDE testing versus last year's status, and a four-fold improvement in fuel cell performance at 0.80 V (36 mA cm^{-2} versus 9 mA cm^{-2}). This catalyst has the majority of Fe sites on the surface of the catalyst and able to adsorb probe molecules and oxygen with a representative active site density of approximately $3 \times 10^{12} \text{ sites cm}^{-2}$ and an ORR turnover frequency of $1.7 \text{ e}^- \text{ site}^{-1} \text{ s}^{-1}$. ORR activity was correlated with FeN_x species content in the catalyst.

- The proposed FeN_x active sites are formed at temperatures as low as 900°C, with higher temperatures causing formation of inactive carbide species and clustering of the atomically-dispersed Fe sites but formation of the more stable graphitic versus amorphous carbon.
- Availability of the (AD)Fe-N-C active sites in a fuel cell electrode was correlated with reduction of the Fe center with a fit redox potential of 0.79 V and ORR reaction order and activation energy of 0.70 kJ/mol and 62 kJ/mol, respectively.
- PGM-free catalyst activity in an MEA of 21 mA cm⁻² at 0.90 V_{iR-free} and hydrogen-air performance of 105 mA cm⁻² were achieved using the CM-PANI-Fe-C(Zn) catalyst.
- Loss of PGM-free electrode performance is primarily due to loss of catalyst ORR activity, with results thus far suggesting activity loss is related to demetallation, likely following the loss of nitrogen coordination through a two-step autocatalytic degradation mechanism.

The following are the remaining challenges and barriers in developing and implementing PGM-free ORR catalysts.

- Insufficient stability of metal organic framework-based catalyst powders and electrodes.
- Limited stability of PGM-free electrodes under steady-state and load-cycling conditions.
- Inadequate understanding of the catalyst and electrode degradation mechanism.
- ORR activity of PGM-free catalysts in continued need of further improvement to reduce cathode thickness and lower cost of other stack components.
- Development of surface-specific characterization techniques and molecular probes for carbon-based materials.
- Electrode design and catalyst-ionomer integration to provide adequate ionic, electronic, and mass transport to and from active sites.
- Replacement of Fe in catalyst with another PGM-free transition metal not catalyzing hydroperoxyl radical formation and ionomer degradation.
- Integration with existing automotive fuel cell stack and system technology.

The focus of future work to address these challenges includes the following.

ElectroCat Development

- Demonstrate or utilize recently selected national laboratory capabilities.
- Incorporate collaborators from DE-FOA-0001874 into ElectroCat and coordinate activities of all ElectroCat partners.
- Populate Data Hub with datasets from national laboratory and FOA partners; implement automated methods for data capture and publication.
- Develop automated artificial intelligence and machine learning techniques for data correlation and experimental design.

Improvement in Performance and Durability of Catalysts and Electrodes

- Further identify primary factors governing the durability of PGM-free catalysts and electrodes, and develop means to prevent performance degradation.
- Advance fuel cell performance of catalysts by maximizing volumetric density and accessibility of active sites, through the development of novel synthesis approaches, using information from in situ characterization techniques; and optimization of hierarchical pore-size and ionomer distribution, using information from imaging, X-ray scattering, and multi-scale modeling efforts.
- Verify synthesis and activity of promising materials (e.g., 900°C, 5 at% Fe) identified in initial screening, scale up synthesis, and test fuel cell performance and durability.
- Continue to develop surface-specific methods for ORR active-site determination (e.g., probe molecules).

SPECIAL RECOGNITIONS AND AWARDS/PATENTS ISSUED

1. 2017 R&D 100 Award for *Clean-Energy Electrocatalysts Without Precious Metals*, Los Alamos National Laboratory, P. Zelenay (PI) (joint entry with Pajarito Powder, LLC).

FY 2018 PUBLICATIONS/PRESENTATIONS

Publications

1. Chung, H.T., D.A. Cullen, D. Higgins, B.T. Sneed, E.F. Holby, K.L. More, and P. Zelenay. "Direct Atomic-Level Insight into the Active Sites of a High-Performance PGM-Free ORR Catalyst." *Science* 357 (6350), 479–484, 2017.
2. Dekel, D.R., M. Page, C. Bae, Y. Yan, P. Zelenay, Y.S. Kim, and S. Gottesfeld. "Anion Exchange Membrane Fuel Cells: Current Status and Remaining Challenges." *J. Power Sources* 375, 351–360, 2018.
3. Kneebone, J.L., S.L. Daifuku, J.A. Kehl, G. Wu, H.T. Chung, M.Y. Hu, E.E. Alp, K.L. More, P. Zelenay, E.F. Holby, and M.L. Neidig. "A Combined Probe-Molecule, Mössbauer, Nuclear Resonance Vibrational Spectroscopy and Density Functional Theory Approach for Evaluation of Potential Iron Active Sites in an Oxygen Reduction Reaction Catalyst." *J. Phys. Chem. C* 121 (30), 16283–16290, 2017.
4. Komini Babu, S., H.T. Chung, P. Zelenay, and S. Litster. "Modeling Electrochemical Performance of the Hierarchical Morphology of Precious Group Metal-Free Cathode for Polymer Electrolyte Fuel Cell." *J. Electrochem. Soc.* 164 (9), F1037–F1049, 2017.
5. Kulesza, P.J., J.K. Zak, I.A. Rutkowska, B. Dembinska, S. Zoladek, K. Miecznikowski, E. Negro, V. Di Noto, and P. Zelenay. "Elucidation of Role of Graphene in Catalytic Designs for Electroreduction of Oxygen." *Curr. Opin. Electrochem.* <https://doi.org/10.1016/j.coelec.2018.05.012> (published online on May 19, 2018).
6. Martinez, U., S. Komini Babu, E.F. Holby, and P. Zelenay. "Durability Challenges and Perspective in the Development of PGM-Free Electrocatalysts." *Curr. Opin. Electrochem.* 10.1016/j.coelec.2018.04.010, 2018 (published on-line April 26, 2018).
7. Mukherjee, S., D.A. Cullen, S. Karakalos, K. Liu, H. Zhang, S. Zhao, K.L. More, G. Wang, and G. Wu. "Metal-Organic Framework-Derived Nitrogen-Doped Highly Disordered Carbon for Electrochemical Ammonia Synthesis Using N₂ and H₂O in Alkaline Electrolytes." *Nano Energy* 48, 217–226, 2018.
8. Thompson, S.T., A.R. Wilson, P. Zelenay, D.J. Myers, K.L. More, K.C. Neyerlin, and D. Papageorgopolous. "ElectroCat: DOE's Approach to PGM-Free Catalyst and Electrode R&D." *Solid State Ionics* 319, 68–76, 2018.
9. Yin, X., L. Lin, H.T. Chung, S. Komini Babu, U. Martinez, G.M. Purdy, and P. Zelenay. "Effects of MEA Fabrication and Ionomer Composition on Fuel Cell Performance of PGM-Free ORR Catalyst." *ECS Trans.* 77 (11) 1273–1281, 2017.

Presentations

1. Cetinbas, C.F., X. Wang, R.K. Ahluwalia, N.N. Kariuki, R. Winarski, V.J. De Andrade, and D.J. Myers. “PEFC Cathode Catalyst Layer Electrode Microstructure Analysis and Transport Modeling” (invited lecture). 21st International Conference on Solid State Ionics (SSI-21), Padua, Italy, June 18–23, 2017.
2. Cetinbas, F., N. Kariuki, R. Ahluwalia, H.T. Chung, P. Zelenay, and D.J. Myers. “PGM-Free Electrode Microstructure Analysis and Transport Modeling.” 232nd Meeting of the Electrochemical Society, National Harbor, Maryland, October 1–5, 2017.
3. Chung, H., D.A. Cullen, B.T. Sneed, H.M. Meyer III, L. Lin, X. Yin, K.L. More, and P. Zelenay. “Atomically Dispersed (AD)Fe-N-C Oxygen Reduction Catalysts for Polymer Electrolyte Membrane Fuel Cells.” 232nd Meeting of the Electrochemical Society, National Harbor, Maryland, October 1–5, 2017.
4. Cullen, D.A., B.T. Sneed, and K.L. More. “Overcoming the Challenges of Beam-Sensitivity in Fuel Cell Electrodes.” Microscopy & Microanalysis 2017, St. Louis, Missouri, August 6–10, 2017.
5. Cullen, D.A., B.T. Sneed, G. Wu, J. Spendelow, H.T. Chung, P. Zelenay, and K.L. More. “Electron Microscopy Observations of Catalyst-Support Interactions in Polymer Electrolyte Membrane Fuel Cells.” 232nd Meeting of the Electrochemical Society, National Harbor, Maryland, October 1–5, 2017.
6. Holby, E.F., U. Martinez, H.T. Chung, and P. Zelenay. “Modeling Durability of PGM-Free Active Site Structures at the Atomic Scale.” 232nd Meeting of the Electrochemical Society, National Harbor, Maryland, October 1–5, 2017.
7. Komini Babu, S., S. Ogawa, H.T. Chung, P. Zelenay, and S. Litster. “Porous Electrode Engineering for Platinum Group Metal-Free Oxygen Reduction Reaction Catalysts” (invited lecture). 231st Meeting of the Electrochemical Society, New Orleans, Louisiana, May 28–June 1, 2017.
8. Komini Babu, S., U. Martinez, H. Chung, L. Lin, X. Yin, and P. Zelenay. “Influence of Transition Metal and Synthesis Methodology on the Active Site Density on the Surface of PGM-Free Catalysts.” 232nd Meeting of the Electrochemical Society, National Harbor, Maryland, October 1–5, 2017.
9. Martinez, U., S. Komini Babu, H.T. Chung, L. Lin, G.M. Purdy, and P. Zelenay. “Structure-Activity-Durability Relationships of (CM+PANI)-Me-C PGM-free Catalysts.” 232nd Meeting of the Electrochemical Society, National Harbor, Maryland, October 1–5, 2017.
10. Myers, D. “Activity, Performance, and Durability of Polymer Electrolyte Fuel Cell Catalysts and Electrodes” (invited lecture). 2nd International Fuel Cells Workshop, Ramat Gan, Israel, October 30–31, 2017.
11. Myers, D., J. Park, N. Kariuki, M. Ferrandon, A.J. Kropf, D. Yang, H. Lv, A. Zakutayev, G. Bender, and H. Dinh. “High-Throughput Experimental Activities in ElectroCat.” ElectroCat Modeling Workshop, Washington, D.C., September 20, 2017.
12. Myers, D.J., M. Ferrandon, A.J. Kropf, D. Yang, N.N. Kariuki, J. Park, and S. Lee. “High-Throughput Synthesis and Characterization of PGM-Free Oxygen Reduction Reaction Electrocatalysts.” 232nd Meeting of the Electrochemical Society, National Harbor, Maryland, October 1–5, 2017.
13. Ogawa, S., S. Komini Babu, E. Padgett, H.T. Chung, P. Zelenay, A. Kongkanand, and S. Litster. “Microstructural Modeling of PEFC Catalyst Layer Performance and Durability.” 232nd Meeting of the Electrochemical Society, National Harbor, Maryland, October 1–5, 2017.
14. Wilson, A.R., D.C. Papageorgopoulos, D.J. Myers, P. Zelenay, H.N. Dinh, and K.L. More. “The Electrocat (Electrocatalysis) Consortium” (invited lecture). 231st Meeting of the Electrochemical Society, New Orleans, Louisiana, May 28–June 1, 2017.
15. Yin, X., H.T. Chung, L. Lin, G.M. Purdy, U. Martinez, and P. Zelenay. “High-Performance PGM-Free Electrocatalysts for the Polymer Electrolyte Fuel Cell Cathode” (invited lecture). 231st Meeting of the Electrochemical Society, New Orleans, Louisiana, May 28–June 1, 2017.

16. Yin, X., L. Lin, H.T. Chung, S. Komini Babu, U. Martinez, G.M. Purdy, and P. Zelenay. “Effects of Porosity and Ionomer Composition on Fuel Cell Performance of PGM-Free ORR Catalysts.” 231st Meeting of the Electrochemical Society, New Orleans, Louisiana, May 28–June 1, 2017.
17. Yin, X., L. Lin, U. Martinez, H.T. Chung, and P. Zelenay. “Organic Molecular Catalyst for Electrochemical Production of Hydrogen Peroxide.” 232nd Meeting of the Electrochemical Society, National Harbor, Maryland, October 1–5, 2017.
18. Zelenay, P. “ElectroCat Overview” (invited lecture). ElectroCat Modeling Workshop, Washington, D.C., September 20, 2017.
19. Zelenay, P. “Electrocatalysis of Oxygen Reduction at Platinum Group Metal-Free Catalysts” (invited lecture). University of California Merced, School of Natural Sciences, Chemistry and Chemical Biology, Merced, California, October 20, 2017.
20. Zelenay, P. “Electrocatalysis Without Precious Metals” (invited lecture). American Chemical Society National Meeting and Exposition, March 18–22, 2018.
21. Zelenay, P. “Introduction to PGM-Free Catalysis and Protocols.” DOE Catalysis-Durability Working Group Meeting, Argonne National Laboratory, Lemont, Illinois, May 2–3, 2017.
22. Zelenay, P. “Oxygen Reduction at Platinum Group Metal-Free Electrocatalysts: Progress in Performance and Understanding of Reaction Mechanism” (invited lecture). Colorado School of Mines, Golden, Colorado, December 8, 2017.
23. Zelenay, P. “PGM-Free Electrocatalysts for Oxygen Reduction Reaction in Fuel Cells: State of the Art and Challenges” (invited lecture). University of California Santa Cruz, Chemistry and Biochemistry, Santa Cruz, California, October 23, 2017.
24. Zelenay, P. “PGM-Free ORR Electrocatalysis: Progress and Challenges on the Path to Viability” (invited lecture). Israel Research Center for Electrochemical Propulsion (INREP) Energy Conference, Bar-Ilan University, Ramat Gan, Israel, May 9–10, 2017.
25. Zelenay, P. “Platinum Group Metal-Free Electrocatalysts for Oxygen Reduction in Fuel Cells” (invited lecture). Milan Polytechnic, Milan, Italy, June 27, 2017.
26. Zelenay, P. “Recent Developments in PGM-Free Electrocatalysis of Oxygen Reduction” (invited lecture). 2nd International Fuel Cells Workshop, Ramat Gan, Israel, October 30–31, 2017.
27. Zelenay, P., and D.J. Myers. “ElectroCat (Electrocatalysis Consortium).” U.S. Department of Energy, Energy Efficiency and Renewable Energy, Fuel Cell Technologies Program, 2017 Merit Review and Peer Evaluation Meeting, Washington, D.C., June 5–9, 2017.
28. Zhang, H., H.T. Chung, D.A. Cullen, K.L. More, P. Zelenay, and G. Wu. “Metal-Organic Framework-Derived Atomic Iron-Dispersed Carbon Electrocatalysts for Oxygen Reduction in Acidic Polymer Electrolyte Fuel Cells.” 231st Meeting of the Electrochemical Society, New Orleans, Louisiana, May 28–June 1, 2017.

Advanced Electrocatalysts Through Crystallographic Enhancement

Jacob S. Spendelow (Primary Contact),
Yung-Tin Pan, Dongguo Li, and Yu Seung Kim
Los Alamos National Laboratory
P.O. Box 1663
Los Alamos, NM 87545
Phone: (505) 667-9434
Email: spendelow@lanl.gov

DOE Manager: Nancy Garland
Phone: (202) 586-5673
Email: Nancy.Garland@ee.doe.gov

Subcontractors:

- Brown University, Providence, RI
- University of Pennsylvania, Philadelphia, PA
- State University of New York at Buffalo, Buffalo, NY
- EWII Fuel Cells, Albuquerque, NM

Project Start Date: October 1, 2016
Project End Date: June 30, 2019

Overall Objectives

- Design and synthesize fully ordered intermetallic MPt (M represents non-precious metals other than iron) nanoparticles.
- Optimize the Pt-support interaction to maximize the catalyst activity and durability.
- Establish effective material interfaces in membrane electrode assemblies (MEAs).
- Scale-up to 50 cm² MEAs and synthesize gram-scale batches of carbon-supported alloy nanoparticles.

Fiscal Year (FY) 2018 Objectives

- Synthesize ordered L1₀-CoPt nanoparticles from Co and Pt precursors and perform initial electrochemical characterization.
- Synthesize at least two distinct nitrogen-doped supports and compare their properties as catalyst supports.

- Demonstrate 0.44 A/mg_{PGM} mass activity in MEA testing with an Fe-free system at 0.9 V, H₂/O₂, 150 kPa_{abs}.
- Develop alternative fct-CoPt synthetic pathway using deposition on Pt nanoparticle seeds.
- Develop atomistic models that attribute reactivity changes to strain, ligand, and crystal structure for L1₀-CoPt system.

Technical Barriers

This project addresses the following technical barriers from the Fuel Cells section of the Fuel Cell Technologies Office Multi-Year Research, Development, and Demonstration Plan¹:

- (A) Durability
- (B) Cost
- (C) Performance.

Technical Targets

Technical targets are detailed in Table 1.

FY 2018 Accomplishments

- Synthesized and tested several classes of L1₀-CoPt nanoparticles.
- Demonstrated mass activity as high as 0.67 A/mg_{PGM} in MEA testing with small L1₀-CoPt nanoparticles (4-nm particle size).
- Demonstrated mass activity as high as 0.56 A/mg_{PGM} and less than 20% loss in mass activity after catalyst accelerated stress test (AST) in MEA testing with large L1₀-CoPt nanoparticles (9-nm particle size).

¹ <https://energy.gov/eere/fuelcells/downloads/fuel-cell-technologies-office-multi-year-research-development-and-22>

Table 1. Progress Toward Meeting Technical Targets for Electrocatalysts and MEAs for Transportation Applications

Characteristic	Units	DOE 2020 Electrocatalyst and MEA Targets	Project Status (5 cm ² cell, differential conditions)
Mass activity	A/mg PGM @ 0.9 mV _{iR-free}	≥0.44	0.67
Mass activity loss after catalyst AST	%	<40	54
Loss at 0.8 A/cm ² after catalyst AST	mV	30	34
MEA performance	mA/cm ² @ 800 mV	≥300	420
MEA performance	mW/cm ² @ rated power (670 mV)	≥1,000	830

INTRODUCTION

Platinum intermetallic nanoparticles recently have been demonstrated as promising catalytic materials for fuel cells and other electrochemical energy technologies [1–3], with initial results suggesting that these intermetallic structures can have greater performance and durability than disordered alloys in electrochemical applications such as fuel cells. Most work to date, however, has used partially-ordered nanoparticles. Scalable synthesis of fully-ordered intermetallics with high surface-to-volume ratio is a key challenge preventing advancement of this field. The goal of this project is to develop novel synthetic routes to prepare monodisperse, highly-ordered, high surface area intermetallics in large quantities with high quality control and with good performance and durability.

APPROACH

The overall approach is to synthesize advanced fuel cell catalysts based on intermetallic alloys and subject them to performance and durability testing in MEAs. The targeted catalysts consist of ordered intermetallic alloy nanoparticles, and they are being developed at Los Alamos National Laboratory (LANL) as well as at the subcontractor facilities, Brown University and University of Pennsylvania. The advanced catalyst nanoparticles are being supported on high-performance nitrogen-doped carbon supports as developed by subcontractor the State University of New York (SUNY) at Buffalo, as well as on commercially-available carbon supports. Catalysts examined include PtFe, PtNi, and PtCo, with subsequent examination of ternary catalyst systems. Although PtFe is being examined as a model catalyst, the project team is working to remove all Fe from the catalyst system to alleviate durability concerns.

By forming ordered intermetallic compounds with $L1_0$ structure, the project team seeks to produce catalysts that retain high activity during durability testing with reduced leaching of base metal components when compared with conventional non-ordered alloys. Theory-based design principles based on a machine-learning technique developed at Brown University are being used to guide the catalyst development.

RESULTS

The team developed several high-performance, durable intermetallic PtCo catalysts in the project in FY 2018. An $L1_0$ -CoPt catalyst with relatively large particle size (9 nm) was the first catalyst developed that met the DOE targets for mass activity and durability. This promising catalyst exhibited highly ordered structure even after the 30,000-cycle DOE catalyst AST, as demonstrated by comparison of X-ray diffraction (XRD) patterns before and after testing (Figure 1). This remarkable stability of the ordered structure and high resistance to Co leaching leads to excellent retention of catalytic activity. High-resolution scanning transmission electron microscopy–energy-dispersive spectroscopy (STEM-EDS) (shows an approximately 1-nm Pt shell surrounding a $Pt_{50}Co_{50}$ core after the AST (total particle composition $Pt_{70}Co_{30}$). High-resolution high angle annular dark field–scanning transmission electron microscopy (HAADF-STEM) shown in Figure 2 reveals that a highly ordered core remains after AST, coated with a ~ 0.7 – 1.0 nm Pt shell (3 to 4 atoms thick), in agreement with the STEM-EDS results. This observation is significant because it demonstrates that atomic-level ordering can be maintained even after durability testing. Co leaching occurs only from surface, forming a Pt shell that protects the particle interior from further leaching. This Pt shell is too thick for significant Co-induced ligand enhancement of oxygen reduction reaction kinetics after the AST, but the kinetic enhancement due to strain remains even after 30,000 cycles.

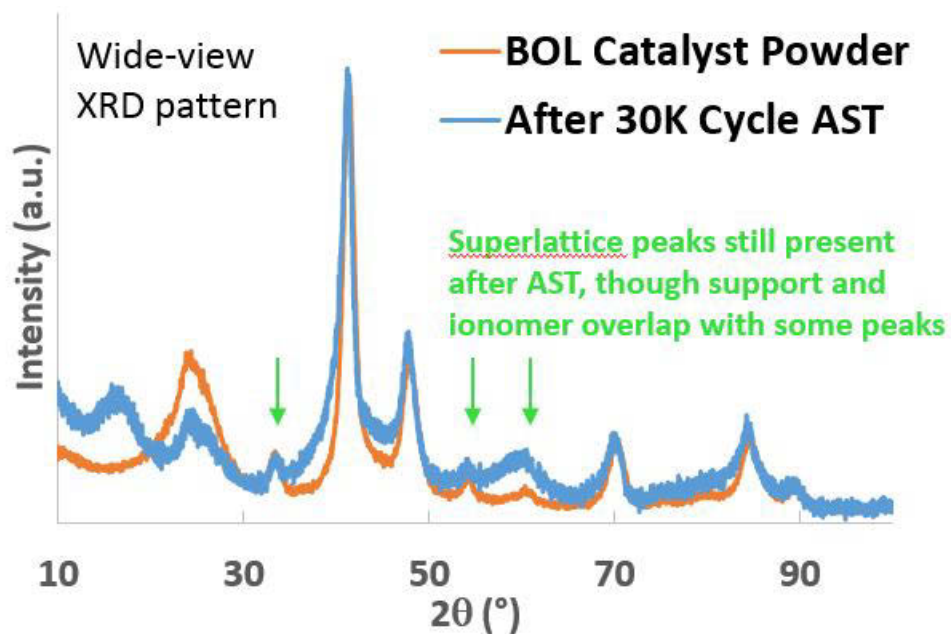


Figure 1. XRD patterns recorded on fresh $L1_0$ -CoPt catalyst powder and on catalyst that had been subjected to the 30,000-cycle catalyst AST reveal similar superlattice peaks, indicating that the ordered structures remain intact even after durability testing

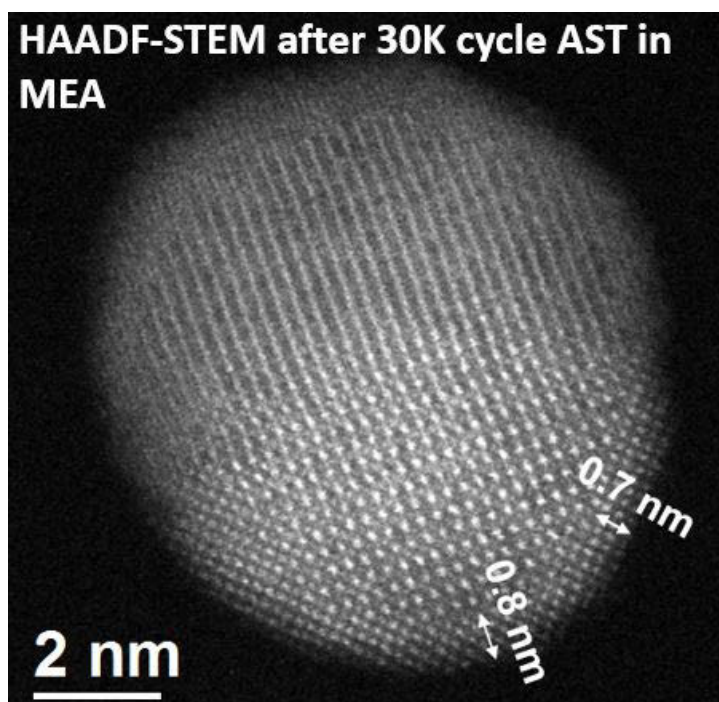


Figure 2. HAADF-STEM image of a particle showing the ordered $L1_0$ -CoPt structure after MEA testing

Though the mass activity and durability were promising, the large particle size of this L1₀-PtCo catalyst leads to low electrochemical surface area and poor performance at high current density. To get around this problem, L1₀-CoPt with smaller particle size is under development in the project. Initial results with 4-nm L1₀-CoPt developed using a novel seed-mediated synthesis and heat treatment approach are highly promising. Mass activity as high as 0.67 A/mg_{PGM}—well above the 0.44 A/mg_{PGM} target—has been demonstrated. More importantly, these catalysts exhibit good performance at high current density (Figure 3). Further work to improve the durability of these catalysts is underway.

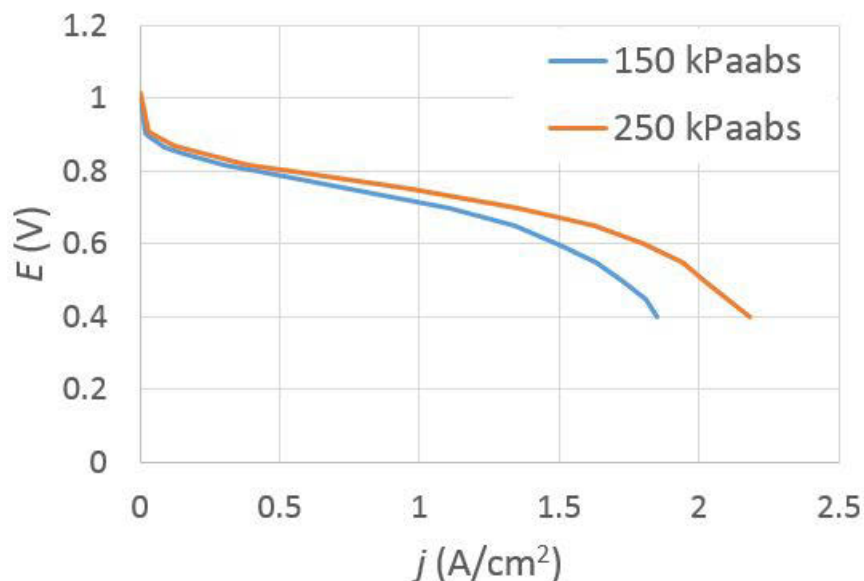


Figure 3. Small particle L1₀-CoPt catalysts provide high performance in fuel cell testing. Test conditions: H₂/air, 80 °C, 150 kPa_{abs}, 100% RH, 0.1 mgPt/cm² on cathode and anode

Computational modeling of base metal leaching using density functional theory calculations to predict the energetics of the diffusion process has been used to build understanding of the factors governing catalyst stability. Results from this work help guide design of more durable catalysts. A key finding in FY 2018 was that formation of a Pt skin on top of an L1₀-CoPt surface can slow down the rate of vacancy-mediated diffusion, leading to a 53-times increase in predicted stability. This improved understanding has guided synthetic efforts, including a greater focus on formation of high-quality Pt skins encapsulating L1₀-CoPt nanoparticles.

Several novel supports based on nitrogen-doped graphitic carbon were synthesized and used as supports for Pt nanoparticles. These catalysts exhibited good activity and stability in rotating disk electrode testing. Pt on carbon support from polyaniline hydrogel precursor was found to provide good polarization performance in MEA testing. Accelerated testing of these materials using the DOE support AST demonstrated little performance loss during the first 500 cycles, and better electrochemical surface area retention than Pt/Vulcan, but further improvement is needed to meet the 5,000-cycle durability target at 80 °C.

CONCLUSIONS AND UPCOMING ACTIVITIES

Results from FY 2018 have demonstrated the viability of the intermetallic L1₀ nanoparticle approach to achieve simultaneous improvements in performance and durability. Highly ordered L1₀ structures have greater resistance to base-metal leaching as compared to random alloys, and this improved leaching resistance is instrumental in providing good MEA durability.

The focus of the project in FY 2019 is on further developing the promising synthetic methods developed in FY 2018 and scaling up the most successful approaches to produce gram-scale batches. These larger batches will

be used to enable further MEA optimization and achievement of good high-current performance along with high mass activity and durability.

FY 2018 PUBLICATIONS/PRESENTATIONS

1. Dave Cullen, Brian Sneed, Karren More, Gang Wu, Jacob Spendelow, Hoon Chung, Ted Holby, Piotr Zelenay, “Electron Microscopy Observations of Catalyst-Support Interactions in Polymer Electrolyte Membrane Fuel Cells,” 232nd ECS Meeting, National Harbor, MD, October 2017.
2. J. Li and S. Sun, “Atomically Thin Pt Coated over Intermetallic FePt Nanoparticles for Efficient Oxygen Reduction Catalysis in Fuel Cells,” 255th ACS National Meeting, New Orleans, LA, March 2018.
3. J. Li, Z. Xi, Y.-T. Pan, J. S. Spendelow, P. N. Duchesne, D. Su, Q. Li, C. Yu, Z. Yin, B. Shen, Y. S. Kim, P. Zhang, S. Sun, “Fe Stabilization by Intermetallic L10-FePt and Pt Catalysis Enhancement in L10-FePt/Pt Nanoparticles for Efficient Oxygen Reduction Reaction in Fuel Cells,” *J. Am. Chem. Soc.* 40 (2018): 2926–2932.
4. Yung-Tin Pan, Yu Seung Kim, Junrui Li, Shouheng Sun, Jacob S. Spendelow, “Fuel Cell Performance and Durability of Intermetallic Oxygen Reduction Catalysts,” 233rd ECS Meeting, Seattle, WA, May 2018.
5. Yung-Tin Pan, Yu Seung Kim, Junrui Li, Shouheng Sun, Jacob S. Spendelow, “Fuel Cell Testing of Intermetallic Oxygen Reduction Catalysts,” 232nd ECS Meeting, National Harbor, MD, October 2017.
6. Shubham Sharma and Andrew Peterson, “Predictions of Oxygen Reduction Reaction (ORR) on Face-Centered Tetragonal (FCT) Platinum-Iron Alloy Surface Using Density Functional Theory,” 10th World Congress of Chemical Engineering, Barcelona, Spain (WCCE 2017).
7. Shubham Sharma and Andrew Peterson, “Predictions of Oxygen Reduction Reaction (ORR) on Face-Centered Tetragonal (FCT) Platinum-Iron Alloy Surface using Density Functional Theory,” Materials Research Society (MRS) Fall Meeting 2017, Boston, MA.
8. Shouheng Sun, “Synthetic Tuning of Nanoparticles to Achieve High Efficiency in Electrocatalysis,” MRS Spring Meeting, Phoenix, AZ, April 2–6, 2018.
9. Xiao Xia Wang, David Cullen, Yung-Tin Pan, Sooyeon Hwang, Maoyu Wang, Zhenxing Feng, Jingyun Wang, Mark Engelhard, Hanguang Zhang, Yuyan Shao, Dong Su, Karren More, Jacob Spendelow, Gang Wu, “Nitrogen Coordinated Single Cobalt Atom Catalysts for Oxygen Reduction in Proton Exchange Membrane Fuel Cells,” *Advanced Materials* 30, no. 11 (2018): 1706758.
10. Gang Wu, “Oxygen-Reduction Active Carbon Supports for Pt Cathode Catalysts in Polymer Electrolyte Fuel Cells,” 231st ECS Meeting, May 2017, New Orleans, LA.

REFERENCES

1. Minh T. Nguyen, Ryo H. Wakabayashi, Minghui Yang, Héctor D. Abruña, and Francis J. DiSalvo, “Synthesis of Carbon Supported Ordered Tetragonal Pseudo-Ternary $Pt_2M'M$ ” ($M = Fe, Co, Ni$) Nanoparticles and Their Activity for Oxygen Reduction Reaction,” *J. Power Sources* 280 (2015): 459–466.
2. Dong Young Chung, Samuel Woojoo Jun, Gabin Yoon, Soon Gu Kwon, Dong Yun Shin, Pilseon Seo, Ji Mun Yoo, Heejong Shin, Young-Hoon Chung, Hyunjoong Kim, Bongjin Simon Mun, Kug-Seung Lee, Nam-Suk Lee, Sung Jong Yoo, Dong-Hee Lim, Kisuk Kang, Yung-Eun Sung, and Taeghwan Hyeon, “Highly Durable and Active PtFe Nanocatalyst for Electrochemical Oxygen Reduction Reaction,” *J. Am. Chem. Soc.* 137 (2015): 15478–15485.
3. Q. Li, Liheng Wu, Gang Wu, Dong Su, Haifeng Lv, Sen Zhang, Wenlei Zhu, Anix Casimir, Huiyuan Zhu, Adriana Mendoza-Garcia, and Shouheng Sun, “New Approach to Fully Ordered Cct-FePt Nanoparticles for Much Enhanced Electrocatalysis in Acid,” *Nano Lett.* 15 (2015): 2468–2473.

Vapor Deposition Process for Engineering of Dispersed Polymer Electrolyte Membrane Fuel Cell Oxygen Reduction Reaction Pt/NbO_x/C Catalysts

James Waldecker
Ford Motor Company
2101 Village Road
Dearborn, MI 48121
Phone: (313) 575-7561
Email: jwaldeck@ford.com

DOE Manager: David Peterson
Phone: (720) 356-1747
Email: David.Peterson@ee.doe.gov

Contract Number: DE-EE0007675

Subcontractors:

- Exothermics, Inc., Amherst, NH
- EWII Fuel Cells, LLC, Albuquerque, NM
- Northeastern University, Boston, MA
- University of Michigan, Ann Arbor, MI

Project Start Date: January 1, 2017
Project End Date: March 31, 2020

Overall Objectives

- Develop a new cathode catalyst powder.
- Improve the catalyst powder manufacturing process.
- Demonstrate the physical vapor deposition (PVD) process is scalable in a cost-effective manner.
- Show ease of integration of catalyst into a membrane electrode assembly (MEA).

Fiscal Year (FY) 2018 Objectives

- Execute subcontracts.
- Demonstrate that oxygen reduction reaction (ORR) catalyst powders from PVD process achieve mass activity (MA) of more than 300 A/g_{Pt}.

- Clarify the interaction between platinum (Pt), niobium oxide (NbO_x), and carbon (C) in PVD Pt/NbO_x/C catalyst powder.

Technical Barriers

This project addresses the following technical barriers from the Fuel Cells section of the Fuel Cell Technologies Office Multi-Year Research, Development, and Demonstration Plan¹:

- (A) Durability
- (B) Cost
- (C) Performance.

Technical Targets

The project seeks to develop an electrocatalyst for oxygen reduction, as well as MEAs containing the electrocatalyst, that meet targets relating to the durability, cost, and performance technical barriers. Targets associated with reducing platinum-group-metal content relate to cost.

FY 2018 Accomplishments

- PVD-processed ORR catalyst powders at Oak Ridge National Laboratory (ORNL), Exothermics, and Ford Motor Company (Ford) were able to produce carbon-supported, NbO_x-templated Pt catalyst (Pt/NbO_x/C) with in-cell mass activities surpassing 300 A/g_{Pt}.
- X-ray absorption spectroscopy (XAS) and transmission electron microscopy (TEM) analysis confirmed the interactions: Pt for the most part physically sits on NbO_x, which distributes homogeneously on nano-size carbon powders. There is no electronic interaction between NbO_x and carbon support, although the electronic interaction between Pt and NbO_x is very sensitive to the morphology of Pt relative to that of NbO_x.

¹ <https://energy.gov/eere/fuelcells/downloads/fuel-cell-technologies-office-multi-year-research-development-and-22>

INTRODUCTION

DOE has set targets (shown in Table 1) for higher-performing catalysts that will address the two major vehicle-related barriers to the commercialization of automotive fuel cell systems: cost and durability. This project seeks to generate new catalysts that meet these targets by applying vapor deposition processes to fabricate catalyst powders and incorporating amorphous NbOx as a secondary support in the powders. The project aims to produce powders—as opposed to a structured catalyst layer—to enhance roughness factor and allow ease of integration into established ink processes at catalyst coated membrane suppliers.

Vapor deposition provides numerous advantages. With a well-controlled, high-volume sputtering process, reproducibility of the catalyst powders should be enhanced as compared to the conventional wet-chemistry process. Targets made for vapor deposition are very pure, limiting the possibility of impurities (e.g., chlorides, iron) being incorporated into the final powder and thus compromising performance or durability. Furthermore, a vapor deposition process may be able to limit the amount of aqueous or solvent waste generated in catalyst powder fabrication, although some estimation of precious-metal reclamation processes still must be considered. Specifically, with regard to NbOx, vapor deposition processes yield an amorphous NbOx, which has not been shown to convert to the electrically insulating, crystalline Nb₂O₅ phase. The NbOx also should provide benefits; numerous studies have shown that the presence of NbOx can enhance either mass-normalized or area-normalized activity by two to three times [1–3]. This project explores whether depositions of NbOx on the surface of porous carbon have the capability to eliminate routes toward platinum-surface coalescence.

APPROACH

The project approach centers on two sources for the production of Pt/NbO_x/C catalysts, beginning with small batch (1–2 g) production at ORNL and scaling up to much larger batch (20–40 g) production at Exothermics. ORNL will establish the procedure needed to make Pt/NbO_x/C catalysts by varying parameters such as carbon type, deposition time, pressure, power applied to the metal targets, and—in the case of reactive sputtering—inert/oxidant ratio in the chamber. Samples then will be evaluated for repeatability in terms of platinum and niobium weight percentages by X-ray fluorescence (XRF), as well as for particle size by transmission electron microscopy. A rotating disk electrode (RDE) will be used to screen which catalyst samples are most active, and X-ray absorption spectroscopy will be used to understand why catalysts are active or durable in the contexts of adsorbates, Pt-Pt and Pt-Nb interatomic distances, and Pt-Pt and Pt-Nb coordination numbers.

Fuel cell testing also will be conducted using the Pt/NbO_x/C catalyst powders according to the protocols and metrics outlined by DOE. Tests will include polarization curves, performance checks at rated power conditions, electrocatalyst cycling at voltages between 0.6 V and 0.95 V, and catalyst support cycling between 1.0 V and 1.5 V. The results expected are that the use of NbOx will prompt adjustments in ink formulations and reveal performance losses at high current density that must be improved. To address these concerns, the project will use limiting current techniques to diagnose non-Fickian mass-transport resistances, as well as pressure-dependent mass-transport resistances. Other diagnostics covering gas crossover, roughness factor, proton conductivity in the catalyst layer, and catalyst activity also will be used in testing.

RESULTS

Project work has focused on fabricating new catalyst powders using PVD systems at Exothermics and ORNL. The carbon supports are high-surface-area carbons Ketjen black or acetylene black (AB). The MA of the processed powders is derived from 50-cm² cell results obtained at EWII and from 5-cm² cell at Ford (as shown in Table 1, together with DOE targets for 2020).

Table 1. Progress Toward Meeting Technical Targets for Electrocatalysts and MEAs for Transportation Applications

MYRDD Table 3.4.5 Technical Targets: MEAs for Transportation Applications			
Characteristic	Units	2020 Target	Project Status
Performance at rated power	mW/cm ² at 150 kPa (abs)	1000	750 ¹ , 720 ²

MYRDD Table 3.4.7 Technical Targets: Electrocatalysts for Transportation Applications			
Characteristic	Units	2020 Target	Project Status
PGM content at rated power	g _{PGM} /kW _{gross} at 150 kPa (abs)	0.125	0.200 ¹ , 0.208 ²
PGM loading	mg _{PGM} /cm ² total	0.125	0.150 ^{1,2}
Mass activity	A/mgPGM at 900 mV _{IR-free}	0.44	0.352 ¹ , 0.335 ²
Electrocatalyst stability (0.6 ↔ 0.95 V)	% mass activity loss after 30K cycles	<40	TBD
Loss at 0.8 A/cm ² (0.6 ↔ 0.95 V)	mV loss after 30K cycles	<30	TBD
Support stability (1.0 ↔ 1.5 V)	% mass activity loss after 5K cycles	<40	TBD
Loss at 1.5 A/cm ² (1.0 ↔ 1.5 V)	mV after 5K cycles	<30	TBD

¹ Measured using Exothermics 180308 (PtCo/NbOx/Ketjen black). High current measurements at 0.6 V, 80 °C (Q/DT=2.44), fully humidified.

² Measured using ORNL-L-013 (Pt/NbOx/acetylene black). High current measurements at 0.6 V, 80 °C (Q/DT=2.44), fully humidified.

Table 2 lists the details of the samples made by ORNL and Exothermics (EXO) that exhibit an MA of more than 300 A/g_{Pt}. It can be seen that in-cell MA of more than 300 A/g_{Pt} has been achieved on NbOx-templated Pt-coated ORR catalysts on both AB and Ketjen black carbons.

Table 2. Sample Details with Mass Activity Greater Than 300 A/g_{Pt}

Sample	Composition (AB = acetylene black) (KB = Ketjen black)	Mass Activity (A/g _{Pt})	Test at:	Cell Size (cm ²)	I/C	Cathode / Anode Loadings (mg/cm ²)
ORNL-L-013	35.8% Pt, 0.61% NbOx, AB	335	Ford	5	0.6	0.1/0.05
Exothermics 180109	19.9% Pt, 1.75% NbOx, KB	328	EWII	50	0.8	0.1/0.05
Exothermics 180302	21.5% Pt, 0.23% NbOx, 1.10% Co, KB	309	EWII	50	0.5	0.1/0.05
Exothermics 180308	28.8% Pt, 0.50% NbOx, 1.54% Co, KB	352	Ford	5	0.6	0.1/0.05

The effects of NbOx in the project has been investigated using TEM and XAS analyses. The high-angle annular dark field and elemental mapping of the ORNL-L-013 sample are shown in Figure 1. It can be seen that NbOx is more dispersed on the surface of carbon (AB); the Pt is more clustered but physically laying on top of the NbOx for the most part, forming the desired morphology for enhanced durability and activity.

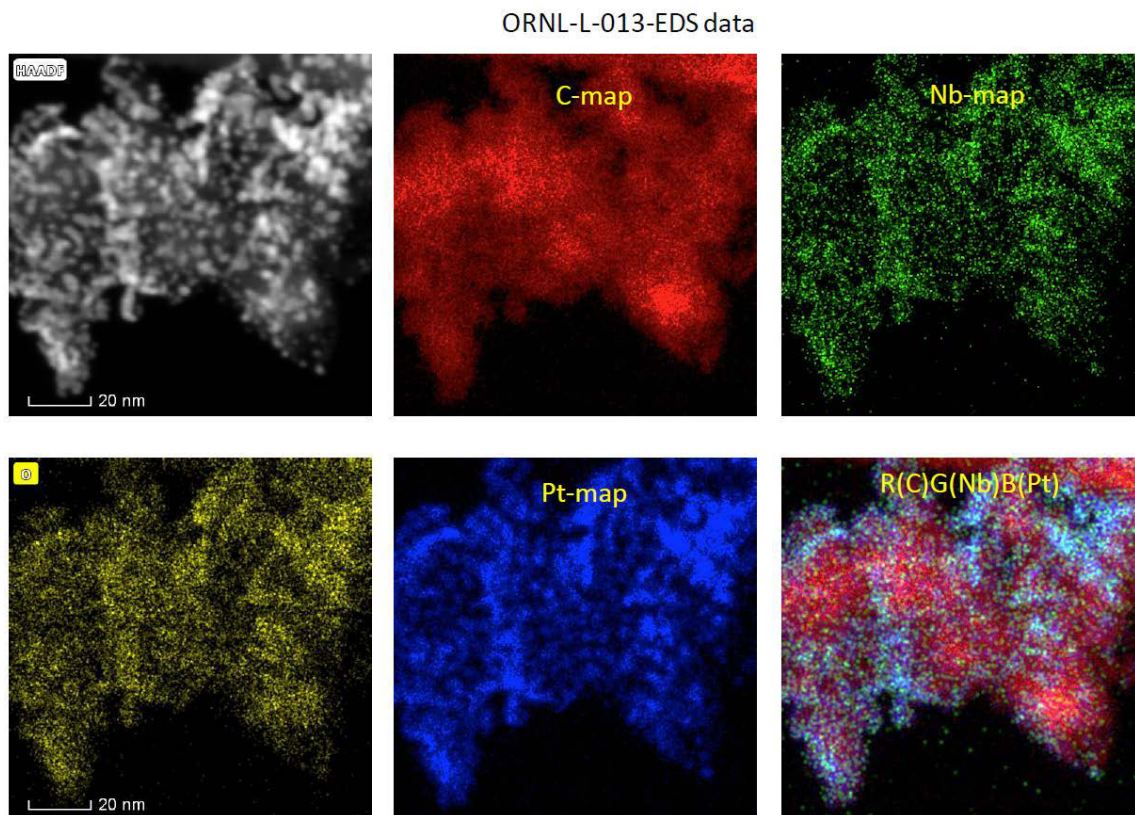


Figure 1. The high-angle annular dark field and elemental mapping in ORNL-L-013 sample

XAS analyses can distinguish the interactions between Pt-C, NbOx-C, and the NbOx and Pt supported on carbon. As a baseline analysis, the XAS is shown in Figure 2a for Tanaka Kikinzoku Kogyo (TKK) Pt (wet-chemical TKK50E) and EXO180209 (26.8 wt% Pt on Ketjen black carbon). The data (Figure 2b) shows that the EXO180209 has slightly shorter Pt-Pt distance than that of commercial TKK 50E but displays very similar numbers of near-neighbor Pt-Pt atoms. The change in Pt-Pt bond distance is not significant, indicating that the type of carbon and the preparation method cannot significantly change the Pt activities as long as the Pt morphology is not significantly altered.

When incorporating NbOx into the catalyst, the first thing that must be determined is whether there is any electronic interaction between NbOx and C. For this purpose, we measured the XAS of vapor processed NbOx on AB carbon (ORNL-L-008, 4.42 wt% NbOx on AB carbon), Pt on NbOx on AB carbon (ORNL-L-013, 0.61 wt% NbOx and 35.8 wt% Pt), and wet-chemically synthesized PtNb/NbOx/AB carbon (5 wt% Nb, 10.6 wt% O, 20.4 wt% Pt, and 64 wt% C).

The Nb X-ray absorption near edge structure (XANES) results are shown in Figure 3, where (a) and (b) are the Nb-XANES analysis, (c) is the derived Nb valence state, and (d) is the Fourier-transformed extended X-ray absorption fine structure (FT-EXAFS) analysis. The results show that the NbOx in ORNL-L-008 is slightly more disordered than Nb₂O₅, but no interaction with C was observed by XAS. The XANES and FT-EXAFS of ORNL-L-013 Pt/NbOx/C is close to that of ORNL-L-008 NbOx/C, and also close to that of Nb₂O₅, but the oxidation state of the Nb in ORNL-L-013 Pt/NbOx/C is 4.6, whereas that in ORNL-L-008 NbOx/C is close to 5. Furthermore, there is no Pt-Nb alloying in the sequentially vapor-deposited Pt/NbOx/C samples, unlike those wet-chemically co-deposited Pt-Nb on carbon [4], where significant Pt-Nb alloying can be observed, as shown on Figure 3(d), which is what is expected based on the processing methods.

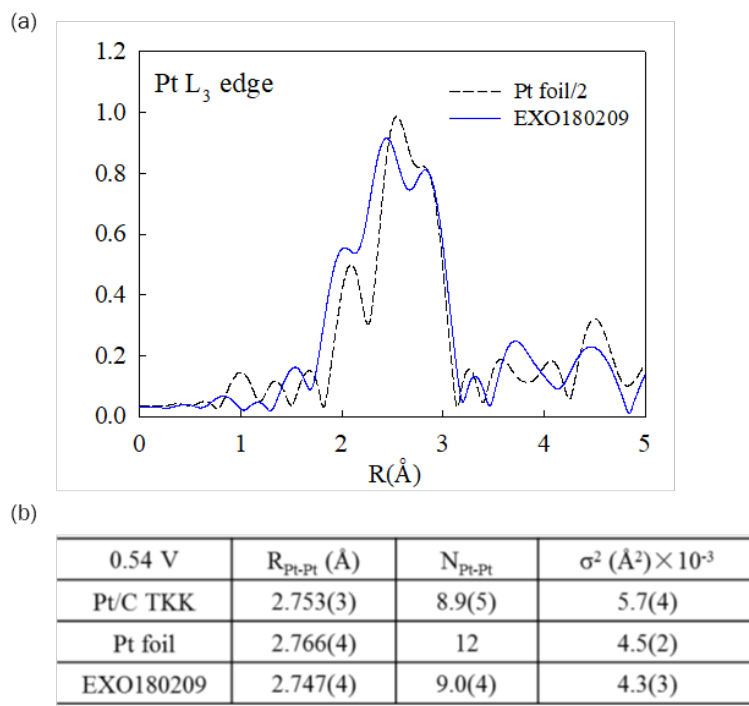


Figure 2. The Pt L3 edge FT-EXAFS comparison at 0.54 V (reversible hydrogen electrode [RHE]) for Pt/C TKK (EA50), Pt foil, and Exothermics 180209 (26.8 wt% Pt on AB carbon)

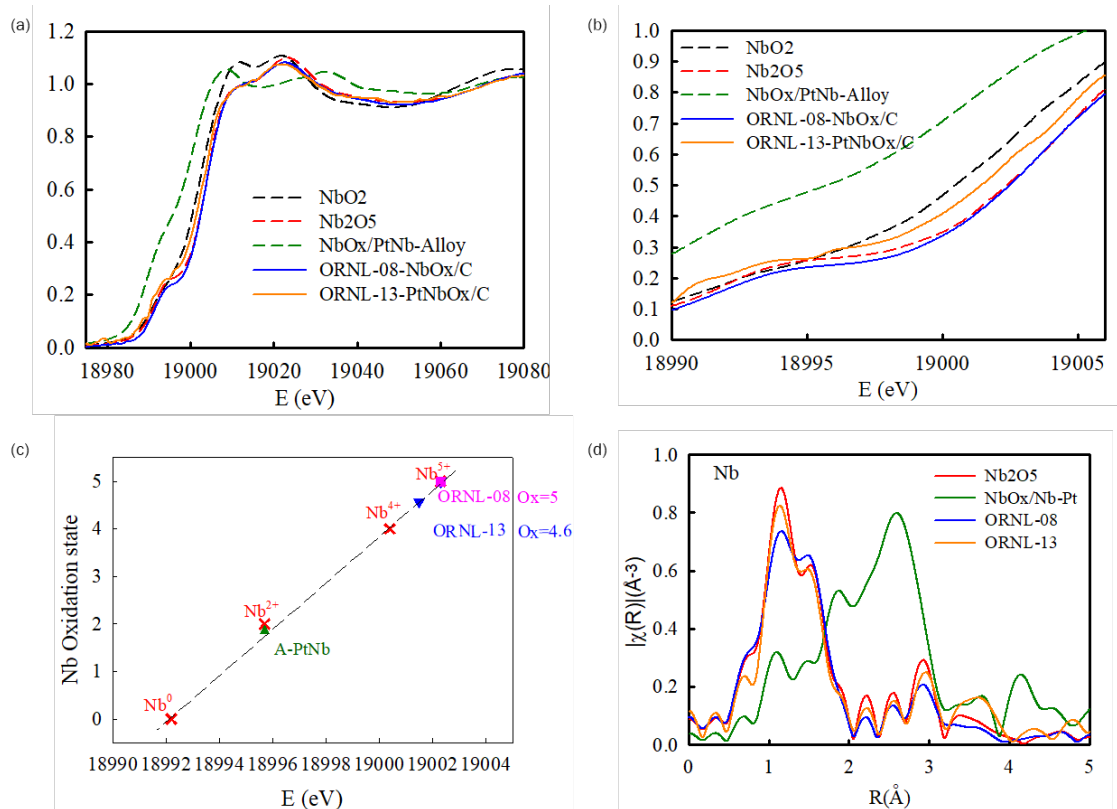


Figure 3. Nb XAS analysis: (a) Nb-XANES analysis, (b) expanded portion for E between 18990 and 19006 eV, (c) quantitative identification of Nb oxidation state from XANES position, and (d) Nb FT-EXAFS comparison

Results of Pt L3-edge XAS analyses on ORNL-L-013 Pt/NbO_x/AB carbon are shown in Figure 4. The presence of Pt-O at 0.54 V and 0.90 V on ORNL-L-013 (Figure 4(a)) indicates the interactions between Pt and the O from the NbO_x rather than from O₂ or H₂O. The presence of Pt-O at 0.54 V in ORNL-13 was further confirmed by XANES (Figure 4(b)), which manifests the charge transfer from Pt to O (ligand effect). As to the Pt-Nb, the data shows that there is no strong interaction between Pt-Nb at 0.54 V (versus RHE, Figure 4(c)), but some interaction between the Pt-Nb at 0.9 V (versus RHE, Figure 4(d)), indicating that the O in NbO_x actively participated in the ORR process. The interaction between Pt and O in the NbO_x could contribute to the ORR activity either positively or negatively depending on the strength of the bonding. If the interaction is weak, then the O in NbO_x acts as a reservoir, facilitating the ORR activity. If the interaction is too strong, then the O from NbO_x holds onto the Pt, preventing the Pt from being actively involved in the ORR reaction, which negatively impacts ORR.

The EXAFS fit results are shown in Table 3 for ORNL-L-013, ORNL-L-019, and EXO180109. The Pt-Pt bond distance in ORNL-L-013 is slightly shortened, probably because of the strong metal-support interaction–induced strain effect as previously shown experimentally by our team and theoretically by other researchers. This could be further improved by engineering the morphology of NbO_x and Pt, the composition of NbO_x, and the extent of disorder on a selected type of carbon support. The templating effects of amorphous NbO_x is one of the main factors that could tremendously enhance ORR activity, as well as durability.

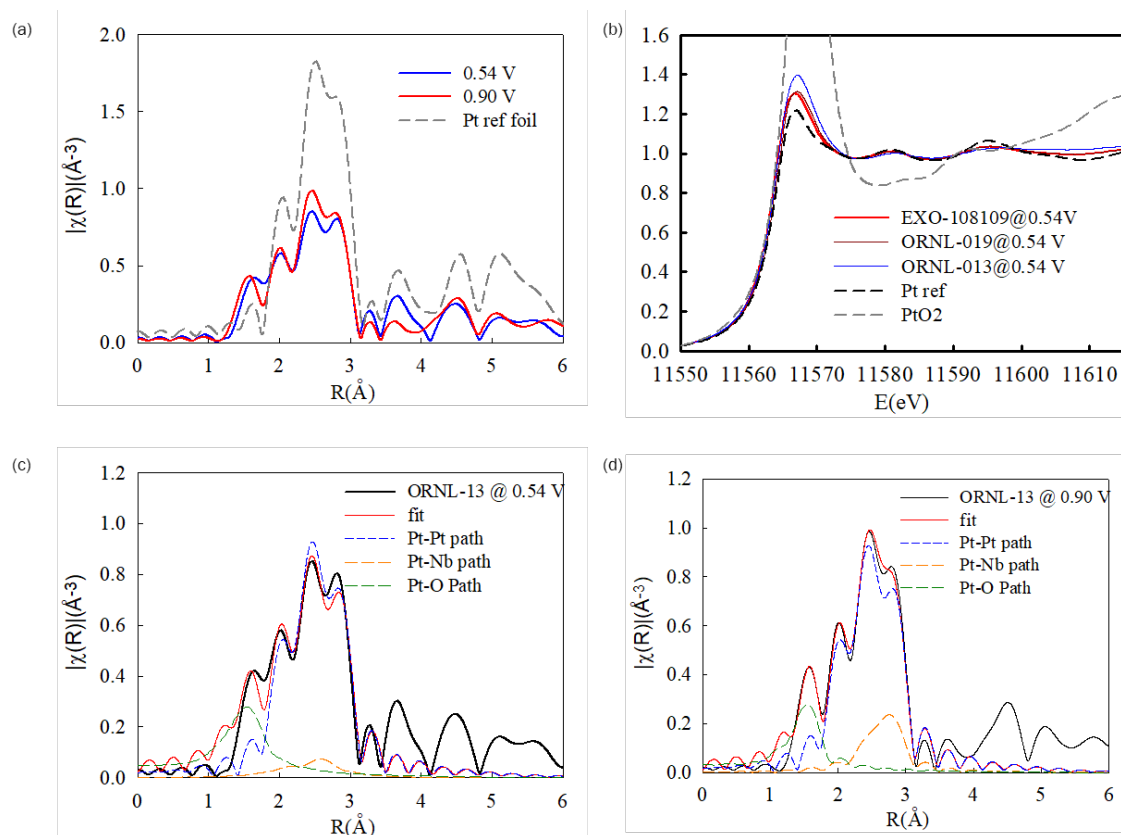


Figure 4. Pt L3-edge XAS; (a) ORNL-L-13 at 0.54 V and 0.9 V (vs. RHE), (b) EXO180109, ORNL-L-019 (37.5 wt% on AB carbon) and ORNL-L-13 at 0.54 V (vs. RHE), (c) EXAFS for ORNL-L-013 at 0.54 V, and (d) at 0.9 V

Table 3. EXAFS Fit Results at 0.9 V Versus RHE

EXAFS 0.9V	Pt-Pt		Pt-Nb		Pt-O	
	N	R (Å)	N	R (Å)	N	R (Å)
Pt foil	12	2.766±0.005	-	-	-	-
ORNL-13	7.8±1.1	2.74±0.01	1.3±0.7	2.86±0.04	0.7±0.5	1.97±0.02
ORNL-19	8.3±0.7	2.75±0.01	-	-	0.6±0.5	1.98±0.02
EXO- 108109	9.3±0.7	2.75±0.01	-	-	0.3±0.3	1.99±0.02

CONCLUSIONS AND UPCOMING ACTIVITIES

During FY 2018, ORNL, Exothermics, and Ford have successfully used PVD in processing carbon-supported, NbOx-templated Pt catalyst (Pt/NbOx/C) powders with in-cell mass activities surpassing 300A/g_{Pt}. XAS and TEM analysis confirmed the interactions: Pt for the most part physically sitting on NbOx, which distributes homogeneously on nano-size carbon powders. There is no electronic interaction between NbOx and carbon support, but the electronic interaction between Pt and NbOx is very sensitive to the morphology of Pt relative to that of NbOx. The next step of the project will focus on durability and the ease of incorporation of the catalysts in single cells.

PUBLICATIONS/PRESENTATIONS

1. Shabroni Ghoshal, Qingying Jia, Michael K. Bates, Jingkun Li, Chunchuan Xu, Kerrie Gath, Jun Yang, James Waldecker, Haiying Che, Wentao Liang, Guangnan Meng, Zi-Feng Ma, and Sanjeev Mukerjee, "Tuning Nb–Pt Interactions to Facilitate Fuel Cell Electrocatalysis," *ACS Catal.* 7, no. 8 (2017): 4936–4946.
2. Qingying Jia, Shraboni Ghoshal, Jingkun Li, Wentao Liang, Guangnan Meng, Haiying Che, Shiming Zhang, Zi-Feng Ma, and Sanjeev Mukerjee, "Metal and Metal Oxide Interactions and Their Catalytic Consequences for Oxygen Reduction Reaction," *J. Am. Chem. Soc.* 139, no. 23 (2017): 7893–7903.
3. James Waldecker, "Vapor Deposition Process for Engineering of Dispersed PEMFC ORR Pt/NbOx/C Catalysts," Presented at the 2018 Department of Energy Annual Review. Washington, D.C. June 14, 2018.

REFERENCES

1. K. Sasaki, L. Zhang, and R.R. Adzic, "Niobium Oxide-Supported Platinum Ultra-Low Amount Electrocatalysts for Oxygen Reduction," *Phys. Chem. Chem. Phys.* 10 (2008): 159–167.
2. T. Trefz, N. Kremliaikova, D. Susac, and J. Jankovic, "Sol-Gel Syntheses of Durable Metal-Oxide Hybrid Platinum Catalysts for PEFC," 224th ECS Meeting, Abstract 1501 (2013).
3. L. Zhang, L. Wang, C.M.B. Holt, T. Navessin, K. Malek, M.H. Eikerling, and D. Mitlin, "Oxygen Reduction Reaction Activity and Electrochemical Stability of Thin-Film Bilayer Systems of Platinum on Niobium Oxide," *J. Phys. Chem. C.* 114 (2010): 16463–16474.
4. Shraboni Ghoshal, Qingying Jia, Michael K. Bates, Jingkun Li, Chunchuan Xu, Kerrie Gath, Jun Yang, James Waldecker, Haiying Che, Wentao Liang, Guangnan Meng, Zi-Feng Ma, and Sanjeev Mukerjee, "Tuning Nb–Pt Interactions to Facilitate Fuel Cell Electrocatalysis," *ACS Catal.* (2017), 7 (8), 4936–4946.

ElectroCat: Durable Mn-Based Platinum-Group-Metal-Free Catalysts for Polymer Electrolyte Membrane Fuel Cells

Hui Xu, (Primary Contact), Fan Yang, Magali Spinetta, Jason Willey (Giner), Gang Wu (UB), Guofeng Wang (UP), Anusorn Kongkanand (GM) Giner, Inc.

89 Rumford Avenue
Newton, MA 02466-1311
Phone: (781) 529-0573
Email: hxu@ginerinc.com

DOE Manager: Nancy Garland
Phone: (202) 586-5673
Email: Nancy.Garland@ee.doe.gov

Subcontractors:

- University at Buffalo (UB), Buffalo, NY
- University of Pittsburgh (UP), Pittsburgh, PA
- General Motors (GM), Pontiac, MI

Project Start Date: October 1, 2017
Project End Date: September 30, 2020

Overall Objectives

- Develop Mn-based catalysts that achieve sufficient activity ($E_{1/2} > 0.85$ V) and stability in acidic media: potential loss of $E_{1/2} < 10$ mV after 30,000 potential (0.6 V to 1.0 V) cycling tests in rotating disk electrode (RDE) tests.
- Demonstrate fuel cell membrane electrode assemblies (MEAs) (25–50 cm²) with a H₂/O₂ mass activity of 0.044 A/cm² at 0.9 V_{IR-free} and H₂/air performance of 0.5 V at 1.0 A/cm², following DOE catalyst performance metrics.
- Limit reduction of catalyst mass activity in 25–50 cm² fuel cell MEAs (<30 mV after 30,000 potential cycles, 0.6–1.0 V in N₂) following DOE's catalyst support durability testing protocols or any other protocols suggested from the ElectroCatalysis Consortium (ElectroCat).
- Acquire a fundamental understanding of the structure-property-performance relationship of the novel Mn-N-C platinum-group-metal (PGM)-free catalysts. The relevant computational data, measurement data, and

publications will be deposited into the database of ElectroCat.

Fiscal Year (FY) 2018 Objectives

- Predict six planar and non-planar Mn-based active sites using computational modeling.
- In RDEs, achieve $E_{1/2} > 0.81$ V and generate 0.25 mA/cm² at 0.9 V. The $E_{1/2}$ drop after 30,000 potential cycles should be less than 30 mV.
- In MEAs, demonstrate H₂/O₂ performance of 0.010 A/cm² at > 0.9 V_{IR-free}.

Technical Barriers

This project addresses the following technical barriers from the Fuel Cells section of the Fuel Cell Technologies Office Multi-Year Research, Development, and Demonstration Plan¹:

- Performance
- Cost
- Durability.

Technical Targets

The DOE 2020 technical targets and our current project status are listed in Table 1 for comparison.

FY 2018 Accomplishments

- Performed density functional theory computations to predict Mn catalysts with the best oxygen reduction reaction (ORR) activity. MnN₄ was found to be the most active among all MnN_x sites.
- Successfully synthesized Mn-based catalysts via various approaches. Strategies to increase catalytic activity have been discovered.
- In RDEs, demonstrated remarkable durability of Mn-based catalysts compared to Fe-based catalysts.

¹ <https://energy.gov/eere/fuelcells/downloads/fuel-cell-technologies-office-multi-year-research-development-and-22>

- In MEAs, demonstrated initial fuel cell performance using Mn catalysts and evaluated different factors to improve fuel cell performance.

Table 1. Progress Toward Meeting Technical Targets for Electrocatalysts and MEAs for Transportation Applications

Characteristic	Units	DOE 2020 Electrocatalyst Targets	Project Status
RDE- $E_{1/2}$	V	≥ 0.85	0.81
RDE- $E_{1/2}$ decrease after 30,000 cycles	mV	≤ 10	17
PGM-free MEA performance (H_2/O_2)	$A/cm^2 @ 0.9 V_{iR-free}$	0.044	0.016
MEA performance (H_2/air)	$V @ 1 A/cm^2$	0.5	0.4
MEA durability (voltage drop)	$mV @ 0.044 A/cm^2$	30	N/A

INTRODUCTION

Development of low-cost and high-performance cathode catalysts for the oxygen reduction reaction in polymer electrolyte membrane fuel cells (PEMFCs) remains a grand challenge for large-scale transportation applications. The primary goal of this project is to significantly reduce the cost of PEMFCs by replacing expensive and rare PGM catalysts with PGM-free catalysts. Among studied PGM-free catalyst formulations, nitrogen and transition metal (M: Fe, Co, or Mn) co-doped carbon (M-N-C) catalysts prepared by high-temperature pyrolysis have demonstrated great promise to replace Pt [1]. Compared to other metals, Fe-N-C catalysts have exhibited the best activity for the ORR in acidic media but suffer from insufficient stability. Furthermore, a major issue associated with Fe-containing catalysts is the production of corrosive $\bullet\text{OH}$ radicals when in contact with H_2O_2 , a product of this two-electron ORR. To address these ionomer/membrane degradation issues due to the intrinsic nature of iron, PGM-free and Fe-free catalysts are highly demanded for low-cost PEMFC technologies.

Motivated by predictions from the first principles density functional theory calculations at the University of Pittsburgh (UP), the team at the University at Buffalo (UB) has successfully prepared active and stable Mn-N-C catalysts. The activity of the Mn-N-C catalysts measured using RDEs in acidic electrolytes is approaching the state-of-the-art Fe-N-C catalysts [1]. More importantly, the Mn-N-C catalysts have demonstrated enhanced stability using potential cycling (0.6–1.0 V) in O_2 -saturated acidic electrolytes. Therefore, in this project, the UP and UB team will collaborate with Giner, Inc. (Giner) and General Motors (GM) to further develop novel Mn-based catalysts and implement them into PEMFCs. Our cohesive efforts will completely address the Fenton reagent issue stemming from currently studied Fe-N-C catalysts and make PGM-free cathode catalysts feasible for PEMFCs.

APPROACH

A strong team has been formed to transform the discovery of low-cost Mn-based catalyst into fuel cell application with expertise in the following areas:

- UP conducts the catalyst modeling to find the most active Mn site for ORR reaction.
- UB synthesizes the highly active Mn-based catalyst based on the modeling predictions from UP.
- Giner designs and optimizes the MEA fabrication process and electrode structure using the Mn-based catalysts delivered from UB.
- GM further validates the system integration of PGM-catalyst-free MEAs.

RESULTS

This is the first year of the project. UP has completed modeling the activity of nine MnN_x sites (x ranging from 2 to 5) for ORR using the first-principles density functional theory calculation methods. Specifically, we predicted the adsorption energy of ORR species (O_2 , OOH , O , OH , and H_2O), free energy evolution following a $4e^-$ ORR pathway, and activation energy for the OOH bond breaking process on various possible active sites. UP predicts that two MnN_4 sites and one MnN_5 sites (shown in Figure 1) are able to catalyze the $4e^-$ ORR process. Moreover, we identified the MnN_4 site near a micropore (Figure 1a) to be the most active site for ORR among all the modeled ones. In contrast, the MnN_x sites with coordinated nitrogen atoms ranging from 2 to 3 are predicted to not promote the $4e^-$ ORR process. These predictions were made based on the thermodynamic analysis of the adsorption energies of ORR species and the free energy evolution of ORR processes.

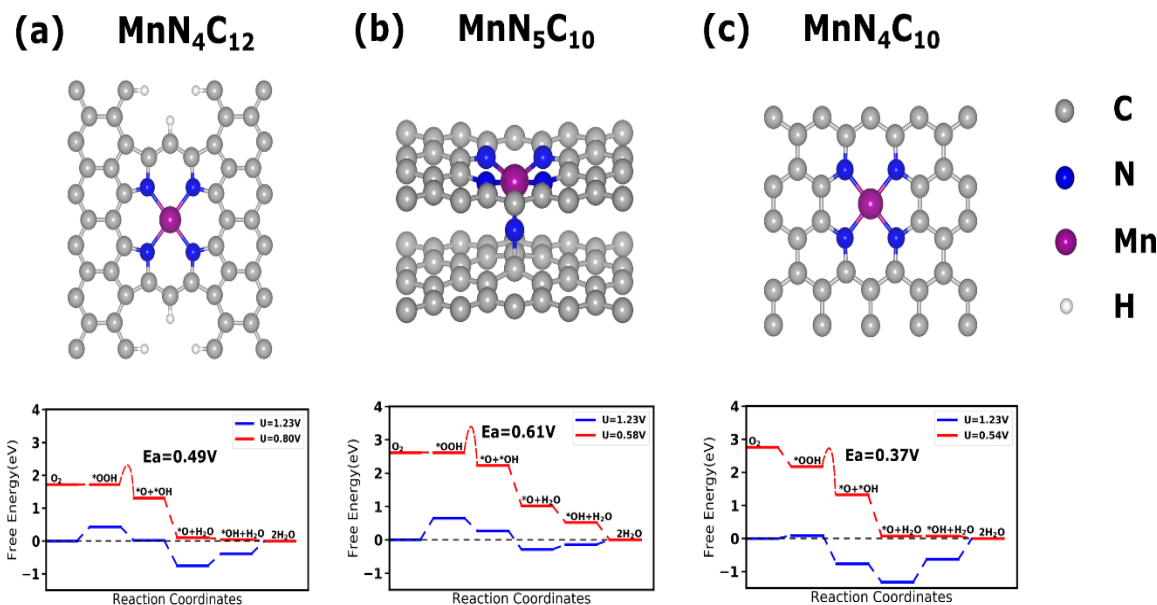


Figure 1. Modeling results of the Mn_x sites for ORR

Based on the prediction from UP, UB successfully synthesized the MnN₄-based catalyst using a two-step chemical doping and adsorption method, which is shown in Figure 2. In the first chemical doping step, Mn-doped zeolitic imidazolate framework (ZIF) precursors were synthesized in a dimethylformamide (DMF) solution. The precursors are identified as nMn-ZIF, where n is the molar ratio of Mn/(Mn+Zn) in the solution. Afterward, Mn and nitrogen co-doped carbon with a three-dimensional porous structure were obtained by pyrolyzing the Mn-containing ZIF precursor. The samples were labeled as nMn-NC. Followed by acid leaching and heat treatment, the obtained powder (labeled as nMn-NC-first) was dispersed in a solution containing Mn salt and additional nitrogen source to carry out the second adsorption step (nMn-NC-second) to introduce more Mn in the catalyst. The subsequent thermal activation can significantly improve the performance, indicating increased density of MnN₄ active sites. Electron microscopy research was conducted at Oak Ridge National Laboratory’s Center for Nanophase Materials Sciences by Dr. Cullen and Dr. More.

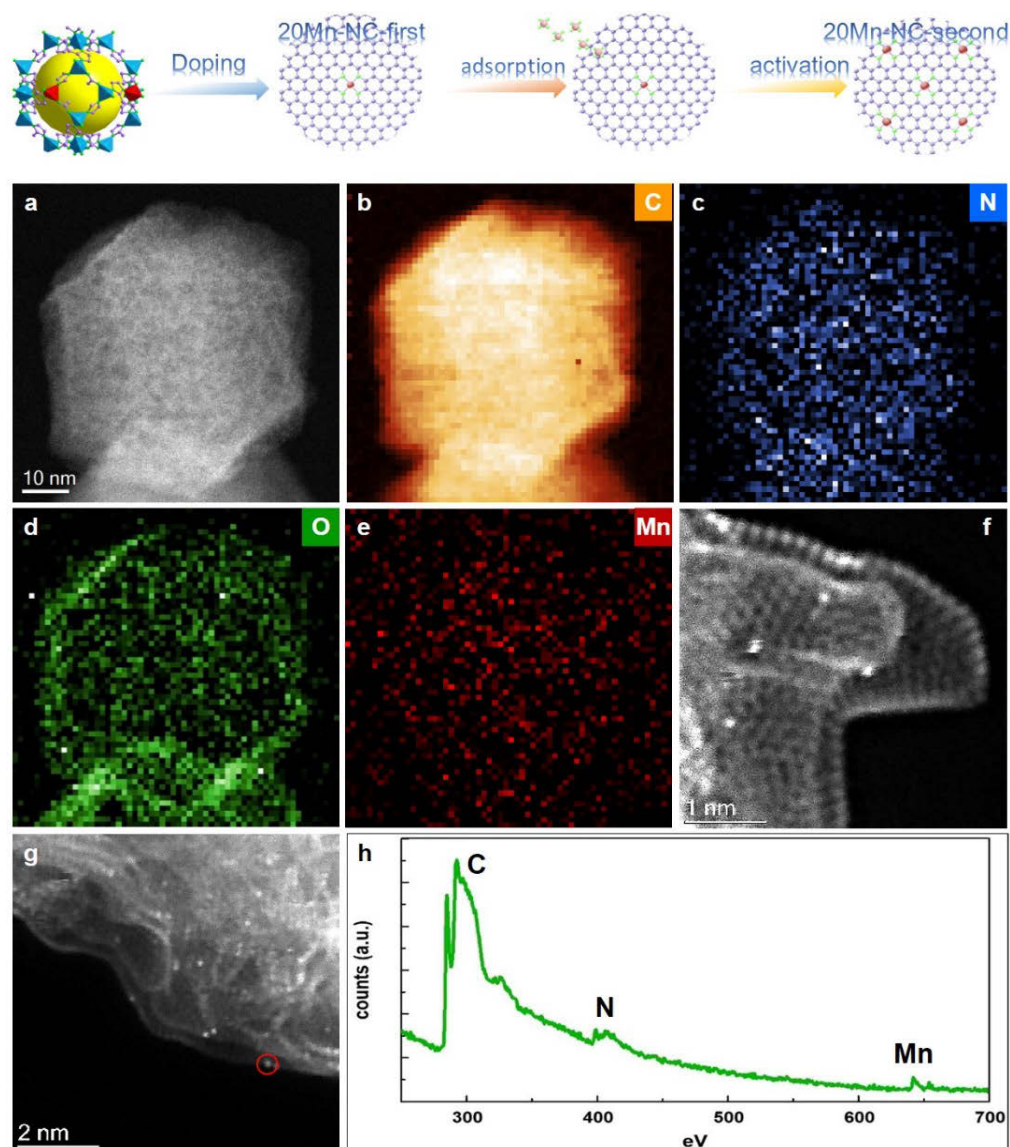


Figure 2. Schematic diagram for two-step doping/adsorbing method to gradually introduce more active sites into the three-dimensional carbon particles derived from Mn-containing ZIF precursors, and microscopy results of 20Mn-NC-second

RDE tests were carried out to compare the electrocatalytic activity of different catalysts. The RDE results are plotted in Figure 3. As can be seen in Figure 3a, the second step can help to improve the half-wave potential by 80 mV (from 0.73 V to 0.81 V). In Figure 3b, the performance of Mn-based catalyst is found to be close to that of the Fe-based catalyst produced with the same procedure. Although the initial performance of the Mn-based catalyst was slightly lower than that of the Fe-based catalyst, the durability of the Mn-based catalyst was significantly better. As can be seen in Figure 3c and 3d, the $E_{1/2}$ of the Mn-based catalyst dropped 17 mV after 30,000 potential cycles (from 0.6 V to 1.0 V), which was much smaller than that of the Fe-based catalyst (29 mV). This result indicates that an Mn-based catalyst has the potential to replace Fe catalyst as a stable PGM-free catalyst in the future with further improvement of the initial performance.

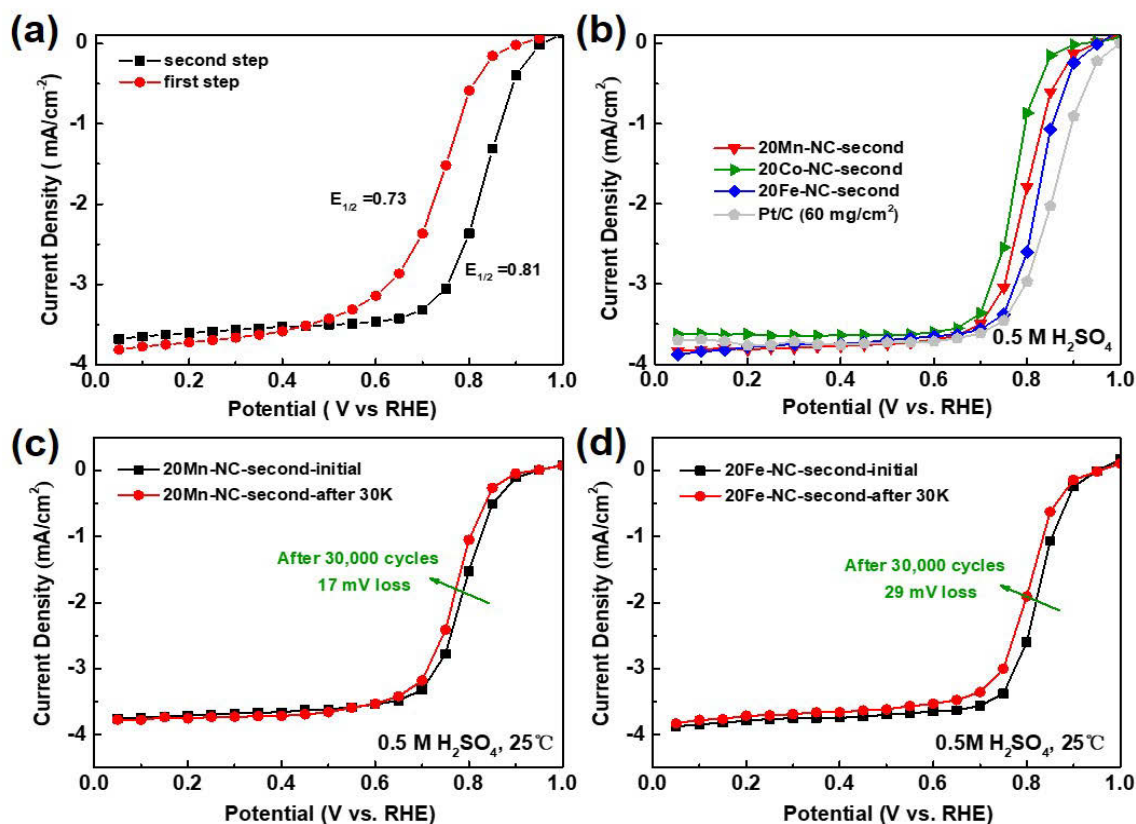


Figure 3. (a) RDE result of the Mn-based catalysts after the first step and second step synthesis; (b) RDE polarization curves of Mn-, Fe-, Co-, and Pt-based catalysts; (c, d) RDE durability tests of Mn- and Fe-based catalysts. The potential cycling is carried out between 0.6 V and 1.0 V for 30,000 cycles with a scan rate of 50 mV/s.

The MEA tests of different Mn-based non-PGM catalysts were carried out at Giner as shown in Figure 4. Figure 4a and Figure 4b show H_2/O_2 and H_2/air polarization curves of Mn-based catalysts from three different synthesis routes: metal-organic-framework (MOF)-based synthesis using DMF, water, and polyaniline hydrogel-based synthesis. Polyaniline hydrogel-based catalyst was obtained by adsorption method as mentioned above. Water-based MOF catalyst was obtained by chemical doping method. The performance rank follows this trend: two-step from DMF > one-step adsorption > one-step from water synthesis. Two-step DMF-based catalyst performed better than the one-step method (hydrogel-based and water synthesis) because the former could introduce more MnN_4 active sites. The benefits of using MOFs to produce highly active Mn-N-C catalysts for ORR are likely due to their well-defined structure, high surface area, and porous structure. From the H_2/O_2 data, the current density @ 0.9 V was about 12 mA/cm^2 . We optimized the MEA fabrication process. As can be seen in Figure 4c, catalyst-coated membranes yielded better performance than gas diffusion electrodes, which likely was due to the better catalyst layer/membrane interface using catalyst-coated membranes. It can also be seen from Figure 4d that the MEA using Aquivion ionomer with a lower equivalent weight in the catalyst layer performed better than the one using Nafion 1100 equivalent weight ionomer. This might be due to the shorter polymer chain of the Aquivion ionomer that could penetrate into the smaller pores of electrodes, thus leading to increased ionomer utilization.

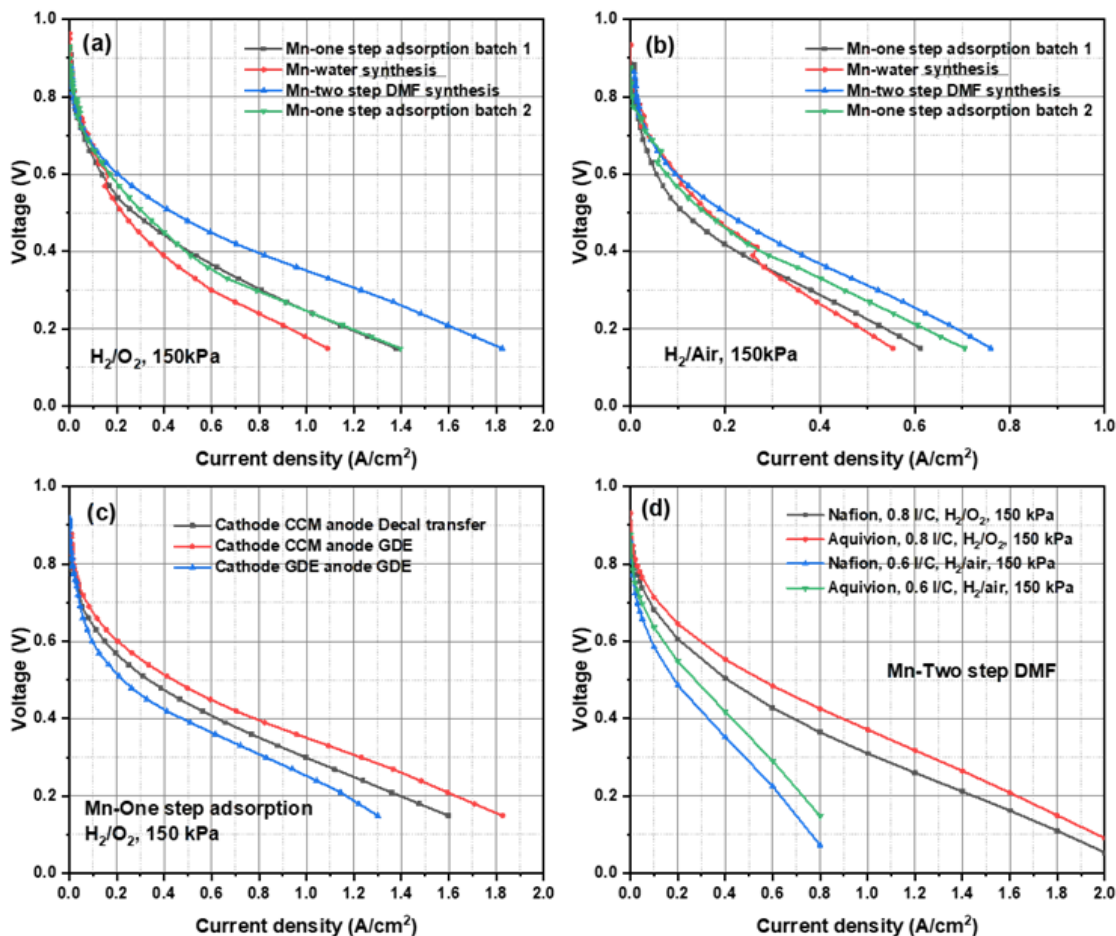


Figure 4. (a-b) IV curve of the MEAs with Mn-based catalysts synthesized via different approaches under H₂/O₂ and H₂/air testing conditions. (c) IV curves of the MEAs with different fabrication process using Mn-one-step adsorption catalyst on cathode. (d) IV curve of the MEAs using different ionomer in the catalyst layer.

CONCLUSIONS AND UPCOMING ACTIVITIES

We have successfully modeled MnN₄ sites in the 4e⁻ ORR process via density functional theory computation, using descriptors like adsorption energy and free energy. Guided by the modeling results, we synthesized Mn-based catalysts to maximize the number of MnN₄ active sites in the catalysts. In the RDE tests, they have demonstrated slightly lower initial performance than Fe catalysts but much better durability. Based on the MEA test results, the two-step DMF approach demonstrated the best performance among all synthesis routes due to increased Mn content in the ZIF structure.

Based on current progress, we have listed our upcoming plan below.

- Catalyst modeling
 - Catalyst: To achieve high activity and durability simultaneously
 - Electrode: Structure affects MEA performance
- Further improve catalyst synthesis

- Increase effective Mn doping
- Improve catalyst synthesis reproducibility
- Scale up catalyst synthesis
- Optimize electrode and MEA design
 - Ink preparation
 - New electrode design (e.g., ionomer-less or -free electrode design)
 - Thick electrode transport studies (O₂ and water)
- Electrode in situ and ex situ characterizations.

FY 2018 PUBLICATIONS/PRESENTATIONS

1. J. Li, M. Chen, Z. Wang, H. Xu, and Gang Wu, “Atomically Dispersed and Nitrogen-coordinated Manganese Catalysts for Oxygen Reduction in Proton Exchange Membrane Fuel Cells,” *Nature Catalysis*, in revision (2018).
2. H. Xu, “Durable Mn-based PGM-Free Catalysts for Polymer Electrolyte Membrane Fuel Cells,” DOE 2018 Hydrogen and Fuel Cells Program Annual Merit Review and Peer Evaluation Meeting, Washington, D.C, June 13–15, 2018.

REFERENCES

1. G. Wu et al., *Science* 332 (2011): 6028.

ElectroCat: Advanced Platinum-Group-Metal-Free Cathode Engineering for High Power Density and Durability

Shawn Litster (Primary Contact), Aman Uddin, Lisa Langhorst, Diana Beltran, Leiming Hu, Reeja Jayan, Laisuos Su, Venkat Viswanathan, Gurjyot Sethi, Hasnain Hafiz
 Carnegie Mellon University
 5000 Forbes Avenue
 Pittsburgh, PA 15213
 Phone: (412) 268-3050
 Email: litster@andrew.cmu.edu

DOE Manager: David Peterson
 Phone: (720) 356-1747
 Email: David.Peterson@ee.doe.gov

Contract Number: DE-EE0008076

Subcontractors:

- University at Buffalo, Buffalo, NY
- Giner, Inc., Auburndale, MA
- 3M Company (3M), St. Paul, MN

Project Start Date: September 1, 2017
 Project End Date: August 31, 2020

Overall Objectives

- Enable high, durable power density with new cathode designs specifically for platinum group metal (PGM)-free catalysts.
- Increase PGM-free catalyst activity and stability through synthesis using a simplified, low-cost method.
- Improve PGM-free mass activity through optimization of the ionomer integration.
- Mitigate PGM-free cathode flooding for fast oxygen transport across thick electrodes.

Fiscal Year (FY) 2018 Objectives

- Establish the synthesis of Fe-doped metal organic framework (MOF)-derived catalysts with high activity and stability.
- Establish cathode and membrane electrode assembly (MEA) fabrication processes for Fe-doped MOF-derived catalysts.

- Optimize the baseline catalyst ink preparation and deposition methods for preparing MEAs.
- Implement a computational model to guide the development of future catalysts and MEAs.

Technical Barriers

This project addresses the following technical barriers from the Fuel Cells section of the Fuel Cell Technologies Office Multi-Year Research, Development, and Demonstration Plan¹:

- (B) Cost
- (C) Performance
- (A) Durability.

Technical Targets

Table 1. Progress Toward Meeting Technical Targets for Electrocatalysts and MEAs for Transportation Applications

Characteristic	Units	DOE 2025 Target	Project Status
PGM-free catalyst activity ^a	$V_{\text{HFR-free}}$ at 0.044 A/cm ²	>0.9	0.89

^a Measured in MEA at 80 °C with 1 atm O₂ partial pressure

FY 2018 Accomplishments

- Synthesized high-activity Fe-doped MOF catalyst tested in rotating disk electrode (RDE), showing half-wave potentials >0.85 V. The stability of these catalysts also is promising, exhibiting a 20 mV half-wave potential loss after 30,000 cycles in RDE.
- Demonstrated an alternative precursor synthesis using water instead of methanol, providing an even lower-cost and environmentally friendly approach. Catalysts produced by this method also exhibited high activity.

¹ <https://energy.gov/eere/fuelcells/downloads/fuel-cell-technologies-office-multi-year-research-development-and-22>

- Demonstrated a method to control catalyst primary particle size with a high resolution without influencing the iron content.
- Discovered the influence of primary particle size on the quality of ionomer integration with the catalyst using nanoscale resolution X-ray computed tomography.
- Optimized the ionomer integration and particle size for baseline MEA performance.
- Achieved a high MEA current density of 28.5 mA/cm² at 0.9 V_{HFR-free} when operating on O₂ at 80°C with 1 atm O₂ partial pressure.
- Demonstrated a high PGM-free power density for 80°C, 1 atm air operation. A power density of 268 mW/cm² at 0.7 V was achieved.
- Implemented a computational-MEA-model-based roadmap to higher MEA power density that accurately reflects catalyst property and cathode design parameters.

INTRODUCTION

PGM-free cathodes have the potential to dramatically transform polymer electrolyte fuel cell (PEFC) commercialization, as their production cost could be 1/10 to 1/100 of those using costly Pt-based catalysts. Unfortunately, PGM-free catalysts and cathodes face two distinct barriers to meeting those targets: (1) PGM-free catalysts typically do not have sufficient activity and stability to replace Pt in most commercial applications; and (2) liquid water flooding and large oxygen and proton transport losses prevent PGM-free cathodes from achieving adequate power density. These losses arise because the lower volumetric cathode activity requires increased thickness of these typically hydrophilic cathode layers. Overcoming those two barriers and ultimately meeting the challenging performance targets requires a comprehensive research and development effort on new PGM-free cathodes. In this project, we are developing catalysts and MEAs for high power density and durability. With a focus on high power density, we concentrate our efforts on PGM-free catalysts that feature iron or cobalt active sites (e.g., FeN₄ active sites) because, to date, they have demonstrated the highest activity and provide adequate currents to facilitate the design and optimization of cathode structures for PGM-free catalysts.

APPROACH

Overcoming those two barriers to PGM-free cathode catalysts and ultimately meeting the challenging performance targets requires a comprehensive research and development effort on new PGM-free cathodes. In this project, we combine three novel and promising approaches, described below.

1. Advanced MOF-derived M-N-C catalysts with high activity and an impressive durability at 0.7 V in fuel cell tests. They feature a streamlined, low-cost synthesis of atomically dispersed active sites at high spatial density.
2. PGM-free specific cathode architectures that address the substantial flooding and transport resistances in thicker catalyst layers by introducing engineered hydrophobicity through additives, coatings, and support layers.
3. Advanced ionomers with high proton conductivity for low ohmic losses across the electrode and more uniform catalyst utilization for better durability. For maximum performance, the development of these strategies and materials will be combined with advanced characterization and modeling.

RESULTS

The team members at the University at Buffalo have developed a new approach to producing highly active Fe-N-C catalysts with uniform morphology and controlled composition via chemical doping of Fe into Zn-zeolitic imidazolate framework (ZIF) precursors that require only one thermal activation step (Figure 1a). The Fe ions added during the ZIF formation were able to chemically dope into the well-defined Zn-ZIF crystals to replace Zn as metal nodes by bridging N-containing ligands, 2-methylimidazole. With only a one-step high-temperature treatment, atomically dispersed Fe catalysts that retain rhombic dodecahedron morphology of individual particles can be obtained with high oxygen reduction reaction (ORR) performance. We have discovered that the Fe content and particle sizes of the catalysts govern the ORR activity of such atomically dispersed Fe catalysts. Because the morphology and porous structure of Fe-ZIF precursors can be directly transferred into the Fe-ZIF catalysts, we are able to tune and correlate the composition and structure of Fe-ZIF precursor to tune their ORR activity.

The ORR activity of Fe-ZIF catalysts in a rotating-ring disk electrode system was investigated as a function of the precursors' Fe content, ranging from 0.05 at% to 9 at% (Figure 1c). The C-xFe-ZIF denotes the nominal Fe atomic percent in the total metal (Fe and Zn) in the synthesis of Fe-ZIF precursors. The ORR activity of these catalysts significantly improved, with an increase of Fe from 0.05 at% to 1.5 at%. The best performing Fe catalysts (C-1.5Fe-ZIF) exhibited a half-wave potential ($E_{1/2}$) of 0.86 V (versus reversible hydrogen electrode), which is achieved by the abundant atomically dispersed Fe-N-C active sites seen in high-angle annular dark field-scanning transmission electron microscope images (Figure 1b). A further increase in Fe content (>1.5

at%) resulted in the gradual decrease of ORR activity. Because Fe atoms tend to aggregate starting from 2.5 at%, the drop in ORR activity for higher Fe content can be attributed to the formation of Fe metallic species.

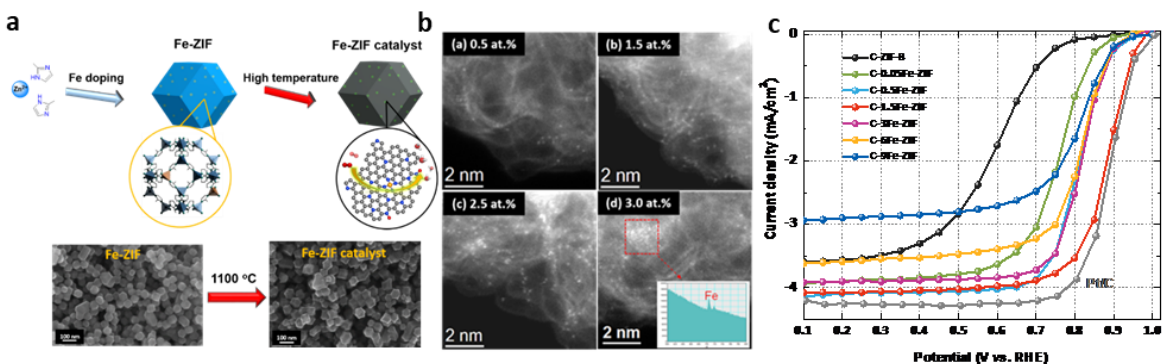


Figure 1. Schematic illustration of the Fe-N-C catalyst synthesis by Fe doping into the formation of Zn-ZIF with a subsequent high temperature treatment (a, top); the scanning electron microscopy (SEM) images of the Fe-N-C catalysts (a, bottom right) derived from Fe-ZIF precursors (a, bottom left); high-angle annular dark field-scanning transmission electron microscope images of atomically dispersed Fe sites in Fe-ZIF catalysts as a function of iron (b); the RDE-measured ORR activity of Fe-ZIF catalysts as a function of iron content (c).

To further enhance the ORR performance of this catalyst, we reduce the internal transport length scales to Fe-N-C active sites by reducing the size of the primary catalyst particles. The University at Buffalo successfully obtained the different size particles—from 1 μm to 80 nm—in catalysts by simply adjusting the reactant concentrations (Figure 2). When the catalyst particle size was submicron (e.g., 1 μm , 200 nm), the ORR performance was insufficient, presumably due to the difficult utilization of active sites inside particles. The catalyst particle size also was carefully tuned in a smaller range (80 nm to 20 nm). For example, the individual particle size of the C-1.5Fe-ZIF catalyst was observed to be approximately 80 nm (Figure 2c). Figure 2f shows the ORR activity of catalysts as a function of their particle size, with the identical Fe content. When the size of particles in the catalyst was reduced to 50 nm, the $E_{1/2}$ of catalysts (50 nm-C-1.5Fe-ZIF) positively shifted to 0.88 V (versus reversible hydrogen electrode) with 1.5 mA/cm² at 0.9 V_{IR-free}. However, with a further reduction of particle size to 20 nm, a decrease in the $E_{1/2}$ to 0.82 V was observed, suggesting a lower number of Fe-N-C active sites in the catalyst. This is possibly explained by the aggregation of particles in 20 nm-C-1.5Fe-ZIF (Figure 4e and inset) compared to the more isolated particles with the 50 nm catalyst (Figure 4d and inset), which may have diminished the number of accessible active sites for ORR. We further evaluated the stability of the best-performing catalysts (50 nm-C-1.5Fe-ZIF). The stability of the catalyst (Figure 2g) was tested by cycling from 0.6 V to 1.0 V in O₂-saturated H₂SO₄ for 40,000 cycles at a scan rate of 50 mV/s. Half-wave voltage losses of 26 mV were observed after 30,000 cycles, revealing this catalyst exhibits good ORR stability in the rotating-ring disk electrode measurement.

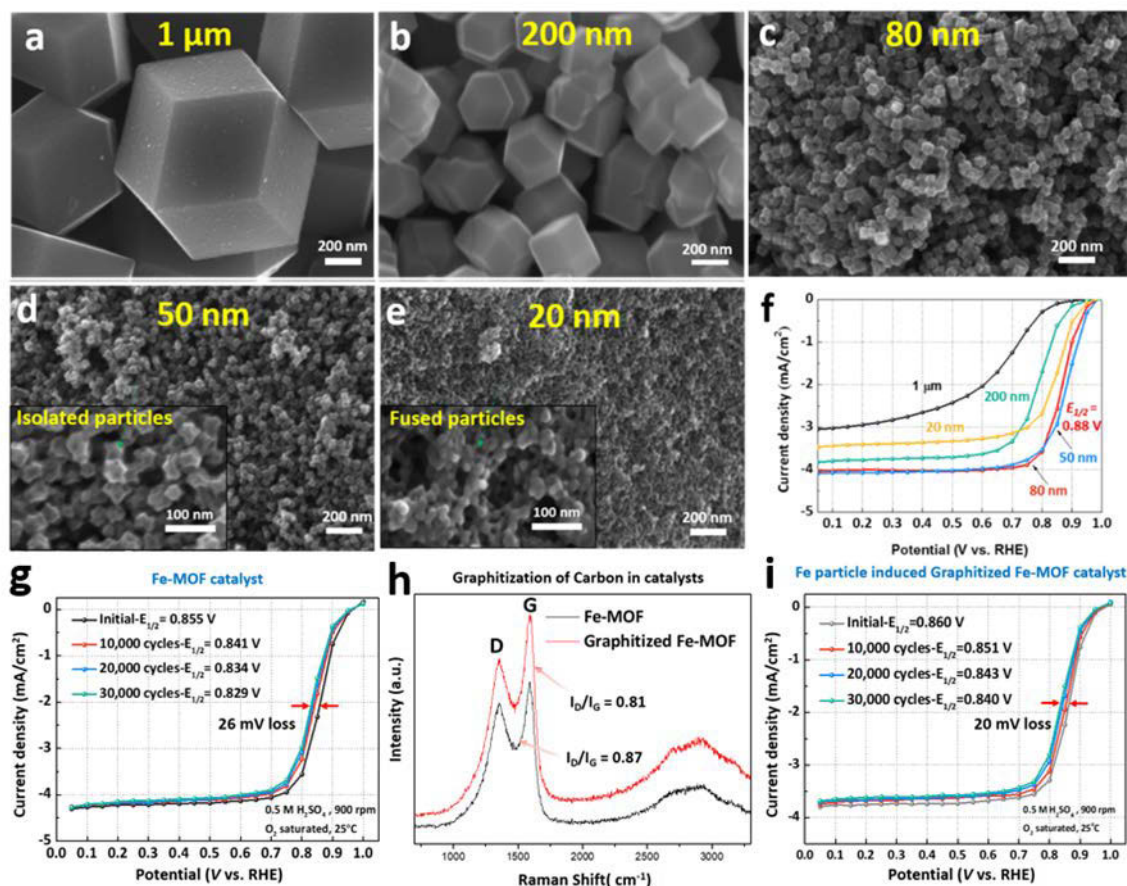


Figure 2. The SEM images of C-1.5Fe-ZIF catalysts in 1 μm (a), 200 nm (b), 80 nm (c), 50 nm in isolated particles (d and inset), and 20 nm in fused particles (e and inset); the ORR activity of Fe-N-C catalysts derived from MOFs as a function of particle size (f); the cycling stability test of Fe-N-C catalyst (g) and graphitized Fe-N-C catalyst (i); Raman spectra of catalysts without or with improved graphitization (h).

To achieve better long-time stability of PGM-free catalysts, we increase the corrosion resistance of the carbon in Fe-N-C catalysts by increasing crystallinity/graphitization of carbon during high-temperature treatment. In the Raman spectra (Figure 2h), the increased graphitization of carbon was observed as the decreased ratio of the intensity of the D band (disordered carbon bonds) to G band (ordered carbon bonds) for the graphitized catalyst (graphitized Fe-MOF: $I_D/I_G = 0.81$) compared to the one without any increased graphitization (Fe-MOF: $I_D/I_G = 0.87$). The Fe-N-C catalysts with improved graphitization (graphitized-Fe-MOF) exhibited a better stability with a half-wave potential loss of only 20 mV after 30,000 cycles. The enhanced stability of the Fe-N-C catalyst is attributed to the increased regularity of carbon structure reducing the rate of oxidation of surface carbon atoms in the catalyst, which leads to the enhanced stability of Fe-N-C catalysts under long-time cycling.

A significant focus of the project is integrating PGM-free catalysts into high-power-density PEFC cathodes. Carnegie Mellon University (CMU) uses a model-based roadmap to higher power density that translates catalyst active site density, primary particle structure, and electrode composition and morphology to the resulting MEA power density, thus giving insights into the leading voltage-loss mechanisms and areas of potential improvement. This also provides a means to generate actionable targets for the catalyst synthesis, including active site density and particle size. As Figure 3a illustrates, this approach uses a combination of a microstructurally consistent cathode model with inputs from multi-modal imaging and a multi-phase computational PEFC model. The model was implemented for the particular structure of the Fe-doped MOF-

derived catalysts, and a baseline model of the initial MEAs prepared at CMU was validated. Figure 3b shows the polarization curve predictions of the model, including the baseline case. The porous electrode design study showed that key changes leading to higher performance are to increase the ionomer effective conductivity and increase the hydrophobicity of the electrode. Both can be achieved by improved ionomer integration within the cathode. Greater conductivity also can be achieved by alternative ionomers with lower equivalent weight. Additionally, greater hydrophobicity can be achieved by using hydrophobic additives and coatings. As shown in Figure 3c, CMU used the model to evaluate the optimal loading of an optimized baseline cathode based on power density at 0.7 V as function of normalized active site density. That study showed a power density of >400 mW/cm² can be achieved with a 50- μ m-thick cathode if the active site density is increased by a factor of four times.

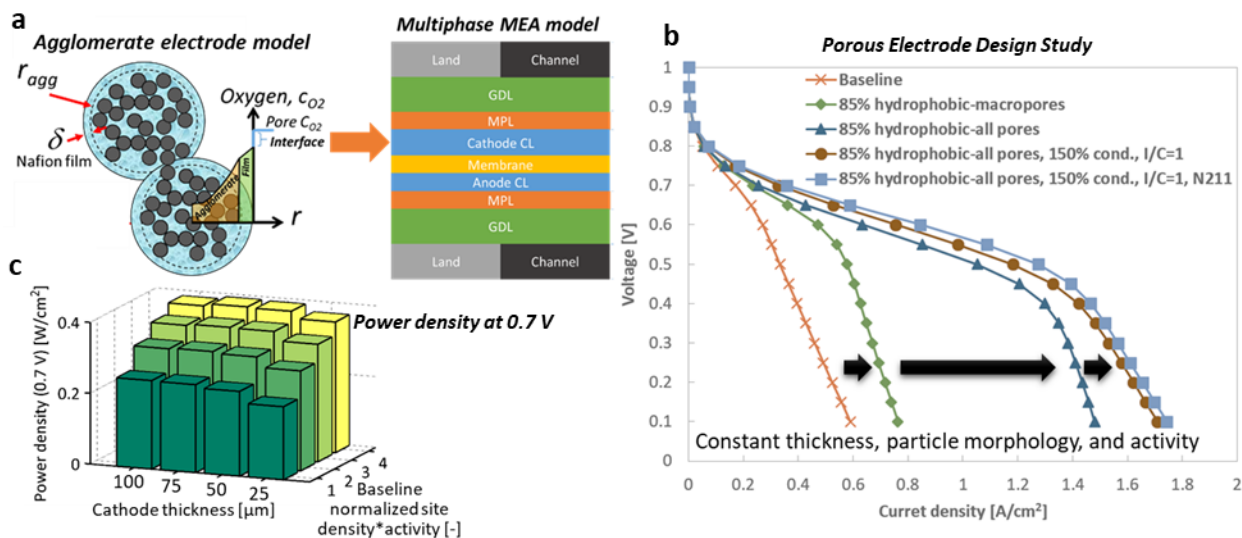


Figure 3. Multi-phase PEFC model with a microstructurally consistent cathode model (a). Polarization curves from a porous electrode density study to identify methods of increasing performance over the experimentally validated baseline case (b). Predicted power density at 0.7 V as a function of normalized active site density and cathode thickness (c).

An experimental study was performed on the integration of ionomers in the cathodes by preparing and testing MEAs at CMU with varying catalyst primary particles sizes synthesized at University at Buffalo, and by varying the ionomer-to-carbon ratio. In addition to MEA testing in PEFC hardware, we performed nanoscale X-ray computed tomography (nano-CT) imaging of the cathodes in the CMU facility. This includes 3-D imaging of the ionomer distribution by absorption contrast imaging of cesium ion-exchanged ionomer. Figure 4 shows the ionomer distribution in cathodes with various particle sizes. With 40 nm catalyst, the interior of the large catalyst aggregates (>5 μ m) is mostly free of ionomer, whereas the 60–100 nm catalysts show better ionomer infiltration. In the case of the 600 nm catalyst, a thick ionomer film formed around the large primary particles because of the reduced surface area available for coating.

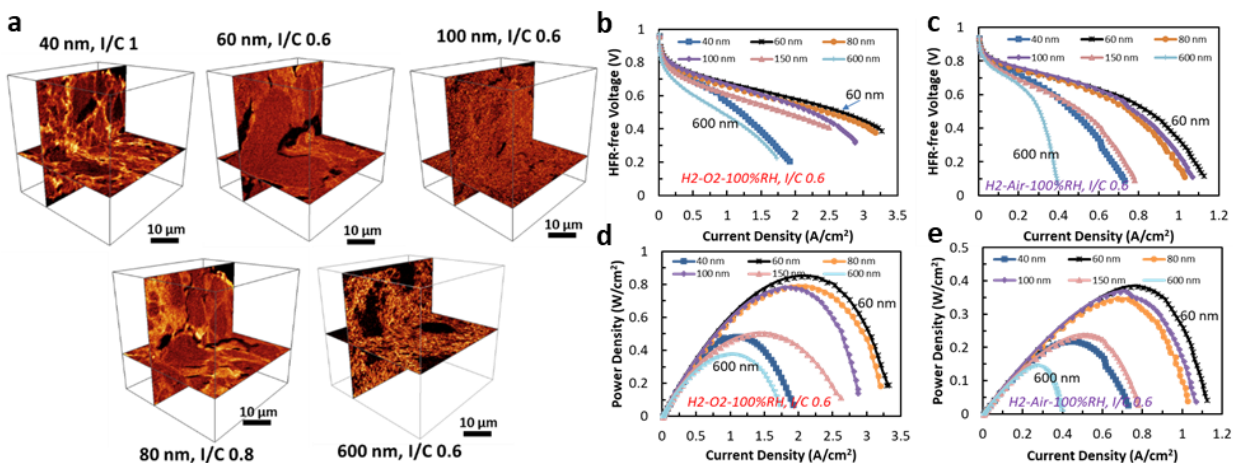


Figure 4. Nano-CT imaging of the ionomer distribution in cathodes of an Fe-MOF catalyst with different primary particle sizes (a). Polarization curves (b, c) and power density curves (d, e) obtained with air and O₂ for MEAs prepared from Fe-doped MOF-derived catalyst with different primary particle sizes. Conditions: catalyst loading: 4 mg/cm²; cell temperature: 80 °C; flow rate H₂/air or O₂: 200/200 sccm, relative humidity: 100%, 1 bar H₂/air or O₂ partial pressure, Nafion 212 membrane.

Figure 4b, 4c, and 4d show the polarization and power density curves obtained under O₂ and air using catalysts with different primary particle sizes with an ionomer-to-carbon ratio of 0.6. The highest activity and best mass transport were achieved using the 60 nm catalyst. With this catalyst, the current density with 1 atm O₂ at a fuel cell voltage of 0.9 V (high-frequency resistance corrected) was 9 mA/cm², and the power density with 1 atm at a fuel cell voltage of 0.7 V was 228 mW/cm². The cell performance with 80 nm and 100 nm catalysts was close to the 60 nm catalyst. A more repeatable MEA performance was achieved with 100 nm catalyst. The PEFC with the 40 nm catalyst performed badly due to the poor ionomer integration, as shown in the nano-CT images. The MEA with a 600 nm catalyst had the lowest apparent activity and lowest maximum current density, possibly due to low surface area; fewer active sites; and thicker, more hydrophilic ionomer films that led to severe flooding. The best FY 2018 performance on 1 atm O₂ achieved was 28.5 mA/cm² at 0.9 V_{HFR-free} at a cell temperature of 80 °C. On 1 atm air, the best current density achieved at 0.8 V was 113 mA/cm², and the highest power density achieved at 0.7 V was 268 mW/cm² (383 mA/cm²) using 100 nm catalyst and an ionomer-to-carbon ratio of 0.8.

CONCLUSIONS AND UPCOMING ACTIVITIES

To date, this project has shown that high activity and stability can be achieved with Fe-doped MOF-derived catalysts. Through integrated catalyst development and MEA design and testing, we discovered the tight connection between particle morphology, ionomer integration, and MEA performance. Through model and imaging guided optimization we have achieved a high power density at PEFC application-relevant voltages. Going forward, the project focus will be to further improve the stability and durability of the catalyst through improvements in the precursor synthesis and its heat treatment at University at Buffalo. This research and development will be supported by density functional theory modeling of the active sites at CMU. The MEA development will focus on increasing the hydrophobicity through additives and coatings, as well as with the use of alternative ionomers from 3M for increased conductivity and improved integration with the catalyst. Giner will support the MEA development through scale-up of the best catalysts identified at University at Buffalo and CMU.

FY 2018 PUBLICATIONS/PRESENTATIONS

1. Xiao Xia Wang, David A. Cullen, Yung-Tin Pan, Sooyeon Hwang, Maoyu Wang, Zhenxing Feng, Jingyun Wang, Mark H. Engelhard, Hanguang Zhang, Yanghua He, Yuyan Shao, Dong Su, Karren L. More, Jacob S. Spendelow, and Gang Wu. “Nitrogen-Coordinated Single Cobalt Atom Catalysts for Oxygen Reduction in Proton Exchange Membrane Fuel Cells.” *Advanced Materials* 30, no. 11 (2018):1706758.
2. Y. He, S. Hwang, D.A. Cullen, M.A. Uddin, L. Langhorst, B. Li, S. Karakalos, A.J. Kropf, E.C. Wegener, J. Sokolowski, M. Chen, D.J. Myers, D. Su, K.L. More, G. Wang, S. Litster, G. Wu, “Highly active atomically dispersed CoN₄ fuel cell cathode catalysts derived from surfactant-assisted MOFs: Carbon-shell confinement strategy.” *Energy and Environmental Science* (2018), doi:10.1039/C8EE02694G.
3. Hanguang Zhang and Gang Wu, “Atomic Iron-Dispersed Electrocatalysts Derived from Metal-Organic Framework for Oxygen Reduction,” AIChE Fall Meeting, Minneapolis, MN, October 29–November 3, 2017.
4. Shawn Litster, “Addressing Transport Losses in Pt-free PEM Fuel Cell Cathodes,” American Chemical Society Spring Meeting, New Orleans, LA, March 20, 2018.
5. Shawn Litster, “Advanced PGM-free Cathode Engineering for High Power Density and Durability,” Presentation at the DOE Hydrogen and Fuel Cells Program Annual Merit Review, Washington, D.C., June 2018.

ElectroCat: Highly Active and Durable Platinum-Group-Metal-Free Oxygen Reduction Reaction Electrocatalysts Through the Synergy of Active Sites

Yuyan Shao (Primary Contact), Xiaohong Xie, Venkateshkumar Prabhakaran, Jian Liu
Pacific Northwest National Laboratory
902 Battle Blvd
Richland WA 99354
Phone: (509) 371-6228
Email: yuyan.shao@pnnl.gov

DOE Manager: Gregory Kleen
Phone: (240) 562-1672
Email: Gregory.Kleen@ee.doe.gov

Subcontractors:

- Washington University in St. Louis, St. Louis, MO
- University of Maryland, College Park, MD
- Ballard Power Systems, Burnaby, BC, Canada

Project Start Date: October 1, 2017
Project End Date: September 30, 2020

Overall Objectives

- Design and fabricate high-performance platinum group metal (PGM)-free oxygen reduction catalysts with increased oxygen reduction active site density and improved mass transport property.
- Design and fabricate highly active H₂O₂ decomposers to decrease H₂O₂ formation in catalyst layer (50%).
- Demonstrate dual active site catalysts (O₂ reduction active sites and H₂O₂ decomposition sites) for improved durability (by 2 times).

Fiscal Year (FY) 2018 Objectives

- Develop two stable H₂O₂ decomposers.
- Identify pathways to produce 200 mg catalysts using thermal shock activation technique.
- Develop two O₂ reduction catalysts with $\Delta E_{1/2} < 65$ mV (vs. Pt/C) under rotating ring disk electrode (RRDE) test.

- Develop dual-site catalysts with H₂O₂ generation no more than 4% under RRDE test.
- Annual milestone: Demonstrate a PGM-free catalyst ≥ 20 mA/cm² at 0.90 V (iR-corrected) in an H₂-O₂ fuel cell and 100 mA/cm² at 0.80 V in an H₂-air fuel cell (measured); maintain partial pressure of O₂ + N₂ at 1.0 bar (cell temperature 80°C).

Technical Barriers

This project addresses the following technical barriers from the Fuel Cells section of the Fuel Cell Technologies Office Multi-Year Research, Development, and Demonstration Plan¹:

- Durability (catalyst)
- Cost (catalyst)
- Performance (catalyst).

Technical Targets

This project focuses on the development of high-performing and durable PGM-free oxygen reduction reaction (ORR) catalysts for polymer electrolyte fuel cells with the potential to meet DOE targets in the Fuel Cells section of the Multi-Year Research, Development, and Demonstration Plan. Our goal is to achieve an activity of 30 mA/cm² at 0.90 V in a polymer electrolyte fuel cell membrane electrode assembly (MEA) by 2020 (Table 1).

FY 2018 Accomplishments

- Developed two H₂O₂ decomposition catalysts that decrease H₂O₂ formation on PGM-free catalysts by up to 50%.
- Developed a PGM-free, Fe-free, atomically dispersed Co catalyst that demonstrated a half-wave potential above 0.81 V (reversible hydrogen electrode [RHE]) (0.6 mg/cm² loading).

¹ <https://energy.gov/eere/fuelcells/downloads/fuel-cell-technologies-office-multi-year-research-development-and-22>

- Identified one key degradation mechanism of PGM-free catalysts by H_2O_2 (radical) attacking of carbon (in collaboration with the Electrocatalysis Consortium (ElectroCat), Los Alamos National Laboratory [LANL]).

Table 1. Progress Toward Meeting Technical Targets for Electrocatalysts for Transportation Applications

Characteristic	Units	DOE 2020 Electrocatalyst Targets	Project Status
PGM-free catalyst activity	$\text{mA}/\text{cm}^2 @ 0.9 \text{ mV}_{\text{iR-free}}$	≥ 44	13

INTRODUCTION

Developing PGM-free ORR catalysts has been an important strategy to decrease the cost of polymer electrolyte fuel cells. One big challenge of PGM-free ORR catalysts is the incomplete reduction of O_2 and formation of H_2O_2 (and radicals). The formation of destructive H_2O_2 (and radicals) not only decreases the activity and stability of PGM-free catalysts, it also damages the membrane and ionomers in the catalyst layer (particularly in the existence of Fe ions that catalyze radical formation from H_2O_2 through the Fenton reaction). The other challenge of PGM-free ORR catalysts is their low active site density. Therefore, the pathway forward is to significantly increase the number of active sites and to decrease/eliminate H_2O_2 formation.

APPROACH

This project is designed to increase PGM-free ORR catalyst activity and improve its durability. Our technical approaches to accomplish these goals include the dual-active site synergy approach, which integrates O_2 reduction active sites and H_2O_2 decomposition active sites, and the unique thermal shock activation technique with extremely fast heating/cooling (16,000 K/s to 400,000 K/s for up to 3,000 K) to increase active site density. The dual-active site synergy approach will minimize or eliminate H_2O_2 , which is believed to be a major source of activity loss [1, 2]. Our close collaboration with the ElectroCat consortium by using advanced capabilities will enable deep understanding of the function mechanisms and degradation mechanisms of the catalysts.

RESULTS

We have developed a PGM-free, Fe-free, atomically dispersed Co catalyst that demonstrated a half-wave potential of ~ 0.81 V (RHE) (Figure 1), which is among the highest ones reported so far for this class of ORR catalyst. We have also demonstrated an MEA ORR activity of 13 mA/cm^2 at 0.90 V in an H_2 - O_2 fuel cell (Figure 1c).

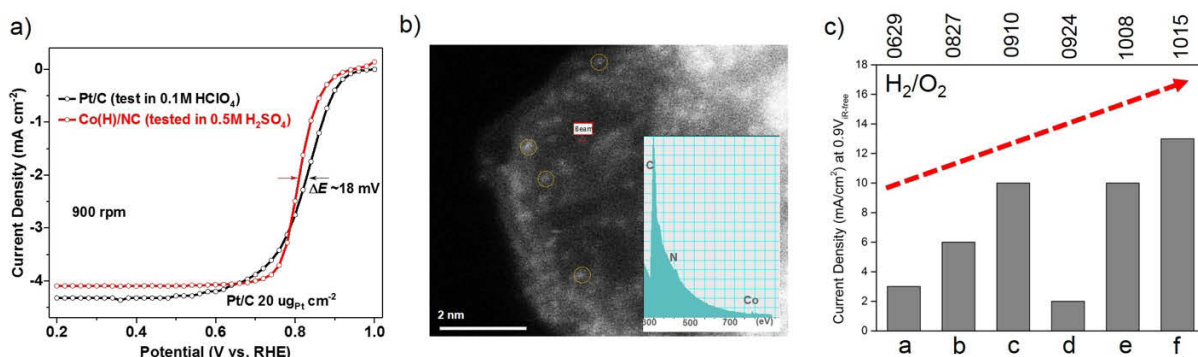


Figure 1. Performance and characterization of Co catalyst. a) RRDE test of Co catalyst (0.6 mg/cm^2 loading) in comparison with Pt/C, b) Scanning transmission electron microscopy image (taken at Oak Ridge National Laboratory) of Co catalyst showing atomic dispersion and the collocation of Co and N, indicating the formation of CoN_4 moieties, c) ORR activity of Co catalyst in MEA showing the progress enabled by MEA optimization.

Through integrating H_2O_2 decomposition catalyst and PGM-free catalyst, we were able to decrease H_2O_2 formation significantly. Figure 2 shows one example of our nitrogen-doped ceria ($N-CeO_x$) with PGM-free catalysts. In collaboration with ElectroCat consortium core team member LANL, we demonstrated significant decrease in CO_2 and F emission in the MEA with the H_2O_2 decomposition catalyst in the catalyst layer (Figure 3). The formation of CO_2 at the cell voltage as low as 0.3 V indicates prominent carbon oxidation by H_2O_2 (radicals) rather than the electrochemical oxidation of carbon, which occurs at electrode potential of 0.9 V and higher. The CO_2 emission measurement confirms that H_2O_2 (radicals) attacking on PGM-free catalysts is one key degradation mechanism that can be controlled using H_2O_2 decomposition catalysts. The decreased F emission (from the degradation of membrane and/or ionomers by H_2O_2 [radicals]) indicates the protection of membrane/ionomers by H_2O_2 decomposition catalysts.

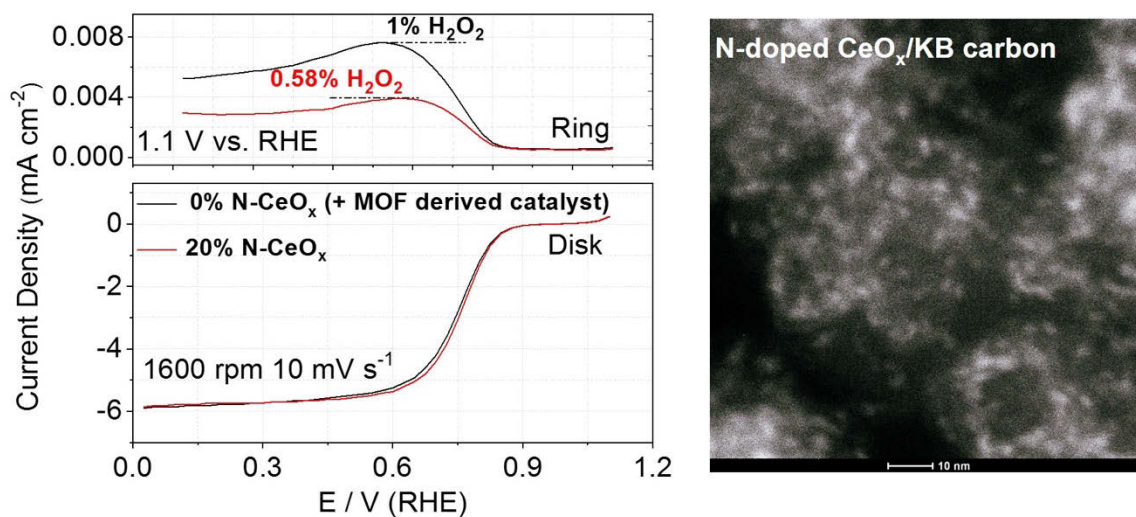


Figure 2. Dual-active site catalysts with decreased H₂O₂ formation and transmission electron microscopy image of an H₂O₂ decomposition catalyst

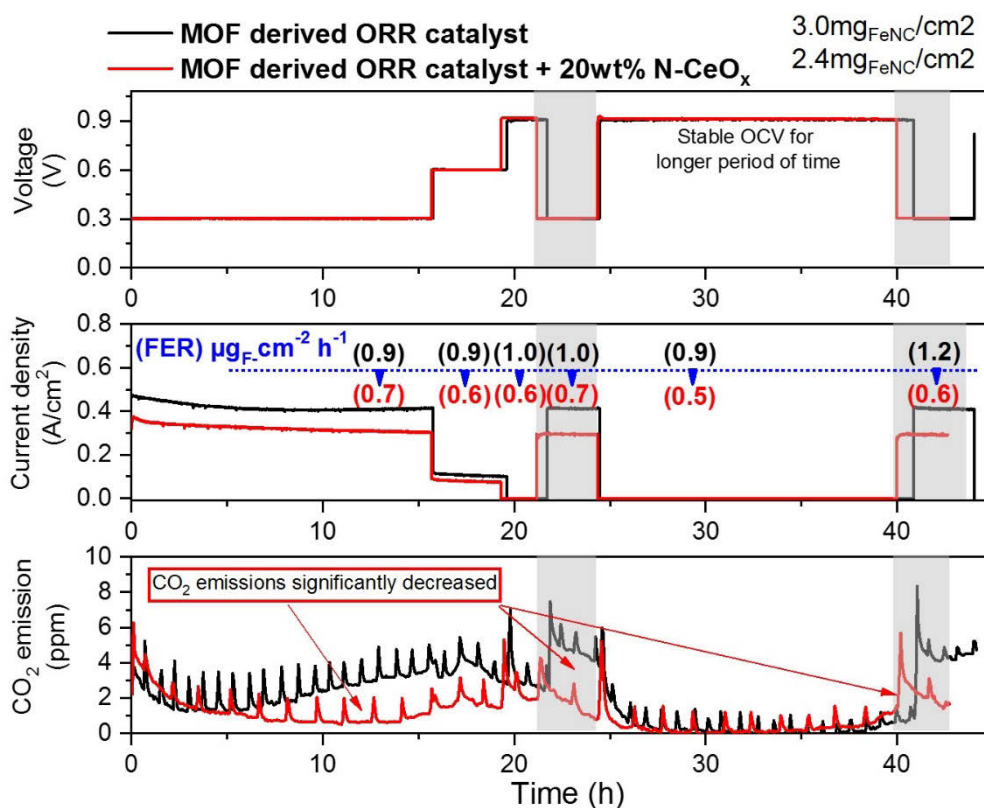


Figure 3. In Situ measurement of CO₂ and F emission in MEA with/without H₂O₂ decomposition catalysts (in collaboration with LANL)

Thermal shock synthesis has been explored to achieve the improved active site density of ORR and H_2O_2 decomposition catalysts. We have synthesized uniformly dispersed, small metal oxide nanoparticles (Figure 4a–b), which will be further functionalized for H_2O_2 decomposition catalysts. Through optimization of thermal shock synthesis, we were able to increase the activity of metal-organic-framework-derived catalysts (Figure 4a), but further improvement is still needed (Figure 4c).

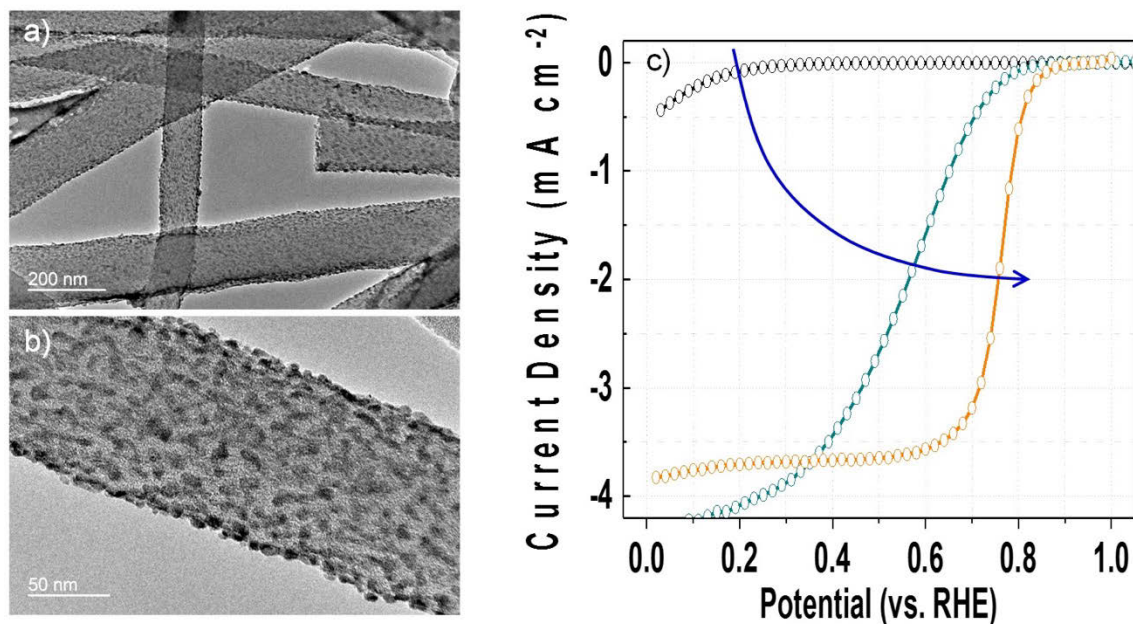


Figure 4. Thermal shock synthesis of H_2O_2 decomposition catalysts and ORR catalysts

CONCLUSIONS AND UPCOMING ACTIVITIES

We have developed a PGM-free, Fe-free Co catalyst that demonstrated a half wave potential of above 0.81 V (RHE) (loading 0.6 mg/cm^2) and 13 mA/cm^2 ORR activity in an $\text{H}_2\text{-O}_2$ cell. We, in collaboration with ElectroCat, identified that H_2O_2 (radical) attack on PGM-free catalysts is one key mechanism for its degradation. With the dual-active sites catalysts (O_2 reduction and H_2O_2 decomposition), we demonstrated the decreased CO_2/F emission, indicating the protection of catalyst and membrane/ionomer by the dual-active site catalysts.

Our upcoming activities include:

- Optimization of catalysts and MEA to achieve activity and performance target of $20 \text{ mA/cm}^2 @ 0.90\text{V}$ (IR-free) in $\text{H}_2\text{-O}_2$ and $100 \text{ mA/cm}^2 @ 0.80 \text{ V}$ in $\text{H}_2\text{-air}$, including catalyst morphology (e.g., particle size, porosity) and ionomer content/distribution in catalyst layer.
- Optimization of thermal shock synthesis to demonstrate its advantages in producing active sites and uniform, smaller particles.
- Integration of dual-active sites for better dispersion of H_2O_2 decomposition catalysts and closer match between ORR sites and H_2O_2 sites.

SPECIAL RECOGNITIONS AND AWARDS/PATENTS ISSUED

1. Clarivate Analytics “Highly Cited Researchers.” Yuyan Shao, November 2017.

FY 2018 PUBLICATIONS/PRESENTATIONS

1. Y. Shao, “Materials Electrochemistry for Energy Conversion and Storage @Scale,” Invited seminar, University of California, Riverside, Department of Chemistry, April 2, 2018.
2. Y. Shao, “Electrochemical Materials and Interface Studies for Improved Activity and Durability in Chemical Transformation Processes,” Invited talk, 39th Symposium on Applied Surface Analysis, Richland, Washington, June 19–22, 2018.
3. Y. Shao, X. Xie, V. Prabhakaran, and J. Liu, “Instability of Fuel Cell Catalysts: Precious Metal and PGM-Free Catalysts,” Invited talk, ACS 2018 Fall Meeting, Boston, Massachusetts, August 19–23, 2018.

REFERENCES

1. Xi Yi and Piotr Zelenay, “Kinetic Models for the Degradation Mechanisms of PGM-Free ORR Catalysts,” *ECS Transactions* 85, no. 13 (2018): 1239-1250.
2. Chang Hyuck Choi, Hyung-Kyu Lim, Min Wook Chung, Gajeon Chon, Nastaran Ranjbar Sahraie, Abdulrahman Altin, Moulay Tahar Sougrati, Lorenzo Stievano, Hyun Seok Oh, Eun-Soo Park, Fang Luo, Peter Strasser, Goran Dražić, Karl Mayrhofer, Hyungjun Kim, and Frederic Jaouen, “Achilles’ Heel of Iron-Based Catalysts During Oxygen Reduction in Acidic Medium,” *Energy Environ. Sci.* (2018).

ElectroCat: Platinum-Group-Metal-Free Engineered Framework Nano-Structure Catalyst

Prabhu Ganesan
Greenway Energy, LLC
301 Gateway Dr.
Aiken, SC 29803
Phone: (803) 447-8319
Email: prabhu.ganesan@greenway-energy.com

DOE Manager: Donna Ho
Phone: (202) 586-8000
Email: Donna.Ho@ee.doe.gov

Contract Number: DE-EE0008077

Subcontractors:

- Savannah River National Laboratory, Aiken, SC
- Northwestern University, Evanston, IL

Project Start Date: September 1, 2017

Project End Date: December 31, 2020

Overall Objectives

- Develop catalysts based on high-surface-area polymers.
- Synthesize platinum group metal (PGM)-free electrocatalysts with well-defined functional groups and structures.
- Characterize PGM-free electrocatalysts to probe any possible correlation between their physical and chemical attributes and their electrochemical performance.
- Active site modeling: model PGM-free engineered framework nano-structure catalyst with ideal structure.
- Conduct membrane electrode assembly (MEA) optimization and fuel cell testing.
- Meet DOE's 2020 activity target: 30 mA cm⁻² at 0.90 V_{IR-free} in an H₂-O₂ fuel cell.
- Deliver six or more MEAs to the Electrocatalysis Consortium (ElectroCat), each with active area ≥50 cm² for independent testing and evaluation.

Fiscal Year (FY) 2018 Objectives

- Greenway Energy, LLC (GWE), Savannah River National Laboratory (SRNL), and Northwestern University (NU) will collaborate to prepare PGM-free engineered framework nano-structure catalysts using a rational catalyst design with well-defined structures and functional groups consisting of “phen”-type coordination sites (e.g., CTFs, MOFs) and porphyrinic type sites (MOFs, POPs).
- Down-select polymeric materials with high surface area, pore volume, and pyridinic N.
- Demonstrate rotating ring-disk electrode (RRDE) performance >1.5 mA cm⁻² at 0.8 V versus reversible hydrogen electrode (RHE) in 0.1 M HClO₄ acid at a loading of 0.6 mg cm⁻².
- GWE consultant Dr. Anderson, in collaboration with Dr. Holby (Los Alamos National Laboratory [LANL] ElectroCat consortium lab), will align modeling tasks with relevant experimental results.
- Initial MEA optimization and fuel cell performance testing will be performed by SRNL and GWE respectively, in collaboration with LANL ElectroCat consortium lab.
- Demonstrate catalyst activity of 20 mA cm⁻² at 0.9 V_{IR-free} in hydrogen/oxygen fuel cell.

Technical Barriers

This project addresses the following technical barriers from Fuel Cells section of the Fuel Cell Technologies Office Multi-Year Research, Development, and Demonstration Plan¹:

- A. Durability
- B. Cost
- C. Performance.

¹ <https://energy.gov/eere/fuelcells/downloads/fuel-cell-technologies-office-multi-year-research-development-and-22>

Technical Targets

Progress toward technical targets for catalyst activity for the oxygen reduction reaction (ORR) is shown in Table 1.

FY 2018 Accomplishments

- Optimized synthesis protocol and scale-up to prepare >400 mg of “phen”-type chelating polymers, porphyrinic polymers, and high N-containing carbon-based materials per batch parameters.
- Down-selected polymeric materials for high-throughput synthesis based on RRDE screening experiments. The three materials selected are azo-polyporphyrin, phenyl-polyporphyrin, and ZIF-8 based catalysts.
- Achieved RRDE performance of 2.78 mA cm⁻² for a phenyl-polyporphyrin-based catalyst.
- Aligned the modeling tasks performed by the LANL ElectroCat consortium laboratory with the ongoing experimental research at GWE, SRNL, and NU.
- Initiated MEA optimization and fuel cell testing studies at GWE, SRNL, and LANL (ElectroCat consortium lab). Significant progress has been made toward achieving the go/no-go metrics demonstrating H₂/O₂ fuel cell performance of 16 mA cm⁻² at 0.9 V_{IR-free} (this is 80% of the target of 20 mA cm⁻²).

Table 1. Progress Toward Technical Targets for Catalyst Activity for the ORR

Metric	Units	Current Status ^a	FY18 Target	2020 DOE Target
Fuel Cell Test: Catalyst Activity	mA cm ⁻² @ 900 mV _{IR-free}	16 ^c 32 ^b	≥20 ^c	≥44 ^b
Fuel Cell Test: Catalyst Activity	mA cm ⁻² @ 800 mV	52.8	NA	NA
RRDE Test: Catalyst Activity	mA cm ⁻² @ 800 mV	2.78	≥1.5 ^d	NA

^a Current status denotes performance measurements recorded up to September 30, 2018.

^b 80 °C H₂/O₂ MEA; fully humidified, total outlet pressure 150 kPa_{abs.}; anode stoich. 2; cathode stoich. 9.5.

^c 80 °C H₂/O₂ in an MEA; total outlet pressure of 100 kPa_{abs.}.

^d 0.1 M HClO₄ acid; catalyst loading of 0.6 mg cm⁻².

INTRODUCTION

Traditional synthesis methodologies that produce durable, highly active PGM-free electrocatalysts typically consist of a top-down approach utilizing a nitrogen-coordinating precursor, a metal precursor, and a support material. Nitrogen-coordinated transition metal complexes typically are absorbed onto a support material, which is then activated via high-temperature pyrolysis. Selection of the support and the nitrogen coordinating precursor has long been the focal point of efforts to maximize the number of accessible, catalytically active sites.

In this project, GWE in collaboration with SRNL and NU will develop durable, highly active, low-cost, PGM-free electrocatalysts for polymer electrolyte membrane fuel cells designed and synthesized using a unique, bottom-up, rationally designed approach. Electrocatalysts are produced via polymerization reaction followed by a high-temperature pyrolysis step. Additionally, this project focuses on catalyst site and ORR mechanistic modeling to better understand the structure-property relationship.

APPROACH

To achieve the overall objectives, the project is divided into three main tasks that encompass the following.

- Task 1. Catalyst development and characterization. Novel electrocatalysts are produced via polymerization reactions using well-defined functional groups and structures. A rational approach is used to better understand PGM-free active site morphology and to enhance the performance of the electrocatalyst by improving active site quantity and morphology.
- Task 2. Active site modeling. Catalyst site and ORR mechanistic modeling will be performed more effectively as we incorporate data on chemical and physical characteristics gained through the bottom-up approach taken in Task 1.
- Task 3. MEA optimization and fuel cell testing. The project will culminate in internal and independent fuel cell tests (deliver six or more MEAs, each with active area ≥ 50 cm², to an ElectroCat core lab for independent testing and evaluation) demonstrating the capability of the novel catalyst materials of achieving DOE project targets and advancing the state of the art.

RESULTS

Task 1.0: Catalyst Development Based on High-Surface-Area Polymers (Month 1–36)

During the first year of the project, a large number of electrocatalysts with well-defined functional groups and structures have been synthesized via polymerization reactions and characterized. Distinct nitrogen functionalities vary among the different material families to rationally target the discovery of the active sites. Possible correlations between physical attributes and electrochemical performance have been examined. Initially, 17 families of materials consisting of “phen”-type chelating polymers, porphyrinic polymers, and high-nitrogen-containing carbon-based materials were synthesized, characterized, and screened by RRDE for oxygen-reduction activity. Subsequently, three materials that met our first year internal ORR activity target measured by RRDE (Table 1), were down-selected for further study and optimization: azo-polyporphyrin, phenyl-polyporphyrin, and ZIF-8 (Figure 1).

Polyporphyrins synthesized using pyrrole and terephthalaldehyde demonstrated the highest performance for catalyzing the ORR and have received the most focus during Budget Period 1 (BP 1). Characterization of phenyl-polyporphyrin by scanning electron microscopy and X-ray photoelectron spectroscopy shows spherical particles of ~200 nm to 300 nm in diameter (Figure 2) with nitrogen content (predominantly pyrrolic) of 11 at%. Following pyrolysis, the Brunauer-Emmett-Teller surface area increases from 16 m²/g to ~1,200 m²/g. Average particle size appears unchanged, but an increase in surface roughness is observed. Additionally, overall N content decreases by half, from 11 at% to about 5.5 at%. After pyrolysis, there is a significant increase in the fraction of pyridinic-N, and Fe content increases from 0.08 at% to about 0.35 at%. RRDE

screening indicates the polyporphyrin-based catalysts exhibit high activity for the ORR, with $E_{1/2}$ typically ranging from 0.78 V to 0.82 V. The highest performance measured for the ORR at 0.8 V versus RHE is 2.78 mA cm^{-2} .

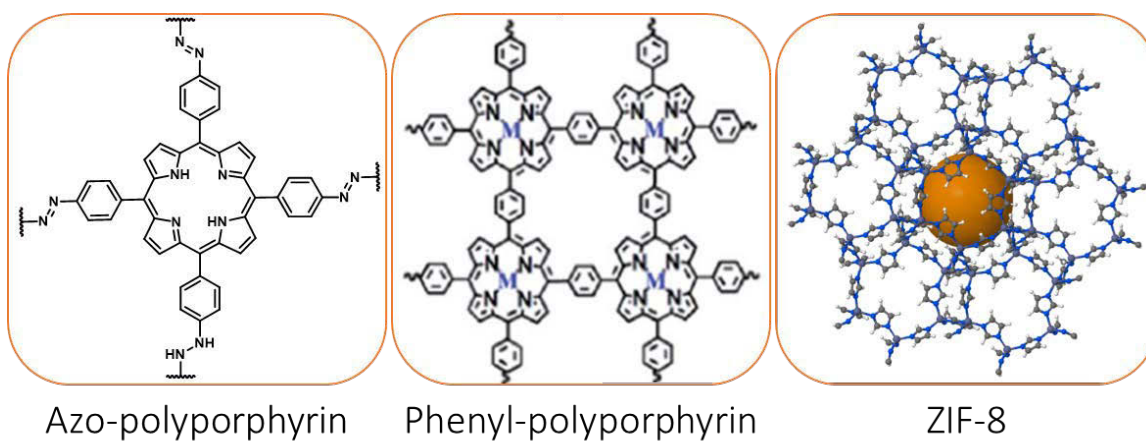


Figure 1. Structures of down-selected polymer-based catalyst precursors

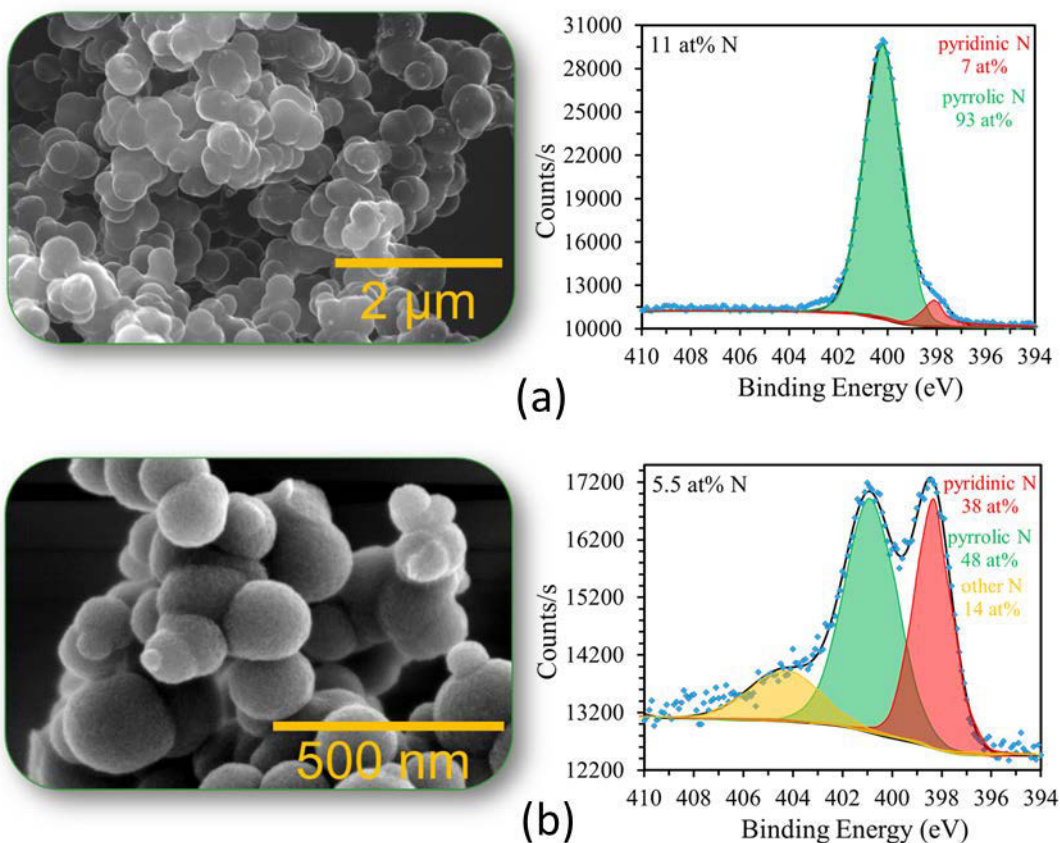


Figure 2. Scanning electron microscopy images and X-ray photoelectron spectroscopy analysis of (a) as-synthesized and (b) heat-treated polyporphyrin materials

Task 2.0: Active Site Modeling (Month 1–30)

The modeling program began with plausible Fe-N-C catalyst structures and H₂O molecules to calculate reversible potentials for steps in the pathway for the oxygen reduction reaction using adsorption energies and the linear Gibbs energy relationship. In coordination with the rational design of catalyst preparation, reactive site modeling will provide insight into the electrochemical mechanisms for the ORR and provide reversible potentials for intermediate steps and overpotentials. For the linear Gibbs energy relationship calculations of approximate reversible potentials for these reactions with intermediates adsorbed on the electrode surfaces, we used the standard experimental reversible potentials for the solution phase potentials and the corresponding Gibbs energy changes shown in Table 2.

Table 2. Solution Phase Potentials and the Corresponding Gibbs Energy Changes for Different ORR Intermediates

Reaction	$U^0(\text{V})$	$\Delta G^0(\text{eV})$
$\text{O}_2(\text{g}) + \text{H}^+(\text{aq}) + \text{e}^- \rightarrow \text{OOH}(\text{aq})$	-0.125	0.125
$\text{OOH}(\text{aq}) + \text{H}^+(\text{aq}) + \text{e}^- \rightarrow \text{O}(\text{aq}) + \text{H}_2\text{O}(\text{l})$	0.21	-0.21
$\text{O}(\text{aq}) + \text{H}^+(\text{aq}) + \text{e}^- \rightarrow \text{OH}(\text{aq})$	2.12	-2.12
$\text{OH}(\text{aq}) + \text{H}^+(\text{aq}) + \text{e}^- \rightarrow \text{H}_2\text{O}(\text{l})$	2.72	-2.72
$\text{O}_2(\text{g}) + 4\text{H}^+(\text{aq}) + 4\text{e}^- \rightarrow 2\text{H}_2\text{O}(\text{l})$	1.23	-4.92

We assume FeN₄ when substituted into graphene is isoelectronic to Fe^{II} in iron porphyrin. Studies of reactions 1–4 over two Fe^{II} sites, two Fe^{III} sites, and two Fe^{IV} sites are the subject of this report. The Fe^{II}, Fe^{III}, and Fe^{IV} sites had the structures as shown in Figure 3. Looking down the columns of adsorption energies tabulated in Figure 3, a trend is evident; all adsorbates bond to the surfaces increasingly weakly as the Fe oxidation state increases. In past work, Dr. Anderson deduced that the ideal adsorption energies for the intermediates during the four-electron reduction of O₂ would be 0.0 eV for O₂ and H₂O and -1.35 eV, -2.49 eV, and -1.38 eV for OOH, O, and OH respectively [2]. Adsorption energies for Fe^{III} edge, Fe^{IV} bulk, and Fe^{IV} edge sites look most promising in this regard. To predict reversible potentials, however, we must use the adsorption energies of both the reactant, for example O, and product, for example OH, simultaneously. The adsorption energies of the H₂O molecule are ~ 0.5 eV, but this energy barrier will be partially offset by the interaction with water because the enthalpy of condensation for H₂O(g) is 0.45 eV.

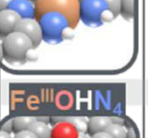
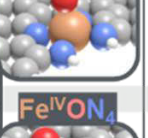
Active sites considered		O ₂	OOH	O	OH	H ₂ O
	Site	Adsorption Energy				
	Fe ^{II} bulk	-1.300	-2.160	-4.825	-3.074	-0.536
	Fe ^{II} edge	-1.053	-1.784	-4.273	-3.033	-0.490
	Fe ^{III} bulk	0.480	-2.429	-3.367	-2.095	-0.807
	Fe ^{III} edge	-0.207	-1.288	-2.864	-2.314	-0.365
	Fe ^{IV} bulk	-0.092	-1.058	-2.543	-1.616	-0.475
	Fe ^{IV} edge	-0.123	-0.805	-2.139	-1.625	-0.371
	Ideal	0.0	-1.35	-2.49	-1.38	-0.0

Figure 3. Schematic representation of various bulk and edge Fe^{II}, Fe^{III}, and Fe^{IV} active sites and adsorption energies (eV) of intermediates over Fe sites

To summarize, of the six catalyst sites explored, bulk Fe^{IV} shows the greatest promise for catalyzing four-electron reduction of O_2 to water because its predicted overpotential 0.29 V is the lowest. Edge Fe^{III} is a close second with its 0.43 predicted overpotential. No other sites are active. An issue is stabilizing Fe^{IV} against reduction to Fe^{III} . Although the calculated reversible potentials are approximate, we think our findings provide helpful guidance for catalyst development. They also correspond nicely to the ~ 0.90 V onset potential for O_2 reduction in the polarization plot for (CM+PANI)-Fe-C catalysts in the work by Chung et al. [1]. The dissociated structure of $\text{OOH}(\text{ads})$ with OH binding to C and O to Fe seen for bulk Fe^{III} and Fe^{IV} sites has not been discussed previously for carbon-based catalysts. The kinetic treatment on the combined electron transfer and bond rearrangement presents a challenge. This form of $\text{OOH}(\text{ads})$ may be important to understanding active site degradation and poisoning.

Task 3.0: MEA Optimization and Fuel Cell Testing (Month 4–36)

Selected catalysts have been successfully synthesized using a scaled-up procedure. Scale-up was necessary for producing the quantities needed for MEA fabrication and optimization. MEA optimization and fuel cell performance evaluation is in progress at LANL, in parallel with in-house fuel cell testing at SRNL and GWE. Fuel cell test results for H_2/O_2 are shown in Figure 4. Evaluation of a polyporphyrin based catalyst at LANL shows 16 mA cm^{-2} at $900 \text{ mV}_{\text{IR-free}}$, at 80°C in an MEA, with a total outlet pressure of 100 kPa (interim FY18 fuel cell target testing parameters). MEAs prepared at SRNL using the same catalyst resulted in a slightly lower performance of 12 mA cm^{-2} with the same testing conditions (Figure 4 [a and b]). Using the 2020 DOE performance target parameters (see Table 1) a current density of 32 mA cm^{-2} was measured (Figure 4 [c and d]).

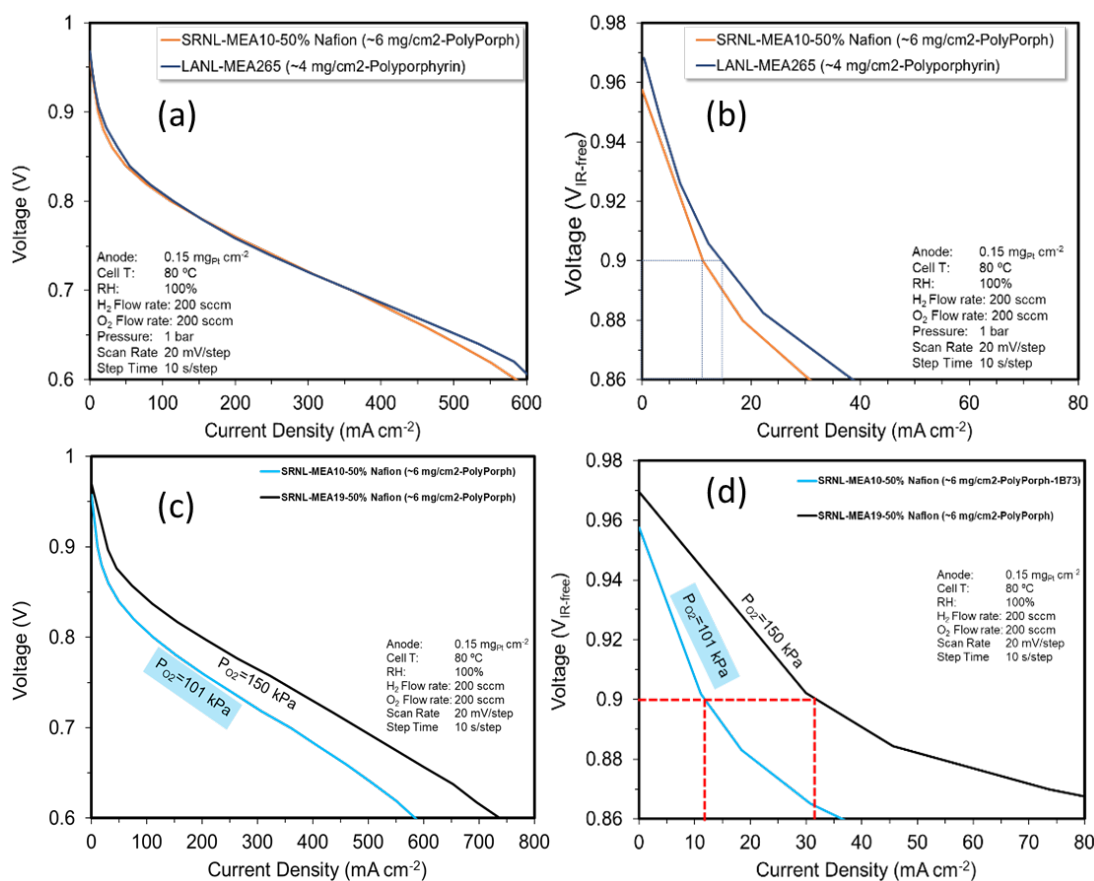


Figure 4. H_2/O_2 fuel cell performances of polyporphyrin-based catalysts at LANL and SRNL/GWE. (a) Uncorrected polarization curves, (b) IR-corrected polarization curves, (c) uncorrected polarization curves obtained at $101 \text{ kPa}_{\text{abs}}$ and $150 \text{ kPa}_{\text{abs}}$ back pressure, and (d) IR-corrected polarization curves obtained at $101 \text{ kPa}_{\text{abs}}$ and $150 \text{ kPa}_{\text{abs}}$ back pressure.

CONCLUSIONS AND UPCOMING ACTIVITIES

A wide range of metal-organic frameworks and covalent-organic frameworks were synthesized using a rational design to impart catalytic activity for the ORR. This was accomplished through the incorporation of FeN₂ moieties, or “phen”-type sites, and FeN₄ moieties, typically porphyrinic functionalities. Of the 17 families of materials screened, polyporphyrins synthesized using pyrrole and terephthalaldehyde demonstrated the highest performance for catalyzing the ORR and were down-selected for further study.

The polyporphyrin-based catalysts, unique to our research team among the ElectroCat consortium core labs and participating project teams, will be the focus during Budget Period 2 (BP 2). The ZIF-8 based catalysts will be utilized as a baseline catalyst for comparison of chemical, electrochemical, and physical properties and in MEA fabrication techniques. Additional analysis of polyporphyrin-based catalysts planned for BP2 includes detailed electron tomography (at Oak Ridge National Laboratory ElectroCat consortium lab), and X-ray techniques such as extended X-ray absorption fine structure and X-ray absorption near edge structure, to better understand the catalyst composition before and after pyrolysis, especially as it pertains to Fe moieties.

Polyporphyrins synthesized using a variety of different precursors, such as those containing 2, 3, and 4 aldehyde functional groups, will be explored during BP2, as well as the effect of different metal centers, especially Mn and Co. Heteroatom addition will be explored to address polymer stability at high potential and to tune hydrophobicity of the catalyst layer. Catalyst performance will be evaluated in H₂/O₂ and H₂/air fuel cell testing with the primary objective of achieving the BP 2 go/no-go metrics of 25 mA cm⁻² at 0.90 V_{IR-free}. Catalyst and MEA stability testing also will be initiated during BP 2.

Models developed during BP 1 will continue to be optimized during BP 2. The kinetic treatment on the combined electron transfer and bond rearrangement presents a challenge. This form of OOH(ads) could be important to understanding active site degradation and poisoning.

FY 2018 PUBLICATIONS/PRESENTATIONS

1. “PGM-Free Engineered Framework Nano-Structure Catalysts,” 2018 DOE Hydrogen Program Fuel Cell Project Progress Report, January 4, 2018, WebEx.
2. “PGM-Free Engineered Framework Nano-Structure Catalysts,” 2018 DOE Hydrogen Program Fuel Cell Project Progress Report, March 27, 2018, Aiken SC.
3. “PGM-Free Engineered Framework Nano-Structure Catalysts,” DOE Hydrogen and Fuel Cells Program Review Presentation, June 13–15, 2018, Washington DC.
4. “PGM-Free Engineered Framework Nano-Structure Catalysts,” Go/No-Go Milestone Presentation, September 06, 2018, Aiken, SC.

REFERENCES

1. H.T. Chung, D.A. Cullen, D. Higgins, B.T. Sneed, E.F. Holby, K.L. More, and P. Zelenay, *Science* 357 (2017): 479.
2. A.B. Anderson, *Phys. Chem. Chem. Phys.* 14 (2012): 1330.

Highly Efficient and Durable Cathode Catalyst with Ultralow Platinum Loading Through Synergetic Platinum/Platinum-Group-Metal-Free Catalytic Interaction

Di-Jia Liu (Primary Contact), Lina Chong
Argonne National Laboratory
9700 South Cass Avenue
Lemont, IL 60439
Phone: (630) 252-4511
Email: djliu@anl.gov

DOE Manager: Dimitrios Papageorgopoulos
Phone: (202) 586-5463
Email: Dimitrios.Papageorgopoulos@ee.doe.gov

Contract Number: DE-EE0007273

Project Start Date: April 3, 2017
Project End Date: September 30, 2019

Overall Objectives

- To develop low-Pt@PGM (platinum group metal)-free (LP@PF) cathode catalysts and membrane electrode assemblies (MEAs) meeting DOE fuel cell performance metrics, particularly at high current/power density region.
- To demonstrate one or more MEAs of total Pt loading $<0.125 \text{ mg/cm}^2$ with mass activity $>0.44 \text{ A/mg-Pt}$, current density $>300 \text{ mA/cm}^2$ at 0.8 V , and $>1,000 \text{ mW/cm}^2$ rated power tested in fuel cell.
- To demonstrate MEA stability of $<40\%$ loss in mass activity or $<30 \text{ mV}$ loss of voltage at 1.5 A/cm^2 after accelerated stress test in fuel cell.
- To gain better understanding on the synergistic catalysis between Pt and PGM-free active sites through computational modeling and advanced characterization.

Fiscal Year (FY) 2018 Objectives

- Demonstrate a MEA containing LP@PF catalyst with current density $>300 \text{ mA/cm}^2$ at 0.8 V and $<40\%$ loss of mass activity when tested under one-bar air in single fuel cell.
- Demonstrate a MEA/fuel cell with mass activity $>0.44 \text{ A/mg-PGM}$ and $<40\%$ loss of mass activity, $<30 \text{ mV}$ loss at 1.5 A/cm^2 in durability, following the accelerated test protocol by DOE.
- Complete LP@PF catalyst structure, electronic state, and surface property characterization using conventional and advanced characterization tools.

Technical Barriers

This project addresses the following technical barriers from the Fuel Cell section of the Fuel Cell Technologies Office Multi-Year Research, Development, and Demonstration Plan¹:

- A. Insufficient fuel cell cathode catalyst durability
- B. High cost due to high Pt loading in fuel cell cathode
- C. Low performance at high fuel cell current density due to insufficient catalytic sites.

Technical Targets

The current project status measured against the DOE 2025 catalyst/MEA performance targets is shown in Table 1.

¹ <https://energy.gov/eere/fuelcells/downloads/fuel-cell-technologies-office-multi-year-research-development-and-22>

FY 2018 Accomplishments

- Argonne National Laboratory's (ANL's) new LP@PF catalysts demonstrated high Pt mass activities up to 3.30 A/mg_{Pt} in fuel cell tests, exceeding the DOE 2025 target.
- Fuel cells containing ANL's LP@PF cathode catalyst with ultralow Pt loading demonstrated current densities >300 mA/cm² at 0.8 V and >1,000 mA/cm² at 0.65 V under one bar air, respectively, meeting the DOE 2025 target.
- Fuel cells containing ANL's LP@PF cathode catalyst with ultralow Pt loading showed 7% loss of mass activity, less than 6 mV voltage loss at 0.8 A/cm² and less than 8 mV voltage loss at 1.5 A/cm² after 30,000 voltage cycle accelerated stress test, meeting the DOE target.
- Advanced characterization and density functional theory (DFT) calculation revealed the catalyst structural properties and synergistic mechanism.

Table 1. Current Project Status Measured Against DOE 2025 Catalyst/MEA Performance Targets

	Units	DOE 2025 Target	Project Inception	Current Status
Pt mass activity @ 900 mV _{iR-free}	A/mg _{PGM}	0.44	1.77	3.30
PGM total loading	mg/cm ²	<0.125 (total)	0.039 (cathode)	0.033 (cathode)
MEA performance @ 800 mV (1 bar air)	mA/cm ²	≥300	273	359
MEA performance @ 675 mV (1 bar air)	mA/cm ²	≥1,000	754	1,005
Loss in mass activity @ 900 mV _{iR-free}	% loss	<40	85%	7%
Loss in performance at 0.8 A/cm ²	mV	<30	50	6
Loss in performance at 1.5 A/cm ²	mV	<30	62	8

INTRODUCTION

This project applies a new approach of preparing highly efficient and stable cathode catalysts containing ultralow Pt on PGM-free catalytic substrate derived from porous organic precursors. It addresses a major challenge in fuel cell catalyst/MEA development—how to improve electrocatalyst/MEA activity and the durability in the full fuel cell operational span using the least possible amount of platinum. The idea stemmed from an early discovery made in our laboratory: a synergistic catalysis exists between ultralow-concentration Pt alloy and its PGM-free catalytic support, leading to high specific activity and stability.

The goal of this project is to deliver one or more such catalysts that can meet DOE fuel cell catalyst/MEA performance metrics, particularly at high current density region. The project addresses several key barriers for polymer electrolyte membrane (PEM) fuel cell technology including cost, efficiency, and durability, aiming at reducing the fuel cell Pt usage to <0.125 g/kW, or <10 g/vehicle. This amount is similar to that currently used in the catalytic converter of the automobile with internal combustion engine. The success of the new catalyst potentially could smooth the transition from internal combustion to fuel cell vehicles without interrupting Pt price and supply. The research also has broader impact to fuel cell technology beyond the transportation sector. The same catalysts and MEAs also can be applied to portable tool, stationary power generation for which the cost reduction is essential to market penetration.

APPROACH

The LP@PF catalysts are prepared using transition metal (TM) based metal-organic frameworks (MOFs) as the precursors that can be converted to PGM-free catalytic substrate upon heat activation. The monometallic or bimetallic MOF is synthesized by either solvothermal or solid-state reaction between the TM ions and nitrogen-containing organic ligands [1, 2]. Upon high-temperature pyrolysis, the ligands are converted to charge-conducting N/C graphitic composite on which the oxygen reduction reaction active site, TM-N_x-C_y, is formed through the coordination between TM ion and the carbonaceous nitrogen. Meanwhile, a fraction of TM is reduced to metallic nanoparticles under the high temperature in reducing environment, which subsequently serve as the seeds to grow Pt-TM core-shell alloy nanoparticles during the following platinum catalyzing and annealing processes. The catalytic activity and durability are tested by the rotating disk electrode (RDE) method and in a fuel cell. In addition to LP@PF catalyst, we also integrated MOFs into nanofiber using the electrospin approach to produce LP@PF catalyst support embedded in nanofiber, LP@PFNF catalysts under this program [3].

RESULTS

During FY 2018, we designed and synthesized nearly 100 LP@PF and LP@PFNF catalysts and tested more than 70 MEAs in fuel cells. We also studied the catalyst structures, electronic states, and surface properties using high-resolution transmission electron microscopy (HR-TEM), X-ray diffraction, X-ray photoelectron spectroscopy, X-ray absorption spectroscopy, and Brunauer-Emmett-Teller surface analysis. Figure 1 shows the HR-TEM images of a representative LP@PF catalyst. The catalyst consists of Pt-Co alloy nanoparticles situated over high-surface-area Co-N_x-C_y substrate (Figure 1A). The Pt-Co nanoparticles have a Pt-Co core and Pt shell of two to three layers of Pt atom (Figure 1B). Amplifying the contrast of the substrate at the background shows the individually dispersed Co atoms embedded in N/C composite (Figure 1C). The oxygen reduction reaction catalysis occurs over Pt-Co nanoparticles and PGM-free sites simultaneously and independently. Meanwhile the unconverted H₂O₂ produced from the TM-N_x-C_y sites can migrate over to nearby Pt-Co nanoparticle surface to be further reduced to H₂O at much faster pace, accomplishing synergistic catalysis and improving Pt utilization.

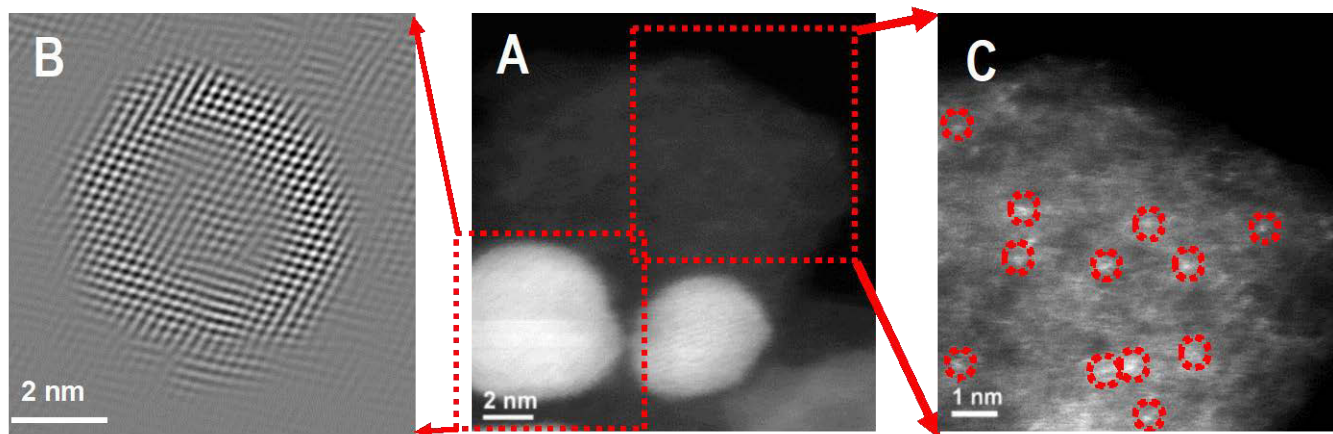


Figure 1. (A) HR-TEM showing a representative LP@PF catalyst with Pt-Co nanoparticles over PGM-free support; (B) core-shell structure of Pt-Co nanoparticles with the Pt-Co core and Pt shell; and (C) PGM-free support showing evenly distributed single Co atoms (red circles) over N/C composite

The LP@PF catalysts were incorporated into MEAs and tested under PEM fuel cell operating condition. Figure 2 shows the current-voltage polarizations tested under one-bar air of PEM fuel cells containing MEAs with LP@PF-11 and LP@PF-12 catalysts at the cathode. The cathodic Pt loadings for the catalysts were $0.033 \text{ mg}_{\text{Pt}}/\text{cm}^2$ and $0.035 \text{ mg}_{\text{Pt}}/\text{cm}^2$, respectively. For comparison, the current-voltage polarizations of two commercial MEAs with 6–10 times the cathodic Pt loading also are plotted. The activity of MEAs with LP@PF cathode catalyst outperformed the commercial products at both high voltage and high current domains of the fuel cell operation, even at substantially less Pt loading.

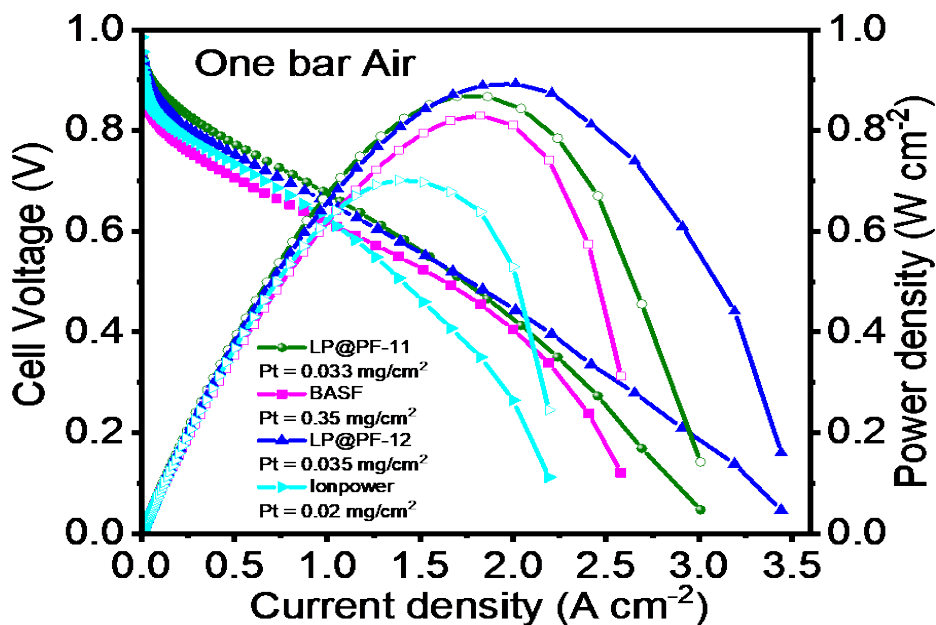


Figure 2. The current-voltage polarizations of fuel cells containing MEAs with LP@PF catalysts at cathode. For comparison, the polarization of two commercial MEAs also is shown. Test condition: 80°C , $P_{\text{air}} = P_{\text{H}_2} = 1 \text{ bar}$, 100% relative humidity, Nafion 211 membrane, MEA area = 5 cm^2 .

The LP@PF catalyst durability also was evaluated under multiple voltage cycling from 0.6 V to 1.0 V, using DOE's accelerated stress test protocol. Figure 3 shows current-voltage polarization of a MEA containing cathodic LP@PF-new catalyst. After 5,000 and 30,000 voltage cycles, the polarization voltage at any given

current density remained nearly unchanged or actually improved somewhat, indicating high stability of the LP@PF catalyst under aging conditions in a fuel cell.

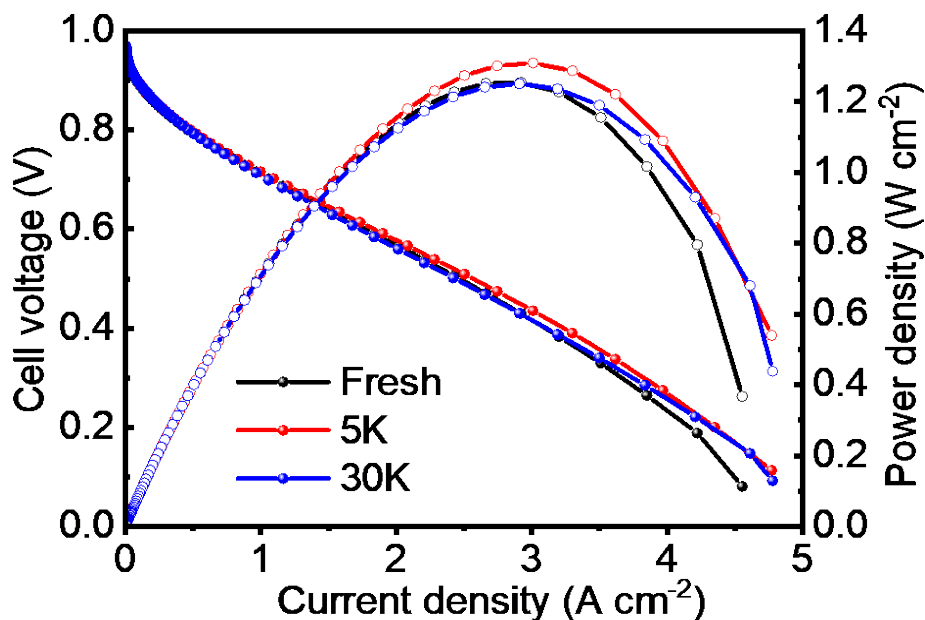


Figure 3. The current-voltage polarizations of fuel cells at different voltage cycles during the accelerated stress test. The MEA has LP@PF-new catalyst at cathode with Pt loading of 0.033 mg/cm². Test condition: 80 °C, P_{air} = P_{H₂} = 1 bar, 100% relative humidity, Nafion 211 membrane, MEA area = 5 cm².

CONCLUSIONS AND UPCOMING ACTIVITIES

Argonne's LP@PF catalysts demonstrated excellent activity and durability when tested in PEM fuel cell, indicating oxygen reduction reaction catalyst performance can be improved through synergistic interaction between ultralow loading of Pt and PGM-free active sites. Further studies include:

- Complete evaluation of new membranes for LP@PF catalyst in MEA H₂-air fuel cell.
- Complete exploration and evaluation of new catalysts and catalytic electrodes for LP@PF and LP@PFNF MEAs.
- Complete optimization of anode/cathode Pt distribution and demonstrate MEA with total Pt loading <0.125 mg/cm².

SPECIAL RECOGNITIONS AND AWARDS/PATENTS ISSUED

1. "Low Platinum Catalyst and Method of Preparation," Di-Jia Liu and Lina Chong, U.S. Patent 9,825,308.

FY 2018 PUBLICATIONS/PRESENTATIONS

1. Lina Chong, Jianguo Wen, Joseph Kubal, Fatih G. Sen, Jianxin Zou, Jeffery Greeley, Maria Chan, Heather Barkholtz, Wenjiang Ding, and Di-Jia Liu, "Ultralow-Loading Platinum-Cobalt Fuel Cell Catalysts Derived from Imidazolate Frameworks," *Science* (2018), DOI:10.1126/science.aau0630.
2. Di-Jia Liu and Lina Chong, "Highly Efficient and Durable Cathode Catalyst with Ultralow Pt Loading Through Synergetic Pt/PGM-Free Catalytic Interaction," 2018 DOE Hydrogen and Fuel Cells Program Annual Merit Review and Peer Evaluation Meeting, June 13–15, 2018, Washington, D.C.

REFERENCES

1. Shengqian Ma, Gabriel Goenaga, Ann Call, and Di-Jia Liu, “Cobalt Imidazolate Framework as Precursor for Oxygen Reduction Reaction Electrocatalyst,” *Chemistry: A European Journal* 17 (2011): 2063–2067.
2. Dan Zhao, Jiang-Lan Shui, Lauren R. Grabstanowicz, Chen Chen, Sean M. Commet, Tao Xu, Jun Lu, and Di-Jia Liu, “Highly Efficient Non-Precious Metal Electrocatalysts Prepared from One-Pot Synthesized Zeolitic Imidazolate Frameworks (ZIFs),” *Advanced Materials* 26 (2014): 1093–1097.
3. Jianglan Shui, Chen Chen, Lauren R. Grabstanowicz, Dan Zhao and Di-Jia Liu, “High-Efficiency Non-Precious Metal Catalyst Containing Metal-Organic Framework Precursor Inside of Carbon Nano-Network,” *Proceedings of National Academy of Sciences* 112, no. 34 (2015): 10629–10634.

FY15 SBIR II Release 2: Ionomer Dispersion Impact on Fuel Cell and Electrolyzer Performance and Durability

Hui Xu (Primary Contact), Chao Lei,
Magali Spinetta
Giner, Inc.
89 Rumford Ave
Newton, MA 02466
Phone: (781) 529-0573
Email: hxu@ginerinc.com

DOE Manager: Donna Ho
Phone: (202) 586-8000
Email: Donna.Ho@ee.doe.gov

Technical Advisor: John Kopasz
Phone: (630) 252-7531
Email: kopasz@anl.gov

Contract Number: DE-SC0011307 (SBIR Phase II TTO)

Collaborators:

- Los Alamos National Laboratory, Los Alamos, NM
- Oak Ridge National Laboratory, Oak Ridge, TN
- University of Connecticut, Storrs, CT

Project Start Date: July 28, 2015

Project End Date: June 27, 2018

Overall Objectives

- Further develop and commercialize Los Alamos National Laboratory's (LANL) nonaqueous solvent-based ionomer dispersion technology.
- Scale-up ionomer and dimensionally stable membrane (DSM) production to allow for continuous roll-to-roll production of low platinum-group metal (PGM) membrane electrode assemblies (MEAs) for fuel cells and electrolyzers.
- Demonstrate the durability of polymer electrolyte membrane (PEM) fuel cell and electrolyzer MEAs at more extensive cycling and operating conditions.

Fiscal Year (FY) 2018 Objectives

- Characterize catalyst ink particle size and electrode layer structure using nonaqueous solvent based ionomer.
- Investigate the influence of the solvent on fuel cell performance and durability.
- Demonstrate the durability advantages of using nonaqueous ionomers in the electrode, and analyze reasons for improved durability.

Technical Barriers

This project addresses the following technical barriers from the Fuel Cell Technologies Office Multi-Year Research, Development and Demonstration Plan¹:

- PEM fuel cell durability
- PEM water electrolyzer durability and cost.

Technical Targets

The targets of this project are to apply ionomer-dispersion technology to make durable fuel cell and electrolyzer MEAs. DOE targets for PEM fuel cells are listed in Table 1.

DOE has not set a target for PGM electrolyzers. Giner's targets are the following:

- Low PGM loading electrolyzer MEA demonstrates less than 20 mV loss (at 1.5 mA/cm²) after 50,000 cycles from 1.4 V to 1.9 V
- Low PGM loading electrolyzer MEA demonstrates less than 20 mV performance loss after 1,000-hour test at 1.5 A/cm².

¹ <https://www.energy.gov/eere/fuelcells/downloads/fuel-cell-technologies-office-multi-year-research-development-and-22>

FY 2018 Accomplishments

- Catalyst ink particle size and rheology characterization were carried out to understand the impacts of solvent and various mixing processes on ink structure. The correlation between ink property and electrode morphology was established.
- Established MEA baseline using an nPA (1-propanol I)/water solvent system, which demonstrated a greatly improved, crack-free morphology; better performance; and more consistent test results than the 2-propanol (isopropanol, IPA) baseline MEA.
- Compared a series of nonaqueous solvents for their impact on ionomer dispersion and fuel cell durability and determined causes for improved fuel cell performance.
- Applied nonaqueous ionomer dispersions to low-Pt (platinum) loading PEM fuel cell MEAs and obtained high-resolution transmission electron microscopy (TEM) images of electrodes with Pt distribution and ionomer distribution. The electrode morphology/structures were correlated to cell performance and durability.

Table 1. Progress Toward Meeting Technical Targets for MEA Durability Targets

Characteristic	Units	DOE 2020 Target
PGM total content (both electrodes)	g/kW	<0.125
PGM total loading (both electrodes)	mg-PGM/cm ² _{geo}	<0.125
Loss in catalytic (mass) activity	% loss	<40
Loss in performance at 0.8 A/cm ²	mV	<30
Loss in performance at 1.5 A/cm ²	mV	<30
Mass activity @ 900 mV _{iR-free}	A/mg-PGM	0.44

INTRODUCTION

LANL has developed a revolutionary method of building an MEA for PEM fuel cells that can significantly reduce manufacturing costs and extend MEA lifetimes. This method incorporates unique polymer dispersions in nonaqueous liquids to produce superior electrode performance, stability, and durability during harsh fuel cell operating conditions [1–2]. The LANL-produced MEA has been evaluated and certified using an accelerated stress test developed by DOE in conjunction with car manufacturers; the voltage loss of LANL’s MEA remained below 30 mV even after 70,000 cycles.

The ionomer dispersion work at LANL has great potential to significantly improve the lifetime of PEM fuel cells [2–4]. However, the ionomer dispersion used was Nafion 1100 equivalent weight (EW); there has been a strong push in the industry towards lower-EW membranes that can increase proton conductivity. Low-EW ionomers are less dimensionally stable and could benefit more from Giner’s well-established DSM technology. Also, the work at LANL has been done with dispersions of ionomer in the salt form, rather than in the proton form. This requires additional processing after membrane production to put the membrane in the acid form. Using dispersions from LANL in the acid form and utilizing Giner’s DSM technology, this Phase II program will validate these technologies for viable commercial applications in advanced fuel cell and electrolyzer systems.

APPROACH

Conventional PEM fuel cell and membrane-based water electrolyzer technology suffers from a lack of durability, high manufacturing costs, and rapid performance degradation. In this project, Giner—in collaboration with LANL—investigates a revolutionary method of building membrane electrode assemblies for PEM fuel cells and water electrolyzers to reduce manufacturing costs and extend the lifetime of the electrochemical devices. In FY 2018, we focused on improving fuel cell durability using nonaqueous solvent-dispersed ionomer. Our approach to obtain good fuel cell durability is to (i) understand ionomer particle morphology in dispersion; (ii) investigate the electrode morphology, catalyst, and ionomer binder distributions in the electrodes; and (iii) evaluate the electrode performance using various electrodes prepared from different dispersing agents. Electrodes were made from different dispersions and tested both at Giner and LANL. Oak Ridge National Laboratory and the University of Connecticut characterized the electrode morphology including polymer electrolyte and catalyst distribution to correlate the beginning of life performance with electrode morphology.

Table 2 summarizes the list of MEAs made at Giner using various ionomer dispersions; these are Nafion 1100 EW dispersed in ethylene glycol (EG), butanediol (BUT), pentanediol (PEN), and 3M low-EW ionomer dispersed in PEN (PEN-3M). Two baselines—IPA/water and nPA/water—also were compared. From our preliminary ionomer to carbon (I/C) ratio study, an I/C of 0.6 was found to provide the best performance when using TKK Pt/C (46.7 wt% Pt on carbon) catalyst. Pt loading for all MEAs was targeted around 0.2 mg/cm² and below and verified by X-ray fluorescence. The Pt loading of five spots on the electrode was measured, with the average value reported as the actual Pt loading.

Table 1. List of Membrane Electrode Assemblies Made at Giner Using Various Dispersing Agents

Sample Abbreviation	Description	I/C	Pt Loading (mg/cm ²)
IPA	Nafion in 2-propanol/water	0.6	0.19
nPA	Nafion in 1-propanol/water	0.6	0.175
EG	Nafion in ethylene glycol	0.6	0.21
BUT	Nafion in butanediol	0.6	0.19
PEN	Nafion in pentanediol	0.6	0.18
PEN-3M	3M 825 EW in pentanediol	0.6	0.17

RESULTS

MEAs were fabricated by a decal transfer process onto Nafion NR-212 membrane. The MEAs were assembled with carbon paper gas diffusion layers (Toray H030). The prepared MEAs were placed in single-cell hardware with triple serpentine flow fields and a 25 cm² active area. The cell was conditioned by alternating between potential holds at 0.2 V (10 minutes) and 0.6 V (10 minutes) until constant currents were obtained at each voltage. The cell was heated to 80°C with humidity bottle temperatures of 80°C for the anode and 75°C for the cathode. The slightly lower cathode humidification temperature was employed to minimize the flooding at the cathode side. Figure 1 shows the dispersing solvent effect on fuel cell performance. The four dispersing agents using nonaqueous ionomers, EG, BUT, PEN, and PEN-3M, are similar in terms of initial performance. The nPA baseline MEA exhibits slightly better performance than all the others, while the IPA baseline displays significantly lower performance, especially in the high-current region. The initial performance ranks as illustrated below are nPA > EG ≈ BUT ≈ PEN ≈ PEN-3M > IPA.

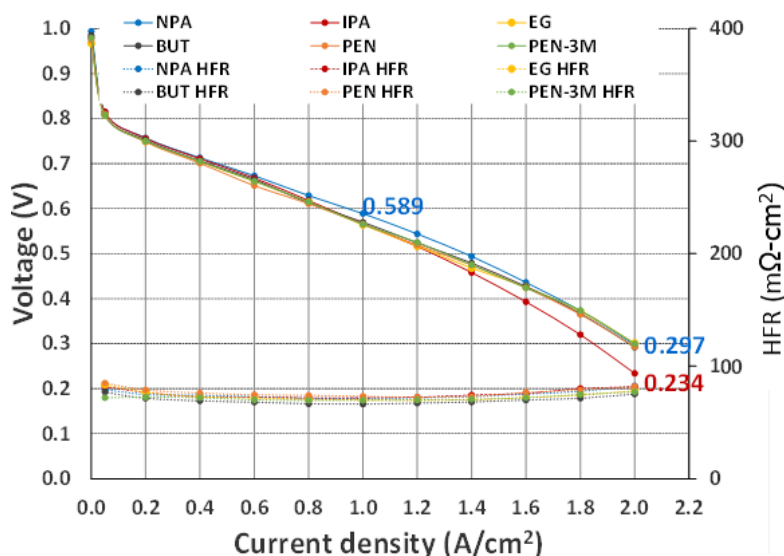


Figure 1. Effect of dispersing agents on initial fuel cell performance. Hydrogen/air fuel cell performance was measured at 80°C and ambient pressure. Membrane: Nafion 212; anode 50 wt% Pt/C (0.25 mg/cm²); cathode 50 wt% Pt/C catalyst; catalyst ink dispersing agent: varied.

Figure 2 shows the electrode durability upon voltage cycling tests up to 30,000 cycles. The voltage loss at 1A/cm² is up to 65–80 mV for the nPA and IPA baselines based on two replicated durability tests for each cathode. On the other hand, both the EG and BUT cathodes demonstrate only 35 mV voltage loss, which is nearly half of those for the two baselines. The good durability in cathodes using nonaqueous solvents EG and BUT could be due to improved electrode morphology and structures that may help to reduce the catalyst degradation.

After durability testing (0.6 V to 1.2 V, 30,000 cycles) under H₂/air, all tested cathodes were subject to particle-size measurements. Figure 3 summarizes the average particle size of Pt in all samples before and after the durability test. All beginning of life samples had comparable Pt particle sizes, 3.0–3.5 nm. After 30,000 voltage cycles, the average Pt particle size increased to 12 nm for both the IPA and nPA baselines, with particle size distribution (PSD) ranging from 5 nm to 30 nm. The BUT and EG cathodes showed a much smaller increase in Pt particle sizes (8–10 nm), with PSD ranging from 3 nm to 20 nm. Nonaqueous solvent-based MEAs demonstrated the least particle size increase. This is consistent with the durability data upon voltage cycling.

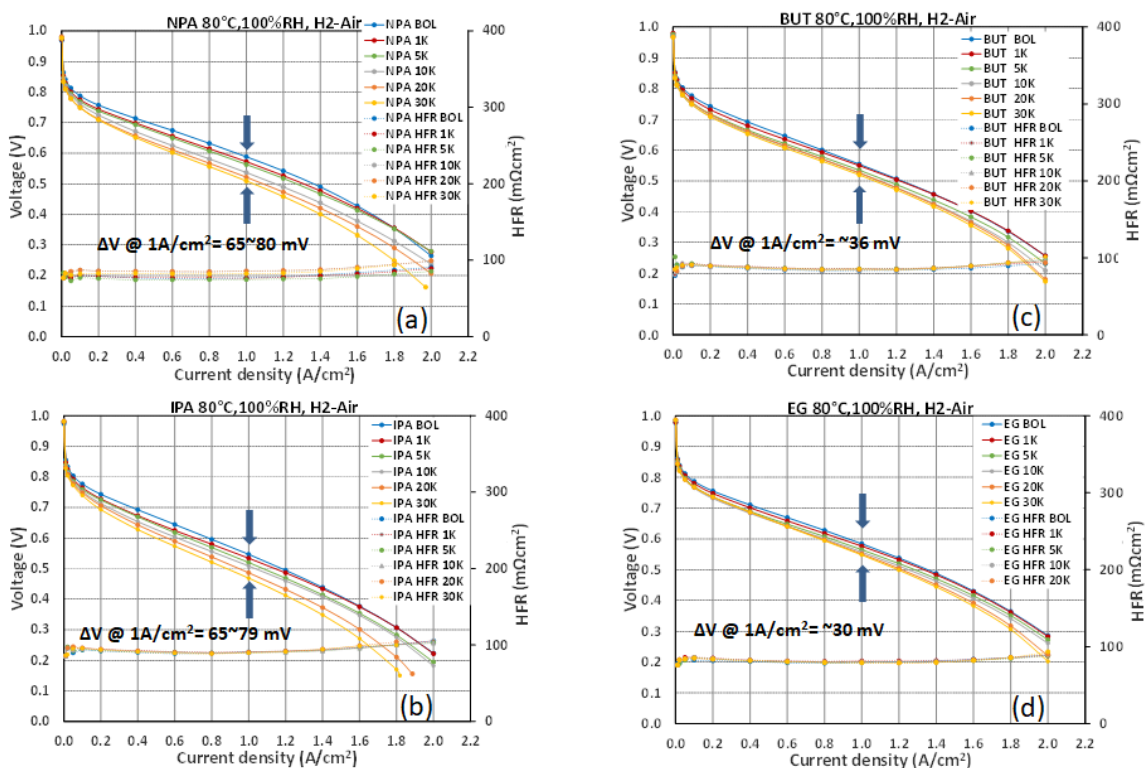


Figure 2. Electrode durability upon voltage cycling test: voltage cycling between 0.6 and 1.0 V. At 80°C, 100% RH, 0.2 SLPM H₂ / 0.075 SLPM N₂ (a) nPA-based MEA; (b) IPA-based MEA; (c) BUT-based MEA; (d) EG-based MEA

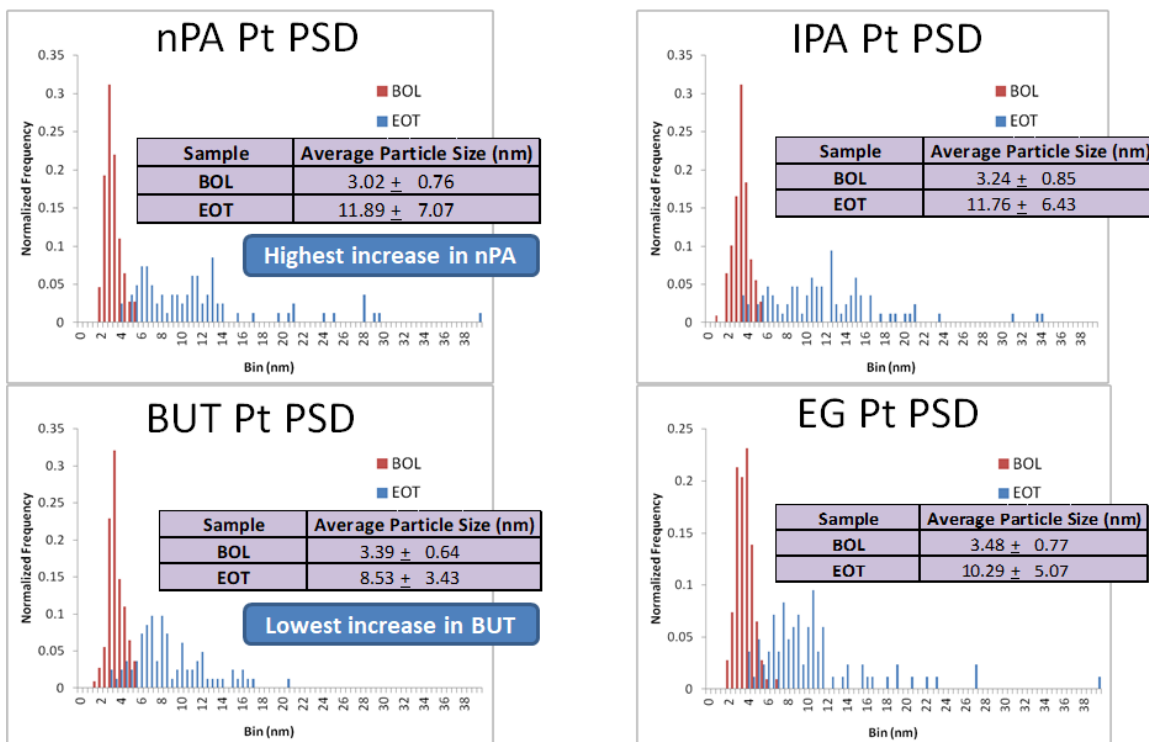


Figure 3. Particle-size measurements of fresh and tested MEAs using ionomers in various solvents

The high-resolution TEM–energy-dispersive X-ray spectroscopy images of the end of testing cathodes are shown in Figure 4. It is shown that there are significantly fewer Pt agglomerations in the BUT and EG samples than in the nPA and IPA baseline. Additionally, in the case of IPA, the electrode almost lost the majority of Pt particles. The loss of catalyst could be due to Pt dissolution and migration. It is also seen that BUT and EG samples have better ionomer distribution than the baseline. The durability benefit of using nonaqueous solvents may result from changed ionomer morphology in these solvents, which can help to prevent catalyst particle agglomeration and migration.

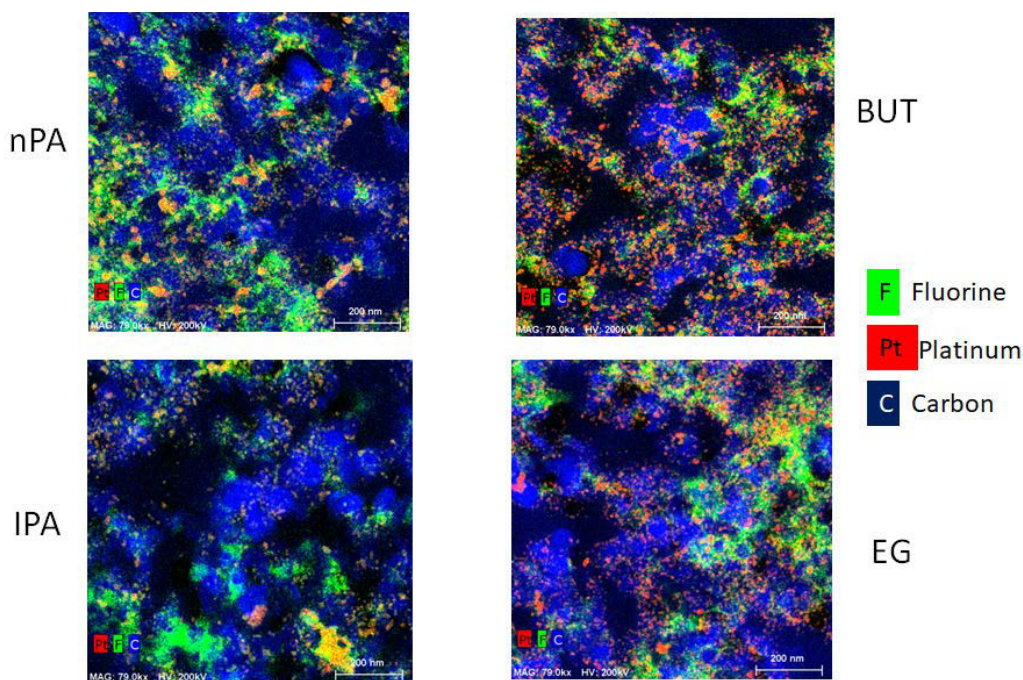


Figure 4. High-resolution TEM- energy-dispersive X-ray spectroscopy images of end-of-testing cathodes prepared from nPA, IPA, BUT, and EG

CONCLUSIONS AND UPCOMING ACTIVITIES

Conclusions

- Nonaqueous solvents affect ionomer morphology and platinum particle size distribution in catalyst inks.
- Nonaqueous solvent–based ionomer dispersions impact the electrode structures by changing the ionomer distribution and pore size distribution.
- Ionomer dispersions influence fuel cell electrode durability, and EG- and BUT-dispersed Nafion ionomers demonstrate the best fuel cell durability.
- The improved fuel cell durability is linked to reduced Pt particle agglomeration and migration, verified by TEM imaging and catalyst particle size distribution measurement.

Upcoming Activities

- Quantitatively characterize catalyst inks and correlate these characteristics to cell performance and durability.
- Investigate interactions between nonaqueous ionomer dispersion/catalysts to develop scalable MEA manufacturing for Giner’s water electrolyzer business.

FY 2018 PUBLICATIONS/PRESENTATIONS

1. H. Xu, “Ionomer Dispersion Impact on Advanced PEM Fuel Cell Performance and Durability,” Oral Presentation, DOE Hydrogen and Fuel Cell Annual Merit Review Meeting, Washington, DC (June 2018).

REFERENCES

1. E. Brosha, F. Garzon, C. Johnston, A. Labourieau, Y.S. Kim, K.-S. Lee, B. Orlor, B. Pivovar, D. Torrace, C. Welch, and H. Xu., “Studies Towards Optimizing Fuel Cell Electrode Structure and Composition,” Canada to USA Fuel Cell and Hydrogen Cluster Connection Workshop, Vancouver, BC, Canada (February 16–17, 2009).
2. Y.S. Kim, K.S. Lee, T. Rockward, U.S. Patent 7981319 B2 (2011).
3. Y.S. Kim, K.S. Lee, T. Rockward, U.S. Patent 8236207 B2 (2012).
4. C. Welch, A. Labouriau, R. Hjelm, B. Orlor, C. Johnston, and Y.S. Kim, “Nafion in Dilute Solvent Systems: Dispersion or Solution?” *ACS Macro Lett.* 1 (2012): 1403–1407.

Advanced Materials for Fully Integrated Membrane Electrode Assemblies in Anion Exchange Membrane Fuel Cells

Yu Seung Kim (Primary Contact), Sandip Maurya, Eun Joo Park
Los Alamos National Laboratory
Los Alamos, NM 87545
Phone: (505) 667-5782
Email: yskim@lanl.gov

DOE Manager: David Peterson
Phone: (720) 356-1747
Email: David.Peterson@ee.doe.gov

Subcontractors:

- Sandia National Laboratories, Albuquerque, NM
- Rensselaer Polytechnic Institute, Troy, NY

Project Start Date: November 2, 2015
Project End Date: November 1, 2018

Overall Objectives

- Synthesize highly conductive and chemically stable hydrocarbon-based anion exchange membrane (AEM).
- Prepare ionomeric electrode binders for the fabrication of anion exchange membrane fuel cell (AEMFC) electrodes.
- Integrate non-precious-metal or low-Pt-metal loading electrocatalysts into membrane electrode assembly (MEA).
- Demonstrate the high performance of AEMFCs.
- Demonstrate AEMFC durability under steady and accelerated stress conditions.

Fiscal Year (FY) 2018 Objectives

- Down-select the hydrogen oxidation reaction (HOR) catalyst and ionomer.
- Integrate the high-performance MEAs to obtain AEMFC peak power density >1 W/cm².

Technical Barriers

This project addresses the following technical barriers from the Fuel Cells section of the Fuel

Cell Technologies Office Multi-Year Research, Development, and Demonstration Plan [1]:

- Durability (polymer electrolytes)
- Cost (non-precious metal catalysts)
- Performance (AEMFCs).

Technical Targets

This project is developing advanced materials for AEMFCs for practical use in power applications. Insights gained from this project will be applied toward the next-stage AEMFC systems. The technical targets for AEMFCs in the Multi-Year Research, Development, and Demonstration Plan [1] are listed below.

- Q2, 2018: AEMFC power density >1 W/cm².
- Q4, 2018: V loss $<10\%$ for 2,000 h at 600 mA/cm².

FY 2018 Accomplishments

- Demonstrated alkaline stability for hexamethyl ammonium functionalized Diels-Alder poly(phenylene) (TMAC6PP): no structural change after 3,600 h in 0.5 M NaOH at 80°C (most stable AEM).
- Explored inhibition mechanism for alkaline HOR, namely, phenyl group adsorption. Additionally, developed the strategies to minimize phenyl adsorption by using rationally designed ionomeric binders, membranes, and less-phenyl-adsorbing PtRu HOR catalysts.
- Demonstrated stable area specific resistance (ASR) of ~ 0.05 Ω cm² of down-selected AEM for 500 h MEA operation at 0.6 A/cm².
- Designed new poly(fluorene) ionomer that exhibited 1.5 W/cm² (H₂/O₂) and 680 mW/cm² (H₂/CO₂-free air) peak power density of AEMFC.
- Implemented alternative Pd-based HOR catalysts in MEAs, which exhibit ~ 1 W/cm² peak power density.

INTRODUCTION

In previous years (2008–2013), we identified that aryl-ether linkage of the polymer backbone is not chemically stable under high pH conditions [2, 3]. Based on this result, we have developed several aryl-ether-free AEMs over the last three years [4–6]. In FY 2016 and FY 2017, hexamethyl ammonium functionalized Diels-Alder poly(phenylene) (TMAC6PP) and alkyl ammonium functionalized poly(terphenylene)s (TPN) were down-selected. We also developed advanced hydrocarbon ionomeric binders for AEMFC electrodes. Electrochemical and spectroscopic analyses are initiated to elucidate major HOR inhibition mechanisms, which helps to design advanced ionomeric binders for the AEMFC anode. In FY 2018, we completed the alkaline stability of the down-selected TMAC6PP AEM in alkaline medium up to 11,000 h. We exploited the HOR inhibition mechanism at MEA scale and made an effort to mitigate the HOR inhibition by the adoption of bimetallic catalysts and the design of new ionomers. We also demonstrated alternative Pd-based HOR catalysts in the integrated MEAs to prove the high-performance construction of the AEMFCs.

APPROACH

Our general approach to preparing stable and highly conductive AEMs is to synthesize cationic group functionalized aryl ether-free polymers. In addition, the strategy involves changing the commonly used benzyl trimethyl ammonium group with more stable alkylammonium. There are several viable synthetic pathways to accomplish synthesizing such polymer structure. Based on research efforts during FY 2016 and FY 2017, two polymers were down-selected, TMAC6PP (Sandia National Laboratories) and TPN (Rensselaer Polytechnic Institute).

Our general approach to preparing advanced high-performing ionomeric binders for AEMFCs is to develop different cationic groups for anode and cathode catalyst layers. For this we evaluated the catalytic activities of Pt and Pt-based bimetallic catalysts using various electrolytes to screen the candidate functional groups. Then the selected candidate functional groups will be employed into a polymeric structure and further structural optimization will be made at the MEA level (Los Alamos National Laboratory). For the anode, the less-phenyl-adsorbing catalyst should be used, such as PtRu or PtNi, in combination with less-phenyl-group-containing ionomers. The performance of the AEMFC components is evaluated in both the individual component and the MEA levels.

RESULTS

Alkaline Stability of Anion Exchange Membranes

Figure 1a compares the hydroxide conductivity change of benzyltrimethylammonium functionalized Diels-Alder poly(phenylene) (ATM-PP) control and TMAC6PP during ex situ stability test at 0.5 M and 4 M NaOH at 80°C. Note that the conductivity of ATM-PP quickly deteriorated within 200 h, but the conductivity of TMAC6PP was stable to 3,600 h and tends to degrade slowly after 4,000 h in 0.5 M NaOH conditions. The life test further proceeded to 11,000 h when the hydroxide conductivity decreased to 5 mS/cm. The chemical stability of the TMAC6PP during AEMFC operation was also measured. During 300 h of operation at a constant voltage of 0.3 V, it was found that the cell ASR tended to increase due to inevitable carbonation. In FY 2018, we developed a replenishing procedure to remove carbonation during the life test and evaluate the stability of the other down-selected AEM, poly(terphenylene). Figure 1b shows the ASR of the cell using the TPN membrane during AEMFC operation at a constant current of 0.6 A cm⁻² and 80°C. The cell was replenished with NaOH at 210, 350, 480, and 550 h of operation, and polarization curves were recorded along with ASR. It was found that the ASR of the cell using TPN was stable (~0.05 Ω cm²), indicating that the AEM remained stable during the long-term test.

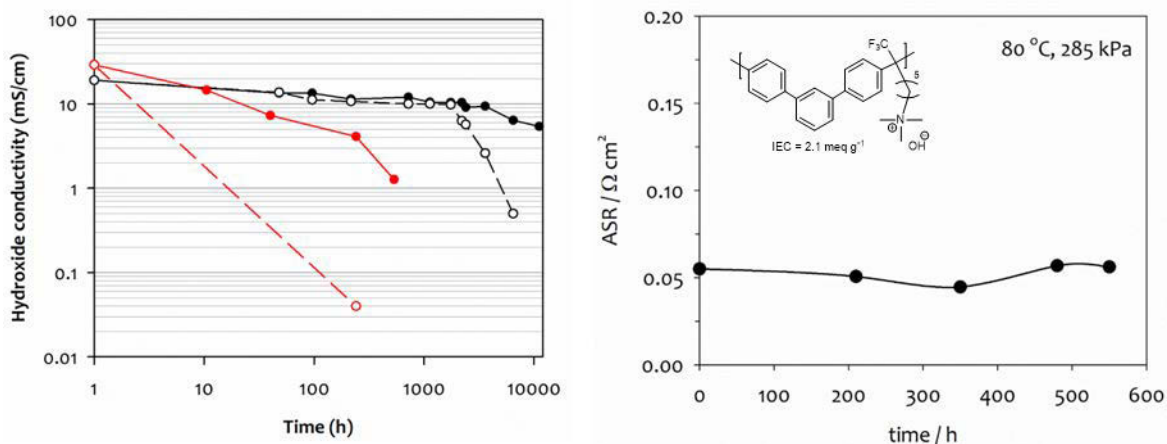


Figure 1. (a) Hydroxide conductivity change of TMAC6PP during ex situ alkaline stability test at 80 °C, (b) hydroxide conductivity change of the TPN membrane during in situ alkaline stability test at 80 °C

Phenyl Group Adsorption and HOR Inhibition

Rotating disk electrode investigation on alkaline HOR indicated that the HOR activity of Pt-based catalysts is greatly hindered by the phenyl adsorption parallel to the Pt surface [7]. We first examined the effect of the catalyst on phenyl group adsorption. It was found that the HOR current density of Pt in 0.1 M benzyltrimethylammonium hydroxide (BTMAOH) showed a peculiar behavior (appearance of inflection point) due to the phenyl group adsorption, the inflection point became less evident with alloying Pt with other transition metal. Less interaction between the phenyl group and catalyst was observed in the order of Mo, Ni, and Ru. The HOR voltammogram of Pt-Ru/C in 0.1 M BTMAOH becomes identical to that of Pt/C in 0.1 M TMAOH (phenyl-group-free solution) with only a slightly lower HOR current density (Figure 2). This result suggests that the phenyl group adsorption may be minimized with Pt-Ru catalysts. Based on this result, we down-selected the Pt-Ru/C catalyst as the HOR catalyst for AEMFCs.

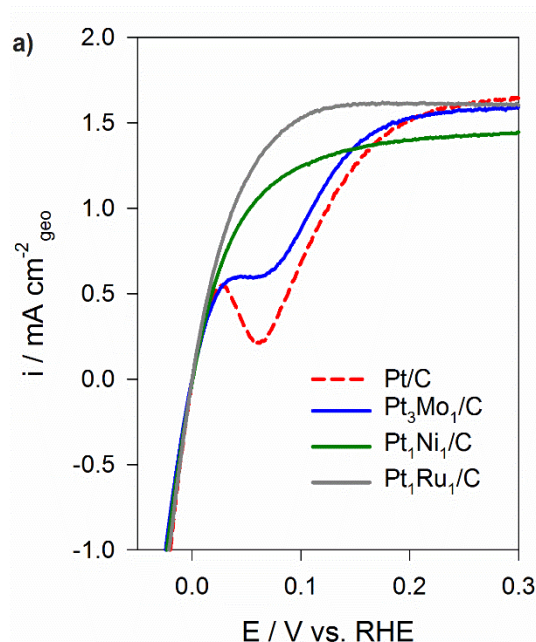


Figure 2. HOR voltammograms of Pt alloy/C catalysts in 0.1 M BTMAOH, measured at 25 °C, rotating speed: 900 rpm, scan rate: 5 mV/s. The graph is reproduced from Maurya et al. [8].

To prevent the phenyl adsorption, we rationally designed and synthesized new ionomeric binders based on poly(fluorene) polymer, that is, FLN [8]. The impact of phenyl group adsorption of FLN and alkyl ammonium functionalized poly(biphenylene) (BPN) ionomer is compared using a microelectrode half-cell. It was found that the HOR voltammogram of the Pt-Ru/C in contact with BPN is significantly suppressed between 0.02 V and 0.7 V, indicating that the phenyl group adsorption substantially inhibits the HOR activity of even low-phenyl-group-adsorbing Pt-Ru/C. In contrast, the HOR voltammogram of the Pt-Ru/C in contact with FLN shows a typical shape like the HOR voltammogram of the catalyst in alkali-metal electrolytes. Based on this result, we down-selected FLN as the electrode ionomer.

AEMFC Performance

Figure 3a shows the progress of AEMFC performance improvement achieved in FY 2018. The AEMFC performance of a control MEA using TMAC6PP was low due to the phenyl group adsorption on the HOR Pt catalyst. The peak power density of the AEMFC is only ~ 300 mW/cm². In FY 2017, the AEMFC performance was improved by using a Pt-Ru catalyst instead of Pt catalyst: ca. the peak power density of ~ 400 mW/cm². When we changed the poly(phenylene) ionomer to FLN, the AEMFC performance improved. The peak power density is $\sim 1,000$ mW/cm². The AEMFC performance further increased with increasing anode flow rate possibly due to the increased hydrogen access to the adsorbed cation layer [9]. The peak power density of the AEMFC reached 1,500 mW/cm² as the anode flow rate increased from 500 sccm to 2,000 sccm. It was also noted that cell high-frequency resistance also improved from ~ 0.07 Ω cm² (FY 2017) to 0.05 Ω cm² (FY 2018). We also examined the fuel cell performance of MEAs using alternative Pd-based HOR catalysts. Figure 3b compares the AEMFC performance of Pt/C, Pt-Ru/C, Pd/C, and Pd/C-CeO₂ anode catalyzed MEAs. Although the performance of the MEAs using the Pt-Ru/C and Pt/C anode catalyzed MEAs is better than Pd-based anode catalyzed MEAs, it was noted that the Pd/C anode catalyzed MEA also reached a peak power density close to 1 W/cm² revealing a benefit associated with the high-hydrogen-absorption characteristics of the Pd/C catalysts.

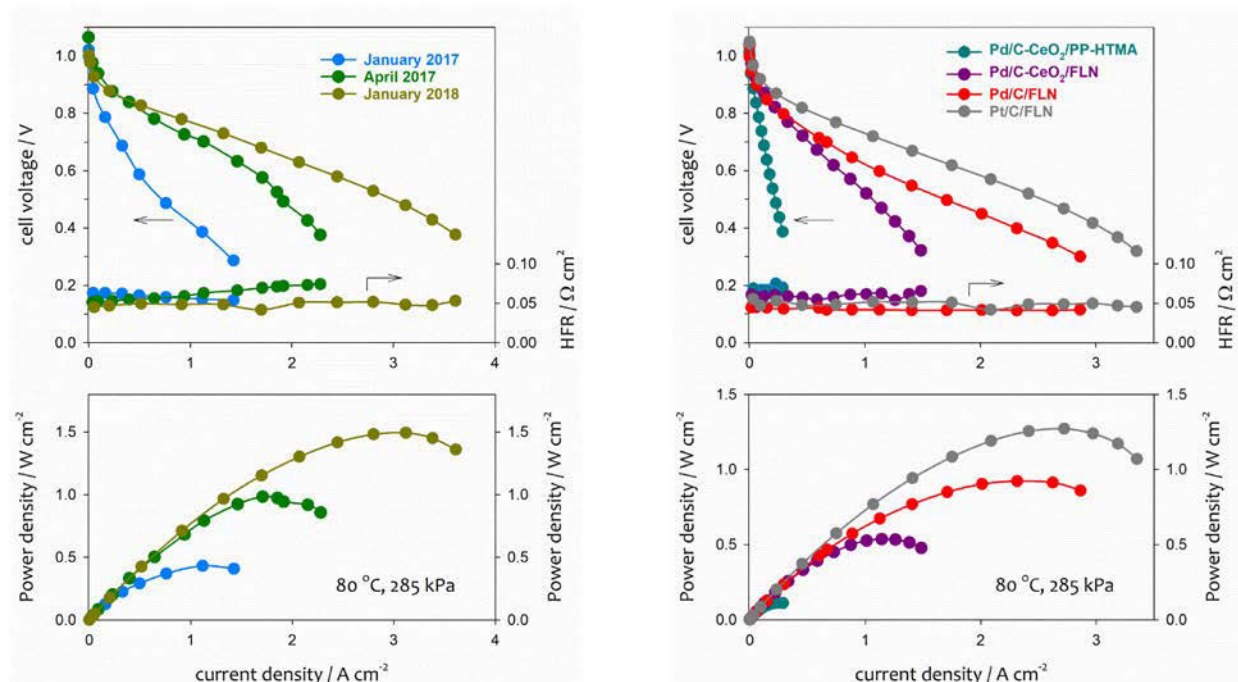


Figure 3. (a) Progress of AEMFC performance improvement; January 2017—AEM: TMAC6PP, anode catalyst: Pt-Ru/C, anode flow rate: 500 sccm; April 2017—AEM: FLN, anode catalyst: Pt-Ru/C, anode flow rate: 500 sccm; January 2018—AEM: FLN, anode catalyst: Pt-Ru/C, anode flow rate: 2,000 sccm. (b) Performance comparison between Pt-based and Pd-based anode catalyzed MEAs. All performance was measured under H₂/O₂ conditions. Cathode catalyst: Pt/C 0.6 mg_{Pt}/cm².

In summary, the major achievement for FY 2018 includes demonstrating high AEMFC performance by the down-selection of bimetallic Pt-Ru catalyst and poly(flourene) ionomer. We have also tested alternative a Pd-based catalyst to investigate the absorption/adsorption phenomena on the HOR catalysts. In the rest of FY 2019, most of the research will be directed toward solving the durability issues and identifying the durability limiting factors.

CONCLUSIONS AND FUTURE DIRECTIONS

- Demonstrated low ASR ($\sim 0.05 \Omega \text{ cm}^2$) of the down-selected AEM for 11,000 h in ex situ test and >550 h for in situ test.
- The HOR inhibition mechanism was further explored and, based on the study, high AEMFC performance (up to 1,500 mW/cm² peak power density) was obtained.
- Designed new poly(flourene) ionomer that exhibited the peak power density of 1.5 W/cm² (H₂/O₂) and 680 mW/cm² (H₂/CO₂-free air).
- Plan to evaluate the AEMFC durability after optimizing the MEAs and fuel cell conditions.
- Plan to evaluate the performance of non-platinum-group-metal HOR and oxygen reduction reaction catalysts.

SPECIAL RECOGNITIONS AND AWARDS/PATENTS ISSUED

1. Yu Seung Kim, Kwan-Soo Lee, and Cy Fujimoto, "Poly(Phenylene)-Based Anion Exchange Polymers and Methods Thereof," US Patent Application Publication, US 2017/0190831, July 6, 2017.
2. Yu Seung Kim, Eun Joo (Sarah) Park, and Sandip Maurya, "Polymer Electrolytes for Alkaline Membrane Fuel Cells," S133606, March 2, 2018.

FY 2018 PUBLICATIONS/PRESENTATIONS

1. Shimshon Gottesfeld, Draio R. Dekel, Miles Page, Chulsung Bae, Yu Shan Yan, Piotr Zelenay, and Yu Seung Kim, “Alkaline Exchange Membrane Fuel Cells—Current Status and Remaining Challenges,” *J. Power Sources* 375 (2018): 170–184.
2. Yu Seung Kim, “Interfacial Behavior of Polymer Electrolytes in Fuel Cell Electrodes,” Fuel Cells Gordon Research Conference, Energizing the Future by Innovation in Fuel Cell Materials, Methods, Modeling, and Manufacture, July 29 to August 3, 2018. Bryant University, Rhode Island.
3. Yu Seung Kim, Sandip Maurya, Ivana Matanovic, Cy Fujimoto, and Chulsung Bae, “Molecular Design Strategy of Polyaromatic Ionomers for AEMFCs,” Workshop on Ion Exchange Membranes for Energy Applications–EMEA2018, June 26–28, 2018, Bad Zwischenahn, Germany.
4. Ivana Matanovic, Hoon Taek Chung, and Yu Seung Kim, “Benzene Adsorption: A Significant Inhibitor for the Hydrogen Oxidation Reaction in Alkaline Conditions,” *J. Phys. Chem. Lett.* 8 (2017): 4918–4924.
5. S. Maurya, H. Chung, C. Fujimoto, I. Matanovic, and Y. S. Kim, “Why Pt-Ru Catalyst Works Better for Alkaline Hydrogen Oxidation Reaction?” Abstract Number: I04-1738, 233rd ECS Meeting, May 13–17, 2018, Seattle, Washington.
6. Sandip Maurya, Cy H. Fujimoto, Michael R. Hibbs, Claudia Narvaez Villarrubia, and Yu Seung Kim, “Toward Improved Alkaline Membrane Fuel Cell Performance Using Quaternized Aryl-Ether Free Polyaromatics,” *Chem. Mater.* 30 (2018): 2188–2192.
7. Sandip Maurya, Joseph H. Dumont, Claudia Narvaez Villarrubia, Ivana Matanovic, Dongguo Li, Yu Seung Kim, Sangtaik Noh, Junyoung Han, Chulsung Bae, Hamish A. Miller, Cy H. Fujimoto, Dario R. Dekel, “Surface Adsorption Affects the Performance of Alkaline Anion-Exchange Membrane Fuel Cells,” *ACS Catalysis* 8 (2018): 9429–9439.
8. Sandip Maurya, Sangtaik Noh, Ivana Matanovic, Eun Joo Park, Claudia Narvaez Villarrubia, Junyoung Han, Chulsung Bae, and Yu Seung Kim, “Rational Design of Polyaromatic Ionomers for Alkaline Membrane Fuel Cells with $> 1 \text{ W cm}^{-2}$ Power Density,” *Energy & Environ. Sci.* (2018), doi:10.1039/C8EE02192A.
9. E.J. Park, S. Maurya, C. Bae, and Y. S. Kim, “Dimethyl Substituted Polyaromatic Alkaline Ionomers for Better Alkaline Hydrogen Oxidation,” 233rd ECS Meeting, May 13–17, 2018, Seattle, Washington.
10. Eun Joo Park and Yu Seung Kim, “Quaternized Aryl Ether-Free Polyaromatics for Alkaline Membrane Fuel Cells: Synthesis, Properties, and Performance—A Topical Review,” *J. Mater. Chem. A.* 6 (2018): 15456–15477.

REFERENCES

1. Fuel Cell Technologies Office Multi-Year Research, Development and Demonstration Plan, <https://energy.gov/eere/fuelcells/downloads/fuel-cell-technologies-office-multi-year-research-development-and-22>.
2. Cy Fujimoto, Dae-Sik Kim, Michael Hibbs, Debra Wroblewski, and Yu Seung Kim, “Backbone Stability of Quaternized Polyaromatics for Alkaline Membrane Fuel Cells,” *J. Memb. Sci.* 423–424 (2012): 438.
3. Yoong-Kee Choe, Cy Fujimoto, Kwan-Soo Lee, Luke T. Dalton, Kathy Ayers, Neil J. Henson, and Yu Seung Kim, “Alkaline Stability of Benzyl Trimethyl Ammonium Functionalized Polyaromatics: A Computational and Experimental Study,” *Chem. Mater.* 26 (2014): 5675.
4. Woo-Hyung Lee, Yu Seung Kim, and Chulsung Bae, “Robust Hydroxide Ion Conducting Poly(biphenyl alkylene)s for Alkaline Fuel Cell Membranes,” *ACS Macro Letters* 4 (2015): 814.
5. Angela D. Mohanty, Chang Y. Ryu, Yu Seung Kim, and Chulsung Bae, “Stable Elastomeric Anion Exchange Membranes Based on Quaternary Ammonium-Tethered Polystyrene-b-poly (Ethylene-co-butylene)-b-polystyrene Triblock Copolymers,” *Macromolecules* 48 (2015): 7085.

6. Woo-Hyung Lee, Angela D. Mohanty, and Chulsung Bae, “Fluorene-Based Hydroxide Ion Conducting Polymers for Chemically Stable Anion Exchange Membrane Fuel Cells,” *ACS Macro Lett.* 4 (2015): 453.
7. I. Matanovic, H. T. Chung, and Y. S. Kim, “Benzene Adsorption: A Significant Inhibitor for the Hydrogen Oxidation Reaction in Alkaline Conditions,” *J. Phys. Chem. Lett.* 8 (2017): 4918.
8. Sandip Maurya, Sangtaik Noh, Ivana Matanovic, Eun Joo Park, Claudia Narvaez Villarrubia, Junyoung Han, Chulsung Bae, and Yu Seung Kim, “Rational Design of Polyaromatic Ionomers for Alkaline Membrane Fuel Cells with $> 1 \text{ W cm}^{-2}$ Power Density,” *Energy & Environ. Sci.* (2018), doi:10.1039/C8EE02192A.
9. Hoon Taek Chung, Ulises Martinez, Ivana Matanovic, and Yu Seung Kim, “Cation-Hydroxide-Water Coadsorption Inhibits the Alkaline Hydrogen Oxidation Reaction,” *J. Phys. Chem. Lett.* 7 (2016): 4464–4469.
10. Sandip Maurya, Joseph H. Dumont, Claudia Narvaez Villarrubia, Ivana Matanovic, Dongguo Li, Yu Seung Kim, Sangtaik Noh, Junyoung Han, Chulsung Bae, Hamish A. Miller, Cy H. Fujimoto, and Dario R. Dekel, “Surface Adsorption Affects the Performance of Alkaline Anion-Exchange Membrane Fuel Cells,” *ACS Catalysis* 8 (2018): 9429–9439.

Advanced Ionomers and Membrane Electrode Assemblies for Alkaline Membrane Fuel Cells

Bryan Pivovar (Primary Contact), Derek Strasser, Kelly Meek, Chris Antunes, Ami Neyerlin, Andrew Park, K.C. Neyerlin, Shaun Alia, Hai Long, and Zbyslaw Owczarczyk
National Renewable Energy Laboratory
15013 Denver West Parkway
Golden, CO 80401
Phone: (303) 275-3809
Email: Bryan.Pivovar@nrel.gov

DOE Manager: David Peterson
Phone: (720) 356-1747
Email: David.Peterson@ee.doe.gov

Subcontractors:

- Lawrence Berkeley National Laboratory, Berkeley, CA
- Colorado School of Mines, Golden, CO
- 3M Company, St. Paul, MN

Project Start Date: October 1, 2015
Project End Date: September 30, 2019

Overall Objectives

- Improve novel perfluoro (PF) anion exchange membrane (AEM) properties and stability.
- Employ high-performance PF AEM materials in electrodes and as membranes in alkaline membrane fuel cells (AMFCs). Apply models and diagnostics to AMFCs to determine and minimize losses (water management, electrocatalysis, and carbonate related).

Technical Barriers

This project addresses the following technical barriers from the Fuel Cells section of the Fuel Cell Technologies Office Multi-Year Research, Development, and Demonstration Plan¹:

- (A) Durability (of membranes and membrane electrode assemblies)
- (B) Cost (of membranes and membrane electrode assemblies)

- (C) Performance (of membranes and membrane electrode assemblies).

Technical Targets

This project will synthesize novel PF AEMs and ionomers and incorporate these into membrane electrode assemblies (MEAs) for fuel cell testing. The project generally supports targets outlined in the Multi-Year Research, Development, and Demonstration Plan in application-specific areas (portable, stationary, transportation). As alkaline membrane fuel cells are at an earlier stage of development, however, specific target tables have not yet been developed. There are four tasks presented by Dimitrios Papageorgopoulos at the AMFC Workshop, April 1, 2016 [1].

- Q2, 2017: Develop anion-exchange membranes with an area-specific resistance ≤ 0.1 ohm cm², maintained for 500 hours during testing at 600 mA/cm² at T >60°C.
- Q4, 2017: Demonstrate AMFC peak power performance >600 mW/cm² on H₂/O₂ (maximum pressure of 1.5 atm_a) in MEA with a total loading of ≤ 0.125 mg-PGM/cm².
- Q2, 2019: Demonstrate AMFC initial performance of 0.6 V at 600 mA/cm² on H₂/air (maximum pressure of 1.5 atm_a) in MEA, a total loading of <0.1 mgPGM/cm², and less than 10% voltage degradation over 2,000-hour hold test at 600 mA/cm² at T >60°C. Cell may be reconditioned during test to remove recoverable performance losses.
- Q2, 2020: Develop non-PGM catalysts demonstrating alkaline membrane fuel cell peak power performance >600 mW/cm² under hydrogen/air (maximum pressure of 1.5 atm_a) in platinum group metal (PGM)-free MEA.

¹ <https://energy.gov/eere/fuelcells/downloads/fuel-cell-technologies-office-multi-year-research-development-and-22>

FY 2018 Accomplishments

- The project has repeatedly demonstrated fuel cell performance greater than 1 W/cm² and durability greater than 500 hours during testing at 600 mA/cm².
- The project has developed novel perfluoro polymers based on sulfonamide linkage chemistry (Generation [Gen] 2), including improving ion exchange capacity and tethering of novel cations (Gen 2+ chemistries).
- PF AEM Gen 3 chemistry was determined to be a no-go due to difficulties in achieving extent of reaction required for viable membrane performance.
- Building on the high performance of ethylene tetrafluoro ethylene polymer (ETFE)-based electrodes, PF AEM electrodes and full PF AEM cells now also have demonstrated performance of greater than 1 W/cm².
- Model development is providing insight into the role of water and carbon dioxide in these systems, allowing the performance potential and limitations of AMFCs to be better understood.

INTRODUCTION

AMFCs are of interest primarily because they enable the use of non-Pt catalysts, the main cost/supply limitation of polymer electrolyte membrane fuel cells (PEMFCs). AMFCs, therefore, offer the potential of greatly decreased polymer electrolyte fuel cell cost. Operating AMFCs under ambient conditions where carbon dioxide is present remains a challenge due to carbonate formation. An approach that has shown promise for carbon dioxide tolerance is increased operating temperature. Unfortunately, the stability of the cation side chains on the membrane polymer and water management within the membrane both become more difficult as temperature rises.

The use of perfluorinated ionomers—similar to those used in PEMFC systems—with tethered cation head groups that allow hydroxide conduction should help improve water-transport properties and offer exceptional chemical durability of the backbone. The significant advances demonstrated in AMFC systems have been accomplished primarily through improving water management and the bonding between membrane and electrode. Both issues can be tackled much more effectively when employing PF AEMs and ionomers. The project consists of three subtasks:

1. Synthesis of novel perfluorinated alkaline ionomers (National Renewable Energy Laboratory [NREL])
2. Characterization of PF AEMs (NREL, Oak Ridge National Laboratory/University of Tennessee Knoxville, Colorado School of Mines)
3. Fuel cell performance and modeling optimization (NREL, Lawrence Berkeley National Laboratory).

APPROACH

The team has focused on achieving higher-temperature, higher-power-density AMFC operation through implementation of novel alkaline PF membranes and ionomeric dispersions. PF materials are expected to enhance water transport capabilities and electrode performance/durability significantly, thereby enabling higher temperature and power density operation. The combination of high current density and high operating temperature will improve the ability of these devices to tolerate ambient CO² and potentially enable tolerance to these conditions. Starting with the sulfonyl fluoride form of current perfluoro ionomers we have identified, and in several cases verified, the ability to convert commercially available precursors into anion exchange polymers and membranes. The synthesized PF ionomers have been cast into membranes, made into polymeric dispersions, and characterized in fuel cell tests. Modeling efforts have been made in parallel to better understand cell performance, loss mechanisms, and mitigation approaches.

RESULTS

Although PF chemistry improves PF sulfonic acid (PFSA) acidity, the strongly electron withdrawing PF backbone creates challenges for anion exchange membranes. From the readily available perfluoro sulfonyl fluoride precursor (PF-SFP), different strategies can be employed to tether cations to the polymer backbone. We have focused on an amide linkage as shown in Figure 1 for our Gen 1 and Gen 2 PF AEMs and an aryl linkage for Gen 3. Although small molecule studies of Gen 3 chemistry showed good chemical stability, we abandoned the approach due to the extent of the reaction difficulties occurring while performing modification to the base polymer, and instead focused on tethering cations with increased stability onto our Gen 2 platform. The advanced cation tethering is in progress, but we have shown the ability to achieve reasonable ion exchange capacity and conductivity with advanced imidazolium-based cations. To date, we have synthesized more than 300 g of Gen 2 PF AEM and have shared this material with more than 20 collaborating institutions.

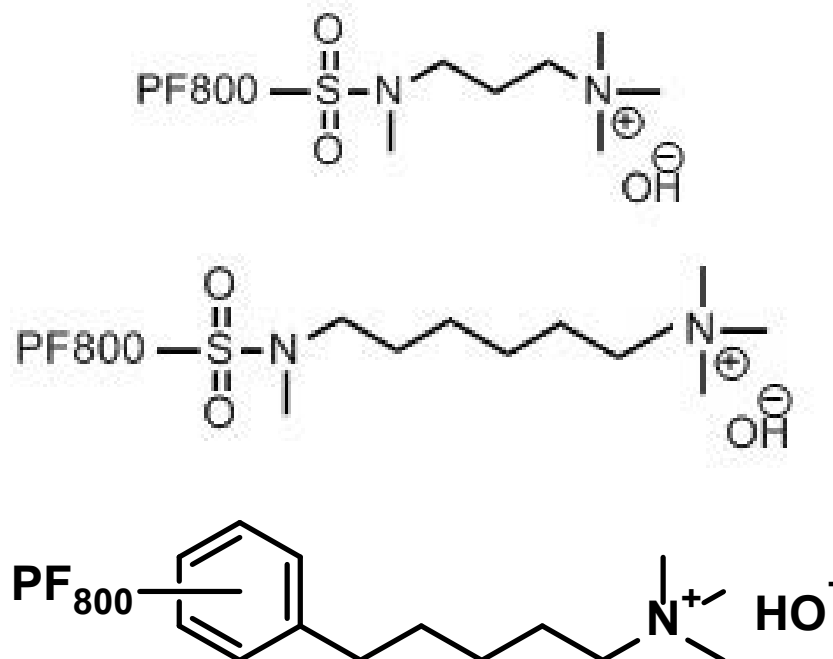


Figure 1. Chemical structures of Gen 1 (top), Gen 2 (middle), and Gen 3 (bottom) PF AEMs

Our Gen 2 PF AEM materials have been tested in AMFCs under a range of conditions and have shown high performance and durability as presented in last year's report. This year we further studied the impact of water management and the influence of different electrodes on AMFC performance. We had two primary electrodes studied, those developed by collaborators Professor Bill Mustain (University of South Carolina) based on ETFE ionomer supplied by Professor John Varcoe (University of Surrey). These electrodes have demonstrated performance above 1.9 W/cm^2 and are based on a hand-milling technique for mixing, followed by air-brush spraying onto gas diffusion layers to obtain gas diffusion electrodes (GDEs) [2]. The AMFC performance and high frequency resistance (HFR) of these MEAs is shown in Figure 2 as a function of reactant gas feed relative humidity (RH). In the tests presented, RH was kept constant in anode and cathode feed for each subsequent test. The results highlight the propensity of these cells to flood and dry out within narrow RH windows. The HFR values obtained allow relative hydration levels to also be probed.

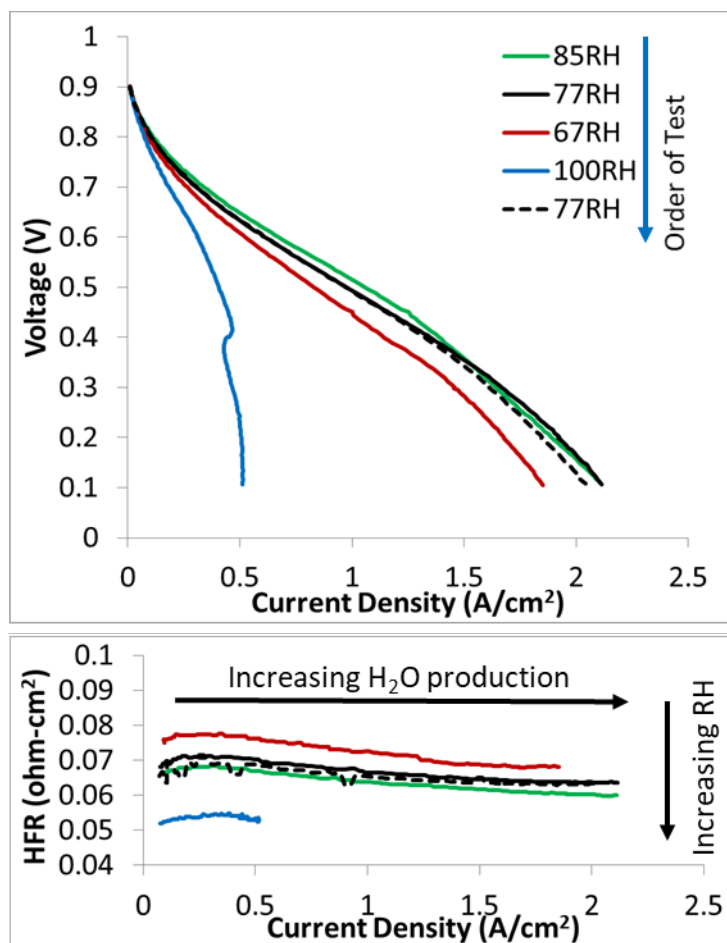


Figure 2. AMFC performance and HFR for PF AEM membranes using ETFE-based GDEs

We greatly expanded our studies of electrodes containing PF AEMs this past year. Figure 3 compares the performance and HFR obtained for different electrodes at optimized RH conditions. The PF AEM electrodes studied were prepared using standard catalyst preparation techniques and a PF AEM Gen 2 dispersion. The performance differences observed for ETFE-based electrodes and PF AEM-based electrodes are quite significant and obvious. For the samples prepared, ETFE greatly outperformed PF AEM samples, with performance being most significant for ETFE at the anode. Durability difference, not shown, was greater for ETFE at the cathode, but in both cases ETFE electrodes were found to be superior. Through modification of fabrication route, we subsequently have improved PF AEM performance significantly. A key observed property in these experiments has been HFR and trends with increasing current density, where flooding and dehydration can be observed.

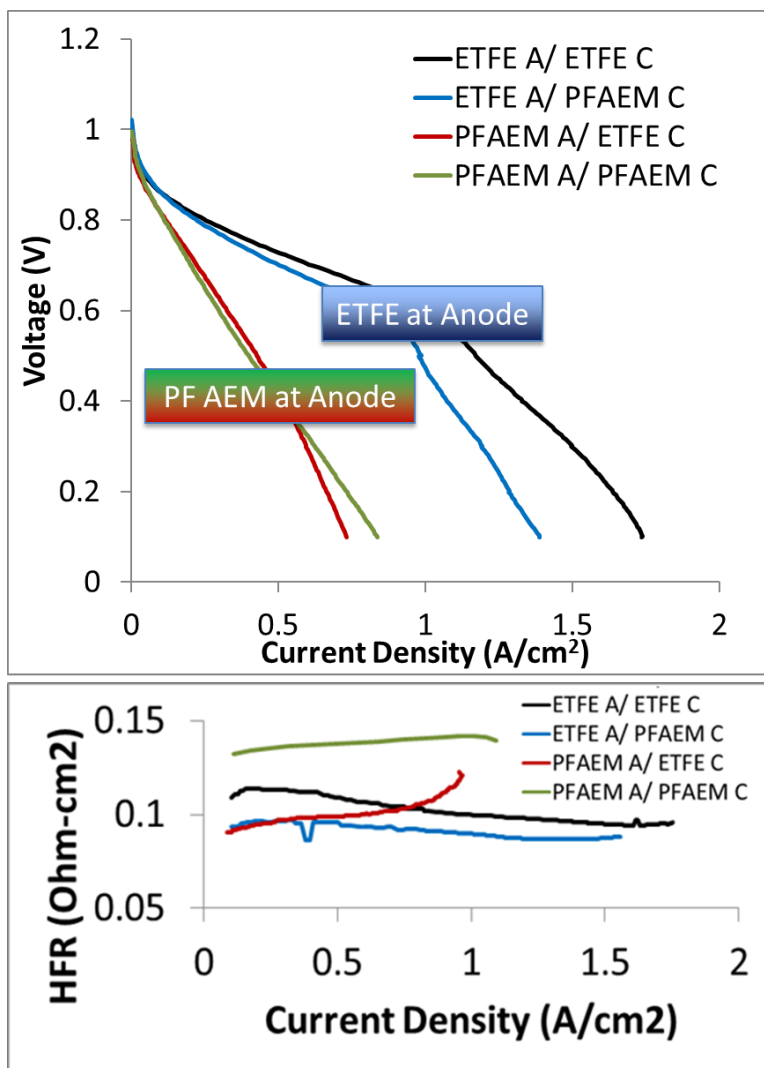


Figure 3. AMFC performance and HFR for PF AEM membranes using ETFE-based GDEs and PF AEM Gen 2 catalyst-coated membranes

To better understand the water-management issues of AMFCs we have focused modeling development in this area. Figure 4 shows the change of water content across an MEA and into the gas diffusion layers and flow channels for small changes in RH (1°C and 2°C changes in dewpoint). The model shows that even with these modest changes in dew point, the accumulation of water in the gas diffusion layer and the anode catalyst layer can be significant. These results are consistent with our observed performance, Figure 2, and in neutron studies performed on these and related AMFCs [2].

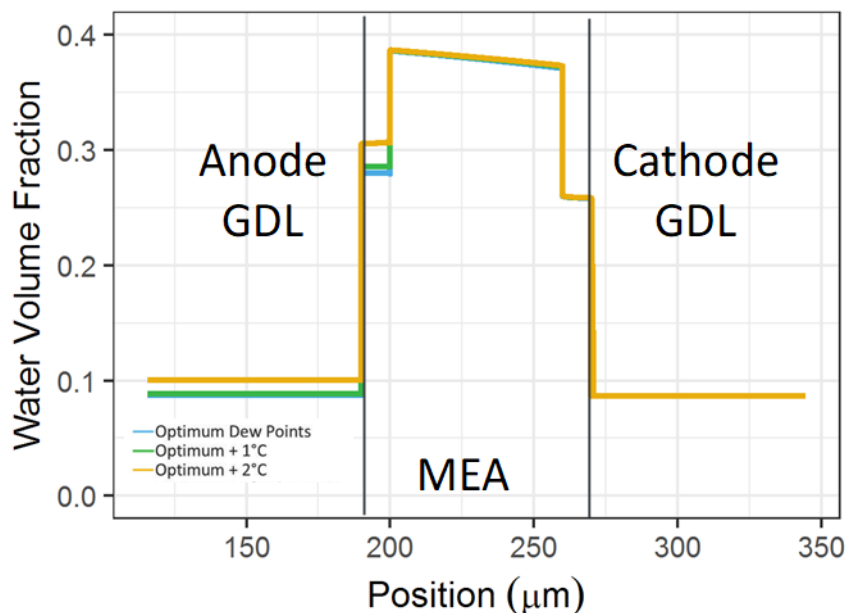


Figure 4. Water-management modeling of AMFC performance with slight variations in RH

CONCLUSIONS AND UPCOMING ACTIVITIES

The project has successfully synthesized PF AEM sulfonamide-linked chemistries for highly OH⁻-conductive AEMs. Extensive characterization has been performed on the polymer. Implementing this polymer into devices yields reasonable AMFC power densities. Modeling and diagnostic techniques are being performed to advance and to optimize AMFC architecture. Future work focuses on the following.

- Polymer synthesis: Gen 2+ polymer development.
- Characterization:
 - Obtaining information about membrane properties (including stability).
 - Continuing studies on stability, conductivity, water transport, and carbonate.
- AMFC implementation, modeling, and diagnostics:
 - Improved performance and durability in cells, closing the gap between experimental and modeling efforts.
 - Segmented cell studies.
 - Electrode optimization and diagnostic studies focused on further characterization of electrodes and elucidating performance loss and durability.
 - In situ: limiting current, RH studies, cyclic voltammetry, and impedance (and water management).
 - Ex situ: microscopic, electrochemical, and spectroscopic analysis.
 - Integration of modeling efforts with cell testing.
 - Further elucidation of the impact of operating conditions (temperature, RH, current density, CO₂ concentration).

FY 2018 PUBLICATIONS/PRESENTATIONS

1. T. Omasta, A. Park, J. LaManna, Y. Zhang, X. Peng, L. Wang, D. Jacobson, J. Varcoe, D. Hussey, B. Pivovar, and W. Mustain, “Beyond catalysis and membranes: visualizing and solving the challenge of electrode water accumulation and flooding in AEMFCs,” *Energy Environ. Sci.* Advance Article (2018), doi: 10.1039/C8EE00122G.
2. Angela D. Mohanty, Steven E. Tignor, Matthew R. Sturgeon, Hai Long, Bryan S. Pivovar, and Chulsung Bae, “Thermochemical Stability Study of Alkyl-Tethered Quaternary Ammonium Cations for Anion Exchange Membrane Fuel Cells,” *J. Electrochem. Soc.* 164, no. 13 (2017): F1279–F1285, doi: 10.1149/2.0141713jes.
3. Ashutosh G. Divekar, Andrew Michael Park, Zbyslaw R. Owczarczyk, Soenke Seifert, Bryan S. Pivovar, and Andrew M Herring, “A Study of Carbonate Formation Kinetics and Morphological Effects Observed on OH- Form of PFAEM When Exposed to Air Containing CO₂,” *ECS Trans.* 80, no. 8 (2017): 1005–1011, doi: 10.1149/08008.1005ecst.
4. Andrew Michael Park, Zbyslaw R. Owczarczyk, L.E. Garner, Ami C. Yang-Neyerlin, Hai Long, C.M. Antunes, Matthew R. Sturgeon, M.J. Lindell, Steven J. Hamrock, Michael Yandrasits, and Bryan S. Pivovar, “Synthesis and Characterization of Perfluorinated Anion Exchange Membranes,” *ECS Trans.* 80, no. 8 (2017): 957–966, doi: 10.1149/08008.0957ecst.
5. Huai-Suen Shiau, Iryna V. Zenyuk, and Adam Z. Weber, “Elucidating Performance Limitations in Alkaline-Exchange- Membrane Fuel Cells,” *J. Electrochem. Soc.* 164, no. 11 (2017): E3583–E3591, doi: 10.1149/2.0531711jes.

REFERENCES

1. D. Papageorgopoulos presentation. AMFC Workshop, Phoenix, AZ, April 1, 2016.
2. T.J. Omasta et al. *Energy Environ. Sci.* 11 (2018): 551–558.

Polymer-Based Fuel Cells that Operate from 80°C to 220°C

Yu Seung Kim (Primary Contact), Albert S. Lee,
Eun Joo Park, Dongguo Li, and Gerie Purdy
Los Alamos National Laboratory
Los Alamos, NM 87545
Phone: (505) 667-5782
Email: yskim@lanl.gov

DOE Manager: Dimitrios Papageorgopoulos
Phone: (202) 586-5463
Email: Dimitrios.Papageorgopoulos@ee.doe.gov

Project Start Date: May 1, 2017
Project End Date: October 30, 2018

Overall Objectives

- Develop ion-pair-coordinated polymer electrolytes to demonstrate a fuel cell that operates from 80°C to 220°C without humidification.
- Density functional theory (DFT) and small-molecule ³¹P nuclear magnetic resonance (NMR) study of the interaction energy between different quaternary ammonium-biphosphate ion-coordinated pairs as a function of phosphoric acid doping level and water content.
- Develop new ion-pair-coordinated electrolyte systems with improved water tolerance.
- Demonstrate membrane electrode assembly (MEA) fabrication and high-performance high-temperature polymer electrolyte membrane fuel cell (HT-PEMFC) performance with newly developed phosphonated ionomer system.

Fiscal Year (FY) 2018 Objectives

- Obtain area specific resistance $\leq 0.1 \Omega \text{ cm}^2$ at 160°C.
- Demonstrate MEA performance with peak power density (H_2/O_2) $> 1,000 \text{ mW cm}^{-2}$.
- Obtain water tolerance $P_{\text{H}_2\text{O}} > 38.5 \text{ kPa}$.
- Achieve cell durability $V_{\text{loss}} < 10\%$ at 160°C.

Technical Barriers

This project addresses the following technical barriers from the Fuel Cells section of the Fuel

Cell Technologies Office Multi-Year Research, Development, and Demonstration Plan [1]:

- (A) Durability
- (B) Cost
- (C) Electrode performance.

Technical Targets

This project aims to develop ion-pair-coordinated polymer electrolytes for HT-PEMFCs operating in the temperature range of 80°–220°C without humidification for practical use in both stationary and automobile applications. Insights gained from this project will be applied towards the next stage HT-PEMFC systems. The technical targets for the developed polymer electrolytes in HT-PEMFCs in the Multi-Year Research, Development, and Demonstration Plan [1] are listed below.

- Q4, 2017: Water tolerance $P_{\text{H}_2\text{O}} > 38.5 \text{ kPa}$.
- Q1, 2018: Area specific resistance (at 160°C) $\leq 0.1 \Omega \text{ cm}^2$.
- Q2, 2018: Peak power density (H_2/O_2) $> 1,000 \text{ mW cm}^{-2}$.
- Q4, 2018: Durability during 80°–180°C AST, $< 10\% \text{ V loss at } 160^\circ\text{C}$.

FY 2018 Accomplishments

- Completed DFT modeling and small-molecule study through ³¹P NMR, demonstrating that guanidinium-phosphate is the best candidate, having strongest interaction between base and phosphoric acid.
- Achieved water tolerance at 80°C, 80% relative humidity (RH) ($P_{\text{H}_2\text{O}} = 38.5 \text{ kPa}$), meeting the go/no-go criteria.
- Demonstrated a peak power density (H_2/O_2) of $1,134 \text{ mW cm}^{-2}$ and area specific resistance of $0.09 \Omega \text{ cm}^2$ at 160°C utilizing a down-selected trimethyl ammonium-functionalized Diels-Alder poly(phenylene)s membrane and phosphonated ionomer.

INTRODUCTION

In FY 2016, we developed a new HT-PEMFC system [2] in which the ion-pair coordination between a quaternary ammonium polymer (QAP) and biphosphate increased the water tolerance of both the membrane and ionomer to widen the operating temperature of HT-PEMFCs to 80°–180°C, a major improvement from commercial phosphoric-acid-doped polybenzimidazole (PBI), which operates from 140°C to 180°C. In FY 2017, a systematic investigation of the ionic interaction strength of various acid-base and ion-pair-coordinated systems were conducted using both computational and ^{31}P NMR studies using small molecules. On the basis of these results, a down-selected trimethyl ammonium-functionalized Diels-Alder poly(phenylene) [2] was used as the QAP membrane and newly applied phosphonated polymer [3, 4] as ionomer supplied from University of Stuttgart. Implementation of these ion-coordinated membranes and phosphonated ionomers gave remarkably improved HT-PEMFC performance and durability.

APPROACH

Our general approach to developing a polymer-based fuel cell that operates at a temperature range of 80°–220°C was to implement a highly conductive, non-leachable solid phosphonated ionomer into the electrodes of HT-PEMFCs with our down-selected phosphoric-acid-doped, ion-pair-coordinated quaternary ammonium polymer membrane. The rationale behind this approach was that the ion-pair-coordinated phosphoric-acid-doped QAP membrane would exhibit high water tolerance and phosphonated ionomer would provide sufficient anhydrous proton conduction at both low and high temperatures without the need for phosphoric acid doping, leading to improvements in both HT-PEMFC performance and durability. For this, we first investigated the interaction energy between different acid-base and quaternary ammonium base–biphosphate system through DFT calculations and ^{31}P NMR. Through these analytical tools, we were able to discern which organic cations have the greatest interaction energies with phosphoric acid, thus giving us a strategy in designing new polymer structures for improved water tolerance and phosphoric acid retention in the membrane. Second, for electrode optimization, a fully solid phosphonated ionomer was utilized as a conductive binder. Through the elimination of leachable liquid phosphoric acid in these electrodes, remarkable improvements in both HT-PEMFC performance and cell durability were able to be attained in tandem with our ion-pair-coordinated membrane.

RESULTS

^{31}P NMR and DFT Study of Acid-Base and Ion-Pair-Coordinated Systems

Figure 1a shows the ^{31}P NMR spectra for various acid-base and ion-pair-coordinated systems with the chemical structures of the investigated organic bases shown in Figure 1b.

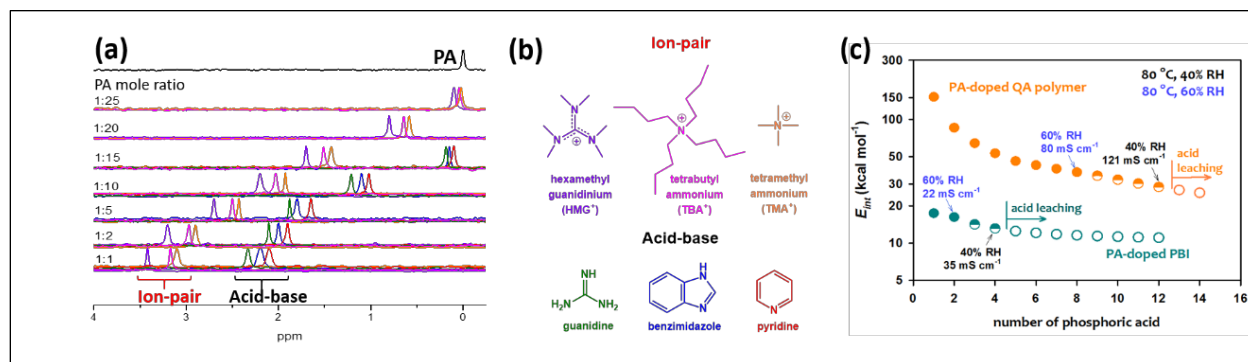


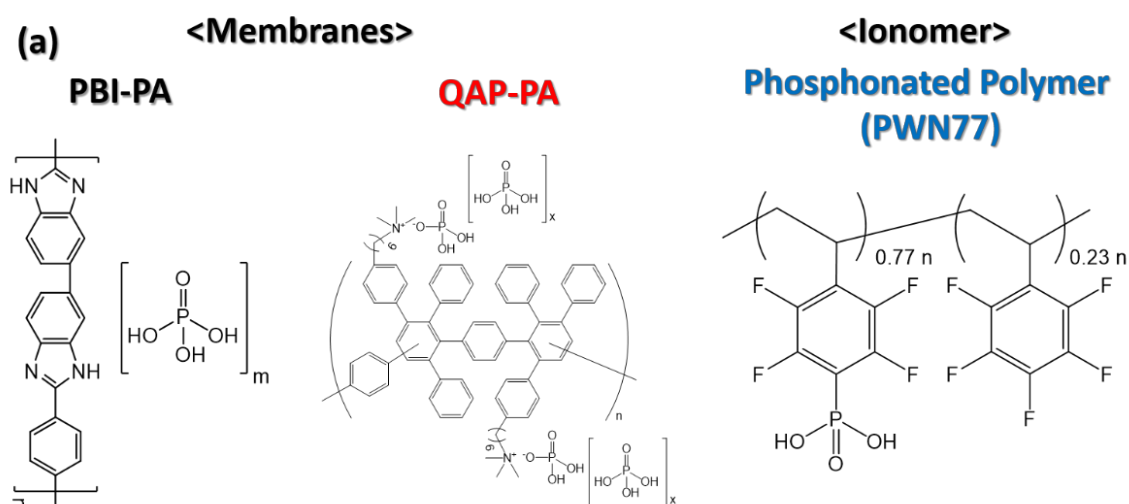
Figure 1. (a) ^{31}P NMR spectra for various ion-pair and acid-base compositions, (b) chemical structures of different bases studied, (c) DFT-derived interaction energies as a function of phosphoric acid doping level

If we consider the ^{31}P NMR chemical shift as an indicator of relative ionic interaction strength relative to pristine phosphoric acid (PA) reference standard at concentration of 5 M, we can observe that the ion-pair-

coordinated systems all exhibit a higher interaction strength compared to the acid-base interactions with these interaction strengths in the following order: hexamethylguanidinium > tetrabutylammonium > tetraalkylammonium > guanidine > benzimidazole > pyridine. Computational works with these small molecules revealed that the water tolerance of the ion-pair-coordinated systems could be greatly increased, as with a greater interaction, the PA-doped QA polymer loses only 2 PA molecules at 80°C, 40% RH, in which the proton conductivity is 121 mS cm⁻¹. In contrast, the PA-doped PBI loses 8 PA molecules at the same condition in which the proton conductivity is 35 mS cm⁻¹.

Rational Design of Ion-Pair-Coordinated Membranes and Phosphonated Ionomers

Figure 2a shows the chemical structures of the various high-temperature polymer electrolytes. A commercial phosphoric-acid-doped PBI membrane as well as QAP-doped PA (QAP-PA) with polyphenylene backbone. It is noteworthy to point out that the polyphenylene backbone was necessary to attain both robust chemical stability at high and low pH (the membrane should be stable in high pH condition for a pretreatment step in alkaline solution as well as low pH when doping in phosphoric acid) and high temperature, as well as excellent mechanical properties. Also, the phosphonated ionomer, phosphonated poly(pentafluorosytre) (PWN77), with a phosphonation degree of 77%, was selected due to its excellent balance in high proton conductivity over lower phosphonated polymers and high chemical resistance [2]. The various physical properties of these materials are shown in Figure 2b.



(b)	Acid—Base System	Ion-Pair Coordinated Polymer	Phosphonated Polymer
	PBI-PA	QAP-PA	PWN77
Concentration of base (mmol/g) before doping	6.5	1.85	0
PA doping level (#acid per base)	12.4	13.5	0
Phosphoric or Phosphonic Acid Concentration (mmol acid/g)	80.6	25.0	2.1
Water Content (#water per PA)	6.0	4.4	-

Figure 2. (a) Chemical structures of developed polymer electrolyte membranes and ionomers, (b) summary of the physical properties of polymer electrolyte membranes and ionomers

As shown, the QAP-PA and phosphonated polymer exhibited drastically lower phosphoric or phosphonic acid concentrations compared to polybenzimidazole phosphoric acid (PBI-PA) acid-base system which may give three main benefits. First, the mechanical properties of ion-pair-coordinated PEMs are significantly better due to lower liquid content [1]. Second, the ion-coordinated PEMs exhibit higher water tolerance. Third, phosphate anion poisoning on the oxygen reduction reaction catalyst is less.

Proton Conductivity and Water Tolerance

The proton conductivities as a function of temperature and RH are shown in Figure 3. The conducting phosphonate groups of PWN77, which are covalently bonded to the polymer backbone, have a significantly lower ionic conductivity at lower temperatures, but at a critical temperature—140°C—the conductivity of PWN77 exceeds that of both commercial polybenzimidazole-doped phosphoric acid and even the ion-pair-coordinated QAP-PA membrane. The phosphonated polymer, PWN77, is inherently dry across all temperatures, thus its proton conductivity is completely anhydrous in nature, which accounts for its relatively low proton conductivity at temperatures less than 100°C as the measured proton conductivities for PWN77, QAP-PA, and PBI-PA at 80°C were 6.5 mS cm⁻¹, 80 mS cm⁻¹, and 86 mS cm⁻¹. Phosphoric acid, however, most commonly used as 85 wt% concentrated aqueous solution, is exceedingly hygroscopic through strong hydrogen-bonding interactions with water and cannot completely rid of itself of water at temperatures lower than 140°C. This propensity to hold water contributes to the relatively higher conductivity at lower temperatures, even for phosphoric-acid-doped PBI systems where the polymer-phosphate acid-base interactions are very weak. It is worth noting that under water-generating conditions of a fuel cell, the conductivity for the phosphonated ionomer also can be boosted by a water-mediated phase, as shown by the RH-dependent conductivity values. Above 140°C, we see that the anhydrous proton conductivity of the phosphonated polymer electrolyte dominates, as a continual increase in conductivity is observed as the temperature reaches 200°C. Specifically, the proton conductivities at 160°C were 168 mS cm⁻¹, 103 mS cm⁻¹, and 125 mS cm⁻¹ for PWN77, QAP-PA, and PBI-PA, respectively. The water tolerance of the selected high-temperature PEMs was examined as a function of RH at 80°C. As shown in Figure 3b, the conductivity of PBI-phosphoric acid showed an immediate and continual decrease in proton conductivity as the RH increased, which we attributed to the instantaneous leaching of phosphoric acid. For the ion-pair-coordinated quaternary ammonium polymer-phosphoric acid system, we found that the proton conductivity increased until reaching 40% RH, as the higher humidity helped promote water-mediated conduction, followed by a similar loss of conductivity through phosphoric acid leaching. The conductivity of the phosphonated polymer, however, steadily increased as the RH increased. As a result, although the absolute proton conductivity was lower at lower RH values, the conductivity increase as a function of RH was attributed to the water-mediated proton conduction process.

HT-PEMFC MEA Performance

MEAs using the ion-pair-coordinated QAP membrane and phosphonated ionomer and reference PWN77 ionomer/PBI-PA membrane cell were prepared with carbon-supported Pt-based catalysts. Catalyst loadings were A/C 0.5/0.6 mg_{Pt}/cm² with both anode and cathode flow and backpressure held at 500 sccm and 10 psi, respectively. Figure 4 shows the H₂/O₂ fuel cell performance of the MEAs at 80°C, 120°C, 160°C, and 200°C. As shown, the PWN77 ionomer MEA showed much better peak-power densities of 1,130 mW/cm² and 1,480 mW/cm² at 160°C and 200°C, and across all temperature ranges. This significant increase in performance of the PWN77 ionomer/ion-pair-coordinated membrane system compared to PBI-PA membrane—despite the 40-fold decrease of phosphonic/PA concentration shown in Figure 2b—was attributed to a combination of lower phosphoric acid poisoning, exceptional water tolerance, and higher anhydrous proton conductivity at elevated temperatures.

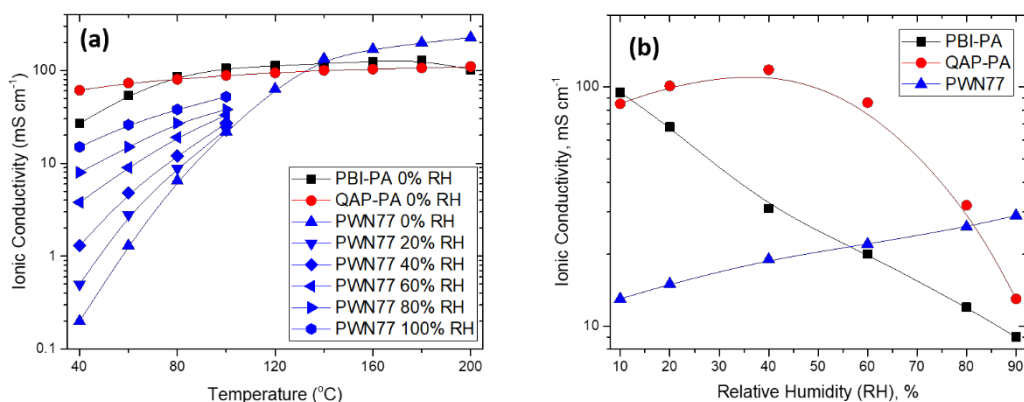


Figure 3. (a) Temperature-dependent and (b) RH-dependent ionic conductivities for various polymer electrolyte systems

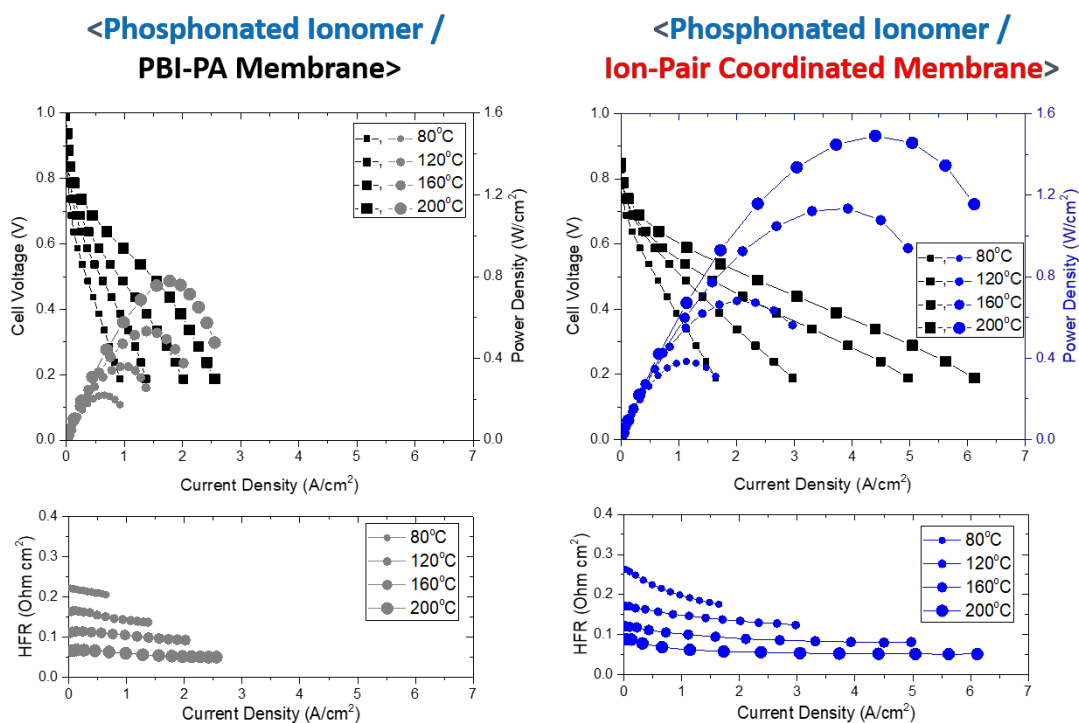


Figure 4. HT-PEMFC MEA performances for (a) phosphonated ionomer/PBI-PA membrane system, and (b) phosphonated ionomer/ion-pair-coordinated membrane at various temperatures

CONCLUSIONS AND UPCOMING ACTIVITIES

- DFT modeling and ³¹P NMR studies of various organic base: phosphoric acid compositions revealed that the ion-coordinated system exhibited a stronger ionic interaction at all phosphoric doping levels, with guanidinium and tetramethylammonium quaternary ammonium bases exhibiting the highest interaction energies.
- Conductivity and water-tolerance measurements revealed that the newly developed ion-pair-coordinated polymer electrolytes exhibited high RH tolerance (up to 40% RH) at 80°C, and the phosphonated ionomer giving stable conductivity for over 200 h at 80°C, 80% RH conditions.

- HT-PEMFC MEA performance using the developed ion-pair-coordinated membrane and phosphonated ionomer was 1,134 mW cm⁻² of peak power density (H₂/O₂) and area specific resistance of 0.09 Ohm cm² at 160°C.
- Durability AST experiments are ongoing and are to be completed before the end of the project term.

SPECIAL RECOGNITIONS AND AWARDS/PATENTS ISSUED

1. Yu Seung Kim and Albert Lee, “Polymer Electrolytes for Fuel Cells,” US Patent Application Publication, Feb. 9, 2018.

FY 2018 PUBLICATIONS/PRESENTATIONS

1. Yoong-Kee Choe, Kwan Soo Lee, Jacob S. Spendelow, Cy Fujimoto, and Yu Seung Kim, 21st International Symposium on Batteries, Fuel Cells and Capacitors, 2017, Fukuoka, Japan, November 14 to November 16.
2. Cy Fujimoto, Eric Sorte, Nelson Bell, Cassandra Poirier, Eun Joo Park, Sandip Maurya, Kwan-Soo Lee, and Yu Seung Kim, “Acid-Catalyzed Benzoylation Reactions of Diels-Alder Polyphenylenes,” *Polymer* (2018). DOI: 10.1016/j.polymer.2018.10.060.
3. Y.S. Kim, K.S. Lee, G. Purdy, Y.-K. Choe, C. Fujimoto, J. Han, and C. Bae, “A New Class of Fuel Cells Based on Ion Pair-Coordinated Proton Exchange Membranes,” Abstract Number 1470 232nd ECS Meeting, Oct. 1–5, 2017, National Harbor, Maryland.
4. Yu Seung Kim, “Interfacial Behavior of Polymer Electrolytes in Fuel Cell Electrodes,” Fuel Cells Gordon Research Conference, Energizing the Future by Innovation in Fuel Cell Materials, Methods, Modeling, and Manufacture, July 29 to August 3, 2018. Bryant University, Rhode Island, USA.
5. David A. Langlois, Albert S. Lee, Natalia Macauley, Sandip Maurya, Marilyn E. Hawley, Sung Dae Yim, and Yu Seung Kim, “A Rejuvenation Process to Enhance the Durability of Low Pt Loaded Polymer Electrolyte Membrane Fuel Cells,” *J. Power Sources* 396 (2018): 345–354.
6. A.S. Lee, E.J. Park, V.M. Atanasov, J. Kerres, H. Jia, and Y.S. Kim, “Phosphonated Ionomers for Ion-Pair Coordinated High Temperature PEMFCs,” Abstract No. I01C-1466, AiMES 2018, Cancun Mexico, September 30 to October 4, 2018.
7. Kwan Soo Lee, Sandip Maurya, Yu Seung Kim, Cortney R. Kreller, Mahlon Scott Wilson, Dennis Larson, S. Elangovan, and Rangachary Mukundan, “Intermediate Temperature Fuel Cells Via an Ion-Pair Coordinated Polymer Electrolyte,” *Energy & Environ. Sci.* 11 (2018): 979–987.

REFERENCES

1. Fuel Cell Technologies Office Multi-Year Research, Development, and Demonstration Plan, <https://energy.gov/eere/fuelcells/downloads/fuel-cell-technologies-office-multi-year-research-development-and-22>.
2. Kwan-Soo Lee, Jacob S. Spendelow, Yoong-Kee Choe, Cy Fujimoto, and Yu Seung Kim, “An Operationally Flexible Fuel Cell Based on Quaternary Ammonium-Biphosphate Ion Pairs,” *Nature Energy* 1 (2016): 1.
3. Vladimir Atanasov and Jochen Kerres, “Highly Phosphonated Polypentafluorostyrene,” *Macromolecules* 44 (2011): 6416.
4. Vladimir Atanasov, Dietrich Gudat, Bastian Ruffman, and Jochen Kerres, *Eur. Polym. J.* 49 (2013): 3977.

FY17 SBIR II Release 1: Novel Hydrocarbon Ionomers for Durable Polymer Electrolyte Membranes

William L. Harrison
NanoSonic, Inc.
158 Wheatland Dr.
Pembroke, VA 24136
Phone: (540) 626-6266
Email: wharrison@nanosonic.com

DOE Manager: Donna Ho
Phone: (202) 586-8000
Email: Donna.Ho@ee.doe.gov

Contract Number: DE-SC0015215 (SBIR Phase II Release 1)

Subcontractor:
Los Alamos National Laboratory, Los Alamos, NM

Project Start Date: April 10, 2017
Project End Date: April 9, 2019

Overall Objectives

- Synthesize and characterize aromatic hydrocarbon proton-conducting membranes based on novel concept of coordinated ion pairs as high-temperature polymer electrolyte membranes in fuel cells for transportation applications.
- Empirically establish structure-property relationships of synthesized materials that will afford optimal membrane properties through monomer selection, and compositional manipulation.
- Measure proton conductivity and fuel cell performance of down-selected proton exchange membrane ionomers.

Fiscal Year (FY) 2018 Objectives

- Develop cost-effective poly(arylene benzonitrile) copolymers as proton-conducting membranes in fuel cells for transportation applications at 120°C.
- Demonstrate improved film-forming capabilities and mechanical properties.

- Measure membrane proton conductivity as a function of relative humidity and temperature as compared to commercial perfluorosulfonic acid membranes.
- Demonstrate fabrication and performance of membrane electrode assemblies.
- Establish and optimize structure-property relationships for enhanced membrane and membrane electrode assembly performance.

Technical Barriers

This project addresses the following technical barriers from the Fuel Cells section of the Fuel Cell Technologies Office Multi-Year Research, Development, and Demonstration Plan¹:

- Maximum Operating Temperature of 120°C
- Low Cost, Non-Perfluorinated Membranes
- Durability: Mechanical and Chemical Stability
- Performance: Stable Proton Conductivity independent of Relative Humidity.

Technical Targets

This project is developmental research toward commercially viable membranes based on a new (2016) ion-pair concept [1] of proton-conducting ionomers. The membrane properties and testing results shall be applied toward the design and fabrication of a proton-conducting ionomer that meet the follow DOE membrane for transportation application targets:

- Maximum operating temperature: 120°C
- Area specific proton resistance: 0.02 Ω cm² at 120°C with 40 kPa water partial pressure, and 0.03 Ω cm² at 30°C with 4 kPa water partial pressure
- Durability: 20,000 cycles
- Cost: \$20/m².

¹ <https://energy.gov/eere/fuelcells/downloads/fuel-cell-technologies-office-multi-year-research-development-and-22>

FY 2018 Accomplishments

- Synthesized a new polymer precursor to allow the synthesis of new functionalized copolymers with tunable ion exchange capacities.
- Demonstrated tailorability of thermooxidative stability of membranes via polymer design.
- Developed a scalable surface treatment for glass substrates that allows for fabrication of very thin membranes (15–30 μm) using simple polymer solutions.
- Demonstrated superior membrane mechanical and dimensional stabilities.
- Demonstrated stable proton conductivity of membranes across a wide range of humidification.
- Successfully fabricated membrane electrode assemblies using NanoSonic’s new functionalized ion-pair copolymers at Los Alamos National Laboratory.
- Demonstrated operation of NanoSonic ion-pair membranes at 120°C and higher (DOE target for 2020).
- Initiated fuel cell test stand durability evaluation of NanoSonic’s down-selected membranes at Los Alamos National Laboratory.

INTRODUCTION

Fuel cells have many attractive features as a sustainable power source, such as high-efficiency energy conversion from a variety of fuels, near-zero greenhouse gas emissions, quiet operation, low air pollution, low maintenance, and scalability based on energy needs (i.e., hand-held/portable devices, vehicular propulsion, stationary power). A critical component necessary to a viable hydrogen-based energy economy is the development of durable, cost-effective proton conducting membranes for fuel cells. Internationally, researchers have focused efforts on various approaches to increase protonic conductivity, minimize electronic conductivity, limit fuel permeability, exhibit the requisite thermal and mechanical properties, and achieve long-term chemical stability. Expensive perfluorinated polymers containing sulfonic acid-type ionomers (e.g., Nafion) remain the leading commercially available membranes. Noted shortcomings of these expensive perfluorinated membranes include limited operation temperature ($\leq 100^\circ\text{C}$), necessity of sufficiently (high) hydration for proton conductivity, and low availability. Fuel cells that operate at higher temperatures ($100^\circ\text{--}120^\circ\text{C}$) would enhance system efficiency, assist with water management, and possibly reduce precious metal catalyst loading levels in the membrane electrode assembly. Most current membrane technologies have a glass transition temperature in the range of 80°C to 120°C and suffer from creep and pinhole formation when subjected to temperatures above that range.

APPROACH

This project demonstrates a new class of hydrocarbon-based polymer ion-pair electrolyte membranes as a viable alternative to expensive perfluorosulfonic acid membranes which are limited to less than 100°C operation. NanoSonic membranes are synthesized via industrial manufacturing procedures and incorporate a new functionalized comonomer precursor. The adaptation of current manufacturing processes should directly affect a cost savings in manufacturing the functional copolymers at scale. The functionalized comonomer polymerization provides a reproducible route to tailored (compositional) copolymers. A low-temperature procedure has been developed to easily convert the functionalized copolymers into quaternary ammonium-ionomeric polymers. Phosphoric acid imbibing occurs quickly (<4 hours) to successfully produce ion-pair membranes.

RESULTS

NanoSonic has continued efforts to further understand important structure-property relationships towards design and fabrication of an optimum fuel cell ionomeric membrane through syntheses and characterization of copolymers. NanoSonic has demonstrated a series of new candidate functionalized copolymers as scalable routes to quaternary ammonium materials via current commercial processes. Currently, perfluorinated sulfonic acid membranes account for a significant cost in the implementation and manufacturing of fuel cell stacks. Therefore, beyond developing a new membrane, reducing the thickness of the membrane should influence the relative cost of the membrane. Beyond the immediate cost impact, there are several kinetic and systematic advantages to utilizing a thinner membrane, including higher through-film proton conductivity, reduced weight, and improved water diffusion, while maintaining the membrane's important function as an effective fuel barrier. Interest in proton conducting membranes on the order of sub- $25\text{-}\mu\text{m}$ thickness has been expressed by potential automotive customers.

NanoSonic has developed a new surface treatment for glass substrates used to solution-cast membranes. This aqueous treatment modifies the surface chemistry of the glass to produce a very hydrophilic surface; treated-glass substrates show improved wettability as compared to the cleaned substrates. Pinhole-free membranes as thin as $15\ \mu\text{m}$ have been produced from 5 wt% to 10 wt% polymer solutions. This is significant, as most proton exchange membranes reported in literature and commercially available are much thicker than this or require some structural support (e.g., mesh, nonwoven backing).

Unsurpassed dimensional stability has been observed for the ion-pair membranes. Alternative hydrocarbon-based membranes with pendant sulfonic acid groups display very large swelling (volumetric) and dimensional changes (300% to 800% reported) as a function of ion exchange capacity. These large dimensional changes

add stress to the membranes and the membrane electrode assembly, effectively limiting their application. The low swelling behavior observed in the ion-pair membranes is nearly negligible with regard to membrane stress. Figure 1 shows dimensional stability of ion-pair membranes. Inferences can be made to the exceptional mechanical durability of the ion-pair membranes. The candidate membranes have successfully demonstrated multiple (20+) wet-dry cycling without signs of mechanical degradation. The superior dimensional stability is attributed to a combination of tailored polymer (compositional) design, targeted copolymer functionalization, and ion-pair doping procedure.



Figure 1. Dimensional stability (low volumetric change) of NanoSonic membranes in dry and wet (hydrated) state

The vast majority of ionomeric membranes require water for reasonable proton conductivity. Also, it is well established that proton conductivity is affected by membrane hydration level and relative humidification within the system. Figure 2 shows the stable proton conductivity of two candidate ion-pair membranes independent of relative humidity at 80°C. As shown, sample 65Qt shows higher or matches the Nafion reference (N212 H⁺) up to 50% relative humidity. The NanoSonic ion-pair membranes does show an influence of ion exchange capacity on proton conductivity, 36Qt <<65Br <65Qt. Testing is ongoing on a NanoSonic membrane with different ion exchange capacity (i.e., degree of functionalization) that may show even more enhanced performance.

Proton-conducting membranes able to operate at or above 120°C offer many benefits for fuel cell operations, including better tolerance to fuel impurities, improved electrode kinetics, higher ionic conductivities, and reduced requirements for heat and water management. Maintaining membrane hydration at the DOE target of 120°C is very difficult, however, which is one reason current commercially available and other alternative/developmental membranes may not work. Experiments investigating the influence of temperature on proton conductivity in membranes are being performed.

Figure 3 shows the influence of temperature and relative humidity on proton conductivity for a NanoSonic ion-pair membrane and Nafion. As expected, Nafion demonstrates good proton conductivity at 100% relative humidity at temperatures up to 100°C (blue line). At 120°C, however, Nafion proton conductivity quickly drops due to membrane dehydration or membrane mechanical failure; 120°C is above Nafion's plasticized glass-transition temperature, as found in literature. Nafion conductivity at 80°C is greatly influenced by relative humidity as observed at 20% and 70% (open blue circles).

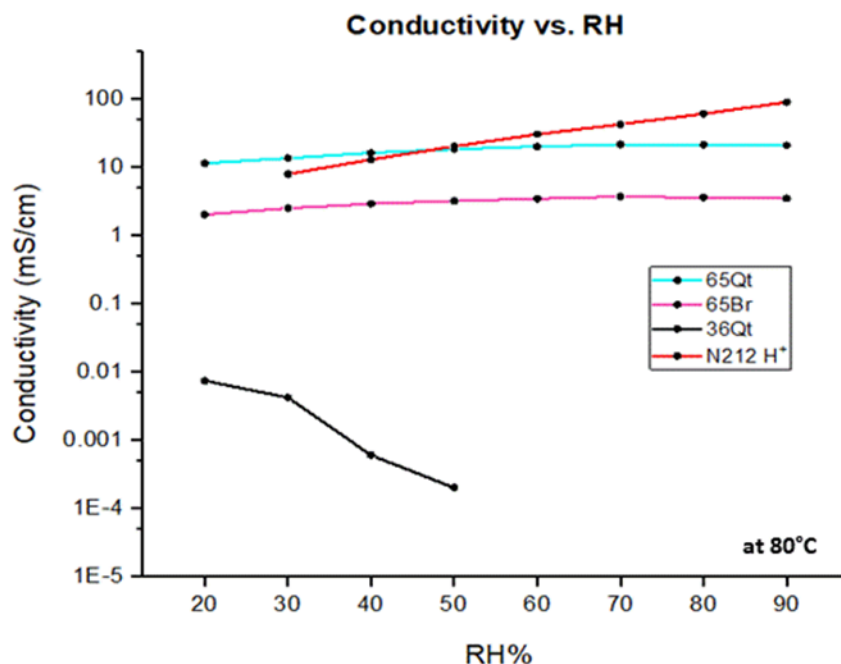


Figure 2. Influence of relative humidity on proton conductivity on NanoSonic ion-pair membranes and Nafion (N212) control

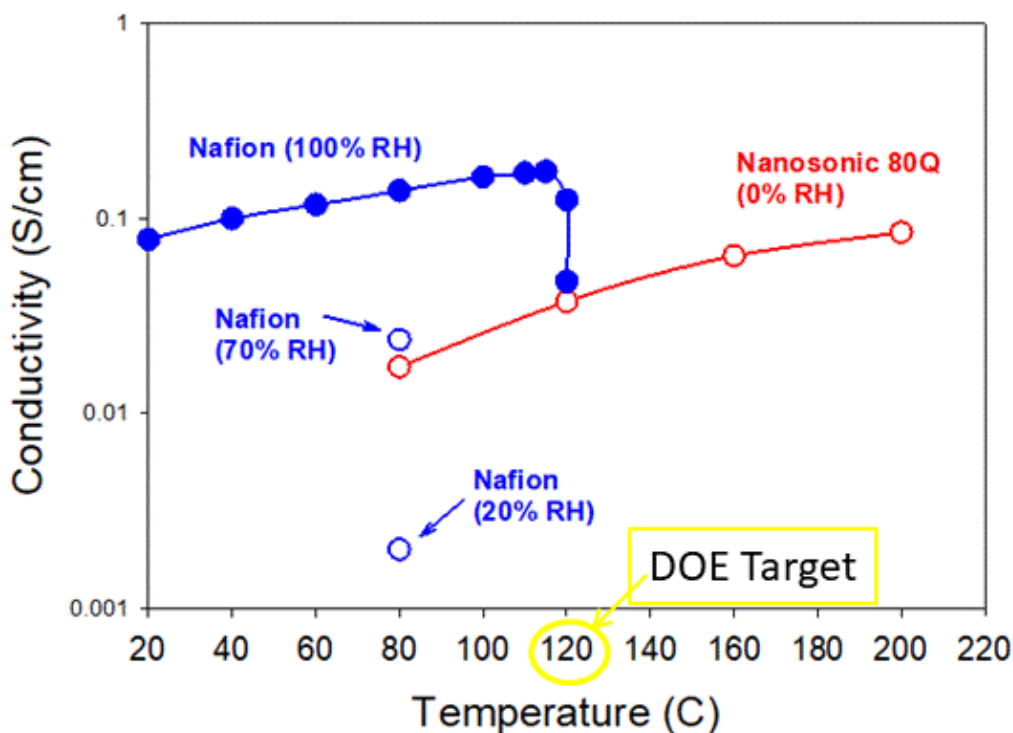


Figure 3. Influence of temperature and relative humidity on proton conductivity on NanoSonic ion-pair membranes and Nafion control

NanoSonic ion-pair membrane “80Q” shows progressively increasing proton conductivity, starting at 120°C even at no humidification (0% relative humidity). Not shown in the graph—but of importance to note—Nafion has no appreciable conductivity at 0% relative humidity. This study is ongoing with down-selected ion-pair membranes with different copolymer compositions and higher initial conductivity. All NanoSonic ion-pair membranes candidates must display hydrated glass-transition temperatures greater than 160°C to account for the plasticization effect of the phosphoric acid and water.

NanoSonic ion-pair membranes have been fabricated into membrane electrode assemblies and demonstrate successful operation at the DOE target temperature, 120°C and higher. Figure 4 displays a NanoSonic ion-pair membrane that was successfully fabricated into a membrane electrode assembly and the preliminary data collected by Yu Seung Kim’s group (our Los Alamos National Laboratory partner). Membrane-to-electrode ionomer interface is critical for efficient operation of the membrane electrode assembly. Progress is being made to optimize membrane electrode assembly fabrication and fuel cell test-stand qualification at Los Alamos National Laboratory.

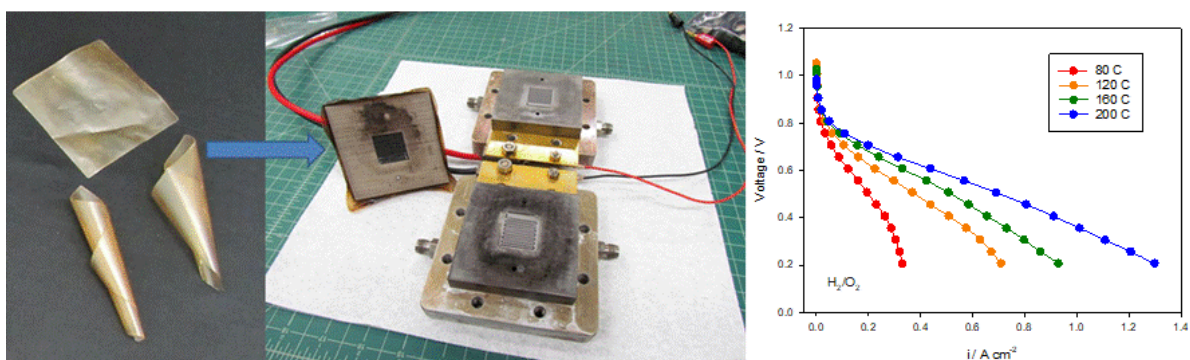


Figure 4. Exemplary NanoSonic ion-pair membrane in a fuel cell test cell with preliminary voltage-current data

CONCLUSIONS AND UPCOMING ACTIVITIES

Proton-conducting membrane copolymers based on a novel ion-pair concept have been developed. A new surface treatment for glass substrates have been employed to fabricate durable, thin membranes (<25 μm) from common laboratory solvents. The ion-pair membranes show exceptional dimensional stability and durability to wet-dry cycling. The ion-pair copolymer membranes show stable proton conductivity independent to relative humidity and at DOE target (120°C) temperature and higher. Fabrication and testing of membrane electrode assemblies of the ion-pair copolymer membranes is ongoing with promising preliminary success. New functionalized copolymer compositions are being synthesized to further understand structure-property relationships as test results are analyzed to guide the development of the optimal proton conduction ion-pair membrane.

REFERENCES

1. K.S. Lee, J.S. Spendelow, Y.K. Choe, C. Fujimoto, and Y.S. Kim, “An Operationally Flexible Fuel Cell Based on Quaternary Ammonium-Biphosphate Ion Pairs,” *Nature Energy* 1, no. 9 (2016): 16120.

FC-PAD: Fuel Cell Performance and Durability Consortium

Rod Borup*¹ (Primary Contact), Adam Weber², Deborah Myers³, K.C. Neyerlin⁴, Ahmet Kusoglu², Rajesh Ahluwalia³, Rangachary Mukundan¹, Karren More⁵

* Author list reflects FC-PAD Directors and Thrust Coordinators only

¹ Los Alamos National Laboratory
MS D429, P.O. Box 1663
Los Alamos, NM 87545
Phone: (505) 667-2823
Email: Borup@lanl.gov

DOE Manager: Gregory Kleen
Phone: (240) 562-1672
Email: Gregory.Kleen@ee.doe.gov

Subcontractors and Collaborators:

- ² Lawrence Berkeley National Laboratory, Berkeley, CA
- ³ Argonne National Laboratory, Argonne, IL
- ⁴ National Renewable Energy Laboratory, Golden, CO
- ⁵ Oak Ridge National Laboratory, Oak Ridge, TN

Project Start Date: October 1, 2015
Project End Date: September 30, 2021

Overall Objectives

Advance performance and durability of polymer electrolyte membrane fuel cells (PEMFCs) primarily at a *pre-competitive* level.

- Improve high-current-density performance at low Pt loadings:
 - Improved electrode structures.
 - Reduced mass transport losses.
 - Loading: ≤ 0.125 mg Pt/cm² total.
 - Performance @ 0.8 V: 300 mA/cm².
 - Performance @ rated power: 1,800 mW/cm².
- Develop knowledge base for more durable and high-performance PEMFC components:
 - Understand science of component integration, for example, ionomer interactions with carbon/interfaces between electrodes and gas diffusion layer (GDL) or membranes.

- Improve component durability (e.g., membrane stabilization, self-healing, electrode-layer stabilization).
- Develop new diagnostics, characterization tools, and models.
- Provide support to DOE-funded FC-PAD projects from funding opportunity announcement DE-FOA-0001412 to develop a knowledge base for both industrial and academic developers.

Fiscal Year (FY) 2018 Objectives

- Understand electrode layer structures:
 - Measure effect of ionomer, catalyst inks, carbon, and cations on electrode structure, catalyst/carbon particle agglomeration, oxygen reduction reaction kinetics, and membrane conductivity and water uptake.
 - Macroscale and microstructure modeling of electrode structure—measure ionomer distribution observations as input data for model development, and define relative electrode resistive losses (e.g., local oxygen transport).
 - Define current state-of-art commercial membrane electrode assemblies (MEAs) to define materials baseline. Analysis of Toyota Mirai components provided by the United States Council for Automotive Research (USCAR).
- Define/measure degradation mechanisms:
 - Define catalyst alloy durability-related particle size agglomeration, alloy dissolution, and mass activity.
 - Define catalyst alloy effect related to carbon corrosion.
 - Define radical scavenger cation migration and diffusion.
- Novel electrode layer design and fabrication:
 - Develop MEAs—ordered arrays, nanowire catalysts, and electrospun electrodes.

Technical Barriers

This project addresses the following technical barriers from the Fuel Cells section of the Fuel Cell Technologies Office Multi-Year Research, Development, and Demonstration Plan¹:

- A. Decrease Cost
- B. Increase Power Density
- C. Simultaneously Improve Durability.

Technical Targets

This project develops MEAs that meet the following targets shown in Table 1.

FY 2018 Accomplishments

- Developed new novel/experimental catalyst-layer architectures.

- Utilized characterization and experimental diagnostics to delineate catalyst-layer interactions.
- Experimentally evaluated degradation mechanisms and conditioning effects.
- Conducted analysis to set baseline and benchmark materials by analysis of Toyota Mirai components.
- Developed diagnostics and models for interpreting critical phenomena and data.
- Explored impact of ionomer and cations from inks to MEAs.

Table 1. FCTT Technical Targets: Membrane Electrode Assemblies for Transportation Applications

Characteristic	Units	2025 Targets
MEA cost	\$/kW	10
Platinum group metal (PGM) total content	g/kW rated	≤0.10
Performance @ 0.8 V	mA/cm ²	300
Performance @ rated power	mA/cm ²	1,800
Durability with cycling	Hours	8,000
Loss in performance at 0.8 A/cm ²	mV	≤30
Loss in performance at 1.5 A/cm ²	mV	≤30

FCTT – Fuel Cell Tech Team

¹ <https://energy.gov/eere/fuelcells/downloads/fuel-cell-technologies-office-multi-year-research-development-and-22>

INTRODUCTION

Although fuel cells are being deployed in cars in limited commercialization, they still fall short of the DOE targets for this technology, which are required for widespread consumer acceptance. The FC-PAD consortium was formed to advance performance and durability of PEMFCs at a pre-competitive level to further enable their commercialization. This consortium coordinates national laboratory activities related to fuel cell performance and durability, provides technical expertise, and harmonizes activities with industrial developers. The consortium serves as a resource that amplifies the Office of Energy Efficiency and Renewable Energy's impact by leveraging the core capabilities of several labs in conducting low-technology-readiness-level research.

The major challenge addressed by this consortium is to develop the knowledge base and understanding to optimize electrode structures for more durable, high-performing PEMFC component technologies, while simultaneously reducing cost. Current research focuses on achieving high performance and durability in low-Pt-loaded PEMFCs.

APPROACH

This consortium incorporates national laboratory investigators with proven experience (developed in prior projects) related to durability, transport, and performance, and combines them into one highly coordinated effort. The consortium formalizes already existing and effective collaborations among the national laboratories that have established leadership in PEMFC performance and durability research and development. Three thrust areas are related to components: (1) Electrocatalysts and Supports, (2) Electrode Layers, and (3) Ionomers, Gas Diffusion Layers, Bipolar Plates, Interfaces; and three thrust areas are cross-cutting in nature: (4) Modeling and Validation, (5) Operando Evaluation: Benchmarking, ASTs, and Contaminants, and (6) Component Characterization and Diagnostics.

FC-PAD is an integrated five-national-laboratory consortia with a large number of contributing staff scientists, research technicians, post-docs and students. For FY 2018, FC-PAD contributors included the following.

- **Argonne National Laboratory (ANL):** Nancy Kariuki, Dennis Papadimas, C. Firat Cetinbas, J-K Peng, Xiaohua Wang, A. Jeremy Kropf, Hemma Mistry, Jaehyung Park
- **Lawrence Berkeley National Laboratory (LBNL):** Lalit Pant, Meron Tesfaye, Anamika Chowdhury, Sarah Berlinger, Andrew Crothers, Peter J. Dudenas, Victoria Ehlinger, Grace Lau, Michael Tucker, Clayton Radke
- **Los Alamos National Laboratory (LANL):** Jacob Spendelow, Andrew Baker, Siddharth Komini Babu, Natalia Macauley, Sarah Stariha, David Langlois, Kavitha Chintam, Roger Lujan, Mahlon Wilson, Sarah Park, Derek Richard, Yu Seung Kim
- **National Renewable Energy Laboratory (NREL):** Guido Bender, Sadia Kabir, Jason Zack, Nihal Shah, Lawrence Anderson, Ellis Klein
- **Oak Ridge National Laboratory (ORNL):** Brian Sneed, Shawn Reeves.

Four FC-PAD projects from DE-FOA-0001412 were announced by DOE during FY 2017. Those projects are led by 3M Company, General Motors, United Technologies Research Center, and Vanderbilt University. The core national laboratory team is supporting those four projects with an equal level of effort utilizing national laboratory capabilities. National lab work for those projects is reported by those projects.

RESULTS

During FY 2018, FC-PAD conducted work in six thrust areas. Much of the work was related to fundamental understanding of the electrode structure and the relative material distribution of materials and how ionomer and ionomeric cations interact with the catalyst and catalyst support. This includes significant characterization

of the electrode structure and modeling to determine the relative impact on performance and durability. Below is a selected subset of these activities during FY 2018.

Carbon Corrosion Effect on Platinum Alloys

To examine the stability of electrode structures and further understand the combined effects of carbon corrosion on performance, we tested various types of carbon support materials, as well as platinum and platinum-alloy catalysts under accelerated stress tests (ASTs). Figure 1a shows the carbon corrosion rate during the DOE/FCTT carbon corrosion AST as measured by CO₂ evolution. The carbon corrosion rate is observed to depend only upon the weight percentage of platinum, and not on the active catalyst being Pt or PtCo. Figure 1b shows the relative carbon remaining during the cycling; while the carbon loss rate is higher for the lower-percentage-Pt catalyst, over these tests, the amount of carbon remaining is still significantly higher. Comparing Pt and PtCo on high-surface-area carbon (HSAC) versus low-surface-area carbon (LSAC), Figure 1c and 1d show that Pt and PtCo follow the same trends for HSAC. HSAC catalysts show a rapid decrease in electrochemical surface area (ECSA) and mass activity, where the Pt catalyst on LSAC has an initial lower ECSA and mass activity; however, the mass activity remains almost unchanged during the carbon corrosion AST. This agrees with the modeling analysis that demonstrates how the change in the carbon corrosion rate coordinates with local mass-transfer resistance increases.

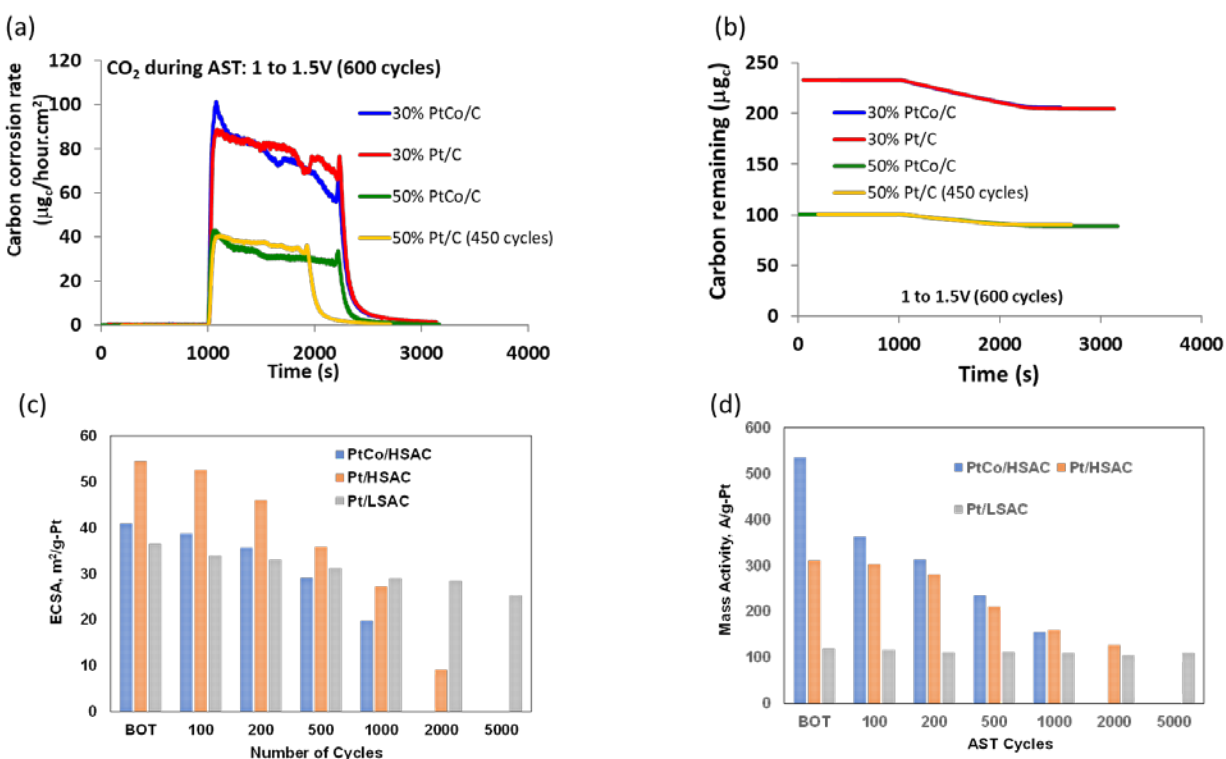


Figure 1. Carbon corrosion measurements comparing 30% and 50% Pt/C and PtCo/C during the DOE/FCTT carbon corrosion AST. (a) Carbon corrosion rate measured by direct CO₂ evolution; (b) calculated remaining carbon after the carbon corrosion and as a function of carbon corrosion cycles for catalysts: PtCo/HSAC, Pt/HSAC; (c) ECSA and (d) mass activity.

Pt and PtCo MEA Conditioning Measurements

FC-PAD has examined the relative performance of MEAs and catalysts in their initial performance compared to their eventual, beginning of life performance, which is generally termed “conditioning.” The conditioning protocol was detailed in the Annual Merit Review (AMR) presentation and consists of high humidity (150% relative humidity), 40°C operation at 0.1 V, with H₂/O₂ followed by H₂/air polarization curves. Figure 2a

shows the catalyst mass activity of a 50% Pt/high-surface carbon (HSC) catalyst during a series of conditioning steps, where the maximum performance is obtained after only two or three conditioning steps. In contrast, a 30 wt% PtCo from Umicore does not reach its maximum mass activity until six to eight conditioning steps. This was measured for three different loadings of Pt: 0.05, 0.10, and 0.15 mgPt/cm². The loading of Pt does not make a significant difference in the conditioning time. The Pt and PtCo particle distribution size (PSD) (Figure 2c) and carbon agglomerate size (Figure 2d) also were measured both before and after conditioning. While the Pt PSD size did not significantly change, the PSD for PtCo increased significantly and the agglomerate size also increased. These measurements show different effects at work during conditioning steps, and variations between different catalysts and MEAs. Thus, care must be taken to appropriately optimize conditioning protocols separately for each material set.

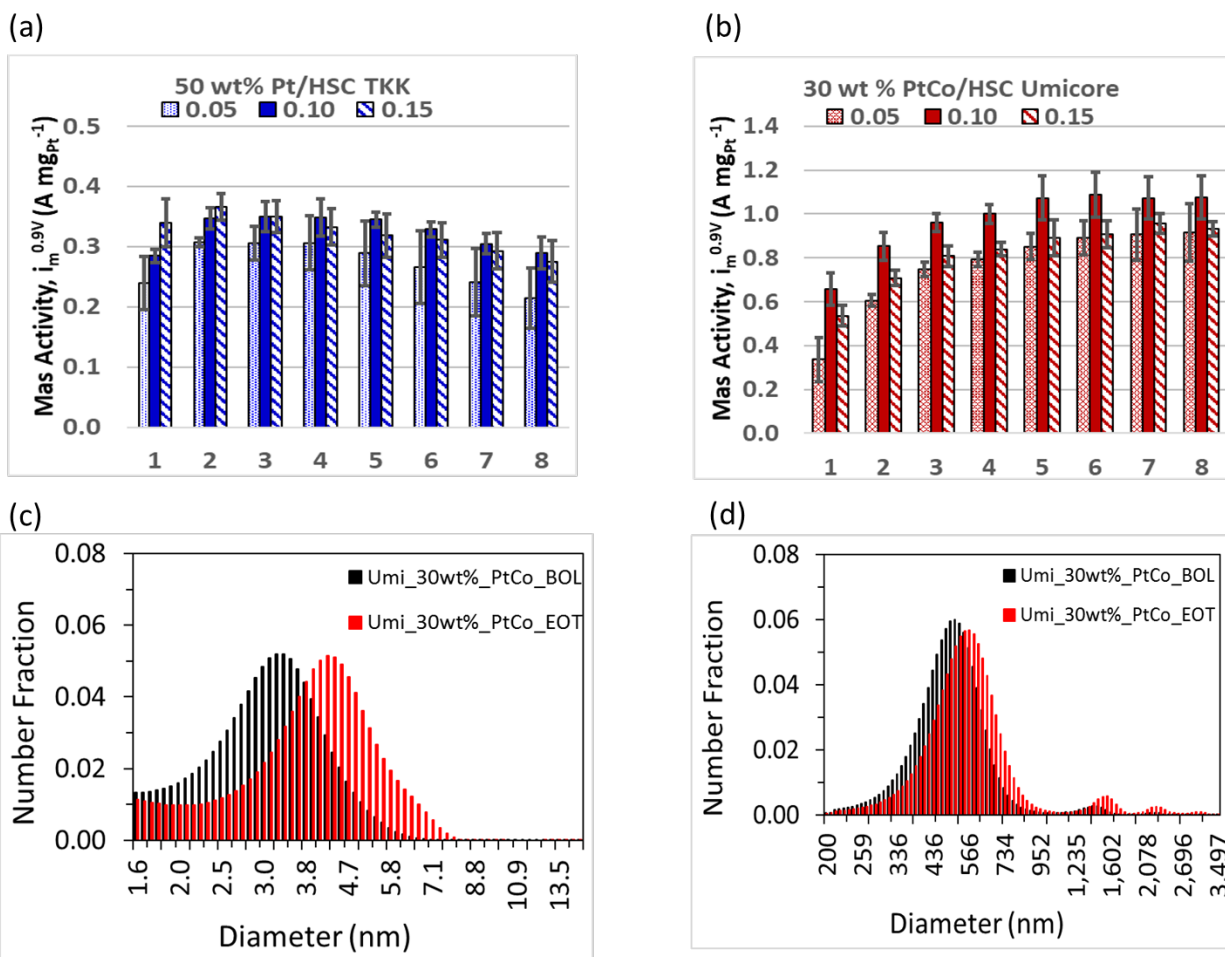


Figure 2. Effect of conditioning cycles on catalyst mass activity for (a) 50 wt% Pt/HSC from TKK and (b) 30 wt% PtCo/HSC from Umicore. Comparison during conditioning protocols at beginning of life (BOL) and end of test (EOT) of PtCo (c) catalyst particle size distribution and (d) carbon agglomerate size.

Array Electrodes

FC-PAD results have demonstrated that state-of-the-art electrode structures are hindered by severe mass-transport limitations during high-power operation at the target low-Pt loadings, resulting in a loss in performance. The ionomer within the electrode adds an additional transport resistance that becomes significant at lower Pt loadings [1]. By separating the different electrode functions into discrete electrode elements, each element can be optimized for its specific function, thereby alleviating the resultant resistances (Figure 3a). We have demonstrated this approach in array electrode through fabrication of freestanding arrays of vertically

oriented ionomer channels with different aspect ratios, and incorporation of these channels into fuel-cell electrodes where they serve as non-tortuous proton-transport highways (Figure 3b). Providing effective proton transport through these low-tortuosity percolating highways allows the catalyst domain to have a lower ionomer/catalyst (I/C) ratio, reducing transport resistance. Proof of concept is demonstrated in Figure 3c where the lower than traditional I/C = 0.5 has a higher performance than a more typical I/C = 0.9 with channels with an aspect ratio of 8. Further work is underway to increase channel aspect ratio and improve integration of channels with the surrounding catalyst layer, leading to further transport improvements and performance increases.

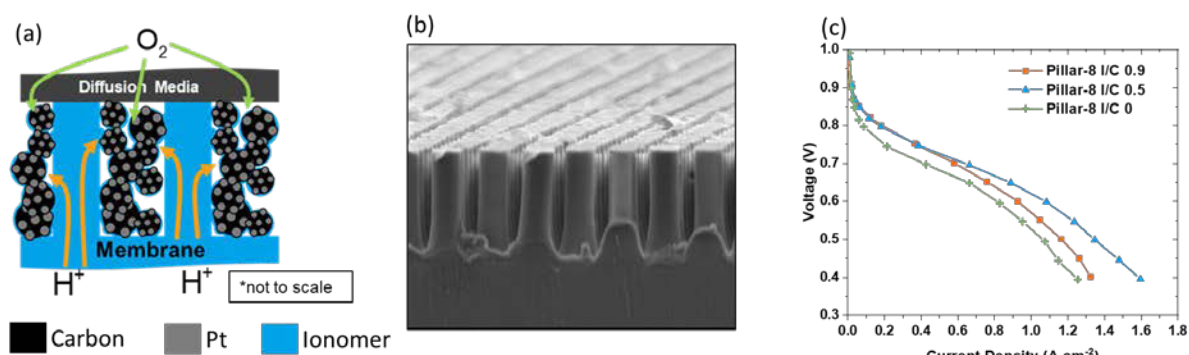


Figure 3. (a) Schematic of the array electrode design, (b) free-standing array of ionomer channels, and (c) polarization performance of array electrode structures with I/C = 0, 0.5, and 0.9

Benchmarking

With limited introduction of commercial fuel cell vehicles initiated, it is important to understand the commercialized state of the art of materials and their limitations to improve upon them. FC-PAD was provided two sets of materials by USCAR from operated Toyota Mirai fuel cell vehicles (300 h and 3,000 h operation). A summary of the MEA components is given in Table 2.

Table 2. Summary of Analysis of Toyota Mirai MEA

	Anode	Cathode
Catalyst	0.05 mgPt/cm ² Pt/C	0.33 mgPt/cm ² PtCo/C
GDL	Fiber substrate (150 micron) with MPL (60 micron) with 120 microgram ceria	Fiber substrate (160 micron) with MPL (40 micron) with 60 microgram ceria
Membrane	10 micron reinforced Nafion	
Bipolar Plate	Carbon-coated Ti	

MPL – microporous layer

To understand the relative durability of the components, the 300-h cell materials were compared to the 3,000-h materials. Little difference was evident; nominally no membrane thinning was measured, and the cathode catalyst particle size was nearly identical at 4.86 nm and 4.96 nm for 300 h and 3,000 h respectively (by small-angle X-ray scattering). Transmission electron microscopy (TEM) analysis of 4.7 nm and 4.8 nm particle size for 300 h and 3,000 h respectively agrees closely with the X-ray measurements. TEM images are shown in Figure 4a and 4b for 300 h and 3,000 h respectively. However, when operating these cells on the DOE/FCTT recommended catalyst ASTs, measurements showed that the materials did not pass the tests. The catalyst particle size increased, and Co was measured to preferentially leach from the catalyst particles (see Figure 4c and 4d). It seems clear that the Toyota Mirai successfully implements mitigation strategies that successfully prevent the vast majority of component degradation, albeit at higher catalyst loadings than the DOE targets.

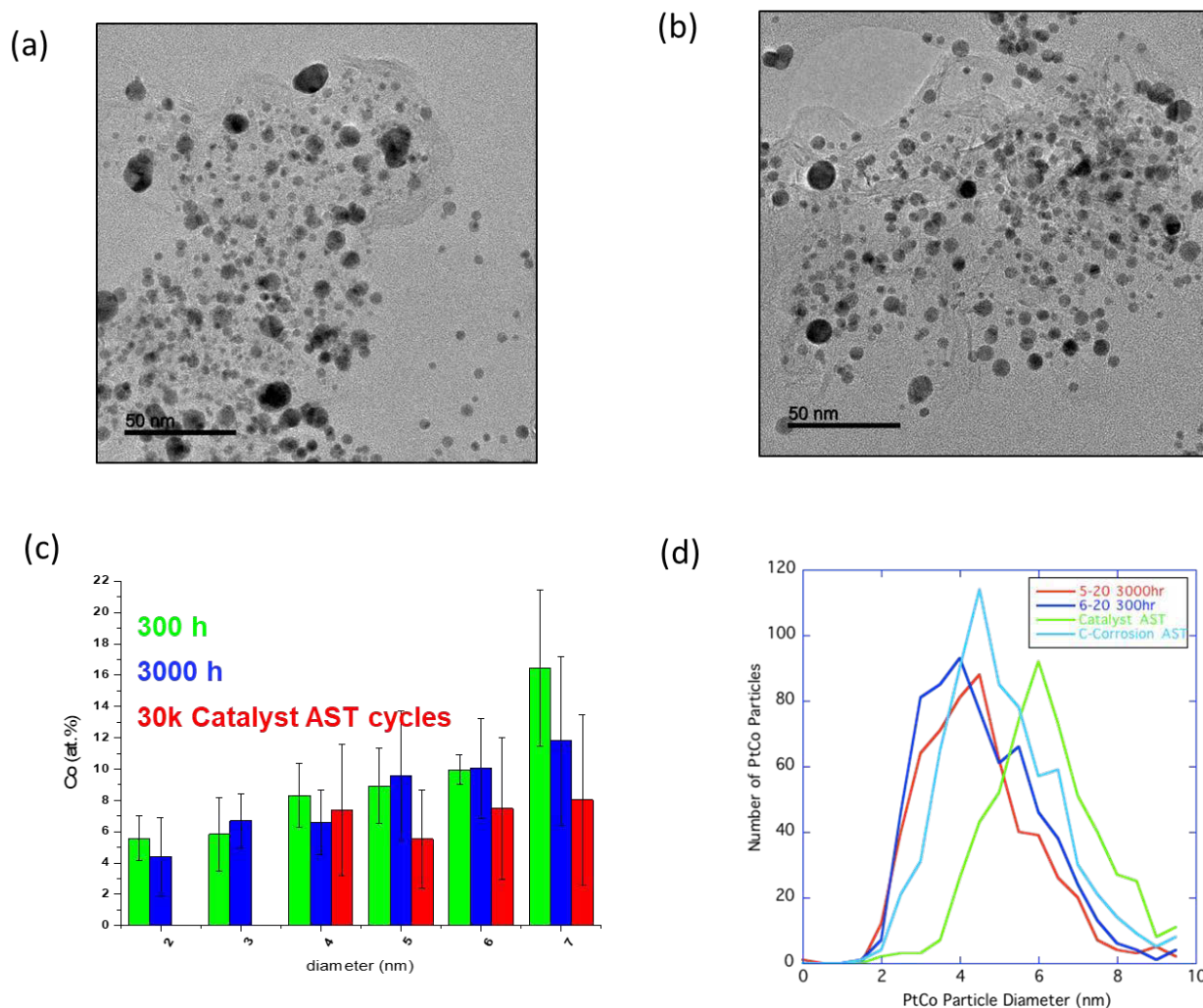


Figure 4. TEM images of the Mirai cathode catalyst after operation of (a) 300 h and (b) 3,000 h. (c) Cobalt % composition for various particle sizes for cells from vehicles operated for 300 h (green), 3,000 h (blue), and after AST (red). (d) PtCo particle size distribution for 300 h (red) and 3,000 h (dark blue), and after the DOE/FCTT recommended catalyst (green) and carbon corrosion (light blue) ASTs.

CONCLUSIONS AND UPCOMING ACTIVITIES

The FC-PAD consortium has conducted significant analysis of MEA electrode structures, analyzed the structures to understand the performance and durability losses, comprehensively defined the current commercial material baseline materials, and used this information to develop new electrode architectures that are designed to minimize existing electrode layer losses. The results and understanding from FC-PAD have been disseminated through 33 peer-reviewed publications and numerous presentations. In addition, the FC-PAD consortium national labs provided support to four DOE-funded projects related to FC-PAD as detailed in their individual project reports.

As a consortium, the future work planned is broad, but concentrates on developing the foundational science to understand MEA component performance and durability.

- Inks and thin films:
 - Examine carbon interactions with different solvents and ionomer chemistry—direct measurement of interaction forces.
 - Measure ionomer thin-film properties under applied potential.
 - Evaluate interfaces and impact of carbon type including durability protocols.
 - Examine impact of cation doping level.
 - Casting and evolution of ionomer thin-film structure.
 - Gas permeability measurements.
- Catalysts:
 - Re-examine intrinsic potential-dependent kinetics—elucidate governing binary interactions, and direct observation of dispersions.
- Catalyst-layer structure:
 - Continue exploration of different catalyst-layer structures—array, electrospun, HSC/VC layered.
 - Incorporation and characterization of novel electrocatalyst materials.
 - Microstructural reconstruction and modeling for catalyst layers including multiphase flow—impact of Pt/C agglomerates.
 - Directly measure ionomer film/carbon in operating electrodes.
 - Local resistance analysis—limiting current under variety of conditions, techniques, ionomers, gases, temperature, humidity.
- Advanced characterization:
 - Multimodal characterization of thin films.
 - New low-voltage cryo-scanning transmission electron microscopy—combinatorial electron energy loss spectroscopy and energy-dispersive X-ray spectroscopy and tomography (4-D scanning transmission electron microscopy), customized in situ cryo-holder to enable improved soft-matter imaging.
- Water and thermal management:
 - Detail model for GDL/channel interface and droplets.
 - Water visualization in various components.
 - Explore impact of carbon type in MPLs.
 - Integrate and evaluate various components to elucidate emergent phenomena.
 - Translational modeling going from ex situ property data to operando performance.

- Durability:
 - Model synergistic mechanical degradation with crossover and performance.
 - Model and measure the movement of chemical scavengers and/or other ions.
 - Examine the effect of aging on electrode microstructure.
 - Develop stabilized systems of radical scavengers.

FY 2018 PUBLICATIONS/PRESENTATIONS

Publications Relevant to FC-PAD from Consortium Members

1. L.M. Pant, Z. Yang, M.L. Perry, and A.Z. Weber, “Development of a Simple and Rapid Diagnostic Method for Polymer-Electrolyte Fuel Cells,” *J. Electrochem. Soc.* 165, no. 6 (2018): F3007–F3014. doi:10.1149/2.0011806jes.
2. R.K. Ahluwalia, D.D. Papadias, N.N. Kariuki, J.-K. Peng, X. Wang, Y. Tsai, D.G. Graczyk, and D.J. Myers, “Potential Dependence of Pt and Co Dissolution from Platinum-Cobalt Alloy PEFC Catalysts Using Time-Resolved Measurements,” *J. Electrochem. Soc.* 165, no. 6 (2018): F3024–F3035. doi:10.1149/2.0031806jes.
3. B.T. Sneed, D.A. Cullen, R. Mukundan, R.L. Borup, and K.L. More, “PtCo Cathode Catalyst Morphological and Compositional Changes after PEM Fuel Cell Accelerated Stress Testing,” *J. Electrochem. Soc.* 165, no. 6 (2018): F3078–F3084. doi:10.1149/2.0091806jes.
4. R. Mukundan, A.M. Baker, A. Kusoglu, P. Beattie, S. Knights, A.Z. Weber, and R.L. Borup, “Membrane Accelerated Stress Test Development for Polymer Electrolyte Fuel Cell Durability Validated Using Field and Drive Cycle Testing,” *J. Electrochem. Soc.* 165, no. 6 (2018): F3085–F3093. doi:10.1149/2.0101806jes.
5. Y. Cai, J.M. Ziegelbauer, A.M. Baker, W. Gu, R.S. Kukreja, A. Kongkanand, M.F. Mathias, R. Mukundan, and R.L. Borup, “Electrode Edge Cobalt Cation Migration in an Operating Fuel Cell: An In Situ Micro-X-ray Fluorescence Study,” *J. Electrochem. Soc.* 165, no. 6 (2018): F3132–F3138. doi:10.1149/2.0201806jes.
6. N. Macauley, D.D. Papadias, J. Fairweather, D. Spornjak, D. Langlois, R.K. Ahluwalia, K.L. More, R. Mukundan, and R.L. Borup, “Carbon Corrosion in PEM Fuel Cells and the Development of Accelerated Stress Tests,” *J. Electrochem. Soc.* 165, no. 6 (2018): F3148–F3160. doi:10.1149/2.0061806jes.
7. D.D. Papadias, R.K. Ahluwalia, N. Kariuki, D.J. Myers, K.L. More, D.A. Cullen, B.T. Sneed, K.C. Neyerlin, R. Mukundan, and R.L. Borup, “Durability of Pt-Co Alloy Polymer Electrolyte Fuel Cell Cathode Catalysts under Accelerated Stress Tests,” *J. Electrochem. Soc.* 165, no. 6 (2018): F3166–F3177. doi:10.1149/2.0171806jes.
8. D.J. Myers, X. Wang, M.C. Smith, and K.L. More, “Potentiostatic and Potential Cycling Dissolution of polycrystalline Platinum and Platinum Nano-Particle Fuel Cell Catalysts,” *J. Electrochem. Soc.* 165, no. 6 (2018): F3178–F3190. doi:10.1149/2.0211806jes.
9. R.K. Ahluwalia, X. Wang, J.-K. Peng, N. Kariuki, D.J. Myers, S. Rasouli, P.J. Ferreira, Z. Yang, A.M. Bonastre, D. Fongalland, and J. Sharman, “Durability of De-Alloyed PtNi/C Catalysts at Low Pt Loadings under Cyclic Potentials,” JESP-18-0204.
10. S. Stariha, N. Macauley, B.T. Sneed, D. Langlois, K.L. More, R. Mukundan, and R.L. Borup, “Recent Advances in Catalyst Accelerated Stress Tests for Polymer Electrolyte Membrane Fuel Cells,” accepted *J. Electrochem. Soc.* (outside of Focus Issue).

11. P.A. García-Salaberri, J.T. Gostick, I.V. Zenyuk, G. Hwang, M. Vera, and A.Z. Weber, “On the Limitations of Volume-Averaged Descriptions of Gas Diffusion Layers in the Modeling of Polymer Electrolyte Fuel Cells,” *ECS Transactions* 80, no. 8 (2017): 133–143. doi: 10.1149/08008.0133ecst.
12. S.A. Berlinger, B.D. McCloskey, and A.Z. Weber, “Understanding Binary Interactions in Fuel-Cell Catalyst-Layer Inks,” *ECS Transactions* 80, no. 8 (2017): 309–319. doi: 10.1149/08008.0309ecst.
13. A. Chowdhury, C.J. Radke, and A.Z. Weber, “Transport Resistances in Fuel-Cell Catalyst Layers,” *ECS Transactions* 80, no. 8 (2017): 321–333. doi: 10.1149/08008.0321ecst.
14. A.R. Crothers, C.J. Radke, and A.Z. Weber, “Nano- and Mesoscale Ion and Water Transport in Perfluorosulfonic-Acid Membranes,” *ECS Transactions* 80, no. 8 (2017): 593–604. doi: 10.1149/08008.0593ecst.
15. A.J. Steinbach, J.S. Allen, R.L. Borup, D.S. Hussey, D.L. Jacobson, A. Komlev, A. Kwong, J. MacDonald, R. Mukundan, M.J. Pejsa, M. Roos, A.D. Santamaria, J.M. Sieracki, D. Spornjak, I.V. Zenyuk, and A.Z. Weber, “Anode-design Strategies for Improved Performance of Polymer-electrolyte Fuel Cells with Ultra-thin Electrodes,” *Joule* (2018). doi: 10.1016/j.joule.2018.03.022.
16. K.B. Hatzell, M.B. Dixit, S.A. Berlinger, and A.Z. Weber, “Understanding Inks for Porous-electrode Formation,” *Journal of Materials Chemistry A* 5, no. 39 (2017): 20527–20533.
17. M. Tesfaye, A.N. MacDonald, P.J. Dudenas, A. Kusoglu, and A.Z. Weber, “Exploring Substrate/Ionomer Interaction under Oxidizing and Reducing Environments,” *Electrochem. Commun.* 87 (2018): 86–90.
18. A.R. Crothers, C.J. Radke, and A.Z. Weber. “Impact of Nano-and Mesoscales on Macroscopic Cation Conductivity in Perfluorinated-Sulfonic-Acid Membranes.” *Journal of Physical Chemistry C* 121, no. 51 (2017): 28262–28274.
19. B.T. Sneed, D.A. Cullen, K.S. Reeves, O.E. Dyck, D.A. Langlois, R. Mukundan, R.L. Borup, and K.L. More, “3D Analysis of Fuel Cell Electrocatalyst Degradation on Alternate Carbon Supports,” *ACS Applied Materials & Interfaces* 9, no. 35 (2017): 29839–29848.
20. S. Stariha, M.S. Wilson, J.M. LaManna, D.L. Jacobson, D.S. Hussey, N. Macauley, J. Rau, and R.L. Borup, “Determining Water Content and Distribution in PEMFCs to Predict Aging While in Storage,” *ECS Transactions* 80, no. 8 (2017): 377–384.
21. D.S. Hussey, J.M. LaManna, E. Baltic, D.L. Jacobson, S. Stariha, D. Spornjak, R. Mukundan, and R.L. Borup, “Membrane/Electrode Assembly Water Content Measured with 2 μm Spatial Resolution Neutron Imaging,” *ECS Transactions* 80, no. 8 (2017): 385–393.
22. A.M. Baker, J.H. Dumont, R. Mukundan, S.G. Advani, A.K. Prasad, D. Spornjak, and R.L. Borup, “The Effects of Cerium Migration on PEM Fuel Cell Performance,” *ECS Transactions* 80, no. 8 (2017): 643–650.
23. J.H. Dumont, A.M. Baker, S. Maurya, Y.-S. Kim, R. Mukundan, D.J. Myers, and R.L. Borup, “Effect of Cerium, Cobalt, and Nickel Contaminants on the Oxygen Reduction Reaction at Platinum Electrodes,” *ECS Transactions* 80, no. 8 (2017): 861–867.
24. A.M. Baker, S. Komini Babu, R. Mukundan, S.G. Advani, A.K. Prasad, D. Spornjak, and R.L. Borup, “Cerium Ion Mobility and Diffusivity Rates in Perfluorosulfonic Acid Membranes Measured via Hydrogen Pump Operation,” *Journal of The Electrochemical Society* 164, no. 12 (2017): F1272–F1278.
25. A.M. Baker, S.T.D. Williams, R. Mukundan, D. Spornjak, S.G. Advani, A.K. Prasad, and R.L. Borup, “Zr-doped Ceria Additives for Enhanced PEM Fuel Cell Durability and Radical Scavenger Stability,” *Journal of Materials Chemistry A* 5, no. 29 (2017): 15073–15079.
26. F.C. Cetinbas, X. Wang, R.K. Ahluwalia, N.N. Kariuki, R.P. Winarski, Z. Yang, J. Sharman, and D.J. Myers, “Microstructural Analysis and Transport Resistances of Low-Platinum-Loaded PEFC Electrodes,” *Journal of The Electrochemical Society* 164, no. 14 (2017): F1596–F1607.

27. B. Ergul, M. Begum, N.N. Kariuki, D.J. Myers, and T. Karabacak, “Oxygen Reduction Reaction Activity of Platinum Thin Films with Different Densities,” *ECS Transactions* 80, no. 8 (2017): 847–852.
28. M. Begum, M. Yurukcu, F. Yurtsever, B. Ergul, N.N. Kariuki, D.J. Myers, and T. Karabacak, “Pt-Ni/WC Alloy Nanorods Arrays as ORR Catalyst for PEM Fuel Cells,” *ECS Transactions* 80, no. 8 (2017): 9191–925.
29. S. Zhao, A. Stocks, B. Rasimick, K.L. More, and H. Xu, “Highly Active, Durable Dispersed Iridium Nanocatalysts for PEM Water Electrolyzers,” *Journal of The Electrochemical Society* 165, no. 2 (2018): F1–F8.
30. P.A. García-Salaberri, I.V. Zenyuk, A.D. Shum, G. Hwang, M. Vera, A.Z. Weber, and J.T. Gostick, “Analysis of Representative Elementary Volume and Through-Plane Regional Characteristics of Carbon-Fiber Papers: Diffusivity, Permeability and Electrical/Thermal Conductivity,” *International Journal of Heat and Mass Transfer* 127 (2018): 687–703
31. A.J. Steinbach, J.S. Allen, R.L. Borup, D.S. Hussey, D.L. Jacobson, A. Komlev, A. Kwong, J. MacDonald, R. Mukundan, M.J. Pejsa, M. Roos, A.D. Santamaria, J.M. Sieracki, D. Spornjak, I.V. Zenyuk, A.Z. Weber, “Anode-Design Strategies for Improved Performance of Polymer-Electrolyte Fuel Cells with Ultra-Thin Electrodes,” *Joule* (April 23, 2018).
32. M. Tesfaye, A.N. MacDonald, P.J. Dudenias, A. Kusoglu, A.Z. Weber, “Exploring Substrate/Ionomer Interaction under Oxidizing and Reducing Environments,” *Electrochemistry Communications* 87 (2018), 86–90.

REFERENCES

1. N. Nonoyama, S. Okazaki, A.Z. Weber, Y. Ikogi, and T. Yoshida, *J. Electrochem. Soc.* 158 (2011): B416.

Novel Ionomers and Electrode Structures for Improved Polymer Electrolyte Membrane Fuel Cell Electrode Performance at Low Platinum-Group-Metal Loadings

Andrew Haug (Primary Contact), Matthew Lindell, John Abulu, Mike Yandrasits, Grant Thoma, Andy Steinbach, Mike Kurkowski, Grant Weatherman, Israr Khan, Fuxia Sun, Matthew Krueger
3M Company, Corporate Research Laboratory
3M Center, Building 201-1W-28
St. Paul, MN 55144-1000
Phone: (651) 737-3579
Email: athaug@mmm.com

DOE Manager: David Peterson
Phone: (720) 356-1747
Email: David.Peterson@ee.doe.gov

Contract Number: DE-EE0007650

Subcontractors:

- Michigan Technological University, Houghton, MI
- Tufts University, Medford, MA
- Lawrence Berkeley National Laboratory, Berkeley, CA
- Oak Ridge National Laboratory, Oak Ridge, TN
- Argonne National Laboratory, Lemont, IL
- National Renewable Energy Laboratory, Golden, CO
- Los Alamos National Laboratory, Los Alamos, NM

Project Start Date: October 1, 2016
Project End Date: September 30, 2019

Overall Objectives

The objective is to develop electrodes containing new ionomers and oxygen reduction reaction (ORR) electrocatalysts that exceed project-specific ionomer targets and the following DOE 2020 targets.

- Mass activity of 0.44A/mg_{PGM} or higher.
- Platinum group metal (PGM) total content (both electrodes) of ≤ 0.125 g/kW.
- PGM total loading (both electrodes) < 0.125 mg_{PGM}/cm².
- Electrocatalyst mass activity durability of $< 40\%$ loss.

- Metal stability accelerated stress test (AST) loss of performance < 30 mV @ 0.8 and 1.5 A/cm².
- 2020 DOE support and start-up–shutdown (SUSD) targets.
- 50% ionomer conductivity and bulk oxygen permeability over 3M825EW.
- Membrane electrode assembly (MEA) robustness $> 70\%$ at cold, hot, and transient conditions.
- Achieve a working electrode model investigating local water and gas transport through cathode electrodes.

Fiscal Year (FY) 2018 Objectives

- Develop an ionomer more conductive and 33% more oxygen permeable than 3M825.
- Achieve power targets of 0.175 g/kW.
- Achieve electrode activity targets of 0.35 A/mg_{PGM} with a nanostructured thin film (NSTF) catalyst greater than 25 m²/g_{PGM}.

Technical Barriers

This project addresses the following technical barriers from the Fuel Cells section of the Fuel Cell Technologies Office Multi-Year Research, Development, and Demonstration Plan¹:

- (A) Durability
- (B) Cost
- (C) Performance
- (D) Operational Robustness.

Technical Targets

Table 1 summarizes 2018 project status against the relevant 2020 DOE targets and project targets. All

¹ <https://energy.gov/eere/fuelcells/downloads/fuel-cell-technologies-office-multi-year-research-development-and-22>

reported status values are measurements made in membrane electrode assembly format.

So far, six of the overall targets have been achieved. This budget period (BP), a new imide-type ionomer (IMIDE#4) demonstrated a bulk oxygen permeability of 93% of the 3M825 baseline while showing 22% more conductivity. Dispersed metal on carbon electrodes containing new ionomers have achieved key performance targets while improving activity and metal stability.

The NSTF Pt/Ir catalysts developed in DE-EE0007077 (Steinbach) retain up to 70% of their metal activity when dispersed in ionomer-containing electrodes. The PtNiRu NSTF catalysts currently have achieved 0.31 A/mg_{PGM} in the DOE 1,000-s hold activity test and higher (0.45 A/mg_{PGM}) in H₂/O₂ Tafel extraction. The NSTF Pt/Ir catalysts have demonstrated as low as 16% surface area loss and 33% activity loss. Dispersed NSTF electrodes with multiple support types have exceeded 5,000 DOE support cycles. Pt and PtCo on graphitized carbon supports have shown up to 45% activity increase (up to 0.30 A/mg Pt) in electrodes utilizing multi-acid side chain (MASC) ionomer at lower ionomer contents, and surface area losses as low as 36%. More active catalysts are being evaluated in this system with the goal of achieving activity and durability targets simultaneously.

FY 2018 Accomplishments

- Generated an imide-based ionomer with 92% more bulk oxygen permeability than the 3M825 baseline.
- Seven other novel ionomer types have been generated but have not shown oxygen permeability gains.
- Reduced electrochemical surface area (ECSA) loss from 90% (baseline) to 55% with base 10V50E and 10VA50E catalyst systems.
- Increased activity of 10VA50E by 45%.
- Tested an 10/10 Pt/Ir NSTF catalyst with 30 m²/g_{PGM} ECSA that showed 15% surface area loss in the DOE metal AST.
- Tufts demonstrated 3M PFIA ionomer is inherently more conductive in an electrode than a perfluorosulfonic acid (PFSA) ionomer of similar ion exchange capacity.
- Identified a key protonic conductivity limitation of dispersed NSTF electrodes with Los Alamos National Laboratory.
- Los Alamos National Laboratory showed correlations between metal -containing and metal-free carbons and agglomeration.
- Michigan Technological University (MTU) correlated ionomer equivalent weight and electrode hydrophilicity.

Table 1. Status Against Technical Targets^a

Metric	Units	Project Target	August 2018
PGM total loading	mg/cm ²	0.125	0.115 ^b
PGM total loading, 150 kPa _{abs}	g/kW	0.125	0.125 ^{b,d}
Mass activity @ 900 mV _{IR-free}	A/mg	0.44+	0.30/0.45
SUSD AST, % ECSA loss	%	<20	N/A
SUSD AST, loss @ 1.2 A/cm ²	mV	<5%	N/A
Support AST, mass activity loss	%	<30	<10% (Pt)
Electrocatalyst AST, mV loss @ 1.5 A/cm ²	mV	<30	80 ^e
Electrocatalyst AST, % mass activity loss	%	<40	40% Pt, 33% Pt/Ir
MEA robustness (cold/hot/cold transient) ^c	%	>70/>70/>70	93/84/90
Ionomer conductivity (80 °C, 50% RH)	S/cm	0.087 (+50%)	0.070 (+22%)
Ionomer bulk O ₂ perm (80 °C, 50% RH)	mol-cm-s ⁻¹ -cm ⁻² -kPa ⁻¹	1.8E-13 (+50%)	2.3E-13 (+92%)

^a All metrics and DOE 2020 targets are taken from DE-FOA-0001412.

^b 0.025 mg Pt/cm² anode.

^c 3M transient protocols used for NSTF testing.

^d At 0.661 V, 80 °/68 °/68 °C, 7.5 psig.

^e At 70 °/70 °/70 °C, 0 psig.

RH – relative humidity

INTRODUCTION

Among the various recommendations for fuel cell performance enhancement at low precious-metal loadings are increasing ionomer and electrode O₂ transport and increasing ionomer hydrophobicity. Further proposed limitations include local (near catalyst) water generation and flooding and transport losses due to alloying (non-platinum) metal dissolution. Additionally, catalysts and electrodes with increased activity and durability are required to meet automotive performance and lifetime targets. The focus of this project is to develop electrode ionomers with improved O₂ transport, integrate these into electrodes containing durable, active NSTF powder, and achieve DOE 2020 power and durability targets.

In Budget Period 2 (BP 2), several electrode-focused ionomers were generated and evaluated. Increased ionomer conductivity has led to improved electrode performance, and lower ionomer content has shown activity and metal stability increases. For the first time, NSTF Pt/Ir catalyst powder is being integrated into a more classic electrode structure and showing good activity and excellent metal stability. Support from the Fuel Cell Consortium for Performance and Durability, Tufts, and MTU is breaking down current NSTF performance limitations, leading to the likelihood that local proton conductivity is limiting in dispersed NSTF systems. Integration and analysis of these novel materials is continuing in Budget Period 3. Model development by MTU and Tufts has resulted in a model that is being validated against data and is probing the transport mechanisms of electrodes containing these novel materials.

APPROACH

The approach is to develop novel electrode-specific ionomers aimed at increasing O₂ permeability, conductivity, and cathode performance. Ionomer development is proceeding along three paths: developing and evaluating multi-acid sidechain materials, imide-only materials (BP 1, BP 2), and more novel O₂-permeable ionomer structures (BP 2, BP 3). NSTF will then be integrated into this ionomer containing electrode framework. The best high-activity, durable ultra-thin film (UTF) alloy powders having a minimal number of monolayers (i.e., maximum ECSA) potentially achieve areas approaching 70 cm²_{PGM}/cm²_{planar} with specific activities as high as 4 mA/cm² with 0.105 mg PGM/cm². This is a theoretical mass activity entitlement of 2.5 A/mg_{PGM}, a 5-fold increase beyond the exceeding the DOE 2020 0.44 A/mg PGM mass activity target. Activity losses stabilizing UTF powder against cyclic decay and integrating UTF powder into an ionomer containing electrode are expected, but such UTFs can lose more than 80% activity and still achieve DOE 2020 targets. Finally, optimizing of the electrode framework containing novel ionomers and optimal NSTF will be completed to achieve the above targets. Guiding this development at every stage will be state-of-the-art characterization and modeling including nanoCT imaging, grazing incident small-angle X-ray spectroscopy (GISAXS), transmission electron microscopy, water imbibition, and pore hydrophobicity/hydrophilicity measurements.

The proposed work is broken down into five tasks: electrode ionomer development and characterization (Task 1), advanced NSTF electrode development and characterization (Task 2), integration of novel ionomers and NSTF into electrodes (Task 3), model development (Task 4), and project management (Task 5). The project contains three 12-month budget periods. NSTF development will focus mainly on the integration of state-of-the-art NSTF catalyst powder into an ionomer-containing electrode architecture.

RESULTS

For Task 1, IMIDE#4 ionomer has been developed that exceed BP 2 targets and meet project targets for bulk oxygen permeability. As shown in Figure 1, IMIDE#4 showed a 92% increase in bulk oxygen permeability over the baseline. In general, the imide-based ionomers have shown increased oxygen permeability with IMIDE#2 and IMIDE#1 (not shown) showing improvements. New materials of this kind are being made in the hopes of furthering these gains. IMIDE#4 is showing the required conductivity improvements over 3M825 as well. Further, Tufts found that for electrodes containing carbon and ionomer, that multi-acid side chains are showing significantly improved conductivity over PFSA (3M825)—even when normalized to ion exchange capacity (Figure 2). Perhaps it is due to larger—and perhaps better—connected—ionic domains as measured by

Lawrence Berkeley National Laboratory using GISAXS. Local oxygen-transport studies conducted by 3M, National Renewable Energy Laboratory, and Lawrence Berkeley National Laboratory have all confirmed that lowering the ionomer content of the electrode decreases local oxygen-transport resistance, which has been directly correlated to high current performance gains. It has not yet been validated that improved bulk oxygen permeability, inherent to the ionomer, results in local oxygen transport gains. That work presently is ongoing. Additional variables, such as choice of carbon support (Vulcan versus graphitized Vulcan), also seem to have an effect on local oxygen transport.

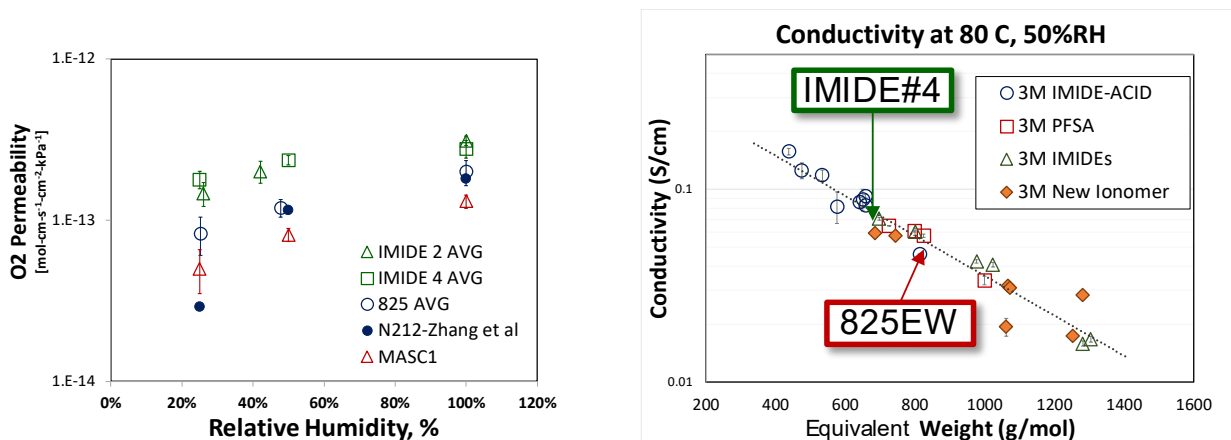


Figure 1. Conductivity (right) and oxygen permeability (left) of baseline PFSA and novel imide ionomers

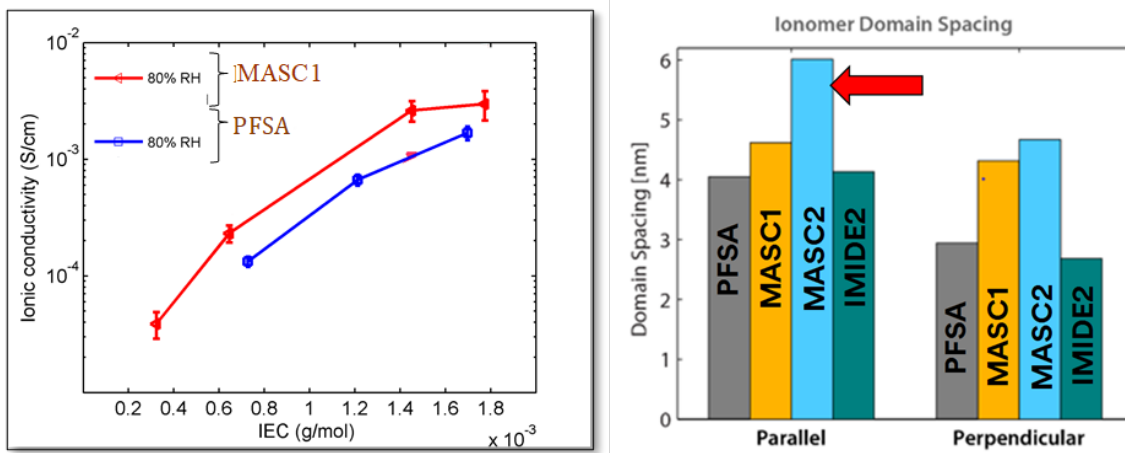


Figure 2. Conductivity normalized to ion exchange capacity of 3M825 PFSA versus multi-acid side chain 1 (MASC#1). Left is work by LBNL showing larger ionomer domains of MASC materials measured by GISAXS.

These gains have allowed less ionomer to be used in the electrode, giving rise to improved local oxygen transport in the electrode and improved performance, as shown in Figure 3. Further, both activity and durability have been improved using these electrodes. Activity gains of 45% have been made with graphitized Pt on C. Metal area loss has been reduced from 91% to 57% as shown in Figure 4. Through Task 3, integration of these ionomers with alloy catalysts has further reduced metal area loss to 36%. Further improvements are expected here with better catalysts, new ionomer integration, and electrode configurations.

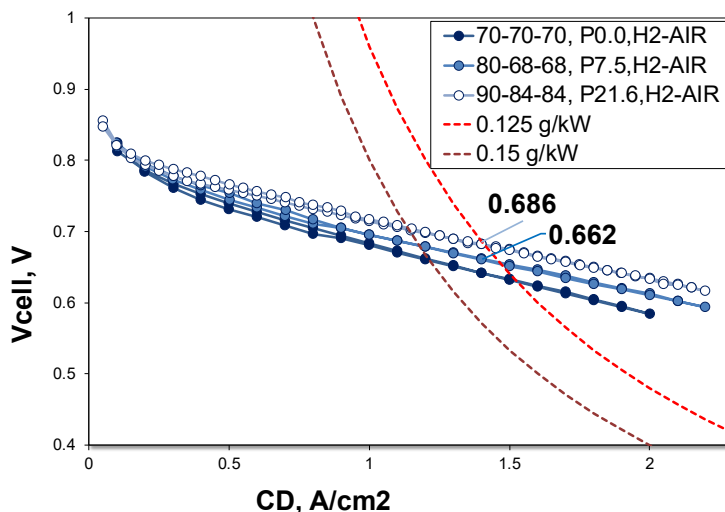


Figure 3. Performance at different conditions for best-in-class alloy at 0.095 mg Pt/cm² cathode loading

Task 2 work with dispersed NSTF electrodes has progressed significantly in BP 2. Integrating new Pt/Ir NSTF alloys has been very promising for several reasons: exceptional metal stability as shown in Figure 4; increased surface area versus Pt-only NSTF electrodes; and the catalyst is transition-metal free, which eliminates the concern for leached transition metals corrupting catalyst-coated membrane performance and water management.

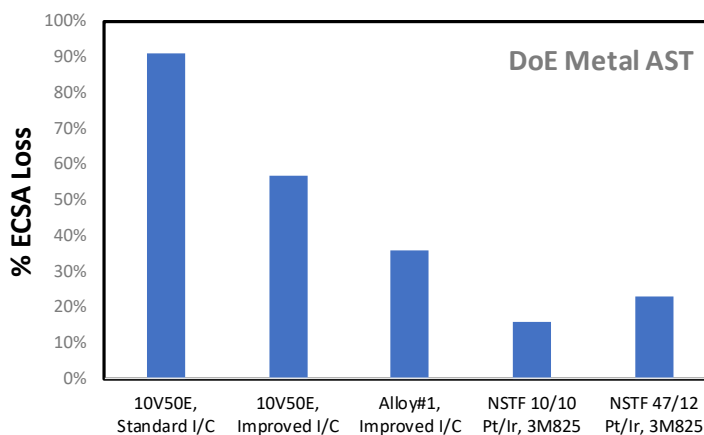


Figure 4. Cathode catalyst surface area loss occurring during DOE 30,000-cycle metal AST test (80 °C, 100% RH, H₂/N₂)

Task 2 work on electrodes has improved the activity retention when comparing classic NSTF Pt/Ir electrodes (whiskers laminated directly to a membrane) to dispersed ionomer-containing NSTF electrodes from ~33% to as much as 71%. Performance of a best-in-class 0.093 mg PGM/cm² NSTF cathode has achieved the target of 0.175 g/kW and demonstration surface area loss of only 23% in the DOE catalyst metal AST. Perhaps of more significance is that, despite the low surface roughness of this material, performance at moderate current densities is maintained, finally breaking the trend of performance versus surface roughness.

Performance of much of the dispersed NSTF materials has been reduced by what seems to be an additional resistance loss. Work with Los Alamos National Laboratory has investigated these materials utilizing advanced impedance techniques with the goal of possibly identifying this limitation. As shown in Figure 5, it is likely that dispersed NSTF electrodes suffer from an additional protonic transport limitation as compared to metal on carbon catalysts such as 10V50E (TKK). Based on the amount of ionomer present in the electrode (and ion

exchange capacity), this limitation more likely would be local to the catalyst. This is consistent with performance improvement seen utilizing lower-equivalent-weight ionomers. Work with multi-acid sidechain ionomers is shown to reduce this resistance loss, and now is being investigated using advanced impedance techniques. Analysis of this local transport loss is ongoing. MTU has used transmission electron microscopy analysis to show that it is highly likely that ionomer is present around the NSTF whisker in dispersed NSTF electrodes. Los Alamos National Laboratory also has demonstrated that gas transport in dispersed NSTF electrodes was quite good even at higher currents. This is consistent with work from Argonne National Laboratory that supports agglomerate more strongly. Agglomerated carbon-ionomer systems have many more regions where gas can pass unhindered by ionomer films, thereby incurring minimal bulk oxygen transport losses.

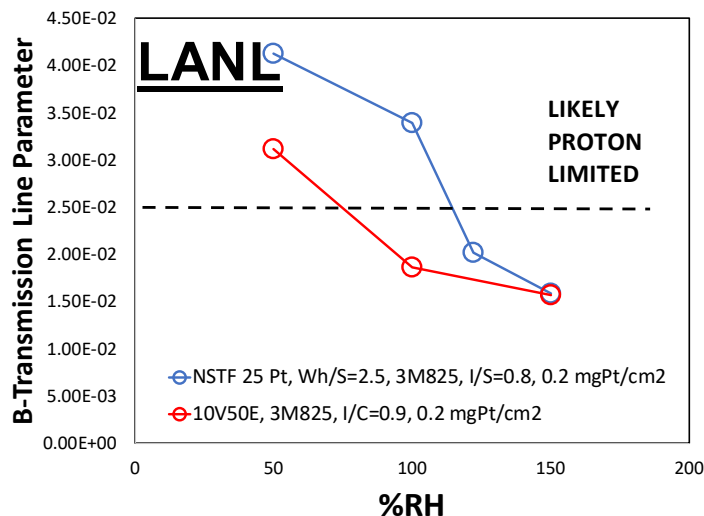


Figure 5. Transmission line impedance analysis of dispersed NSTF versus metal on carbon (10V50E) cathode electrodes performed by Los Alamos National Laboratory

In BP 2, Task 4 model development continued in collaboration with Tufts and MTU. Water generation and migration is being captured in the electrode. It is now being fitted against various data and parameters to better understand liquid water generation for different systems with different wettabilities.

CONCLUSIONS AND NEXT STEPS

New electrode ionomer development has exceeded oxygen permeability project targets with conductivity approaching overall targets. Led by understanding gained in multi-acid side chain ionomers in the electrode, local oxygen transport in the electrode has been reduced and performance increased. Metal-on-carbon stability has been improved by incorporating new ionomers. Dispersed NSTF stability and activity has been improved and local transport understanding is leading to performance gains. Key next steps are to continue the learning in the areas of local transport in electrodes and then apply this learning to best integrate the new ionomers and NSTF materials into the electrode in BP 3.

FY 2018 PUBLICATIONS/PRESENTATIONS

1. Abbou, S., K. Tajiri, E.F. Medici, and J. S. Allen, "Liquid Water Uptake and Contact Angle Measurement of Proton Exchange Membrane Fuel Cell (PEMFC) Electrodes," *Journal of the Electrochemical Society* (submitted).
2. Haug, A.T., "Novel Ionomers and Electrode Structures for Improved PEMFC Electrode Performance at Low PGM Loadings," USCAR Fuel Cell Tech Team, September 11, 2018, Detroit, MI.

3. Haug, A.T., 2018 Annual Merit Review, DOE Hydrogen and Fuel Cell Vehicles Technology Programs, Presentation FC143, June 2018, Washington, D.C.
4. Kusoglu, A., M. Tesfaye, D. Kushner, B. McCloskey, and A. Weber, "Thermal Transitions in Perfluorosulfonated Ionomer Thin Films," ACS Macro Letters (submitted).
5. Liu, J., and I.V. Zenyuk, "Bridging Micro and Nano Scales in Fuel Cell Electrodes Using Multi-Modal Imaging and Scale-Bridging Method," InterPore 10th Annual Meeting and Jubilee, May15, 2018, New Orleans, LA.
6. Normile, S.J., and I.V. Zenyuk, "Imaging Ionomer in Fuel Cell Electrodes with Two-Energies Transmission X-ray Microscopy Approach," *Solid State Ionics* (Under Review, 2018).
7. Sabarirajan, D., and I.V. Zenyuk, Telluride Science Research Center Workshop: Interfacial Chemistry and Charge Transfer for Energy Conversion and Storage, July 22–27, Telluride, CO.
8. Saha, P., D. Sabarirajan, and I.V. Zenyuk, Gordon Research Conference: Electrochemistry, January 7–12, 2018, Ventura, CA.
9. Zenyuk, I.V., 3rd International Fuel Cells Workshop, Fuel Choices and Smart Mobility Summit, October 29–30, 2018, Tel Aviv, Israel.
10. Zenyuk, I.V., Electrochemical Society Meeting, October 1, 2018, Cancun, Mexico (PEFC&E 18 Symposia Plenary).
11. Zenyuk, I.V., Gordon Research Conference, Fuel Cells, July 29–August 3, 2018, Smithfield, RI.
12. Zenyuk, I.V., University of California, Irvine, Department of Chemical Engineering and Materials Science Engineering, February 23, 2018, Irvine, CA.
13. Zenyuk, I.V., University of South California, Aerospace and Mechanical Engineering, March 7, 2018, Los Angeles, CA.
14. Zenyuk, I.V., D. Sabarirajan, and P. Saha, "Understanding Ion Transport at Charged Interfaces with Application to Polymer Electrolyte Fuel Cells," 69th Annual Meeting of the International Society of Electrochemistry, September 5th, 2018, Bologna, Italy.

Durable High-Power Membrane Electrode Assemblies with Low Platinum Loading

Swami Kumaraguru (Primary Contact),
Srikanth Arisetty, Frank Coms, Craig Gittleman,
Vinaykumar Konduru, Yeh Hung Lai,
Ashley McQuarters, Nagappan Ramaswamy
General Motors Company (GM)
850 N Glenwood Avenue
Pontiac, MI 48340-2920
Phone: (585) 683-8413
Email: swami.kumaraguru@gm.com

DOE Manager: Gregory Kleen
Phone: (240) 562-1672
Email: Gregory.Kleen@ee.doe.gov

Contract Number: DE-EE0007651

Subcontractors:

- University of Texas, Austin, TX
- Giner, Inc., Newton, MA

Project Start Date: April 1, 2017
Project End Date: March 31, 2020

Overall Objectives

- Identify best-in-class materials and generate a state-of-the-art (SOA) membrane electrode assembly (MEA) that meets DOE 2020 performance and cost targets.
- Study the impact of operating conditions on durability of SOA MEAs in differential cell conditions supported with advanced electrochemical and analytical characterization.
- Develop a predictive model for electrode and membrane degradation and recommend implementable benign operating conditions to prolong MEA durability to >5,000 h.

Fiscal Year (FY) 2018 Objectives

- Down-select and integrate best-in-class catalyst, ionomer, and membranes to generate SOA MEAs that will meet DOE 2020 performance and cost targets. Deliver 5-cm² and 50-cm² SOA MEAs to Fuel Cell

Consortium for Performance and Durability (FC-PAD) partners for durability studies.

- Conduct a systematic study to understand the role of catalyst and ionomer properties on measured polarization curve, activity, and transport properties of the catalyst layer.
- Initiate H₂-N₂ voltage cycling to study the effect of operating conditions on durability.
- Develop a combined accelerated chemical and mechanical stress test for membrane degradation. Explore degradation mechanisms.

Technical Barriers

This project addresses the following technical barriers from the Fuel Cells section of the Fuel Cell Technologies Office Multi-Year Research, Development, and Demonstration Plan¹:

(A) Durability

(B) Cost

(C) Performance.

Technical Targets

Table 1 shows the DOE technical targets and current project status.

FY 2018 Accomplishments

- Several best-in-class catalysts, ionomers, and membranes were tested for activity and performance. The best-in-class materials were integrated to generate a SOA MEA.
- The final SOA MEA design exhibits >1.0 W/cm² and Q/ΔT <1.45 and platinum group metal (PGM) content (g/kW rated) of ~0.1 mg/cm² MEA or 10 kW/g PGM. Additional DOE metrics are shown in Table 1.
- Roles of carbon support on activity and transport properties were identified. Carbon micropore and macropore surface area was found to impact both oxygen and proton

¹ <https://energy.gov/eere/fuelcells/downloads/fuel-cell-technologies-office-multi-year-research-development-and-22>

- transport resistance. The expectation for an ideal carbon support was laid out.
- Performance variation due to ionomer distribution for different catalysts (HSC-a vs. HSC-g) and ink formulations (low to high alcohol fraction) was demonstrated by catalyst layer ionomer mapping studies at Oak Ridge National Laboratory.
 - Among different ionomer chemistries studied, the equivalent weight (EW) of the ionomer was the dominant factor in determining ionomer solution properties, catalyst ink properties, and catalyst layer performance. The side chain lengths considered in this study did not have a significant impact.
 - A combined highly accelerated chemical and mechanical stress test (HAST) was developed. The HAST indicates that higher mechanical stress can accelerate chemical degradation.
 - Several analytical methods involving Fourier transform infrared spectroscopy (FTIR), ultraviolet, and X-ray fluorescence (XRF) were developed to monitor Ce^{3+} movement. A two-chamber relative humidity (RH) gradient cell was devised at Giner to measure Ce^{3+} movement via convection.
 - Ce^{3+} movement via both diffusion and convection was measured. Initial studies indicate convection to be the dominant process.
 - Demonstrated use of X-ray computed tomography at Lawrence Berkeley National Laboratory for identifying shorts due to gas diffusion layer fibers in MEAs.

Table 1. Progress Toward Meeting Technical Targets for Electrocatalysts and MEAs for Transportation Applications

Characteristic	Units	DOE 2020 Catalyst and MEA Targets	Project Status (50 cm ² cell) 94 °C, 250 kPaa	Project Status (50 cm ² cell) 80 °C, 150 kPaa
Mass activity	A/mg _{PGM} @ 0.9 mV _{iR-free}	≥0.44	0.65	0.65
Specific activity	μA/cm ² _{PGM} @ 0.9 mV _{iR-free}	≥720	1,477	1,477
I @ 0.8 V	A/cm ²	0.3	0.44	0.30
MEA performance	mW/cm ² _{geo} @ 675 mV	≥1,000	1,275	1,000
Durability with cycling	Hours @ <10% V loss	5,000	TBD	TBD
Q/ΔT	KW/°C	1.45	1.45	1.94
PGM total loading	mg-PGM/cm ² _{geo}	≤0.125	≤0.125	≤0.125
PGM content	g/KW rated mg/cm ² MEA	≤0.125	0.1	0.125

INTRODUCTION

GM and other automotive MEA developers have achieved very impressive beginning-of-life performance using low-Pt (0.05–0.1 mg_{Pt}/cm²) loaded cathodes with PtCo alloys and thin (10–15 micron) membranes. Unfortunately, these MEAs are subject to life-limiting degradation during operation, especially at peak power, because of complex degradation mechanisms that are highly sensitive to the materials, MEA design, and fuel cell operating strategy. Specifically, power degradation of the cathode occurs via Pt and Co dissolution as well as deterioration of O₂ transport properties. Additionally, thin membranes are subject to failure due to manufacturing defects in the adjacent gas diffusion media and electrodes and the formation of membrane-attacking radical species caused by high gas crossover. This project is designed to systematically study these degradation phenomena in a SOA MEA, applying and extending diagnostic and modeling tools available at GM, its partners, and the FC-PAD consortium.

APPROACH

The project approach is based on our understanding that there is substantial opportunity to select operating conditions and voltage waveforms to reduce life-limiting electrode and membrane degradation rates. In this project, we intend to map the impact of operating conditions on SOA MEA durability for proton exchange membrane fuel cells (PEMFCs). This will be achieved by systematic durability studies relying on advanced characterization tools, degradation mechanism model development, and validation. Specifically, the project approach is to improve MEA performance and durability by executing the following work elements: (1) integrating the BIC materials to generate an SOA MEA in Budget Period (BP) 1, (2) incorporating systematic durability studies to assess the impact of operating conditions on MEA life, (3) conducting extensive postmortem characterization of MEAs to provide mechanistic understanding of MEA degradation along with developing and validating models to predict electrode and membrane degradation, and (4) recommending benign, yet realistic operating conditions to extend MEA durability past the 5,000-hour DOE 2020 durability target.

RESULTS

The goal of BP 1 was to generate a SOA MEA that meets or exceeds the DOE 2020 performance targets. Accordingly, in 2018, the SOA MEA was generated with use of BIC materials. As illustrated in Table 1 and Figure 1, the SOA MEA performance exceeds the criteria of 1 W/cm² at rated cell voltage of 0.67 V. The final SOA MEA design exhibits >1.275 W/cm² and Q/ΔT <1.45 and PGM content of 0.1 g/kW rated (10 kW/g PGM) at 250 kPaa and 94°C. The SOA MEA meets 1.0 W/cm² (rated 0.67 V) even at 80°C, 150 kPaa conditions, albeit at a less stringent heat rejection criteria of Q/ΔT = 1.94. The 5-cm² and 50-cm² MEAs were provided to the National Renewable Energy Laboratory (NREL) for confirmation testing and follow-up studies. As shown in Figure 1, the performance loss terms were quantified with differential cell diagnostics and use of an improved 1-D model. Such high performance, exceeding DOE targets, was achieved by systematic down-selections of catalysts (six), ionomers (nine), and membranes (three), followed by optimization using a design of experiment approach. The final SOA MEA design included a 12 μm perfluorosulfonic acid membrane with expanded polytetrafluoroethylene reinforcement, 30% PtCo/HSC-a on the cathode electrode with mid side chain ionomer (825 EW) at 0.9 I/C.

In addition to down-selection of the materials, one of the main objectives was to attain insights into the activity and transport properties of the catalyst layers. Measurements were conducted in 5-cm² differential cells with electrochemical diagnostics such as H₂-N₂ impedance for proton transport resistance [1], limiting current for oxygen transport resistance [2], CO measurements as a function of RH for Pt accessibility [3], and O₂ pol curve for activity measurements. Catalyst candidates were also characterized by transmission electron microscope measurements (University of Texas Austin) for particle size distribution and Brunauer-Emmett-Teller measurements for pore size distribution. The catalyst candidates are ~30 wt% PtCo (3:1 atomic ratio) supported on different carbon supports, both solid and porous carbon. Transmission electron microscope measurements indicate distinct advantage for porous high-surface-area carbon supports for a more uniform and smaller nanoparticle distribution. It is also reflected in the ECSA and mass activity measurements.

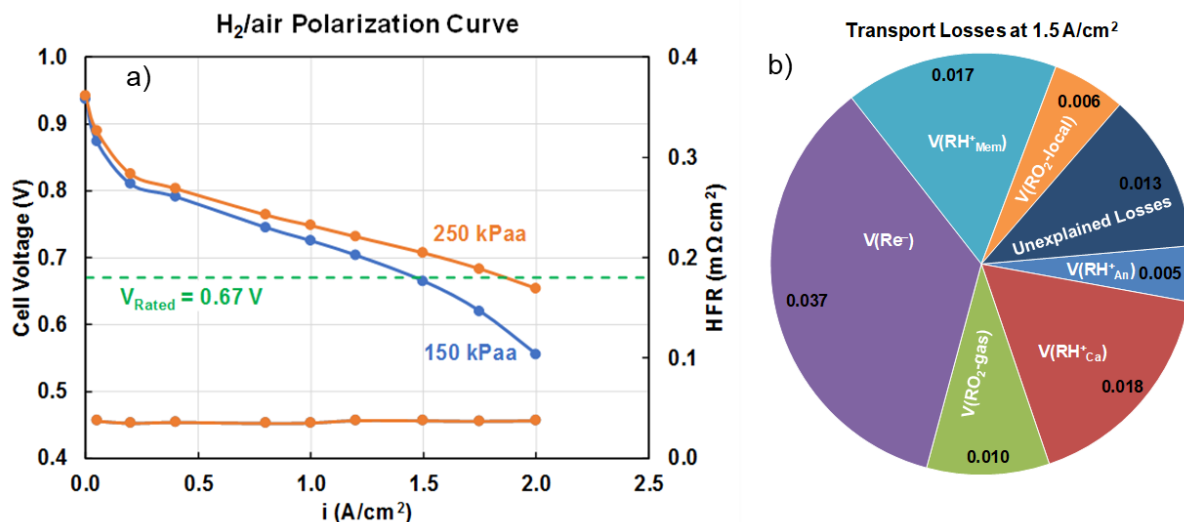


Figure 1. (a) Performance of SOA MEA as measured in 50-cm² cell. Conditions: 150 kPaa, 80 °C, 100% RH; and 250 kPaa, 65% RH, 94 °C. (b) Transport losses at 1.5 A/cm².

One important insight from this study is the impact of the carbon support on transport properties. Figure 2a shows the dependence of oxygen transport resistance and proton transport resistance on carbon surface area properties. Oxygen transport resistance is significantly reduced for catalysts with lower micropore surface area (<2 nm). Similarly, the proton transport resistance scales with macropore carbon surface area. In this study, macropore surface area is defined as pore size greater than 8 nm. So, an ideal carbon support should have a higher total surface area and mesopore surface area (4–7 nm) and lower micropore (<2 nm) and macropore (>8 nm) surface area.

For the ionomer study, several ionomer candidates at different EW and side chain length were considered. The ionomer solutions were characterized by advanced characterization methods such as ultra-small-angle X-ray scattering (USAXS) (at Argonne National Laboratory), grazing-incidence small-angle X-ray scattering (at Lawrence Berkeley National Laboratory), and other properties like molecular weight by size-exclusion chromatography, viscosity measurements, proton conductivity, and water uptake. All the measurements indicate that the impact of side chain length and chemistry considered in this study had minimal impact. The property variation was dominated by the equivalent weight of the ionomer. Scatterer size (nm) (from USAXS) indicative of ionomer aggregates was found to increase with EW. The lower scatterer size and smaller aggregates were found to reduce the particle size distribution of catalyst ink as measured by laser diffraction studies. For MEA tests, the ionomer content (I/C) was normalized to account for the difference in EW. The lower-EW ionomer had a significant improvement on performance at high current density as shown in Figure 2b. Despite I/C normalization in the catalyst layer, the lower-EW ionomers exhibited lower proton transport resistance and most of the performance improvement for lower-EW ionomers could be explained by the decreased transport resistance.

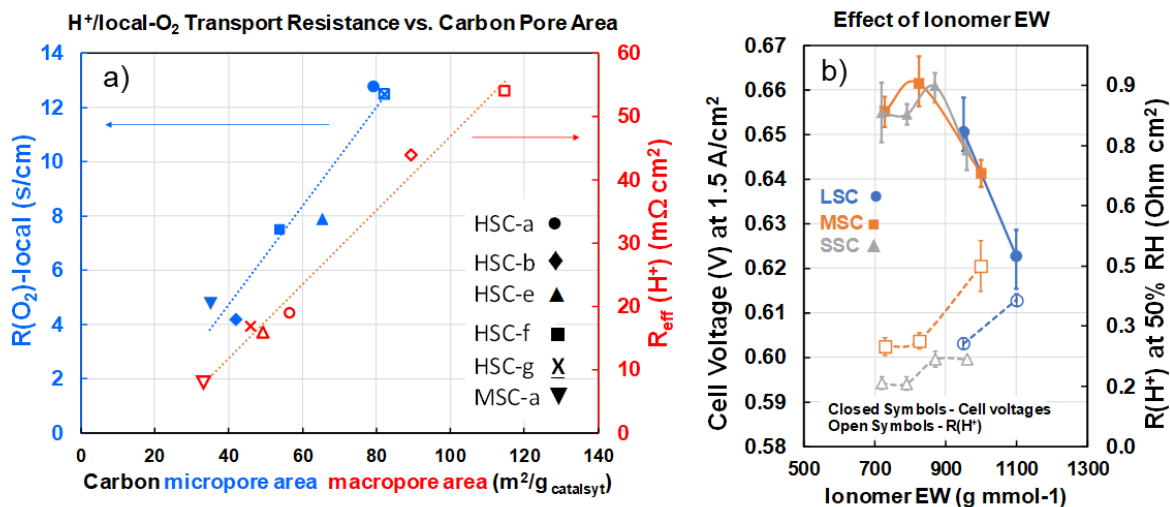


Figure 2. (a) Local oxygen transport resistance (closed symbols) and proton transport resistance (open symbols) dependence on carbon micropore and macropore surface area. (b) Proton transport resistance and cell voltage at 1.5 A/cm² as a function of ionomer EW.

A highly accelerated stress test (HAST) was developed to generate local stressful conditions that are both chemical and mechanical in nature. HAST involves a 50-cm² cell cycled between 0.05 A/cm² and 1.2 A/cm² with a low inlet RH in the co-flow configuration. This results in maximum chemical stress occurring near the gas inlets and the maximum mechanical stress near the outlets. The HAST was conducted using a current distribution tool providing a quantitative measure of mechanical stress (high frequency resistance [HFR]) and state of health (X-over measurement). Current, HFR, voltage, and water content (λ) profiles of the HAST are shown in Figure 3. The results indicate severe membrane thinning (chemical degradation in nature) at the outlet region where mechanical stress is high due to severe membrane hydration cycling. It was also found that the Ce concentration (measured by XRF) was depleted at the location of membrane failure (cathode outlet), possibly from the stronger water flux. To ascertain whether the chemical degradation of membrane was from Ce depletion due to stronger water flux, or increased mechanical stress due to humidity cycling, the test was repeated without the chemical mitigant—Ce. Preliminary tests of non-Ce-containing membranes exhibit chemical degradation at the same location indicating possible interaction between mechanical stress and chemical degradation.

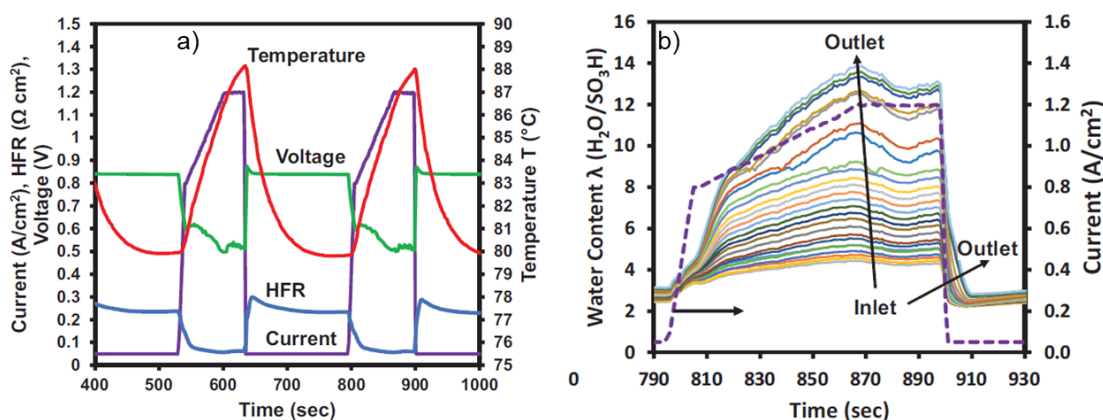


Figure 3. (a) HAST profiles of cell current, HFR, temperature, and voltage. (b) Close up of λ (solid) and current (dashed line) profiles from 790 to 930 sec.

The rapid movement of Ce^{3+} resulted in additional studies to quantify the Ce^{3+} migration mechanism as well as quantify migration rates due to diffusion and convection. Ce^{3+} diffusion measurements were conducted by applying a droplet of Ce^{3+} solution of known concentration and monitoring its movement with the FTIR method. The FTIR method uses the linear relationship between percentage Ce^{3+} complexation and absorbance at $1,726 \text{ cm}^{-1}$ [4]. Figure 4a shows the strong dependence of Ce^{3+} diffusion coefficient on RH (λ) and temperature. A 25-fold change in magnitude was observed between 100% and 50% RH followed by a further significant drop at lower RH. To quantify Ce^{3+} movement via convection, a two-chamber RH gradient cell as shown in Figure 4b was used. A thin strip of membranes with localized Ce was exposed to RH gradient in this cell and Ce^{3+} movement was monitored with the FTIR method. As shown in Figure 4c, the localized Ce^{3+} of Sample 1 near the RH gradient exhibited rapid movement from the high RH chamber to the low RH chamber. Sample 2 also exhibited movement to the low RH chamber after 36 h (not shown). The rapid movement due to RH gradient is indicative of the dominant role of convection in Ce^{3+} movement.

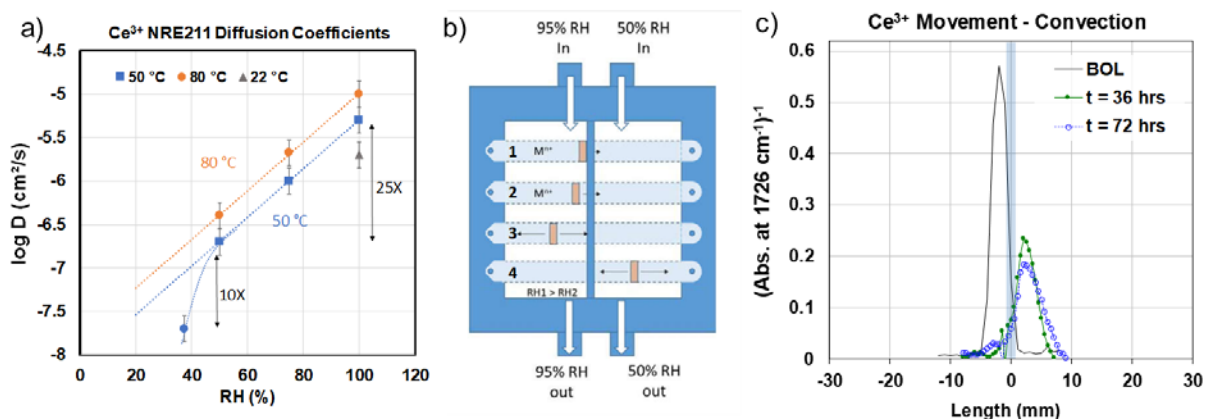


Figure 4. (a) Ce^{3+} diffusion coefficients as function of RH and temperature. (b) Two-chamber RH gradient cell. (c) Ce^{3+} profile as a function of time in the two-chamber RH gradient cell.

UPCOMING ACTIVITIES

For the remainder of 2018 and Budget Period 2, the project will focus on electrode and membrane durability studies. Key activities will be conducted in collaboration with FC-PAD partners and are as follows:

- H_2 - N_2 voltage cycling tests in various voltage waveforms and operating conditions at the National Renewable Energy Laboratory. Electrochemical diagnostics, including limiting current and others, to quantify voltage loss terms of the end-of-test MEA (GM/National Renewable Energy Laboratory).
- End-of-test MEA characterization for platinum dissolution, cobalt dissolution, particle size distribution quantification (GM/University of Texas Austin), and alloy structural changes (Oak Ridge National Laboratory).
- PtCo dissolution measurements at different potentials using an online inductively coupled plasma–mass spectrometer (Argonne National Laboratory).
- Confirm dominant Ce migration mechanism and quantify diffusion and convection coefficient to support Ce migration model and its incorporation in combined chemical and mechanical stress model.
- Open circuit voltage and H_2O_2 vapor cell tests to understand impact of membrane thickness on chemical degradation rates and mechanism.
- Conduct X-ray computed tomography on pre-shortened MEAs to visualize shorting and its propagation under HAST conditions (GM/Lawrence Berkeley National Laboratory).

FY 2018 PUBLICATIONS/PRESENTATIONS

1. N. Ramaswamy and S. Kumaraguru, “Materials and Design Selection to Improve High Current Density in PEMFC,” *ECS Transactions* 85, no. 13 (2018): 835–842.
2. F. Coms, S. Schlick, and M. Danilczuk, *The Chemistry of Membranes Used in Fuel Cells: Degradation and Stabilization* (Hoboken: Wiley, 2018): 75–106.
3. Y. Lai, K. Rahmoeller, J. Hurst, R. Kukreja, M. Atwan, A. Maslyn, and C. Gittleman, “Accelerated Stress Testing of Fuel Cell Membranes Subjected to Combined Mechanical/Chemical Stressors and Cerium Migration,” *J. Electrochem. Soc.* 165, no. 6 (2018): F3217–F3229.
4. F. Coms and A. McQuarters, “Determination of Ce^{3+} and Co^{2+} Diffusion Coefficients in NR211 membrane,” *ECS Transactions* 86, no. 13 (2018): 395–405.
5. C. Gittleman, Y. Lai and F. Coms, “Durability of Polymer Electrolyte Membranes for Automotive Application,” Invited presentation, AiMES 2018, Cancun, Mexico, October 2018.
6. N. Ramaswamy, V. Konduru and S. Kumaraguru, “Effect of Ionomer EW and Side Chain Length on Catalyst Layer Transport Resistances,” AiMES 2018, Cancun, Mexico, October 2018.

REFERENCES

1. R. Makharia, M. Mathias, and D. Baker, “Measurement of Catalyst Layer Electrolyte Resistance in PEFCs Using Electrochemical Impedance Spectroscopy,” *J. Electrochem. Soc.* 152, no. 5 (2005): A970–A977.
2. T. Greszler, D. Caulk, and P. Sinha, “The Impact of Platinum Loading on Oxygen Transport Resistance,” *J. Electrochem. Soc.* 159, no. 12 (2012): F831–F840
3. E. Padgett, N. Andrejevic, Z. Liu, A. Kongkanand, K. Moriyama, S. Kumaraguru, Y. Jiang, and D. Mueller, “Connecting Fuel Cell Catalyst Nanostructure and Accessibility Using Quantitative Cryo-STEM Tomography,” *J. Electrochem. Soc.* 165, no. 3 (2018): F173–F180.
4. F. Coms and A. McQuarters, “Determination of Ce^{3+} and Co^{2+} Diffusion Coefficients in NR211 membrane,” *ECS Transactions* 86, no. 13 (2018): 395–405.

High-Performance Polymer Electrolyte Membrane Fuel Cell Electrode Structures

Mike L. Perry
United Technologies Research Center
411 Silver Lane
East Hartford, CT 06118
Phone: (860) 610-7339
Email: perryml@utrc.utc.com

DOE Manager: David Peterson
Phone: (720) 356-1747
Email: David.Peterson@ee.doe.gov

Contract Number: DE-EE0007652

Subcontractors:

- Ion Power Inc., New Castle, DE
- University of Arkansas at Little Rock, Little Rock, AR

Project Start Date: October 1, 2016

Project End Date: June 30, 2020

- Fabricate sufficient thin-film catalyst to fabricate an MEA with a cell active area of $\geq 12.5 \text{ cm}^2$.

Technical Barriers

This project addresses the following technical barriers from the Fuel Cells section of the Fuel Cell Technologies Office Multi-Year Research, Development, and Demonstration Plan¹:

- (A) Durability (improved understanding of initial transport losses is required to mitigate)
- (B) Cost (MEAs with ultra-low PGM loadings have relatively large transport losses)
- (C) Performance (reduced transport losses are required to meet high power density targets).

Technical Targets

This project is ultimately focused on developing high-performance MEAs with ULCLs. To date, the team has focused on MEAs with Pt-only catalysts (i.e., not Pt-alloy catalysts that have higher activities), because these MEAs are less complex, are inherently more stable, and exhibit similar transport losses at ULCLs using Pt particles that are similar in size to those used with Pt-alloy catalysts. Analogously, the team is utilizing MEAs that do not utilize SOA catalyst loadings for the anodes (e.g., $\leq 0.025 \text{ mg-PGM/cm}^2$), because the key remaining barrier is improving cathode performance with ULCLs.

FY 2018 Accomplishments

- Developed and demonstrated MEAs with improved transport losses with CCLs that meet the 2020 target (i.e., MEAs with 0.1 mg-Pt/cm^2 on the cathode exhibited superior performance to the team's FY 2017 MEAs with 0.2 mg-Pt/cm^2 on the cathode at high current densities).
- Completed the development of a new hierarchical model of the CCL, which was

Overall Objectives

- Develop improved understanding of the various transport losses in polymer electrolyte fuel cell (PEFC) cathode catalyst layers (CCLs) with state-of-the-art (SOA) ultra-low catalyst loadings (ULCLs) of platinum-group metals (PGMs).
- Obtain this fundamental understanding by developing and validating a detailed microstructural CCL model.
- Utilize the validated CCL model to develop and demonstrate membrane electrode assemblies (MEAs) that potentially can meet all of DOE's 2020 technical targets for MEAs.

Fiscal Year (FY) 2018 Objectives

- Complete development of microstructural CCL model, and implement this key component model into the Fuel Cell Performance and Durability Consortium (FC-PAD) model of a complete PEFC.
- Validate this new CCL model using data from MEAs with ULCLs and SOA performance.

¹ <https://energy.gov/eere/fuelcells/downloads/fuel-cell-technologies-office-multi-year-research-development-and-22>

successfully validated using both the team's data and multiple data sets in literature on ULCL MEAs.

- Completed an extensive assessment of how various CCL models compare with experimental data. Results show that the United Technologies Research Center (UTRC) hierarchal model provides the best physical representation of an SOA CCL, and the most

quantitatively reasonable predictions for transport resistances.

- Fabricated a complete MEA with a novel thin-film catalyst that demonstrated reasonable performance for a first-of-a-kind MEA with ULCL (0.096 mg-PGM/cm² on cathode).

Table 1. Progress Toward Meeting MEA Technical Targets for Transportation

Characteristic	Units	DOE 2020 Targets	Project Status (Differential Operating Conditions)
PGM total loading	mg-PGM/cm ² _{geo}	≤0.125	≈ 0.2 total (≈ 0.1 per electrode)
MEA performance	mA/cm ² _{geo} @ 0.8 V	≥300	304 (Pt-only catalyst)
MEA performance	mW/cm ² _{geo} @ 0.675 V	≥1,000	805 (Pt-only catalyst)

INTRODUCTION

MEAs with ULCLs of highly active Pt-alloy catalysts already have been demonstrated to exceed DOE's 2020 high-efficiency target of $>0.3 \text{ A/cm}^2$ at 0.8 V [1]. Meeting the rated-power target of 1 W/cm^2 with these MEAs, however, has been far more challenging because mass-transport losses in conventional PEFC CCLs increase as the amount of catalyst is decreased [2]. Therefore, what primarily is needed to fully realize DOE's 2020 targets is mitigation of these transport losses, which is the focus of this project.

The initial focus of this project is to improve the fundamental understanding of transport losses in PEFC CCLs, because the sources of these losses historically have not been sufficiently understood, as evidenced by disagreement about the key mechanisms [3]. Subsequently, this improved fundamental understanding shall be used to design advanced MEAs that have significantly reduced mass-transport losses. This ultimately should enable the achievement of simultaneous requirements of high mass activity, low PGM loading, and high power density.

APPROACH

The project objective will be realized by first developing and validating a detailed microstructural CCL model. CCLs are complex structures and there are many constituents and mechanisms within this critical layer that may make significant contributions to the observed transport losses [4]. Further, the relative importance of processes could vary with operating conditions. To discern transport-loss mechanisms, it is necessary to first differentiate between the wide variety of possible microstructures and phases within the electrodes with sufficient geometric detail. A sufficiently detailed geometric model of the CCL can be used to uniquely determine what components and mechanisms are major contributors to transport losses in the CCL. This model and its performance-prediction capabilities then can be validated using a variety of CCL-characterization methods to measure the key geometric details included in the model, as well as by testing a variety of MEAs under various operating conditions.

The core project team has the capability to fabricate SOA MEAs using conventional carbon-support catalysts. Additionally, the University of Arkansas at Little Rock (UALR) has unique capabilities to fabricate thin-film catalyst architectures, which can be used to fabricate CCLs with alternative electrocatalyst structures. Therefore, the team can make and test both SOA MEAs and novel catalyst materials. These capabilities are being used to design innovative catalyst-layer morphologies to achieve high performance at both high and low power densities. Discerning the sources and magnitudes of the various losses requires testing a matrix of CCLs that provide sufficient variations in the underlying parameters to highlight the different losses. Each CCL variant must be subjected to a battery of diagnostic tests that help to quantify the different overpotentials. An iterative process is used to develop high-performance MEAs (depicted in Figure 1). In addition to the core team, the world-class material-characterization capabilities of FC-PAD are being used to help the team measure key geometric details of the CCLs.

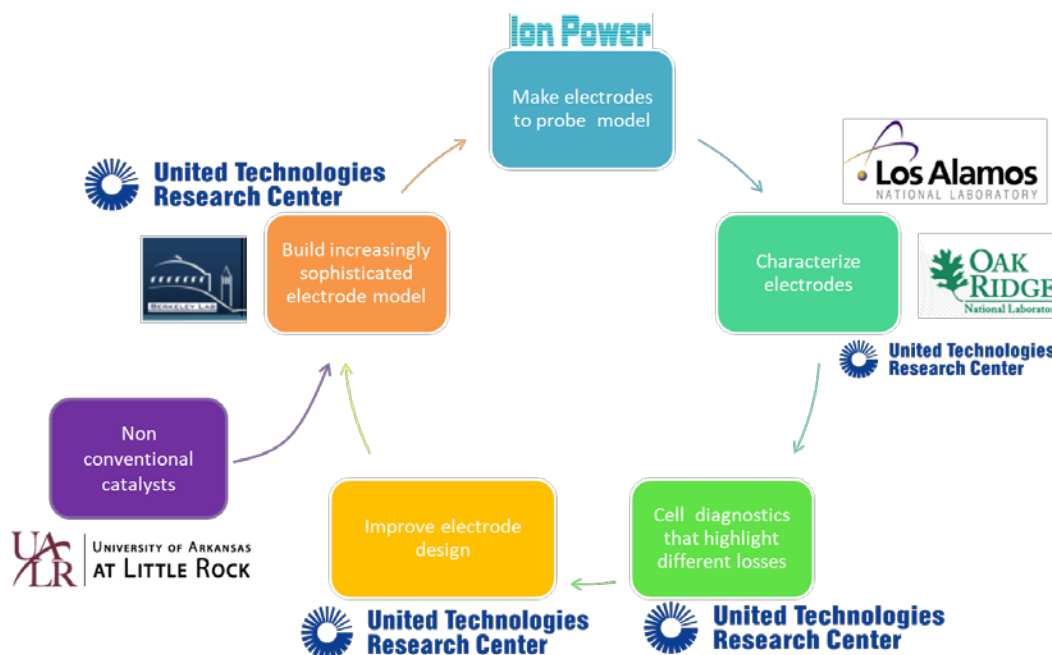


Figure 1. Simple graphical summary of the team’s approach to achieving the project’s objectives

RESULTS

UTRC has developed and validated a new type of hierarchal CCL model [5]. Conceptually, the model treats the catalyst layer as an assembly of representative spherical volume elements (i.e., agglomerates) that contain supported catalyst particles and are flooded with electrolyte as depicted schematically in Figure 2. Uniquely, this hierarchal model includes both spherical diffusion losses at the scale of platinum particles, as well as transport processes at the scale of the agglomerates—which is the only scale normally considered in many CCL transport models. This hierarchal approach was motivated by the realization that very large fluxes occur on catalyst particles near the outer surface of agglomerates at high overpotentials. The agglomerate in Figure 2 (not to scale) contains an interior core comprised of platinum (light grey) on carbon (dark grey) separated by ionomer (dark blue), and an exterior ionomer film (light blue). Relatively large pores between agglomerates—often called secondary pores—are available for gas transport.

The structure is largely determined by the morphology of the carbon black support. Carbon blacks in fuel cells typically contain significant amounts of micro-, meso-, and macroporosity. Electrolyte occupies the mesoporosity, and the macroporosity remains open for gas transport. It is interesting to note that, historically, fuel-cell modelers have found it very beneficial to utilize agglomerate models to effectively treat the complex processes that occur in gas-diffusion electrodes over two different length scales that vary by approximately 20X (i.e., the electrode thickness and the agglomerate diameter). A somewhat analogous treatment of the agglomerate and catalyst particles had not been done previously, however, even though the ratio of these two length scales is twice as large (i.e., approximately 42X using the dimensions shown in Figure 2). UTRC’s hierarchal-agglomerate model incorporates—for the first time—spherical diffusion losses at the scale of the platinum particles to the processes at the scale of the agglomerate that are normally considered in a conventional agglomerate model.

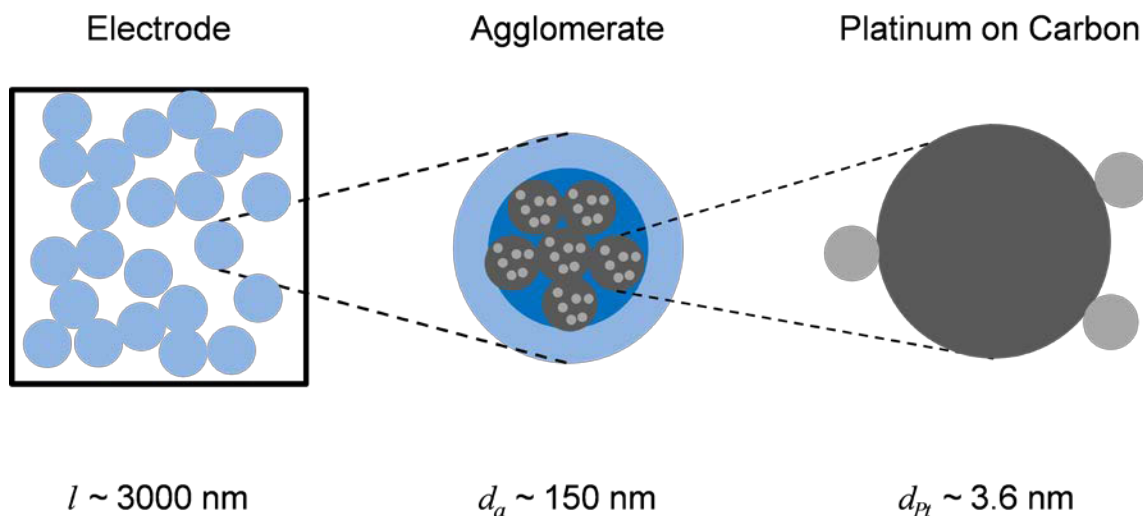


Figure 2. From left to right: schematic representations of agglomerates in a gas-diffusion electrode; an individual agglomerate consisting of a core containing platinum, carbon, and ionomer surrounded by an ionomer film; and platinum on a primary carbon particle

Predictions from this hierarchical model agree semi-quantitatively with published experimental investigations into the effect of platinum loading on cell performance. One example of this agreement is shown in Figure 3; more examples can be found in Darling et al. [5], which compares transport resistances as introduced by researchers at General Motors [6] predicted for agglomerate diameters ranging from 50 nm to 200 nm, to the experiments of Owejan et al. [7], Ono et al. [8], and Nonoyama et al. [2], as summarized by Weber and Kusgolo [9], along with the data fit of Greszler et al. [10] at 150 kPa. All resistances were calculated at 80°C and 90% relative humidity. Qualitatively, the model and experiment show similar trends of decreasing transport resistances with increasing platinum loading. Quantitative comparisons are only appropriate for the data of Owejan et al. and Greszler et al. because they used Pt on Vulcan, which is what has been modeled by UTRC to date. Nonoyama et al. did not disclose their carbon support, and Ono et al. used a high-surface-area support (TKK's TEC10E50E). The model simulations with agglomerate diameters in the range of 100 nm to 150 nm compare quite favorably with the data reported by Greszler et al. In general terms, the model appears to effectively explain why transport losses increase as platinum content decreases.

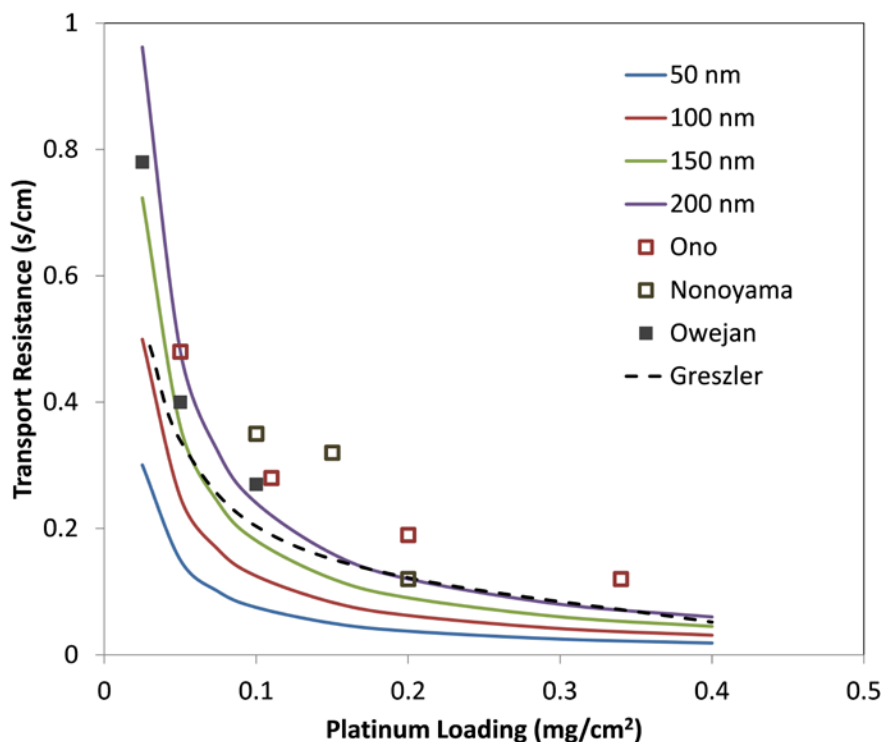


Figure 3. Measured and predicted transport resistances as functions of catalyst loading. Predictions are shown for agglomerate diameters ranging from 50 nm to 200 nm.

Using cell performance data, UTRC also has successfully validated this hierarchical model on both the ULCL MEAs fabricated and characterized by the project team, and multiple data sets reported in the literature on MEAs with ULCLs [5]. Although UTRC's model is only a CCL model, it can be used to predict complete polarization curves by doing the following.

1. Use methodology developed by General Motors to isolate the transport resistance of the gas-diffusion layer (GDL) via experiments with dilute O_2/N_2 . We used a transport resistance of 0.65 s/cm to describe the GDL when comparing to UTRC's polarization curves at the specified operating conditions.
2. Subtract the resistance of the membrane to convert the measured voltages to cathode voltages.
3. Use UTRC's CCL model to predict the current as a function of cathode voltage and oxygen content.

An example of the results from this analysis are shown in Figure 4. With minimal fitting parameters, the model successfully predicts performance of an Ion Power MEA tested at UTRC on oxygen, air, and "half air" (10.5% oxygen in nitrogen). The project's first year go/no-go milestone was for the model to predict the current density of polarization curves to within 50% at 0.8 V and 0.6 V. The measured current density at 0.8 V (IR-free, as modeled) was 35 mA/cm² and the model value was 40 mA/cm², which is 14% larger. The measured current density at 0.6 V (IR-free) was 1.145 A/cm² and the model value was 1.130 A/cm², which is 1.3% smaller. The agreement between the model and the data therefore exceeded the go/no-go milestone criteria.

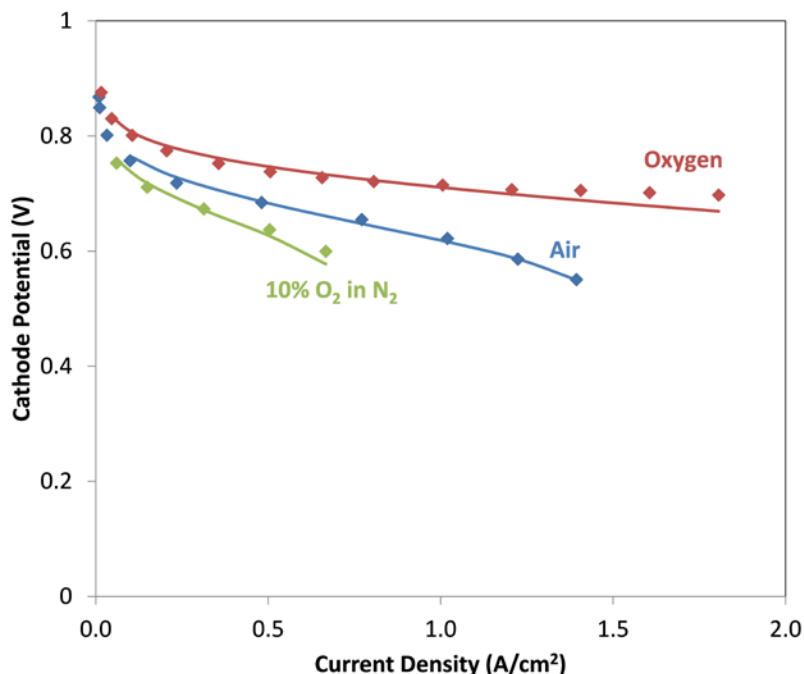


Figure 4. Comparison of model (solid lines) to polarization data measured by UTRC on an Ion Power MEA with a CCL catalyst loading of 0.046 mg/cm² Pt. The ORR activity on air was increased to 2.5 A/m² from 1.9 A/m² on oxygen to fit low current data; no other model parameters were fit.

Other commonly applied models do not qualitatively match all of the empirically observed trends. This is an important point and is worth emphasizing rigorously for this new model to gain broad acceptance within the fuel-cell community. Therefore, during the past quarter, UTRC completed an extensive comparison of various CCL-transport models; a very brief summary of the results is presented here (these different transport models are fully described in Weber et al. [5] and are beyond the scope of this report). Table 1 summarizes how the different expressions for the transport resistance (R_{Pt}), described in 11 different models of transport in the CCL, vary with three electrode descriptors L_{Pt} , M_{Pt} , and I/C , as well as the overpotential $U-V$. Where $R_{Pt} = \Gamma_{Pt} * R_{CL}$, is a convenient derived quantity that should not vary with platinum loading; R_{CL} is the transport resistance (s cm⁻¹); Γ_{Pt} is the platinum area divided by macroscopic area of electrode; L_{Pt} is the amount of platinum in electrode (mg/cm²), M_{Pt} is the mass fraction of platinum in a supported catalyst, and I/C is the ionomer to carbon ratio (by mass). The next-to-last column summarizes whether a particular model is in directional agreement with all relevant experimental observations summarized in Table 2, and the final column gives quantitative estimates for R_{Pt} . Unfortunately, experimental observations regarding how R_{Pt} varies with M_{Pt} , and I/C are sparse and, in the case of I/C , are inconsistent. Nevertheless, it is possible to conclude that many of the simplest and most common models for transport in a CCL cannot correctly describe the experimental data.

Table 2. Qualitative Comparisons of Different CCL Models to Experimental Results

Case	How does RPt respond to increases in:	LPt	MPt	I/C	U-V	Match	RPt
–	Experiment	↔	↑	↑	↔	–	12
1	Through electrode thickness	↑	↓	↑	↓	✗	2.3
2	To isolated catalyst nanoparticles	↔	↔	↔	↔	✗	2.2
3	Diffusion through thin ionomer film	↔	↓	↑	↔	✗	0.8
4	Adsorption onto platinum from ionomer	↔	↔	↔	↔	✗	12.0
5	Dissolution, primary carbon particles	↔	↑	↔	↔	✗	?
6	Dissolution, agglomerates	↔	↑	↓	↔	✗	?
7	Diffusion in film around agglomerates	↔	↑	↑	↔	✓	4.6
8	Diffusion inside agglomerates	↔	↑	↔	↓	✗	0.02
9	Agglomerate core + shell	↔	↑	↑	↔	✓	1.2
10	Agglomerate core + shell + nanoscale	↔	↑	↑	↔	✓	15.0

Only three of the ten models in Table 2 match the experimentally observed dependencies on L_{Pt} , M_{Pt} , I/C , and $U-V$. Of the three directionally correct models, the model incorporating nanoparticle limitations associated with either localized diffusion to or adsorption on the platinum particles (i.e., Case 10, UTRC’s hierarchal model) provides the best fit to the experimental data. One example of this is the R_{Pt} values shown in Table 2.

In conclusion, the sensitivities of different analytical models for transport resistances in the air electrode of PEFCs were qualitatively and semi-quantitatively compared to empirical data. Seven of the ten models examined do not qualitatively reproduce the experimentally observed responses to changes in mass fraction of platinum and ratio of ionomer to carbon. Of the three qualitatively correct models, the model incorporating both nanoscale transport effects to the agglomerate plus external diffusion gives the best physical representation of a CCL, and provides quantitatively reasonable predictions for transport resistances.

The team also demonstrated the capability to fabricate MEAs using unique thin-film electrocatalysts produced by UALR. UALR has developed the capability to make density-modulated platinum-thin-film (Pt-TF) catalysts using high-pressure sputtering deposition. Change of working gas pressure of the sputtering system results in various Pt-TF catalysts with different densities and porosities. UALR also has developed the capability to deposit Pt-TF catalysts directly onto either GDLs or membranes. UTRC tested an MEA that was fabricated by using a GDL with an MPL (SGL-25BC), which UALR had coated with Pt-TF catalyst, and integrating this gas-diffusion electrode with “half MEA” that had a conventional catalyst layer on only one side of the membrane. The results successfully demonstrated that the team can fabricate and test functional MEAs with thin-film catalysts, which will be a focus of both experimental and modeling work going forward.

CONCLUSIONS AND UPCOMING ACTIVITIES

The first objective of this project has successfully been completed; specifically, a detailed microstructural model has been successfully developed and validated. UTRC’s hierarchal model matches the experimentally observed responses of conventional MEAs with ULCLs in a manner that is clearly superior to other CCL-transport models. The team now is using this hierarchal CCL model to guide the development of advanced MEAs which utilize conventional carbon-supported catalysts. The team also has developed the capability to fabricate and test MEAs with thin-film electrocatalysts. UTRC also plans to develop a microstructural model for these types of CCL architectures—which are very different than MEAs with conventional carbon-supported catalysts. This work should lead to the development of improved PEFCs, which ultimately can meet both the cost and performance targets established by DOE for transportation applications.

FY 2018 PUBLICATIONS/PRESENTATIONS

1. R.M. Darling, “A Hierarchical Model for Oxygen Transport in Agglomerates in the Cathode Catalyst Layer of a Polymer-Electrolyte Fuel Cell,” *J. Electrochem. Soc.* 165 (2018): F571.

2. R.M. Darling, “A Hierarchical Model for Oxygen Transport Within Agglomerates in the Cathode Catalyst Layer of a Polymer Electrolyte Fuel Cell,” Presented at FC PAD Meeting at NREL, April 2018.
3. R.M. Darling, “High Performance PEFC Electrode Structures,” Presented at Fuel Cell Tech Team Meeting, Detroit, Michigan, September 2018.
4. M.L. Perry, “High Performance PEFC Electrode Structures,” Presented at FCTO AMR Meeting, Project ID FC157, June 2018.

REFERENCES

1. D. Myers et al., FCTO AMR Meeting presentation, Project ID# FC106 (2015).
2. N. Nonoyama et al., *J. Electrochem. Soc.* 158 (2011): B416.
3. M. Eikerling et al., *Sustain. Energy & Fuels* 6 (2018): 1189.
4. A. Weber et al., *J. Electrochem. Soc.* 161 (2014): F1254.
5. R. M. Darling, *J. Electrochem. Soc.* 165 (2018): F571.
6. Baker et al., *J. Electrochem. Soc.* 156 (2009): B991.
7. Owejan et al., *J. Electrochem. Soc.* 160 (2013): F824.
8. Ono et al., *ECS. Transactions*, 28 (2010): 69.
9. Weber and Kusgolo, *J. Mater. Chem. A* 2 (2014): 17207.
10. Greszler et al., *J. Electrochem. Soc.* 159 (2012): F831.

Fuel Cell Membrane Electrode Assemblies with Ultra-Low-Platinum Nanofiber Electrodes

Peter N. Pintauro
Vanderbilt University
PMB 351604
3201 Vanderbilt Place
Nashville, TN 37235
Phone: (615) 343-3878
Email: pn.pintauro@vanderbilt.edu

DOE Manager: Donna Ho
Phone: (202) 586-8000
Email: Donna.Ho@ee.doe.gov

DOE Technical Advisor: John Kopasz
Phone: (630) 252-7531
Email: kopasz@anl.gov

Contract Number: DE-EE0007653

Subcontractors:

- Nissan Technical Center North America, Farmington Hills, MI
- Georgia Institute of Technology, Atlanta, GA
- 3M Company, St. Paul, MN

Project Start Date: January 1, 2017
Project End Date: December 31, 2020

Overall Objectives

- Fabricate, characterize, and evaluate membrane electrode assemblies (MEAs) with nanofiber mat cathodes containing highly active oxygen reduction reaction (ORR) catalysts for H₂/air fuel cells.
- Generate useful correlations and insightful understandings regarding nanofiber electrode electrospinning.
- Develop collaborations with Fuel Cell Performance and Durability Consortium (FC-PAD) researchers at national laboratories.

Fiscal Year (FY) 2018 Objectives

- Synthesize and evaluate shape-controlled platinum-alloy catalyst (at Georgia Tech).

- Evaluate/characterize nanofiber anode and cathode MEAs with new binders, TKK (Tanaka Kikinokogyo) PtCo/C and PtNi/C cathode catalysts, and Pt/C anode catalyst (Vanderbilt and Nissan Technical Center North America).
- Begin to electrospin nanofiber electrodes on commercial equipment at eSpin Technologies, Inc.

Technical Barriers

This project addresses the following technical barriers from the Fuel Cells section of the Fuel Cell Technologies Office Multi-Year Research, Development, and Demonstration Plan¹:

- (A) Durability (aging and degradation of fuel cell electrodes).
- (B) Cost (reducing the material and manufacturing costs of high-performance electrodes and MEAs).
- (C) Performance (fabricating MEAs that generate higher power at lower precious-metal loading, with special emphasis on the cathode).

Technical Targets

The 2020 DOE technical targets and project status are shown in Table 1.

FY 2018 Accomplishments

- MEAs were fabricated with electrospun particle/polymer nanofiber mat cathodes (0.1 mg_{Pt}/cm² PtCo/C or PtNi/C) and anodes (0.1 mg_{Pt}/cm² Pt/C), where the binder was a mixture of Nafion and poly(acrylic acid) or neat Nafion (for the latter, a new carrier polymer was utilized that could be easily removed from the fibers after electrospinning).
- MEA performance was verified at Nissan and at an FC-PAD lab (Los Alamos National Laboratory).

¹ <https://energy.gov/eere/fuelcells/downloads/fuel-cell-technologies-office-multi-year-research-development-and-22>

- A 5 cm² MEA with a PtCo/C nanofiber cathode performed very well and produced 906 mW/cm² at rated power (95°C, 200 kPa_{abs}, and 0.20 mg/cm² total Pt loading) and 809 mW/cm² at rated power (95°C, 200 kPa_{abs}, and 0.115 mg/cm² total Pt loading).
- There was a modest power loss after a metal dissolution, load-cycling accelerated stress test (AST) (30,000 voltage cycles); power loss was within the DOE target of 20%–30% loss in max power, and only a 12% loss in power when a recovery protocol was used. This power loss is significantly less than that in a conventional slurry electrode MEA.
- Energy dispersive X-ray spectroscopy experiments found that there was greater retention of Co in a PtCo/C nanofiber cathode after a metal dissolution load-cycling AST, as compared to the retention in a conventional sprayed cathode (61% versus 49% Co retention). High Co retention is an indicator of improved durability.
- A nanofiber MEA with a PtCo/C cathode and Pt/C anode (each at 0.1 mg/cm² Pt loading) produced high power at high- and low-relative humidity (RH) conditions: 1.1 W/cm² at 100% RH and 0.967 W/cm² at 40% RH (all data collected at 80°C and 200 kPa_{abs} pressure).
- Preliminary fiber characterization work was carried out at Oak Ridge National Laboratory, Los Alamos National Laboratory, and the Nissan Technical Center North America. Results from scanning transmission electron microscopy experiments show that fibers are ~30% porous with a uniform distribution of catalyst and binder (minimal agglomerates of catalyst or binder); the O₂ mass-transfer resistance is low in a nanofiber cathode (35 versus 52 s/m for a sprayed cathode); the ionomer resistance of a nanofiber cathode was substantially less than that of a sprayed particle/Nafion electrode.
- Shape-controlled Pt_{2.6}Co catalyst was prepared at Georgia Tech and showed good mass activity in a slurry cathode MEA after four recovery cycles (0.384 A/mg_{Pt}) with high fuel cell power densities (e.g., a maximum power of 0.73 W/cm² after recovery).
- The following Year 2 go/no-go milestones were met: (1) nanofiber MEA with >280 mA/cm² at 0.8V (see Figure 3); (2) rated power >900 mW/cm²; and (3) <40% drop in ORR mass activity after load cycling (see Table 4). Milestones associated with start up–shut down and drive cycle durability were not met (<10% drop in voltage at 1.2 A/cm² after start up–shut down and <20% loss in rated power after drive cycle durability) because these tests were not performed; they were not deemed to be of critical importance given the other technical accomplishments in 2018.

Table 1. Progress Toward Meeting Technical Targets for Electrocatalysts and MEAs for Transportation Applications

Characteristic	Units	DOE 2020 Electrocatalyst and MEA Targets	Project Status
Mass activity	A/mg _{PGM} @ 0.90 V _{IR-free}	0.44	0.464 ^a
PGM total loading (both electrodes)	mg-PGM/cm ² _{geo}	0.125	0.20
Loss in performance @ 0.80 A/cm ² after a load-cycling AST (30,000 voltage cycles)	mV	<30	68 ^b
Loss in performance @ 1.5 A/cm ² after a load-cycling AST (30,000 voltage cycles)	mV	<30	32 ^b
MEA performance @ 0.80 V	mA/cm ² _{geo}	300	402 ^b
MEA performance @ rated power (150 kPa _{abs})	mW/cm ² _{geo}	1,000	945 ^c

^a Measured at Los Alamos National Laboratory.

^b 5 cm² MEA, TKK PtCo/C cathode catalyst, Pt/C anode catalyst, Nafion + poly(acrylic acid) binder, Nafion 211 membrane, T = 80 °C, 200 kPa_{abs}, 100% RH.

^c 10 cm² MEA, TKK PtCo/C cathode catalyst, TKK Pt/C anode catalyst, Nafion binder, Nafion 211 membrane, T=95 °C, 200 kPa_{abs}, 100% RH.

INTRODUCTION

Despite widespread literature demonstration of excellent oxygen reduction reaction activity of some new catalysts in rotating disk electrode experiments, almost none of them have shown promising performance in fuel cell MEAs. This is because MEA fabrication remains centered on decal, catalyst-coated membrane, and catalyst-coated gas diffusion electrode methodologies, with little or no control over the macro-scale organization of catalyst particles and polymer binder. Features such as electrode macroporosity, microporosity, and particle and binder interconnectivity become more critical when high-performance nanomaterials are used in electrodes. Consequently, new electrode fabrication techniques are needed for next-generation MEAs, which accommodate and control the multi-scale arrangement of catalyst and binder for improved power output and durability.

Building from strong initial data showing electrospinning as a viable approach to the design and fabrication of fuel cell electrodes [1–3], this project seeks to fabricate MEAs with electrospun nanofiber electrodes containing Pt and Pt-alloy catalyst powders and selected perfluorosulfonic acid ionomer binders with the capability of meeting the DOE 2020 performance and durability targets for MEAs and catalyst layers.

APPROACH

The research approach for this project directly addresses three critical issues: (1) the use of high-activity PtNi/C and PtCo/C catalysts in hydrogen/air fuel cell MEA cathodes; (2) the organization of Pt-alloy catalytic nanoparticles into intelligently designed nanofiber mat electrodes via particle/polymer electrospinning, in which the fiber volume fraction, nanoparticle loading, binder type, fiber diameter, and mat thickness are independently controlled; and (3) the identification of the optimum composition and structure of nanofiber electrode MEAs which meet the DOE 2020 performance, Pt-loading, and durability targets.

The project has five major tasks: (1) prepare and evaluate MEAs with commercial Pt-alloy cathodes at ultra-low Pt loading with various perfluorinated ionomer-based binders; (2) synthesize Pt-alloy octahedra catalysts with high oxygen reduction activity; (3) incorporate the octahedra Pt-alloy catalysts into nanofiber and sprayed electrode MEAs; (4) optimize the nanofiber cathode mat composition and mat morphology to maximize fuel cell performance and durability at high and low relative humidity conditions; and (5) provide catalyst powder, electrospun cathode mats, MEAs, experimental skills, and the team's electrospinning knowledgebase to our FC-PAD collaborators.

RESULTS

H₂/air fuel cell polarization curves for nanofiber electrode MEAs at 80°C with different cathode catalysts are shown in Figure 1. The Pt cathode and anode loadings were each 0.1 mg/cm², and the electrode binder was a mixture of Nafion and poly(acrylic acid) (PAA). The PtCo (I/C = 1.08) and PtNi (I/C = 1.08) catalysts were from TKK (TEC36E52 and TECNiE52) and the Pt/C catalyst (I/C = 0.90) was from Johnson-Matthey (HiSPEC 4000). As expected, the Pt-alloy cathodes worked best with a maximum power density >1.0 W/cm². The performance of the three different MEAs is summarized in Table 2; a higher power output for the alloy catalysts is associated with a higher mass activity.

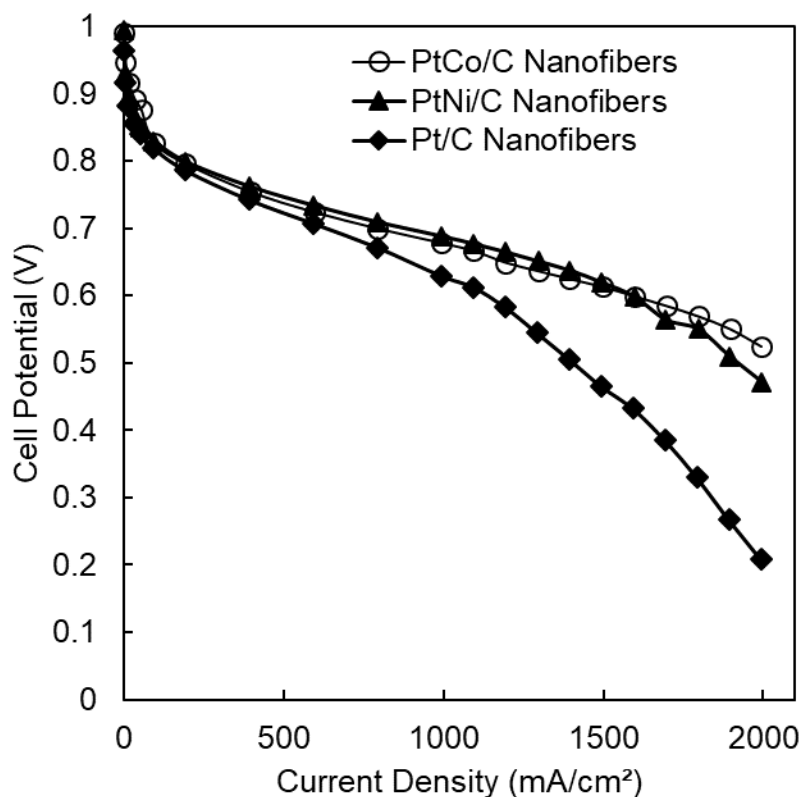


Figure 1. H₂/air fuel cell polarization curves for nanofiber MEAs with different cathode catalysts and with a catalyst binder of Nafion + PAA. All cathodes are 0.1 mg_{Pt}/cm² (TKK PtCo/C and PtNi/C and J-M Pt/C, as listed in Table 2); 80 °C; 200 kPa_{abs}; 90% RH; Nafion 211 membrane; and 4/8 L/min H₂/air flow rates.

Table 2. Cathode Electrochemical Surface Area (ECSA) and Mass Activity and Fuel Cell Power Results for Nanofiber Electrode MEAs with Different Cathode Catalysts (0.1 mg_{Pt}/cm²) and an Anode of Pt/C (J-M HISPEC 4000 at 0.1 mg_{Pt}/cm²). Fuel Cell Operating Conditions Are Listed in the Caption for Figure 1.

Cathode Catalyst	ECSA (m ² /g _{Pt})	Mass Activity (mA/mg _{Pt})	Power Density at 0.65 V (mW/cm ²)	Max Power Density (mW/cm ²)
Pt/C (J-M HISPEC 4000)	45	160	579	704
PtNi/C (TKK TECNiE52)	46	266	840	988
PtCo/C (TKK TEC36E52)	48	270	803	1,034

Nanofiber electrode MEAs with a TKK PtCo/C cathode, a TKK Pt/C anode, and a Nafion binder performed exceptionally well at both high- and low-relative-humidity fuel cell conditions, as shown in Figure 2. Power output was high over a wide range of feed gas relative humidities, where the fuel cell temperature was 80°C, the pressure was 200 kPa_{abs}, and the total MEA Pt loading was either 0.20 mg/cm² or 0.115 mg/cm².

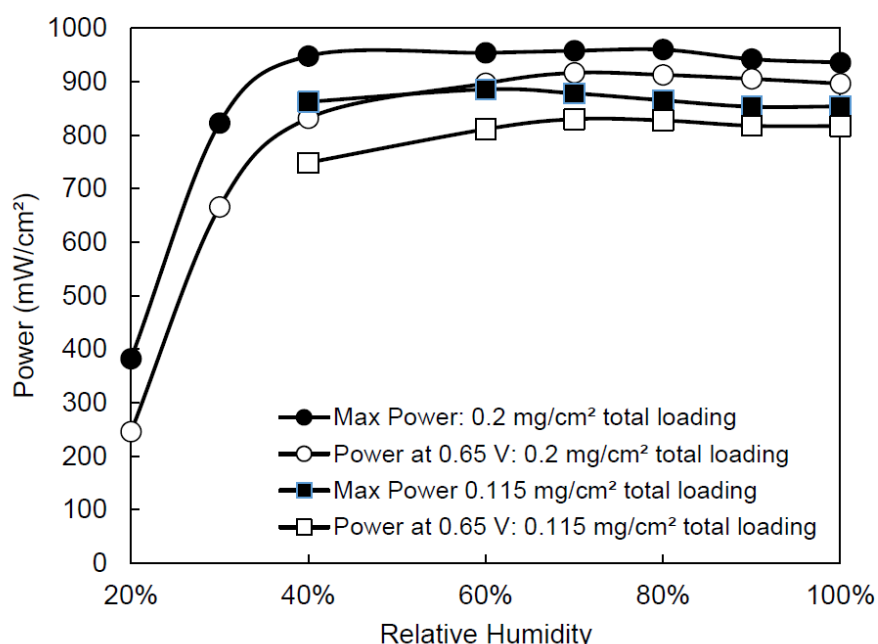


Figure 2. H₂/air fuel cell power output for nanofiber MEAs operating at different feed gas relative humidities, with a PtCo/C cathode (TKK TEC36E52) and a Pt/C anode (TKK TEC10F50E). MEA with 0.2 mg_{Pt}/cm² loading: 0.098 mg_{Pt}/cm² cathode and 0.102 mg_{Pt}/cm² anode. MEA with 0.115 mg_{Pt}/cm² loading: 0.096 mg_{Pt}/cm² cathode and 0.019 mg_{Pt}/cm² anode. 80 °C; 200 kPa_{abs}; Nafion 211 membrane; 125/500 standard cubic centimeters per minute H₂/air flow rates.

Rated power was found from fuel cell polarization data, at a voltage given by Equation 1, where the stack power was selected to be 90 kW, $Q/\Delta T$ was fixed at 1.45 kW/°C, the fuel cell operating temperature was set at 95°C, the pressure was 200 kPa_{abs}, and the ambient temperature was 40°C. At rated power (0.663 V, according to Equation 1), the power density of a nanofiber MEA with a Nafion binder and a total Pt loading of 0.117 mg/cm² (TKK TEC36E52 PtCo/C cathode at 0.095 mg_{Pt}/cm² and TKK TEC10F50E Pt/C anode at 0.022 mg_{Pt}/cm²) was 945 mW/cm², which exceeds the project's 2018 go/no-go target.

$$Q/\Delta T = \frac{\left[\text{Stack Power (kW)} \times \frac{(1.25 - V @ \text{rated power})}{V @ \text{rated power}} \right]}{\text{Cell Operating Temperature (°C)} - \text{Ambient Temperature (°C)}} \quad (1)$$

Voltage cycling metal dissolution ASTs were performed with nanofiber electrode MEAs, where the nanofiber cathode/anode was a mixture of Nafion + PAA or neat Nafion. H₂/air fuel cell polarization curves before and after 30,000 voltage cycles between 0.6 V to 0.95 V are shown in Figure 3. The fuel cell operating pressure during collection of polarization data was 200 kPa_{abs}, the feed gas flow rates were 500 cm³/min for H₂ and 2,000 cm³/min for air, the temperature was 80°C, and the RH was fixed at 100%. Both the anode and cathode Pt loadings were 0.1 mg/cm². Beginning-of-life (BoL) and end-of-life (EoL) fuel cell performance data are summarized in Table 3.

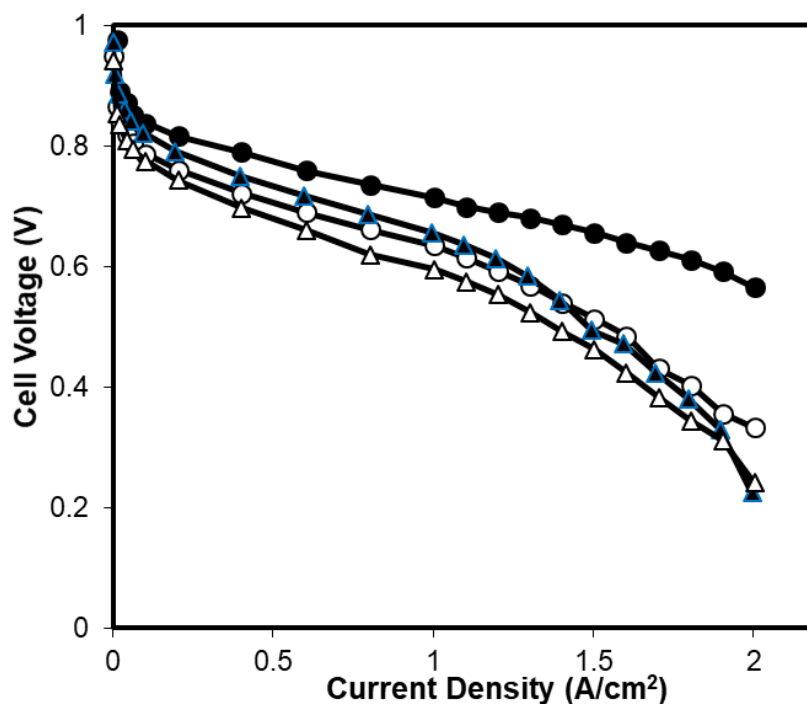


Figure 3. Fuel cell polarization results before and after a metal dissolution AST (end-of-life after 30,000 voltage cycles, 0.6 V to 0.95 V) for nanofiber electrode MEAs with a PtCo/C cathode (0.1 mg_{Pt}/cm² TKK TEC36E52) and a Pt/C anode (0.1 mg_{Pt}/cm² Johnson-Matthey HISPEC 4000). Nafion + PAA binder: ▲ (BoL) and △ (EoL); Nafion binder: ● (BoL) and ○ (EoL). 80 °C; 200 kP_{abs}; 100% RH; Nafion 211 membrane; 0.5/2.0 L/min H₂/air flow rates.

Table 3. Nanofiber Fuel Cell Performance Before and After a Metal Dissolution Voltage Cycling AST for Two Different Binders. Summary of Result from Figure 3.

Nanofiber Binder	Beginning of Life (BoL)		End of Life (EoL)	
	Max Power (mW/cm ²)	Power at 0.65 V (mW/cm ²)	Max Power (mW/cm ²)	Power at 0.65 V (mW/cm ²)
Nafion + PAA	759	661	695	419
Nafion	1,132	998	777	575

The durability of the nanofiber MEAs was excellent, with EoL maximum power losses of 8.4% (for a Nafion + PAA binder) and 31% (for Nafion binder). When a recovery step (a low-temperature hydrogen pump) was added to the AST, the deleterious effects of metal dissolution were mitigated, as shown in Table 4. Thus, after 15,000 voltage cycles and a single recovery step, the MEA was restored to its original condition in terms of cathode mass activity and power output. After 30,000 voltage cycles with a recovery, the drop in power density as compared to that at BoL was small (only 12%). Overall, it can be concluded that recovery has little effect on cathode ECSA but it does partially/totally restore the cathode mass activity for ORR and the MEA power density.

Table 4. The Use of a Recovery Step to Improve the Power Output of a Nanofiber Electrode MEA After a Metal Dissolution Voltage Cycling Accelerated Stress Test

	ECSA (m ² /g _{Pt})	Mass Activity (A/mg _{Pt})	Max Power Density (W/cm ²)
BoL	40	0.464	0.900
After 15,000 cycles	27	0.236	0.740
15,000 cycles + recovery	31	0.496	0.905
After 30,000 cycles	26	0.202	0.734
30,000 cycles + recovery	22	0.296	0.793

CONCLUSIONS AND UPCOMING ACTIVITIES

Nanofiber electrode MEAs produce high power at low platinum loadings, over a wide range of feed gas relative humidities and after a metal dissolution voltage cycling accelerated stress test. Power densities at or above 1.0 W/cm² were measured for an MEA with a total Pt loading of 0.2 mg/cm². Rated power at 95°C, 200 kPa_{abs} pressure, and a total MEA Pt loading of 0.115 mg/cm² was >900 mW/cm². High power with improved durability after a metal dissolution AST is associated with a more uniform distribution of binder and catalyst particles throughout the fiber mat electrode (no agglomerates), which results in higher catalytic activity for the ORR, low gas-transport resistance for O₂, and low ionic resistance in the catalyst layer. Additionally, fibers with neat Nafion binder appear to hold water at low feed-gas humidity conditions, resulting in high power at 40% RH.

Future work will focus on the following.

- Working with FC-PAD collaborators at national labs to probe the structure of electrospun particle/polymer nanofiber electrodes with Nafion/PAA and neat Nafion binder to better understand why fiber electrodes work well in a fuel cell.
- Optimizing the nanofiber anode and cathode composition and MEA hot pressing conditions for optimal power and durability at a total Pt loading of 0.125 mg/cm².
- Preparing and evaluating nanofiber cathodes and anodes that are electrospun on commercial equipment at eSpin Technologies, Inc.

FY 2018 PUBLICATIONS/PRESENTATIONS

1. P.N. Pintauro, “Recent Progress on Improving the Performance of Nanofiber Electrodes in a Hydrogen/Air Fuel Cell” (invited talk), 8th International Fuel Cell Workshop, Yamanashi University, August 2018.
2. John Slack, Krysta Waldrop, Ryszard Wycisk, Cenk Gumeci, Nilesh Dale, and Peter N. Pintauro, “Electrospun Fiber Mat Electrode MEAs for Hydrogen/Air Fuel Cells,” Electrochemical Society Fall Meeting, Cancun, Mexico, October 2018.
3. Krysta Waldrop, John Slack, Peter N. Pintauro, and Ryszard Wycisk, “Electrospun Particle/Polymer Fiber Mats as Hydrogen/Air Fuel Cell Electrodes,” American Institute of Chemical Engineers Annual Meeting, Pittsburgh, PA, November 2018.

REFERENCES

1. W. Zhang, and P.N. Pintauro, “High Performance Nanofiber Fuel Cell Electrodes,” *Chem. Sus. Chem.* 4 (2011): 1753–1757.
2. M. Brodt, R. Wycisk, and P.N. Pintauro, “Nanofiber Electrodes with Low Platinum Loading for High Power Hydrogen/Air PEM Fuel Cells,” *J. Electrochem. Soc.* 160 (2013): F744–F749.
3. M. Brodt, T. Han, N. Dale, E. Niangar, R. Wycisk, and P. Pintauro, “Fabrication, In-Situ Performance, and Durability of Nanofiber Fuel Cell Electrodes,” *J. Electrochem. Soc.* 162 (2015): F84–F91.

Facilitated Direct Liquid Fuel Cells with High-Temperature Membrane Electrode Assemblies

Emory S. De Castro (Primary Contact),
Ryan Pavlicek, and Manav Sharma
Advent Technologies, Inc.
One Mifflin Place, Suite 400
Cambridge, MA 02138
Phone: (857) 264-7035
Email: EmoryDeCastro@Advent-Energy.com

DOE Manager: Gregory Kleen
Phone: (240) 562-1672
Email: Gregory.Kleen@ee.doe.gov

Contract Number: DE-EE0006959

Subcontractor:
Los Alamos National Laboratory, Los Alamos, NM

Project Start Date: October 1, 2015
Project End Date: June 30, 2019

Overall Objectives

- Demonstrate the potential of direct liquid fuel cells by exploiting features of high-temperature membrane electrode assemblies (MEAs).
- Show feasibility that direct dimethyl ether (DME) oxidation at a high-temperature MEA performs significantly better than direct methanol fuel cells (DMFC) operating at less than 100°C when compared across metrics such as anode specific current, platinum group metal (PGM) loading, power output, durability, and crossover losses.
- Leverage a highly active ternary catalyst for high-temperature direct dimethyl ether fuel cells.

Fiscal Year (FY) 2018 Objectives

- Establish enhanced kinetics for DME oxidation at the higher temperatures.
- Demonstrate DME oxidation anode specific current (A/g_{PGM}) equivalent to or better than that obtained for the state-of-the-art DMFC.

Technical Barriers

This project addresses the following technical barriers from the Fuel Cells section of the Fuel Cell Technologies Office Multi-Year Research, Development, and Demonstration Plan [1], using DMFC systems as a reference fuel cell system:

- Cost (catalyst, system)
- Performance (catalyst, electrodes, MEAs)
- Durability (catalyst, membrane).

Technical Targets

This program falls under DOE's incubator initiative, which explores high-impact research in new areas. Thus, the technical targets for this program were created relative to the state-of-the-art DMFC system, the only other viable direct fuel oxidation system at this time. Progress toward meeting the technical targets for direct DME oxidation is shown in Table 1.

FY 2018 Accomplishments

- Identified zero-order anode reaction kinetics impeding reaction rate.
- Overcame kinetic limitations for anode mass-specific activity for direct DME oxidation with commercial catalysts through higher-temperature operation ($>200^{\circ}\text{C}$).
- Demonstrated highest anode mass-specific activity for a direct fuel cell ($94 A/g_{\text{PGM}}$ at 0.5 V) operating with a total PGM loading less than $5 \text{ mg}_{\text{PGM}}/\text{cm}^2$.

Table 1. Progress Toward Meeting Technical Targets for Direct DME Oxidation

Key Performance Indicator (this period)	Units	Current DMFC	Target	Program Status (5-cm ² cell)
Total PGM loading	mg _{PGM} /cm ²	5	3	4.5
Anode mass-specific activity	A/g _{PGM} at 0.5 V	50	75	94
Crossover current	mA/cm ²	60–120 ^a	<60	6
Maximum power	mW/cm ²	160	270	135 ^b

^a 60 mA/cm² with 0.5 M methanol, 80 °C, Nafion 117; 120 mA/cm² with 1.0 M methanol

^b Using 4.6 mg_{PGM}/cm²

INTRODUCTION

In searching for an exemplary carbon-neutral fuel, DME may be one of the most appealing candidates. This simplest of the ethers can be readily produced from renewably sourced hydrogen and CO₂, making it an effective hydrogen carrier. Being both nontoxic and easy to liquefy under moderate pressure, DME closely matches diesel and has been run in trucks. Los Alamos National Laboratory (LANL) has demonstrated the potential for direct oxidation of DME in a fuel cell [2]. Thus, DME could bridge both internal combustion and fuel cell technologies, while remaining carbon neutral with low or no ancillary emissions.

LANL has identified a highly active catalyst for direct oxidation of DME that already, in the early phase of development, allows for matching performance of the DMFC when using typical low-temperature perfluorosulfonic acid membranes. However, the output is not sufficient to approach commercial acceptance targets for higher-power applications with considerable precious metal cost. More importantly, the LANL work has noted an acute sensitivity of the DME oxidation rate to temperature increase. High-temperature MEAs, based on phosphoric acid-imbibed membranes, operate at 160°C to 180°C without additional water and are highly tolerant to carbon monoxide—an intermediate of DME oxidation. This work is to exploit a novel ternary LANL anode catalyst with the features of high-temperature operation to produce high-power, low-cost direct DME MEAs. We envision the use of such systems as auxiliary electrical power for transport applications.

APPROACH

The project consists of three phases. In the first phase we demonstrated direct oxidation of DME at a lab-scale (5 cm²) MEA with a commercial catalyst. In the second phase we focused on increasing the anode specific current using this commercial catalyst to achieve a key program go/no-go milestone to show concept feasibility. In the last phase, we will evaluate the assemblies for durability, optimize structures for the ternary catalyst, and demonstrate improved power output. Throughout the program we employ two kinds of high-temperature membranes. One is polybenzimidazole (PBI), which is characterized as a high-acid, low-solids material. The other is referred to by a generic Advent trademark TPS and, relative to PBI, is a low-acid, high-solids material based on pyridine and polysulfone. Throughout the three experimental phases, key performance indicators, such as power output, amount of precious metal employed, and durability will be compared to the state of the art DMFC and incorporated as project milestones. We currently finished the second phase, which is summarized in the results below.

RESULTS

Identification of Anode Rate-Limiting Step

The objective of this program has been to demonstrate superior anode activity for direct oxidation of a high-energy-content fuel. Last year we reported a substantial improvement in DME oxidation current by increasing the *cathode* platinum loading from 0.8 mg Pt/cm² to 2.2 mg Pt/cm², implying we had not selected conditions that allowed us to isolate the anode reaction. Having achieved that goal, we evaluated the impact of DME pressure (concentration) on anode performance. If the oxidation kinetics were limited by the oxidation rate, then an increase in DME pressure should increase the current density. Figure 1 shows how changing pressure nearly eight-fold *does not* improve performance. This behavior infers the oxidation mechanism is “zero order,” meaning there is a step after the initial oxidation that limits the overall reaction. For example, DME oxidation could result in reaction products other than carbon dioxide such as carbon monoxide or other carbon-containing poisons for the anode. In this case, the reaction is limited by our ability to clear the poison from the anode catalyst.

Overcoming Rate-Limiting Anode Step

Kinetically limited processes are facilitated by increasing temperature. Thus, we systematically increased our cell temperature from 180°C to 240°C. Over this temperature range and for a given pressure of DME, the current and power output increased. Figure 2 shows this increase in power output versus temperature. Having confirmed the temperature relationship, we selected operation at the highest temperature (240°C) and

systematically varied the pressure of DME from 3.5 psig to 30 psig. Unlike that shown in Figure 1, Figure 3 now clearly shows a current dependence on DME pressure and confirms we have switched the reaction rate into first order, effectively inducing a rapid removal of electrode-blocking reaction products.

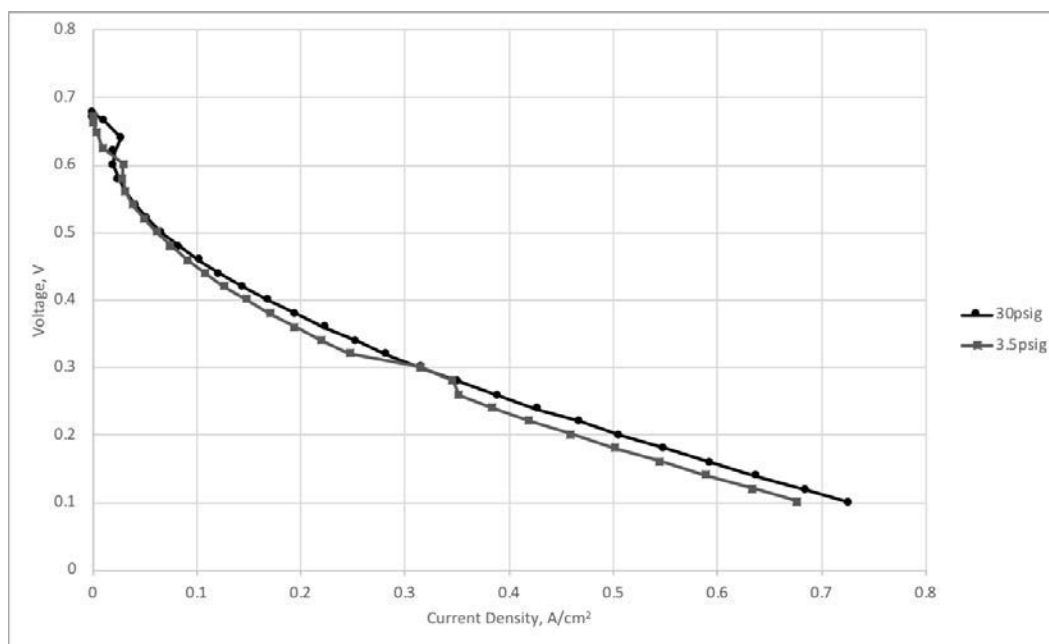


Figure 1. Lack of DME pressure dependence on current-voltage. Test MEA composed of cathode with Pt-alloy/C 2.3 mg_{Pt}/cm²; anode 12100 HiSPEC PtRu/C 2.23 mg_{Pt}/cm²; and PBI membrane. Test cell operated at 180°C with air 500 sccm, backpressure 3.5 psig and DME 125 sccm, humidified DME:water = 1:3 at the backpressure indicated.

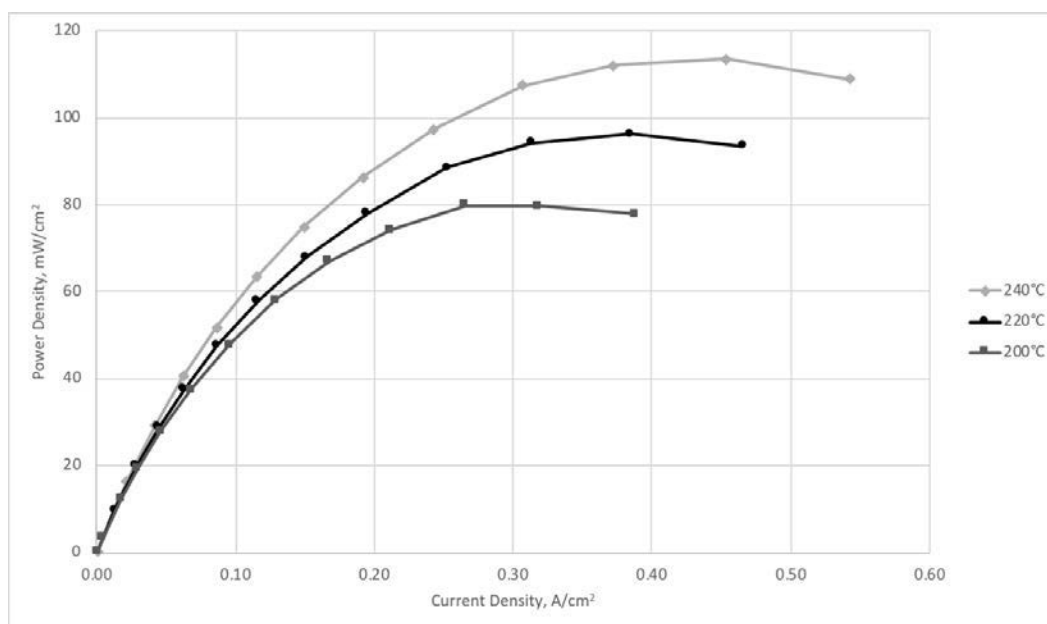


Figure 2. Power density over various temperatures. Test MEA composed of cathode with Pt-alloy/C 2.9 mg_{Pt}/cm²; anode 12100 HiSPEC PtRu/C 1.6 mg_{Pt}/cm²; and PBI membrane. Test cell operated at indicated temperatures with air 500 sccm, DME 125 sccm humidified at DME:water = 1:3 at 30 psig.

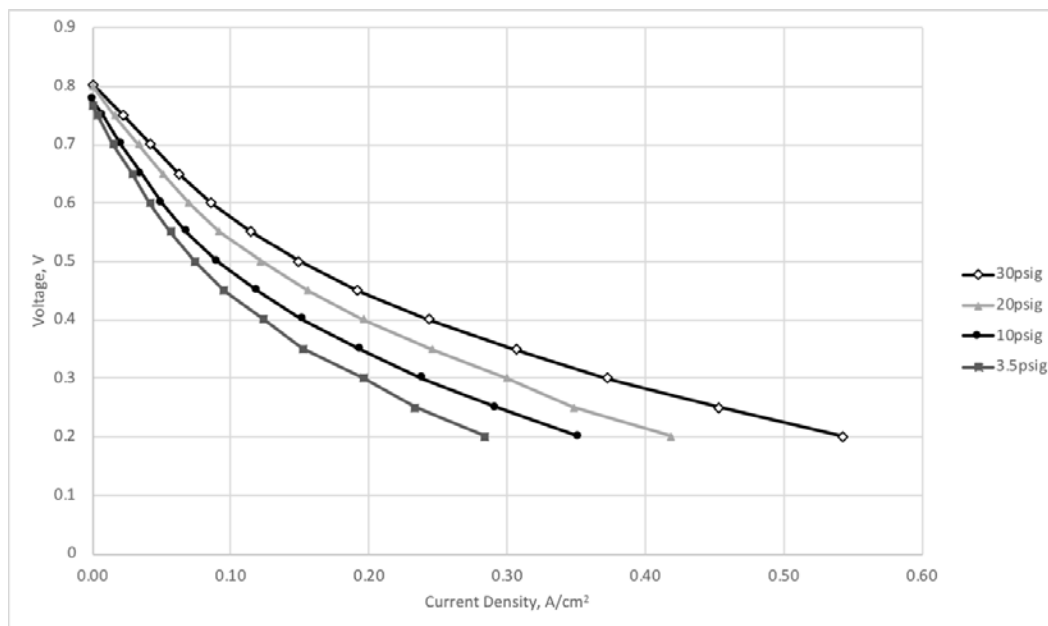


Figure 3. Current-voltage curves versus pressure of DME at higher temperature. Test MEA composed of cathode with Pt-alloy/C 2.9 mg_{PtGM}/cm²; anode 12100 HiSPEC PtRu/C 1.6 mg_{PtGM}/cm²; and PBI membrane. Test cell operated at 240°C with air 500 sccm, DME 125 sccm humidified at DME:water = 1:3 at indicated pressures.

Improvement in Anode Mass-Specific Activity

By combining previously reported advances in the cathode configuration with operating at the higher temperature, we were able to incorporate the benchmark PtRu anode catalyst in various configurations with the objective of maximizing activity and minimizing mass transport resistance. The process of developing architectures for catalysts involves a materials approach whereby a key performance indicator, anode mass-specific activity, is gauged as a function of electrode-layer porosity, hydrophobicity, and phosphoric acid loading. Citing the results of Figure 4, we note several salient observations. First, we confirm that operating at higher temperature results in an improved anode mass specific activity (compare Figure 4 square “Low Temperature” with filled circle “2016”). Second, with a combination of higher cathode catalyst loading and improved electrode structure, we have almost doubled the anode specific current from 32 A/g_{PtGM} in 2016 to 50 A/g_{PtGM} at 0.5 V in 2017 (compare filled circle to triangle). And finally, when combining higher cathode loadings and higher temperature, we greatly exceeded our target of 75 A/g_{PtGM} at 0.5 V with 94 A/g_{PtGM}. This last result included two other improvements as well. One involved building thinner microporous layers to facilitate gas transport. The other improvement came from a careful balance of optimum anode and cathode catalyst loadings to optimize reaction rates while at the same time remaining under the target total catalyst loading of 5 mg_{PtGM}/cm².

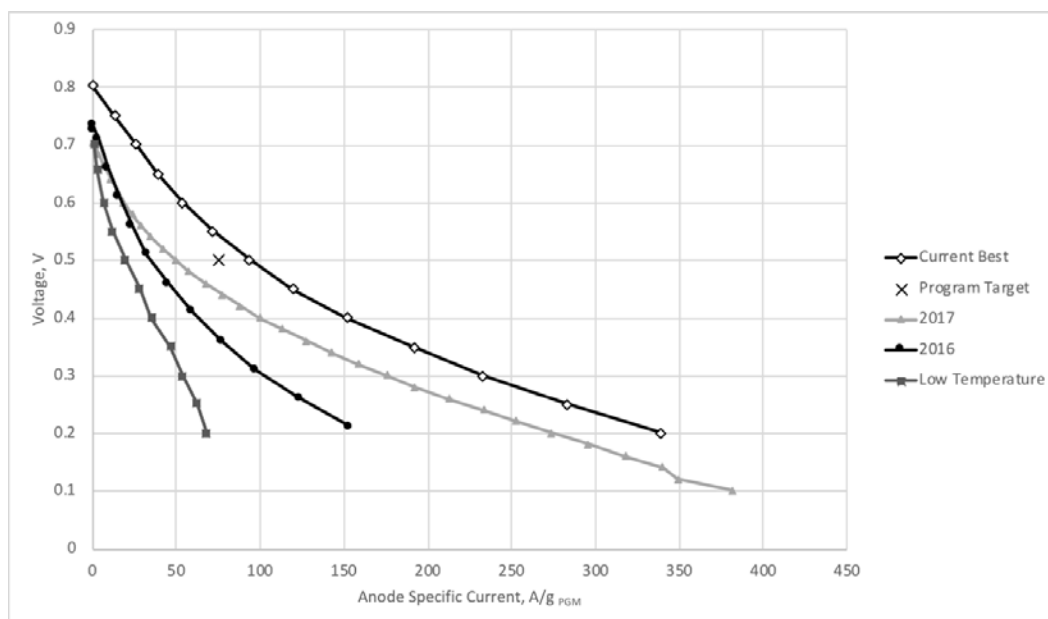


Figure 4. Improvement in anode mass-specific current

Open circles: replotted data from Figure 3 (30 psig) as anode-specific current. Single X: program target. Filled triangles: 2017 results showing impact of higher cathode catalyst loading using for anode HiSPEC 12100 PtRu/C 1.9 mg_{PGM}/cm², cathode Pt-alloy/C 2.2 mg_{PGM}/cm², at 180 °C and DME pressure 3.5 psig. Filled circles: 2016 results showing initial impact of higher operating temperature versus lower temperature using for anode HiSPEC 12100 PtRu/C 1.9 mg_{PGM}/cm², cathode Pt-alloy/C 0.8 mg_{PGM}/cm², at 180 °C and DME pressure 3.5 psig. Filled squares: LANL data from prior program, DME at HiSPEC 12100 PtRu/C, 80 °C, total 8 mg_{PGM}/cm², 26 psig. All with PBI membrane except for low-temperature black squares, which is Nafion. All with air 500 sccm, DME 125 sccm humidified at DME:water = 1:3.

CONCLUSIONS AND UPCOMING ACTIVITIES

Based on the target-exceeding anode mass-specific current, very low crossover currents, and reasonable power output, direct DME fuel cells offer great potential to exceed the performance of the state-of-the-art DMFC. While we have gone far without yet realizing the potential of the ternary catalyst, the morphology of this material is significantly different than that of our benchmark PtRu, and additional electrode optimization is needed. Upcoming efforts are focused on revising electrode processing conditions to fully realize the expected activity of the ternary catalyst, and benchmarking durability performance.

REFERENCES

1. Multi-Year Research, Development and Demonstration Plan: Section 3.4 Fuel Cells, Fuel Cell Technologies Office, 2016. http://energy.gov/sites/prod/files/2016/06/f32/fcto_myrd_fuel_cells_0.pdf.
2. Q. Li, X. Wen, G. Wu, H.T. Chung, and P. Zelenay, "High-Activity PtRuPd/C Catalyst for Direct Dimethyl Ether Fuel Cell," *Angew. Chem. Int. Ed.* 54 (2015): 1–6.

Advanced Catalysts and Membrane Electrode Assemblies for Reversible Alkaline Membrane Fuel Cells

Hui Xu (Primary Contact), Shuai Zhao
Giner, Inc.
89 Rumford Ave
Newton, MA 02466
Phone: (781) 529-0573
Email: hxu@ginerinc.com

DOE Manager: David Peterson
Phone: (720) 356-1747
Email: David.Peterson@ee.doe.gov

Contract Number: DE-EE0006960

Subcontractors:

- State University of New York at Buffalo (SUNY-Buffalo), Buffalo, NY
- National Renewable Energy Laboratory, Golden, CO

Project Start Date: June 1, 2015
Project End Date: June 30, 2018

Fiscal Year (FY) 2018 Objectives

- To further develop highly efficient bifunctional electrocatalysts related to spinel structures.
- To test the bifunctional catalysts under both fuel cell and electrolyzer modes to demonstrate their performance and to meet the reversible fuel cell targets.
- To operate regenerative fuel cell membrane electrode assemblies (MEAs) using as-developed bifunctional catalysts and alkaline membranes.

Technical Barriers

This project addresses the following technical barriers from the Fuel Cells section of the Fuel Cell Technologies Office Multi-Year Research, Development, and Demonstration Plan¹:

- (A) Durability (catalysts, electrode layers)
- (B) Cost (catalyst, MEAs)
- (C) Performance (catalysts, electrodes, MEAs).

Technical Targets

This project is developing novel bifunctional oxygen reduction reaction (ORR) and oxygen evolution reaction (OER) cathodes for reversible alkaline fuel cells. The new materials will be achieving the following targets at the end of the project for viable applications:

- In RDE, demonstrate ORR activity >1 mA/mg at iR -free 0.9 V, and OER activity >15 mA/mg at iR free 1.6 V.
- Achieve reversible current density of 600 mA/cm² at 0.55 V for fuel cell and 2.0 V for electrolyzer.
- Achieve fuel cell and electrolyzer life of 500 hours with less than 10% performance decay.

FY 2018 Accomplishments

During this period, we have achieved the following accomplishments:

- Co_xNi_yO_z and advanced carbon-based bifunctional ORR/OER catalysts were developed for OER durability in electrolysis cell mode with diluted potassium hydroxide (KOH) solution. The electrolysis cell was operated at 500 mA/cm² and the voltage was below 2.0 V, without any performance decay for 500 hours.
- Co_xNi_yO_z and advanced carbon-based bifunctional ORR/OER catalysts were investigated for ORR durability in fuel cell mode at 200 mA/cm² for 50 hours. There was only slight voltage decay in the initial 24 hours, but it recovered after reconditioning.
- The reversibility test in KOH solution (compared with that in water system) exhibited the good reversible catalyst activity for the ORR and OER, indicating the majority of performance loss in the fuel cell test was caused by the anion exchange materials.

¹ <https://energy.gov/eere/fuelcells/downloads/fuel-cell-technologies-office-multi-year-research-development-and-22>

INTRODUCTION

The primary goal of this project is to design advanced bifunctional non-platinum group metal (PGM) catalysts based MEAs for a reversible alkaline membrane fuel cell (AMFC). Water is split into H_2 and O_2 to be stored in electrolyzer mode and reversibly, the gases can be utilized by fuel cell mode to produce electricity. The performance of the innovative reversible AMFC technologies greatly relies on a bifunctional oxygen electrode capable of high activity for the ORR and the OER. The development of highly efficient bifunctional cathode catalysts derived from earth-abundant elements faces two grand challenges. The first is that the optimal active sites for the ORR differ from those for the OER. The second is stability during the high potential/voltage (>1.6 V) of the OER. As a result, most of the studied traditional carbon catalysts likely suffer from significant performance loss during ORR-OER dual-operation modes. In FY 2016, Giner and SUNY-Buffalo have developed transition metal-based oxide nanocomposites and heteroatom-doped graphene tube (GT) catalysts with high ORR/OER activities and limited durability. In the past year, the stability of nanocarbon catalysts has been tremendously enhanced by the doping of Mn into nanocarbon. The developed catalysts were integrated with selected anion-exchange ionomers and membranes. The MEAs were tested under both fuel cell and electrolyzer operating modes.

APPROACH

The development of highly efficient bifunctional cathode catalysts derived from earth-abundant elements faces the two challenges identified above. This incubator project addresses these catalyst challenges by developing PGM-free cathodes for reversible alkaline fuel cells coupled with anion exchange membranes and ionomers. Therefore, special emphasis is given to exploring highly stable oxides and nanocarbons under appropriate accelerated stress tests. As shown in Figure 1, our overall approach is to integrate active transition-metal-based oxides with highly graphitized and stable nanocarbons to maximize the ORR/OER activity and stability in alkaline media.

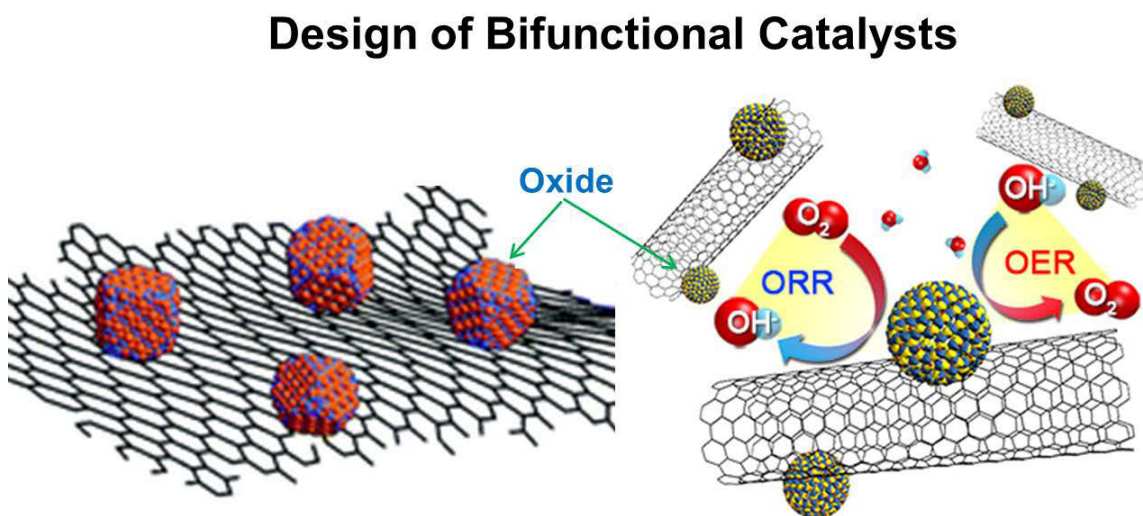


Figure 1. Proposed schemes of ORR/OER bifunctional cathode catalysts consisting of active oxide nanocrystals onto highly stable graphene (left) and carbon tubes (right)

RESULTS

As shown in Figure 2a, the core-shell structured $\text{Co}_x\text{Ni}_y\text{O}_z$ particles were prepared in situ via a hydrothermal process in the presence of the highly active and stable GTs derived from CoNi. The particle size is around 50 nm (Figure 2b) with a surface area $\sim 50 \text{ m}^2/\text{g}$. The bifunctional nanocomposite catalyst showed enhanced OER and ORR activity relative to the individual components separately (i.e., the $\text{Co}_x\text{Ni}_y\text{O}_z$ and N-GT alone), as shown in Figure 2c, in terms of the mass activity determined at 1.6 V and 0.9 V for the corresponding OER and ORR. More importantly, sufficient stability was achieved during the harsh potential cycling tests (0–1.9 V) (Figure 2d).

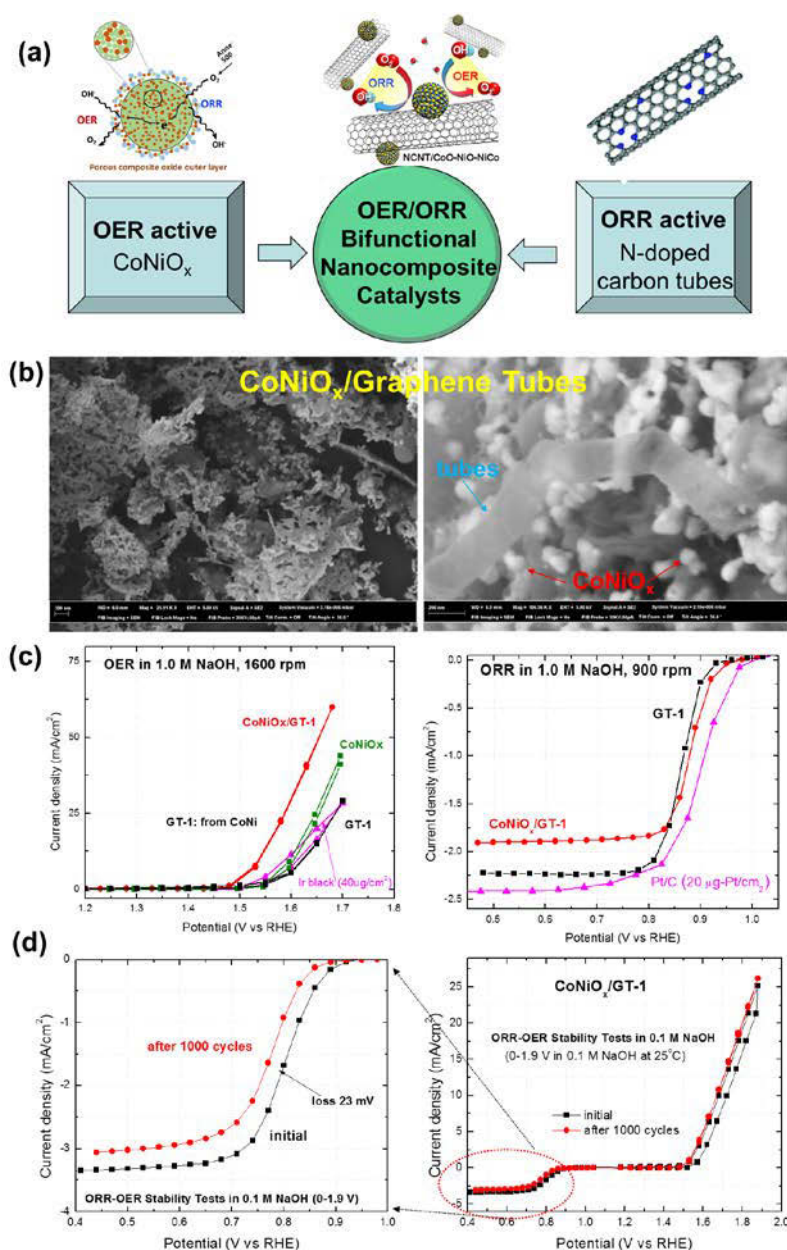


Figure 2. Design and synthesis of nanocomposite bifunctional catalysts by using GT-supported $\text{Co}_x\text{Ni}_y\text{O}_z$ and their ORR/OER activity and stability (a) integration scheme, (b) non-uniform morphology showing significant agglomeration of $\text{Co}_x\text{Ni}_y\text{O}_z$ nanoparticles, (c) ORR and OER activity in 1.0 M NaOH electrolyte, and (d) stability tests by using potential cycling stabilities in 0.1 M NaOH electrolyte, 0–1.9 V vs. reversible hydrogen electrode, 500 mV/s at room temperature

This is the first successful demonstration that nanocarbon-based catalysts can be very active and stable for ORR/OER dual-mode operation. However, scanning electron microscopy images of the $\text{Co}_x\text{Ni}_y\text{O}_z/\text{GT}$ nanocomposite indicate that oxide particles are significantly agglomerated without good dispersion onto the GTs in contrast to the ideal configuration. Therefore, our future efforts will be focused on nanocomposite synthesis with uniform oxide particle distribution onto ORR active GTs.

The $\text{Co}_x\text{Ni}_y\text{O}_z$ OER durability of the combined advanced carbon tubes and transition-metal oxide bifunctional catalyst developed by Giner was first investigated in a 0.1 M KOH-fed single electrolysis cell for 600 hours at different current densities (see Figure 3).

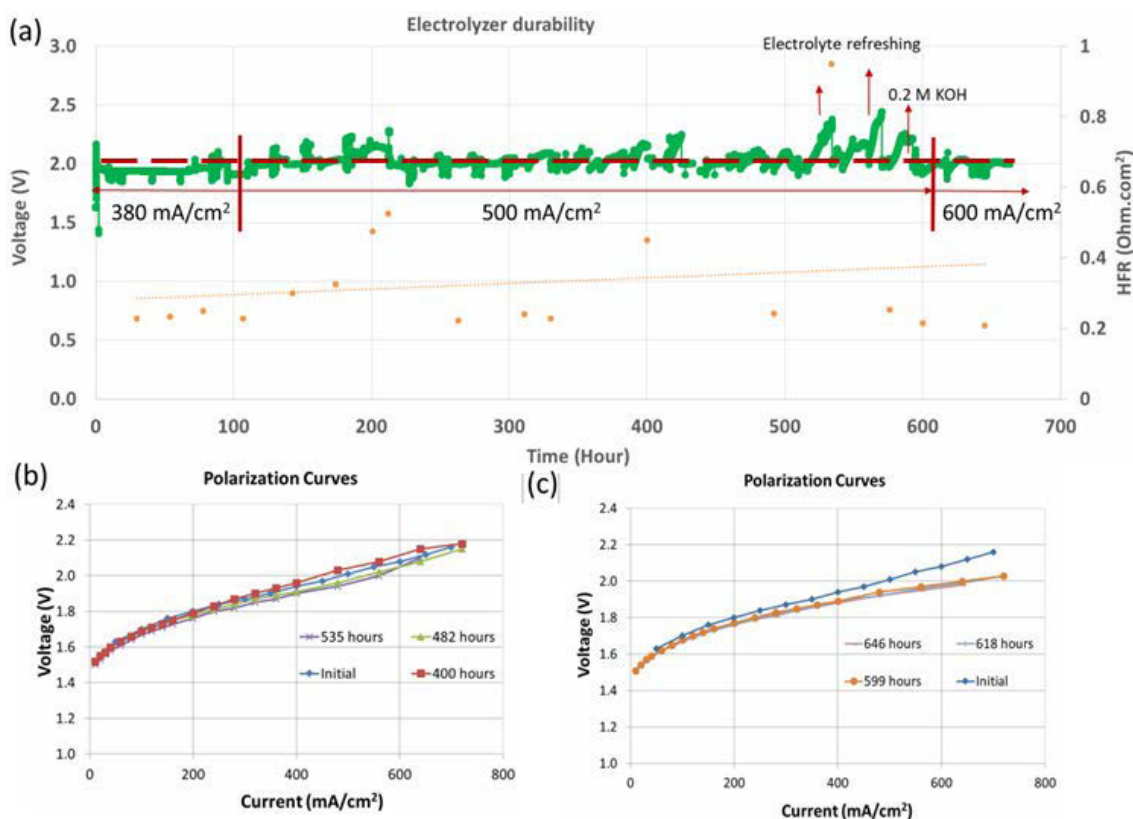


Figure 3. (a) Chronopotentiometry for 600 hours at different current densities; (b) polarization curves at different hours during durability test; (c) hydroxide solution concentration influence on bifunctional ORR/OER-based electrolysis cell. Electrolysis cell test conditions: 60 °C, 0.1 M KOH (0.2 M KOH after 500 hours) solution on both electrodes; cathode: $\text{Co}_x\text{Ni}_y\text{O}_z$ advanced carbon materials (2 mg/cm², ionomer=20 wt%); anode: PtRu/C (0.72 mg/cm², ionomer=26 wt%).

The membrane and ionomer were Tokuyama A201. The H_2 electrode for all the following MEA tests was identical: PtRu/C (0.7 mg PtRu/cm², I/C=0.8). The bifunctional catalyst loading on the O_2 electrode was 2 mg/cm², with 20 wt% ionomer. An initial screening current density of 380 mg/cm² was used for the first 100 hours in the chronopotentiometry. The performance was very stable; no frequent replenishing of the KOH solution was required to maintain the performance. From 100 hours to 600 hours, the current density was fixed at 500 mg/cm². The voltage was stable until around 200 hours, where it climbed to around 2.2 V, with the high frequency resistance (HFR) increasing from 256 to 450 mOhm-cm² for a few hours. This was likely caused by poor contact due to the gradual oxidation of the carbon paper, which was observed after opening the cell. Therefore, a piece of platinum-plated titanium paper was assembled into the original cell for continuous testing, with the HFR returning to approximately 0.25 Ohm-cm². After 300-hour operation, the membrane required a more frequent electrolyte replenishing due to increased HFR as the hydroxide ions were depleted in the recycled electrolyte. However, the catalyst performance was always recovered as shown in the polarization

curves after each electrolyte replenishing. Lastly, a higher concentration (0.2 M) of KOH was applied that helped to maintain the stable voltage after 500 hours. A much more stable voltage profile was therefore obtained as expected. The current density was increased to 600 mA/cm², without voltage increase, for an additional 50 hours. This long-term durability test proved the excellent OER activity and longevity of our bifunctional catalyst under the harsh environment and oxidizing voltage as high as 2.0 V.

To prove the reversibility of the bifunctional catalysts in reversible fuel cells, pure water (no KOH) was first used as the feedstock. First, the cell was operated in fuel cell mode; then the operation was switched to electrolyzer mode and held for 30 minutes at 2.0 V. Finally, the operation was switched back to the fuel cell operation mode. It clearly shows that the electrolyzer operation deteriorated rapidly with the pure water. More severely, when it was finally switched back to fuel cell operation, the fuel cell performance also decreased tremendously. HFRs under different operations are also compared in Figure 4. The initial HFR for fuel cell mode was 0.22 Ohm·cm² and barely changed after it was switched to the electrolyzer operation. However, the HFR increased to 0.4 Ohm·cm² only after 30 minutes, most likely due to decayed membrane and ionomer. The HFR changed little after it was switched back from electrolyzer operation to fuel cell operation. However, overall the HFR doubled from the initial fuel cell operation to final fuel cell operation. Again, this confirms that the decayed membrane and ionomer in the electrode affected not only electrolyzer operation but also fuel cell operation.

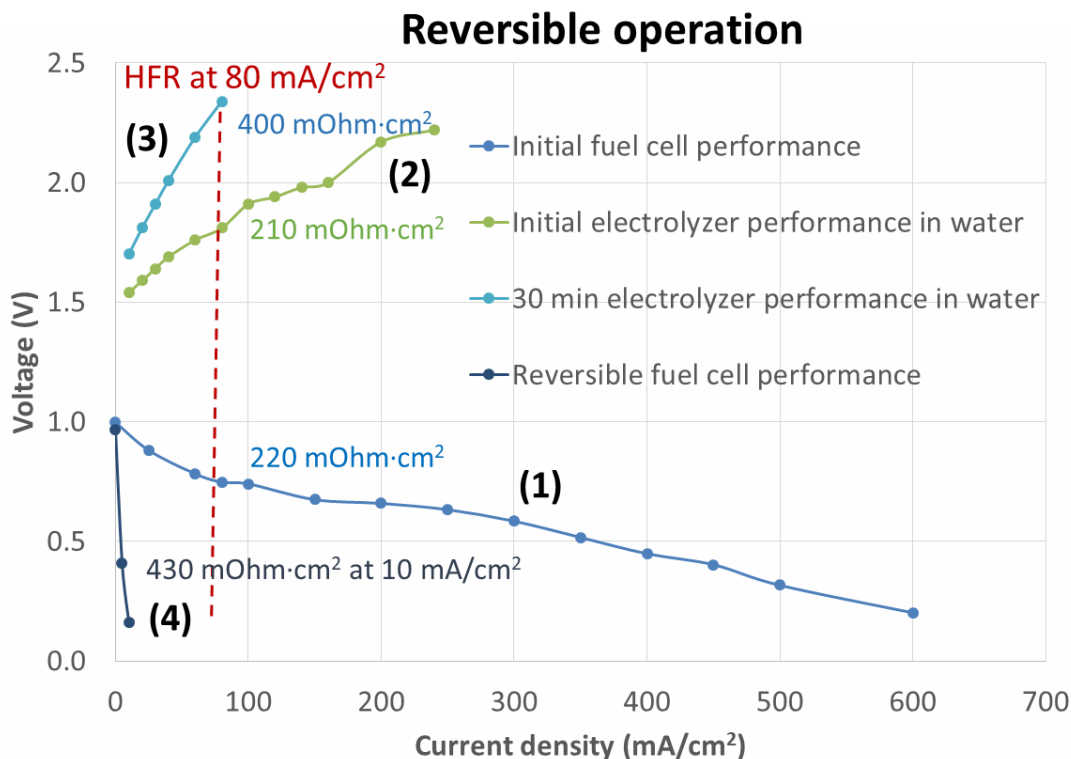


Figure 4. Reversible operation of fuel cell and electrolysis cell based on an oxygen electrode composed of Co_xNi_yO₂ advanced carbon materials with Ag addition. Cathode: Co_xNi_yO₂ advanced carbon materials (2 mg/cm², BP-60 ionomer=20%); anode: PtRu/C (0.7 mg/cm², ionomer=26%). Fuel cell test conditions: H₂/O₂ flow rate 1,500/3,000 ccm/min, T 60 °C, anode/cathode temperature-57 °/60 °C, and H₂/O₂ backpressure 35 psia. Electrolysis cell test conditions: 60 °C, pure deionized water on both electrodes.

CONCLUSIONS AND UPCOMING ACTIVITIES

Conclusions

- High-performance $\text{Co}_x\text{Ni}_y\text{O}_z$ /nanocarbon bifunctional OER and ORR catalysts have demonstrated remarkable reversibility and stability under harsh voltage cycling from 0.0 V to 1.9 V.
- MEA testing shows that alkaline membrane and ionomer degraded rapidly at high electrolysis voltages. Thus, hydroxide ion transfer paths across the membrane and in the electrodes were largely blocked.
- The introduction of diluted carbonate salt (e.g., NaHCO_3) or base (e.g., KOH) solutions can help to retain the electrolysis operation to some degree, although it leads to flooding and complicates the reversible fuel cell system.

Future Work

- Develop oxidation (high voltage) alkaline membrane and ionomer.
- Complete dual-operation durability test up to 500 hours after the integration of fuel cell and electrolyzer test station.

FY 2018 PUBLICATIONS/PRESENTATIONS

1. Shuai Zhao et al., “Recent Progress and Perspectives of Bifunctional Oxygen Reduction/Evolution Catalyst Development for Unitized Regenerative Anion Exchange Membrane Fuel Cells,” *Nano Energy* 47 (2018): 172–198
2. S. Zhao, B. Rasimick, W. Mustain, and H. Xu, “Highly durable and active Co_3O_4 nanocrystals supported on carbon nanotubes as bifunctional electrocatalysts in alkaline media.” *Applied Catalysis B: Environmental* 203 (2017): 138–145.
3. S. Gupta, S. Zhao, O. Ogoke, Y. Lin, H. Xu, and G. Wu, “Engineering Favorable Morphology and Structure of Fe-N-C Oxygen-reduction Catalysts via Tuning Nitrogen/Carbon Precursors,” *ChemSusChem* 10 no. 4 (2017): 774–785.
4. H. Zhang, H. Osgood, X. Xie, Y. Shao, and G. Wu, “Engineering nanostructures of PGM-free oxygen-reduction catalysts using metal-organic frameworks.” *Nano Energy* 31 (2017): 331–350.

FY16 SBIR II Release 1: Regenerative Fuel Cell System

Paul Matter (Primary Contact), Minette Ocampo, Michael Beachy, Chris Holt, Nora Shaheen, Monica Chan, and Jimmy Gaydos
pH Matter, LLC
6655 Singletree Dr.
Columbus, OH 43229
Phone: (614) 396-7820
Email: info@phmatter.com

DOE Manager: Donna Ho
Phone: (202) 586-8000
Email: Donna.Ho@ee.doe.gov

Contract No: DE-SC0013111 (SBIR Phase II Release 1)

Subcontractors:

- Giner, Inc., Newton, MA
- National Renewable Energy Laboratory, Golden, CO

Project Start Date: April 12, 2016
Project End Date: April 11, 2018

Overall Objectives

- Demonstrate a reversible 25-cm² anion exchange membrane fuel cell (AEMFC) for 1,000 cycles (42% round-trip efficiency; >250 mA/cm² power generation; >50 mA/cm² energy storage).
- Incorporate membrane electrode assemblies (MEAs) into a regenerative stack.
- Perform economic analysis on reversible AEMFC system following DOE guidelines for candidate grid load-leveling technologies.

Fiscal Year (FY) 2018 Objectives

- Demonstrate a reversible 25-cm² AEMFC for 1,000 cycles (42% round-trip efficiency; >250 mA/cm² power generation; >50 mA/cm² energy storage).
- Incorporate MEAs into a regenerative stack.
- Perform economic analysis on reversible AEMFC system following DOE guidelines for candidate grid load-leveling technologies.

Technical Barriers

This project addresses the following technical barriers from the Fuel Cell section of the Fuel Cell Technologies Office Multi-Year Research, Development, and Demonstration Plan,¹ with respect to alkaline fuel cells for energy storage:

- (A) Durability: Increase the durability of reversible fuel cell electrodes for stationary load cycles
- (B) Cost: Develop low-platinum group metal (PGM) and PGM-free catalysts and electrodes for reversible anion-exchange membrane fuel cells (oxygen and hydrogen electrodes)
- (C) Performance: Optimize reversible anion-exchange membrane fuel cell and stack performance while maintaining cost and durability.

Technical Targets

This Phase II Small Business Innovation Research (SBIR) project is developing new catalyst materials and MEAs for a regenerative alkaline fuel cell stack. The materials being developed address the following technical targets for energy storage applications:

- 1,000 cycles at target current density and above the efficiency targets
- 42% efficiency; >250 mA/cm² power generation; >50 mA/cm² energy storage.

FY 2018 Accomplishments

The following work related to the technical objectives has been accomplished on this SBIR Phase II project:

- In 25-cm² reversible cell testing, demonstrated 360 cycles between target fuel cell and electrolysis current density at 50°C with cell that achieves performance and economic model cost and efficiency targets; demonstrated >1,000 cycles of stable performance (below

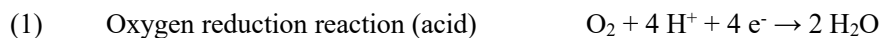
¹ <https://www.energy.gov/eere/fuelcells/downloads/fuel-cell-technologies-office-multi-year-research-development-and-22>

efficiency target); demonstrated 250 hours of simulated load cycle operation.

- Demonstrated 3-cell 25-cm² stack that simultaneously achieves performance and the economic model cost targets using low-cost platinum-free hydrogen and oxygen electrode catalysts; demonstrated 200 cycles.
- Further refined an economic model based on the assumptions developed by Steward et al. [1] and the Phase II targets. The model includes a sensitivity analysis for key cell parameters being developed (i.e., current density, efficiency, lifetime, and fuel cell cost).

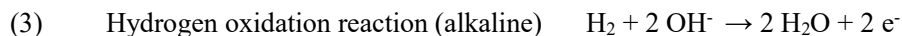
INTRODUCTION

Low-temperature fuel cells, such as proton exchange membrane (PEM) and alkaline fuel cells, offer an efficient and clean means of energy conversion of hydrogen to electricity. However, PEM fuel cells typically require platinum (Pt) in the cathode to operate at high power density and high efficiency, which hurts the economics for this technology. Pt is used as an electrocatalyst for the oxygen reduction reaction (ORR); the cathode side half reaction is shown below for acidic and alkaline electrolytes, respectively:



The slow kinetics in the cathode is one of the largest sources of inefficiency in fuel cells, thus high platinum catalyst loadings are needed to prevent even more voltage losses (or overpotential). At commercial scale, precious metals in the cathodes of PEM fuel cells would comprise a significant portion of the entire stack cost [1, 2]. Additionally, Pt-based ORR catalysts can degrade quickly under fuel cell operating conditions, such as frequent load cycling.

More recently, there has been renewed interest in alkaline fuel cells for stationary applications as development of commercial anion exchange membranes (AEMs) is helping to alleviate system-level problems with alkaline fuel cells, such as pressure balance. Further, recent published results at Los Alamos National Laboratory have shown that alkaline fuel cells could potentially operate at high efficiency with PGM-free ORR catalysts [3]. Alkaline fuel cells are of particular interest for energy storage applications that do not have volume limitations, such as grid load leveling. In an alkaline fuel cell, oxygen is reduced by reaction (2) above, and hydrogen is oxidized by reaction (3) below.



Alkaline fuel cells could potentially be operated in a reversible manner, allowing renewable energy to be stored in the form of hydrogen. This would be particularly valuable when coupled with renewable energy generation (wind or solar) to provide energy storage and load leveling. However, when operating in regeneration mode, cathode degradation is even more pronounced for conventional ORR catalysts because of the high voltages required for the oxygen evolution reaction (OER), the reverse of reaction (2) above. Consequently, in existing reversible systems, separate cell stacks for fuel cell and electrolysis operation are used, adding to the already high system cost. If a low-cost regenerative stack could be developed, it would be a key breakthrough in the commercial viability of energy storage systems [4]. In this project, pH Matter, LLC, is partnering with Giner, Inc., and the National Renewable Energy Laboratory (NREL) to develop and demonstrate a low-cost regenerative alkaline fuel cell.

APPROACH

The overall objective of the project is to develop and demonstrate a regenerative fuel cell stack technology that is economically viable in stationary energy storage. Researchers at pH Matter synthesized a matrix of PGM-free hydrogen oxidation reaction (HOR) / hydrogen evolution reaction (HER) catalysts, and gas diffusion electrodes based on these materials. Researchers at NREL synthesized a matrix of low-PGM hydrogen electrode materials. The HOR/HER materials and gas diffusion electrodes were characterized and tested under cycling conditions to determine performance and stability. Additionally, pH Matter optimized ORR/OER electrodes previously developed in Phase I for improved performance and durability at higher temperatures and pressures. The hydrogen and oxygen electrodes were then demonstrated in 25-cm² single cells for up to 1,000 cycles using a novel unitized reversible cell design at pH Matter. Materials that degraded during cycling were characterized by pH Matter and NREL to determine degradation mechanisms. Engineers at Giner tested cells in parallel using a commercial electrolyzer design. Down-selected cells were then incorporated into fuel cell and/or electrolyzer stacks and demonstrated in simulated application testing at pH Matter and Giner. The project establishes a foundation for future work, where the technology will be incorporated into a prototype

regenerative fuel cell system. Additionally, a design and economic model of the regenerative fuel cell system were built to verify advantages of the approach compared to available energy storage technologies.

RESULTS

In previous work, the team developed novel PGM-free oxygen electrode and low-PGM (Pt-free) hydrogen electrode catalysts, and optimized electrodes for regenerative cell operation. Regenerative cells showed excellent stability for cycling for up to 360 cycles above the target performance. This year, work was expanded to longer cycle numbers, simulated operation, and stack testing. After initial degradation and break-in at 60°C, 25-cm² cells were shown to be stable for more than 1,000 cycles. Although the performance fell below the project targets during the break-in period, the long-term stability at 60°C and 70°C was found to be exceptional. Figure 1 shows the stability of a cell cycling between 150 mA/cm² and 50 mA/cm² over 1,000 times in accelerated degradation tests. Cells were also operated for up to 250 hours under simulated load cycling. The load cycle tests were designed to simulate operation of the cells within an energy storage device, such as seasonal solar storage. In these tests, the cells operated for 15 hours under electrolysis operation at 50 mA/cm², followed by 5 hours of fuel cell operation at 150 mA/cm². An example of the load cycling is shown in Figure 2. Finally, cells were loaded into a 3-cell stack at pH Matter. The stack was based on pH Matter's unique patent-pending reversible unitized cell design. The initial current-density performance in the stack matched the project targets, and the stack was cycled 200 times, as shown in Figure 3.

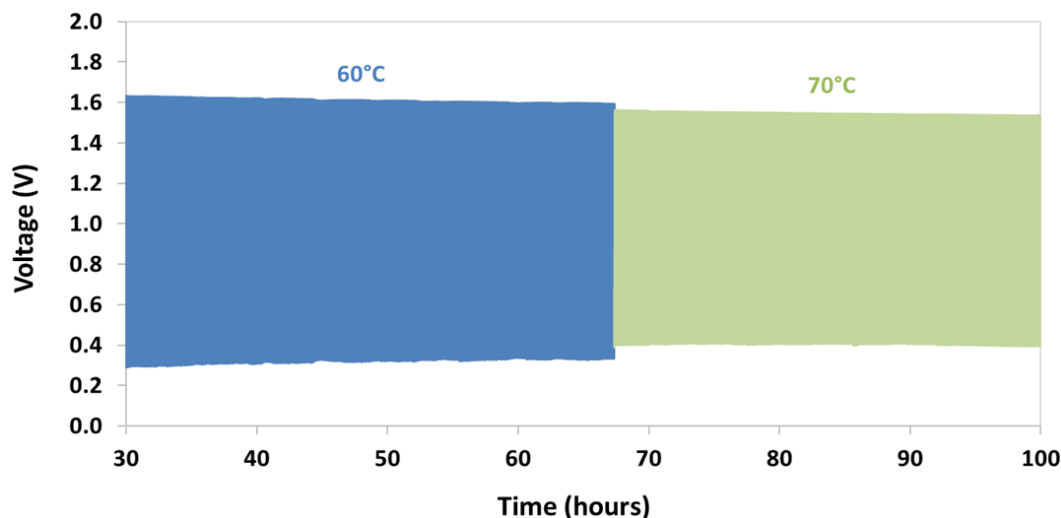


Figure 1. Accelerated degradation testing of 25-cm² unitized reversible cell containing down-selected low-PGM hydrogen electrode and PGM-free oxygen electrode showing stability for >1,000 cycles

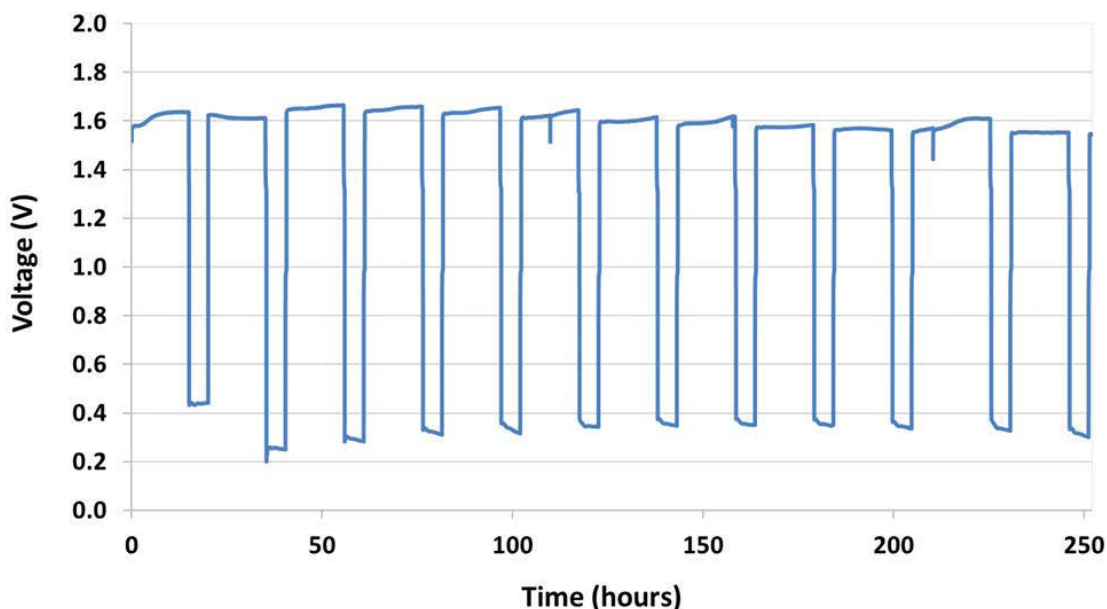


Figure 2. Simulated load cycling at 60°C of 25-cm² unitized reversible cell containing down-selected low-PGM hydrogen electrode and PGM-free oxygen electrode showing stability for >250 hours

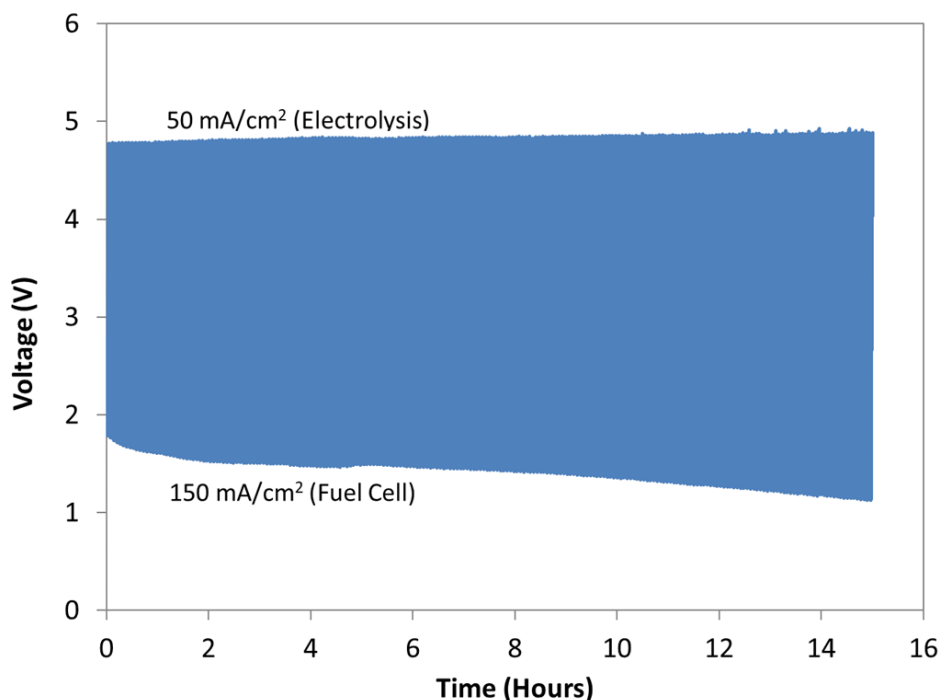


Figure 3. Accelerated degradation testing at 50°C of 25-cm² unitized reversible 3-cell stack containing down-selected low-PGM hydrogen electrode and PGM-free oxygen electrode showing stability for >200 cycles

In fiscal year 2018, NREL supported testing and characterization on the project by examining the degradation of components. In general, degradation was found to occur during electrolysis operation of the oxygen electrode. NREL examined long-term oxygen-side degradation for 3 days each at progressively higher voltages (1.6, 1.7, and 1.8 V). Recoverable degradation was found to occur from carbonation of the electrolyte. After 9

days of operation minimal electrolysis performance degradation occurred, although a small increase in high frequency resistance and catalyst resistance was detected. These results were reported in this year’s Annual Merit Review presentation. Giner supported the project by testing 50-cm² cells and a 4-cell stack in a commercial electrolyzer design. Cells with pH Matter’s down-selected electrodes showed stable performance for electrolysis in the single cells for >100 hours. A 4-cell stack was demonstrated for 700 hours under simulated load operation with the down-selected electrode materials in the commercial design. These results were also reported in the Annual Merit Review presentation. Additionally, Giner provided input for economic modeling.

The economic model was updated this year to project electricity costs for energy stored with a reversible alkaline fuel cell system. The guidelines for the model and assumptions generally followed those used by Steward et al. [1] and assumed a unitized reversible alkaline fuel cell system operating at up to 2,000 psi storage pressure for 4 years. The delivered electricity cost for this scenario was determined to be \$0.175/kWh. The system was compared to a discrete storage system with a PEM fuel cell stack and an alkaline membrane electrolyzer. The discrete electrolyzer was the same cost and performance as the unitized reversible stack while the PEM stack cost and performance were based on DOE estimates [5]. The discrete system required only hydrogen storage, as the PEM stacks were assumed to operate with air. For the discrete case, the delivered electricity cost was determined to be \$0.223/kWh. Table 1 breaks down the economic comparison. However, the discrete system may have advantages with longevity, customizable sizing for load cycles, and lower PEM fuel cell cost with future automotive adoption. Likewise, the unitized system may have unaccounted size/weight advantages for certain applications. Consequently, the advantages of a discrete versus unitized reversible fuel cell system will ultimately depend on the application.

Table 1. Economic Comparison of a Discrete versus a Unitized Fuel Cell Storage System

	Discrete	Unitized
Upfront Power Cost (\$/kW)	Fuel Cell + Electrolyzer	Reversible Cell Stack
Storage Capacity Cost (\$/kWh)	\$23	\$35
Round-Trip Efficiency	43%	43%
Delivered Energy (\$/kWh)	0.223	0.175

CONCLUSIONS AND UPCOMING ACTIVITIES

The following conclusions can be drawn from work completed on this project:

- The novel PGM-free oxygen electrode developed on this project shows performance comparable to precious metal catalysts, good stability during cycling from ORR to OER voltages, and excellent stability during long-term electrolysis or fuel cell operation.
- PGM-free electrodes developed on this project show higher over-potential than commercial Pt/Ru but excellent stability. The novel low-PGM hydrogen electrodes developed on this project show similar over-potential as commercial Pt/Ru and excellent stability but require further optimization for high current density operation.
- Full 25-cm² cells that meet the project cost and performance targets have been demonstrated for 360 cycles above the go/no-go operating conditions.
- Full 25-cm² cells that meet the project cost targets, but are below the performance targets after initial break-in at 60°C, have been demonstrated for >1,000 cycles with exceptional stability.
- Performance results measured in 25-cm² accelerated degradation tests were demonstrated in long-term simulated load cycling for more than 250 hours.

- The performance results in 25-cm² cells were replicated in a 3-cell stack, and durability for 200 cycles was demonstrated.
- NREL confirmed the stability of the oxygen-side electrodes in electrolysis testing and found electrolyte carbonation to be the main source of electrolysis degradation. This degradation was mostly recoverable with replacement of liquid electrolyte.
- Giner demonstrated operation of the hydrogen and oxygen electrodes in a 50-cm² 4-cell alkaline membrane electrolyzer stack for more than 500 hours.
- Economic modeling suggests that the reversible AEMFC concept would be an excellent energy storage option for grid load leveling if performance targets can be achieved at the system level. The unitized system has potential cost and size advantages versus a discrete system.

Although the project was completed in 2018, future planned work on the reversible cell technology will include:

- Further improve economics with further optimization of electrodes for higher power and improvement of catalysts for lower over-potential.
- Incorporate novel membranes into the cells to increase cell lifetime.
- Improve mechanical integrity of the cells to enable demonstration of higher-pressure operation at the cell and stack levels.
- Demonstrate long-term operation over thousands of hours and under various load cycle conditions.
- Demonstrate the stack at the kW scale.
- Integrate the stack into a system with energy storage in gas cylinders.

FY 2018 PUBLICATIONS/PRESENTATIONS

1. S.M. Alia, C. Ngo, S. Shulda, S. Pylypenko, B.S. Pivovar, “Platinum-Nickel Nanowires as Electrocatalysts in Alkaline Hydrogen Oxidation and Evolution,” 230th ECS Meeting (Honolulu, HI, 2016) 2787.
2. S.M. Alia, C. Ngo, S. Shulda, S. Pylypenko, B.S. Pivovar, “Platinum-Nickel Nanowires as Electrocatalysts in Alkaline Hydrogen Oxidation and Evolution,” AIChE Annual Meeting (San Francisco, CA, 2016) 474452.
3. P. Matter, M. Ocampo, C. Holt, M. Beachy, N. Shaheen, M. Chan, and J. Gaydos, “Reversible Fuel Cell System for Energy Storage,” Hydrogen Symposium at the 2017 TechConnect World Innovation Conference (May 2017).
4. P. Matter, “Reversible Fuel Cell System for Energy Storage and Hydrogen Production,” Solar Power International (Las Vegas, NV, September 2017).
5. P. Matter, M. Ocampo, C. Holt, M. Beachy, N. Shaheen, M. Chan, M. Galliger, J. Gaydos, H. Xu, S. Zhao, S. Alia, A. Park, and B. Pivovar, “Low-Cost Reversible Alkaline Fuel Cell,” Fuel Cell Seminar (Long Beach, CA, November 2017).

REFERENCES

1. D. Steward, G. Saur, M. Penev, and T. Ramsden, *Lifecycle Cost Analysis of Hydrogen Versus Other Technologies for Electrical Energy Storage*. NREL Report NREL/TP-560-46719 (2009). Accessed July 23, 2015. <http://www.nrel.gov/docs/fy10osti/46719.pdf>.

2. Brian D. James, Jennie M. Moton, and Whitney G. Colella, *Mass Production Cost Estimation of Direct H₂ PEM Fuel Cell Systems for Transportation Applications: 2013 Update*. Accessed July 23, 2015. http://energy.gov/sites/prod/files/2014/11/f19/fcto_sa_2013_pemfc_transportation_cost_analysis.pdf.
3. H.T. Chung, J.H. Won, and P. Zelenay, “Active and stable carbon nanotube/nanoparticle composite electrocatalyst for oxygen reduction.” *Nature Communications* 4 (2013). Accessed July 23, 2015. doi: 10.1038/ncomms2944.
4. R.J. Remick and D. Wheeler, *Reversible Fuel Cells Workshop Summary Report*. Accessed July 23, 2015. http://www1.eere.energy.gov/hydrogenandfuelcells/pdfs/rev_fc_wkshp_report.pdf
5. A. Wilson, G. Kleen, and D. Papageorgopoulos, “Fuel Cell System Cost – 2017,” DOE Hydrogen and Fuel Cells Program Record 17007. Accessed at https://www.hydrogen.energy.gov/pdfs/17007_fuel_cell_system_cost_2017.pdf.

Performance of Advanced Automotive Fuel Cell Stacks and Systems with State-of-the-Art d-PtCo/C Cathode Catalyst in Membrane Electrode Assemblies

Rajesh K. Ahluwalia (Primary Contact),
Xiaohua Wang, and J-K Peng
Argonne National Laboratory
9700 South Cass Avenue
Lemont, IL 60439
Phone: (630) 252-5979; Fax: (630) 252-5161
Email: walia@anl.gov

DOE Manager: Nancy L. Garland
Phone: (202) 586-5673
Email: Nancy.Garland@ee.doe.gov

Project Start Date: October 1, 2003
Project End Date: Project continuation and
direction determined annually by DOE

Overall Objectives

- Develop a validated model for automotive fuel cell systems, and use it to assess the status of the technology.
- Conduct studies to improve performance and packaging, to reduce cost, and to identify key R&D issues.
- Compare and assess alternative configurations and systems for transportation and stationary applications.
- Support DOE/U.S. DRIVE automotive fuel cell development efforts.

Fiscal Year (FY) 2018 Objectives

- Modify the reference fuel cell system (FCS) configuration to include controls for extended stack durability on operational, start-up, and shut-down transients.
- Quantify the impact of low-platinum group metal (PGM) alloy catalysts on the performance of automotive stacks and fuel cell systems.

- Provide modeling support to Strategic Analysis, Inc. in annual update of progress in meeting technical targets, including FCS cost.

Technical Barriers

This project addresses the following technical barriers from the Fuel Cells section of the Fuel Cell Technologies Office Multi-Year Research, Development, and Demonstration Plan¹:

- (A) Durability
- (B) Cost
- (C) Performance.

Technical Targets

This project focuses on conducting system-level analyses to address the following DOE 2020 technical targets for automotive fuel cell power systems operating on direct hydrogen:

- Energy efficiency: 60% at 25% of rated power
- $Q/\Delta T$: 1.45 kW/°C
- Power density: 850 W/L for system, 2,500 W/L for stack
- Specific power: 850 W/kg for system, 2,000 W/kg for stack
- Transient response: 1 second from 10% to 90% of maximum flow
- Start-up time: 30 seconds from -20°C and 5 seconds from +20°C ambient temperature
- Precious-metal content: 0.125 g/kW_e rated gross power.

¹ <https://www.energy.gov/eere/fuelcells/downloads/fuel-cell-technologies-office-multi-year-research-development-and-22>

FY 2018 Accomplishments

- Projected 46.0 ± 0.7 $\$/kW_e$ FCS cost at 500,000 units per year, and 8.5 ± 0.4 kW_e/g FCS Pt utilization with state-of-the-art (SOA) d-PtCo/C cathode catalyst, reinforced 14- μm 850 equivalent weight membrane, and $Q/\Delta T = 1.45$ $kW/^\circ C$ constraint.
- Verified that the SOA catalyst system can achieve $1,180 \pm 55$ mW/cm^2 stack power density, exceeding the target $1,000$ mW/cm^2 at low Pt loading (0.125 $mg-Pt/cm^2$ total).
- Projected $<5\%$ penalty in power density if the cathode humidifier is removed, and $\sim 15\%$ penalty if stack inlet pressure is reduced to 2 atm from 2.5 atm.
- Showed that parasitic power approaches 25 kW_e if the compressor discharge pressure is raised to 4 atm.
- Modified the reference system configuration to include valves and controls for protected shutdown, safe startup from sub-freezing temperatures, and limiting cell voltage to 0.85–0.875 V during idle.

INTRODUCTION

While different developers are addressing improvements in individual components and subsystems in automotive fuel cell propulsion systems (i.e., cells, stacks, balance-of-plant components), we are using modeling and analysis to address issues of thermal and water management, design-point and part-load operation, and component-, system-, and vehicle-level efficiencies and fuel economies. Such analyses are essential for effective system integration.

APPROACH

Two sets of models are being developed. The GCtool software is a standalone code with capabilities for design, off-design, steady-state, transient, and constrained optimization analyses of fuel cell systems. A companion code, GCtool-ENG, has an alternative set of models with a built-in procedure for translation to the MATLAB/SIMULINK platform commonly used in vehicle simulation codes, such as Autonomie.

RESULTS

For extended durability, we modified the reference system to incorporate valves (see Figure 1) and controls for protected shutdown, safe startup from below-freezing temperatures, and limiting cell voltage at idle. We developed a model to show that the cell voltage can be maintained below 0.85 V during idle by reducing the cathode stoichiometry to 1.05, or by increasing the stack temperature to more than 80°C, while limiting the minimum stack power to 2.8–3.0 kW_e. We analyzed the possibility of further decreasing the idle cell voltage with wider latitude in minimum power by decreasing O₂ concentration at stack inlet by recycling cathode spent air and bypassing the stack. We also developed a protected shutdown algorithm that involves closing the stack bypass and isolation valves to deplete O₂ in the cathode channels during shutdown, ensuring that damaging H₂-air fronts cannot form in the anode channels during subsequent start-up. Following our earlier work [1], we are analyzing a method of preventing icing by maximizing in-stack heat production during sub-freeze start by operating at low cell voltages.

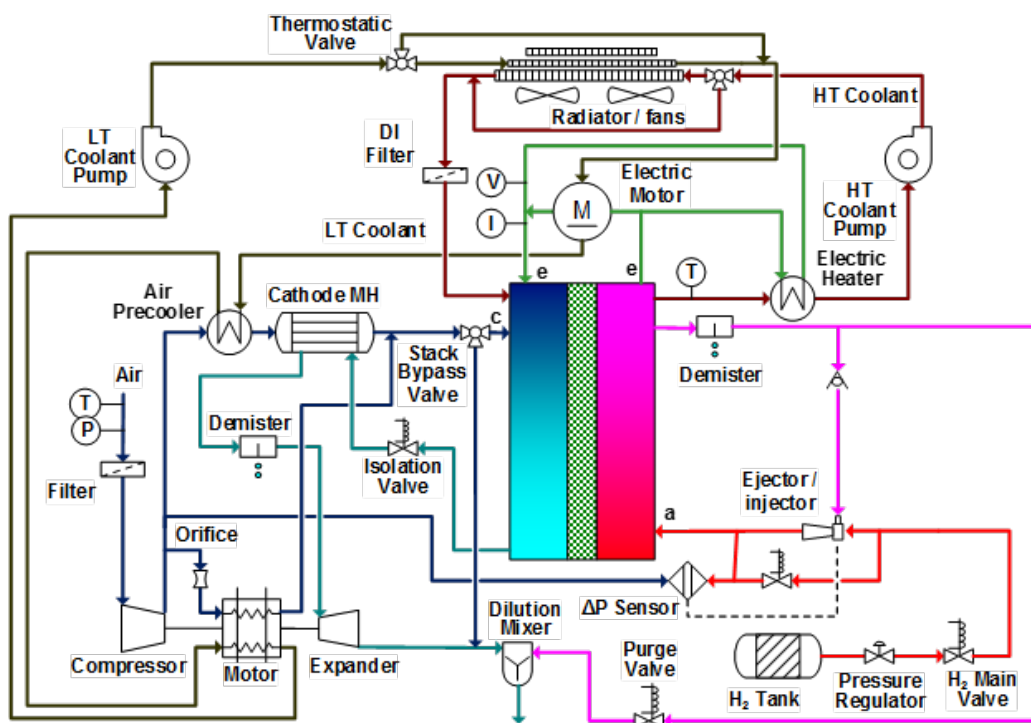


Figure 1. Argonne 2018 FCS configuration with controls

We evaluated the performance of a SOA d-PtCo catalyst supported on high-surface-area carbon in cathode and Pt catalyst supported on Vulcan carbon in anode. The Pt loadings are 0.1 mg/cm² in the cathode catalyst and 0.025 mg/cm² in the anode catalyst. Figure 2a lists other attributes of the membrane electrode assembly (MEA) containing these catalysts. We collaborated with the Fuel Cell Consortium for Performance and Durability (FC-PAD) funding opportunity announcement project led by General Motors in testing cells with this MEA on a United States–European Union (U.S.-EU) differential cell hardware shown in Figure 2b. The tests were run using two different protocols, random and controlled. The random protocol used semi-statistical ordering of a test matrix with multiple variables, forward scans, and a 3-minute hold at each cell voltage. The controlled protocol used model-guided single-variable tests with some two-variable tests, forward scans, and 3-minute hold at each cell voltage. As in earlier work [2], we determined the kinetic performance of d-PtCo/C catalyst by using the measured polarization data at low-current densities together with the ionic conductivity (σ_c) of the cathode catalyst layer (CCL) derived from the galvanostatic impedance data obtained in H₂/N₂, and a transient solid solution model for oxide coverage (θ) as a function of potential, relative humidity (Φ), and temperature (T). Figure 2c lists the derived kinetic constants appearing in the following distributed kinetic model for the oxygen reduction reaction (ORR).

$$\eta_c = \eta_s^c + iR_{\Omega}^c \left(\frac{i\delta_c}{b\sigma_c} \right)$$

$$i + i_x = i_0 S_{Pt} (1 - \theta) e^{-\frac{\omega\theta}{RT}} e^{\frac{\alpha n F}{RT} \eta_s^c}$$

$$i_0 = i_{0r} e^{-\frac{\Delta H_s^c}{R} \left(\frac{1}{T} - \frac{1}{T_r} \right)} P_{O_2}^{\gamma} \Phi^{\beta}$$

Figure 2d compares the mass activity of the cathode catalyst calculated using the kinetic model with the data for other catalyst systems investigated in this project. Some main conclusions from this comparison are highlighted below.

- d-PtCo/C has 2 times the modeled mass activity of the annealed Pt catalyst (a-Pt/C) that has nearly the same particle size.
- d-PtCo/C and d-PtNi/C alloy have comparable mass activities.
- Both low-PGM alloy catalysts (d-PtNi/C and d-PtCo/C) meet the mass activity targets of 440 A/g_{Pt}.

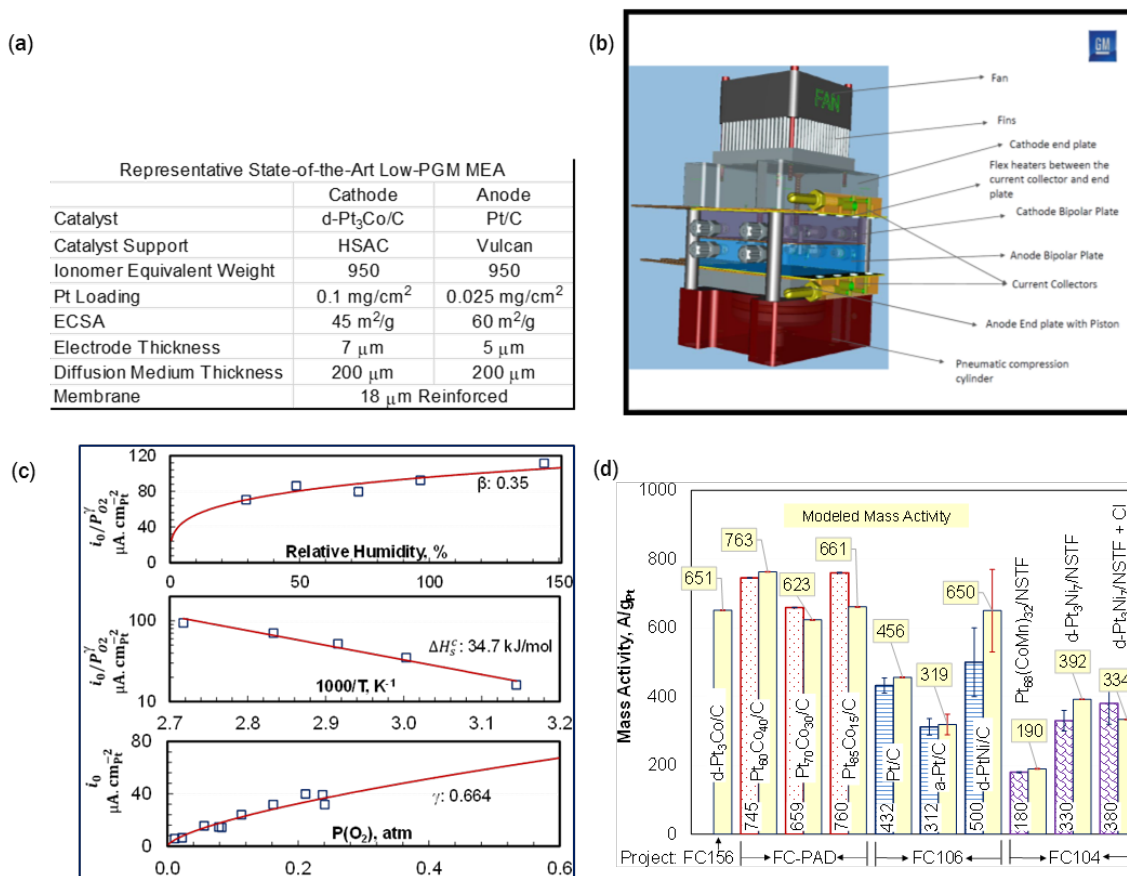


Figure 2. ORR kinetics model: (a) representative state-of-the-art low-PGM MEA; (b) U.S.-EU differential cell hardware; (c) modeled kinetics of ORR on SOA d-PtCo/C catalyst; and (d) comparison of mass activity with other dispersed Pt and Pt alloy catalysts and binary and ternary nanostructured thin film catalysts. Solid fills are modeled values from ORR kinetic model; pattern fills are measured mass activities in H₂/O₂.

We characterized the high-current-density performance of the MEA by developing a correlation for mass transfer overpotential (η_m) in terms of the limiting current density (i_L) at which η_m equals 400 mV. The limiting current density was modeled as a function of pressure, CCL temperature (T_c), CCL relative humidity (Φ_c) and O₂ partial pressure (P_{O_2}) in gas channel (see Figure 3a). We formulated heat and mass transfer models to determine T_c and Φ_c as functions of bipolar plate temperature, Nernst potential, cell voltage, current density, and water transport across membrane. Some conclusions from the results in Figure 3 are noted below.

- For given pressure (P), i_L in Figure 3b increases with increase in $P(O_2)$. However, for given $P(O_2)$, i_L in Figure 3b and 3c is smaller at greater pressures because of the inverse dependence of O₂ gas phase diffusivity on pressure. The decrease in i_L is less than proportional to 1/P, implying that non-Fickian diffusion controls mass transport resistance.
- At constant $X(O_2)$, i_L in Figure 3d increases with increase in pressure because of higher $P(O_2)$. The increase in i_L is somewhat less than proportional to $P(O_2)$, implying that mass transport resistance also increases with $P(O_2)$.
- Dependence of i_L on T_c in Figure 3e is greater than $T^{3/2}$, confirming that processes other than Fickian diffusion are rate controlling, particularly O₂ permeability through the ionomer film on the catalyst particles.

- For given T_c , i_L in Figure 3f is highest at an intermediate relative humidity in CCL (ϕ_c^*) indicating that CCL floods for $\phi_c > \phi_c^*$. Figure 3f shows that ϕ_c^* increases at higher T_c .

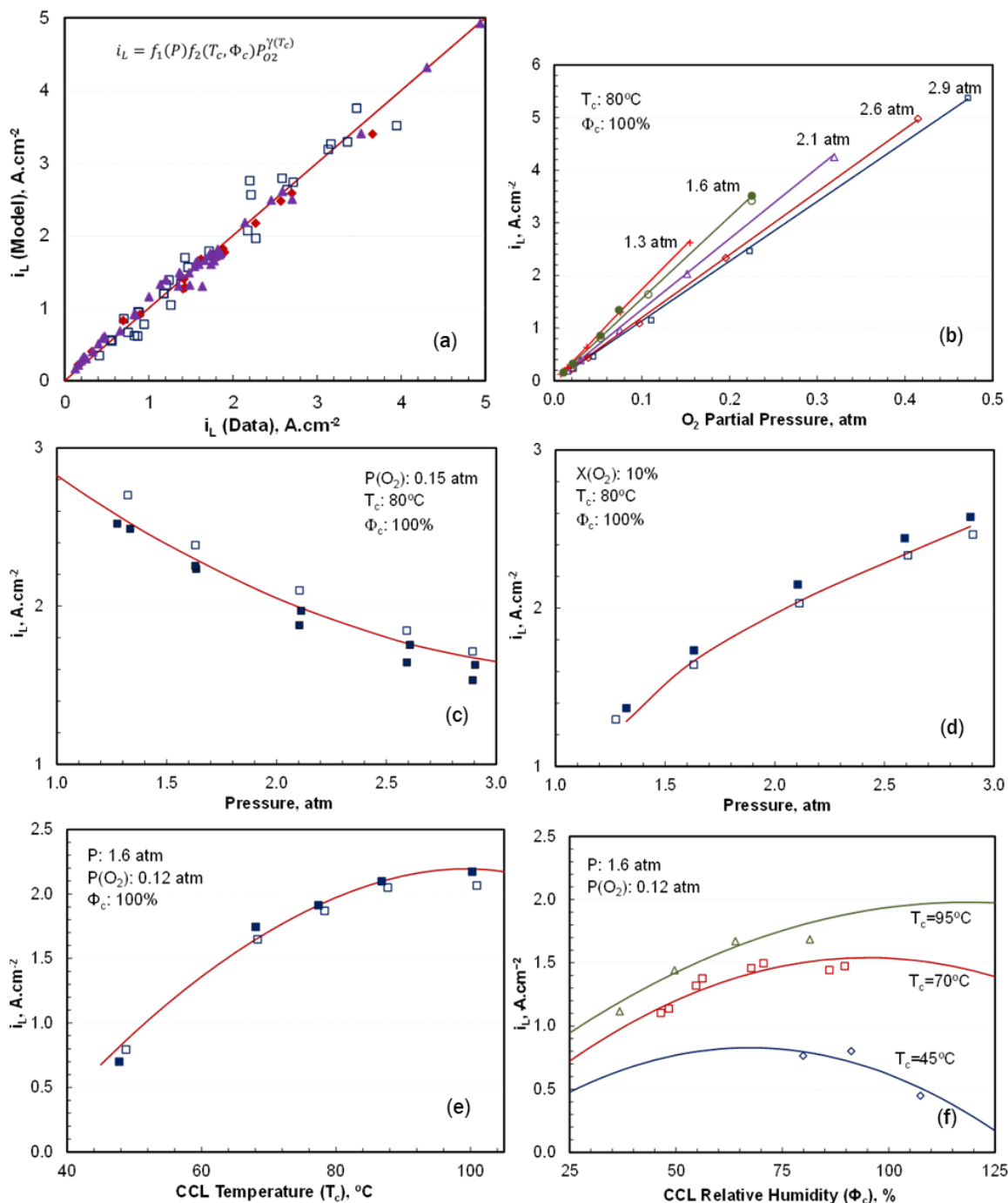


Figure 3. Oxygen mass transfer and limiting current density: (a) limiting current density model calibration; (b) effect of operating pressure and oxygen partial pressure; (c) effect of operating pressure for fixed $P(O_2)$; (d) effect of operating pressure for fixed $X(O_2)$; (e) effect of CCL temperature; and (f) effect of CCL relative humidity

Following the methodology formulated previously [2, 3], we developed an integral cell model using the differential cell data in Figure 2 and Figure 3 to evaluate the performance and cost of an automotive fuel cell system with the SOA d-PtCo/C catalyst relative to 2020 targets of 65% peak efficiency, $Q/\Delta T$ of 1.45 kW/K,

and \$40/kW cost. The Pt loadings are 0.1 mg/cm² in the cathode catalyst and 0.025 mg/cm² in the anode catalyst. The 850-EW PFSA membrane is 14 μm thick, chemically stabilized, and mechanically reinforced. All other main attributes of the system components and operating conditions are summarized in Table 1.

Table 1. Rated Power Performance of FCS with SOA Alloy Catalysts

Stack Parameters	2018 FCS with d-PtCo/C Catalyst	2017 FCS with d-PtNi/C Catalyst
Membrane	Ionomer: 850 EW PFSA with chemical additive Substrate: Mechanical reinforcement Thickness: 14 μm	Ionomer: 850 EW PFSA with chemical additive Substrate: Mechanical reinforcement Thickness: 14 μm
Cathode Catalyst	d-Pt ₃ Co/C (0.1 mg _{Pt} /cm ²), EW=950, I/C=1.0	Electrode: d-PtNi ₃ (0.1 mg _{Pt} /cm ²), acid washed Ink: organic, EW=850, I/C=1.0
Anode Catalyst	Pt/C (0.025 mg _{Pt} /cm ²)	Pt/C (0.025 mg _{Pt} /cm ²)
Stack Gross Power	88.5 kW	88.1 kW
Stack Voltage (Rated)	250 V	250 V
Number of Active Cells	380 cells (also 381 cooling cells)	377 cells (also 376 cooling cells)
Stack Gross Power Density	3.07 kW/L	2.84 kW/L
Stack Gross Specific Power	3.73 kW/kg	3.45 kW/kg
Stack Inlet Pressure	2.5 bar	2.5 bar
Stack Coolant Temperature	85°C (inlet), 95°C (outlet)	84°C (inlet), 94°C (outlet)
Stack Air Inlet/Outlet RH	Inlet: 51% RH at 85°C; Outlet: 77% RH at 95°C	Inlet: 75% RH at 84°C; Outlet: 100% RH at 94°C
Stack Fuel Inlet/Outlet RH	Inlet: 42% RH at 95°C; Outlet: 160% RH at 85°C	Inlet: 42% RH at 94°C; Outlet: 100% RH at 84°C
Cathode/Anode Stoichiometry	1.5 (cathode) / 2.0 (anode)	1.5 (cathode) / 2.0 (anode)
Cell Area	197 cm ² (active), 320 cm ² (total)	213 cm ² (active), 346 cm ² (total)
Cell Voltage	657.1 mV	663 mV
Current Density	1.8 A/cm ²	1.651 A/cm ²
Crossover Current Density	4.2 mA/cm ² @ 80°C, 100% RH, 1 atm P _{H₂}	4.2 mA/cm ² @ 80°C, 100% RH, 1 atm P _{H₂}
Power Density	1183 mW/cm ²	1095 mW/cm ²
Balance of Plant		
Humidifier Membrane Area	0.68 m ²	0.8 m ²
Air Pre-cooler Heat Duty	6.3 kW	6.3 kW
CEM Motor and Motor Controller Heat Duty	3.1 kW	3.0 kW
Main Radiator Heat Duty	87.3 kW	78.9 kW
CEM Power	Compressor shaft power: 10.4 kW Expander shaft power out: 4.5 kW Net motor and motor controller: 7.4 kW _e	Compressor shaft power: 10.3 kW Expander shaft power out: 4.7 kW Net motor and motor controller: 7.0 kW _e
Fan and Pump Parasitic Power	0.6 kW _e (coolant pump), 0.3 kW _e (H ₂ recirculation pump), 0.345 kW _e (radiator fan)	0.5 kW _e (coolant pump), 0.3 kW _e (H ₂ recirculation pump), 0.345 kW _e (radiator fan)

Figure 4a presents the cost of the fuel cell system at different stack inlet pressures and stack coolant outlet temperatures. The results in Figure 4a confirm the FY 2017 landmark conclusion that at high manufacturing volume (500,000 units/year), the projected system cost can be 46.0 ± 0.7 \$/kW_e at 2.5 atm stack inlet pressure and 95°C stack coolant outlet temperature. Removing the membrane humidifier slightly reduces the system cost at 2.5 atm stack inlet pressure. These results are based on Strategic Analysis, Inc.’s 2018 cost correlation that includes a \$2.01/kW_e increase for manufacturing bipolar plates and MEAs, added controls for extended durability, and compressor-expander-motor module price inflation [4].

Pending model validation against data from a 50-cm² integral cell, the results in Figure 4a should be regarded as preliminary. The error bars reflect variance of kinetic data in random and controlled tests and include degradation between the two series of tests. We also estimated the system cost at lower manufacturing volumes as 51 \$/kW_e at 100,000 units/year, and 88 \$/kW_e at 10,000 units/year.

In Figure 4, (b) and (c) present the modeled stack and FCS platinum utilization and confirm the FY 2017 results that the stack Pt utilization (9.5 ± 0.5 kW_e/g) with the SOA catalyst exceeds the DOE target (8.0 kW_e/g). Even on a system basis, the modeled FCS Pt utilization (8.5 ± 0.4 kW_e/g) exceeds the stack target. The results indicate that stack inlet pressures greater than 2.0 atm are needed to meet the Pt utilization target.

Figure 4d presents the modeled stack power density and confirms the FY 2017 result that with the SOA catalyst the gross stack power density ($1,180 \pm 55 \text{ mW/cm}^2$) greatly exceeds the target ($1,000 \text{ mW/cm}^2$) at low Pt loading (0.125 mg-Pt/cm^2 total). Also, stack inlet pressures greater than 2.0 atm are needed to meet the power density target.

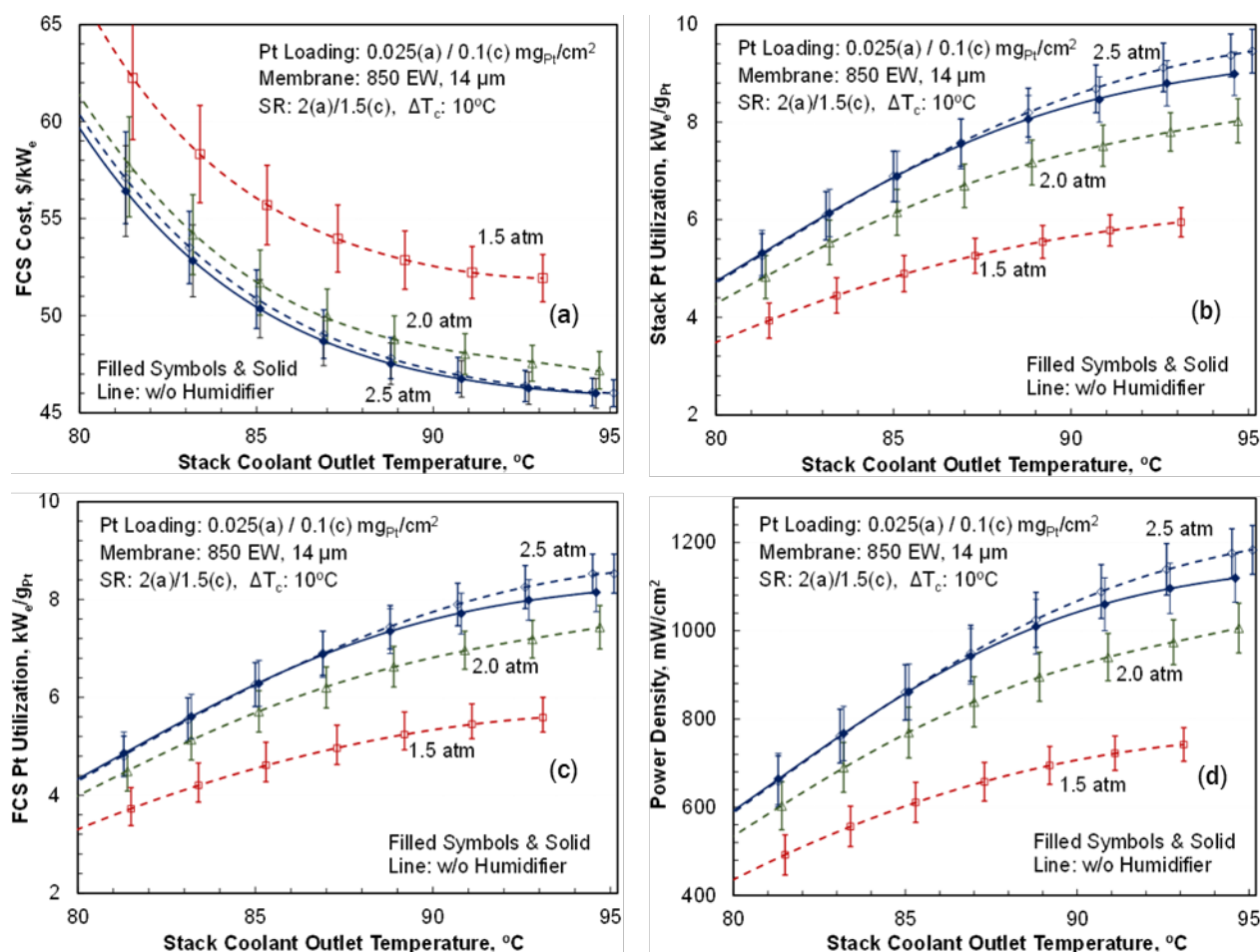


Figure 4. FCS performance with SOA d-PtCo/C cathode electrode: (a) FCS cost at high-volume manufacturing (50,000 units/year); (b) stack Pt utilization; (c) FCS Pt utilization; (d) stack power density

CONCLUSIONS AND UPCOMING ACTIVITIES

- We have shown that minimal controls are needed to extend stack durability by maintaining the cell voltage below 0.85 V during idle and to implement protected shutdown strategies by depleting O₂ in the cathode channels during shutdown, ensuring that damaging H₂-air fronts cannot form in the anode channels during subsequent start-up.
- We demonstrated that SOA d-Pt₃Co/high-surface-area carbon cathode catalysts in MEAs can lead to power densities exceeding the 2020 target of $1,000 \text{ mW/cm}^2$ at 0.125 g/kW_e PGM content under operating conditions (95°C , $<100\%$ outlet relative humidity, SR(c) = 1.5, 2.5 atm stack inlet pressure) required to meet the heat rejection constraint ($Q/\Delta T = 1.45 \text{ kW/}^\circ\text{C}$). We also showed that stack Pt utilization exceeding the target of $8.0 \text{ kW}_e/\text{gPt}$ can be achieved with this catalyst system.
- We confirmed the FY 2017 landmark conclusion that at high manufacturing volume (500,000 units/year), the projected system cost can be $46.0 \pm 0.7 \text{ } \$/\text{kW}_e$ at 2.5 atm stack inlet pressure and 95°C stack coolant outlet temperature. This projection is based on Strategic Analysis, Inc.’s 2018 cost

correlation that includes \$2.01/kW_e increase for manufacturing bipolar plates and MEAs, added controls for extended durability, and compressor-expander-motor module price inflation. At reduced manufacturing volumes, the projected costs increase to \$51/kW_e at 100,000 units per year and \$88/kW_e at 10,000 units per year.

- Our future work will focus on durability of low-loaded d-PtCo/C catalysts under cyclic potentials and on automotive drive cycles.

FY 2018 PUBLICATIONS/PRESENTATIONS

1. R.K. Ahluwalia, “Performance and Durability of Advanced Automotive Fuel Cell Stacks and Systems with Dispersed Alloy Cathode Catalyst in Membrane Electrode Assemblies,” 2017 Technology Collaboration Program on Advanced Fuel Cells—Topical Meeting on Catalysis, Berlin, Germany, November 14, 2017.
2. R.K. Ahluwalia and N. Garland, “Reports from the Annexes: Annex 34: Fuel Cells for Transportation,” 55th ExCo Meeting, Berlin, Germany, November 14–17, 2017.
3. R.K. Ahluwalia, D.D. Papadias, N.N. Kariuki, J.-K. Peng, X. Wang, Y. Tsai, D.G. Graczyk, and D.J. Myers, “Potential Dependence of Pt and Co Dissolution from Platinum-Cobalt Alloy PEFC Catalysts Using Time-Resolved Measurements,” *Journal of the Electrochemical Society* 165, no. 6 (2018): F3024–F3035.
4. R.K. Ahluwalia, F.C. Cetinbas, J.-K. Peng, N.N. Kariuki, and D.J. Myers “Reconstruction and Modeling of Electrode Microstructure Using Nano X-ray Computed Tomography,” 2017 Fuel Cell Consortium for Performance and Durability Meeting, Southfield, Michigan, July 19, 2017.
5. R.K. Ahluwalia, X. Wang, and D.D. Papadias, “Performance and Stability of Bipolar Plates for Automotive Fuel Cells,” Shanghai Jiaotong University, Shanghai, China, September 26, 2017.
6. R.K. Ahluwalia, X. Wang, and J.-K. Peng, “Performance and Durability of Advanced Automotive Fuel Cell Stacks and Systems with Dispersed Alloy Cathode Catalyst in Membrane Electrode Assemblies,” FY 2017 Annual Progress Report, DOE Hydrogen and Fuel Cells Program, DOE/GO-102017-5042, February 2018.
7. R.K. Ahluwalia, X. Wang, and J.-K. Peng, “Performance and Durability of Advanced Automotive Fuel Cell Stacks and Systems with Dispersed Alloy Cathode Catalyst in Membrane Electrode Assemblies,” Topical Meeting on Catalysis, IEA Energy Technology Network, Technology Collaboration Program on Advanced Fuel Cells, Berlin, Germany, November 15, 2017.
8. R.K. Ahluwalia, X. Wang, J.-K. Peng, and D.D. Papadias, “Fuel Cell System Modeling and Analysis,” US Drive Fuel Cell Tech Team Meeting, Southfield, Michigan, February 21, 2018.
9. R.K. Ahluwalia, X. Wang, J.-K. Peng, N.N. Kariuki, D.J. Myers, S. Rasouli, P.J. Ferreira, Z. Yang, A. Martinez-Bonastre, D. Fongalland, and J. Sharman, “Durability of De-Alloyed Platinum-Nickel Cathode Catalyst in Low Platinum Loading Membrane-Electrode Assemblies Subjected to Accelerated Stress Tests,” *Journal of the Electrochemical Society* 165, no. 6 (2018): F3316–F3327.
10. R.L. Borup, R. Mukundan, S. Stariha, D.A. Langlois, R. Ahluwalia, D.D. Papadias, B. Sneed, K.L. More, and S.S. Kocha, “Cathode Carbon Corrosion and Electrode Layer Compaction in PEM Fuel Cells,” 232nd Electrochemical Society Meeting, National Harbor, Maryland, October 1–6, 2017.
11. F.C. Cetinbas, N.N. Kariuki, R.K. Ahluwalia, H.T. Chung, P. Zelanay, and D.J. Myers, “PGM-Free Electrode Microstructure Analysis and Transport Modeling,” 232nd Electrochemical Society Meeting, National Harbor, Maryland, October 1–6, 2017.
12. F.C. Cetinbas, X. Wang, R.K. Ahluwalia, N.N. Kariuki, R.P. Winarski, Z. Yang, J. Sharman, and D.J. Myers, “Microstructural Analysis and Transport Resistances of Low-Platinum-Loaded PEFC Electrodes,” *Journal of the Electrochemical Society* 164, no. 14 (2017): F1596–F1607.

13. N. Kariuki, D.D. Papadias, D.J. Myers, and R.K. Ahluwalia, "Insights into Platinum-Cobalt Electrochemical Dissolution from Platinum-Cobalt Alloy Polymer Electrolyte Fuel Cell Fuel Cell Cathode Catalysts Using Online ICP-MS," 232nd Electrochemical Society Meeting, National Harbor, Maryland, October 1–6, 2017.
14. L. Osmieri, X. Wang, F. Cetinbas, H.T. Chung, X. Yin, S. Kabir, D.J. Myers, P. Zelenay, R. Ahluwalia, and K.C. Neyerlin, "Operando Determination of Oxygen Reduction Reaction Kinetics on PGM-Free Electrocatalysts in a PEFC," 233rd Electrochemical Society Meeting, Seattle, Washington, May 13–17, 2018.
15. D.D. Papadias, R.K. Ahluwalia, N.N. Kariuki, D.J. Myers, K.L. More, D.A. Cullen, B. Sneed, R. Mukundan, R.L. Borup, K.C. Neyerlin, and S.S. Kocha, "Durability of Pt-Co Alloy Cathode Catalysts for PEM Fuel Cells Under Cyclic Potentials," 232nd Electrochemical Society Meeting, National Harbor, Maryland, October 1–6, 2017.
16. D.D. Papadias, R.K. Ahluwalia, N.N. Kariuki, D.J. Myers, K.L. More, D.A. Cullen, B.T. Sneed, K.C. Neyerlin, R. Mukundan, and R.L. Borup, "Durability of Pt-Co Alloy Polymer Electrolyte Fuel Cell Cathode Catalysts Under Accelerated Stress Tests," *Journal of the Electrochemical Society* 165, no. 6 (2018): F3166–F3177.
17. X. Wang, J.-K. Peng, and R.K. Ahluwalia, "Using Differential Cell Data to Predict the Performance of Integral Automotive Fuel Cells," Shanghai Jiaotong University, Shanghai, China, September 26, 2017.
18. X. Wang, R.K. Ahluwalia, J.-K. Peng, F.C. Cetinbas, and D.D. Papadias, "Performance and Durability of Automotive Fuel Cell Stack and System," Research & Advanced Technology, SAIC Motor Corporation Limited, Shanghai, China, September 25, 2017.
19. L. Xin, F. Yang, J. Xie, Z. Yang, N. N. Kariuki, D. J. Myers, J.-K. Peng, X. Wang, R.K. Ahluwalia, K. Yu, P.J. Ferreira, A.M. Bonastre, D. Fongalland, and J. Sharman, "Enhanced MEA Performance for PEMFCs under Low Relative Humidity and Low Oxygen Content Conditions via Catalyst Functionalization," *Journal of the Electrochemical Society* 164, no. 6 (2017): F674–F684.

REFERENCES

1. R.K. Ahluwalia, and X. Wang, "Rapid Self-Start of Polymer Electrolyte Fuel Cell Stacks from Subfreezing Temperatures," *J. Power Sources* 162 (2006): 502–512.
2. R.K. Ahluwalia, X. Wang, and J.-K. Peng, "Fuel Cell System Modeling and Analysis," DOE Hydrogen and Fuel Cells Program, 2017 Annual Merit Review and Evaluation Meeting, FC017, Washington, D.C., June 5–9, 2017.
3. R.K. Ahluwalia, X. Wang, and A.J. Steinbach, "Performance of Advanced Automotive Fuel Cell Systems with Heat Rejection Constraint," *J. Power Sources* 309 (2016): 178–191.
4. B.D. James, J.M. Huya-Kouadio, and C. Houchins, "Fuel Cell Systems Analysis," 2018 DOE Hydrogen and Fuel Cells Program Review, FC163, Washington, D.C., June 15, 2018.

Fuel Cell Systems Analysis

Brian D. James (Primary Contact),
Jennie M. Huya-Kouadio, Cassidy Houchins,
Daniel A. DeSantis
Strategic Analysis, Inc.
4075 Wilson Blvd Suite 200
Arlington, VA 22203
Phone: (703) 778-1114
Email: bjames@sainc.com

DOE Manager: Gregory Kleen
Phone: (240) 562-1672
Email: Gregory.Kleen@ee.doe.gov

Contract Number: DE-EE0007600

Subcontractors:

- Argonne National Laboratory, Lemont, IL
- National Renewable Energy Laboratory, Golden, CO

Project Start Date: October 1, 2016
Project End Date: September 30, 2021

Overall Objectives

- Provide thorough, annually updated assessment of the technical status of current on-road and advanced (2020 and 2025) proton exchange membrane (PEM) fuel cell (FC) power systems for light-duty, medium-duty, and heavy-duty vehicles (LDVs, MDVs, HDVs) and buses, detailed to the extent necessary to track system performance and manufacturability.
- Report cost estimates of the fuel cell systems (FCSs) described above to reflect optimized components and manufacturing processes at various rates of production, and update these on an annual basis.
- Conduct sensitivity analyses of FCS cost and identify key system cost parameters with the goal of fully understanding the cost drivers.
- Identify most promising pathways to system/life cycle cost reduction.
- Perform review of all components of the analysis, both internally and with the help of perspectives external to the project, and document analysis assumptions and results

through presentations and a complete, comprehensive report.

Fiscal Year (FY) 2018 Objectives

- Update 2017, 2020, and 2025 automotive FCS cost projections to reflect the latest performance data and system design information.
- Conduct an MDV fuel cell electric truck (FCET) cost analysis based on system design and performance studies completed in 2017.
- Evaluate the cost of electrospun materials for use in the membrane electrode assembly.

Technical Barriers

This project addresses the following technical barrier from the Fuel Cells section of the Fuel Cell Technologies Office Multi-Year Research, Development, and Demonstration Plan¹:

(B) Cost.

Technical Targets

Table 1 shows the DOE technical targets and current project status.

FY 2018 Accomplishments

- Projected the FCS cost for an 80 kW_{net} LDV application using a Design for Manufacture and Assembly (DFMA) methodology to be \$47/kW_{net} for 2018, \$44/kW_{net} for 2020, and \$39/kW_{net} for 2025 at 500,000 vehicles produced per year, reaching the DOE target of \$40/kW_{net} by 2025.
- Cost modeled an MDV FCS (160 kW_{net}), resulting in \$98/kW_{net} for 2018, \$91/kW_{net} for 2020, and \$80/kW_{net} for 2025 projections at an annual production rate of 100,000 vehicles per year.

¹ <https://energy.gov/eere/fuelcells/downloads/fuel-cell-technologies-office-multi-year-research-development-and-22>

Table 1. DOE Technical Targets for 80-kWe (net) (kW_{net}) Integrated Transportation Fuel Cell Power Systems Operating on Direct Hydrogen

Characteristic	Units	Project Status	DOE 2025 Targets	DOE Ultimate Target
Cost of transportation fuel cell power systems ^a	\$/ kW_{net}	47	40	30
Cost of transportation fuel cell stacks ^a	\$/ kW_{net}	19	20	15
Cost of bipolar plates ^a	\$/ kW_{net}	5	3	NA
Air compression system cost ^a	\$/system	850	500	NA
Cathode humidifier system cost ^a	\$/system	60	100	NA

^a Based on high production volume of 500,000 vehicles per year

INTRODUCTION

This project assesses the cost and performance impact of research advancements on fuel cells for transportation using a DFMA-style [1] cost analysis methodology. Results from this analysis provide assistance to the Fuel Cell Technologies Office in assessing the impact of current project portfolios and in identifying areas where R&D is still needed to address shortfalls in meeting cost targets. Low-temperature PEM FCSs operating on hydrogen with peak electrical capacities of current (2018) and future (2020 and 2025) of 80 kW_{net} for LDV and 160 kW_{net} for MDV applications are analyzed. Onboard compressed hydrogen storage, battery energy storage, and traction drive motor subsystems are not included in this cost assessment. To examine the difference between a nascent and a mature product manufacturing base, LDV FCSs are analyzed at 1,000, 10,000, 20,000, 50,000, 100,000, and 500,000 FCSs per year. MDV FCSs are analyzed at 200, 500, 1,000, 10,000, 50,000, and 100,000 FCSs per year.

Fuel cell stack and balance of plant designs and performance parameters are discussed, and the methods of modeling each are explained. New technologies, materials data, and optimization modeling are incorporated to provide updated system cost. Cost trends are evaluated in terms of the capital costs per unit of installed electrical capacity (\$/kW_{net}) and system annual production rate.

APPROACH

A DFMA-style analysis is conducted to estimate the manufacturing cost of PEM FCSs for 80 kW_{net} LDVs. Argonne National Laboratory (ANL) first principles fuel cell performance models [2] and Strategic Analysis, Inc. (SA) DFMA cost models are used to identify cost and performance optimized conditions, which are then vetted by the U.S. DRIVE Fuel Cell Tech Team. Output from the ANL model provides insight into cell voltage, stack pressure, cathode catalyst loading, air stoichiometry, and stack outlet coolant temperature. The DFMA cost model provides insight into cost and performance tradeoffs. The FCS is sized to provide 80 kW_{net} based on rated power operating parameters. System performance is based on performance estimates of individual components, built up into an overall system energy budget.

DFMA process-based cost estimation techniques are applied to the major system components (and other specialty components) such as the fuel cell stack, membrane humidifier, air compressor/expander/motor unit, and hydrogen recirculation ejectors. For each of these, a manufacturing process train details the specific manufacturing and assembly machinery, and processing conditions are identified and used to assess component cost. The costs of lesser components are determined by price quote or analogy to similar commercial components.

RESULTS

The final 2018 system cost results for the LDV and MDV FCSs are described in this report. Full analysis assumptions and results are available in SA's 2018 Final Report [3]. A graphical comparison of system cost results at all production volumes appears in Figure 1.

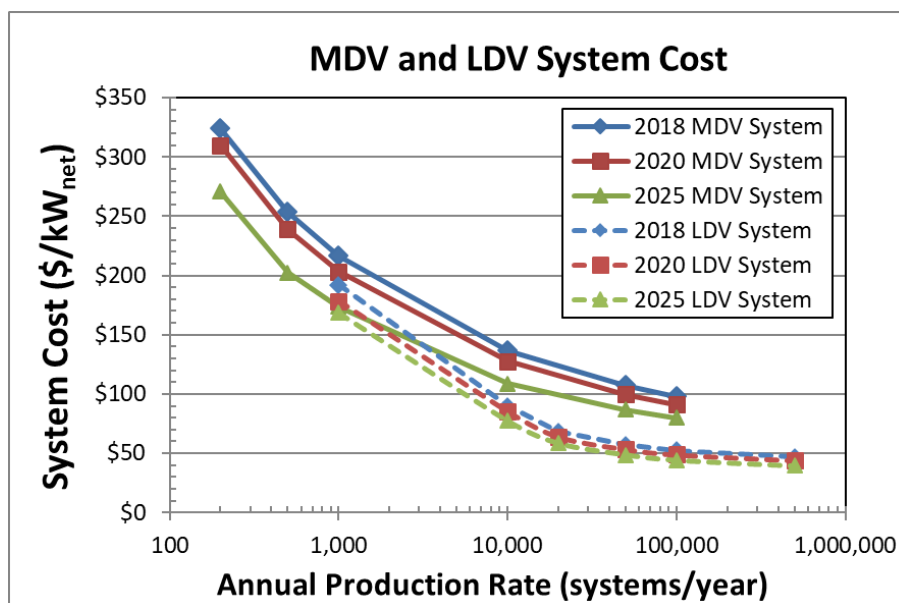


Figure 1. MDV and LDV system cost at each production rate for 2018, 2020, and 2025 systems

2018 Baseline Automotive System Cost

The operating conditions and assumptions used to project costs for the 2018, 2020, and 2025 auto systems are summarized in Table 2. An overall increase in projected system cost occurred between 2017 and 2018 (previously \$45/kW_{net}, now \$47/kW_{net} at 500,000 systems per year [sys/yr]). The same catalyst utilized in 2017 (de-alloyed platinum cobalt on high-surface-area carbon [PtCo/HSC]) [4] was used for 2018; however, more relevant experimental data of this catalyst provided by General Motors was incorporated into ANL's performance model. This led to an increase in power density from 1,095 mW/cm² to 1,183 mW/cm², reducing total system cost ~\$0.90/kW_{net}. Despite this reduction in cost, multiple changes were made in 2018 to improve the validity of the cost model resulting in an overall cost increase for the 2018 system. Air valves were added to prevent air backflow and to provide stack isolation during shutdown. The largest cost impact was inflation adjustment of the air compression system cost, ~\$1.70/kW_{net}, which had been erroneously constant for multiple years. Although this does not reflect a technological advancement, it is necessary in order to project a realistic cost for the 2018 LDV FCS. The air compression system is one of the most cost-sensitive components in the FCS, as seen in the tornado chart in Figure 2.

2020 and 2025 Future Automotive System Cost

The system parameters chosen for the 2020-year analysis assume reasonable and attainable performance and manufacturing methods that have been demonstrated at lab scale. In contrast, the system parameters for the 2025-year system are based on aggressive/optimistic technology advances, that is, advances that might be possible in approximately 2025 if there was a focused/well-funded effort (or possibly in a later year if development efforts are not focused or well-funded).

Between the current and future year studies, performance is assumed to increase while simultaneously reducing Pt loading. Assuming 1,500 mW/cm² power density with only 0.088 mg/cm² Pt loading, the 2025 auto system cost (\$39/kW_{net} at 500,000 sys/yr) now meets the 2025 DOE target of \$40/kW_{net}. However, achievement of the 2025 power density target may require a new higher-performing and/or lower-loaded catalyst.

Table 2. PEM Fuel Cell Auto Systems Operating Conditions and Assumptions

Auto System Year	2017	2018	2020	2025
System gross power (kW _{net})	87.90	88.37	88.37	88.37
System net power (kW _{net})	80	80	80	80
Power density (mW/cm ²)	1,095	1,183	1,260	1,500
Cell voltage (mV)	663	657	657	657
Stack temp. (coolant exit temp.) (°C)	94	95	95	95
Pressure (atm)	2.5	2.5	2.5	2.5
Pt loading (mg/cm ²)	0.125	0.125	0.125	0.088
Platinum group metal total content (g/kW _{gross})	0.124	0.115	0.108	0.064
Air stoichiometry	1.5	1.5	1.5	1.5
Cathode catalyst system ^a	Disp. PtCo/HSC	Disp. PtCo/HSC	Disp. PtCo/HSC	Disp. adv. high perf. catalyst
Cells per system	377	380	380	380
Total system cost (\$/kW _{net}) (100,000 sys/yr)	\$50	\$52	\$49	\$44
Total system cost (\$/kW _{net}) (500,000 sys/yr)	\$45	\$47	\$44	\$39

^a Disp. = Dispersed. All years assume dispersed Pt/C on the anode.

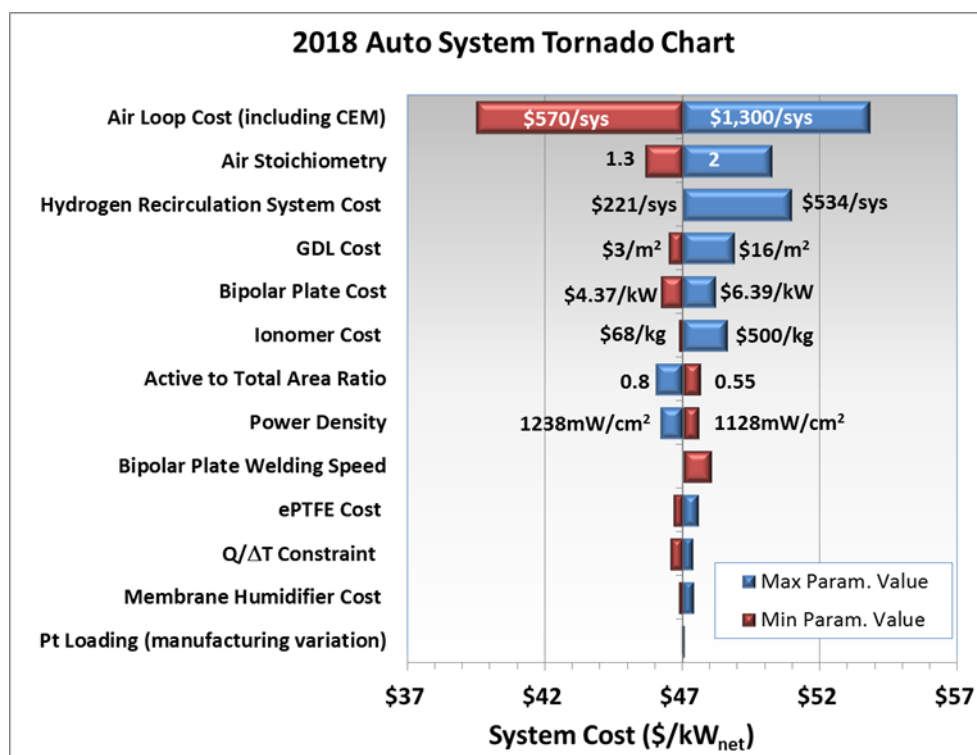


Figure 2. 2018 auto system tornado chart showing air loop cost (including compressor/expander/motor [CEM]) being the most sensitive cost component

2018 MDV Fuel Cell Electric Truck System Cost

To determine the system design for MDV FCETs and to assess their similarities to bus FCSs, information was gathered on current FCET demonstration projects. SA chose a fuel-cell-dominant 160 kW_{net} Class 6 MDV system as the baseline type of truck on which to perform a detailed DFMA cost analysis. In a fuel-cell-dominant system, the fuel cell is sized for the peak sustained power and the battery is only for short-term power augmentation. The system utilizes two 80-kW stacks and thus offers synergies with LDV stacks. Feedback from bus FCS manufacturers suggests that the FCSs in buses, with minor adjustments, could be used in FCETs. From this input, the system was designed to be quite similar to a fuel cell bus system. The parameters contained in Table 3 were used to define the systems analyzed for the 2018 DFMA cost estimate. Because the Toyota Mirai stacks have been demonstrated in a fuel cell heavy-duty truck [5], a few of the operating parameters for the truck system (such as Pt loading ~30 g Pt/stack [6], stack pressure, and temperature) were aligned with the Mirai system. Similar to the bus system, the FCET operating temperature is lower than that of the LDV system so as to reduce degradation and increase longevity of the stack. The power density was derived from ANL's performance modeling for the de-alloyed PtCo/HSC catalyst. A range in production volume from 200 to 100,000 systems per year reflects a demonstration size fleet (at the low end) up to a mass-produced system (at the high end) likely supplied to multiple truck integrators.

Table 3. PEM Fuel Cell Bus and MDV FCET Systems Operating Conditions and Assumptions

System Analyzed	2016 Bus	2018 MDV	2020 MDV	2025 MDV
Annual production (FCSs/year)	200–1,000	200–100,000	200–100,000	200–100,000
Target stack durability (hours)	25,000 [7]	25,000 [7] / 5,000 [8]	25,000 [7] / 5,000 [8]	25,000 [7] / 5,000 [8]
Total Pt loading (mg Pt/cm ² total area)	0.5	0.35	0.35	0.3
PGM total content (g/kW _{gross})	0.719	0.321	0.316	0.242
Power density (mW/cm ²)	739	1,178	1,200	1,350
Cell voltage (V/cell)	0.659	0.68	0.68	0.68
Net power (kW _{net})	160	160	160	160
Gross power (kW _{gross})	195	196	189	185
Operating pressure (atm)	1.9	2.4	2.4	2.4
Stack temp (coolant exit temp) (°C)	72	63 ^a	63 ^a	63 ^a
Total system cost (\$/kW _{net}) (100,000 sys/yr)	NA	\$97	\$90	\$81

^a Lower temperature selected for durability

2020 and 2025 MDV Fuel Cell Electric Truck System Cost

Given that FCETs are in their infancy, currently only used in demonstration projects, there is interest and uncertainty as to the configuration and technology for future year systems. Compared to the 2018 FCET baseline system design, the modeled 2020 and 2025 systems assume a more advanced air compression system with an expander. The gross power is thus smaller than for the baseline, leading to lower-cost systems. The assumed performance projections are based on the team's best engineering judgment, with consideration of current Mirai performance, assumed truck operating conditions, and the improvements expected in LDV polarization performance.

Electrospun Membrane and Catalyst Materials

As a side study to the baseline system, SA analyzed three different electrospun material sets: (1) membrane support (direct replacement of expanded polytetrafluoroethylene [ePTFE]), (2) co-spun membrane support and ionomer, and (3) Pt catalyst. Many of the assumptions used in the analysis came from open source documentation [9, 10] and discussions with experts from 3M and Vanderbilt University. Quotes for high-volume electrospinning production equipment were obtained from Inovenso and Elmarco.

Electrospun nanofiber mats made of a polyphenylsulfone (PPSU) membrane support material are projected to be \sim $\$1/\text{m}^2$ compared to $\$6/\text{m}^2$ for the price of ePTFE mats at high production volume. These electrospun membrane supports are projected to replace ePTFE for the 2020 and 2025 LDV FCSs. A co-spun support and ionomer membrane is modeled as a dense Nafion layer reinforced with PPSU nanofibers. It is compared to the baseline ePTFE-supported Nafion membrane manufactured using a Gore Direct-Coat method. The electrospun catalyst is modeled as d-PtCo/HSC and is compared to a slot die coating process. Figure 3 shows various combinations of the three material sets to estimate the total price of a catalyst-coated membrane. The lowest price ($\$/\text{m}^2$) catalyst-coated membrane at 500,000 sys/yr is comprised of an electrospun PPSU support with a Gore Direct-Coat membrane coating technique to coat Nafion, and slot die coated catalyst for the cathode and anode. All methods listed in Figure 3 have similar cost at high manufacturing rates. If electrospun materials perform better than conventional catalyst-coated membranes (seen in work by Vanderbilt [11]), there can be a reasonable cost savings in the stack.

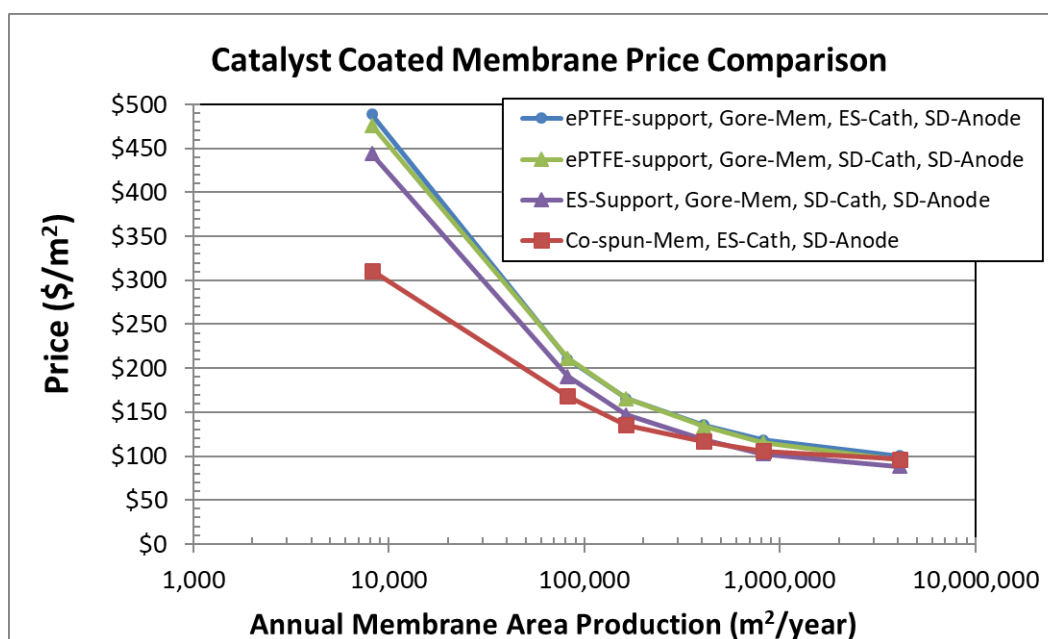


Figure 3. Comparison of catalyst-coated membrane prices with electrospun or conventional components (ES – electrospun, SD – slot die coated)

CONCLUSIONS AND UPCOMING ACTIVITIES

- The estimated cost for an $80 \text{ kW}_{\text{net}}$ automotive FCS is $\$47/\text{kW}_{\text{net}}$ at 500,000 sys/yr . When projecting the cost utilizing future year technology, it is estimated to be $\$44/\text{kW}_{\text{net}}$ in 2020, and $\$39/\text{kW}_{\text{net}}$ in 2025, meeting the DOE 2025 target of $\$40/\text{kW}_{\text{net}}$.
- FCSs for MDV/HDV trucks are expected to be very similar to buses. When designed for fuel-cell-dominant operation, a $160 \text{ kW}_{\text{net}}$ MDV FCS is estimated to cost $\$97/\text{kW}_{\text{net}}$ at 100,000 sys/yr . Future projections for MDV FCS cost are $\$90/\text{kW}_{\text{net}}$ for 2020 and $\$81/\text{kW}_{\text{net}}$ for 2025 at 100,000 sys/yr .
- Electrospun PPSU fibrous supports can be lower price compared to an ePTFE membrane support. Co-spun Nafion and support membranes and electrospun catalysts are estimated to be very similar in price to conventional membranes and electrodes. Given the same or better performance, electrospun materials can present a price reduction opportunity for the stack.

- Future work includes evaluation of high-speed roll-to-roll cell assembly (2-D manufacturing), review of the cost impact of various stack durability methods, estimation of the cost to recycle and dispose a fuel cell membrane electrode assembly, and continued evaluation of air compression systems.

FY 2018 PUBLICATIONS/PRESENTATIONS

1. B.D. James, J.M. Huya-Kouadio, and C. Houchins, “Mass Production Cost Estimation of Direct H₂ PEM Fuel Cell Systems for Transportation Applications: 2017 Update,” Strategic Analysis report for DOE Fuel Cell Technologies Office, September 30, 2017.
2. J.M. Huya-Kouadio, B.D. James, and C. Houchins, “Meeting Cost and Manufacturing Expectations for Automotive Fuel Cell Bipolar Plates,” Presentation at the 2017 Fuel Cell Seminar, November 2017.
3. B.D. James, J.M. Huya-Kouadio, and C. Houchins, “Medium & Heavy-Duty PEM Fuel Cell Electric Truck Analysis: A Comparison with Fuel Cell Electric Buses and Light-Duty Vehicles and Their Potential to Lower Costs in Early Market,” Presentation at the 2017 Fuel Cell Seminar, November 2017.
4. J.M. Huya-Kouadio, B.D. James, and C. Houchins, “Meeting Cost and Manufacturing Expectations for Automotive Fuel Cell Bipolar Plates,” Fuel Cell Seminar Conference Article, *Electrochemical Society Transactions*, December 2017.
5. B.D. James, J.M. Huya-Kouadio, and C. Houchins, “Fuel Cell Vehicle Cost Analysis,” Presented to the Fuel Cell Technical Team, Southfield, MI, February 21, 2018.
6. B.D. James, “2018 Cost Projections of PEM Fuel Cell Systems for Automobiles and Medium-Duty Vehicles,” DOE Fuel Cell Technologies Office webinar presentation, April 25, 2018.
7. B.D. James, J.M. Huya-Kouadio, C. Houchins, and D.A. DeSantis, “2017 DOE Hydrogen and Fuel Cells Program Review: Fuel Cell Systems Analysis,” Presented at the 2018 DOE Hydrogen and Fuel Cells Program Annual Merit Review Meeting, Washington, DC, June 15, 2018.

REFERENCES

1. Geoffrey Boothroyd, Peter Dewhurst, and Winston A. Knight, *Product Design for Manufacture and Assembly, Third Edition* (Boca Raton: CRC Press, Taylor & Francis Group, 2011).
2. Rajesh Ahluwalia, “Fuel Cell Systems Analysis,” Presented at the DOE Fuel Cell Tech Team, Southfield, MI, February 21, 2018.
3. B.D. James, J.M. Huya-Kouadio, and C. Houchins, “Mass Production Cost Estimation of Direct H₂ PEM Fuel Cell Systems for Transportation Applications: 2018 Update,” Strategic Analysis report for DOE Fuel Cell Technologies Office, December 31, 2018.
4. Anusorn Kongkanand and Mark F. Mathias, “The Priority and Challenge of High-Power Performance of Low Platinum Proton-Exchange Membrane Fuel Cells,” *Physical Chemistry Letters* 7 (2016): 1127–1137.
5. “Toyota Opens a Portal to the Future of Zero Emission Trucking,” Toyota News Release (April 19, 2017). Accessed June 21, 2018: <http://corporatenews.pressroom.toyota.com/releases/toyota+zero+emission+heavyduty+trucking+concept.htm>.
6. P. Ruiz, “Three Challenges Confronting the Toyota Mirai Fuel Cell Vehicle,” *The Fuze* (November 10, 2015). Accessed June 21, 2018: <http://energyfuse.org/three-challenges-confronting-the-toyota-mirai-fuel-cell-vehicle/>.
7. Jacob Spendelow and Dimitrios Papageorgopoulos, “Fuel Cell Bus Targets,” DOE Fuel Cell Technologies Program Record #12012 (September 12, 2012). Accessed June 27, 2018: https://www.hydrogen.energy.gov/pdfs/12012_fuel_cell_bus_targets.pdf.
8. “Medium- & Heavy-Duty Fuel Cell Electric Truck: Action Plan for California,” Report written by the California Fuel Cell Partnership (October 2016). Accessed June 27, 2018: <http://cafcp.org/sites/default/files/MDHD-action-plan-2016.pdf>.

9. Peter Pintauro, “Composite Membranes, Methods of Making Same, and Applications of Same,” U.S. Patent 9,350,036 B2, filed August 6, 2012, and issued May 24, 2016.
10. Jason Ballengee, “Preparation of Nanofiber Composite Proton Exchange Membranes from Dual Fiber Electrospun Mats,” *Journal of Membrane Science* 442 (2013): 187–195.
11. Peter Pintauro, “Fuel Cell Membrane-Electrode-Assemblies with Ultra-Low Pt Nanofiber Electrodes,” Presented at the DOE Hydrogen and Fuel Cells Program Annual Merit Review Meeting, Washington DC, June 6, 2017.

Technology Acceleration and Hydrogen Infrastructure R&D Overview

INTRODUCTION

Technology Acceleration and Hydrogen Infrastructure R&D focuses on accelerating the transition of early-stage hydrogen and fuel cell research to subsequent stages of development and leveraging the private sector to enable commercialization and deployment. Examples include integration of hydrogen production technologies with the electricity grid, lowering the cost of manufacturing hydrogen and fuel cell technologies, reducing the cost of hydrogen transport and distribution, and reducing the cost and improving reliability of hydrogen fueling stations and the supporting infrastructure component supply chain. Key focus areas of early-stage R&D include (1) enabling hybrid energy systems that integrate nuclear power with hydrogen production, (2) evaluating and improving the long-term durability of megawatt-scale electrolyzer and fuel cell technologies, (3) reducing the costs of manufacturing electrolyzers and fuel cells through innovations in membrane synthesis and coating, as well as novel methods of quality control and assurance during the manufacturing process, (4) developing novel approaches to enhance efficiency and scalability of hydrogen liquefaction, (5) developing affordable, efficient, and reliable methods of hydrogen compression (such as non-mechanical methods), (6) improving the accuracy and reliability of hydrogen fueling station technologies, and (7) enhancing materials compatibility to improve durability and lower cost of key components of hydrogen infrastructure (e.g., pipelines, dispensing hoses, and storage vessels). Techno-economic analysis is used to identify drivers of hydrogen cost and barriers to widespread growth, which inform Program planning and portfolio development.

In fiscal year (FY) 2018, Technology Acceleration and Hydrogen Infrastructure R&D accomplishments included advances in hydrogen compression and liquefaction, and in hydrogen fueling for medium- and heavy-duty applications. For example, the National Renewable Energy Laboratory (NREL) completed experimental validation of the innovative pressure consolidation strategy developed by Argonne National Laboratory (ANL). Pressure consolidation is an approach to optimize the operation of hydrogen fueling stations that are supplied by tube trailers, such that the capital cost of compression at the station can be reduced by up to 40%.¹ Additionally, R&D projects in the formerly named Technology Validation subprogram portfolio completed more than 15,000 hours of durability testing of low-temperature electrolyzer technologies and collected data on 27 fuel cell electric buses, demonstrating that fuel cell buses have exceeded the DOE and U.S. Department of Transportation durability targets.

In August 2018, the Program hosted the H2@Scale End Use Applications Fuel Cell Truck Powertrain R&D Activities and Target Review with subject matter experts and stakeholders to assess the status, challenges, and opportunities for fuel cell truck applications. This meeting was used to inform technical targets for the use of hydrogen and fuel cells in medium- and heavy-duty transportation. Additionally, in September 2018, the Program hosted the annual International Hydrogen Infrastructure Workshop to identify the current status of technology and key R&D challenges through feedback from key industry and government stakeholders in the United States, Japan, Germany, and Scandinavia. Feedback from these meetings and workshops is being used to guide Program strategy in FY 2019.

OBJECTIVES

Key objectives for Technology Acceleration and Hydrogen Infrastructure R&D include the following.

- By 2019, achieve compression of hydrogen to 875 bar using electrochemical cells and metal hydride materials at ≤ 4 kWh/kg.

¹ For more information, please see: https://www.energy.gov/sites/prod/files/2017/11/f46/cto_nov17_h2_scale_session_elgowainy.pdf

- By 2020, establish the potential for magnetocaloric technologies to liquefy hydrogen at twice the energy efficiency of conventional liquefaction plants.
- By 2020, develop manufacturing techniques to reduce the cost of automotive fuel cell stacks at high volume (500,000 units/year) to \$20/kW (from the 2008 value of \$38/kW).
- By 2025, conduct early-stage R&D to enable technologies that reduce the cost of hydrogen delivery and dispensing to \$7/kg.

FY 2018 TECHNOLOGY STATUS AND ACCOMPLISHMENTS

In FY 2018, Technology Acceleration and Hydrogen Infrastructure R&D made significant progress to advance cost-competitive hydrogen production and delivery technologies and establish the viability of hydrogen use in emerging applications. The current cost of hydrogen production and delivery ranges from \$13–\$16/gge (gallon of gasoline equivalent, approximately equal to 1 kg of hydrogen on a lower heating value basis).² The Fuel Cell Technologies Office’s target for the cost of hydrogen production and delivery is \$7/gge by 2025.³ The targeted cost of hydrogen production is \$2/gge,⁴ and the target cost of hydrogen delivery and dispensing therefore is \$5/gge. In support of this target, Program R&D focused on enabling hydrogen production within hybrid energy systems and improving the reliability and lowering the footprint of hydrogen fueling station technologies. The Program also completed an analysis identifying one R&D pathway to achieving the Program’s target for the cost of hydrogen production and delivery by 2025 (see Figure 1).⁵

A key focus of the DOE’s H2@Scale initiative is advancing technologies that can be used in hybrid energy systems, wherein hydrogen production is integrated with electricity generators and transmission to lower cost and support grid resiliency. Previous accomplishments in this area have included technology acceleration R&D that established the ability of electrolyzers to meet the performance requirements for responsive load and ancillary services on the grid. In 2018, R&D focus areas were broadened to include development of test capabilities for emerging high-temperature electrolysis technologies that can monetize process heat from nuclear power plants. Integration of high-temperature electrolysis with nuclear power can increase the capacity factors of nuclear power generators and reduce the electrical energy consumption of electrolysis by up to 25%.⁶ Another key R&D focus was to enable manufacturing technologies that can reduce the capital cost of electrolyzers at the scales needed for emerging applications. While electrolyzers are commonly manufactured at kilowatt scales for small-scale (<100 kg/day) consumers of hydrogen, megawatt-scale units are required in emerging applications, such as the integration of electrolyzers with the grid (i.e., “power-to-gas”) and hydrogen fueling stations. An additional R&D focus area was to lower the costs of hydrogen distribution and fueling infrastructure. Project goals included improving the reliability of hydrogen compression and dispensing, improving the accuracy of hydrogen meters, and reducing the footprint of hydrogen fueling stations.

² https://www.hydrogen.energy.gov/pdfs/15011_low_volume_production_delivery_cost.pdf

³ https://www.hydrogen.energy.gov/pdfs/15012_hydrogen_early_market_cost_target_2015_update.pdf

⁴ https://www.hydrogen.energy.gov/pdfs/12001_h2_pd_cost_apportionment.pdf

⁵ This analysis is documented in Hydrogen and Fuel Cells Program Record 18003:

https://www.hydrogen.energy.gov/pdfs/18003_current_status_hydrogen_delivery_dispensing_costs.pdf

⁶ For more information on the electrical energy consumption of low- and high-temperature electrolysis, please see the H2A case studies available here: <https://www.nrel.gov/hydrogen/h2a-production-case-studies.html>

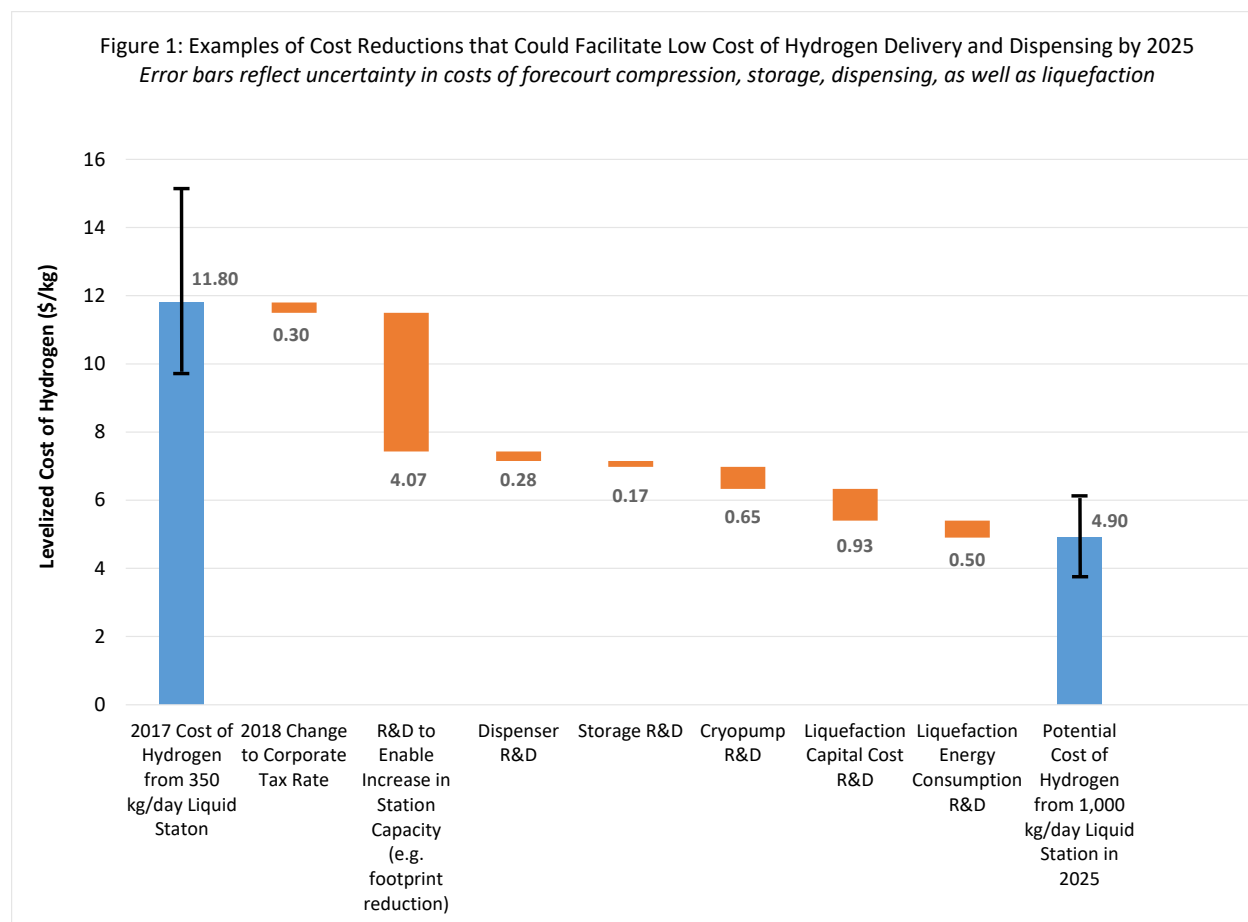


Figure 1. Examples of R&D that can reduce the cost of hydrogen delivery and dispensing to \$5/kg by 2025, from the 2017 projected cost of \$11.80/kg from a 350 kg/day station supplied by liquid hydrogen. Detailed information is included in the DOE Hydrogen and Fuel Cells Program Record 18003.

ACCOMPLISHMENTS

Technology Acceleration and Hydrogen Infrastructure R&D accomplishments in FY 2018 include the following.

- The Program awarded three new projects through the Small Business Innovation Research program, focused on developing novel membranes with sufficient durability for 875-bar electrochemical hydrogen compression, and non-destructive evaluation technologies for stationary pressure vessels.
- In collaboration with the Hydrogen Fuel R&D and Fuel Cell R&D subprograms and with industry input, the Program developed technical targets for the cost and performance of medium- and heavy-duty vehicles powered by fuel cells. Key metrics included fuel cell costs, vehicle fill time, storage cycle life, and fuel cell life.
- In collaboration with the Safety, Codes and Standards and Hydrogen Fuel R&D subprograms, the Program initiated activities to launch the Hydrogen Materials Compatibility (H-Mat) national laboratory consortium. H-Mat will conduct materials research to reduce the costs and enhance the durability of steels and polymers in hydrogen service.
- One of the 27 prototype fuel cell electric buses undergoing performance evaluation by NREL exceeded DOE's ultimate target for fuel cell durability of 25,000 hours. Twelve have exceeded 19,000 hours to

date. NREL has been collecting data on bus maintenance costs and hydrogen consumption and completed its annual report on status versus targets.⁷

Key project-level accomplishments in FY 2018 include the following.

Station Technologies

- GVD Corporation determined that its novel coatings for hydrogen compressor seals reduce seal erosion by 70%. GVD's coatings comprise polymeric and inorganic layers that enhance seal flexibility and lubricity and are expected to reduce hydrogen permeation by 10-fold.
- Giner ELX achieved the highest known efficiency of 350-bar electrochemical hydrogen compression: 4 kWh/kg, at an inlet pressure of 100 bar and outlet pressure of 350 bar. Giner's compressor concept relies on novel aromatic membranes that achieve 30% less drag than conventional perfluorosulfonic acid membranes and 50% less back diffusion.
- Ivys Energy Solutions established that its approach to wireless communication between vehicles and fueling stations, using digital short-range communication, can exceed the requirements of the SAE International J2799 standard. Ivys also established that its novel metering technology, based on Coriolis meters, can achieve an accuracy of at least 2%.

Materials Compatibility

- Researchers at Sandia National Laboratories, Oak Ridge National Laboratory, and the National Institute of Standards and Technology completed fatigue testing of X100 base metal and welds in 210-bar hydrogen. The data generated can be used to enable use of X100 steels in hydrogen pipelines, which could reduce initial capital cost by more than 40% relative to conventional X52 steels. The team's analyses also identified microstructural features of steel, such as high-angle grain boundaries, that may reduce crack growth rates by 4–5 times.

Liquid Hydrogen Technologies

- Pacific Northwest National Laboratory designed an approach to integrate variable diversion flow valves with a regenerator for magnetocaloric materials that will ultimately be used to liquefy hydrogen at twice the efficiency of conventional liquefaction. Variable diversion flow valves enable optimization of the amount of heat transfer fluid that passes through each layer of materials. Each layer achieves a different temperature when the regenerator is operating and experiences different amounts of heat transfer from the layers above and below. The ability to precisely control the amount of fluid that each layer experiences is therefore essential to the concept's success.

Manufacturing R&D

- NREL and Gore scanned two rolls of fuel cell membrane material on a web-line optical research apparatus at NREL to obtain a 2-dimensional thickness map (at ~1 mm spatial resolution). This map can be easily analyzed to locate where thickness is above or below defined thresholds for quality control. In-line mapping of thickness will help enable high-volume manufacturing and cost reduction of membranes for fuel cells and electrolyzers. Preliminary discussions to perform a more extensive study of membrane thickness distributions have begun.
- NREL used roll-to-roll coating to develop gas diffusion electrodes approximately 200 times faster and with superior performance compared to spray-coated electrodes. Electrodes manufactured with roll-to-roll techniques, unlike spray coating, do not require an ionomer film to be sprayed onto the catalyst layer

⁷ The report summarizing data on fuel cell bus performance is available here: <https://www.nrel.gov/docs/fy19osti/72208.pdf>

to maximize performance, which eliminates additional material costs (no need for extra ionomer and solvents) and reduces manufacturing time (fewer processes).

- Mainstream Engineering, NREL, and the Georgia Institute of Technology deployed prototype optical systems using cross-polarized light to monitor membrane films continuously for simultaneous film thickness mapping and defect detection at speeds up to 300 ft/min on polyethylene terephthalate. This technique provides real-time automated in-line defect and thickness mapping and will help improve the manufacturing process by providing real time feedback, increasing reproducibility, and reducing labor costs.

Fuel Cell Technology Validation

- ANL completed performance evaluation of the Toyota Mirai under varying conditions, including outside temperature (-7°C to 35°C). A final report from the project has been published here: <https://publications.anl.gov/anlpubs/2018/06/144774.pdf>.

Hybrid Energy Systems R&D

- Idaho National Laboratory completed installation of a test stand for 25-kW high-temperature electrolyzers. High-temperature electrolyzers have the potential to utilize heat from nuclear power plants to produce hydrogen with up to 30% less electricity than low-temperature electrolysis. Key metrics that must be validated include long-term durability, particularly when energy supply is variable.
- Significant innovations were incorporated into the development and operation of a hydrogen fueling station operated by the Natural Energy Laboratory Hawaii Authority (NELHA). For instance, the Hawaii Natural Energy Institute developed a tool to simulate electrolyzer performance as a function of key parameters (e.g., operating pressure and temperature, current density, membrane thickness, hydration factor) and developed another tool that simulates grid integration of electrolysis. The team also integrated a booster compressor with NELHA's fueling station that can recover up to 90% of the hydrogen in 450-bar tube trailers, reducing delivery costs by up to 50%.

New Project Selections

In FY 2018, the Program added the following new projects through a funding opportunity announcement (FOA).

- Four projects will focus on integration of electrolyzers with renewable energy and hydrogen distribution infrastructure, electrolysis of wastewater, production of synthetic fuels, and autonomous fueling of vehicles.⁸ (Equilon Enterprises, dba Shell Oil Products US; Plug Power; Giner, Inc; Skyre, Inc.)
- Four projects will conduct R&D that reduces the costs of manufacturing electrolyzer components, using advanced techniques such as additive manufacturing. (3M Company; University of Tennessee Space Institute; University of Connecticut; Clemson University)
- One project will develop innovative concepts to improve efficiency and reduce the capital cost of hydrogen liquefaction, using a vortex tube concept. (Washington State University)
- Two projects will develop innovative cryocooler concepts to reduce the footprint of hydrogen fueling stations. (NREL; Gas Technologies Institute).
- One project will perform metal hydride materials discovery for nonmechanical hydrogen compression, in collaboration with the Hydrogen Materials Advanced Research Consortium. (Greenway Energy)

⁸ Projects were selected to comply with FY 2018 congressional direction.

BUDGET

The FY 2018 budget for Technology Acceleration and Hydrogen Infrastructure R&D projects totaled about \$35 million. The funding breakout is shown in Figure 2 and includes \$19 million appropriated for Technology Acceleration, which includes \$3 million for Manufacturing R&D. Hydrogen delivery R&D funding (\$16 million) is included in the breakout below to be consistent with the President's budget request and FY 2019 appropriations, both of which defined a new Hydrogen Infrastructure R&D subprogram line item, which includes hydrogen delivery R&D. The budget emphasized new project selections in the areas of electrolyzer manufacturing, integrated energy systems, hydrogen chillers, compressors, and liquefaction technologies, in support of H2@Scale and congressional direction. In some cases, such as liquefaction and compression, FY 2018 funding is minimal because ongoing projects are being funded by prior year appropriations. The budget also represents launch of the H-Mat consortium on early-stage materials compatibility R&D via a lab call at the end of FY 2018. Finally, the budget included ongoing R&D from FOA selections in previous years in fueling station technologies and fuel cell manufacturing.

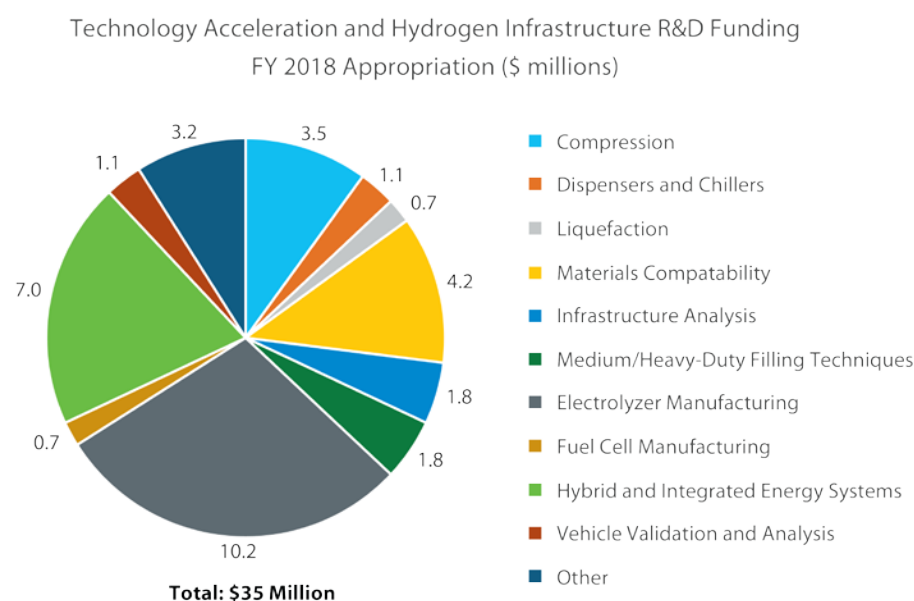


Figure 2. Technology Acceleration and Hydrogen Infrastructure R&D FY 2018 appropriation

UPCOMING ACTIVITIES AND PLANS

The future plans for Technology Acceleration and Hydrogen Infrastructure R&D, pending funding appropriations, include the following.

- Expand early-stage R&D on materials compatibility through the H-Mat Consortium. R&D beginning in FY 2019 focuses on enhancing the toughness of high-strength steels with potential for use in 875-bar pressure vessels, enhancing the durability of polymers used in hydrogen seals, and understanding the effects of water vapor on hydrogen embrittlement in aluminum alloys. A key focus in FY 2019 will be expanding stakeholder engagement with H-Mat.
- Expand R&D on technologies for medium- and heavy-duty hydrogen filling. Efforts in FY 2019 will be guided by technical targets for filling technologies and techniques that were developed in FY 2018 through analysis and stakeholder engagement. R&D will build on filling techniques being investigated in

a cooperative research and development agreement project that was selected for DOE cost match in FY 2018.

- Continue to leverage cross-office and cross-agency R&D opportunities and resources, including expanded collaboration with the National Science Foundation, the DOE Office of Basic Energy Sciences, and Advanced Research Projects Agency-Energy.

Fred Joseck

Technology Acceleration and Hydrogen Infrastructure R&D Manager

Fuel Cell Technologies Office

Office of Energy Efficiency and Renewable Energy

U.S. Department of Energy

1000 Independence Ave., SW

Washington, DC 20585-0121

Phone: (202) 586-7932

Email: Fred.Joseck@ee.doe.gov

Fuel Cell Membrane Electrode Assembly Manufacturing R&D

Michael Ulsh (Primary Contact), Guido Bender, Peter Rupnowski, and Scott Mauger
National Renewable Energy Laboratory (NREL)
15013 Denver West Parkway
Golden, CO 80401
Phone: (303) 275-3842
Email: michael.ulsh@nrel.gov

DOE Manager: Nancy Garland
Phone: (202) 586-5673
Email: Nancy.Garland@ee.doe.gov

Subcontractors:

- Lawrence Berkeley National Laboratory, Berkeley, CA
- Colorado School of Mines, Golden, CO
- Tufts University, Medford, MA
- General Motors, Pontiac, MI
- W.L. Gore & Associates, Elkton, MD
- Mainstream Engineering, Rockledge, FL
- Proton OnSite, Wallingford, CT

Project Start Date: July 16, 2007

Project End Date: Project continuation and direction determined annually by DOE

Overall Objectives

- Perform early-stage development of real-time characterization techniques relevant to membrane electrode assembly (MEA) component critical material properties and validate these techniques under relevant fabrication conditions.
- Study the effects of MEA component fabrication variations on MEA performance and lifetime to understand the required characteristics of real-time characterization systems.
- Develop models to predict the effects of local variations in MEA properties and to improve our understanding of excitation modes during real-time characterization.
- Study material-process-performance relationships for MEA materials in scalable processes, providing guidance for new process development to partners.

Our development activities will continue to be fully informed by input from industry. As new technologies emerge and needs change, the directions of this project will be adjusted.

Fiscal Year (FY) 2018 Objectives

- Complete in situ drive cycle testing on MEAs with membrane defects.
- Demonstrate coating of electrodes using processes with different shear behaviors to understand the impact of process shear on catalyst layer morphology and performance.
- Complete the design, construction, and operation of a test bed to facilitate studies of illumination, detection, and material interactions for membrane thickness imaging.
- Perform initial ink development and coating of unsupported catalyst systems.
- Characterize the influence of catalyst ink composition on ink rheology and stability.
- Determine the feasibility of using an optical-reflectance-based technique for imaging the loading of Pt in standard Pt/C electrodes, in accordance with the following criteria: (1) electrodes having loading within the range of 0.05–0.4 mg Pt/cm², (2) sensitivity to differences in loading of 0.1 mg Pt/cm², and (3) imaging at a speed of at least 1 inch/sec.

Technical Barriers

This project addresses the following technical barriers from the Manufacturing R&D section of the Fuel Cell Technologies Office Multi-Year Research and Development Plan¹:

- (A) Lack of High Volume MEA Processes
- (E) Lack of Improved Methods of Final Inspection of MEAs
- (H) Low Levels of Quality Control.

¹ <https://www.energy.gov/eere/fuelcells/downloads/fuel-cell-technologies-office-multi-year-research-development-and-22>

Contribution to Achievement of DOE Manufacturing Milestones

This project contributes to the achievement of the following DOE milestones from the Manufacturing R&D section of the Fuel Cell Technologies Office Multi-Year Research and Development Plan:

- Milestone 1.6: Develop fabrication and assembly processes for polymer electrolyte membrane fuel cell (PEMFC) MEA components leading to an automotive fuel cell stack that costs \$20/kW. (4Q, 2020)
- Milestone 5.5: Develop correlations between manufacturing parameters and manufacturing variability, and performance and durability of MEAs. (4Q, 2018)
- Milestone 5.6: Demonstrate methods to inspect full MEAs and cells for defects prior to assembly into stacks in a production environment. (4Q, 2018)
- Milestone 5.7: Develop areal techniques to measure platinum (and other catalyst metals) quantitatively in an MEA. (4Q, 2018)

FY 2018 Accomplishments

NREL accomplished the following in FY 2018:

- Demonstrated high sensitivity of thermal scanning to the thickness of membranes already attached/laminated to gas diffusion electrodes (GDEs) using half-cell materials fabricated by General Motors (GM).
- Completed the design, construction, and operational testing of an in-line test bed for real-time membrane thickness imaging and demonstrated the technique in-line using a state-of-the-art reinforced membrane.
- Performed full-width, full-length high-resolution optical imaging of Gore membrane production rolls, and developed automated defect detection and classification algorithms.
- Designed and built an optical inspection apparatus on the web-line, creating a highly flexible test bed for reflectance or transmission measurements.

- Performed in situ studies of the impacts of electrode and membrane irregularities on the performance and failure of MEAs, supported by X-ray computed tomography (XCT) measurements made by Lawrence Berkeley National Laboratory (LBNL).
- Coated electrodes under different shear conditions to understand the impact of process physics on morphology and performance.
- Performed rheology, zeta potential, and stability studies of unsupported (low-temperature electrolysis [LTE] and platinum-group metal [PGM]-free) and supported catalysts.
- Completed feasibility study of optical methods to image loading in Pt/C electrodes.
- Demonstrated roll-to-roll casting of ionomer membranes.
- Assisted Mainstream Engineering in validating their prototype optical inspection system in-line on our coating line using as-cast membrane materials.
- Demonstrated the through-plane reactive excitation (TPRE) technique on the research web-line; LBNL modeled improved methodologies.
- Continued collaboration with our industry partners in accordance with our project charter.

INTRODUCTION

In FY 2005–FY 2007, NREL provided technical support to DOE in developing a new key program activity: manufacturing R&D for hydrogen and fuel cell technologies. This work included a workshop on manufacturing R&D, which gathered inputs on technical challenges and barriers from the fuel cell industry, and subsequent development of a roadmap for manufacturing R&D. In late FY 2007, NREL initiated a project to assist the fuel cell industry in addressing these barriers, initially focusing on in-line quality control of MEA components.

APPROACH

NREL and its partners are addressing the DOE manufacturing milestones listed above by performing early-stage R&D in the areas of real-time characterization, understanding the performance and lifetime impacts of irregularities in MEA materials originating during fabrication and handling, and elucidating how material and fabrication parameters impact MEA performance. We utilize industry relationships to understand MEA material, structure, and processing directions and challenges. We then develop real-time characterization techniques, using computational modeling to (a) assist in the development and optimization of unique measurement techniques, and (b) predict the effects of material irregularities on performance. These techniques are validated under simulated processing conditions. In parallel, we use specialized in situ testing to perform detailed parametric studies of the effects of material irregularities on performance and lifetime. We also explore material-process-performance relationships in the scalable fabrication of MEA materials.

RESULTS

We continued our effort to study the in situ effects of pinholes, using membrane samples mechanically punched using a 120 μm micro-needle. We completed an initial set of spatial initial performance (with the segmented cell), prolonged performance, and accelerated stress test (AST)/failure studies. Figure 1 shows results from the catalyst-coated membrane (CCM)-type samples. Figure 1 (left) is an XCT image of a fabricated MEA, showing the as-tested morphology of the pinhole. Figure 1 (center) shows the spatial initial performance effect of the pinhole (located in the center of the MEA) from the segmented cell testing, where red color indicates a decrease in performance in that segment in the defected cell as compared to a pristine cell. Figure 1 (right) shows the results of a combined chemical-mechanical AST, where we see earlier failure of the pinhole MEA as compared to the pristine MEA. And in drive cycle testing (not shown), we see increased performance degradation of the pinhole MEA compared to the pristine MEA. We also studied the impact of electrode defects, namely thin and thick spots. For thin spots, we observed similar performance degradation to that of bare spots, including failure in the drive cycle test when using a 25 μm membrane (as opposed to a 50 μm membrane, which did not fail). Interestingly, this brings up the possibility that the effects of these defects may be due to behaviors at the edges or interfaces of the defects, rather than absolute reduction in catalyst material. For thick spots, we observed high levels of performance degradation, almost always leading to failure during the cycling test (where the pristine did not fail).

We studied the feasibility of using an optical-based technique for imaging the loading of Pt in standard Pt/C electrodes ranging in Pt loading from 0.05 to 0.4 mg/cm^2 . We explored both reflectance and transmission modes and obtained different results for different cases of measurement mode, configuration, and sample type. Ultimately, methods with the criteria sensitivity (to variations of 0.1 mg/cm^2) at the criteria measurement speed (at least 1 m/min) were successfully developed. As an example, Figure 2 shows optical reflectance signal as a function of Pt loading for a series of ultrasonically sprayed CCMs. Over a range of loading from 0.5 to 0.35 mg/cm^2 , the differences in the data at 0.1 mg/cm^2 intervals were statistically significant.

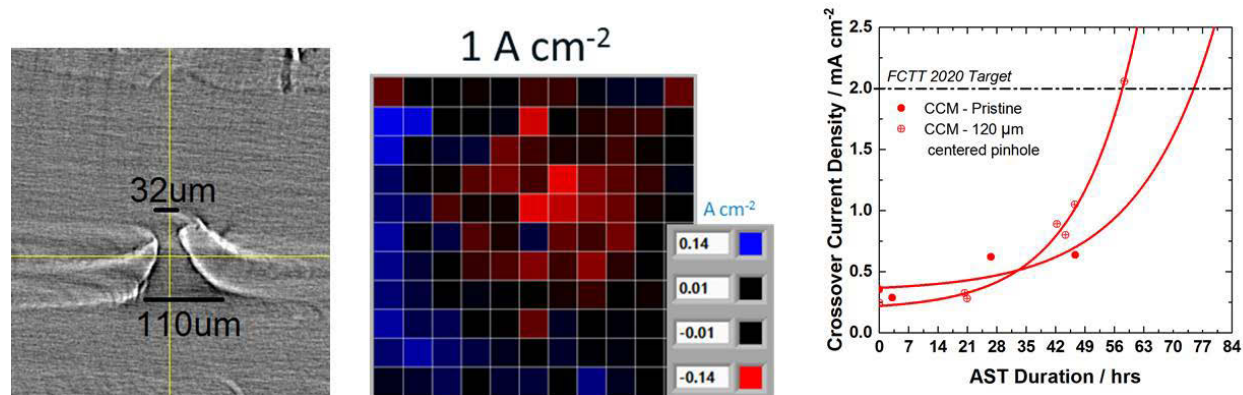


Figure 1. XCT imaging of the pinhole in the fabricated MEA (left), segmented cell data showing local performance variation resulting from the pinhole (center), and results from the AST test, showing measured hydrogen crossover current density as a function of AST hours (right)

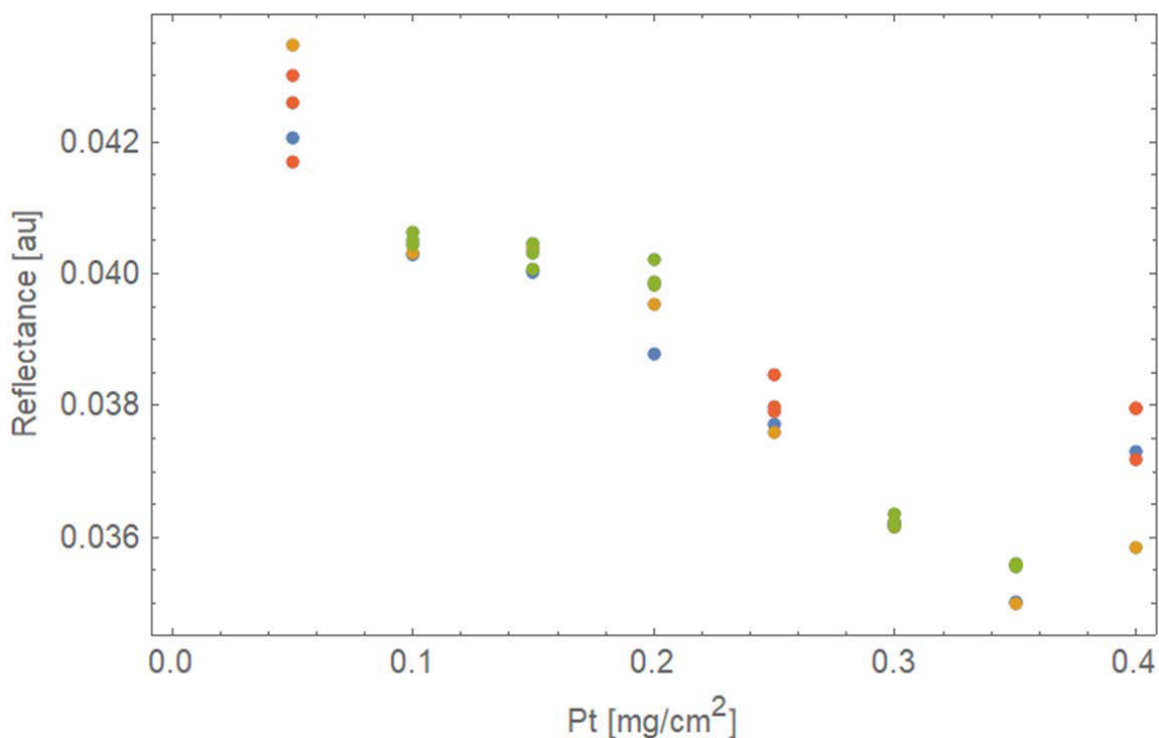


Figure 2. Optical reflectance signal as a function of Pt loading for CCM samples

With regard to our work on infrared methods, we demonstrated a moving-substrate configuration for TPPE using a web sample with individual catalyst-coated sections with pinholes in the membrane. Thermal responses due to the pinholes were detected; however, they were typically less than 1°C. Subsequent modeling at LBNL indicated that small increases in reactive gas hydrogen concentration results in significant increases in temperature rise, so a follow-on experiment is contemplated using such gas mixtures to further explore the potential for the technique. Other beneficial modifications to the equipment setup were also modeled. We also performed analysis of the thermal scanning data from the new series of half-cell (membrane on GDE) samples fabricated by GM. The analysis showed that the responses were statistically significant and proportional to thickness.

We initiated a study of the rheology and stability of unsupported catalyst inks in a 1:1 water/n-propanol solvent. Figure 3 shows rheology as a function of solids loading (left) and zeta potential as a function of ionomer-to-carbon (I:C) ratio (right). Similar to Pt/C inks, we see an increase in structure (agglomeration) and shear-thinning behavior with increasing solids loading. We also observe the change from shear-thinning to Newtonian behavior with the addition of ionomer. We also studied the rheology of Ni-C and Ni-Fe catalyst inks. Similar to the case of supported catalysts, we observe that water-rich inks have lower viscosity than alcohol-rich inks. However, we see the unexpected result that unsupported catalysts with high surface area do not always behave similarly to inks made with carbons of similar surface area.

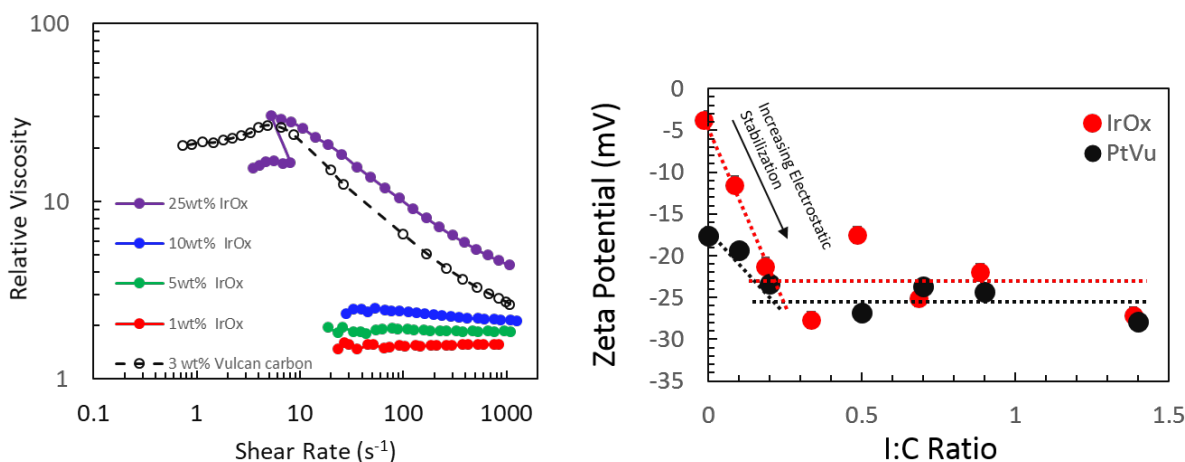


Figure 3. Relative viscosity of IrOx inks of different solids loading as a function of shear rate (left) and zeta potential of IrOx (red) and Pt/Vulcan (black) catalysts as a function of I:C

Finally, we characterized the influence of ink composition stability. We have also begun studying the physical stability of various catalyst inks and how different catalysts and formulations affect the rate of agglomeration and sedimentation of catalyst particles. For this work, we built a new measurement setup to continuously monitor the optical transmission of catalyst inks. Figure 4 shows results of an IrO_x catalyst ink, where initially the catalyst particles are well dispersed, and transmission is low. However, at around 20 minutes after cessation of ink mixing, the top of the vial has very high transmission, indicating that the catalyst particles have already sedimented out of this region.

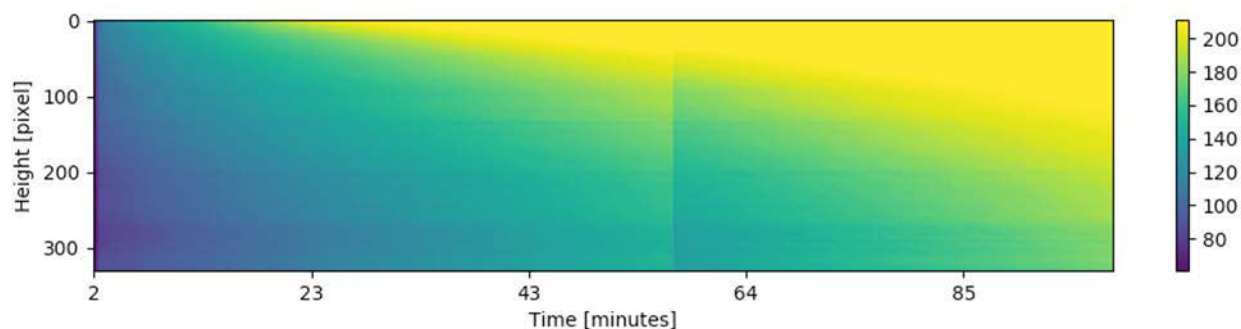


Figure 4. Temporal data for transmission of an IrOx ink from the ink stability testing device

CONCLUSIONS AND UPCOMING ACTIVITIES

- Perform ink development studies of unsupported LTE catalysts to understand the influence of solvent and catalyst materials on ionomer-catalyst interactions.
- Perform initial defect detection tests for LTE membranes using existing test beds.

- Perform studies to understand the impact of electrode coating irregularities and pinholes in membranes, with particular focus on how their effects are modulated by aspects of membrane architecture, e.g., thickness and presence of reinforcing material (in coordination with modeling and/or XCT characterization with project partner LBNL).
- Perform hyperspectral imaging of membrane thickness, exploring x-y resolution, z resolution, and percentage of coverage, and evaluate the effect of line speed, with milestone criteria: physical resolution of 100 μm or smaller, thickness ranges: 50–200 μm (LTE) and 12–50 μm (PEMFC), line speed of 2 ft/min or faster.
- Evaluate ink formulations, drying conditions, and substrates to reduce crack formation in fuel cell and electrolysis catalyst layers coated using scalable methods.

FY 2018 PUBLICATIONS AND PRESENTATIONS

1. P. Rupnowski and M. Ulsh. Thickness mapping using multispectral imaging. U.S. Patent Application no. 15/830,585, filed June 7, 2018.
2. A. Phillips, M. Ulsh, K.C. Neyerlin, J. Porter, and G. Bender. “Impacts of electrode coating irregularities on PEMFC lifetime using quasi in-situ infrared thermography and accelerated stress testing.” *Int. J. Hydrogen Energy* 43 (March 22, 2018): 6390–6399.
3. A. Phillips, J. Mackay, N. Shrivastava, J. Porter, T. Harris, M. Ulsh, and G. Bender. “The Effect of Membrane Casting Irregularities on Initial Fuel Cell Performance.” Oral presentation IO1C-1484 at the ECS Fall Meeting, National Harbor, MD, October 2017.
4. A. Phillips, J. Mackay, J. Porter, M. Ulsh, and G. Bender. “The Effect of Catalyst Layer Coating Irregularities on Fuel Cell Performance Over Time.” Oral presentation IO1A-1412 at the ECS Fall Meeting, National Harbor, MD, October 2017.
5. S. Mauger, K.C. Neyerlin, A.C. Yang-Neyerlin, G. Bender, M. Ulsh, B. Green, and K. More. “Material-Process-Performance Relationships for Roll-to-Roll Coated Fuel Cell Electrodes.” Oral presentation IO1B-1441 at the ECS Fall Meeting, National Harbor, MD, October 2017.
6. S. Mauger, S. Khandavalli, K.C. Neyerlin, J. Stickel, K. Hurst, and M. Ulsh. “Rheological Characterization of Interparticle Interactions in Fuel Cell Catalyst Dispersions.” Oral presentation IO1A-1382 at the ECS Fall Meeting, National Harbor, MD, October 2017.
7. S.A. Mauger, S. Khandavalli, J. Stickel, K.E. Hurst, K.C. Neyerlin, and M. Ulsh. “Rheological Properties and Interparticle Interactions in Fuel Cell Catalyst Dispersions.” Poster presentation at the 89th Annual Meeting of the Society of Rheology, Denver, CO, October 2017.
8. M. Ulsh. “Fuel Cell MEA Manufacturing R&D.” Oral presentation at the Hydrogen and Fuel Cell Program Annual Merit Review and Peer Evaluation Meeting, Washington, DC, June 2018.
9. M. Ulsh and S. Mauger. “Material-Process-Performance Relationships in PEM Catalyst Inks and Coated Layers.” Poster presentation at the Hydrogen and Fuel Cell Program Annual Merit Review and Peer Evaluation Meeting, Washington, DC, June 2018.
10. S. Khandavalli, J. Stickel, K. Hurst, N.N. Kariuki, J.H. Park, D.J. Myers, K.C. Neyerlin, M. Ulsh, and S.A. Mauger. “Rheological Investigation of Catalyst Inks for Roll-to-Roll Processing of Fuel Cell Electrodes.” Poster presentation at the Fuel Cells Gordon Research Conference, Smithfield, RI, July 2018.
11. S. Khandavalli, J. Stickel, K. Hurst, N.N. Kariuki, J.H. Park, D.J. Myers, K.C. Neyerlin, M. Ulsh, S.A. Mauger. “Rheological Investigation of Catalyst Inks for Roll-to-Roll Processing of Fuel Cell Electrodes.” Oral presentation at the International Symposium of Coating Science and Technology, Long Beach, CA, September 2018.

12. S.A. Mauger, K.C. Neyerlin, A.C. Yang-Neyerlin, K.L. More, and M. Ulsh. “Gravure Coating for Roll-to-Roll Manufacturing of Proton-Exchange-Membrane Fuel Cell Catalyst Layers.” *J. Electrochem. Soc.* 165.11 (September 11, 2018): F1012–F1018.

Clean Energy Supply Chain and Manufacturing Competitiveness Analysis for Hydrogen and Fuel Cell Technologies

Patrick Valente
Ohio Fuel Cell Coalition (OFCC)
151 Innovation Drive, Suite 240D
Elyria, OH 44035
(614) 542-7308
Email: pat.valente@fuelcellcorridor.com

DOE Manager: Nancy Garland
Phone: (202) 586-5673
Email: Nancy.Garland@ee.doe.gov

Contract Number: DE-EE0006931

Subcontractors:

- Connecticut Center for Advanced Technology, East Hartford, Connecticut
- DJW Technology, Inc., Dublin, Ohio
- National Renewable Energy Laboratory, Golden, Colorado
- National Fuel Cell Research Center, Irvine, California

Project Start Date: September 1, 2015
Project End Date: March 31, 2019

Overall Objectives

- Objective 1. Establish regional Technical Exchange Centers to increase communication between original equipment manufacturers (OEMs) and hydrogen and fuel cell component and subsystem suppliers.
- Objective 2. Establish a readily web-accessible database containing inputs from suppliers and OEMs along with supplier contact lists.
- Objective 3. Standardize component and subsystem component specifications.
- Objective 4. Develop strategies for lowering cost, increasing performance, and improving durability of components and subsystem components.

Fiscal Year (FY) 2018 Objectives

- Continue operation of the four regional Technical Exchange Centers and host

supplier/OEM/informational events in the various regions.

- Plan the 2018 Ohio Fuel Cell Symposium, scheduled for October 2–3, 2018, at Stark State College in North Canton, Ohio. A supply chain exchange and networking event will be held during the symposium.
- Finalize working groups, which will assist with the projections of cost reduction and initiation of component fabrication based on standardization of specifications, and determine components to be standardized. The objective is to identify components common to multiple designs of fuel cell systems that can be manufactured in high volume by Tier 1 and Tier 2 suppliers.
- Continue evaluation of organizations/companies for potential event participation and database inclusion.
- Conduct a National Supply Chain Exchange at the Fuel Cell Seminar and Energy Exposition in November 2017.

Technical Barriers

This project addresses the following technical barriers from the Fuel Cells section of the Fuel Cell Technologies Office Multi-Year Research, Development, and Demonstration Plan¹:

- Durability
- Cost
- Performance.

This project also addresses the following technical barrier from the Manufacturing R&D section of the Fuel Cell Technologies Office Multi-Year Research, Development, and Demonstration Plan:

- Lack of Standardized Balance-of-Plant Components.

¹ <https://www.energy.gov/eere/fuelcells/downloads/fuel-cell-technologies-office-multi-year-research-development-and-22>

FY 2018 Accomplishments

- Held the Colorado CleanTech Manufacturing Forum and Rocky Mountain regional supply chain event with almost 90 participants; also hosted a successful ride and drive and made quality connections.
- Held the Northeast Hydrogen Highway Summit with partner Proton OnSite at their facilities in Wallingford, Connecticut. There was an unveiling and ribbon cutting of the first retail hydrogen refueling station on the East Coast and a panel discussion and meeting to explore how to lay the foundation for building the Northeast Hydrogen Highway.
- Planned and executed a National Supply Chain Exchange at the Fuel Cell Seminar and Energy Exposition in Long Beach, California.
- Coordinated arrangements for finalizing the agenda and events surrounding the 2018 Ohio Fuel Cell Symposium, to be held October 2–3, 2018, at Stark State College in North Canton, Ohio; speakers include industry leaders from DOE, LG Fuel Cell Systems, Plug Power, FuelCell Energy, and the National Fuel Cell Research Center, and the OFCC will host a supply chain exchange during the symposium.
- Completed a supply chain brochure detailing this project and listing OEM needs; the brochure will be given to suppliers to better match their capabilities with the OEMs needs.
- Completed identification and initial mapping of the supply chain for hydrogen fueling stations.
- Made progress in establishing OEM working groups and efforts toward component standardization.
- Continued meeting and discussions to broaden the Midwest Technical Exchange Center for supply chain and manufacturing, including possible relationships in the Michigan and Pennsylvania areas.

INTRODUCTION

The project goal is to facilitate the development of a robust supply chain for fuel cell and hydrogen systems that will benefit manufacturing and the supply chain with accelerated mass production, cost reduction, and improved performance and durability of these systems. The project will identify and address the critical gaps in the needs and capabilities of the fuel cell supply chain. This will contribute to the United States maintaining a competitive advantage and global leadership in the industry.

This project builds on existing manufacturing infrastructure to help reverse the decline in and/or create new manufacturing jobs, and it acts as an economic lever for additional technology development. The benefits that will be gained from addressing the manufacturing barriers (cost, performance, and mass production) and product standardization will facilitate commercialization of hydrogen and fuel cell technologies and promote energy efficiency and renewable energy.

APPROACH

Our Technical Exchange Centers continued to research and catalog company and product information for our regional and national database. We have begun marketing our supply chain assistance and resources more formally than just word-of-mouth. We are having companies and organizations reach out to us with their needs. We promote the communication between suppliers and OEMs through a number of avenues—industry events, one-on-one interactions, and addressing the needs and capabilities of the fuel cell supply chain.

While a longer process than anticipated, we have identified and reached out to acquire participants for our OEM and supplier working groups and to obtain their recommendation for components and subsystems to be standardized. Emphasis remains on North American companies related to automotive, stationary power, and motive applications with respect to polymer electrolyte membrane fuel cells. We developed a questionnaire with 55 component and materials for OEM evaluation, of which 28 were identified. We will use the OEM recommendations to contact companies with manufacturing capabilities that meet the top three OEM recommendations.

RESULTS

The four regional Technical Exchange Centers continue to be the catalyst for this project. One of the main components of this project is to increase communication between fuel cell OEMs and fuel cell component/subsystem suppliers. We held a number of events, from Connecticut to Colorado, reaching a broad and varied audience of more than 250 participants from across the country.

All four regional Technical Exchange Centers worked together to execute a National Supply Chain Exchange at the Fuel Cell Seminar and Energy Exposition. We had 22 suppliers and six integrators that included industry leaders Ballard, FuelCell Energy, and Doosan as integrators as well as Johnson Matthey and Saint Gobain, among others, as suppliers. Our post-event survey indicated 75% made new contacts they otherwise would not have and 64% are continuing dialogue for potential relationships.

Concerning our working group/standardization efforts:

- A number of OEMs were contacted, including several major automakers, to identify balance-of-plant components for standardization. Those contacted have responded and completed the component questionnaire with their recommendations for which components to standardize.
- Components have been ranked based on information obtained from the integrators. We hope to have one-on-one interactions to discuss what components and to what level of standardization we should work toward. After discussion held with several OEMs, about six of the 19 components originally on the list to be considered for standardization have been eliminated.

- The two highest-ranked components to standardize are humidifiers and AC/DC converters, a unanimous choice by the participants. We want to be sure of the components so we do not dilute our efforts over multiple choices.

Relative to the database, the Northeast Technical Exchange Center continues to build theirs with the addition of specialization in hydrogen refueling, a demo, and searchable map database. They are wrapping up work with the Hydrogen Safety Panel, have written white papers for fuel cell electric vehicles and light-duty vehicles and buses, and are working on a third white paper for refueling.

The work detailed above is a necessary stepping stone to help the United States and our fuel cell industry to be a competitive and global leader in the fuel cell market. The formation of resources, such as the regional and national databases, and communication between fuel cell component and subsystem suppliers, both individually and within working groups, is a must to achieve the goal to develop a robust supply chain, standardize and improve functionality and performance, and maintain competitive pricing.

CONCLUSIONS AND UPCOMING ACTIVITIES

It is more than clear that our networking and contacts are a driving force for progress in the fuel cell industry. We have seen a number of partnerships develop, such as the Honda and General Motors announcement to jointly produce fuel cells for both their companies, that benefit not only the automakers but the industry as a whole. While there are still a number of gaps between OEM needs and supplier capabilities, this project has helped make the introductions and, in some cases, build the relationships that will eventually help to bridge these gaps.

The next budget year will also determine if we are able to continue to support our Technical Exchange Centers through other avenues once this project is completed. For example, the Colorado Hydrogen Coalition is developing a plan to continue the project and house the Rocky Mountain Region Technical Exchange Center going forward using industry funding and stakeholder sponsorships, and the Colorado Advanced Manufacturing Alliance has submitted a proposal to provide support through business-to-business networking sessions in conjunction with established manufacturing events in the region.

While we planned most of the 2018 Ohio Fuel Cell Symposium during FY 2018, it will actually be held in FY 2019, and we are very excited to hear the messages that will be presented by our speakers—industry leaders Plug Power, FuelCell Energy, the National Fuel Cell Research Center, and LG Fuel Cell Systems. We will also be hosting a Supply Chain Exchange Event where these organizations will also participate.

While the working group and standardization components of this project have moved slower than anticipated, we are now in a position to move forward toward our final goals of standardizing component specifications to improve cost efficiency and improve durability and performance of the fuel cell components and subsystems.

FY 2018 PUBLICATIONS/PRESENTATIONS

1. Participated in the Annual Merit Review, June 13–15, 2018, in Washington DC. The OFCC had a poster presentation and we took part in a panel discussion.
2. U.S. Department of Energy, Ohio Fuel Cell Coalition, *Hydrogen and Fuel Cells Regional Technical Exchange Centers Brochure* (2017), <https://www.fuelcellcorridor.com/doe-ofcc-tec-brochure>.

Hydrogen Fuel Cell Nexus Business-to-Business Website

Alleyn Harned (Primary Contact) and
Matthew Wade
Virginia Clean Cities at James Madison University
1401 Technology Drive MSC 4115
Harrisonburg, VA 22807
Phone: (540) 568-8896
Email: aharned@vacleancities.org

DOE Managers:
Nancy Garland
Phone: (202) 586-5673
Email: Nancy.Garland@ee.doe.gov

Greg Kleen
Phone: (240) 562-1672
Email: Greg.Kleen@ee.doe.gov

Contract Number: DE-EE0006932

Subcontractors:

- Birch Studio, Charlottesville, VA
- Breakthrough Technologies Institute, Woodbridge, VA

Project Start Date: July 1, 2015

Project End Date: September 30, 2018

Overall Objectives

- Expand the domestic supply chain of hydrogen components and systems.
- Scale up the fuel cell and hydrogen supply chain by building and populating a comprehensive communications database.
- Drive U.S. companies to the free website via an engaging outreach campaign.
- Advance hydrogen fuel cell suppliers in the transportation, utility, industrial, commercial, and residential sectors, with a focus on the transportation sector in fuel and infrastructure supply chain systems.
- Contribute to a more diverse and efficient energy balance.

Fiscal Year (FY) 2018 Objectives

- Develop interface to allow fuel cell and hydrogen companies to post their needs and specifications, and allow potential supply chain companies to post their capabilities. The idea is

to stimulate a dialogue and encourage supplier-to-end-manufacturer connections.

- Update the Hydrogen Fuel Cell Nexus (HFC Nexus) continuously and technical specifications quarterly and, if necessary, revise and update the interface based on user experience. The number of suppliers/components added during each quarter will be included in the quarterly reports.
- Mine the traffic on the website, compile information gained during outreach efforts, and discuss with DOE and fuel cell industry leaders to identify critical gaps in the supply chain and develop a response plan.
- Identify the fuel cell system gaps and cater the opportunity center to narrow the gaps identified. Deliver a preliminary assessment.
- Seek information biannually from additional suppliers not previously captured.
- Collect data and research suppliers.
- Open a dialogue with potential partners through dissemination of the developed materials. The project team will track the materials distribution by using actual numbers of printouts distributed, website hits, webinar participants, and video views.
- Seek opportunities for information placement in trade journals, which often make space available for nonprofits.
- Create and advance a sustainability program for long-term continued life of the website and database and for continued upkeep and enhancement of data. This will include exploring collaboration with industry, federal agencies, and national laboratories.

Technical Barriers

This project addresses the crosscutting technical barriers of supply chain transparency and business and product information of the Fuel Cell Technologies Office Multi-Year Research, Development, and Demonstration (MYRDD)

Plan.¹ The project also addresses the following specific barrier from the Education and Outreach section of the MYRDD Plan:

- (A) Lack of Readily Available, Objective, and Technically Accurate Information.

Contribution to Achievement of DOE Milestones

This project will directly contribute to achievement of DOE milestones from the Education and Outreach section of the Fuel Cell Technologies Office MYRDD Plan. The project is a cross-cutting effort to publish available supply chain business content and connect industry partners. As such, milestones associated with development and demonstration in the Manufacturing R&D section are supported, and this project takes those milestones to deployment.

FY 2018 Accomplishments

- The HFC Nexus has 356 fuel cell and hydrogen companies.
- The HFC Nexus has 104 active user accounts.
- Using Google Analytics to track the website traffic, Virginia Clean Cities (VCC) can report that the directory saw 7,877 users, 9,629 sessions, and an average of 21 daily active users (Figure 1). This is an increase from 6,100 users, 8,000 sessions, and an average of 8 daily active users (DAUs) from July 1, 2016, through June 30, 2017. A DAU is the number of unique users who had at least one session within a 30-day period.
- The project team created an HFC Nexus news blog (hfcnexus.com/blog) dedicated to promoting news about events, conferences, grants, trainings, and new technologies in the hydrogen fuel cell industry.
- The project team launched the HFC Nexus advertising module.

Sessions by country



Figure 1. Sessions by country in the past 12 months. Dark blue—Between 10% and 50% of sessions; light blue—less than 10% of sessions; gray—no sessions.

¹ <https://www.energy.gov/eere/fuelcells/downloads/fuel-cell-technologies-office-multi-year-research-development-and-22>

INTRODUCTION

The Fuel Cell and Hydrogen Opportunity Center, renamed the Hydrogen Fuel Cell Nexus (and live at www.hfcnexus.com and www.hfcnexus.org, Figure 2) sought to expand the domestic supply chain of components and systems necessary for the manufacture and distribution of hydrogen and fuel cell equipment. The supply chain has benefited through the development of a comprehensive online database. This effort advanced hydrogen fuel cell suppliers in the transportation, utility, industrial, commercial, and residential sectors, with a focus on the transportation sector in fuel and infrastructure supply chain systems.



Figure 2. www.HFCnexus homepage

APPROACH

VCC and project partners addressed the main objective of the Fuel Cell and Hydrogen Opportunity Center project by collaboratively identifying gaps and developing elements of interest for a comprehensive supplier tool, gathering national supplier information to fill the database, identifying and encouraging new suppliers to become engaged in the hydrogen industry, and releasing and maintaining a public directory tool for interaction with the data. Birch Studio developed the user interface for the website. VCC populated the database with U.S. companies from the FuelCells2000 directory. After the website was launched, VCC began an aggressive outreach campaign using trade association outreach, webinars, social media, and personal contact to drive companies to this resource. The mechanism for the project to continue with a sustainable stream of revenue through advertisements and donations has been created. No revenue has been raised through this mechanism to date.

RESULTS

The efforts of the Fuel Cell and Hydrogen Opportunity Center project team began with the release of a live and interactive website directory on July 11, 2016. The website directory has grown from an initial population of 220 companies to 356. These companies were verified as active in the hydrogen or fuel cell industries. Phone numbers, email addresses, and mailing information for employees at each company were uploaded for each company to provide a method for website users to contact the company (Figure 4). The website has grown from zero user accounts to 104 active user accounts in 2018.

HYDROGEN GENERATION/SUPPLY

Companies that make and sell hydrogen generation systems or supplies hydrogen in a gas or liquid form.



Air Liquide aims to deliver innovative gas solutions and technologies to a wide range of customers, driving their performance and helping them reduce their environmental impact. No matter where, we make sure our solutions are safe, reliable, cost-effective and sustainable.

ALSO LISTED IN: [Hydrogen Fuel](#), [Hydrogen Generation/Supply](#), [Hydrogen System Integrator](#) [Edit](#)
 UPDATED: January 31, 2017



Air Products is the world's largest supplier of hydrogen. A commercial developer, supplier and operator of turnkey hydrogen on-site plants, Air Products is in the forefront of developing hydrogen fueling stations for clean transportation applications.

ALSO LISTED IN: [Hydrogen Generation/Supply](#), [Hydrogen Station](#), [Hydrogen Storage](#), [Hydrogen System Integrator](#) [Edit](#)
 UPDATED: January 25, 2017

Figure 3. Example category page

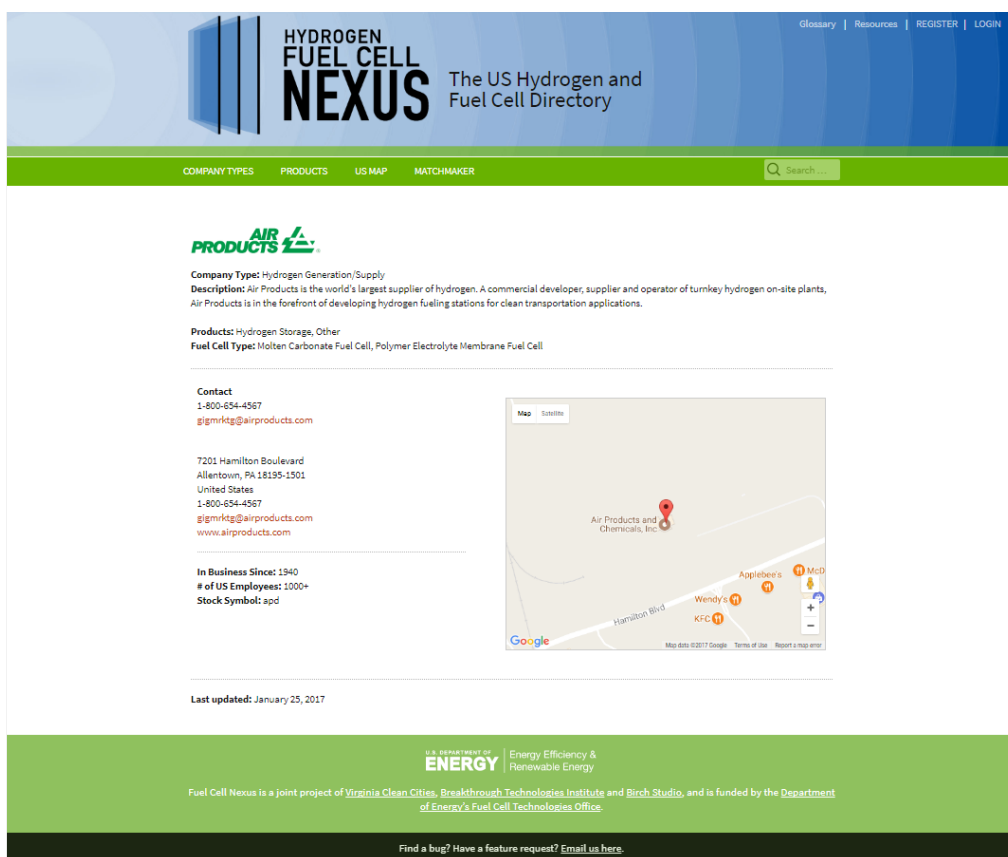


Figure 4. Example of company page

CONCLUSIONS

During the final project year, the project team was active in several areas of the project related to improving the website and adding companies. The project team continued verifying data and company information and revising as needed. The project team engaged in direct marketing and outreach to hydrogen and fuel cell companies. During this period, VCC developed and disseminated marketing and outreach materials that described the website and how to utilize it. Birch Studio developed the news blog for providing important updates on developments in the hydrogen and fuel cell industry. Birch Studio began a maintenance and iteration phase to continue improving the website interface. VCC staff continued promoting the database at events and collected data on hydrogen and fuel cell companies to include in the database. Project staff continued website branding with DOE guidance. The project team engaged in an outreach campaign to drive appropriate suppliers to the site by initiating friendly partnerships with business-to-business marketing associations and other business associations in areas of critical need.

The database and website tools have three main areas: public access, supplier secure access, and system administrator’s access. Figure 4 is an example of a company page. This page is useful to the user because it provides information on the company, including products, address, and contact information. The content is accessible 24 hours a day, 7 days a week. A news blog was added to generate additional content for the Nexus (Figure 5).

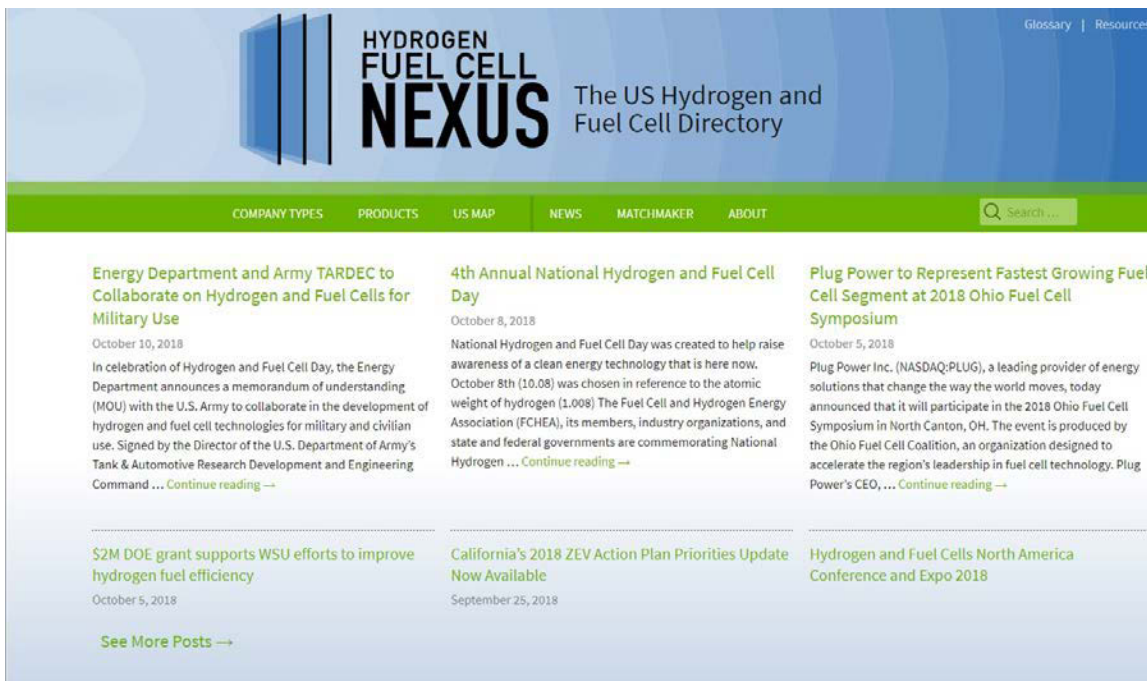


Figure 5. Example of news blog page

Continuous Fiber Composite Electrofusion Coupler

Brett Kimball

Automated Dynamics, Part of Trelleborg Group
2 Commerce Park Dr
Niskayuna NY 12211
Phone: 518-377-6471 x239
Email: brett.kimball@trelleborg.com

DOE Manager: Nancy Garland
Phone: (202) 586-5673
Email: Nancy.Garland@ee.doe.gov

Contract Number: DE-EE0007274

Subcontractors:

- NOV Fiberglass Systems, Houston, TX
- Savannah River National Laboratory, Aiken, SC

Project Start Date: December 1, 2015

Project End Date: April 30, 2019

Overall Objectives

- Quantify:
 - Various mechanical characteristics of coupler: burst strength, axial strength, leak rates, fatigue characteristics.
 - Manufacturing costs of coupler.
- Optimize:
 - Mechanical design of composite coupler: maximize strength characteristics while constraining costs.
- Demonstrate:
 - Coupler without O-ring sealing components, which would require underground maintenance.
 - Manufacturability of a robust coupler that reduces cost and complexity of hydrogen pipeline installation.
 - Advanced electrofusion coupler meets mechanical requirements for pipeline designed to transport hydrogen at 100 bar (and pass test at 350 bar).

Fiscal Year (FY) 2018 Objectives

- Demonstrate a functioning coupler that passes the required fatigue test consistently (burst and leak tests already passed). Fatigue test goal is minimum 10,000 cycles, R=0.5, 1,500 psi.
- Optimize the electrofusion process cycle performed with non-standard electrofusion equipment.
- Analyze failure modes upon leaking for insight into potential improvements in coupler.

Technical Barriers

This project addresses the following technical barriers from the Hydrogen Delivery section of the Fuel Cell Technologies Office Multi-Year Research, Development, and Demonstration Plan¹:

D. High As-Installed Cost of Pipelines.

Contribution to Achievement of DOE Technology Acceleration Milestones

This project will contribute to achievement of the following DOE milestones from the Hydrogen Delivery section of the Fuel Cell Technologies Office Multi-Year Research, Development, and Demonstration Plan:

- Milestone 1.5: Coordinating with the Hydrogen Production and Storage subprograms, identify optimized delivery pathways that meet a hydrogen delivery and dispensing cost of <\$2/gge for use in consumer vehicles. (4Q, 2020)
- Milestone 6.3: By 2020, reduce the cost of hydrogen delivery from the point of production to the point of use in consumer vehicles to <\$2/gge of hydrogen for the gaseous delivery pathway. (4Q, 2020)

FY 2018 Accomplishments

- Implemented the improved design, reducing the number of components and corresponding number of bond zones and leak paths by a factor of 2. The prior design required two

¹ <https://www.energy.gov/eere/fuelcells/downloads/fuel-cell-technologies-office-multi-year-research-development-and-22>

separate bonding layers, each of which was a hydrogen leak path in the coupler.

- Implemented a custom electrofusion process to achieve sufficient power to melt and fuse the coupler's components. Prior equipment did not output enough voltage for the modified design; it was short by more than 50% voltage capacity. The modified design required increased resistance, and therefore voltage, because of decreased wire size. Wire size decreased by over 50% effective area, significantly increasing the surface area available for bonding. This was needed due to prior fatigue test failures at the bond zone. An off-the-shelf electrofusion system with higher voltage would be used in practice.

INTRODUCTION

Traditional pipe couplers considered for a non-metallic buried hydrogen pipeline employ elastomeric sealing components, such as O-rings. The American Society of Mechanical Engineers code committee responsible for hydrogen piping and pipelines has expressed concerns that such underground maintenance would be problematic and unsatisfactory.

The proposed coupler design under this project will eliminate the need for such elastomeric seals. This coupler seals adjacent non-metallic composite pipes by the electrofusion of two adjacent cylindrical plastic surfaces (applying heat via electrical current). State-of-the-art electrofusion couplers are rated at too low of a pressure for the hydrogen pipeline proposed. Therefore, a new design is required.

APPROACH

This research draws from existing electrofusion pipe coupling technology but extends it to be suitable for use on a variety of materials available for composite pipelines. Automated Dynamics' (now part of Trelleborg Group) technology is well-suited to couple thermoplastic bonded pipes (where each of the pipe's radial adjacent layers are bonded to each other) by our fiber placement technology that bonds continuous media (fiber reinforced composite, plastic coated wire) on the fly without need for post-curing, as well as thermoset pipes, which require a different coupler design employing metal mechanical wedge grips and coupling threads. The coupler designed in this project shall be available for such pipes and for non-bonded pipes. Existing electrofusion couplers do not allow for the continuous fiber composite reinforcement necessary to achieve the high pressures sought by DOE. Our coupler will employ this continuous fiber thermoplastic or thermoset composite as a structural layer for high pressures and high induced axial loads.

RESULTS

The project has been focused on achieving the following results:

- **Passed tensile test requirements**, failing pipe before failing coupler, on average at 11,000 lb.
- **Passed burst test requirements**, failing pipe before failing coupler, on average at 5,400 psig.
- **Passed leak-rate test requirements**, achieving 10×10^{-5} cm He/s leak rate.
- **Still working toward passing fatigue test at minimum 10,000 cycles, R=0.5, 1,500 psi.**

These results are the key milestones toward commercial viability. Passing the fatigue test remains the singular most difficult hurdle. Currently, parts are in-test at Savannah River National Laboratory.

CONCLUSIONS AND UPCOMING ACTIVITIES

We expect to pass the last of the three milestones (fatigue testing) in 2018 to nearly finalize the scope of work of the active project. Minimal repeat testing will be available for statistically significant results. This is due to the greater complexity of fatigue requirements than initially considered in 2015. Additionally, the manufacturing and quality plans will become more detailed, which will aid in the evolving commercialization plan.

SPECIAL RECOGNITIONS AND AWARDS/PATENTS ISSUED

1. "Continuous fiber reinforced composite and metal electrofusion coupler," Patent application #16/175,018 (filed October 30, 2018).

FY 2018 PUBLICATIONS/PRESENTATIONS

1. David Hauber and Brett Kimball, "Continuous Fiber Composite Electrofusion Coupler," Presentation at the DOE Annual Merit Review and Peer Evaluation Meeting, Washington, D.C., June 2018.

In-Line Quality Control of Polymer Electrolyte Membrane Materials

Paul Yelvington (Primary Contact),
Andrew Wagner
Mainstream Engineering
200 Yellow Place
Rockledge, FL 32955
Phone: (321) 631-3550
Email: pyelvington@mainstream-engr.com

DOE Manager: Nancy Garland
Phone: (202) 586-5673
Email: Nancy.Garland@ee.doe.gov

Contract Number: DE-SC0013774

Subcontractors:

- National Renewable Energy Laboratory, Golden, CO
- Georgia Tech, Atlanta, GA

Project Start Date: Phase I and II: June 8, 2015,
Phase IIb: August 27, 2018

Project End Date: Phase I and II: July 31, 2018,
Phase IIb: August 26, 2020

Overall Objectives (Phase I/II)

- Identify membrane defect size that leads to cell failure.
- Create a production-intent prototype automated vision system to perform quality control and demonstrate it on a full-speed membrane web line.
- Detect defects down to 4 microns at 100 ft/min.
- Determine membrane thickness to 0.5-micron resolution.
- Achieve a 5σ false-positive rate (FPR) and false-negative rate (FNR).

Fiscal Year (FY) 2018 Objectives

- Determine impact of line speed on detection rate and autonomous software operation.
- Demonstrate prototype on a full-speed membrane web line and a coating line.

- Conduct web-line runs to determine FPRs and FNRs.
- Identify final image analysis parameters for defect and thickness resolution.

Technical Barriers

This project addresses the following technical barriers from the Manufacturing R&D section of the Fuel Cell Technologies Office Multi-Year Research, Development, and Demonstration Plan (FCTO MYRDD) Plan¹:

- Lack of Improved Methods of Final Inspection of Membrane Electrode Assemblies (MEAs)
- Low Levels of Quality Control.

Contribution to Achievement of DOE Manufacturing R&D Milestones

This project will contribute to achievement of the following DOE milestones from the Manufacturing R&D section of the FCTO MYRDD Plan:

- Milestone 1.3: Develop continuous MEA manufacturing processes that increase throughput and efficiency and decrease complexity and waste. (4Q, 2017)
- Milestone 1.6: Develop fabrication and assembly processes for polymer electrolyte membrane fuel cell (PEMFC) membrane electrode assembly (MEA) components leading to an automotive fuel cell stack that costs \$20/kW at high volume (500,000 units/year). (4Q, 2020)
- Milestone 5.2: Demonstrate improved sensitivity, resolution, and/or detection rate for MEA inspection methods. (4Q, 2016)
- Milestone 5.4: Design and commercialize an in-line quality control device for PEMFC MEA materials based on the National Renewable

¹ <https://www.energy.gov/eere/fuelcells/downloads/fuel-cell-technologies-office-multi-year-research-development-and-22>

Energy Laboratory's (NREL's) optical reflectance technology. (4Q, 2017)

- Milestone 5.6: Demonstrate methods to inspect full MEAs and cells for defects prior to assembly into stacks in a production environment. (4Q, 2018)
- Milestone 5.8: Implement demonstrated in-line quality-control techniques on pilot or production lines at PEMFC MEA material manufacturers. (4Q, 2020)

FY 2018 Accomplishments

- The smallest detectable defect was identified as 10 microns in Nafion-211 and Nafion-HP.
- Mainstream brought online an inspection winder that could run up to 550 ft/min.
- The inspection system was tested and demonstrated operating in real time on two coating web lines up to 10 ft/min and on two inspection web lines up to 550 ft/min.
- FPRs and FNRs were achieved at 4σ under all conditions for defects 250 microns and larger, and at 5σ at 30 ft/min with a 127-micron-thick Nafion-115 membrane

INTRODUCTION

Fuel cells stand on the cusp of commercialization for large-scale applications such as zero-pollution automotive systems. They are held back by high manufacturing costs and expensive catalysts. The membrane alone accounts for as much as 45% of the total material cost of a commercial fuel cell system at 1,000 units/year and 12% at 500,000/year [1]. Moreover, manufacturing defects in the membrane not only lead to wasted expensive materials but they also cause cell failures that can cascade into complete stack failure. This requires additional labor to rework the stack and results in the loss of expensive catalyst and gas diffusion electrode materials. Current inspection methods look for defects after batch production of the membrane, leading to delayed correction of issues with the membrane and membrane electrode fabrication process. Reaching the quality targets for fuel cell system manufacturing requires a new, high-efficiency, real-time quality control system. Mainstream Engineering is developing a real-time optical quality control system, which we call the Mantis Eye, that provides increased resolution, improved accuracy, and increased detection speeds over existing optical scanners for the examination of fuel cell and other membranes.

APPROACH

Mainstream's overall technical approach to create the Mantis Eye prototype was to rigorously prove out the patent-pending optical technique with a wide range of commercially available membranes, upgrade to imaging hardware tailored for Nafion, prove out the defect detection abilities of the hardware, automate the software, and build the prototype. A wide range of typical defects were induced and examined in the Nafion membranes and characterized with the machine vision system. Pinholes down to 5 microns were the focus during the first year and the limits of detection were determined for the upgraded hardware. During this time, NREL and Georgia Tech created defective membrane samples and tested them to determine the smallest defect that impacts cell performance. Then the custom vision software was fully automated to image the membrane, detect defects, log the defects, track the defect location, and print an identifying marker beside the defect. The machine vision software was programmed on an industrial microcontroller. The system was then deployed and tested on multiple web lines and coating lines to demonstrate its capabilities and identify areas needing refinement. Many defects including pinholes, scratches, folds, ribbing, and streaking were identified on the rollstocks. The Mantis Eye prototype was tested with freshly cast membrane and on a custom inspection winder at speeds up to 550 ft/min.

RESULTS

Developed and Tested High-speed Inspection Winder

The Mantis Eye optical scanner was originally developed with static samples and a small 3-inch web line in Phase I. Operation on the small web line showed that tension control and web steering are critical in web converting equipment, especially for the quality-control section. To achieve the best web imaging, the web needs to be free of wrinkles and sagging, have equal tension across the web width, and run straight to maintain proper camera alignment and eliminate roll telescoping. Mainstream had a custom winder/unwinder built to our specifications that is capable of bidirectional winding and unwinding a 14-inch membrane roll thousands of feet long (depending on thickness) at speeds up to 550 linear ft/min. In Figure 1, the inspection winder is shown with the Mantis Eye mounted on it. The winder uses active tension control to maintain proper tension and avoid any of the aforementioned web-line issues. The machine includes a removable splice table and a pneumatically actuated, backlit inspection platform. It is capable of maintaining tension and winding in the forward and reverse directions. The main plate has provisions for mounting the Mantis Eye camera, encoder, printer, and machine vision light. In addition, the web material passes extremely close to the light source. This provides the best possible vision conditions and allows for imaging at a realistic line speed. Using this inspection machine, detailed statistics were generated to allow calculation of the FPR and FNR. For dust control, the machine was installed in a soft-walled ISO Class 7 clean room.



Figure 1. Mainstream’s Mantis Eye prototype detector installed on Mainstream’s inspection winder

The Mantis Eye system was tested on multiple materials on the inspection winder with a focus on polyethylene terephthalate (PET) film due to its availability in long rolls and ease of handling compared to Nafion. The field of view, line speed, and vision algorithms were tested to optimize system performance and defect resolution as well as determine reliability statistics. The system successfully operated in real time and marked 100- μm defects at up to 550 ft/min. As the speed increased beyond 300 ft/min, the camera’s exposure time began to limit defect detection as motion blur caused the defects to cover multiple pixels per exposure. This effect is seen in Figure 2; when the line speed exceeded 300 ft/min, the defect appears dimmer and larger. Thus the camera hardware became the limiting element at high line speeds. If speeds above 300 ft/min are required, cameras capable of shorter exposure times or multiple cameras can be used to prevent motion blur. The defect logging and printer were able to operate up to 550 ft/min with no issues. Reliability test rolls of PET and Nafion were made with known defects of different sizes and were run on the inspection winder.

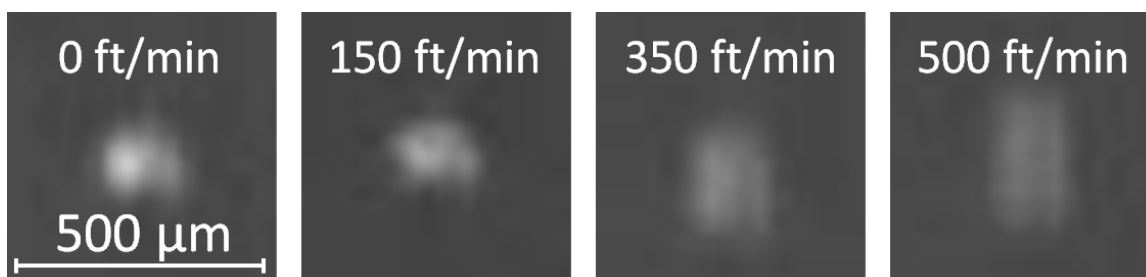


Figure 2. Pinhole defect images in PET taken with the Mantis Eye detector at different speeds

Reliability Statistics

The FPR and FNR were determined by inducing a wide range of defects across a roll of material and scanning it with the Mantis Eye. A 1,000-ft roll had defects induced in a 100-ft test section. Zero to three pinhole defects that were 250, 500, or 640 microns in diameter were randomly induced every 4 inches. A key was made for the location and size of the defects. The roll was then run for the entire length and the location and number of defects logged. The run was repeated multiple times with the camera set up to image a full 14-inch-wide web. A data set was generated and analyzed to find the optimized image processing and logging settings. For these runs, a no-defect negative condition was defined as one inch of web with no defects assuming that is the minimum practical length that could be removed if a defect was found. The FPR was then defined as the number of incorrect positive defect marks (“false alarms”) for every inch of web divided by the total number of inches of web without a defect. The FNR was defined as the number of incorrect negative marks (“misses”) for every inch of web divided by the total number of inches of web with a defect. Using this information, the FPR and the FNR were identified. For PET at 100 ft/min, the FPR and FNR hit 4σ levels (0.62%) for 250–640-micron defects. For Nafion at 30 ft/min, the FPR and FNR hit 5σ levels (0.023%) for 100-micron defects. The FPR and FNR depend on algorithm parameters, such as the brightness/size thresholds or requirements for multiple image captures that can be optimized based on a cost function that appropriately weights false positives (false alarms) or false negatives (misses) for the specific manufacturing process.

Coating Line Deployment and Testing

The prototype Mantis Eye system was installed on Georgia Tech’s lab-scale coater and NREL’s pilot coating line. On Georgia Tech’s system, Nafion was coated at up to 10 ft/min with observed defects including ribbing, streaking, pinholes, blobbing, and dust. The optical scanner was able to accurately observe defects as they were generated, but at the time of the Georgia Tech deployment these defects had not been observed previously by the team and were not part of the real-time processing capabilities. The software was upgraded to identify these larger defects and not just small pinholes. In addition, multiple edge-detection features were added to determine spots and streaking. The deployment onto NREL’s line allowed for the Nafion web to be dried before or after the inspection location and is shown in Figure 3. This allowed for images of freshly cast Nafion both wet and dry. In addition, the NREL deployment had the camera underneath the web, imaging through the PET, which was the first time it was deployed in this manner. Freshly cast, defective membrane is shown before and after image processing in Figure 4. The streaking and ribbing were successfully outlined and identified.

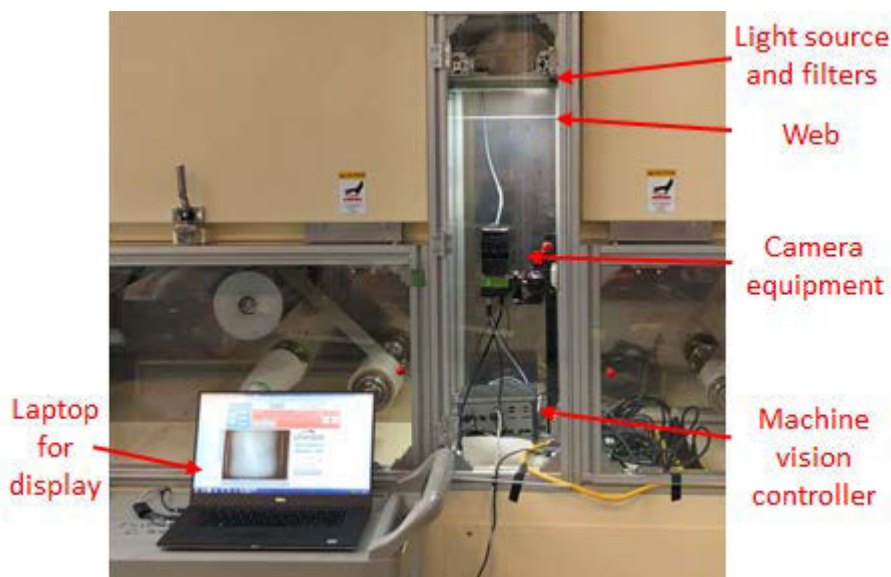


Figure 3. Mainstream's Mantis Eye prototype on NREL's pilot coating line

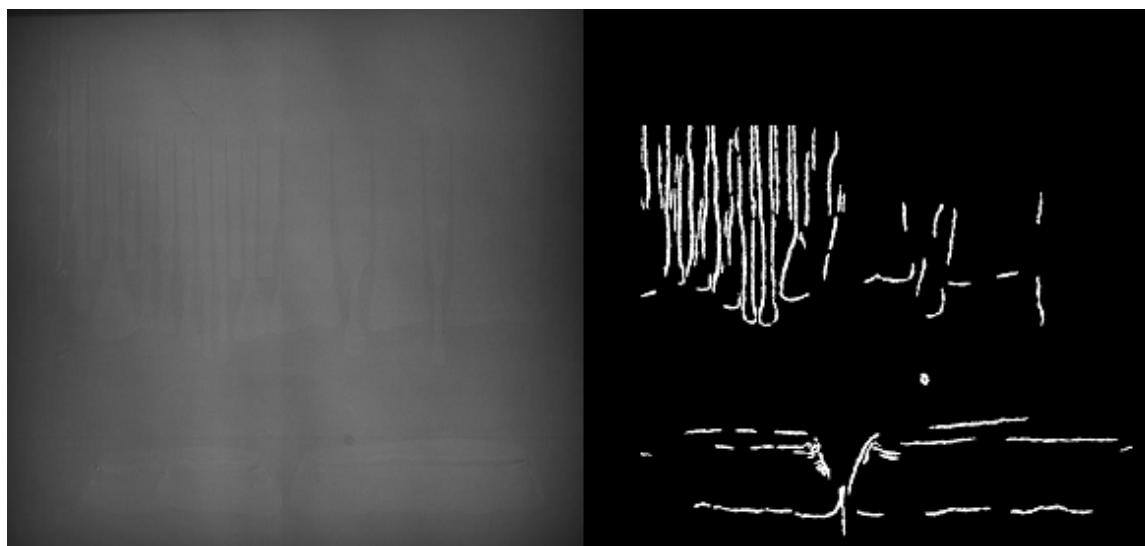


Figure 4. Raw image (left) and processed image (right) from Mantis Eye scanner on freshly cast Nafion membrane with streaking defects

CONCLUSIONS AND UPCOMING ACTIVITIES

The overall goal of the Phase II program was to research, develop, and commercialize an in-line quality control system for roll-to-roll membrane manufacturing. Mainstream Engineering developed the Mantis Eye inspection system, a low-cost, real-time optical detector for quality control using continuous analysis of membranes for PEMFC MEAs. The inspection system samples, logs, and marks the location on the roll of material such that defects in MEA materials can be addressed prior to assembly into complete cells. A prototype system was developed and tested on Mainstream's inspection winder, NREL's research web line, Georgia Tech's research coating line, and NREL's pilot-scale coating line. These deployments allowed for optimization of the software to detect both small and large defects. In addition, NREL determined that pinhole defects smaller than 10 microns caused no immediate cell performance issues, while defects larger than 50 microns did. For the Phase IIb project, the overall goal is to develop and commercialize a suite of instruments that provides a full turnkey inspection package for MEA production, including analysis of catalyst-coated

membrane and other opaque materials. For FY 2019, the goal will be to transition reflectance technology from NREL and use it on a web line at full production speed for MEA material quality control.

SPECIAL RECOGNITIONS AND AWARDS/PATENTS ISSUED

1. P.E. Yelvington and A. Wagner, “Method and Apparatus for Cross-Polarized, Optical Detection of Polymer Film Thickness and Defects Using Polarimetric Thickness Mapping,” U.S. Patent Application Serial No. 15/894,172 (2018).

FY 2018 PUBLICATIONS/PRESENTATIONS

1. A. Wagner, T. Lasko, and P.E. Yelvington, “In-Line Quality Control of PEM Materials,” presented at the DOE Hydrogen and Fuel Cells Program 2018 Annual Merit Review and Peer Evaluation Meeting, Washington, D.C., June 2018.

REFERENCES

1. G.J. Kleen, “Membrane Development in the U.S. DOE Fuel Cell Technologies Program,” Fuel Cell Seminar and Exhibition, Orlando, Florida, 2011.

Manufacturing Competitiveness Analysis for Hydrogen Refueling Stations

Ahmad Mayyas (Primary Contact), Margaret Mann
National Renewable Energy Laboratory
15013 Denver West Parkway
Golden, CO 80401
Phone: (303) 384-7446
Email: Ahmad.Mayyas@nrel.gov

DOE Manager: Nancy Garland
Phone: (202) 586-5673
Email: Nancy.Garland@ee.doe.gov

Project Start Date: April 6, 2015
Project End Date: September 30, 2018

Overall Objectives

- Develop manufacturing cost models for the key components in a hydrogen refueling station such as the compressors, dispenser, and on-site hydrogen production systems (proton exchange membrane [PEM] and alkaline electrolyzers).
- Identify cost drivers associated with manufacturing of the key systems in the hydrogen refueling station and on-site production systems to highlight potential cost reduction areas.

Fiscal Year (FY) 2018 Objectives

- Develop a bottom-up manufacturing cost model for the on-site hydrogen production systems (PEM and alkaline electrolyzers).
- Identify potential cost reductions in the manufacturing of PEM and alkaline electrolysis systems.

Technical Barriers

This project addresses the following technical barriers from the Manufacturing R&D section of the Fuel Cell Technologies Office Multi-Year Research, Development, and Demonstration Plan¹:

(A) Lack of High-Volume MEA Processes

(B) Lack of High-Speed Bipolar Plate Manufacturing Processes

(F) Manual Stack Assembly.

Contribution to Achievement of DOE Manufacturing R&D Milestones

This project will contribute to achievement of the following DOE milestones from the Manufacturing R&D section of the Fuel Cell Technologies Office Multi-Year Research, Development, and Demonstration Plan:

- Milestone 1.4: Demonstrate processes for direct coating of electrodes on membranes. (4Q, 2019)
- Milestone 1.5: Demonstrate processes for highly uniform continuous lamination of MEA components. (4Q, 2019)

FY 2018 Accomplishments

- Developed a new set of maps for the major international manufacturers of hydrogen refueling station parts and water electrolysis systems.
- Developed a manufacturing cost model for PEM electrolyzers using different sizes (in kilowatts) and different annual production rates (ranging from 10 to 50,000 electrolyzers per year).
- Developed a manufacturing cost model for alkaline electrolyzers using different sizes (in kilowatts) and different annual production rates (electrolyzers per year).

¹ <https://www.energy.gov/eere/fuelcells/downloads/fuel-cell-technologies-office-multi-year-research-development-and-22>

INTRODUCTION

This study is one of a few studies that discuss cost of hydrogen infrastructure. While other studies focus on the big picture by assessing the effect of capital cost reductions on the hydrogen prices, this study provides a detailed bottom-up manufacturing cost analysis for the key systems in the hydrogen refueling station (compressors, pressure vessels, chillers, heat exchangers, and dispensers) and on-site hydrogen production systems (PEM and alkaline electrolyzers). Cost analysis for the key parts and systems in the hydrogen refueling station was completed in FY 2017. In FY 2018, we also developed sets of manufacturing competitiveness analyses for PEM and alkaline electrolyzers to study the effect of cost components (e.g., labor, facilities, and energy costs) in different countries on the electrolyzer cost.

APPROACH

This study is centered around three main analyses: manufacturing competitiveness analysis, supply chain analysis, and effect of qualitative factors on the selection of the manufacturing facility locations for manufacturing of parts and systems used in the hydrogen refueling station and on-site hydrogen production systems. These analyses were completed for the hydrogen refueling station in FY 2015 to FY 2017. In FY 2018, we primarily focused on the manufacturing competitiveness analysis for on-site hydrogen production systems to evaluate relative manufacturing cost in selected countries in North America, Europe, and Asia. The goal of this comparative analysis is to study the advantage of the U.S.-based manufacturers relative to other international manufacturers who could enjoy benefits of the low labor cost, low facilities cost, or low energy cost such as in China and Mexico.

RESULTS

Manufacturing Cost Model

Manufacturing cost models were developed for the key parts in the PEM and alkaline stacks. Table 1 shows important parameters used in developing these cost models for 1-MW systems.

For the PEM electrolyzer stack, we assumed that the catalyst-coated membrane (CCM) is made by depositing catalyst layers (platinum group metals) on both sides of the purchased Nafion membrane² to form cathode and anode layers. The porous transport layer (PTL) is made from sintered titanium via a powder metallurgy process. This process allows us to adjust the compaction pressure to get the desired porosity in the PTL (in this analysis, porosity is assumed to be 30% by volume). The CCM and PTL represent the so-called membrane electrode assembly (MEA). Parts in the MEA are held together by the frame that is made from polyphenylene sulfide (PPS) resin mixed with 40% glass fiber. The PPS-based frame provides the flexibility required to hold the MEAs and durability to withstand relatively high operating temperature inside the stack (80°–120°C).

² Nafion is a registered trademark for DuPont.

Table 1. Some Parameters Used in Developing Cost Model for PEM Electrolyzer Stack

Part	PEM		Alkaline	
	Assumptions	Notes	Assumptions	Notes
Membrane	Nafion 117 (purchased part)	Alternatives include PFSA (PEEK, PBI) membranes ^a	Tokoyama A201 28 μm (purchased part)	Alternatives include mPBI, LDPE ^a
Catalyst	Pt price = \$1,500/tr.oz	DOE current value platinum loadings: Anode = 7 g/m ² (Pt), Cathode = 4 g/m ² (Pt-Ir)	n/a	n/a
Electrodes	Slot-die coating of catalyst to get CCM		Raney-Nickel	PVD ^b and selective leaching to get the required porosity
PTL	Sintered porous titanium Ti price = \$4.5/kg	Porosity = 30%	Pure nickel sheets	Nickel has good corrosion resistance in alkaline solution
Frame	PPS-40GF or PEEK	0.635 cm from each side for MEA bonding	PPS-40GF or PEEK ^c	
Plates	Stainless steel 316L	Coated (plasma nitriding)	Nickel plates	Surface treatment of high-purity Ni sheets

^a PFSA – perfluorosulfonic acid, PEEK – polyetheretherketone, PBI – polybenzimidazole, LDPE – low density polyethylene

^b PVD – physical vapor deposition

^c PPS-40GF – polyphenylene sulfide with 40% glass fiber filler

The alkaline electrolyzer stack consists of Raney-Nickel electrodes on both sides and Tokoyama A201 membrane in the middle (alternative membranes include mPBI and asbestos-based membranes, see [1–3] for discussion on characteristic and performance of these membrane technologies in the alkaline electrolyzers). Nickel is known to have good corrosion resistance to the alkaline solutions and good current densities [4]. Seal and frame are made from PPS-40GF: polyphenylene sulfide with 40% glass fiber filler (alternative membrane technologies include perfluorosulfonic acid and PEEK).

The PEM stack cost curve in Figure 1 shows the effect of the annual production rates on the total PEM stack cost. Generally, we can see that stack cost is decreasing with the annual production rates. This figure also shows that PEM stack cost is dominated by the CCM cost, followed by these parts in order from high cost to low cost contributions: PTL, assembly and end-plates, bipolar plates, and frame/seal. We should remember that CCM consists of Nafion membrane and platinum group metals, and both are high-cost materials.

The cost curve and cost breakdown for the alkaline stack as a function of the annual production rate are shown in Figure 2. We can see that the stack cost is dominated by the membrane cost followed by the cost of the following parts in order from high cost to low cost contributions: electrodes, bipolar plates, balance of stack (wiring, housing, insulation, etc.) and assembly and end-plates.

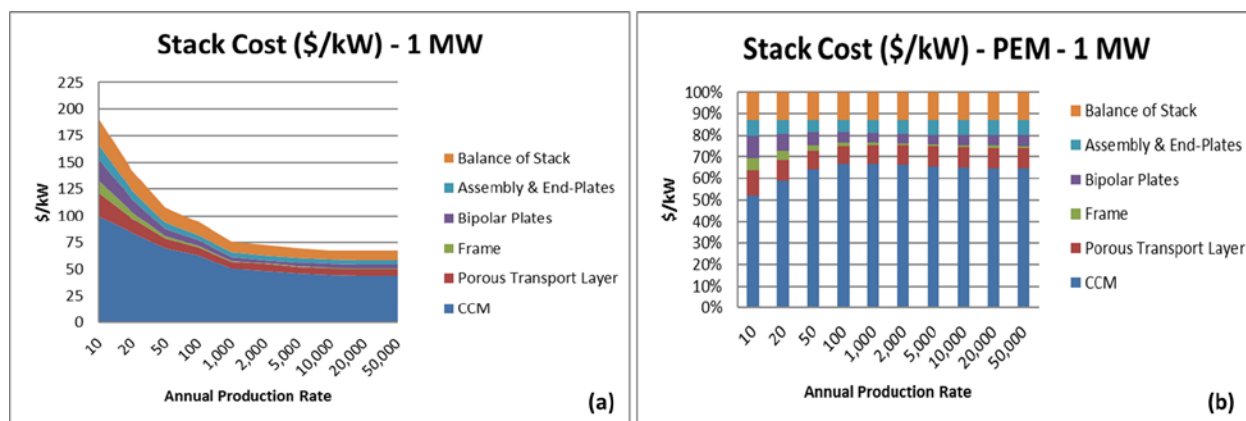


Figure 1. (a) Manufacturing cost curve for 1-MW PEM electrolyzer stack. (b) Cost breakdown for this system at different annual production rates (production capacity = 170 Nm³/h [367 kg/day]).

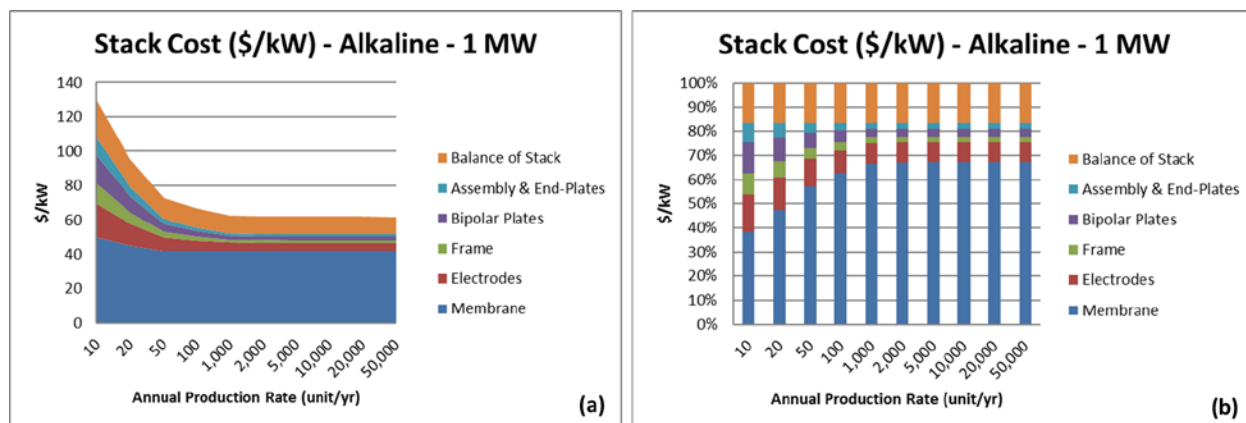


Figure 2. (a) Manufacturing cost curve for 1-MW alkaline electrolyzer stack. (b) Cost breakdown for this system at different annual production rates (production capacity = 110 Nm³/h [237 kg/day]).

The PEM system cost and cost breakdown are shown in Figure 3a and 3b respectively. Balance of plant (BOP) dominates the total system cost at different annual production rates. Here, we assumed that BOP parts are outsourced from part vendors, so we do not expect economies of scale to have the same impact as in the case of a stack that is manufactured in-house. Power supplies (AC/DC rectifier) dominate the balance of plant cost followed by the deionized water circulation unit, which contains an expensive water/oxygen separation tank that separates oxygen and water coming out of the stack.

The alkaline electrolyzer system cost and cost breakdown are shown in Figure 3c and 3d, respectively. Like the PEM electrolysis system, the alkaline electrolysis system cost is dominated by the BOP (major contributor is the power supplies). The hydrogen processing unit and electrolyte circulation subsystem each contribute to about 10%–15% in the total system cost.

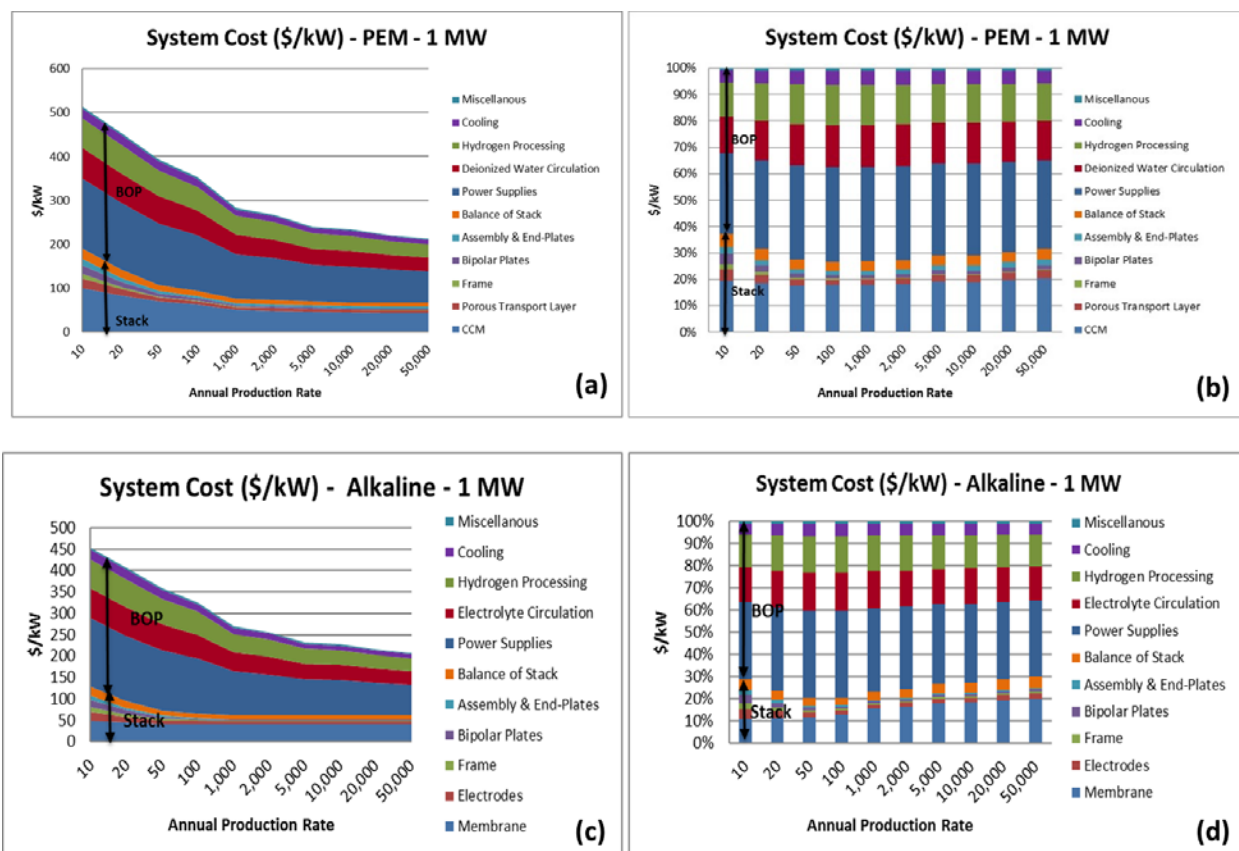


Figure 3. (a) Cost curve for 1-MW PEM electrolyzer system showing cost of the stack and BOP. (b) Cost breakdown for 1-MW PEM electrolyzer at different annual production rates. (c) Cost curve for 1-MW alkaline electrolyzer system showing cost of the stack and BOP. (d) Cost breakdown for 1-MW alkaline electrolyzer at different annual production rates. (Note: Hydrogen production capacity for 1-MW PEM electrolyzer is 170 Nm³/h [367 kg/day], and hydrogen production capacity for 1-MW alkaline electrolyzer is 110 Nm³/h [237 kg/day].)

Manufacturing Competitiveness Analysis

Manufacturing competitiveness analysis was used to examine the relative cost of manufacturing PEM and alkaline stacks in several countries and to study the cost advantages of the U.S.-based manufacturers over other international manufacturers. Figure 4 shows the manufacturing cost for 1-MW PEM and alkaline stacks. By looking at these charts we can see that China’s advantage relative to the United States is driven by lower labor (including stack assembly, which is a labor-intensive process), building, and energy costs. Mexico’s advantage relative to the United States is driven by lower labor (including assembly) and building costs. Relative cost of the stack is higher in Europe because of the higher labor and energy costs. Similarly, the relative cost of the stack is higher in Japan (relative to the United States) because of the higher labor costs in Japan.

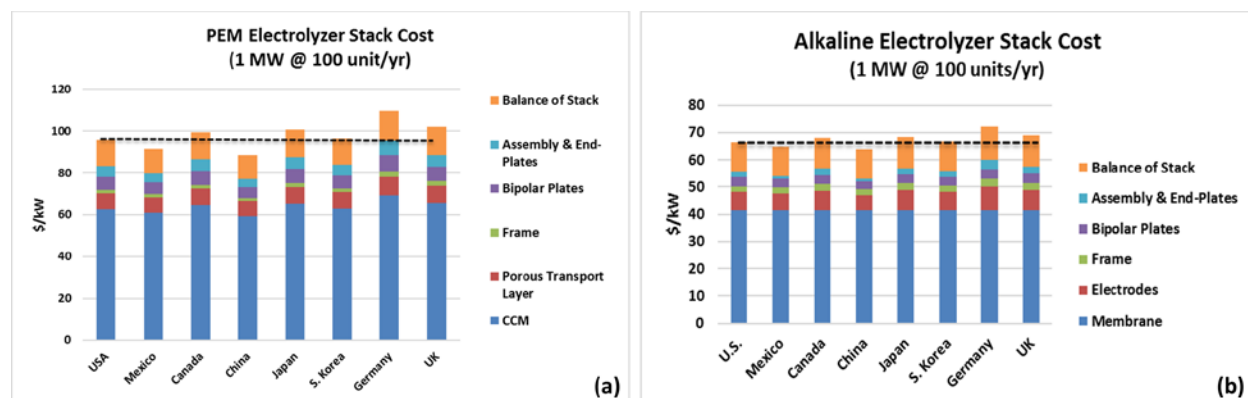


Figure 4. (a) Manufacturing cost for 1-MW PEM electrolyzer stack (production capacity 170 Nm³/h [367 kg/day]). (b) Manufacturing cost for 1-MW alkaline electrolyzer stack (production capacity 110 Nm³/h [237 kg/day]).

CONCLUSIONS AND UPCOMING ACTIVITIES

This project discusses manufacturing competitiveness analysis for the hydrogen refueling stations including on-site hydrogen production systems. In FY 2018, we focused on the on-site hydrogen production systems (PEM and alkaline). Bottom-up cost models were developed for the major parts in PEM and alkaline stacks. For a 1-MW system, we found that system costs (total of the stack and BOP) for both PEM and alkaline electrolyzers are dominated by the BOP cost at higher production rates. At the stack level, the CCM in the PEM stack and membrane in the alkaline stack dominates the stack cost.

This project was concluded in September 2018, but we believe that there are many areas that need further investigations to direct future R&D efforts in stack manufacturing and BOP standardization. Roll-to-roll manufacturing of CCM and increasing the automation level in the stack assembly are two important areas where we can see cost reductions in stack manufacturing. Standardization of BOP parts is another area where R&D efforts can be made to lower the cost of BOP, which contributes about two-thirds of the cost of a 1-MW PEM electrolyzer.

FY 2018 PUBLICATIONS/PRESENTATIONS

1. Ahmad Mayyas, “Manufacturing Competitiveness Analysis for Hydrogen Refueling Stations,” Presentation at the Annual Merit Review, Washington, D.C., June 4, 2018.
2. Ahmad Mayyas and Margaret Mann, “Emerging Manufacturing Technologies for Fuel Cells and Electrolyzers,” Accepted for publication in *Procedia Manufacturing* (2018).
3. Ahmad Mayyas, Margaret Mann, and Mark Ruth, “Manufacturing Competitiveness Analysis for PEM and Alkaline Water Electrolysis Systems,” Fuel Cell Seminar and Energy Exposition, Long Beach, CA, November 7–9, 2017.

REFERENCES

1. M. Bodner, A. Hofer, and V. Hacker, “H₂ Generation from Alkaline Electrolyzer,” *WIREs Energy Environ* 4 (2015): 365–381, doi:10.1002/wene.150.
2. M.R. Kraglund, D. Aili, K. Jankova, E. Christensen, Q. Li, and J.O. Jensen, “Zero-Gap Alkaline Water Electrolysis Using Ion-Solvating Polymer Electrolyte Membranes at Reduced KOH Concentrations,” *Journal of The Electrochemical Society* 163, no. 11 (2016): F3125–F3131.
3. U.F. Vogt, M. Gorbar, M. Schlupp, G. Kaup, A. Bonk, A. Hermosilla, and A. Züttel, “Membranes Development for Alkaline Water Electrolysis,” 4th European PEFC and H₂ Forum, Luzern, Switzerland, July 2–5, 2013.

4. D. Symes, B. Al-Duri, W. Bujalski, and A. Dhir, “Cost-effective design of the alkaline electrolyser for enhanced electrochemical performance and reduced electrode degradation,” *International Journal of Low-Carbon Technologies* 10 (2015): 452–459.

Roll-to-Roll Advanced Materials Manufacturing Lab Consortium

Claus Daniel (Primary Contact), Scott Mauger, David Wood, Greg Krumdick, Vince Battaglia, Michael Ulsh
Oak Ridge National Laboratory
1 Bethel Valley Rd.
Oak Ridge, TN 37830
Phone: 865-946-1544
Email: danielc@ornl.gov

DOE Manager: Nancy Garland
Phone: (202) 586-5673
Email: Nancy.Garland@ee.doe.gov

Partners:

- Argonne National Laboratory, Lemont, IL
- Lawrence Berkeley National Laboratory, Berkeley, CA
- National Renewable Energy Laboratory, Golden, CO
- Eastman Business Park, Rochester, NY
- Proton OnSite, Wallingford, CT

Project Start Date: October 1, 2016
Project End Date: September 30, 2019

Overall Objectives

Oak Ridge National Laboratory (ORNL), Argonne National Laboratory (ANL), Lawrence Berkeley National Laboratory (LBNL), and the National Renewable Energy Laboratory (NREL) in collaboration with Eastman Kodak Business Park (Kodak) formed a Roll-to-Roll Advanced Materials Manufacturing (R2R-AMM) multi-lab collaboration to:

- Broadly disseminate materials, process science, and advanced technologies to industry in R2R manufacturing.
- Enable advanced R2R manufacturing R&D to demonstrate a materials genomic approach to optimization of process parameters for finding new transformational improvements in manufacturing technologies enabling clean energy applications.

Fiscal Year (FY) 2018 Objectives

For its fuel cell core lab project, the multi-lab collaboration will:

- Develop ink formulations and understand interparticle interactions and the impact of dispersion methods using rheology, zeta potential, and ultra-small-angle X-ray scattering (USAXS) measurements.
- Initiate a rheological model for inks containing carbon-supported platinum catalysts, ionomer, and solvents.
- At various scales and using different processes, coat phase-segregated and multi-layer ionomer-rich-surface (IRS) gas-diffusion electrodes (GDEs).
- Perform advanced ex situ characterization, including X-ray computed tomography (XCT), of coated GDEs to understand the impact of formulation and process parameters on electrode morphology.
- Perform in situ testing to understand the impact of formulation and process parameters on membrane electrode assembly (MEA) performance.
- Initiate a new cooperative research and development agreement (CRADA) project in the hydrogen and fuel cells space.

Technical Barriers

This project addresses the following technical barriers from the Manufacturing R&D section of the Fuel Cell Technologies Office Multi-Year Research, Development, and Demonstration Plan¹:

- (A) Lack of High Volume MEA Processes.

¹ <https://www.energy.gov/eere/fuelcells/downloads/fuel-cell-technologies-office-multi-year-research-development-and-22>

Contribution to Achievement of DOE Manufacturing Milestones

This project contributes to the achievement of the following DOE milestones from the Manufacturing R&D section of the Fuel Cell Technologies Office Multi-Year Research, Development, and Demonstration Plan:

- Milestone 1.6: Develop fabrication and assembly processes for polymer electrolyte membrane (PEM) fuel cell MEA components leading to an automotive fuel cell stack that costs \$20/kW. (4Q, 2020)

FY 2018 Accomplishments

The multi-lab collaboration accomplished the following in FY 2018:

- Performed USAXS measurements of inks in situ during mixing, with different supported catalysts, ionomer ratios, solvent mixtures, and dispersing methods to elucidate the impact of these variables on the time required to fully disperse the supported catalysts and the level of agglomeration in the ink.
- Performed Kelvin probe measurements of the R2R gravure-coated IRS GDEs to understand the impact of formulation and drying parameters on enabling segregation of the ionomer during the drying process.
- Performed in situ testing (polarization, mass activity, transport resistance) of the same GDEs to understand the correlation between achieving an ionomer-rich surface and achieving target MEA performance.
- Developed an open-source software tool to perform equivalent-circuit modeling for the analysis of fuel cell electrochemical impedance spectroscopy (EIS) measurements.
- Performed XCT of IRS GDEs to understand the impact of ink and process parameters on ionomer, pore size, and solid-particle size distributions in the electrode.
- Initiated the development of a fuel cell catalyst ink rheology model to elucidate particle-ionomer-solvent interactions.

- Studied high-solids ink formulation, mixing, and the resulting particle size to support initial slot-die coating studies.
- Awarded a new CRADA project with Proton OnSite to collaborate on high-volume methods for PEM electrolysis MEA fabrication.

INTRODUCTION

GDEs are recently garnering high interest in the industry as an alternate or possibly combined fabrication pathway for MEAs, as opposed to the more standard catalyst-coated membrane (CCM) approach. GDEs provide a different set of fabrication and performance variables that may provide improved performance and lifetime in some cases. However, fabrication of MEAs based on GDEs can require different material structures than CCMs, and, for scaling of GDE-based MEAs, this means potentially different process techniques and conditions. For example, an additional layer of ionomer, which would require another processing step, is often required between the GDE catalyst layer and membrane to achieve comparable performance to CCMs. The goal of this project is to explore, understand, and optimize material and process parameters for scalable processes to support increased throughput, increased quality, and reduced cost for high-volume production of MEAs by developing single-process methodologies to coat IRS GDEs via R2R processes with comparable performance to baseline CCMs.

APPROACH

The approach is to understand the fundamental (nano- and micro-scale) interactions in the heterogeneous electrode ink that lead to macro-scale properties determined by rheology, which ultimately impact coating and drying parameters as well as device performance (NREL and ORNL). NREL and ORNL will leverage coating technologies across several scales to fabricate IRS GDEs. Advanced characterization tools at ANL and ORNL (USAXS and XCT at ANL's Advanced Photon Source [APS] and electron microscopy at ORNL) will be leveraged to understand the dispersion of particles and polymer in the ink and to image the morphology through the thickness of the electrode layer as a function of material, ink, and process parameters. Modeling capabilities at LBNL will be leveraged to help understand the complex interparticle interactions in the electrode that impact rheology, coatibility, and the electrode layer morphology. NREL will utilize standard in situ testing to quantify impact of ink and process parameters on performance.

RESULTS

We performed USAXS measurements of inks with different catalyst supports, ionomer-to-carbon ratios (I:C), and solvent mixtures at the APS at ANL. The measurements were made in an in situ apparatus, designed such that samples of the ink could be directly measured during the dispersing process as a function of time. Figure 1 (a) shows the raw USAXS intensity data as a function of the scattering vector (Q), where increasing Q is associated with decreasing particle size. In this example, data for four different durations of bath sonication are shown. Figure 1 (b) then shows the USAXS intensity as a function of time for the Q values associated with nominally $3\ \mu\text{m}$ ($Q = 0.0002$) and nominally $300\ \text{nm}$ ($Q = 0.002$) structures. We observe that, for the first 10 minutes of sonication, larger agglomerates are broken up, leading to an increase in smaller, aggregate particles. After 10 minutes of sonication, no further breakup of particles is observed. MEAs were made with inks of the same formulations, and in situ polarization and mass activity results indicated that a 10-second tip sonication prior to bath sonication resulted in improved performance over that of bath sonication alone, and that, subsequent to a 10-second tip sonication, 20 minutes of bath sonication led to higher performance and mass activity than for 5- and 1-minute bath sonication durations.

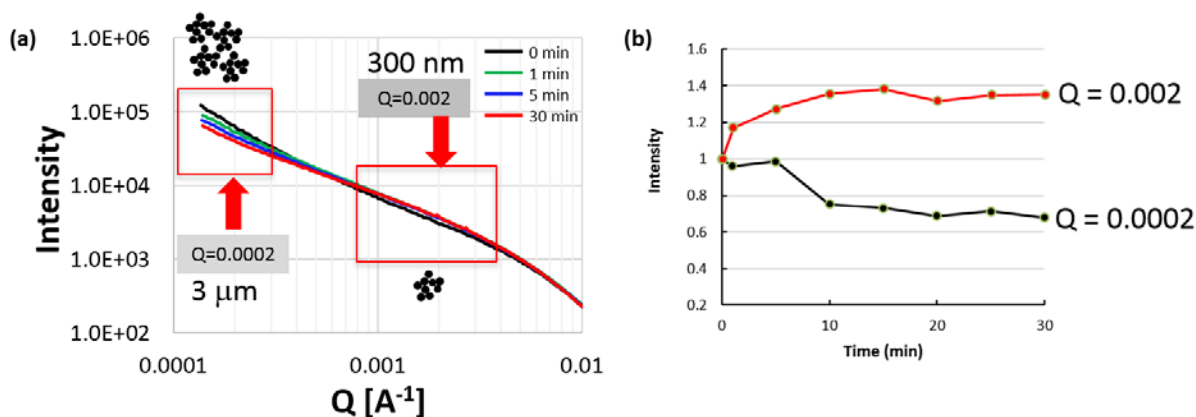


Figure 1. (a) Raw USAXS intensity data for an example ink sonicated for four different durations, and (b) USAXS intensity data associated with agglomerate ($Q = 0.0002$) and primary aggregate ($Q = 0.002$) particles in the ink as a function of mixing time

We also performed unique NREL-developed oxygen-transport limiting current analysis and EIS to understand the oxygen transport (non-Fickian) resistance and bulk catalyst layer resistances in these MEAs. We observed that the optimal case (10-s tip + 20-min bath) had a lower resistance than a comparator (1-min bath) case, which experienced ineffective dispersion and thus had larger catalyst agglomerates. Similarly, the EIS measurements indicated that the 10-s tip + 20-min bath and 20-min bath cases had the least catalyst layer proton resistance. The 20-min tip sonication case had higher resistance due to excessive sonication that detached Pt from the carbon support, whereas the 1-min bath case had the highest resistance due to insufficient dispersion. To assist with data analysis for these in situ studies, we developed a methodology and associated open-source code to perform equivalent-circuit modeling of fuel cell MEA EIS data. This code helps us to understand the resistances in the various MEA layers as a function of the various ink and process parameters, including protonic resistance of the cathode. The open-source code has been provided to the community via NREL's website.

We performed Kelvin probe measurements of R2R gravure-coated GDEs, which provide a rapid indication of the amount of ionomer on the surface of the electrode. Figure 2 (a) shows these results, which indicate that higher I:C and higher fraction of water in the water/1-propanol solvent mixture lead to higher surface content of ionomer. We then performed in situ testing of MEAs made from these GDEs. Figure 2 (b) and (c) show that the oxygen-reduction-reaction mass activity and H_2 /air polarization performance, respectively, both improve for conditions that optimize ionomer content on the GDE surface.

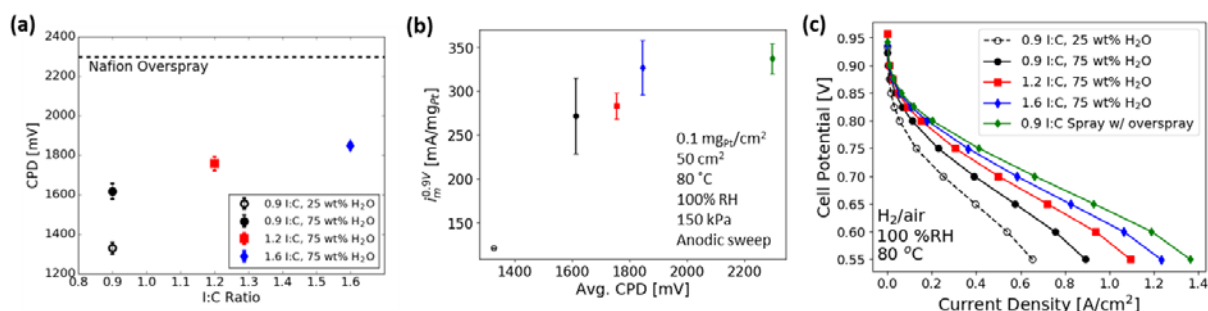


Figure 2. (a) Kelvin probe contact potential difference as a function of I:C for inks with different I:C and solvent ratio, (b) mass activity as a function of contact potential difference for MEAs made from the same four inks as well as for the comparator GDE with a separate ionomer overcoat (same legend as [c]), and (c) H_2 /air polarization for the same MEAs

XCT of these GDEs was also performed at the APS to understand how ink and process parameters impact the morphology of the electrode. Figure 3 (a) shows a 3-D reconstruction of the microstructure of one of the electrodes. Figure 3 (b) shows profiles of ionomer distribution through the normalized thickness of the electrode as a function of water/1-propanol mixture and I:C. The electrodes cast from the water-rich solvent (solid data lines) have a more uniform distribution because the ionomer associated with the catalyst particle is not mobile during the drying of the electrode. We also see that higher I:C leads to an increase in the ionomer surface content. In the electrode cast from the 1-propanol-rich dispersion, the ionomer is not associated with the catalyst, so it is more mobile and can redistribute itself within the electrode as it dries.

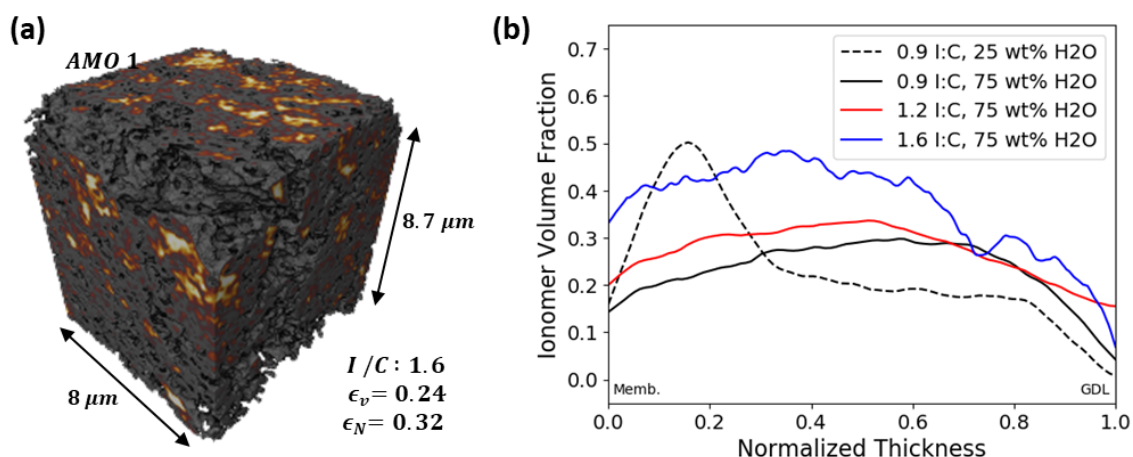


Figure 3. (a) 3-D visualization of the example electrode, and (b) through-the-thickness ionomer profiles from XCT

In preparation for slot-die coating of catalyst inks, we performed rheology and particle-size studies of high-solids-loading carbon-only inks to understand processing limitations with these materials. Figure 4 (a) shows rheology data for three of the carbon-only inks, with solids loadings between 10% and 13%. The rheological behavior of all three inks is shear thinning, and the viscosity is seen to increase with solids loading. Figure 4 (b) shows an image of the slot-die-coated carbon ink on the coating line at ORNL.

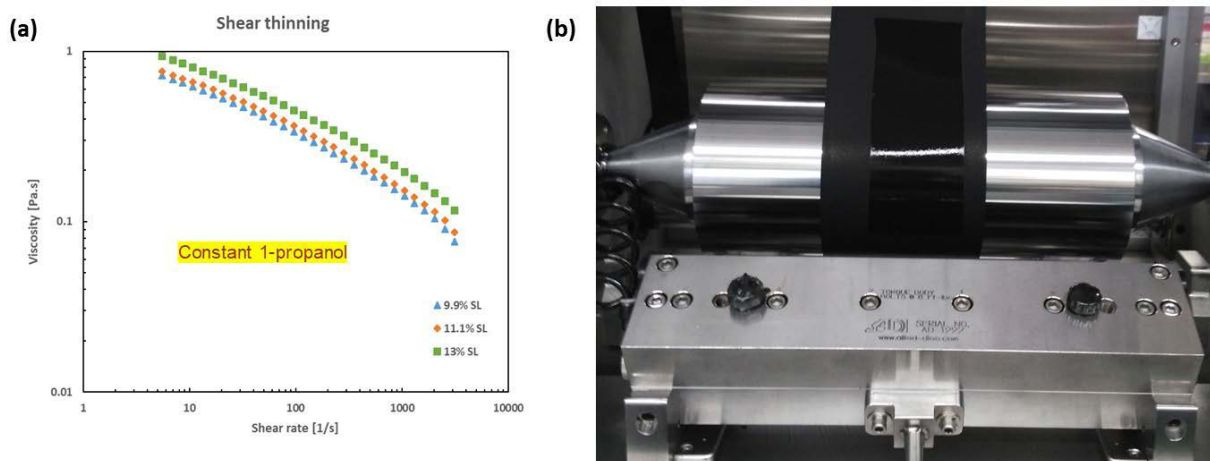


Figure 4. (a) High-solids-loading ink viscosity as $f(\text{shear rate})$, and (b) image of slot-die coated carbon-only ink

CONCLUSIONS AND UPCOMING ACTIVITIES

- As shown in Figure 2, the R2R-coated IRS GDEs to date have demonstrated equivalent mass activity to the baseline CCM, although the high-current-density performance is not yet comparable. These data show strong potential for meeting the goal of replacing a two-layer (electrode + ionomer overcoat), two-process-step GDE fabrication methodology with one having a single layer and comparable performance to the CCM baseline.
- Future work under consideration toward fully meeting the project goals (depending on future funding and prioritization) includes dual-slot simultaneous two-layer coating of the electrode and ionomer layers, single-layer segregated coatings at higher drying temperature and using alternate solvents, further development of the fuel cell ink rheology model, and initiation of consolidation and coating physics models.

FY 2018 PUBLICATIONS/PRESENTATIONS

1. P. Rupnowski, M. Ulsh, B. Sopori, B.G. Green, D.L. Wood III, J. Li, and Y. Sheng, “In-line monitoring of Li-ion battery electrode porosity and areal loading using active thermal scanning – modeling and initial experiment,” *J. Power Sources* 375 (2018):138–148.
2. B.L. Sopori, M.J. Ulsh, P. Rupnowski, G. Bender, M.M. Penev, J. Li, D.L. Wood III, and C. Daniel, “Batch and Continuous Methods for Evaluating the Physical and Thermal Properties of Thin Films,” U.S. Patent Application no. 15/554,551, March 8, 2018.
3. J. Park, N. Kariuki, D.J. Myers, S.A. Mauger, K.C. Neyerlin, and M. Ulsh, “In Situ X-Ray Scattering Characterization of PEMFC Catalyst Ink Microstructure during Ink Processing,” Oral presentation MA2018-01 at the 233rd ECS Meeting, Seattle, WA, May 2018.
4. C. Daniel, S. Mauger, G. Krumdick, R. Prasher, M. Ulsh, and D. Wood, “Roll-to-roll Advanced Materials Manufacturing Lab Consortium,” Oral presentation at the Hydrogen and Fuel Cell Program Annual Merit Review and Peer Evaluation Meeting, Washington DC, June 2018.
5. M. Ulsh, S. Mauger, S. Khandavalli, J. Pfeilsticker, M. Wang, K.C. Neyerlin, D. Wood III, J. Li, M. Wood, D. Myers, N. Kariuki, J. Park, C.F. Cetinbas, R. Ahluwalia, G. Krumdick, A. Weber, F. Ma, and R. Prasher, “PEM Fuel Cell Gas-diffusion Electrodes with Ionomer-rich Surface Layer,” Poster presentation at the Advanced Manufacturing Office Peer Review Meeting, Washington DC, July 2018.
6. S.A. Mauger, C.F. Cetinbas, J.H. Park, K.C. Neyerlin, R.K. Ahluwalia, D.J. Myers, S. Khandavalli, L. Hu, S. Litster, and M. Ulsh, “Control of ionomer distribution and porosity in roll-to-roll coated fuel cell catalyst layers,” Poster presentation at the Fuel Cells Gordon Research Conference, Smithfield, RI, July 2018.
7. S.A. Mauger, C.F. Cetinbas, R.K. Ahluwalia, D.J. Myers, J. Park, K.C. Neyerlin, L. Hu, S. Litster, and M. Ulsh, “Control of ionomer distribution and porosity in roll-to-roll coated fuel cell catalyst layers,” Oral presentation at the International Symposium of Coating Science and Technology, Long Beach, CA, September 2018.

Hydrogen Energy Systems as a Grid Management Tool

Richard (Rick) E. Rocheleau (Principal Investigator), Mitch Ewan (Primary Contact)
Hawaii Natural Energy Institute (HNEI)
School of Ocean and Earth Science and Technology
University of Hawaii at Manoa
1680 East-West Road, POST 109
Honolulu, HI 96822
Phone: (808) 956-2337; (808) 956-8346
Email: ewan@hawaii.edu; rochelea@hawaii.edu

DOE Manager: Peter Devlin
Phone: (202) 586-4905
Email: Peter.Devlin@ee.doe.gov

Technical Advisor: Karen Swider-Lyons
Naval Research Laboratory
Phone: (202) 404-3314
Email: karen.lyons@nrl.navy.mil

Contract Number: DE-EE0002811

Project Start Date: September 30, 2010
Project End Date: September 29, 2015

(NELHA) to support the operation of the hydrogen system.

- Install, commission, and operate the hydrogen system at NELHA.
- Install a 350-bar hydrogen fuel dispenser at NELHA to fuel the MTA fuel cell electric vehicle (FCEV) shuttle bus.
- Install a 350-bar hydrogen fuel dispenser at HAVO to fuel two HAVO shuttle buses.
- Develop a HAVO compressor boost system to extract up to 90% of the hydrogen from the hydrogen transport trailers and reduce hydrogen transport cost by 50%.
- Recertify three hydrogen transport trailers to extend operations for another 5 years.
- Complete the conversion of the MTA bus and install an export power unit to supply 110/220 VAC power for civil defense emergency power.

Overall Objectives

- Demonstrate the use of electrolyzers to mitigate the impacts of intermittent renewable energy by regulating grid frequency.
- Characterize performance and durability of commercially available electrolyzers under dynamic load conditions.
- Supply hydrogen to fuel cell shuttle buses operated by County of Hawaii Mass Transit Agency (MTA) and Hawaii Volcanoes National Park (HAVO).
- Conduct performance and cost analysis to identify benefits of integrated system including grid ancillary services and off-grid revenue streams.
- Evaluate effect on reducing overall hydrogen costs offset by value-added revenue streams.

Fiscal Year (FY) 2018 Objectives

- Install site improvements and utilities at Natural Energy Laboratory Hawaii Authority

Technical Barriers

This project addresses the following technical barriers from the Market Transformation section of the Fuel Cell Technologies Office Multi-Year Research, Development and Demonstration Plan¹:

- (A) Inadequate Standards and Complex and Expensive Permitting Procedures
- (B) High Hydrogen Infrastructure Capital Costs
- (C) Inadequate Private Sector Resources Available for Infrastructure Development
- (F) Inadequate User Experience for Many Hydrogen and Fuel Cell Applications
- (G) Lack of Knowledge Regarding the Use of Hydrogen Inhibits Siting
- (H) Utility and Other Stakeholders Lack Awareness of Potential Hydrogen Production and Storage Applications.

¹ <https://www.energy.gov/eere/fuelcells/downloads/fuel-cell-technologies-office-multi-year-research-development-and-22>

Technical Targets

No specific technical targets have been set.

FY 2018 Accomplishments

- Completed installation of site improvements and utilities at NELHA to support the operation of the hydrogen system.
- Installed 350-bar hydrogen fuel dispenser at NELHA to fuel the MTA FCEV bus.
- Completed the conversion of the MTA bus and installed the 110/220 VAC export power unit.
- Replaced the original MTA bus 30 kW fuel cell power system with a new technology US Hybrid 40 kW fuel cell power system.
- Completed recertification of three hydrogen transport trailers.
- Completed the development of a dynamic simulation model of the hydrogen production system.
- Completed the development of the HAVO compressor boost system.

INTRODUCTION

While solar and wind resources offer a major opportunity for supplying energy for electrical grid electricity production and delivery systems, their variability and intermittency can raise challenges for the cost-effective and high-reliability integration of these renewable sources on electrical grids. In Hawaii, the curtailment and grid management-related challenges experienced by these renewable sources are a challenge at today's level of generation capacity and will hinder the substantive additional penetration of electricity generation supplied by these renewable resources. We believe hydrogen production through electrolysis may provide an opportunity to mitigate curtailment and grid management costs by serving as a controllable load allowing real-time control in response to changes in electricity production. The renewable hydrogen product can also create new and incremental revenue streams to the power producers through the sale of hydrogen products to customers outside of the electricity delivery system. Accordingly, hydrogen energy production at utility scale offers the potential for increasing the levels of variable renewable energy that can be harnessed by the power producers or systems operators.

APPROACH

This project evaluates the value proposition of using electrolyzers to both regulate the grid and use the product hydrogen for transportation applications. An electrolyzer system is being installed at NELHA on the Big Island. The electrolyzer will be ramped up and down to simulate frequency regulation. Data will be collected to analyze the optimum electrolyzer ramp rates and determine its durability and performance under dynamic operating conditions over time. The hydrogen produced by the system will be used to fuel three hydrogen-fueled buses. It is planned to deliver hydrogen to HAVO to support two HAVO buses. The third bus will be operated in Kailua-Kona. A schematic of the project concept is shown in Figure 1.

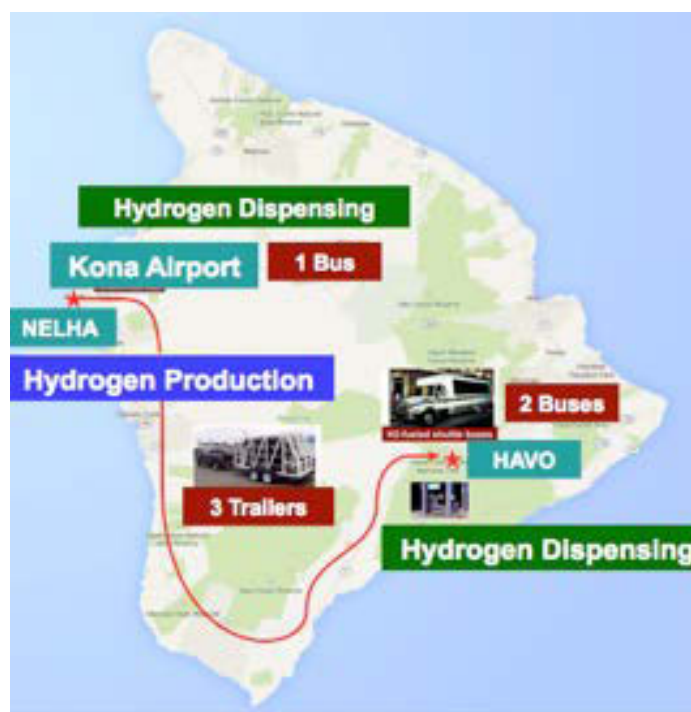


Figure 1. Hydrogen production and delivery concept

RESULTS

Considerable progress was made in FY 2018. With the permitting approved in FY 2017, the site improvements and installation of the hydrogen system equipment (Figures 2, 3, and 4) were completed in May 2018.



Figure 2. NELHA site infrastructure



Figure 3. Entrance to NELHA hydrogen site

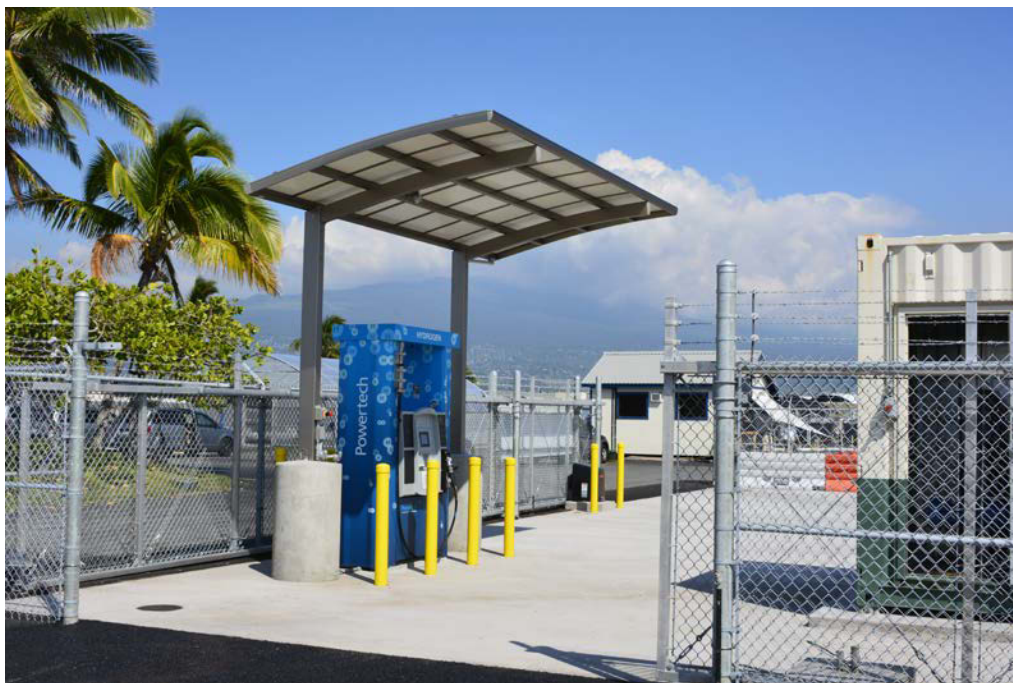


Figure 4. NELHA 350-bar dispenser

This was followed by commissioning the electrolyzer and compressor systems by their respective suppliers/manufacturers. The recertification of the hydrogen transport trailers (HTTs) was completed by Luxfer, the cylinder manufacturer; however, the requirement to install an upgraded design of the thermal pressure relief devices resulted in a significant additional expense and delays in obtaining the new devices, and it has delayed shipping the units to Hawaii. This also impacted the completion of the final commissioning of the overall system by several months because the HTTs are a significant component of our infrastructure design. In parallel, work was completed on the conversion of the three hydrogen buses including installation of a new technology 40 kW US Hybrid fuel cell on the MTA bus. The MTA bus was also retrofitted with a US Hybrid power export unit that converts the stored energy on the bus to 110/220 VAC power for up to 30 hours. The bus can then be refueled with hydrogen for another 30 hours of power. This effectively converts the bus into a mobile power supply that supports civil defense during environmental emergencies such as hurricanes. The delivery of hydrogen to HAVO will be accomplished via the three hydrogen transport trailers using a “drag and drop” strategy. Using a cascade fill would result in the trailers being able to dispense only ~50% of their contents. Given the high cost of transportation, it was decided to develop a compressor system that could extract more hydrogen from the trailer. This was accomplished through the development of a compressor boost system, which will allow ~90% of the hydrogen being dispensed, resulting in a reduction of hydrogen transport costs of ~50%. The boost compressor system has been completed but cannot be shipped until it has completed testing with each of the hydrogen transport trailers. In May 2018 Mother Nature struck a major blow to the project with the eruption of the Kilauea volcano at HAVO, causing significant damage to HAVO’s infrastructure. After 3 months, the eruption finally stopped in August; however, volcanologists have stated there is no guarantee that the eruption will not start again. The HAVO segment of the project is currently on hold until the situation has been clarified.

CONCLUSIONS AND UPCOMING ACTIVITIES

This project has coordinated the efforts of a diverse group of stakeholders to provide a technology solution to facilitate integration of intermittent renewable energy sources on an electrical grid while producing hydrogen for transportation. The project has identified and provided valuable solutions to the many non-technical barriers associated with introducing hydrogen technology into a community for the first time. Lessons learned from this project will make the way easier for projects that follow.

It is concluded that a hydrogen energy system (HES) is a valuable grid frequency management tool capable of controlling intermittent renewable sources of energy for grid frequency management applications. While the HES is not as fast as the battery energy storage system (BESS), the performance measured with the modified control system under different load demands is much closer to the BESS performance. However, our current thinking is that replicating the exact operational response time as the BESS cannot be achieved with an electrolyzer. The data shows that the electrolyzer can only be used for slower-acting changes (1 Hz to 0.5 Hz). A potential solution is to design an electrolyzer/BESS hybrid system and develop a modeling program to find the optimum mix of battery and electrolyzer to provide the maximum grid regulation services at minimum cost. Additional work is required to develop a control scheme that can manage power distribution between the electrolyzer and BESS.

While the DOE participation in the project formally ended in 2015, the project is being continued using other funding. Future work involves following:

- Operating hydrogen production systems and dispensing infrastructure at the NELHA site
- Operating the 29-passenger fuel cell electric bus based at the NELHA site
- Transporting hydrogen in hydrogen transport trailers from the NELHA production site to the HAVO dispenser to support the two HAVO buses
- Collecting and analyzing hydrogen system and FCEV bus performance data
- Preparing performance reports and sharing them with project sponsors and industry
- Conducting outreach activities with the public to inform them about hydrogen technologies.

FY 2018 PUBLICATIONS/PRESENTATIONS

1. M. Ewan and R. Rocheleau, “Hydrogen Energy Systems as a Grid Management Tool,” Oral presentation at the DOE Hydrogen and Fuel Cells Program Annual Merit Review, Washington, DC, June 14, 2018.
2. M. Ewan, “Supporting a Hawaii Hydrogen Economy,” Oral presentation at First International Hydrogen Forum, San Jose, Costa Rica, August 13, 2018.

Fuel-Cell-Powered Airport Ground Support Equipment Deployment

Joe Blanchard
Plug Power, Inc.
15913 E. Euclid Ave.
Spokane, WA 99316
Phone: (509) 280-7741
Email: jblanchard@plugpower.com

DOE Managers:
Peter Devlin
Phone: (202) 586-4905
Email: Peter.Devlin@ee.doe.gov

Michael Hahn
Phone: (240) 562-1551
Email: Michael.Hahn@ee.doe.gov

Contract Number: DE-EE0006093

Project Start Date: January 2013
Project End Date: May 2018

Overall Objectives

- To create a hydrogen fuel cell-based solution for airport ground support equipment (GSE) that is cost competitive and more energy efficient compared to incumbent internal combustion engine-powered alternatives.
- To enable airport end users to accomplish daily tasks with a hydrogen fuel cell solution while reducing consumption of gasoline and diesel fuels, reducing U.S. demand for petroleum.
- To demonstrate lower carbon emissions with fuel cells.
- To demonstrate a value proposition that shows decreased energy expenditures when compared to diesel-powered airport vehicles.

Fiscal Year (FY) 2018 Objectives

- Complete redesign of fuel cell system to incorporate the Plug Power stack.
- Redeploy updated fuel-cell-powered cargo tractors at Memphis Airport to continue operation.

- Collect operational and performance data throughout FY 2018.

Technical Barriers

This project addresses the following technical barriers from the Technology Validation section of the Fuel Cell Technologies Office Multi-Year Research, Development, and Demonstration Plan¹:

- Lack of Fuel Cell Electric Vehicle and Fuel Cell Bus Performance and Durability Data.

It also addresses the following technical barriers from the Market Transformation section of the Fuel Cell Technologies Office Multi-Year Research, Development, and Demonstration Plan:

- Inadequate user experience for many hydrogen and fuel cell applications.

Contribution to Achievement of DOE Milestones

This project will contribute to achievement of the following DOE milestones from the Systems Analysis section of the Fuel Cell Technologies Office Multi-Year Research, Development, and Demonstration Plan:

- Milestone 1.16: Complete analysis of program performance, cost status, and potential use of fuel cells for a portfolio of commercial applications. (4Q, 2018)
- Milestone 1.17: Complete analysis of program technology performance and cost status, and potential to enable use of fuel cells for a portfolio of commercial applications. (4Q, 2018)
- Milestone 1.18: Complete life cycle analysis of vehicle costs for fuel cell electric vehicles compared to other vehicle platforms. (4Q, 2019)
- Milestone 1.19: Complete analysis of the potential for hydrogen, stationary fuel cells, fuel cell vehicles, and other fuel cell

¹ <https://www.energy.gov/eere/fuelcells/downloads/fuel-cell-technologies-office-multi-year-research-development-and-22>

applications such as material handling equipment including resources, infrastructure and system effects resulting from the growth in hydrogen market shares in various economic sectors. (4Q, 2020)

It also contributes to achievement of the following DOE milestones from the Market Transformation section of the Fuel Cell Technologies Office Multi-Year Research, Development, and Demonstration Plan:

- Milestone 2.11: Develop installation and permitting templates for airport ground support equipment. (1Q, 2015)

FY 2018 Accomplishments

- Completed redesign of GSE fuel cell with Plug Power stack.
- Completed fleet redeployment of 14 fuel-cell-powered tractors at Memphis. One system was held at Plug Power for ongoing testing.
- Demonstrated performance of fleet at Memphis met objectives established in original statement of project objectives.
- Provided data set on performance through January 2018.
- Completed decommission of Memphis operation and hydrogen infrastructure.
- Received commitment from FedEx to relocate two fuel cell systems at Albany Airport for expanded weather testing.
- Established logistics between FedEx at the Albany Airport and Plug Power Headquarters to use Plug Power's hydrogen filling station for the remainder of the program.
- Installed the hydrogen filling station to support the FedEx Express Hydrogen Fuel Cell Extended-Range Battery Electric Vehicles program (DE-EE00006522).
- Revised statement of project objectives and budget period 3 plans to reflect change to Albany Airport.
- Began preparations of fuel cells, GSE tractors, and hydrogen fueling station to be operational in the fourth quarter of calendar year 2018.

INTRODUCTION

The airside operations at an airport significantly contribute to the overall emissions and fuel consumption of an airport operator. Identifying alternative power solutions for airport GSE that reduce emissions while maintaining economic and productivity objectives is an ongoing challenge. Battery-powered GSE support improvements in emissions but introduce potential performance shortcomings as well as require a charging infrastructure.

Fuel cells have been identified as a potential solution to meet the demanding operational needs of airport GSE as well to address the need to reduce emissions. This program converted 15 battery electric GSE baggage tractors to hydrogen fuel cell power to demonstrate the simplicity and functionality of hydrogen as an alternate zero-emission solution.

APPROACH

The project approach was to design and test a fuel cell solution that effectively replaces a lead-acid battery pack for an existing electric-drive GSE unit. The project also required the participants to establish a hydrogen infrastructure that included compression, storage, and dispensing of 350 bar hydrogen. There will be 15 fuel-cell-powered GSE cargo tractors deployed in the FedEx operation allowing real world data to be collected with a reasonably large sample size.

Operational and maintenance data will be analyzed according to project objectives. The data will support both the fundamental evaluation of fuel cell technology in new applications as well as the commercial decision-making process of the project participants.

RESULTS

During FY 2018 the demonstration phase at the Memphis airport continued and data was compiled and submitted through January 2018. Unfortunately, in early calendar year 2018 the plans to decommission the hydrogen infrastructure brought a premature conclusion to the demonstration phase. In April 2018, the systems were decommissioned, and fuel cells were returned to Plug Power and the electric GSE baggage tractors were returned to Charlotte.

The performance criteria and results during the demonstration phase at the Memphis Airport are shown in Table 1. The performance objectives during budget period 2 were achieved once the fuel cell stacks and systems were upgraded by Plug Power.

Table 1. Fuel-Cell-Powered Ground Support Equipment—Year 1

Criteria	Metric	Demonstrated Performance
Power	Capable of 5,000 lb drawbar capacity	Tugs demonstrated the ability to pull 50,000 lb
Availability	>80%	90.5% (February to October 2017) (mitigation actions of all failures have been identified, leading to improved availability)
Run Time	>1 shift	Tugs achieved 304 shifts before running out of fuel
Reliability—Mean Time between Failures	>100 hours	218 hours (36 failures over 7,844 hours)

Plans were undertaken to relocate two of the baggage tractors to the Albany International Airport where FedEx operates a limited-scale freight operation. There were two main benefits of locating in Albany. First is that it provides a true northern winter climate to test and verify the fuel cell GSE during below-freezing weather. Second, the location did not require new hydrogen infrastructure as the Plug Power facility with a hydrogen dispenser is within 1.5 miles of the FedEx operation at Albany airport.

Activities from April 2018 to the end of FY 2018 have centered around the relocation and restart of the program. The go/no-go to move into budget period 3 was originally requested in January 2018. At the end of FY 2018 the approval to proceed to budget period 3 was still pending but expected soon in FY 2019.

CONCLUSIONS AND UPCOMING ACTIVITIES

- Completed the redesign and validation of the fuel cell systems with the Plug Power stack.
- Collected and reported on performance data that meets the objectives of the program.
- Completed and wrapped up operation at Memphis at the beginning of the third quarter of FY 2018.
- Finalized decision to move program to the FedEx cargo operation at the Albany International Airport and continue demonstration throughout budget period 3 using two of the fuel-cell-powered cargo tractors through the winter months.
- Began preparations for the move of equipment, including cold weather preparation and maintenance on both the cargo tractors and fuel cell systems.
- Defined and secured the hydrogen fueling plan using existing infrastructure at Plug Power’s headquarters.

The upcoming activities in budget period 3 include:

- Further work to enhance cold weather storage, starting, and operation of the fuel-cell-powered cargo tractors.
- Continued operational performance and climate data gathering.
- Preparation of reports, including updated technical and economic analysis, and project close out.

The original scope of the project included 15 fuel-cell-powered GSE; as such, Plug Power and our project partners will continue to investigate a suitable location to deploy the remainder of the fleet.

FY 2018 PUBLICATIONS/PRESENTATIONS

1. Larry Pitts, “Fuel Cell Powered Airport Ground Support Equipment,” presented at the DOE Annual Merit Review, Washington, DC, June 13–15, 2018.

Maritime Fuel Cell Generator Project

Lennie Klebanoff
Sandia National Laboratories
PO Box 969, MS-9052
Livermore, CA 94551
Phone: (925) 294-3471
Email: lekleba@sandia.gov

DOE Manager: Peter Devlin
Phone: (202) 586-4905
Email: Peter.Devlin@ee.doe.gov

Subcontractor:
Hydrogenics, Mississauga, Ontario, Canada

Project Start Date: September 15, 2013
Project End Date: Project continuation and direction determined annually by DOE

Overall Objectives

- Lower the technology risk of future port fuel cell deployments by providing performance data of hydrogen proton exchange membrane (PEM) fuel cell technology in this environment.
- Lower the investment risk by providing a validated economic assessment for this and future potential projects.
- Enable easier permitting and acceptance of hydrogen fuel cell technology in maritime applications by assisting the U.S. Coast Guard and the American Bureau of Shipping develop hydrogen fuel cell codes and standards.
- Engage potential adopters/end users of hydrogen fuel cells to enable more widespread acceptance of the technology.

Fiscal Year (FY) 2018 Objectives

- Repair and upgrade the 100-kW maritime fuel cell (MarFC) unit based on prior deployment experience in Hawaii.
- Locate another deployment partner that can advantageously use the MarFC unit while satisfying hydrogen safety requirements. Deploy the unit if all requirements are met.

Technical Barriers

This project addresses the following technical barriers from the Market Transformation section of the Fuel Cell Technologies Office Multi-Year Research, Development, and Demonstration Plan¹:

- (A) Inadequate standards and complex and expensive permitting procedures
- (E) A lack of flexible, simple, and proven financing mechanisms
- (F) Inadequate user experience for many hydrogen and fuel cell applications.

Technical Targets

No specific technical targets have been set.

FY 2018 Accomplishments

- Repaired and upgraded the MarFC unit based on prior deployment in Hawaii.
- Completed unit testing both indoors and in cold weather, proving the MarFC works reliably.
- Engaged with the Port of Massachusetts, Curtin Maritime, and the Scripps Institution of Oceanography (SIO) for deployment of the unit, and down-selected SIO for the next deployment site.
- Successfully negotiated with the legal department of SIO to gain full approval for the MarFC deployment.
- Hydrogenics and Sandia visited and successfully reviewed the SIO Nimitz Marine Facility site for compatibility with unit operation and refueling. The MarFC unit will be used to provide shore power for the Robert Gordon Sproul research vessel in FY 2019.

¹ <https://www.energy.gov/eere/fuelcells/downloads/fuel-cell-technologies-office-multi-year-research-development-and-22>

INTRODUCTION

Fuel costs and emissions in maritime ports are an opportunity for transportation energy efficiency improvement and emissions reduction efforts. Ocean-going vessels, harbor craft, and cargo handling equipment are still major contributors to air pollution in and around ports. Diesel engine costs continually increase as tighter criteria pollutant regulations come into effect and will continue to do so with expected introduction of carbon emission regulations. Diesel fuel costs will also continue to rise as requirements for cleaner fuels are imposed. Both aspects will increase the cost of diesel-based power generation on the vessel and on shore.

Although fuel cells have been used in many successful applications, they have not been technically or commercially validated in the port environment. One opportunity to do so was identified in Honolulu Harbor at the Young Brothers Ltd. wharf. At this facility, barges sail regularly to and from neighboring islands and containerized diesel generators provide power for the reefers while on the dock and on the barge during transport, nearly always at part load. Due to inherent efficiency characteristics of fuel cells and diesel generators, switching to a hydrogen fuel cell power generator was found to have potential emissions and cost savings.

Deployment in Hawaii showed the unit needed greater reliability in the start-up sequence, as well as an improved interface to the end user, thereby presenting opportunities for repairing/upgrading the unit for deployment in another locale. In FY 2018, the unit was repaired and upgraded based on the Hawaii experience, and another deployment site was identified for another 6-month deployment of the 100-kW MarFC.

APPROACH

This project developed and demonstrated a nominally 100 kW, integrated fuel cell prototype for marine applications (Figure 1).



Figure 1. The 100-kW maritime fuel cell generator (MarFC), with integrated hydrogen storage, PEM fuel cell power generation, and power conditioning equipment

This project brought together industry partners in this prototype development as a first step toward eventual commercialization of the technology. To be successful, the project incorporated interested industry and regulatory stakeholders: an end user, technology supplier and product integrator, and land- and maritime-based safety and code authorities. Project costs were shared by the primary stakeholders in the form of funds, in-kind

contribution, and material/equipment either loaned or donated to the project. Co-funding was provided by the U.S. Department of Transportation, Maritime Administration's Maritime Environmental and Technical Assistance program.

The project had five phases:

1. Establishment and specification (September 2013–December 2013)
2. Detailed design and engineering (January 2014–March 2015)
3. Prototype fabrication/site construction (October 2014–June 2015)
4. Demonstration at Young Brothers and analysis (August 2015–June 2016)
5. Deployment of a repaired/upgraded MarFC unit at a site to be determined.

RESULTS

Early in the project year, Hydrogenics completed its upgrade and repair of the MarFC unit, as well as testing of the unit in cold weather. The improvements included the following:

1. Reliability problems with the MarFC conditioning electronics upon start-up were resolved by providing a converter solution that is robust with no start-up concerns. Working with ABB's maritime group based in Finland, Hydrogenics modified the MarFC to include a proven ruggedized HESS-880 converter solution. The complete solution includes other electronic components including a 440 VAC to 230 VAC step-down transformer and filtering of the AC output.
2. A ruggedized system display was installed, making it easy for the operator to ascertain the state of the MarFC, especially during start-up (Figure 2).
3. System heaters and controls were added to allow the MarFC to operate in weather down to -25°C (Figure 3) in anticipation of a future deployment in cold weather.



Figure 2. Installation of a ruggedized system display, making it easy for the operator to ascertain the state of the MarFC, especially during start-up



Figure 3. System heaters and controls that were installed to allow the MarFC to operate in weather down to -25°C in anticipation of a future deployment in cold weather

After completion of the repairs/upgrades, the unit was tested both indoors as well as outdoors in cold weather at the Hydrogenics site in Mississauga, Ontario, Canada (Figure 4).



Figure 4. (L) Indoor testing of the MarFC unit at Hydrogenics after system repair and upgrade; (R) outdoor testing of the MarFC unit in cold weather at the Hydrogenics site in Mississauga, Ontario, Canada, December 2017

Different test data were logged during the outside test, including output power and temperatures of the fuel cell and inverter coolants and container interior (Figure 5). An upgrade/testing report was written by Hydrogenics and delivered to Sandia. Pending identification of a suitable deployment site, Hydrogenics moved the unit to a temperature-controlled storage facility nearby the Hydrogenics site.

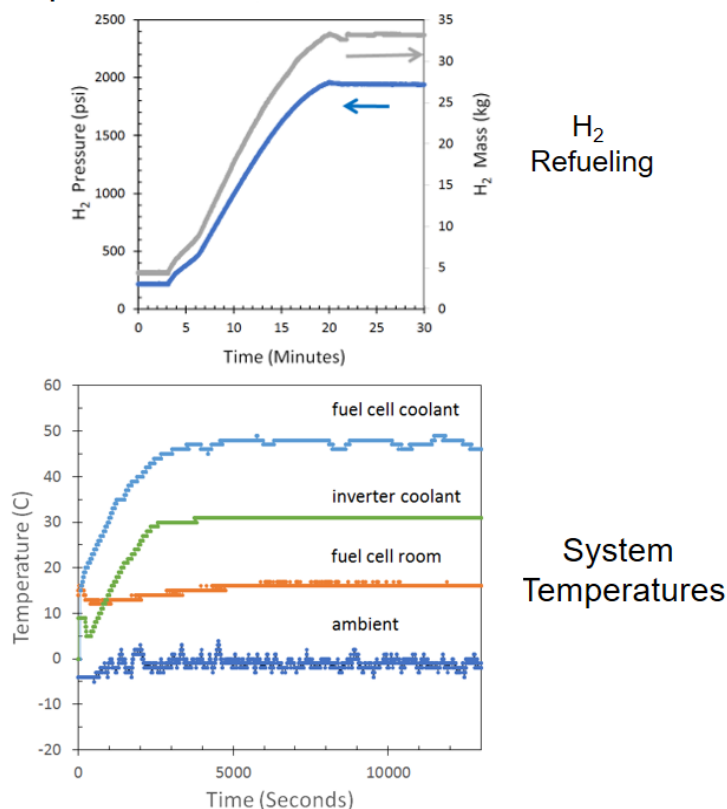


Figure 5. Test data logged during the outside MarFC test. (Top) Hydrogen refueling rate data; (Bottom) MarFC system temperatures during operation.

Initially, the Port of Massachusetts (Massport) was identified as a possible deployment location for the powering of refrigerated units, so called “reefers.” Unfortunately, Massport and Sandia could not come to agreement on the legal and insurance terms and conditions. At the recommendation of the Port of Long Beach, Curtin Maritime (a tenant at the Port of Long Beach) was contacted. Unfortunately, due to the narrow geometry of the Curtin lot, as well as various “no-go” regions of the lot which could not be used for the unit, there was no location on the site that could satisfy the required offsets for storing hydrogen.

The Scripps Institution of Oceanography (SIO) expressed interest in using the unit to cold-iron the research vessel Robert Gordon Sproul when in port. This vessel requires ~50 kW of shore power during the day, with a reduced ~14 kW of shore power at night. Legal terms and conditions were discussed and approved, and the Nimitz Marine Facility at SIO satisfied the site locations for the storage and delivery of hydrogen. However, the Scripps vessel requires 480 VAC power, whereas the MarFC unit is wired for 208 VAC power. In FY 2019, the unit will be upgraded to provide 480 VAC power and deployed at SIO for use with the Robert Gordon Sproul. Figure 6 shows the research vessel Robert Gordon Sproul in port at the Nimitz Marine Facility of SIO, as well as the MarFC unit indicated notionally.



Figure 6. The SIO research vessel Robert Gordon Sproul, in port at the Nimitz Marine Facility of the SIO, San Diego, California. The blue box notionally indicates the future deployment and location of the MarFC.

CONCLUSIONS AND FUTURE DIRECTIONS

Last year's deployment in Hawaii pointed to several ways the unit could be improved and items needing repair. These upgrades and repairs were implemented and tested, with the result being a unit that is much more reliable and easier for the operators to use. Several deployment sites were identified for the next use of the MarFC unit, with SIO satisfying the legal and regulatory requirements, as well as providing a strong test of the unit. In FY 2019, the unit will be upgraded to provide the 480 VAC power required by the research vessel Robert Gordon Sproul, and the unit will be deployed for 6 months at SIO.

FY 2018 PUBLICATIONS/PRESENTATIONS

1. L.E. Klebanoff, "H₂ Maritime Webinar," U.S. Department of Transportation/MARAD, U.S. Department of Energy Fuel Cell Technologies Office, California Air Resources Board, California Energy Commission, and Bay Area Air Quality Management District Joint Webinar (August 23, 2018).
2. L.E. Klebanoff, "Maritime Fuel Cell Generator Project," DOE Hydrogen and Fuel Cells Program Annual Merit Review, Washington DC (June 14, 2018).

Demonstration of Fuel Cell Auxiliary Power Unit to Power Truck Refrigeration Units in Refrigerated Trucks

Kriston Brooks
Pacific Northwest National Laboratory
P.O. Box 999
Richland, WA 99352
Phone: (509) 372-4343
Email: kriston.brooks@pnnl.gov

DOE Manager: Peter Devlin
Phone: (202) 586-4905
Email: Peter.Devlin@ee.doe.gov

Subcontractors:

- Nuvera Fuel Cells, Billerica, MA
- Ballard Power Systems, Burnaby, BC

Project Start Date: June 1, 2012
Project End Date: September 30, 2018

Overall Objectives

- Demonstrate the technical viability of fuel cell-based transport refrigeration units (TRUs) for refrigerated Class 8 trailers.
- Assess the performance of the fuel cell-based TRUs by demonstrating these systems with 800–1,000 hours of commercial deliveries.
- Use the demonstration data and market assessment to develop a business case that will determine if life cycle cost parity can be achieved with incumbent technologies.

Fiscal Year (FY) 2018 Objectives

- Direct subcontract teams led by Nuvera Fuel Cells and Ballard Power Systems as they each develop a fuel cell-based TRU for a refrigerated Class 8 trailer.
- Complete Phase I of the Ballard subcontract team development effort by producing a business case, a safety plan, and a preliminary design.
- Complete Phase II of the Nuvera subcontract team development effort by performing an 8-hour integrated laboratory demonstration of the

fuel cell system, power electronics, and transport refrigeration unit.

Technical Barriers

This project addresses the following technical barriers from the Market Transformation section of the Fuel Cell Technologies Office Multi-Year Research, Development, and Demonstration Plan¹:

- High hydrogen fuel infrastructure capital costs for polymer electrolyte membrane fuel cell applications
- Inadequate private sector resources available for infrastructure development
- A lack of cycle cost and performance data to demonstrate low investor risks
- Inadequate user experience for fuel cell applications.

Contribution to Achievement of DOE Market Transformation Milestones

This project contributes to achievement of DOE milestones from the Market Transformation section of the Fuel Cell Technologies Office Multi-Year Research, Development, and Demonstration Plan by developing a pathway for the introduction of fuel cell technologies into the TRU market. This niche market will increase hydrogen usage, reduce hydrogen cost, and further establish the hydrogen infrastructure at food distribution centers.

These demonstrations provided valuable data on the performance of the technology in real-world operations and can be used to benchmark the benefits of the technologies. Both the TRU manufacturers and demonstrators provided input into the business case to create a clear picture of the value proposition of this new technology.

¹ <https://www.energy.gov/eere/fuelcells/downloads/fuel-cell-technologies-office-multi-year-research-development-and-22>

FY 2018 Accomplishments

- Nuvera integrated the fuel cell system (including stack, packaged balance of plant, and power electronics) with a Thermo King Precedent TRU and tested it in a laboratory environment at both refrigeration and freezer temperature conditions.
- Nuvera completed the Phase II go/no-go decision and wrote a final report describing the results of Phase II development and testing achieved during Phase II.
- Ballard completed the Phase I go/no-go decision and wrote a final report describing the system design and market assessment results achieved during Phase I.
- Pacific Northwest National Laboratory prepared a final summary report describing the results of project.

INTRODUCTION

A TRU is a high-powered air conditioning system used in cooling cold goods during loading, on-road transport, and delivery. It is generally powered by a separate diesel engine. Replacing this diesel engine with a fuel cell will address recent state and federal environmental mandates to reduce emissions, address noise restrictions found in many urban areas, reduce system maintenance, and improve the overall energy efficiency of the system. The initial market for this application would be food distribution centers where vehicles return to a central facility for refueling and where fuel cell lift trucks have already been established. This market will further expand the hydrogen usage at these sites and increase fuel cell market penetration.

The purpose of this project was to perform two demonstrations of fuel cell-based TRUs using two separate fuel cell teams as shown in Table 1. These demonstrations could provide user experience for over-the-road fuel cell applications that will mitigate commercial risk in developing this new technology.

Table 1. Fuel Cell-Based TRU Demonstration Teams

Project Role	Nuvera Team	Ballard Team
Fuel Cell Supplier, System Integrator	Nuvera	Ballard
TRU Supplier	Thermo King	Carrier Transicold
Demonstration Partner	H-E-B	Walmart

APPROACH

Each team consisted of a fuel cell system supplier and integrator, a TRU system manufacturer, and a demonstration site. During FY 2018, Ballard completed Phase I of the development effort. Phase I involved the development of a preliminary business case, a safety plan, and the design of the fuel cell system. Nuvera completed Phase II of the development effort. Phase II involved an 8-hour test of the integrated fuel cell system, power electronics, and TRU. Phase II also included an updated business case analysis. Although not performed by either team, Phase III of the project was to include a demonstration of 800 to 1,000 hours duration that would include actual deliveries of cold goods at the demonstration partner's site.

RESULTS

FY 2018 was the conclusion of the project. The Nuvera team completed Phase II and the Ballard team completed Phase I. In both cases, a “no-go” decision was made to progress this work further. The work that was performed during FY 2018 is described in more detail below.

Nuvera Fuel Cell System Development

The Nuvera team completed their packaging of the fuel cell system using an existing shell of a Thermo King SGSM 3000 diesel genset that is undermounted on a Class 8 trailer as the equipment enclosure. The fuel cell stack and balance of plant was packaged in this shell and the system controls, software, and communication were finalized to allow its integration with the Thermo King Precedent C-600 TRU. This particular TRU is a plug-in hybrid system that allows the use of either the diesel-generated power or 480 VAC 3-phase shore power during operations.

One significant challenge that was successfully overcome during the Nuvera design was the power electronics. Conversion from the fuel cell's DC power to 480 VAC power requires inverters and boost converters. It also requires signal conditioning components such as filters to prevent premature failure of the electrical components. The integrated test setup with the Nuvera fuel cell, power electronics (inverter), and Thermo King TRU are shown in Figure 1.

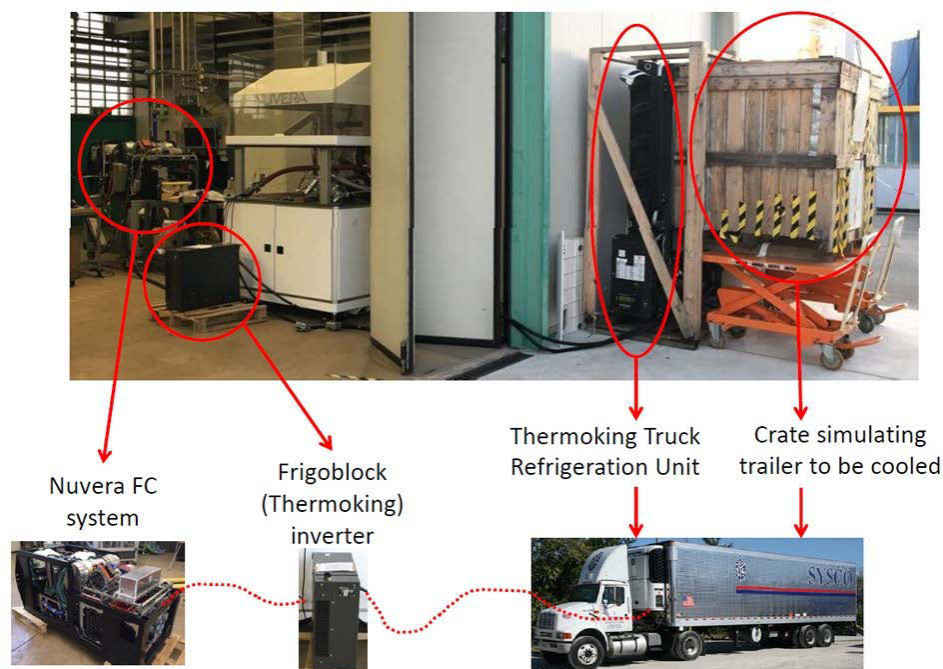


Figure 1. Nuvera integrated test setup

The test was done using a crate to simulate an actual trailer (box) to be cooled. The use of a test crate causes the TRU to cycle (because without the crate, the TRU would run at maximum power continuously). This crate methodology is a standard method commonly used by Thermo King for endurance testing and allowed Thermo King to compare the performance to their internal testing of non-fuel-cell-powered units. Although the crate was insulated, the insulation effectiveness was less than what would be installed in a typical well-insulated refrigerated trailer, resulting in more ambient heat flowing into the test crate than would flow into a conventional refrigerated trailer. Because of this, temperature cycling is more frequent using the test crate; therefore, the test is more severe than a test performed using a standard trailer.

The integrated laboratory demonstration was performed successfully for 8 hours. The test consisted of operations at a setting of 1°C (34°F) cooling temperature for the first 4.5 hours and then -20°C (-4°F) for the remaining 3.5 hours. During the entire duration of this testing, the temperature set point was reached and maintained as seen in Figure 2. The fuel cell system produced up to 15 to 23 kW maximum power with a resultant system efficiency of approximately 47% (lower heating value). It should be noted that the peaks in the data correspond to defrost and heat events generated by the TRU that will drive the crate temperature above and below the set point. These peaks are a result of excessive cycling caused by the box configuration of the test and would be eliminated in a full-sized trailer.

In addition to the integrated test, Nuvera also provided an updated economic analysis comparing a Thermo King diesel-powered TRU with a fuel cell-powered version. The analysis identified the “tipping point” between positive, marginal, and negative net present values (NPVs) as shown in Figure 3. With the 30% investment tax credit, the diesel fuel cost at \$3/gallon (February 2018 price), and the incremental cost of the fuel cell at \$33,600 (i.e., best case scenario), the NPV is positive only when the cost of hydrogen is \$6/kg or less. As diesel prices rise, the NPV becomes positive as hydrogen costs fall.

As a result of the negative estimated NPV life cycle cost comparison to the diesel engine TRU, the Nuvera team decided to not continue the project into Phase III nor perform their originally planned demonstration. Instead, they wrote a final report and closed out the subcontract.

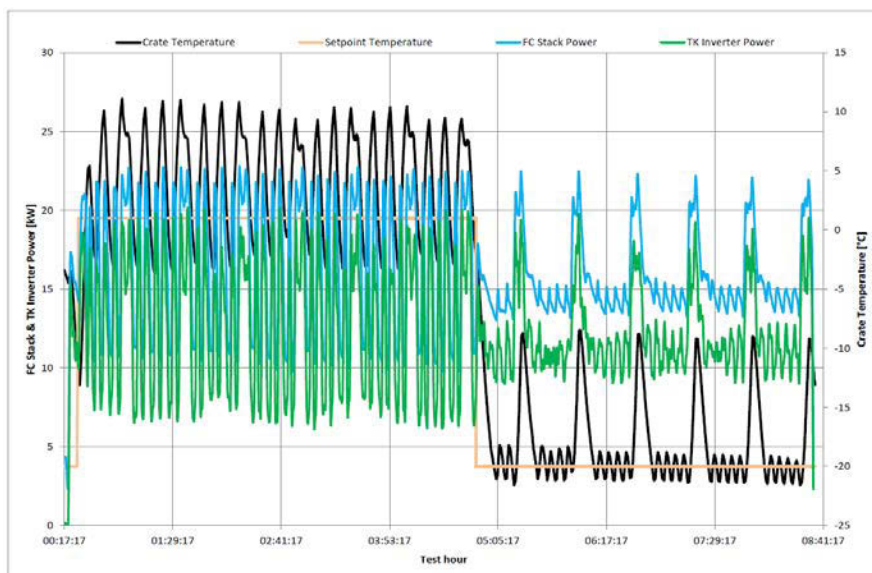


Figure 2. Power and temperature results from the Nuvera laboratory integrated 8-hour test

INC. COST \$ 33,600		\$ 3.00	\$ 4.00	\$ 6.00	\$ 8.00	
	HYDROGEN (\$/kg)	\$ 2.50	45,432	71,482	123,581	175,680
		\$ 4.00	25,669	51,719	103,818	155,917
		\$ 6.00	(681)	25,368	77,467	129,566
		\$ 8.00	(27,032)	(982)	51,117	103,216
		\$10.00	(53,382)	(27,332)	24,767	76,866
\$12.00		(79,732)	(53,683)	(1,584)	50,515	
INC. COS \$ 42,000		\$ 3.00	\$ 4.00	\$ 6.00	\$ 8.00	
	HYDROGEN (\$/kg)	\$ 2.50	36,563	62,612	114,711	166,811
		\$ 4.00	16,800	42,850	94,949	147,048
		\$ 6.00	(9,550)	16,499	68,598	120,697
		\$ 8.00	(35,901)	(9,851)	42,248	94,347
		\$10.00	(62,251)	(36,202)	15,897	67,996
\$12.00		(88,602)	(62,552)	(10,453)	41,646	
INC. COS \$ 50,400		\$ 3.00	\$ 4.00	\$ 6.00	\$ 8.00	
	HYDROGEN (\$/kg)	\$ 2.50	27,694	53,743	105,842	157,941
		\$ 4.00	7,931	33,980	86,079	138,178
		\$ 6.00	(18,420)	7,630	59,729	111,828
		\$ 8.00	(44,770)	(18,721)	33,379	85,478
		\$10.00	(71,120)	(45,071)	7,028	59,127
\$12.00		(97,471)	(71,421)	(19,322)	32,777	

Figure 3. NPV of fuel cell vs. diesel-powered TRU developed by Thermo King and Nuvera

Ballard Fuel Cell System Development

During FY 2017, the Ballard team completed their Phase I milestones including a preliminary design, safety strategy, and market assessment. The market assessment performed by Ballard resulted in a similar negative NPV life cycle cost comparison to the diesel engine TRU. As a result of the negative estimated NPV life cycle cost comparison to the diesel engine TRU, the Ballard team (including Walmart and Carrier) decided not to continue the project into Phase II. Instead they wrote a final report and closed out the subcontract.

Final Fuel Cell TRU Report

The results of the development work performed by both Nuvera and Ballard were summarized in a final report. This report compared the designs of the two teams. The initial designs exhibited many similarities, suggesting that the lessons learned would be applicable to any potential TRU system. These included the approach to power conditioning, the required electrical power to the TRU, the use of an electric hybrid architecture for the TRU, and the decision for an underslung location on the trailer of the fuel cell system.

The report also enumerated both the market drivers and the remaining challenges of successful market penetration of a fuel cell-powered TRU from the two teams. Once again, the drivers and challenges from the market assessments were similar. The negative NPV identified by both teams under current conditions and the lack of strong environmental regulations were the largest challenges that led both teams not to continue. Given the high costs and lack of strong customer pull for a zero-emission TRU alternative, TRU manufacturers selected not to embark on further development programs.

The report concludes that the project provided TRU manufacturers an opportunity to understand fuel cell technology: both its benefits and the areas of needed development. Through the development of a business case, specific metrics have been established for evaluating the market for its readiness to implement the technology. Finally, the project has given the fuel cell companies an opportunity to interface with the TRU manufacturers and potential customers to better understand their needs and value propositions.

CONCLUSIONS AND UPCOMING ACTIVITIES

Pacific Northwest National Laboratory agreed with the assessment of the manufacturers. The fuel cell-powered TRU technology is sound and has the potential to be implemented into existing TRUs to create a new, efficient, and environmentally friendly product offering. However, the business case is not yet strong enough to be implemented across the grocery and cold food distribution market. As the cost of the hydrogen, the fuel cell, and power conditioning decrease and regulatory drivers strengthen, this market should be revisited. It is also possible that niche markets, such as small specialty food distributors like organic produce and seafood, may exist now that are less sensitive to cost where these systems could be implemented.

At this point there are no plans for upcoming activities in FY 2019 with this scope.

FY 2018 PUBLICATIONS/PRESENTATIONS

1. K.P Brooks and D.T. Howe, *Fuel Cell Transport Refrigeration Unit Report*, PNNL-27809 (Richland, WA: Pacific Northwest National Laboratory, 2018).

FedEx Express Hydrogen Fuel Cell Extended-Range Battery Electric Vehicles

Phillip C. Galbach
Federal Express Corporation (FedEx)
3690 Hacks Cross Rd. Bldg I
Memphis, TN 38125
Phone: (901) 434-5725
Email: pccgalbach@fedex.com

DOE Manager: Peter Devlin
Phone: (202) 586-4905
Email: Peter.Devlin@ee.doe.gov

Contract Number: DE-EE00006522

Subcontractors:

- Workhorse Technologies Inc., Loveland, OH
- Plug Power Inc., Latham, NY

Project Start Date: October 15, 2015
Project End Date: September 30, 2020

Overall Objectives

- To convert an existing electric parcel delivery unit into a zero-emission extended range electric vehicle by utilizing hydrogen fuel cell technology.
- Understand, demonstrate, and deploy hydrogen fuel cell technologies in a real-world environment.

Fiscal Year (FY) 2018 Objectives

- Create fueling strategy for vehicle in Latham, New York.
- Work with Menands station on route selection, charging, and maintenance.
- Complete integration of fuel cell and electric vehicle communication.
- Prepare vehicle for on-road testing and implementation.
- Complete and submit safety plan.
- Conduct durability testing.
- Deliver vehicle to station.

- Train FedEx drivers and maintenance technicians on hydrogen safety.
- Start and continue data collection through Budget Period (BP) 1.
- Transmit data to the National Renewable Energy Laboratory (NREL) regularly.

Technical Barriers

This project addresses the following technical barriers from the Market Transformation section of the Fuel Cell Technologies Office Multi-Year Research, Development, and Demonstration Plan¹:

- High hydrogen fuel infrastructure capital costs for polymer electrolyte membrane fuel cell applications
- Market uncertainty around the need for hydrogen infrastructure versus timeframe and volume of commercial fuel cell applications
- Inadequate user experience for many hydrogen and fuel cell applications
- Insufficient numbers of trained and experienced servicing personnel
- Lack of qualified technicians for maintenance
- Lack of certified service providing organizations for installation and maintenance.

Contribution to Achievement of DOE Market Transformation Milestones

This project will contribute to achievement of the following DOE milestones from the Market Transformation section of the Fuel Cell Technologies Office Multi-Year Research, Development, and Demonstration Plan:

- Milestone 1.8: Complete deployment and evaluation of short haul/drayage trucks and range extenders. (1Q, 2014)

¹ <https://www.energy.gov/eere/fuelcells/downloads/fuel-cell-technologies-office-multi-year-research-development-and-22>

FY 2018 Accomplishments

- Proposed plans for truck fueling at Plug Power Latham.
- Build plans for hydrogen dispenser in Latham.
- Planned route selection, driver selection, charging, and maintenance with Menands management.
- Installed fuel cell systems and converter in truck engine compartment.
- Created control strategy for battery charging.
- Created software for communications between fuel cell system and truck.
- Installed/debugged remaining items on truck.
- Provided electric vehicle supply equipment charger for truck to Menands ship center.
- Registered vehicle.
- Submitted safety plan to DOE.
- Conducted durability test.
- Received permit for hydrogen dispenser at Plug Power.
- Installed outdoor hydrogen dispenser at Plug Power.
- Delivered truck to Menands ship center.
- Trained FedEx employees on hydrogen safety.
- Started data collection.
- Sent first set of data to NREL.
- Sent request for extension of BP 1 to DOE.
- Extended BP 1 to the end of February 2019.
- Continuing with data collection and working with NREL to determine how to analyze the data.

INTRODUCTION

The ability to reduce fuel consumption and emissions while delivering packages is an immense challenge, particularly with the available technology. This is further complicated by the diversity of the different duty cycles utilized by the pick-up and delivery vehicles (PUDs) at FedEx. This has created enormous opportunities for an extended-range, zero-emission electric PUD.

As a part of this project, we will be converting 20 existing electric vehicles (EVs) into hydrogen fuel cell powered extended-range electric vehicles (eREVs) in two different phases/BPs.

Successful utilization of fuel cell technologies in real world environments will help foster a better understanding while providing the opportunity to identify and utilize additional duty cycles, eventually reducing costs by achieving economies of scale, while providing clean, safe, secure, and affordable energy.

APPROACH

The first step was to find industry partners that had the experience, capabilities, and knowledge to collaborate with us in embarking on this project. As a result, we are collaborating with Workhorse, the EV manufacturer, Plug Power, the fuel cell manufacturer, and Morgan Olson, the body manufacturer for the eREV.

The project is divided into two separate phases/BPs (BP 1 and BP 2). The first period concentrates on the conversion of just one asset. This will enable the project team to test, analyze, and measure the performance. BP 2 will only be launched if the first phase is considered successful and the team will utilize the lessons learned and implement those in the second phase.

We have made significant progress in BP 1 and are close to launching the first eREV PUD. The identification of the ideal route and location for the first PUD was completed. The optimized charge strategy and power generation for the fuel cell was implemented. The fabrication, validation, and testing of the fuel cells has successfully been completed. The various integration activities between the EV and fuel cell are completed. The ideal hydrogen tank size, packaging, and compartment locations are finalized and being utilized. The body for the PUD was installed on the electric chassis. The safety and venting testing has been initiated. Next, the eREV will be taken through a series of durability tests before it is placed in active service.

The second phase is launched if the first phase is considered successful and will convert an additional 19 EVs into fuel cell eREV PUDs.

RESULTS

This has been an ongoing project. There has been much accomplished to get the vehicle on the road for real-world testing. A fueling strategy was worked out with Plug Power to fuel the vehicle at the Plug Power facility. Durability testing was conducted by Plug Power for a couple of months. The vehicle was commissioned and put into service on January 30, 2018. There have been some challenges at the beginning of the real-world validation. In the first months, there were various problems with both the fuel cell and the electric vehicle. Figure 1 depicts out-of-service time by system, in days. The last three months of service, September not depicted, have been nearly perfect.



Figure 1. Availability by month

Figure 2 shows the overall availability of the vehicle by system. The target for the fuel cell and fuel cell integration reliability is less than 7% down time. Because of a few incidences we have not hit that target.

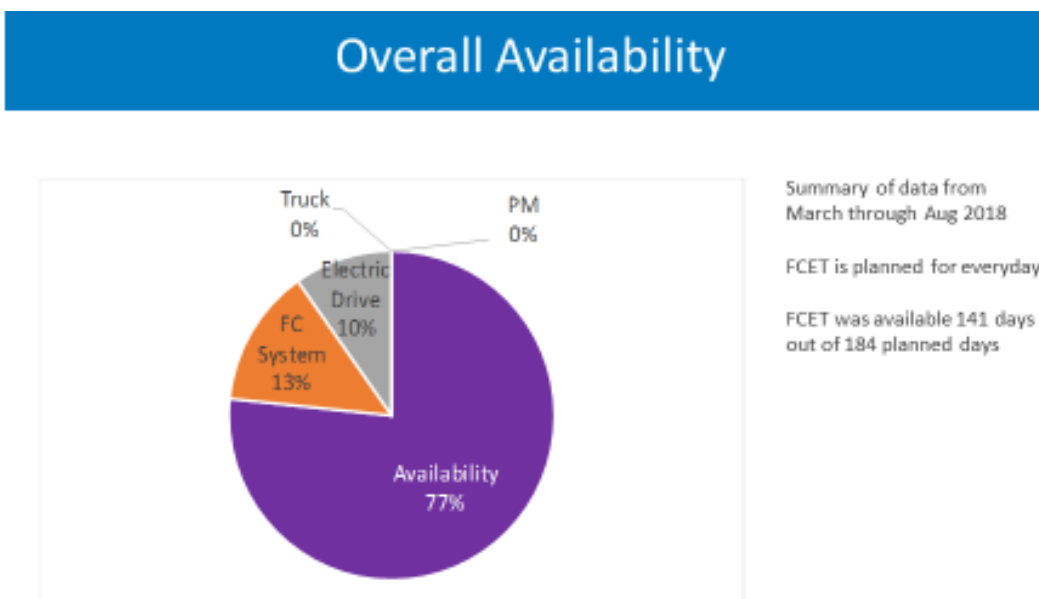


Figure 2. Overall availability

CONCLUSIONS AND UPCOMING ACTIVITIES

Because of the early issues and challenges, DOE has told us to extend BP 1 to collect more data and determine its reliability. We have requested an extension to collect data until February 28, 2019. This will give us a full year's worth of data to analyze before making a go/no-go recommendation.

FY 2018 PUBLICATIONS/PRESENTATIONS

1. Phillip Galbach, “FedEx Express Hydrogen Fuel Cell Extended Range Battery Electric Vehicles,” presented at the DOE Annual Merit Review, Washington, DC, June 13–15, 2018.
2. Phillip Galbach, “FedEx Express—Fleet Logistical Considerations,” presented at the H2@Scale DOE Truck Workshop, Chicago, IL, July 30–31, 2018.

Northeast Demonstration and Deployment of FCRx200

Abas Goodarzi
US Hybrid
445 Maple Ave
Torrance, CA 90503
Phone: (310) 212-1200
Email: abas@ushybrid.com

DOE Manager: Peter Devlin
Phone: (202) 586-4905
Email: Peter.Devlin@ee.doe.gov

Contract Number: DE-EE0007276

Subcontractor:
Nissan North America, Inc., Franklin, TN

Project Start Date: September 1, 2016
Project End Date: February 28, 2022

Overall Objectives

- Design, develop, test, and demonstrate one fuel cell range-extended plug-in hybrid utility vehicle (FCRx200) at the operator's site.
- Given a DOE "go" approval, deploy and operate a minimum of 20 FCRx200s for at least 5,000 hours per vehicle at the operator's site.
- Conduct an economic assessment, including a payback analysis cost per unit and payback time, concerning the use of hydrogen-fueled fuel cells for range extenders used in commercial operations.

Fiscal Year (FY) 2018 Objectives

- Complete design and integration of prototype vehicle.
- Validate vehicle's performance.
- Demonstrate FCRx200 at operator's site.

Technical Barriers

This project addresses the following technical barriers from the Market Transformation section of the Fuel Cell Technologies Office Multi-Year Research, Development, and Demonstration Plan¹:

(A) Durability

(B) Cost

(C) Performance

- Cell Issues
- Stack Water Management
- System Thermal and Water Management
- System Air Management
- System Start-Up and Shutdown Time and Energy/Transient Operation.

Contribution to Achievement of DOE Market Transformation Milestones

This project will contribute to achievement of the following DOE milestones from the Market Transformation section of the Fuel Cell Technologies Office Multi-Year Research, Development, and Demonstration Plan:

- Milestone 1.8: Complete deployment and evaluation of short haul/drayage trucks and range extenders. (1Q, 2014)
- Milestone 1.12: Complete test and business case analysis for onboard fuel cell rechargers for battery electric vehicles. (1Q, 2015)

The FCRx200 features Nissan's Li-Ion battery, which is entirely housed under the cargo floor. This project meets U.S. customer duty cycles using proven Nissan LEAF battery technology in the FCRx200 and UTC-derived proton exchange membrane fuel cell technology. The FCRx200's 24 kWh battery is similar to the Nissan LEAF's, but with a revised module layout for packaging requirements and with the addition of an active battery cooler to accommodate the higher quick charging and driving load demands expected in commercial usage. By more than doubling the range, the FCRx200 will be a deployment that can demonstrate fuel cell range extenders for battery-based electric vehicles in Class 1 vehicle platforms. It is an enabling technology that makes electric-powered cargo vehicles a viable solution for a wide range of applications, including passenger transportation services, light freight

¹ <https://www.energy.gov/eere/fuelcells/downloads/fuel-cell-technologies-office-multi-year-research-development-and-22>

transport, and dispatch utility operations where electric drive transportation systems are beginning to be introduced commercially.

FY 2018 Accomplishments

- Completed comprehensive vehicle component placement and packaging designs.

INTRODUCTION

US Hybrid utilized an in-house-fabricated fuel cell power plant (FCRx) to hybridize and range-extend the modified e-NV200 drivetrain prototype. Fuel cell stack sizing, balance of plant, and its configuration with the battery were designed in detail during the project's design phase. The fuel cell will be powered and refueled with pressurized hydrogen gas stored in on-board tanks. The integrated design with innovative balance of plant technology enables robust performance with reduced system complexity, weight, and volume to extend operation life and provide lower total cost of ownership (TCO). With a compact volume, the FCPx (Figure 1) is engineered specifically for an automotive application and was designed to be installed under the hood of conventional vehicles. The FCPx offers more than 50% efficiency over wide load range.

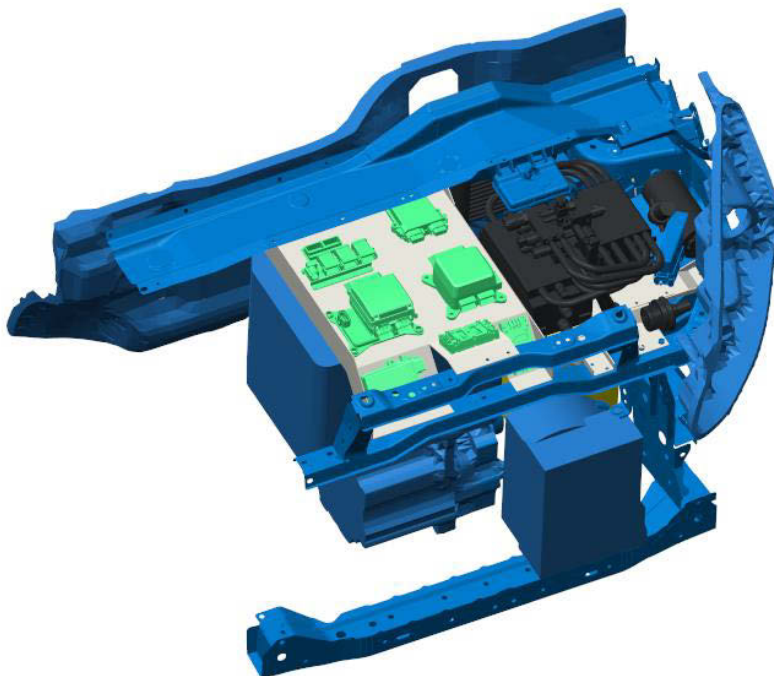


Figure 1. US Hybrid range extender fuel cell system

APPROACH

US Hybrid led the design and development of the FCRx200. It was responsible for the design, development, and manufacturing of the fuel cell power plant range extender subsystem, fueling (storage and fill), and planned integration of the vehicle. US Hybrid also led the controls integration and battery hybridization work.

RESULTS

In FY 2018, US Hybrid continued work on modeling and optimization, FCPx and balance of plant design, and vehicle packaging. This included hydrogen tank placement and packaging, fill port component location, system radiator location, cooling package, and range extender system enhancements and packaging (Figures 2–4).

After discussing limits of Nissan's cooling package, it was decided that installing another radiator directly in front of Nissan's existing cooling package would detrimentally impact the performance of Nissan's cooling package. Installing two auxiliary radiators behind daytime running light holes will allow for fresh air to flow through radiators and not introduce any detrimental heat rejection problems. Nissan confirmed no problem with removing daytime running lights. Also, they are not needed according to transportation laws.

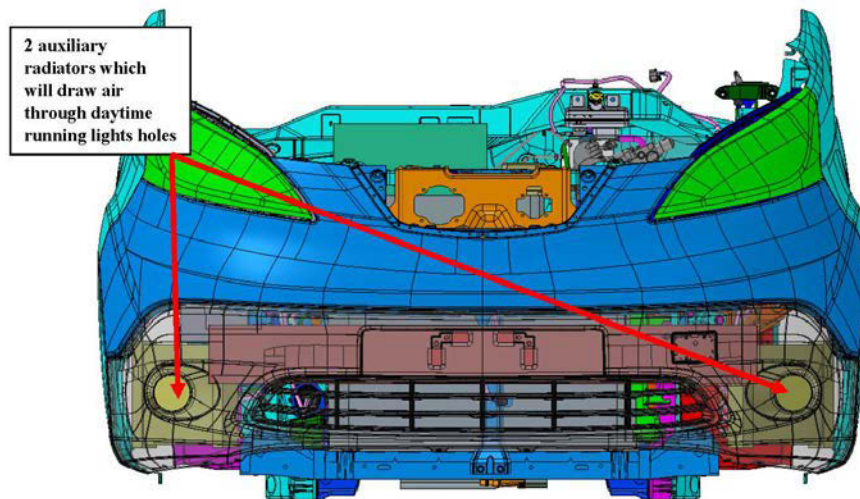


Figure 2. Cooling package

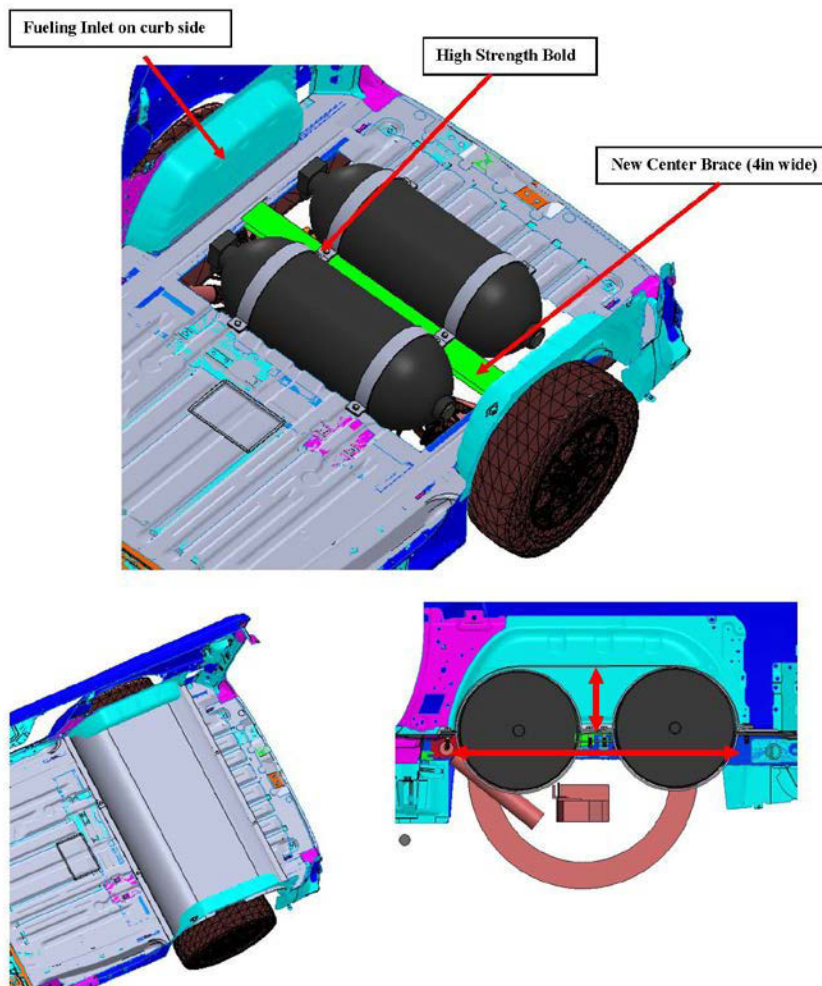


Figure 3. Hydrogen tank packaging and enclosure

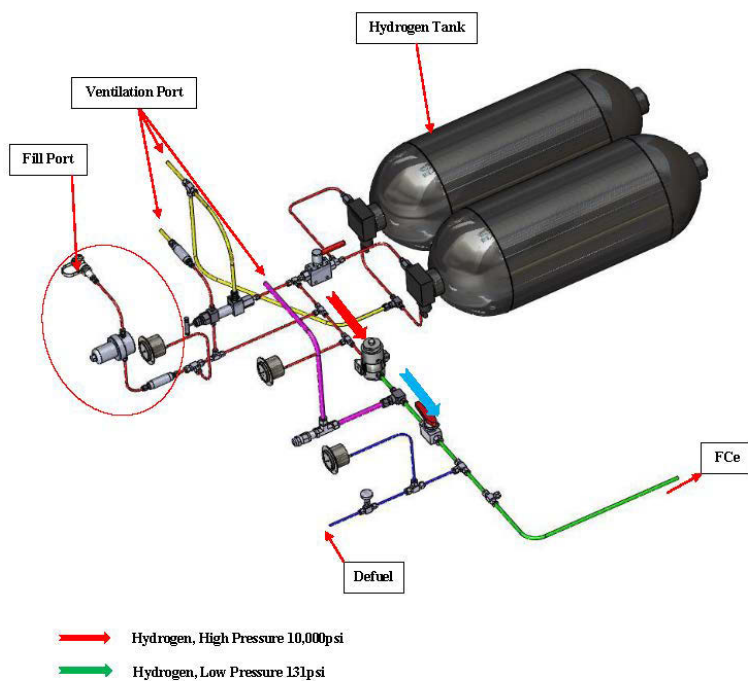


Figure 4. Piping and instrumentation diagram

CONCLUSIONS AND UPCOMING ACTIVITIES

FY 2019 proposed activities include:

- Complete integration of prototype vehicle
- Validate vehicle's performance
- Demonstrate FCRx200 at operator's site.

Information that was gathered this year from designs will be utilized in wrapping up design and fabrication of the FCPx, DC-DC power converter, hydrogen storage, and other subsystem components. The components will then be integrated into the vehicle, tested, and validated for performance criteria.

Technology Validation: Fuel Cell Bus Evaluations

Leslie Eudy (Primary Contact), Matthew Post,
Matthew Jeffers
National Renewable Energy Laboratory (NREL)
15013 Denver West Parkway
Golden, CO 80401
Phone: (303) 275-4412
Email: Leslie.Eudy@nrel.gov

DOE Manager: Jason Marcinkoski
Phone: (202) 586-7466
Email: Jason.Marcinkoski@ee.doe.gov

Project Start Date: March 2001
Project End Date: Project continuation and
direction determined annually by DOE

Overall Objectives

- Validate fuel cell electric bus (FCEB) performance and cost compared to DOE and U.S. Department of Transportation targets and conventional technologies
- Coordinate with the U.S. Department of Transportation Federal Transit Administration (FTA) on the data collection for the National Fuel Cell Bus Program and with international work groups to harmonize data collection methods and enable the comparison of a wider set of vehicles.

Fiscal Year (FY) 2018 Objectives

- Document performance results from each current FCEB demonstration site
- Complete an annual status report comparing results from the different demonstrations.

Technical Barriers

This project addresses the following technical barriers from the Technology Validation section of the Fuel Cell Technologies Office Multi-Year Research, Development, and Demonstration Plan¹:

(A) Lack of Fuel Cell Electric Vehicle and Fuel Cell Bus Performance and Durability Data

(D) Lack of Hydrogen Fueling Infrastructure Performance and Availability Data.

Contribution to Achievement of DOE Technology Validation Milestones

This project has contributed to achievement of the following DOE milestone from the Technology Validation section of the Fuel Cell Technologies Office Multi-Year Research, Development, and Demonstration Plan:

- *Milestone 2.3: Validate fuel cell electric vehicles achieving 5,000-hour durability (service life of vehicle) and a driving range of 300 miles between fuelings. (4Q, 2019)*
Through FY 2018, NREL collected data on 27 FCEBs. NREL documented 12 fuel cell power plants (FCPPs) with operation hours in excess of 20,000 hours. One of these systems has logged more than 29,000 hours in service, and four additional systems have surpassed 25,000 hours. Bus fuel economy is dependent on duty cycle. Based on in-service fuel economies of 5.6 miles per kilogram, the hybrid FCEBs currently in service can achieve a range of approximately 260 miles per fill.

FY 2018 Accomplishments

- Published reports on performance and operational data covering 27 full-size FCEBs in revenue service in the United States.
- Documented more than 29,000 hours on a single FCPP.

¹ <https://www.energy.gov/eere/fuelcells/downloads/fuel-cell-technologies-office-multi-year-research-development-and-22>

INTRODUCTION

Transit agencies continue to aid the FCEB industry in developing and optimizing fuel cells for buses. These in-service demonstration programs are vital to validate the performance of fuel cell systems in buses and to determine issues that require resolution. Using fuel cells in a transit application can help accelerate the learning curve for the technology because of the high mileage accumulated in short periods of time. During the last year, the project teams have made progress in transitioning training to transit staff and improving the ability to troubleshoot issues. More work is still needed to improve reliability, lower capital and operating costs, and improve parts availability.

APPROACH

NREL uses a standard evaluation protocol to provide:

- Comprehensive, unbiased evaluation results of advanced technology vehicle development and operations
- Evaluations of hydrogen infrastructure development and operation
- Descriptions of facility modifications required for the safe operation of FCEBs
- Detailed FCEB performance and durability results to validate status against technical targets, educate key stakeholders, and further DOE goals.

The evaluation protocol includes collecting operation and maintenance data on the buses and infrastructure. The analysis, which consists of economic, technical, and safety factors, focuses on performance and use, including progress over time and experience with vehicle systems and supporting infrastructure. The data are compared to DOE and FTA technical targets and to conventional baseline buses in similar service.

RESULTS

During FY 2018, NREL collected and analyzed data on the following FCEB demonstrations at four U.S. transit agencies and one university transit system:

- American Fuel Cell Bus (AFCB) Project—SunLine Transit Agency (Thousand Palms, California) is operating four EIDorado National 40-foot buses with a BAE Systems hybrid propulsion system using Ballard Power Systems fuel cells and lithium batteries.
- University of California, Irvine (UCI)—UCI operates one AFCB in its fleet.
- Orange County Transportation Authority (OCTA) AFCB—Orange County Transportation Authority is operating an AFCB in Southern California.
- Stark Area Regional Transit Authority (SARTA) AFCB Project—SARTA is operating five AFCBs in Canton, Ohio.
- Zero Emission Bay Area (ZEB) Demonstration—Five Bay Area transit agencies led by AC Transit (Oakland, California) are demonstrating thirteen 40-foot Van Hool buses with 120 kW fuel cells in a Siemens hybrid system. The hybrid system was integrated by Van Hool and uses lithium ion batteries from EnerDel. NREL has ended the full evaluation of this fleet. Current data collection is limited to fuel cell hours, mileage, and miles between roadcall analysis.

These projects involve fuel-cell-dominant hybrid buses. A summary of selected results is included in this report. The results are also compared to technical targets for FCEB performance established by DOE and FTA and published in a Fuel Cell Technologies Program Record in September 2012 [1]. Tables 1 through 5 provide a summary of the reported results from the operation at each agency, including data from the baseline buses.

Table 1. FY 2018 Summary Data Results for SunLine

Vehicle Data	AFCB	CNG
Number of buses	7	5
Data period	Mar 2012–Jul 2018	Jan 2017–Jul 2018
Number of months	77	19
Total fleet miles	506,496	516,105
Average miles per month	2,323	5,433
Total FC hours	38,304	-
Fuel economy (mi/kg or gge)	5.59	3.44
Fuel economy (mi/dge)	6.31	3.84
Average speed (mph)	15.1	16.8
Availability (%)	74	88

FC – fuel cell

CNG – compressed natural gas

gge – gasoline gallon equivalent

dge – diesel gallon equivalent

Table 2. FY 2018 Summary Data Results for UCI

Vehicle Data	AFCB
Number of buses	1
Data period	Jan 2016–Jul 2018
Number of months	31
Total fleet miles	52,065
Average miles per month	1,680
Total FC hours	5,917
Fuel economy (mi/kg)	5.20
Fuel economy (mi/dge)	5.88
Average speed (mph)	9.2
Availability (%)	78

Table 3. FY 2018 Summary Data Results for OCTA

Vehicle Data	AFCB	CNG
Number of buses	1	10
Data period	Jun 2016–Jul 2018	Jun 2016–Jun 2018
Number of months	26	26
Total fleet miles	36,808	857,036
Average miles per month	1,416	3,296
Total FC hours	3,027	-
Fuel economy (mi/kg or gge)	6.49	3.56
Fuel economy (mi/dge)	7.33	3.98
Average speed (mph)	14.8	17.0
Availability (%)	55	85

Table 4. FY 2018 Summary Data Results for SARTA

Vehicle Data	AFCB	CNG	Diesel Hybrid
Number of buses	5	4	3
Data period	Oct 2017–Jul 2018	Oct 2017–Jul 2018	Oct 2017–Jul 2018
Number of months	10	10	10
Total fleet miles	92,524	182,536	88,453
Average miles per month	2,056	4,563	3,402
Total FC hours	6,786	-	-
Fuel economy (mi/kg or gge)	4.83	4.15	-
Fuel economy (mi/dge)	5.46	4.64	4.71
Average speed (mph)	13.6	N/A	N/A
Availability (%)	65	77	86

Table 5. FY 2018 Summary Data Results for ZEB

Vehicle Data	FCEB	Diesel
Number of buses	13	10
Data period	Sep 2011–Mar 2017	Jul 2013–Mar 2017
Number of months	59	45
Total fleet miles	1,773,305	2,029,503
Average miles per month	2,456	4,510
Total FC hours	204,639	-

One performance target set by DOE and FTA is for a FCPP durability of 4–6 years (or 25,000 hours), which would be approximately half the life of the bus. The FCPP would be rebuilt or replaced at that time—similar to what transit agencies typically do for diesel engines. Over the last year, NREL collected data on 27 FCPPs including eight new buses at two different agencies. Figure 1 shows the total hours accumulated on individual FCPPs for the current projects tracked by NREL. The 2016 and ultimate targets are included on the graph as lines along with the average of 21,023 hours. As of July 2018, the highest-hour FCPP had reached 29,028 hours. Twelve FCPPs have surpassed the 2016 target of 18,000 hours. Of those FCPPs, five have surpassed the ultimate target of 25,000 hours. Agencies report that the FCPPs are proving reliable and that issues with the system are typically attributed to balance of plant components.

The transit industry measures reliability as mean distance between failures, also known as miles between roadcall (MBRC). Figure 2 tracks the MBRC over time for all five demonstrations and includes the MBRC for the bus as a whole and MBRC for the fuel cell system. The targets for each category are included on the chart. Reliability has shown a steady increase over time, reaching the ultimate targets for both bus MBRC and fuel cell system MBRC. Roadcalls due to bus-related issues—such as problems with doors and air conditioning—made up 45% of the total failures. Fuel-cell-related issues made up approximately 22% of the roadcalls during the period.

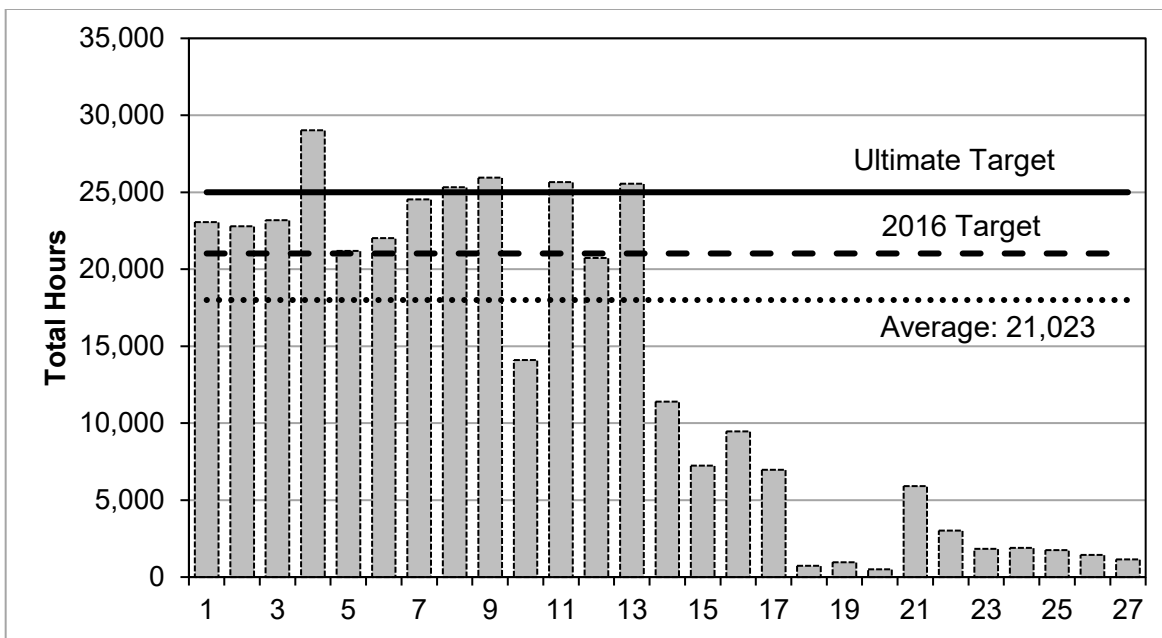


Figure 1. Total fuel cell hours accumulated on each FCPP

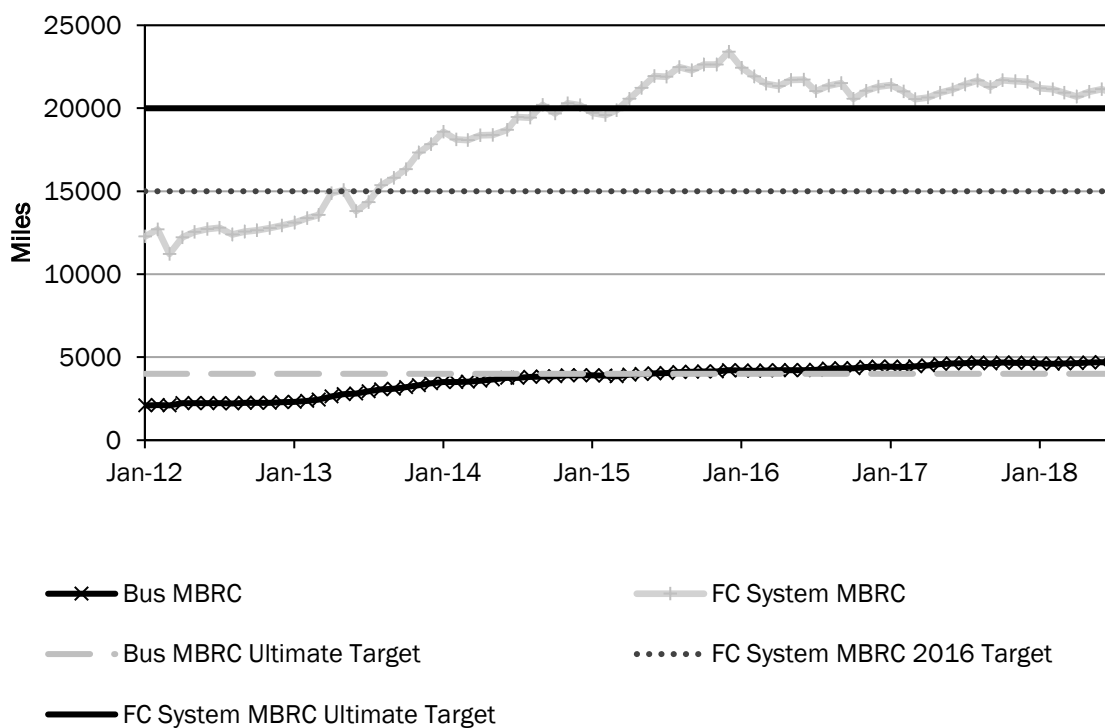


Figure 2. Miles between roadcall

CONCLUSIONS AND UPCOMING ACTIVITIES

Fuel cell propulsion systems in buses have continued to show progress, with increasing durability and reliability of FCEBs and the primary components. The current technology meets the ultimate reliability target for roadcall frequency of both the overall bus and the fuel cell system. The fuel cell systems on five buses have surpassed the ultimate target for power plant lifetime and six additional fuel cell systems have surpassed the 2016 target. Table 6 summarizes the current status compared to the DOE and FTA performance targets. Transit agencies have made major progress over the last 2 years toward transitioning maintenance to staff. There are still challenges to overcome before fuel cell buses can match the current performance standard of diesel buses. These include:

- Continuing operation to validate durability and reliability of the fuel cell systems and other components to match transit needs
- Completing the transfer of all maintenance work to transit personnel
- Lowering the costs of purchasing, operating, and maintaining buses and infrastructure
- Scaling up the introduction and operation of larger numbers of FCEBs.

Table 6. FY 2018 Summary of Progress Toward Meeting DOE and FTA Targets

	Units	2018 Status (Range)	2016 Target	Ultimate Target
Bus lifetime	Years/miles	0.2–8/ 500–222,000 ^a	12/500,000	12/500,000
Power plant lifetime	Hours	500–29,000 ^a	18,000	25,000
Bus availability	%	55–88	85	90
Roadcall frequency (bus/FC system)	Miles between roadcall	2,500–5,700/ 13,000–36,800	3,500/15,000	4,000/20,000
Operation time	Hours per day/days per week	7–21/5–7	20/7	20/7
Maintenance cost	\$/mile	0.22–0.73	0.75	0.40
Fuel economy	Miles per dge	5.8–7.8	8	8
Range	Miles	199–348	300	300

^a Accumulation of miles and hours to date—not end of life

Future work by NREL includes:

- Continuing data collection, analysis, and reporting on performance data for FCEBs in service at the following sites:
 - SunLine
 - UCI
 - AC Transit ZEB A FCEB demonstration (limited parameters)
 - Additional sites as funding allows.
- Investigating reliability, durability, and life cycle of FCEBs as a part of ongoing evaluations
- Coordinating with FTA to collect data on the demonstrations funded under the National Fuel Cell Bus Program.

FY 2018 PUBLICATIONS/PRESENTATIONS

1. L. Eudy, “Fuel Cell Electric Buses: Progress Toward Meeting Technical Targets,” Presentation at a Denver Regional Transportation District Meeting, August 2018.
2. L. Eudy, “Technology Validation: Fuel Cell Bus Evaluations,” Presentation at the DOE Hydrogen and Fuel Cells Program Annual Merit Review, Washington, D.C., June 2018.
3. L. Eudy, “Fuel Cell Electric Buses: Progress Toward Meeting Technical Targets,” Presentation for a DOE Webinar, May 2018.
4. L. Eudy, M. Post, and M. Jeffers, “Fuel Cell Buses in U.S. Transit Fleets: Current Status 2017,” National Renewable Energy Laboratory, Golden, CO, NREL/TP-5400-70075, November 2017.
5. L. Eudy, M. Post, and M. Jeffers, “Zero Emission Bay Area (ZEBA) Fuel Cell Bus Demonstration Results: Sixth Report,” National Renewable Energy Laboratory, Golden, CO, NREL/TP-5400-68413, September 2017.

REFERENCES

1. Fuel Cell Technologies Program Record #12012, September 2012, www.hydrogen.energy.gov/pdfs/12012_fuel_cell_bus_targets.pdf.

Hydrogen Station Data Collection and Analysis

Sam Sprik (Primary Contact), Jennifer Kurtz,
Shaun Onorato, Genevieve Saur, Mike Peters
National Renewable Energy Laboratory
15013 Denver West Parkway
Golden, CO 80401-3305
Phone: (303) 275-4431
Email: Sam.Sprik@nrel.gov

DOE Manager: Jason Marcinkoski
Phone: (202) 586-7466
Email: jason.marcinkoski@ee.doe.gov

Project Start Date: October 1, 2011
Project End Date: Project continuation and
direction determined annually by DOE

Overall Objectives

- Analyze current, state-of-the-art hydrogen infrastructure using several metrics including efficiency, performance, cost, and reliability of station components and systems.
- Perform an independent assessment of technology in real-world operating conditions, focusing on hydrogen infrastructure for on-road vehicles.
- Leverage and develop the data processing and analysis capabilities at the National Renewable Energy Laboratory's (NREL's) National Fuel Cell Technology Evaluation Center (NFCTEC).
- Publish aggregated results for existing hydrogen stations in the form of composite data products (CDPs).

Fiscal Year (FY) 2018 Objectives

- Obtain/collect data from state-of-the-art hydrogen fueling facilities that receive funding through DOE, the California Energy Commission (CEC) awards, and others, to enrich the analyses and the set of publicly available CDPs on hydrogen fueling infrastructure.
- Work with codes and standards activities and fueling facility owners/operators to benchmark

performance of the fueling events relative to current SAE procedures.

- Perform analysis and provide feedback on sensitive data from hydrogen infrastructure for industry and DOE. Aggregate these results for publication.
- Participate in technical review meetings and site visits with industry partners to discuss results from NREL's analysis.
- Provide input to the Alternative Fuels Data Center station locator for accurate and up-to-date hydrogen station information through close partnership with CEC, California Fuel Cell Partnership, and station providers, including efforts in the northeastern United States.
- Publish a set of aggregated results for all stations including stations that are not considered retail and another set for just the retail stations that are open to all original equipment manufacturer fuel cell electric vehicle (FCEV) customers.

Technical Barriers

This project addresses the following technical barrier from the Technology Validation section of the Fuel Cell Technologies Office Multi-Year Research, Development, and Demonstration Plan¹:

- Lack of Hydrogen Refueling Infrastructure Performance and Availability Data.

FY 2018 Accomplishments

- Published fall 2017 and spring 2018 CDPs based on the available station data.
- Internally processed and analyzed quarterly infrastructure data in the NFCTEC for inclusion in the two sets of published CDPs and the detailed data products shared with those providing data.
- Shared the infrastructure data collection templates with external partners including new station providers.

¹ <https://www.energy.gov/eere/fuelcells/downloads/fuel-cell-technologies-office-multi-year-research-development-and-22>

- Analyzed data from CEC on their awarded retail stations.
- Kept NREL Fleet Analysis Toolkit code up to date, fixed bugs, integrated with latest releases of MATLAB, and revised import tools to accept data in multiple formats from stations.
- Provided input to the Alternative Fuels Data Center to keep the hydrogen station information up to date through close partnership with California Fuel Cell Partnership, CEC, station providers, and the northeastern U.S. stations.
- Presented results at the 2017 Fuel Cell Seminar and the 2018 Annual Merit Review.

INTRODUCTION

There are 35 retail stations in California serving more than 5,000 FCEVs. Additionally, in California, there are 29 more stations in the works at various stages from planning to commissioning for a potential of 64 retail stations by 2020. The funding of the network of stations has been carefully planned out by California and station providers to cover strategic geographic areas in the state including connector and destination stations for the consumer to feel confident about finding fuel for their FCEV as they travel about. In the northeast United States, efforts are under way to build out a network of 12 stations, with several near completion, to begin covering that geographic region. Counting retail and non-retail stations together, there are 40 stations open in the United States. As these stations roll out and serve more and more customers, there are many opportunities to learn and improve on previous designs and efforts.

California is not stopping at 64 stations. It's planning to co-fund the first 100 stations to help get the network to a point where it can support itself with growth from private investments. The most recent notice of proposed awards from the CEC came through GFO-15-605, announced in February 2017, proposing \$33 million for 16 additional retail stations. California's funding of hydrogen stations comes through the CEC's Alternative and Renewable Fuel and Vehicle Technology Program.

For a better understanding of the status of these stations and to inform research and development needs, this project aims to gather, analyze, and publish data and results for the hydrogen community. The aggregated results are shared publicly, and individual results go back to the providers of the data. The type of data needed is defined using data templates that are provided to the station operators. Working with station operators and funders such as California, we demonstrate the importance of station assessments and propose data requirements through their funding mechanisms.

APPROACH

This project documents the innovations and equipment performance used in hydrogen fueling, explores how well customer needs are met, and identifies areas that need improvement. This includes analysis that captures the technology capability (such as back-to-back filling or impact of precooling the hydrogen fuel) as well as the customer perspective (such as fueling times and rates, safety, and availability). Individual components, such as compressors, will be evaluated with the available data to establish status and research needs. Station locations will be evaluated within the context of both available vehicles and future vehicles and their fueling patterns. NREL will also use the analysis results to support DOE in identifying trends from the data that will help guide DOE's research and development activities.

Data analysis will be performed on sensitive industry hydrogen fueling data within the confines of the NFCTEC and recommendations will be provided to DOE on opportunities to refocus or supplement research and development activities. Aggregation of the analyzed data allows for the creation of composite results for public dissemination and presentation. All this involves working with industry partners to create and publish CDPs that show the current technology status without revealing proprietary data. Feedback to industry takes the form of detailed data products (protected results) and provides direct benefit from the NREL analysis performed on industry data. We will continue exercising the fueling analysis functionality of the NREL Fleet Analysis Toolkit to preserve and archive a snapshot of the analysis results from each quarter. This allows a deeper level of results to be stored in an easy-to-access form within the NFCTEC.

Using unique analysis capabilities and tools developed at NREL, researchers are providing valuable technical recommendations to DOE based on real-world experiences with the technology. NREL will continue to provide multiple outputs in the form of CDPs and presentations and papers at technical conferences.

RESULTS

Using data reported to NREL from 29 retail and 9 non-retail stations, more than 90 CDPs were created for the retail group of stations and more than 90 CDPs were created by combining the retail and non-retail stations. Additionally, detailed data products were created for each station showing its data relative to the aggregated

data. Selected public results were presented at the DOE Annual Merit Review and at the Fuel Cell Seminar. All the aggregated results were published to NREL's website and cover several analysis categories including deployment, performance, reliability, utilization, safety, energy use, and hydrogen quality.

Fueling Performance

For 2017, the amount of hydrogen dispensed from the retail stations that were reporting data was 438,352 kg, more than four times the amount dispensed in 2016, which was 104,981 kg. Each quarter since the third quarter of 2015 has seen an increase in the amount dispensed by quarter, with the fourth quarter of 2017 at 143,900 kg. This is because more FCEVs are on the road with more stations opening to support them. The average amount dispensed per station in 2017 Q4 was 4,963 kg, with some stations approaching 10,000 kg in a quarter. The average amount of time spent fueling per vehicle in December 2017 was 3.2 minutes and fueling rates for that month averaged 1.02 kg/min. The amount of fuel dispensed per vehicle averaged 3.2 kg at the end of 2017. Most stations are precooling the fuel down to a nominal temperature of -40°C , which allows for faster fills while not overheating the vehicle tank.

Utilization

At first, the focus of early stations was to have good geographic coverage so early FCEV customers could drive within and between the clusters of stations without worrying about fuel availability. To that end, most of the stations are on the smaller size (<200 kg per day) and can fill only one vehicle at a time. As more vehicles are introduced, now numbering more than 5,000, the stations are seeing demand and in some cases the demand exceeds the intended daily capacity of the stations. As the demand continues to increase, these stations will not be able to support the vehicles and will have to upgrade their equipment and add dispensers, or more stations would be needed nearby to cover the demand. To see how the stations are being utilized, we have developed several CDPs showing amount dispensed by month, quarter, day, and hour of day. We also track the average utilization by quarter relative to their nominal daily capacity, the max quarterly capacity utilization, and the max daily capacity utilization. We have seen four stations near or over their nominal daily capacity for at least one day with several approaching 80%. For the maximum quarterly capacity utilization, there are two stations that have exceeded 80% for a quarter and the average daily utilization shows two stations over 50% with the highest at 63.4%.

Availability

There have been times this year where stations were down either because of maintenance needs or insufficient fuel availability in the network to support the demand. This can be frustrating to customers who already have a limited network of stations. Analysis was done this year to show missed opportunities based on a station being down compared to what it would normally fuel during that same time frame. For the station downtime, we used California Fuel Cell Partnership State of the State Survey data that records when a station is offline. The normal fueling demand was based on averages of what the station normally sees based on fueling records. Figure 1 is a two-dimensional histogram binned by hour of day and day of the week showing how much fuel would normally have been dispensed if stations were not offline. We see that for the fourth quarter of 2017 for 22 stations, they missed fueling 4,683 kg of fuel because they were offline. The highest missed opportunity bins for that quarter are on Wednesdays from noon to 2 p.m. and then from 5–6 p.m.

Maintenance

In the past, we have seen most of the maintenance events and labor time performed on compressors at the stations. We are gradually seeing a shift from compressor issues, as operators learn to avoid failures through preventative maintenance and upgrades while responding more quickly to compressor issues and shifting to dispenser issues. There were many maintenance items related to the chiller that is responsible for cooling the hydrogen fuel down to -40°C . The temperature swings from ambient to -40°C could be causing issues related to leaks at fittings, freezing conditions from moisture in the air, and other issues with the chiller equipment. Figure 2 shows maintenance by equipment type with 46% of events and 31% of labor hours addressing dispenser items, followed by compressor items at 21% of events and 13% of labor hours, with chiller maintenance events at 11% and 14% of labor hours.

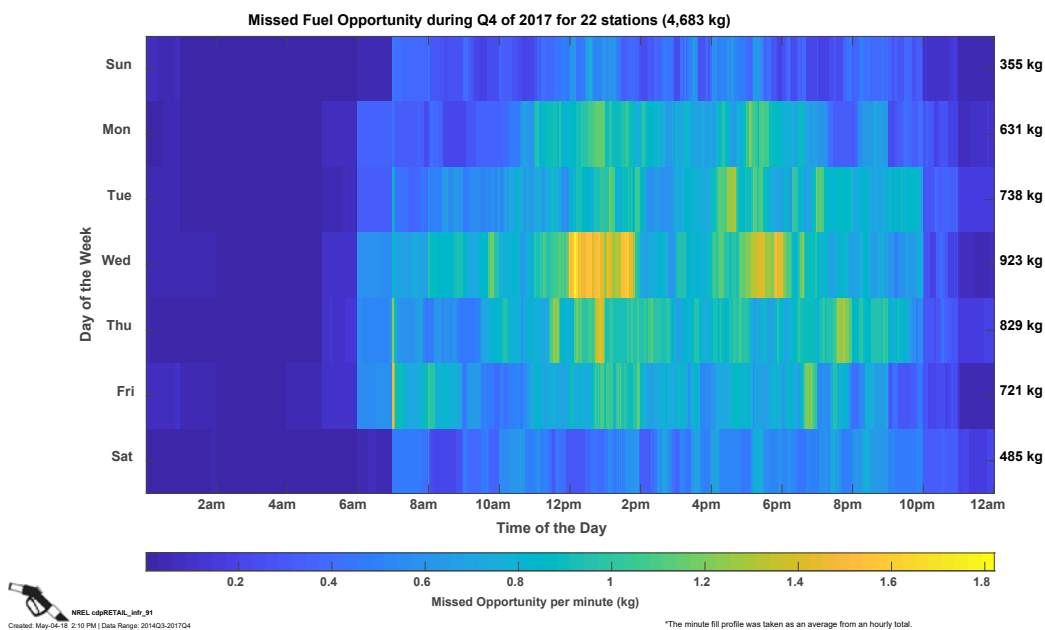


Figure 1. Missed fueling opportunity

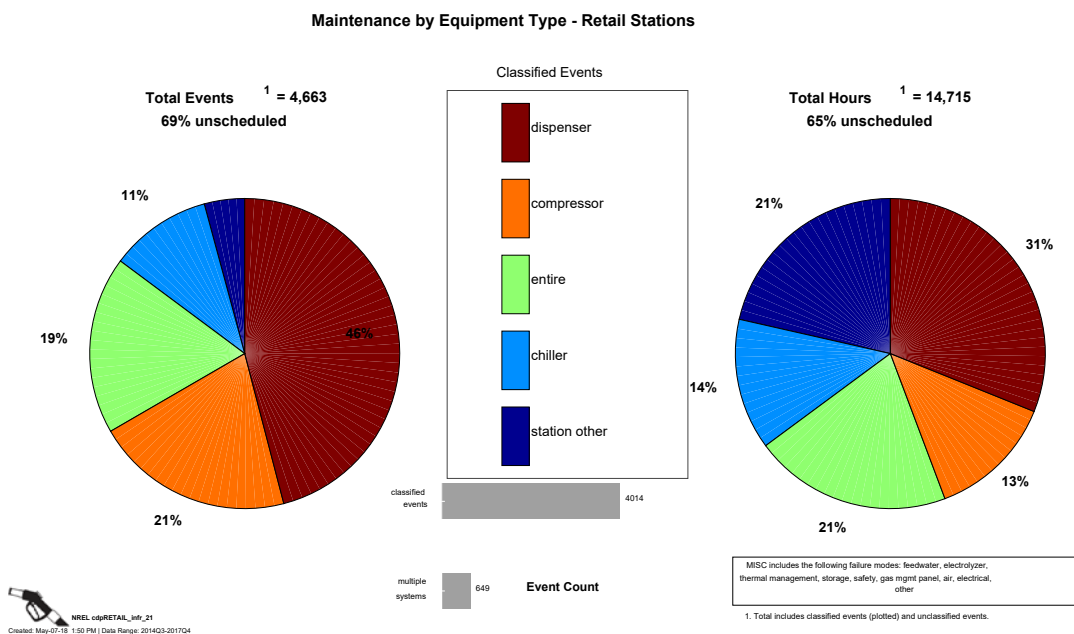


Figure 2. Maintenance by equipment type

Electricity Cost

For stations reporting electricity bills each month, CDPs were developed showing the electrical cost per kilogram of hydrogen dispensed by month. Figure 3 shows the cost per kg by station type. We see the cost coming down over time, most likely due to the increase in fuel dispensed. For December 2017, the average electricity cost per kg for delivered liquid hydrogen stations was \$1.74 per kg, for delivered compressed it was \$1.70 per kg, and for the stations with delivered compressed as well as on-site electrolysis, it was \$4.53 per kg.

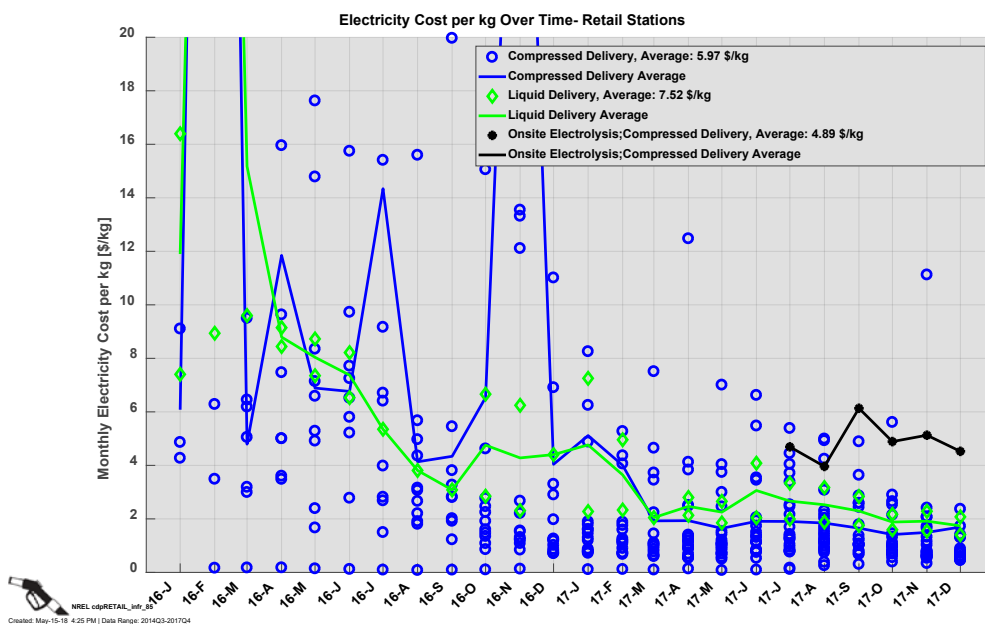


Figure 3. Electricity cost per kilogram hydrogen dispensed

Hydrogen Price at the Pump

The price of hydrogen displayed at the dispenser has been relatively high for these early stations. This may not be a concern for early customers that have fuel included with the lease of their FCEVs but may be an issue as drivers start paying for their own fuel at the pump. Figure 4 shows the range of prices at the stations over time and weighted by the amount of fuel sold. For the last quarter of 2017, the weighted price at the pump for 70 MPa hydrogen fuel was \$16.31 per kg of hydrogen.

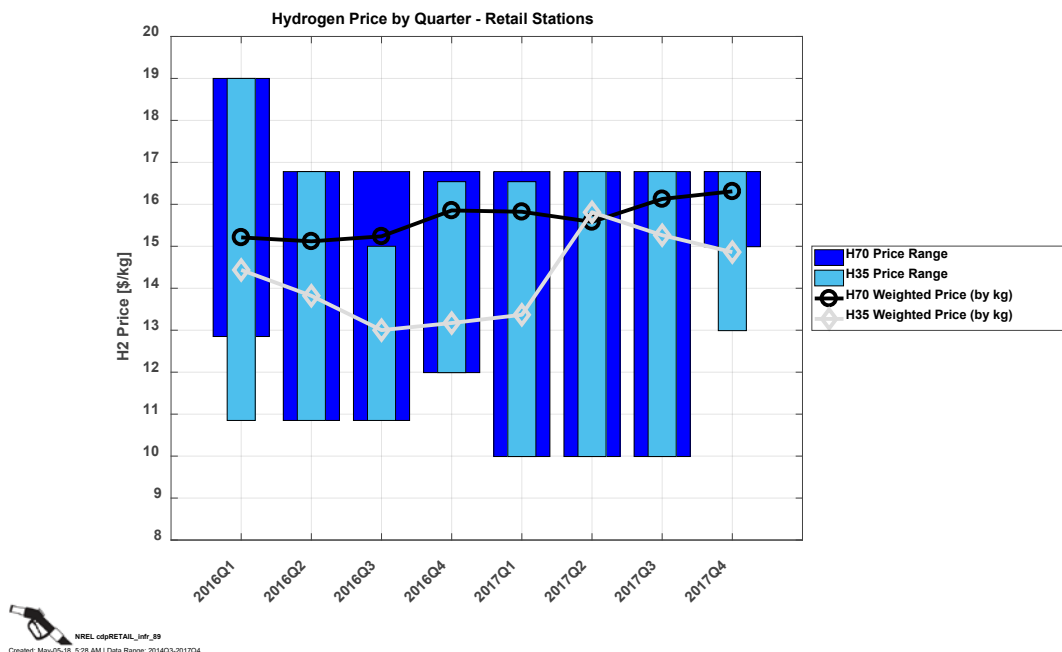


Figure 4. Price of hydrogen dispensed

Hydrogen Quality

Hydrogen is sampled at the stations periodically for impurity analysis. CDPs based on the data from the lab analysis are created for each individual constituent showing the range of values for each impurity seen at stations. For example, the lab results for carbon monoxide show a range from 0.5 to 10 parts per billion at the stations. This is well below limits of 200 parts per billion but is useful for fuel cell developers to see what their equipment will be exposed to at these stations. Impurity CDPs are available for all the constituents listed in the SAE J2719 standard.

The results discussed here were based on a subset of the CDPs developed by this project and are available on NREL's website alongside the complete set of CDPs for retail stations and the set for the combination of non-retail and retail stations.

CONCLUSIONS AND UPCOMING ACTIVITIES

As the network of stations grows, we expect to see new technologies deployed at larger stations with multiple fueling positions as well as the continual operation of the existing stations. Their performance and availability will affect how successfully they support the current and upcoming fleet of fuel cell vehicles. Continual data collection, analysis, and feedback will provide DOE and the hydrogen and fuel cell community with awareness of the benefits and shortcomings of the current technology and identify areas for further research and development. This project will continue to add timely analysis topics and work toward a more automated system for recurring analysis that is desired and useful for the community. For the near term, activities include the next set of CDPs planned to be available in the fourth quarter of 2018.

As more hydrogen markets open for applications such as long-haul and medium-duty trucks, the knowledge from existing stations will serve to inform the development of infrastructure for these applications.

FY 2018 PUBLICATIONS/PRESENTATIONS

1. Sam Sprik, Jennifer Kurtz, Chris Ainscough, Genevieve Saur, Shaun Onorato, and Matt Ruple, "TV017: Hydrogen Station Data Collection and Analysis" (presented at the 2018 DOE Annual Merit Review and Peer Evaluation Meeting, Washington, DC, June 14, 2018).
2. Sam Sprik, Jennifer Kurtz, Genevieve Saur, Shaun Onorato, Matt Ruple, and Chris Ainscough, "Next Generation Hydrogen Station Composite Data Products: All Stations (Retail and Non-Retail Combined), Data through Quarter 4 of 2017" (May 2018), http://www.nrel.gov/hydrogen/proj_infrastructure_analysis.html.
3. Sam Sprik, Jennifer Kurtz, Genevieve Saur, Shaun Onorato, Matt Ruple, and Chris Ainscough, "Next Generation Hydrogen Station Composite Data Products: Retail Stations, Data through Quarter 4 of 2017" (May 2018), http://www.nrel.gov/hydrogen/proj_infrastructure_analysis.html.
4. Sam Sprik, Jennifer Kurtz, Chris Ainscough, Genevieve Saur, and Michael Peters, "Next Generation Hydrogen Station Composite Data Products: All Stations (Retail and Non-Retail Combined), Data through Quarter 2 of 2017" (November 2017), http://www.nrel.gov/hydrogen/proj_infrastructure_analysis.html.
5. Sam Sprik, Jennifer Kurtz, Chris Ainscough, Genevieve Saur, and Michael Peters, "Next Generation Hydrogen Station Composite Data Products: Retail Stations, Data through Quarter 2 of 2017" (November 2017), http://www.nrel.gov/hydrogen/proj_infrastructure_analysis.html.
6. Sam Sprik, Jennifer Kurtz, Chris Ainscough, Genevieve Saur, Mike Peters, and Keith Wipke, "Performance of Existing Hydrogen Stations" (presented at the 2017 Fuel Cell Seminar and Energy Exposition, Long Beach, CA, November 8, 2017).

Performance and Durability Testing of Volumetrically Efficient Cryogenic Vessels and High-Pressure Liquid Hydrogen Pump

Salvador M. Aceves (Primary Contact),
Guillaume Petitpas, Julio Moreno-Blanco,
Juan Manuel Garcia-Guendulain
Lawrence Livermore National Laboratory
7000 East Avenue
Livermore, CA 94550
Phone: (925) 422-0864
Email: aceves6@llnl.gov

DOE Manager: Jason Marcinkoski
Phone: (202) 586-7466
Email: jason.marcinkoski@ee.doe.gov

Subcontractor:
Linde LLC, Hayward, CA

Project Start Date: January 2014
Project End Date: September 2018

Overall Objectives

- Characterize cryogenic vessel and liquid hydrogen (LH₂) pump performance by modeling important performance parameters including: refuel density, boil-off, hydrogen temperature and pressure during fill, and system (volumetric and gravimetric) storage density.

Fiscal Year (FY) 2018 Objectives

- Characterize LH₂ pump performance by modeling vessel fill experiments.
- Determine vessel fill density, weight and volume storage performance, and vent losses by modeling typical vehicle utilization patterns.

Technical Barriers

This project addresses the following technical barriers from the Technology Validation section of the Fuel Cell Technologies Office Multi-Year Research, Development, and Demonstration Plan¹:

- (C) Hydrogen Storage
- (D) Lack of Hydrogen Infrastructure Performance and Availability Data.

Contribution to Achievement of DOE Technology Validation Milestones

This project will contribute to achievement of the following DOE milestones from the Technology Validation section of the Fuel Cell Technologies Office Multi-Year Research, Development, and Demonstration Plan: Milestone 3.4: Validate station compression technology provided by delivery team (4Q, 2018).

FY 2018 Accomplishments

- Developed a thermodynamic model to determine fill density for any initial vessel condition.
- Determined vessel fill density for typical vehicle utilization and refueling patterns.
- Demonstrated very low potential for vent losses even under extreme vehicle utilization scenarios.
- Evaluated volumetric and gravimetric cryogenic vessel storage performance for typical utilization conditions.

¹ <https://www.energy.gov/eere/fuelcells/downloads/fuel-cell-technologies-office-multi-year-research-development-and-22>

INTRODUCTION

Cryogenic pressure vessels (also known as cryo-compressed vessels) have fundamental thermodynamic advantages enabling high-density hydrogen storage without the boil-off losses typical of cryogenic systems. High density is critical for practical hydrogen-fueled transportation, enabling vehicles with similar driving autonomy and refueling time as today's gasoline vehicles while producing zero regulated and climate-changing emissions. High density enables storage of a large amount of fuel in a small package that occupies less space onboard the vehicle and weighs less, therefore reducing system cost by reducing the need for expensive structural materials (carbon fiber and metals). Low vessel cost combined with effective LH₂ distribution, storage at the station, and dispensing results in minimum cost of ownership among existing approaches for automotive hydrogen storage. Safety is also improved because cryogenic hydrogen has lower internal energy and therefore expands less in case of vessel failure. An outer vacuum jacket provides an extra layer of protection and volume for hydrogen expansion, reducing expansion pressure and thrust.

Cryogenic pressure vessel refueling also is thermodynamically favored. A two-stage LH₂ pump manufactured by Linde enables direct pressurization of dense LH₂, therefore minimizing compression work (hence low electricity consumption) and enabling high throughput (100 kg/h, enough for 5-minute automobile refuels) from a small displacement (0.36 liters) two-stage piston pump. Additionally, refueling at densities higher than LH₂ at the dewar (65 g/L) is possible due to the high compressibility of LH₂.

APPROACH

We developed a thermodynamic model capable of predicting cryogenic vessel fill pressure and temperature (and therefore density) for any initial condition. The model has been validated by comparison with the results of 24 cryogenic pressure vessel fill experiments with a LH₂ pump manufactured by Linde and installed at the Lawrence Livermore National Laboratory campus [1]. The LH₂ piston pump takes LH₂ from the station dewar at near ambient pressure (3 bar) and very low temperature (24.6 K) and pressurizes it to the vessel pressure in two stages of compression, up to 875 bar. Experiments spanned initial vessel temperatures from ambient to 22 K, enabling pump testing over a broad range of conditions.

We also conducted a comprehensive evaluation of all factors affecting cryogenic vessel fill density in an effort to evaluate system performance versus operational parameters over a broad range of conditions. The model considers use patterns, insulation performance, vessel characteristics, liquid hydrogen pump performance, and para-hydrogen to ortho-hydrogen conversion [2].

Lastly, we evaluated cryogenic vessel *system* storage performance, including volumetric (g H₂/L), gravimetric (H₂ weight fraction), and vent losses over a broad range of conditions.

RESULTS

Key results from this year's effort include the following.

- Fill densities are well predicted (RMS error = 0.7 g/L) with a thermodynamic fill model that assumes constant 10 kJ/kg K inlet vessel entropy.
- The thermodynamic fill model has been applied to generate diagrams that can be used for directly reading fill density for any initial vessel condition (Figure 1).
- Fill density increases monotonically with driving distance (Figure 2). The main effect determining this behavior is heat transfer from the environment. Increased driving distance rapidly depletes hydrogen in the vessel, reducing time available for heat transfer, leading to colder vessels that fill to higher density. This is synergistic with hydrogen storage needs of frequently driven vehicles—more capacity in the vehicles that most need it.

- Para-hydrogen to ortho-hydrogen (P-O) conversion absorbs heat and cools down the vessel, leading to significant increases in fill density (up to 5.3%). P-O conversion is most active for vehicles driven 20–60 km/day, and therefore will have a major effect on most personal vehicles (Figure 2).
- Cryogenic vessel system density (defined as hydrogen stored divided by total system volume) is greatest for 700-bar vessels. There is little gain (1 g/L or less) in increasing pressure beyond 500 bar, however, and maximum fill density at 150 km/day driving distance (42 g/L) is equal for 500-bar and 700-bar vessels (Figure 3).
- A 350-bar vessel can store hydrogen at system density up to 40.5 g/L and appears a reasonable alternative with average system density only 2.5 g/L less on average than 700-bar vessels (Figure 3).
- Weight fraction (hydrogen mass divided by total system mass) is greatest (7.4%) for 150 bar and 250 bar, and a 350-bar vessel is nearly as weight efficient (7%). For 500- and 700-bar vessels, the weight fraction drops to 6.4% and 5.6% due to thicker composite walls (Figure 4).
- Results indicate that 250–350 bar appears to be a superior design space for cryo-compressed storage due to lower composite mass (and therefore lower cost) than 500- to 700-bar vessels, while maintaining nearly as high system density (Figure 3, Figure 4). A full economic and functional evaluation is necessary, however, to determine “optimum” design pressure for cryogenic vessels.
- Cryogenic vessels with a working vacuum insulation are unlikely to have any vent losses during normal operation. Venting only occurs when the vehicle is continuously driven for many hours, filled to maximum capacity at the end of the trip, and used infrequently (10 km to 30 km per day) after fill. Vessels 350 bar and stronger do not lose hydrogen if driven 10 km/day or more. Losses can be avoided by educating drivers to not fill the vessel to full capacity after a long drive if they anticipate infrequent use of the vehicle in the following days.

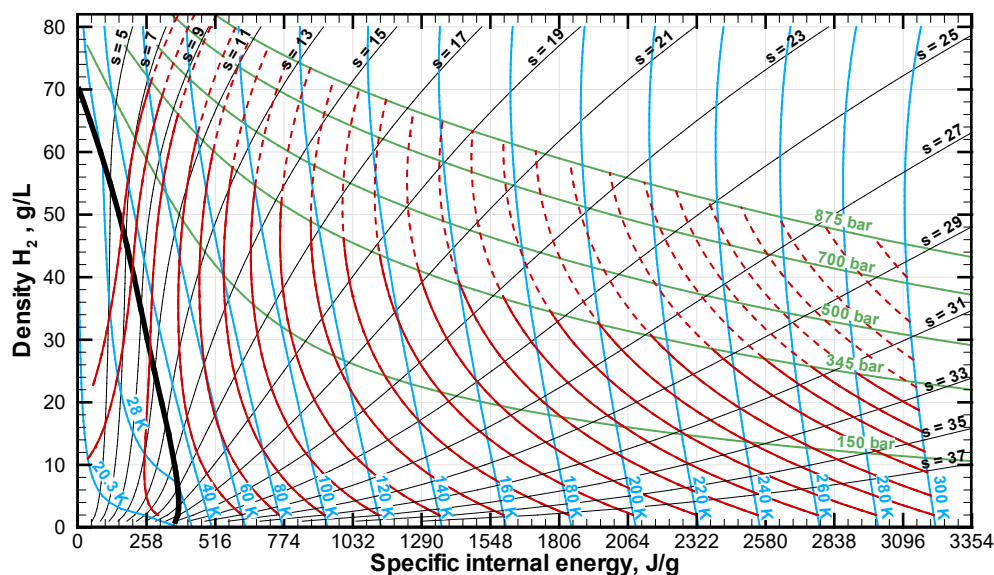


Figure 1. Hydrogen phase diagram showing liquid hydrogen pump fill lines in red. To calculate fill density, identify the initial condition (p_0 , T_0) in the diagram, and follow the red line from p_0 , T_0 to the final fill pressure. Fill lines assume constant vessel inlet entropy $s_{H_2} = 10$ kJ/kg-K and thermal equilibrium between the experimental vessel and hydrogen inside the vessel.

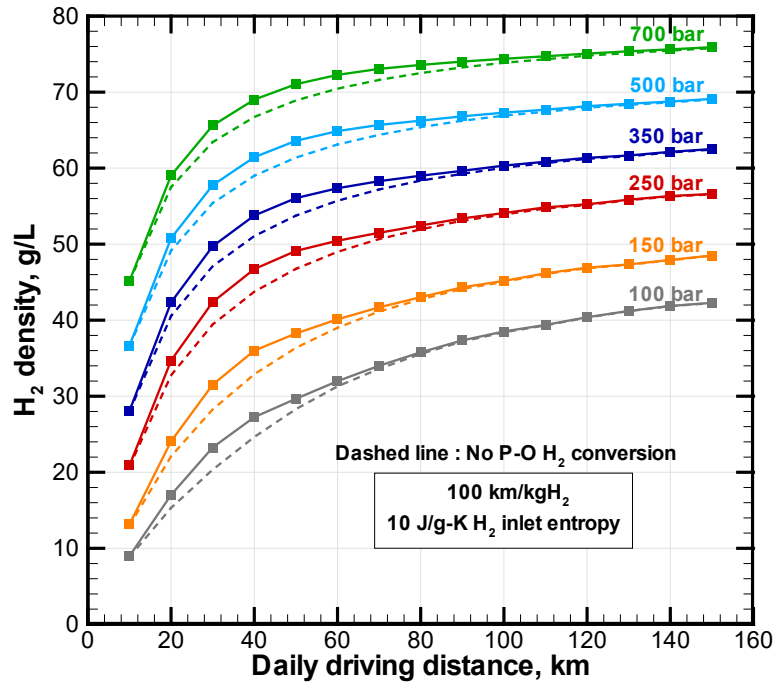


Figure 2. Steady-state fill density for 100-bar to 700-bar vessels continuously driven the same daily distance. In addition to the predicted fill density (solid), the figure shows a dashed line indicating fill density if P-O conversion is absent [2].

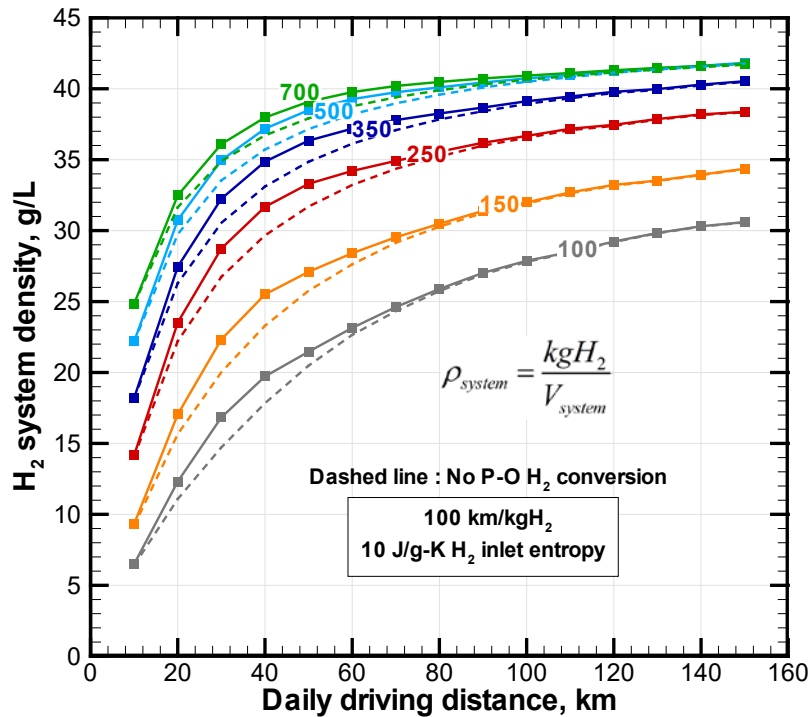


Figure 3. Steady-state system storage density (hydrogen mass divided by total system volume) as a function of daily driving distance and design pressure. Dashed lines indicate system density if P-O conversion is absent.

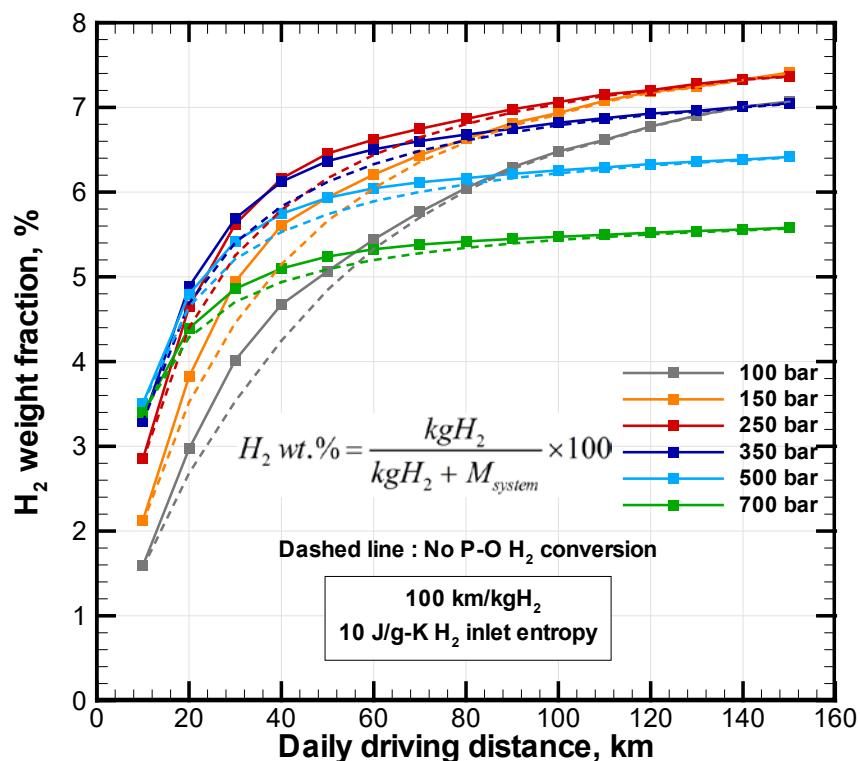


Figure 4. Steady-state system hydrogen weight fraction (hydrogen mass divided by total system weight) as a function of daily driving distance and design pressure. Dashed lines indicate hydrogen weight fraction if P-O conversion is absent.

CONCLUSIONS AND UPCOMING ACTIVITIES

The results confirm previous experiments and models indicating that cryogenic vessels have maximum system density of all available storage technologies and avoid vent losses in all but the most extreme situations. Design pressures in the 250 bar to 350 bar range seem most advantageous due to high system density and low weight and cost, although determining an optimum pressure demands a complete economic and functional analysis.

SPECIAL RECOGNITIONS AND AWARDS/PATENTS ISSUED

1. Cryogenic pressurized storage with hump-reinforced vacuum jacket, Salvador M. Aceves, Francisco Espinosa-Loza, Guillaume Petitpas, Vernon A. Switzer, Elias Rigoberto Ledesma-Orozco, Victor Alfonso Alcantar-Camarena, US Patent 10,082,246, September 25, 2018.

FY 2018 PUBLICATIONS/PRESENTATIONS

1. V. Alcántar, S. Ledesma, S.M. Aceves, E. Ledesma, A. Saldana. “Optimization of Type III Pressure Vessels Using Genetic Algorithm and Simulated Annealing.” *International Journal of Hydrogen Energy* 42 (2017): 20125–20132.
2. V. Alcántar, S.M. Aceves, E. Ledesma, S. Ledesma, and E. Aguilera. “Optimization of Type 4 Composite Pressure Vessels Using Genetic Algorithms and Simulated Annealing.” *International Journal of Hydrogen Energy* 42 (2017): 15770–15781.
3. J.C. Moreno-Blanco, F. Elizalde-Blancas, A. Gallegos-Muñoz, and S.M. Aceves. “The Potential for Avoiding Hydrogen Release from Cryogenic Pressure Vessels after Vacuum Insulation Failure.” *International Journal of Hydrogen Energy* 43 (2018): 8170–8178.

4. G. Petitpas and S.M. Aceves. “Liquid Hydrogen Pump Performance and Durability Testing Through Repeated Cryogenic Vessel Filling to 700 Bar.” *International Journal of Hydrogen Energy* 43, no. 39 (2018): 18403–18420.
5. Guillaume Petitpas, Julio Moreno-Blanco, Francisco Espinosa-Loza, and Salvador M. Aceves. “Rapid High-Density Cryogenic Pressure Vessel Filling to 345 Bar with a Liquid Hydrogen Pump.” *International Journal of Hydrogen Energy* 43, no. 42 (2018): 19547–19558.

REFERENCES

1. Guillaume Petitpas, Julio Moreno-Blanco, Francisco Espinosa-Loza, and Salvador M. Aceves, “Rapid High-Density Cryogenic Pressure Vessel Filling to 345 Bar with a Liquid Hydrogen Pump,” *International Journal of Hydrogen Energy* 43, no. 42 (2018): 19547–19558.
2. Julio Moreno-Blanco, Guillaume Petitpas, Francisco Espinosa-Loza, Francisco Elizalde-Blancas, Joel Martinez-Frias, and Salvador M. Aceves, “The Fill Density of Automotive Cryo-Compressed Hydrogen Vessels,” *International Journal of Hydrogen Energy* (2018) (in press).
3. Julio Moreno-Blanco, Guillaume Petitpas, Francisco Espinosa-Loza, Francisco Elizalde-Blancas, Joel Martinez-Frias, and Salvador M. Aceves, “The Storage Performance of Automotive Cryo-Compressed Hydrogen Vessels,” *International Journal of Hydrogen Energy* (2018) (submitted for publication).

Grid Integration and Hydrogen Energy Generation: Modeling and Validation of Electrolyzers in Real-Time Grid Simulation

Rob Hovsopian (Primary Contact),
Manish Mohanpurkar, Yusheng Luo,
Anudeep Medam, Rahul Kadavil
Idaho National Laboratory
750 University Blvd.
Idaho Falls, ID 83406
Phone: (208) 526-8217
Email: rob.hovsopian@inl.gov

DOE Manager: Jason Marcinkoski
Phone: (202) 586-7466
Email: Jason.Marcinkoski@ee.doe.gov

Subcontractors:

- Humboldt State University, Arcata, CA
- Florida State University, Tallahassee, FL

Project Start Date: October 1, 2017
Project End Date: September 30, 2020

Overall Objectives

- Validate electrolyzer network capability to support utility needs for stability with high penetration of renewables.
- Create control logic and communications for networked electrolyzer operation based on stability and economics.
- Quantify the benefit of electrolyzer operation to the power system stability and generalize its impact for multiple units connected in single- and multiple-distribution networks.
- Provide experimental data to H2@Scale modeling, simulation, and analysis team for performance, reliability, durability, and economic assumptions.

Fiscal Year (FY) 2018 Objectives

- Expand the grid modeling to accommodate futuristic hydrogen refueling stations (H2@Scale) providing energy storage for very high renewable energy penetration in digital real-time simulations. This platform will be

used to assess the value of electrolyzers by providing hydrogen storage under varying renewable energy penetrations including solar and wind.

- Implement the “front end controller” (FEC) that interprets solar and wind profiles of varying penetration levels to make logical decisions to enable hydrogen-based storage. Additional capabilities of the FEC include the accurate interpretation of sample utility signals and safe control of the operation of the hydrogen refueling station. Ensure the control signals generated by FEC for the lower level controller respond to different utility signals and hence can participate in demand response and ancillary service programs.
- Perform real-time simulation within which the future hydrogen refueling station is controlled by the FEC to provide local fast loop support and macro grid-level slow loop support. The hydrogen refueling station hardware at NREL will be used as power-hardware-in-the-loop (HIL) to perform real-time simulation and extend the potential of H2@Scale support for renewable energy penetration.
- Test and validate the performance of single and multiple electrolyzers (MW scale) in providing local voltage and frequency support when integrated with the FEC.
- Test the performance of the FEC in driving the electrolyzer to account for the variability of varying penetration levels of wind and solar that is connected at diverse locations within the power grids.

Technical Barriers

This project addresses the following technical barriers from the Technology Validation section of the Fuel Cell Technologies Office Multi-Year Research, Development, and Demonstration Plan¹:

¹ <https://www.energy.gov/eere/fuelcells/downloads/fuel-cell-technologies-office-multi-year-research-development-and-22>

(B) Lack of Data on Stationary Fuel Cells in Real-World Operation

(G) Hydrogen from Renewable Resources

(H) Hydrogen and Electricity Co-Production.

Contribution to Achievement of DOE Technology Validation Milestones

This project will contribute to achievement of the following DOE milestone from the Systems Analysis and Technology Validation sections of the Fuel Cell Technologies Office Multi-Year Research, Development, and Demonstration Plan:

- Milestone 3.9: Validate large-scale system for grid energy storage that integrates renewable hydrogen generation and storage with fuel cell power generation by operating for more than 10,000 hours with a round-trip efficiency of 40%. (4Q, 2020)

FY 2018 Accomplishments

Modeling and Validation of Electrolyzers in Real-Time Grid Simulation

- To accomplish the objectives of this project, Idaho National Laboratory (INL), the National Renewable Energy Laboratory (NREL), and Sandia National Laboratories (SNL) utilized several core capabilities related to hydrogen and real-time simulations with HIL:
 - Real-time connectivity between the real-time simulators and electrolyzer at the two labs
 - Advanced grid modeling, hydrogen components and systems, control systems development, and optimization.
- The team completed the implementation of the FEC on a processor board and interfaced with the real-time simulator to develop a real-time test bed for rapid prototyping of the functionalities of the FEC. This platform serves as the verification and validation platform for the FEC development and testing.
- A paper related to electrolyzers and grid interaction assessment was published in *Energies MDPI*. Title: “Electrolyzers Enhancing Flexibility in Electric Grids,”

Manish Mohanpurkar, Yusheng Luo, Danny Terlip, Fernando Dias, Kevin Harrison, Joshua Eichman, Rob Hovsopian, and Jennifer Kurtz.

- An urban city model, within which hydrogen fuel cell electric vehicles (FCEVs) have a large-scale adoption and are used for public transportation, was built using the data provided by the New York Taxi and Limousine Commission. The study results and discussion were published as a peer-reviewed paper and presented at the IEEE conference, Probabilistic Methods Applied to Power Systems, Boise, Idaho, June 2018. Title: “Optimal Scheduling of Electrolyzer in Power Market with Dynamic Prices,” Yusheng Luo, Min Xian, Manish Mohanpurkar, Bishnu P. Bhattarai, Anudeep Medam, Rahul Kadavil, and Rob Hovsopian.
- A “renewable energy module” was built and integrated into the FEC that was iteratively built in the past-funded project by the Fuel Cell Technologies Office. This renewable energy module can predict the renewable energy output of a desired plant and, in turn, provide control for the hydrogen electrolyzers. The outcome of this research direction enables a controllable and relatively predictable renewable energy output to the grid.
- Two power grid representations were utilized to understand the potential of H2@Scale to provide energy storage for renewable energy assimilation—San Diego Gas and Electric and Pacific Gas and Electric. IEEE models were also adopted for analysis.
- NREL, INL, and SNL had a technical interchange meeting in June 2018 to gauge the progress of the project and increase the effort on areas of testing and the development of the FEC in line with the optimization-based findings of the cost of hydrogen.
- The performance of multiple FECs that cohesively operate distributed electrolyzers in providing MW-level storage to renewable energy was tested and validated. Centralized and distributed electrolyzers connected to the test grids at different locations provide grid support based on FEC action.
- Varying levels of renewable energy penetrations (20%, 30%, and 50%) for the

electric grids were investigated for the test grids to assess the energy storage potential of H2@Scale infrastructure.

Topic 1A. Experimental and Core Capability Related to H2@Scale

- A programmable high-power source for controlled AC and DC output and frequency conversion as well as product tests relative to high-temperature electrolysis stacks were procured.

INTRODUCTION

This project aims to quantify the value of hydrogen refueling stations from a grid integration perspective to provide energy storage for accommodating renewable energy. Significant emphasis is on assessing the potential of H₂@Scale (MW level) to provide hydrogen energy-based storage to reduce the variability of renewable energy sources. The anticipated value of electrolyzers stems from the fact that they are a controllable load with fast response. They are typically coupled with hydrogen energy storage, dispensers, and compressor units to form hydrogen refueling stations. They provide the flexibility to meet hydrogen demand with stored hydrogen when responding to the grid demand and store more hydrogen when the grid power demand is low. In addition to this complementary approach, local energy storage potential from hydrogen infrastructure can be established. The input resource for electrolyzers is electricity, which allows flexible co-placement of electrolyzers with other distribution energy sources in a power system network, leading to an optimal value of the objective function. Real-time simulations of power systems that include renewable energy modeling with HIL of the electrolyzer and supplementary systems representing the hydrogen refueling station form the test setup of this project.

This project leverages the existing work at INL, NREL, and SNL in the areas of power systems, electrolyzers, power markets, optimization, and control systems. The 250-kW modular electrolyzer stack is utilized for performing real-time simulations and HIL to generate high-accuracy data and results. The FEC developed in this research helps integrate the operations of the electrolyzer with the grid management systems and adds stability as the variability in renewable energy is reduced. The flexibility on account of controllability is utilized to assimilate renewable energy, manage distribution loads, and provide grid support. The adoption of the FEC developed and tested in this project will drive down the cost of generating hydrogen while maintaining the requisite reserves to meet demands for power.

APPROACH

The team developed and worked on an optimization-based approach to create the “renewable energy module” that provides the FEC the necessary information related to renewable energy penetration on the grid. There are two ways to address renewable energy penetration at very high levels and accommodate renewable energy sources’ variability and unpredictability. The first one is to let the utility or operator directly control and hence manage the output of the renewable energy plant. At very high penetration levels of renewable energy, the grid operators need significant flexibility to manage the variability and uncertainty.

The second approach includes coordinating the operation of the renewable energy plant and local hydrogen storage with the grid operator or utility to improve predictability and lessen uncertainty. This will ultimately reduce cost and stress as well as augment the stability of the electric grids. Numerous instances have been recorded in which the excess renewable energy is spilled and hence underutilized. For such instances, hydrogen operators can get electricity for free or even get paid to consume it to maintain stability. This ultimately adds to the revenue of the hydrogen station operators, reduces the costs of producing hydrogen, and makes the market more viable.

This project experimentally verified the response of the FEC controlling the operation of the electrolyzer in response to renewable energy-related information with the optimal location and sizing of the electrolyzer. Advanced optimization techniques are being utilized for assessing the feasibility of sizing of hydrogen infrastructure for a given level of renewable energy. Several other grid scenarios related to grid dynamics and transients were also simulated in real time to assess the coordinated operation of FECs and electrolyzers. For these cases, the FEC and electrolyzer demonstrated voltage and frequency support to the grid in addition to the renewable energy assimilation. Voltage support by the FEC and electrolyzer in providing grid services using the hardware stack was also demonstrated.

The key takeaway is the optimal location and sizing of electrolyzers can greatly affect the performance of electrolyzers in providing local support, so optimization plays a key role. From past Fuel Cell Technologies Office-funded projects, the FEC had two major functional modules represented by two control loops—slow

and fast loops. The slow loop is associated primarily with the cost optimization of hydrogen, whereas the fast loop deals with the provision of grid services by the stack. The “renewable energy module” was added to the existing two loops to provide the functionalities shown in Figure 1.

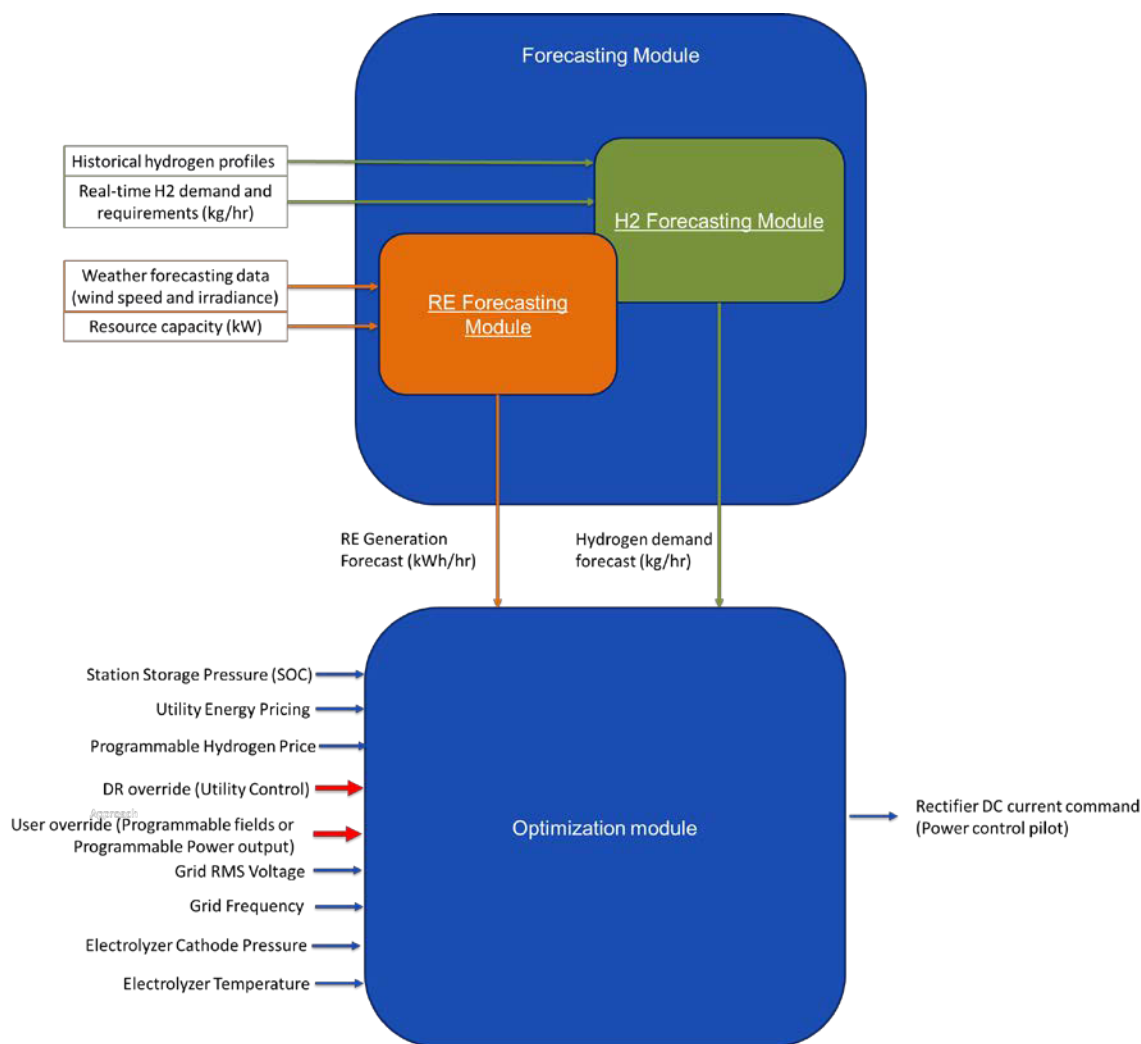


Figure 1. Data exchange between forecasting module and optimization module

Figure 2 provides detailed functionalities and expected data for all modules with inputs and outputs for the entire FEC. The regional power grid models, FEC, distributed real-time simulations, and connectivity between INL and NREL enabled the assessment of hydrogen-based energy storage for renewable energy. The selection and modeling of renewable energy penetration of diverse levels (20%, 30%, and 50 %) were integrated into the regional grids. Existing NREL databases related to renewable energy (solar and wind) were studied for the same penetration levels.

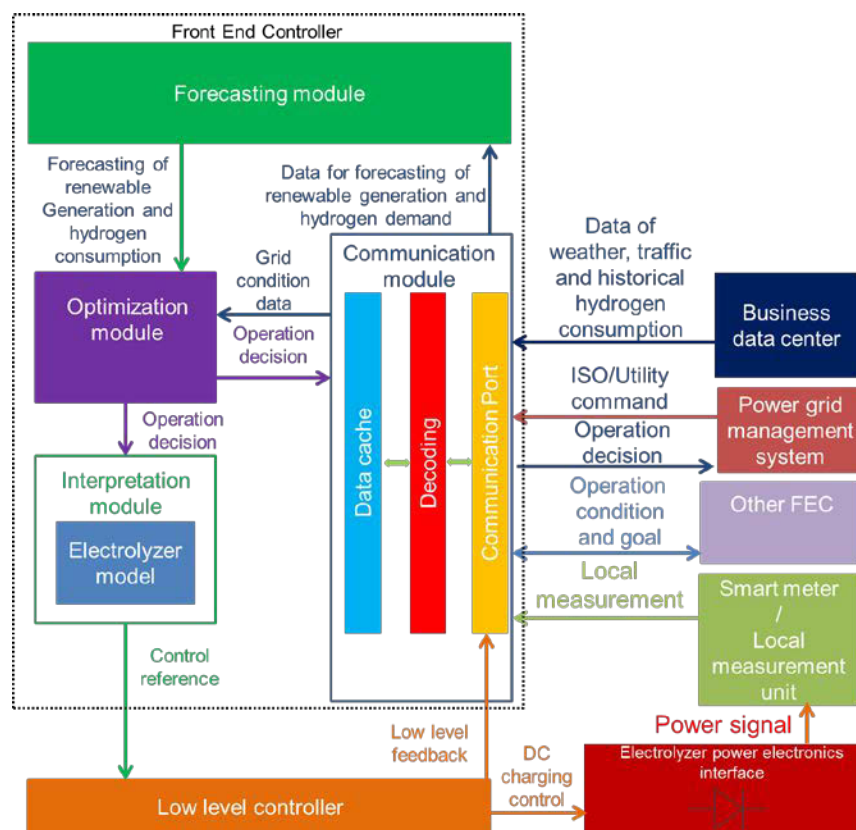


Figure 2. Updated FEC configuration with the integration of renewable energy module

Distributed real-time simulations and HIL were performed utilizing the 250-kW electrolyzer stack and a hardware implementation of the FEC. The functionalities of the electrolyzer stack responding to control signals from the FEC were verified for applications including grid services within the required time resolutions. An IEEE 34-bus test system and Pacific Gas and Electric representation in a real-time environment was created to understand and assess the performance of the integrated FEC and electrolyzer stack. Regional power grid models, including Arizona, southwest California, and the Bay Area, leverage existing models from the IEEE standard systems library that are directly derived from existing power grids around the United States.

The test results demonstrated the capability of the electrolyzer to provide local grid services and the ability of the FEC as hardware to control the electrolyzer. Economic optimization in the FEC has also been developed and implemented. This allows the FEC to make optimal decisions under different market rates and structures to generate hydrogen at a low cost. The optimization developed for the electrolyzer and implemented in the FEC hardware serves the purpose of striking a balance between providing support to the grid operations and increasing the profit of the hydrogen producer. Economic results were discussed and presented last year and are not included here. The distributed real-time simulations between INL and NREL involved controlling the electrolyzer hardware stack using the FEC implemented on the PI-card (a processor card). The data transmission for controlling the stack power consumption was 100 Hertz. This testing was important to verify the communication between the FEC on the PI-card with the hardware stack. This integrated platform was utilized to test the controllability of electrolyzer stacks based on the functionalities defined in the FEC under dynamic grid conditions. The electrolyzer stack controlled via the FEC on the PI-card demonstrated voltage and frequency support to the grid based on varying grid conditions including renewable energy variations.

Solar Forecasting Module in the FEC

The solar photovoltaic (PV) time-series forecasting is based on a popular linear regression forecasting model that uses the SARIMAX (Seasonal Autoregressive Integrated Moving Averages with eXogenous regressors) process in order to account for the inherent seasonal effect of PV power output time series. The SARIMAX model allows for integration of exogenous variables such as weather data for temperature in the future to improve the forecasting accuracy. Real-world PV output time-series data for 1 year is used to perform the day-ahead prediction. The time-series data is split into two parts—the training part, which makes up about 90% of the input data and will be used to train the model, and the remaining 10%, the test part, which will be used to evaluate the accuracy of the trained SARIMAX model as shown in Figure 3.

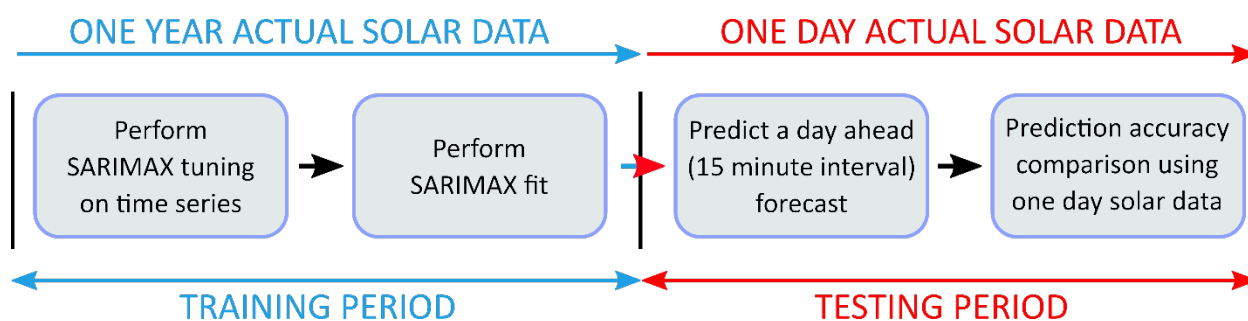


Figure 3. Prediction process utilized in the FEC for interpreting PV

The seasonal ARIMAX model is generally referred to as SARIMAX (p, d, q) x (P, D, Q, s), where p, d, q and P, D, Q, s are non-negative integers that refer to the polynomial order of the autoregressive (AR), integrated (I), moving average (MA), and periodicity parts of the nonseasonal and seasonal components of the model. In the training phase, a grid-based search is performed to estimate the orders for (p, d, q) and (P, D, Q) that result in the best fit mainly based on the Akaike Information Criterion, which is an estimator of the relative quality of the fitted model for the given training data set. Comparison of the training data with the fitted data obtained from the SARIMAX (1, 0, 1) x (1, 1, 1, 12) model as shown in Figure 4 suggests that the SARIMAX model is able to obtain a good fit.

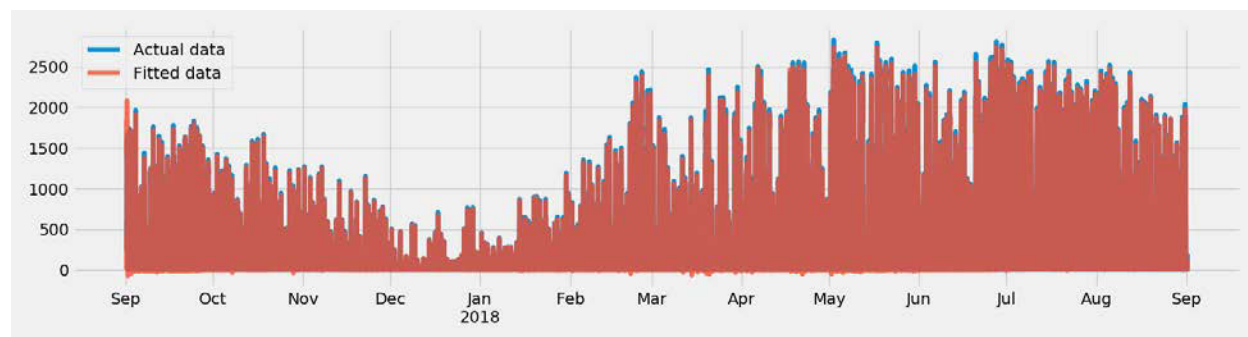


Figure 4. SARIMAX model fitted with training data

The trained model is then used to perform a day-ahead prediction with a time resolution of 15 minutes as the input data set. The day-ahead prediction is then compared against the test data set to measure the effectiveness of the PV prediction using root mean square error technique. To demonstrate the H2@Scale renewable energy penetration in a grid, the available power from the renewable energy source, “Pset,” is obtained from the solar forecast module of the FEC and sent to the electrolyzer. The electrolyzer should then be able to consume the power as requested. The project ran several cases and combinations of 20%, 30%, and 50% PV penetration (concentrated and distributed) on the test systems with suitably scaled hydrogen infrastructure to support the storage. A sample case of 20% PV penetration is discussed here, in which the electrolyzer is centralized, but we have simulated an array of distributed PV cases as well.

RESULTS

For the 20% penetration case: As shown in Figure 5, all the PV is located at 808, electrolyzers are located at 806, and the total power rating of the electrolyzer is 200 MW. Due to the spatiotemporal characteristics, variability, and uncertainty of renewable energy sources, their generation cannot be flexibly adjusted to match the demand from the load side. Excessive generation can even exert negative impact on the power grid when there is mismatch between generation and load. Hence localized storage in the form of hydrogen can play a significant role. Generating hydrogen with excess renewable energy generation is can help relieve certain stressful conditions. From this perspective, an observability of PV is created in the existing FEC in the form of a renewable energy module. This module enables the FEC to control the electrolyzer operations to complement the PV generation to soften the transients as shown in further results. The 20% PV penetration case along with the actual and forecast generation from the renewable energy module is shown in Figure 6. The load profile is shown in Figure 7. Figure 8 demonstrates the role of electrolyzers that are being controlled by the FEC with the renewable energy module.

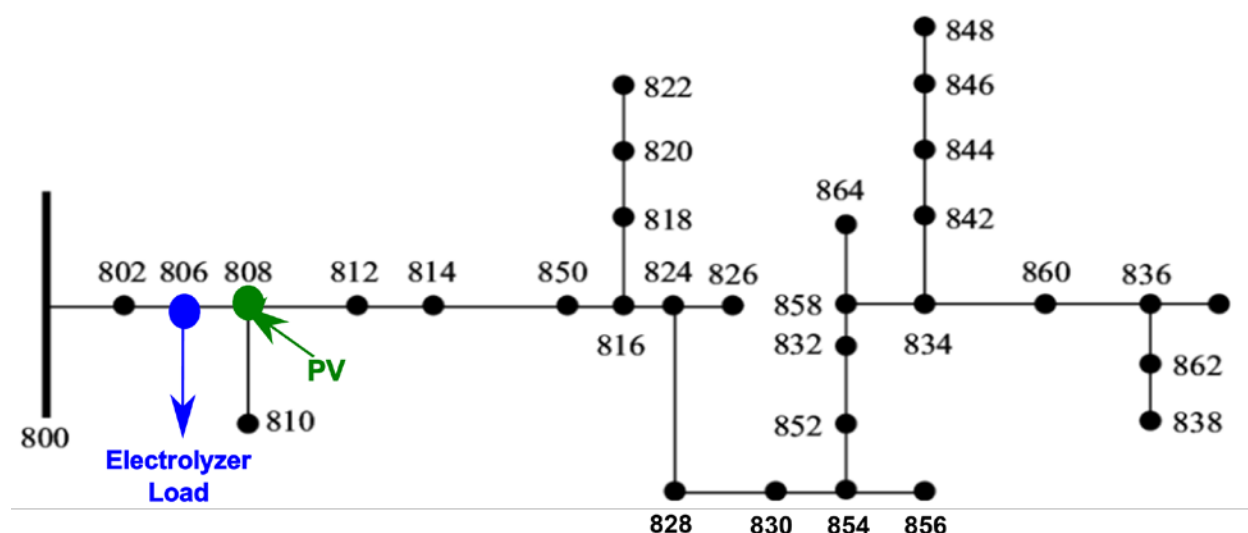


Figure 5. Test system for 20% penetration of PV and electrolyzers

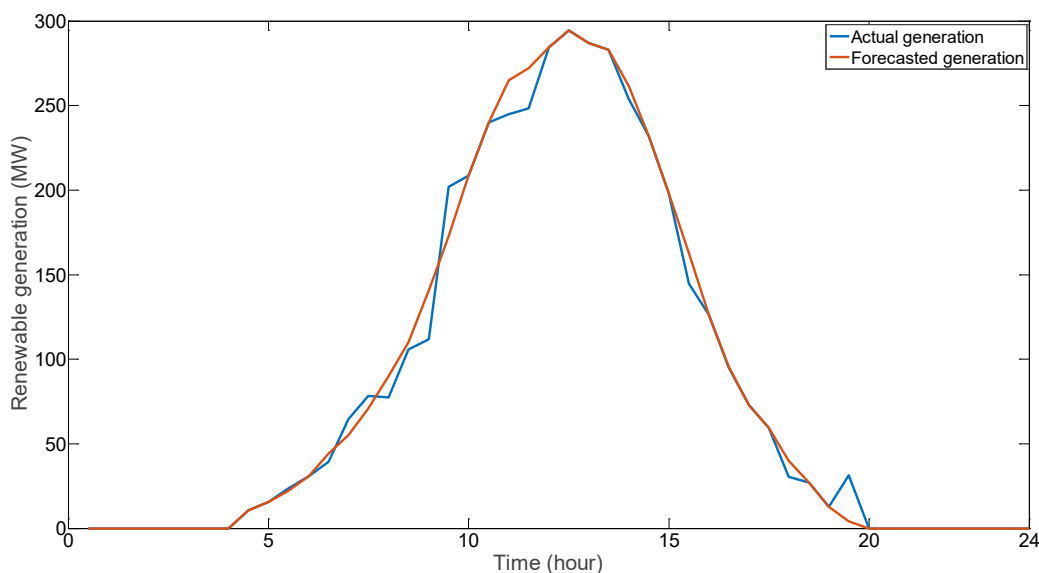


Figure 6. Actual amount versus forecast amount of renewable generation (PV) for a given day

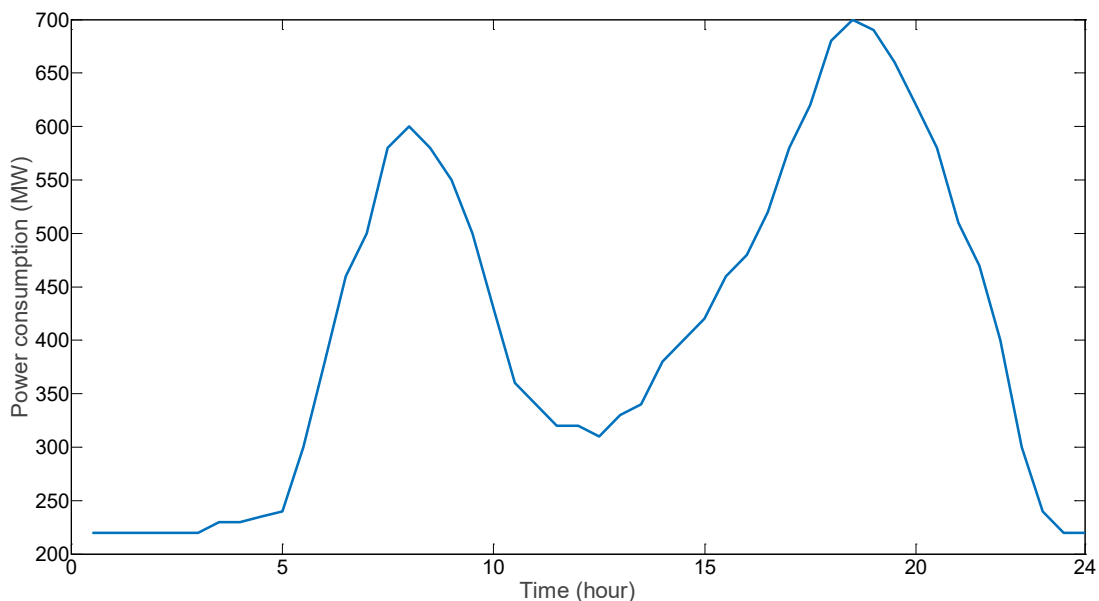


Figure 7. Load profile in test case of 20% renewable penetration

Observations for the 20% PV penetration case: Power consumed by electrolyzers can be leveraged as a balancing tool. As shown in Figure 8, the blue curve is the actual renewable generation for the 20% renewable penetration case. As the energy consumption of electrolyzers can be adjusted by FEC to the amount shown in the shadowed area, then the renewable generation injected to the grid will be shaped as the green curve, which is relatively flat. A flatter renewable energy generation is much easier to control and even dispatch for certain grid applications. The total hydrogen produced by the electrolyzer is directly a function of the energy consumed, and the FEC ensures typical hydrogen demand is satisfied. Figure 9 shows the comparison of impact to frequency stability during the transient noted in Figure 8. Without FEC-controlled electrolyzers, frequency can deviate up to 0.28 Hz. When electrolyzers are driven by FEC to offset the impact of excessive renewable generation, frequency deviation can be limited to within 0.006 Hz. Such a transient happens four times in this daily PV profile and is compensated for by the FEC-controlled electrolyzers.

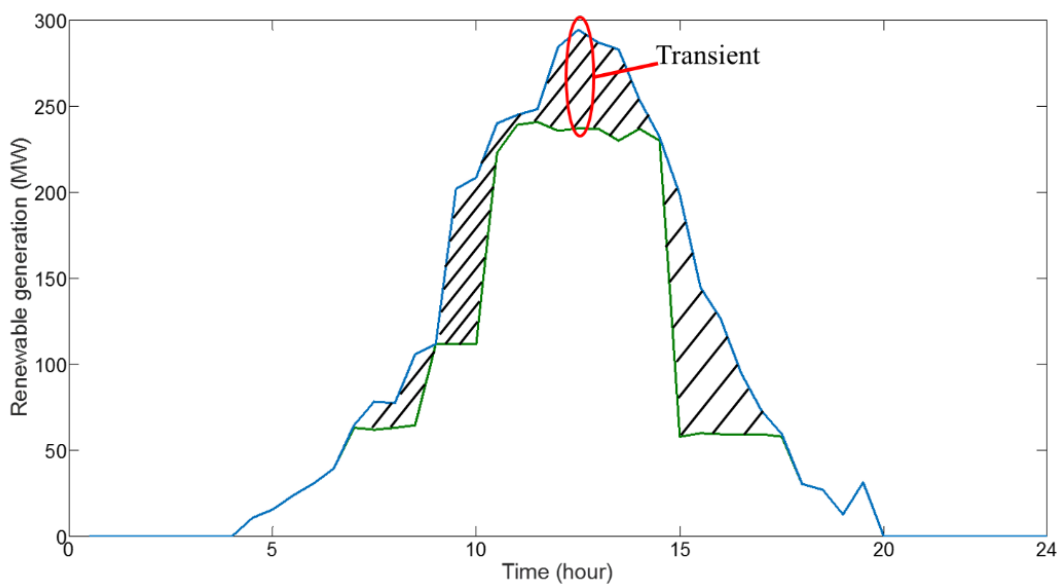


Figure 8. FEC-controlled electrolyzers modify the profile of renewable generation (20% renewable energy penetration)

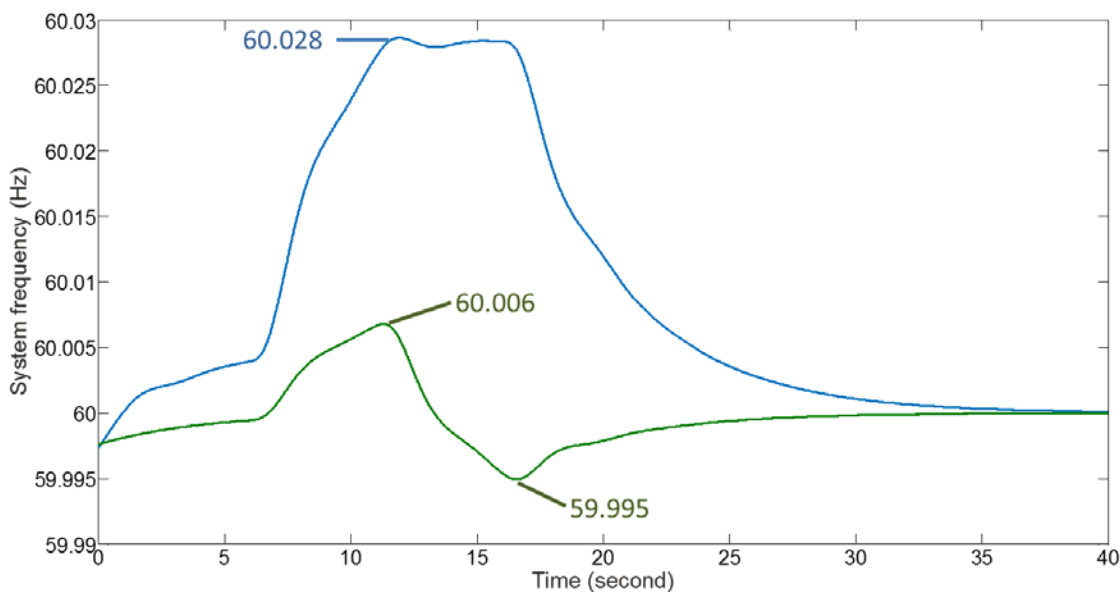


Figure 9. Comparison of system stability during transient with/without FEC-controlled electrolyzer (20% renewable energy penetration)

CONCLUSIONS AND UPCOMING ACTIVITIES

The capability of an electrolyzer as a controllable load and provider of grid services was demonstrated to be significant and was experimentally verified in a real-time environment. A special focus on the real-time simulations, inter-lab connectivity, HIL, and advanced grid modeling was used to assess the potential of H2@Scale infrastructure to provide energy storage for renewable energy.

The controllability of an electrolyzer was enabled by a vendor-neutral approach—the FEC. The FEC ensures an optimal response of the electrolyzer to provide essential grid support in the form of voltage and frequency support. An FEC is a set of generic controls that can be integrated with existing controllers of electrolyzers that are available in the market. The objective of developing FECs is to demonstrate the immense flexibility that electrolyzers can add to the power grid operations as well as to lower hydrogen costs. An FEC from a past-funded activity was leveraged to add a renewable energy module to enable the prediction and control of electrolyzers considering the physical constraints of electrolysis. The FEC tries to minimize the cost of production of hydrogen by participating in grid services and providing storage for the assimilation of renewable energy.

Integrated FEC configurations were tested in both large centralized electrolyzer plants and smaller distributed ones. Another combination of distributed and concentrated renewable energy was also explored. The 250-kW stack at NREL was used as the building block to extrapolate and assess the potential of H2@Scale to provide storage. Both configurations performed and provided essential flexibility and energy storage to the grid under dynamic renewable energy conditions. Additionally, the FEC can drive the hydrogen production cost lower by considering different utility rate structures, participating in demand response programs, and interfacing with market signals. Hardware-based testing in real time was used to infer and augment the understanding of the role electrolyzers can play in markets for additional revenue. The FEC is now implemented on a hardware controller card and its functionality testing with the electrolyzer stack (250 kW) is also completed.

Topic 1A. Experimental and Core Capability Related to H2@Scale

A vendor technical data sheet for the programmable high-power source purchased for installation in the INL Systems Integration Lab was developed. The power converter was purchased from AMETEK Programmable Power, California Instruments RS Series. This power conversion unit can connect the INL Digital Real-Time

Power and Energy Lab to a high-temperature steam electrolysis pilot plant ranging up to 250 kWe DC input. This enables INL to repeat the dynamic response testing performed using the NREL low-temperature electrolyzer. This activity was limited to specification of requirements, procurement, and delivery to INL. Testing will be completed in FY 2019 and the results will be compared to the low-temperature electrolyzer results measured in FY 2017 and FY 2018.

Fuel Cell Hybrid Electric Delivery Van

Jason Hanlin
Center for Transportation and the Environment
730 Peachtree Street, Suite 760
Atlanta, GA 30308
Phone: (404) 808-6489
Email: Jason@cte.tv

DOE Manager: Peter Devlin
Phone: (202) 586-4905
Email: Peter.Devlin@ee.doe.gov

Contract Number: DE-EE0006523/0004

Subcontractors:

- Hydrogenics USA, San Diego, CA
- United Parcel Service, Sandy Springs, GA
- Unique Electric Solutions, Stony Brook, NY
- The University of Texas at Austin—Center for Electromechanics, Austin, TX
- Lithium Werks, Austin, TX

Project Start Date: July 15, 2014

Project End Date: November 30, 2020

Overall Objectives

- Increase the zero-emission driving range and commercial viability of medium-duty electric drive trucks.
- Phase 1—Develop a fuel cell hybrid electric delivery van and validate its design and construction through in-service operation.
- Phase 2—Build the Phase 1 delivery van at pre-commercial volume (up to 15 additional vehicles) and perform at least 5,000 operation hours of in-service demonstration.
- Develop an economic/market opportunity assessment for medium-duty fuel cell hybrid electric trucks.

Fiscal Year (FY) 2018 Objectives

- Complete major component and final system integration into the base electric vehicle.
- Test and validate the vehicle according to DOE contractual specifications.

- Complete pre-deployment training and education at the demonstration site in West Sacramento.
- Begin demonstration of vehicle by deploying it into United Parcel Service (UPS) fleet service.

Technical Barriers

This project addresses the following technical barriers from the sections of the Fuel Cell Technologies Office Multi-Year Research, Development, and Demonstration Plan listed below.¹

Technology Validation

(A) Lack of Fuel Cell Electric Vehicle and Fuel Cell Bus Performance and Durability Data

Market Transformation

(D) Market uncertainty around the need for hydrogen infrastructure versus timeframe and volume of commercial fuel cell applications

(F) Inadequate user experience for many hydrogen and fuel cell applications

Contribution to Achievement of DOE Market Transformation Milestones

This project directly addresses Market Transformation subprogram targets. It provides a pathway for the introduction of fuel cell technologies into the medium-duty vehicle market. The project has a technology validation phase and a follow-on deployment of a pre-commercial volume of the vehicles in parcel delivery service. The project is built upon the initial structure that DOE prescribed in the Funding Opportunity Announcement and is augmented by the active participation and guidance of a major commercial fleet operator, UPS. UPS operates 46,000 medium-duty vehicles worldwide. Further, the vehicles will be deployed in California to take advantage of that state's focused growth of fueling infrastructure and desire to deploy zero-emission vehicles. The Center for Transportation and the Environment

¹ <https://www.energy.gov/eere/fuelcells/downloads/fuel-cell-technologies-office-multi-year-research-development-and-22>

(CTE) has coordinated with station providers early in the project to identify and overcome fueling station barriers for this emerging application of fuel cell technologies, such as the limitation of J2601 fueling protocol described below. This project further leverages the resources and support of the State of California.

The project team has also focused on upfront design to ensure that selection the fuel cell size will take advantage of volume growth from other applications and markets, and that the design will meet the needs of our commercial fleet operator by matching the performance of incumbent technologies, while meeting the range requirements for more than 97% of delivery van duty cycles.

FY 2018 Accomplishments

- Completed the vehicle build. All systems were integrated and the first iteration of the vehicle control software was implemented.
- Conducted stationary testing of the fuel cell power system.
- Began driving tests to validate vehicle performance parameters prior to delivery to fleet operator.
- Began detailed vehicle demonstration preparation tasks, such as coordinating hydrogen fueling tests, drafting a fueling agreement between UPS and the fuel provider, and developing a training matrix for all necessary deployment training.
- Received a preliminary funding award from California Air Resources Board (CARB) for all remaining funds required to deploy the 15 additional vehicles in Phase 2.

INTRODUCTION

Parcel delivery van fleets currently are dominated by diesel- and compressed natural gas-powered Class 3–6 trucks. In recent years, some parcel delivery services have integrated battery-electric trucks into their fleets; however, these battery-electric vehicles have been unable to match the performance of existing delivery vans, and their limited range significantly impacts deployment strategy. The intent of this project is to develop a hydrogen fuel cell hybrid electric van that provides fleet operators with a zero-emission vehicle capable of meeting route range requirements while matching the performance characteristics of existing fleet vehicles. According to Fleet DNA project data compiled by the National Renewable Energy Laboratory (NREL), a vehicle with a 125-mile range will meet 97% of Class 3–6 daily delivery driving distances [1]. Meeting this 125-mile range threshold will increase the attractiveness of zero-emission trucks to fleet operators and increase their commercial viability.

APPROACH

This project aims to develop and demonstrate a hydrogen fuel cell hybrid electric van with a 125-mile operational range and validate the vehicle through in-service deployment in a California UPS fleet. This project has two phases:

1. Develop a fuel cell hybrid electric delivery van and validate its design and construction through in-service operation.
2. Build the Phase 1 delivery van at pre-commercial volume (up to 15 additional vehicles) and perform at least 5,000 operation hours of in-service demonstration.

During Phase 1, real-world delivery van route data is collected to define the expected duty-cycle requirements. All potential fuel cell hybrid electric van powertrain configurations then are modeled and simulated on the duty cycles to assess vehicle performance and aid final design. Trade studies (including cost and projected costs at high volumes) are accomplished and vehicle components then are down-selected and the physical layout is completed. The first delivery van then can be built and validated through in-service operation. If the delivery van meets Phase 1 performance requirements, then the project team will build and deploy up to 15 additional vans in Phase 2. All of the vans will be demonstrated in California. Vehicle performance data during the demonstration periods will be collected and provided to NREL's National Fuel Cell Technology Evaluation Center for analysis.

The project team benefits from having members with extensive hydrogen fuel cell experience, including the University of Texas at Austin—Center for Electromechanics (UT-CEM), Hydrogenics, and one of the largest medium-duty truck fleet operations in the world, UPS. UPS has deployment experience with delivery vans powered by various fuels, including gasoline, diesel, compressed natural gas, and battery-electric. This experience gives them a unique perspective on the commercial viability of alternative fueled vehicles and their project contributions are invaluable. Project funding is provided by DOE, the California Energy Commission, and the South Coast Air Quality Management District. UPS is providing cost-sharing during the demonstration periods by supplying operation, maintenance, and fueling costs.

RESULTS

During FY 2018, the project team completed the vehicle design, received the last remaining long lead-time components, completed component integration and vehicle build, began vehicle acceptance testing, and made preparations for Phase 1 vehicle deployment. The project team also submitted and was preliminarily awarded all remaining funds required to deploy the 15 additional vehicles in Phase 2 under the CARB Zero- and Near Zero-Emission Freight and Facilities (ZANZEFF) program.

The battery pack was assembled, balanced, tested, and integrated with the power electronics hardware and motor required for the base electric drive van assembly and commissioning. The switched reluctance traction motor was tested, and a new motor cradle was designed, fabricated, and installed to dampen the motor

vibration and noise identified during testing. The fuel cell power system components were validated and integrated. Figure 1 shows the project team monitoring the fuel cell power system during stationary testing.



Figure 1. Hydrogenics, Unique Electric Solutions, and UT-CEM monitoring the fuel cell power system during bench tests

Some issues arose during component and acceptance testing, but the project team worked cooperatively to resolve them in a timely manner, and design improvements were implemented to prevent the issues from recurring. As a result of project risk analysis, the team keeps spare equipment on hand in case a DC-to-DC converter or fuel cell pump blower fails during the Phase 1 demonstration period. Figure 2 shows the vehicle undergoing preliminary driving tests, and vehicle acceptance testing will continue into FY 2019.



Figure 2. Unique Electric Solutions and UT-CEM conducting drive test of vehicle

The project team is preparing for the upcoming Phase 1 demonstration period that includes fueling tests, training, and data-collection procedures. Fueling agreements have been drafted, and there is a plan in place for an initial fueling test when the vehicle arrives in West Sacramento. All upcoming training activity has been documented in a responsibility matrix and assigned to project team members. A data-collection procedure is in place and is overseen by NREL.

CONCLUSIONS AND UPCOMING ACTIVITIES

The Fuel Cell Hybrid Electric Delivery Van project is utilizing team member experience with hydrogen fuel cell technologies, alternate fuel vehicle fleet familiarity, and stakeholder feedback to develop commercially viable zero-emission medium-duty trucks. The team has:

- Finished building the Phase 1 vehicle
- Completed stationary subsystem and vehicle-level testing
- Begun driving tests to validate contract parameters
- Developed a strategy to ease UPS fleet acceptance and fueling procedures.

Future work includes:

- Complete vehicle acceptance testing
- Deliver vehicle to West Sacramento, where UPS will operate the vehicle
- Train UPS operations and maintenance personnel and local first responders
- Operate the vehicle for 6 months in parcel delivery service
- Update the vehicle design based on lessons learned from 6-month demonstration
- Execute a contract with CARB for the remaining funds required to build and demonstrate 15 additional Phase 2 vehicles
- Build 15 additional fuel cell hybrid electric delivery vans
- Coordinate hydrogen fueling availability at other deployment sites
- Deploy and support additional vans as they are deployed in UPS California fleets
- Collect and evaluate operating data during deployment
- Develop an economic/market opportunity assessment for the vehicles.

FY 2018 PUBLICATIONS/PRESENTATIONS

1. Maria Gallucci. “UPS to Deploy Fuel Cell/Battery Hybrids as Zero-Emission Delivery Trucks.” *IEEE Spectrum: Technology, Engineering, and Science News*. August 24, 2018. <https://spectrum.ieee.org/green-tech/fuel-cells/ups-to-deploy-fuel-cellbattery-hybrids-as-zeroemission-delivery-trucks> (accessed November 19, 2018).
2. J. Hanlin. Fuel Cell Hybrid Electric Delivery Van Project (2018).

REFERENCES

1. K. Walkowicz, K. Kelly, A. Duran, and E. Burton. *Fleet DNA Project Data*. National Renewable Energy Laboratory (2014). <http://www.nrel.gov/fleetdna> (accessed February 25, 2019).

Innovative Advanced Hydrogen Mobile Fueler

Sara Odom (Primary Contact), Spencer Quong
Electricore, Inc.
27943 Smyth Drive, Suite 108
Valencia, CA 91355
Phone: (661) 607-0260
Email: sara@electricore.org

DOE Manager: Jason Marcinkoski
Phone: (202) 586-7466
Email: Jason.Marcinkoski@ee.doe.gov

Contract Number: DE-EE0007275

Subcontractors:

- Air Liquide, Houston, TX
- Hydrogen Technology & Energy Corporation, Vancouver, BC, Canada
- Quong & Associates, Inc., San Francisco, CA
- Manta Consulting, Carmel, CA

Project Start Date: July 1, 2016

Project End Date: December 31, 2020

Overall Objectives

- Design and build an advanced hydrogen mobile fueler (AHMF).
- Deploy the AHMF to support a network of hydrogen stations and vehicles in the United States.
- Gather and analyze fueling data for the National Renewable Energy Laboratory (NREL) technology validation team.

Fiscal Year (FY) 2018 Objectives

- Procure key components and long-lead items for the AHMF.
- Complete the procurement of components, build subsystems, and begin assembly of the AHMF.

Technical Barriers

This project addresses the following technical barriers from the Technology Validation section of the Fuel Cell Technologies Office Multi-Year Research, Development, and Demonstration Plan¹:

(C) Hydrogen Storage

(D) Lack of Hydrogen Refueling Infrastructure Performance and Availability Data

(E) Codes and Standards.

Contribution to Achievement of DOE Technology Acceleration Milestones

This project will contribute to achievement of the following DOE milestones from the Technology Validation, Hydrogen Delivery, and Hydrogen Safety, Codes and Standards sections of the Fuel Cell Technologies Office Multi-Year Research, Development, and Demonstration Plan.

Technology Validation

- Milestone 2.3: Validate fuel cell electric vehicles achieving 5,000-hour durability (service life of vehicle) and a driving range of 300 miles between fuelings.
- Milestone 3.4: Validate station compression technology provided by delivery team.
- Milestone 3.8: Validate reduction of cost of transporting hydrogen from central production to refueling sites to <\$0.90/gallon gas equivalent.

Hydrogen Delivery

- Milestone 2.1 and 6.2: By 2015, reduce the cost of hydrogen delivery from the point of production to the point of use for emerging regional consumer and fleet vehicle markets to <\$4/gallon gas equivalent.
- Milestone 2.4 and 6.3: By 2020, reduce the cost of hydrogen delivery from the point of production to the point of use in consumer vehicles to <\$2/gallon gas equivalent.

Hydrogen Safety, Codes and Standards

- Milestone 2.19: Validate inherently safe design for hydrogen fueling infrastructure.

¹ <https://www.energy.gov/eere/fuelcells/downloads/fuel-cell-technologies-office-multi-year-research-development-and-22>

- Milestone 3.4: Develop hydrogen material qualification guidelines, including composite materials.

FY 2018 Accomplishments

- Completed design specifications and parameters for the AHMF and its components. The final design reflects target specifications identified for storage, fueling, performance, and usage.
- Purchased and received major components and subsystems for the AHMF including the 45-ft custom trailer, diesel generator, heat exchanger, dispenser, and compressor.
- Created detailed manufacturing and testing plans for AHMF.
- Received special permit approval from the U.S. Department of Transportation for 95-MPa transport high-pressure storage.

INTRODUCTION

This project will design, develop, deploy, and analyze the economic viability of a mobile fueling system for hydrogen. The project team proposed use of the AHMF to support a network of stations in the United States. As part of the design activity, the project team was to define, in collaboration with an automaker, the preferred network of stations. The team has selected a northeast United States network, specifically that resulting from a collaboration between Air Liquide and Toyota. The automaker(s) will support the project by providing specifications based upon vehicle requirements and support the evaluation of the AHMF with respect to compliance with specific fueling performance criteria. The AHMF will have the capacity to fuel 10–20 fuel cell vehicles per day, consistent with the requirements of the H70 fueling category. The AHMF will operate without remote power connections, be modular for easy transport and deployment, and have the ability to provide expanded daily capacity and multiday operations through the use of delivered gaseous hydrogen.

APPROACH

The project comprises two primary phases, each consisting of several key tasks and milestones.

The first phase will involve the design, development, and construction of the AHMF, moving from the conceptual design through to completion of assembly and testing so the AHMF is ready to deploy. The first phase will contain two key decision points—the final design review and construction and testing of the AHMF.

The second phase will demonstrate the AHMF over 18 months at multiple site locations and gather key data in collaboration with participating automotive companies. Fueling data will be provided to NREL quarterly for review and analysis; economic data will be included in the project's final report.

RESULTS

The AHMF project has completed the design stage and is currently in construction at the Hydrogen Technology & Energy Corporation's (HTEC's) Vancouver manufacturing facility. The team solicited input from selected automotive companies (potential users of the AHMF) and DOE to determine crucial design specifications and parameters for the AHMF and its components. The team decided to use Air Liquide's C100 station as the base design for this project. The design utilizes several components from the C100, with appropriate modifications to accommodate the AHMF specifications and mobile approach. The AHMF will be a self-contained, full-performance, mobile hydrogen station.

Based upon the final design, the team continues to procure necessary components and equipment for construction including:

- Custom 45-ft dual axle trailer
- Diesel generator
- HTEC Powercubes (2)
- Compressor
- Liquid nitrogen Blueeze system
- Liquid nitrogen cooling system components
- Heat exchanger
- Hydrogen flow meter
- Nozzle assembly

- Dispenser and point-of-sale hardware.

Air Liquide and a vendor (Hexagon Lincoln) have completed all of the required testing and received approval for the U.S. Department of Transportation Special Permit for 95-MPa transport. The tanks have already been manufactured and set aside for this project. The team has done preliminary work on the frame and fire protection for the high-pressure storage and is ready to issue the purchase order.

The team has been in discussions with automotive companies about possible site locations of the AHMF demonstration, but decisions are delayed until plans for the introduction of the fuel cell vehicles in the northeast United States are finalized.

Table 1. AHMF Specifications

Specification	Description
Pressure Class	H70 (70 MPa) after compressing high bank storage
Precooling	T30 (-30 °C) or T40 (-40 °C)
Performance	Up to 15 kg per hour, 100–120 kg in 8–10 hours
Fueling Protocol	SAE J2601-2014 table based for 2–7 kg tanks SAE J2799-2014
Setup	1 hour for limited performance, 8 hours for full performance
Storage	Up to 170 kg hydrogen at 45 MPa with ability to connect to external storage
Power	Onboard 480-V AC, low-noise, low-emissions diesel generator with option of using external power
Usage	Dispenser human-machine interface allows fueling by minimally trained users

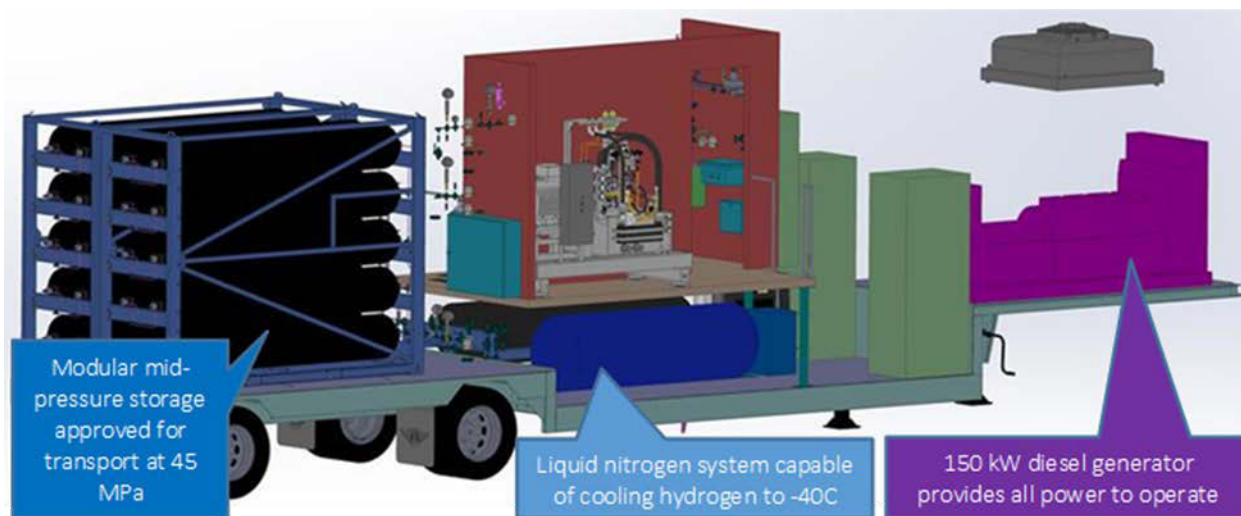


Figure 1. AHMF—passenger’s side view without trailer walls

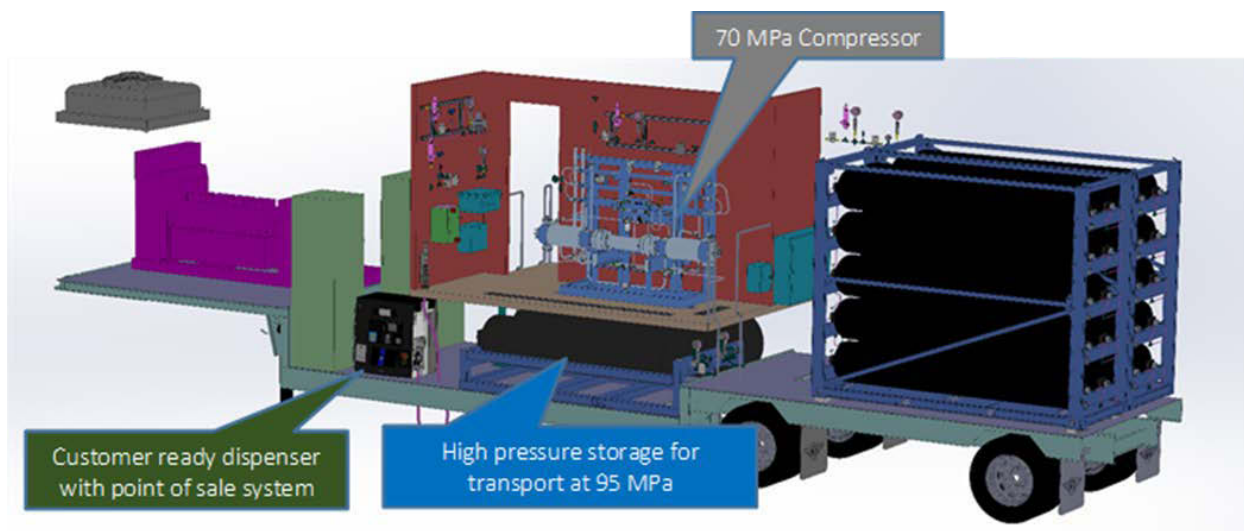


Figure 2. AHMF—driver's side view without trailer walls

CONCLUSIONS AND UPCOMING ACTIVITIES

The team is currently preparing for subsystem assembly and integration into the AHMF. Planned activities include assembly, testing of subsystems and full system, and site selection.

FY 2018 PUBLICATIONS/PRESENTATIONS

1. Sara Odom, "Innovative Advanced Hydrogen Mobile Fueler," Presentation at the 2018 DOE Hydrogen and Fuel Cells Program Annual Merit Review and Peer Evaluation Meeting, Washington, D.C., June 2018.

High-Temperature Electrolysis Test Stand

James O'Brien (Primary Contact),
Richard Boardman
Idaho National Laboratory (INL)
MS 3870
2525 Fremont Ave.
Idaho Falls, ID 83415
Phone: (208) 526-9096
Email: james.obrien@inl.gov

DOE Manager: Jason Marcinkoski
Phone: (202) 586-7466
Email: jason.marcinkoski@ee.doe.gov

Subcontractor:
L&L Mechanical, Inc., Blackfoot, ID

Project Start Date: August 1, 2016
Project End Date: Project continuation and
direction determined annually by DOE

Overall Objectives

- Deploy a 25-kW high-temperature electrolysis (HTE) flexible test facility at the Idaho National Laboratory (INL) Energy Systems Laboratory.
- Integrate the HTE system with colocated thermal energy systems, including a high-temperature, high-pressure water flow loop and a thermal energy storage system.
- Integrate the HTE test station with colocated digital real-time simulators for dynamic performance evaluation and hardware-in-the-loop simulations.
- Perform HTE stack testing using hardware obtained from industry partners; focus on flexible intermittent and reversible operation and the effects of flexible operation on long-term performance.
- Work with HTE industry partners to demonstrate performance of flexible intermittent operation of large HTE systems.

Fiscal Year (FY) 2018 Objectives

- Complete installation of 25-kW HTE system including:

- Mechanical and electrical utilities/infrastructure to support operation of the 25-kW HTE flexible test station
- Installation of experiment components within a Perma-Con enclosure; electrical hookups and process piping
- Installation of system instrumentation: mass flow controllers, pressure transducers, thermocouples, etc.
- Prepare and submit experiment laboratory instruction to review committee for approval of research operations and activities.
- Complete configuration and Labview programming of data acquisition/instrument control system.
- Conduct stand-alone testing of components to verify expected performance.
- Conduct system checkout and shakedown testing.

Technical Barriers

This project addresses the following technical barriers from the Technology Validation section of the Fuel Cell Technologies Office Multi-Year Research, Development, and Demonstration Plan¹:

(G) Hydrogen from Renewable Resources

(H) Hydrogen and Electricity Co-Production.

Contribution to Achievement of DOE Technology Validation Milestones

This project will contribute to achievement of the following DOE milestones from the Technology Validation section of the Fuel Cell Technologies Office Multi-Year Research, Development, and Demonstration Plan:

- Milestone 3.5: Validate distributed production of hydrogen from renewable liquids at a projected cost of \$5.00/gasoline gallon equivalent and from electrolysis at a projected

¹ <https://www.energy.gov/eere/fuelcells/downloads/fuel-cell-technologies-office-multi-year-research-development-and-22>

cost of \$3.70 with an added delivery cost of <\$4/gasoline gallon equivalent. (4Q, 2018)

- Milestone 3.9: Validate large-scale system for grid energy storage that integrates renewable hydrogen generation and storage with fuel cell power generation by operating for more than 10,000 hours with a round-trip efficiency of 40%. (4Q, 2020)

FY 2018 Accomplishments

- Completed installation/assembly of laboratory mechanical and electrical utilities/infrastructure.
- Completed welding of high-temperature SS 310 pipe fittings.
- Completed installation of experiment components and support systems within the Permacon enclosure, including electrical power and process piping.
- Submitted laboratory instruction governing HTE research activities and operations for approval.
- Completed installation of system instrumentation and development of the Labview data acquisition/system controller program.
- Completed development of Labview-based data acquisition and instrument control system.
- Completed testing of all major components.
- Demonstrated hydrogen recycle operations.

INTRODUCTION

High-temperature electrolysis of steam for hydrogen production is an advanced water-splitting technology that exhibits high electric-to-hydrogen efficiency, especially when coupled to an integrated high-temperature process heat source. INL developed a world-class HTE laboratory and test capability under the DOE Office of Nuclear Energy Nuclear Hydrogen Initiative during the 2002–2012 time period. The focus of the current project is to establish a new HTE research and demonstration facility at INL to enhance the existing INL core capability in HTE and to support systems integration, systems operation, HTE model validation, and technical performance characterization of advanced hydrogen production by high-temperature water splitting. The initial thrust of this project is the development of a 25-kW flexible test station to support integrated operation of state-of-the-art HTE stack technologies from multiple industry partners. Establishment of the 25-kW HTE system will be followed by deployment of a test skid with infrastructure support for up to 250-kW HTE turnkey systems.

The new HTE test capability will be designed for integrated operation with the INL Power Systems Test Bed (comprising real-time digital/real-time simulation units and a renewable-power microgrid) and the forthcoming Dynamic Energy Transport and Integration Laboratory (DETAIL). The HTE system will be colocated with a high-temperature high-pressure pressurized water reactor flow loop, which will be thermally integrated with the HTE system via a Thermal Energy Distribution System (TEDS) that is currently in the final detailed engineering design phase, with funding from the DOE Office of Nuclear Energy, under the Nuclear-Renewable Hybrid Energy Systems initiative. TEDS will have its own high-temperature (up to 340°C) heater to support independent operation as a heat source. It will also include a large (200-kWh) thermal energy storage system based on a packed-bed thermocline tank with a solid alumina particulate sensible heat storage medium. System integration will enable assessment and characterization of dynamic HTE operation to simulate load-leveling capability with intermittent power from renewables and a fluctuating demand profile. This project leverages emerging and demonstrated high-temperature water splitting by HTE and high-temperature solid oxide cell technology, which may include reversible HTE/solid oxide fuel cell operation.

APPROACH

The new HTE Technology Validation capability under development at INL will include a 25-kW flexible HTE test station as well as infrastructure support for up to 250-kW HTE turnkey systems. At the 25-kW scale, this approach will enable thermal integration with colocated thermal energy sources as well as integrated operation with the INL Power Systems Test Bed. The 25-kW system will be flexible, allowing HTE operation from the 5-kW to the 25-kW scale, with support for intermittent and reversible operation. INL will work with various industrial partners to supply the HTE stacks and to design the test matrices. The 250-kW infrastructure installation will support demonstration and testing of industry-supplied pilot-scale turnkey systems with grid integration and variable operation.

The flexible HTE test station has been designed to support HTE operations in the 5- to 25-kW range. At the 25-kW scale, the hydrogen production rate will be approximately 135 standard liters per minute or 12.1 g/min. For a typical solid oxide electrolysis cell active area and current density of 144 cm² and 0.67 A/cm², respectively, and four stacks, the current and voltage will be 96.5 A and 65 V per stack. The test station includes four DC power supplies, each rated at 100 V and 100 A to supply electrolysis power to the stacks. The HTE system was assembled on a skid with all the hydrogen components positioned inside of a ventilated enclosure with an active gas monitoring system that is interlocked to the hydrogen production process for safety.

RESULTS

Assembly of the 25-kW HTE system has been completed. An overview photograph of the installation is provided in Figure 1. Major system components include a large top-hat furnace, steam generator/superheater, air compressor, chiller, hydrogen compressor, air-cooled hydrogen outlet finned tube array, water-cooled condensers, a hydrogen storage tank, plus associated instrumentation including mass flow controllers, pressure

transducers, and thermocouples. The ventilation exhaust duct from the experiment enclosure is visible in the top of Figure 1. A blower that is mounted outside of the building draws air from the surrounding high bay laboratory through the experiment enclosure and through the exhaust duct to the outside blower. The hydrogen vent line can also be seen in the top of Figure 1.



Figure 1. Overview of the 25-kW HTE experiment skid and enclosure within the INL System Integration Laboratory

The steam generator is an inductively heated unit that delivers high-temperature superheated steam (up to 900°C) directly from an inlet flow of room-temperature liquid deionized water. The HTE system will also include a heat exchanger option (Phase II) for process-heat-based steam generation when the DETAIL thermal network is complete. The furnace that will house the HTE stacks has a movable top hat that lifts up to expose the hot zone for installation of test articles. The electrolysis stacks will be positioned within the hot zone for testing at 800°C. The steam generator and furnace are shown installed inside the experiment enclosure in Figure 2. The inlet flow to the electrolysis stacks will include steam plus hydrogen. Hydrogen must be included on the inlet side in order to maintain reducing conditions on the electrolysis cell cathodes. During start-up, hydrogen will be supplied from compressed gas cylinders, but for long-term operation, a fraction of the hydrogen that is produced by steam electrolysis is recycled from the electrolyzer outlet flow back to the inlet after steam is removed by a combination of low-pressure condensation, compression, and high-pressure condensation. Condensation is aided by cooling the condenser units and the counterflow heat exchanger using chilled water at 5°C delivered from a refrigerated chiller. A finned-tube air-cooled natural convection heat exchanger is used for the initial cooling of the outlet hydrogen/steam flow that exits the hot zone at high temperature. The finned-tube array and the chilled-water-cooled condensers are shown in Figure 3. The hydrogen recycle system, including the compressor and hydrogen storage tank, is shown in Figure 4. Nitrogen is included as an inert carrier gas and a purge gas. Air is supplied to the anode side of the HTE stacks as a sweep gas to remove electrolytically produced oxygen from anode side of the stacks. Compressed air is produced by an air compressor, metered by a precision mass flow controller, and preheated to 800°C using a high-temperature in-line gas heater prior to entering the hot zone.



Figure 2. Superheated steam generator and high-temperature furnace in experiment enclosure



Figure 3. Finned-tube steam coolers and water-cooled condensers



Figure 4. Hydrogen recycle compressors system compressor, storage tank, and counterflow heat exchanger

In terms of safety, because this system has been deployed in a large, high-bay laboratory, all hydrogen-related components are positioned inside a ventilated enclosure (12 ft x 14 ft x 10 ft), which includes a gas monitoring system. The enclosure is shown in Figure 1. The gas monitoring system is interlocked to the hydrogen gas supply and the electrolyzer power supplies such that hydrogen gas inlet flows and hydrogen production in the electrolyzer are both terminated in the event of a hydrogen gas alarm. An alarm condition will also initiate the flow of “safe gas” through the cathode side of the stacks. Safe gas is a mixture of nitrogen and hydrogen (3.96% H₂) that will continue to flow through the cathode side of the electrolysis stacks to prevent oxidation damage to the cathodes until normal operations can be resumed or the system is shut down. The ventilation system also includes an airflow switch that will generate an alarm signal in the event of loss of ventilation flow. In addition to the automated interlock features of the gas monitoring system, the system will notify laboratory occupants of the presence of a potentially hazardous buildup of these gases. The system has relay outputs, display readout, visual and audible alarms, and an autodialer.

CONCLUSIONS AND UPCOMING ACTIVITIES

A new 25-kW flexible HTE test station has been installed at INL in the Energy System Laboratory Building, Systems Integration Laboratory. This test station will serve as an experimental platform for the advancement of HTE technology as well as system integration studies. The test station has been designed for stand-alone operation, but it will also be thermally integrated with colocated systems via a thermal energy distribution system, and electrically integrated with a controllable microgrid, allowing for demonstration and characterization of dynamic hybrid energy concepts.

Fully integrated non-electrolysis operational testing of all HTE systems will be completed by the end of November 2018. Initial electrolysis testing at the 5-kW scale will be performed in the February 2019 time frame. A request for proposals has been released to three domestic suppliers of solid-oxide electrolysis stacks for bid. Procurement of stacks for support of 25-kW testing will be pursued, budget permitting, later in FY 2019, with full-scale testing to follow. Thermal integration of the HTE test stand with the high-temperature water loop will be implemented during FY 2020, after the installation and qualification of TEDS. This integration will require procurement of a heat exchanger to support boiling of the liquid water feedstock, plus a separate steam superheater.

FY 2018 PUBLICATIONS/PRESENTATIONS

1. J.E. O'Brien, "A 25-kW High-Temperature Electrolysis Facility for Flexible Operation and System Integration Studies," conference paper in preparation, 2018.

Modular Solid Oxide Electrolysis Cell System for Efficient Hydrogen Production at High Current Density

Hossein Ghezal (Primary Contact), Casey Brown, Stephen Jolly, Micah Casteel, Eric Tang, Tony Wood
FuelCell Energy, Inc.
3 Great Pasture RD
Danbury, CT 06813
Phone: (203)825-6048
Email: hghezal@fce.com

DOE Manager: David Peterson
Phone: (720) 356-1747
Email: David.Peterson@ee.doe.gov

Contract Number: DE-EE0007646

Subcontractor:
Versa Power Systems, Calgary, Alberta, Canada

Project Start Date: October 1, 2016
Project End Date: September 30, 2019

- Complete detailed design of a >4 kg H₂/day SOEC demonstration system with estimated overall efficiency >75%.

Technical Barriers

This project addresses the following technical barriers related to hydrogen generation by water electrolysis from the Hydrogen Production section of the Fuel Cell Technologies Office Multi-Year Research, Development, and Demonstration Plan¹:

- (F) Capital Cost
- (G) System Efficiency and Electricity Cost
- (J) Renewable Electricity Generation Integration.

Contribution to Achievement of DOE Technology Acceleration Milestones

This project will contribute to achievement of the following DOE milestones from the Hydrogen Production—Advanced Electrolysis Technologies section of the Fuel Cell Technologies Office Multi-Year Research, Development, and Demonstration Plan:

- Milestone 2.9: Verify the balance of plant's ability to meet the 2020 system efficiency targets. (Q1, 2018)
- Milestone 2.10: Create modularized designs for optimized central electrolysis systems projected to meet 2020 capital and hydrogen production cost targets. (Q3, 2018)
- Milestone 2.11: Verify the stack and system efficiencies against the 2020 targets. (Q1, 2020)

Overall Objectives

- Demonstrate the potential of solid oxide electrolysis cell (SOEC) systems to produce hydrogen at a cost of less than \$2.00/kg.
- Enhance cell and stack durability to enable dynamic load profiles associated with intermittent renewable integration (>1 A/cm² operation).
- Develop and validate a modular SOEC system that demonstrates proof of concept of both technical and economic objectives.

Fiscal Year (FY) 2018 Objectives

- Complete 1,000-hour test of a single cell demonstrating voltage degradation rate of ≤2%/1,000 h.
- Complete testing of a solid oxide electrolytic stack for ≥1,000 h validating electrical efficiency ≥95% (lower heating value based) at ≥1 A/cm² and degradation rate ≤4%/1,000 h.

¹ <https://www.energy.gov/eere/fuelcells/downloads/fuel-cell-technologies-office-multi-year-research-development-and-22>

FY 2018 Accomplishments

- Demonstrated performance degradation rate of $\leq 2\%/1,000$ h resulting from long-term tests ($\sim 16,000$ h) of a High Power Density (HiPoD) SOEC operating continuously at 1 A/cm^2 .
- Verified performance of a 45-cell Compact SOEC Architecture (CSA) stack with less than $0.4\%/1,000$ h degradation rate over $\sim 4,000$ h of tests under simulated system conditions with electrical efficiency $>95\%$ (based on lower heating value of hydrogen) at $\geq 1 \text{ A/cm}^2$.
- Completed the detailed design of a >4 kg H_2 /day prototype unit to demonstrate the system efficiency metrics ($>90\%$ electric) and to verify the operability of SOEC using intermittent renewables.

INTRODUCTION

The overall objective of the project is to demonstrate the potential of SOEC systems to produce hydrogen at a cost of \$2.00/kg H₂ or less (excluding delivery, compression, storage, and dispensing). An additional objective of the project is to enhance stack endurance and impart subsystem robustness for operation on load profiles compatible with intermittent renewable energy sources. Advanced high-temperature electrolysis systems have the capabilities to vary the composition of energy input between thermal and electrical energy, which offers the possibility of upgrading low-value waste heat into high-value hydrogen. This feature enables SOEC systems with extremely high electricity-to-hydrogen conversion efficiency, which is not feasible by conventional low-temperature electrolysis.

The project work plan, focused on achieving the techno-economic targets, includes research and development in a wide range of disciplines, including cell performance and stability improvements through system design, modeling, optimization, and performance verification. Cell and stack endurance are planned to be improved by reducing cell degradation rates to <1%/1,000 h and stack degradation to <2%/1,000 h. These reduced degradation rates will be achieved at current densities greater than 1 A/cm² to meet capital cost targets. System efficiencies will exceed 95% stack electrical efficiency, 90% system electrical efficiency, and 75% total (electric + thermal) efficiency. This corresponds to less than 37 kWh electricity consumed per kilogram of hydrogen produced, with the remainder of energy supplied thermally. A modular system architecture will reduce system cost, increase scalability, and impart the required flexibility and robustness to operate on dynamic load profiles such as those supplied by intermittent energy sources.

APPROACH

The approach to meeting the objectives of the project consists of both cell and stack technology development as well as system design and verification.

Cell development activities include materials development, single cell testing, and post-test microstructural analysis. In particular, the optimal intersection between system operational parameters, cell performance, and degradation will be thoroughly investigated. This includes the effect of inlet steam concentration and utilization, operating temperature, current density, system pressure, anode flush gas composition, and load cycling effects. Stack development efforts will focus on manufacturability, thermal management, and scale-up. A novel stack architecture will be utilized for electrolysis operation at moderate current density operation (1–2 A/cm²). Stack manufacturing, testing, and validation will seek to demonstrate a 4 kg hydrogen per day production rate at greater than 95% electrical efficiency with less than 2%/1,000 h degradation.

System development and techno-economic analysis will focus on system architecture, operational parameter selection, and tradeoff analyses to determine an optimal system layout and operating regime. Due to the broad range of potential operating conditions, a baseline system will be developed for comparison purposes in the examination of potential system architectures. Quantitative comparative metrics will be developed to determine the relative effects of different operating conditions on the overall system performance, cost, and flexibility. A breadboard demonstration system (>4 kg H₂/day) will be designed, manufactured, and tested to validate the system performance. Finally, techno-economic analyses will be performed throughout the system development process to investigate the cost and performance impact of system operation parameters and layout.

RESULTS

Research work was continued on improving the performance endurance of the SOEC cells. FuelCell Energy's HiPoD cells [1], based on optimized cathode porosity, have shown superior performance at high current densities up to 6 A/cm². A HiPoD cell recently completed nearly two years of continuous operation at 1 A/cm² (17,051 hours) as shown in Figure 1. This cell achieved a degradation rate of 32 mV/1,000 h, following an initial stabilization period of ~1,200 h. Prior to an uncontrolled shutdown of the cell at approximately 16,000 h of operation (due to test stand malfunction), the cell performance degradation was below the target 2%/1,000 h. The project activities were also focused on establishing operating conditions (e.g., steam concentration and

utilization) that may result in higher performance stability and endurance. A recent cell operating on higher steam utilization (50%)—but lower steam concentration (60%)—has shown a significantly lower degradation rate of 9 mV/1,000 h over the last 4,300 h (0.72%/1,000 h) of operation.

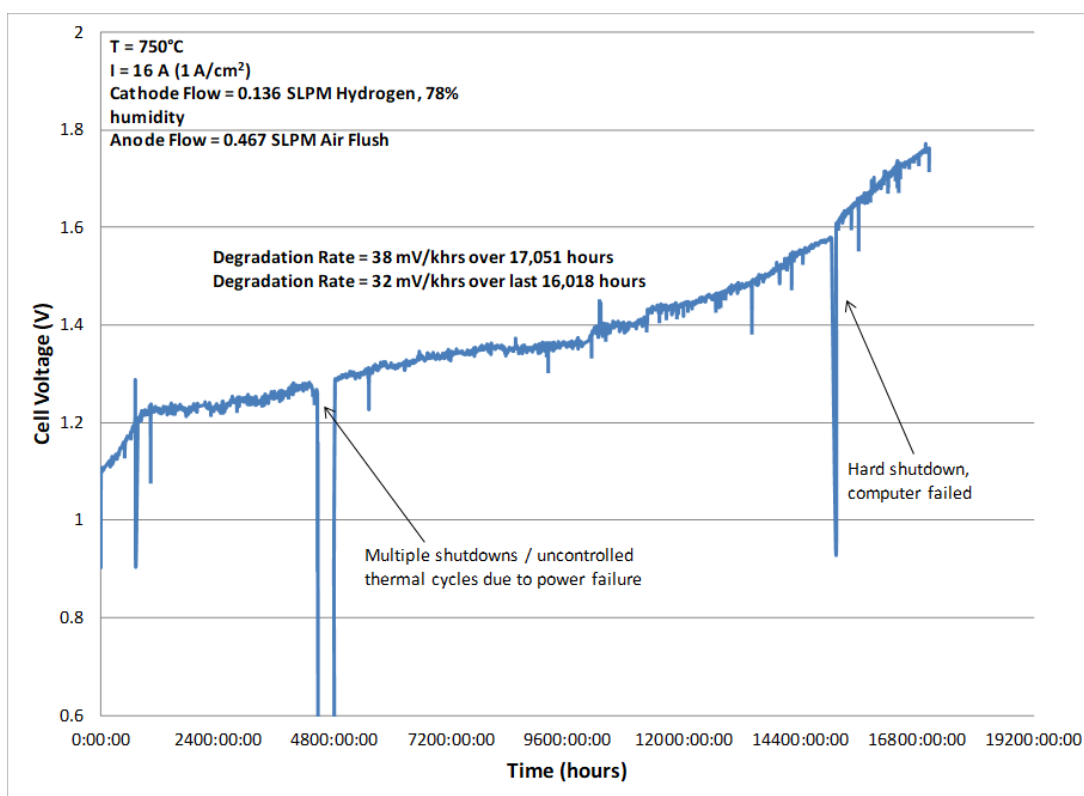


Figure 1. Test of HiPoD cell (5 cm x 5 cm x 0.03 cm) at 1 A/cm² demonstrated voltage degradation rate of less than 2%/1,000 h over ~16,000 h of operation

A 45-cell CSA stack, shown in Figure 2, was built with 300- μ m-thick HiPoD cell technology. This stack ran for nearly 4,800 h on load with efficiency and degradation that exceeded the program targets. During operation, the stack underwent several unintended and uncontrolled thermal cycles. For the first 4,000 h elapsed time of operation, as shown in Figure 3, the stack was operated at 1 A/cm² with an average degradation rate of 4.4 mV or 0.35%/1,000 h. During that period, the stack exhibited a voltaic (dc) efficiency greater than 95% lower heating value of hydrogen. For the final 800 h of operation, the stack was transitioned to the higher current operating point of 1.22 A/cm², thereby increasing the hydrogen production rate to 4 kg/day, meeting another milestone for the project.

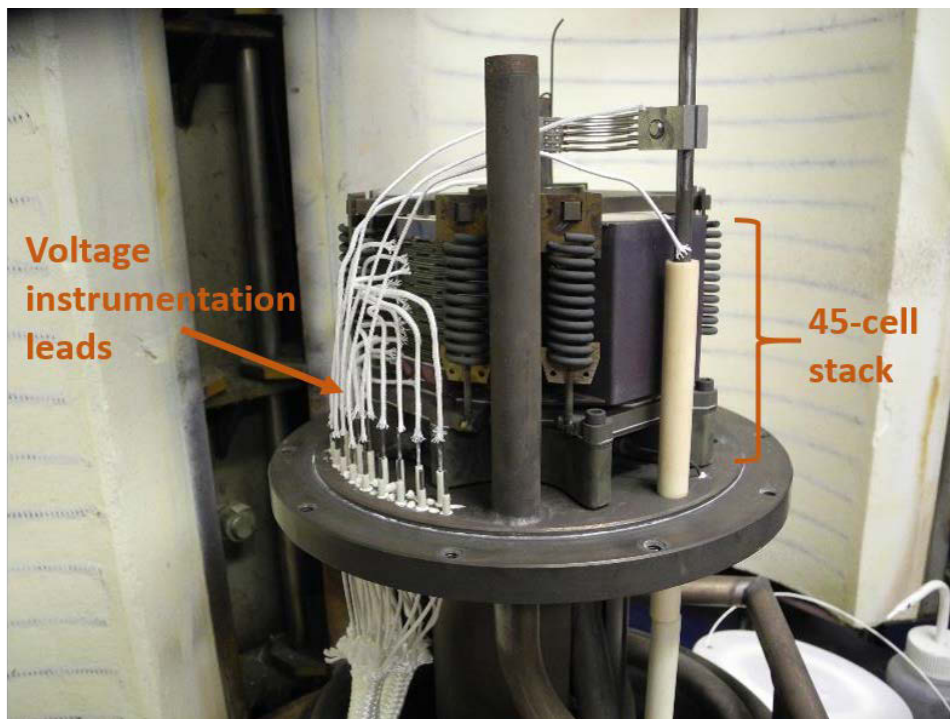


Figure 2. Picture of 45-cell CSA stack fabricated via an automated manufacturing process

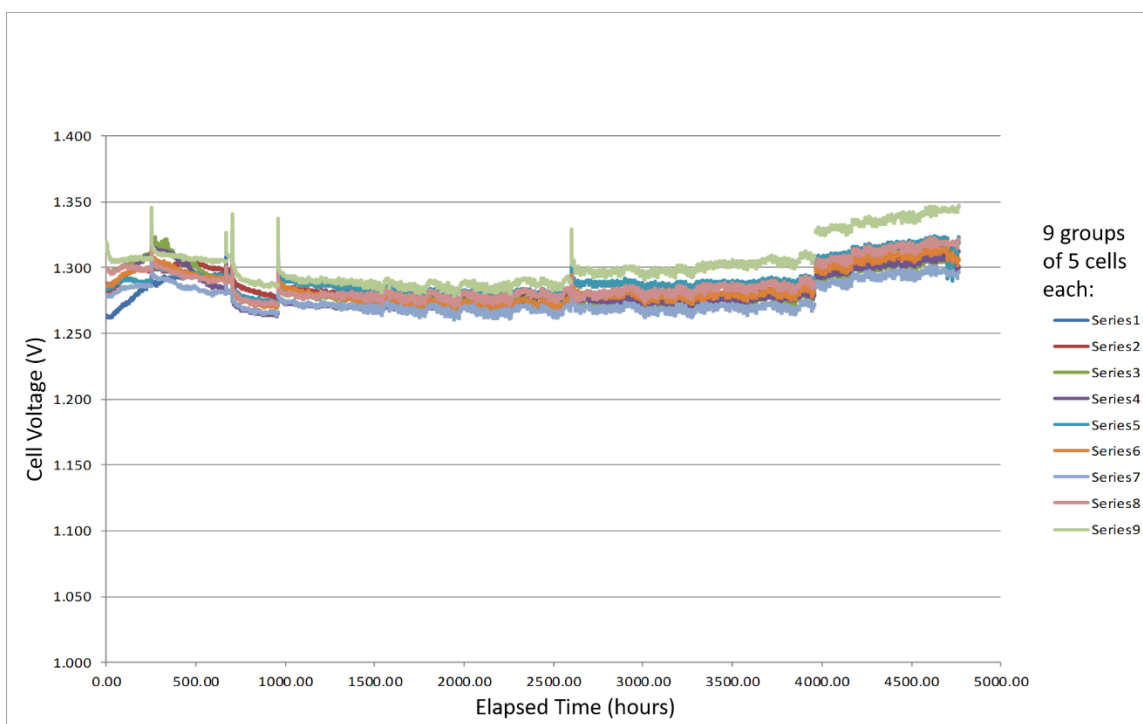


Figure 3. 45-cell CSA stack produced 3.3 kg/day hydrogen at 1 A/cm² and verified performance degradation of less than 2%/1,000 hours for a period of nearly 4,000 h

The detailed design for a >4 kg H₂/day demonstration system was completed. The design includes process models over a range of operating modes, piping and instrumentation diagrams, and 3-D module conceptual models. The process diagrams include the electrolyzer module, heat exchangers, recycle loops, instrumentation, and the control loops for pressure, temperature, and flow. Thermal integration within the demonstration system consists of heat recovery from the electrolyzer effluents (anode and cathode outlet streams) using heat exchangers to maximize the overall efficiency of the system. To simulate the integration of waste heat recovery from low-grade sources, electric heaters are incorporated in the design. The goal of the system demonstration is to show >75 % system efficiency and the ability to operate on intermittent load profiles. The demonstration system is based on an integrated electrolysis stack vessel, which includes balance of plant components that are more efficiently close-coupled with the stack thermal zone within the pressure boundary. Figure 4 shows the 3-D design concept developed for the >4 kg H₂/day demonstrator to be fabricated and tested in the next year of the project.



Figure 4. Rendering of the integrated 4 kg H₂/day pilot demonstration system consisting of a single vessel containing the SOEC module and balance-of-plant equipment

CONCLUSIONS AND UPCOMING ACTIVITIES

During FY 2018, work was continued on improving the SOEC robustness and performance stability. The very low performance degradation of the HiPoD technology was demonstrated by both single cell testing for a period of two years as well as a 45-cell stack producing >3 kg H₂/day. Additionally, the detailed design of a high-temperature water splitting demonstration unit capable of producing >4 kg H₂/day with expected overall efficiency (thermal + electric) of 75% (lower heating value hydrogen) was completed.

The future work on the cell and stack technology consists of studies to determine the operating conditions and cell material modifications that will further reduce cell degradation. Continued improvements in cell and stack manufacturing are anticipated to result in further reduction of stack degradation. The techno-economic analysis of a forecourt system (1,500 kg H₂/day) will be developed using the H2A (Hydrogen Analysis) methodology.

The system design and performance will be based on the lessons learned from stack tests. The system design optimization will be supported by the operation of the >4 kg H₂/day modular SOEC demonstration unit, which will be fabricated in the coming year. The modular SOEC system has the objective of demonstrating stable system operation over >1,000 h of steady-state testing, as well as showing successful operation on load profiles relevant to intermittent renewable energy sources.

FY 2018 PUBLICATIONS/PRESENTATIONS

1. H. Ghezel-Ayagh, “Modular SOEC System for Efficient H₂ Production at High Current Density,” U.S. Department of Energy Hydrogen and Fuel Cells Program, 2018 Annual Merit Review and Peer Evaluation Meeting (AMR), Washington, D.C, June 13–15, 2018.
2. H. Ghezel-Ayagh, “SOFC Development Update at FuelCell Energy,” NETL 19th Annual Solid Oxide Fuel Cell (SOFC) Project Review Meeting, Washington, D.C, June 13–15, 2018.

REFERENCES

1. A. Wood, H. He, T. Joia, M. Krivy, and D. Steedman, “Communication—Electrolysis at High Efficiency with Remarkable Hydrogen Production Rates,” *Journal of Electrochemical Society* 163, no. 5 (2016): F327–F329.

Optimal Stationary Fuel Cell Integration and Control (Energy Dispatch Controller)

Genevieve Saur
National Renewable Energy Laboratory
15013 Denver West Parkway
Golden, CO 80401-3305
Phone: (303) 275-3783
Email: genevieve.saur@nrel.gov

DOE Manager: Jason Marcinkoski
Phone: (202) 586-7466
Email: Jason.Marcinkoski@ee.doe.gov

Subcontractors:

- Washington State University, Pullman, WA
- University of Colorado at Boulder, Boulder, CO

Project Start Date: June 1, 2016
Project End Date: September 30, 2019

Overall Objectives

- Create an open-source tool set to foster growth in fuel cell integrated buildings with emphasis on optimal dispatch control.
- Objective 1: Energy dispatch controller (EDC)—Implement an open-source dispatch and load-control tool for building management that can communicate and transact with a fuel-cell-integrated building system and with the grid for optimized dispatch of building components.
- Objective 2: System planning tool—Implement a planning tool for optimal component selection and sizing based on optimal resource control for distributed energy systems and smart building components using location-specific energy markets, building energy modeling, and chosen dispatch control strategy.

Fiscal Year (FY) 2018 Objectives

- Improve and refine optimization for the EDC optimization.
- Develop methods for improving the building reduced order model (ROM) used for the optimization.

- Begin closed-loop testing and validation of modules in co-simulation with EnergyPlus.
- Create optimizations and start integration of the planning tool for building component sizing.
- Build and refine communications agents for implementation of VOLTTRON communication framework.

Technical Barriers

This project addresses the following technical barriers from the Grid Modernization Initiative Multi-Year Program Plan [1]:

- 4.2.3: Utilizing open standards and middleware software approaches to enable integration of EMS, DMS, and BMS.
- 4.3.3: Develop efficient linear, mixed-integer, and nonlinear mixed-integer optimization solution techniques customized for stochastic power system models, novel bounding schemes to use in branch and bound, and structure-exploiting algorithms. Demonstrate the cost-benefit achieved by these techniques relative to existing ones.

Contribution to Achievement of DOE Technology Validation Milestones

This project will contribute to achievement of the following DOE milestones from the Technology Validation section of the Fuel Cell Technologies Office Multi-Year Research, Development, and Demonstration Plan¹:

- Milestone 1.5: Demonstrate processes for highly uniform continuous lamination of membrane electrode assembly (MEA) components. (4Q, 2019)
- Milestone 1.6: Develop fabrication and assembly processes for polymer electrolyte membrane fuel cell MEA components leading to an automotive fuel cell stack that costs \$20/kW. (4Q, 2020)

¹ <https://www.energy.gov/eere/fuelcells/downloads/fuel-cell-technologies-office-multi-year-research-development-and-22>

FY 2018 Accomplishments

- Testing and validation of EDC was begun in co-simulation. Some promising results were used to demonstrate the dispatch controller techniques at a high-performance building conference.
 - Closed-loop testing and validation activities were ongoing using an EnergyPlus simulation for feedback.
 - Improvements were made to the optimization formulation using results from co-simulation testing.
 - Developed significant improvements to the ROM. Validation testing with first- and second-order ROMs were evaluated for accuracy and speed.
 - Fuel cell start-up/shut down functionality introduced.
- Design and integration of the planning tool for sizing building components was begun. Several methods for discrete and continuous sizing were implemented with an initial graphical user interface.
- Developed and revised several VOLTTRON agents needed for a comprehensive communication platform. Showed successful communication with five agents for initial proof-of-concept.

INTRODUCTION

Current building control strategies can rely on arbitrary assignment of value to assets and be simplistic, needing prior-analysis for set control strategies. This project will create open-source tools for dynamic building energy management, an EDC capable of supervisory control, and a planning tool for component sizing of distributed generation and storage components using simulated dispatch. The controllable components within a building can be equipment such as a fuel cell, chiller, or water heater, or the thermal mass of the building envelope as controlled through the temperature. Constraints to the energy management can be thermal comfort or required operations of specific equipment.

The project aims to modernize building energy management by holistically integrating control of building elements for optimal operation, including maximizing benefit of distributed generation and storage. The project will also aid grid modernization by characterizing the potential of buildings to participate in ancillary grid services and positioning building operators to participate in ancillary grid services markets as they are available.

APPROACH

The project is using a cross-functional approach with team members who have expertise in fuel cells, power systems, commercial buildings, and building-communication networks. We are leveraging prior knowledge with tools and research from the different areas to create a novel controller and planning tool.

The EDC optimization utilizes a strategy using model predictive control. This approach allows forecasting of building loads and predicted building operation, which facilitates participation in grid ancillary service markets. The planning tool then will use simulated optimal dispatch to size added components into the system.

RESULTS

In the second year of the project we have taken the foundational work on optimization formulations from the first year and begun testing, validation, refinement, and integration. Using closed-loop simulation with EnergyPlus [2] we have begun testing of different modules of the optimization. This has led to improvements in the EDC optimization formulation, the building ROMs, and co-simulation environment. Work also has begun on the development of the planning tool, which integrates the functionality of the EDC to evaluate building component sizing. Development of a comprehensive communications framework resulted in the development and refinement of several VOLTTRON agents and demonstrated successful communication between agents.

The model predictive control strategy for building dispatch control allows prediction of the building operation, which facilitates participation in ancillary grid services. The forecast provides knowledge of expected capacity for providing services at different times; it takes in inputs such as current temperature, equipment states, utility costs, weather prediction, and load forecasting. The EDC optimization then determines an optimal operation over the next 24-hour period and implements set points for the next one hour. The optimization runs again each hour over a rolling 24-hour period. Variation between scheduled and actual operation occur due to building feedback and variability in actual building loads versus the forecast.

The initial dispatch controller optimization formulation was improved to include allowance of fuel cell startup and shutdown during optimization. This required moving to mixed integer linear programming for the algorithm formulation. The fuel cell model also was improved to include the ability to reject heat into the hot-water loop for additional combined heat and power applications.

Testing and validation work using a co-simulation environment (Figure 1) supported improvement in several areas of the project. Using EnergyPlus for the closed-loop simulation we moved from simpler single-zone reference building models to multi-zone models of both a large office building and a large hotel. In testing we identified significant ROM mismatches (Figure 2), which led to a collaborative effort in ROM development between NREL, Washington State University, and Pacific Northwest National Laboratory. The ROM is

needed by the dispatch controller to forecast the building load, generation, and storage and to optimize their operation. A ROM mismatch causes non-optimal solutions, but a perfect ROM is impossible due to the uncertainties of the elements that go into it (Figure 3). However, there are methods for reducing the impact of error through improvements to the ROM and forecasting.

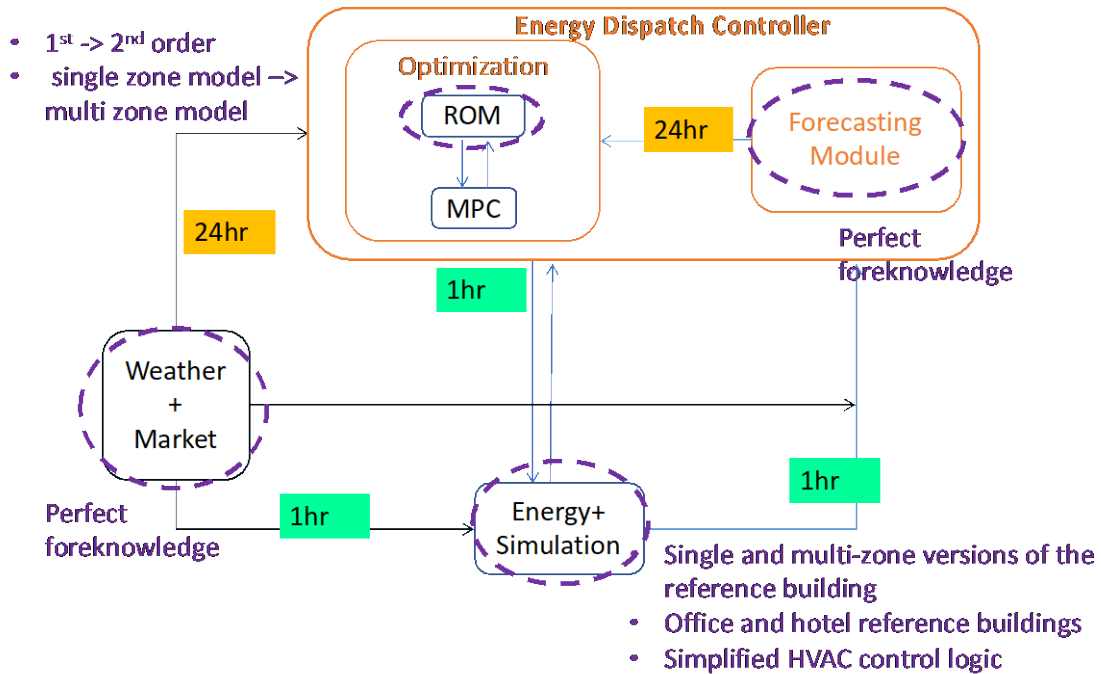


Figure 1. Co-simulation environment

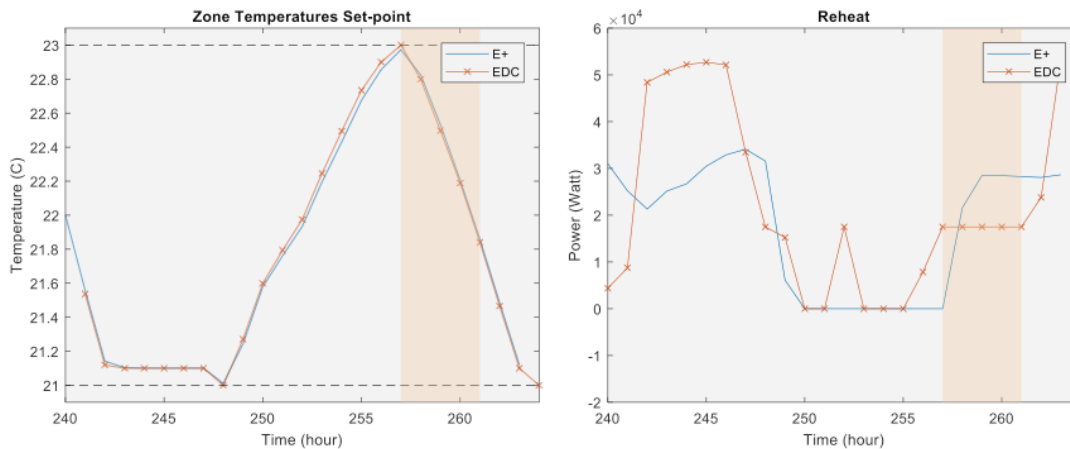


Figure 2. Example of ROM mismatch: temperature tracks well but power for reheat does not

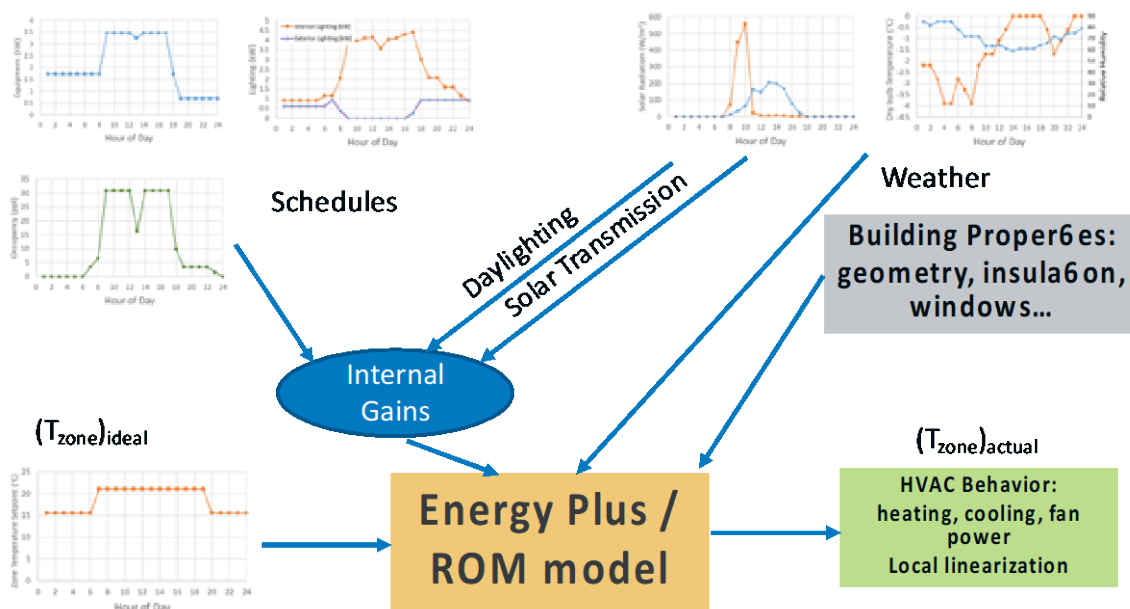


Figure 3. Elements that go into ROM development

Multiple iterations of ROM improvement were accomplished. Some of the outcomes included moving from a first-order ROM to a second-order with local linearization. The time-step selection was shown to be an important factor due to the difference in response time between wall zones (slow response rate) and air zones (fast response rate). It was shown that undesirable temperature oscillations could occur when the time steps were too short, but not enough information was captured about the changes if the time step was too large. The team developed methods for reducing undesirable effects in the ROM.

Some preliminary results were completed for the single-zone office building, which showed the operation of different modules and promising prospects for use of the dispatch controller with a fuel cell-integrated building. Several scenarios were developed to test various aspects of the optimization. Table 1 has results for a low-gas-cost scenario, which shows a significant cost improvement for the FC- and EDC-operated building. However, there is still work to be done to quantify the benefit that the fuel cell has with and without optimized control to isolate the source of the improvement. We also need to validate with the multi-zone building models and improved ROM.

Table 1. Preliminary Results for a Single-Zone Office Building Running with the EDC and Fuel Cell, Low-Gas-Cost Scenario

Low NG cost scenario	Total cost	Electricity cost	Natural gas cost	Ancillary services payment
EDC	398	81	321	5
EDC, no FC	733	611	127	5
No EDC, no FC, 1 set-point	747	594	153	
No EDC, no FC, 2 set-points	691	572	119	

A comprehensive communication bus that can simplify integration with a building is being developed with Pacific Northwest National Laboratory using VOLTTRON [3]. Required agents were identified and developed. In several cases previous work was adapted and expanded to serve the needs of the project, including identifying gaps in the OpenADR agent for serving non-demand-response grid ancillary services, revising a weather agent to use a non-subscription-based weather forecast, and evaluating others for their use in the project. A communications network was set up to demonstrate the agents functioning together.

Initial formulations for a planning tool that can optimally size several building components given the expected optimal operation of the building were developed. The building components for on-site generation and storage included fuel cells, batteries, and thermal storage. Methods for discrete and continuous sizing were implemented. This was coupled with a graphical user interface that will be expanded to include inputs and visualizations for the EDC.

CONCLUSIONS AND UPCOMING ACTIVITIES

The second year of the project built upon the foundational work of the first year to include initial testing and validation. The framework for a suite of novel tools for building energy management and component sizing is functioning though additional work is needed to integrate all the modules into one complete package.

Third and final year activities include the following.

- Settle upon a formulation for the optimization and ROM that can be thoroughly evaluated and quantify benefits for building operations as well as grid services.
- Develop a package of test scenarios that can adequately map how the controller performs. These scenarios may include spark spread (difference between electricity and natural gas prices), geography, building types, combined heat and power opportunities, and grid service environments.
- Integrate the planning tool sizing to demonstrate the combined benefit of optimal component sizing and building operation.

- Complete hardware-in-the-loop testing to validate co-simulation results.
- Complete a transition to python to facilitate graphical user interface development and use of open-source solvers in the optimization problems.

FY 2018 PUBLICATIONS/PRESENTATIONS

1. Y. Lin, D. McLarty, A. Pratt, B. Ball, G. Henze, and G. Saur. “Optimal Dispatch Controller for Fuel Cell Integrated Building.” 5th International High Performance Buildings Conference at Purdue, West Lafayette, Indiana, July 9–12, 2018.
2. Genevieve Saur. “Optimal Stationary Fuel Cell Integration and Control (Energy Dispatch Controller).” Presented at the DOE Hydrogen and Fuel Cells Program 2018 Annual Merit Review and Peer Evaluation Meeting, Washington, D.C., June 13–15, 2018.
3. Genevieve Saur, Annabelle Pratt, Yashen Lin, Dustin McLarty, Zhiwen Ma, Brian Ball, Jereme Haack, Venkatesh Chinde, Nathaniel Jones, and Haley Mikeska. “Optimal Stationary Fuel Cell Integration and Control (Energy Dispatch Controller) (GMLC0252).” Presented at the U.S. Department of Energy’s Grid Modernization Initiative Second Peer Review, Washington, D.C., September 4–7, 2018.

REFERENCES

1. Grid Modernization Initiative Multi-Year Program Plan, <https://energy.gov/sites/prod/files/2016/01/f28/Grid%20Modernization%20Multi-Year%20Program%20Plan.pdf>.
2. EnergyPlus is a whole building energy simulation program that engineers, architects, and researchers use to model both energy consumption—for heating, cooling, ventilation, lighting, and plug and process loads—and water use in buildings. <https://energyplus.net/>.
3. VOLTTRON is a real-time, scalable platform for transactive energy control and other applications. <https://bgintegration.pnnl.gov/volttron.asp>.

Integrated Systems Modeling of the Interactions between Stationary Hydrogen, Vehicles, and Grid Resources

Sam Saxena (Primary Contact), Cong Zhang, Max Wei, Jeff Greenblatt, Josh Eichman,^a Matteo Muratori,^a Omar J Guerra,^a Anudeep Medam^b
Lawrence Berkeley National Laboratory
1 Cyclotron Road
Berkeley, CA 94720
Phone: (510) 269-7260

Email: SSaxena@lbl.gov

^aNational Renewable Energy Laboratory

^bIdaho National Laboratory

DOE Manager: Jason Marcinkoski

Phone: (202) 586-7466

Email: Jason.Marcinkoski@ee.doe.gov

Project Start Date: October 1, 2016

Project End Date: September 30, 2019

Overall Objectives

- Provide an integrated modeling capability—the Hydrogen Vehicle to Grid Integration (H2VGI) Model—to quantify the interactions between stationary hydrogen generation, fuel cell vehicles, and grid support resources.
- Quantify potential grid support and balancing resources from flexible hydrogen systems (e.g., dispatchable production of hydrogen by electrolysis).
- Develop methods to optimize the systems configuration and operating strategy for grid-integrated hydrogen systems.

Fiscal Year (FY) 2018 Objectives

- Realistic integration of hydrogen resources into grid models to capture potential benefits and impacts for hydrogen technologies.
- Refine input values into economic models for hydrogen resources from available data and literature (e.g., fuel cell vehicle, electrolyzer, and fueling station costs).
- Garner industry feedback for project modeling strategy and results.

- Submit economic case study quantifying the scale of the opportunity from hydrogen-vehicle-grid integration for several utility regions in the Western Interconnect for both central and distributed electrolyzer operation and station configuration/storage sizing.
- Quantify the value of hydrogen production for fuel cell electric vehicles (FCEVs) in the Western Electricity Coordinating Council (WECC) area to support renewable supply integration.
- Draft a short report on testing and validation of an H2VGI economic modeling case study with key graphs and figures summarizing findings.

Technical Barriers

This project addresses the following technical barriers from the Systems Analysis section of the Fuel Cell Technologies Office Multi-Year Research, Development, and Demonstration Plan¹:

- (A) Lack of Fuel Cell Electric Vehicle and Fuel Cell Bus Performance and Durability Data
- (D) Insufficient Suite of Models and Tools.

Contribution to Achievement of DOE Systems Analysis Milestones

This project will contribute to the achievement of the following DOE milestones from the Systems Analysis section of the Fuel Cell Technologies Office Multi-Year Research, Development, and Demonstration Plan:

- Milestone 1.5: Complete evaluation of hydrogen for energy storage and as an energy carrier to supplement energy and electrical infrastructure. (4Q, 2012)
- Milestone 1.9: Complete analysis and studies of resource/feedstock, production/delivery, and existing infrastructure for technology readiness. (4Q, 2014)

¹ <https://www.energy.gov/eere/fuelcells/downloads/fuel-cell-technologies-office-multi-year-research-development-and-22>

FY 2018 Accomplishments

- Submitted a paper to explore the opportunity for providing balancing support to the grid. This shows the potential impact that hydrogen systems can have on a large grid system.
- Refined the refilling behavior according to realistic data.
- Established a concept model in PLEXOS to perform the economic analysis.
- Assessed several utility regions in the Western Interconnect with all assumptions and methods vetted
- Forecasted FCEVs, which were used to estimate the hydrogen consumption.
- Compared the economic cost for the central and distributed hydrogen generating scenarios.
- Created the PLEXOS model to compare the economic cost for different electrolyzer sizes.

INTRODUCTION

The goal of this multiyear project is to establish the available capacity, value, and impacts of interconnecting hydrogen infrastructure and FCEVs to the electric grid. The first objective is to quantify the opportunity of utilizing flexibility from hydrogen systems to support the grid. This includes provisions for vehicle and station controllable loads. The second objective is to develop and implement methods to assess the optimal system configuration and operating strategy for grid-integrated hydrogen systems. This involves developing a modeling framework that can analyze the value of optimally dispatching resources based on grid needs while respecting hydrogen production and vehicle travel requirements. The third objective is to develop the economic model to evaluate the cost in different hydrogen production scenarios. For example, both the centralized and the distributed hydrogen stations are analyzed to evaluate the cost difference. By exploring different electrolyzer sizes, variations in system cost are investigated using PLEXOS in the WECC area. These results can form the basis for future hydrogen station installations and provide a reference for future electricity grid planning.

APPROACH

There are two key topics to be investigated: (1) explore the cost difference between the centralized and distributed hydrogen stations, considering the delivering process; and (2) explore the cost difference as a function of electrolyzer size in the whole WECC area by using PLEXOS. First, vehicle and station rollout scenarios will be developed using the Scenario Evaluation and Regionalization Analysis (SERA) model [1]. Individual vehicle models, energy demands from large numbers of FCEVs, and backup power capacity for grid services will be developed using the Lawrence Berkeley National Laboratory V2G-Sim modeling framework [2, 3]. The National Renewable Energy Laboratory will lead the development of individual hydrogen generation/station models and aggregate hydrogen generation capacity allocation for grid services [4]. Finally, vehicle and hydrogen generation data will be integrated into external grid models (e.g., vehicle operating characteristics and historical market prices) to quantify the economic impacts of flexible hydrogen resources on grid operation. After estimating hydrogen consumption volume, central and distributed hydrogen production options will be analyzed. For both the United States and California scenarios, the hydrogen station operation cost will be analyzed. In the PLEXOS model [5], the hydrogen consumption rate will be used to calculate the volume of electricity needed to generate the hydrogen. Then, the pumped hydroelectric storage capability of PLEXOS will be used to simulate the hydrogen generation and utilization process. Finally, the electrolyzers will be connected to nodes and interact with the whole grid system to supply the hydrogen generation.

RESULTS

Fuel cell vehicle models have been formulated and calibrated for use using V2G-Sim, which has been extended to include FCEVs. The FCEV models allow hydrogen consumption to be predicted for any trip, given speed and terrain versus time profiles for the trip and the prediction of hydrogen demand from large collections of vehicles based on travel itinerary data using National Household Travel Survey data [6]. The coupled sub-models include calibrated fuel cell vehicle models and a preliminary refueling sub-model, which governs when individual vehicles are refueled within their travel itineraries.

Using the hydrogen FCEV demand sub-models, preliminary results have been found for the hydrogen demand, electrolyzer cycling profiles, and grid power demand at the hydrogen fueling station for nearly 3,000 vehicles driving and refueling over 40 days. This capability to predict and aggregate FCEV hydrogen demand is a key building block for determining temporally and spatially resolved hydrogen fueling demand as a function of adoption scenario.

We plotted the refueling probability as the red line in Figure 1 to show a clear comparison with our previous assumption. There is a probability that refueling will occur when the tank level is lower than 100% and that probability grows as the tank level reduces.

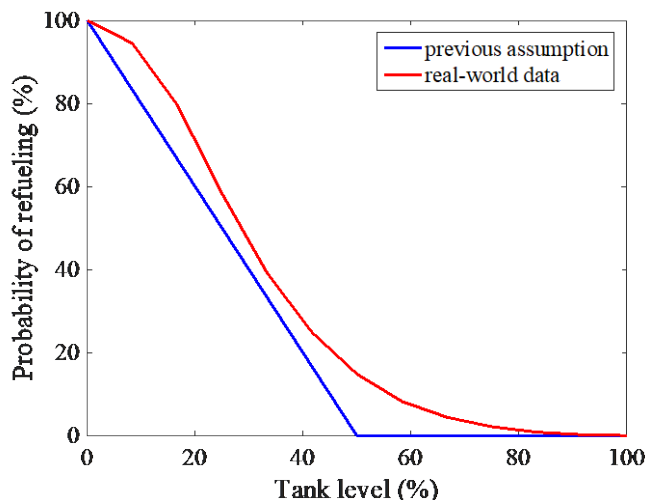


Figure 1. FCEV refueling behavior assumption in our previous work

Using the H2VGI toolkit, the value of central versus distributed production was explored for the entire hydrogen production-distribution-dispensing network, largely with the SERA model, and also for individual stations within the network using V2G-Sim. For individual hydrogen stations, the electricity consumption is highly dependent on the type of station (e.g., gaseous delivered, liquid delivered, gaseous on-site production). An on-site electrolysis station's electricity consumption is dominated by the electrolyzer. The consumption for the other components is an order of magnitude less than for the electrolyzer. Without considering electrolyzer consumption, a liquid delivered hydrogen station has the highest consumption, followed by the on-site electrolysis station, and, last, the gaseous delivered hydrogen station. This is because both the liquid and on-site electrolysis stations require additional electricity to compress the hydrogen into medium-pressure tanks, while the gaseous delivered station gets pressurized hydrogen into the medium-pressure tanks.

Figure 2 shows the total cost to operate the entire hydrogen network. The cost increases for each successive year as more hydrogen infrastructure is installed and more hydrogen is delivered to customers. Regarding electrolysis, for the entire United States, the cost for central electrolysis is lower than for distributed electrolysis due to large economies of scale; however, in California the cost for central electrolysis is higher than distributed electrolysis for all years considered due to the limited market size. This is attributed to the market conditions in California (e.g., fuel prices for trucks and large travel distances due to cities being spread out).

Figure 3 shows the annual total generation cost and average price of the WECC load. Three points can be made:

- The flexible hydrogen generation scenarios can optimize the hydrogen production process, which appears to reduce the total generation cost.
- The total generation cost can be reduced as the electrolyzer size becomes larger in flexible scenarios.
- The average price has a similar trend as the total generation cost.

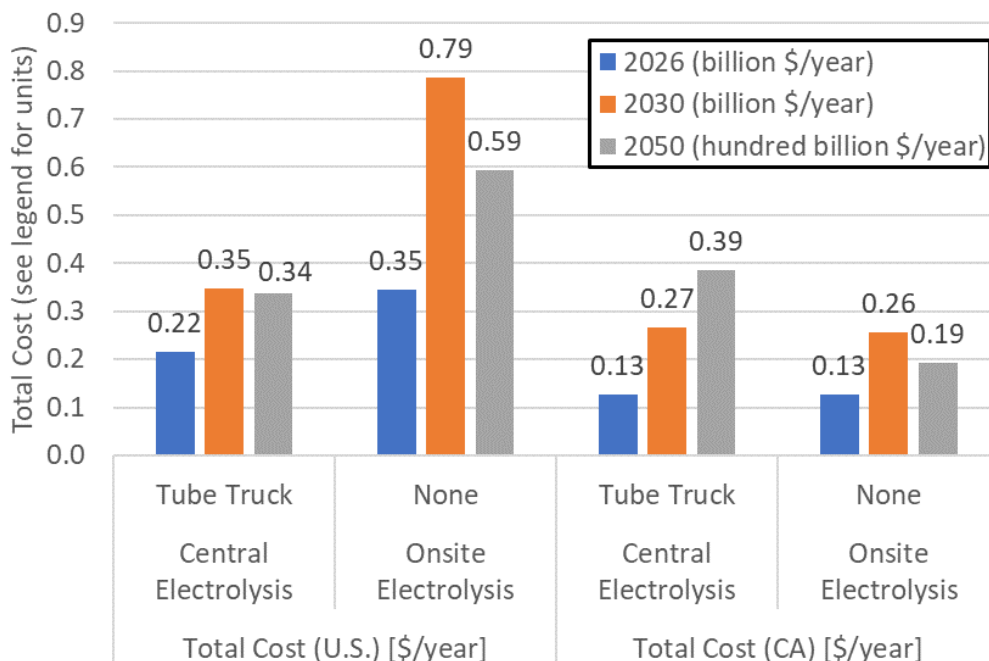


Figure 2. Total cost of operating hydrogen network

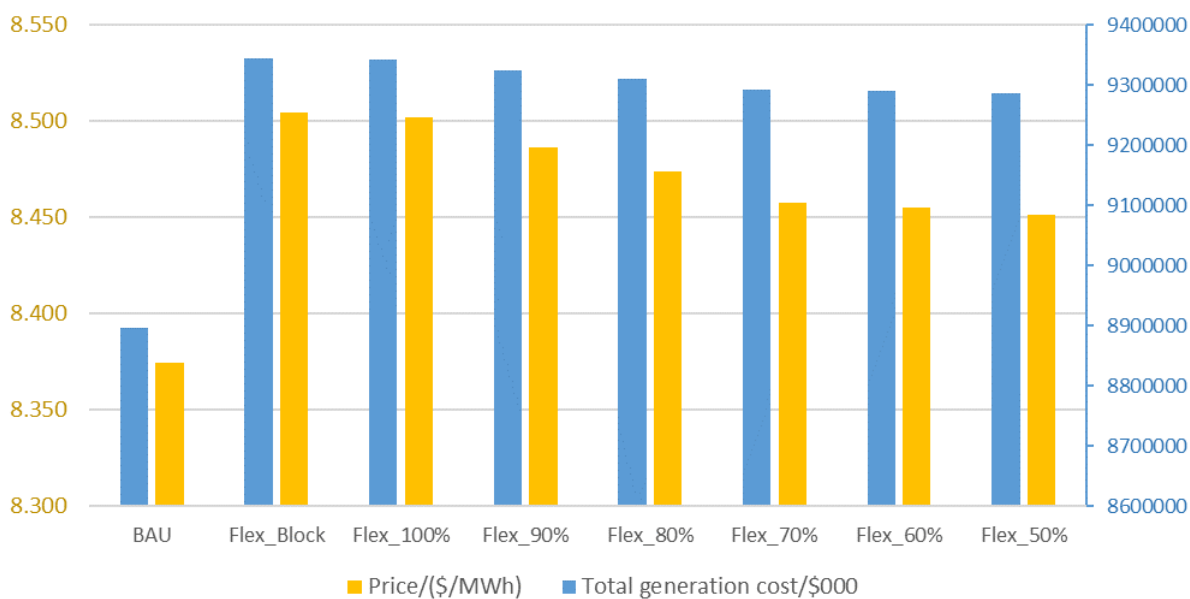


Figure 3. The annual total generation cost and average price of the WECC grid

As is shown in Figure 4, CO₂ emissions are also a significant parameter to evaluate to determine whether the electricity generators are environmentally friendly. Although CO₂ emissions increase after including the flexible hydrogen generating load, the CO₂ emissions decrease again as the electrolyzer size increases. It means that the larger flexible load can be more helpful in decreasing CO₂ emissions.

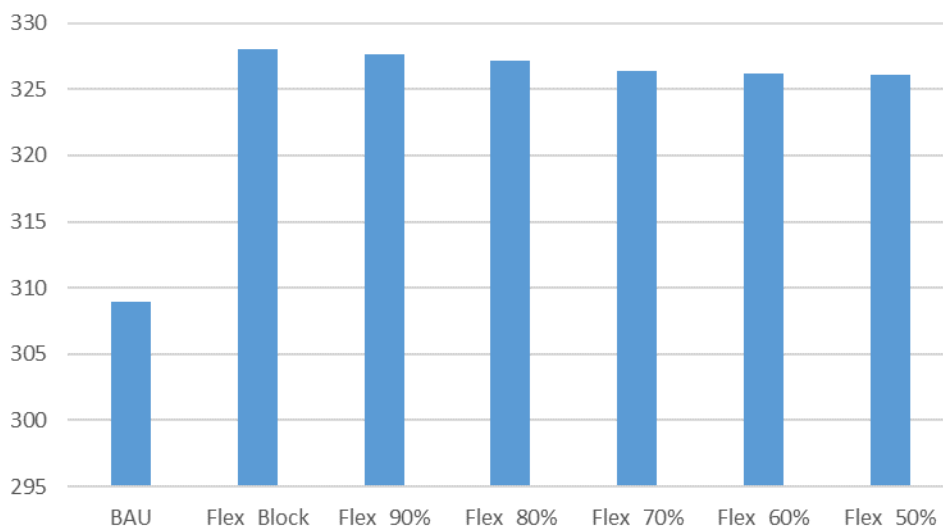


Figure 4. The CO₂ emissions of the WECC grid

CONCLUSIONS AND UPCOMING ACTIVITIES

The team has made progress on developing several sub-models for the H2VGI toolkit that include vehicle deployment scenarios, FCEV drivetrain models, fueling demand from large vehicle populations, modeling of fuel station electricity demand components, and an initial case study of the potential economic influence on the grid electricity price. In addition, for the centralized and distributed hydrogen stations, a cost comparison is also given for different scenarios.

Upcoming activities include publishing initial results on the PLEXOS case study to quantify the economic opportunity of FCEVs and developing more comprehensive scenarios to quantify the economic opportunity for FCEVs (e.g., light, medium, and heavy duty) to provide grid services within the larger alternative fuel vehicle opportunity space. A key output will be a simulation matrix defining the number of scenarios and parametric variations to be explored in each scenario. We will also estimate the hydrogen demand for FCEVs (light, medium, and heavy duty) and calculate the time-dependent hydrogen production load profiles, by implementing scenarios in PLEXOS to quantify the economic opportunity for FCEVs (light, medium, and heavy duty) to provide grid services within the larger alternative fuel vehicle opportunity space. Key outputs of this activity will be a set of H2VGI+PLEXOS models to simulate each of the defined scenarios. We will generate comprehensive results from H2VGI+PLEXOS for each of the chosen scenarios, and scenarios will include high fractions of intermittent renewable generation (e.g., 30%, 40%) and increasing adoption of hydrogen-powered vehicles (e.g., 10%, 20%, 30% of the light-duty vehicle fleet and up to 30% of the heavy-duty vehicle fleet). For this activity, we will compare the relative economic benefits and renewables integration opportunities across the different scenarios of light, medium, and heavy-duty FCEV adoption.

FY 2018 PUBLICATIONS/PRESENTATIONS

Publications:

1. Dai Wang, Matteo Muratori, Joshua Eichman, Max Wei, Samveg Saxena, Cong Zhang, “Quantifying the Flexibility of Hydrogen Production Systems To Support Large-Scale Renewable Energy Integration,” *Journal of Power Sources* 399 (2018): 383-391.

Presentations:

1. Sam Saxena (Primary Contact), Max Wei, Cong Zhang, Josh Eichmana, Matteo Muratoria, Fernando Dias, Stevic Svetomir, “Integrated Systems Modeling of the Interactions between Stationary Hydrogen, Vehicles, and Grid Resources,” presented at the 2017 DOE Annual Merit Review and Peer Evaluation Meeting, Washington, DC, June 13, 2018.

2. Sam Saxena (Primary Contact), Dai Wang, Jeff Greenblatt, Max Wei, Cong Zhang, Josh Eichmana, Matteo Muratoria, Fernando Dias, Stevic Svetomir, “Integrated Systems Modeling of the Interactions between Stationary Hydrogen, Vehicles, and Grid Resources,” Online webinar for the industry, March 28–30, 2018.

REFERENCES

1. B. Bush, M. Melaina, M. Penev, and W. Daniel, “SERA Scenarios of Early Market Fuel Cell Electric Vehicle Introductions: Modeling Framework, Regional Markets, and Station Clustering,” NREL/TP-5400-56588 (Golden, CO: National Renewable Energy Laboratory, 2013).
2. D. Wang, M. Muratori, J. Eichman, M. Wei, S. Saxena, and C. Zhang, “Quantifying the flexibility of hydrogen production systems to support large-scale renewable energy integration,” *Journal of Power Sources* 399 (2018): 383–391.
3. V2G-Sim model (Lawrence Berkeley National Laboratory, 2017), <http://v2gsim.lbl.gov/>.
4. J. Eichman and F. Flores-Espino, *California Power-to-Gas and Power-to-Hydrogen Near-Term Business Case Evaluation*, Technical Report NREL/TP-5400-67384 (Golden, CO: National Renewable Energy Laboratory, December 2016).
5. Energy Exemplar (2018), <https://energyexemplar.com/>.
6. National Household Travel Survey, “National Household Travel Survey” (2009).

H2@Scale: Experimental Characterization of Durability of Advanced Electrolyzer Concepts in Dynamic Loading

Shaun Alia (Primary Contact), Guido Bender,
Bryan Pivovar
National Renewable Energy Laboratory
15013 Denver West Parkway
Golden, CO 80401
Phone: (303) 275-3748
Email: Shaun.Alia@nrel.gov

DOE Manager: Jason Marcinkoski
Phone: (202) 586-7466
Email: jason.marcinkoski@ee.doe.gov

Subcontractor:
Los Alamos National Laboratory, Los Alamos, NM

Project Start Date: October 2017
Project End Date: Project continuation and
direction determined annually by DOE

Overall Objectives

- Evaluate and quantify the impact of catalyst loss mechanisms—including constant, intermittent, and start-stop operation—on low-temperature electrolysis.
- Evaluate mitigation strategies, including materials and system controls, to minimize durability losses at low loading and under intermittent operation.

Fiscal Year (FY) 2018 Objectives

- Demonstrate low-temperature electrolysis in situ testing and durability capabilities.
- Quantify the impact of low loading and intermittent operation on low-temperature electrolysis durability.

Technical Barriers

This project addresses the following technical barriers from the Technology Validation section of the Fuel Cell Technologies Office Multi-Year Research, Development, and Demonstration Plan¹:

- Reducing the cost of hydrogen production by electrochemical water splitting
- Durability losses at low cost and the impact on the price of hydrogen production.

FY 2018 Accomplishments

- Demonstrated more than 15,000 hours of durability testing in low-temperature electrolysis.
- Established baseline performance and durability in ex situ and in situ testing to guide catalyst and electrode development efforts.
- Evaluated the impact of low loading, intermittent operation, water quality, and catalyst choices on single-cell durability and catalyst layer degradation.

¹ <https://www.energy.gov/eere/fuelcells/downloads/fuel-cell-technologies-office-multi-year-research-development-and-22>

INTRODUCTION

While hydrogen is a significant chemical commodity, low-temperature electrolysis is a relatively small contributor due to high hydrogen production cost. Low-temperature electrolyzers currently use high quantities of iridium at the anode, to avoid performance loss with extended operation and because the hydrogen cost is driven by the power-input cost. To meet electrolysis cost targets, however, electrolysis must be coupled with low-cost power sources and reduce catalyst loadings to address the increased capital cost at lower capacity.

Reducing the iridium loading previously has been found to accelerate the observation of durability losses. During FY 2018, work was completed to quantify the impact of operation profiles (constant, intermittent operation) on electrolysis durability and catalyst layer degradation to assess how renewable electrolysis affects catalyst/electrode development efforts and hydrogen production cost targets.

APPROACH

The National Renewable Energy Laboratory (NREL) has developed standard testing and durability protocols to establish:

- Reasonable metrics for ex situ and in situ testing performance and durability
- How catalyst loading impacts the onset of durability loss observations
- The relative impact of input profiles, including constant (current, steady input), square-wave (wind input), and triangle-wave (solar input) on electrolysis durability.

Approach development included setting conditioning and test procedures to establish initial performance baselines for catalyst and electrode development projects. Durability testing was used while varying singular parameters (loading, water quality, input profile) to evaluate their relative impact on long-term operation. Various techniques including cell performance, diagnostics, and microscopy were used establish degradation modes and suggest methods for mitigating performance loss.

RESULTS

As baseline materials, NREL evaluated iridium black (metal/hydroxide) and oxide (thermally oxidized) in ex situ and in situ testing (Figure 1). Although iridium produced high oxygen evolution activity in rotating disk electrode half-cells, the performance benefit generally was not observed in membrane electrode assemblies due to surface and near-surface oxidation during single-cell conditioning. Iridium oxidation was observed in half-cell tests, where activity and metallic features (hydrogen underpotential deposition) were lost at moderate potential (1.6 V). These losses, however, were not related to dissolution and were recoverable after extended operation at reducing conditions. Unrecoverable iridium losses were higher than oxides in half- and single-cells due to the relatively higher dissolution rate of metal/hydroxide as compared to oxide. Although iridium metal/hydroxide-based materials often are a focus of catalyst development efforts, thermal oxides might be better suited for low-temperature electrolysis due to the lower durability losses.

Membrane electrode assembly evaluations focused on iridium oxide due to the slower dissolution kinetics. Electrode spraying method and ink composition influenced catalyst layer uniformity and the resulting performance and durability of single-cell tests. In general, a balance was needed in ionomer content to ensure ink uniformity while minimizing contaminant effects; a balance also was required in spray rate and temperature to produce evenly coated catalyst layers. Ensuring uniform coating appeared critical in obtaining reproducible durability experiments, because membrane electrode assemblies with undercoated or weak points in the catalyst layer might have accelerated degradation and performance decline.

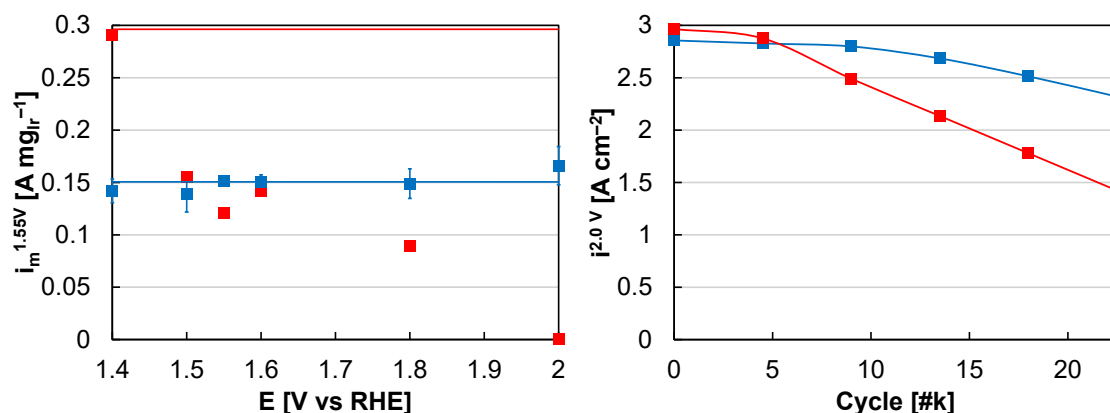


Figure 1. Durability losses of iridium (red) and iridium oxide (blue) nanoparticles in (a) rotating disk electrodes and (b) membrane electrode assemblies

Catalyst loading and operating potential were found to significantly impact membrane electrode assembly durability (Figure 2). Although iridium dissolution and loss occurred at higher loading (0.4 mg cm^{-2}), thicker catalyst layers masked loss observations and lower loading (0.1 mg cm^{-2}) was needed to observe durability losses during a reasonable amount of time. Reaching operating potentials of 2 V and greater was also necessary to accelerate iridium dissolution, and lower potential appeared to minimize loss or delay the impact of iridium degradation on cell performance.

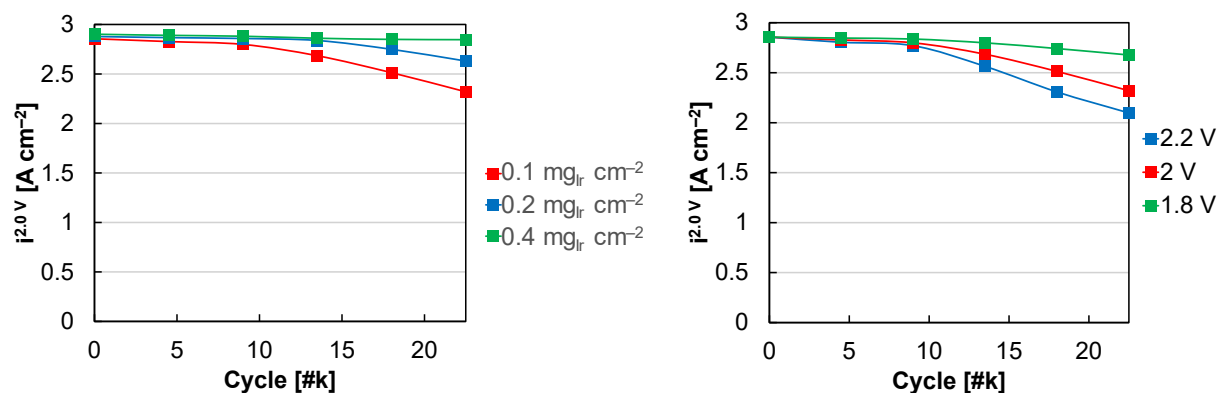


Figure 2. The impact of (a) loading and (b) upper potential on membrane electrode assembly durability. Durability tests were completed using square-waves, between 1.45 V and (a) 2.0 V or (b) as specified in the figure legend.

In an effort to minimize the length of single-cell durability tests (16 days), membrane electrode assemblies were used with low loadings (0.1 mg cm^{-2}) and with an upper potential of 2.0 V. A variety of power input profiles were evaluated to quantify their impact on device durability, and loss increased in the following order: constant/hold, triangle-wave, and square-wave (Figure 3). In rotating disk electrodes, high potential accelerated loss due to an increased dissolution rate. Potential cycles, however, did not accelerate loss because the potential range of interest did not include a redox transition, and resulted in lower loss rates because less time was spent at elevated potential. In single-cell tests, the higher loss rate likely was due to differences between the potential applied to the catalyst layer and observed at the current collectors. Cycling potential likely resulted in nonuniform potentials at catalyst sites and accelerated loss due to potential spikes increasing the dissolution rate. Potential cycling further resulted in thinner catalyst layers and decreases in the iridium oxide equivalent pore diameter.

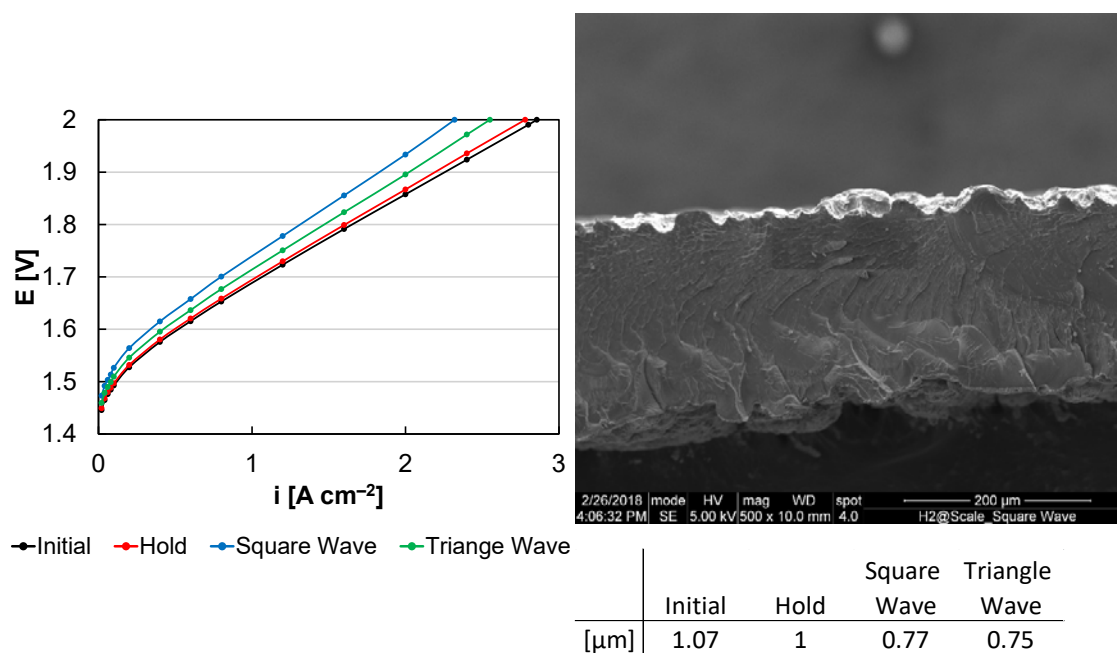


Figure 3. (a) Membrane electrode assembly performance, initially and following durability, and (b) microscopy of a cross-sectioned membrane electrode assembly following a square-wave durability testing; anode (iridium oxide) catalyst layer thicknesses initially and following durability

Although potential cycling resulted in higher durability losses than potential holds, the square-wave profile also produced greater losses than the triangle wave. Sawtooth profiles were used to identify the source of increased loss—whether due to the sudden increase or decrease in applied current (Figure 4). The hard-up profile (sudden increase to 2.0 V, gradual decrease to 1.45 V) produced loss similar to the square wave. Conversely, the hard-down profile (sudden decrease to 1.45 V, gradual increase to 2.0 V) produced loss similar to the triangle wave. Although adding intermittency increased the rate of performance loss, the sudden increase in power input appeared to be more detrimental with continued operation. The sudden increase may have resulted in greater variation of potentials within the catalyst layer, accelerating catalyst dissolution and performance loss.

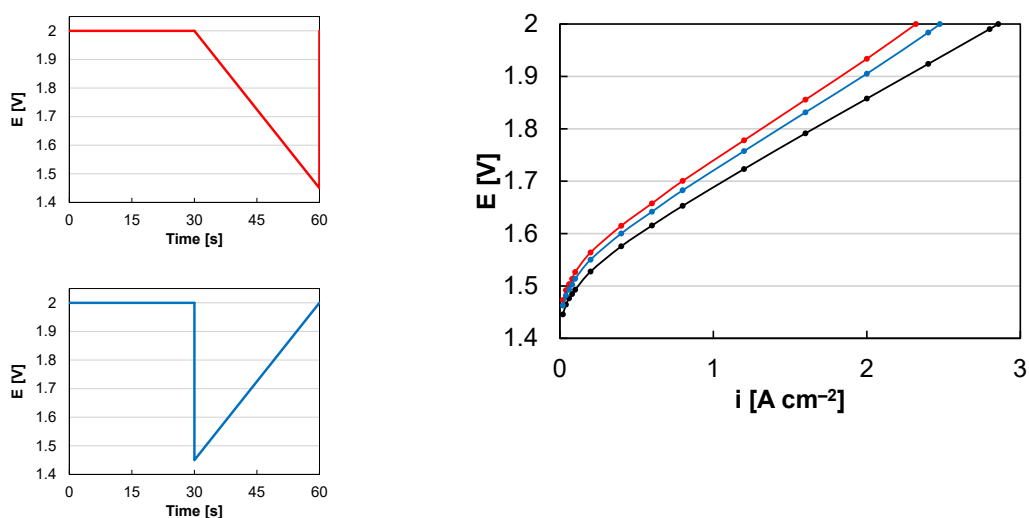


Figure 4. (a) Sawtooth test profiles and (b) membrane electrode assembly performance, initially and following durability

Water quality also was studied as a test concern, to evaluate how contaminants affect the measured performance and durability of membrane electrode assemblies. When the conductivity of the water increased, several observations were made: a hysteresis was found between anodic and cathodic polarization curves; initial membrane electrode assembly performance decreased; and durability losses increased under the same input profiles.

Nickel was found to be the primary contaminant source in these studies, and different effects may be observed with other contaminants. An expanded contaminant effort is underway in half- and single-cells to better understand the effect of likely system contaminants on cell performance and durability.

CONCLUSIONS AND UPCOMING ACTIVITIES

Project findings indicate that significant durability losses are observed at low loading when adding intermittent power inputs. Mitigation strategies, including catalyst improvements to reduce the upper operating potential, moderate loading, or system control to limit the upper operating potential will be critical in extending device lifetime when adjusting electrolysis operation for lower hydrogen production cost.

Continuing efforts have expanded upon constant and intermittent operation to include potential excursions and controlled or uncontrolled stops. These situations are being evaluated to assess the relative durability impact of iridium redox on cell durability, and how combined processes (hydrogen crossover, iridium reduction, increasing dissolution rates) influence electrolysis durability. NREL is developing a rainbow stack testing capability to increase the rate of data acquisition and gain improved statistics of these degradation process. Simulated wind and solar profiles also are being added to assess how square- and triangle-wave durability compares to more realistic models of power inputs.

FY 2018 PUBLICATIONS/PRESENTATIONS

1. Shaun M. Alia. “H₂@Scale: Experimental Characterization of Durability of Advanced Electrolyzer Concepts in Dynamic Loading.” Poster at the DOE Hydrogen and Fuel Cells Program Annual Merit Review, Washington, D.C. (June 2018).
2. Shaun M. Alia and Grace C. Anderson. “Iridium Oxygen Evolution Activity and Durability Baselines in Rotating Disk Electrode Half-Cells.” *Journal of the Electrochemical Society* (submitted 2018).
3. Shaun M. Alia, Sarah Stariha, Rod L. Borup, and Bryan S. Pivovar. “H₂@ Scale: The Effect of Loading, Test Parameters, and Oxides on Electrolyzer-Catalyst Durability.” In *Meeting Abstracts*, no. 46, 1604–1604. The Electrochemical Society (2018).
4. Shaun M. Alia and Bryan S. Pivovar. “The Effect of Loading, Test Parameters, and Oxides on Electrolyzer-Catalyst Durability.” AICHE Annual Meeting 2018. In *Meeting Abstracts*, no. 46, 1604–1604. The Electrochemical Society (2018) 83a.

Hydrogen Stations for Urban Sites

Brian Ehrhart (Primary Contact),
Gabriela Bran-Anleu, Ethan Hecht, Alice Muna,
Ethan Sena, Chris LaFleur
Sandia National Laboratories
PO Box 5800, MS 0748
Albuquerque, NM 87185
Phone: (505) 284-4906
Email: bdehrha@sandia.gov

Carl Rivkin
National Renewable Energy Laboratory
Golden, CO 80401

DOE Manager: Neha Rustagi
Phone: (202) 586-8424
Email: Neha.Rustagi@ee.doe.gov

Project Start Date: March 2017
Project End Date: July 2019

Overall Objectives

- Create compact gaseous and delivered liquid hydrogen reference station designs appropriate for urban locations, enabled by hazard/harm mitigations, near-term technology improvements, and layouts informed by risk (performance-based design).
- Disseminate results and obtain feedback through reports and a workshop with stakeholders representing code/standard development organizations, station developers, code officials, and equipment suppliers.
- Identify and provide designs for compact station concepts that enable siting of three times the number of stations in the dense urban example of San Francisco.

Fiscal Year (FY) 2018 Objectives

- Produce layouts for base case stations, modified delivery stations, stations adhering to new National Fire Protection Association (NFPA) 2 requirements, risk-informed stations, and underground storage and provide to NFPA 2 collaborators for review and feedback.

- Disseminate draft results including base case designs, modified delivery stations, stations adhering to new NFPA 2 requirements, designs informed by risk, stations with underground storage, and rooftop storage at a workshop. Include at least three designs with equivalent risk to the baseline designs and obtain feedback at the workshop with at least 10 stakeholders representing code/standard development organizations, station developers, code officials, authorities having jurisdiction, and equipment suppliers.

Technical Barriers

This project addresses the following technical barriers from the Hydrogen Delivery section of the Fuel Cell Technologies Office Multi-Year Research, Development, and Demonstration Plan¹:

- A. Lack of Hydrogen/Carrier and Infrastructure Options Analysis
- I. Other Fueling Site/Terminal Operations
- K. Safety, Codes and Standards, Permitting.

Contribution to Achievement of DOE Delivery Milestones

This project will contribute to the achievement of the following DOE milestones from the Hydrogen Delivery section of the Fuel Cell Technologies Office Multi-Year Research, Development, and Demonstration Plan:

- Milestone 1.4: Go/no-go on the use of liquid hydrogen carriers as an effective means of hydrogen delivery. (4Q, 2019)
- Milestone 6.3: By 2020, reduce the cost of hydrogen delivery from the point of production to the point of use in consumer vehicles to <\$2/gallon gas equivalent of hydrogen for the gaseous delivery pathway. (4Q, 2020)

This project will help to inform and enable siting of hydrogen fueling stations into dense urban areas, which will greatly improve the station economics. These siting challenges are especially

¹ <https://www.energy.gov/eere/fuelcells/downloads/fuel-cell-technologies-office-multi-year-research-development-and-22>

acute for delivered liquid hydrogen stations, and this project addresses this issue directly.

FY 2018 Accomplishments

- Completed preliminary designs for delivered gas, delivered liquid, and on-site electrolysis production stations for base case, alternate delivery, new NFPA 2, underground storage, rooftop storage, gasoline colocation, and risk-informed stations.
- Performed risk-informed hazard analysis for base case stations and for alternate methods, indoor location, and alternate pipe size designs.
- Presented preliminary results and obtained feedback at workshop in Livermore, California.

INTRODUCTION

Additional fueling stations need to be constructed in the United States to enable the widespread adoption of fuel cell electric vehicles. A wide variety of private and public stakeholders are involved in the development of this hydrogen fueling infrastructure. Each stakeholder has particular needs in the station planning, development, and operation process that may include evaluation of potential sites and requirements, understanding the components in a typical system, and/or improving public acceptance of this technology. Publicly available templates of representative station designs can be used to meet many of these stakeholder needs. These “reference stations” help reduce the cost and speed the deployment of hydrogen stations by providing a common baseline with which to start a design, enabling quick assessment of the suitability of a particular site for a hydrogen station, and identifying contributors to poor economics and research and development areas for certain station designs.

This project builds on past and current reference station design tasks. The Reference Station Phase 1 design task identified desirable fueling station parameters (e.g., capacity, consecutive fills) and down-selected many permutations to five economically favorable layouts, two of which stored hydrogen as a liquid. These layouts and stations would meet projected near-term market needs using current or near-term technology. One of the recommendations from this work was the need for science-based methods to reduce the setback requirements for liquid stations if they are to achieve market penetration in urban areas. The Phase 2 Reference Station design task considered hydrogen production (and delivery) costs, and modular station design layouts, but not for stations that store hydrogen as a liquid, and only using current technology and fire code separation distances.

APPROACH

In this project, we are continuing the previous reference station efforts by developing realistic potential layouts of gaseous and liquid hydrogen stations (both greenfield and colocated with gasoline) in compact footprints suitable for deployment in dense urban centers. In contrast to previous efforts, the Reference Stations for Urban Sites project considers stations that may not be attainable with today’s technology or permissible with current prescriptive codes and standards. These reference stations include justification of their safety (e.g., through a risk assessment) and/or identify high-priority development needs (e.g., revision of the fire codes) to enable these designs to be approved by local authorities having jurisdiction now or in the near future. In particular, this project includes footprint reduction by considering alternative gaseous and liquid hydrogen delivery vehicle designs, the impact of proposed changes to NFPA 2-prescribed setback distances (which are currently under review), station layouts informed by risk assessment rather than prescriptive setback distances, layouts with gaseous or liquid hydrogen storage underground, and rooftop installations.

We do not attempt to redesign existing hydrogen fueling station equipment in this project but rather focus on the application and layout of that equipment. The tools developed by the Fuel Cells Technology Office Safety Codes and Standards effort at Sandia National Laboratories are used in this project to engineer reference station designs. Whereas the Sandia National Laboratories safety codes and standards efforts are focused on development of models and tools for assessing risk, this Hydrogen Fueling Infrastructure Research and Station Technology (H2FIRST) project effort is focused on application of these tools to real-world designs. As with other reference station projects, cost models will also be developed for these designs. Because the reference stations in this project may include the use of equipment that has not yet been developed, some cost determinations will be estimates based on component-level modifications of previous reference station projects.

RESULTS

Initially, the work focused on creating and refining designs and assessing the associated safety of three base stations with delivered gas, delivered liquid, and on-site production via electrolysis. This involved sizing the stations to accommodate 600 kg of hydrogen dispensed per day, including sizing of storage tanks, pipe sizes, and equipment. Additionally, the fueling stations incorporate a number of design choices not related to the

hydrogen system itself: traffic flow, parking, the delivery truck path, and a convenience store. Any changes to design choices or assumptions required an update to all aspects of the designs (including the calculation of setback distances and footprint) as well as the risk hazard scenario calculations. The base case for a delivered gas station design is shown in Figure 1.

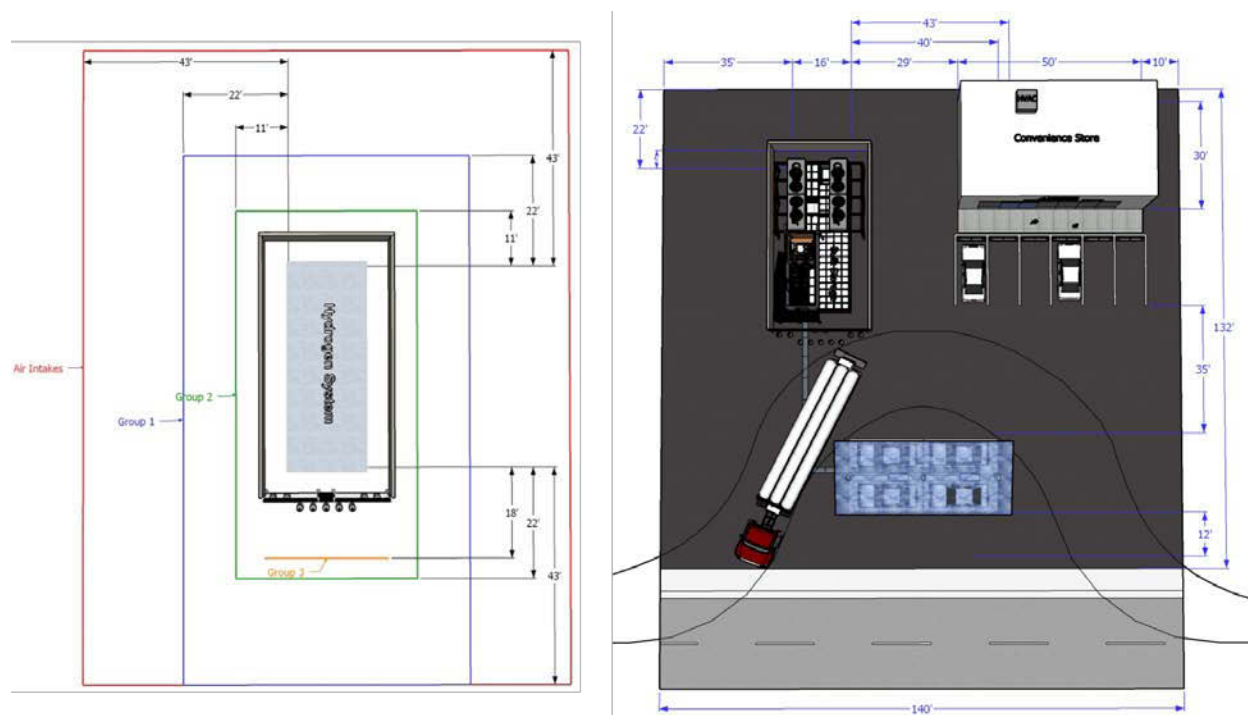


Figure 1. Delivered gas base case footprint, showing NFPA 2 setback distances on the left and full station footprint on the right

Subsequent designs deviated from these base cases for comparison purposes. A review of NFPA 2 requirements cited in the base cases was used to look for proposals to NFPA 2 that may affect these requirements in the next edition of the code. These proposals are currently under review and subject to change, so these analyses may or may not be valid when the next NFPA 2 edition is released. However, it is still useful to consider changes in the next version of the code in order to see how this would affect the reference station designs. Many requirements appear to be unchanged in the next (draft) edition of the code (at least as of this writing), but bulk gaseous setback distances have been reduced significantly, especially Group 1 exposures (which include air intakes and lot lines). Additionally, bulk liquid storage systems that also have bulk compressed hydrogen gas are currently treated as liquid-only (a peculiarity pointed out by this project team); this has been changed in the next (draft) edition. Both of these changes affect the setback distances that the hydrogen system uses and have an impact on station footprint. The effects of these changes are shown in Figure 2.

Although the overall project considers only over-the-road (not pipeline) hydrogen delivery to refueling stations, the assumptions made in the delivery pressure, delivery capacity, and physical dimensions of the delivery truck can have a significant impact on the reference station design and footprint. Low-pressure (and low-capacity) gaseous delivery means that the delivered gaseous reference station would need an unrealistically high number of deliveries to operate near capacity. High-pressure (and higher capacity gaseous) deliveries would alleviate this. Additionally, the higher pressure allows for a smaller physical footprint of the delivery truck, meaning it could be much more maneuverable within the station area. Conversations with experts indicated that, especially for urban sites, the truck should be able to maneuver within the station footprint, rather than assuming the truck can pull directly in or out of the station. Current delivery trucks for

liquid hydrogen tend to be very large, with more than enough capacity for multiple stations. Therefore, considering a smaller truck (with still more than enough capacity for an individual station) will similarly increase maneuverability within the station footprint. The largest reduction in delivery truck size considered was for liquid hydrogen delivery; the effect of this modified truck path on station footprint is illustrated in Figure 3.

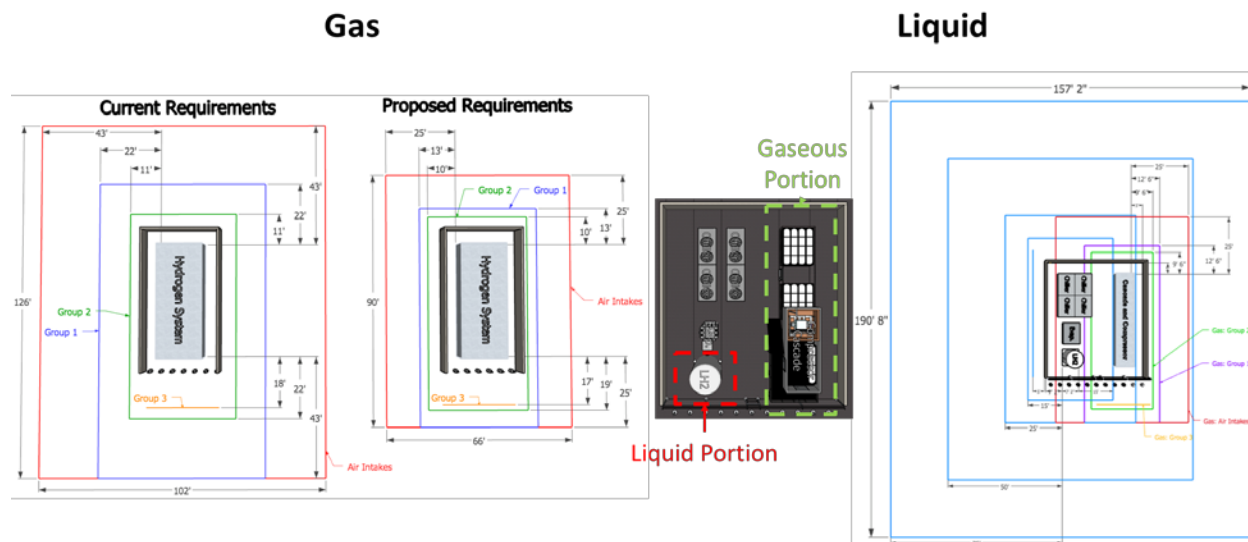


Figure 2. Proposed changes to NFPA 2 setback distances for bulk gaseous hydrogen storage on the left and bulk liquid hydrogen storage on the right

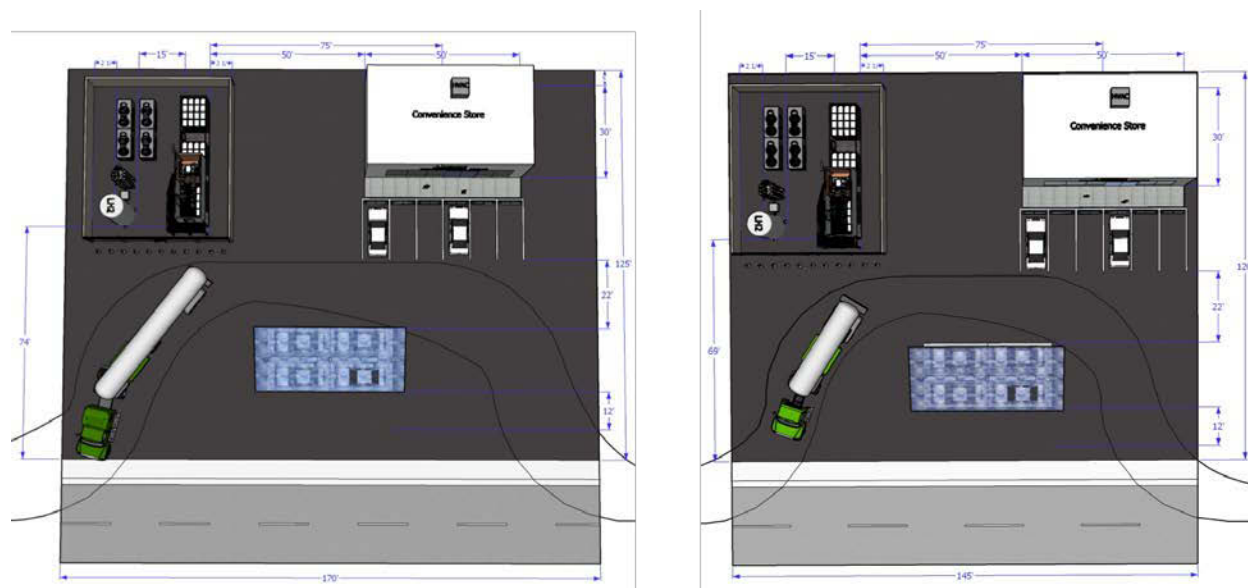


Figure 3. Effect of smaller delivery truck path on full station layout for delivered liquid base case on the left and alternate delivery truck size on right

Another set of designs focused on storing the hydrogen either below ground (direct buried or in a vault) or above ground on an elevated platform. It is expected that both methods would increase the capital cost of the station, although this has not been specifically evaluated yet. Both methods achieved reductions in the refueling station lot size, but the way NFPA 2 is currently written, both of these station designs would need to locate equipment in nonintuitive ways. For example, the underground direct-bury system designs had a very

large layout of underground pressure vessels, each of which needed to be connected to the central at-grade equipment enclosure via welded pipes that are also underground. By contrast, the elevated designs required a huge amount of very heavy equipment be located a significant distance off the ground; it is not clear if any advantage to reducing setback distances can be gained from such a design.

Another set of designs considered the collocation of hydrogen refueling systems on the same lot as gasoline vehicle refueling. This led to larger lot sizes due to the additional fueling capacity, but the gas and liquid hydrogen systems that had delivery did not have a significant increase due to the fact that the gasoline delivery truck could use the same truck path as the hydrogen. By contrast, the electrolysis system with no hydrogen delivery had a large increase in lot size because the gasoline delivery truck needed a large path to be incorporated. The full layouts for delivered gas and electrolysis hydrogen refueling stations collocated with conventional fueling stations are shown in Figure 4.

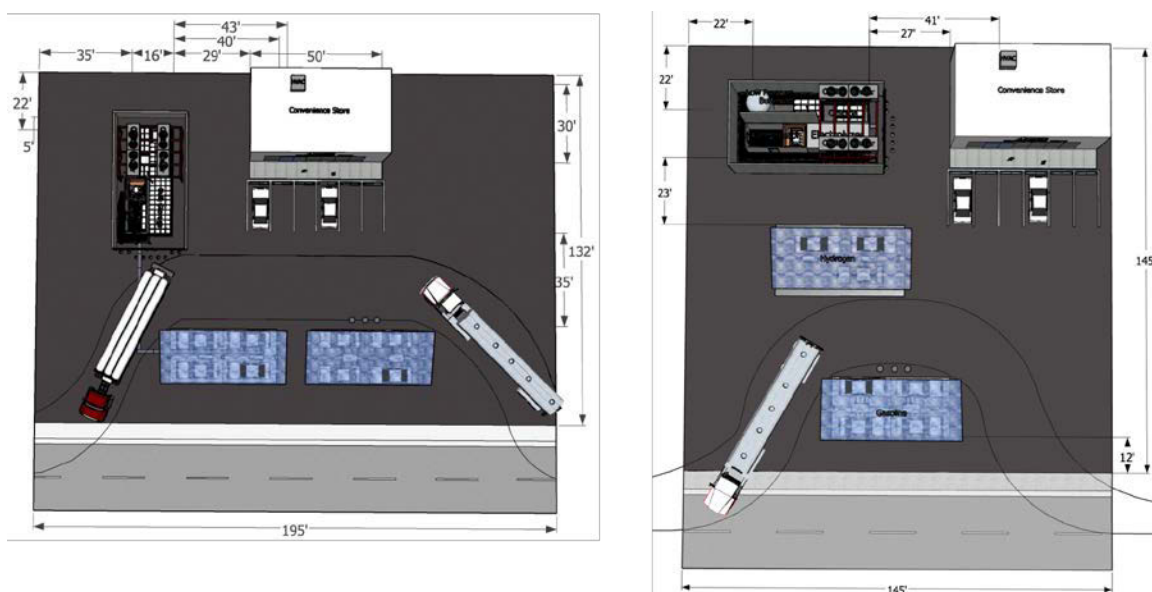


Figure 4. Collocation of hydrogen and conventional refueling stations for delivered gas on the left and electrolysis on the right

A final set of designs focused on other designs that use a performance-based design framework to justify alternate means for not meeting particular setback distances. This was applied to a bulk delivered liquid system that did not meet some of the longest setback distances, but still needed to achieve equivalent levels of safety risk. This analysis led to the identification of some specific issues with the current methodology (as outlined in NFPA 2), which will be addressed next FY. Other designs considered in this category actually met code requirements but seemed to be nonstandard in other ways, such as locating the bulk hydrogen system indoors or changing pipe sizes to reduce the pipe diameter (and associated setback distance). All of these designs achieved refueling station footprint reductions, but it is not clear if they would be technically realistic or economically viable.

Preliminary results for all of these designs and analyses were presented at a workshop in Livermore, California, to various industry experts and stakeholders. This workshop helped identify issues in the analysis that will be addressed next FY but also helped to give confidence to other designs that did not seem to have any significant issues. The preliminary station footprint area values are shown in Table 1, along with how those areas compare to the base case. These values will change as the designs are updated and modified in the next FY.

Table 1. Summary of Preliminary Hydrogen Refueling Station Lot Sizes and Comparison to Base Case Designs

Scenario	Total Lot Area (ft ²)	Reduction from Base Case
Base Case Gas	18,480	–
New NFPA Separation Distances	16,240	12.1%
New Delivery Single Truck	16,500	10.7%
New Delivery Double Truck	16,500	10.7%
Gasoline Colocation	25,740	39.2% (Increase)
Underground Direct-Bury	15,400	16.7%
Underground Vault	13,720	25.8%
Rooftop Storage	16,000	13.4 %
Non-Prescriptive Gas	14,950	19.1%
Base Case Liquid	21,250	–
New NFPA Separation Distances	18,252	14.1%
New Liquid Delivery	17,400	18.1%
Gasoline Colocation	22,040	3.7% (Increase)
Underground Direct-Bury	15,515	27.0%
Rooftop Storage	19,840	6.63 %
Non-Prescriptive Liquid	12,992	38.9%
Base Case	12,051	–
New NFPA Separation Distances	9,180	23.8%
Gasoline Colocation	21,145	75.5% (Increase)
Rooftop	11,020	8.5%

CONCLUSIONS AND UPCOMING ACTIVITIES

On-site production, smaller delivery truck paths, upcoming NFPA 2 requirements, and underground storage can all achieve significant station footprint reduction to varying extents. The economic trade-offs to these design choices have not yet been evaluated.

In the next FY, feedback from the workshop will be incorporated into the station designs. This will also include modifications to the performance-based framework used to justify alternate risk-informed methods for meeting NFPA 2 requirements. An economic evaluation will be performed on the station designs to illustrate trade-offs for various designs that can reduce station footprint. This will also help to show the economic value of reducing the footprint in addition to the ability to site stations in more locations. Similarly, a national siting study will be performed to identify how different amounts of footprint reductions can increase the number of potential sites available for hydrogen fueling stations. The improvements to the risk assessment, economic evaluation, and national siting study will help to identify and inform future needs to further efforts to expand hydrogen fueling infrastructure.

FY 2018 PUBLICATIONS/PRESENTATIONS

1. B.D. Ehrhart, G. Bran-Anleu, E.S. Hecht, C. Rivkin, A. Muna, E. Sena, “Reference Stations for Urban Sites Workshop,” Presented preliminary results and obtained feedback from stakeholders in Livermore, CA, September 6, 2018. SAND2018-9895 PE.

Toyota Mirai Testing

Henning Lohse-Busch (Primary Contact),
Kevin Stutenberg
Argonne National Laboratory
9700 South Cass Ave.
Lemont, IL 60439
Phone: (630) 252-1978
Email: hlb@anl.gov

DOE Manager: Jason Marcinkoski
Phone: (202) 586-7466
Email: Jason.Marcinkoski@ee.doe.gov

Project Start Date: October 1, 2017
Project End Date: September 30, 2018

Overall Objectives

This is the technology assessment of a 2017 Toyota Mirai fuel cell (FC) vehicle using a chassis dynamometer in a controlled laboratory environment and in-depth instrumentation. The objectives are to:

- Establish vehicle level energy consumption, efficiency, and performance data on varying drive cycles at ambient temperatures ranging from 20°F (-7°C) to 95°F (35°C) with a stretch goal of testing a cold start at 0°F (-18°C).
- Generate an efficiency map of the FC system.
- Establish the performance envelope and synergies between the FC system and the hybrid system (including FC system idle).
- Publish an independent data set of a production automotive FC system as a public reference for researchers at DOE, national laboratories, original equipment manufacturers (OEMs), suppliers, standards committees, and academia.

Fiscal Year (FY) 2018 Objectives

This is a one-year project.

Technical Barriers

This project addresses the following technical barrier from the Technology Validation section of

the Fuel Cell Technologies Office Multi-Year Research, Development, and Demonstration Plan¹:

- (A) Lack of Fuel Cell Electric Vehicle and Fuel Cell Bus Performance and Durability Data.

Contribution to Achievement of DOE Technology Validation Milestones

This project will contribute to achievement of the following DOE milestone from the Technology Validation section of the Fuel Cell Technologies Office Multi-Year Research, Development, and Demonstration Plan:

Milestone 2.3: Validate Fuel Cell electric vehicles achieving 5,000-hour durability (service life of vehicle) and a driving range of 300 miles between fuelings (4Q, 2019).

FY 2018 Accomplishments

The chassis dynamometer testing of a fully instrumented vehicle yielded the following accomplishments.

- Determined the performance envelope and synergies between the FC system and the hybrid system.
- Generated an efficiency map of the FC system.
- Measured the hydrogen consumption of the 2017 Toyota Mirai on the standard North American certification drive cycles (EPA Urban Dynamometer Driving Schedule [UDDS], Highway, and US06) at three conditions: 20°F (-7°C); 72°F (25°C), and 95°F (35°C) with 850 W/m² of solar load.
- Determined the FC system idle fuel flow rate.
- Characterized the FC system start-up behavior on a UDDS drive cycle after weekend cold soak at 0°F (-18°C).
- Posted the test data and comprehensive analysis report at www.anl.gov/d3.

¹ <https://www.energy.gov/eere/fuelcells/downloads/fuel-cell-technologies-office-multi-year-research-development-and-22>

INTRODUCTION

The research community is lacking public and independent laboratory-grade data of production automotive FC vehicles. The FC stack and system performance and efficiency data generated in this work serve to refine and validate modeling and simulation work, inform the research target-setting process, and highlight potential challenges that necessitate further research. The testing of the vehicle generated 10-Hz-resolved FC stack, FC system, and hybrid system data to determine component performance envelopes, component efficiencies, and overall control strategies for a range of thermal conditions.

APPROACH

Argonne has been providing technology assessment of advanced technology powertrain vehicles to the DOE Vehicle Technologies Office since the early 2000s. To evaluate a vehicle in a variety of real-world conditions, the team used a chassis dynamometer in a thermal chamber. The test conditions were based on the EPA 5-cycle fuel economy procedures, which included ambient temperatures of 20°F (-7°C), 72°F (25°C), and 95°F (35°C) with 850 W/m² of radiant sun energy. Testing also occurred at 0°F (-17°C). The test cell is set up with passive and active hydrogen safety systems and it is fully equipped to test hydrogen-powered vehicles. The instrumentation focus was on measuring the power flows between the major powertrain components as shown in Figure 1. A Hioki high-precision power analyzer was used to measure the electrical power flows. The hydrogen mass flow was measured with two Micro Motion Coriolis mass flow meters integrated into the test cell. More than 400 significant signals were recorded at 10 Hz for the more than 100 tests. For more detail on the chassis dynamometer testing and the instrumentation approach review Argonne’s “Chassis Dynamometer Testing Reference Document” [1].

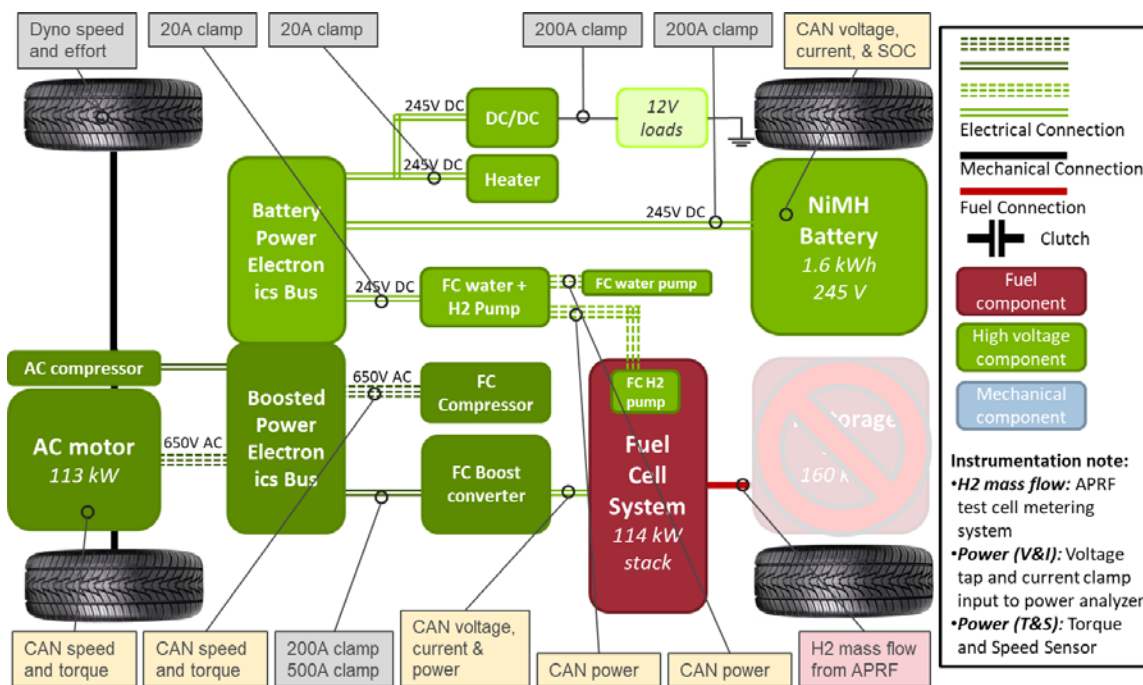


Figure 1. Power flow instrumentation summary

This technology assessment was a collaboration with Transport Canada, which provided a 2017 Toyota Mirai. Table 1 provides some relevant vehicle details.

Table 1. Data Parameters and Powertrain Specifications of the 2017 Toyota Mirai

Vehicle Architecture	FC series hybrid vehicle
Test Weight^a	4,250 lb (1,928 kg)
Road Load^a	A = 32.325 lbf B = 0.20003 lbf/mph C = 0.018292 lbf/mph ²
FC System^b	Solid polymer electrolyte fuel cell 370 cells in stack 114 kW, 3.1 kW/L, 2.0 kW/kg
Battery^b	Nickel-metal hydride, 1.6 kWh, 245 V DC

^a EPA data

^b Manufacturer data

RESULTS

Fuel Cell System and Hybrid System Operation

This powertrain is a FC-dominant hybrid. Similar to the internal combustion engine in a mild hybrid electric vehicle, the FC stack provides the majority of the traction power, the FC stack typically does not operate while the vehicle is stopped, and the FC stack has the ability to turn “off” or idle to enable the car to operate as an electric vehicle momentarily. The open circuit voltage slowly decreases as the FC system idles. Figure 2 illustrates these different powertrain operating modes on the New European Driving Cycle. This drive cycle requires relatively low power (20 kW or less) from the vehicle and at these low power levels the air compressor power consumption is only a few hundred watts, which results in high average FC system efficiency.

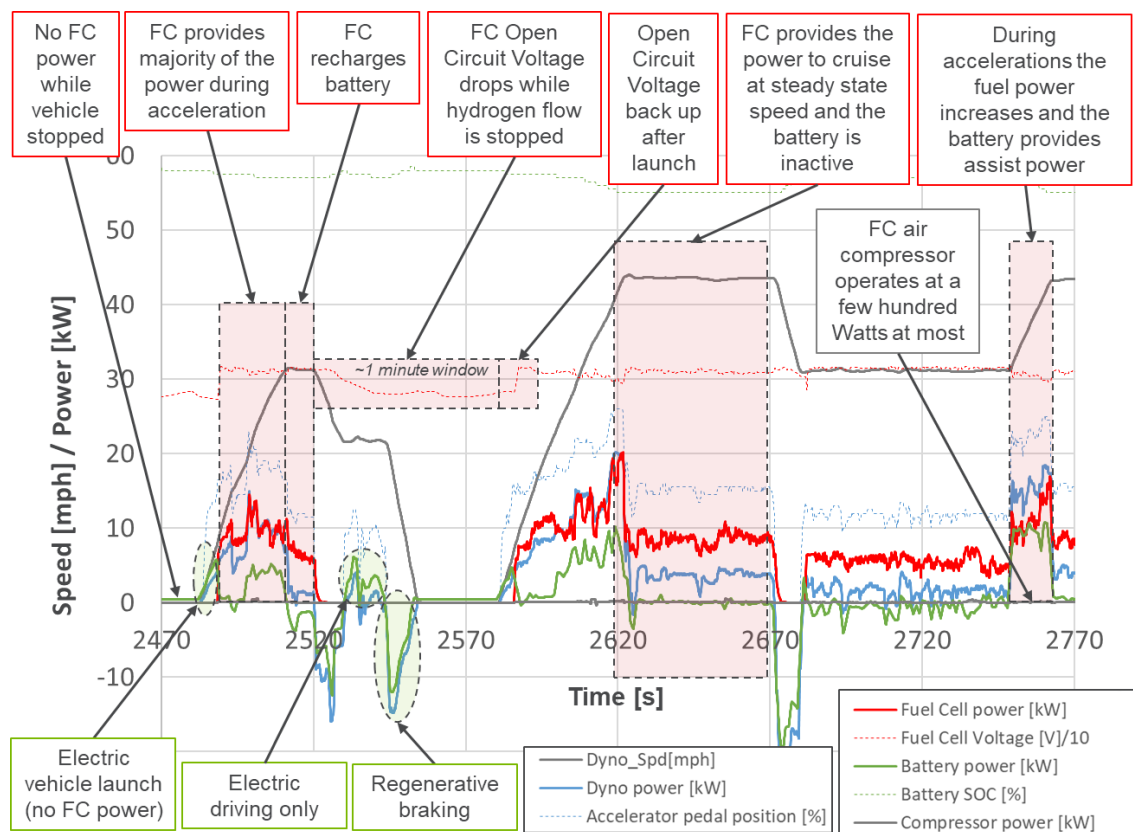


Figure 2. Powertrain and FC system operation in different drive modes on the linear segment drive cycle

On a high-power-demand drive cycle—such as the US06—the FC system demonstrates a great dynamic response that meets the high and fast power swings imposed on the powertrain. The power consumption of the air compressor at high FC stack loads can be up to 15 kW, which negatively impacts the FC system efficiency.

Fuel Cell Stack and System Efficiency Map

The vehicle also was tested at different steady-state speeds and steady-state load points to establish an FC stack and system efficiency map. The FC stack, FC system, and boost converter efficiencies, shown in Figure 3, were derived from the 10 Hz data. Figure 1 defines the system boundaries used to define the FC stack and the FC system.

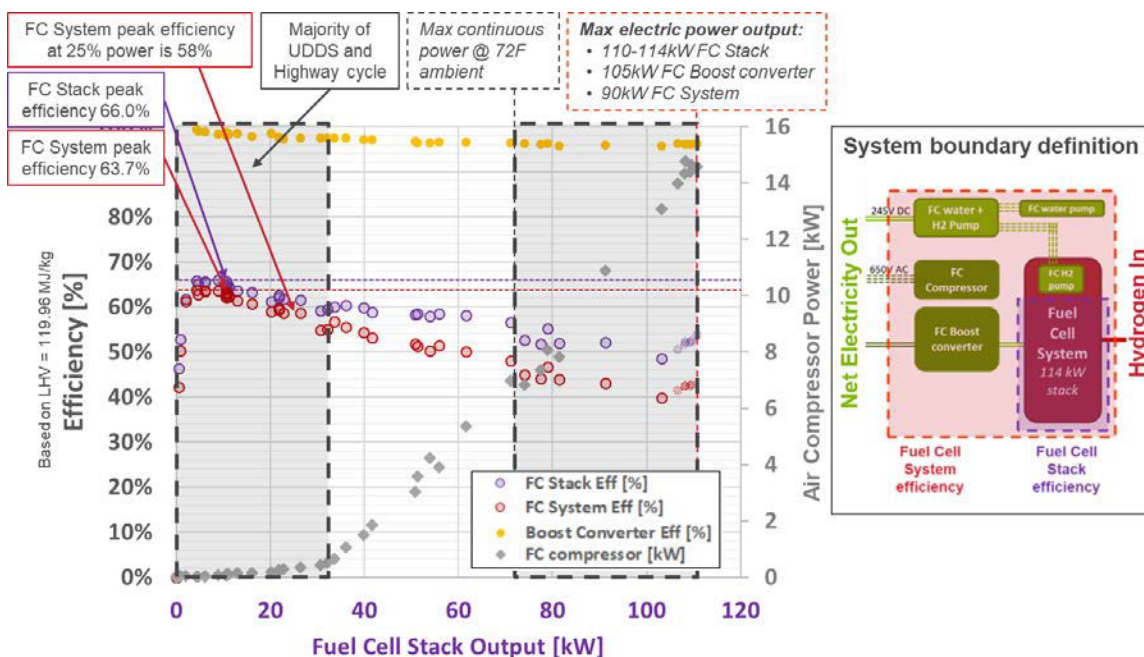


Figure 3. FC stack and FC system efficiency as a function of electric power output of the stack

The measured FC stack peak efficiency is 66.0%. The measured FC system peak efficiency is 63.7%. The FC system efficiency at 25% of maximum power is 58%. The low air-compressor power consumption of a few hundred watts at low stack power (<30 kW) results in high system efficiencies. The majority of the certification drive cycles, as well as typical driving conditions, are characterized by such low power demands, therefore the FC system typically operates in its most efficient range. Toyota redesigned the air-management system and anode flow channels to minimize the auxiliary power losses to the air compressor in this generation FC system [2].

The maximum power output of the fuel cell stack was measured around 110 kW to 114.6 kW depending on the thermal conditions. At these high power levels, the air-compressor consumption is up to 15 kW, which penalizes the FC system efficiency at those conditions. The peak power and the duration of continuous power are highly dependent on the cooling conditions such as ambient temperature and relative wind speed. All the testing was performed with a variable-speed fan that matched the vehicle speed. At 72°F (25°C) on a simulated 25% grade, the fuel cell stack produced 112 kW for 30 seconds and the continuous FC stack power settled at 73 kW with a vehicle speed of 27 mph.

Hydrogen Energy Consumption on Standard Drive Cycles Across Different Temperatures

The hydrogen energy consumption is shown in Figure 4. The energy consumption at 72°F (25°C) for the UDDS and Highway drive cycles are similar. On these low-load drive cycles, the losses attributed to the air compressor and boost converter are almost insignificant. On the higher-power US06 cycle, the boost converter and air compressor losses become significant. The overall average FC system efficiency on the UDDS is 61.8% as compared to 48.1% on the US06. The drop in efficiency is driven by low stack efficiency and higher air-compressor power at the higher loads.

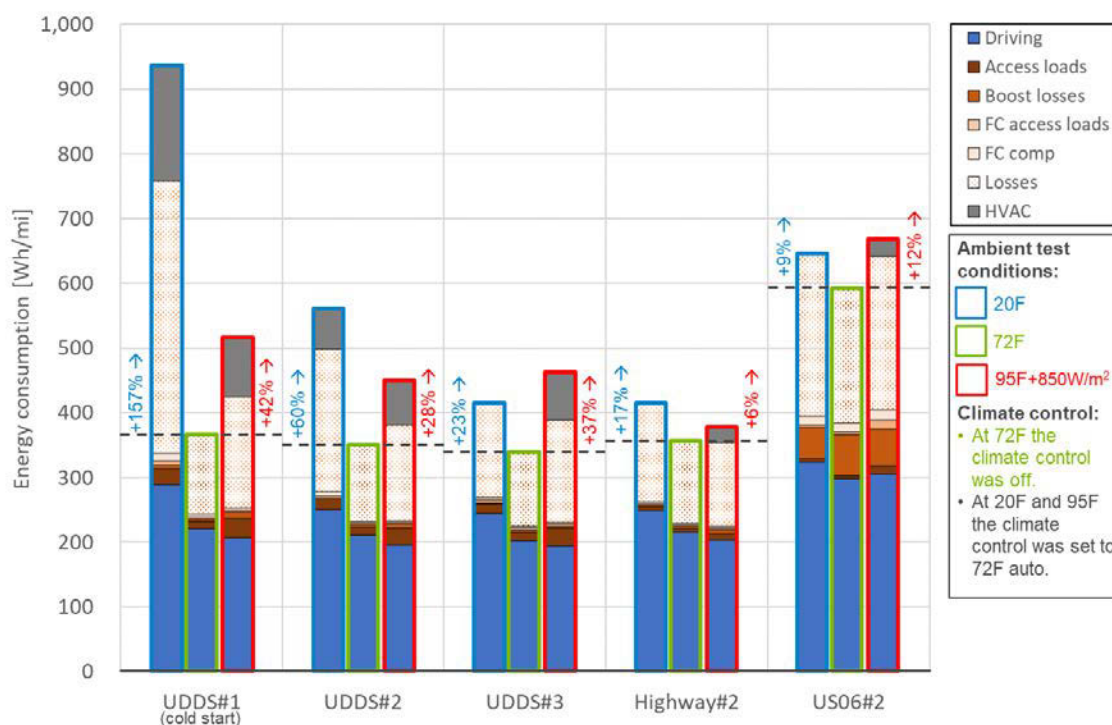


Figure 4. Hydrogen energy consumption and energy breakdown for different drive cycles across different temperatures

Results for the different ambient conditions also are presented in Figure 4. A cold-start test means that the vehicle, and therefore the powertrain, was soaked at the target ambient temperature for more than 12 hours before the start of the test. The Toyota Mirai purges the water from the FC stack when the vehicle is turned off and again when the temperature drops to freezing conditions. The cold-start UDDS cycle energy consumption at 20°F (-7°C) is 1.5 times greater than at 72°F (25°C) due to the electric heating of the FC system and the cabin, as well as the hydrogen used to recondition the dried-out proton exchange membranes. It is noteworthy that the FC system generates enough heat to maintain the cabin temperature at 72°F (25°C) on the third UDDS cycle. The increase in energy consumption at 95°F (35°C) ambient temperature with the 850 W/m² solar energy is driven by the power demand of the high-voltage refrigerant compressor for the climate control system.

Cold Start After a Weekend-Long Thermal Soak at 0°F (-18°C) Ambient Temperatures

The vehicle was temperature soaked over a full weekend at 0°F (-18°C). On the cold-start UDDS cycle, the driving starts 20 seconds after the vehicle is turned on. The electric heater warms up the FC system and extra hydrogen is used to recondition the dry proton exchange membranes. The standard open circuit voltage is achieved after 150 seconds of operation. The FC stack power is limited during these first 150 seconds of the drive cycle and the battery pack provides extra power to meet the acceleration demands. The fuel economy on the 0°F (-18°C) cold-start UDDS cycle is 30 mi/kg/mi of hydrogen, which is 60% less than at 72°F (25°C), as shown in Table 2.

Table 2. Fuel Economy Results in Kilogram of Hydrogen per Mile [mi/kg]

Ambient Conditions	0°F (-18°C)	20°F (-7°C)	72°F (25°C)	95°F (35°C)
UDDS#1 (cold start)	30.0	35.6	91.5	64.5
UDDS#1	39.8	59.5	95.3	74.2
UDDS#3	40.4	80.0	98.7	71.8
Highway	N/A	80.1	94.1	88.6
US06	N/A	51.6	56.1	50.0

Fuel Cell System Idle Fuel Flow Rate

As noted, the FC system turns “off” when FC power is not needed. This FC idle condition produces zero electric power output. To investigate this idle operation, a special 1-hour test was performed. After 505 seconds of driving, the vehicle was put in park and left “on.” The FC system produced no electric power for 1,400 seconds. The data shows that the FC stack is starved for hydrogen to maintain an open circuit stack voltage around 74 V (typical open circuit voltage is 315 V). Periodically, a small amount of hydrogen is released in the system and some air is pushed into the stack. Over the 1,400 seconds of idle, 1.71 grams of hydrogen were consumed, which results in an idle fuel flow rate of 4.39 g/h. The low idle fuel flow rate enables the FC system to have enough reactants in the channels to provide immediate power when needed. After the 1,400 seconds of idling, the state of charge of the high-voltage battery pack had dropped low enough that the FC system produced power to recharge the battery pack.

More Detailed Analysis and Public Data Access

A comprehensive analysis is available in the full report titled *Technology Assessment of a Fuel Cell Vehicle: 2017 Toyota Mirai* [3]. The report along with data files are posted at www.anl.gov/d3. The analysis report provides in-depth details on the following topics:

- Vehicle overview and instrumentation details
- Fuel cell hybrid powertrain operation overview
- Fuel cell stack and system efficiency (steady load mapping)
- Energy and efficiency analysis of certification drive cycle testing and results at 72°F
- Fuel cell system operation (including system operation, idle mode, maximum power analysis)
- Impact of temperatures: 0°F, 20°F, 72°F, and 95°F + 850 W/m² (includes energy analysis, FC system shut down and start up at cold start, power delivery, and hill-climb test).

CONCLUSIONS AND UPCOMING ACTIVITIES

This work was an in-depth technology assessment of a 2017 Toyota Mirai FC vehicle using a chassis dynamometer in a controlled laboratory environment and in-depth instrumentation. The FC stack had a high dynamic response, which enabled this powertrain to be an FC-dominant hybrid electric vehicle. The measured peak efficiency was 66.0% and 63.7% for the stack and FC system, respectively. The maximum stack power output was measured as approximately 110 kW to 114 kW. The overall average FC system efficiency on the UDDS drive cycle (mild city driving) was 61.8% as compared to 48.1% on the US06 drive cycle (aggressive high-speed driving). The FC system efficiency at high load suffered from the air compressor load, which could be as much as 15 kW. The cold-start UDDS cycle energy consumption at 20°F (-7°C) was 1.5 times greater than at 72°F (25°C) due to the electric heating of the FC system and the cabin, as well as the hydrogen used to recondition the dried-out proton exchange membranes. At 0°F (-18°C), the FC stack power was limited during these first 150 seconds of the drive cycle and the battery pack provided extra power to meet the acceleration

demands. The FC system had an idle fuel flow rate of 4.39 g/h while producing zero power output. The low idle fuel flow rate enabled the FC system to have enough reactants in the channels to provide immediate power when needed.

All the raw 10 Hz data along with an in-depth analysis report is available to the public for download at www.anl.gov/d3. This provides much-needed public reference data on an automotive FC system for the research community.

This project is completed. Argonne stands ready to perform a technology assessment on other fuel cell vehicles or advanced technology vehicles for DOE.

ACKNOWLEDGEMENTS

This project is complete. Argonne thanks Transport Canada for its collaboration.

FY 2018 PUBLICATIONS/PRESENTATIONS

1. H. Lohse-Busch, “Technology Assessment of a Fuel Cell Vehicle: 2017 Toyota Mirai,” 2018 DOE Hydrogen and Fuel Cells Program Annual Merit Review and Peer Evaluation Meeting, Project TV149 (June 13, 2018).
2. H. Lohse-Busch, K. Stutenberg, M. Duoba, S. Iliev, M. Kern, B. Richards, and M. Christenson, *Technology Assessment of a Fuel Cell Vehicle: 2017 Toyota Mirai*, ANL Report ANL/ESD-18/12 (Argonne National Laboratory, June 2018).

REFERENCES

1. H. Lohse-Busch et al., “Chassis Dynamometer Testing Reference Document” (July 2013), <https://anl.app.box.com/s/5tllld40tjhhhtoj2tg0n4y3fkwdbs4m3>.
2. T. Hasegawa, H. Imanishi, M. Nada, and Y. Ikogi, “Development of the Fuel Cell System in the Mirai FCV,” SAE Technical Paper 2016-01-1185 (2016). doi:10.4271/2016-01-1185.
3. H. Lohse-Busch, K. Stutenberg, M. Duoba, S. Iliev, M. Kern, B. Richards, and M. Christenson, *Technology Assessment of a Fuel Cell Vehicle: 2017 Toyota Mirai*, ANL Report ANL/ESD-18/12 (Argonne National Laboratory, June 2018).

Fatigue Performance of High-Strength Pipeline Steels and Their Welds in Hydrogen Gas Service

Joseph Ronevich (Primary Contact),^a Zhili Feng,^b
Andrew Slifka,^c Robert Amaro,^d Eun Ju Song,^a
Yanli Wang^b

^a Sandia National Laboratories (SNL)

^b Oak Ridge National Laboratory (ORNL)

^c National Institute of Standards and Technology (NIST)

^d University of Alabama

7011 East Avenue

Livermore, CA 94550

Phone: (925) 294-3115

Email: jaronev@sandia.gov

DOE Manager: Neha Rustagi

Phone: (202) 586-8424

Email: Neha.Rustagi@ee.doe.gov

Project Start Date: October 1, 2015

Project End Date: September 30, 2018

Overall Objectives

- Enable the use of high-strength steel hydrogen pipelines, because significant cost savings can result by implementing high-strength steels as compared to lower-strength pipes.
- Demonstrate that girth welds in high-strength steel pipe exhibit fatigue performance similar to lower-strength steels in high-pressure hydrogen gas.
- Identify pathways for developing high-strength pipeline steels by establishing the relationship between microstructure constituents and hydrogen-accelerated fatigue crack growth (HA-FCG).

Fiscal Year (FY) 2018 Objectives

- Provide a comprehensive study of high-strength steel weld performance in high-pressure hydrogen gas by completing triplicate HA-FCG measurements in multiple high-strength alternate-consumable arc welds at constant hydrogen pressure, load-cycle frequency, and R-ratio = 0.5. (SNL/ORNL)
- Assess viability of lower-cost joining process for high-strength steels by completing triplicate

HA-FCG measurements of friction stir weld at 3,000 psi, load-cycle frequency of 1 Hz, and R-ratio of 0.5. (SNL/ORNL)

- Define microstructure for an “optimized” high-strength steel suitable for pipeline use (i.e., a steel with targeted strength exceeding 100 ksi and HA-FCG similar to lower-strength steels). (SNL)
- Measure elastic-crack tip strains in representative compact-tension (CT) specimen in air and hydrogen and quantify dislocation accumulation at and near strained-crack tip in air and hydrogen (NIST). Calibrate cyclic large-scale plasticity model to measured crack tip strains, and perform parametric modeling study to determine the coupled load-rate and hydrogen diffusion-rate interactions.

Technical Barriers

This project addresses the following technical barriers from the Hydrogen Delivery section of the Fuel Cell Technologies Office Multi-Year Research, Development, and Demonstration (MYRDD) Plan¹:

(D) High As-Installed Cost of Pipelines

(K) Safety, Codes and Standards.

Technical Targets

This project impacts the following technical targets for hydrogen delivery components from the Fuel Cell Technologies Office MYRDD Plan related to pipelines for gaseous hydrogen delivery:

- Total capital investment: 695,000 \$/mile (FY 2020)
- Transmission pressure: 100 bar (FY 2020)
- Lifetime: 50 years (FY 2020).

Direct reductions in capital costs would be realized if higher-strength steels with thinner-wall pipes were permitted in ASME code (ASME B31.12 [1])

¹ <https://www.energy.gov/eere/fuelcells/downloads/fuel-cell-technologies-office-multi-year-research-development-and-22>

for hydrogen pipelines. Furthermore, understanding the performance baseline of high-strength welds in high-pressure hydrogen is necessary to gaining acceptance of high-strength hydrogen pipelines.

FY 2018 Accomplishments

- Completed at least two fatigue crack growth rate tests on four different high-strength X100 pipeline welds (W1, W3, W4, and a friction stir weld (FSW)). Tests were completed under 21 MPa hydrogen gas at 1 Hz and R=0.5, and results were compared to original X100 weld and lower-strength welds that showed only slightly higher fatigue crack growth rates (FCGR) in high-strength welds compared to lower-strength welds.
- Measured residual stresses in collaboration with University of California Davis on X100 weld and heat-affected zone, and published a paper in *Engineering Fracture Mechanics*.
- Examined influence of microstructure on HA-FCG based on gradient microstructures, microstructure orientation, and grain-size effects. Found that microstructure orientation has the largest (up to 5X) influence on HA-FCG compared to microstructure constituents and grain size (2X). This suggests that microstructural control of grain-boundary interfaces could affect HA-FCG performance in pipeline steels.
- Quantified elastic-crack tip strains as a function of distance in front of a crack tip in representative CT specimens. Measurements conducted in both air and 5.5 MPa pressurized hydrogen by use of Argonne National Laboratory's synchrotron X-ray source. Data collected were also used to determine dislocation density as a function of distance in front of the crack tip.
- Fatigue and fracture damage model was implemented in the finite-element code ABAQUS. The damage model predicts the onset of crack growth as a function of strain fields resulting from a crack tip.

INTRODUCTION

Steel pipelines represent an economical means of transporting gaseous hydrogen over long distances; however, it is well known that these carbon-manganese steels are susceptible to hydrogen degradation. Current steel pipeline codes (e.g., ASME B31.12 [1]) place limitations on higher-strength pipes due to the assumption that higher-strength pipes are more susceptible to hydrogen embrittlement than lower-strength grades. Recent testing [2–4] of pipeline steels with a range of specified minimum yield strength (SMYS) from 358 MPa to 689 MPa have not exhibited this trend and suggest that HA-FGR may not increase with strength. Given the recent results, the B31.12 code committee is reassessing the current limitations placed on higher-strength pipes, which would help reduce material and installation costs.

This project focuses on developing a pathway to enable the use of high-strength steel pipes. One means to accomplishing this goal is to assess the fatigue performance of high-strength steel pipelines under high-pressure hydrogen gas. The fatigue crack growth rate (da/dN) versus stress-intensity factor range (ΔK) relationship is a necessary input to structural integrity models applied to steel hydrogen pipelines. One specific assessment methodology for steel hydrogen pipelines is published in ASME B31.12 code [1], which requires testing of the base metal, weld, and heat-affected zone. One of the gaps is the fatigue performance of high-strength steel welds and whether the behavior will follow the same trends that the base metal exhibited over the SMYS range. The performance of the steel base metals or welds may vary as function of microstructure; therefore, development of physics-based relationships between FCGRs and microstructure would greatly enhance the structural integrity models and drastically reduce the test-burdening required to qualify materials for hydrogen use. The relationships between microstructures, contained in high-strength steels and welds, and hydrogen-assisted fatigue are evaluated in this study.

APPROACH

The objectives for this project are the following: (1) evaluate if girth welds in high-strength steel pipe exhibit fatigue performance similar to lower-strength steels in high-pressure hydrogen gas and (2) identify pathways for developing high-strength pipeline steels by establishing the relationship between microstructure constituents and HA-FCG. Based on these project objectives, the technical tasks are designed to furnish innovative high-strength steel products for evaluation and to measure performance metrics for these high-strength steel products (i.e., FCGRs under hydrogen gas) with high reliability. In this work, five different high-strength welds were examined to provide overall assessment of high-strength weld behavior in hydrogen. Included in this weld study was examination of a friction stir weld (FSW), an alternative that uses a non-consumable tool for welding, which provides a possible lower-cost joining option. Completion of these tasks will assist in reaching the goal of this work: the deployment of steel pipe with reduced wall thickness, which can lower costs for hydrogen pipeline installation.

RESULTS

Rate tests of HA-FCG were performed under 21 MPa hydrogen gas at $R=0.5$ and test frequency of 1 Hz for four high-strength pipeline welds. The welds were fabricated by ORNL using the same X100 base metal. Three different filler metals were used to fabricate welds: W1, W3, and W4. Additionally, an FSW was fabricated, which is an autogenous weld (e.g., no filler metal added). Test coupons were extracted from the center of each weld in the orientation such that the crack would extend radially outward through the wall. A minimum of two tests were performed for each weld as well as the heat affected zone of the FSW and X100A welds. The results are shown in Figure 1 for the high-strength welds compared to previously tested lower-strength welds. The results show some variability in the FCGR of the higher-strength welds; however, collectively, the higher-strength welds exhibit slightly higher FCGR compared to the lower-strength welds. The red dashed line in Figure 1 represents the ASME B31.12 design curve [6], which was recently approved for design of steels up to SMYS of 70 ksi and pressures of 21 MPa. The results show that most of the weld data fall below this design curve, which suggests potential use of these higher strengths in the future.

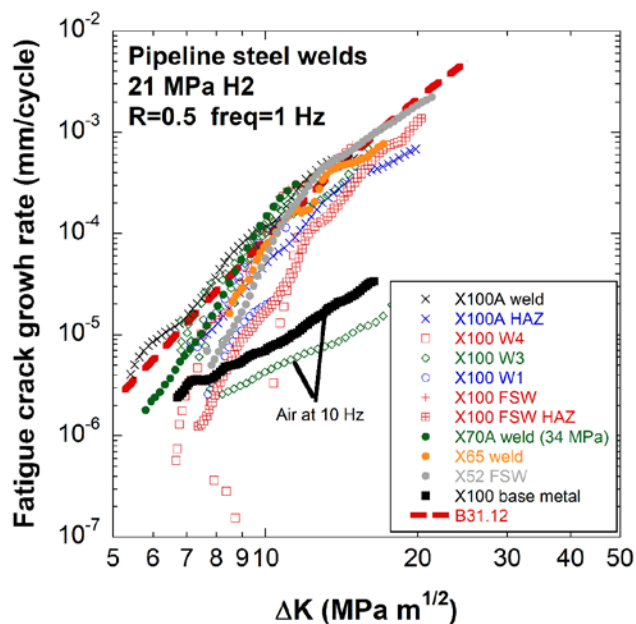


Figure 1. FCGR (da/dN versus ΔK_{app}) curves for high-strength pipeline steel welds compared to low-strength welds tested in 21 MPa H₂ gas. Tests performed in air at 10 Hz are shown for comparison along with B31.12 curve.

Residual stresses can be quite large in welds, particularly higher-strength welds; therefore, measurements of residual stress were conducted in collaboration with the University of California Davis to determine their magnitude and effect on FCGR. Figure 2a shows the residual stress influence on stress intensity factor (K_{res}) for duplicate measurements of the high-strength welds. Using the K_{res} , the FCGR curves were corrected such that the influence of residual stress was removed. The corrected FCGR curves (da/dN vs ΔK_{corr}) shown in Figure 2b exhibit a slightly narrower band compared to the raw data shown in Figure 1. The results suggest that higher-strength welds exhibit a range of FCGRs that are only slightly higher compared to lower-strength welds. Note that the residual stress was not measured on lower-strength welds.

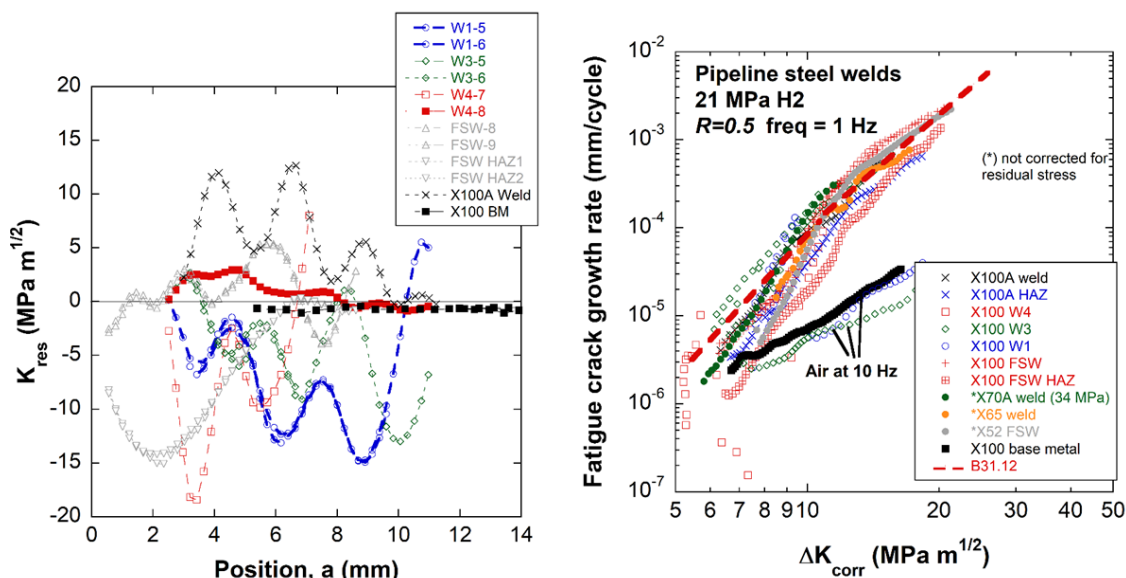


Figure 2. (a) Residual stress effects on K (e.g., K_{res}) as a function of position for high-strength steel welds. (b) FCGR curves for high-strength welds tested in 21 MPa hydrogen gas corrected for residual stress.

A Gleeble sample was fabricated and residual stresses were removed through a 2% rolling reduction on the sample. A constant ΔK test was performed at $10 \text{ MPa m}^{1/2}$ at $R=0.5$ and 1 Hz. The FCGR results are shown in Figure 3a. Microscopy was performed on select regions that demonstrated variations in FCGR as shown in Figure 3a. Region A consisted of coarse ferrite/bainite, region B was fine ferrite/bainite, and region C was ferrite/martensite. It is clear from the microscopy that the regions contained significantly different microstructural features, yet the difference in da/dN was less than a factor of 2, which suggests that the microstructural constituents examined have a small effect on FCGR.

The role of grain size and orientation of crack propagation were examined on X60 and X100 steels. The as-received X60 steel microstructure consisted of equiaxed 7- μm grain-size polygonal ferrite that was isotropic in nature, as shown in the inset image of Figure 3b. Tests were performed in T and R directions, which showed very similar FCGR in a hydrogen environment. The sample was heat treated at 1,100°C for 2 h to obtain a microstructure of 70- μm grain size. Tests were performed in the T direction and compared to the finer grain size. The coarse (70- μm) material exhibited slightly lower FCGR at lower ΔK and slightly higher FCGR above $\Delta K = 10 \text{ MPa m}^{1/2}$. Overall, the differences observed with testing orientation and grain size were less than a factor of 2. The X100 steel consists of an anisotropic microstructure of bainite with finer grain size (e.g., features less than 1 μm). Specimens were tested in both the L and R orientations, as shown in Figure 3c. The microstructure was elongated, due to the rolling process, in the L orientation, which means that a propagating crack in the L direction would be parallel to the elongated features and a crack in the R direction would be perpendicular to these features. The resulting FCGR measurements were significantly different in the two orientations. The measured FCGRs were nearly 5 times slower in the R direction than in the L direction, which suggests that interfaces play an important role in controlling FCGR.

The elastic-crack tip strains in a CT specimen were measured as a function of distance in front of the crack tip and ΔK . The measurements were performed in air and 5.5 MPa hydrogen by use of a novel test apparatus created at NIST and at the high-energy X-ray source at Argonne National Laboratory. The data were then used to determine the spatial dislocation density in a CT specimen. Data were also used in conjunction with strain-controlled test results to calibrate a large-scale cyclic plasticity material deformation model implemented in the finite-element platform ABAQUS. In the absence of the ability to quantify plastic strains within the crack-tip plastic zone, the solutions of models having varying crack-tip radii were compared to the measured strain solution. The CT-specimen strains resulting from a model having a blunted crack tip of 5- μm radius match the experimentally measured strains in the far field, so this work has provided sufficient evidence to support the use of a blunted crack tip, on the order of 5 μm , when modelling cracks in ABAQUS. Using this information, a fatigue and fracture-damage model has been implemented in ABAQUS. The damage model predicts the onset of crack growth as a function of strain fields resulting from a crack tip.

Constant $\Delta K = 10 \text{ MPa m}^{1/2}$

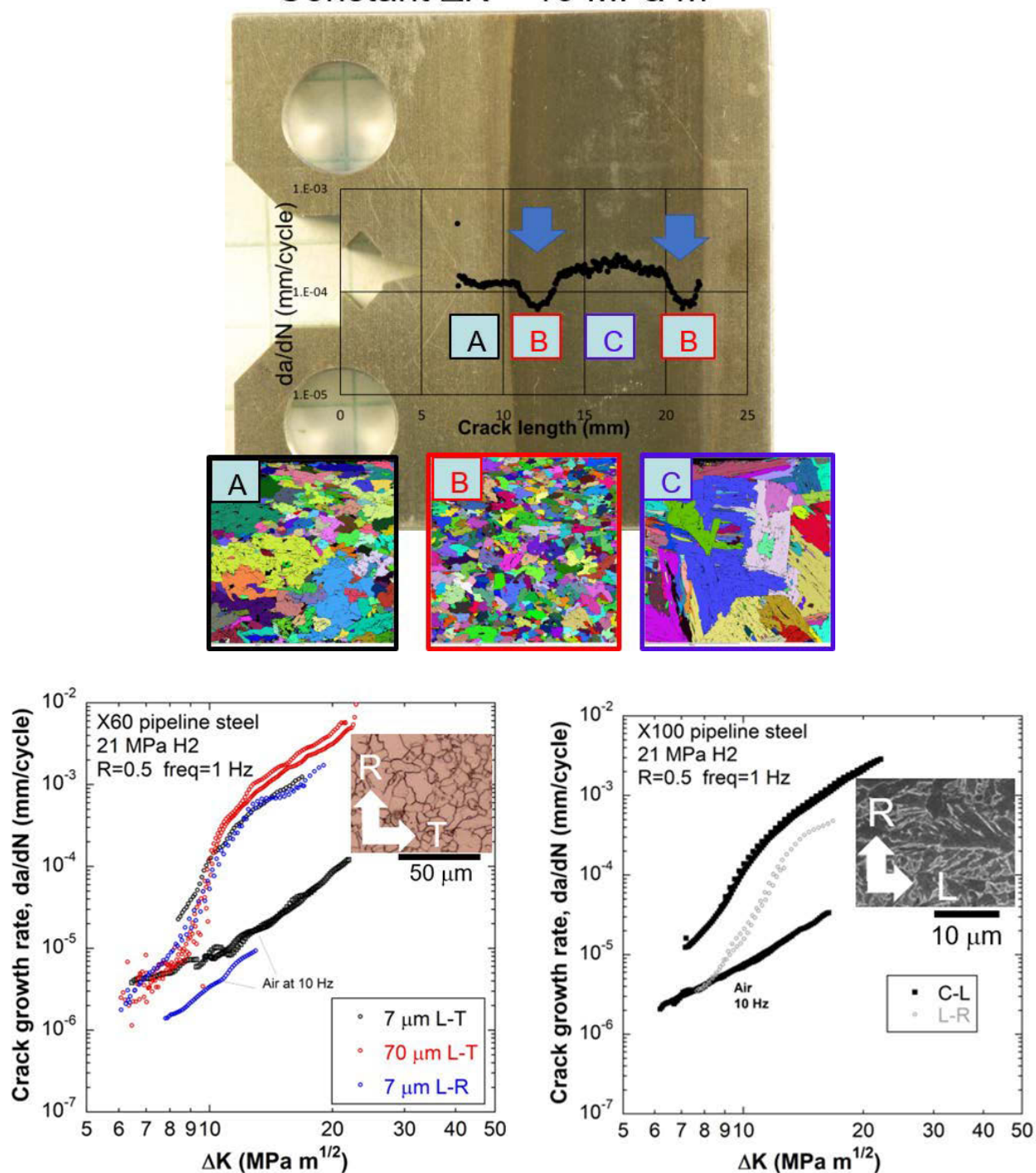


Figure 3. (a) Compact tension specimen with fatigue crack growth rate curve overlaid to show changes in da/dN as a function of microstructure. Region A consisted of coarse ferrite/bainite, region B consisted of fine ferrite/bainite, and region C consisted of ferrite/martensite. (b) da/dN curves of X60 pipeline steel in 21 MPa hydrogen showing differences in FCGR with grain size (7 and 70 μm) and orientation (L-R vs L-T). (c) da/dN curves of X100 pipeline steel in 21 MPa hydrogen comparing differences in FCGR with orientation (L-R vs C-L).

Parametric studies were performed using the calibrated deformation model to determine the effect of crack extension-hydrogen diffusion interactions. Results of the first parametric study indicate that the differences in hydrogen diffusivities exhibited by the common microstructures found in pipeline and pressure-vessel steels were insufficient to cause an effect on HA-FCG. Specifically, the first study indicates that the rate of hydrogen diffusion to the crack tip was dominated by the rate of loading and frequency of loading of the crack tip rather than the individual microstructure diffusivities. Subsequent parametric studies were performed in which the steel matrix was saturated with hydrogen. This boundary condition is indicative of in-service conditions for carbon steels because the diffusivities are sufficiently high to fill the lattice trap sites within minutes or hours. The second study found that the rate of change of the hydrogen diffusion trends with the rate of change of crack extension (per cycle) for ΔK values below about $15 \text{ MPa}\cdot\text{m}^{1/2}$ as shown in Figure 4. Once the ΔK values exceed about $15 \text{ MPa}\cdot\text{m}^{1/2}$, the rate of change of hydrogen diffusion saturates and therefore lags behind the rate of change of crack extension (per cycle). The studies indicate that the rate of hydrogen flux to the front of a moving crack tip is driven by the crack-tip loading rate and not by the material diffusivity. As the loading rate increases, up to a critical value (about $15 \text{ MPa}\cdot\text{m}^{1/2}$ per cycle), the rate of hydrogen flux to the crack tip also increases. Above the critical loading rate, the effect of the stress-driven hydrogen flux rate saturates. These results suggest that the transition in HA-FCG behavior exhibited by most steels at about $15 \text{ MPa}\cdot\text{m}^{1/2}$ results from the interaction of FCGR and stress-driven hydrogen flux rates, and not from material diffusivity (for diffusivities found in pressure-vessel and pipeline steel microstructures). The results were compared for loading frequencies of both 1 Hz and 0.01 Hz. Ultimately, the combined results of the two parametric studies suggest that the rate of change of the crack-growth driving force is the primary indicator of HA-FCG morphology. These statements above are merely correlations, but the parametric studies from this project have provided the ability to explore these theories beyond what experimental testing can provide. For example, testing at very low frequencies or the effects of a wide range of diffusivities cannot easily be performed in a laboratory; but these simulations allow us to explore the effects on hydrogen to theorize the role that these variables have in hydrogen accumulation.

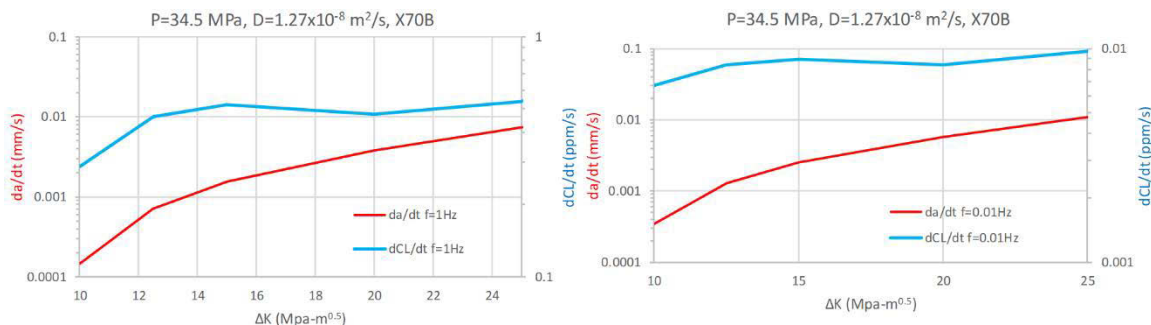


Figure 4. Results of parametric modeling study to determine the interaction between fatigue crack growth rate and hydrogen diffusion, as a function of applied ΔK and load frequency. Results indicate that the hydrogen diffusion rate saturates at an applied ΔK of $\sim 15 \text{ MPa}\cdot\text{m}^{1/2}$. Beyond this value of ΔK , the change in hydrogen diffusion rate no longer keeps pace with the change in FCGR. (a) Study results for load frequency of 1 Hz. (b) Study results for load frequency of 0.01 Hz.

CONCLUSIONS AND UPCOMING ACTIVITIES

- A comprehensive study of fatigue performance of high-strength pipeline steel welds was performed on five different X100 pipeline welds in high-pressure hydrogen gas. Variability in FCGR was attributed to residual stress in welds compared to the base metals. High-strength welds were observed to have only slightly higher FCGR compared to lower-strength welds, which suggests that higher-strength welded pipes could be used for hydrogen with proper design.
- (Future) One distinct gap that was identified was the lack of fracture-toughness data on pipeline welds. This is likely due to the challenges associated with extracting valid tests from localized regions. Sandia

is planning to perform fracture testing on a variety of strength welds using carryover funds from this project in FY 2019.

- Laboratory-controlled microstructures were developed using a Gleeble and specialized heat treatments to examine the role of microstructural constituents, grain size, and grain orientation on susceptibility to HA-FCG. Of all the variables tested, microstructural orientation (e.g., induced from the rolling process) was observed to have the most dramatic effect on reducing HA-FCG. When the crack was oriented perpendicular to the rolling direction, HA-FCG was reduced up to 5 times compared to when the crack was oriented parallel to the rolling direction. This suggests that the role of interfaces (e.g., grain boundary) have a significant effect on suppressing HA-FCG.
- Elastic strain fields were characterized for the CT specimen crack tip as a function of ΔK , distance in front of the crack tip, and environmental conditions. Dislocation density was characterized for CT specimen crack tip as a function of ΔK , distance in front of the crack tip, and environmental conditions. A large-scale cyclic plasticity material model was implemented and calibrated to strain-field measurements in air. A crack initiation/extension damage model has been implemented in ABAQUS and calibrated to experimental results in air.
- (Future, as a function of ongoing work with the U.S. Department of Transportation) Large-scale cyclic plasticity material model to be calibrated to strain-field measurements in hydrogen. Crack initiation/extension damage model to be calibrated to experimental results in hydrogen.

SPECIAL RECOGNITIONS AND AWARDS/PATENTS ISSUED

1. R&D100 Award: Feng, Z., Yu, X., Wang, Y., David, S., Tzelepis, D.A., Gerth, R. J., Anderson, J., Douglas, J. “Filler Materials for Welding and 3D Printing.”

FY 2018 PUBLICATIONS/PRESENTATIONS

1. J.A. Ronevich, C.R. D’Elia, M.R. Hill, “Fatigue crack growth rates of X100 steel welds in high pressure hydrogen gas considering residual stress effects,” *Engineering Fracture Mechanics* 194 (2018): 42–51.
2. M. Connolly, P. Bradley, A. Slifka, D. Lauria, E. Drexler, “In situ synchrotron X-ray measurements of strain fields near fatigue cracks grown in hydrogen,” *Materials Research Proceedings* 4 (2018): 17–22.
3. J.A. Ronevich et al., “Fatigue performance of high-strength pipeline steels and their welds in hydrogen gas service,” Presentation at the DOE Hydrogen and Fuel Cells Program Annual Merit Review, Washington D.C., June 2018.
4. J. Ronevich et al., “Hydrogen Accelerated Fatigue Crack Growth of Multiple X100 Pipeline Steel Welds,” International Conference on Metals and Hydrogen, May 29, 2018.
5. E.J. Song et al., “Correlating Steel Pipeline Microstructure to Fatigue Crack Growth Rates in High Pressure Hydrogen Gas,” International Conference on Metals and Hydrogen, May 29, 2018.
6. E.J. Song, J.A. Ronevich, “Orientation dependence of hydrogen accelerated fatigue crack growth rates in pipeline steels,” PVP2018-84835. Proceedings of ASME 2018 Pressure Vessel & Piping Conference, July 2018.
7. J. Ronevich et al., “Fatigue Performance of High-Strength Pipeline Steels and Their Welds in Hydrogen Gas Service,” Hydrogen Delivery Tech Team meeting, February 28, 2018.
8. G. Rawls, J. Ronevich, A. Slifka, “Lowering costs of hydrogen pipelines through use of fiber reinforced polymers and modern steels,” Fuel Cell Technologies Office Webinar, September 27, 2017.
9. J. Ronevich, R. Amaro, “Enhancing reliability and reducing costs of steels in hydrogen service through predictive computational modeling, advanced imaging, and high-pressure experimentation,” Inter-agency Working Group presentation, April 17, 2018.

10. R.L. Amaro, C.P. Looney, M.J. Connolly, T.C. Cauthen, A.V. Woods, A.J. Slifka, “Parametric study of hydrogen diffusion in steel alloys through macroscopic and mesoscopic finite element modeling,” 12th International Conference on Fatigue Damage of Structural Materials, September 16–21, 2018, Hyannis, MA.
11. C.P. Looney, Z.M. Hagan, E.S. Drexler, P.E. Bradley, A.J. Slifka, R.L. Amaro, “Modelling the test methods used to determine material compatibility for hydrogen pressure vessel service,” 12th International Conference on Fatigue Damage of Structural Materials, September 16–21, 2018, Hyannis, MA.

REFERENCES

1. ASME. B31.12 Hydrogen Piping and Pipelines (New York, NY: ASME, 2011).
2. A.J. Slifka et al., “Fatigue crack growth of two pipeline steels in a pressurized hydrogen environment,” *Corrosion Science* 78 (2014): 313–321.
3. J.A. Ronevich, B.P. Somerday, C.W. San Marchi, “Effects of microstructure banding on hydrogen assisted fatigue crack growth in X65 pipeline steels,” *Int. J. of Fatigue* 82 (2016): 497–504.
4. C. San Marchi, B.P. Somerday, K.A. Nibur, D.G. Stalheim, T. Boggess, S. Jansto, “Fracture Resistance and Fatigue Crack Growth of X80 Pipeline Steel in Gaseous Hydrogen,” in ASME Pressure Vessels & Piping Division (Baltimore, Maryland: ASME, 2011).
5. J.R. Fekete, J.W. Sowards, R.L. Amaro, “Economic impact of applying high strength steels in hydrogen gas pipelines,” *International Journal of Hydrogen Energy* 40 (2015): 10547–10558.
6. ASME. B31.12 Hydrogen Piping and Pipelines (New York, NY: ASME, 2018 expected).
7. R.L. Amaro, E.S. Drexler, A.J. Slifka, “Fatigue crack growth modeling of pipeline steels in high pressure gaseous hydrogen,” *International Journal of Fatigue* 62 (2014): 249–257.

700-bar Hydrogen Dispenser Hose Reliability Improvement

Kevin Harrison (Primary Contact), Owen Smith
National Renewable Energy Laboratory
15013 Denver West Parkway
Golden, CO 80401-3305
Phone: (303) 384-7091
Email: Kevin.Harrison@nrel.gov

DOE Manager: Neha Rustagi
Phone: (202) 586-8424
Email: Neha.Rustagi@ee.doe.gov

Project Start Date: July 2013
Project End Date: Project continuation and direction determined annually by DOE

Overall Objectives

- Characterize and improve the reliability of 700-bar hydrogen refueling hose assemblies, and ultimately reduce the cost of dispensing hydrogen into fuel cell electric vehicles, by working closely with original equipment manufacturers (OEMs), such as SpirStar and others developing advanced high-pressure hydrogen hoses, to identify points of failure.
- Operate a fully automated test system that unifies the four stresses of pressure, temperature, time, and bending.
- Identify compounding impacts of high-volume 700-bar fuel cell electric vehicle refueling that has yet to be experienced in today's low-volume market.
- Determine any relative changes in bulk properties and degradation mechanisms of the inner hose liner due to the stress of repeated fueling events using pre- and post-cycling chemical and physical analysis.

Fiscal Year (FY) 2018 Objectives

- Continue hose cycling toward 25,000 cycles or until failure using the test apparatus that unifies the stresses to which the hose is subjected during high-volume fueling events.
- Gather and analyze data on hydrogen leakage rates, timing, and sources through the use of a vacuum sampling pump system with combustible gas detectors and the deployment of chemochromic leak-indication tape.
- Use data and observations to help inform preventative-maintenance schedules and standards development for hydrogen stations.
- Perform post-failure materials testing on failed field samples to further understand potential design flaws and stressors on the inner layer.

Technical Barriers

This project is conducting applied research, development, and demonstration to reduce the cost of hydrogen delivery systems. This project addresses the following technical barriers from the Hydrogen Delivery section of the Fuel Cell Technologies Office Multi-Year Research, Development, and Demonstration Plan¹:

- (I) Other Fueling Site/Terminal Operations
- (J) Hydrogen Leakage and Sensors.

Technical Targets

This project aims to generate data that will help OEMs and hose developers improve reliability and replacement intervals for high-pressure gaseous hydrogen dispenser hoses. The data provided by this project ultimately will reduce the cost of hydrogen delivery from the point of production to the point of use in consumer vehicles by providing robust dispenser operation with reduced

¹ <https://www.energy.gov/eere/fuelcells/downloads/fuel-cell-technologies-office-multi-year-research-development-and-22>

maintenance costs and improved customer satisfaction.

- Target hose replacement interval: 25,000 cycles
- DOE ultimate target cost of hydrogen delivery: <\$2.00/gge.

FY 2018 Accomplishments

- Completed more than 5,000 cycles on Hose Assembly #2, running various cases of SAE J2601 H70-T40. Upgrades were implemented to the hose test stand to add hydrogen recycling and full-flow tankless capability analogous to SAE J2601 mass flow rates.
- Analyzed failed sample from field deployment of hydrogen refueling hose.
 - Pinhole leak observed at ~1,000–2,000 cycles, located 35 mm from nozzle end crimp fitting. Leak occurred despite using bend restrictors on hoses.
 - Steel overwrap braid layers observed as intact. Polyoxymethylene core around pinhole leak appeared to have significant impression damage from steel braids.

- Using optical microscopy and depth composition at 1,000-times magnification, groove impression depths were measured at 18 μm to 21 μm , a factor of 6 to 7 times deeper than a sample of pre-cycled hose with 2.5–3.2 μm impressions.
- Examined failure mode of pinhole leak and found evidence of plastic deformation and expanded polymer fibers near one end of pinhole. Other areas of pinhole exhibited sharp edges and loose fibers consistent with shear failure.
- Explored for evidence of high-density blistering on polyoxymethylene inner wall caused by hydrogen decompression. High-density blistering results were inconclusive, but large blister was observed 5 mm from failure with an area of 1,375 μm^2 , protruding 17 μm into hose core.
- Disseminated results and findings to OEMs, field station operators, and codes and standards groups to help inform inspection requirements and standards development.

INTRODUCTION

Operation and maintenance costs of dispensing are a large part of the cost of hydrogen stations. The National Renewable Energy Laboratory (NREL) has found that about 41% of maintenance hours for hydrogen fueling retail stations are associated with dispensers, with about 10% of those hours attributed to failed parts. This data can be found in NREL's infrastructure composite data products (CDPs) CDP-INFR-21 and CDP-INFR-24 [1]. These CDPs provide an early look at maintenance and reliability issues of the retail 700-bar vehicle refueling stations. Station operators have reported that they are replacing the high-pressure hoses earlier than expected, in intervals of a few months. Although high-pressure hoses are not a high-capital-cost item as compared to the nozzle and breakaway, the frequency of replacement could result in the high-pressure hoses becoming a significant lifetime cost over 10 years. This project focuses on accelerating the cycle rate, monitoring the leakage patterns, and continuing past the point of typical replacement to supply the OEMs with valuable data on post-cycled specimens to improve reliability.

APPROACH

This project aims to perform long-duration, accelerated life testing on commercial or prototype hose assemblies using high-pressure, low-temperature hydrogen to achieve realistic precooled fueling conditions closely following the SAE International J2601-2014 fueling protocol. This work is unique and goes beyond standard OEM and certification standards agency acceptance testing in that it simultaneously stresses the hose assembly by applying mechanical bending and twisting stress to the hose and nozzle assembly to simulate people refueling vehicles. The short time in between back-to-back fills simulates a busy station where the dispensing equipment is kept cold most of the time and subjected to frequent decompression and thermal cycles.

A hose reliability test stand, shown in Figure 1, was developed to support full 700-bar fueling simulation capabilities. The test stand uses a six-axis robot with pre-programmed motion paths to capture realistic stresses resulting from human interaction with the hose assembly while maintaining a compact footprint to safely operate in the high-pressure test bay, which offers a safe and controlled environment to test components to failure under high pressure while minimizing dangers to personnel or equipment. The test stand closely mirrors an actual dispenser in its design and pressure-ramping capabilities. A tankless control algorithm was successfully developed using the interaction of an air-loaded pressure regulator on the dispenser side of the test apparatus and flow control valves on the vehicle side. In FY 2018, upgrades were performed on the stand to add hydrogen recirculation capability and boost flow rates from 200 g/fill to 3–5 kg/fill.

The leakage rate of the hose is monitored over time using a hydrogen vacuum-pump sampling system attached to an outer protective sleeve near each flared crimp fitting to identify leaks as they occur. The flow rate is set to 400 mL/min and was calibrated to measure delayed response times. Chemoschromic leak-indication tape is wrapped over the hose end assemblies to further identify exact points of leakage, and potential inspection methods are verified at regular intervals. Data collected from the hose reliability test stand include pressure, temperature, and real-time leakage rates from crimp fitting areas. These data can be used to explore the dependency of leak intensity on current pressure and temperature.

Permeation of hydrogen through the polymer inner layers is a potential source of non-destructive leakage. Permeation activity typically follows the Arrhenius rate equation and is reduced with lower temperatures. However, temperatures that drop close to the glass transition temperature increase the brittleness of the polymer and the likelihood of internal damage to the polymer, allowing for easier permeation. Plotting the natural logarithm of the permeability rate and the inverse temperature allows correlation to the Arrhenius relationship and insights into the activation energy, or the ease of permeation of hydrogen through the polymer. Similar relationships have been tabulated for comparable polymers, but no study previously has been carried out for hydrogen and polyoxymethylene [2].



Figure 1. Hose reliability test stand

The project also includes analysis of the physical and mechanical property changes of the inner hose liner due to long-duration hydrogen cycling. Tests previously identified and performed on pre-cycled specimens include optical microscopy at 1,000- to 5,000-times magnification, and scanning electron microscopy to ultimately identify blistering and other surface damage. Superficial changes are expected due to several cycles of hydrogen permeation and rapid decompression during vent cycles.

Dynamical mechanical analysis is the primary characterization testing to identify material degradation and compositional changes by examining changes in thermal viscoelastic properties—including glass transition points—in response to applied stresses and temperature sweeps from -75°C to 150°C . These tests are repeated on post-cycled samples to compare any changes or degradations in the bulk polymer properties.

RESULTS

Hose Sample #2 had limited cycles this FY due to hydrogen station availability. Minor leaks continue to be observed. The amount of hydrogen lost per cycle was relatively small, with a mass loss rate of up to 500 microgram/s. Because the leak was smaller than many instrumentation tolerances, pressure checks did not fail and such a leak would go undetected in the field. There currently is only one code that has defined numerical criteria for leakage thresholds, set as 10 ccN/h, or 3,235 micrograms per second [3].

A failed field sample was sent to NREL from an operator of a hydrogen fueling station, who reported that hoses “were still experiencing through-wall failures. Blisters form on the ID which ultimately leads to a hole in the inner liner. The braids maintain hose integrity but not pressure integrity. Mean time before failure (MTBF) is on the order of 1,000–2,000 cycles.” The hose sample supplied had 250 mm long, 16 mm ID rigid bend restrictors installed on both ends. However, the leak was observed approximately 35 mm from the nozzle end, under the bend restrictor, in the same general location as the leaks observed in Hose Sample #2.

During disassembly of hose layers, each layer was inspected. The outer polyamide layer had a 25-mm large blister rupture due to buildup of leaking gas. All the steel overwrap braid layers were intact and undamaged. The polyoxymethylene inner core had significant damage, with an irregular through-wall hole and impressions on the external surface caused by the innermost steel overwrap braiding (Figure 2). There is no protective layer

between the innermost steel overwrap and the polyoxymethylene core. There was some extrusion of polymer material observed between the braids close to the failure location.

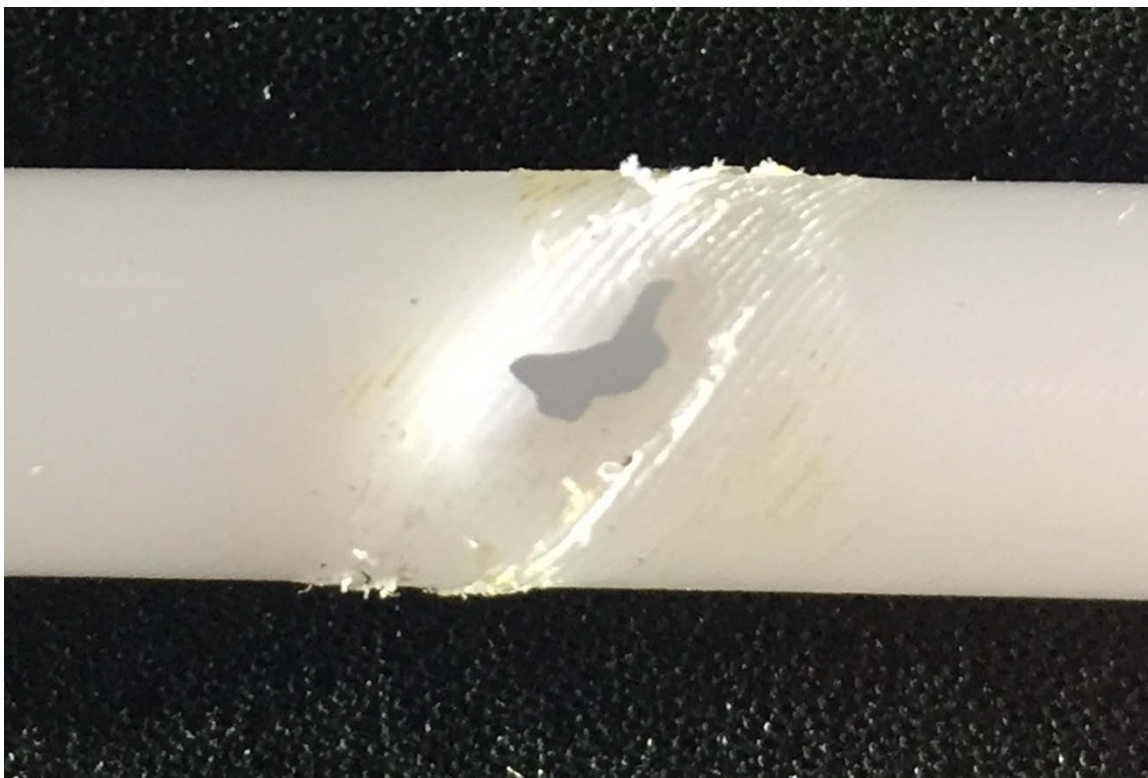


Figure 2. Hose inner-core pinhole leak and general damage

A Keyence VHX-5000 optical microscope with 1,000X lens and depth composition was used to measure the impression depths from the steel overwrap, compared to a pre-cycled specimen. The post-cycled failed sample was examined on the reverse side from the failure point. The measured impressions were 18–21 μm , and the pre-cycled specimen had impressions measured at 2.5 μm to 3.2 μm deep in the mid-hose (Figure 3). This is a factor of 6 to 7 times greater than pre-cycled, suggesting that continuous flexing of the inner braiding is impacting the core wall thickness and strength.

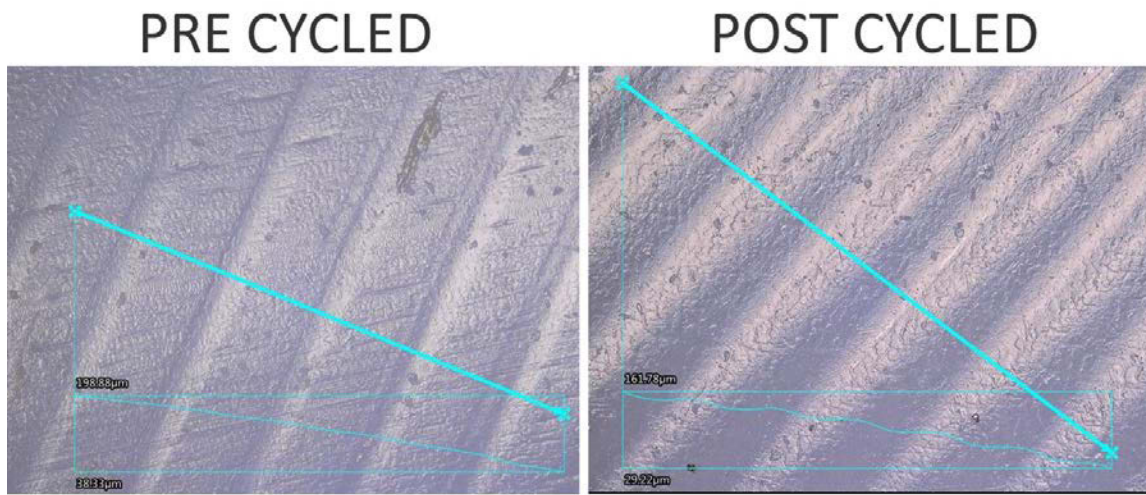


Figure 3. Comparison of wire-overwrap impressions on pre-cycled and post-cycled hose core

The pinhole leak was examined from the inside by cutting the core open, and evidence of plastic deformation and expanded polymer fibers was found near one end of the pinhole. Other areas of the pinhole inner wall exhibited sharp edges and loose fibers consistent with shear failure, suggesting that the pinhole leak started at soft spots in the wall and proceeded to expand through the core wall due to shear action of escaping hydrogen as shown in Figure 4. Small particulates from 90–300 μm were found on the outside wall, but no major particulates were found in the inner wall. The polyoxymethylene inner wall also was examined for evidence of high-density blistering caused by hydrogen decompression. Results were inconclusive at 1,000X compared to pre-cycled specimens, though some large isolated blisters were observed near the failure location. The largest blister observed was 5 mm from the failure location, with an area of 1,375 μm^2 , protruding 17 μm into the hose core.

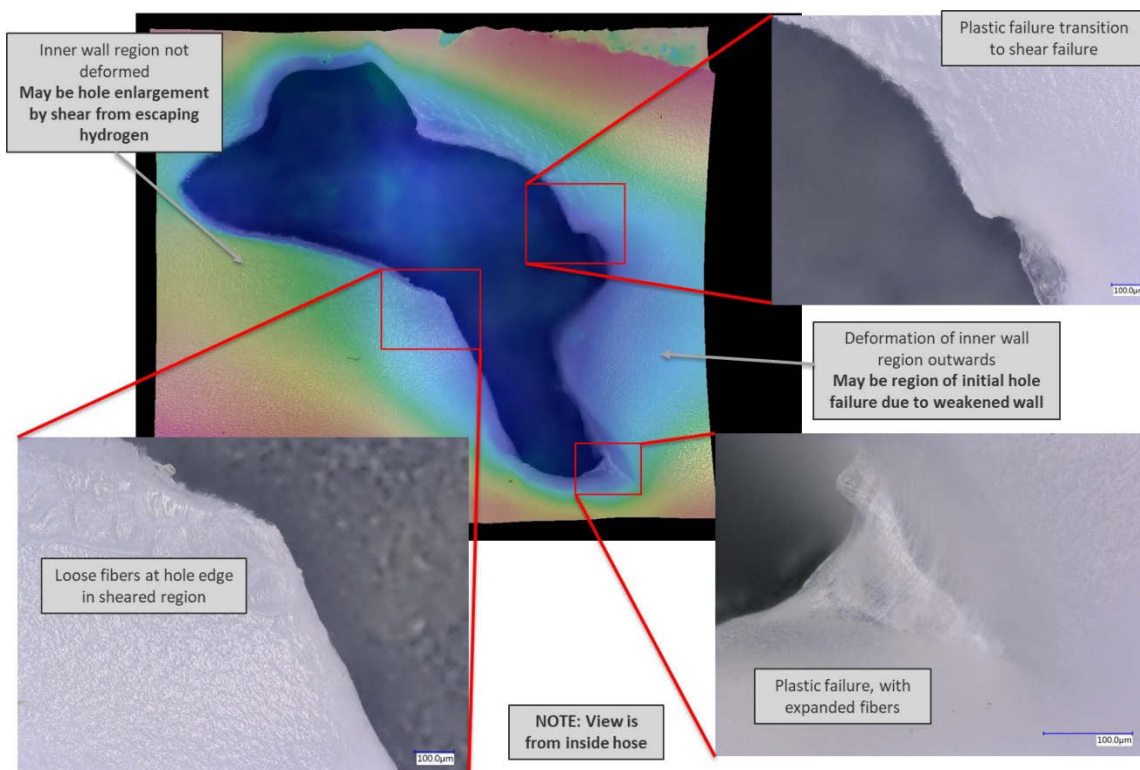


Figure 4. Analysis of pinhole leak failure modes

Data from these studies have been shared with the hose OEM, field station operators, and with standards groups such as the International Organization for Standardization to help inform standards development (e.g., ISO 19880-5 WG22).

CONCLUSIONS AND UPCOMING ACTIVITIES

- Conclusion:** Failures in the field occur in similar locations as those found in Sample #2, with damage observed from innermost steel-wire overwrap. These similarities indicate that test conditions at NREL simulate in-field conditions well. Large blisters were discovered on the inner layer, but the cause of high-density blistering is still inconclusive. There is evidence that plastic deformation led to initial failure.
- Upcoming:** Pull Sample #2, which has not failed but has a confirmed leak, to dissect and compare it to failed and pre-cycled samples. Using existing funding, set up dynamic mechanical analysis (Thermo-Fisher HAAKE MARS 60 with extended temperature chamber) to perform identified tests to measure viscoelastic response on failed hose, Sample #2, and pre-cycled samples.

- **Upcoming:** With future external funding, hoses from additional manufacturers can be tested and verified under similar test conditions and materials testing. The addition of high-flow controls and hydrogen recirculation will allow test profiles to be brought closer to real-world conditions and increase potential for thermal shocking.

REFERENCES

1. Sam Sprik, Jennifer Kurtz, Chris Ainscough, Genevieve Saur, Michael Peters, and Matthew Jeffers. “Next Generation Hydrogen Station Composite Data Products—Data Through Quarter 4 of 2016” (National Renewable Energy Laboratory, May 2017). <http://www.nrel.gov/docs/fy17osti/66555.pdf>.
2. C. San Marchi and B.P. Somerday. “Technical Reference for Hydrogen Compatibility of Materials.” Technical Report SAND2012-7321 (Sandia National Laboratories, September 2012).
3. CSA Group. “Hoses for Compressed Hydrogen Fuel Stations, Dispensers and Vehicle Fuel Systems.” ANSI/CSA HGV 4.2-2013 (2013).

Hydrogen Compression Application of the Linear Motor Reciprocating Compressor

Eugene L. Broerman (Primary Contact), Norm Shade (ACI Services), Klaus Brun, Jeffrey Bennett, Nathan Poerner, Adrian Alvarado, Diana Strickland, Jerome Helffrich, Shane Coogan, Aaron Rimpel, Pablo Bueno
Southwest Research Institute
6220 Culebra Rd
San Antonio, TX 78238
Phone: (210) 522-2555
Email: EBroerman@swri.org

DOE Manager: Neha Rustagi
Phone: (202) 586-8424
Email: Neha.Rustagi@ee.doe.gov

Contract Number: DE-EE0006666

Project Start Date: September 5, 2014
Project End Date: September 4, 2019

Overall Objectives

- Develop and evaluate the linear motor reciprocating compressor (LMRC) by integrating individually developed components.
- Achieve a higher efficiency than conventional reciprocating compression using an LMRC that also has lower capital and maintenance costs.
 - Improve isentropic efficiency above 73% by minimizing aerodynamic losses and using low-friction bearings (goal is above 95%).
 - Reduce capital costs to half those of conventional reciprocating compressors by minimizing part count.
 - Reduce required maintenance by simplifying the compressor design to eliminate common wear items.
- Meet the design requirements for all three stages of compression: compress hydrogen from 290 psia (20 bar) to 12,690 psia (875 bar) with flow rates greater than 22 lbm/h (10 kg/h) and an isentropic efficiency of compression above 73%.

- Meet the test requirements for the first stage of compression: compress hydrogen from 290 psia (20 bar) to 1,030 psia (71 bar) with flow rates greater than 22 lbm/h (10 kg/h) and an isentropic efficiency of compression above 73%.
- Meet the Fiscal Year (FY) 2018 additional test requirement for the first stage of compression: achieve an overall system specific energy of 1.6 kWh/kg or lower.

FY 2018 Objectives

- Commission bench-scale system.
- Test the bench-scale system.
- Analyze the single stage test results.

Technical Barriers

This project addresses the following technical barriers from the Hydrogen Delivery section of the Fuel Cell Technologies Office Multi-Year Research, Development, and Demonstration (MYRDD) Plan¹:

(B) Reliability and Costs of Gaseous Hydrogen Compression.

Technical Targets

During the proposal phase and kick-off of the project, the DOE technical targets were based on the 2012 MYRDD Plan. A 2015 MYRDD Plan was updated in August of 2015. Table 1 compares the predicted characteristics of the LMRC design with 2020 targets from both MYRDD reports.

FY 2018 Accomplishments

- Commissioned bench-scale system.
- Tested the bench-scale system.
- Analyzed the single stage test results.

¹ <https://www.energy.gov/eere/fuelcells/downloads/fuel-cell-technologies-office-multi-year-research-development-and-22>

**Table 1. Progress Toward Meeting Technical Targets for Hydrogen Delivery with Small Compressors: Fueling Sites
(~100 kg H₂/h peak flow)**

Characteristic	Units	2015 MYRDD Target for 2020	LMRC 2020 Status (Predictions)
Reliability		NA	High
Availability	%	≥85	TBD
Compressor Efficiency	isentropic %	NA	80% – all three stages
Compressor Specific Energy	kWh/kg	100 bar inlet: 1.6 500 bar inlet: 1.4	100-bar inlet pressure: 1.45 (projected to be achievable given optimizations to LMRC)
Loss of Hydrogen Throughput	% of flow	0.5%	<0.4%
Uninstalled Capital Cost (based on 750 kg/d station, ~100 kg H ₂ /h peak compressor flow)	\$	100-bar inlet: \$275,000 500-bar inlet: \$90,000 (1 compressor, no backup)	100-bar to 875-bar inlet: \$195,000 500-bar inlet: \$105,000 (1 compressor, no backup)
Annual Maintenance Cost	% of installed capital cost	4%	1.2% of uninstalled capital cost
Outlet Pressure Capability	bar	950	875
Compression Power	kW	NA	170 (20 bar at inlet) (compressor required power)

NA – not applicable

TBD – to be determined

100-bar inlet – pipeline delivery of gas to the compressor

500-bar inlet – tube trailer delivery of gas to the compressor

INTRODUCTION

Southwest Research Institute and ACI Services, Inc. are developing an LMRC to meet DOE's goal of increasing the efficiency and reducing the cost of forecourt hydrogen compression. The proposed advanced compression system utilizes a novel and patented concept of driving a permanent magnet piston inside a hermetically sealed compressor cylinder through electromagnetic windings. The LMRC is an improvement over conventional reciprocating compressors as it minimizes the mechanical part count, reduces leakage paths, and is easily modularized for simple field installation [1].

APPROACH

The LMRC is a novel concept compared to conventional reciprocating compression technology. The compression system replaces the functions of an electric motor drive and reciprocating compressor with an integrated, linear, electrically actuated piston. The LMRC design includes a magnetic piston within a cylinder and a gas compression chamber at each end of the piston. The compressor cylinder comprises an electromagnetic coil that operates with the piston to convert an input of electrical power to a reciprocating movement of the piston. This uses the same technology seen in magnetic bearings of turbomachinery and does not require oil for lubrication. Since the driver and compressor are integrated into the same hermetically sealed component, there is a significant reduction in the number of parts and materials needed to construct this device. In addition, the simplicity of the design reduces required maintenance, minimizes seal leakages and wear, and allows for oil-free operation.

The LMRC system minimizes parasitic losses by using: reduced piston speeds, low-pressure-drop contoured valves, and inter-stage cooling manifolds. Working at low reciprocating speeds of approximately 300 cycles per minute (5 Hz), the LMRC prototype is expected to meet an isentropic efficiency goal of greater than 95% per stage [2]. That efficiency can be compared with current state-of-the-art technology that typically has an efficiency closer to 73%. The improved isentropic efficiency and reduced mechanical losses result in an increase in overall efficiency for the LMRC system.

RESULTS

Initial commissioning efforts revealed that due to a hardware change in the control circuitry made to protect the electric driver, the ability to switch the polarity of the current flows was limited to no faster than ~10 ms. Regardless, a timed sequence of duty cycles was successful in generating cyclic motion of the LMRC. Initial tests with this sequence compressing nitrogen gas rarely ran for more than 2–3 simultaneous cycles before the piston was unable to move far enough past the zero-force point near the middle of the stroke to successfully complete the stroke, and the piston would subsequently become stuck. One example of this issue is shown in Figure 1.

The next test step used helium as the test gas instead of nitrogen. Results revealed that the piston traveled much more freely than with the nitrogen, such that greater lengths of travel would occur for similar inputs of energy. Alternatively, the same amount of travel could be achieved with lower inputs of energy. This is due to the flow performance of the compressor valves and other flow-restricting devices with the smaller molecular size of the helium gas. As a result, longer continuous operation (i.e., a greater number of simultaneous cycles) could be obtained. Subsequent testing was performed to improve the performance of the LMRC by optimizing the performance of the electrical controls and timing of the software controls system.

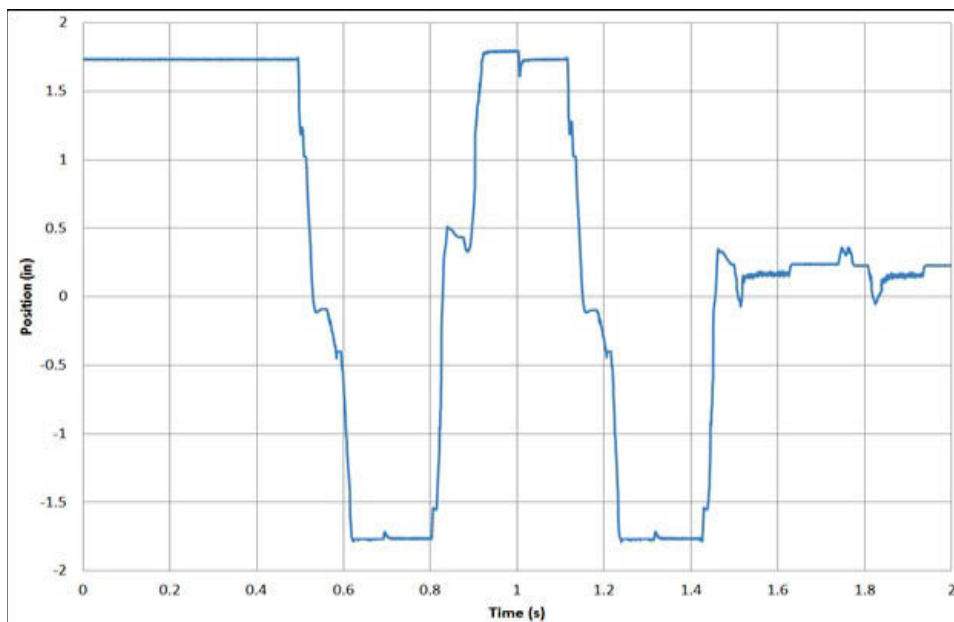


Figure 1. Commissioning issues: failed continuous cycle

Successful operation of the compressor was achieved with the use of helium as the working fluid after performing the numerous modifications to the system to resolve or improve the commissioning issues. One example of these tests is shown in Figure 2. At this point, the compressor was running at about 280 cycles per minute, with a compression ratio of 3.76 (suction line pressure of 73 psia and discharge line pressure of 274 psia).

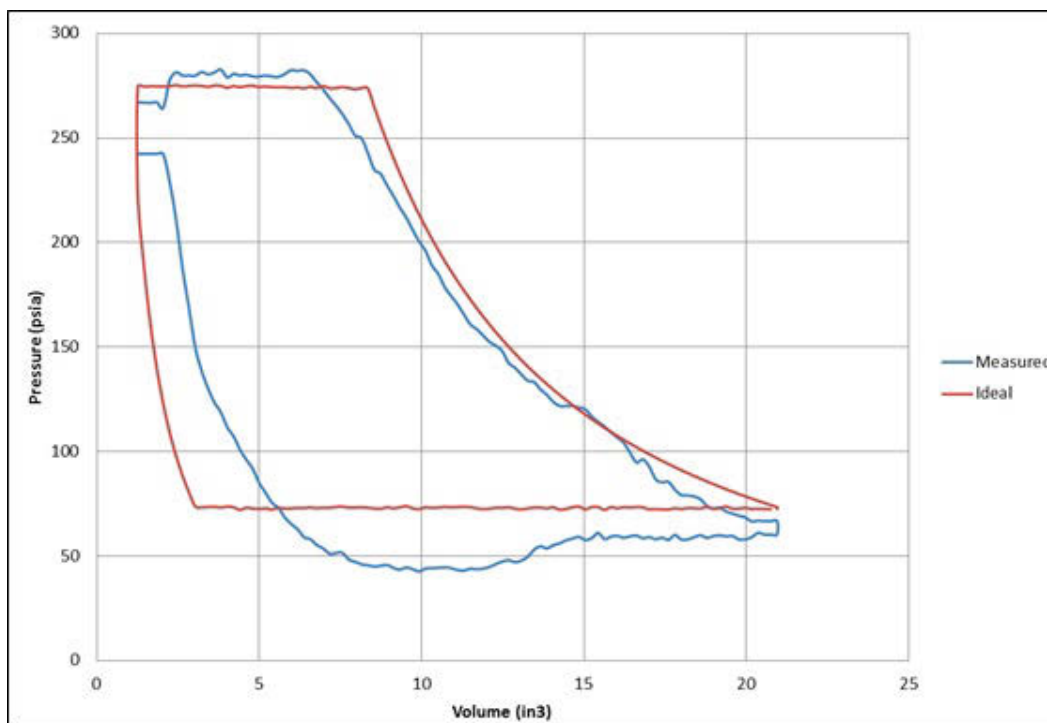


Figure 2. Pressure-volume (PV) card for helium

Of the testing performed with hydrogen gas, the test case that came the closest to the design conditions is presented in Figure 3. For this test, the compressor was operating at 456 cycles per minute, a compression ratio of 3.5 (suction pressure at 137 psia and discharge pressure at 478 psia), and flow rate of approximately 8.2 kg/h.

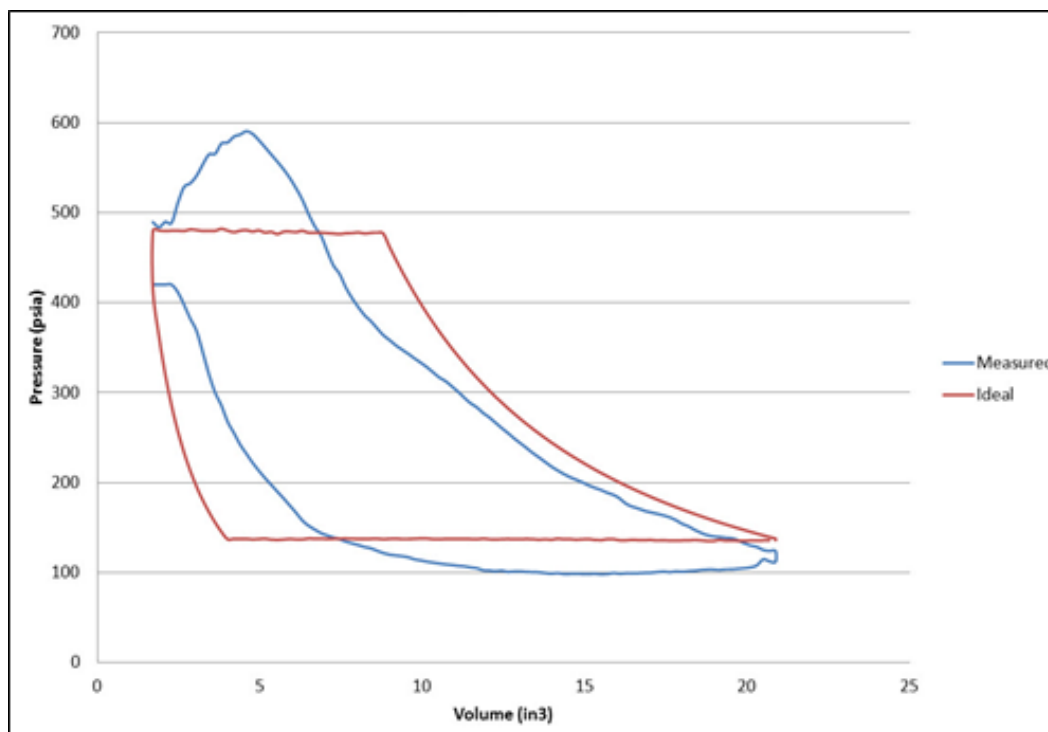


Figure 3. PV card for hydrogen

CONCLUSIONS AND UPCOMING ACTIVITIES

Conclusions derived from the work conducted in FY 2018 are:

- Testing indicates that high-efficiency hydrogen compression is possible with an LMRC used for the compression process. Modifications to the LMRC will be needed to achieve target efficiencies.
- Inconsistent currents, “slow” switching speeds (due to performance issues with the electronics controller), and inaccurate position measurements led to inaccurate motor control.
- Inaccurate motor control prevented the LMRC from achieving the goals.

Future work in Project Year 5 (FY 2019; Budget Period 3) will include:

- Redesign the motor portion of the low-pressure LMRC such that the overall system will have a specific energy significantly closer to 1.6 kWh/kg
- Fabricate and assemble the more efficient low-pressure LMRC
- Commission the test bench using an inert gas and following the plan previously defined
- Complete testing of improved LMRC system according to the defined test matrix with hydrogen
- Analyze the results from the improved low-pressure system testing.

REFERENCES

1. U.S. Patent 8,534,058. Issued Sept. 17, 2013. “Energy Storage and Production Systems, Apparatus and Methods of Use Thereof.” Patented in United States of America.
2. D. Deffenbaugh, et al. “Advanced Reciprocating Compression Technology.” DOE Award No. DE-FC26-04NT42269, Southwest Research Institute Contract No. 18.11052, December 2005.

Magnetocaloric Hydrogen Liquefaction

Jamie Holladay (Primary Contact), Kerry Meinhardt, Evgueni Polikarpov, Ed Thomsen, John Barclay,^a Corey Archipley,^a Jun Cui,^{b,c} Sam Wolf,^c and Iver Anderson^c

Pacific Northwest National Laboratory
PO Box 999, MS: K1-90
Richland, WA 99352
Phone: (509) 371-6692

Email: Jamie.Holladay@pnl.gov

^a Emerald Energy Northwest, LLC

^b Pacific Northwest National Laboratory

^c Ames Laboratory

DOE Manager: Neha Rustagi

Phone: (202) 586-8424

Email: Neha.Rustagi@ee.doe.gov

Subcontractor:

Emerald Energy Northwest, LLC, Redmond, WA

Project Start Date: October 1, 2015

Project End Date: Project continuation and direction determined annually by DOE

Overall Objectives

- Quantify and incorporate novel configurations to achieve simpler, more efficient liquefier designs for liquid hydrogen.
- Identify, characterize, and fabricate magnetic materials in shapes suitable for high-performance active magnetic regenerators (AMRs) operating between 280 Kelvin (K) and 20 K.
- Fabricate and characterize improved multilayer magnetocaloric regenerator performance.
- Design, fabricate, test, and demonstrate a lab-scale magnetocaloric hydrogen liquefier (MCHL) system.
- Demonstrate a lab-scale hydrogen liquefier that defines how to achieve a figure of merit (FOM) increase from 0.3 up to >0.5.
- Perform techno-economic analysis on a commercial-scale (30 metric tons per day of liquid hydrogen) system.

Fiscal Year (FY) 2018 Objectives

- Resolve regenerator design and assembly issues such as unexpected spike in thermal expansion coefficient for ferromagnetic rare-earth refrigerants near Curie temperature.
- Demonstrate controlled start-up, cool-down, and steady-state operation of a multilayered regenerator.
- Minimize force imbalance in a reciprocating dual magnetic regenerator design and reduce extra cooling required for flux-jump heat generation from internal current changes due to flux conservation in superconducting magnets during reciprocating AMR cycles.
- Complete detailed efficiency analysis of efficiency-reducing mechanisms within generic magnetic liquefiers to show the means to achieve an FOM >0.65.
- First achievement of 80 K temperature decrease with a four-layer AMR design starting at 280 K.
- Increase spherical particle yield to >85%, a 40% increase over the original design, in the upgraded rotating disk atomizer (RDA).

Technical Barriers

This project addresses the following technical barrier from the Hydrogen Delivery section of the Fuel Cell Technologies Office Multi-Year Research, Development, and Demonstration Plan [1]:

(H) High Cost and Low Energy Efficiency of Hydrogen Liquefaction.

Technical Targets

Conventional hydrogen liquefiers, at any scale, have a maximum FOM of ~0.35 due primarily to the intrinsic difficulty of rapid, efficient compression of either hydrogen or helium working gases (depending on the liquefier design). The novel approach of this MCHL project uses solid magnetic working refrigerants cycled in and out of high magnetic fields to execute an efficient AMR liquefaction cycle that avoids the use of gas

compressors. Numerical simulation modeling of high-performance MCHL designs indicates certain achievable designs show promise for simultaneously lowering installed capital costs per unit capacity and increasing thermodynamic efficiency from a FOM of ~0.35 toward 0.5–0.6. Results from experimental prototypes should support the design and deployment of hydrogen liquefier plants that meet the DOE hydrogen production and delivery targets (Table 1).

FY 2018 Accomplishments

- Achieved controlled start-up and operation of a four-layer AMR with cooling to ~200 K from room temperature (280 K).
- Reduced net force imbalance in reciprocating dual, multilayer regenerator prototype in ~6 Tesla (T) field changes from >1,000 lb to <100 lb.

- Used force balance to reduce changes in magnetic induction in reciprocating AMR prototype to sufficiently reduce internal heating in a 6-T persistent-mode superconducting magnet due to flux conservation so the existing cryocooler could keep the magnet at <5 K during steady-state operation.
- Improved RDA spherical particle yield by 42% to achieve a yield of spherical particles of 88% for gadolinium (Gd) sphere synthesis.
- FOM >0.7 predicted by detailed analysis for two-stage MCHL 30 tonne/day hydrogen liquefier.
- Identified a series of five magnetocaloric materials with tunable compositions ($Gd_xEr_{1-x}Al_2$ and $Dy_xEr_{1-x}Al_2$) with thermomagnetic characteristics for a 120 K to 20 K operation range to complement existing magnetocaloric materials for 280 K to 120 K operation.

Table 1. Pacific Northwest National Laboratory (PNNL) Magnetocaloric Hydrogen Liquefaction Technical Targets

30 tonne/day (Small Facility)	Claude Cycles (Current) [1]	PNNL's MCHL Targets	2020 DOE Target [1]
Efficiency	<40%	70~80%	N/A
FOM	<0.3 (small facility) 0.35~0.37 (large facility)	~0.6 (small facility) ~0.65 (large facility)	N/A
Operation and maintenance cost	4%	2.8%	--
Energy input	10–15 kWh/kg H ₂	5~6 kWh/kg H ₂	12 kWh/kg H ₂

INTRODUCTION

MCHL technology promises cost-effective and efficient hydrogen liquefaction because it eliminates gas compressors—the largest source of inefficiency in traditional Claude cycle liquefiers—as well as the use of liquid nitrogen to precool the hydrogen. The Claude cycle liquefier is the current industrial choice for hydrogen liquefaction and uses a variety of configurations with processes that use helium, hydrogen, or gas mixtures as coolants. In the case of hydrogen as the refrigerant gas and the process gas, the hydrogen feed to the process is first cooled by liquid nitrogen, and then further cooled in counterflow heat exchangers in which the cooling power is provided by turbo expansion of a portion of the precooled hydrogen stream. Liquefaction of the precooled, high-pressure hydrogen stream is finally accomplished by throttling a Joule-Thomson valve into a phase-separator collection vessel. Conventional liquefier technology for hydrogen is limited to an FOM of ~0.35 for a large facility, and typically less than 0.3 for a smaller facility.

The current MCHL design is an AMR system that uses regions of high or low magnetic field and reciprocating magnetocaloric materials to transfer heat between hot and cold thermal reservoirs. In one step of the AMR cycle, the magnetic material in a high-performance regenerator is adiabatically placed in a high magnetic field. The conservation of total entropy in this adiabatic process requires the magnetic refrigerants in the regenerators to increase in temperature to compensate for the increased magnetic order (lower entropy) among the material's magnetic moments. The increased thermal energy is transferred to a heat sink by the cold-to-hot flow of heat transfer fluid (HTF). After the cold-to-hot HTF flow is completed, the magnetic material is adiabatically removed from the high magnetic field, resulting in an increase in entropy among the magnetic moments of the refrigerant in the regenerators (maintaining constant total entropy), and the temperature of the magnetic refrigerants decreases in the magnetic regenerators. During the subsequent hot-to-cold flow of the HTF at constant low magnetic field, the colder magnetic regenerator cools the HTF before it exits the regenerator and accepts heat from the thermal load, thereby cooling the hydrogen process stream. At the end of this flow, the AMR cycle is repeated at the operating frequency. A more complete description, including a simplified process flow diagram (PFD) and schematics, is found in the FY 2016 Annual Progress Report (APR).

The AMR cycle can be highly efficient because the magnetization/demagnetization temperature changes are only a fraction of the adiabatic temperature changes of a gas compression process and the magnetic regenerators can be designed to have much higher effectiveness than a gas-to-gas counterflow heat exchanger. The MCHL project is developing liquefier designs that use magnetocaloric refrigeration to achieve an efficient thermodynamic liquefaction cycle. Detailed modeling of the MCHL technology coupled with experimental validation in prototypes indicate this technology has the potential to simultaneously decrease liquefier installed capital costs per unit capacity—thereby reducing delivery cost—and increase thermodynamic efficiency from an FOM of ~0.3 toward 0.5–0.6.

APPROACH

At a high level, the critical path for the MCHL project can be summarized as:

1. Identify, synthesize, and characterize magnetocaloric materials.
2. Develop an approach to understand the magnitude of the thermomagnetic properties and how to utilize the second order phase transition characteristic in many magnetocaloric materials to improve liquefier FOM while minimizing cost. The heat capacity below the second order phase transition in ferromagnetic refrigerants is ~10% larger at high magnetic fields than at low magnetic fields. We use this unique characteristic to enable the “bypass of a portion heat-transfer fluid operation” described in the FY 2016 APR as well as in the current report.
3. Investigate layered material operation to understand how temperature changes within the layers and coupled HTF flows through layers impact performance. This will include detailed simulation models using the materials properties measured as well as experiments.

4. Apply well-known catalysts to efficiently execute the ortho-para hydrogen conversion for liquefaction; this will include system design options to best integrate catalysts into compact, micro-channel process heat exchangers.
5. Demonstrate hydrogen liquefaction in an MCHL with appropriate ortho-para (o-p) hydrogen conversion catalysts integrated into the heat exchanger and continuously cooled by bypass heat transfer gas.

This project builds upon work first pioneered by Dr. John Barclay at Emerald Energy Northwest LLC. We have modified the design and updated the previously developed models. The approach is to develop and demonstrate a two-stage system that liquefies hydrogen starting at room temperature (Figure 1). We have several major efforts occurring simultaneously to complete the critical path for this project's magnetocaloric hydrogen liquefaction research goals.

(1) In-house synthesized alloy ingots are used for the materials characterization using Ames Laboratory's (Ames) magnetic materials characterization capabilities. For use in the MCHL, the materials need to be spherical with diameters in the range of 150–250 μ m. We are using Ames' RDA, a tunable, low-cost material synthesis technique, to make kilogram batches of spheres with adjustable diameters from different compositions. The RDA-synthesized materials will be tested in PNNL's versatile, unique reciprocating dual regenerator research system. Details of the dual regenerator design and schematics as well as initial bypass operation are found in the FY 2016 APR.

(2) Bypass operation was tested and identified as a key to achieving high-performance operation with minimal materials (FY 2016 APR).

(3) The proprietary layered regenerator and system design efforts were pursued via modeling and experimental efforts. The materials properties were used in an advanced modeling subtask to understand the performance and improve the system design (FY 2017 APR). The model was validated against experimental data from PNNL's research system as reported in the FY 2017 APR. A second-generation dual regenerator design was developed to test the understanding of layering of different magnetic refrigerants coupled with bypass operation. Layered regenerators are not a new approach; however, expected performance with layered AMRs has not been previously achieved. We hypothesized the reason for this is that each layer needs to be considered as an individual magnetic Brayton cycle refrigerator coupled to adjacent refrigerators with different refrigerants. To accomplish this coupled design means the amount of materials required for each layer must be carefully determined and the corresponding HTF flow for each layer must simultaneously be varied. This hypothesis was tested in the second-generation multilayer design constrained to operate using several of the subsystems from the initial test apparatus. During testing of the new design in FY 2017, challenges regarding magnetic force imbalance, resultant additional heating in the superconducting (s/c) magnet due to flux conservation in persistent-mode s/c magnets, and the need for increased HTF control during start-up, cool-down, and steady-state operation were identified. These challenges were solved in FY 2018 and are reported here.

(4 and 5) Based on the results of the previous work from 280 K to 120 K, the MCHL stage operating between 120 K and 20 K will be designed and built. It will include integration of o-p catalysts into compact, high-performance hydrogen process heat exchangers for the lower-temperature MCHL stage for actual liquefaction tests to be done. This integration and research will be part of the future work on this project. Finally, a more detailed techno-economic analysis update was done to indicate progress against the DOE's efficiency and cost performance targets. An initial techno-economic analysis was reported in FY 2016; this one was done in much more detail using lessons learned and new results from experiments. A detailed FOM analysis was completed in FY 2018.

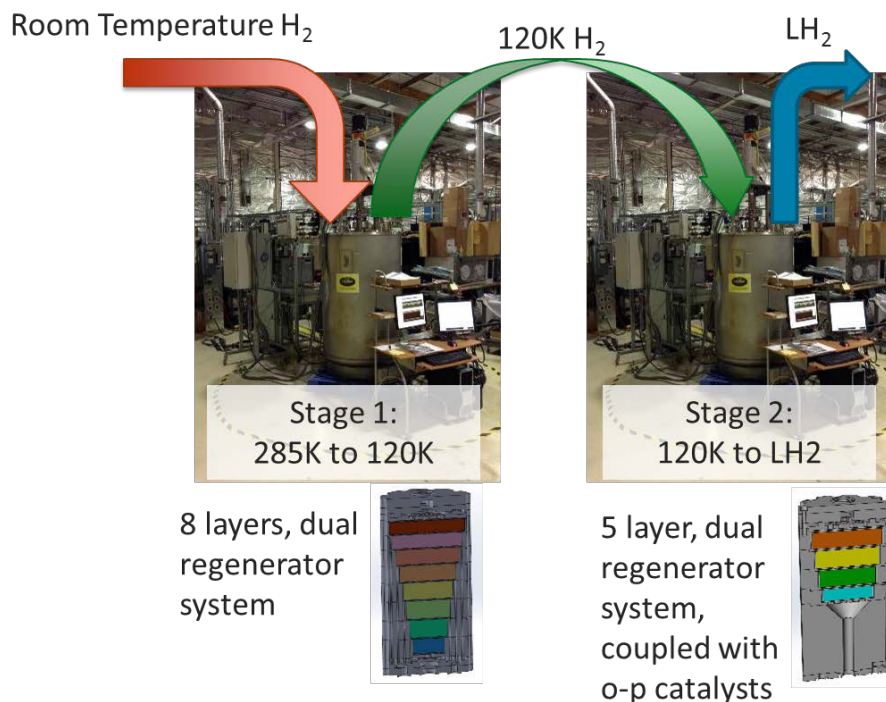


Figure 1. Two-stage, multilayer regenerator, reciprocating magnetocaloric system concept

RESULTS

Minimization of Force Imbalance and Improved Flux Conservation Achieved for Proper Operation

During the MCHL system operation in FY 2017, a net force from the two opposing attractive forces of the magnetic refrigerants toward the center of the high-field, solenoidal magnet occurred as the regenerators move into and out of the magnetic field. In the absence of refrigeration, the dual regenerators at the same temperature and an appropriate distance apart should experience almost the same magnitude force but in opposite directions so the net large compressive forces between the two regenerators should almost cancel each other. In an AMR refrigerator, the average temperature of one regenerator will be several K lower than the other regenerator as they enter and leave the high field region of the cycle. The different temperatures cause a different magnetization entering and leaving the high magnetic field region, which creates a net force imbalance. This is inherent in reciprocating designs because the magnetic work for the AMR cycle is input in this manner into the regenerator. This additional power is provided by an axial linear drive mechanism in MCHL operation.

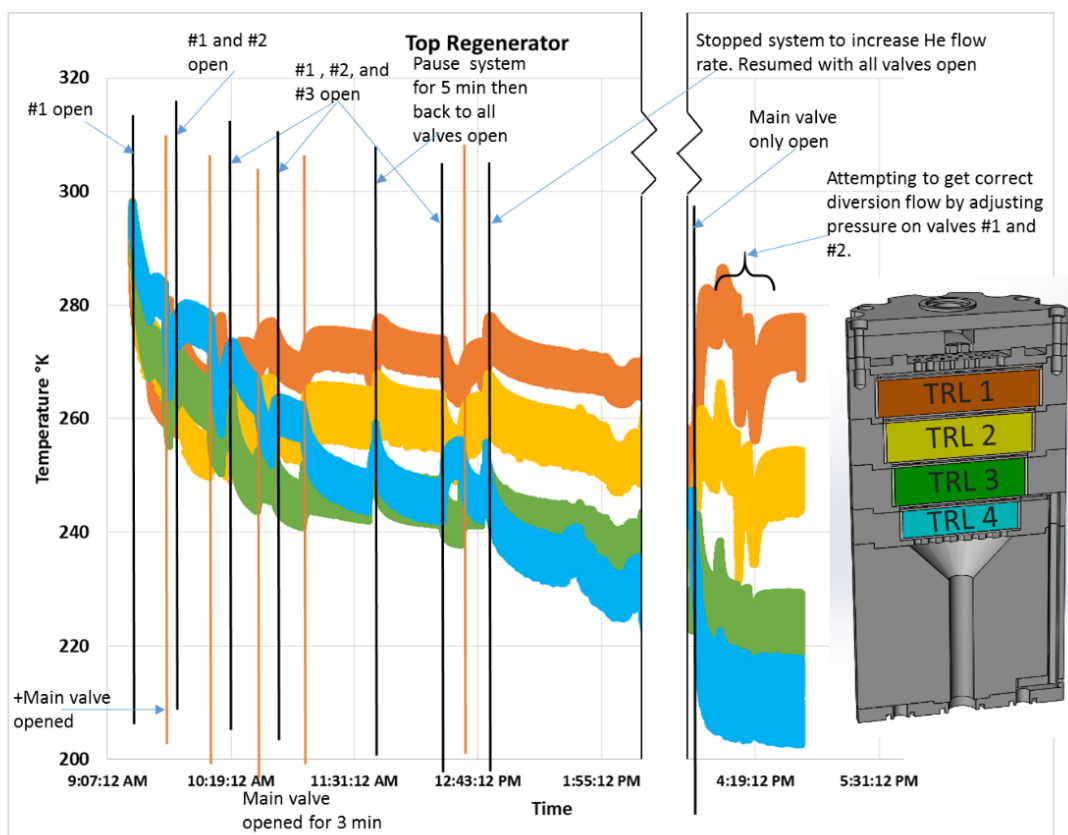
However, this AMR cycle force imbalance is magnified in reality because dual magnetic regenerators are separated “lumped” sources of magnetization that must go through the axial magnetic induction (B) gradients that are offset axially entering and leaving a solenoidal magnet. The net magnetic force increases accordingly to several hundreds or even a thousand pounds.

The second effect of different lumped magnetization moving in and out of a persistent-mode superconducting magnet (a constant magnetic flux device) is an increase or decrease in free current field (H) to keep B constant during the AMR cycle. This detrimental change in H causes heating due to flux-jumping as currents change in the s/c magnet. Therefore, a change in the magnetization of the material being moved in and out of the magnetic field is compensated by changing the magnetic field strength H generated by the circulating electric current in the s/c magnet. These changes in the electric current cause the magnet to heat up due to Joule heating and—if the magnet heats up too much—it will quench (at ~ 5.8 K on the solenoid). During operation in FY 2017, a substantial force imbalance, at times in exceeding 1000 lb_f , was measured. This limited the s/c magnet operation to ~ 3 T and cycle frequency to ~ 0.25 Hz. During FY 2018, we developed a generic

optimization program to design an addition of shaped pieces of Fe between, above, and below the dual regenerators. The model indicated that if the right mass of Fe of the correct shape was placed in the correct location, the force imbalance could be minimized to less than 50 lb_f [2]. Due to space constraints within the existing magnetic refrigerator prototype, the ideal shape and placement could only be approximated, but the force imbalance was decreased to less than 100 lb_f (a 90% reduction) and, more importantly, the flux-jump heating in the solenoid was sufficiently reduced to enable the cryocooler to keep the magnet below ~5 K even when operating at 6 T and 0.25 Hz.

200 K Temperature Achieved with Innovative HTF Control

Improved HTF flow in the regenerators was achieved by using PNNL-designed and built controllable pneumatic diversion-flow valves to enable control of helium heat transfer gas through each layer as required for proper cool-down and at steady-state operation. (There were no commercially available pneumatic valves that met design requirements.) Several previous attempts by several different groups have been unable to cool to below the Curie temperature of the colder layers of magnetic material. We experienced this result in our initial multilayer magnetic regenerator prototype. After installing compact controllable diversion-flow valves between each set of layers of refrigerants, we were able to use these diversion-flow valves to achieve a start-up from room temperature to steady-state operation with temperature spans for each layer that are below their respective Curie temperatures (293 K, 274 K, 253 K, and 235 K). For start-up, the valves control the flow so that each layer is sequentially cooled down below its respective Curie temperature before the heat transfer gas is adjusted to that required for steady-state operation. During operation, the valves allowed HTF flow control to optimize the temperature distribution in the regenerator (Figure 2), which in turn would increase the efficiency.



Gas inlet T= 285K

Figure 2. Regenerator temperature profile using adjustable valves to achieve ~200 K

RDA Upgrades Improved Yield of Gd Spherical Particles (150–250 μm) to 88%, a 42% Improvement

Ames' RDA was originally designed for more easily quenched materials, leaving it undersized for the current task of producing rare earth powders, leaving cooling times too small, and allowing flake formation. However, the system for magnetocaloric materials worked, but the yield of spherical material in the desired size range was lower than expected. Recent system upgrades were made to add consistency between runs and improve the quality of powder. The major upgrade was increasing the quench drum diameter by nearly 40% from 12 to 16.5 in. This increases the flight path and cooling time of the droplets, reducing flakes and extending the range of useful disc speeds and superheats. An atomization of pure Gd using the pre-upgraded system was rerun in the upgraded system using identical superheat and disc speed to assess the upgrade. Quantitatively, data gathered from the flake removal process show powder in the desired size range (150–250 μm) is 38% flake in the pre-upgraded system, while the upgraded system reduced the flake to 12% (Figure 3). This is a 42% increase in spherical particles and a spherical particle yield of 88%. Therefore, the upgrade to the RDA has proven effective in improving the quality of the produced powders. We anticipate similar improvement for other alloys.

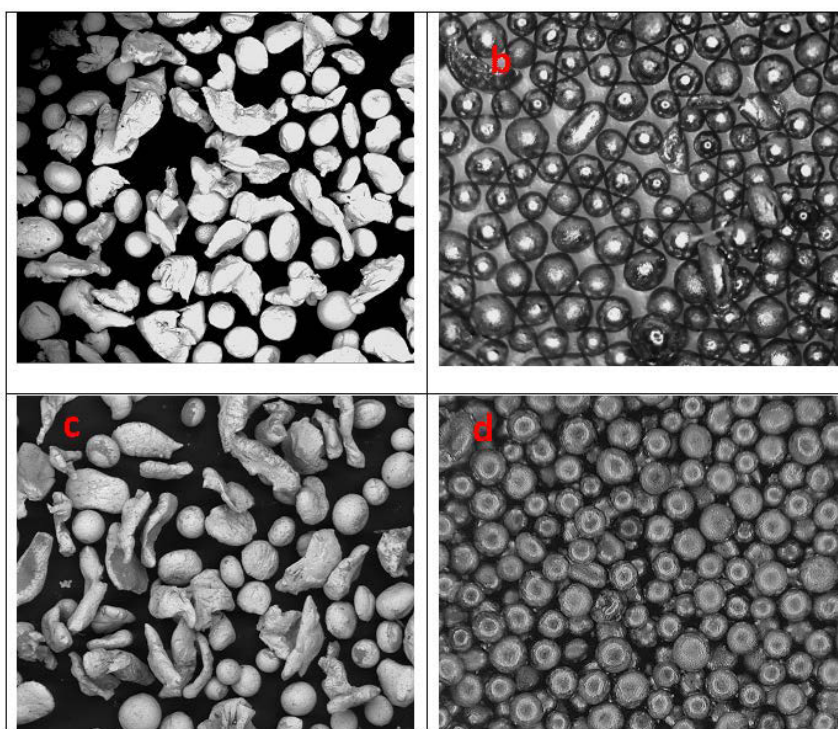
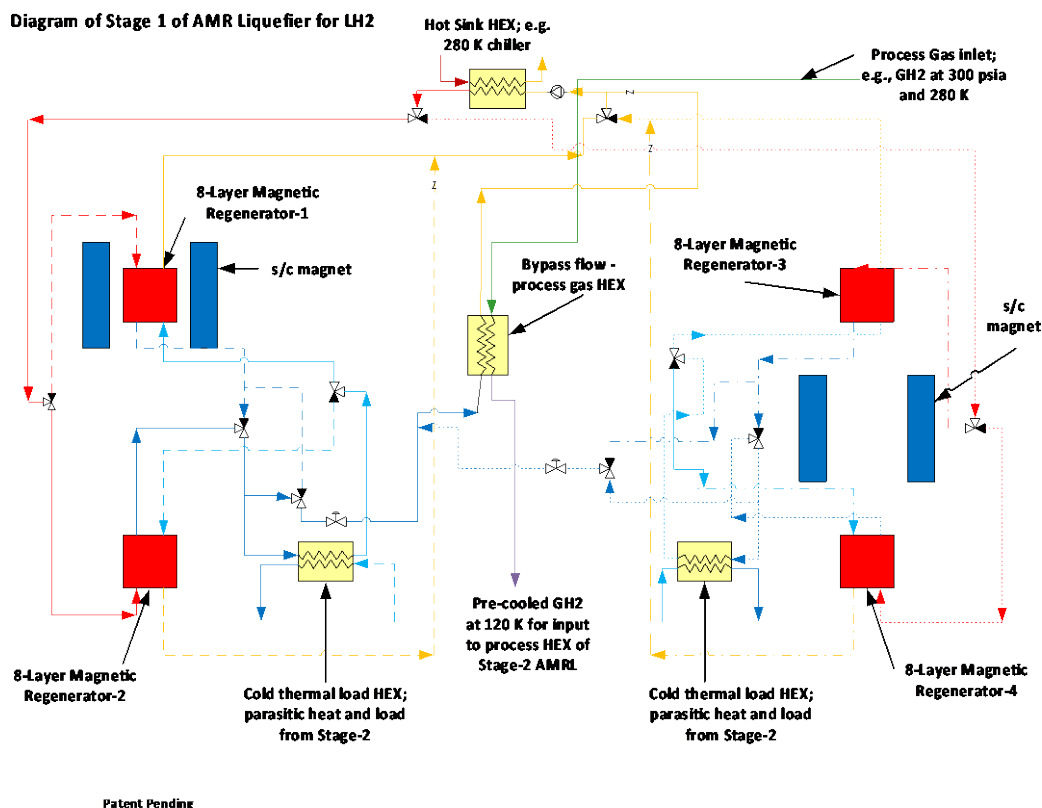


Figure 3. Comparison of 150–250 μm Gd powders produced by the RDA (a) pre-upgrade with flake, (b) post-upgrade with flake, (c) pre-upgrade flake removed, and (d) post-upgrade flake removed

FOM Analysis Shows 0.7 Is Feasible

Finally, a detailed FOM analysis for a 30 tonne H_2 /day magnetocaloric-based liquefier was completed. To do the analysis, a PFD was produced for a combination of two modules of quad-regenerator reciprocating refrigerators: one module operating from 280 K to 120 K, in series with the second module operating from 120 K to 20 K. Each quad consisted of two sets of reciprocating dual regenerators with a 90 phase difference in their respective drive actuators and with synchronized 3-way valve control of the flow of HTF through the process heat exchanger to provide continuous cooling to the incoming gaseous hydrogen at 300 psia. The warmer module used liquid propane as the HTF and eight different magnetic refrigerants, each spanning 20 K. The colder module used helium gas at ~ 800 psia as the HTF and five different magnetic refrigerants, each spanning 20 K (Figure 4). The PFD was used to identify all the mechanisms of the system that contribute to

the thermodynamic efficiency. We then calculated the ideal work rate, real work rates, and the resultant FOM for all major sources of inefficiency. The MCHL used 13 refrigerants in two modules to enable bypass flow to continuously cool the 300-psi hydrogen process stream from 280 K to 20 K. The MCHL operated at 1 Hz and 6 T. The real work rate included Carnot work rate/layer; estimates of the parasitic heat leak; cold work sources (e.g., 2nd stage He circulator as part of the HTF); external work input from cryocooler compressor for the s/c; reciprocating drives for the regenerators; HTF pumps; and internal irreversible entropy such as heat transfer between the HTF and magnetic materials, friction within HTF flow with pressure drop, longitudinal thermal conduction in the HTF with mixing effects, and eddy current heating from time-dependent magnetic field as regenerators reciprocate. Table 2 contains the estimated values and the calculated FOM of 0.7.



Stage 1 (Room temperature to 120K)

Figure 4. PFD of Stage 1 and Stage 2 of AMR for hydrogen liquefaction

HEX – heat exchanger

Table 2. Inputs for FOM Calculation

	Work Range (kW)
Carnot work for 2-stage, 13-layer device (with bypass flow but without irreversible entropy in regenerators)	2,649
Internal irreversible entropy sources in regenerators	1,075
Parasitic heat leak + cold work sources (e.g., 2nd stage He circulator @ 50% efficiency)	0.6+1.9
Reciprocating drives for regenerators (@ 90% efficiency)	372
HTF pumps at room temperature (@ 50% efficiency)	4.1
Cryocooler compressor power (2 each for 30 tonne/day)	16
Total real work	4,119
Total ideal work	2,996
$FOM = \frac{\dot{W}_{Ideal}}{\dot{W}_{Real}}$	0.73

CONCLUSIONS AND UPCOMING ACTIVITIES

This project has made progress toward the ultimate goals of increasing the system efficiency while maintaining or decreasing the capital cost of hydrogen liquefaction technologies. In FY 2018, we made progress along the critical path in that we:

1. Were the first to achieve cool-down and steady-state operation of a 4-layer dual AMR refrigerator with a temperature decrease to 200 K from 280 K
2. Completed a detailed FOM analysis resulting in a projected FOM of >0.7 for a 30 tonne H₂/day system
3. Developed novel small pneumatic-controlled valves compatible with the cryogenic conditions and effective operation in a high magnetic field
4. Demonstrated controllable diversion flow of HTF in the layered regenerators using the PNNL-developed valves
5. Developed properly shaped and positioned high-permeability materials that—when integrated into the dual regenerator system—reduce the magnetic force imbalance significantly by reducing changes in B required to satisfy flux conservation in s/c solenoids without excessive Joule heating in the magnet
6. Upgraded the RDA to improve the spherical shaped material yield to 88%
7. Identified a good series of tunable magnetic refrigerants for 120 K to 20 K operation with projected thermomagnetic performance for high-performance regenerators.

Upcoming activities will include:

- Demonstrate the stage 1 operation to achieve a temperature of 120 K from 280 K
- Use the lessons learned from stage 1 to complete the design of the stage 2 system operating from 120 K to 20 K
- Characterize and synthesize the remaining materials for the second stage
- Build and test the second stage
- Update techno-economic analysis prepared in Q4 FY18.

SPECIAL RECOGNITIONS AND AWARDS/PATENTS ISSUED

1. Non-Provisional U.S. Patent Application: Production of Liquid Natural Gas and Other Cryogenics Using a Multi-Stage Active Magnetic Regenerative Liquefier. Application date 7/2018.
2. Non-Provisional U.S. Patent Application: Active Magnetic Regenerative Processes and Systems Employing Hydrogen as Heat Transfer Fluid and Process Gas. Application date 7/2018.
3. Non-Provisional U.S. Patent Application: Advanced Multi-Layer Active Magnetic Regenerator Systems and Processes for Magnetocaloric Liquefaction. Application date 3/2018.
4. Foreign Patent Application: Active Magnetic Regenerative Processes and Systems Employing Hydrogen as Heat Transfer Fluid and Process Gas. Application date 3/2018.
5. Foreign Patent Application: Advanced Multi-Layer Active Magnetic Regenerator Systems and Processes for Magnetocaloric Liquefaction. Application date 3/2018.

FY 2018 PUBLICATIONS/PRESENTATIONS

Publications

1. J.D. Holladay, R.P. Teyber, K.D. Meinhardt, E. Polikarpov, E.C. Thomsen, C. Archipley, J. Cui, et al. “Investigation of Bypass Fluid Flow in an Active Magnetic Regenerative Liquefier.” *Cryogenics* 93 (2018); doi:10.1016/j.cryogenics.2018.05.010.
2. R.P. Teyber, K.D. Meinhardt, E.C. Thomsen, E. Polikarpov, J. Cui, A. Rowe, J.D. Holladay, et al. “Passive Force Balancing of an Active Magnetic Regenerative Liquefier.” *Journal of Magnetism and Magnetic Materials* 451 (2018); doi:10.1016/j.jmmm.2017.11.002.
3. J.A. Barclay, K.P. Brooks, J. Cui, J.D. Holladay, K.D. Meinhardt, E. Polikarpov, and E.C. Thomsen. “Propane Liquefaction with an Active Magnetic Regenerative Liquefier.” *Cryogenics* (Submitted and in Review 2018).
4. R.P. Teyber, J.D. Holladay, K.D. Meinhardt, E. Polikarpov, E.C. Thomsen, J. Cui, et al. “Performance investigation of a high-field active magnetic regenerator.” *Applied Energy* (Submitted and in Review 2018).

Presentations

1. J.D. Holladay, K.D. Meinhardt, E.C. Thomsen, E. Polikarpov, J.A. Barclay, J. Cui, and I.E. Anderson. “MagnetoCaloric Gas Liquefaction: A New High-Efficiency, Low-Cost Gas Liquefaction Technology.” Presented by Jamie D. Holladay at Hydrogen and Fuel Cells Working Group, December 8, 2017.
2. J.D. Holladay, K.D. Meinhardt, E.C. Thomsen, E. Polikarpov, J.A. Barclay, C. Archipley, J. Cui, I.E. Anderson, and S. Wolf. “MagnetoCaloric Hydrogen Liquefaction.” Presented by Jamie D. Holladay at the DOE Hydrogen and Fuel Cells Program Annual Merit Review, Washington, DC, June 2018.

REFERENCES

1. DOE. “Multi-Year Research, Development and Demonstration Plan” (2015). <https://www.energy.gov/eere/fuelcells/downloads/fuel-cell-technologies-office-multi-year-research-development-and-22>.
2. R.P. Teyber, K.D. Meinhardt, E.C. Thomsen, E. Polikarpov, J. Cui, A. Rowe, J.D. Holladay, et al. “Passive Force Balancing of an Active Magnetic Regenerative Liquefier.” *Journal of Magnetism and Magnetic Materials* 451 (2018); doi:10.1016/j.jmmm.2017.11.002.

Electrochemical Compression

Monjid Hamdan
Giner ELX, Inc.
89 Rumford Ave.
Newton, MA 02466
Phone: (781) 329-0306
Email: mhamdan@ginerelx.com

DOE Manager: Neha Rustagi
Phone: (202) 586-8424
Email: Neha.Rustagi@ee.doe.gov

Contract Number: DE-EE0007647

Subcontractors:

- National Renewable Energy Laboratory, Golden, CO
- Rensselaer Polytechnic Institute, Troy, NY
- Gaia Energy Research Institute LLC, Arlington, VA

Project Start Date: October 1, 2016
Project End Date: June 30, 2020

Overall Objectives

Develop and demonstrate an electrochemical hydrogen compressor (EHC) to address critical needs of higher-durability compressors.

Fiscal Year (FY) 2018 Objectives

- Fabricate aromatic membranes with enhanced properties for use in EHCs; evaluate performance of aromatic membranes operating at 5,000 psi (350 bar).
- Improve EHC water and thermal management.
 - Develop water-management membranes (WaMM) for use in EHCs.
 - Engineer stack and cell components for high-pressure operation.
- Optimize stack hardware and demonstrate cell performance of ≤ 0.250 V/cell at current densities $\geq 1,000$ mA/cm² at pressures of 5,000 psi (350 bar).

Technical Barriers

This project addresses the following technical barriers from the Hydrogen Delivery section of the Fuel Cell Technologies Office (FCTO) Multi-Year Research, Development, and Demonstration Plan¹:

- (B) Reliability and Costs of Gaseous Hydrogen Compression.

Technical Targets

Table 1. Progress Toward Meeting Technical Targets for Hydrogen Compressors for Fueling Sites

Characteristics	Units	2020 Target ^a	2018 Giner ELX Status
Compressor Specific Energy	kWh/kg	1.62 ^b	2.72 ^c (<1.2) ^d
Uninstalled Cap. Cost ^b	\$	170k	<450 k
Outlet Pressure Capability	bar	950	350

^a FCTO Multi-Year Research, Development, and Demonstration Plan, Hydrogen Delivery section.

^b 100-bar delivery/commercial mechanical compressors are >6 – 8 kWh/kg (@7-bar delivery).

^c Operation at 2-bar delivery.

^d Projected at 100-bar delivery.

FY 2018 Accomplishments

Membrane Optimization:

- Reduced hydrogen back-diffusion in perfluorosulfonic acid (PFSA) membranes by $>50\%$ —applicable to aromatic membranes.
- Improved EHC efficiency—aromatic membrane: cell efficiencies to 2.7 kWh_e/kg-H₂ (@ 1,000 mA/cm²), 2-bar feed.
- Fabricated flexible WaMM compatible with high-pressure operation—significantly improves water management and cell voltage stability at high operating pressures.

¹ <https://www.energy.gov/eere/fuelcells/downloads/fuel-cell-technologies-office-multi-year-research-development-and-22>

Stack/System Hardware Development:

- Completed preliminary review of EHC system with Intertek (product testing and certification company).
- Established appropriated standards, component classifications, and operating requirements for certification.
- Initiated 875+ bar stack design and procurement of components.

INTRODUCTION

Hydrogen compression represents a key technical challenge for the widespread commercialization of fuel cell electric vehicles. To dispense hydrogen to fuel cell electric vehicles tanks, hydrogen must be compressed to a minimum of 875 bar. Conventional compressors account for more than half of the refueling station's cost and have insufficient reliability [1–3]. EHCs utilize direct current to electrochemically compress hydrogen to high pressures. Recent developments in membrane technology promise a new generation of very efficient, low-cost EHCs. The emergence of PEM-based solid-state EHCs eliminates many of the issues associated with mechanical compression; however, current state-of-the-art EHCs are challenged by issues related to membrane sealing and low operating current density attributed to poor water and heat management.

APPROACH

The work conducted in this program exploits the use of three novel technologies that include:

(1) dimensionally stable aromatic membranes, engineered with low electro-osmotic drag and low hydrogen diffusivity, that exhibit high durability and sealing properties; (2) a WaMM that enables passive water feed and cell voltage stability; and (3) an advanced high-pressure stack design optimized for safe high-pressure gas compression. The aim of this project is to further develop and implement these technologies to improve water and thermal management within EHCs and enable high current density operation to reduce compressor cost.

RESULTS

Membrane Development

Perfluoroalkylsulfonate (BP-ArF4) and biphenylsulfonic acid polymers with 50% disulfone units (BPSH) were synthesized and cast into membranes with dimensions of 5.5" x 5.5". The strength of the membranes is enhanced via the addition of thermoplastic support structures. Membrane electrode assemblies (MEAs) were fabricated by bonding anode and cathode electrode structures to opposite sides of the membranes. The MEAs then were assembled into EHC stack hardware and individually tested. Evaluations initially were conducted using PFSA membranes to optimize the catalyst, flow-distributors (to improved heat and water management), and the WaMMs. The improvements then were incorporated into the EHC stack hardware design and used to evaluate and optimize the aromatic membranes developed during this program. Optimization studies were conducted at low pressure (280 psi). Select MEAs then were evaluated at pressures of up to 5,000 psi (350 bar). In all tests, hydrogen was fed to the inlet of the EHC stack at a pressure of 35 psi (~2 bar) and electrochemically compressed to the final pressure. Utilizing this test methodology, an EHC cell voltage reduction of 0.6 V/cell (0.700 V/cell to 0.100 V/cell) at an operating current density of 1,000 mA/cm² was demonstrated at 280 psi (~20 bar) operation. Aromatic membranes, BP-ArF4 and BPSH, exhibited the best cell performance (lowest cell voltage) of 0.100 V/cell at an operating current density of 1,000 mA/cm² (Figure 1).

Following optimization studies at low operating pressures, aromatic membranes then were evaluated in EHC stack hardware rated for 5,200 psi (360 bar). Hydrogen was fed to the inlet of the EHC stack at a pressure of 35 psi (~2 bar) and electrochemically compressed to 5,000 psi (350 bar). Utilizing a back-pressure regulator attached to the outlet of the stack, hydrogen pressure was gradually increased while monitoring cell voltage at a constant current density of 1,000 mA/cm². During evaluation, MEAs fabricated with BP-ArF4 membranes exhibited a voltage of 0.217 V/cell at a current density of 1,000 mA/cm²: **The highest efficiency demonstrated by a single-stage EHC operating at 5,000 psi (350 bar)**. Under similar operating conditions, the cell voltage of a baseline PFSA membrane of similar thickness and ionic conductivity was measured at ~0.3 V/cell. Improvements in cell voltage of the aromatic membranes at high operating pressures are attributed to improved water management (high water content and lower electro-osmotic drag). In addition to improved cell voltage and efficiency, the aromatic membranes also demonstrated a significant reduction in hydrogen back-diffusion as compared to baseline PFSA membranes. The MEAs fabricated with BP-ArF4 membranes demonstrate a back-diffusion loss of 7% at an operating pressure of 5,000 psi (350 bar), compared to 27% when utilizing PFSA membranes (Figure 2).

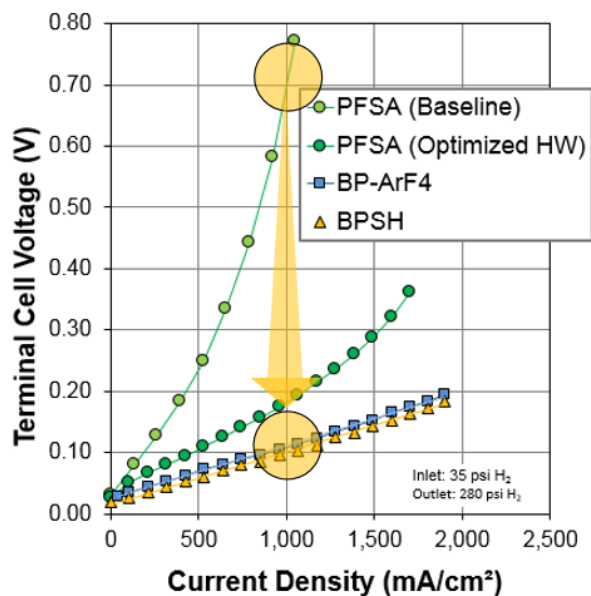


Figure 1. EHC cell optimization and performance at 280 psi (~20 bar)

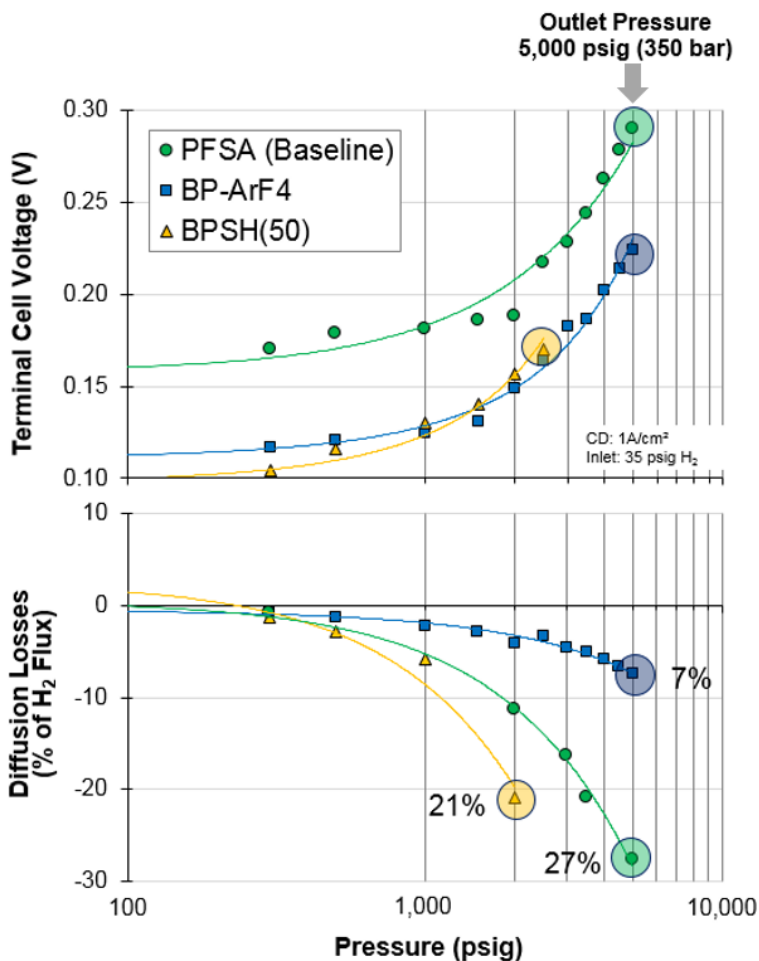


Figure 2. Performance of aromatic membranes at 5,000 psi (350 bar) operation

Separate testing demonstrated that hydrogen back-diffusion in PFSA membranes can be improved at elevated operating pressures. To illustrate this, membranes consisting of a mix of PFSA and synthesized polymers were evaluated in an operating EHC up to a pressure of 5,000 psi (350 bar). As shown in Figure 3, back-diffusion in the modified PFSA membranes was reduced by >50% as compared to “unmodified” PFSA. A trade-off between back-diffusion and cell voltage is realized depending on the amount and type of synthesized polymer. In one test, the modified-PFSA (Mod A) exhibited an improvement in cell voltage from ~0.300 V/cell to 0.240 V/cell at an operating current density of 1,000 mA/cm² and pressure of 5,000 psi (350 bar). Modifications that were implemented on PFSA membranes to reduce back-diffusion will be investigated on aromatic membranes under development in the upcoming year.

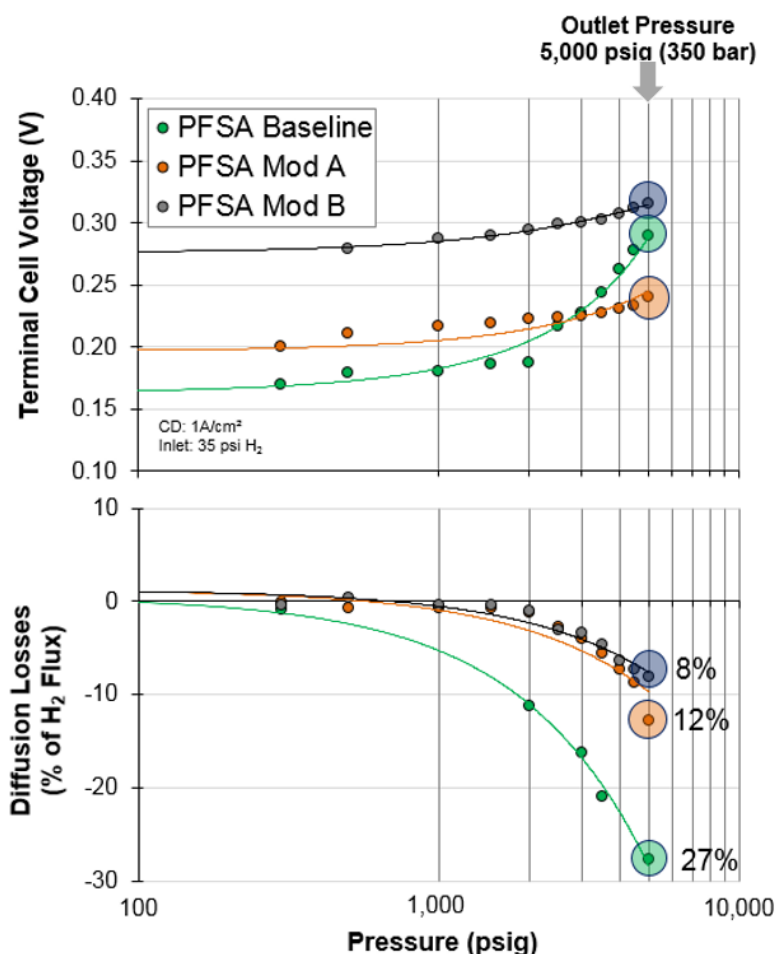


Figure 3. Performance of PFSA membranes at 5,000 psi (350 bar) operation

Electrochemical Hydrogen Compressor Stack Design

The mechanical challenge superimposed on the electrochemical design is the development of a cell-stack configuration that can tolerate high differential pressure across the membrane, cell components, and the outside environment. Giner has demonstrated differential pressures in excess of 5,000 psi (350 bar) using current stack technology. The ability to contain the overall pressure of the stack at an operating pressure of 875 bar requires the use of thicker end-plates to limit deflection, and an improvement in cell component strength.

A preliminary design of a scaled up (300 cm²) 875-bar stack design has been completed. Additionally, a 50 cm² version of the 300 cm² 875-bar stack design was machined, complete with all internal cell components.

Each of the 50 cm² 875-bar stack endplates (Figure 4) was designed to a thicknesses and diameter of 7 inches and 17 inches, respectively. As a comparison, the 50 cm² 350-bar hardware previously used to validate membrane performance at 5,000 psi (350 bar) has thicknesses and diameter of 4 inches and 12 inches, respectively. The 50 cm² 875-bar stack is currently undergoing proof pressure testing to 1,400 bar. The operational data (mechanical and electrochemical) obtained during stack evaluations will be used to validate the final design of the scaled-up 300 cm² 875-bar EHC stack. Issues related to sealing and cell performance can then be fine-tuned into the final scaled up design prior to fabrication.



Figure 4. 875 bar EHC stack (50 cm²)

Electrochemical Hydrogen Compressor System Design

This project requires the assembly of an EHC system, designed as a complete factory-packaged unit so that only minimal site preparation and installation work will be required. Operation will be completely automated, with a computerized control system providing load-following capability, safety interlocks, as well as remote control and monitoring. The EHC system will be pressure tested to the ASME standards, but special considerations will be taken into account for specialized fittings that will be certified to ANSI /HG V 4.10 (standard for fittings for compressed hydrogen gas and hydrogen rich mixtures).

A preliminary system piping and instrumentation diagram (separated into hazardous and non-hazardous zones), component selection, and layout have been initiated. With assistance from Intertek, a description of the applicable standards and codes required for certification were generated. Giner has initiated the procurement of equipment that will be used in the high-pressure operation of the stacks (for the testbed and system). The components are UL listed and rated for operation in classified hazardous areas zoned for Class 1, Division 2, Group B.

CONCLUSIONS AND UPCOMING ACTIVITIES

Significant progress has been made in the EHC membrane development. Giner and its team members have demonstrated membrane reproducibility and durability as well as a significant improvement in EHC cell efficiency. The progress made during this program has enabled EHC stack efficiencies in the range of 2.7 kWh_e/kg-H₂ (flux). Additionally, development efforts conducted under this project have resulted in cost reductions of PEM-based EHC stacks and systems. Future plans include the following.

- Membrane: Complete investigation on aromatic membranes.
 - Continue optimization to reduce back-diffusion in aromatic membranes.
 - Scale up aromatic membranes from 50 cm² to 300 cm².
- Stack: Fabricate and test high-pressure 12,688 psi (875 bar) stack hardware.
 - Initiate 875+ bar testing in 50 cm² hardware, then in 300 cm² hardware.
- System: Initiate assembly of prototype system design.
 - Complete preliminary design of lab-scale prototype unit (piping and instrumentation diagram, process flow diagram, electrical, layout, hazard and operability study).
 - Complete selection and procurement of system components.
 - Review and certify EHC design with third-party nationally recognized testing laboratory (Intertek).

FY 2018 PUBLICATIONS/PRESENTATIONS

1. W. Colella and M. Hamdan, “Energy Systems, Thermodynamic, and Financial Analysis of Low Temperature, Proton-Conducting Electrochemical Hydrogen Compressors (EHCs) for Distributed Energy Storage,” 233rd ECS Meeting, May 13–17, 2018.
2. M. Hamdan, “Advanced Electrochemical Hydrogen Compression,” 2018 International Hydrogen Infrastructure Workshop, Presentation, September 11–12, 2018.
3. M. Hamdan, “Advanced Electrochemical Hydrogen Compressor,” 234th ECS and SMEQ Joint International Meeting, October 2, 2018.
4. M. Hamdan, “Electrochemical Compression,” 2018 Hydrogen Annual Program Merit Review Meeting, Presentation PD136, June 14, 2018.

REFERENCES

1. Fuel Cell Technologies Office Multi-Year Research, Development, and Demonstration Plan: Hydrogen Delivery. http://energy.gov/sites/prod/files/2015/06/f22/fcto_myrrdd_delivery.pdf.
2. G. Parks et al., Hydrogen Station Compression, Storage, and Dispensing Technical Status and Costs (NREL Independent Review, May 2014).
3. “Hydrogen Fueling Infrastructure Analysis.” National Renewable Energy Laboratory. <https://www.nrel.gov/hydrogen/hydrogen-infrastructure-analysis.html>.

Hybrid Electrochemical Hydrogen/Metal Hydride Compressor

Scott Greenway (Primary Contact), Theodore Motyka, Claudio Corgnale, Martin Sulic
Greenway Energy, LLC
301 Gateway Dr., Ste 183
Aiken, SC 29803
Phone: (803) 381-1818
Email: scott@greenway-energy.com

DOE Manager: Neha Rustagi
Phone: (202) 586-8424
Email: Neha.Rustagi@EE.Doe.Gov

Contract Number: DE-EE0007648

Subrecipients:

- Skyre LLC
- Savannah River National Laboratory

Project Start Date: October 1, 2016
Project End Date: September 30, 2019

Overall Objectives

- Combine two novel technologies, an electrochemical hydrogen compressor (EHC) and a metal hydride compressor (MHC), into a new hybrid solid-state hydrogen compressor system.
- Evaluate the hybrid system for hydrogen refueling and other potential commercial hydrogen applications.
- Perform a techno-economic analysis against DOE cost and performance targets.
- Develop modeling tools to guide small-scale experimental testing for both the EHC and the MHC components as well as for the design and testing of a prototype hybrid compressor unit.
- Design, fabricate and test a 1–5 kg/day prototype unit and validate the models for future full-scale application of this technology.

Fiscal Year (FY) 2018 Objectives

- Demonstrate an EHC bench-scale system able to reach the required operating conditions.

- Demonstrate the technical feasibility of the selected hybrid compressor system under partial load and transient conditions.
- Develop a detailed transport model to demonstrate the proposed prototype system for partial load and transient conditions.
- Identify at least one large-scale hybrid compressor system that meets the FOA techno-economic targets under steady state and nominal conditions and design of a prototype.

Technical Barriers

This project addresses the following technical barrier from the Hydrogen Delivery section of the Fuel Cell Technologies Office Multi-Year Research, Development, and Demonstration Plan¹:

(B) Reliability and Costs of Gaseous Hydrogen Compression.

Technical Targets

Hydrogen refueling station compression systems currently have a high capital cost per unit throughput. Today's mechanical compression technology requires frequent maintenance, resulting in the need for redundancy to minimize downtime and leading to high cost. Because of this, DOE is evaluating alternatives to mechanical compressors for refueling station systems up to 100 kg/h. DOE targets for hydrogen compression include achieving output pressures over 875 bar; energy consumption and efficiencies better than today's three-stage mechanical compressors and on a path to approach 1.4 kWh/kg, and a reliability of 80% with a leak rate <0.5%. A preliminary techno-economic model developed during the first half of this fiscal year has shown a hybrid EHC/MHC configuration with good potential of meeting many of DOE's compressor targets.

¹ <https://www.energy.gov/eere/fuelcells/downloads/fuel-cell-technologies-office-multi-year-research-development-and-22>

FY 2018 Accomplishments

- High-temperature membranes were selected so that waste heat from the EHC stage can be used to drive the MHC stage.
- Nafion 117 was selected as the baseline membrane and evaluated at high temperature (150°C) and high pressure (100 bar) with promising results for 100 hours.
- HP2 and HP3 metal hydride (MH) materials (TiCrMn type) were selected as the best candidate materials based on their operating conditions, cost, and availability.
- HP3 was down-selected as the first candidate MH.
- The performance of new MH vessel design, showing substantial performance and cost improvement over standard shell and tube designs, was modeled and successfully verified.
- Nafion 117 operating at high temperatures (>120°C) was found to have suitable waste heat to drive the MH stage, identifying a thermally self-sustaining configuration.
- An initial design was identified for the prototype and large-scale configurations.
- The techno-economic analysis of the new hybrid integrated system identified the current techno-economic performance of the system and a viable path to reach the DOE targets.

INTRODUCTION

Various alternatives to traditional mechanical compressor systems have been considered, including metal MHCs and EHCs. Both MHCs and EHCs are solid-state systems that have no moving parts other than valves. Both are quiet and have low maintenance requirements. However, strength and material issues as well as water and heat management issues have challenged EHCs, especially when operated at very high pressures. Similarly, low efficiency, especially when staging is required to attain high pressure ratios, has challenged MHCs and has made them too complex and expensive. Material degradation due to hydrogen impurity effects has also created issues for MHCs.

One novel alternative evaluated here is to combine EHC and MHC technologies in a way to maximize their advantages and to minimize each of their challenges to improve the overall systems performance on a path to meet or exceed current DOE targets. A hybrid EH/MH compressor takes advantage of lower maintenance/operating costs as well as increased reliability associated with both the MHC and EHC technologies over traditional mechanical compressors. Neither the MHC nor the EHC has any moving parts other than valves. The hybrid system also takes advantage of the higher efficiency and lower cost of the EHC by operating at lower delivery pressures combined with the robust and simple operation of a single-stage MH compressor at higher pressures. Both MHC and EHC technologies are scalable and can be used for a variety of hydrogen compression and delivery applications.

APPROACH

This project integrates an EHC unit with an MHC system into an overall hybrid compressor system. The hybrid compressor will be designed to compress a hydrogen flow rate of 10 kg/h (scalable to 100 kg/h) with an outlet pressure of 875 bar. A prototype hybrid unit will be designed based on the results obtained from system models and detailed models developed to simulate the overall full-scale hybrid compressor system. During Period 2, a prototype will be built and tested for a hydrogen flow rate of 1–5 kg/day and an outlet pressure of 875 bar. The modeling activities (along with selected experimental tests) will represent the basis to design larger scale (10–100 kg/h) hybrid systems and assess their performance against the DOE techno-economic targets.

RESULTS

Screening Analysis of Candidate Hybrid Compressor Systems

The initial techno-economic model developed during FY 2017 has been refined to include:

- Additional balance-of-plant equipment (heat exchangers, valves, humidifiers, and dryers), with the main objective to humidify the hydrogen feeding the EH compressor and dehumidify the hydrogen flow feeding the MH compressor.
- Enthalpy balance equations to assess the efficiency of the EHC system and consequently the available waste heat to be used to desorb hydrogen from the MHC system.
- Volumetric efficiency of the MH compressor system, identifying the additional MH material to be included in the system to assure the continuity and steady state operation performance of the overall compressor.

A schematic of the two-stage compression system is shown in Figure 1. A humidifier unit is placed before the EHC stage to provide the hydrogen flow with the right water content (especially for the Nafion membrane EHC). Two parallel EHC units compress the hydrogen up to pressures on the order of 100–200 bar. The hydrogen flow is then dehumidified in a dryer unit, and the water is collected, pumped, and reused in the humidifier units. The dried hydrogen feeds the MHC units (two parallel units) that compress the hydrogen up to a final pressure of 875 bar.

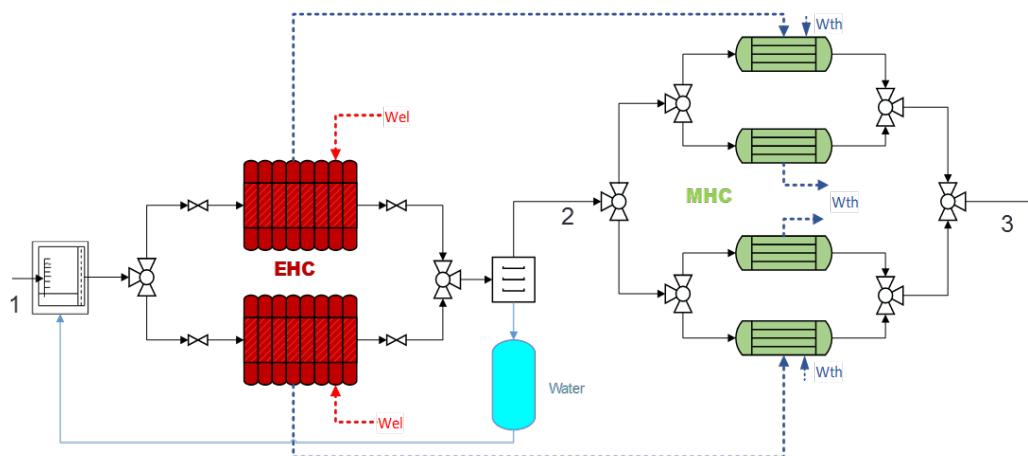


Figure 1. Hybrid compressor schematic (first stage: EHC; second stage: MHC)

Previous techno-economic analyses of the Nafion membrane and PBI membrane systems showed potential cost advantages for a higher temperature PBI system over Nafion. However, further exploration into materials compatibility has revealed potential cost challenges with the phosphoric acid used in PBI systems. Alternatively, recent experimental results indicate an expanded temperature window for Nafion to 150°C, thus maintaining the availability of high-quality waste heat to power the MH cycle. A final membrane down-selection was made in favor of Nafion over PBI membranes due to several disadvantages over Nafion, which include a 4x increase in cell hardware cost to make the hardware compatible with the PBI membranes and swelling of the membrane during doping causing membranes to tear. Nafion was also found to offer the following benefits over PBI membranes for this application:

- Significant experience with Nafion.
- Cell hardware rated for 6,000 psi.
- Application is suited for pressurized water operation.
- Anode and cathode pressure suppress steam.
- Membrane remains hydrated.
- Material stability (below $T_m \sim 190^\circ\text{C}$).
- Demonstrated 100 hours of cell operation at 150°C.

A final decision was made to down-select Nafion 117 for the membrane system for the reasons described above and based on testing described below. The opportunity exists to evaluate Nafion 115 (thinner membranes) in the future as a further cost reduction

EHC Bench-Scale Experimental Tests

Previous testing of Nafion at 150°C was limited to a maximum output pressure of 200 psig. During FY 2018, a high-pressure pump was installed on the test stand to allow testing up to 1,750 psig (120 bar). Figure 2 shows a range of test conditions tested on a single cell stack operating at 500 mA/cm² over a period of 95 run hours. Voltage remained constant at fixed conditions. During the high-temperature testing with Nafion reaching 150°C and 120 bar output pressure, the team leveraged a proprietary hydration and thermal management approach. Future actions for performance improvement include investigation of thinner membranes, membrane pretreatment at high temperature for higher water uptake, and redesign of the flow field for better gas distribution.

Test Point	Temperature (°C)	Anode Pressure (psig)	Cathode Pressure (psig)
A	130	75	200
B	135	75	200
C	140	75	200
D	145	75	200
E	150	75	200
F	150	75	1750
G	150	100	1450
H	150	100	1450

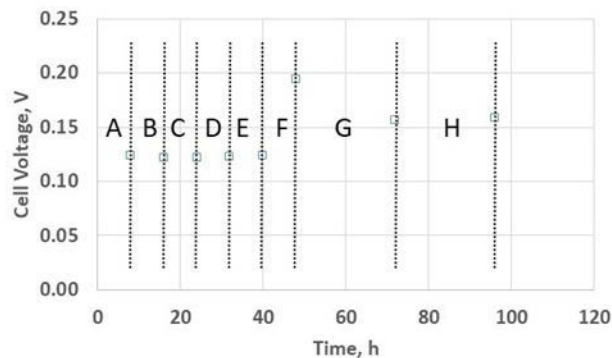


Figure 2. Nafion 117 cell test results during 95-hour operation at elevated temperatures

MH Bench-Scale Experimental Tests

An automated Sieverts apparatus was designed and fabricated for this project during FY 2017. This apparatus, which can operate at pressures greater than 875 bar and temperatures greater than 170°C, has been used to evaluate several high-pressure MH candidates identified last year (TiCr, TiCrMn, TiCrMnFe) as well as several identified in collaboration with the Sandia National Laboratories project team investigating similar high-pressure materials (TiCrMnFeV). Figure 3 shows the results for the characterization of one of our candidate MH materials, HP3 (TiCrMn). Figure 3a shows absorption and desorption isotherms from 22°C to 170°C, while Figure 3b shows van't Hoff plots for the same material, which is used to determine the enthalpy (ΔH) and entropy (ΔS) for the material. HP3 was selected as our best candidate MHC material thus far but additional testing to evaluate alternative annealing methods for this alloy are underway to improve its performance at higher pressures and lower temperatures.

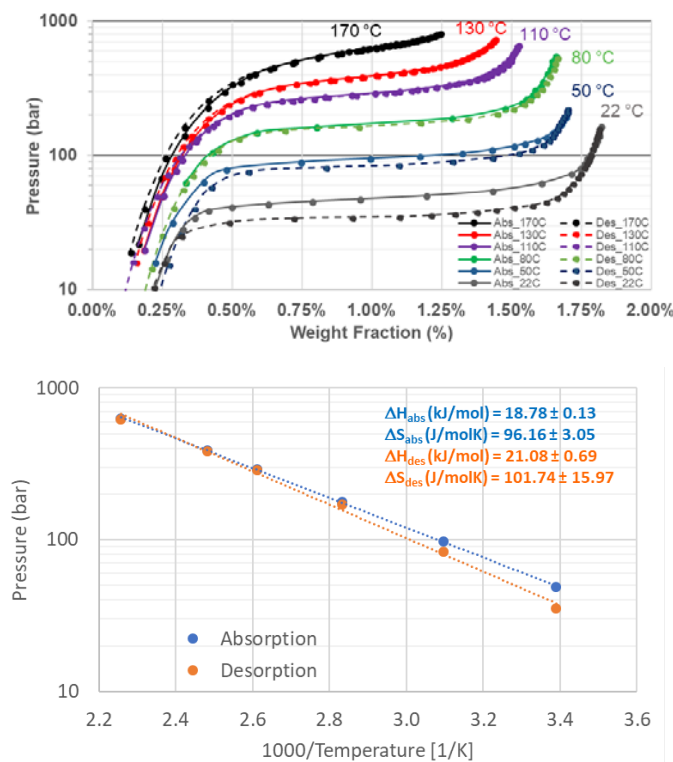


Figure 3. Characterization of MHC candidate HP3 (TiCrMn): (top) absorption and desorption isotherms; (bottom) van't Hoff plot

Hybrid Compressor System Model Development and Application

Global models were developed for the hybrid compressor system. The models are capable of both transient and steady-state calculations and consist of mass and energy equations that are coupled to equations for the thermodynamics of the EHC and the kinetics and thermodynamics of the MHC. Real gas properties were obtained by interfacing dynamically with the National Institute of Standards and Technology REFPROP [1] software. Characteristic parameters for the compressor are based on available data and MH properties that are similar to those anticipated for the actual material. The model for the MHC applies to a transient start-up from an initial MH concentration of 1,000 mol/m³ and an initial discharged metal concentration of 12,000 mol/m³ at the start of the first cycle.

In summary, the models demonstrated the capability of the hybrid compressor system to meet the performance targets for hydrogen flow and pressure at nominal conditions and its ability to rapidly recover from an off-normal state. Additionally, it was shown that the hybrid system can operate under partial feed conditions, as well as partial load, and could exceed 80% of the targets for the compressed gas. Based on model calculations, the 1-hour time allotted for certain stages of the MHC cycle can be significantly reduced provided the size of the MH bed is properly adjusted. The current model was used with our most recent material and system results to predict the performance of our final proposed hybrid compressor system configuration for our go/no-go milestone at the end of the period.

MH Tank Detailed Model Development

A detailed model was developed in Comsol and predicts temperature, pressure, hydrogen flowrate, chemical kinetics, and state of charge for the MH bed. Energy consumption, efficiency, and exergy can be computed from the model. Moreover, the model has the flexibility to be applied to a number of system designs and to various MHs with their accompanying kinetics. The EHC stage couples with the MH stage through boundary conditions on the inlet hydrogen stream and on the heat transfer fluid for the MH stage. An application of the MHC model to a single tube in an MHC stage is provided as a demonstration of the model. The tube wall, MH bed, and adjacent heat transfer fluid are a representative periodic region within the MHC. In the model, the temperature of the MH was controlled by changing the inlet temperature of the heat transfer fluid.

Figure 4 shows the initial design simulated. It consisted of a cylindrical MH bed at the center of the compressor tube, contained by a stainless-steel tube wall with four short fins protruding radially inward from the tube into the MH to promote effective heat transfer. The analysis showed excellent performance with insulation between the external wall and the MH material. Steady state was obtained after three cycles. Additional tests with enhanced finned structure and sensitivity analysis on the insulation are in progress.

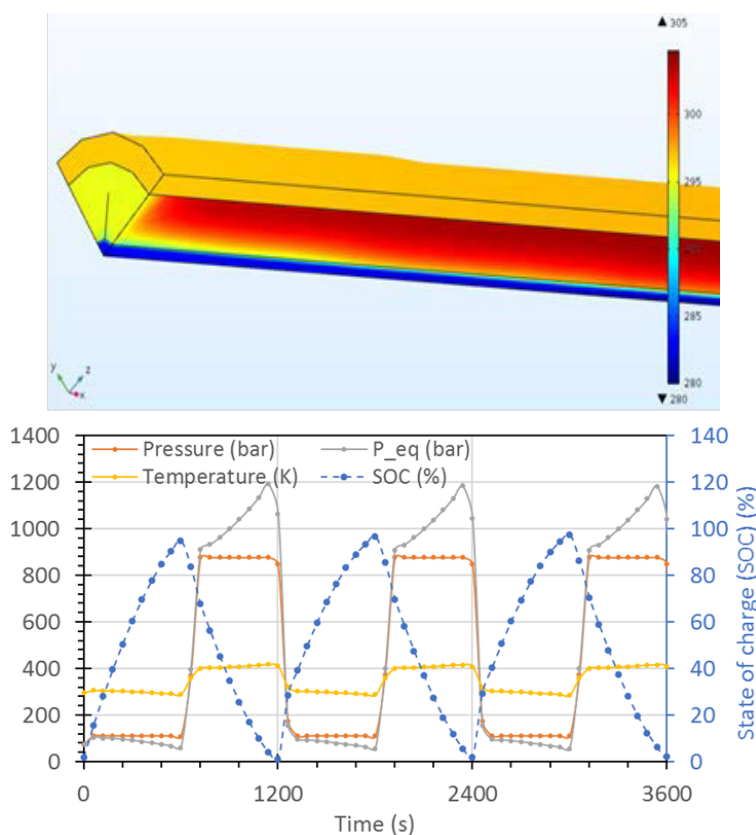


Figure 4. Detailed MH tank simulation: (top) temperature profile—charging cycle at 150 s; (bottom) pressure, temperature, and state of charge plots for three 20-minute cycles

Hybrid Compressor Prototype Design

A prototype, hybrid compressor system (for 1–5 kg/day) was designed and modeled. Several MH compositions (including amendments to enhance thermal conductivity), bed geometries, and heat exchange surface configurations were examined and compared to select the best MH tank format in terms of techno-economic performance. Skyre provided the required details for the EHC system based on the current or advanced high-temperature EHC technology. Figure 5 shows the overall system high level piping and instrumentation diagram schematic. The waste heat available from the electrochemical system membrane electrode assembly is recovered to provide the required heating power to the MH high pressure system. Initial calculations carried out demonstrated the technical feasibility of the integrated approach. The fluid flow rates required to discharge the thermal power produced in the electrochemical system match the flow rates required to transfer the heating thermal power to the MH system. The MH system comprises two parallel units, working in opposite mode (one unit is charging hydrogen and the other unit is discharging hydrogen) to assure continuity. The cooling power is provided through water, operating at about room temperature. The hydrogen processed by the electrochemical unit is stored in a small buffer tank at 100 bar. A three-way valve directs the hydrogen flow to the MH unit working in charging mode. The hydrogen is compressed up to 875 bar through the thermal MH system.

be validated during prototype testing in Phase 2 and used to provide a preliminary design for a full-scale hybrid compressor system.

EHC-MHC Techno-Economic Analysis

- The techno-economic analysis for the new hybrid integrated system identified the current cost and performance of the system and a viable path to reach the DOE targets.

Upcoming activities during Phase 2 include assembling and demonstration of the prototype hybrid compressor system, detailed model update and validation against the prototype data, and optimization of the hybrid compressor system to reach DOE targets.

FY 2018 PUBLICATIONS/PRESENTATIONS

1. C. Corgnale, et al. “Technical Performance of a Hybrid Thermo-Electrochemical System for High Pressure Hydrogen Compression.” *ECS Transactions* 80, no. 10 (2017): 41–54.
2. C. Corgnale, et al. Abstract submitted to the ECS AIMES meeting (September 2018).
3. C. Corgnale, et al. “Techno-Economic Analysis of High-Pressure Metal Hydride Compression Systems.” *Metals* 8, no. 6 (2018): 469.

REFERENCES

1. National Institute of Standards and Technology Standard Reference Database 23, Version 9.0. E.W. Lemmon, M.L. Huber, M.O. Mc Linden. Thermophysical Properties Division (Copyright 2010).

Metal Hydride Compression

Terry Johnson (Primary Contact), Anne Mallow, Robert Bowman,^a Barton Smith,^a Lawrence Anovitz,^a Craig Jensen^b
Sandia National Laboratories
7011 East Avenue
Livermore, CA 94551-0969
Phone: (925) 294-2512
Email: tjohns@sandia.gov
^a Oak Ridge National Laboratory
^b Hawaii Hydrogen Carriers LLC

DOE Manager: Neha Rustagi
Phone: (202) 586-8424
Email: Neha.Rustagi@ee.doe.gov

Subcontractor:
Hawaii Hydrogen Carriers LLC, Honolulu, HI

Project Start Date: October 1, 2016
Project End Date: September 30, 2019

Overall Objectives

- Develop and demonstrate, on a laboratory scale, a two-stage metal hydride (MH) compressor with a feed pressure of approximately 100 bar delivering high purity hydrogen gas at an outlet pressure ≥ 875 bar.
- Demonstrate an increase in the technology readiness level of this technology from 2 to 5 and enable the development of a comprehensive cost analysis for a production system scaled to 100 kg H₂/h flow rate.
- Demonstrate, through engineering analysis, that the compressor design is capable of an energy efficiency of < 4.0 kWh/kg.

Fiscal Year (FY) 2018 Objectives

- Down-select to one MH alloy for each stage that meets system-level requirements based on laboratory characterization.
- Complete the detailed design of prototype compressor beds for both stages based on trade studies.
- Demonstrate a compressor design that can achieve an energy consumption of ≤ 4.0

kWh/kg-H₂ under 100–875 bar operation using a system-level model of the compressor.

Technical Barriers

This project addresses the following technical barriers from the Hydrogen Delivery section of the Fuel Cell Technologies Office Multi-Year Research, Development, and Demonstration Plan¹:

(B) Reliability and Costs of Gaseous Hydrogen Compression.

Technical Targets

This project is developing MH compressor technology that is currently at a technology readiness level of 2. The results of this project will address several of the DOE technical targets for small, forecourt compressors, specifically:

- Specific energy: The 2020 target for hydrogen compression from 100 bar inlet is 1.6 kWh/kg. Our project goal is to demonstrate that a MH compressor can achieve a specific energy of less than 4.0 kWh/kg as a first step towards this target.
- Uninstalled capital cost: The 2020 target for 100 bar pipeline delivery is \$275,000. An FY 2019 cost analysis for a commercial system will address the R&D needed to achieve this target.
- Outlet pressure capability: The 2020 and ultimate targets are 950 bar. We plan to demonstrate a prototype compressor concept capable of > 875 bar pressure with a goal of ultimately achieving 950 bar.

FY 2018 Accomplishments

- In collaboration with Greenway Energy Inc., characterized seven different MH alloys for use in the high-pressure stage of the compressor. Demonstrated two alloys that could produce > 875 bar pressure at reasonable temperatures.

¹ <https://www.energy.gov/fuelcells/downloads/fuel-cell-technologies-office-multi-year-research-development-and-22>

- Identified the compressor bed design with the best efficiency, manufacturability, and heat transfer through a comprehensive trade study.
- Completed the detailed design of compressor beds based on a helical tube heat exchanger to maximize performance and energy efficiency.
- Engaged several suppliers for the compressor beds and heat exchangers and received quotes for fabrication. Completed final down-selection and ordered components.
- Performed small-scale thermal conductivity and hydrogen cycling experiments to verify stability and effective thermal conductivity of cycled MH/graphite composites.
- Completed the design of the compressor bed loading procedure.
- Completed the design for the compressor test facility, including the hydrogen supply and recirculation system and the temperature control system consisting of hot and cold oil circulation systems, and assessed safety through a failure modes effects and criticality analysis.
- Updated the system-level compressor model with measured thermodynamics and kinetics of the alloys to be used in the prototype compressor as well as the design of the compressor beds. Simulations were then run to demonstrate that the system could meet our go/no-go criteria.

INTRODUCTION

Conventional hydrogen compressors often constitute more than half the cost of hydrogen stations and exhibit insufficient reliability. Fatigue associated with their moving parts, including cracking of diaphragms and failure of seals, leads to failure in conventional compressors, which is exacerbated by the repeated starts and stops expected at fueling stations. Furthermore, the conventional lubrication of these compressors with oil is generally unacceptable at fueling stations due to potential fuel contamination. MH technology offers an alternative to both conventional (mechanical) and newly developed (electrochemical, ionic liquid pistons) methods of hydrogen compression. Advantages of MH compression include simplicity in design and operation, absence of moving parts, compactness, and potential for high reliability.

MH hydrogen compression utilizes a reversible heat-driven interaction of a hydride-forming metal alloy with hydrogen gas to form the MH phase and is a promising process for hydrogen energy applications [1, 2]. To deliver hydrogen continuously, each stage of the compressor must consist of multiple MH beds with synchronized hydrogenation and dehydrogenation cycles. Multistage pressurization allows achievement of greater compression ratios using reduced temperature swings compared to single stage compressors. The objectives of this project are to investigate and demonstrate, on a laboratory scale, a two-stage MH hydrogen gas compressor with a feed pressure of >100 bar and a delivery pressure ≥ 875 bar of high purity hydrogen gas using the scheme shown in Figure 1. Progress to date includes the selection of metal hydrides for each compressor stage based on experimental characterization of their thermodynamics, kinetics, and hydrogen capacities for optimal performance with respect to energy requirements and efficiency. Additionally, final bed designs have been completed based on trade studies and all components have been ordered. The prototype two-stage compressor will be fabricated, assembled, and experimentally evaluated in FY 2019.

APPROACH

The approach for this project is split into three phases to meet the project objectives: (1) feasibility assessment and system design, (2) prototype fabrication, and (3) prototype performance evaluation. In the first phase, candidate hydride materials are selected based on literature review and team experience. Absorption and desorption isotherms of selected hydrides are then measured and compared to system-level requirements to demonstrate feasibility. In parallel, trade studies are performed on different design configurations for the prototype compressor beds and a down selection made. Finally, a system-level compressor model is developed and used for feasibility assessment of the hydride materials and bed designs.

In the second phase, component fabrication and assembly drawings for compressor beds are developed based on the down selected designs. Procurement of hydride alloys and fabrication of bed components follows. Once received, the integrated prototype compressor is assembled.

In the third and final phase of the project, the prototype compressor is integrated with the test facility and performance testing of the prototype is conducted. This testing assesses the impact of heating rates, state of charge, and temperature ranges on compressor performance as well as degradation behavior. This will include up to 300 hours of operation. Results of the prototype characterization will be documented and used for the conceptual design and cost analysis for a 100 kg H₂/h system in a final report to DOE.

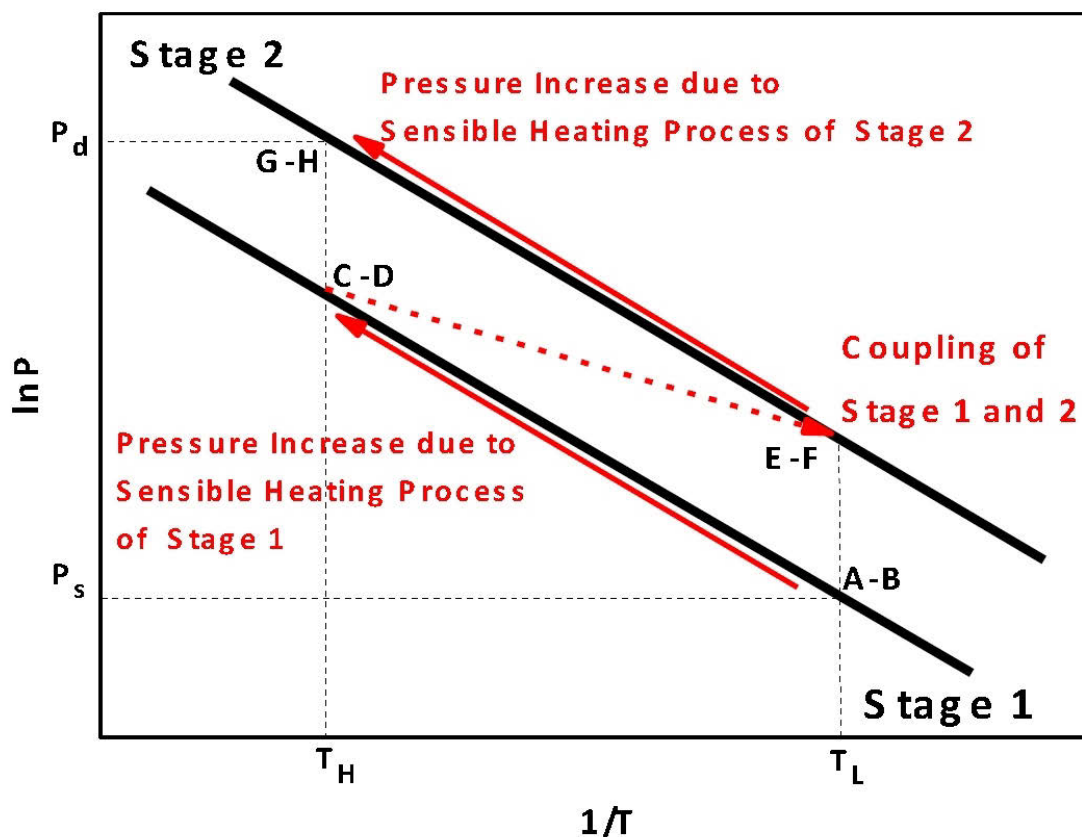


Figure 1. van't Hoff plots illustrating the operation of a two-stage metal hydride hydrogen compression system from the low temperature T_L to the high temperature T_H . The black lines represent the van't Hoff plot for the hydrogenation process for stage 1 (lower black line) and for stage 2 (upper black line). The dashed red line represents the coupling between stage 1 and stage 2. The compression cycle is summarized as follows: Step A: A low-pressure hydrogen supply (e.g., an electrolyzer or pipeline) is attached to the first stage, at pressure P_s . The temperature of stage 1 is maintained at T_L during hydrogenation. Steps B-C: A sensible heating process raises the bed temperature to T_H , increasing the pressure of the stage 1 vessel. Steps D-E: Coupling between stage 1 (dehydrogenation at T_H) and stage 2 (hydrogenation at T_L) occurs. Steps F-G: Stage 2 hydride bed undergoes sensible heating in order to achieve the delivery pressure of P_d . Step H: During dehydrogenation of stage 2 high pressure hydrogen is released from the compressor at P_d .

RESULTS

Metal Hydride Selection and Characterization

The focus in FY 2018 was to identify the best MH for the high-pressure stage of the prototype compressor. To do so required experimental characterization of the pressure-composition-temperature (PCT) behavior of candidate materials. In FY 2017, Oak Ridge National Laboratory (ORNL) had designed and assembled a custom, high-pressure Sievert's apparatus capable of accurate isotherm measurements up to 1,000 bar and 175°C. This system was used in FY 2018 to characterize several high-pressure alloys chosen based on literature data and synthesized by the Materials Preparation Center at Ames Laboratory (Iowa State University). Three alloy samples were fabricated for this purpose, all of which were titanium-based AB_2 -type MHs: (1) $Ti_{0.95}Zr_{0.05}Cr_{1.2}Mn_{0.75}V_{0.05}$, (2) $Ti_{0.8}Zr_{0.2}Fe_{1.6}V_{0.4}$, and (3) $TiCrMn_{0.7}Fe_{0.2}V_{0.1}$. These will be referred to as Ames #1, #2, and #3 for brevity. An additional alloy was produced by Ames based on the Ames #2 material, but with nickel substitution for the iron. This material was formulated to try to produce flatter plateau pressures with somewhat lower pressure than Ames #2 and will be referred to as Ames #4.

In addition, our team collaborated with Greenway Energy, the lead for a related hybrid electrochemical-MH compressor project, to characterize several other materials. For their high-pressure stage, Greenway had identified three different materials. These were also titanium-based AB₂ MHs and included Ti_{1.1}CrMn, (Ti_{0.97}Zr_{0.03})_{1.1}Cr_{1.6}Mn_{0.4}, and TiCr_{1.55}Mn_{0.2}Fe_{0.2}. Greenway had assembled their own high-pressure Sievert's apparatus in early FY 2018 and performed characterization of PCT isotherms on their three materials along with two of our team's alloys.

The following is a brief summary of the results of the characterization of these seven alloys. Of the four alloys chosen by our team, Ames #1 showed a room-temperature absorption isotherm consistent with literature data indicating that it could easily be filled by our low-pressure stage at a reasonable temperature. Desorption pressure from the alloy was then measured at up to 180°C displaying desorption pressures in excess of 875 bar. Although complete isotherms were not measured at these temperatures, the discrete measurements indicated that the alloy was a potential candidate for the high-pressure stage of the compressor. However, the measured desorption pressures would require higher temperature operation than the preliminary design of the compressor assumed.

Ames #2 was found to have the highest desorption pressure capability of all of the alloys tested. Isotherms of this alloy were measured at ORNL and Greenway. As Figure 2 shows, room-temperature absorption requires >400 bar pressure to reach a capacity greater than 1.5 wt%, but at greater than 875 bar, hydrogen can be desorbed from the alloy at 150°C. The figure indicates that while the alloy is viable for the high-pressure stage, highly sloping isotherms prevent it from reaching an ideal compression ratio. In an attempt to correct this characteristic, Ames #4 was produced with the intent that the nickel substitution would flatten and slightly lower the plateau pressures. Unfortunately, the results at Greenway showed that the desorption pressure was lowered too significantly and both the absorption and desorption isotherms remained highly sloped.

Based on literature data, Ames #3 held the most promise for our application with flat plateau pressures that spanned the range of interest for the high-pressure stage of the compressor. However, characterization by Greenway showed that the sample tested did not produce as high a pressure as anticipated. Based on the measurements, the material could be filled at room temperature with about 150 bar hydrogen but might only provide 500–600 bar pressure at 150°C, requiring a higher than desired operating temperature to achieve 875 bar.

Similar results were found by Greenway when characterizing their selected materials. Two of their materials had very sloped isotherms that prevented them from being viable. The third material, Ti_{1.1}CrMn, had relatively flat plateau pressures, but provided lower desorption pressures than anticipated. At 170°C, this material only produced 400–500 bar pressure over a reasonable capacity.

Based on the inability of either team to find an ideal high-pressure stage candidate, it was decided that our prototype compressor would maintain the goal of >875 bar output and use the Ames #2 material for our high-pressure stage. This required shifting our low-pressure stage material from Hydralloy C5 to the Ames #3 material. This material would require 150 bar supply pressure but could provide a high enough pressure to fill the Ames #2 alloy.

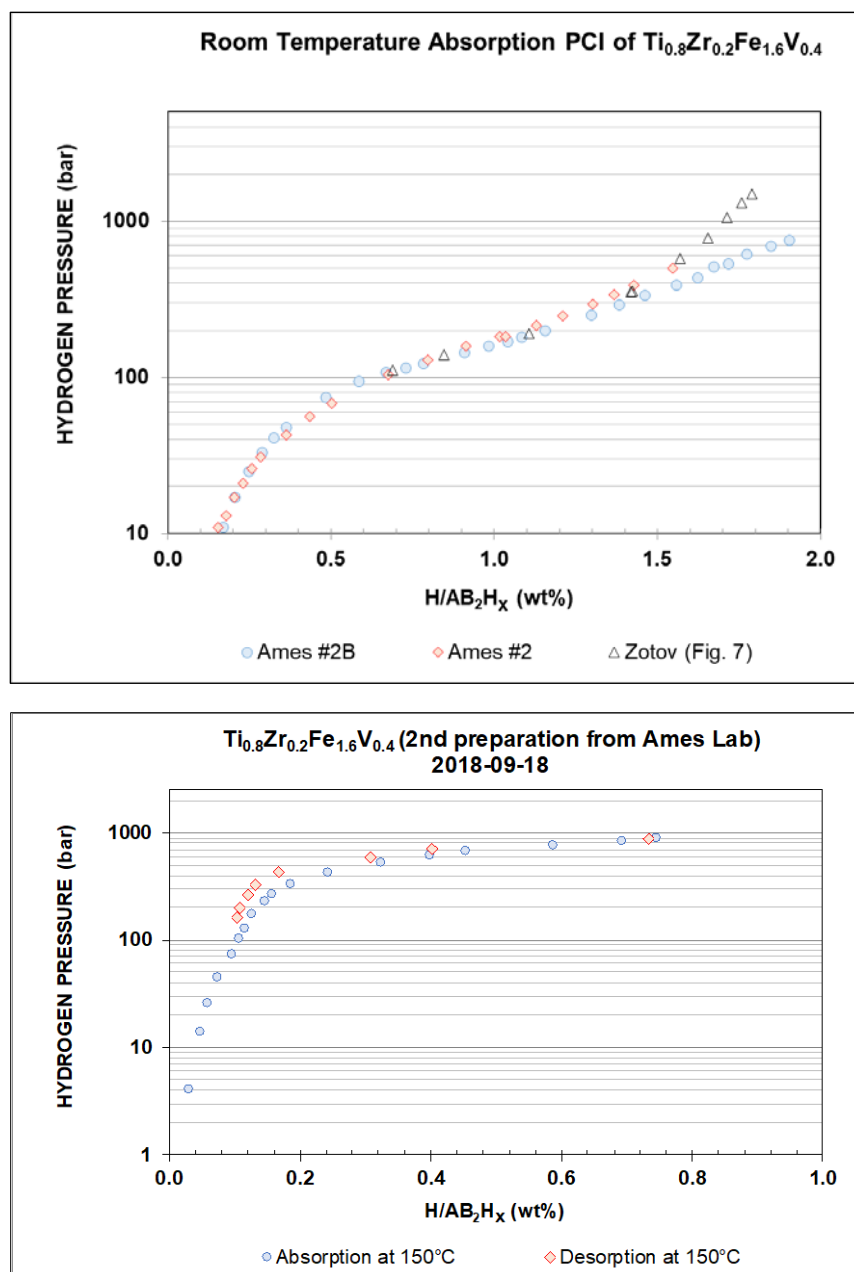


Figure 2. Hydrogen absorption and desorption isotherms measured at ORNL for two preparations of alloy $Ti_{0.8}Zr_{0.2}Fe_{1.6}V_{0.4}$ (Ames #2). Room-temperature data is shown in the top panel along with PCT data obtained by Zotov et al. [3]. Data at 150°C is shown in the bottom panel.

System Design

An extensive trade study was carried out for the compressor bed designs to determine the best design for each stage. Configurations considered include a shell and tube design with external heating/cooling, a closed ended vessel with internal heating/cooling, and an open-ended vessel with internal heating/cooling. A down-selection to a single design for both low- and high-pressure compressor beds was made in Q1 FY 2018. It was determined that an open-ended vessel with a helical tube heat exchanger had the greatest potential to meet goals for heat transfer, target pressure range (50 bar suction and 875 bar discharge), and energy consumption (4.0 kWh/kg H_2). Scalability of the design to 100 kg/h hydrogen flow and cost for high volume manufacturing was also considered.

The final helical tube design for the prototype compressor is depicted in Figure 3 and consists of a single heat exchanger tube that enters through the pressure vessel lid, spirals through the MH, and exits through the vessel bottom. The helical shape of the tube provides optimal heat transfer distribution within the vessel and requires no manifolds, external or internal. Due to this fact, this heat exchanger design provides the lowest energy burden of the options considered. In addition to the helical tube, the cross-sectional view in Figure 3 shows the hydrogen inlet/outlet at the vessel bottom with a hydrogen distribution tube running the length of the vessel. A Teflon liner, also shown in Figure 3, surrounds the helical tube and MH to thermally insulate the hydride from the vessel, improving energy efficiency. The vessel lid and seal consist of a two-piece design with the T-shaped piece providing the seal with a polymer or metal gasket and the large annular threaded nut providing the force to hold the seal in place. This is a standard design for suppliers of high-pressure reactors such as HiP and Parker/Autoclave, for example.

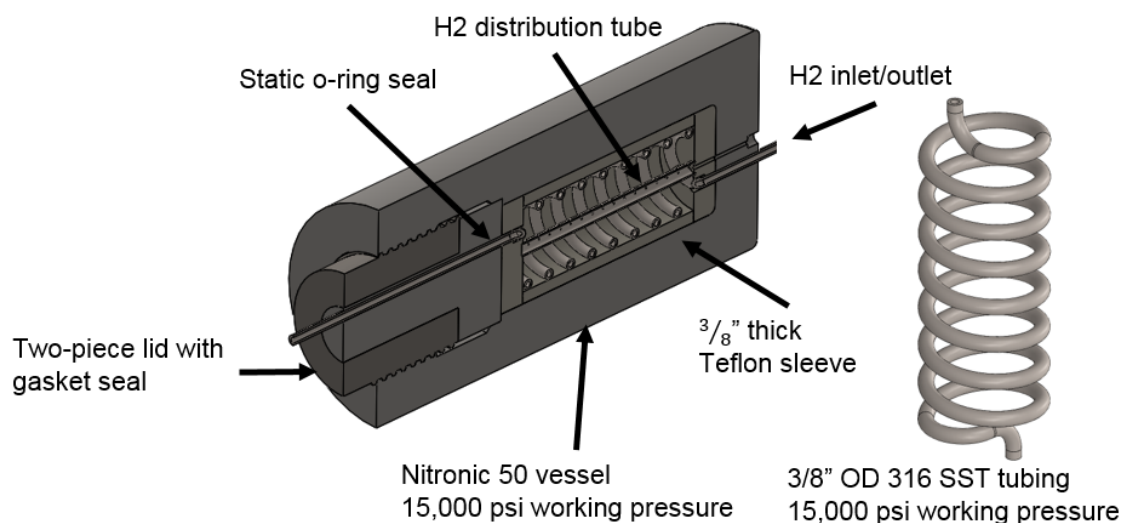


Figure 3. Prototype compressor bed and helical coil heat exchanger

The original design for the compressor prototype included two beds per stage with each bed containing approximately 25 kg of MH. However, due to budget constraints, the prototype was descoped in two ways. Firstly, it was decided that the proof-of-concept could be demonstrated with just one bed per stage. This would not allow for the quasi-continuous flow of hydrogen from the compressor and would cut the flow rate in half but would allow for the demonstration of all other aspects of the system. The second scope change was to reduce the scale of the prototype beds from 25 kg of MH per bed to approximately 3 kg. This required a redesign of the compressor beds but reduced the cost of the prototype significantly and still maintained all of the key design aspects.

A process was identified in FY 2017 to enhance the thermal conductivity of the MH materials using expanded natural graphite (ENG). Enhanced thermal conductivity is necessary to achieve good performance from the compressor beds, which must be alternately heated and cooled to drive the thermodynamic cycles of the MHs. In FY 2018, experiments were carried out to determine the type and amount of ENG to add to the MHs and the required compression force to create robust MH/ENG compacts with good thermal conductivity. Small test compacts (1-inch diameter, 0.25-inch thick) were pressed using a hydraulic press in an argon glove box. These compacts were then measured to verify the thermal conductivity enhancement of the graphite additive. Measurements were made using the transient plane source (TPS) method with a Hot Disk Thermal Analyzer (ThermTest, Inc. TPS2500). This instrument allows for the measurement of anisotropic thermal conductivity (radial and through-thickness), which is expected from compacted ENG, and graphite flake to a lesser degree. Compacts made from Hydralloy C5 and 10% by weight ENG have shown radial conductivity up to 29 W/mK prior to cycling. Based on literature data [4] and tests performed on cycled compacts at Sandia National

Laboratories (SNL), the thermal conductivity is expected to drop by 50% or more after 10 to 20 cycles before stabilizing.

Test Facility

A test facility has been designed to permit performance testing of the prototype 2-stage compressor that operates between 100 bar and 875 bar. The test facility will consist of three primary systems: a high-pressure hydrogen manifold, a temperature control system with hot and cold oil recirculation loops, and a data acquisition and control system.

The high-pressure hydrogen manifold was designed to allow for supply of hydrogen to the prototype compressor at 50 to 150 bar, compression of hydrogen from the low-pressure to the high-pressure stage, delivery of hydrogen from the high-pressure stage at 875 bar, and closed-loop recirculation of the hydrogen back to the supply volumes. The system makes use of existing infrastructure at Sandia's Hydrogen Effects on Materials Laboratory facility including the supply volumes and associated manifold and the manifold and test stand within the high-pressure test cell. The additional manifold section connecting the two beds to each other and the rest of the system is shown in Figure 4.

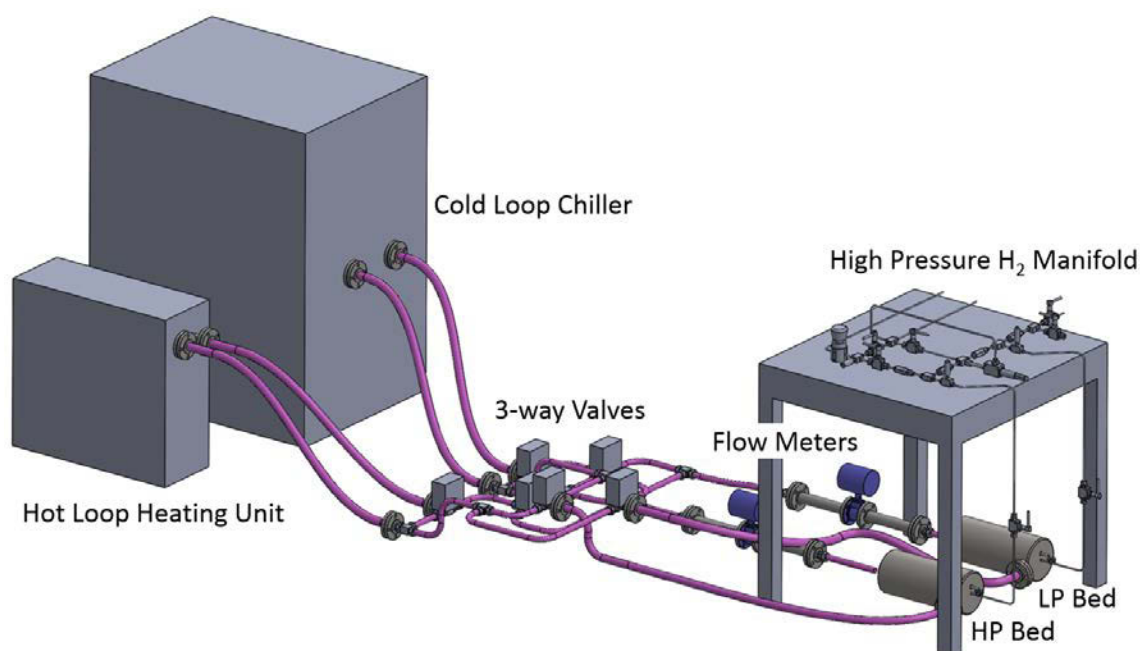


Figure 4. High-pressure hydrogen manifold and temperature control system for the prototype compressor

The temperature control system for the compressor prototype, also shown in Figure 4, consists of two oil recirculation loops, one at a low temperature and one at a high temperature. The low-temperature loop consists of a chiller with self-contained pump and heat exchanger. The chiller circulates heat transfer fluid at a specified temperature through the oil manifold and has a cooling capacity of 3 kW. The high-temperature loop is operated with another self-contained unit with a pump to flow heat transfer fluid and a 6-kW resistive heater. The unit has an internal expansion tank to allow for expansion of the fluid at high temperature. Flow from the two oil loops is directed to either the low- or high-pressure bed through a series of 3-way valves for heating and cooling.

A simple data acquisition and control system will be assembled for the system. Data collected will consist of the flow rate and temperature of the two oil loops, supply pressure, intermediate pressure, and delivery pressure of the compressor, internal and external temperatures of the two compressor beds, and delivered hydrogen flow rate. Control of hydrogen flow through the compressor is achieved through the pressure

differences across a set of check valves between the supply and the low-pressure bed, the low- and high-pressure beds, and the high-pressure bed and a back-pressure regulator set to 875 bar. The pressure of the beds is, in turn, controlled by the temperature of the two hydride beds, which is achieved by directing the flow of the two fluid loops using a series of pneumatically actuated valves. These valves will be controlled by a timer and relay circuit that triggers valves to open or close at preset time intervals chosen based on the desired cycle time of the compressor.

Operation of the system will include a number of hazards including high pressure, high temperature, air-sensitive metal alloys, a combustible liquid, and combustible gases. To ensure the operational safety of the system a failure modes, effects, and criticality analysis was carried out to examine the system for potential failure modes and their associated effects as well as to analyze their relative criticality and risk with respect to safety and programmatic impact. Results from the analysis were used to assist in finalizing and improving the system design and associated testing procedures.

Overall, 346 failure mode effects were identified for the MH compressor system. Out of those, 266 were identified as being negligible in terms of severity. Of the other 70 failure mode effects, one was identified as catastrophic but improbable and 37 were identified as critical. These critical failure modes have been considered further, but none of them have greater than a remote chance of occurring. In all cases, procedures and both passive and active controls and safeguards will be important to insure safe operations. A list of procedures and safeguards has been developed based on this analysis. Procedures will be documented and posted where appropriate. All trained operators will be required to read, understand, and follow these procedures. Safeguards will be fully tested prior to operating the system. We believe that these procedures and controls will prevent or mitigate any significant risks.

CONCLUSIONS AND UPCOMING ACTIVITIES

Work completed in FY 2018 demonstrated that although an ideal combination of MHs for the low- and high-pressure stages of the compressor was not found from the selected candidates, several combinations were viable given either a higher supply pressure or a lower delivery pressure. In addition, a three-stage design was identified based on the measured materials that could compress from 50 to 875 bar. These options were presented to the project sponsor and a final alloy selection was made to deliver 875 bar hydrogen with a two-stage design and 150 bar supply pressure.

The hydride characterization work proved to be much more difficult than anticipated. This points to the need for additional fundamental materials discovery for viable high-pressure MH alloys for this application.

Through the compressor bed design trade study, it was concluded that the helical coil heat exchanger design provided the best combination of performance, manufacturability, and cost. A final detailed design of the bed and heat exchanger was completed and suppliers were engaged to carry out the fabrication for a reduced-scale prototype. Based on system-level simulations, the reduced-scale system should produce a hydrogen flow rate of approximately 120 grams/hour at 875 bar.

The compressor beds and heat exchangers were ordered at the end of Q4 FY 2018 along with the test facility components. In FY 2019, the temperature control system and hydrogen manifold will be assembled, leak checked, and tested. The data acquisition and control system will be designed, procured, and assembled. The custom die sets for the MH/ENG compacts will be fabricated and assembled while the alloys are being produced by Ames Laboratory. Once the alloys are received, they will be processed at Hawaii Hydrogen Carriers where they will be ball milled to a fine powder. The ball milled hydride will then be shipped to SNL for final processing. At SNL, the hydride powder will be mixed with graphite and compacted into shapes for loading into the compressor beds in an argon glove box. Once loaded, the compressor beds will be leak and pressure tested prior to integration in the test facility.

With bed integration complete, system checkout and safety assessments will be carried out prior to hydride activation and initial cycling. The primary performance testing of the prototype MH compressor will then take place. In parallel with this effort, conceptual design and cost analysis for a 100 kg/h commercial system will be carried out by Hawaii Hydrogen Carriers. The performance testing results and cost analysis will then be documented in a final report.

FY 2018 PUBLICATIONS/PRESENTATIONS

1. T. Johnson, “Metal Hydride Compression,” Oral presentation at Joint HSTT-HDTT-CSTT Meeting, Southfield, MI, March 28, 2018.
2. T. Johnson, “Metal Hydride Compression,” Oral presentation at DOE Annual Merit Review, Washington DC, June 2018.

REFERENCES

1. M.V. Lototsky, Y.A. Yartys, B.G. Pollet, and R.C. Bowman Jr., “Metal hydride hydrogen compressors: A review,” *Int. J. Hydrogen Energy* 39 (2014): 5818.
2. V.A. Yartys, M.V. Lototsky, V. Linkov, D. Grant, A. Stuart, J. Eriksen, R. Denys, and R.C. Bowman, Jr., “Metal hydride hydrogen compressors: Recent advances & future prospects,” *Appl. Phys. A* 122 (2016): 415.
3. T.A. Zotov, R.B. Sivov, E.A. Movlaev, S.V. Mitrokhin, and V.N. Verbetsky, “IMC hydrides with high hydrogen dissociation pressure,” *J. Alloys Compds.* 509S (2011): S839.
4. M. Dieterich, C. Pohlmann, I. Burger, M. Linder, and L. Rontzsch, “Long-term cycle stability of metal hydride-graphite composites,” *Int. J. Hydrogen Energy* 40 (2015): 16375–16382.

Dispenser Reliability

Michael Peters (Primary Contact), Josh Martin, Matt Ruple, Kevin Hartmann, Cory Kreutzer, Daniel Leighton, William Buttner
National Renewable Energy Laboratory
15013 Denver West Parkway
Golden, CO 80401-3305
Phone: (303) 524-0864
Email: Michael.Peters@nrel.gov

DOE Manager: Neha Rustagi
Phone: (202) 586-8424
Email: Neha.Rustagi@EE.Doe.Gov

Project Start Date: October 1, 2016
Project End Date: Project continuation and direction determined annually by DOE

Overall Objectives

- Explore the costs and benefits of an increase in the pre-chilled temperature during light-duty hydrogen vehicle fueling.
- Improve hydrogen dispenser reliability through accelerated life testing.
- Perform fill testing of hydrogen tanks at elevated temperature to look at pre-chilled temperature effects on final state of charge.

Fiscal Year (FY) 2018 Objectives

- Complete the commissioning of the research dispenser and recirculation loop.
- Determine the optimal hydrogen sensor placement and setpoints.
- Finish the buildout of the “device under test apparatus.”

Technical Barriers

This project addresses the following technical barriers from the Technology Validation and Safety, Codes and Standards sections of the Fuel Cell Technologies Office Multi-Year Research, Development, and Demonstration Plan.¹

Technology Validation Barriers

D. Lack of Hydrogen Refueling Infrastructure Performance and Availability Data

Safety, Codes and Standards Barriers

G. Insufficient Technical Data to Revise Standards

FY 2018 Accomplishments

- Achieved numerous flow tests on the research dispenser and recirculation loop as part of the commissioning process.
- Determined the optimal location, number, and response time for the hydrogen sensors.
- Finalized the buildout of 10 interchangeable dispenser systems.

¹ <https://www.energy.gov/eere/fuelcells/downloads/fuel-cell-technologies-office-multi-year-research-development-and-22>

INTRODUCTION

Hydrogen station reliability currently lags far behind consumer expectations. To support widespread fuel cell electric vehicle (FCEV) deployment, operators must improve reliability. One of the largest contributors to station reliability problems is the dispenser, in particular the components exposed to prechilled hydrogen. The National Renewable Energy Laboratory's (NREL's) 700-bar station has shown that 65% of its entire station component failures happen within the prechilled portion of the station. An improved understanding of component life cycles at low temperatures is needed so that resources can be allocated to redesign unreliable parts. If the -40°C temperature requirement could be increased to -20°C or even 0°C , station reliability could also be improved. Increasing the low temperature requirement may be possible through alternative fueling protocols, informed by validated fueling models, or through redesigned (or reassessment of the temperature limits of) vehicle tanks that can handle higher temperature excursions.

APPROACH

NREL is performing accelerated life testing of components typically found in the prechilled section of the dispenser. The objective is to measure the mean fills between failures and mean kilograms between failures of hydrogen components subjected to pressures, ramp rates, and flow rates similar to light-duty FCEV fueling at numerous temperatures: -40°C , -20°C , and 0°C . The five types of components under test include nozzles, breakaways, filters, normally closed valves, and normally open valves. Devices from two manufacturers for each component type will be tested at the three temperature levels. Therefore, the testing will yield 30 different mean fills between failures and mean kilograms between failures results by the end of the experiment.

The experiment is broken into variable and fixed factors and levels. The main variable factor that is controlled is the hydrogen temperature delivered to the components. The hydrogen temperature factor consists of three different levels: -40°C , -20°C , and 0°C . The type of component and the manufacturer part number fall within the controlled factors section. Uncontrolled variable factors include ambient temperature and ambient relative humidity. These factors will be measured, recorded, and analyzed for each fill. The fixed factors that will remain the same for each fill are the ramp rate, flow rate, and pressure range of the hydrogen delivered to the components. The expected response variables are whether the hydrogen leaks, number of fills before failure, number of kilograms before failure, and hydrogen leak rate.

The accelerated life testing will allow for eight “dispenser-like” systems to be tested simultaneously. The systems are packaged with two dispenser sets in series and four sets in parallel to complete the full system. A single test setup is shown in Figure 1. The figure shows the five components under test in addition to a pressure transducer and temperature transducer on each individual test setup; these instruments help determine the leak rate of components. The accelerated testing is achieved by putting multiple test setups into one test apparatus and testing them all simultaneously. Figure 2 shows how the individual test setups are positioned in the test apparatus to achieve accelerated life testing. Note that a controllable research dispenser and a recirculation loop were implemented into the test apparatus on the front end and back end respectively.

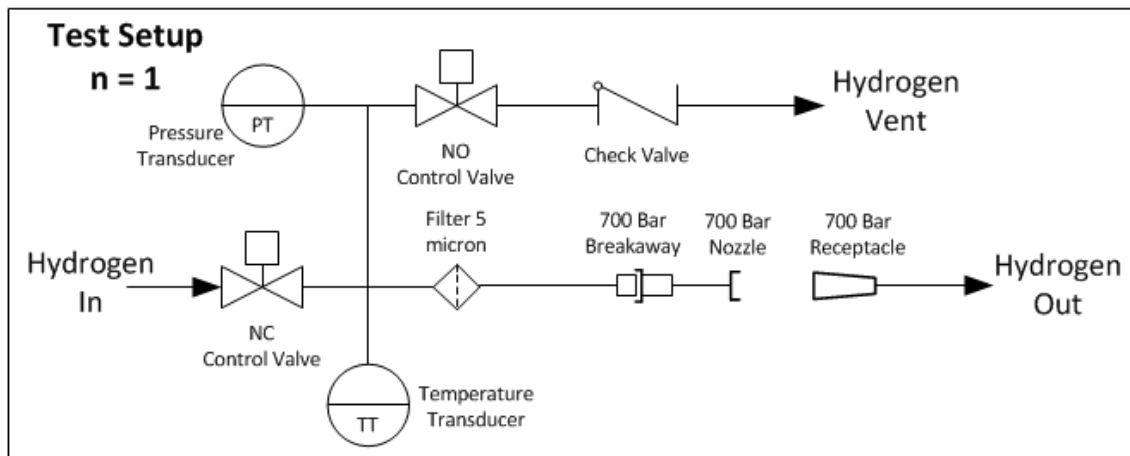


Figure 1. Overview of one test setup

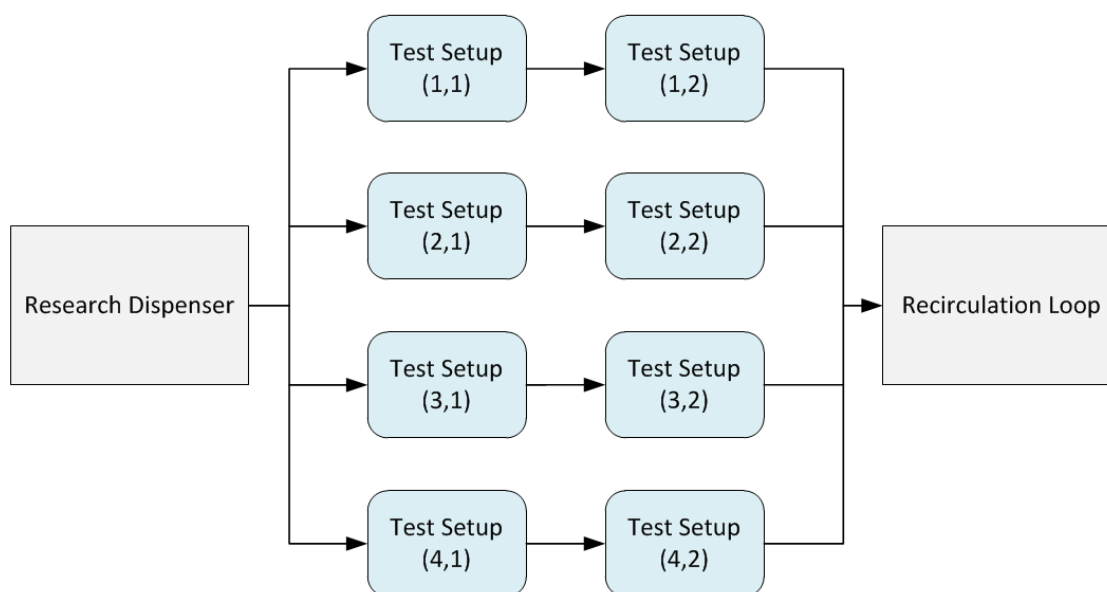


Figure 2. Complete system with eight dispenser test setups

RESULTS

Leak Testing

It is important for the test apparatus to identify any leaks from the components as quickly as possible to determine the true lifetime of the components. There are two different ways the system checks for leaks: hydrogen sensors and a mass calculation using the pressure, temperature, and volume of a given section.

For the sensor approach NREL used its Hydrogen Wide Area Monitoring (HyWAM) apparatus to determine the optimal sensor placement, response time, and warning/fault set points. The testing concluded that two hydrogen sensors were needed per compartment. The test apparatus is broken up into four compartments, each with two dispenser systems, so there is a total of eight hydrogen sensors in use for this experiment. Figure 3 shows the test setup used for determining the optimal sensor placement and response time.

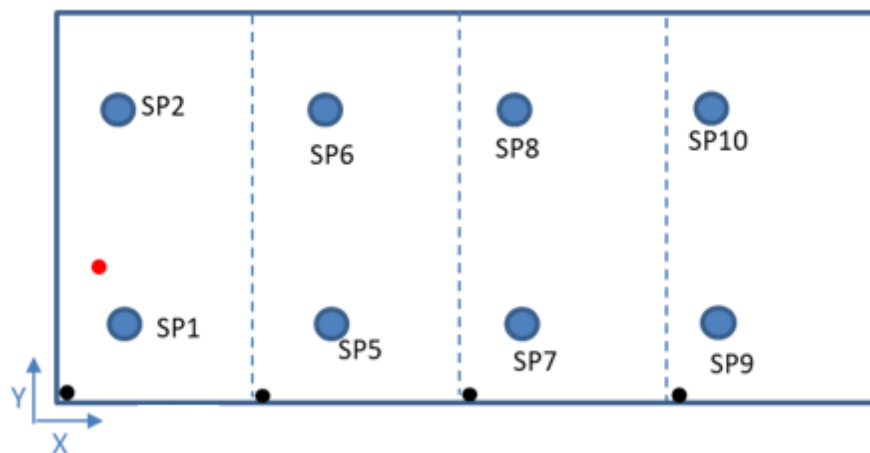


Figure 3. HyWAM sensor placement

In addition to using sensors, a leak rate can be determined by calculating the mass in each section with the corresponding pressure and temperature transducers. The system performs four different leak checks during a fill and it uses that time to determine if there is a small leak that the sensors are not picking up. This leak check method is standard to SAE J2601 fills and is a redundancy to the sensor method that has been implemented.

Research Dispenser and Recirculation Loop Commissioning

NREL designed, built, and commissioned a research dispenser and recirculation loop to support the flow rates, ramp rates, and temperatures required for this testing. The research dispenser supplies high-pressure hydrogen to the system, controls pressure ramp rate, and is used to dial in the hydrogen temperature to the device under test. The recirculation loop acts as a high pressure to low pressure crossover to make a closed system for testing that allows for no consumption of hydrogen. The recirculation loop also controls the flow rate of the test. Figure 4 shows a commissioning fill that was exploring the interaction between the research dispenser and the recirculation loop. The desired ramp rate corridor is represented on the primary y-axis in red and the test pressure ramp rate is in blue. This test showed good agreement between the desired ramp rate and the actual rate. On the secondary y-axis is the gas temperature leaving the system. The black dotted lines show the J2601 requirement window of -33°C to -40°C and the orange line is the actual temperature. The fill reached the required temperature in enough time and the temperature hovered around the warmest part of the temperature corridor.

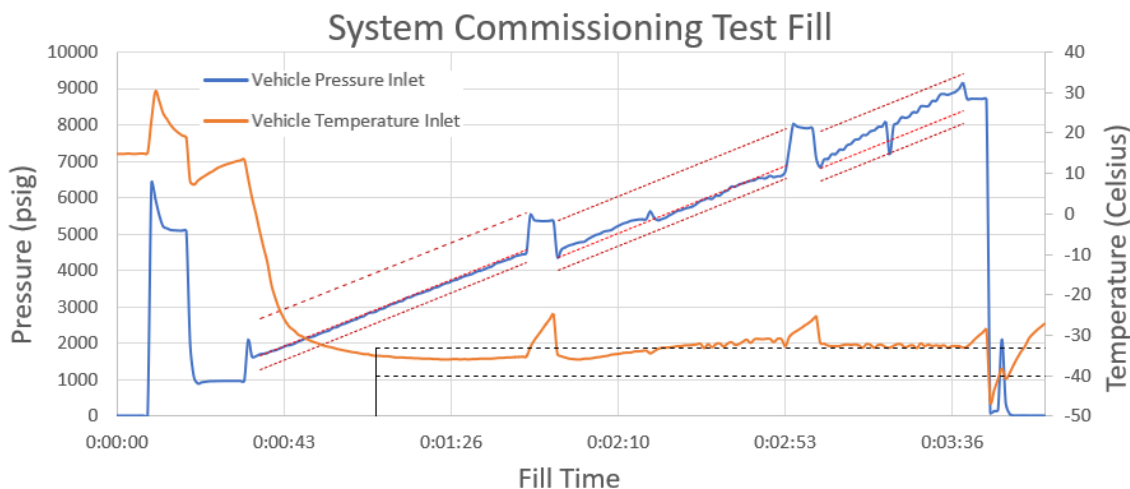


Figure 4. System commissioning test

Device Under Test Buildout

NREL was able to obtain components from two different manufacturers for each device under test. The device under test apparatus was built to accommodate eight dispenser-like systems at once with two dispenser systems going into a single compartment. The apparatus was modeled after an electrical rack where components can easily be slid in or out based on the need to replace a component. Spare parts are on hand to ensure the quick transition of the apparatus when parts fail; this allows for continued testing while the failure analysis is being conducted. Figure 5 shows the device under test apparatus after buildout was complete.



Figure 5. Device under test apparatus

CONCLUSIONS AND UPCOMING ACTIVITIES

NREL will complete the accelerated life testing on the components at -40°C , -20°C , and 0°C .

FY 2018 PUBLICATIONS/PRESENTATIONS

1. M. Peters, N. Menon, K. Hartmann, and J. Martin, “Dispenser Reliability,” presentation at the DOE Hydrogen and Fuel Cells Program 2018 Annual Merit Review and Peer Evaluation Meeting, June 2018, Washington, DC.

Advancing Hydrogen Dispenser Technology by Using Innovative Intelligent Networks

Darryl Pollica (Primary Contact), Bryan Gordon,
Chris O'Brien

Ivys Energy Solutions
303 Wyman Street, Suite 300
Waltham, MA 02451
Phone: (781) 812-6772
Email: darryl.pollica@ivysinc.com

DOE Manager: Neha Rustagi
Phone: (202) 586-8424
Email: Neha.Rustagi@ee.doe.gov

Contract Number: DE-EE0007273

Subcontractors:

- Air Liquide Advanced Technologies (US), Houston, TX
- Rheonik GmbH, Oldehausen, Germany
- National Renewable Energy Laboratory, Golden, CO

Project Start Date: June 1, 2016
Project End Date: June 30, 2019

Fiscal Year (FY) 2018 Objectives

- Improve reliability of vehicle-to-dispenser communication with the use of emerging connected-vehicle-to-infrastructure wireless communication technologies employed for Intelligent Transportation Systems, using the secure IEEE 1609 vehicle communications protocol.
- Achieve consistent 2% or better metering accuracy of the dispenser system through tight design control of flow dynamics and thermal response of the meter, as well as improved thermal mass flow regulation enabled by advanced fueling event notification.
- Reduce cost and complexity of dispenser hardware, such as hydrogen pre-cooling systems, via intelligent and predictive controls incorporating individual vehicle data, and, where possible, area-wide fleet data to allow more appropriately sized equipment.

Overall Objectives

- Improve reliability of vehicle-to-dispenser communication with the use of emerging connected-vehicle-to-infrastructure wireless communication technologies employed for intelligent transportation systems, using the secure IEEE 1609 vehicle communications protocol.
- Achieve consistent 2% or better metering accuracy of the dispenser system through tight design control of flow dynamics and thermal response of the meter, as well as improved thermal mass flow regulation enabled by advanced fueling event notification.
- Reduce cost and complexity of dispenser hardware, such as hydrogen pre-cooling systems, via intelligent and predictive controls incorporating individual vehicle data, and, where possible, area-wide fleet data to allow more appropriately sized equipment.

Technical Barriers

This project addresses the following technical barriers from the Hydrogen Delivery section of the Fuel Cell Technologies Office Multi-Year Research, Development, and Demonstration (MYRDD) Plan¹:

(I) Other Fueling Site/Terminal Operations.

Technical Targets

This project will develop an SAE J2601-compliant dispenser system that aims to address reliability concerns with vehicle-to-dispenser communication, compliance with weights and measures standards for commercial fueling, and dispenser cost and complexity. Specifically, the project team will develop, test, and demonstrate dedicated short-range communication (DSRC) hardware for vehicle-to-station communication as opposed to the current infrared communication standard, as well as engineer a new high-accuracy Coriolis flow meter specifically designed to

¹ <https://www.energy.gov/eere/fuelcells/downloads/fuel-cell-technologies-office-multi-year-research-development-and-22>

maintain an accuracy of 4% or better in automotive hydrogen-refueling conditions. This meter will be integrated with the prototype dispenser in an optimized way to ensure that accuracy is maintained, enabling a pathway for NIST Handbook 44 compliance of dispenser systems. Lastly, the project will engineer and develop novel methods for hydrogen pre-cooling, flow control, and predictive control algorithms to decrease system complexity and cost. Technical targets are detailed in Table 1.

FY 2018 Accomplishments

- Successfully completed the first project go/no-go and passed into Budget Period 2 with updated budget proposal.
 - Tested improved hydrogen meter hardware to demonstrate $\leq 2\%$ accuracy of technology using hydraulic bench tests and SAE J2601 H70-T30-compliant refueling.
 - Completed bench testing of DSRC wireless system with over 1 million SAE J2799-compliant messages sent and capability of roadside unit (RSU) to support multiple nozzles.
 - Updated project budget allocation to reflect increased use of contract services to aid in design of innovative dispenser system and DSRC wireless communication.
- Froze the design of innovative dispenser in preparation for hardware build, which included:
 - Collaboration with project partners (National Renewable Energy Laboratory

- [NREL] and Air Liquide) to assess design hazards of dispenser, heat exchanger, and DSRC wireless communication using structured what-if method.
- Finite-element analysis (FEA) to assess ability of dispenser housing to withstand drive-off events.
- Completion of mechanical and electrical design package including process and instrumentation diagrams, wiring schematics, bill of materials, and assembly drawings for use by U.S.-based contract manufacturing/assembly house.
- Completion of mechanical design package of heat-exchanger system.
- Verification of component functional operating limits to design verification and reporting plan.
- Executed agreement with contract manufacturer for the build of dispenser and low-cost ASME heat exchanger with about 45% build completion to date.
- Executed agreement with contract software developer well-versed in DSRC implementation to develop full-scale prototype wireless communication system.
- Presented update on DSRC wireless communication and demonstration plan to the SAE Interface Task Force.

Table 1. Hydrogen Dispenser Targets Compared to Corresponding MYRDD Targets

Category	Project Target	MYRDD	Project Status
Dispenser Capital Cost	\$150,000 at low volume	\$40,000 by 2020 at high volume	Less than \$200K at prototype stage
Communication Method	DSRC using IEEE 1609 protocols	N/A	Demonstrated capability at bench scale
Meter Accuracy	$\leq \pm 2\%$ accuracy at temperatures between -40° and 85° C and flow rates between 0.6 and 60 g/s	N/A	$\leq 2\%$ accuracy with 95% confidence
Cooling System Cost	\leq \$100,000 at low volume	\$70,000 by 2020	In progress—will be determined after prototype is built

INTRODUCTION

This project aims to improve early adoption of fuel cell electric vehicles (FCEVs) by addressing technical obstacles and high costs associated with SAE J2601/1-compliant hydrogen dispenser systems. The team will focus on three main areas: (1) robustness of vehicle-to-dispenser (SAE J2799) communication, (2) ability to comply with NIST Handbook 44, and (3) complexity of system design associated with hydrogen cooling and flow control. The team intends to address these issues by improving hydrogen-meter accuracy, replacing infrared communication with wireless technology used for vehicle-to-vehicle and vehicle-to-infrastructure communication, and implementing improved modeling and controls around thermal and flow management.

APPROACH

The team will design, develop, and deploy an advanced hydrogen dispenser that incorporates DSRC wireless communication and improved hydrogen-meter accuracy to a minimum of $\leq 4\%$. During the beginning phases of the project, demonstration of core technologies will occur at the bench level along with detailed system modeling. Testing will include wireless communication of refueling protocol messages using DSRC hardware and bench-scale demonstration of hydrogen-meter accuracy of at least 4% over varying temperatures, pressures, and flow conditions.

After bench validation, a prototype dispenser will be designed and manufactured for full-scale simulated-environment testing at the NREL Hydrogen Infrastructure Testing and Research Facility (HITRF). The goals of this phase are to validate compliance with SAE J2601/1 (2016), demonstrate hydrogen-meter accuracy of $\leq 4\%$ when integrated in a dispenser, and show wireless communication of refueling messages from a simulated vehicle to the dispenser control unit. Lastly, the prototype dispenser will be installed at an Air Liquide station for up to a 6-month test to validate the advanced communication, meter accuracy, and dispenser performance under real environmental operating conditions fueling FCEVs.

RESULTS

The team successfully demonstrated two key technologies as part of the first project go/no-go: (1) the wireless-to-vehicle communication, which uses DSRC wireless technology customized for this application to transmit SAE J2799 fueling messages, and (2) the hydrogen metering system, which provides highly accurate measurement of hydrogen mass delivered during vehicle fueling events with an accuracy of $\leq 4\%$. In addition to completing this major project milestone, the dispenser design was completed, 100% of components have been procured, and hardware build is about 45% completed.

To demonstrate the go/no-go goal of $\leq 4\%$ hydrogen flow accuracy, the team conducted more than 100 tests with a wide range of conditions. Led by Rheonik, these tests included hydraulic flow accuracy measurements and simulated refueling events in two separate SAE J2601 H70-T30 compliant dispensers. Twenty Coriolis mass flow meters were tested using Rheonik's standard hydraulic test by flowing water through each meter at 10, 8, 4, 2, and 0.2 kilograms per minute. The meter's digital-pulse output channel, typically used for sealed custody-transfer applications such as those in hydrogen refueling, was electronically recorded. Pulsed-flow measurements were then compared to a NIST-calibrated gravimetric device to calculate meter accuracy. As shown in Figure 1, the hydraulic test demonstrated $< 4\%$ accuracy when scaled for hydrogen (10:1 ratio).

Additional meter accuracy testing was performed under a number of SAE J2601 H70-T30 refueling events and validated using an EU metrology device used to measure hydrogen-meter accuracy for fielded systems. In total, 30 tests were performed to quantify meter accuracy over a varying range of pressures, flow rates, total mass dispensed, pre-cool temperatures, and meter placement relative to the heat exchanger (e.g., upstream or downstream). Results from these tests were analyzed using various statistical methods: moving range, one-way analysis of variance (ANOVA), and process capability. Results from these tests demonstrated repeatable accuracy of $\leq 2\%$ with 95% confidence over all conditions tested, as shown in Figure 2, and the capability of the meter to meet DOE's MYRDD target of $\leq 2\%$ meter accuracy. Additional tests that quantify zero-point shift, meter stability, and temperature effects further validate the meter's ability to maintain high accuracy in demanding hydrogen refueling applications.

Test Flow Rate	Average % Error	Standard Deviation	Standard Error
10 kg/min	0.044%	0.054%	0.01%
8 kg/min	0.038%	0.073%	0.02%
4 kg/min	-0.017%	0.079%	0.02%
2 kg/min	0.011%	0.108%	0.02%
0.20 kg/min	0.033%	0.108%	0.02%
Overall Average	0.022%	0.032%	0.01%

Figure 1. Results of hydrogen-meter flow accuracy using hydraulic test method

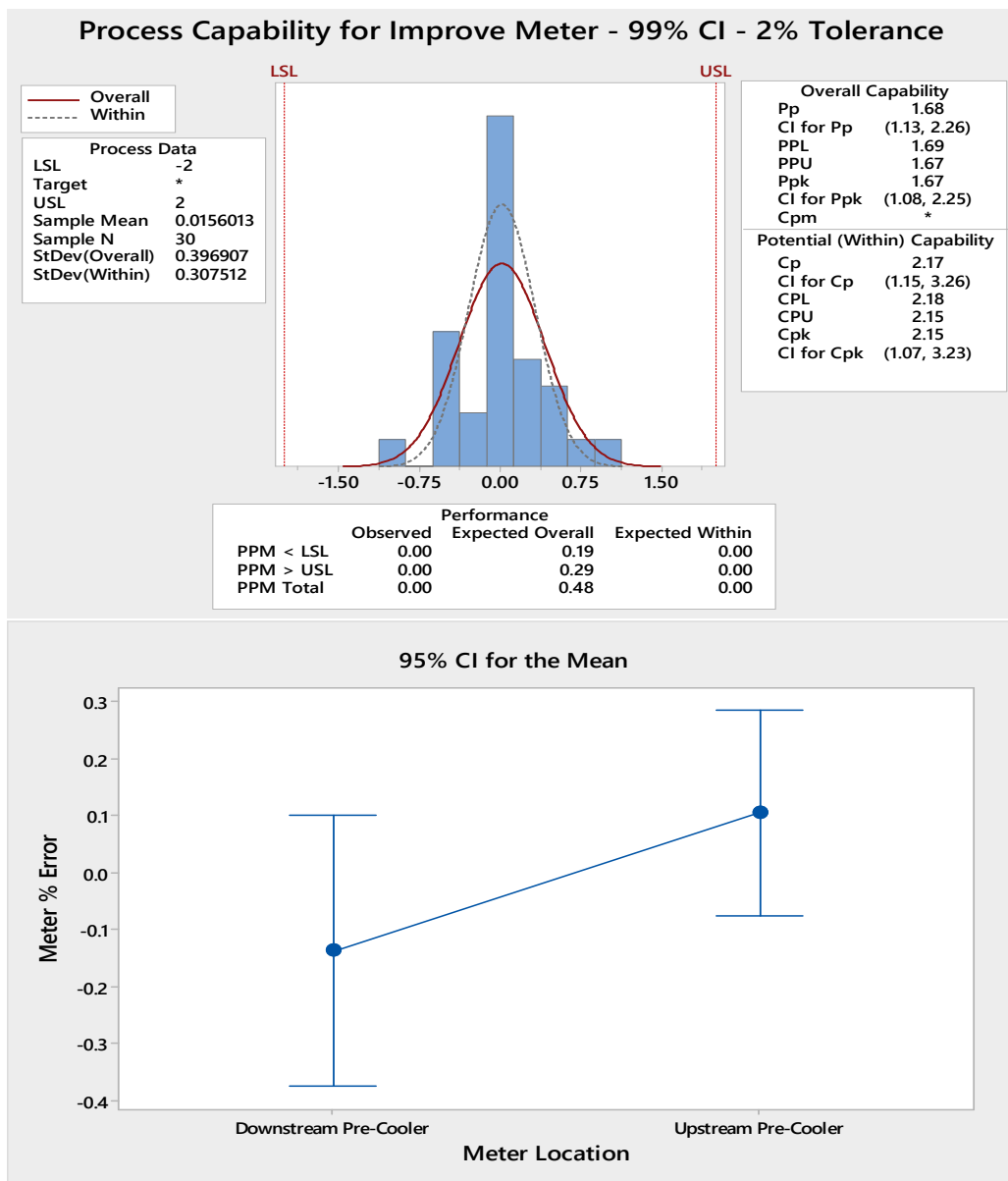


Figure 2. Results of hydrogen-meter accuracy in SAE J2601 H70-T30-compliant refueling

Vehicle-to-dispenser wireless communication was validated at the bench scale, successfully demonstrating DSRC’s capability to send SAE J2799 messages using commercially available hardware. Validation included

development of custom message generation and transmitting applications to send and receive J2799 messages. The onboard unit (OBU) application was designed to read and transmit randomly generated, simulated fueling event messages from a source file. Each message was encoded into a network packet (or payload) and broadcasted by the OBU (vehicle) using WAVE protocols through IEEE 1609 [1] stacks and IEEE 802.11p [2] radios on designated channels. Packets were then received by a corresponding RSU (dispenser), decoded back to ASCII formats, and transmitted to a desktop computer. Each message included a randomly generated set of SAE J2799 string to simulate refueling events, which included randomly varying protocol version, tank volume, pressure, temperature, and fueling commands. Additional information such as message timestamp, send/receive latency, and a unique identifier were also added to each packet. Two other parameters were varied during the test: distance between the OBU and RSU, and the number of messages transmitted per second. For most testing, the distance was about 1.5 meters, as shown in Figure 3; for longer-distance tests, the separation was increased to more than 20 meters, with a wall in between each radio. Message transmission frequency was varied from a low end of 10 messages per second (per requirements in SAE J2799) to a high end of 300 messages per second to simulate multiple simultaneous refueling events.

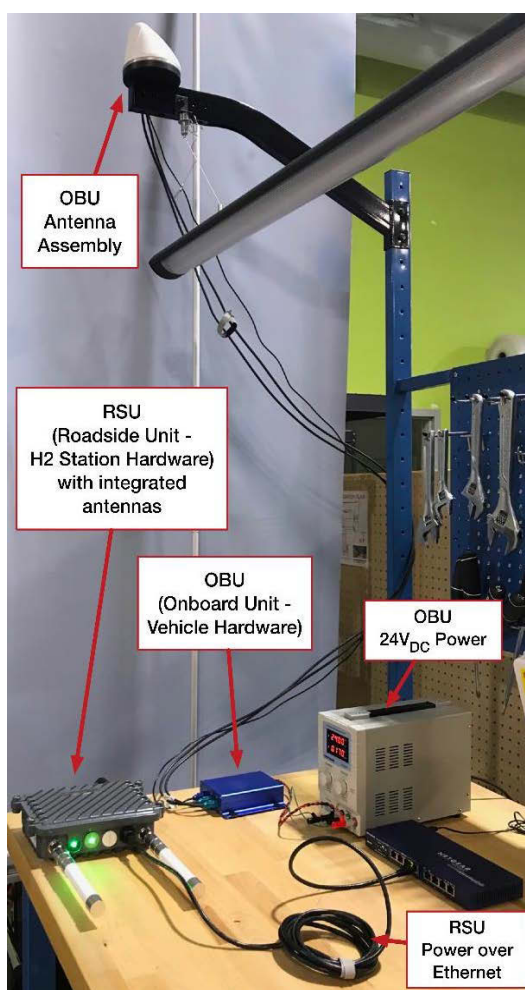


Figure 3. DSRC vehicle-to-dispenser wireless communication test apparatus

Results of the DSRC vehicle-to-dispenser bench testing are summarized in Table 2. In total, 117 individual tests were performed, amounting to more than 1 million messages exchanged, or the equivalent of more than 160 complete refueling events. Over all of these tests, a total of 127 messages (0.01%) were missed with a maximum delay of less than 300 ms; however, all the messages successfully received showed zero errors and

complete cyclic redundancy checks (CRCs) when compared bit by bit over the entire test set. Testing results far exceeded requirements specified in SAE J2799, thus allowing completion of this go/no-go milestone.

Table 2. Summary of DSRC Vehicle-to-Dispenser Communication Bench Testing Results

Test	# of Tests / # of Messages per Test	Message Send Period (ms)	Missed Messages / Total Messages	Longest Delay between Messages (ms)
5-Minute Refueling – Set 1	31 / 6,000	100	31 / 186,000	300
5-Minute Refueling – Set 2	30 / 6,000	100	1 / 180,000	200
High-Data-Rate Test 100 Hz	10 / 6,000	10	0 / 60,000	10
High-Data-Rate Test 300 Hz	10 / 6,000	3.3	7 / 60,000	19
70,000-Message Data Set 10 Hz	1 / 70,000	100	13 / 70,000	300
Long-Distance Test 50 Hz (distance >20 m through wall)	1 / 6,000	20	1 / 6,000	40
Long-Distance Test 300 Hz (distance >20 m through wall)	1 / 74,000	3.3	48 / 74,000	54
Halt and Abort Tests (1 message per 100 has FC=Halt; 1 message per 100 has FC=Abort)	3 / 65,000	4	13	24
Transmission Pause Tests (insert 1 sec pause every 6K messages)	30 / 6,000	4	13	31
<i>Summary</i>	<i>117 tests / 1,011,000 total messages</i>	<i>3.3–100</i>	<i>127 / 1,011,000</i>	<i>Max. 300</i>
<i>Go/No-Go Requirements</i>	<i>Min. 5 tests / Min. 30,000 total messages</i>	<i>100 or faster</i>	<i>N/A (Message content error rate = 0)</i>	<i>500 or less</i>
<i>Result</i>	<i>Pass</i>	<i>Pass</i>	<i>Pass</i>	<i>Pass</i>

The team completed the design and component verification of the prototype intelligent dispenser system, which integrates DSRC vehicle-to dispenser communication, high-accuracy hydrogen metering, and lower-cost hydrogen dispensing equipment for testing at NREL’s HITRF. Design activities included developing manufacturing-ready assembly drawings for mechanical and electrical systems, bill of material, hazard analysis, and FEA analysis. A major piece of this activity was the detailed hazard analysis led by Ivys with support from NREL and Air Liquide. More than 150 man-hours were spent assessing the design using a combination SWIFT/PHA analysis technique, covering various hazards associated with mechanical, electrical, fire, explosion, software, and operator error. Risks identified from this analysis have been mitigated by various design changes implemented before freezing the design. Local manufacturers with expertise in high-pressure gas-system assembly and hazardous-area electrical systems have since begun assembly of the prototype dispenser, which is 45% complete.

Lastly, Ivys presented the proposed DSRC wireless-communication method, testing, and results during the SAE Interface Task Force meeting held on June 6, 2018, in Torrance, California. This SAE team oversees the development and approval of various standards governed by SAE, including fueling protocols, nozzle

requirements, and communication protocols used in hydrogen systems. The presentation was well received by various automotive original equipment manufacturers (OEMs) and station providers, and feedback was used to update existing design and verification plans. An additional white paper was provided to three automotive OEMs to help begin internal discussion and to provide further feedback. The project team hopes that with cooperation from the industry, this project can assist in providing initial test data for use by the industry to influence long-term viability and acceptance of wireless vehicle-to-dispenser communication protocols.

CONCLUSIONS AND UPCOMING ACTIVITIES

In the second year of this project, significant progress was made to validate key technologies, far surpassing the requirements of the go/no-go and demonstrating the ability to meet DOE's MYRDD long-term targets. The dispenser-system design and hazard analysis have been completed, and the design was frozen before beginning build of the prototype dispenser system for testing in early 2019 at NREL's HITRF. Future planned activities include:

- Complete build of dispenser hardware that integrates high-accuracy hydrogen flow metering technology, improved variable-orifice flow control and wireless vehicle-to-dispenser communication.
- Complete a low-cost heat-exchanger system including initial factory testing and ASME certification.
- Install and validate prototype dispenser for compliance to SAE J2601/1 at NREL's HITRF.
 - Demonstrate $\leq 4\%$ accuracy of flow measurement during simulated filling events.
 - Demonstrate $\leq 2.5\%$ accuracy of flow measurement in secondary bench testing using hydrogen-meter qualification equipment at NREL at pressures up to 700 bar, flow rates up to at least 30 grams per second, and ambient hydrogen temperature.
 - Demonstrate transmission of SAE J2601/1 refueling messages from a simulated vehicle to the dispenser control unit per the requirements of SAE J2799.
- Install and validate prototype dispenser under real environmental operating conditions with FCEVs including the following:
 - Demonstrate $\leq 4\%$ hydrogen metering accuracy with a stretch goal of $\leq 2\%$ using the Hydrogen Field Standard dispenser accuracy verification.
 - Demonstrate successful wireless connection from FCEV to prototype dispenser and exchange of refueling event data using DSRC wireless communication.

FY 2018 PUBLICATIONS/PRESENTATIONS

1. Bryan Gordon, "Alternatives to IrDA using Dedicated Short Range Communication (DSRC)," SAE Interface Task Force Conference, 6 June 2018, Honda R&D Americas Inc, Torrance, CA.
2. Bryan Gordon, "Summary of Alternatives to IrDA using Dedicated Short Range Communication (DSRC)," Honda R&D Americas Inc., 19 June 2018.
3. Chris O'Brien, Bryan Gordon, and Darryl Pollica, "Advancing Hydrogen Dispenser Technology by Using Innovative Intelligent Networks," presented at the 2018 DOE Annual Merit Review and Peer Evaluation Meeting, Washington D.C., June 2018.

REFERENCES

1. IEEE 1609 series of standards define security and communication stacks (e.g., MAC and PHY layers) used by DSRC hardware.
2. IEEE 802.11p defines wireless-communication protocols.

Cryogenically Flexible, Low-Permeability Hydrogen Delivery Hose

Jennifer Lalli (Primary Contact) and William Harrison
NanoSonic, Inc.
158 Wheatland Drive
Pembroke, VA 24136
Phone: (540) 626-6266
Email: jhlalli@nanosonic.com

DOE Manager: Neha Rustagi
Phone: (202) 586-8424
Email: Neha.Rustagi@ee.doe.gov

Contract Number: DE-SC0010162

Subcontractors:

- National Renewable Energy Laboratory, Golden, CO
- Pacific Northwest National Laboratory, Pasco, WA
- Cardinal Rubber & Seal, Roanoke, VA
- LifeGuard Technologies, Springfield, PA

Project Start Date: June 30, 2017
Project End Date: October 2019

Overall Objectives

NanoSonic's overall objectives for hydrogen dispenser technologies mirror those of the DOE Office of Energy Efficiency and Renewable Energy (DOE-EERE) Fuel Cell Technologies Office's hydrogen delivery program to realize hydrogen as a safe, reliable, and cost-competitive replacement for gasoline. Outcomes of this project will include:

- A highly durable hose that can reliably perform at 875 bar (for H70 service, 70 MPa delivery) and over a temperature range of -40°–85°C.
- A new class D hydrogen dispensing hose, for use on station-side applications, that is chemically engineered to survive 51,240 fills (70 fills/day, 2 years) and meets the requirements outlined in ANSI/CSA HGV 4.2-2013, with a dispenser compliant with SAE TIR J2601 and NIST Handbook 44.
- A state-of-the-art, metal-free hose based on a unique fiber-reinforced, high-performance, cryogenically flexible polymer to resist

hydrogen embrittlement, survive the Joule-Thompson effect thermal cycles, perform consistently at pressures greater than 875 bar, and endure mechanical wear and fatigue at the pump.

- An alternative to the German-made hydrogen dispenser hose that is currently qualified for H70 service, although it does not meet the service requirement of 25,550 fills/year, nor allow for a cost of \$2–\$4 per gallon of gas equivalent.

Fiscal Year (FY) 2018 Objectives

- Demonstrate a new fitting for H70 service with NanoSonic's hydrogen hose.
- Model and down-select a metal-free, fiber-reinforced hose as a function of fiber material, angle, and filament wind design.
- Quantify the burst strength of the new hydrogen hose with the new fitting.
- Demonstrate durability via pressure-cycle testing.
- Verify durability, purity, and consumer ease of use at dispensing stations.

Technical Barriers

This project addresses the following technical barriers from the Hydrogen Delivery section of the Fuel Cell Technologies Office Multi-Year Research, Development, and Demonstration Plan¹:

- (A) Lack of Hydrogen/Carrier and Infrastructure Options Analysis
- (C) Reliability and Costs of Liquid Hydrogen Pumping
- (E) Gaseous Hydrogen Storage and Tube Trailer Delivery Costs
- (I) Other Fueling Site/Termination Operations.

¹ <http://www.energy.gov/eere/fuelcells/downloads/fuel-cell-technologies-office-multi-year-research-development-and-22>

Technical Targets

The goals of this project mirror those of DOE-EERE to advance hydrogen delivery-system technologies toward the DOE hydrogen delivery program's 2017 delivery targets. NanoSonic has reduced the cryogenic flexibility of our hydrogen hose by decreasing the glass transition temperature (T_g) to -100°C and increasing upper thermal stability to 350°C to enable a wide service-use temperature range of -50°C to 90°C . Burst strength has been increased from 9,000 psi to $>31,000$ psi during first-quarter testing on hoses with fittings crimped in-house. The burst strength will be increased in FY 2019 to 51,000 psi, which is four times the maximum allowable working pressure (MAWP) of 12,690 psi, by modifying the fitting and the application methodology.

NanoSonic modeled, produced, and down-selected a filament-wound hose that survived 50,000 cryogenic cycles at -40°C conducted at a working pressure of 12,000 psi. This same hose also survived nearly 2,000 cycles at 85°C prior to failure due to fitting slippage rather than burst. The new fitting is expected to survive 100,000 combined pressure and thermal cycles over -40°C to 85°C . A novel ceramer coupling agent with a T_g of -65°C was developed, and it demonstrated an increase of 25% burst strength with all fittings. Solvent and abrasion resistance are being tested per the targets outlined in ANSI/CSA HGV 4.2-2013, and evolved gas analysis and quality are being tested per the targets outlined in SAE J2719 and ISO/PDTS 14687-2. Current cost projections based on materials for 300 meters of hose are two times less than the competitor. Cost savings based on durability and normalized for lifetime predict a 4x savings. NanoSonic can produce 16 metal-free hydrogen hoses, each 3 meters in length, in an 8-hour work shift. NanoSonic's planned scale-up

method predicts an 8x cost savings normalized for lifetime and 600 m hose, per targets given in Table 1.

FY 2018 Accomplishments

- Modeled, produced, and down-selected a metal-free filament-wound hose.
- Demonstrated hydrostatic burst strength $\sim 36,000$ psi for three types of non-metal fiber filament-wound composite hoses.
- Demonstrated 25% weight reduction for composite hydrogen hose relative to metal-reinforced hose.
- Demonstrated enhanced flexibility for composite hose relative to metal-reinforced hose for increased durability and an enhanced consumer experience.
- Crimped fittings onto metal-free composite hose and demonstrated burst strengths $\sim 36,000$ psi; failure due to fitting slippage rather than burst.
- Demonstrated a metal-free composite hose that survives 50,000 cycles at 12,000 psi at -40°C .
- Demonstrated an additional $>1,900$ cycles at 12,000 psi at 85°C .
- Developed low- T_g ceramer coupling agent that enhances crimp survivability by $>25\%$ and increased compression strength, exhibits compression strength $>11,200$ psi.
- Reduced cost to $\$300/\text{m}$ via scale-up.
- Collaborating with gas-distribution original equipment manufacturers, fittings manufacturers, national laboratories, and safety standards groups to qualify the hose for H70 service.

Table 1. Progress Toward Meeting Technical Targets for Durable Hydrogen Hose for Fuel Cell Vehicles

Characteristic	Units	2019 Targets	NanoSonic
Tg for Cryogenic Service Temperature	°C	-50	meets
TGA 5% Weight Loss for Upper Service Temperature	°C	90	meets
Burst Strength	psi	51,000	> 36,000, failure due to fitting slippage rather than burst
Cycle Pressure Test	cycles	50,000 cycles at MAWP at -40 °C	meets
Cycle Pressure Test	cycles	50,000 cycles at MAWP at 85 °C	> 1900
Compression Strength	psi	12,690	meets
Hose Cost	\$/m	<200	<60

INTRODUCTION

NanoSonic is developing and manufacturing a cost-effective new hose to offer reliable delivery of hydrogen for fuel cell vehicles as a safe, reliable, and cost-competitive replacement for gasoline per the DOE-EERE hydrogen delivery goals. This American-made hose will meet DOE-EERE's technical targets to enable the hydrogen economy through enhanced safety and durability. There is need for a highly durable hose that can reliably perform at 875 bar (for H70 service, 70 MPa delivery) and over a temperature range of -50°C to +90°C.

NanoSonic has worked during this DOE Small Business Innovation Research program to produce a new class D hydrogen dispensing hose for use on station side applications. NanoSonic's hose was systematically and chemically engineered to survive 51,240 fills, or 70 fills/day for a period of at least 2 years. Our state-of-the-art hose is based on a unique fiber-reinforced, high-performance, cryogenically flexible polymer to resist hydrogen embrittlement, survive the Joule-Thompson effect thermal cycles, perform consistently at pressures greater than 875 bar, and endure mechanical wear and fatigue at the pump. Currently, there is only one hydrogen dispenser hose that is qualified for H70 service. This non-U.S., German-made hose from Spir Star is rated for a working pressure of 875 bar, although it does not meet the service requirement of 25,550 fills/year, nor does its price allow for a cost of \$2–\$4 per gallon of gas equivalent.

APPROACH

The new hydrogen hose involves an all-polymer material approach, in contrast to the currently qualified hose that uses steel as its reinforcing agent. The unique polymer-fiber reinforcement design will meet the current burst-strength requirements and surpass the durability of steel-based hoses, which are susceptible to weakening and catastrophic failure via hydrogen embrittlement. NanoSonic's state-of-the-art hose is based on a unique fiber-reinforced, high-performance, cryogenically flexible polymer to resist hydrogen embrittlement, survive the Joule-Thompson effect thermal cycles, perform consistently at pressures greater than 875 bar (for H70 service, or 700 bar with a safety overpressure), and endure mechanical wear and fatigue at the pump. The polymer core is based on an ultra-low- T_g backbone for cryogenic flexibility and modified for adhesion to the fiber-reinforcing agents and ceramer inclusions for enhanced compression strength.

NanoSonic's manufacturing approach toward cost savings and enhanced durability is three-fold. First, a unique filament winding additive manufacturing technique allows for rapid, reproducible, and reliable production of composite hoses with tailored angular designs. Second, NanoSonic has two large-scale reactors that allow for the cost-effective production of 55-gallon- and 200-gallon-drum batches of our low- T_g and low-hydrogen-permeable nanocomposite resins. Finally, NanoSonic has invested in a crimper to integrate the end-connection fittings directly onto our hoses; and we have partnered with a hose-assembly company to assist with swaged fittings. This allows for enhanced adhesion and mechanical fit between the fitting and the hose. Crimping in-house and with our local partners also yields a product with complete fit and finish for qualification and distribution.

RESULTS

NanoSonic's major focus during FY 2018 was on demonstrating high burst strength and pressure-cycle survivability for filament-wound composite hoses with new fibers. Our 2018 metal-free composite hose is shown in Figure 1. NanoSonic produced hoses >3 meters in length, as shown in Figure 2, and fitted 15"-long sections with end connectors in-house for hydrostatic burst-strength testing, and 5' in length, as determined by their 9" bend radius, for pressure-cycle testing at CSA's laboratory. CSA was contracted to perform the two rounds of pressure evaluations on NanoSonic's high-pressure hoses. The scheduled tests were (a) Hydrostatic Strength and (b) Pressure Cycle Test. Each test is described below.



Figure 1. NanoSonic’s hydrogen delivery hoses demonstrating cryogenic flexibility at the National Renewable Energy Laboratory

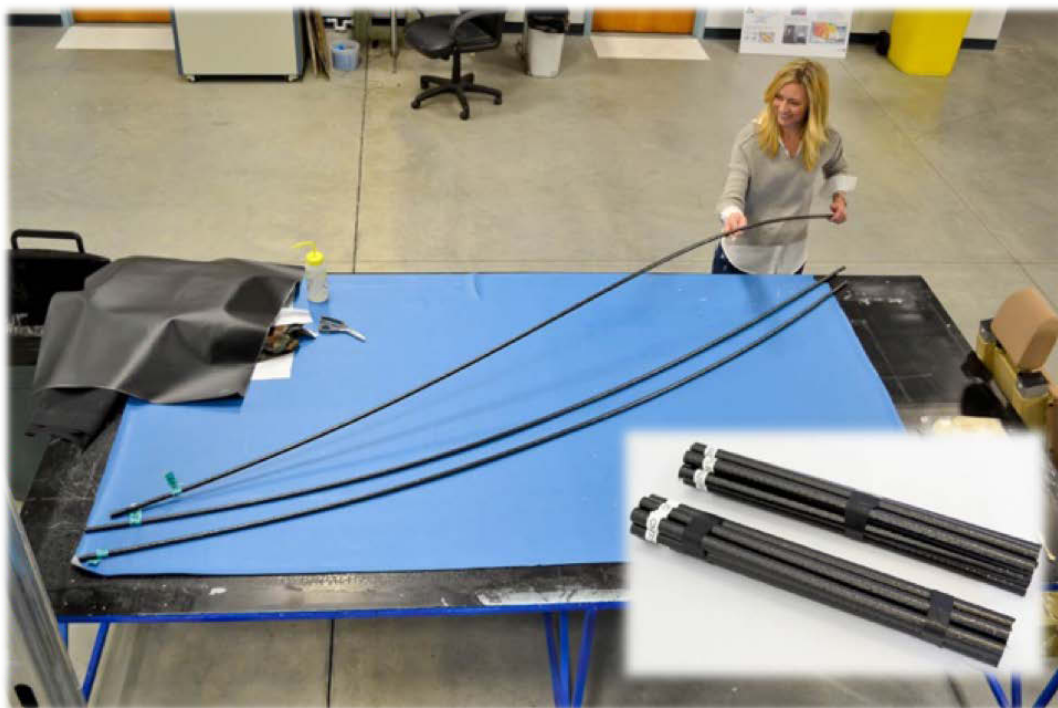


Figure 2. NanoSonic 3-m-length hoses for dispenser integration and 15-in.-length for testing

A. Hydrostatic Strength (section 2.4) of ANSI/CSA HGV 4.2-2013: *Standard for hoses for compressed hydrogen fuel stations, dispensers and vehicle fuel systems*. Requires a 1-min hold without burst or visible loss of fluid at a hydrostatic pressure of 4 times the manufacturer’s specified maximum allowable working pressure (MAWP), up to a 10,000 psi MAWP hose assembly. Two production-assembly samples of each model at 12-inches in length are required.

B. Pressure Cycle Test (section 2.17) of ANSI/CSA HGV 4.2-2013: *Standard for hoses for compressed hydrogen fuel stations, dispensers and vehicle fuel systems*. Requires 50,000 cycles with MAWP (assuming 10,000 psi) at -40°C and 50,000 cycles with MAWP (assuming 10,000 psi) at 85°C, followed by compliance testing to Leakage (section 2.2a) and Electrical Conductivity (section 2.5). Two production-assembly samples of each model hose length of “ $\pi(\text{minimum bend radius}) + 2(\text{hose O.D.})$ ” are required and are shown in Figure 3.

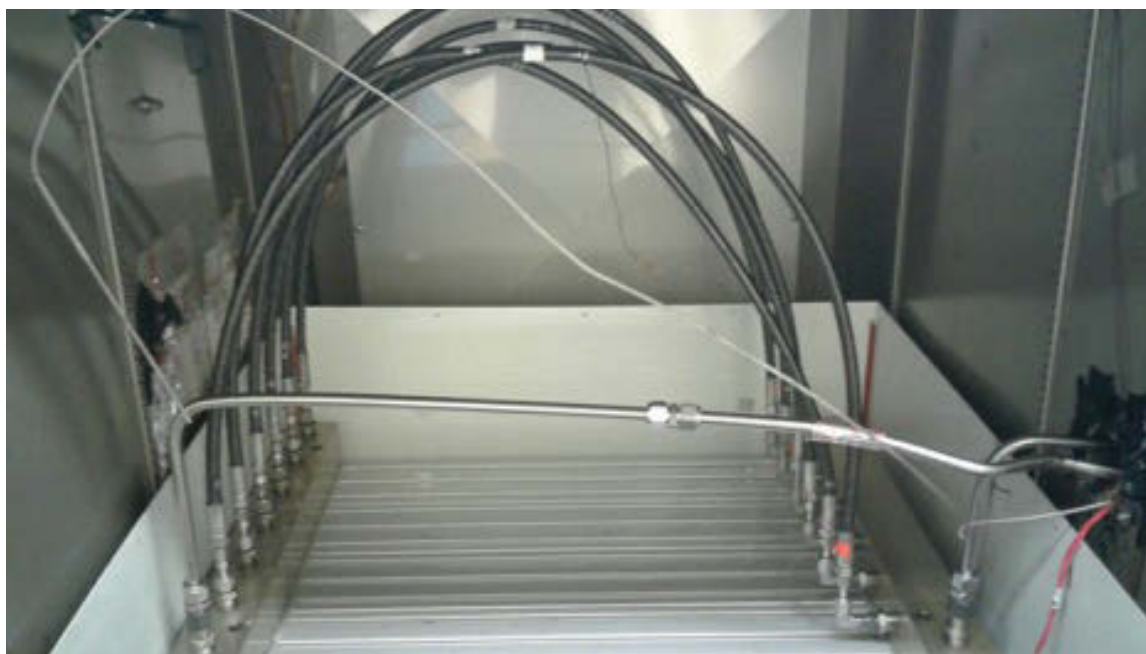


Figure 3. NanoSonic hydrogen hoses in pressure-cycle testing system

First, NanoSonic developed a ceramer coupling agent to enhance the bond strength between the hose and the fitting. It was first demonstrated with a commercial hose and two types of commercial hose fittings. NanoSonic’s ceramer resulted in increased burst strengths that ranged from 10%–50% for each hose (Table 2).

Table 2. NanoSonic Ceramer Coupling Agent Effect on Hose Burst Strength

Hose Type	Hose ID	Fitting	Fitting OD (mm)	Ceramer	Burst Strength (psi)	Failure Mode
commercial	41A	A	16.1	yes	21,191	Burst
commercial	41B	A	16.1	no	10,096	Burst
commercial	WH208-9C20893	A	15.9	yes	58,449	Burst
commercial	WH208-9A20891	A	15.9	no	52,959	Burst
commercial	WH208-9D20894	B	15.9	yes	26,136	Burst
commercial	WH208-9B20892	B	15.9	no	9,635	Burst

NanoSonic used our ceramer with all NanoSonic hydrogen hoses based on the burst-strength enhancements documented with commercial hoses. In 2018, NanoSonic produced a series of metal-free, carbon, and two additional fiber-reinforced hoses on our filament winder that exhibited hydrostatic burst-strength values consistent with H35 service (Table 3). Hose failure occurred for each of these hoses at the end near the fitting.

The fitting crimp recipe was found to influence the burst strength, and NanoSonic hoses with highest burst strength of 35,981 psi failed due to fitting slippage (Figure 4). It was also found that the failure mechanism of commercial hoses was burst. Also of importance, NanoSonic's hoses weigh 25% less than commercial hoses, each with fittings.

Table 3. NanoSonic Hydrostatic Burst-Strength Values for H35 Hoses

Hose ID	Fiber	Ceramer	Fitting	I.D. (in)	Length (in)	Burst (lbs/in ²)
2	C	yes	A	¼	14	26,418
3	C	yes	A	¼	14	25,242
4	C	yes	A	¼	14	25,228
5	C	yes	A	¼	14	30,515
6	C	yes	A	¼	14	28,715
7	C	yes	A	¼	14	30,224
8	C	yes	A	¼	14	31,776
10	C	yes	A	¼	14	30,609
11	C	yes	A	¼	14	35,295
12	C	yes	A	¼	14	35,981
13	D	yes	A	¼	14	26,259
21	E	yes	A	¼	14	31,790
23	E	yes	A	¼	14	29,052
24	E	yes	A	¼	14	29,641

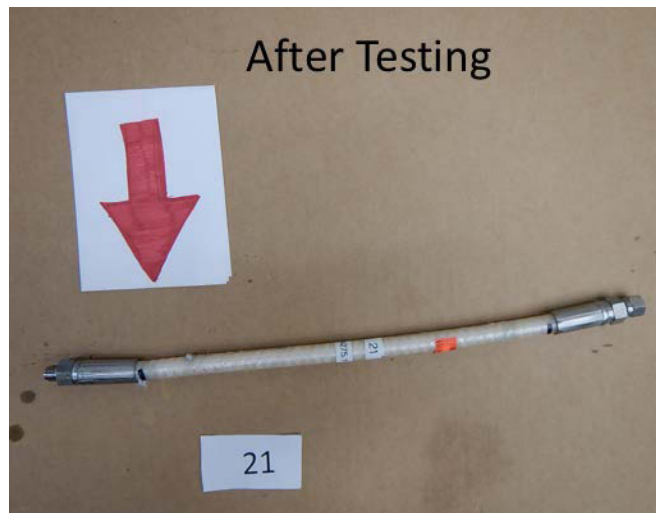


Figure 4. NanoSonic H35 hose with fitting failure

NanoSonic submitted six composites (three types, two of each) for pressure-cycle testing at CSA Group (Figure 3). Each of these specimens was 5' in length, and the architecture consisted of a low-hydrogen-permeable core with a carbon fiber-wound overwrap infused with our low- T_g polymer matrix resin. Each filament-wound architecture varies as a function of the overwrap angle. The Pressure Cycle Test (section 2.17) of ANSI/CSA HGV 4.2-2013 was conducted per the following schedule:

- 50,000 cycles at 12,000 psi (827 bar) at -40°C.

- 50,000 cycles at 12,000 psi (827 bar) at 85°C.

Our down-selected material design survived the following:

- 50,000 cryogenic cycles at (-40°C) conducted at 12,000 psi.
- This same specimen also survived nearly 2,000 cycles (at 185°F) prior to failure due to the fitting slipping off.
- Failure occurred at the 1,988th cycle.
- Failure mode was fitting slippage (Figure 4).

CONCLUSIONS AND UPCOMING ACTIVITIES

Conclusions derived from the work in FY 2018 are the following:

- NanoSonic’s hydrogen hoses meet burst-strength values for H35 service with multiple fibers and are expected to meet H70 service with the appropriate fittings.
- NanoSonic’s ceramer results in increased hydrostatic burst strength.
- Fitting crimp recipe and type influence burst strength.
- NanoSonic’s metal-free hydrogen hose exhibits values of hydrostatic strength of ~36,000 psi and fails due to fitting slippage rather than burst.
- NanoSonic’s metal-free hydrogen hose survives >51,900 pressure cycles at 12,000 psi per 50,000 impulses at -40°C, and >1,900 impulses at 85°C; failure was due to fitting slippage rather than burst.
- NanoSonic is currently testing our hose with new fittings produced locally per internal designs with Cardinal Rubber & Seal, Techsburg, and LifeGuard Technologies.
- Benchmark testing against emerging potential commercial competitors will commence in the next quarter, such as Yokohama Rubber/Iwatani Industrial Gases, ContiTech, and Togawa Rubber. Yokohama’s hose is rated for 70 MPa and the Togawa hose is rated for 35 MPa. There are few details given for ContiTech products.
- Environmental robustness and fuel quality are being established through testing with CSA, Pacific Northwest National Laboratory and the National Renewable Energy Laboratory.

FY 2018 PUBLICATIONS/PRESENTATIONS

1. J. Lalli, “Cryogenically Flexible, Low Permeability H₂ Delivery Hose,” DOE Hydrogen and Fuel Cells Program Annual Merit Review and Peer Evaluation Meeting (2018).

Advanced Barrier Coatings for Harsh Environments

W. Shannan O'Shaughnessy (Primary Contact),
Chris Thompson, and Scott Morrison
GVD Corporation
45 Spinelli Place
Cambridge, MA 02155
Phone: (617) 661 0060 x15
Email: soshaughnessy@gvdcorp.com

DOE Manager: Neha Rustagi
Phone: (202) 586-8424
Email: Neha.Rustagi@ee.doe.gov

Contract Number: DE-SC0011339

Subcontractors:

- Oak Ridge National Laboratory, Oak Ridge, TN
- National Renewable Energy Laboratory, Golden, CO

Project Start Date: April 6, 2015

Project End Date: April 5, 2019

Overall Objectives

- Optimize a flexible hydrogen barrier coating to be vacuum deposited onto elastomeric materials to reduce seal failure due to damage from hydrogen permeation.
- Demonstrate prolonged life of seals and gaskets in compression systems by increasing seal lubricity with a thermally initiated chemical vapor deposition polytetrafluoroethylene (PTFE) coating.
- Demonstrate feasibility of a high throughput, mass manufacturing system for coated O-rings and seals.

Fiscal Year (FY) 2018 Objectives

- Quantify materials characteristics of polymeric and oxide layers as a function of deposition conditions.
- Identify best candidate materials for barrier coating.
- Quantify improved lifetime of PTFE-coated gaskets in hydrogen compressors and dispensers.

Technical Barriers

This project addresses the following technical barriers from the Hydrogen Delivery section of the Fuel Cell Technologies Office Multi-Year Research, Development, and Demonstration Plan¹:

(B) Reliability and Costs of Gaseous Hydrogen Compression

(I) Other Fueling Site/Terminal Operations

(J) Hydrogen Leakage and Sensors.

Technical Targets

This project addresses the failure of seals in hydrogen compression, storage, and delivery operations. Large pressure and temperature variations in the hydrogen station operation compromises seals and gaskets. Barrier film coatings address failures due to hydrogen permeation into elastomeric seal materials. PTFE lubricious coatings address failure due to friction wear on both hard-plastic gaskets and elastomeric seals. Results are aggregated into Table 1.

The objective of this project is to increase the lifetime of seals and gaskets, thereby reducing failures and maintenance downtime of systems. Success in this project will create significant movement toward the stated DOE goal of enabling a delivered hydrogen cost of \$7/gallon gas equivalent in early markets by 2025.

FY 2018 Accomplishments

- Correlated chemical structure of gas barrier material to process conditions. Identified material with lowest defect density, greatest electrochemical stability, and best adhesion to test substrates. It is expected that these properties are aligned with good gas barrier characteristics.
- Improved the mechanical properties of the polymeric layer deposited by plasma activation

¹ <https://energy.gov/eere/fuelcells/downloads/fuel-cell-technologies-office-multi-year-research-development-and-22>

- (instead of thermal activation) so that manufacturing can be economized.
- Established protocols for lubricious coating testing with the National Renewable Energy Laboratory (NREL) to obtain continuous, quantitative comparisons of coated seals with uncoated seals in hydrogen compressors (high-temperature, high-pressure application).
 - Began lifetime testing of coated O-rings in hydrogen dispensers with Takaishi Industry Co. Ltd. (low-temperature, high-pressure application).

Table 1. Progress Toward Meeting Technical Targets for Advanced Barrier Coatings for Harsh Environments

Characteristic	Units	Current Status
Average permeation reduction (helium)	Percent reduction (%)	53%
Average permeation reduction (hydrogen)	Percent (%)	N/A
Compression gasket failure (incumbent benchmarking)	Pass/fail	Pass
Dispenser seal lifetimes	Relative lifetime	Testing in progress

INTRODUCTION

In order to realize the full potential of zero-emission fuel cell electric vehicles, a critical hurdle that has yet to be overcome is achieving viable cost for hydrogen compression, storage, and dispensing. Current hydrogen systems within fuel cell electric vehicles and the supporting infrastructure to compress, store, and deliver hydrogen fuel are prone to systemic inefficiencies and poor reliability. Many of these reliability problems stem from the failure of plastic and elastomer seals (including O-rings, gaskets, and piston seals), which results in significantly increased labor costs for rebuilds and excessive equipment downtime. One cause of failure is that seal components leak and weaken as hydrogen molecules saturate these materials under conditions of extreme temperature and high hydrogen pressure. Another important mechanism of failure is simple frictional wear, which stems from insufficient lubricity and is exacerbated by extreme temperatures and pressures. Thus, there is a need for improved polymer seals with prolonged lifetimes and improved performance in extreme temperature (-40°C to 200°C) and high-pressure (>875 bar) hydrogen environments to enable reliable operation of hydrogen systems. This need has been emphasized in two recent meetings sponsored by the DOE's Fuel Cell Technologies Office [1, 2], hydrogen compressor manufacturers, fuel cell electric vehicles automakers, and two leading seal manufacturers. In this program, GVD addresses the challenges of hydrogen saturation and frictional wear, using its proprietary gas barrier coatings and lubricious coatings (Figure 1).

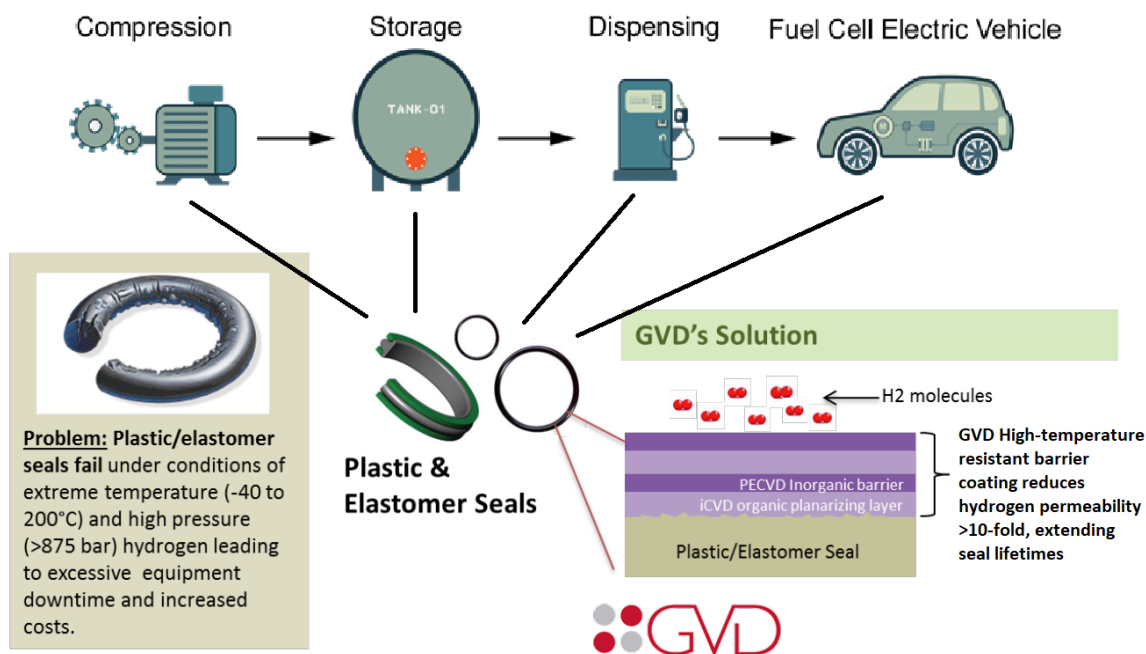


Figure 1. Plastic and elastomeric seals are central to all aspects of hydrogen generation and delivery. GVD's gas barrier and lubricious coatings promise to extend the lifetime and improve the reliability of seals in hydrogen compression, storage, and dispensing equipment.

APPROACH

This project aims to upgrade current state-of-the-art gaskets by applying a vapor deposited film on the outside of the gasket. This can be accomplished using initiated or plasma enhanced chemical vapor deposition. A glass-like oxide material is used to prevent hydrogen ingress into the sample; however, because glass is not a flexible material, it needs to be thin to prevent microfractures that compromise the coating. Dyads of thin glass-like oxides are alternated with polymeric layers to allow the material more flexibility and create a more tortuous path should any cracks form.

One application that GVD is targeting with its coatings is seals used in hydrogen compression. It is important to note that, depending on the application, seals can exhibit a wide range of different pressures and temperatures. Seals fail commonly in high-pressure compression service and must subsequently be replaced because leaks can create both economic and safety concerns. GVD is investigating coating seals with a novel PTFE material to reduce wear. As the compressors run, they heat up due to friction. This heat causes the polymeric material to expand much faster than the metal compressor housing. This expansion leads to increased wear on the plastics. When the compressor is switched to the “off” state and cools, the components constrict to room-temperature size. However, the plastics lose material from abrasion while running and fail to seal at room temperature due to a size mismatch. A PTFE coating adds lubricity to the gasket, preventing friction wear that causes material loss. GVD is partnering with NREL and Takaishi Co. Ltd. to directly test the wear rates of coated seals in industrial hydrogen compressors under harsh conditions.

RESULTS

Following promising helium permeability reduction for a multi-material gas barrier coating, GVD has carried out optimization of the two material types used in the multi-dyad barrier coatings. These are:

1. The glass-like oxide material formed by the decomposition of the precursor. The gas permeability of the oxide material depends on the extent of crosslinking, elemental composition, and surface coverage of the oxide, all of which are controlled by process conditions.
2. The polymeric material that is used as a spacer between the oxide layers. The polymeric material serves to decouple defects in the oxide layer and improve the overall flexibility of the coating, so that cracking is avoided.

Rather than using gas permeability of the complete multilayer coating as a metric for optimization, GVD optimized the two materials separately, using as metrics the properties desirable for each layer. For the oxide, these are stability, adhesion, surface coverage, and a highly crosslinked structure. For the polymeric layer, the metrics are flexibility and smoothness.

For the oxide layer, GVD used Fourier transform infrared (FTIR) spectroscopy and two electrochemical analytical tests, developed specially for this purpose, to evaluate the chemical structure, surface coverage, and stability. FTIR spectroscopy revealed that the deposition conditions explored yielded a wide range of chemical compositions and crosslinking within the film. Electrochemical testing showed that the oxide coatings were able to reject ionic species in solution, indicating that they are pinhole-free. In addition, most of the coatings, though not all, resisted electrochemical degradation, which bodes well for the long-term stability and mechanical properties of the final multilayer coating. Furthermore, there was a strong correlation between the stability and chemical structure of the films; higher levels of crosslinking and high inorganic character led to better film stability and better performance in the electrochemical tests.

One of the main thrusts of this project is the development of a plasma-deposited polymeric layer inspired by a highly flexible overcoat deposited using thermal initiation deposition. Because the oxide layer requires plasma activation, using a plasma process for the polymeric layer offers simplified and accelerated manufacturing. In earlier phases of the program, GVD arrived at a plasma-deposited material that was deemed appropriate for use. However, further testing showed that the plasma-deposited polymeric layer was more brittle than the thermally deposited material. By tuning the energy inputs, reactant mixture, and reaction times, GVD has been able to improve the flexibility of the polymeric material. This work is still ongoing, but FTIR spectroscopy has revealed that the more flexible plasma-deposited material was more similar in its chemical structure to the thermally deposited material. Higher flexibility should lead to greater cracking resistance of the overall coating.

Gaskets coated with GVD's lubricious coating were tested against uncoated gaskets in Hydropac gas compressors at NREL. In earlier phases, GVD saw promising reductions in mass loss of coated gaskets. Since then, GVD has begun testing at NREL, where more standardized testing with continuous monitoring of seal

performance is possible. An aggressive testing procedure was developed to differentiate between controls and test samples. The test procedure involves repeated temperature cycling between ambient temperature and 120°C (cycle time is approximately 1 hour) in addition to real-time monitoring of leak rates. Temperature cycling is expected to maximize the degradation of seals. Real-time leak rate measurements allow for continuous, quantitative comparison between controls and seals with a lubricious coating. The test procedure was checked for repeatable temperature ramp rates and flow rates, and the first round of tests are currently underway. Testing automation introduced in 2018 has improved the repeatability and reliability of the measurements and will allow unmonitored operation of the rig to accelerate futures tests.

In addition, testing of GVD-coated O-rings is currently being carried out by Takaishi Co. Ltd. (of Japan) in low-temperature applications. GVD’s lubricious coatings are being characterized for their effect on the lifetime of O-rings used in hydrogen dispenser equipment. The first round of testing is being performed presently.

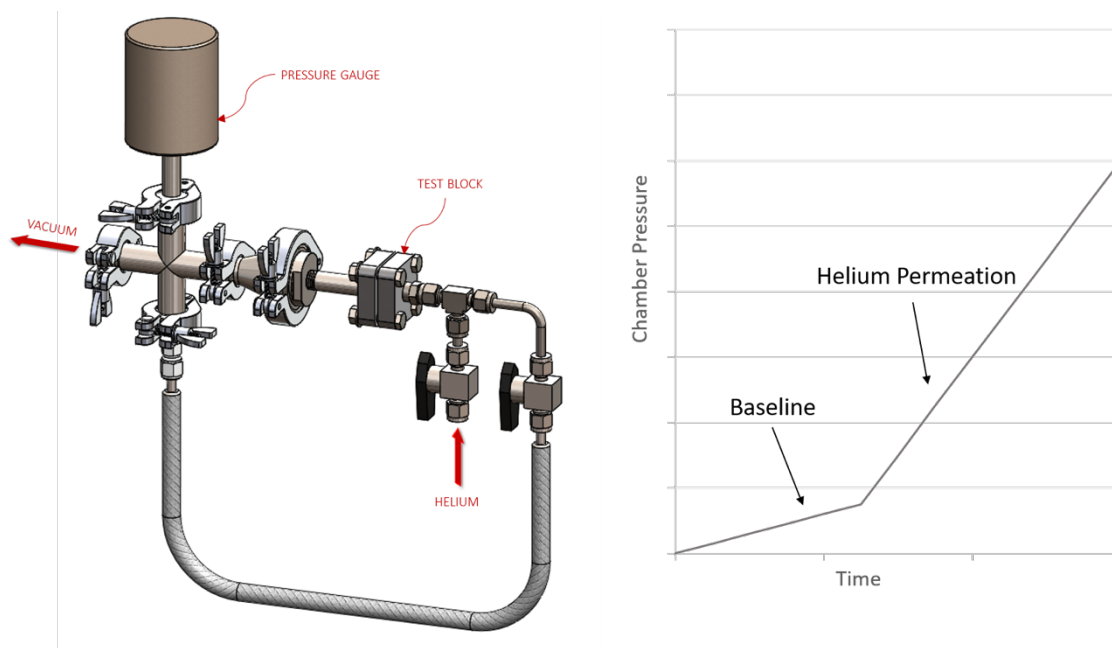


Figure 2. Schematic of the helium permeability testing setup at GVD and a theorized plot of pressure vs. time in a typical permeability measurement

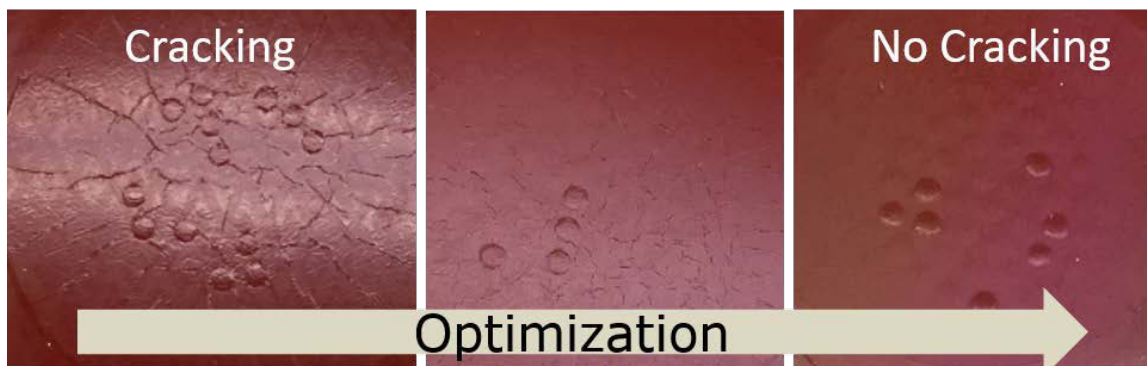


Figure 3. Effect of deposition conditions on the cracking of GVD’s polymeric coating on a silicone substrate

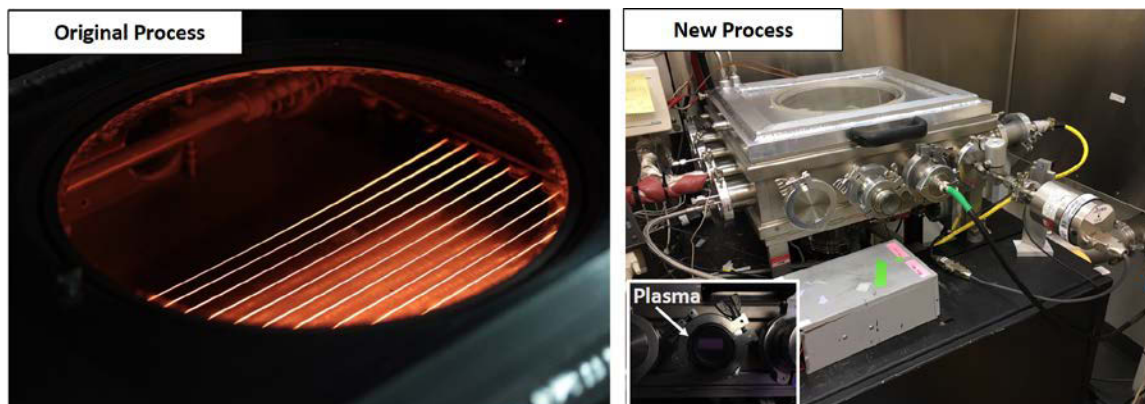


Figure 4. Image of the reactor used for the thermally initiated vapor deposition (left) and that for the plasma chemical vapor deposition process (right)

CONCLUSIONS AND UPCOMING ACTIVITIES

In 2018, GVD has identified the best potential candidate materials (determined by deposition conditions) for the oxide layer and has improved the mechanical properties of a polymeric spacer material that can be manufactured using a plasma activated process. Consequently, future tests of the hydrogen permeability at high temperatures and pressures are more likely to give positive results.

Next, GVD will optimize the geometry of the multi-material coating to achieve the greatest barrier properties and mechanical stability. The considerations include the total thickness as well as the thickness of a surface-passivation layer, a planarization layer, the subsequent oxide layers, and the subsequent polymeric layers. The barrier properties of the coating for hydrogen will then be validated, and optimized manufacturing equipment will be designed. GVD's testing of lubricious coatings for seals and gaskets with NREL will continue, as will the testing of the lubricious coating for low-temperature environments in conjunction with Takaishi Co. Ltd. Feedback from the testing currently underway will provide a starting point for optimization of the PTFE coating.

FY 2018 PUBLICATIONS/PRESENTATIONS

1. Shannan O'Shaughnessy, "Advanced Barrier Coatings for Harsh Environments," Hydrogen Storage and Delivery Tech Team, Golden, CO, February 2018.
2. Shannan O'Shaughnessy, "Advanced Barrier Coatings for Harsh Environments," DOE Hydrogen and Fuel Cells Program 2018 Annual Merit Review, Washington, DC, June 2018.

REFERENCES

1. "Polymer and Composite Materials Used in Hydrogen Service," Meeting Proceedings (Oct. 2012). Accessed Aug 20, 2013. http://www1.eere.energy.gov/hydrogenandfuelcells/pdfs/poly_comp_materials_proceedings.pdf.
2. S. Ahmed, E. Sutherland, *2013 Hydrogen Compression, Storage, and Dispensing Cost Reduction Workshop Final Report* (April 2013). Accessed August 21, 2013. http://www1.eere.energy.gov/hydrogenandfuelcells/pdfs/2013_csd_workshop_report.pdf.

Low-Cost Magnetocaloric Materials Discovery

Robin Ihnfeldt (Primary Contact), Renkun Chen
(University of California San Diego), Sungho Jin
General Engineering & Research
10459 Roselle St. Ste. A
San Diego, CA 92121
Phone: (858) 736-5069
Email: rihnfeldt@geandr.com

DOE Manager: Neha Rustagi
Phone: (202) 586-8424
Email: Neha.Rustagi@ee.doe.gov

Technical Advisor: Sungho Jin
Phone: (858) 945-2030
Email: Jin1234jin@gmail.com

Contract Number: DE-SC0015932

Subcontractor:
University of California San Diego, San Diego, CA

Project Start Date: July 31, 2017
Project End Date: July 30, 2019

Overall Objectives

Discover, develop, and commercialize low-cost high-performance magnetocaloric alloys to enable magnetic refrigeration to move from prototype to production.

Fiscal Year (FY) 2018 Objectives

- Discover low-cost magnetocaloric materials which function at temperatures greater than 50K.
- Characterize ΔT of materials and confirm second-order response.
- Optimize composition and processing to achieve high-performance (ΔT equivalent or better than gadolinium [Gd]), low-cost (target <\$400/kg at large scale), and high-stability form useful for magnetic refrigeration (spheres and/or thin plates).
- Commercialize magnetocaloric materials products on www.geandr.com webstore.

Technical Barriers

This project addresses the following technical barriers from the Hydrogen Delivery section of the Fuel Cell Technologies Office Multi-Year Research, Development, and Demonstration Plan¹:

(H) High-Cost and Low Efficiency of Hydrogen Liquefaction.

Technical Targets

The transportation and storage of hydrogen is safer and more economical when it is in liquid form, but getting it into liquid form and keeping it in liquid form is not easy. Despite significant efforts to improve compression-based liquefaction systems, they remain too inefficient and expensive to meet the DOE hydrogen production and delivery targets shown in Table 1. Therefore, exploration of new refrigeration technologies—such as magnetic refrigeration—is needed.

General Engineering & Research (GE&R) is supporting the DOE effort to develop magnetic refrigeration technologies for high-efficiency hydrogen liquefaction. Our goal is to discover, develop, and commercialize low-cost high-performance magnetocaloric effect (MCE) alloys to enable magnetic refrigeration to move from prototype to production. Targets for our MCE materials have been defined as follows:

- Cost: \$400/kg or less, at large scale
- Performance: Equivalent or better than Gd ($\Delta S \geq 6$ J/kg K in 3T field)
- Forms: Sub-mm sized spheres and thin plates.

FY 2018 Accomplishments

- Discovered low-cost MCE material set with novel second-order response for temperature range 9–340 K.
- Increased performance for sub-80 K MCE materials from $\Delta S \sim 4$ J/kg K in 3T field (Phase I) to $\Delta S \geq 10$ J/kg K in 3T field, which exceeds the project targets.

¹ <https://www.energy.gov/eere/fuelcells/downloads/fuel-cell-technologies-office-multi-year-research-development-and-22>

- Measurable ΔT verified at room temperature and consistent with second-order response.
- In-house small-scale manufacturing processes set up, with initial line of MCE materials products commercialized on www.geandr.com webstore.
- Alloys tested on rotating disk atomization process, with sub-mm sized spheres obtained and MCE properties maintained.
- Discovered that compositional doping improves both MCE performance and material stability in air.

Table 1. DOE Hydrogen Liquefaction Technical Targets

DOE Current Targets	FY 2015 Status	FY 2020 Target	Ultimate Target
Small-Scale Liquefaction (30,000 kg H₂/day)			
Installed Capital Cost (\$)	70 million	70 million	—
Energy Required (kWh/kg of H ₂)	15	12	—
Large-Scale Liquefaction (300,000 kg H₂/day)			
Installed Capital Cost (\$)	560 million	560 million	142 million
Energy Required (kWh/kg of H ₂)	12	11	6

INTRODUCTION

Magnetic refrigeration utilizes the MCE, which is the temperature variation of a magnetic material after exposure to a magnetic field (see Figure 1) [1]. The MCE is an intrinsic property of a magnetic solid. The thermal response of the MCE material to the application or removal of a magnetic field is typically maximized when the material is near its magnetic ordering temperature, also known as the Curie temperature (T_c). The useful portion of the MCE usually spans about 25 degrees on either side of the material's T_c [2]. Therefore, to span a wide temperature range, a refrigerator must contain several different MCE materials arranged according to their T_c .

There are several issues that must be solved before the technology of magnetic refrigeration can move forward from prototypes to mass production. One of these issues is the lack of commercially available low-cost MCE materials that will function—for a long period—in a magnetic refrigeration environment, such as the active magnetic regenerator (AMR), which is being developed by several entities [3–7]. Synthesizing MCE materials is not easy, and the known materials are expensive rare-earth based or poor performance. Our goal is to discover, develop, and commercialize low-cost, high-performance magnetocaloric alloys to enable magnetic refrigeration to move from prototype to production.

APPROACH

The MCE occurs due to either a second-order phase transition (magnetic), or a first- and second-order phase transition (structural and magnetic, respectively). Materials with second-order transitions are entirely reversible, and materials with first-order transitions are not. Over the last two decades, the approach to MCE materials development has been to maximize entropy change (ΔS) and to reduce or eliminate rare-earth materials from the composition. Materials such as GdSiGe-, LaFeSi-, and MnFeAs-based alloys have been discovered that exhibit a giant magnetocaloric effect (large ΔS), but it is due to a first-order phase transition. In previous work, our team synthesized many of the known MCE materials and built MCE devices. We found major issues occur when using MCE materials with first-order transitions, including low ΔT and cracking due to volume changes when exposed to numerous magnetization cycles [8]. We also found that MCE materials without a rare-earth component were useless in actual devices because their performance was too low. Based on this experience, our approach to discovering better MCE alloys included the following requirements: (1) only second-order response, and (2) use low-cost rare-earth elements (Ce, Nd, Gd) to keep costs reasonable while still maintaining high performance. CeSi ($T_c \sim 9$ K) and NdSi ($T_c \sim 45$ K) alloys with second-order only MCE properties were reported by two different groups a few years ago [9, 10]. During Phase I, we synthesized ternary compounds of $Ce_xNd_{1-x}Si$ where $0 < x < 1$ and showed high performance MCE properties from 10 K to 45 K [11]. Our Phase II approach has been to systematically test compositional and processing effects on this alloy set to achieve functionality at higher temperature ranges, and demonstrate large-scale manufacturability.

RESULTS

During FY 2018 we systematically synthesized and characterized hundreds of alloys of various compositions. Figure 1a shows the interesting results of doping of the $Nd_{1.0}Si_{0.9}M_{0.1}$ where M is Fe, Cu, Co, Ni, Zn, Cr, Mn, Sn, and Al. With replacement of the silicon with Fe, Cu, Co, Ni, Zn, and Cr, the T_c was increased to ~ 75 K, and replacement with Mn increased T_c to ~ 125 K. Synthesis and characterization of $Gd_{1.0}Si_{0.8}Mn_{0.1}$ (Figure 1b) showed T_c of ~ 340 K, and similar to the Phase I Ce-Nd-based compounds, it was discovered that variation in the T_c from 125 K to 340 K can be achieved by varying the Nd-Gd concentration. From this discovery, we now have a novel MCE material set with second-order only response that uses only low-cost elements and has functionality over the entire temperature range, 9–340 K. A new patent application has been filed to cover the novel compositions discovered this year.

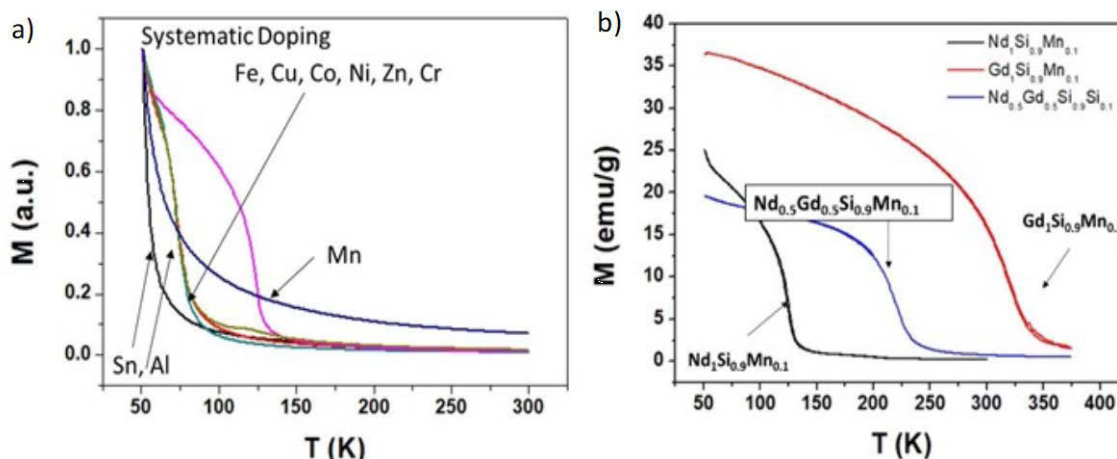


Figure 1. Magnetization versus temperature for (a) $Nd_{1.0}Si_{0.9}Mn_{0.1}$ compounds, where M is Fe, Cu, Co, Ni, Zn, Cr, Mn, Sn, and Al; and (b) Nd-Gd based compounds.

Effects of composition on MCE performance was tested. Figure 2 shows the change in entropy (ΔS) versus temperature for various compositions with different doping concentrations and elements. Thus far, the best performance is achieved with replacement of 20 at% of the Si with Cr or Mn, or some combination of these elements. Error on the ΔS measurements is ± 0.5 J/kgK.

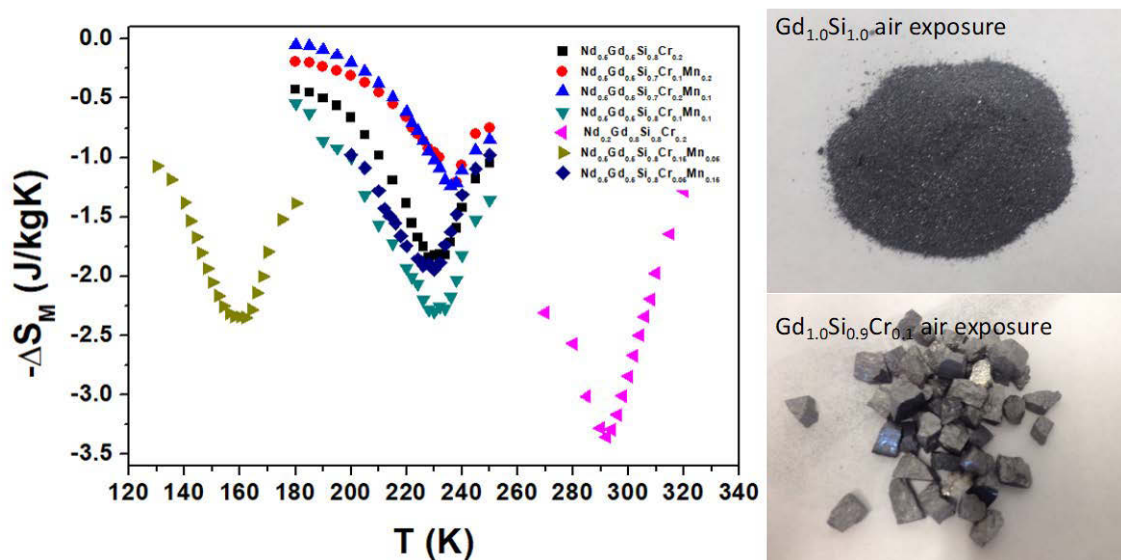


Figure 2. ΔS versus temperature for various magnetocaloric compositions. Images show presence of Cr eliminates long-term oxidation degradation of MCE materials with exposure to air.

X-ray diffraction (XRD) data (Figure 3) indicates the optimal performance may be due to a dual structural phase occurring at the 20 at% concentration, as only single phase occurs with higher or lower concentrations. Interestingly, the MCE properties (T_c and peak ΔS) are affected similarly with doping of Cr or Mn, where either element can be used to achieve desired T_c and peak ΔS performance as long as the 20 at% composition is maintained. The materials stability in air is significantly improved with presence of Cr, however, which is not the case with Mn. Compounds with no Cr after several weeks of exposure to air slowly degraded to an oxidized powder, whereas alloys with Cr showed little to no oxidation when exposed to air (see Figure 2). Many of the currently available or known MCE materials also degrade with exposure to air, and thus must be handled only in inert atmospheres, which makes it much more difficult to build systems. The ability to provide

MCE materials that are stable in air at room temperature is a major improvement that will significantly lower the cost and time needed to develop devices. Further, testing of other elemental doping to improve performance is in progress.

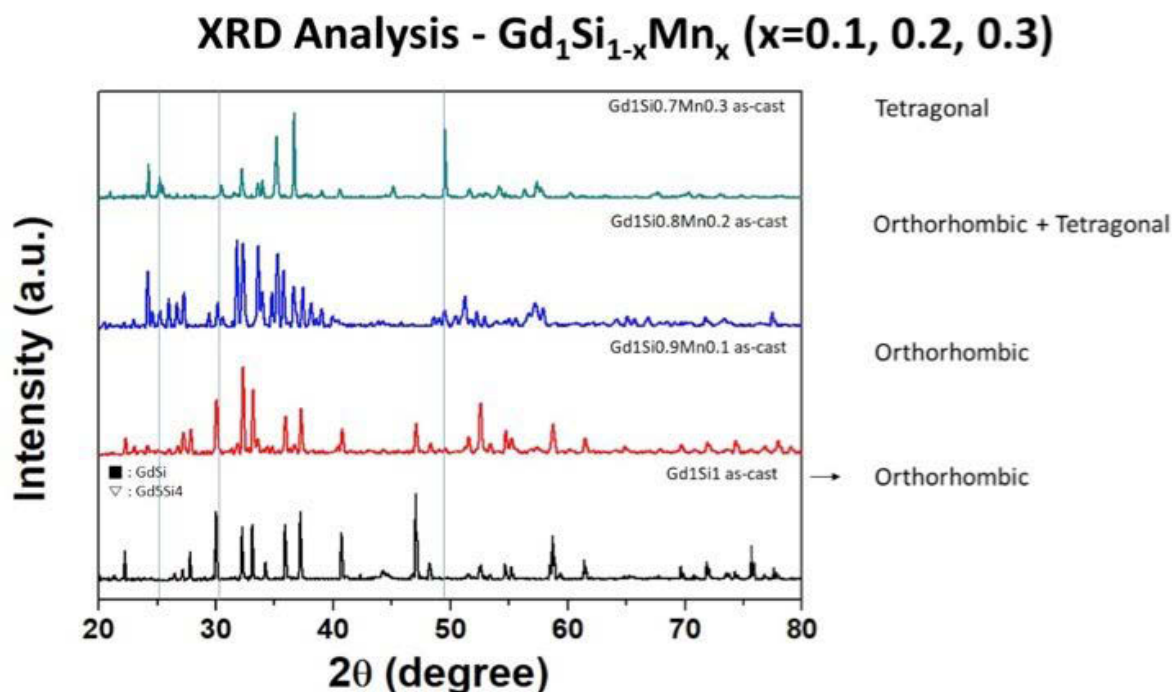


Figure 3. XRD data for various magnetocaloric compositions

Effects of processing on MCE properties also has been investigated. The alloys can be formed using a number of different melting techniques. An arc melt process is economical for quickly synthesizing small quantities of alloys. However, arc melt furnaces operate at $>5,000^\circ\text{C}$ temperatures, which often leads to evaporative loss of material. This loss can be difficult to control, thus batch-to batch-variation is significant. We have installed an induction melt system, which shows good performance can be achieved with this technique. Temperatures during induction melting are better controlled, and typically $<2,000^\circ\text{C}$, which eliminates the possibility of evaporation losses. The challenge with induction melting is finding compatible crucibles and casting processes for rare-earth metals. In our current setup, we are able to enclose the material in tantalum foil during melting to achieve the desired alloy, however this is not practical for large-scale manufacturing. There also may be benefits to rapid quenching of the alloys. Both arc melt and induction melt systems are available for large-scale manufacturing. We are currently working with several alloy manufacturers that have both types of equipment available along with several different casting and quenching techniques.

Figure 4 shows the current best performance (ΔS) of GE&R material set versus temperature. Figure 4 also shows a ΔT measurement of our MCE material with peak performance near room temperature. The ΔT measurement was performed in air, using a thermal couple attached to a ~ 10 -gram piece of MCE material and magnetic field generated by a 1T Halbach Array magnet. The $\Delta T \sim 1^\circ\text{C}$ is consistent with a second-order reversible response. Aside from elemental Gd, which only works at room temperature, we believe our materials are the highest performance (largest ΔT) commercially available. They are the only materials on the market with functionality below 180 K, the only materials on the market that are supplied with certificate of analysis verifying performance (ΔS versus T), and the only materials on the market with second-order-only transitions (totally reversible and no cracking issues).

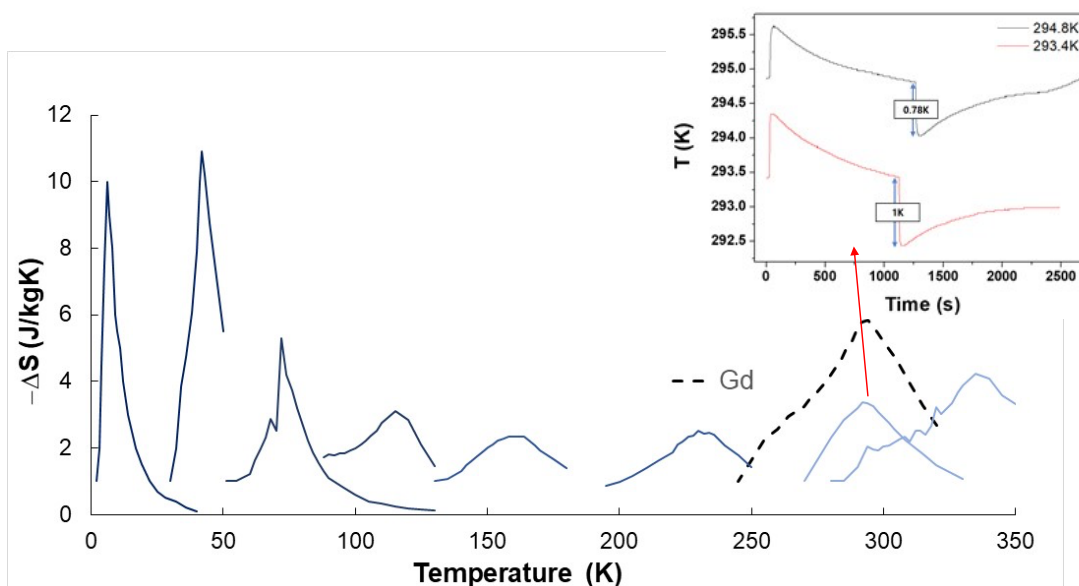


Figure 4. GE&R magnetocaloric materials performance (ΔS) versus temperature at 3T magnetic field (inset is ΔT measurement of GE&R room temperature composition with exposure to 1T magnetic field)

The intent of making these materials available as soon as possible is to allow other entities in R&D to begin testing and working with the materials, and potentially to provide us feedback on performance or other issues we need to address. The materials with working temperature below ~ 80 K show the highest performance with $\Delta S > 10$ J/kg K, which exceeds our target performance (that of Gd). The high performance was obtained by annealing the materials at 950°C for 6 weeks. The materials with working temperatures of more than 80 K are also in process of annealing, which we expect to improve performance. However, these long high-temperature anneals are expensive and time consuming. The anneals act to homogenize the materials, whereas phase separation during cooling may be occurring. We are investigating different casting and quenching techniques with several alloy manufacturers to see if this will allow reduced anneal time or eliminate the need for anneals altogether.

Initial feedback from potential customers of our MCE materials includes a request to form these materials into various shapes. We currently only are selling these in 5-g quantities in the form of small pieces (3–5 mm). Shapes such as sub-mm sized spheres, thin plates, and large ingots have been requested. Working with Arc Cast, Inc., we were able to successfully synthesize sub-mm sized spheres using their rotating disk atomization process [11]. The initial composition showed no degradation in performance. Additional compositions need to be tested on this process to ensure the higher-performance materials continue to maintain high performance. Processing optimization also needs to be done to better control the spherical size distribution. Formation of larger ingots (>500 g ingot) is in process, and machining into thin plates will be tested once large ingots with good MCE performance are successfully formed.

CONCLUSIONS AND UPCOMING ACTIVITIES

This project has made progress towards the ultimate goals of increasing the efficiency and reducing the capital cost of hydrogen liquefaction. In FY 2018 we have made progress along the critical path in support of developing magnetocaloric refrigeration technologies in that we have:

- Discovered a magnetocaloric material set that meets the target cost and has functionality over the entire temperature range from 9 K to 340 K

- Optimized composition and processing to exceed target performance for materials that function below 80 K
- Developed multiple synthesis pathways to achieve large-scale manufacturing goals
- Commercialized initial line of magnetocaloric materials on our webstore
- Demonstrated compatibility of rotating disk atomization process to form sub-mm sized spheres.

Upcoming activities will include:

- Continued investigation of compositional variation to improve performance
- Work with different alloy manufacturers to investigate effects of various casting and quenching techniques to improve performance and reduce anneal time
- Work with different alloy manufacturers to provide larger-scale manufacturing of ingots (>500 g/batch)
- Optimize rotating disk atomization process for narrower sub-mm sized distributions and meet cost targets
- Develop methods to form materials into thin plates.

SPECIAL RECOGNITIONS AND AWARDS/PATENTS ISSUED

1. Awarded a Phase I CALSeed grant from the California Energy Commission for business-development efforts of magnetocaloric technologies.
2. Awarded “Best Emerging Technology” in the Western Region Cleantech Open Competition.
3. Accepted into the San Diego Regional Energy Innovation Network, which is an incubator/accelerator program for clean technology startups.
4. Filed international patent application (US2018/012836) for our ternary-based compounds.
5. Filed new provisional applications (US 62/634078 and US 62/693719) to cover our novel compositions that function from 10 K to 340 K.

FY 2018 PUBLICATIONS/PRESENTATIONS

1. R. Ihnfeldt, R. Chen, E. Kim, X. Xu, and S. Jin, “Low Cost High Performance Magnetocaloric Materials for Hydrogen Liquefaction Applications.” Poster Presented at the 62nd Annual Conference on Magnetism and Magnetic Materials, Pittsburgh, PA, November 8, 2017.
2. R. Ihnfeldt, S. Jin, R. Chen, X. Xu, E. Caldwell, and E. Kim, “High Efficiency Magnetic Refrigeration Enabling Economic and SAFE Hydrogen Fuel.” Presented at the 2017 Cleantech Open Western Region Awards and Innovation Showcase, Fremont, CA, October 17, 2017.
3. R. Ihnfeldt, S. Jin, R. Chen, X. Xu, E. Caldwell, and E. Kim, “High Efficiency Magnetic Refrigeration Enabling Economic and SAFE Hydrogen Fuel.” Presented to the San Diego Regional Energy Innovation Network, San Diego, CA, November 14, 2017.
4. R. Ihnfeldt, S. Jin, R. Chen, X. Xu, E. Caldwell, and E. Kim, “High Efficiency Magnetic Refrigeration Enabling ZERO Emission Hydrogen Transportation.” Invited Presentation at Thermag VIII International Conference on Caloric Cooling, Darmstadt, Germany, September 19, 2018.
5. R. Ihnfeldt, S. Jin, R. Chen, X. Xu, E. Caldwell, and E. Kim, “High Performance Low Cost Magnetocaloric Materials,” Presented at Hydrogen Delivery Technical Team Review, Golden, CO, on February 28, 2018.

6. R. Ihnfeldt, S. Jin, R. Chen, X. Xu, E. Caldwell, and E. Kim, “Low-Cost Magnetocaloric Materials Discovery.” Poster Presentation at Fuel Cell Technologies Annual Merit Review, Washington, DC, on June 14, 2018.
7. E. Kim, X. Xu, R. Ihnfeldt, R. Chen, S. Jin, and C. Yoon, “The Mechanical Stability of La-Fe-Si Plate Over Magnetic Cycling.” Poster Presented at the 62nd Annual Conference on Magnetism and Magnetic Materials, Pittsburgh, PA, November 8, 2017.

REFERENCES

1. E.J.R. Plaza and J.C.P. Campoy, *J. Magnetism and Magnetic Mat.* 321 (2009): 446.
2. Y. Chuke, M. Bobade, Yavatmal, and P. Wardha, *International Engineering Journal for Research & Development* 1, no. 3, E-ISSN No: 2349-0721.
3. <http://machinedesign.com/energy/magnetic-refrigeration-heats> (accessed 12/07/2016).
4. <http://www.forbes.com/sites/hilarybrueck/2015/05/06/magnet-fridge/#1a13678648ca> (accessed 12/07/2016).
5. <http://www.cooltech-applications.com/magnetic-refrigeration-system.html> (accessed 12/07/2016).
6. R. Bjork, A. Smith, C.R.H Bahl, and N. Pryds, *International Journal of Refrigeration* 34, no. 8 (2011): 1805.
7. O. Gutfleisch, T. Gottschall, M. Fries, D. Benke, I. Radulov, K.P. Skokov, H. Wende, M. Gruner, M. Acet, P. Entel, and M. Farle, “Mastering Hysteresis in Magnetocaloric Materials,” <https://arxiv.org/ftp/arxiv/papers/1604/1604.08487.pdf> (accessed 11/23/2016).
8. E. Kim, X. Xu, R. Ihnfeldt, R. Chen, S. Jin and C. Yoon, “The Mechanical Stability of La-Fe-Si Plate Over Magnetic Cycling,” Poster Presented at the 62nd Annual Conference on Magnetism and Magnetic Materials, Pittsburgh, PA, November 8, 2017.
9. L.C. Wang, Q.Y. Dong, J. Lu, X.P. Shao, Z.J. Mo, Z.Y. Xu, J.R. Sun, F.X. Hu, and B.G. Shen, *Journal of Alloys and Compounds* 587, no. 10 (2014).
10. Q.M. Zhang, R.L. Gao, L. Cui, L.C. Wang, C.L. Fu, Z.Y. Xu, Z.J. Mo, W. Cai, G. Chen, and X.L. Deng, *Physica B* 456, no. 258 (2015).
11. R. Ihnfeldt, S. Jin, R. Chen, X. Xu, E. Caldwell, and E. Kim, “Low-Cost Magnetocaloric Materials Discovery,” Poster Presentation at Fuel Cell Technologies Annual Merit Review, Washington, DC, June 14, 2018.

Novel Membranes for Electrochemical Hydrogen Compression Enabling Increased Pressure Capability and Higher Pumping Efficiency

Taoli Gu (Primary Contact), Sora Lee, Scott Fackler, Bamdad Bahar
Xergy Inc.
299 Cluckey Dr. Ste A
Harrington, DE 19952
Phone: (302) 629-5768
Email: taoli.gu@xergyinc.com

DOE Manager: Neha Rustagi
Phone: (202) 586-8424
Email: Neha.Rustagi@ee.doe.gov

Contract Number: DE-SC0018456

Subcontractor:
Rensselaer Polytechnic Institute

Project Start Date: April 9, 2018
Project End Date: January 8, 2019

Overall Objectives

This project is conducting fundamental studies of novel membranes for electrochemical hydrogen compression (EHC) application. Insights gained from these studies will be applied toward the synthesis of ionomers and fabrication of membranes that meet the following ultimate targets:

- Hydrogen stream: ≥ 1 kg/h
- Specific energy consumption: 1.4 kWh/kg
- Inlet pressure: 100 bar
- Outlet pressure: 875 bar.

Fiscal Year (FY) 2018 Objectives

- Synthesize biphenyl-quaternary ammonium (QA) ionomers enabling cell operation at higher temperature with better humidity tolerance and higher pressure.
- Prepare reinforced composite proton exchange membranes (PEMs) by impregnating QA-

functionalized polymers into a mechanically robust matrix.

- Evaluate properties of polymer and composite membranes with reference to the technical milestones.

Technical Barriers

This project addresses the following technical barriers from the Hydrogen Delivery section of the Fuel Cell Technologies Office Multi-Year Research, Development, and Demonstration Plan¹:

- Reliability and Costs of Hydrogen Compression.

Technical Targets

- Efficiency of 1.4 kWh/kg at an inlet pressure of 100 bar, outlet pressure of 875 bar, and flow rate of 1 kg/h.

FY 2018 Accomplishments

- Designed and synthesized four ionomers for EHC performance test.
- Discovered that polyethylene (PE)-reinforced membranes were more flexible with larger elongation at break and less Young's modulus compared to their free-standing counterparts.
- Studied the relationship between equilibrium proton conductivity and relative humidity (RH) for phosphoric acid (PA)-doped QA functionalized biphenyl-based polymer (BPN1)-trimethylamine (TMA), BPN1-piperidine (Pip) and BPN1-pyridine (Pyr) ion-pair ionomer membranes. The results showed that these membranes had moisture tolerance up to 90% RH without a significant conductivity drop.
- Studied the relationship between equilibrium proton conductivity and temperature. It is observed that high conductivity (>100 mS/cm)

¹ <https://www.energy.gov/eere/fuelcells/downloads/fuel-cell-technologies-office-multi-year-research-development-and-22>

can be achieved under relatively low RH (~50%) at elevated temperature (80°C).

- Identified that PA-doped BPN1 composite membranes have better water tolerance compared to commercially available Nafion XL.

INTRODUCTION

EHC has the potential for use in compressing hydrogen at refueling stations that serve hydrogen fuel cell vehicles. The pressure of compression required depends on the vehicle tank type and is currently either 350 or 700 bar. It is desirable for an EHC to have high proton conductivity (for high operating efficiency), large elongation at break (such that it can reliably withstand the pressure difference at both sides), and high durability (to reduce the maintenance required). Rensselaer Polytechnic Institute (RPI) is developing promising polymer candidates for EHC. For example, RPI created PA-doped BPN1 ion-pair ionomer membrane for EHC application with proton conductivity enabled by an excess of PA molecules surrounding the QA-dihydrogen phosphate ion pair [1]. Figure 1 shows the chemical structures of four proposed ionomers. The ion-pair interaction and PA-retention can be tuned by the QA groups with different basicity and size. Together, Xergy, a leading company in the field of electrochemical compression, and RPI are working together to create novel EHC membranes. The group has generated a performance map based on ionomer structures and membrane fabrication variables to down-select the ionomers based on expected long-term durability and enabling DOE targets. Using those polymer resins as active material, Xergy has manufactured both free-standing and reinforced composite membranes. The team has made progress in testing membranes for compressor performance.

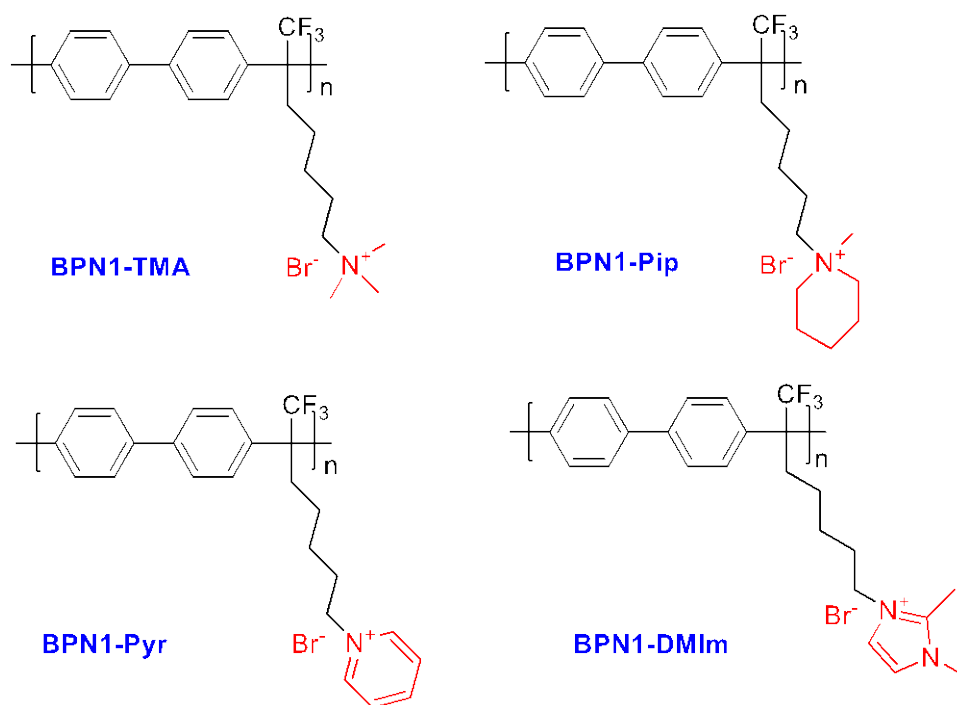


Figure 1. Chemical structures of ionomers with various quaternary ammonium groups

APPROACH

- Synthesize four ionomers (BPN1 series).
- Fabricate membrane: free-standing membranes and reinforced membranes.
- Characterize membrane (PA doping level by acid-base titration, equilibrium conductivity at different temperatures and RHs, and mechanical property by dynamic mechanical analysis).
- Test EHC at different temperatures and RHs.

- Generate performance maps as a function of membrane and operating condition variables.
- Down-select optimal ionomer(s).
- Test long-term durability of membranes made of optimal ionomer(s).
- Test EHC performance using optimal ionomer(s), and compare with DOE targets.

RESULTS

During FY 2018, RPI synthesized four ionomers by reacting BPN1-100 with TMA, Pip, Pyr, and 1,2-dimethylimidazole (DMIIm). The chemical structures are shown in Figure 1. Xergy fabricated membranes from the RPI ionomers, including both free-standing and reinforced composite membranes. Hand-cast samples were prepared at sizes of approximately 15 x 15 cm (225 cm²) or greater with thickness uniformity of $\pm 10\%$ (i.e., $20 \pm 2 \mu\text{m}$).

The mechanical properties of both free-standing and PE-reinforced membranes of BPN1-TMA and BPN1-Pip were evaluated. Since the membrane in EHC systems faces a significant pressure difference at inlet (low pressure) and outlet (high pressure) side, elongation at break is considered the most important mechanical property. Table 1 and Figure 2 indicate that PE-reinforced membranes have larger percentages for elongation at break and lower pressures for Young's modulus compared to their free-standing counterparts. The improved membrane flexibility is a result of the stretchability of the PE mesh. Therefore, further property studies for this project focused on the PE-reinforced membranes.

Table 1. Mechanical Properties for BPN1-TMA and BPN1-Pip at 30 °C and 0% RH

Ionomer	Type	Elongation at Break (%)	Tensile Strength (MPa)	Young's Modulus (MPa)
BPN1-TMA	Free-standing	145	15.9	75.7
	PE-reinforced	269	13.0	11.7
BPN1-Pip	Free-standing	119	13.5	96.9
	PE-reinforced	331	17.6	11.7

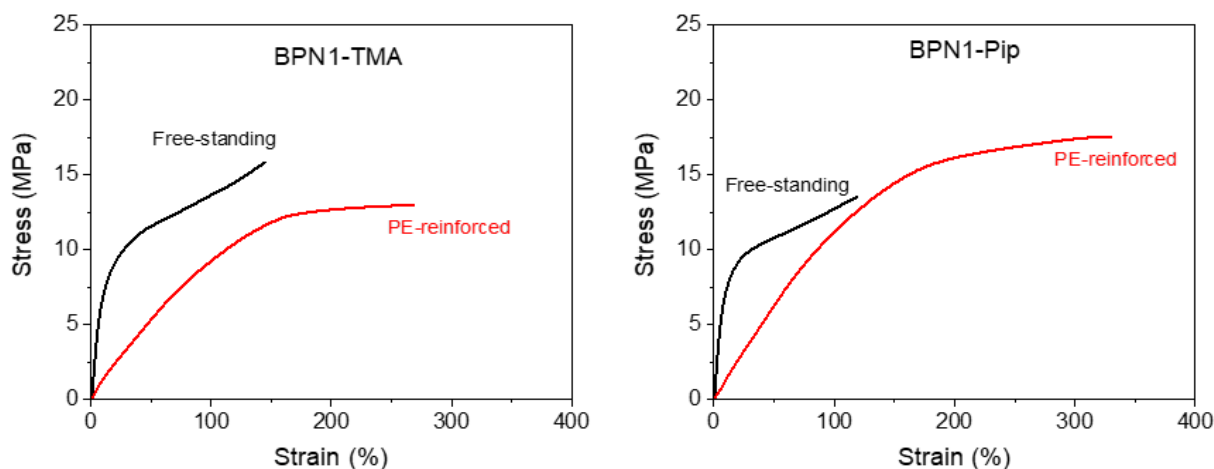


Figure 2. Stress-strain curve for (a) BPN1-TMA, and (b) BPN1-Pip at 30 °C and 0% RH

Four BPN1-based reinforced membranes with different cation groups were prepared for EHC performance test. The four cation groups have different basicity and size, which affect the interaction with PA. The membrane was first immersed in a 1M NaOH aqueous solution for 12 hours followed by immersion in a PA

aqueous solution (85 wt%) for 6 hours. Since proton conductivity is highly dependent on the PA content, the doping level (defined as the average number of PA molecules per cation group) was studied by acid-base titration. The results are summarized in Table 2. BPN1-TMA and BPN1-Pip exhibited similar doping levels due to the almost identical basicity of trimethylamine and piperidine. BPN1-Pyr, however, showed a lower doping level since pyridine is less basic. Thus, the pyridinium-dihydrogen phosphate ion-pair interaction is weaker than with the others.

Table 2. Doping Level of BPN1-TMA, BPN1-Pip and BPN1-Pyr

Ionomer	Doping Level
BPN1-TMA	8.3
BPN1-Pip	8.2
BPN1-Pyr	4.8

Acid-doped membranes typically show inadequate performance under humidified conditions [2]. To select the optimal ionomer for EHC performance testing, it is important to consider the extent of moisture tolerance as well as the equilibrium conductivity at different RHs and temperatures. We studied the equilibrium conductivity at 30°C (the common operating temperature for EHC) with RH ranging from 50% to 100%. The data were obtained after keeping the membrane at a fixed RH for at least 4 h before recording the conductivity value. As shown in Table 3, the equilibrium conductivity increases with as RH increases up to 90% but then drops significantly at 100% RH for all the three ionomers. The increasing conductivity is due to moisture facilitating proton transportation within the membrane. The conductivity, however, decreases under fully humidified conditions (at 100% RH) due to PA loss. To further confirm the tolerance of 90% RH, an extended test time of up to 14 h was applied, and no obvious conductivity drop was observed. Therefore, we conclude that PA-doped BPN1-TMA, BPN1-Pip, and BPN1-Pyr ionomers can be operated at up to 90% RH without significant PA leakage issues.

Table 3. Equilibrium Conductivity at 30°C under Various RH

Ionomer	Equilibrium Conductivity (mS/cm)					
	50% RH	60% RH	70% RH	80% RH	90% RH	100% RH
BPN1-TMA	49	65	77	126	136	63
BPN1-Pip	48	60	77	95	122	97
BPN1-Pyr	44	59	82	99	98	90

Conductivity usually increases under elevated temperatures because of the enhanced internal mobility of protons. Table 4 shows that the equilibrium conductivity of BPN1-TMA was higher at 80°C compared to that at 30°C under the same RH conditions. Additionally, it is worth noting that proton conductivity over 100 mS/cm can be reached even at 50% RH at 80°C. This finding provided us with an opportunity to explore EHC performance at high temperature and low RH conditions, which cannot be applied to the commercially available PEM Nafion, to improve the operating efficiency and ease the water management requirements.

Table 4. Equilibrium Conductivity of BPN1-TMA at 30°C and 80°C under Various RH

Temperature	Equilibrium Conductivity (mS/cm)								
	20% RH	30% RH	40% RH	50% RH	60% RH	70% RH	80% RH	90% RH	100% RH
30°C	N/A	N/A	N/A	49	65	77	126	136	63
80°C	62	78	96	114	139	171	175	190	155

EHC testing was carried out on both PE-reinforced BPN1 and Nafion XL. The initial polarization curve (Figure 3a) reveals that the BPN1-Pyr and BPN1-Pip composite membranes operate significantly better than

the Nafion XL, initially presumed to be due to their better conductivity at lower moisture levels. However, it appears this is actually due to the fact that the cells had not been “broken in” yet. As the Nafion XL membrane becomes activated throughout the following tests (i.e., the membrane becomes more hydrated and the contact resistances in the cell are lessened by pressurizations), its performance increases to the order of the BPN1-Pyr and the BPN1-Pip. The polarization curve after the first (Figure 3b) and second pressurization (Figure 4a) shows consistent, nearly linear performance of the BPN1-Pyr and BPN1-Pip membranes. The Nafion XL membrane, however, shows a rapid deterioration at higher current densities. Since the protons require water molecules to be transported through the membrane, it is likely that the Nafion XL rapidly fails at higher current densities due to a lack of replenishment of water, whereas the BPN1-Pyr and BPN1-Pip membranes, which do not require as much water, do not exhibit this. In the long-term polarization curves (Figure 4b), the Nafion XL membrane shows higher total performance within the time-frame tested. However, if the slope of the curves is estimated by a fitting function, it shows that the rate at which the current is dropping per unit time for the Nafion XL membrane is greater than for the BPN1-Pyr and BPN1-Pip membranes. This suggests that, given a long enough time, the performance of the Nafion XL membrane will drop below that of both the BPN1-Pyr and BPN1-Pip membranes. This again could be due to the water requirements of the Nafion XL versus the BPN1-Pyr and BPN1-Pip.

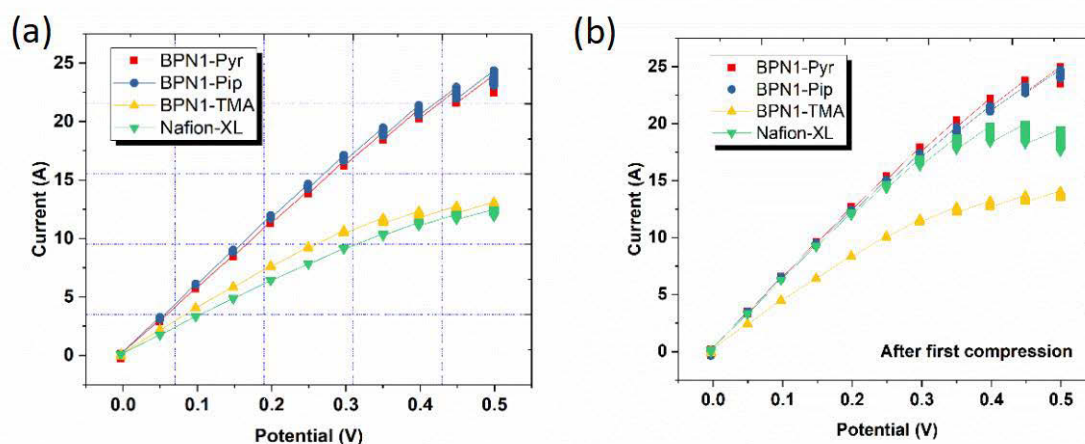


Figure 3. ECC testing results: (a) initial results; (b) after first compression

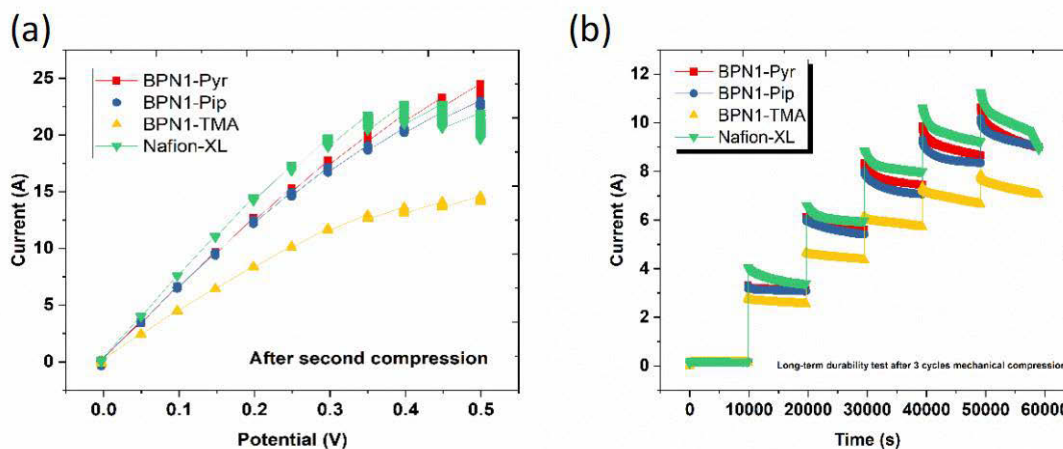


Figure 4. ECC testing results: (a) after second compression; (b) long-term durability test

CONCLUSIONS AND UPCOMING ACTIVITIES

Conclusions

- Four ionomers (BPN1-TMA, BPN1-Pip, BPN1-Pyr, and BPN1-DMIm) were synthesized and characterized.
- The PE-reinforced membrane outperformed the free-standing membrane in terms of elongation at break.
- The PA-doped ion-pair ionomer membrane exhibited moisture tolerance up to 90% RH.
- The elevated temperature can help achieve high conductivity at lower RH range.
- PE-reinforced BPN1 outperforms Nafion XL at high current densities in EHC due to better water management.

Upcoming Activities

The project teams have made major progress over the last months. There are still tasks to be completed before the electrochemical compressors can match DOE's target performance. These include, but are not limited to, the following items:

- Down-selecting the best candidate polymer and evaluating its long-term stability
- Preparing reinforced membranes with down-selected polymer
- Testing EHC performance and long-term stability, iterating key variables including ionomer structure, temperature, and RH
- Continuing to validate compressor performance at different temperatures
- Continuing data collection, analysis, and reporting on performance data to meet DOE targets.

REFERENCES

1. W.-H. Lee, Y.S. Kim, and C. Bae. *ACS Macro Lett.* 4 (2015); 814–818.
2. K.-S. Lee, J.S. Spendelow, Y.-K. Choe, C. Fujimoto, and Y.S. Kim. *Nat. Energy* 1 (2016): 16120.

Safety, Codes and Standards Subprogram Overview

INTRODUCTION

The Safety, Codes and Standards subprogram identifies and performs early-stage research and development (R&D) that provides a fundamental understanding of the relevant physics, critical data, and safety information used to develop and revise technically sound and defensible codes and standards. These codes and standards provide the scientific basis to facilitate and enable the safe widespread deployment and commercialization of hydrogen and fuel cell technologies. The subprogram identifies and evaluates safety and risk management measures that can be used to define requirements and close the gaps in codes and standards in a timely manner. Additionally, the subprogram promotes collaboration among government, industry, codes and standards development organizations (CDOs and SDOs), universities, and national laboratories in an effort to harmonize regulations, codes, and standards (RCS) both internationally and domestically. An emphasis on communication and collaboration among codes and standards stakeholders, the federal government, industry, and national labs maximizes the impact of the subprogram's early-stage R&D.

In fiscal year (FY) 2018, the Safety, Codes and Standards subprogram continued to make substantial progress in the area of hydrogen behavior and risk assessment, completing validation of the ColdPlume model for cryogenic hydrogen behavior using a world-first imaging diagnostic. This validation, combined with modeling and other experimental data, will ultimately enable a reduction in the separation distance requirements in current editions of the code.¹ To expand on this progress, experimental designs were completed for large-scale optical measurement of the concentration of hydrogen from real-world releases. The diagnostic is expected to provide key measurements of liquid hydrogen vent stack dispersion and vaporization profiles from liquid hydrogen pools. In the area of hydrogen sensing, an updated gap analysis identified critical R&D gaps while validated computational fluid dynamic models enabled profiling of indoor hydrogen releases for an improved understanding of indoor hydrogen dispersion. The subprogram also made significant progress in the area of materials compatibility R&D. A newly developed universal design curve for pressure vessel steels will enable pressure vessel design for high-pressure hydrogen service without further testing requirements. Metallic materials compatibility R&D enabled a test methodology proposal to the UN Global Technical Regulation (GTR) 13 Phase II Working Group. A testing program for model elastomer compounds led to the development of a first-of-its-kind database of the behavior of various polymers for hydrogen service. In hydrogen safety, a new partnership with the American Institute of Chemical Engineers to establish the Center for Hydrogen Safety will broaden the impact of the Hydrogen Safety Panel and safety knowledge resources.² Other critical R&D areas that made progress in FY 2018 include hydrogen fuel quality R&D, work to enable the integration of R&D with the domestic and international codes and standards community, and activities that support the H2@Scale initiative through RCS development.

GOALS

The subprogram's key goals are to provide the validated scientific and technical basis required for the development of codes and standards; to promulgate safety practices and procedures to allow for the safe deployment of hydrogen and fuel cell technologies; and to ensure that best safety practices are followed in Hydrogen and Fuel Cells Program activities.

¹ NFPA 2: Hydrogen Technologies Code, 2016 Edition, <https://www.nfpa.org/codes-and-standards/all-codes-and-standards/list-of-codes-and-standards/detail?code=2>

² The Center for Hydrogen Safety, <https://www.aiche.org/CHS>

OBJECTIVES

The subprogram's key objectives are to:

- Support and facilitate development and promulgation of essential codes and standards to enable widespread deployment and market entry of hydrogen and fuel cell technologies and completion of all essential domestic and international RCS
- Conduct early-stage R&D to provide critical data and information needed to define requirements in developing codes and standards
- Ensure that best safety practices underlie activities supported through DOE-funded projects
- Develop and enable widespread sharing of safety-related information resources and lessons learned with first responders, authorities having jurisdiction, and other key stakeholders.

FY 2018 TECHNOLOGY STATUS AND ACCOMPLISHMENTS

The subprogram continues to perform early-stage R&D to provide the scientific basis for codes and standards development with projects in a wide range of areas, including fuel specifications, separation distances, materials and components compatibility, and hydrogen sensor technologies. Using the results from these R&D activities, the subprogram continues to actively participate in discussions with SDOs such as the National Fire Protection Association (NFPA), the International Code Council (ICC), SAE International, the CSA Group, and the International Organization for Standardization (ISO) to promote domestic and international collaboration and harmonization of RCS.

A number of codes and standards relevant to the hydrogen industry were developed or revised during FY 2018. These RCS are listed below³:

- ISO 19880-3:2018 Gaseous hydrogen – Fueling stations – Part 3: Valves (published June 2018)
- ISO 16111:2018 Transportable gas storage devices – Hydrogen absorbed in reversible metal hydride (published August 2018)
- SAE J2579: Standard for Fuel Systems in Fuel Cell and Other Hydrogen Vehicles (revised June 15, 2018)
- IEC 62282-5-100 Portable Fuel Cell Power Systems – Safety: Ed 3 (published April 2018)
- SAE J3089: Characterization of On-board Vehicular Hydrogen Sensors Technical Information Report (passed second ballot in FY2018)
- ANSI FC 5 – CSA ballot for U.S. adoption of ISO 16110: Portable Hydrogen Generators (approved and published in mid-2018).

The H2Tools website⁴ provides up-to-date information relevant to the status of the subprogram's activities and enables dissemination of key safety knowledge resources, including:

- Technical Reference for Hydrogen Compatibility of Materials

³ The full text of the RCS listed can be found at their respective CDO and SCO websites: International Organization for Standardization (<https://www.iso.org/home.html>); SAE International (<https://www.sae.org/>); International Electrochemical Commission (<https://www.iec.ch/>); and the American National Standards Institute (<https://www.ansi.org/>).

⁴ H2Tools, <http://h2tools.org>

- Safety Planning for Hydrogen and Fuel Cell Projects
- Hydrogen Lessons Learned Database
- Hydrogen Safety Best Practices Manual
- National Hydrogen and Fuel Cell Emergency Response Training Resource
- Introduction to Hydrogen for Code Officials
- Hydrogen Safety for First Responders
- Codes and Standards – Permitting Tools, including the National Permitting Guide.

SAFETY, CODES AND STANDARDS ACCOMPLISHMENTS

In FY 2018, the Safety, Codes and Standards subprogram continued to make progress in several key areas. Some of the highlights are described below.

Hydrogen Behavior, Risk Assessment (Sandia National Laboratories [SNL])

- Published a report documenting a hydrogen fuel cell electric vehicle (FCEV) tunnel safety study, which provided a scientific basis for allowing FCEVs in tunnels. The report is intended to enable the adoption of FCEVs in the northeast region.
- Completed a draft of the Hydrogen Risk Assessment Model (HyRAM) 2.0, which includes the customization of quantitative risk assessment analysis and will expand HyRAM capabilities beyond indoor refueling stations.
- Signed a cooperative research and development agreement with FirstElement Fuel to demonstrate a performance-based approach to a hydrogen refueling station design.
- Completed validation of the ColdPlume model with model comparisons to data collected using a unique, world-first, cryogenic hydrogen imaging diagnostic for 15 experimental release conditions, including five conditions with simultaneous velocity data. The validated model can be used to predict hazard distances from liquid hydrogen system leaks.
- Developed an optical design for light collection for a large-scale diagnostic enabling the measurement of hydrogen concentration for real-world releases from a stand-off distance of at least 20 ft. This first-of-its-kind diagnostic will be used to measure liquid hydrogen vent stack dispersion and vaporization profiles from liquid hydrogen pools. The data will be used to validate models and enable reductions to liquid hydrogen fueling station footprints.

Hydrogen Sensors (National Renewable Energy Laboratory [NREL])

- Filed a provisional patent (NREL Prov 17-94A: Interface for a High-Pressure Hydrogen Dispenser, 2018, W. Buttner and K. Harrison) that specifically addresses a means to provide gas samples at low-pressure gas compatible for analysis by all potential on-site hydrogen contaminant detectors.
- Published a gap analysis for hydrogen safety sensors that identified critical gaps in hydrogen safety sensor performance.
- Collaborated with the U.S. Department of Transportation to design, build, and demonstrate an analyzer capable of verifying that hydrogen levels in FCEV exhaust are within the levels as prescribed by GTR 13.

- Profiled indoor hydrogen releases through the development of empirically validated computational fluid dynamic models to enable an improved understanding of indoor hydrogen dispersion. This work is anticipated to be incorporated into NFPA 2 as a guidance document on sensor placement.
- Led the development of SAE Technical Information Report J3089 (Characterization of On-board Vehicular Hydrogen Sensors) under the auspices of the SAE Fuel Cell Standard Committee. The Technical Information Report passed ballot and has been published as a formal SAE document.

Hydrogen Quality (Los Alamos National Laboratory)

- Completed the planning and installation of an inline fuel analyzer in the field (H2Frontier) and conducted on-site baseline measurements while adding wireless capabilities for remote testing.
- Developed a method to create a strategy to externally humidify the analyzer and produce a stable baseline to implement the technology at hydrogen refueling stations where no water is available.
- Demonstrated an analyzer response time of <5 minutes using flow rates of 100 and 200 standard cubic centimeters per minute with 500 parts per billion and 50 parts per million carbon monoxide/hydrogen concentrations. The analyzer's response time is less than the time required to refuel two FCEVs.
- Successfully conducted testing with 200 parts per billion carbon monoxide/hydrogen (SAE level) and met the goal of obtaining a response within 2.5 minutes by adjusting the alarm trigger level.

Hydrogen Safety Panel, Databases, Props, and First Responders (Pacific Northwest National Laboratory [PNNL])

- Partnered with the American Institute of Chemical Engineers to establish the Center for Hydrogen Safety enabling long-term sustainability and broader impact of the Hydrogen Safety Panel and safety knowledge resources.
- Updated the National Hydrogen and Fuel Cell Emergency Response Training Resource in support of in-person training conducted in the Northeast United States in early 2018.

Materials Compatibility (SNL, PNNL, Oak Ridge National Laboratory)

- Developed and proposed design curves for American Society of Mechanical Engineers (ASME) pressure vessel steels (applicable to both Cr-Mo and Ni-Cr-Mo steels) to the ASME Pressure Vessel Committee as the basis for a code case that will allow pressure vessel design for high-pressure hydrogen without additional testing burden.
- Performed round-robin testing with international partners to show consistency in fatigue life measurements in high-pressure gaseous hydrogen at low temperature (in context of materials requirements for the SAE J2579 standard).
- Proposed a materials testing methodology for hydrogen compatibility to the UN GTR 13 Phase II Informal Working Group.
- Developed six ethylene propylenediamene (EPDM) and six nitrile butyl rubber (NBR) model compound materials for investigation of hydrogen effects with fillers. Carbon and silica fillers indicated a 10 parts per million hydrogen absorption in the material.
- Performed R&D to determine that the desorption rate of the EPDM polymer is nearly five times faster than the NBR polymer without any additives or fillers. The compression set of NBR was significantly influenced by hydrogen with a 37% increase whereas EPDM compression set was insignificant.

Coordination of Codes and Standards Development, Domestic and International, and Codes and Standards Outreach (SNL, NREL, Fuel Cell and Hydrogen Energy Association):

- Developed new permitting and codes and standards training tools for hydrogen technologies deployment that includes an overview of NFPA 2 at H2Tools.org.

BUDGET

The subprogram received an appropriation of \$7 million in FY 2018. FY 2018 funding has allowed for continued support of codes-and-standards-related R&D and of the domestic and international collaboration and harmonization efforts for codes and standards that are essential to enable the safe and timely deployment of hydrogen and fuel cell technologies. Figure 1 shows subprogram funding in FY 2018. The Hydrogen Behavior and Risk category includes hydrogen behavior R&D, risk assessment, and modeling and validation R&D. The Materials Compatibility category includes metallic and non-metallic materials compatibility R&D for service in the hydrogen environment. Component R&D includes sensor R&D, hydrogen fuel quality, and station R&D to enable footprint reduction. The Safety Resources and Support category includes the Hydrogen Safety Panel and safety knowledge resources. The Codes and Standards Harmonization category includes work to integrate R&D learnings into codes and standards, collaboration with the Federal Energy Management Program, and support of international harmonization of RCS.

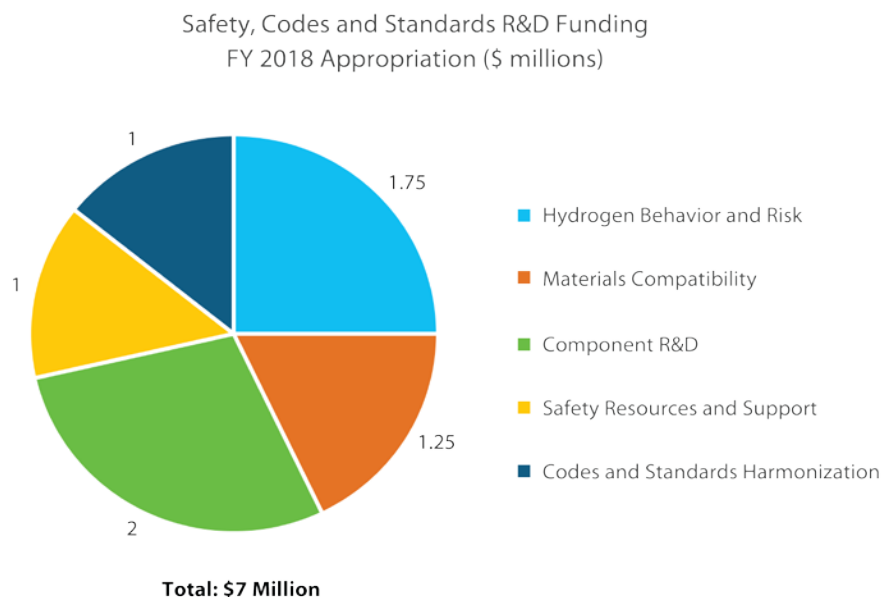


Figure 1. Safety, Codes and Standards subprogram FY 2018 appropriation

UPCOMING ACTIVITIES AND PLANS

The Safety, Codes and Standards subprogram will continue to support early-stage R&D to enable safe deployment of hydrogen technologies through materials compatibility R&D, hydrogen behavior and risk R&D, component failure R&D, safety R&D, and hydrogen fuel quality analysis. The subprogram will continue to work with CDOs and SDOs to ensure that the R&D performed enables science-based hydrogen-specific codes and standards.

The Hydrogen Materials Compatibility Consortium (H-Mat) will launch in FY 2019 to assemble world-class expertise and facilities in materials compatibility R&D at the national laboratories and leverage these

capabilities in priority R&D tasks led by industry and academia. H-Mat has two primary R&D thrusts: hydrogen effects in metals, led by SNL, and hydrogen effects in polymers, led by PNNL.

The subprogram will also continue to perform R&D necessary to promote the domestic and international harmonization of test protocols as well as the harmonization of RCS for hydrogen fuel quality and other key international standards. This will be enabled by working with the appropriate domestic and international organizations such as the NFPA, ICC, SAE International, the CSA Group, and ISO.

Laura Hill

Safety, Codes and Standards Project Manager
Fuel Cell Technologies Office
Office of Energy Efficiency and Renewable Energy
U.S. Department of Energy
1000 Independence Ave., SW
Washington, DC 20585-0121
Office: (202) 586-8384
Email: Laura.Hill@ee.doe.gov

National Codes and Standards Development and Outreach

Carl Rivkin
National Renewable Energy Laboratory (NREL)
15013 Denver West Parkway
Golden, CO 80401
Phone: (303) 275-3839
Email: carl.rivkin@nrel.gov

DOE Manager: Laura Hill
Phone: (202) 586-8384
Email: Laura.Hill@ee.doe.gov

Subcontractor:
Crystallogly Consulting, Los Angeles, CA

Project Start Date: October 1, 2002
Project End Date: Project continuation and direction determined annually by DOE

Overall Objectives

- Support the deployment of hydrogen technologies for hydrogen fuel cell vehicles and associated infrastructure, industrial trucks, and stationary fuel cell applications.
- Integrate safety research into codes and standards.
- Make critical safety information readily available through webinars, training sessions, safety reports, online training, and technical presentations.
- Inform key stakeholders of the safety, codes, and standards requirements for the safe use of hydrogen technologies.
- Work with potential infrastructure developers to accelerate the deployment of hydrogen fueling stations and other key infrastructure.
- Identify and resolve safety issues associated with hydrogen technologies infrastructure.
- Support the continuous improvement of codes and standards through incorporating research and field data into the code development process.

Fiscal Year (FY) 2018 Objectives

- Publish papers on the large-scale hydrogen systems and multi-fuel alternative fuel stations.

- Support the deployment efforts through participation in H2USA's Market Support and Acceleration Working Group.
- Support the development of the National Fire Protection Association (NFPA) 2 Hydrogen Technologies Code by chairing the Technical Committee on Hydrogen Technology, directing the various task groups formed under the committee.
- Support NFPA 502 Standard for Road Tunnels, Bridges, and other Limited Access Roadways by incorporating fire safety analysis into document annex.
- Develop outreach products for permitting hydrogen technologies including web-based regulations, codes, and standards (RCS) training materials.
- Implement continuous codes and standards improvement (CCSI) process by evaluating field data to determine codes and standards development priorities through an NREL technical report on safety research needs.
- Provide codes and standards information to critical stakeholders such as code officials through in-person training, updated online training, NREL technical reports posted on DOE websites, and development of relevant videos.
- Support the coordination of international and domestic hydrogen standards such as participating in International Organization for Standardization/Technical Committee 197 Hydrogen Technologies, hydrogen component development working groups, and domestic standards organizations such as the CSA Group.

Technical Barriers

This project addresses the following technical barriers from the Hydrogen Safety, Codes and Standards section of the Fuel Cell Technologies Office Multi-Year Research, Development, and

Demonstration Plan¹: (A) Safety Data and Information: Limited Access and Availability

(D) Lack of Hydrogen Knowledge by AHJs

(F) Enabling National and International Markets Requires Consistent RCS

(G) Insufficient Technical Data to Revise Standards

(H) Insufficient Synchronization of National Codes and Standards

(I) Lack of Consistency in Training of Officials

(K) No Consistent Codification Plan and Process for Synchronization of R&D and Code Development

(L) Usage and Access Restrictions

Contribution to Achievement of DOE Hydrogen Safety, Codes and Standards Milestones

This project will contribute to achievement of the following DOE milestones from the Hydrogen Safety, Codes and Standards section of the Fuel Cell Technologies Office Multi-Year Research, Development, and Demonstration Plan:

- Milestone 4.6: Completion of standards for critical infrastructure components and systems. (4Q, 2014)
- Milestone 4.7: Complete risk mitigation analysis for advanced transportation infrastructure systems. (1Q, 2015)
- Milestone 4.8: Revision of NFPA 2 to incorporate advanced fueling and storage systems and specific requirements for infrastructure elements such as garages and vehicle maintenance facilities. (3Q, 2016)
- Milestone 4.9: Completion of GTR Phase 2. (1Q, 2017)

FY 2018 Accomplishments

- Implemented CCSI through several projects including:

- Inter-Laboratory Research Integration Group (IRIG) assigned priorities to research and code development projects.
- Successfully submitted code amendments in IRIG priority areas, as defined by the group rating projects, to NFPA 2, NFPA 55, and NFPA 502.
- Led NFPA Hydrogen Technologies Technical Committee as committee chair in producing the 2020 edition of NFPA 2 Hydrogen Technologies Code.
- Led the NFPA Standard Permit Task Group to develop permitting tools for hydrogen fueling stations and links in the annex of NFPA 2 to connect these tools to the code.
- Developed new permitting and codes and standards training tools for hydrogen technologies deployment that includes overview of NFPA 2 at H2Tools.org.
- Collaborated effectively with other DOE laboratories, including Sandia National Laboratories and Pacific Northwest National Laboratory, to develop training materials and code proposals. Proposals include annex material to NFPA 502 on hydrogen releases in tunnels, which was successfully moved to the final ballot stage in FY2018.
- Documented safety lessons learned on deployment of hydrogen projects through collaboration with NREL's Environmental, Health, and Safety group.

¹ <https://www.energy.gov/eere/fuelcells/downloads/fuel-cell-technologies-office-multi-year-research-development-and-22>

INTRODUCTION

The fundamental purpose of this work is to support the safe deployment of hydrogen technologies. To achieve this objective, codes and standards must be in place to protect public safety and any significant safety issues must be resolved before deployment proceeds. The primary focus of this project is to identify research needs to support codes and standards development and integrating that research into the appropriate documents.

The work under this project has helped develop a national set of codes and standards to safely deploy hydrogen technologies. Additionally, key safety issues have been identified and are in the process of being resolved. Safety, codes, and standards information has been distributed to interested parties using a variety of techniques including webinars, NREL technical reports, workshops, in-person presentations, videos, online training tools, and web-based products.

APPROACH

The project approach involves integrating the efforts from as many key stakeholders as possible in codes and standards development and coordination and outreach activities to achieve maximum impact. These stakeholders include industry partners, standards development organizations, research organizations including other national laboratories, authorities having jurisdiction, local government in locations where projects will be deployed, and trade organizations involved in technology development and deployment.

RESULTS

NREL, at the direction of DOE, has helped develop a baseline set of codes and standards for the deployment of hydrogen technologies. This accomplishment helps meet several DOE milestones, including 4.4 and 4.8.

The next step in this codes and standards development process after the promulgation of the baseline set of codes and standards is monitoring the field performance of these documents, determining where modifications are required (including the research required to support these modifications), and supporting the implementation of those modifications. Examples of these modifications achieved in FY 2018 include adding allowances for using active safety measures for bulk liquefied hydrogen storage systems in NFPA 2 and the references to NREL work on hydrogen fueling system installation methods to reduce the probability of system fouling. This helps DOE meet milestone 4.5.

This modification process is illustrated in Figure 1. The process consists of evaluating field deployment of hydrogen technologies through use of NREL data and site visits, determining whether there are issues with codes and standards based on this information, and developing modified codes and standards requirements to resolve these issues. This process also integrates NREL (and other DOE laboratories) laboratory research activities involving hydrogen technologies safety by using this research to address codes and standards issues.

The CCSI process produced results in the following areas:

1. The NFPA Hydrogen Standard Permit Task Group submitted a public comment to include a permit for a hydrogen fueling station employing both bulk gaseous and liquid hydrogen storage, and this comment was accepted in the form of a pointer in the code to standard permit documents.
2. The NFPA Hydrogen Storage Task Group developed a public comment to differentiate between bulk liquid and bulk gaseous portions of hybrid storage systems so that the safety separation distances could be significantly reduced and allow for more options in hydrogen fueling station siting.

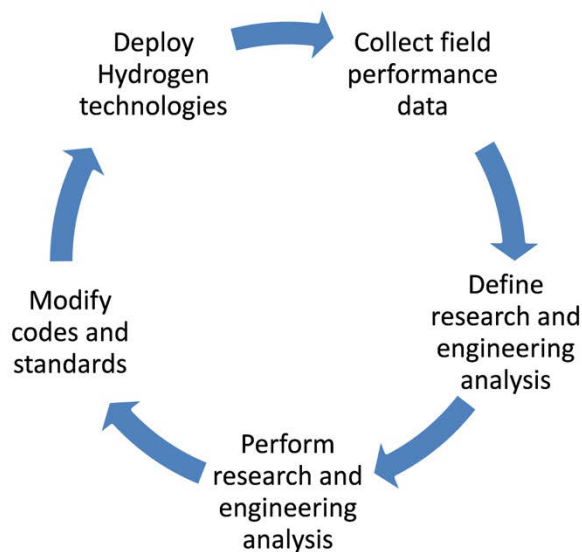


Figure 1. CCSI process

NREL completed codes and standards and permitting training tools such as the “NFPA 2 Hydrogen Technologies Code Overview” posted to the H2Tools.org website.

NREL supported the work of H2USA by participating as a member of the Market Support and Acceleration Working Group.

NREL has acted as Task Group Leader for the NFPA Hydrogen Storage Task Group and the Standard Permit Task Group, which will develop new requirements for bulk gaseous and liquefied hydrogen and associated safety mitigation measures for the next edition of NFPA 55/2. This supports DOE milestone 4.9.

CONCLUSIONS AND UPCOMING ACTIVITIES

Conclusions

- Codes and standards
 - The CCSI process is effective at modifying key codes to incorporate research results and define required research, such as characterization of liquid hydrogen releases.
 - Integration of DOE (and other) research into hydrogen codes and standards is a priority to ensure DOE safety research achieves the greatest possible impact on public safety by integration in widely used safety documents.
 - Ongoing coordination of the fire and building codes and key hydrogen codes and standards is a priority.
 - Field deployment information will help set codes and standards development priorities and improve the quality and relevance of codes as this information is incorporated through the American National Standards Institute-prescribed revision process.
 - Coordination of U.S. infrastructure codes and international standards is an increasing priority as infrastructure proceeds to commercial deployment

- Outreach
 - Outreach deployment support has been reduced to focus limited resources on IRIG (research integration) efforts.
 - Deployment support focused on infrastructure at locations with project activity and concrete deployment plans; for example, jurisdictions in California and the Northeast can be effective at moving projects forward, but this is a labor-intensive effort.
 - These goals can only be accomplished through collaborations with key stakeholders at all levels.
 - NREL supports the deployment of hydrogen and fuel cell technologies through programs such as technical reports, webinars, safety reviews, and the web-based information compendium. NREL has developed permitting tools that address the different needs of stakeholders and are readily accessible through various DOE websites including H2Tools.org. These Internet accessible tools have provided permitting support for all types of users from the infrequent user to more knowledgeable users.
 - NREL will use its status as a national research laboratory with independent status to provide safety information and to bring together safety officials from different jurisdictions.

Upcoming Activities

- Codes and standards
 - Focus on the IRIG project of integrating safety research into codes and standards. Key project areas will be station siting requirements, high-risk component safety, critical infrastructure such as tunnels and garages, and codes and standards streamlining to reflect higher levels of infrastructure deployment.
 - Support H2@Scale work by identifying gaps in safety knowledge and research required to fill these gaps, as well as coordinating this research where possible.
 - Continue work to coordinate codes and standards with special focus on taking information from deployment projects back to code development committees.
 - Resolve infrastructure codes and standards issues such as hydrogen setback distances in NFPA codes.
 - Continue coordination between NFPA codes and International Code Council codes, as well as International Organization for Standardization hydrogen component standards and domestic hydrogen component standards.
 - Support efforts to adopt NFPA 2 Hydrogen Technologies Codes (and other key codes), such as the work done by California's Office of the State Fire Marshal to adopt NFPA 2 earlier than adoption of the International Fire Code would dictate. This effort will begin focus on areas of deployment outside of California as the deployment process proceeds nationally.
 - Continue to incorporate research into codes through the CCSI process using the IRIG as the primary mechanism to achieve these incorporations.
 - Support efforts to develop standard permits and similar tools for hydrogen infrastructure projects to streamline project permitting efforts.

- Outreach
 - Continue to publish NREL technical reports, deliver webinars, and provide web-based information on key safety issues required to support hydrogen technologies deployment.
 - Assist code officials, project developers, and other interested parties in use of new codes and standards and safety information through outreach activities, with special focus on key jurisdictions such as California and the Northeast.
 - Utilize NREL hydrogen fueling station for training purposes such as videos on hydrogen fueling operations and maintenance.
 - Work with interested parties to provide information to assist in infrastructure deployment.
 - Provide in-person codes and standards training or consultation in key locations such as California, New York, Massachusetts, and other zero-emission vehicle states.

FY 2018 PUBLICATIONS/PRESENTATIONS

1. C. Rivkin. “Overview: NFPA 2 Hydrogen Technologies Code Requirements.” H2tools.org. 2018.
2. C. Rivkin. “National Codes and Standards Development and Outreach.” Presented at DOE Annual Merit Review, Washington, DC, June 2018.
3. C. Rivkin. “NFPA 2 National Hydrogen Code 2020 Edition Update.” Presented at 2017 Fuel Cell Seminar, Long Beach, CA, November 2017.
4. C. Rivkin, R. Burgess, W. Buttner. “Regulations, Codes, and Standards (RCS) for Large Scale Hydrogen Installations.” NREL/CP-5400-70929. Proceedings of the 7th International Conference on Hydrogen Safety (ICHS 2017), 11–13 September 2017, Hamburg, Germany (published July 2018).

R&D for Safety, Codes and Standards: Materials and Components Compatibility

Chris San Marchi
Sandia National Laboratories
7011 East Ave
Livermore, CA 94550
Phone: (925) 294-4880
Email: cwanma@sandia.gov

DOE Manager: Laura Hill
Phone: (202) 586-8384
Email: Laura.Hill@ee.doe.gov

Project Start Date: October 1, 2003
Project End Date: Project continuation and direction determined annually by DOE

Overall Objectives

- Optimize the reliability and efficiency of test methods for structural materials and components in hydrogen gas.
- Generate critical hydrogen compatibility data for structural materials to enable technology deployment.
- Create and maintain information resources such as the “Technical Reference for Hydrogen Compatibility of Materials” and the “Database for Hydrogen Compatibility of Materials.”
- Demonstrate leadership in the international harmonization of standards for qualifying materials and components for high-pressure hydrogen service.

Fiscal Year (FY) 2018 Objectives

- Provide the American Society of Mechanical Engineers (ASME) technical community with the technical basis for generalized assessment of fatigue crack growth of pressure vessel steels for high-pressure hydrogen service.
- Demonstrate fatigue life measurements at low temperature in high-pressure hydrogen with international partners to corroborate results from various testing institutions.

- Establish the technical basis for simplified fatigue life test methods to enable materials selection for hydrogen service in low-cycle applications (such as vehicle fuel systems).
- Obtain international consensus on materials testing methods and metrics for the SAE J2579 standard and for inclusion in the United Nations (UN) Global Technical Regulation (GTR no. 13 Phase II).

Technical Barriers

This project addresses the following technical barriers from the Hydrogen Safety, Codes and Standards section of the Fuel Cell Technologies Office Multi-Year Research, Development, and Demonstration Plan¹:

- (A) Safety Data and Information: Limited Access and Availability
- (F) Enabling National and International Markets Requires Consistent RCS
- (G) Insufficient Technical Data to Revise Standards.

Contribution to Achievement of DOE Hydrogen Safety, Codes and Standards Milestones

This project will contribute to the achievement of the following DOE milestones from the Hydrogen Safety, Codes and Standards section of the Fuel Cell Technologies Office Multi-Year Research, Development, and Demonstration Plan:

- Milestone 2.9: Publish technical basis for optimized design methodologies of hydrogen containment vessels to account appropriately for hydrogen attack. (4Q, 2014)
- Milestone 2.16: Demonstrate the use of new high-performance materials for hydrogen applications that are cost-competitive with aluminum alloys. (4Q, 2017)

¹ <https://www.energy.gov/eere/fuelcells/downloads/fuel-cell-technologies-office-multi-year-research-development-and-22>

- Milestone 2.18: Implement validated mechanism-based models for hydrogen attack in materials. (4Q, 2018)
- Milestone 3.3: Reduce the time required to qualify materials, components, and systems by 50% relative to 2011 with optimized test method development. (1Q, 2017)
- Milestone 3.4: Develop hydrogen material qualification guidelines including composite materials. (Q4, 2017)
- Milestone 4.9: Completion of the GTR Phase 2. (1Q, 2017)
- Milestone 5.2: Update materials compatibility technical reference. (4Q, 2011–2020)
- Milestone 5.4: Develop and publish database for properties of structural materials in hydrogen gas. (2Q, 2013)

FY 2018 Accomplishments

- Developed design curves for ASME pressure vessel steels (applicable to both Cr-Mo and Ni-Cr-Mo steels).
- Proposed design curves to ASME Pressure Vessel Committee as the basis for a code case that will allow pressure vessel design for high-pressure hydrogen without additional testing burden.
- Established the methods and the technical basis for materials acceptance criteria in the context of fuel systems for fuel cell electric vehicles with international experts.
- Performed round-robin testing with international partners to show consistency in fatigue life measurements in high-pressure gaseous hydrogen at low temperature (in context of materials requirements for SAE J2579 standard).
- Proposed materials testing methodology for hydrogen compatibility to UN GTR no. 13 Phase II Informal Working Group.
- Negotiated general consensus for the UN GTR with materials experts from the United States, Japan, Germany, European Union, Korea and China (a few details are still actively being negotiated, but general concepts have been accepted).

INTRODUCTION

A principal challenge to the widespread adoption of hydrogen infrastructure is the lack of quantifiable data to define safety margins and to mitigate potential hazards. To convince regulatory officials, local fire marshals, fuel suppliers, and the public at large that hydrogen refueling is safe for consumer use, the risk to personnel and bystanders must be quantified and minimized to an acceptable level. Such a task requires strong confidence in the safety performance of high-pressure hydrogen systems. Developing meaningful materials characterization and qualification methodologies in addition to enhancing understanding of the performance of materials is critical to eliminating barriers to the development of safe, low-cost, high-performance, high-pressure hydrogen systems for the consumer environment. This activity develops scientifically defensible, accelerated testing strategies and critically evaluates test methodologies for quantifying hydrogen effects on materials. Additionally, the program engages the international scientific community to harmonize test methods, provide guidance on materials selection for hydrogen service, and disseminate the latest scientific knowledge on the hydrogen compatibility of materials and suitability of components.

APPROACH

The materials and components compatibility element of the Safety, Codes and Standards subprogram leverages decades of experience in high-pressure hydrogen systems, well-developed industry partnerships, and a core capability in hydrogen-materials interactions anchored by the Hydrogen Effects on Materials Laboratory. In this laboratory, we focus on three critical activities:

1. Optimizing materials characterization methodologies
2. Generating critical hydrogen compatibility data for materials to enable technology deployment
3. Providing international leadership by assembling and maintaining a technical reference and database that compile technical data relevant to understanding the effects of hydrogen on materials.

To achieve these goals, the Hydrogen Effects on Materials Laboratory develops and maintains unique hardware and test methods for measuring fracture and fatigue behavior of materials in high-pressure gaseous hydrogen environments over a range of temperatures. This program element also leverages state-of-the-art materials science characterization tools to advance the understanding of hydrogen-materials interactions in both structural and functional materials.

RESULTS

Design Curves for Pressure Vessels

Nearly all of the fatigue data used to design high-pressure vessels for stationary hydrogen storage according to the ASME Boiler and Pressure Vessel Code was developed as part of this program in previous years. In general, stationary storage vessels for hydrogen are manufactured from SA-372 Grade J steel because, until recently, comprehensive data did not exist for any other steel. Recent work [1] contributed fatigue data for several high-hardenability steels (such as SA-723 Ni-Cr-Mo steels), which enables thicker vessel walls and larger sizes of storage vessels. Additionally, these recent data expanded the data range that can be used in design, essentially eliminating the overly conservative extrapolation of data to small defect sizes. A re-assessment of the older data sets for the Grade J steel and the newer data for Ni-Cr-Mo steels revealed consistency of the fatigue crack growth data for all of these steels, greatly expanding the parameter space for which fatigue crack growth data is available.

The new data were used to develop simplified design curves that bound the fatigue crack growth data for all the tested pressure vessel steels. The new design curves combine both the driving force (ΔK) and the load ratio (R) in a simple engineering relationship that appears to be relevant for a range of ASME pressure vessel steels. Formulation of these design curves was reported to the relevant ASME code committee and the concept was quickly embraced as a useful tool to advance pressure vessel design and eliminate, in some cases, the need and

cost for additional testing. While a few fine points are still being discussed within the committee, a code case has been drafted that will significantly enable the design of high-pressure vessels for storage at hydrogen fueling stations.

The master design curves can be split into a family of design curves as shown in Figure 1. While previously only the upper envelope of data was available (i.e., $\Delta K > 10 \text{ MPa m}^{1/2}$), the new design curves capture the behavior at lower ΔK and the transition between the two generalized regimes. By employing the design curves at lower ΔK , a significantly longer design life is allowed by design calculations (which are known to be conservative) because the crack growth rates have been shown to be lower than extrapolated from the upper curve alone. Additionally, the new data demonstrates limitations on the performance of high-strength steels and the need to advance our understanding of hydrogen effects on these steels to enable their use in hydrogen, for example through microstructural design.

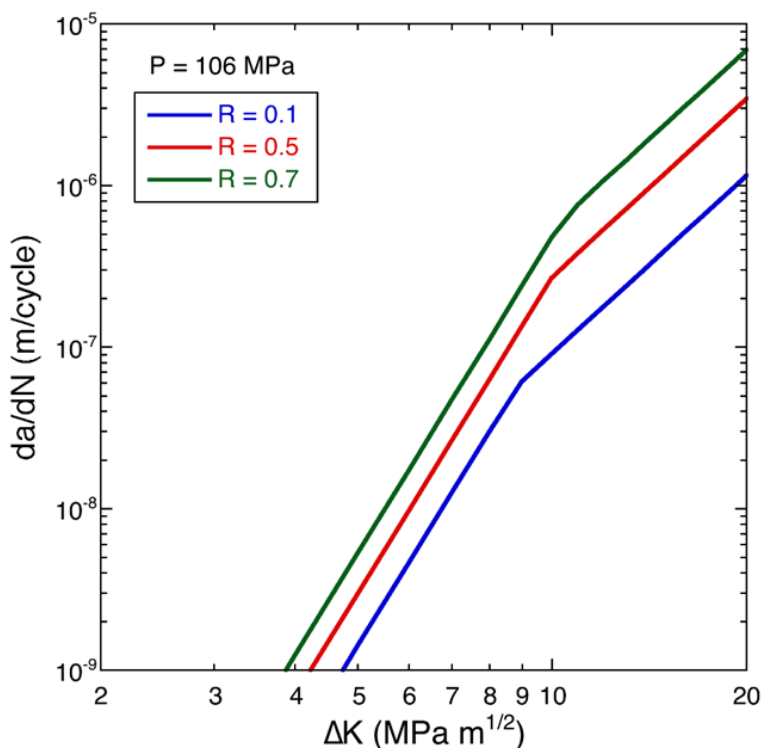


Figure 1. Master design curves for Cr-Mo and Ni-Cr-Mo pressure vessel steels at several load ratios (R)

Fatigue Life Methods

Fatigue life methods are an important and, in some cases, necessary alternative to fracture-mechanics-based design methods. Unlike the ASME codes, which specify design basis, many industries use performance-based requirements, which are design agnostic. Vehicle standards, for example, define performance requirements of components and systems rather than specifying design requirements. Performance-based standards allow for design innovation when components and systems can be tested, such as in vehicle crash tests. Performance-based standards, however, can be difficult to realize for structural materials because the transference of the performance of a structural material to the performance of a component is generally design specific. Nevertheless, with understanding of the application and the system performance requirements, it is possible to identify simple relevant performance metrics that materials must satisfy without specifying the design.

We have led an international team of materials experts for several years with the aim of developing performance-based materials testing requirements for hydrogen compatibility. While initial activities of the expert team on materials compatibility identified a long list of testing requirements that would have been

overly burdensome to manufacturers, the team negotiated comparatively simple test metrics specific to the vehicle application. These metrics have been formalized in the SAE J2579 standard with technical justification and have been proposed to the GTR no.13 Phase II Informal Working Group. For the first time, this definition of test metrics enables relatively simple screening of materials for hydrogen compatibility, as discussed in a joint publication with materials experts from the United States, Japan, and Germany [2]. While the developed test metrics are specific to the vehicle application, the performance-based concept for hydrogen compatibility can be extended to other applications where the design is not defined by the standard or code.

As part of the international activity to develop a performance-based protocol for hydrogen compatibility of materials, a modest test program was developed such that the participating laboratories could compare results on identical specimens. This activity provided a common understanding of the testing requirements, challenges with execution of the tests, and consistency of test results from different laboratories. The results are summarized in Ref. [2], along with rationale for the methods. An important outcome of this testing activity was a consensus that the limiting temperature for fatigue performance for austenitic stainless steels is room temperature. Previously, it was assumed that hydrogen effects are greatest at low temperature (around 220 K), close to the lower end of the temperature range specified for the application space (usually considered to be 233 K). Through this testing activity (and subsequently corroborated by complementary testing activities [3]), it was realized collectively that fatigue life in this class of materials is similar or shorter at room temperature than at low temperature, both in air and in hydrogen (Figure 2). While this idea had been proposed previously, it was the collective testing activity that enabled consensus among the hydrogen compatibility experts. As a result, the testing protocols were simplified, requiring fatigue life testing at room temperature in hydrogen, which is already challenging enough, but less challenging than testing at low temperature in high-pressure hydrogen.

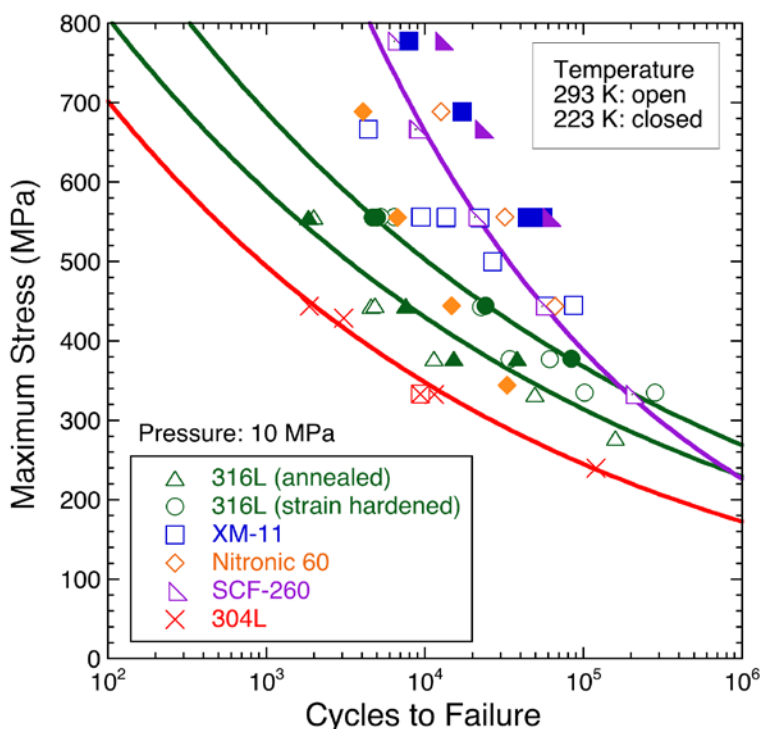


Figure 2. Fatigue life curves for several austenitic stainless steels, showing effect of temperature of fatigue in gaseous hydrogen at pressure of 10 MPa

In summary, working closely with international materials experts and SAE, consensus was reached for the first time on a simple performance-based protocol for screening materials for high-pressure hydrogen service. A collaborative testing activity across multiple test laboratories aided consensus building and further

simplification of the testing protocols. The protocols have been proposed for inclusion in GTR no. 13 Phase II and there is general agreement among materials testing experts participating in the GTR discussions (including United States, Japan, European Union, Korea, and China). Acceptance of welded components remains an open question and should be a focus of continued work.

CONCLUSIONS AND UPCOMING ACTIVITIES

- A variety of common pressure vessel steels show similar fatigue behavior in high-pressure gaseous hydrogen, and this behavior can be captured with a relatively simple set of design curves that account for the load ratio.
- The fatigue design curves developed for pressure vessels are the basis for a code case being debated in the ASME committee on high-pressure vessels.
- Materials requirements for hydrogen compatibility in the fuel system of vehicles have been developed in collaboration with an international team of materials experts; the requirements have been incorporated into SAE J2579 and are being negotiated for inclusion in the UN GTR no. 13.
- A scientific paper on performance-based materials requirements for the high-pressure components on the vehicle was jointly authored with international experts from Japan and Germany.
- Hydrogen-assisted fatigue and fracture of welded austenitic stainless steels and aluminum alloys represent high-priority research topics based on discussion with standards organizations and industry participants; in particular, demonstration that welded stainless steel can meet similar requirements as base materials may enable the replacement of fittings with welded joints, while validation of testing protocols for the unique characteristic fracture behavior of aluminum alloys is still needed.

FY 2018 PUBLICATIONS/PRESENTATIONS

1. J. Ronevich, C. San Marchi. “Effects of Gaseous Hydrogen on Austenitic Stainless Steel Welds.” Presented at International Hydrogen Infrastructure Workshop Bilateral Safety Meeting, 13 September 2018, Boston, MA. SAND2018-10200PE.
2. C. San Marchi. “Master Curves for Fatigue Crack Growth of Ferritic Steels in Gaseous Hydrogen.” Presented at meeting of Study Group on Materials Testing and Qualification for Hydrogen Service, 20 July 2018, Prague, Czech Republic. SAND2018-8867PE.
3. J. Ronevich, et al. “Effects of Gaseous Hydrogen on Austenitic Stainless Steel Welds.” Presented at meeting of Study Group on Materials Testing and Qualification for Hydrogen Service, 20 July 2018, Prague, Czech Republic. SAND2018-8850PE.
4. C. San Marchi, J. Yamabe, M. Schwarz, H. Matsunaga, S. Zickler, S. Matsuoka, H. Kobayashi. “Global Harmonization of Fatigue Life Testing in Gaseous Hydrogen.” *Proceedings of the 2018 ASME Pressure Vessels & Piping Conference*, 15–20 July 2018, Prague, Czech Republic. Paper PVP2018-84898.
5. C. San Marchi (in collaboration with SAE Fuel Cell Safety Task Force). “Proposed Test Method to Establish Hydrogen Compatibility of Materials for Fuel Cell Vehicles.” Presented by Glenn Scheffler to GTR no. 13 Phase 2 informal working group, June 2018, Seoul, Korea. SAND2018-6478PE.
6. C. San Marchi. “R&D for Safety, Codes and Standards: Materials Compatibility.” Presented at Joint Tech Team Meeting, Delivery, Storage and Safety, Codes and Standards, 28–29 March 2018, Troy, MI. SAND2018-3050C.
7. C. San Marchi (invited), J. Ronevich. “Dispelling Myths about Gaseous Hydrogen Environmental Fracture and Fatigue.” Presented at TMS Annual Meeting, 11–15 March 2018, Phoenix, AZ. SAND2018-2718C.

8. C. San Marchi, J. Ronevich. “Basis of FCGR Laws for Fatigue Crack Growth of PV Steels in Gaseous Hydrogen.” Presented at ASME Boiler and Pressure Vessel Committee Code Week, 2–9 February 2018, Las Vegas, NV. SAND2018-1098PE.
9. C. San Marchi (in collaboration with SAE Fuel Cell Safety Task Force). “Proposed Test Method to Establish Hydrogen Compatibility of Materials for Fuel Cell Vehicles.” Presented to GTR no. 13 Phase 2 informal working group, 5–7 February 2018, Torrance, CA. SAND2018-0857PE.
10. C. San Marchi, P. Gibbs, J. Foulk, K. Nibur. “Fatigue Life of Austenitic Stainless Steels in Hydrogen Environments.” Paper presented at 43rd MPA Seminar, 11–12 October 2017, Stuttgart, Germany (co-sponsored).

REFERENCES

1. C. San Marchi, P. Bortot, J. Felbaum, Y. Wada, J.A. Ronevich. “Fatigue and Fracture of High-Hardenability Steels for Thick-Walled Hydrogen Pressure Vessels.” Presented at International Conference on Hydrogen Safety, Hamburg, Germany, 11–13 September 2017.
2. C. San Marchi, J. Yamabe, M. Schwarz, H. Matsunaga, S. Zickler, S. Matsuoka, H. Kobayashi. “Global Harmonization of Fatigue Life Testing in Gaseous Hydrogen.” *Proceedings of the 2018 ASME Pressure Vessels & Piping Conference*, 15–20 July 2018, Prague, Czech Republic. Paper PVP2018-84898.
3. T. Iijima, H. Enoki, J. Yamabe, B. An. “Effect of High Pressure Gaseous Hydrogen on Fatigue Properties of SUS304 and SUS316 Austenitic Stainless Steel.” *Proceedings of the 2018 ASME Pressure Vessels & Piping Conference*, 15–20 July 2018, Prague, Czech Republic. Paper PVP2018-84267.

Fuel Quality Assurance Research and Development and Impurity Testing in Support of Codes and Standards

Tommy Rockward (Primary Contact), Eric Brosha, Chris Romero, and Rangachary Mukundan
Los Alamos National Laboratory (LANL)
P.O. Box 1663
Los Alamos, NM 87545
Phone: (505) 667-9587
Email: trock@lanl.gov

DOE Manager: Laura Hill
Phone: (202) 586-8384
Email: Laura.Hill@ee.doe.gov

Project Start Date: October 1, 2006
Project End Date: Project continuation and direction determined annually by DOE

Overall Objectives

- Develop a low-cost, fast-response device (analyzer) to measure impurities in a dry hydrogen fuel stream at or above the SAE J2719 levels.
- Test the analyzer in real-world environments.
- Develop a better understanding of the analyzer's workings to identify best materials and device configurations for improved analyzer performance.

Fiscal Year (FY) 2018 Objectives

- Develop an external humidification system and evaluate membrane hydration state as a function of membrane thickness, gas diffusion layer composition, and gas flow rate.
- Investigate the role of ionomer in the electrode in order to optimize conditioning time and improve the analyzer's signal to noise.
- Evaluate adsorption/desorption characteristics of carbon monoxide (CO) in order to implement a clean-up strategy for resetting the analyzer.
- Identify location for field trials and plan the system installation.

- Install the analyzer at a hydrogen station and demonstrate a viable operating mode.

Technical Barriers

This project addresses the following technical barriers from the Hydrogen Safety, Codes and Standards section of the Fuel Cell Technologies Office Multi-Year Research, Development, and Demonstration (MYRDD) Plan¹:

- (G) Insufficient Technical Data to Revise Standards
- (K) No Consistent Codification Plan and Process for Synchronization of R&D and Code Development.

Contribution to Achievement of DOE Hydrogen Safety, Codes and Standards Milestones

This project will contribute to achievement of the following DOE milestones from the Hydrogen Safety, Codes and Standards section of the Fuel Cell Technologies Office MYRDD Plan. The MYRDD milestones that align with LANL's work are 2.2, 2.6, 2.15, 2.17, and 3.2.

- Investigate the causes of drift in the baseline current of the analyzer in order to identify the mechanism of current degradation and develop strategies to stabilize the baseline. (1Q, FY 2018)

FY 2018 Accomplishments

- Developed a method to create a strategy to externally humidify the analyzer and produce a stable baseline in order to implement our technology at hydrogen refueling stations where no water is available.
- Enhanced the electrode performance by reducing ionomer content by a factor of 10, which inherently increased access to platinum (Pt) sites and lowered its resistance by an order

¹ <https://www.energy.gov/eere/fuelcells/downloads/fuel-cell-technologies-office-multi-year-research-development-and-22>

of magnitude and increased the overall performance from 5 mA to well above 25 mA.

- Tested a novel operating mode that incorporated a clean-up strategy and implemented that in the field.
- Demonstrated analyzer response time of <5 min using 100 and 200 sccm flow rates with 500 ppb and 50 ppm CO/H₂ concentrations. Analyzer's response time is less than the time required to refuel two fuel cell vehicles.
- Successfully conducted testing with 200 ppb CO/H₂ (SAE International level) and met the goal of obtaining a response within 2.5 min by adjusting the alarm trigger level.
- Completed the planning and installation of analyzer in the field (H2Frontier) and conducted on-site baseline measurements while adding wireless capabilities for remote testing.

INTRODUCTION

In 2012 two hydrogen fuel specifications (SAE J2719 and ISO 14687-2) were developed. These specifications outlined the allowable non-hydrogen constituents' levels for hydrogen fuel to be used for fuel cell road vehicles. Research indicates that several of these non-hydrogen constituents can be harmful to fuel cell performance in trace amounts and recommends avoiding them. And, as hydrogen refueling stations are being built, there is an immediate need to implement fuel quality assurance measures to prevent damage to fuel cell vehicles or fleets. While the hydrogen grade at these filling stations would be certified periodically, having a low-cost, fast-responding hydrogen contaminant detector to measure impurities at or above the levels in the fuel specification would be invaluable to vehicle owners, station owners, and fuel suppliers. In FY 2015, LANL scientists demonstrated proof-of-concept for a fuel quality analyzer and are now (FY 2018) in the planning and development stages for field trial testing their device. The results of the field trials testing guide the research on the fundamental understanding of the working mechanism of the analyzer to enable advances in this technology.

APPROACH

Research on fuel impurities conducted over the years at LANL indicates fuel cells with membrane electrode assemblies (MEAs) made of low-surface-area Pt-type electrodes as being the best sensors for detecting surface-adsorbing contaminants such as CO and hydrogen sulfide (H₂S). Both of these contaminants can chemisorb onto active Pt sites and reduce activity for hydrogen dissociation and inherently the overall fuel cell performance. Our findings demonstrated that the overall performance was impacted more as the contaminant concentration increased. In order to mitigate or minimize performance losses due to these species, the Pt loading was increased or Pt-alloys were introduced. Our work here proposes a device that uses an asymmetric MEA that has ultra-low-loaded Pt as the working electrode to detect minuscule amounts of adsorbates and a relatively higher amount of Pt or PtRu (platinum;ruthenium) at the reference electrode to alleviate impacts of impurities and maintain stability. We operated the device as an electrochemical hydrogen pump because there is no continuous source of oxygen or water at the hydrogen refueling station, and this method does not require oxygen. However, it does require proper membrane and electrode hydration. To overcome this challenge, we developed a wicking scheme to provide the necessary hydration.

RESULTS

LANL scientists have continued to make progress on the development and deployment of a hydrogen contaminant detector. Several fundamental improvements and hardware modifications were made to enhance the analyzer's performance while also incorporating the appropriate measures for field trials. Fundamental improvements such as optimizing the ionomer content improved Pt access, allowing larger baseline currents to be obtained while simultaneously reducing the conditioning time. The implementation of periodically applying 1.5 V was proven effective as a clean-up strategy for desorbing surface contaminants. These findings (shown in Figures 1, 2, and 3) made it possible to demonstrate an operating mode for the analyzer to be used during the field test trials.

Figure 1 shows the response of the analyzer when exposed to 100 sccm flow rate of ultra-high-purity hydrogen followed by the addition of two different CO concentrations (500 ppb and 50 ppm) with 1.5 V applied for 30 seconds every 15 minutes. The analyzer operated at 30°C and ambient pressure with a dry hydrogen stream. By applying the external voltage using a Gamry potentiostat, we were able to maintain performance within an operating window and establish an alarm trigger level. We set the alarm trigger level to 30 mA and monitored the time required for the performance to drop below it during CO exposure. Our desired response time was set for less than 5 minutes. During the challenge with 500 ppb CO in hydrogen, our analyzer responded in 2.79 minutes while the 50 ppm CO challenge yielded a response time of 33 seconds; both times met our desired response time goal.

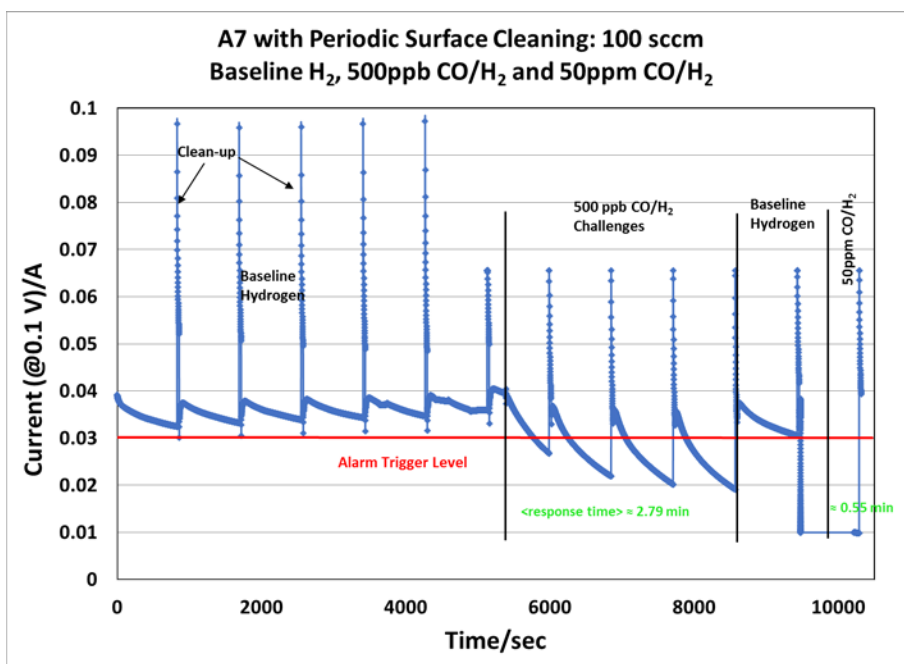


Figure 1. Analyzer exposed to 500 ppb and 50 ppm CO/H₂ using 100 sccm flow rate with periodic 1.5 V clean-up steps

Figure 2 shows the impact of flow rate on the analyzer response time using identical conditions and operating parameters as mentioned above. We increased the flow rate to 200 sccm. These results unexpectedly showed a lower baseline current while operating on the ultra-high-purity hydrogen; this is possibly due to membrane drying. We observed that the response times at both concentrations met our goal but had increased from the times measured using 100 sccm as the flow rate. The response times were 3.48 and 1.5 minutes for 500 ppb and 50 ppm CO concentrations, respectively.

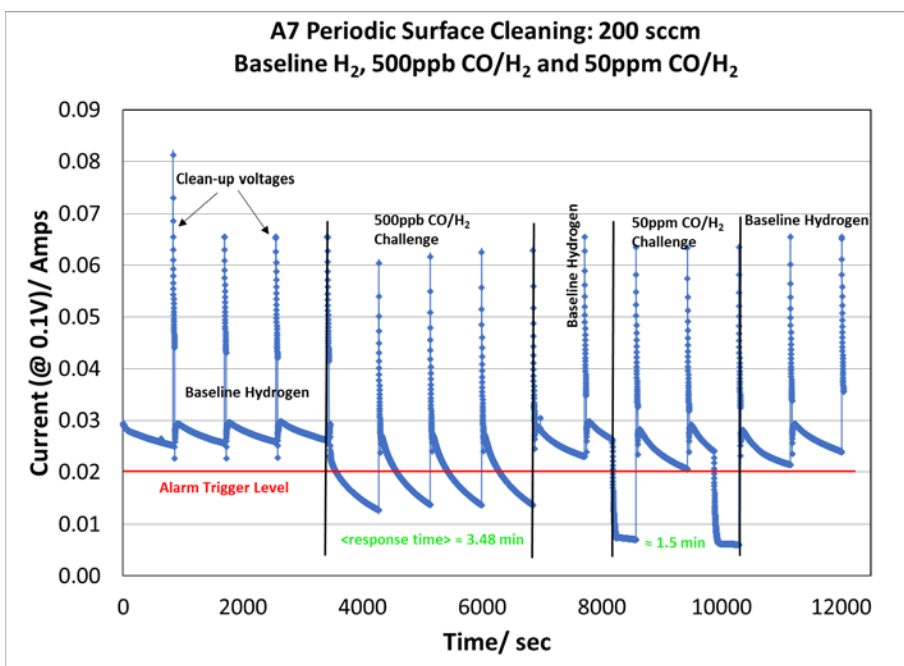


Figure 2. Analyzer exposed to 500 ppb and 50 ppm CO/H₂ using 200 sccm flow rate with periodic 1.5 V clean-up steps

Results shown in Figures 1 and 2 were useful in helping to determine an operating mode for our field trials; however, the CO concentrations used were above the SAE level. In Figure 3, we challenged the analyzer using 200 ppb CO in hydrogen. Using identical conditions as previously stated, we observed the analyzer performance began to slowly decay, which is indicative of its sensitivity to 200 ppb CO. We also found the current drop did not fall below the initial trigger alarm level within the desired response time goal of 5 minutes. The average response time to surpass the alarm trigger level was measured at 6.9 minutes. In order to achieve our response time target we were able to adjust the trigger level, which reduced the average response time to 2.5 minutes.

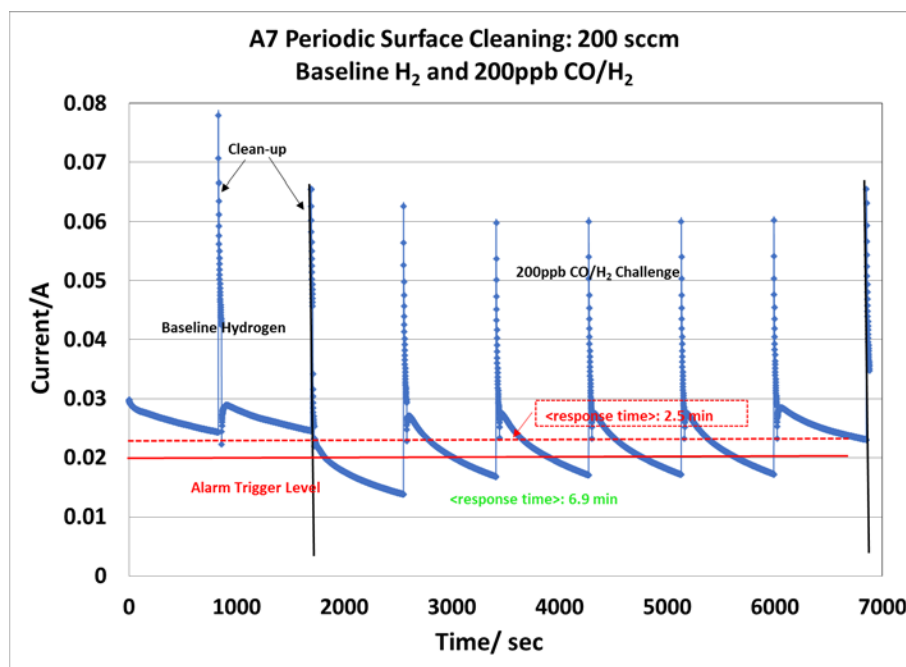


Figure 3. Analyzer exposed to 200 ppb CO/H₂ using 200 sccm flow rate with periodic 1.5 V clean-up steps

During FY 2018, LANL was successful in identifying a partner to allow field testing for the analyzer. H2Frontier, Inc. in Burbank, California, a long-time collaborator of LANL’s sensor team, agreed to provide fuel sampling to our device. In preparation for the field trials, several phases were established to ensure safety and compliance as well as a functional system. In July 2017, LANL staff visited the H2Frontier site to discuss the installation and planning phase. The team identified several potential constraints in the field such as temperature control of the enclosure, gas access ports, system location, remote monitoring and testing, etc., and established timely solutions to each in order to successfully install and test the device in March 2018. The analyzer in the field is currently equipped with remote monitoring and control with experiments being designed and controlled from LANL.

CONCLUSIONS AND UPCOMING ACTIVITIES

In FY 2018, we successively made improvements to the analyzer prototype. We modified components to stabilize the membrane hydration (i.e., high-frequency resistance), varied the ionomer content to stabilize the baseline as well as improve conditioning, and implemented a clean-up strategy to reset the device after exposure to contaminants. In doing so, we were able to demonstrate sensitivity to 200 ppb CO in dry H₂ in less than the 5 minutes. Our efforts also included identifying a location in the field for the analyzer to be tested and its successful installation and testing. Furthermore, our staff also installed remote access software and a valve control system to operate experiments from Los Alamos.

We have decoupled our upcoming activities into two sections—field experiments and R&D.

1. In the field experiments conducted at H2Frontier, we will:

- Validate baseline stability and identify factors affecting stability
- Test analyzer periodically with challenges of CO and during reformer startup to assess response stability
- Develop Gen 2 analyzer and electronics design
- Look for industrial partners to transition this work to.

2. Our R&D will consist of the following:

- Eliminate the humidification system by using advanced membranes
- Improve our understanding of analyzer working mechanisms (based on field trials feedback)
- Extend analyzer work to include H₂S and ammonia (NH₃)
- Incorporate impedance spectroscopy into analyzer
- Design analyzer for operation under pressure.

SPECIAL RECOGNITIONS AND AWARDS/PATENTS ISSUED

1. 2017 R&D 100 winner for hydrogen safety sensor work.

FY 2018 PUBLICATIONS/PRESENTATIONS

1. R. Mukundan, et al. “Electrochemical Approaches to Hydrogen Contaminant Detection.” International Hydrogen Infrastructure Workshop, Boston, MA, September 2018.

R&D for Safety, Codes and Standards: Hydrogen Behavior

Ethan S. Hecht (Primary Contact),
Bikram Roy Chowdhury, Anthony H. McDaniel,
Scott Bisson
Sandia National Laboratories
P.O. Box 969, MS 9052
Livermore, CA 94550
Phone: (925) 294-3741
Email: checht@sandia.gov

DOE Manager: Laura Hill
Phone: (202) 586-8384
Email: Laura.Hill@ee.doe.gov

Project Start Date: October 1, 2003
Project End Date: Project continuation and
direction determined annually by DOE

Overall Objectives

- Develop a science and engineering basis for the release, ignition, and combustion behavior of hydrogen across its range of use (including high pressure and cryogenic).
- Facilitate the assessment of the safety (risk) of hydrogen systems and enable use of that information for revising regulations, codes, and standards (RCS) and permitting hydrogen fueling stations.

Fiscal Year (FY) 2018 Objectives

- Finalize validation of a cryogenic hydrogen dispersion model using data from lab-scale experiments.
- Develop a diagnostic that can measure large-scale and/or real-world cryogenic hydrogen dispersion including cryogenic hydrogen venting and vaporization from pools.

Technical Barriers

This project addresses the following technical barriers from the Hydrogen Safety, Codes and Standards section of the Fuel Cell Technologies Office Multi-Year Research, Development, and Demonstration (MYRDD) Plan¹:

- Safety Data and Information: Limited Access and Availability
- Insufficient Technical Data to Revise Standards.

Contribution to Achievement of DOE Milestones

This project will contribute to achievement of the following DOE milestones from the Hydrogen Safety, Codes and Standards section of the Fuel Cell Technologies Office MYRDD Plan:

- Milestone 2.13: Develop and validate simplified predictive engineering models of hydrogen dispersion and ignition. (4Q 2015)
- Milestone 2.19: Validate inherently safe design for hydrogen fueling infrastructure. (4Q, 2019)
- Milestone 4.8: Revision of NFPA 2 to incorporate advanced fueling and storage systems and specific requirements for infrastructure elements such as garages and vehicle maintenance facilities. (3Q, 2016)

FY 2018 Accomplishments

- Completed validation of the ColdPlume model with model comparisons to data collected using a unique, world-first, cryogenic hydrogen imaging diagnostic for 15 experimental release conditions, including five conditions with simultaneous velocity data. The validated model can be used to predict hazard distances from liquid hydrogen system leaks.
- Developed an optical design for light collection for a large-scale diagnostic enabling the measurement of hydrogen concentration for real-world releases from a stand-off distance of at least 20 ft. This first-of-its kind diagnostic will be used to measure liquid hydrogen vent stack dispersion and vaporization profiles from liquid hydrogen pools. The data will be used to validate models and enable reductions to liquid hydrogen fueling station footprints.

¹ <https://www.energy.gov/eere/fuelcells/downloads/fuel-cell-technologies-office-multi-year-research-development-and-22>

INTRODUCTION

Fire codes govern the required distances between hydrogen sources (e.g., a liquid hydrogen tank at a fueling station) and hazards (e.g., ignition sources). Revisions to the fire code distances require justification, which is facilitated by analysis that include physical models. These models must be validated by carefully controlled experiments, under relevant conditions, which can include high pressures (10,000 psi) or cryogenic temperatures (20 K). Over the course of this project, a range of experiments have been designed, developed, and executed to provide validation data for models. Models have been developed and exercised to inform the fire codes. This work has enabled quantitative risk assessments of hydrogen systems and subsequent reduction of setback distances from high-pressure hydrogen sources. More recently, our efforts have focused on developing a scientific basis for modeling dispersion and flames from cryogenic (liquid) hydrogen sources. There are currently large distances required by the fire codes around liquid hydrogen tanks, hindering the development and construction of hydrogen fueling stations with liquid hydrogen on site, an economically viable station design for large-capacity stations needed in urban areas. Validated models and targeted experiments from this project will be exercised to provide a technical basis for the revision of fire codes related to liquid hydrogen.

APPROACH

The goals of this work are to develop and validate scientific models to accurately predict hazards and consequences from hydrogen releases and combustion/flames. In this project, we previously developed one-dimensional and engineering models of hydrogen dispersion and flames that can run quickly on a PC. While these models are one dimensional, they include enough physics (e.g., the effect of buoyancy) to be accurate under a wide range of scenarios. These models are able to characterize the hazards from hydrogen releases and flames and are fast enough that they can be run multiple times and incorporated into a quantitative risk assessment framework that includes probabilities of leak frequency and size, and probabilistic harm models. While the models we used to inform fire codes have been validated, carefully controlled experiments are required to validate and develop new models for cryogenic hydrogen to have an impact on liquid hydrogen separation distances. Advanced optical and laser diagnostics are used, along with more conventional diagnostics (e.g., thermocouples) to characterize the dispersion and flame properties of releases, at a lab scale. The temperature, pressure, and orifice of the unignited releases and flames are controlled while characteristics are measured (e.g., concentration, flame temperature, radiative heat flux). For liquid hydrogen, some phenomena, such as releases from vent stacks and measurements of vaporization and pooling rates, require larger-scale experiments, and we are currently developing diagnostics and experimental platforms to measure these phenomena.

RESULTS

With the focus on developing a large-scale diagnostic, one of the first tasks this fiscal year was surveying the literature for diagnostics capable of measuring hydrogen concentration with reasonable resolution suitable for model validation. One option is using sensors, either within the flow or on samples extracted from the flow. Sensors are reasonably low cost and straightforward to implement. However, there are several drawbacks to sensors. Placing either the sensors or sampling probes in the flow can disturb the flow field of interest. Sensors lead to point measurements of concentration making it challenging to get spatial resolution, and most sensors have poor temporal response (and hence poor temporal resolution). Finally, depending on the technology (e.g., electrochemical, thermal conductivity, catalytic), sensors are often not specific to hydrogen and can be affected (e.g., drift, have reduced accuracy) by other environmental factors (e.g., temperature). Optical diagnostics, on the other hand, can provide high spatial and temporal resolution and are nonintrusive, but optical methods of detecting hydrogen are very challenging (i.e., there are no strong absorption features or fluorescence transitions). Nonetheless, due to the perceived benefits, and our experience using optical hydrogen diagnostics in the laboratory, we decided to pursue the scale-up of our lab-scale method of measuring Raman scattering.

Raman scattering is inelastic scattering of light off molecules. Different molecules have different Raman transitions and hence different Raman bands. In the laboratory, we reshape a high-powered laser beam into a

sheet and image Raman scattered light off hydrogen and nitrogen molecules to calculate the two-dimensional hydrogen concentration and temperature fields of turbulent jets, as shown in Figure 1. We have specific light filters to only collect Raman shifted light that is scattering off of the molecules of interest and can reduce the signal due to ambient light (a serious issue when trying to measure in the sunlight) and light scattered at the excitation wavelength (the laser wavelength—a large signal for cryogenic plumes where there is condensed moisture scattering a lot of light).

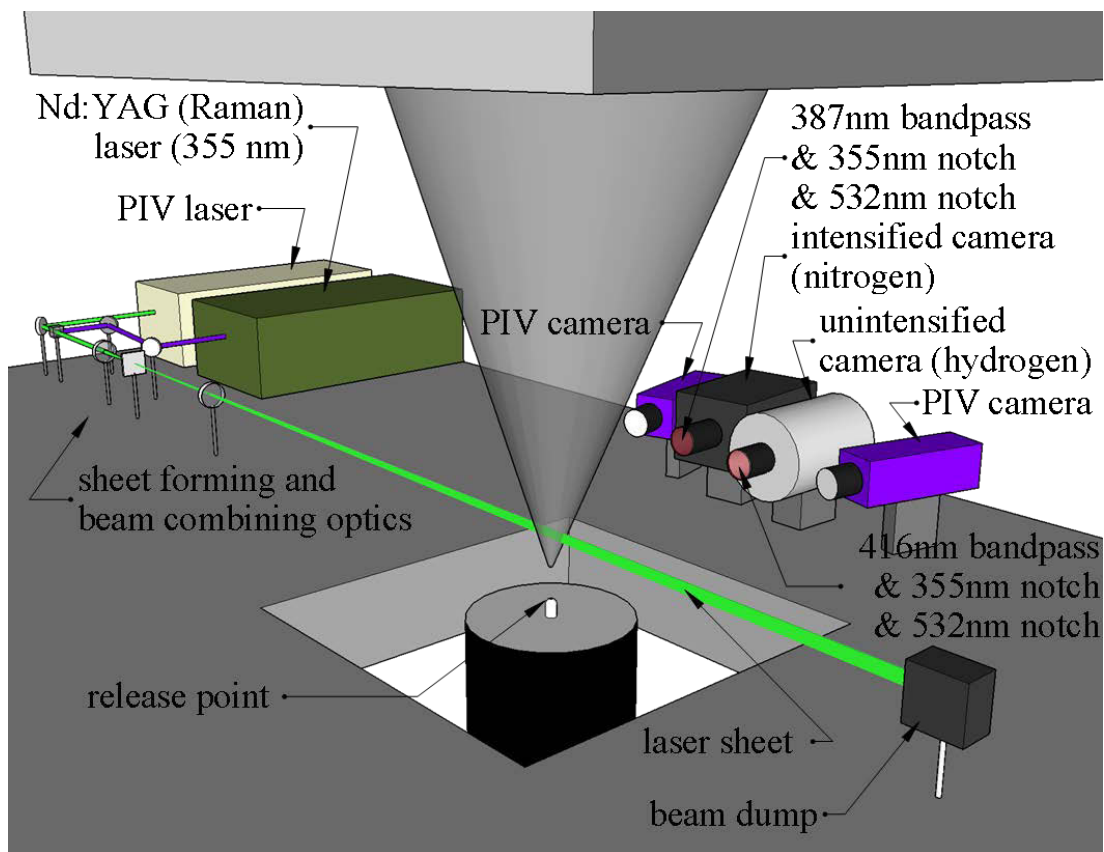


Figure 1. Laboratory setup for simultaneous Raman scattering measurements and particle imaging velocimetry measurements of cryogenic hydrogen jets. This setup enables the measurement of two-dimensional fields of species concentrations, temperatures, and velocity.

The intensity of Raman scattered light is inversely proportional to the wavelength of light to the fourth power and therefore the intensity increases greatly when smaller wavelengths of light are used to excite the molecules. However, the sensitivity of detectors (e.g., cameras, diodes) is often poorer at lower wavelengths and if using a laser, converting the higher wavelengths to lower wavelengths reduces the laser power output. Nonetheless, moving to the ultraviolet wavelengths can boost the signal-to-noise ratio, both in the lab and in moving toward the large-scale diagnostic. Figure 2 demonstrates this relationship using the laser system in the laboratory and several camera options that we currently have in the laboratory. As shown, by using the same cameras, we expect to achieve over 3 times the current signal-to-noise level by using the third harmonic of our Nd:YAG laser at 355 nm instead of the second harmonic at 532 nm.

Efforts toward experimentally demonstrating this signal-to-noise boost in the lab were delayed by several challenges. Ultraviolet light at 355 nm, even at lower laser energy, is much more damaging to optical coatings than visible light at 532 nm. This required us to develop a more even distribution of laser energy from the oscillator cavity by replacing optics and develop less temporal energy fluctuations by seeding the laser. We also determined a maximum laser power, less than the peak power, to prevent damage to optics. To maintain

the total power needed to achieve the signal boost shown in Figure 2, we are adding a second laser that will temporally lag the first laser, but it will still produce spontaneous Raman scattering that will be captured by our cameras. Although the laser energy at 355 nm was lower than the energy at 532 nm, the photon energy is higher, and we found that we were igniting the flows when using the ultraviolet light. For this reason, we reduced the peak energy by temporally stretching the laser pulses by constructing delay cavities.

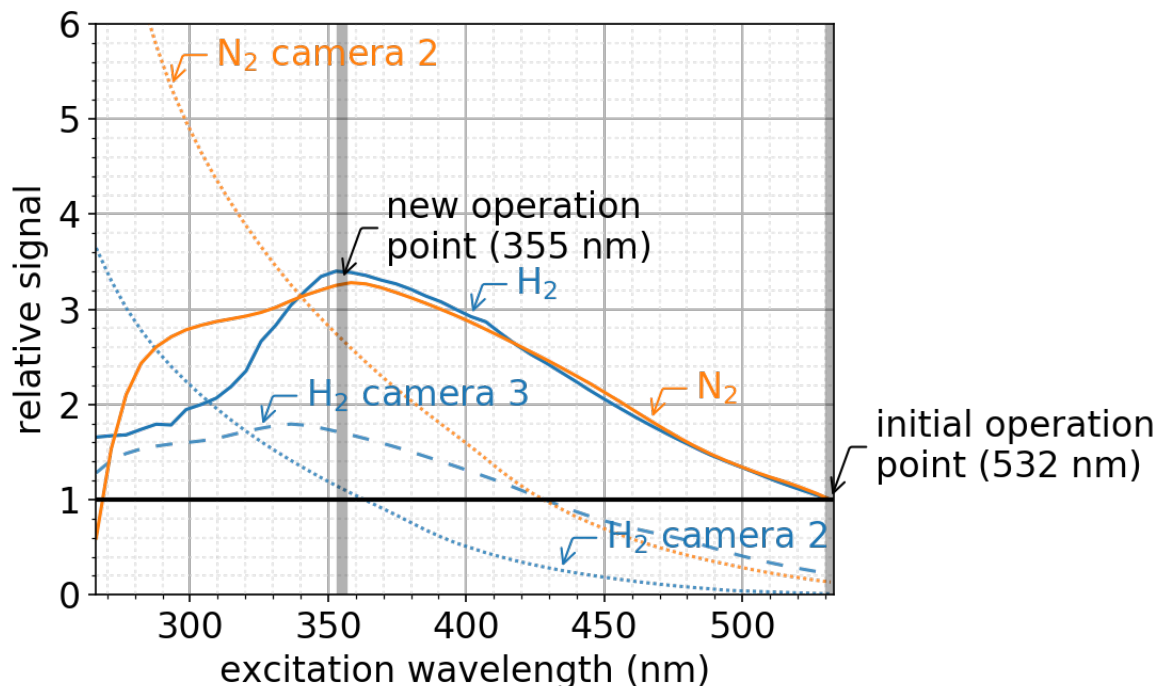


Figure 2. Relative signal that can be achieved for measuring Raman scattering from hydrogen and nitrogen molecules as a function of excitation light wavelength using several scientific cameras available in the laboratory

We developed plans for the light collection system of the large-scale diagnostic and proved several concepts in the lab this fiscal year. The goals of the large-scale diagnostic are extremely challenging to meet, and we used ray-tracing software to specify the necessary optics, as shown in Figure 3. There are several important characteristics of the system. First, we are using the full 10-in. ($f/0.8$) aperture afforded by a Fresnel lens (which reduces cost and time to develop large, custom optics) maximizing the solid angle of light collection. Second, there is a region of parallel light rays between the imaging lens and the achromatic focusing lens that enables placement of the wavelength filter, which has an angular response to light rejection/throughput. Finally, we have carefully chosen the focal lengths to reduce the image size so that it can fit on a small sensor. We used the system shown in Figure 3 to successfully measure Raman scatter off a pure 3-in. section of hydrogen from over 20 ft away. This proves that our light collection system has the potential to work in the field, measuring hydrogen concentration from a large standoff distance.

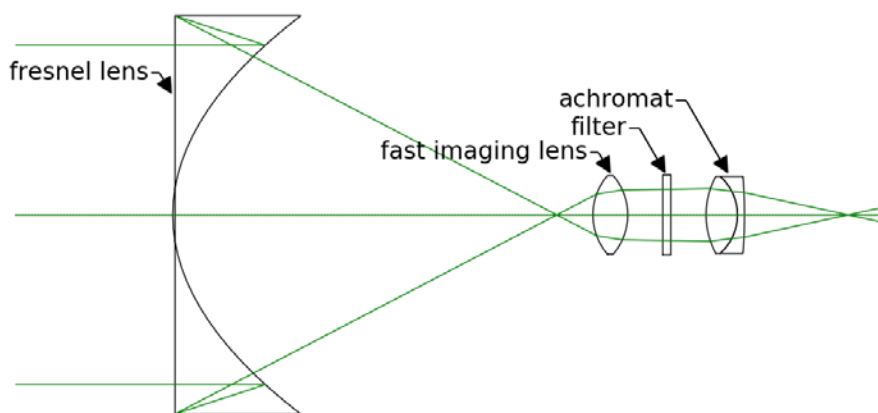


Figure 3. Ray trace diagram of large-scale cryogenic hydrogen dispersion diagnostic

A final result from this fiscal year was the completion of a lab-scale experimental campaign collecting simultaneous concentration, temperature, and velocity fields from cryogenic hydrogen releases. We then compared this new data, along with data collected last fiscal year, to a model of cryogenic hydrogen dispersion. The model and data showed very good agreement, validating the modeling approach. The model can now be used with confidence to predict the dispersion and mixing of cryogenic hydrogen jets and plumes with air. This model can be incorporated into our quantitative risk assessment toolkit and used to assess the safety of hydrogen fueling stations with liquid hydrogen.

CONCLUSIONS AND UPCOMING ACTIVITIES

Significant progress was made this fiscal year toward the development of an optical diagnostic that will be used to measure the dispersion from large-scale cryogenic hydrogen releases. The light collection system was developed and the concept was proved to measure Raman scattered light from hydrogen molecules from over 20 ft. This optical collection system needs some refinement, including additional light rejection at the excitation wavelength and the use of a field lens to increase the field of view. The illumination system for the large-scale diagnostic also still needs development before this diagnostic can be applied to a large-scale cryogenic hydrogen release. This is the thrust of our work moving forward; completing the assembly of the large-scale diagnostic and using this diagnostic to measure the real-world dispersion of cryogenic hydrogen. Next fiscal year, our first use of this diagnostic will be to measure the dispersion of cryogenic hydrogen from a liquid hydrogen vent stack. This information will be used to provide justification for the reduction of the 75 ft setback distance (in NFPA 2: Hydrogen Technologies Code) from liquid hydrogen bulk storage to air intakes and the general footprint for hydrogen fueling stations with liquid hydrogen.

FY 2018 PUBLICATIONS/PRESENTATIONS

1. E.S. Hecht. "October 2017 Codes and Standards Tech Team Update: Building Knowledge of Cryogenic Hydrogen Behavior." Presented to the DOE Codes and Standards Tech Team, October 12, 2017. SAND2017-11032PE.
2. E.S. Hecht. "Hazard and Consequence Modeling Applicable to Safety Codes and Standards." Presented at the US-Korea Joint Research Meeting, Long Beach, CA, November 6, 2017. SAND2017-12044 PE.
3. E.S. Hecht. "Current Research and Future Outlook for Behavior and Consequence Modeling." Presented at the US-Korea Joint Research Meeting, Long Beach, CA, November 6, 2017. SAND2017-12045 PE.
4. E.S. Hecht. "November Update on the Separation Distance for Liquid Hydrogen Storage Project." Presented to the Liquid Hydrogen CRADA contributors, November 28, 2017. SAND2017-12948 PE.

5. E.S. Hecht, B. Roy Chowdhury. “Experimental Validation of a Model for Cryogenic Hydrogen Jet Dispersion.” Presented at the 255th American Chemical Society National Meeting, New Orleans, LA, March 20, 2018. SAND2018-2834 C.
6. E.S. Hecht. “Hydrogen Behavior R&D for Safety, Codes and Standards at Sandia National Labs.” Presented to the NFPA 2 Hydrogen Storage Task Group, April 3, 2018. SAND2018-3518 PE.
7. E.S. Hecht, B. Roy Chowdhury, S.E. Bisson, A.H. McDaniel. “How to See and Quantify Hydrogen Concentration (and Cryogenic Hydrogen) using Optical Diagnostics.” Presented at the PreSLHy Kick-Off Meeting in Karlsruhe, Germany, April 16–20, 2018. SAND2018-4000 PE.
8. E.S. Hecht, B. Roy Chowdhury, A.H. McDaniel, S.E. Bisson. “R&D for Safety, Codes and Standards: Hydrogen Behavior.” Presented at the U.S. Department of Energy’s Hydrogen and Fuel Cells Program 2018 Annual Merit Review and Peer Evaluation Meeting, Washington, DC, June 13–15, 2018. SAND2018-4001 PE.
9. E.S. Hecht. “Safety, Codes and Standards and the HyRAM Toolkit.” Presented to representatives of the State Power Corporation of China Research Institute in Livermore, CA, August 6, 2018. SAND2018-5847 PE.
10. E.S. Hecht, P. Panda. “Mixing and Warming of Cryogenic Hydrogen Releases.” *International Journal of Hydrogen Energy*. In Press 2018. <https://doi.org/10.1016/j.ijhydene.2018.07.058>
11. E.S. Hecht. “Cryogenic Hydrogen Behavior and Research Priorities.” Presented at PreSLHy LH2 Research Priority Workshop in Buxton, England, September 17–21, 2018. SAND2018-10121 PE.
12. E.S. Hecht, B.D. Ehrhart, G.A. Bran Anleu. “Summary of Liquid Hydrogen Research at Sandia National Laboratories.” Presented by Jay Keller at the 2nd International Workshop on Liquefied Hydrogen in Kobe, Japan, October 24–25, 2018. SAND2018-10664 C.

Hydrogen Quantitative Risk Assessment

Alice Muna (Primary Contact), Brian Ehrhart, Ethan Hecht, Gabriela Bran-Anleu, Myra Blaylock, John Reynolds (SAIC), Cianan Sims (Sims Industries), Chris LaFleur
Sandia National Laboratories
P.O. Box 5800 MS 0748
Albuquerque, NM 87185
Phone: (505) 844-2580
Email: amuna@sandia.gov

DOE Manager: Laura Hill
Phone: (202) 586-8384
Email: Laura.Hill@ee.doe.gov

Project Start Date: October 1, 2003
Project End Date: Project continuation and direction determined annually by DOE

Overall Objectives

- Develop algorithms, models, and data to enable industry-led codes and standards revisions to be based on a strong, traceable science and engineering basis.
- Develop hydrogen-specific quantitative risk assessment (QRA) and consequence models and methods to support regulations, codes, and standards decisions and to enable alternate means of code compliance, such as performance-based design.
- Develop the Hydrogen Risk Assessment Model (HyRAM) toolkit to provide a rigorous, documented basis for analyzing hydrogen infrastructure safety with QRA and consequence modeling.

Fiscal Year (FY) 2018 Objectives

- Develop additional QRA capability to enable HyRAM to be applied to a larger variety of hydrogen applications.
- Update National Fire Protection Association (NFPA) 55/2 gaseous separation distances using scientific justification for risk criteria.
- Provide the necessary information to authorities in the Northeast Corridor to determine whether

fuel cell electric vehicles (FCEVs) will be permitted in tunnels.

- Leverage foundational R&D capabilities in QRA and materials to characterize and calculate risk associated with a key hydrogen infrastructure gap (storage).

Technical Barriers

This project addresses the following technical barriers from the Hydrogen Safety, Codes and Standards section of the Fuel Cell Technologies Office (FCTO) Multi-Year Research, Development, and Demonstration Plan¹:

- (A) Safety Data and Information: Limited Access and Availability
- (F) Enabling National and International Markets Requiring consistent RCS
- (K) No Consistent Codification Plan and Process for Synchronization of R&D and Code Development
- (L) Usage and Access Restrictions—parking structures, tunnels and other usage areas.

Contribution to Achievement of DOE Hydrogen Safety, Codes and Standards Milestones

This project will contribute to achievement of the following DOE milestones from the Hydrogen Safety, Codes and Standards section of the FCTO Multi-Year Research, Development, and Demonstration Plan:

- Milestone 2.4: Publish a methodology for estimating accident likelihood. (2Q, 2013)
- Milestone 2.8: Publish risk mitigation strategies. (2Q, 2014)
- Milestone 2.11: Publish a draft protocol for identifying potential failure modes and risk mitigation. (4Q 2014)

¹ <https://www.energy.gov/eere/fuelcells/downloads/fuel-cell-technologies-office-multi-year-research-development-and-22>

- Milestone 2.13: Develop and validate simplified predictive engineering models of hydrogen dispersion and ignition. (4Q 2015)
- Milestone 2.19: Validate inherently safe design for hydrogen fueling infrastructure. (4Q, 2019)
- Milestone 4.7: Complete risk mitigation analysis for advanced transportation infrastructure systems. (1Q, 2015)
- Milestone 4.8: Revision of NFPA 2 to incorporate advanced fueling storage systems and specific requirements for infrastructure elements such as garages and vehicle maintenance facilities. (3Q, 2016)

FY 2018 Accomplishments

- Published report documenting a Hydrogen Fuel Cell Electric Vehicle Tunnel Safety Study, which provided a scientific basis for allowing FCEVs in tunnels. The report is intended to enable the adoption of FCEVs in the northeast region.
- Completed a draft of HyRAM 2.0, which includes the customization of QRA analysis and which will expand HyRAM capabilities beyond indoor refueling stations.
- Signed a cooperative research and development agreement (CRADA) with FirstElement Fuel to demonstrate a performance-based approach to a hydrogen refueling station design.
- Addressed public comments and proposed edits to gaseous separation distance tables and annex information to the second draft of NFPA 2 and 55 enabling reduced gaseous hydrogen fueling station footprint.

INTRODUCTION

DOE has identified consistent safety, codes, and standards as a critical need for the deployment of hydrogen technologies, with key barriers related to the availability and implementation of technical information in the development of regulations, codes, and standards. Advances in codes and standards have been enabled by risk-informed approaches to create and implement revisions to codes, such as NFPA 2, NFPA 55, and International Organization for Standardization (ISO) Technical Specification (TS)-19880-1. This project provides the technical basis for these revisions, enabling the assessment of the safety of hydrogen fuel cell systems and infrastructure using QRA and physics-based models of hydrogen behavior. The risk and behavior tools that are developed in this project are motivated by, shared directly with, and used by the committees revising relevant codes and standards, thus forming the scientific basis to ensure that code requirements are consistent, logical, and defensible.

APPROACH

This work leverages Sandia's unique experimental and modeling capabilities and combines these efforts with stakeholder engagement and international leadership. Sandia develops the algorithms and methods for performing QRA, including scenario development, likelihood and consequence analysis, and risk quantification. Sandia's Turbulent Combustion Laboratory develops and validates predictive engineering models for flame initiation, flame sustainment, radiative heat flux, and overpressures. The resulting QRA and hydrogen behavior models are integrated into the HyRAM toolkit to enable consistent, traceable, and rigorous risk and consequence assessment. HyRAM's hydrogen behavior and QRA models are then applied to relevant technologies and systems to provide insight into the risk level and risk mitigation strategies with the aim of enabling the deployment of fuel cell technologies through revision of hydrogen safety, codes, and standards.

RESULTS

Northeast Corridor Tunnel Updates

The need to understand the risks and implications of traffic incidents involving hydrogen fuel cell vehicles in tunnels is becoming important with the increased deployment of these vehicles, particularly in the Northeast Corridor. The goal of this work was to provide the necessary information to authorities having jurisdiction in the Northeast Corridor to determine whether FCEVs will be permitted in tunnels. A risk analysis was performed to capture potential scenarios that could occur in the event of a crash and provide a quantitative calculation for the probability of each scenario. The scenario with the potential for increased consequence due to hydrogen was determined to be an FCEV crash where the thermally-activated pressure relief device activates due to temperatures from an external fire. This scenario was modeled in three different tunnels and the results determined that there may be localized concrete spalling, but no effect to the structure of the tunnels. The risk and modeling analysis was documented in a Sandia report and published in October 2017. A briefing on the analysis and results was given to the New York and New Jersey Port Authority and Massachusetts Department of Transportation engineers.

Chris LaFleur and DOE/FCO staff met with Bill Bergeson of the Federal Highway Administration as well as staff from the National Highway Traffic Safety Administration (NHTSA) who have been working with fuel cell vehicles for many years to discuss FCEVs and tunnels. The path forward discussed was to create a comprehensive alternative fuel vehicle tunnel safety roadmap that will collect and address all stakeholders' concerns. This roadmap will include light-, medium-, and heavy-duty vehicles powered by hydrogen fuel cells, compressed natural gas, propane, and advanced chemistry batteries. Sandia will draft an outline for this roadmap in FY 2019, and FCO and the Federal Highway Administration (FHWA) will form a stakeholder group to collect and address all concerns. This effort will also involve other Office of Energy Efficiency and Renewable Energy offices, such as the Vehicle Technologies Office, as well as NHTSA. The combined federal effort will allow forward progress, with public safety as a priority. Chris LaFleur also led the International Partnership for Hydrogen and Fuel Cells in the Economy Regulations Codes Standards & Safety working group meeting on tunnels in conjunction with the Research Priorities Workshop at the Health and Safety Laboratory in Buxton, United Kingdom, in September.

HyRAM 2.0 Updates

The HyRAM toolkit integrates state-of-the-art models and data for assessing hydrogen safety. HyRAM provides a common platform for stakeholders conducting quantitative risk assessment and consequence analysis for hydrogen systems. The resulting information provides the scientific basis to ensure code requirements are consistent, logical, and defensible.

In FY 2018, the HyRAM development team focused their efforts on developing a customizable QRA analysis to expand HyRAM's analysis capabilities beyond an indoor refueling station. The team determined that the best way to accomplish this goal was not to integrate an existing event/fault tree software but instead leverage the plethora of free, publicly available fault tree software and provide a method for the user to enter in the risk results. To accomplish this, updates to the QRA source code were made, including the conversion of this part of the software from C# to Python. The graphical user interface text and images have been updated to display the new QRA options. Figure 1 illustrates the updated image that will be inserted into HyRAM showing the editable portions of the analysis.

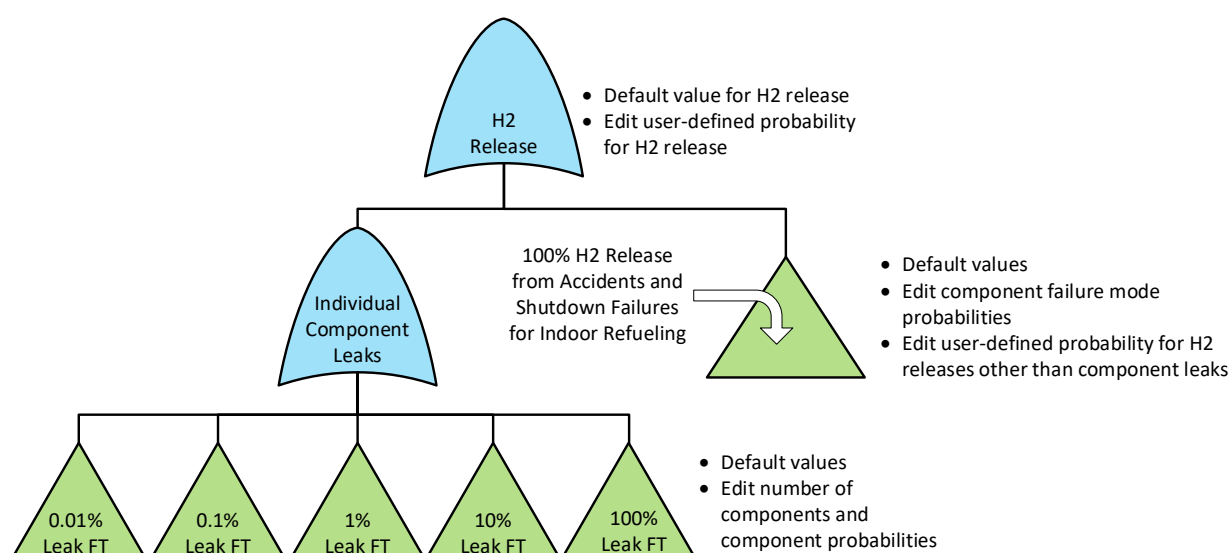


Figure 1. Updated HyRAM fault tree showing editable portions of the QRA

The HyRAM QRA analysis has also been updated to include two new generic components. The intent of this update is that systems with a unique component would be able to enter in reliability data for their component and that would be added to the existing QRA framework. A component failures table in HyRAM is used to compute the accidental and shutdown failure parameters for the 100% leak release calculation only (and not in the other four fault trees with other leak sizes). This table has been updated so a user can edit the distribution type and parameters, as needed. A new tab has been added that displays the distributions for user ease of use. The scenario stats (output of QRA calculation) have also been updated in HyRAM. First, the scenario rankings have added a branch line probability to ease in the creation of an event tree, if needed. Additional significant digits were added to provide for more clarity in the average number of events per year and the potential loss of life (PLL) contribution calculations. The cut sets were also edited for clarity and ease. Instead of listing only the 100% leak cut sets, there are now five tables, corresponding to the five fault trees, with each cut set probability listed. The interface between the C# and the Python was also edited to directly pass the C# inputs into Python without converting them into a text file as an intermediate. This updated framework runs faster and will reduce errors.

The HyRAM QRA updates are currently in test form and will be debugged in Q1 of FY 2019. The goal is that HyRAM 2.0 will be re-issued a copyright and be available for release in FY 2019. The HyRAM team also

published SAND2018-0749, titled “HyRAM V1.1 User Guide.” This document captures the main features of HyRAM version 1.1 and is based upon the HyRAM V1.0 User Guide.

Real-World Application of Alternate Means

Sandia executed an in-kind CRADA with FirstElement Fuel on March 14, 2018. The statement of work for this CRADA is to develop a performance-based design for a hydrogen refueling station, utilizing Sandia’s QRA methodology. The first task for this CRADA is to collaborate to prepare station permitting documents and submit to an applicable authority having jurisdiction for approval. The second task is to develop a final report documenting the technical results/accomplishments for the project. FirstElement Fuel has 19 planned liquid-hydrogen-based refueling stations and work has begun to develop calculations to support an alternate means justification to challenge separation distances. This justification will be presented to an authority having jurisdiction.

NFPA 2/55 Technical Committee Support

Sandia has worked closely with the NFPA 2 and 55 technical committees and task groups to update the gaseous storage separation distances based on a risk-informed process. In FY 2018, the public comments submitted to NFPA 2 and 55 were reviewed and necessary changes were identified in the code. Public comments were submitted to fix the errors. Sandia attended the second draft of NFPA 2 and 55 technical committee meetings to vote on public comments as members of the committees. All of Sandia’s public comments were accepted in both NFPA 2 and 55, which included the following: fixing errors within the separation distance table calculations, correcting annex material to reflect the same information in both NFPA 2 and 55, and updating the history of the risk-informed approach taken to derive separation distances.

CONCLUSIONS AND UPCOMING ACTIVITIES

Sandia will continue to provide information to authorities and other interested parties on our tunnel analysis. In addition, Sandia will work on developing a tunnel safety roadmap for light-, medium-, and heavy-duty vehicles powered by hydrogen fuel cells, compressed natural gas, propane, and advanced chemistry batteries. This work will be in conjunction with a combined federal effort from DOE FCTO, DOE Vehicle Technologies Office, NHTSA, and FHWA.

The HyRAM toolkit provides a platform with state-of-the-art hydrogen models for assessing the risk of hydrogen systems and the consequences of hydrogen releases and fires to enable industry-led analyses. We plan to add modules for consequence modeling, including the ability to calculate the physical effects of liquid hydrogen releases, cold plumes, and subsequent ignitions, pending the results from Sandia’s liquid hydrogen experiments and modeling.

FY 2018 PUBLICATIONS/PRESENTATIONS

1. C.B. LaFleur, G.A. Bran Anleu, A.B. Muna, B.D. Ehrhart, M.L. Blaylock, W.G. Houf. “Hydrogen Fuel Cell Electric Vehicle Tunnel Safety Study.” Sandia National Laboratories, October 2017. SAND2017-11157.
2. C.B. LaFleur. “Hydrogen Fuel Cell Tunnel Analysis.” Presented to Massachusetts Department of Transportation Engineers, October 20, 2017. SAND2017-8177 O.
3. A. Muna. “Hydrogen Quantitative Risk Assessment 2017 Update and Path Forward.” Presented at US DRIVE Hydrogen Codes & Standards Tech Team Meeting, October 12, 2017.
4. A.B. Muna. “QRA and Physics Mode Flow Charts.” SAND2017-11836.
5. A.B. Muna. “Hydrogen Quantitative Risk Assessment 2017 Update and Path Forward.” Presented at Codes and Standards Technical Team Meeting, October 12, 2017. SAND2017-10867 PE.
6. A.B. Muna. “Hydrogen Quantitative Risk Assessment.” Presented at meeting with KGS and Hoseo University in Long Beach, CA, November 6–7, 2017. SAND2017-11689 PE.

7. A.B. Muna. “Hydrogen Quantitative Risk Assessment Path Forward.” Presented at meeting with KGS and Hoseo University in Long Beach, CA, November 6–7, 2017. SAND2017-11690 PE.
8. E.A. Sena, B.D. Ehrhart, A.B. Muna. “HyRAM 1.1 User Guide.” Sandia National Laboratories, January 2018. SAND2018-0749.
9. B.D. Ehrhart. “Hydrogen Risk Assessment Models (HyRAM) Overview.” Virtually presented at the HySA Hydrogen Safety Awareness Meeting, University of the Western Cape, South Africa. May 25, 2018. SAND2018-5511 PE.
10. G.A. Bran-Anleu. “Quantitative Risk Analysis to Guide Station Design.” Presented at the International Infrastructure Workshop, September 11, 2018.
11. C.B. LaFleur. “Hydrogen Fuel Cell Tunnel Analysis.” Presented at the IPHE Regulations Codes Standards & Safety working group meeting, September 18, 2018. SAND2017-8177 O.

Hydrogen Safety Panel, Safety Knowledge Tools, and First Responder Training Resources

Nick Barilo
Pacific Northwest National Laboratory (PNNL)
P.O. Box 999
Richland, WA 99352
Phone: (509) 371-7894
Email: nick.barilo@pnnl.gov

DOE Manager: Laura Hill
Phone: (202) 586-8384
Email: Laura.Hill@ee.doe.gov

Subcontractors:

- Santa Monica Fire Department, Santa Monica, CA
- UL, Northbrook, IL
- Air Products and Chemicals, Inc., Allentown, PA
- Becht Engineering, St. Louis, MO
- CSA Group, Langley, BC, Canada
- California Fuel Cell Partnership, West Sacramento, CA
- City of Santa Fe Springs, CA
- Proton OnSite, Wallingford, CT
- GWS Solutions of Tolland, LLC, Tolland, CT
- Witte Engineered Gases, Seminole, FL
- Firexpro, Wellesley, MA

Project Start Date: 2004
Project End Date: Project continuation and direction determined annually by DOE

Overall Objectives

- Enable the safe and timely transition to hydrogen and fuel cell technologies.
- Provide expertise and recommendations to help identify safety-related technical data gaps, best practices, and lessons learned.
- Help integrate safety planning into funded projects to ensure that projects address and incorporate hydrogen safety practices.
- Collect information and share lessons learned from hydrogen incidents and near misses to help prevent similar safety events in the future.
- Capture vast and growing knowledge base of hydrogen experience and make it publicly available to the hydrogen community and stakeholders.
- Support implementation of hydrogen and fuel cell technologies by providing technically

accurate hydrogen safety and emergency response information to first responders.

Fiscal Year (FY) 2018 Objectives

- Develop a long-term sustainability plan for the Hydrogen Safety Panel (HSP) and its resources
- Participate in outreach events on hydrogen safety aimed at a variety of stakeholder groups to emphasize available tools and resources.
- Participate in stakeholder meetings with the Connecticut Center for Advanced Technologies to identify potential HSP reviews.
- Update the Hydrogen Tools Portal content management system and user interface.

Technical Barriers

This project addresses the following technical barriers from the DOE Fuel Cell Technologies Office (FCTO) Multi-Year Research, Development, and Demonstration (MYRDD) Plan [1]:

Safety, Codes, and Standards

- (A) Safety Data and Information: Limited Access and Availability
- (C) Safety Is Not Always Treated as a Continuous Process
- (D) Lack of Hydrogen Knowledge by Authorities Having Jurisdiction
- (E) Lack of Hydrogen Training Materials and Facilities for Emergency Responders
- (F) Insufficient Technical Data to Revise Standards.

Education and Outreach

- (A) Lack of Readily Available, Objective and Technically Accurate Information
- (D) Lack of Educated Trainers and Training Opportunities.

Contribution to Achievement of DOE Milestones

This project contributes to achievement of the following DOE tasks and milestones from the FCTO MYRDD Plan:

Safety, Codes, and Standards

- Task 1: Address Safety of DOE Research and Development (R&D) Projects (ongoing)
- Task 5: Dissemination of Data, Safety Knowledge, and Information (ongoing)
- Milestone 5.1: Update Safety Bibliography and Incidents Databases (4Q, 2011–2020)

Education and Outreach

- Task 1: Educate Safety and Code Officials (ongoing)
- Milestone 1.1: Update “Introduction to Hydrogen Safety for First Responders” Course for First Responders (biannually)

FY 2018 Accomplishments

- Partnered with the American Institute of Chemical Engineers (AIChE) to establish the Center for Hydrogen Safety enabling long-term sustainability and broader impact of the Hydrogen Safety Panel and Safety Knowledge resources.
- Updated the National Hydrogen and Fuel Cell Emergency Response Training Resource in support of in-person training conducted in the Northeast United States in early 2018.
- Held the 24th Hydrogen Safety Panel meeting in Cambridge, Massachusetts, September 26–28, 2017, which included consideration of timely and relevant safety issues and the engagement of key hydrogen infrastructure stakeholders.
- Conducted 20 reviews (including safety plans and project designs) from July 1, 2017, to September 30, 2018, and provided timely feedback to support the safe completion of project activities.

- Provided outreach and educational sessions for a variety of audiences including the DOE Energy Exchange Conference, Green Transportation Summit and Expo, Hydrogen South Africa, and stakeholder meetings in the Northeast United States to familiarize participants with hydrogen fuel cell technologies, safe practices and safety resources, and reduce barriers to technology acceptance.

INTRODUCTION

Safety is essential for realizing the “hydrogen economy”—safe operation in all of its aspects from hydrogen production through storage, distribution, and use; from research, development, and demonstration to deployment and commercialization. As such, safety is given paramount importance in all facets of the research, development, demonstration, and deployment work of the DOE FCTO. This annual report summarizes activities associated with three project tasks: the HSP, Safety Knowledge Tools, and First Responder Training Resources.

Recognizing the nature of the DOE FCTO program and the importance of safety planning, the HSP was formed in December 2003 to assemble a broad cross-section of expertise from the industrial, government, and academic sectors to help ensure the success of the program. The panel’s experience resides in industrial hydrogen production and supply, hydrogen R&D and applications, process safety and engineering, materials technology, risk analysis, accident investigation, and fire protection. The panel provides expertise and recommendations on safety-related issues and technical data gaps, reviews individual DOE-supported projects and their safety plans, and explores ways to develop and disseminate best practices and lessons learned, all broadly benefiting the FCTO program. The panel currently has 15 members with a total of over 400 years of industry and related experience (see Table 1 for FY 2018 panel membership).

Table 1. Current Hydrogen Safety Panel Membership

Nick Barilo, Program Manager	PNNL
Richard Kallman, Chair	City of Santa Fe Springs, CA
Eric Binder	Santa Monica Fire Department
Ken Boyce	UL
David Farese	Air Products and Chemicals
Don Frikken	Becht Engineering
Livio Gambone	CSA Group
Aaron Harris	Air Liquide
Chris LaFleur	Sandia National Laboratories
Miguel Maes	NASA White Sands Test Facility
Steve Mathison	Honda Motor Company
Larry Moulthrop	Proton OnSite
Glenn Scheffler	GWS Solutions of Tolland, LLC
Tom Witte	Witte Engineered Gases
Robert Zalosh	Firexplo

Widespread availability and communication of safety-related information are crucial to ensuring the safe operation of future hydrogen and fuel cell technology systems. The entire hydrogen community benefits if knowledge on hydrogen safety is openly and broadly shared. To that end, PNNL continues to improve the safety knowledge software tools and develop new techniques for disseminating this information. This report covers the Hydrogen Tools Portal (<http://h2tools.org>), the Hydrogen Lessons Learned database (<http://h2tools.org/lessons/>), and the Hydrogen Safety Best Practices online manual (<https://h2tools.org/bestpractices>). These resources are key to reaching, informing, and educating users and stakeholders whose contributions will help enable the deployment of new hydrogen and fuel cell technologies.

Suitably trained emergency response personnel are essential to a viable infrastructure. FCTO has placed a priority on training emergency response personnel, not only because these personnel need to understand how to respond to a hydrogen incident, but also because firefighters and other emergency responders are influential in their communities and can be a positive force in the introduction of hydrogen and fuel cells into local markets. This report covers emergency response training for hazardous materials to provide a tiered hydrogen safety education program for emergency responders. The effort started with development and distribution of the awareness-level online course in FY 2006–2007. An operations-level classroom curriculum was developed

in FY 2008–2009, including design, construction, and operation of a fuel cell vehicle prop for hands-on training. PNNL and the California Fuel Cell Partnership collaborated to develop a national hydrogen safety training resource for emergency responders, which was made publicly available in September 2014.

APPROACH

The HSP strives to raise safety consciousness most directly at the project level through organizational policies and procedures, safety culture, and priorities. The panel reviews project safety plans and design documents to encourage thorough and continuous attention to safety aspects of the specific work being conducted. Panel safety reviews focus on engagement, learning, knowledge sharing, and active discussion of safety practices and lessons learned, rather than being audits or regulatory exercises. Through this approach, the HSP is promoting safe operation, handling, and use of hydrogen and hydrogen systems for all projects.

The panel's approach for disseminating safety knowledge in FY 2018 focused on adding resources to the existing Hydrogen Tools Portal and participating in impactful outreach activities. The portal brings together and enhances the utility of a variety of tools and web-based content on the safety aspects of hydrogen and fuel cell technologies. It is intended to help inform those tasked with designing, approving, or using systems and facilities, as well as those responding to incidents. Additional discussion is provided in the Results section of this report.

PNNL collaborates with subject matter experts in hydrogen safety and first responder training to develop, review, and revise training materials as needed. The PNNL project team works with DOE to inform stakeholder groups of training opportunities and to provide in person training when appropriate. The online awareness-level course provides a basic understanding of hydrogen properties, uses, and appropriate emergency response actions. The operations-level classroom/hands-on prop-based course has been presented at the Volpentest Hazardous Material Management and Materials Response Federal Training Center in Richland, Washington, and at several fire-training centers in California, Hawaii, and the Northeastern United States. This has enabled the panel to reach larger audiences in areas where hydrogen and fuel cell technologies are being deployed. The National Hydrogen and Fuel Cell Emergency Response Training Resource provides a consistent source of accurate information and current knowledge to ensure that training organizations have the information needed to develop or supplement their own courses. As part of this resource, a training template has been developed to guide the delivery of a variety of training regimens to various audiences.

RESULTS

A significant activity in FY 2018 was identifying long-term sustainability of the HSP and project safety resources. The goal is to make the HSP more readily available to industry and agencies, and to improve contracting efforts by making them less cumbersome and time consuming. PNNL evaluated three organizations and entered into significant talks with AIChE. The discussions resulted in a partnership between PNNL and AIChE to establish the Center for Hydrogen Safety (CHS). CHS will be a not-for-profit, non-biased membership organization within AIChE that promotes the safe operation, handling, and use of hydrogen and hydrogen systems across all installations and applications. The CHS will identify and addresses concerns regarding the safe use of hydrogen:

- As a sustainable energy carrier
- In commercial and industrial applications
- In hydrogen and fuel cell technologies.

Benefits to CHS members will include:

- Access to the U.S. Hydrogen Safety Panel for reviews and support
- Accredited education, training, and outreach materials
- Conferences and networking opportunities.

Membership in CHS will also demonstrate to stakeholders and the public that safety is a priority for the member organizations. This will be important messaging as infrastructure is more broadly deployed in locations where stakeholders are less familiar with hydrogen and fuel cell technologies.

The 24th HSP meeting was held in Cambridge, Massachusetts, September 26–28, 2017. The meeting provided opportunities to consider timely and relevant safety issues. The topics discussed and outcomes achieved at the meeting are detailed in the meeting minutes [2]. Significant activities during the meeting included interaction with a certification organization and discussion on sustainability of the HSP. The HSP guidance document, “Safety Planning for Hydrogen and Fuel Cell Projects,” was discussed along with proposed changes. These changes were incorporated, and the revised document was released in November 2017 [3]. The document was also reconfigured so that it could be used for both DOE and non-DOE projects.

During the past year, the HSP has provided safety reviews and support to 20 projects (Table 2). Since 2004, the panel has participated in 494 project reviews (including safety plans, site visit reviews, follow-up phone interviews, and design review work). In addition to reviewing safety plans for DOE, the HSP performed a site visit at Argonne National Laboratory to evaluate proposed changes to their gas blending system for turbines and engines using 100% hydrogen as a fuel. The visit included meetings with representatives from the project team and supporting organizations and a tour of the facility. Comments and recommendations were provided to the project team in September 2018. In March 2018, the HSP participated in an outreach event in Berkeley, California, to help the public become acquainted with specifics on the proposed Berkeley hydrogen fueling station. The PNNL project manager presented on the HSP’s role in deployment of the California hydrogen fueling station infrastructure.

In FY 2018, PNNL entered into a cooperative research and development agreement (CRADA) with the Connecticut Center for Advanced Technologies to raise the awareness of the HSP and identify projects that would benefit from safety reviews, outreach, and engagement with stakeholders. Stakeholder meetings were conducted in Connecticut, Rhode Island, and New Jersey in September 2018. In conjunction with these meetings, PNNL led hydrogen safety training focusing on fundamental safety knowledge and available safety resources.

At the request of the California Energy Commission (CEC), the HSP initiated a task group on mobile applications. The task group is evaluating the safety of mobile hydrogen and fuel cell applications (mobile auxiliary power units, mobile fuelers, multi-cylinder trailer transport, refrigeration units, etc.). The effort includes examination of the applications, requirements, and performance of mobile hydrogen to understand how safety considerations are applied. A report summarizing HSP activities, conclusions, and recommendations will be provided to the CEC and likely will be made available on the Hydrogen Tools Portal.

The HSP issued two white papers in FY 2018. The first, “Safety issues associated with the use of alternative fuel tanks: What can the hydrogen community learn from the CNG experience?” was published in June 2018 [4]. This paper (1) considered historical data from compressed natural gas (CNG) tank failures, including tank design and failure modes; (2) further evaluated vehicle fires and localized effects on tanks; and (3) identified research and testing gaps that the hydrogen industry should consider. The panel published a second white paper, “Qualified Individual for Liquefied Hydrogen,” on the Hydrogen Tools Portal in April 2018 [5]. This white paper is intended to help develop and implement practices and procedures that would ensure safety in the operation, handling, and use of hydrogen and hydrogen systems.

The Hydrogen Tools Portal was made publicly available in June 2015 and continues to grow in popularity. Based on current Google Analytics, the portal is becoming an international resource, as more than half of user sessions are from outside of the United States. Activities during 2018 focused on updating the portal from Drupal 7 to Drupal 8, improving the user interface, and revising the HSP site.

Table 2. HSP Project Safety Work July 1, 2017, to September 30, 2018

Work	Project Title	Contractor
Site Visit	Gas Blending System Hydrogen Modifications	Argonne National Laboratory
Safety Plan	PGM-Free Engineered Framework Nano-Structure Catalyst	Greenway Energy, LLC
Safety Plan	Super Metallated Frameworks as Hydrogen Sponges	University of California Berkeley
Safety Plan	Thin-Film, Metal-Supported High-Performance and Durable Proton-Solid	UTRC
Safety Plan	Characterization and Accelerated Life Testing of a New Solid Oxide Electrolysis Cell	Northwestern University
Safety Plan	Proton-Conducting Solid Oxide Electrolysis Cells for Large-Scale Hydrogen Production at Intermediate Temperatures	University of Connecticut
Safety Plan	Advanced PGM-Free Cathode Engineering for High Power Density and Durability	Carnegie Mellon University
Safety Plan	Best-in-Class Platinum Group Metal-Free (PGM-Free) Catalyst Integrated Tandem Junction Photoelectrochemical (PEC) Water Splitting Devices	Rutgers
Safety Plan	Vapor Deposition Process for Engineering of Dispersed PEMFC ORR Pt/NbO _x /C Catalysts	Ford
Design Review	Overview of the Medium Pressure Reactor System Design	University of Hawaii
Safety Plan	Hydrogen Fuel Cell Range Extender for Battery Electric Vehicle	FedEx
Design Review	Carbon Free Data Center	National Renewable Energy Laboratory
Safety Plan	Innovative Non-PGM Catalysts for CHP Relevant Proton Conducting Membrane Fuel Cells	Northeastern University
Safety Plan	CEC-2016-09-Revised	FirstElement
Safety Plan	High Performance PEFC Electrode Structures	UTRC
Safety Plan	Modular SOEC System for Efficient Hydrogen Production at High Current Density	FuelCell Energy
Safety Plan	High Temperature Alkaline Water Electrolysis	Giner, Inc.
Safety Plan	Solid Oxide Based Electrolysis and Stack Technology with Ultra-High Electrolysis Current Density (>3 A/cm ²) and Efficiency	FuelCell Energy
Safety Plan	Hybrid Electrochemical Hydrogen/Metal Hydride Compressor	Greenway Energy, LLC

Disseminating safety information continues to be an important aspect of this project. In addition to the CRADA activities described above, PNNL participated in outreach to personnel that construct, operate, and maintain energy-efficient and cost-effective federal facilities and fleets in the United States. Working with the Federal Energy Management Program (FEMP), PNNL participated in an outreach at the 2017 Energy Exchange Training and Trade Show in Tampa, Florida, in August 2017. The 90-minute presentation on fuel cell technologies was professionally recorded and made into a training course that has been deployed on FEMP's website. PNNL also collaborated with Clean Cities to co-present "Hydrogen Fuel Cells and Fuel Cell Electric Vehicles: Emerging Applications and Safety Management" at the Green Transportation Summit and Expo on April 17, 2018, in Tacoma, Washington. The event was well attended and included a good interactive discussion with participants.

PNNL's leadership in hydrogen safety is reinforced through its international collaborations. PNNL worked with Hydrogen South Africa, the International Association for Hydrogen Safety (HySafe), and the United Kingdom's Health and Safety Laboratory to provide an online hydrogen safety awareness webinar/panel discussion for code officials and stakeholders in South Africa in May 2018. PNNL also presented on the HSP and project learnings at the 2017 International Conference on Hydrogen Safety in Hamburg, Germany, in September 2017, and participated in the HySafe Research Priorities workshop in Buxton, United Kingdom, in September 2018.

First responder outreach activities for FY 2018 were limited to updating the National Hydrogen and Fuel Cell Emergency Response Training Resource (<https://h2tools.org/fr/nt>) in February 2018 and providing limited support to Frontier Energy's first responder training activities in the Northeast during the spring of 2018.

CONCLUSIONS AND UPCOMING ACTIVITIES

The HSP will continue to focus on how safety knowledge, best practices, and lessons learned can promote the safe conduct of project work and the deployment of hydrogen technologies and systems in applications of interest and priority in the DOE FCTO. The HSP can also be used more broadly as an asset for safe commercialization by reaching out to new stakeholders and users involved in early deployment, as shown by the panel's successful activities in California.

HSP initiatives over the next year will include the following:

- PNNL will work with AIChE to make the HSP available through AIChE.
- Continue to support the CEC's rollout of California's hydrogen fueling station infrastructure.
- Engage non-DOE entities to identify opportunities to use the panel to review hydrogen and fuel cell initiatives and promote safety.
- Continue to evaluate the panel membership to maintain its leadership role in hydrogen safety through an appropriate mix of safety expertise and perspective to perform safety reviews and address relevant issues.

Hydrogen safety knowledge tools help remove barriers to the deployment and commercialization of hydrogen and fuel cell technologies. The introduction of the Hydrogen Tools Portal opens opportunities to share new information and reach broader audiences. The primary focus in FY 2019 will be to maintain the portal in an operating state with minimal change.

The project's First Responder Training Resources can help ensure a safe transition to fuel cell vehicles and a hydrogen infrastructure and pave the way for broader public acceptance. This resource and associated props will be transitioned to the CHS in FY 2019, consistent with the President's direction toward a focus on early-stage R&D for DOE laboratories. To ensure a successful transition and long-term impact, the resource will be updated prior to the transfer.

FY 2018 PUBLICATIONS/PRESENTATIONS

1. Barilo, N.F. 2017. "Hydrogen Fuel Cells and Fuel Cell Electric Vehicles: Emerging Applications and Safety Management." Richland, WA: Pacific Northwest National Laboratory. Video, PNNL-SA-130157.
2. Barilo, N.F. 2018. "Safety issues associated with the use of alternative fuel tanks: What can the hydrogen community learn from the CNG experience?" PNNL-SA-132793. Richland, WA: Pacific Northwest National Laboratory.
3. Barilo, N.F. November 1, 2017. "Assuring Safety for Deployment of Hydrogen and Fuel Cell Technologies." Paris, France. PNNL-SA-129784.
4. Barilo, N.F. November 8, 2017. "Safety Learnings from Hydrogen Light Duty Vehicle Fueling Station Projects." Presented at Fuel Cell Seminar, Long Beach, California. PNNL-SA-130058.

5. Barilo, N.F. February 22, 2018. “Safety Planning for Hydrogen and Fuel Cell Projects.” Presented at California GFO-17-602 Webinar, “Online Conference,” United States. PNNL-SA-132444.
6. Barilo, N.F. May 25, 2018. “Hydrogen Safety Resources.” Presented at Hydrogen South Africa Hydrogen Safety Awareness. PNNL-SA-135026.
7. Barilo, N.F. 2017. “Hydrogen Safety Panel, Safety Knowledge Tools and First Responder Training Resources.” PNNL-SA-127936. Richland, WA: Pacific Northwest National Laboratory.
8. Barilo, N.F. March 30, 2018. “Hydrogen Safety Panel Activities in California Hydrogen Infrastructure Rollout.” Berkeley, CA. PNNL-SA-133425.
9. Barilo, N.F. August 15, 2017. “Hydrogen Fuel Cells and Fuel Cell Electric Vehicles, Emerging Applications and Safety Management.” Tampa, FL. PNNL-SA-127986.
10. Barilo, N.F. 2017. “Safety Planning for Hydrogen and Fuel Cell Projects.” PNNL-25279-1. Richland, WA: Pacific Northwest National Laboratory.
11. Barilo, N.F. June 15, 2018. “Hydrogen Safety Panel, Safety Knowledge Tools, and First Responder Training Resources.” Presented at DOE Annual Merit Review, Washington, DC. PNNL-SA-133744.
12. Barilo, N.F. September 12, 2018. “Introducing the Hydrogen Safety Panel and Safety Resources.” Presented at DOE CCAT Stakeholder Meetings, New York, NY. PNNL-SA-137746.
13. Barilo, N.F. September 19, 2018. “Hydrogen Safety Panel Learnings and Gaps.” Presented at HySafe Research Priorities Workshop, Buxton, United Kingdom. PNNL-SA-137902.
14. Barilo, N.F. September 12, 2018. “Introduction to Hydrogen and Fuel Cell Technologies and Safety Considerations.” Presented at stakeholder meetings in the Northeast U.S., New York, NY. PNNL-SA-137745.
15. Barilo, N.F. September 12, 2017. “U.S. Hydrogen Safety Panel Experience.” Presented at International Conference on Hydrogen Safety, Hamburg, Germany. PNNL-SA-128907.
16. Barilo, N.F. September 14, 2017. “Addressing the Hydrogen Infrastructure Safety Challenge.” Presented at Air Liquide, Paris, France. PNNL-SA-128908.

REFERENCES

1. U.S. Department of Energy, “Fuel Cell Technologies Office Multi-Year Research, Development and Demonstration (MYRD&D) Plan,” <http://energy.gov/eere/fuelcells/downloads/fuel-cell-technologies-office-multi-year-research-development-and-22>.
2. Barilo, N.F. to Farese, D. et al., “24th Hydrogen Safety Panel Meeting Minutes,” November 10, 2017.
3. “Safety Planning for Hydrogen and Fuel Cell Projects,” PNNL-25279-1, November 2017, https://h2tools.org/sites/default/files/Safety_Planning_for_Hydrogen_and_Fuel_Cell_Projects-November2017_0.pdf.
4. “Safety issues associated with the use of alternative fuel tanks: What can the hydrogen community learn from the CNG experience?,” November 2017, https://h2tools.org/sites/default/files/Safety_Planning_for_Hydrogen_and_Fuel_Cell_Projects-November2017_0.pdf.
5. “Qualified Individual for Liquefied Hydrogen,” April 2018, https://h2tools.org/sites/default/files/HSP_White_Paper-LH2_Qualified_Individuals.pdf.

NREL Hydrogen Sensor Testing Laboratory

William Buttner
National Renewable Energy Laboratory
15013 Denver West Parkway
Golden, CO 80401
Phone: (303) 275-3903
Email: William.Buttner@nrel.gov

DOE Manager: Laura Hill
Phone: (202) 586-8384
Email: Laura.Hill@ee.doe.gov

Subcontractors:

- Element One, Boulder, Colorado
- A.V. Tchouvelev & Associates, Inc. (AVT), Mississauga, Ontario, Canada

Project Start Date: October 1, 2010

Project End Date: Project continuation and direction determined annually by DOE

Overall Objectives

- Support the safe implementation of hydrogen as an alternative fuel by assuring the availability of gas detection technology.
- Quantify performance of commercial and developing hydrogen sensors relative to DOE metrics.
- Support infrastructure and vehicle deployment by providing expert guidance on the use of hydrogen sensors and analyzers.
- Support development and assess performance of advanced hydrogen sensor technologies, including hydrogen wide area monitoring (HyWAM)¹ [1].
- Develop active monitoring as a mitigation strategy for more efficient facility designs with improved safety.
- Support development and updating of hydrogen safety codes and standards.
- Educate the hydrogen community on the proper use of hydrogen sensors.

Fiscal Year (FY) 2018 Objectives

- Enable safe infrastructure deployment by providing sensor testing capability and guidance to stakeholders in the hydrogen energy field.
- Quantify performance metrics of commercial as well as emerging and novel developmental sensor technologies.
- Support the U.S. Department of Transportation (DOT) on the development of the Federal Motor Vehicle Safety Standard (FMVSS) for hydrogen fuel cell electric vehicles (FCEVs), especially with regard to hydrogen detection requirements identified in the Global Technical Regulation (GTR) 13 [2].
- Facilitate safe deployment of FCEVs through participation in the SAE Fuel Cell Standard Committee and by developing the SAE Technical Information Report J3089, “Characterization of On-board Vehicular Hydrogen Sensors” [3].
- Advance the science of hydrogen safety by empirically profiling hydrogen releases (indoor and outdoor) for the validation of hydrogen plume dispersion models.
- Enable science-based revisions of hydrogen codes and standards by active participation within standard and code development organizations and committees and by research and development activity to support codes and standards development.

Technical Barriers

This project addresses the following technical barriers identified in the Hydrogen Safety, Codes and Standards section of the Fuel Cell Technologies Office Multi-Year Research, Development, and Demonstration Plan.²

- (A) Safety Data and Information: Limited Access and Availability

¹ HyWAM may be defined as the 3-dimensional temporal and spatial profiling of planned or unintentional hydrogen releases.

² <https://www.energy.gov/eere/fuelcells/downloads/fuel-cell-technologies-office-multi-year-research-development-and-22>

- (C) Safety is Not Always Treated as a Continuous Process
- (D) Lack of Hydrogen Knowledge by AHJs
- (F) Enabling National and International Markets Requires Consistent RCS
- (G) Insufficient Technical Data to Revise Standards
- (H) Insufficient Synchronization of National Codes and Standards
- (K) No Consistent Codification Plan and Process for Synchronization of R&D and Code Development.

Contribution to Achievement of DOE Hydrogen Safety, Codes, and Standards Milestones

This project will contribute to the achievement of the following DOE milestones from the Hydrogen Safety, Codes and Standards section of the Fuel Cell Technologies Office Multi-Year Research, Development, and Demonstration Plan.

- Milestone 2.15: Develop holistic design strategies. (4Q, 2017)
- Milestone 2.19: Validate inherently safe design for hydrogen fueling infrastructure. (4Q, 2019)
- Milestone 3.1: Develop, validate, and harmonize test measurement protocols. (4Q, 2014)
- Milestone 4.9: Completion of GTR Phase 2. (1Q, 2017)
- Milestone 5.1: Update safety bibliography and incidents databases. (4Q, 2011–2020)

FY 2018 Accomplishments

- **Provisional Patent (NREL Prov 17-94A):** Filed “Interface for a High-Pressure Hydrogen Dispenser” (2018), which specifically addresses a means to provide gas samples at low-pressure gas compatible for analysis by all potential on-site hydrogen contaminant detectors (W. Buttner and K. Harrison).
- **NREL Record of Invention (ROI):** Filed NREL ROI “Wide Area Monitor for Hydrogen Releases within Hydrogen Facilities (HyWAM)” (2018, W. Buttner), which

describes the use of a distributed network of point sensors (chemical, physical, and environmental) as a basis for HyWAM. This ROI formed the basis of a DOE Technology Commercialization Fund project [4].

- **Hydrogen Safety Sensor Gap Analysis:** Published a gap analysis for hydrogen safety sensors [5]. The gap analysis, which identified critical gaps in hydrogen safety sensor performance, was an outcome of a workshop which was jointly organized by NREL, the European Joint Research Centre (JRC), and the Fuel Cell and Hydrogen Joint Undertaking (FCH JU).
- **FCEV Exhaust Gas Measurement Technology:** The NREL Sensor Laboratory collaborated with DOT to design, build, and demonstrate an analyzer capable of verifying that hydrogen levels in FCEV exhaust are within the levels as prescribed by GTR 13 [2].
- **Characterization of Indoor Hydrogen Releases:** Profiled indoor hydrogen releases through the development of empirically validated computational fluid dynamics (CFD) models in collaboration with A. V. Tchouvelev & Associates, Inc. (AVT) to enable an improved understanding of indoor hydrogen dispersion. This work is anticipated to be incorporated into NFPA 2 [6] as a guidance document on sensor placement.
- **SAE Technical Information Report (TIR) J3089, “Characterization of On-board Vehicular Hydrogen Sensors”:** SAE J3809 development was led by the NREL Sensor Laboratory under the auspices of the SAE Fuel Cell Standard Committee. The TIR passed ballot and has been published as a formal SAE document [3].

INTRODUCTION

Hydrogen sensors are an enabling technology to assure the safe use of hydrogen as an alternative renewable fuel. To assure the availability of reliable safety sensors and their proper use, the DOE Fuel Cell Technologies Office established the NREL Hydrogen Sensor Testing Laboratory [7]. The NREL Sensor Laboratory provides stakeholders (e.g., sensor developers and manufacturers, end users, and code officials) a resource for an independent, unbiased evaluation of hydrogen sensor performance. Sensor evaluations are performed using test protocols that were guided by the requirements in national [8] and international sensor standards [9], as well as by the sensor performance targets established by DOE [10]. In addition to laboratory assessment, the NREL Sensor Laboratory strives to assure the proper use of hydrogen sensors through outreach activity such as participation on code and standards development organizations (CDOs/SDOs), safety committees, workshops, conferences, and webinars. The NREL Sensor Laboratory further facilitates deployment by partnering directly with end users to assist in the design and implementation of their sensor system. An emerging mission of the NREL Sensor Laboratory is to develop HyWAM strategies to support H₂@Scale [11] and to characterize hydrogen dispersion as a means to improve facility safety [12].

APPROACH

The NREL Sensor Laboratory research, development, and demonstration (RD&D) effort is guided by the needs of the hydrogen community, which is evolving as infrastructure strives to accommodate the growing FCEV fleet of commercial vehicles. Although the mission of the NREL Sensor Laboratory is evolving, the unbiased and confidential performance evaluation of hydrogen sensors has been a core activity within the NREL Sensor Laboratory. In this function, the NREL Sensor Laboratory supports sensor developers, end users, as well as permitting officials and standard and code developers. This expertise also supports the qualification of sensors for specialized application, such as HyWAM. Sensor evaluations are performed using a custom-built sensor test apparatus (Figure 1), which was designed with advanced capabilities, including simultaneous testing of multiple hydrogen sensors, sub-ambient to elevated temperature, sub-ambient to elevated pressure, active humidity control, and accurate control of gas parameters with multiple precision digital mass flow meters operating in parallel. In addition, other test fixtures have been developed for life tests and chemical poison studies, as well as for specialized applications. The test apparatuses are fully automated for control and monitoring of test parameters and for data acquisition with around-the-clock operation capability. Test sensors are subjected to an array of tests to quantify the impact of variation of environmental parameters and chemical matrix on performance. Although standard protocols have been developed (e.g., [3] and more recently [13]), these can be adapted for specialized requirements. Results are reported back to the client to support their future development work. NREL sensor testing also supports end users by qualifying sensor technology for their application (e.g., [14]) and by educating the hydrogen community on the proper use of hydrogen sensors.

The NREL Sensor Laboratory maximizes its impact by direct collaborations with stakeholders in the hydrogen community; this is achieved in part through formal agreements with industrial partners, including nondisclosure agreements, technical service agreements, and cooperative research and development agreements. Strategic partnerships have also been maintained with other government organizations, most notably with the JRC in Petten, Netherlands, under which the respective sensor test facilities collaborated on hydrogen sensor research projects of common interests. Currently, this collaboration is formalized under a DOE-JRC agreement [15] and has led to multiple publications including several cited in this report (e.g., [5], [12]). Such collaborations provide a platform for the international distribution of the NREL sensor research and development.

In addition to sensor performance assessment, the scope of the NREL Sensor Laboratory has expanded its active participation on a variety of national and international codes and standards development organizations and safety committees, including National Fire Protection Association (NFPA) 2, International Standards Organization (ISO) Technical Committee (TC) 197, SAE Fuel Cell Standards Committee, UL, Compressed Gas Association (CGA), ASTM International, HySafe, and the GTR. The type of support provided by the

NREL Sensor Laboratory to SDOs, CDOs, and safety committees includes (1) pre-normative research to support code and standard requirements; (2) document development; (3) development and deployment of verification technology; and (4) expert guidance and recommendations. Increasingly, the NREL Sensor Laboratory uses its expertise to develop sensor-based tools for the hydrogen community; currently this includes developing HyWAM for hydrogen plume profiling to support NFPA 2 and a hydrogen analyzer to verify compliance of FCEV exhaust requirements as prescribed in the GTR. Dissemination of results is through a variety of venues, including participation on international hydrogen safety committees, presentations at international conferences and workshops, publications in the open literature, and direct outreach to the hydrogen community.

Finally, the NREL Sensor Laboratory has an ongoing commitment to training young scientists and engineers in the field of renewable energy. Accordingly, the NREL Sensor Laboratory has for several years provided internship opportunities to undergraduate engineering majors. While supervised by the director of the NREL Sensor Laboratory, interns are assigned a specific project. Responsibilities include experimental design and data analysis, as well as direct interaction with clients. Interns have made significant contributions to numerous projects within the NREL Sensor Laboratory, including several described in this report. They are included as coauthors on numerous presentations and papers.



Figure 1. The NREL hydrogen sensor test apparatus

RESULTS

Although activity of the NREL Sensor Laboratory was hindered somewhat by FY 2018 budget uncertainties, significant progress was achieved. Highlights are discussed below.

Support of the GTR 13 and FMVSS

GTR 13 [1] is the defining document regulating hydrogen vehicle safety requirements. GTR 13 has been formally implemented by the international regulatory community, and as such, national authorities overseeing development and enforcement of vehicle regulations are to endeavor to harmonize their national regulations with the GTR. Within the United States, the national authority for vehicle safety is the DOT and the prevailing regulatory code is the FMVSS. Included within the GTR are safety requirements on allowable hydrogen levels in FCEVs. The NREL Sensor Laboratory, in cooperation with DOT, has been developing an off-vehicle

exhaust gas analyzer and analytical methods for compliance verification to the hydrogen emission requirements specified in the GTR. In the past year, the analyzer was deployed on an FCEV operating under simulated road conditions using a dynamometer (testing was performed at an original equipment manufacturer facility under a non-disclosure agreement). Figure 2 shows a series of hydrogen pulses that were discharged from the FCEV during operation, all of which were within compliance to the GTR regulations. The NREL analyzer was configured to be compatible with a gas collection system used by a vehicle test facility identified by DOT (Air Quality Division, Environment and Climate Change Canada). Plans are being formulated to deploy the NREL analyzer on a commercial FCEV at the Environment and Climate Change vehicle test facility.

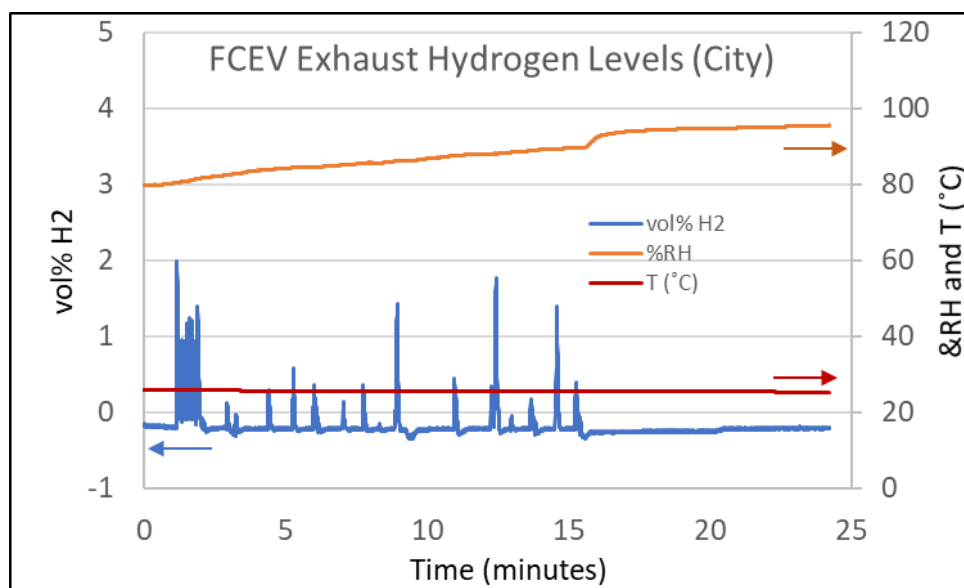


Figure 2. Hydrogen concentrations as measured from an actual FCEV operating under simulated load conditions (using a dynamometer) as measured with the NREL Exhaust Gas Analyzer. Although hydrogen transients were observed, they were within the regulated levels prescribed by GTR 13 [2].

The NREL Sensor Laboratory has also supported DOT on the upcoming revision of GTR 13. Currently within the GTR, one proposed means to quantify hydrogen in closed spaces (e.g., passenger compartments, trunks) is through oxygen displacement. Earlier work by NREL and the JRC has shown this method to be insufficiently accurate and plagued with potential false readings for regulatory purposes [6]. It was thus jointly proposed by NREL and the JRC that reference within GTR 13 to the proposed use of oxygen displacement as a means to quantify hydrogen or helium buildup in the FCEV be removed in future revisions. This recommendation was made to the representative on the GTR development committee (Nha Nguyen/DOT).

Characterization of Outdoor Liquid Hydrogen Releases with HyWAM

Cold hydrogen plumes formed during liquid hydrogen (LH2) releases are currently not well understood because field data is essentially nonexistent. This lack of understanding leads to overly conservative safety distances at LH2 facilities. To address this need, the NREL Sensor Laboratory, in collaboration with the NFPA 2 Hydrogen Storage Task Group, developed the prototype Hydrogen Plume Analyzer to empirically monitor LH2 storage tank venting. The prototype analyzer, which consisted of multiple sampling points for gas (e.g., hydrogen and oxygen) and physical (e.g., temperature and humidity) sensors, could form the basis for a Hydrogen Wide Area Monitor (HyWAM) [16]. A HyWAM is now being developed for research purposes and general deployment. Active monitoring has been identified by the NFPA 2 Hydrogen Storage Task Group as a mitigation strategy to alleviate the large setbacks associated with LH2 storage.

Characterization of Indoor Hydrogen Releases:

Sensors are mandated by both the International Fire Code [17] and NFPA 2 [6] for numerous indoor hydrogen infrastructure applications. However, no guidance is provided on the selection or use of sensor technology. Rational sensor placement guidance requires an understanding of hydrogen dispersion behavior within the deployment environment, which in turn requires the development of validated models. Working in collaboration with the NREL Sensor Laboratory, AVT performed CFD modeling of a leak scenario associated with an electrolyzer system housed within a 20 foot ISO container. Independent CFD modeling was performed by the JRC under a collaboration agreement [15]. In this study, CFD modeling of the hydrogen dispersion was validated by the NREL Sensor Laboratory using a HyWAM system based upon an array of point sensors. As expected, it was shown that the dispersion of indoor hydrogen releases is predicated upon the facility ventilation flow patterns. Somewhat unexpectedly, however, the modeling demonstrated that optimal sensor placement may be achieved in locations of low ventilation flow within the facility (as modeled by CFD), and that in doing so, leaks can be more predictably and quickly detected than by placing the sensor in front of a ventilation exhaust system as is currently more frequently performed. Furthermore, low-level leaks can be detected that would have been undetectable by other means (e.g., pressure sensors mounted on pneumatic lines). Detection is achieved before dangerous levels of hydrogen can accumulate. A more thorough analysis will be presented at the 2019 International Conference on Hydrogen Safety (www.hysafe.info/ichs2019/). The effectiveness of optimized sensor placement to reduce hazards has not yet been quantified by a quantitative risk analysis (QRA). Expansion of indoor releases to other larger facilities and incorporation into QRA tools, such as HyRAM [18], is planned.

SAE Technical Information Report J3089 [3]

SAE TIR J3089, “Characterization of On-board Vehicular Hydrogen Sensors,” was prepared under the auspices of the SAE Fuel Cell Standards Committee. The TIR passed ballot and was approved for publication. The TIR provides original equipment manufacturers and sensor suppliers with a common set of test protocols to be performed by the manufacturer for the assessment of sensor performance.

CONCLUSIONS AND UPCOMING ACTIVITIES

The NREL Sensor Laboratory has been a resource to the national and international hydrogen community since 2010. The unbiased and confidential performance evaluation of hydrogen sensors remains a core capability for the NREL Sensor Laboratory. In this function, the NREL Sensor Laboratory continues to support sensor developers, end users, and permitting officials as well as SDO and CDOs. The NREL Sensor Laboratory remains active on CDOs and SDOs, including UL, CGA, NFPA, SAE, and ISO, as well as safety committees such as HySafe. However, the mission of the NREL Sensor Laboratory is evolving. Increasingly, the NREL Sensor Laboratory is using its expertise to develop sensor-based tools for improved safety and risk reduction in hydrogen infrastructure. Currently this includes developing HyWAM for indoor and outdoor hydrogen plume profiling, and the hydrogen analyzer to verify compliance of FCEV exhaust requirements as prescribed in the GTR.

The NREL Sensor Laboratory is actively participating with the NFPA 2 Hydrogen Storage Task Group, which was formed to facilitate the use of LH2 at commercial fueling facilities. Active monitoring, such as with HyWAM, has been identified by the task group as a potential mitigation strategy to alleviate the prohibitive setbacks associated with LH2 storage, which can be as high as 75 feet [6]. This setback precludes the use of LH2 storage in many urban fueling stations. The current LH2 setbacks appear to have been established on consensus rather than a scientific basis. This is because of an inadequate understanding of hydrogen plume behavior, especially cold hydrogen plumes, which in turn is due, in part, to a lack of real-world data on hydrogen cold plume dispersions. There are two main themes to be addressed for the use of HyWAM and sensors in active monitoring for LH2 storage. First, it has been recognized that to implement mitigation strategies to lower the prescribed setbacks it will be necessary to more fully elucidate the behavior of real-world hydrogen releases, especially cold hydrogen releases; in part this is to identify the deployment number and location of measurement points. Thus, one critical role for sensors is the empirical characterization of real-

world hydrogen dispersion behavior, which in turn can then be used to validate theoretical models and integrated into QRA to guide the design of a facility to optimize and quantify the effectiveness of active monitoring as a mitigation strategy. To do this, the NREL Sensor Laboratory is forming strategic partnerships to deploy HyWAM technology during planned LH2 releases; several of these were identified through participation in the HySafe Workshop [19] and include the Health and Service Laboratory (Buxton, United Kingdom) and Karlsruhe Institute of Technology (Karlsruhe, Germany). There are in addition studies within the United States investigating LH2 release behavior and being planned by the Compressed Gas Association and by Lawrence Livermore National Laboratory. NREL also has a pending partnership with a developer of commercial hydrogen fueling stations (First Element) through the DOE Technology Commercialization Fund project [4]. In addition to validating the fundamental behavior of released hydrogen dispersion, sensors will also be needed for deployment within and around a facility as elements in the active monitor. Thus, in addition to validating the fundamental behavior of released hydrogen dispersion (e.g., a “research HyWAM”), sensors will also be used in a deployed monitoring system (e.g., a “deployed HyWAM”). Cost and ease of operation are critical metrics for the deployed HyWAM. Hydrogen safety sensors have been part of a hydrogen safety system for many years to assure safety integrity level compliance and because they were prescribed in codes such as NFPA 2 and the International Fire Code. As with the conventional use of hydrogen sensors in a facility safety system, the elements of an active monitoring system must cost-effectively meet stakeholder expectations with respect to critical performance metrics that must be validated through performance testing. The distinction and interrelation between the two sensor applications and the role of the NREL Sensor Laboratory are illustrated in Figure 3. At present, however, there is no viable HyWAM technology available, although various approaches have been proposed [1] and even demonstrated, although usually under highly controlled conditions. HyWAM may be based upon stand-off strategies, such as Raman [20], Schlieren [21], and acoustic, or through a distributed network of point sensors [12]. The NREL Sensor Laboratory has developed a hydrogen analyzer that can simultaneously measure hydrogen concentration (and other parameters) from multiple locations; this system can form the basis of a HyWAM. The development of HyWAM for assurance of hydrogen safety is a critical component in the FY 2019 NREL Sensor Laboratory RD&D program.

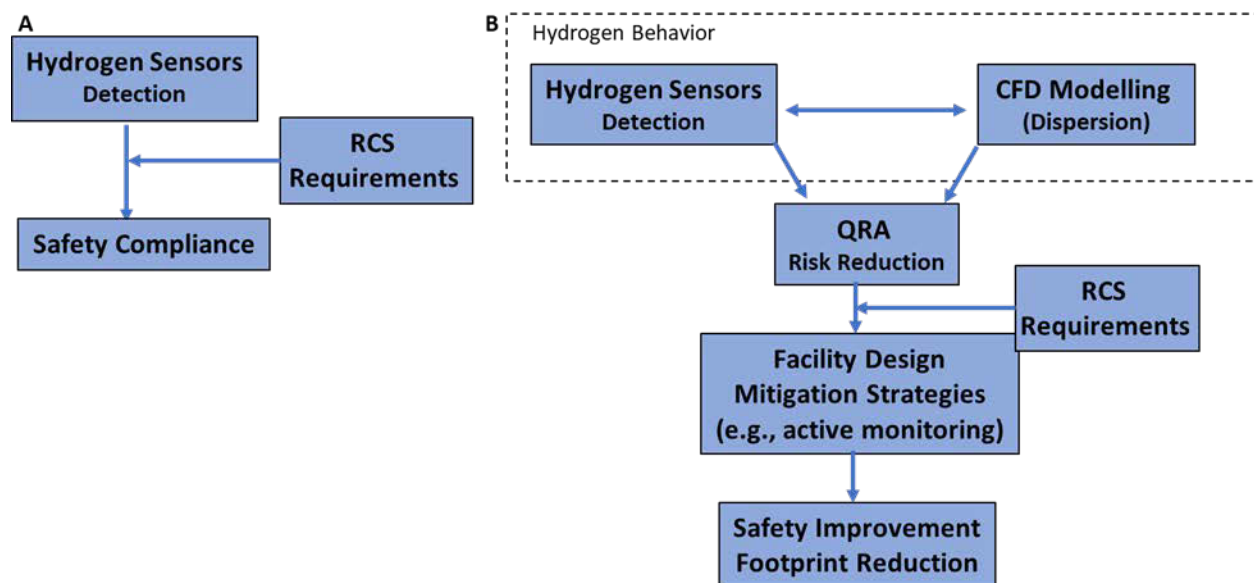


Figure 3. Evolving mission of the NREL Sensor Laboratory. (A) Hydrogen sensors have been routinely used as part of a facility safety system to achieve an appropriate safety integrity level and at the same time to assure compliance to prescriptive code requirements. (B) Detection is also needed to verify released hydrogen behavior (e.g., using HyWAM) to validate dispersion models and for a facility active monitoring system. Coupled with other mitigation strategies, active monitoring can assure improved safety in smaller footprints.

The previous discussion focused on outdoor LH2 applications. Elucidation of hydrogen dispersion is germane for indoor and outdoor gaseous hydrogen and LH2 operations. Understanding hydrogen dispersion behavior can also improve safety of indoor hydrogen operations, and the NREL Sensor Laboratory is also actively working on improving safety of indoor operations. Indoor sensor placement guidance requires an understanding of hydrogen behavior within the deployment environment, which in turn requires the development of validated models. In our recent study on an indoor gaseous hydrogen facility, CFD modeling of the hydrogen dispersion was independently cross-verified by two groups (AVT and the JRC). The specific system was a hydrogen production system housed within a ventilated ISO container housing. The models were validated by the NREL HyWAM system, which is based upon an array of point sensors (preliminary results were briefly presented in [22]). As expected, it was shown that the dispersion of indoor hydrogen releases is predicated upon the facility ventilation flow patterns. Somewhat unexpectedly, however, the modeling demonstrated that optimal sensor placement may be achieved in locations of low ventilation flow within the facility (as modelled by CFD), and that in doing so, leaks can be more predictably and quickly detected than by placing the sensor in front of a ventilation exhaust system as is currently more frequently performed. Furthermore, low-level leaks can be detected that would have been undetectable by other means (e.g., pressure sensors mounted on pneumatic lines). A more thorough analysis will be formally presented at the 2019 ICHS in a paper to be coauthored by AVT, JRC and the NREL Sensor Laboratory. The effectiveness of optimized sensor placement to reduce hazards is to be quantified by a QRA. It is also planned to expand this study to larger-scale indoor hydrogen facilities.

The analytical performance of the NREL FCEV Exhaust Gas Analyzer has been demonstrated. The DOT has supported development of the analyzer and to perform real-world measurements on an FCEV. A probe that integrates the exhaust gas collection system to the analyzer was developed by NREL and tested on an FCEV operating under simulated load conditions using a dynamometer. It is planned to deploy the integrated system on an FCEV at a certified vehicle test facility identified by DOT (currently this is planned to be within the Air Quality Division, Environment and Climate Change Canada in Ontario, Canada).

SPECIAL RECOGNITIONS AND AWARDS/PATENTS ISSUED

1. 2018 DOE Hydrogen and Fuel Cells Program R&D Award in recognition “For outstanding dedication and contributions to hydrogen safety, sensor technologies, and the global hydrogen refueling community”.
2. “EERE Success Story—NREL-KPA-Toyota Collaboration Facilitates Permitting of FCEV Repair Facilities,” <https://www.energy.gov/eere/success-stories/articles/eere-success-story-nrel-kpa-toyota-collaboration-facilitates>, February 15, 2018.
3. Invited speaker and session organizer (Mitigation, Sensors, Hazard Prevention, and Risk Reduction) for the 2018 HySafe Research Safety Priorities Workshop, Buxton, United Kingdom, September 18–20, 2018.
4. W. Buttner, NREL Record of Invention ROI-18-28, “Wide Area Monitor for Hydrogen Releases within Hydrogen Facilities (HyWAM),” 2018.
5. W. Buttner and K. Harrison, NREL Provisional Patent PROV-17-94A, “Interface for High Pressure Dispensers,” 2018.

FY 2018 PUBLICATIONS/PRESENTATIONS

Talks and Presentations

1. W. Buttner, E. Weidner, R. Ortiz-Cebolla, and C. Bonato, “Safety Sensors for the Hydrogen Infrastructure,” Fuel Cell Seminar and Energy Exposition, Long Beach, CA (November 7–9, 2017).
2. W. Buttner, H. Wright, A. Tchouvelev, D. Meleido, D. Baraldi, and E. Weidner, “The NREL Hydrogen Sensor Laboratory—Indoor Sensor Placement Study and Hydrogen Wide Area Monitoring,” DOE FCTO Codes and Standards Tech Team (2017).

3. R. Ortiz-Cebolla, E. Weidner, C. Bonato, W. Buttner, and H. Wright, “Hydrogen Safety Sensor Stability Testing—Impact of the Chemical Environment,” European Hydrogen Energy Conference, Costa del Sol, Spain (March 14–16, 2018).
4. J. Stetter, V. Patel, W. Buttner, and H. Wright, “Characterization of a Selective, Zero Power Sensor for Distributed Sensing of H₂ in Energy Applications,” International Meeting on Chemical Sensors, Vienna, Austria (July 15–19, 2018). This work was a summary of collaborative work performed under the DOE Small Business Voucher Program [23].
5. W. Buttner, A. Tchouvelev, D. Meleido, and L. Gardner, “Mitigation, Sensors, Hazard Prevention, and Risk Reduction,” HySafe Hydrogen Safety Research Priorities Workshop, Buxton, United Kingdom, (September 19–22, 2018).
6. F. Markert, D. Cironne, N. Barilo, I. Azkarate, Iñaki, and W. Buttner, “General Aspects of Hydrogen Safety,” HySafe Hydrogen Safety Research Priorities Workshop, Buxton, United Kingdom (September 19–22, 2018).
7. W. Buttner, “The NREL Hydrogen Sensor Testing Laboratory,” DOE Hydrogen and Fuel Cells Program 2018 Annual Merit Review and Peer Evaluation Meeting, Washington, DC (June 13–15, 2018).

Publications

1. W. Buttner, M. Ciotti, K. Hartmann, K. Schmidt, H. Wright, and E. Weidner, “Empirical Profiling of Cold Hydrogen Plumes formed from Venting of LH₂ Storage Vessels,” *International Journal of Hydrogen Energy* (in press) (2018).
2. R. Ortiz-Cebolla, E. Weidner, C. Bonato, W. Buttner, K. Hartmann, and K. Schmidt, “Test Methodologies for Hydrogen Sensor Performance Assessment: Chamber vs. Flow-Through Test Apparatus,” *International Journal of Hydrogen Energy* (in press) (2018).
3. R. Ortiz-Cebolla, E. Weidner, C. Bonato, and W. Buttner, *Summary Report for a Hydrogen Sensor Workshop—Hydrogen Safety Sensors and Their Use in Applications with Hydrogen as an Alternative Fuel*, EUR 28852 EN, Brussels, Belgium (2017), <https://ec.europa.eu/jrc/en/publication/summary-report-hydrogen-sensor-workshop-hydrogen-safety-sensors-and-their-use-applications-hydrogen>.
4. SAE Technical Information Report, “J3089: Characterization of On-Board Vehicular Hydrogen Sensors,” SAE (2018); completed under the auspices of the SAE Fuel Cell Standard Committee, https://saemobilus.sae.org/content/J3089_201810.
5. W. Buttner, “Wide Area Monitor for Hydrogen Releases within Hydrogen Facilities (HyWAM),” NREL Record of Invention ROI-18-28 (2018).
6. W. Buttner and K. Harrison, “Interface for High Pressure Dispensers,” NREL Provisional Patent PROV-17-94A (2018).
7. EERE Success Story, “NREL-KPA-Toyota Collaboration Facilitates Permitting of FCEV Repair Facilities” (February 15, 2018), <https://www.energy.gov/eere/success-stories/articles/eere-success-story-nrel-kpa-toyota-collaboration-facilitates>.
8. W. Buttner, “NREL Hydrogen Sensor Testing Laboratory,” DOE Hydrogen and Fuel Cells Program FY 2017 Annual Progress Report (2018), https://www.hydrogen.energy.gov/pdfs/progress17/viii_7_buttner_2017.pdf.

REFERENCES

1. Zalosh, R. and Barilo, N., “Wide Area and Distributed Hydrogen Sensors,” Proceedings of the 3rd International Conference on Hydrogen Safety, Ajaccio, Corsica (2009).
2. Global Technical Regulation No. 13—Global Technical Regulation on Hydrogen and Fuel Cell Vehicles, ECE/TRANS/180/Add.13, United Nations: 115 (2013).

3. SAE Technical Information Report, “J3089 2018: Characterization of On-Board Vehicular Hydrogen Sensors,” SAE (2018).
4. Department of Energy Announces Technology Commercialization Fund Projects (2018).
5. Ortiz Cebolla, R., Weidner, E., Bonato, C., and Buttner, W., “Summary Report for a Hydrogen Sensor Workshop—Hydrogen Safety Sensors and Their Use in Applications with Hydrogen as an Alternative Fuel,” EUR 28852 EN, Brussels, Belgium (2017).
6. NFPA 2: Hydrogen Technologies Code (2016).
7. Buttner, William, “The NREL Hydrogen Sensor Laboratory—Safety Sensor Testing Laboratory,” National Renewable Energy Laboratory (NREL), Golden, CO (October 2017).
8. UL 2075—Standard for Gas and Vapor Detectors and Sensors, UL, Northbrook, IL: 144 (2013).
9. ISO 26142—Hydrogen Detector Apparatus for Stationary Applications, ISO 26142, International Standards Organization: 36 (2010).
10. Hydrogen, Fuel Cells & Infrastructure Technologies Program Multi-Year Research, Development and Demonstration Plan, Planned program activities for 2005–2015, U.S. DOE Office of Renewable Energy and Efficiency (2005).
11. DOE, “H2@Scale” (2017), <https://www.energy.gov/eere/fuelcells/h2-scale>.
12. Buttner, W., Ciotti, M., Hartmann, K., Schmidt, K., Wright, H., Schmidt, K., and Weidner, E., “Empirical Profiling of Cold Hydrogen Plumes formed from Venting of LH2 Storage Vessels,” *International Journal of Hydrogen Energy* (In Press 2018).
13. Standard Hydrogen Test Protocols for the NREL Sensor Testing Laboratory (2011), <https://www.nrel.gov/docs/fy08osti/42666.pdf>.
14. Buttner, William, “Hydrogen-Powered Vehicles—A Safe Alternative to Traditional Gasoline Internal Combustion Engines” (March, 2017), <https://www.kpaonline.com/ehs/hydrogen-powered-vehicles-safe-alternative-traditional-gasoline-internal-combustion-engines/>.
15. Collaboration Arrangement for Research and Development in Energy-Related Fields between the U.S. Department of Energy and the Joint Research Centre of the European Commission (signed June 2, 2016), https://eeas.europa.eu/headquarters/headquarters-homepage/2817/node/2817_nl.
16. Buttner, W., “Wide Area Monitor for Hydrogen Releases within Hydrogen Facilities (HyWAM),” NREL Record of Invention ROI-18-28 (2017).
17. 2015 International Fire Code (IFC) (2015).
18. Groth, K., “Hydrogen Quantitative Risk Assessment,” DOE Hydrogen and Fuel Cells Program Annual Merit Review, Washington, DC (2016).
19. Coldrick, Simon, Dolci, Francesco, Hawksorth, Stuart, Jordan, Thomas, Buttner, William, Azkarate, Inaki, Barthelemy, Herve, Hooker, Phil, Keller, Jay, and Tchouvelev, Andrei, “2018 HySafe Safety Research Priority Workshop Summary Report (in preparation),” Buxton, United Kingdom (2019).
20. Hecht, E.S. and Panda, P.P., “Mixing and Warming of Cryogenic Hydrogen Releases,” *International Journal of Hydrogen Energy* (2018), <https://doi.org/10.1016/j.ijhydene.2018.07.058>.
21. Kebler, A., Ehrhardt, W., and Langer, G., “Hydrogen Detection: Visualisation of Hydrogen Using Non Invasive Optical Schlieren Technique BOS,” Proceedings of the HySafe International Conference on Hydrogen Safety, Pisa, Italy (2005).
22. Buttner, W., “NREL Sensor Testing Laboratory,” U.S. Department of Energy Hydrogen and Fuel Cells Program 2018 Annual Merit Review and Peer Evaluation, Washington, DC (2018).
23. Small Business Voucher—U.S. Department of Energy (2017), <https://www.sbv.org/>.

Compatibility of Polymeric Materials Used in the Hydrogen Infrastructure

Kevin L. Simmons (Primary Contact), Wenbin Kuang (Pacific Northwest National Laboratory), Nalini Menon (Sandia National Laboratories), Barton Smith (Oak Ridge National Laboratory), Amit Naskar (Oak Ridge National Laboratory), Mike Veenstra (Ford Motor Company)
Pacific Northwest National Laboratory (PNNL)
PO Box 999
Richland, WA 99352
Phone: (509) 375-3651
Email: kl.simmons@pnnl.gov

DOE Manager: Laura Hill
Phone: (202) 586-8384
Email: Laura.Hill@ee.doe.gov

Subcontractor:
Ford Motor Company, Detroit, MI

Project Start Date: October 1, 2015
Project End Date: September 30, 2018

Overall Objectives

- Provide scientific and technical basis to enable full deployment of hydrogen and fuel cell technologies by filling the critical knowledge gap for polymer performance in hydrogen environments.
- Develop an understanding of material interaction with hydrogen to mitigate impacts on reliability and durability.
- Develop experimental test methodologies that provide material performance under hydrogen infrastructure environments.
- Disseminate material characteristics to the community to begin discussions on how to improve materials in the hydrogen infrastructure environment.

Fiscal Year (FY) 2018 Objectives

- Complete the test methodology for in-situ high pressure hydrogen testing of friction and wear of polymers.

- Investigate the effects of fillers in nitrile butyl rubber (NBR) and ethylene propylenediamene (EPDM) model elastomer compounds.
- Disseminate test methodologies in hydrogen testing through Compressed Hydrogen Materials Compatibility 2 (CHMC 2) polymers standards.
- Complete high-pressure hydrogen cycling design and installation for testing polymers.
- Disseminate information to the hydrogen community by participating in committees, journal articles, and conferences.

Technical Barriers

This project addresses the following technical barriers from the Hydrogen Safety, Codes and Standards section of the Fuel Cell Technologies Office Multi-Year Research, Development, and Demonstration Plan¹:

- (A) Safety Data and Information: Limited Access and Availability
- (G) Insufficient Technical Data to Revise Standards
- (J) Limited Participation of Business in the Code Development Process
- (K) No Consistent Codification Plan and Process for Synchronization of R&D and Code Development.

Contribution to Achievement of DOE Hydrogen Safety, Codes and Standards Milestones

This project will contribute to achievement of the following DOE milestones from the Hydrogen Safety, Codes and Standards section of the Fuel Cell Technologies Office Multi-Year Research, Development, and Demonstration Plan:

- Milestone 5.2: Update materials compatibility technical reference. (4Q, 2011–2020)

¹ <https://www.energy.gov/eere/fuelcells/downloads/fuel-cell-technologies-office-multi-year-research-development-and-22>

FY 2018 Accomplishments

- Developed six EPDM and six NBR model compound materials for investigation of hydrogen effects with fillers. Carbon and silica fillers indicate 10 ppm of hydrogen absorption in the material.
- Performed friction and wear testing on all 12 compounds in ambient air, high-pressure argon, and hydrogen environmental conditions.
- Performed R&D to determine that the desorption rate of the EPDM polymer is nearly five times faster than that of the NBR polymer without any additives or fillers. Compression set of NBR is significantly influenced by hydrogen with a 37% increase whereas EPDM compression set was insignificant.

INTRODUCTION

Polymers are critical to hydrogen infrastructure applications to reduce cost and eliminate the design constraints of metallic components. However, unlike metals that have been studied extensively in high-pressure hydrogen, there is a significant knowledge gap in understanding polymer performance under these conditions. Standardized qualification methodologies, databases of acceptable conditions, and hydrogen-compatible polymers are not available to the hydrogen design community to guide material selection. The overall goal of this project is to fill this knowledge gap and support stakeholders in the safe selection of polymers for use in the wide range of required applications and conditions.

This will be done by developing a technical foundation to understand the effects of hydrogen on polymers and composites to enable the development of appropriate test protocols for evaluating materials for hydrogen service. The information generated from these tests of target polymeric materials will be disseminated to hydrogen users and standard and code development organizations.

APPROACH

The project consists of four main tasks: (1) gather information from stakeholders, (2) develop test methodologies, (3) characterize polymers, and (4) disseminate the information generated. The information gathered from stakeholders will be used to ensure that the materials being evaluated, the range of conditions of study, and the testing protocols being developed as part of this project will benefit stakeholders from polymer, component, and system manufacturers. The aim of the test methodologies being developed is to mimic the conditions of interest and accelerate the process to produce meaningful results in a reasonable timeframe. Because properties differ widely for a single polymeric material based on its additives and processing approach, testing results would be meaningless unless key polymer characteristics are understood. The project will fully characterize the polymers to allow others to compare their materials to those that were tested. Finally, the information generated, both the test protocol and the compatibility results, will be disseminated through material databases, standards organizations, and peer-reviewed journals.

RESULTS

The team has been working with stakeholders on the Canadian Standards Association (CSA) committee for developing the new CHMC 2 standard for hydrogen compatibility in polymers. The scope of this standard is to provide uniform test methods for the industry to compare the performance of polymers in applications utilizing hydrogen. During this fiscal year, significant progress was made in advancing the test methods from conceptual approaches to a comprehensive document that is being prepared for an industry review and ballot. The committee consists of more than 25 stakeholders from various parts of the hydrogen community. There were numerous opportunities to exchange experiences in the area of test method development under the auspices of the CSA CHMC 2 committee's meetings that benefited the community and the project team. The development of the CSA CHMC 2 document for hydrogen polymer capability is greatly benefiting from the leadership and technical contribution of this project team.

This fiscal year, the team worked with Kyushu University on developing a set of model material compounds of NBR and EPDM for investigating the effects of known additives and fillers in the elastomer materials with hydrogen. There was a total of six compounds for each material:

- No filler, crosslinked elastomer
- Crosslinked elastomer with plasticizer only
- Crosslinked elastomer with carbon black only
- Crosslinked elastomer with silica filler only
- Crosslinked elastomer with plasticizer, carbon black, and silica filler
- Crosslinked elastomer with carbon black and silica filler.

Kyushu University provided thermal desorption data (Figure 1) to the team on their hydrogen content as a function of pressure, time after decompression, and their volume change. The results of the thermal desorption data demonstrate the effects of the polymer, plasticizer, and the fillers. The desorption rate of the EPDM polymer is nearly five times faster than that of the NBR polymer without any additives or fillers. The addition of the plasticizer significantly increased the desorption of hydrogen in the EPDM, whereas the data was inconclusive for NBR due to a measurement error. The inorganic fillers of silica and carbon black show an absorption behavior in both materials (of 10 ppm of hydrogen), which will be investigated in the future.

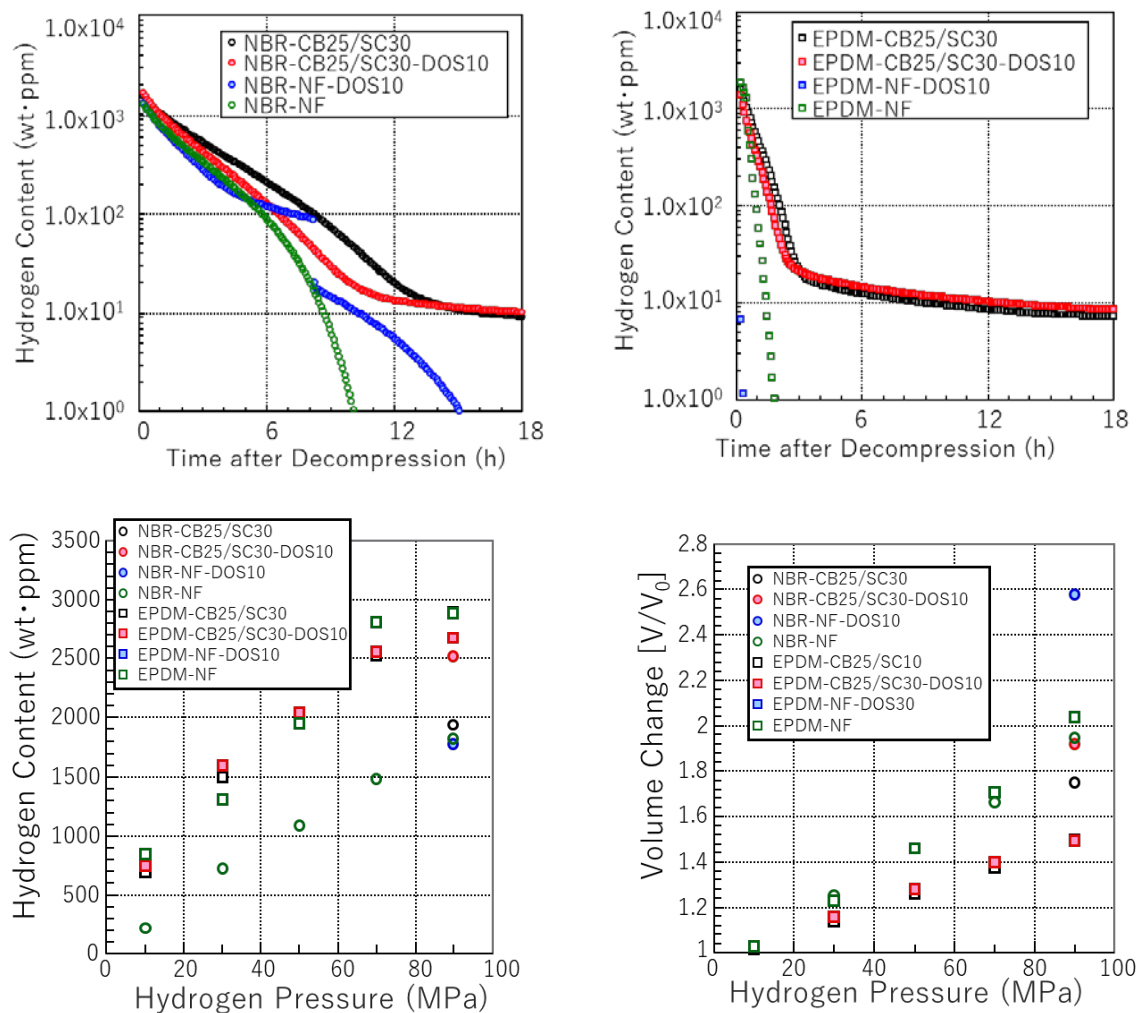


Figure 1. Hydrogen thermal desorption and hydrogen effects related to pressure

The filler material used in these model material compounds shows a decrease in volume change for NBR by 10% and 30% in EPDM from unfilled baseline compound, while the plasticizer only increased by nearly 40% in volume at 90 MPa.

A final draft has been developed for the in-situ friction and wear testing capability at PNNL. The test methodology was an adaptation of ASTM G-133 and has demonstrated differences in hydrogen, argon, and ambient air. This fiscal year all 12 of the model material compounds were tested following a newly developed test method using the in-situ friction and wear testing capability. Results of the test shown in Table 1 demonstrate the effect that hydrogen has on NBR and EPDM. The hydrogen exposure actually decreased the coefficient of friction (CoF) with the exception of compound N6. These results are different than what has

been compared to in the past with commercial off-the-shelf material and indicate that the compounds can alter the performance of the materials’ frictional and wear behavior.

Table 1. Tribology Results of Ambient Air and High-Pressure Hydrogen

EPDM	PNNL#E1	PNNL#E2	PNNL#E5	PNNL#E6
Features	No filler No plasticizer	No filler Plasticizer	Carbon black Inorganic Plasticizer	Carbon black Inorganic No plasticizer
Air In-situ Tribo (CoF)	1.24	1.01	1.65	1.57
HP-H2 In-situ Tribo (CoF)	1.11	0.84	1.04	1.26
NBR	PNNL#N1	PNNL#N2	PNNL#N5	PNNL#N6
Air In-situ Tribo (CoF)	2.17	1.47	1.44	1.15
HP-H2 In-situ Tribo (CoF)	1.74	1.12	.681	2.73

Tribo – tribology

HP-H2 – high-pressure hydrogen

The development of the high-pressure in-situ dynamic mechanical analysis (DMA) was designed and an autoclave was procured. The autoclave frame was constructed, and the autoclave was mounted in place. The DMA components for the internal design are in fabrication. The new in-situ DMA will allow research into the effects of polymer property changes in relation to gas and pressure effects. This will provide insight into compressibility of materials of during charging and discharging, volume changes in material during high-pressure soaking as gas diffuses into the polymer, and material expansion during decompression.

The compression set of NBR compounds N1, N2, N5, and N6 and EPDM compounds E1, E2, E3, and E4 were investigated for polymer property changes before and after hydrogen. N1 and E2 were rubbers with no filler or plasticizer, N2 and E2 had filler and no plasticizer, N5 and E5 had both filler and plasticizer, and N6 and E6 had fillers and no plasticizer. The compression set for the filled, plasticized EPDM system is insignificant. However, the compression set increased by ~37% due to hydrogen exposure for the filled plasticized NBR system. The material systems were then analyzed with DMA storage modulus measurements. In general, both EPDM and NBR show a decrease in storage modulus upon hydrogen exposure. A 20% decrease in modulus was seen in the filled plasticized EPDM after hydrogen exposure, whereas the modulus change in the NBR equivalent system was insignificant. There were also no indications of changes to the glass transition temperatures in all the compounds tested before and after exposure. For unexposed and exposed rubbers, fillers contribute heavily to the storage modulus of EPDM and NBR whereas plasticizers significantly lower the glass transition temperature.

The volumetric change before and after exposure was significantly different between the two model compounds. The NBR material expansion after exposure increased in volume by 72% of the filled plasticized compound compared to 8% in the EPDM (Table 2). It was observed that the volume change was much slower in recovery with the NBR compared to the EPDM, which correlates to the desorption curves discussed above. For filled and unfilled EPDM and NBR, volume change was lower with filler present than with no filler.

Micro-computed-tomography images of the NBR and EPDM rubbers were compared. For EPDM formulation E1, a large number of cracks that were not aligned in any particular direction were seen all over the sample after hydrogen exposure. When filled, EPDM E6 showed complete crack mitigation after hydrogen exposure. For exposed N1 samples, far fewer cracks (again not aligned in any particular direction) were seen in the sample. Overall, NBR seemed more resistant to hydrogen exposure without filler or plasticizer help, whereas for EPDM, filler addition is a must for crack mitigation.

Table 2. Filler Effects on Volumetric Changes after Hydrogen Exposure

		Filler	Plasticizer	Percent increase in volume	Recovery in volume
NBR	N1	No	No	79%	99%
	N2	No	Yes	85%	97%
	N5	Yes	Yes	72%	97%
	N6	Yes	No	55%	101%
EPDM	E1	No	No	4%	102%
	E2	No	Yes	2%	103%
	E5	Yes	Yes	8%	100%
	E6	Yes	No	16%	102%

CONCLUSIONS AND UPCOMING ACTIVITIES

The team has contributed to the advancement of test methodologies for polymer compatibility in hydrogen with involvement in the CSA CHMC 2 standard. The model material compounds provided detailed insight as to the difference in hydrogen diffusion behaviors between polymers and fillers. The carbon and silica fillers both indicate a hydrogen absorption around 10 ppm hydrogen. The plasticizer additive increases the hydrogen diffusion with its addition. The coefficient of friction decreased in hydrogen atmosphere with these specific compounds compared to past off-the-shelf commercial materials, indicating that the filler materials in hydrogen can influence the wear and friction of the material compounds. The effect of filler and plasticizer as additives with respect to hydrogen exposure of NBR and EPDM rubbers were studied, and conclusions useful toward compression set, volumetric swelling, and mitigating damage accumulation were drawn.

The upcoming activities include the following:

- Build up material properties in a database
- Long term aging effects of hydrogen
- Material contamination of hydrogen
- Complete neutron scattering experiments on pressure cycle aged polymers
- Material damage effects from hydrogen and pressure
- Polymeric material damage model
- New material development approaches for improved durability of elastomers.

FY 2018 PUBLICATIONS/PRESENTATIONS

1. K.L. Simmons, “Hydrogen Compatibility of Polymers Program,” 2018 HYDROGENIUS Research Symposium, Fukuoka, Japan (February 2, 2018).
2. N.C. Menon, “Compatibility of Polymeric Materials in Hydrogen Service,” 2018 HYDROGENIUS Research Symposium, Fukuoka, Japan (February 2, 2018).
3. N. Menon, K. Simmons, D. Smith, A. Naskar, M. Veenstra, “Influence of Fillers and Plasticizers on Polymer Behavior in High-Pressure Hydrogen Environments,” Poster presentation to Material Science Research Foundation External Review Board, Sandia National Laboratories, Albuquerque, NM (April 19, 2018).
4. K.L. Simmons, N. Menon, D. Smith, A. Naskar, M. Veenstra, “Compatibility of Polymeric Materials Used in the Hydrogen Infrastructure,” 2018 Hydrogen and Fuel Cells Program Annual Merit Review, Washington, DC (June 2018).

Advancing Fuel Cell Electric Vehicles in San Francisco and Beyond

Jessie Denver (Principle Investigator),
Suzanne Loosen (Primary Contact)
City and County of San Francisco
Department of the Environment
1 Dr. Carlton B. Goodlett PL, Room 300
San Francisco, CA 94102-4694
Phone: 415-355-3720
Email: Jessie.denver@sfgov.org

DOE Manager: Gregory Kleen
Phone: (240) 562-1672
Email: Gregory.Kleen@ee.doe.gov

Contract Number: DE-EE0007599

Subcontractors:

- Frontier Energy (formerly known as BKi)
- Newcomb Anderson McCormick
- Business Council on Climate Change

Project Start Date: October 1, 2017

Project End Date: March 31, 2019

Overall Objectives

- Provide community outreach and technical assistance to station developers in areas of station development.
- Update and harmonize best practices in permitting and inspection of hydrogen fueling stations among Bay Area authorities having jurisdiction (AHJs).
- Deliver hydrogen safety and best practice education to elected officials and planning, building inspection, and public safety professionals across the Bay Area.
- Increase community awareness of the availability and value of hydrogen and fuel cell electric vehicles (FCEVs).
- Drive market demand for FCEVs through an established, public-facing, group procurement program.

Fiscal Year (FY) 2018 Objectives

- Ongoing implementation of training and outreach plan.
- Continued community engagement.
- Conduct outreach to AHJs to facilitate hydrogen fueling station development.
- Reporting and dissemination.
- Continued implementation of SunShares group procurement program.

Technical Barriers

This project addresses the following technical barriers from the Education and Outreach section of the Fuel Cell Technologies Office Multi-Year Research, Development, and Demonstration Plan¹:

- (A) Lack of Readily Available, Objective, and Technically Accurate Information
- (D) Lack of Educated Trainers and Training Opportunities.

Contribution to Achievement of DOE Milestones

This project will contribute to achievement of the following DOE milestones from the Education and Outreach section of the Fuel Cell Technologies Office Multi-Year Research, Development, and Demonstration Plan:

- Task 1: Educate Safety and Code Officials
- Task 2: Educate Local Communities
- Task 3: Educate State and Local Government Representatives
- Task 4: Educate Potential End-Users.

¹ <https://energy.gov/eere/fuelcells/downloads/fuel-cell-technologies-office-multi-year-research-development-and-22>

FY 2018 Accomplishments

- Implemented training and outreach schedule.
- Implemented community engagement plan.
- Conducted outreach to AHJs to streamline permitting processes.
- Completed project reporting and dissemination.
- Implemented FCEV group-buy program.

INTRODUCTION

This program supports the introduction of FCEVs and retail hydrogen fueling stations in San Francisco and the nine-county Bay Area. Per a January 2018 Executive Order from the Governor’s office, California has a goal of 5 million zero-emission vehicles on the roads by 2030. To support deployment of zero-emission vehicles, the state also is working to develop 200 hydrogen stations by 2025. By applying lessons learned from the market transformation the solar industry experienced the last decade, we are working on reducing soft costs tied to two primary barriers. The first is the cost and complexity of permitting and inspection processes associated with hydrogen station development among multiple AHJs, and the second is a lack of consumer awareness of hydrogen and FCEVs.

APPROACH

To address the cost and complexity of permitting, we provided training and technical assistance to AHJs and station developers in proposed project areas. This included organizing and facilitating pre-application meetings, documenting permitting and inspection processes among AHJs, publishing a newsletter, and developing specialized trainings. As stations near project completion, we will organize local community awareness events in partnership with the AHJ and station developer.

To address the lack of consumer awareness, we worked with the SunShares group procurement program to provide discounts on FCEVs coupled with consumer workshops for residents throughout the greater Bay Area, leveraging established communication channels to reach consumers (e.g., affiliate groups, employers, and local government). We also have incorporated FCEVs in our annual Clean Cities workshops and local ride-and-drive events.

RESULTS

Our work supports hydrogen station development in San Francisco and the nine-county Bay Area. Figure 1 shows stations that are open or in development as of Fall 2018.

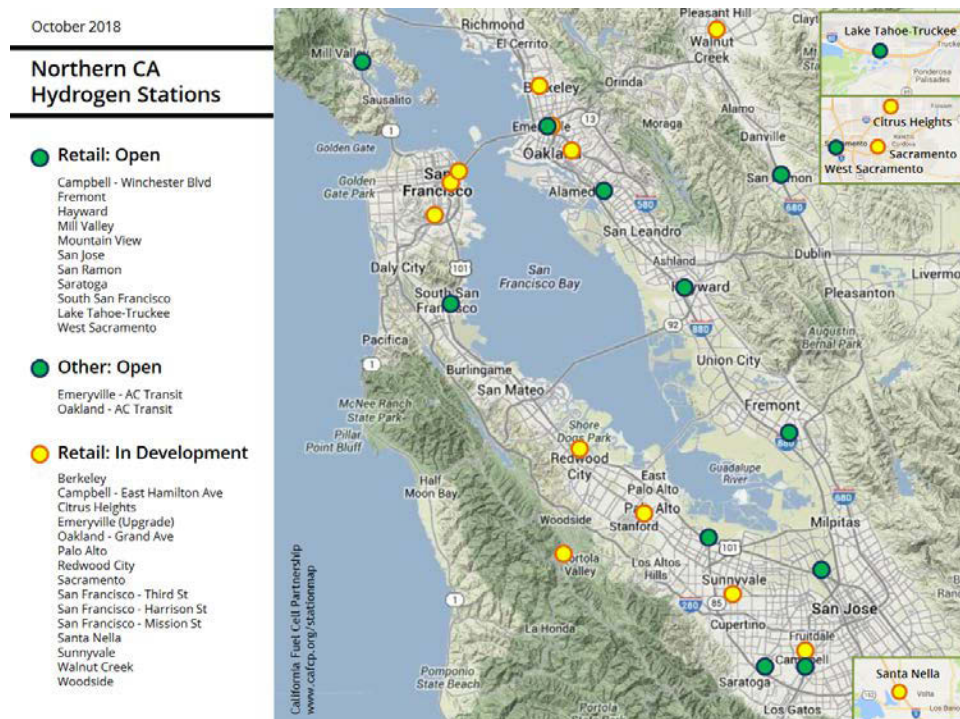


Figure 1. Map of San Francisco Bay Area hydrogen stations, Fall 2018

To accommodate delays in the station development schedule for San Francisco-specific projects, a six-month, no-cost extension was applied for and granted by DOE. This allowed us to schedule first-responder trainings, which are highlighted in Table 1. It also enabled us to ensure we could hold community meetings closer to station opening, a best practice according to the California Fuel Cell Partnership.

In addition to planned events, we found a unique opportunity to present an overview of hydrogen fueling station development and technical resources to the Steering Committee of the Bay Area Planning Directors Association. Following the presentation, we provided a summary of technical resources to the Steering Committee, which was sent to Bay Area Planning Directors Association members representing most municipalities in the Bay Area.

Table 1. Training and Outreach Schedule

Topic	Audience	Date	Type
Hydrogen Safety for Permitting Authorities	Building officials, planning and sustainability staff	July 19, 2017	Webinar
Regional Briefings on Fuel Cell Electric Vehicles and Hydrogen Station Development—South Bay	Elected officials, municipal staff, public	January 23, 2018	Half-day workshop
Regional Briefings on Fuel Cell Electric Vehicles and Hydrogen Station Development—North Bay	Elected officials, municipal staff, public	January 26, 2018	Half-day workshop
Overview of Hydrogen Fueling Station Development and Technical Resources	Bay Area Planning Directors Association	July 13, 2018	Presentation to Steering Committee and mailing to membership
Hydrogen Safety Training for First Responders—North Bay	Public safety and fire department first responders	October 3, 2018	Full-day training session
Hydrogen Safety Training for First Responders—South Bay	Public safety and fire department first responders	October 4, 2018	Full-day training session

To increase community awareness, we also participated in a broad range of outreach events that included static displays of FCEVs and vehicle test drives (see Table 2).

Table 2. Community Engagement Schedule

Topic/Event	Audience	Date	Type
SEMICON West Conference, San Francisco	Microelectronics conference and exhibition attendees	July 10–13, 2017	Static FCEV display
Intersolar North America, San Francisco	Conference and exhibition attendees	July 12–13, 2017	Static FCEV display
National Drive Electric Week	Public, elected officials	September 23, 2017	Test drives
East Bay Regional Park District Green Expo	Staff and supporters of regional parks	October 4, 2017	Static FCEV display
Fleet Week	Public, elected officials	October 6–7, 2017	Static FCEV display, test drives
Proposed Hydrogen Station—Berkeley	Public, elected officials, municipal staff	March 30, 2018	Public meeting (evening)
Earth Day San Francisco	Public, elected officials	April 21, 2018	Static FCEV display

To increase awareness of hydrogen and FCEVs beyond the Bay Area, we scheduled presentations at three regional or national events. Those are included in Table 3.

Table 3. Dissemination Schedule

Topic	Audience	Event	Date	Co-Presenter
Overview of Fuel Cell Electric Vehicles and Hydrogen Station Development	Fleet managers, public	Northern California Alt Car Expo, Oakland, CA	March 21, 2018	UC Berkeley Transportation Sustainability Research Center
Overview of Fuel Cell Electric Vehicles and Hydrogen Station Development	West coast fleet managers, technical and government staff	Green Transportation Summit and Expo, Tacoma, WA	April 17, 2018	Hydrogen Safety Council
Overview of Fuel Cell Electric Vehicles and Hydrogen Station Development	Clean Cities coordinators and stakeholders	DOE Clean Cities Annual Peer Exchange, Cocoa Beach, FL	November 7, 2018	Greater New Haven Clean Cities Coalition

The monthly *SF Clean Cities Hydrogen and Fuel Cell Electric Vehicle Newsletter* now has 350 subscribers and will likely continue beyond the project term as a Clean Cities project. Content includes a summary of a top news story, along with videos and links to news articles, and an update on California hydrogen fueling station development.

Our no-cost extension also facilitated the participation in an additional year of the SunShares group procurement program. SunShares offers pre-vetted discounts on residential solar photovoltaic systems and zero-emission vehicles. For the three years covered (2016–2018), the program featured the Toyota Mirai. The program conducts outreach to consumers through 40–50 public- and private-sector affinity groups (e.g., municipalities and large employers), which means that thousands of Bay Area residents learned about the benefits of longer range and ease of fueling associated with FCEVs. Program results have been documented in a case study.

CONCLUSIONS AND UPCOMING ACTIVITIES

The project has been successful in educating AHJs, elected officials, and the public about hydrogen and FCEVs. We have offered robust technical assistance to AHJs and delivered technical resources to decision makers across the Bay Area.

One of the objectives of the project was to harmonize permitting practices among AHJs. This approach has been successful in the past for reducing soft costs and supporting market transformation of residential solar photovoltaic installations, so that project developers have a consistent set of requirements across the cities they work in.

In practice, we found that permitting for gaseous fueling stations is context-dependent in AHJs, based on local knowledge and political environment. For example, one community allowed parallel planning, building, and fire safety review and issued permits within a few months. Another community allowed project review only in series and required an outside consultant to conduct an extensive environmental review, adding several months to the permitting process. Both proposed sites were existing petroleum fueling stations, and both AHJs had participated in a pre-application meeting according to best practice and California Energy Commission grant requirements.

We also found that AHJs in general were not receptive to documenting existing permitting processes for compressed natural gas stations (as proposed) or in participating in a standardized permitting process. Documentation of our experience with this task will be included in a case study.

Upcoming activities include hydrogen safety training for first responders and a San Francisco community meeting in January 2019. The community meeting will include presentations by the station developer, California Energy Commission, and the Governor’s Office of Business Development. In addition, another case study will be developed on training and community engagement.

Systems Analysis Subprogram Overview

INTRODUCTION

The Systems Analysis subprogram supports the decision making of the Fuel Cell Technologies Office (FCTO) by providing a greater understanding of technology gaps, options, and risks for early-stage research and development (R&D). The analytical effort provides techno-economic analysis of fuel production to utilization on a life-cycle basis for light-, medium- and heavy-duty fuel cell electric vehicles (FCEVs) and supports the H2@Scale concept. Analysis is also conducted to assess cross-cutting issues, such as integration of hydrogen and fuel cells with the electric grid for energy storage development and hydrogen technologies that support infrastructure development through innovative R&D. The goal is to provide system-level analysis to support hydrogen and fuel cell technologies development and technology readiness by evaluating technologies and pathways including resource requirements to guide the selection of research, development, and demonstration (RD&D) projects and estimate the potential value of specific early-stage R&D efforts. The subprogram also collaborates with industry and other federal offices and agencies (such as Fossil Energy and Nuclear Energy) to leverage outside activities, coordinate efforts, and build opportunities for new technology applications and input.

The Systems Analysis subprogram made several significant contributions to the Hydrogen and Fuel Cells Program in fiscal year (FY) 2018. The hydrogen cost target—to represent the hydrogen fuel cost at which hydrogen FCEVs are projected to become competitive on a cost-per-mile basis with the competing fuel/vehicle combination, gasoline in hybrid-electric vehicles—was updated and determined to be \$7/gasoline gallon equivalent (gge) (untaxed) in 2025 and ultimately less than \$4/gge (untaxed). The impact of improving the fuel cell efficiency on the costs of the fuel cell and storage systems for medium- and heavy-duty FCEV performance was studied. The Greenhouse gases, Regulated Emissions, and Energy use in Transportation (GREET) model continues to be enhanced for the analysis of water consumption for multiple hydrogen pathways on a life-cycle basis. The integration of hydrogen delivery with onboard storage was examined to understand impacts of novel storage systems on the levelized cost of hydrogen and program targets.

GOAL

The goal of the Systems Analysis subprogram is to provide system-level analysis to support hydrogen and fuel cell technologies development and technology readiness by evaluating technologies and pathways including resource requirements to guide the selection of early-stage RD&D projects and estimate the potential value of specific RD&D efforts.

OBJECTIVES

- By 2018, complete an assessment of fuel cell cost and power requirements for multiple medium- and heavy-duty truck applications.
- By 2018, update the risk analysis process for FCTO technologies, prepare a risk analysis plan for FCTO, and apply the process to at least one FCTO program.
- By 2018, complete a preliminary resource analysis supporting the H2@Scale initiative and identify excess hydrogen generation capacity available for hydrogen fueling or other applications.
- By 2019, complete a sustainability analysis of FCTO metrics and develop a method of incorporating metrics in program targets.
- By 2019, complete an analysis of the potential for hydrogen, stationary fuel cells, fuel cell vehicles, and other fuel cell applications such as grid services. The analysis will address necessary resources, hydrogen production, and performance of stationary fuel cells and vehicles.

- Provide milestone-based analysis, including risk analysis and independent reviews, to support the fuel cell technologies' needs prior to technology readiness.
- Periodically update the life-cycle energy and petroleum use analysis for technologies and pathways for fuel cell technologies to include technological advances or changes.

FY 2018 STATUS

The Systems Analysis subprogram focuses on examining the economics, benefits, opportunities, and impacts of fuel cells and renewable fuels with a consistent, comprehensive analytical framework. Analysis conducted in FY 2018 included updating the hydrogen cost target, examining the life-cycle cost of various vehicle platforms including fuel cell vehicles with the Vehicle Technologies Office, analyzing the impact of novel onboard storage systems interaction with hydrogen delivery systems on hydrogen pathway levelized cost of driving, studying the improvement of fuel cell and storage system costs as a result of improved fuel cell efficiency, and analyzing life-cycle water use for multiple hydrogen and conventional light-duty fuel/vehicle pathways. The Systems Analysis subprogram leverages the key models shown in Figure 1. These models have been developed in prior years for critical program analyses.

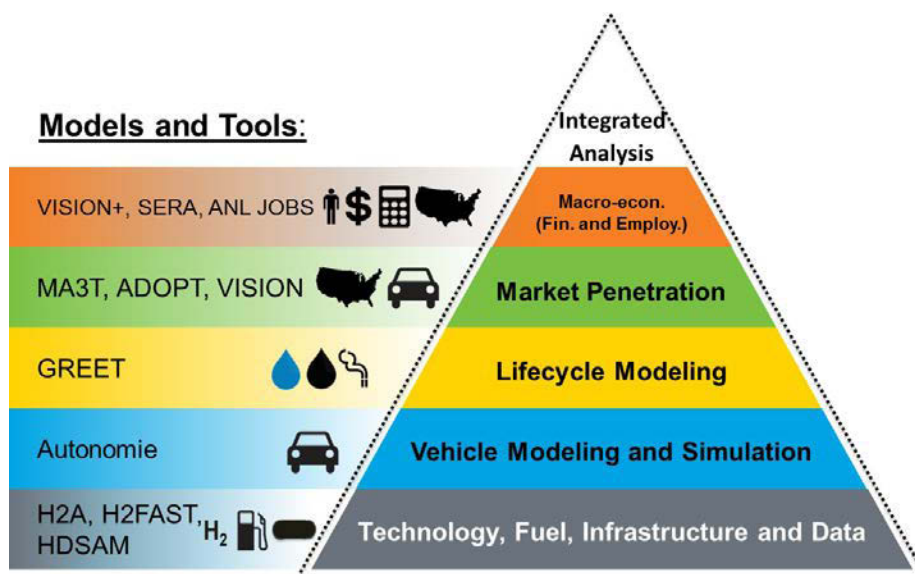


Figure 1. Systems analysis models and tools

Model description fact sheets: <http://www.energy.gov/eere/fuelcells/systems-analysis>

FY 2018 ACCOMPLISHMENTS

Studies and Analysis

H2@Scale Analysis

This analysis updated the estimate of the maximum hydrogen demand market size to be 151 million metric tonnes (MMT) annually, including demands from refineries and the chemical processing industry, metals refining, ammonia production, hydrogen use for biofuels refining, hydrogen use for synthetic fuels production, direct injection into the nation's natural gas system, light-duty FCEVs, other transportation including medium-duty and heavy-duty trucks, and seasonal energy storage for the electricity grid.

Also, the study developed four national supply and demand curves for hydrogen consisting of supplies from steam reforming natural gas, high-temperature electrolysis using nuclear energy, and low-temperature electrolysis of otherwise curtailed electricity. The scenarios vary based on varying assumptions of natural gas

prices, low-temperature electrolyzer prices, and electricity market structures. The national demand curves for the hydrogen demands varied depending upon assumptions regarding the evolution of the U.S. electricity system and the U.S. metals industry. The results quantified the national economic potential for H2@Scale ranging from 22 MMT/yr to 45 MMT/yr over five scenarios with various technology and market assumption.

Sustainability Analysis: Hydrogen Regional Sustainability

This project developed and implemented an analytic framework that integrates Argonne National Laboratory's GREET model and the National Renewable Energy Laboratory's Scenario Evaluation and Regionalization Analysis (SERA), Automotive Deployment Options Projection Tool, and Future Automotive Systems Technology Simulator models, updating results to reflect current model capabilities.

The analysis compared petroleum fuel impacts from the four FCEV case study life cycles to the life-cycle impacts from conventional gasoline vehicles, hybrid-electric vehicles, and battery-electric vehicles, all with 400-mile range. Result indicate the FCEVs require the least amount of petroleum over the vehicle life cycle. The analysis included the monetized social benefits of air pollution reductions associated with FCEV adoption in the H2USA scenarios, which were found to range from \$1.2 billion to \$2.2 billion in the Urban Markets and the State Success scenarios, respectively.

Market Segmentation Analysis of Medium- and Heavy-Duty Trucks with a Fuel Cell Emphasis

This study developed a total cost of ownership systems analysis framework for several medium- and heavy-duty trucks that included both direct costs (purchase price, fuel, operating and maintenance) and indirect costs (dwell time costs due to refueling/recharging and payload opportunity costs from forgone revenue due to the truck being weight limited). By incorporating dwell time and payload opportunity costs, this analysis more accurately analyzes fuel cells for commercial applications than previous studies have done.

A comparative total cost of ownership evaluation was completed for five different truck powertrain technologies (diesel, diesel hybrid-electric, compressed natural gas, battery electric, and fuel cell electric) for three different truck applications (Class 8 long haul, Class 8 short haul, and Class 4 parcel delivery) and for different technology statuses (2018, 2020, 2040). Several scenarios for fuel cell powertrain trucks to have the lowest total cost of ownership of all powertrains by 2020 if FCTO program cost and performance targets are met were included in the evaluation. The analysis shows strong commercial application opportunities for fuel cell powertrains in Class 4 parcel delivery and Class 8 long haul trucking applications.

Regional Supply

This analytical project produced an optimization framework for supply chain deployment for more than 3,000 cities in the United States in 5-year investment increments through the year 2040 with the use of the SERA model. The optimization included a new algorithm for intra-urban pipeline distribution to hydrogen stations from semi-central hydrogen production units and three scenarios: National Expansion (high demand growth), State Success (medium growth), and Urban Markets (low growth).

The analysis produced regionalized cost of hydrogen based on regionally optimal supply chains and illustrated substantial potential for retail adoption and economic and functional advantages of employing high-pressure pipeline intra-city hydrogen distribution. The SERA model estimates that the average U.S. dispensed hydrogen cost is \$16/kg (2016 real dollars) in 2018 but drops to \$4.6/kg by 2040 driven by economies of scale. The results indicate that existing hydrogen capacity in the Gulf Coast is used to meet demand in California. However, by 2030, new production plants are built across the United States and concentrated in California and the Northeast to support the nearly 50 tonne/day hydrogen demand. Cumulative capital investment opportunity by 2040 is ~\$28 billion, indicating a large market for new firms to enter the industry. Additionally, the growth of FCEVs results in the displacement of 4.0 billion gallons of gasoline each year. Finally, a novel hydrogen distribution pathway was shown to be economically competitive by 2030 with more than 50% of stations joining the pipeline network in eight urban areas by 2040.

Analysis of Cost Impacts of Integrating Advanced Onboard Storage Systems with Hydrogen Delivery

This study evaluated the potential of reducing fueling-station costs by reducing compressor, storage, and/or refrigeration costs, assuming hypothetical vehicle onboard storage options that require a combination of dispensing pressure and temperature that satisfies the same onboard hydrogen storage capacity and fill rate. In particular, this study evaluated a dispensing pressure much lower than the baseline 700 bar (e.g., 100 bar) and either cryogenic temperatures (e.g., liquid hydrogen or liquid nitrogen temperatures, such as these preferred by metal organic framework onboard storage systems) or near-ambient temperatures (300 K, e.g., temperatures preferred by metal hydride onboard storage systems). The hydrogen delivery and refueling cost is strongly impacted by the pressure and temperature requirements of the FCEV onboard storage system. Low-pressure and near-ambient-temperature dispensing can significantly reduce hydrogen dispensing cost to FCEV customers. These onboard storage options, including their respective boundary conditions, will be integrated with hydrogen delivery technologies to evaluate the cost impact on the hydrogen pathways.

Analysis of Program Benefits

Hydrogen Cost Target

The hydrogen cost target that was developed to assist DOE in focusing and prioritizing R&D options was updated in 2018. The cost target represents the cost at which hydrogen FCEVs are projected to become competitive on a cost-per-mile basis with the competing fuel/vehicle combination: gasoline in internal combustion engine vehicles and hybrid-electric vehicles. The ultimate hydrogen R&D cost target is set at \$4/gge (approximately equal to 1 kg of hydrogen on a lower heating value basis), untaxed and dispensed at the pump; a 2025 cost target is set at \$7/gge (targets expressed in 2016\$). The methodology and assumptions used to calculate the hydrogen cost targets are documented in a peer-reviewed DOE program record.¹

Water Life Cycle Analysis

This analysis focused on identifying water use impact of electricity generation and large-scale deployment of hydrogen FCEVs. The results illustrate that regional variation exists for water use impact of electricity generation and FCEV deployment. The spatial trend of electricity generation suggests that the power sector has already adapted to varying water availability by using non-freshwater resources (wind/solar/nuclear/reclaimed water) in water-stressed regions. The analysis found a majority of power plants (80%) are located in water-abundant regions. At the state level, Texas, Arizona, Colorado, and Kansas contributed 73% of the water scarcity footprint of thermal power generation in water-stressed regions. For hydropower electricity, Nevada, Arizona, Nebraska, and California contributed 88% of the water scarcity in water-stressed regions. For future energy systems deployment, such as FCEVs, any marginal increase in water demand in water-stressed regions will magnify the impact on water stress. This study provides a systematic approach to evaluate the sustainability of various energy systems in terms of water use and their impact on water stress in various regions in the United States.

Patents Resulting from DOE-Sponsored R&D

The commercial impact of FCTO funding continues to be analyzed by tracking the patents and patent applications resulting from FCTO-funded R&D projects. More than 738 patents were awarded by 2017 as a result of research funded by FCTO in the areas of storage, hydrogen production and delivery, and fuel cells. The patent application analysis identified 893 patent applications related to FCTO-funded R&D and found that approximately 80% of these applications received patent awards. These results were highlighted in the FY 2017 Pathways to Success: Innovations Enabled by the U.S. Department of Energy Fuel Cell Technologies Office report (prepared by Pacific Northwest National Laboratory).

¹ Hydrogen R&D Cost Target Calculation—2018 Update, Program Record (Hydrogen and Fuel Cells Program) 18004, 2018, https://www.hydrogen.energy.gov/pdfs/18004_h2_cost_target_calculation_2018.pdf

BUDGET

The FY 2018 appropriation for the Systems Analysis subprogram was \$3 million (Figure 2).

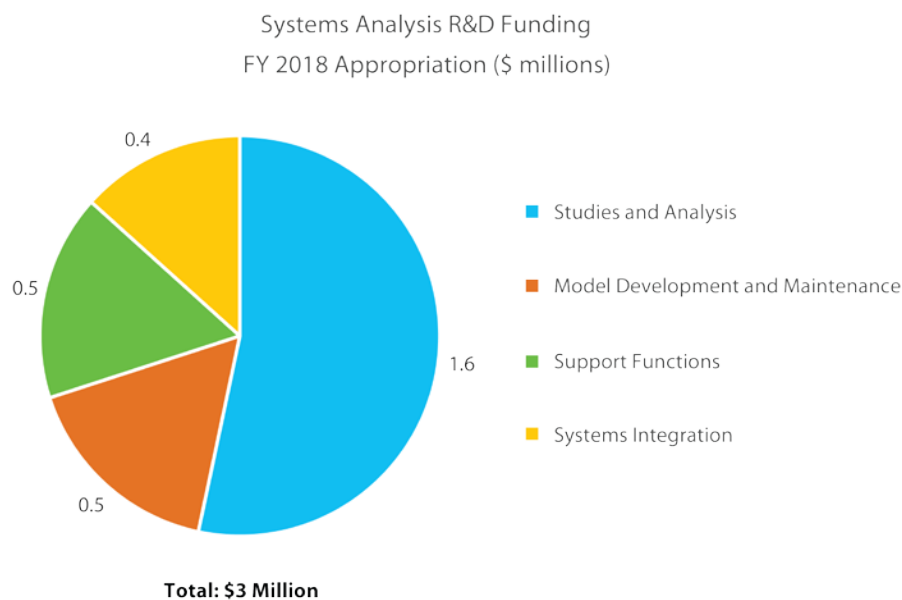


Figure 2. Systems Analysis subprogram FY 2018 appropriation

Funding continues to focus on conducting analysis using the models developed by the program. In particular, analysis projects are concentrated on:

- Analyzing market segmentation of fuel cell technology applications for light-, medium-, and heavy-duty vehicles
- Analyzing life-cycle water use for hydrogen production technology pathways for light-duty vehicles
- Calculating the cost of onboard hydrogen storage options
- Estimating the reduction in greenhouse gas emissions and petroleum use based on various hydrogen pathways for medium- and heavy-duty trucks
- Estimating the hydrogen production from diverse domestic energy resources (natural gas, coal, uranium, biomass, wind, solar) required for potential future FCEV demand
- Performing hydrogen fueling station business assessments
- Studying hydrogen's use as an energy carrier with applications across sectors (e.g., industrial, grid services, in addition to vehicles) and energy storage supporting the H2@Scale initiative
- Analyzing hydrogen supply and demand for multiple application to support H2@Scale
- Integrating with nuclear hybrid systems
- Integrating delivery and onboard storage systems.

Fred Joseck

Systems Analysis Subprogram Manager
Fuel Cell Technologies Office
Office of Energy Efficiency and Renewable Energy
U.S. Department of Energy
1000 Independence Ave., SW
Washington, DC 20585-0121
Phone: (202) 586-7932
Email: Fred.Joseck@ee.doe.gov

Regional Water Stress Analysis with Hydrogen Production at Scale

Amgad Elgowainy (Primary Contact), Uisung Lee, Hui Xu, Michael Wang
Argonne National Laboratory
9700 South Cass Avenue
Lemont, IL 60439
Phone: (630) 252-3074
Email: aelgowainy@anl.gov

DOE Manager: Fred Joseck
Phone: (202) 586-7932
Email: Fred.Joseck@ee.doe.gov

Project Start Date: April 2013
Project End Date: Project continuation and direction determined annually by DOE

Overall Objectives

- Incorporate water consumption associated with hydrogen production as a transportation fuel for use in fuel cell electric vehicles (FCEVs).
- Compare water consumption of hydrogen for use in FCEVs with other fuel or vehicle systems on a life cycle basis.
- Identify major contributors in upstream supply chain to water consumption.
- Analyze the technology environmental impacts on regional water stress for hydrogen and fuel cell deployment scenarios.

Fiscal Year (FY) 2018 Objectives

- Quantify and compare water consumption and water stress impacts of electricity generation in different regions of the United States.
- Evaluate the impacts hydrogen FCEV deployment will have on regional water stress in the United States.
- Improve the Available water remaining for the United States (AWARE-US) water stress index.

Technical Barriers

This project directly addresses Technical Barriers B, C, and D in the System Analysis section of the Fuel Cell Technologies Office Multi-Year Research, Development, and Demonstration Plan.¹ These barriers are as follows.

- (B) Stove-Piped/Siloed Analytical Capability
- (C) Inconsistent Data, Assumptions, and Guidelines
- (D) Insufficient Suite of Models and Tools.

Contribution to Achievement of DOE Systems Analysis Milestones

This project contributes to achievement of the following DOE milestones from the Systems Analysis section of the Fuel Cell Technologies Office Multi-Year Research, Development, and Demonstration Plan:

- Milestone 1.13: Complete environmental analysis of the technology environmental impacts for hydrogen and fuel cell scenarios and technology readiness.
- Milestone 2.2: Annual model update and validation. (4Q, 2011 through 4Q, 2020)

FY 2018 Accomplishments

- Improved the AWARE-US water stress index with new ground water recharge data.
- Estimated water consumption and water use impact of electricity generation in different regions of the United States.
- Performed water consumption impact analysis for the large-scale deployment scenarios of hydrogen FCEVs.

¹ <https://www.energy.gov/eere/fuelcells/downloads/fuel-cell-technologies-office-multi-year-research-development-and-22>

INTRODUCTION

Hydrogen is a zero-carbon energy carrier that can be produced from a variety of domestic feedstock sources. Hydrogen is also important for FCEVs and the processing and upgrading of other fuels. Production of energy and transportation fuels, including hydrogen, typically requires the use of freshwater resources. However, freshwater resources available to human use vary substantially across the United States. Large-scale deployment of energy systems in water-stressed regions has the potential to exacerbate water-resource competition among various uses, such as ecosystem services and food and energy production. This means water consumption of energy systems may cause negative environmental and social impacts in water-stressed regions. Thus, water stress analysis at a regional level is critical for a sustainable future of new energy systems.

The objective of this study is to evaluate the impacts of deploying new energy systems (e.g., hydrogen) on the regional water resources in the United States by considering local water supply and demand. Because electricity is a key resource for generating or compressing hydrogen, we evaluated water consumption and water stress impacts associated with electricity generation in the United States using facility-level water consumption data and the newly developed county-level water stress index (AWARE-US). We then analyzed the regional impact of hydrogen production at scale scenarios for FCEVs on water stress. This study contributes information that can be used to guide sustainable water management decisions.

APPROACH

The project includes three major parts: (1) updating the county-level water stress index (AWARE-US), (2) evaluating water stress impacts of hydro and thermoelectricity generation at the regional level, and (3) evaluating regional water stress impacts of hydrogen production associated with 2040 FCEV deployment scenarios. To improve reliability of AWARE-US, we incorporated the latest high-resolution (800 m) groundwater recharge data from the United States Geological Survey (USGS).

To evaluate water use impact of electricity generation, we consider spatial variations in both water consumption and regional water supply because impact of the same amount of water consumption on water stress varies widely across the United States [1]. In this analysis, water use impact is quantified as water scarcity footprint [2]. Water scarcity footprint is calculated as the product of facility-level water consumption factors [3] and county-level characterization factors (CFs) from the updated AWARE-US index [1]. The resulting water scarcity footprint is expressed in terms of U.S. equivalent gallons of water consumption [1]. One U.S. equivalent gallon indicates the impact of one gallon of water consumption in a region that has the U.S. average amount of water availability. Because water consumption in different regions can be expressed as equivalent gallons of water consumption, AWARE-US enables systematic comparison of the water consumption impacts across regions. Finally, Argonne evaluated the regional water use impact associated with hydrogen demand for FCEVs by combining estimated water consumption for hydrogen production and the AWARE-US index. Consistent with the H2@Scale initiative, we assume electricity is used for hydrogen production when wind/solar/nuclear is used for electricity generation. When renewable resources are not available, steam methane reforming (SMR) of natural gas is used for hydrogen production.

RESULTS

Figure 1 shows improvements in the groundwater recharge (GWR) data used in AWARE-US. Previously, we used the 1950–1980 annual GWR data (Figure 1a) from USGS, which was the only national data available at the time when we initially developed AWARE-US. To reflect more recent data, we incorporated the latest national-level, high-resolution (800 m) GWR data from USGS [4] (Figure 1b). We found overall patterns are similar between the old and updated GWR datasets, but large differences are observed when examined at the county level. Specifically, differences in annual GWR can be as high as 300 mm/year (Figure 1c). Comparing to the old dataset, the updated GWR rate is much lower (difference >100 mm/year) for many counties in southeastern states, northern California, and western Oregon, but much higher (difference >150 mm/year) in the Corn Belt and New England regions (Figure 1c). In AWARE-US, GWR is part of the natural runoff (renewable freshwater resources). In certain areas, usage of groundwater may exceed GWR, which means non-

renewable water resources will be used. This may cause problems like groundwater depletion and ecosystem degradation. Improved GWR data allows us to better differentiate human water consumption sourced from renewable versus non-renewable groundwater. It also improves reliability of AWARE-US, especially in regions relying on groundwater resources.

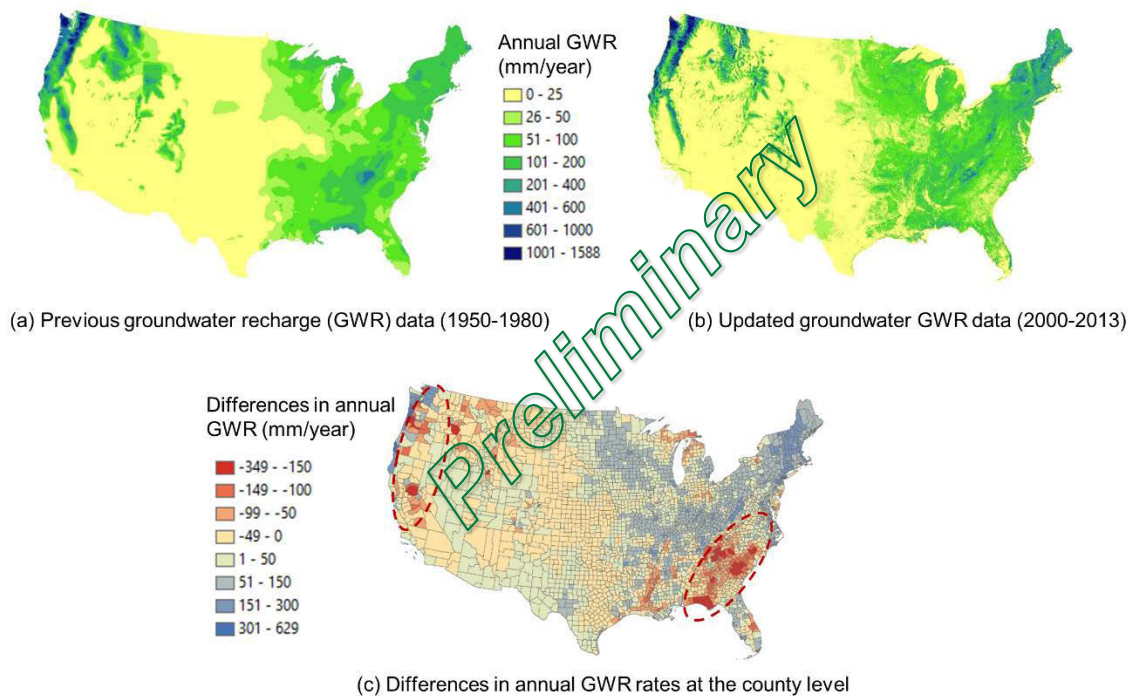


Figure 1. Updated groundwater recharge data for AWARE-US

Figure 2 illustrates the regional trend of electricity generation, which indicates that the power sector has adapted to varying energy resources and freshwater availability. We found regions in water-stressed areas tend to use technologies not involving freshwater consumption for electricity generation (Figure 2a). For instance, wind-power plants are concentrated in the High Plains and Texas where water stress is much higher than neighboring regions. There are some wind-power clusters in Midwestern states like Iowa, but these clusters are driven more by wind resources and policies rather than by shortages of water resources. In the southwestern United States, solar, wind, and non-freshwater (e.g., reclaimed water) resources have been utilized to address water shortage issues in this region. Although non-freshwater power generation has already been deployed in various semi-arid regions, electricity generation from these facilities is still small compared to traditional thermal and hydropower generations. For power plants relying on freshwater, those with the highest capacities ($\geq 1,000$ MWh) are mostly located in the eastern United States (Figure 2b). Because freshwater water is relatively abundant in this area, once-through technology is still widely used for thermoelectricity generation, but circulating technology is also a popular option. In the Western United States, thermal power generation mostly uses recirculating rather than once-through technology.

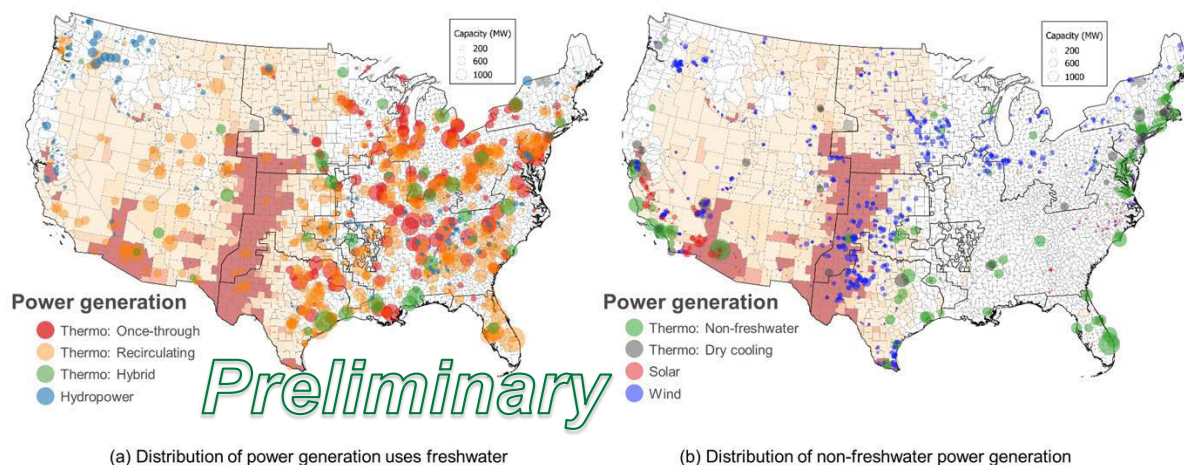


Figure 2. Spatial distribution of power generation by energy source and technology

When regional water stress is considered, we found that a majority of existing thermal and hydropower plants that use freshwater are located in water-abundant regions (AWARE-US $CF < 1$) (Figure 3). However, about 23% of thermal power plants and 18% of hydropower plants (by power generation) are located in water-stressed regions (AWARE-US $CF > 1$). For the 23% thermal power plants, about 91% have already adopted recirculation-cooling technology to reduce cooling water withdrawal. Due to varying water stress, spatial distribution patterns of water consumption versus water use impact are very different, especially in the western United States, where water use impact can be 100 times higher than indicated by water consumption. While water consumption of thermal power generation is higher in the eastern United States, water use impact (water scarcity footprint) is higher in the southwestern United States, primarily due to limited freshwater supply. At the state level, Texas, Arizona, Colorado, and Kansas contributed the most to the overall water scarcity footprint (73%) (Figure 3b), but they only contribute 17% of total thermal power generation. For hydropower, we found constrained water resources make the water scarcity footprint of hydropower amplify water constraints in water-stressed regions (e.g., Colorado River, San Joaquin River). Spatially, due to high evaporation rate, water consumption for hydropower (evaporation from reservoirs) is higher in the southern United States. At the state level, 86% of the total hydropower water scarcity footprint comes from Nevada, Arizona, Nebraska, and California. Reducing hydropower water consumption can be difficult because evaporation rates are primarily determined by local climate. In addition, large reservoirs used for hydropower generation are often built for multiple purposes (e.g., navigation, irrigation, flood control). Thus, reducing the water impact of multipurpose dams requires coordinated efforts of all stakeholders.

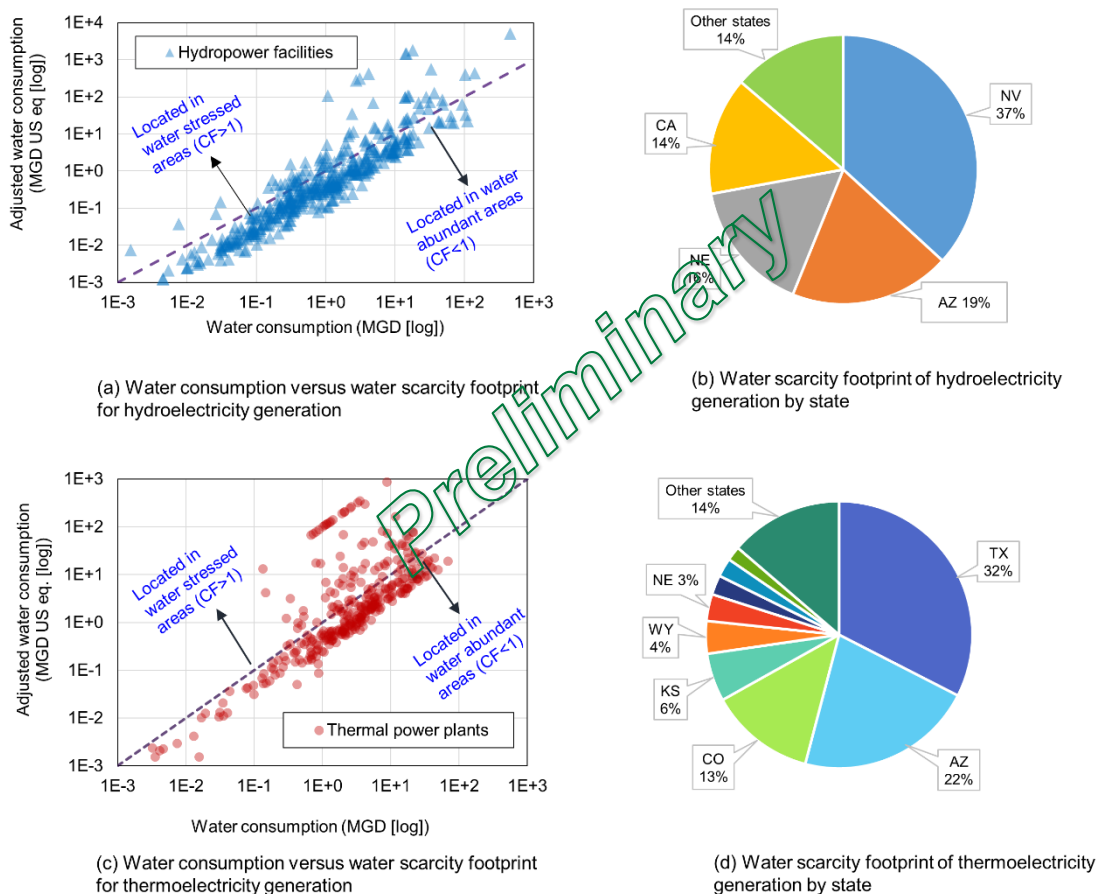


Figure 3. Water consumption and water scarcity footprint for hydroelectricity (a,b) and thermoelectricity generation (c,d)

Figure 4 shows water consumption and water use impact of FCEV deployment scenarios at the county level. Water demand of hydrogen production includes local water consumption and upstream water input (e.g., water embedded in electricity). Comparison of water consumption (Figure 4a) and water use impact (Figure 4b) suggests that implications of water consumption on regional water stress for hydrogen FCEV deployment differ by region. We found that water consumptions of hydrogen production are highest in the Pacific coastal and the northeastern coastal areas (Figure 4a), primarily due to the projected distribution of FCEVs [1]. Water consumption alone, however, does not reflect differences in regional water stress. Figure 4b represents water use impact of FCEVs at the county level and considers both consumption and water stress, expressed in water scarcity footprint. The results suggest that the western United States would have much higher water use impact compared to the eastern United States. For example, using one FCEV deployment scenario, California consumes only 1.3 times the volume of freshwater consumed in New York in order to meet the hydrogen demand in their respective states. However, the water consumption impact in California is 27 times higher compared to New York due to higher water stress status in California.

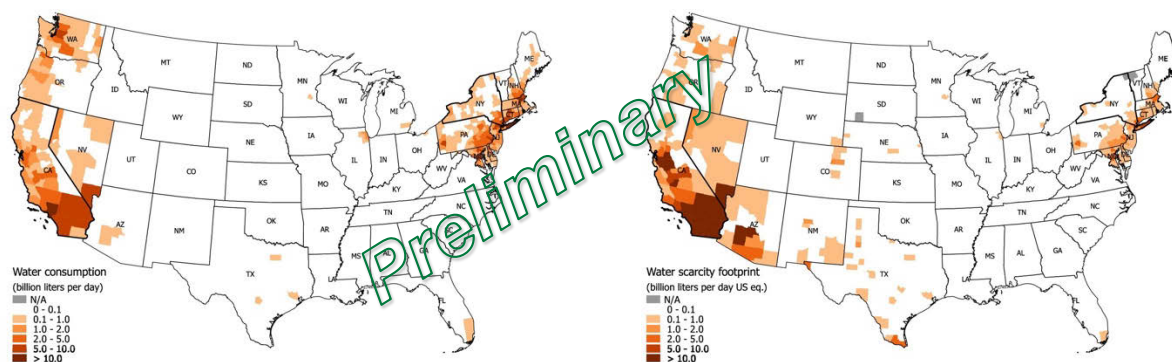
a) Water consumption for H₂ FCEVsb) Water scarcity footprint for H₂ FCEVs

Figure 4. County-level water consumption versus water scarcity footprint for hydrogen production used for FCEVs in 2040

CONCLUSIONS AND UPCOMING ACTIVITIES

This analysis focused on identifying water use impact of electricity generation and large-scale deployment of hydrogen FCEVs. The results illustrate that regional variation exists for water use impact of electricity generation and FCEV deployment. The spatial trend of electricity generation suggests that the power sector has already adapted to varying water availability by using non-freshwater resources (wind/solar/nuclear/reclaimed water) in water-stressed regions. We found a majority of power plants (80%) are located in water-abundant regions. At the state level, Texas, Arizona, Colorado, and Kansas contributed 73% of water scarcity footprint of thermal power generation in water-stressed regions. For hydropower electricity, Nevada, Arizona, Nebraska, and California contributed 88% of the water scarcity in water-stressed regions. For future energy systems deployment, such as FCEVs, any marginal increase in water demand in water-stressed regions will magnify the impact on water stress. This study provides a systematic approach to evaluate the sustainability of various energy systems in terms of water use and its impact on water stress in various regions in the United States.

For upcoming activities, we will focus on three major areas: (1) updating AWARE-US with the latest water consumption data, (2) developing a monthly/seasonal AWARE-US database, and (3) developing regional supply-demand databases. Accurate and timely human water consumption estimates are critical for evaluating water stress conditions. Currently AWARE-US uses 2010 withdrawal data along with consumption factors derived from the 1995 water use report. In FY19, we will upgrade AWARE-US with water consumption data from the 2015 water use report. Furthermore, current AWARE-US evaluates water use impact on an annual basis, but both water demand and water supply can vary substantially from month to month. To address this issue, subsequent studies will develop a monthly version of AWARE-US to enable seasonal water impact analysis in FY19. Finally, we will start to build a regional database that shows supply and demand of major fuels (hydrogen, electricity, gasoline, diesel, and biofuel) at a regional level. We will estimate water consumption and water use impact associated with the production of each fuel and incorporate them into the regional database.

FY 2018 PUBLICATIONS/PRESENTATIONS

1. Uisung Lee, Hui Xu, Jesse Daystar, Amgad Elgowainy, and Michael Wang “AWARE-US: Quantifying Water Stress Impacts of Energy Systems in the United States.” *Science of The Total Environment* 648 (January 2019): 1313–22.
2. Amgad Elgowainy, Uisung Lee, Hui Xu, and Michael Wang. “Regional water stress analysis with hydrogen production at scale.” Poster presentation, DOE Hydrogen and Fuel Cells Program Annual Merit Review, Washington DC, June 14, 2018.

REFERENCES

1. Uisung Lee, Hui Xu, Jesse Daystar, Amgad Elgowainy, and Michael Wang. “AWARE-US: Quantifying Water Stress Impacts of Energy Systems in the United States.” *Science of The Total Environment* 648 (January 2019): 1313–22. <https://doi.org/10.1016/j.scitotenv.2018.08.250>.
2. ISO. “14046 Water Footprint—Principles, Requirements and Guidelines,” (2014).
3. Uisung Lee, Jeongwoo Han, Amgad Elgowainy, and Michael Wang. “Regional Water Consumption for Hydro and Thermal Electricity Generation in the United States.” *Applied Energy* 210 (January 2018): 661–72. <https://doi.org/10.1016/j.apenergy.2017.05.025>.
4. M. Reitz, W.E. Sanford, G.B. Senay, and J. Cazenias. “Annual Estimates of Recharge, Quick-Flow Runoff, and Evapotranspiration for the Contiguous U.S. Using Empirical Regression Equations.” *JAWRA Journal of the American Water Resources Association* 53 (August 2017): 961–83. <https://doi.org/10.1111/1752-1688.12546>.

Analysis of Technology Improvement in Fuel Cell Vehicles

Aymeric Rousseau (Primary Contact),
Ram Vijayagopal, Ehsan Islam
Argonne National Laboratory
9700 S. Cass Ave
Lemont, IL 60439
Phone: (630) 252-7261
Email: arousseau@anl.gov

DOE Manager: Fred Joseck
Phone: (202) 586-7932
Email: Fred.Joseck@ee.doe.gov

Project Start Date: October 1, 2017
Project End Date: September 30, 2018

Overall Objectives

- Quantify the impact of system improvements on energy consumption and economic viability of light-duty fuel cell electric vehicles (FCEVs).
- Expand the analysis to medium- and heavy-duty vehicles by developing the assumptions, sizing algorithms, and test processes.

Fiscal Year (FY) 2018 Objectives

- Quantify the impact of technology progress on light duty FCEVs.
- Estimate the technology progress assumptions applicable for fuel cell electric trucks (FCETs) and their impact on energy consumption and cost of the vehicle.

Technical Barriers

This project addresses the following technical barriers from the System Analysis section of the Fuel Cell Technologies Office (FCTO) Multi-Year Research, Development, and Demonstration Plan¹:

- (A) Future Market Behavior
- (C) Inconsistent Data, Assumptions, and Guidelines
- (D) Insufficient Suite of Models and Tools.

Contribution to Achievement of DOE Systems Analysis Milestones

This project will contribute to achievement of the following DOE milestones from the Systems Analysis section of the FCTO Multi-Year Research, Development, and Demonstration Plan:

- Milestone 1.1: Complete an analysis of the hydrogen infrastructure and technical target progress for hydrogen fuel and vehicles.
- Milestone 1.17: Complete analysis of program technology performance and cost status, and potential to enable use of fuel cells for a portfolio of commercial applications. (4Q, 2018)
- Milestone 2.2: Annual model update and validation. (4Q, 2011 through 4Q, 2020)

FY 2018 Accomplishments

A comprehensive section on light-duty FCEVs was added to the Baseline Scenario (BaSc) analysis report published by Argonne. Analysis was extended to medium- and heavy-duty vehicles as well. Class 4 and Class 6 delivery trucks and Class 8 line-haul trucks were included in this analysis. Fuel cell- and storage-specific assumptions for trucks were developed for 2017–2050. Preliminary results on fuel consumption and cost are available now. This is being reviewed internally to support the work related to life cycle cost analysis.

¹ <https://www.energy.gov/eere/fuelcells/downloads/fuel-cell-technologies-office-multi-year-research-development-and-22>

INTRODUCTION

Fuel cell technologies have achieved incremental improvements in cost reduction and durability since 2004 with DOE funding. Testing of commercial FCEVs reveals the peak efficiency of the fuel cell system to be close to 64%. Future technology improvements will reduce the cost of fuel cell stacks and improve their durability. In the analysis of light-duty vehicles, the primary task is to estimate when FCEVs will be economically more attractive to consumers. For this, various assumptions are made for future technology improvements. A detailed analysis of this is published in the BaSce report of 2018 [1].

Fuel cells also are getting more attention from the commercial vehicle segments (Class 4–8 trucks), as this provides a cleaner alternative to petroleum products. In comparison to other alternative technologies such as batteries, fuel cells provide a cleaner and cheaper way to drive longer distances without any downtime for charging. Several fuel cell truck prototypes developed with DOE funding are showing promising results. This study looks at how the technology would change in the future and estimates the impact on commercial viability of such trucks.

APPROACH

Light-Duty Vehicles

The National Highway Traffic Safety Administration (NHTSA) issued a notice of proposed rulemaking guidelines for the light-duty vehicles, and Argonne updated the vehicle models according to those guidelines. Various other assumptions related to vehicle attributes and vehicle component weights were also updated in consultation with NHTSA. In previous years, our analysis considered just five broad vehicle classes. Argonne expanded this list to 10 vehicle classes, with subcategories based on performance. This would adequately cover the breadth of light duty vehicles sold in the U.S. market. Table 1 details the different vehicle classifications along with the definition of the different performance categories used in the study.

Table 1. Vehicle classification and performance categories

Vehicle Class	Performance Category	0–60 mph time (s)
Compact	Base (Non Performance)	10.0
Compact	Premium (Performance)	8.0
Midsize	Base (Non Performance)	6.0
Midsize	Premium (Performance)	9.0
Small SUV	Base (Non Performance)	9.0
Small SUV	Premium (Performance)	7.0
Midsize SUV	Base (Non Performance)	10.0
Midsize SUV	Premium (Performance)	7.0
Pickup	Base (Non Performance)	7.0
Pickup	Premium (Performance)	7.0

Light-weighting is applied across all glider systems except for those related to safety. Light-weighting is also applied to the wheels, except for tires. The details for each of the assumptions can be found in the report to NHTSA. For simplicity of the analysis of the report, only the assumptions for Midsize Base (Non Performance) vehicle are highlighted. The midsize base vehicle characteristics are as shown in Table 2.

Table 2. Vehicle characteristics for Midsize (Non Performance) FCEV

Vehicle Attributes	Value
Vehicle mass (kg)	1,653
Drag coefficient	0.300
Rolling resistance	0.0090
Frontal area (m ²)	2.35

Fuel Cell Assumptions

Figure 1 illustrates the main assumptions for fuel cell vehicles from 2020 to 2045 lab years. The assumptions reflect the “high” technology progress case only.

Fuel Cell Assumptions [Preliminary]

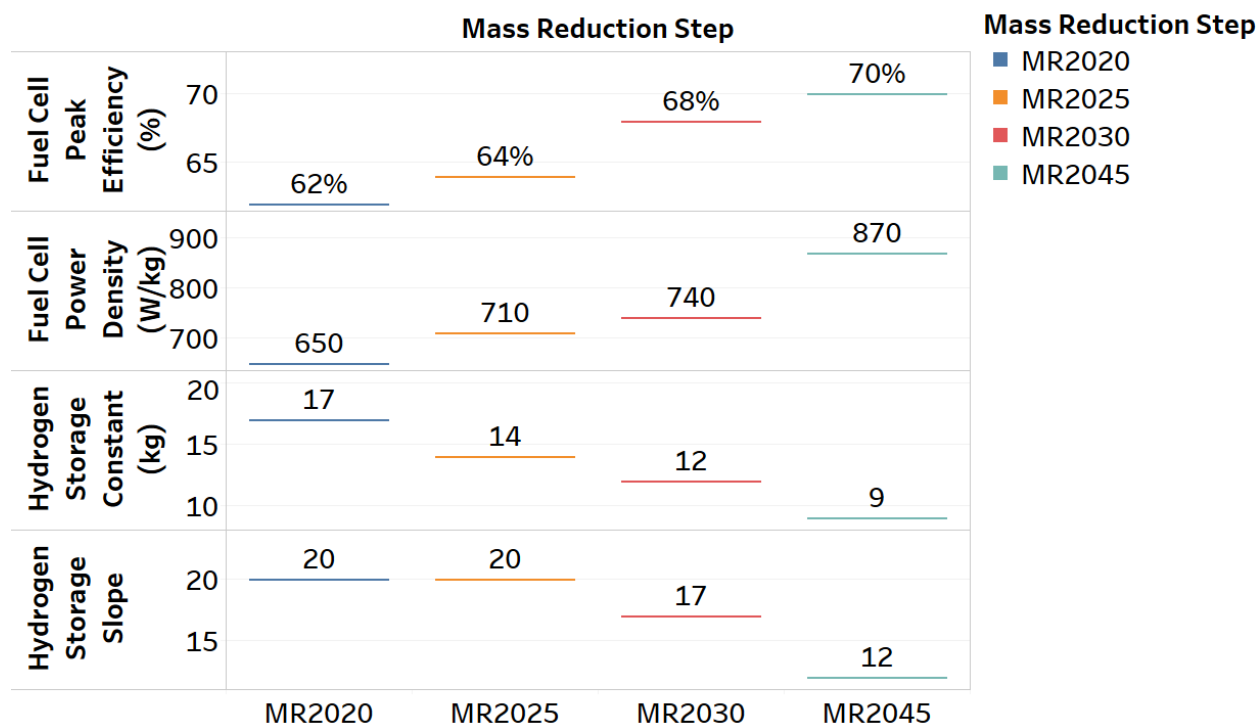


Figure 1. Fuel cell assumptions

RESULTS

Simulation Results

For simplicity of the analysis, only the midsize vehicle results (for both performance categories) are displayed in this section. Figure 2 shows the simulation results for midsize fuel cell vehicles from 2020 to 2045 lab years, followed by effectiveness of the same across lab years in Figure 3. For each lab year, the technologies that are expected to be available are implemented on the vehicle, and the power and energy requirements of various components are revised based on the sizing logic. For example, a lighter hydrogen tank will make the vehicle lighter, and this would help in reducing the fuel cell power and onboard hydrogen requirements.

To quantify the impact of the technologies we look at the reduction in fuel cell power requirement and improvement in overall fuel economy. Figure 3 shows the impact of the technology changes from 2020 to 2045. Fuel cell power requirement drops by about 20% for the midsize sedans if technology progresses as we assume. This would result in about 40% mass reduction of the fuel cell system. The lighter vehicle and more efficient component will improve the fuel economy of the vehicles. The fuel economy on city driving (UDDS) improves by about 37% and that on highway driving (HWFET) improves by about 29%. In a similar manner the effectiveness impact is quantified for all vehicles considered in this study.

Fuel Cell Simulation Results [Preliminary]

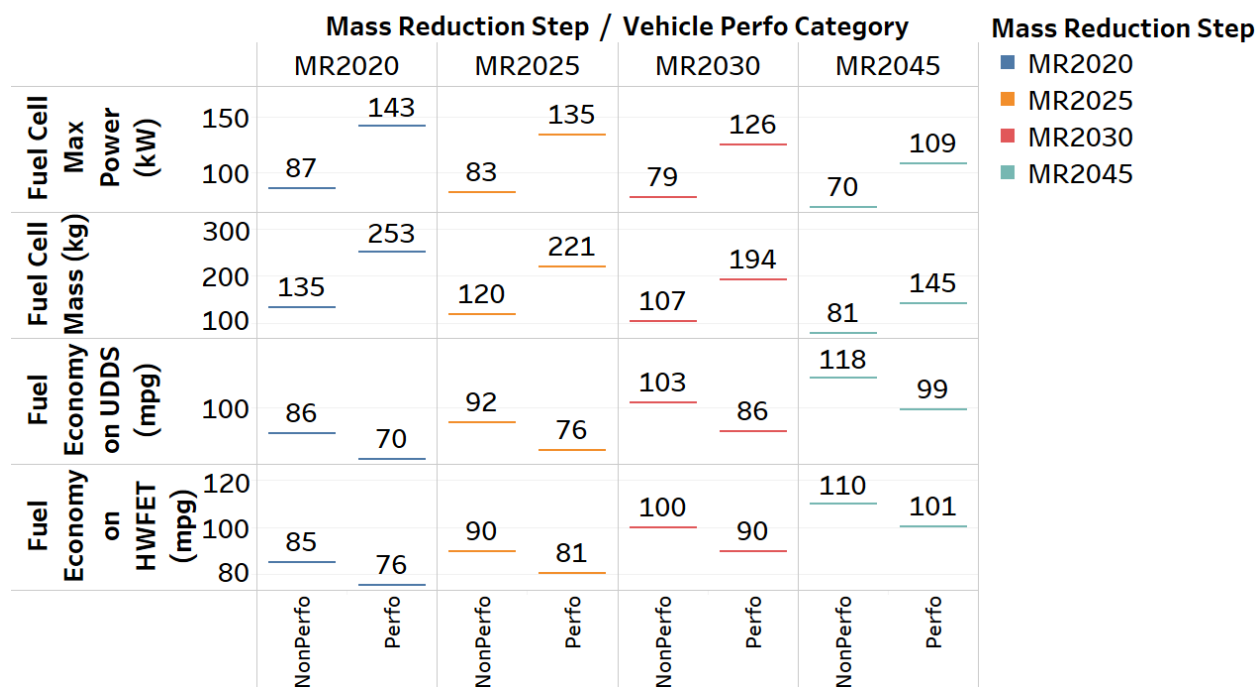


Figure 2. FCEV results across lab years for midsize vehicle class

Fuel Cell Simulation Results Analysis [Preliminary]

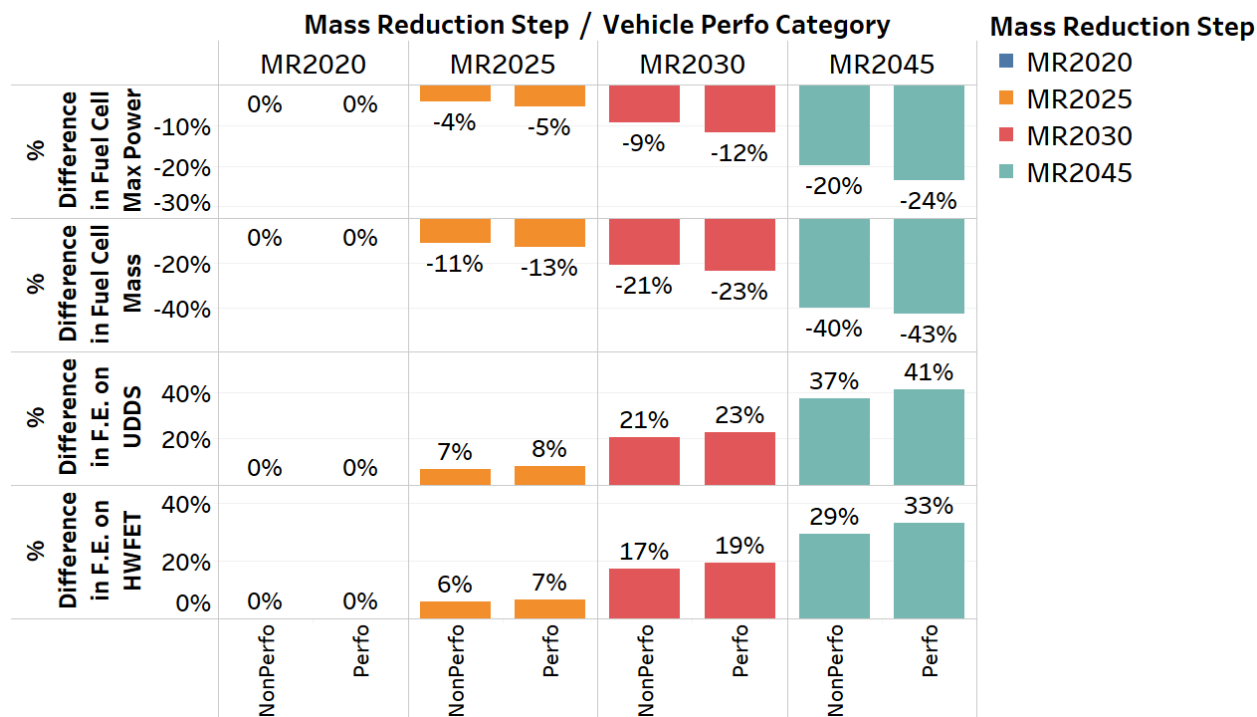


Figure 3. FCEV effectiveness across lab years for midsize vehicle class

Medium- and Heavy-Duty Vehicles

The analysis of medium- and heavy-duty vehicles follows the same methodology as in the case of the light duty vehicles. It starts with technology improvement assumptions. While light-duty fuel cell assumptions have been widely reviewed and agreed upon by experts from DOE and industry, such assumptions are under development and review for FCETs. The workshop organized by FCTO at Argonne to identify the barriers and challenges to the use of fuel cells in trucks was a useful step toward developing these assumptions.

Technology Progress Assumptions for Trucks

Prior work from Argonne had shown that the cost reduction of fuel cells and storage systems is more important than the improvements in efficiency or weight for light-duty applications. This may not be entirely applicable to the commercial vehicle segment, as cargo weight and volume is of critical importance in this application. In the case of both fuel cell and storage technologies, the impact of any present investment is not expected for the year 2020. The ‘low’ case estimates the technology progress without any DOE involvement, and the ‘high’ case sets the goals DOE is expected to achieve. All the years shown here are production years.

Figure 4 shows the assumptions made on fuel cell technology goals for the future. While light-duty systems have cost goals of ~\$40/kW by 2025, the commercial vehicle fuel cells are likely to cost a lot more due to the much tougher operational and durability requirements. Figure 5 shows the hydrogen storage goals. The light-duty vehicle tank costs are estimated for storing 5–6 kg of hydrogen. Prior work on FCETs has shown that a 15 kg tank could meet the operational requirements of a wide variety of trucks, and two such tanks could store enough hydrogen to cover almost all applications except the Class 8 line-haul trucks, so the tank costs are estimated for 15 kg of hydrogen storage. The assumptions and equations related to the storage pressure, material design, and cost are kept the same as in the light duty BaSce analysis.

Preliminary Fuel Cell Assumptions

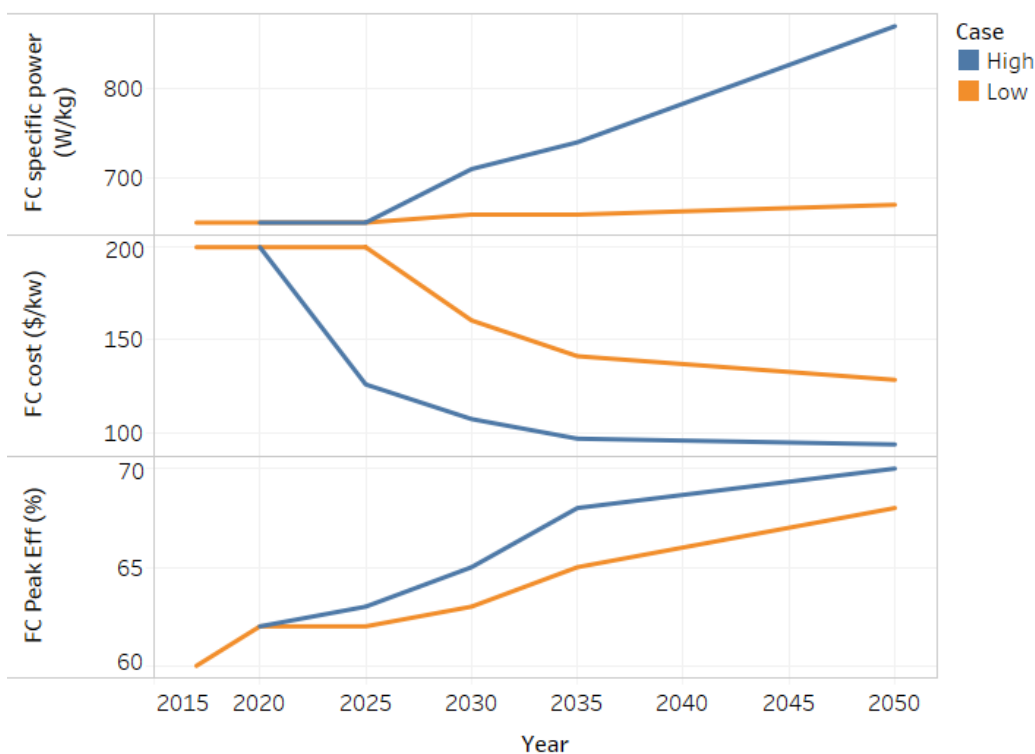


Figure 4. Fuel cell assumptions for trucks

Preliminary Storage Assumptions

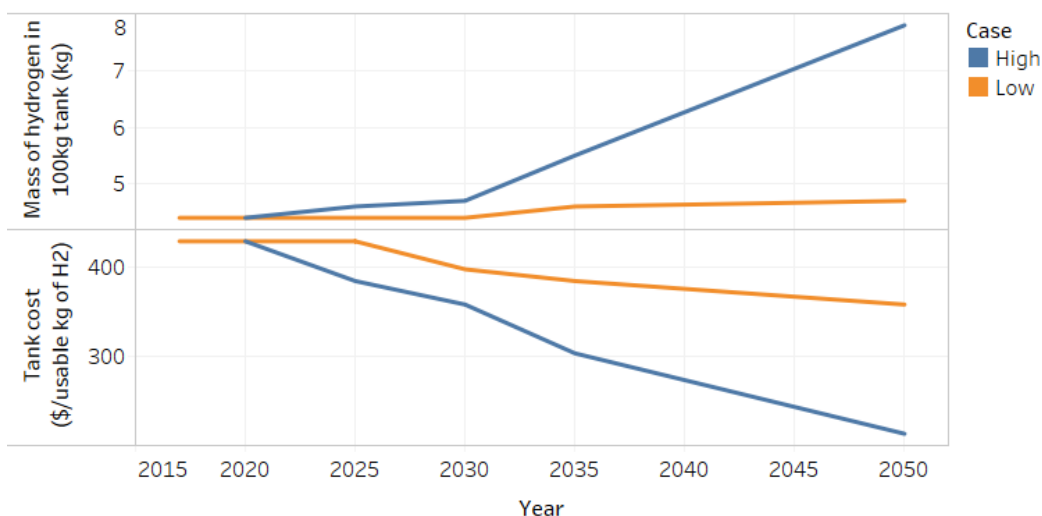


Figure 5. Storage technology assumptions for trucks

Vehicle Assumptions

For analysis, two vehicles are identified from the vast array of commercial vehicles. Class 4 delivery vehicles and Class 8 line-haul trucks are chosen to evaluate the impact of technology. They are two extreme cases in terms of the operational requirements. A Class 4 delivery truck normally runs under 100 miles a day and returns to its operational base at least once a day. The yearly driving distance is typically within 15,000 miles. As vehicle miles traveled is low, fleets tend to own such trucks for a long time, and 10- to 15-year-old trucks are not uncommon in this use case (e.g., last-mile delivery trucks of USPS, UPS, FedEx). The line-haul trucks have entirely different operational requirements. They should be able to drive at least 500 miles without stops to be commercially competitive. They should also be able to drive more than 100,000 miles a year and should have a useful life over 1 million miles. In both cases, the weight and volume of the fuel cell system is critical. It should not reduce the cargo carrying capacity of these vehicles.

Vehicle performance requirements for these vehicles are shown in Table 3.

Table 3. Performance Requirements from Medium- and Heavy-Duty vehicles

Class	Purpose	0-30 mph (s)	0-60 mph (s)	6% grade speed (mph)	Max. Speed (mph)	Daily Driving Range (miles)
4	Delivery	10	28.5	40	70	150
8	Tractor	18	66	30	65	500

As part of the BaSce analysis, conventional, hybrid, plug-in, and electric vehicles are also evaluated along with FCETs. All these vehicles have to achieve or exceed the above-mentioned performance requirements.

Sizing Process

Sizing process is adapted from the methodology developed for another FCTO-funded study [2]. The vehicle models are developed using Autonomie [3]. The recent workshop conducted by FCTO at Argonne on identifying the barriers for FCETs also informed this process. While the earlier method accounted for sizing one vehicle using off-the shelf components, this new analysis extends it to using projected technology improvements.

A full report on sizing and fuel consumption estimates will only be ready after the simulations for energy consumption are carried out. A preliminary draft is being prepared and expected to be issued by Q2 of FY19.

CONCLUSIONS AND UPCOMING ACTIVITIES

On light-duty vehicles, this study shows the relation between improvement in technology and the benefits realized at the vehicle level. By 2050, the fuel cell size requirements will come down by ~20% for midsize cars. The improvement in efficiency and reduction in mass could result in 30%–40% improvement in fuel economy.

On medium- and heavy-duty vehicles, the assumptions for technology improvements and cost are under review. The sizing process is published and reviewed. The detailed analysis of energy consumption and ownership costs will be available after the simulations are completed. This is expected by mid FY19.

FY 2018 PUBLICATIONS/PRESENTATIONS

1. E. Islam, N. Kim, A. Moawad, and A. Rousseau. *An Extensive Study on Sizing, Energy Consumption, and Cost of Advanced Vehicle Technologies*. Report to the U.S. Department of Energy. ANL/ESD-17/17 (August 2018).

REFERENCES

1. E. Islam, N. Kim, A. Moawad, and A. Rousseau. *An Extensive Study on Sizing, Energy Consumption, and Cost of Advanced Vehicle Technologies*. Report to the U.S. Department of Energy. ANL/ESD-17/17 (August 2018).
2. J. Marcinkoski et al. “Medium and Heavy Duty Fuel Cell Electric Truck Component Sizing.” Presented at EVS 2017, Canada.
3. Autonomie, available from www.autonomie.net.

Sustainability Analysis: Hydrogen Regional Sustainability (HyReS)

Elizabeth Connelly (Primary Contact),
Chad Hunter, Maggie Mann
National Renewable Energy Laboratory (NREL)
15031 Denver West Parkway
Golden, CO 80401
Phone: (303) 275-3836
Email: Elizabeth.Connelly@nrel.gov

DOE Manager: Fred Joseck
Phone: (202) 586-7932
Email: Fred.Joseck@ee.doe.gov

Project Start Date: October 1, 2015
Project End Date: September 30, 2018

Overall Objectives

- Develop a regional hydrogen sustainability analysis (HyReS) assessment framework that can be applied to hydrogen supply and fuel cell systems and is consistent with a broad range of existing sustainability assessment tools used by relevant stakeholders.
- Apply the framework as an enhancement to the existing suite of hydrogen systems analysis models developed for the Fuel Cell Technologies Office (FCTO).
- Refine the framework to incorporate the latest developments in the field of sustainable development assessment, including recent data and analytic approaches, and to capture current issues relevant to key stakeholders.
- Implement the framework through a user interface that is accessible to target audiences, including private sector sustainability managers, industry stakeholders, government and non-government agencies, and potential investors.

Fiscal Year (FY) 2018 Objectives

- Complete HyReS framework as part of the Scenario Evaluation and Regionalization Analysis (SERA) modeling outputs.

- Assess scenarios corresponding to H2USA light-duty vehicle demand, H2@Scale hydrogen demand, and FCTO Multi-Year Research, Development, and Demonstration (MYRDD) Plan targets.
- Benchmark the full life cycle impacts of 400-mile range fuel cell electric vehicles (FCEVs) against conventional vehicles, hybrid electric vehicles (HEVs), and battery electric vehicles (BEVs) that are modeled to have a 400-mile range using the Future Automotive Systems Technology Simulator (FASTSim).
- Apply the Sustainability Accounting Standards Board (SASB) framework to HyReS results to address the business community perspective.

Technical Barriers

This project addresses the following technical barriers from the Systems Analysis section of the FCTO MYRDD Plan¹:

- Future Market Behavior
- Stove-piped/Siloed Analytical Capability
- Insufficient Suite of Models and Tools.

Contribution to Achievement of DOE Systems Analysis Milestones

This project will contribute to achievement of the following DOE milestones from the Systems Analysis section of the FCTO MYRDD Plan:

- Milestone 1.19: Complete analysis of the potential for hydrogen, stationary fuel cells, fuel cell vehicles, and other fuel cell applications such as material handling equipment including resources, infrastructure and system effects resulting from the growth in hydrogen market shares in various economic sectors. (4Q, 2020)
- Milestone 2.2: Annual model update and validation. (4Q, 2011 through 4Q, 2020)

¹ <https://www.energy.gov/eere/fuelcells/downloads/fuel-cell-technologies-office-multi-year-research-development-and-22>

FY 2018 Accomplishments

- Developed and implemented an analytic framework that integrates Argonne National Laboratory's Greenhouse gases, Regulated Emissions, and Energy use in Transportation (GREET) model and the National Renewable Energy Laboratory's SERA, Automotive Deployment Options Projection Tool (ADOPT), and FASTSim models, updating results to reflect current model capabilities (Milestone 2.2).
- Compared petroleum fuel impacts from the four FCEV case study life cycles to the life cycle impacts from conventional gasoline vehicles, HEVs, and BEVs all with 400-mile range. Results indicate the FCEVs require the least amount of petroleum over the vehicle life cycle.
- Calculated monetized social benefits air pollution reductions associated with FCEV adoption in the H2USA scenarios. Benefits range from \$1.2 billion to \$2.2 billion from the Urban Markets to the State Success scenarios, respectively.

INTRODUCTION

The Hydrogen Regional Sustainability (HyReS) project examines environmental burdens in a regional life cycle assessment approach that takes into account the economic and social aspects of hydrogen supply chains and FCEV production and operation. The HyReS framework enhances, extends, and complements the capabilities of a number of analytic models developed for the U.S. Department of Energy, including the SERA and GREET models [1–3]. The HyReS framework will also incorporate data and analytic capabilities from other models relevant to sustainability assessment, such as the Billion-Ton Study [4], the Renewable Electricity Futures (REF) Study [5], and the Estimating Air pollution Social Impact Using Regression (EASIUR) model [6]. The integrated framework will address a number of sustainability metrics, such as petroleum and fossil fuel energy usage, water usage, life cycle costs, and air pollution emissions and the impacts on human health.

Progress to date has involved reviewing the sustainability literature and engaging with stakeholders to better understand how the HyReS framework can interface with and be useful to key stakeholders. The result is a set of proposed HyReS indicators, which include “material” sustainability factors identified by SASB to inform investors [7]. The HyReS framework is integrated into the SERA modeling capabilities and is being used in scenario analysis of the H2USA [8] and H2@Scale [9] demand scenarios. Additionally, the FASTSim model [10] is used to simulate FCEVs, conventional vehicles, HEVs, and BEVs all with a 400-mile range and similar performance attributes for a more apples-to-apples comparison of future vehicle life cycle impacts.

APPROACH

In order to assess regional sustainability impacts of hydrogen supply to FCEVs, HyReS relies upon an analytical framework that integrates the following capabilities: hydrogen demand based upon a detailed geospatial vehicle stock model (SERA) [2], optimized, least-cost hydrogen infrastructure supply chain networks (SERA) [1], life cycle fuel and vehicle impacts based upon GREET [3], market adoption of FCEVs based upon the ADOPT model [8,11], and a health benefits mapping and analysis of criteria pollutant emissions using the EASIUR model [6].

The HyReS framework is used to compare the three H2USA [8] scenarios: Urban Markets, State Success, and National Expansion. Estimating gasoline displacement (and using petroleum and water intensity for a gallon of gasoline) for each scenario results in calculations of net petroleum and water consumption. In addition, sensitivity scenarios relating to FCTO MYRDD goals and REF scenario electric grid mixes are assessed for the “State Success” scenario. The FASTSim model [10] is used to simulate model year (MY) 2010 and 2025 vehicles with a range of 400 miles, and the petroleum consumption over the lifecycle of various vehicle-fuel systems are compared.

RESULTS

Using FASTSim to model MY 2010 and MY 2025 vehicles with 400-mile ranges of similar size and performance, there is an increase in the vehicle cycle energy intensity of the GREET-default BEV300 to the modeled BEV400. On the other hand, because the total vehicle weights of the other FASTSim-modeled vehicles are less than the GREET-default weights, the vehicle cycle energy intensity for the FASTSim-based FCEV, ICEV, and HEV is less, especially for MY 2025. Based on the FASTSim results for MY 2025 vehicles, FCEVs require the least amount of petroleum fuel over the vehicle cycle. Figure 1 presents the lifecycle (A) petroleum and (B) water intensity of the GREET-default vehicles and the FASTSim-based vehicles for MY 2025. Looking at the yellow section indicating the vehicle cycle portion, it is clear that the vehicle cycle water consumption is more variable across vehicle types than petroleum consumption, where ICEVs and HEVs have the lowest vehicle cycle water consumption, though FCEVs consume less water than BEVs.

FASTSim results on the estimated fuel economies of the 400-mile range vehicles is used to calculate the fuel cycle (fuel production and vehicle operation) impacts. The red and blue portions of Figure 1 show the fuel cycle (A) petroleum and (B) water consumption of MY 2025 400-mile-range vehicles. The results show that the FCEV with hydrogen produced from wind electrolysis results in the least consumption of both. The FCEVs

and BEVs, regardless of fuel feedstock, realized approximately 95% reductions in life cycle petroleum consumption when compared to conventional gasoline ICEVs. On the other hand, the vehicles fueled by corn, corn stover, poplar, or grid electricity are estimated to consume more water over the vehicle lifetime than conventional ICEVs.

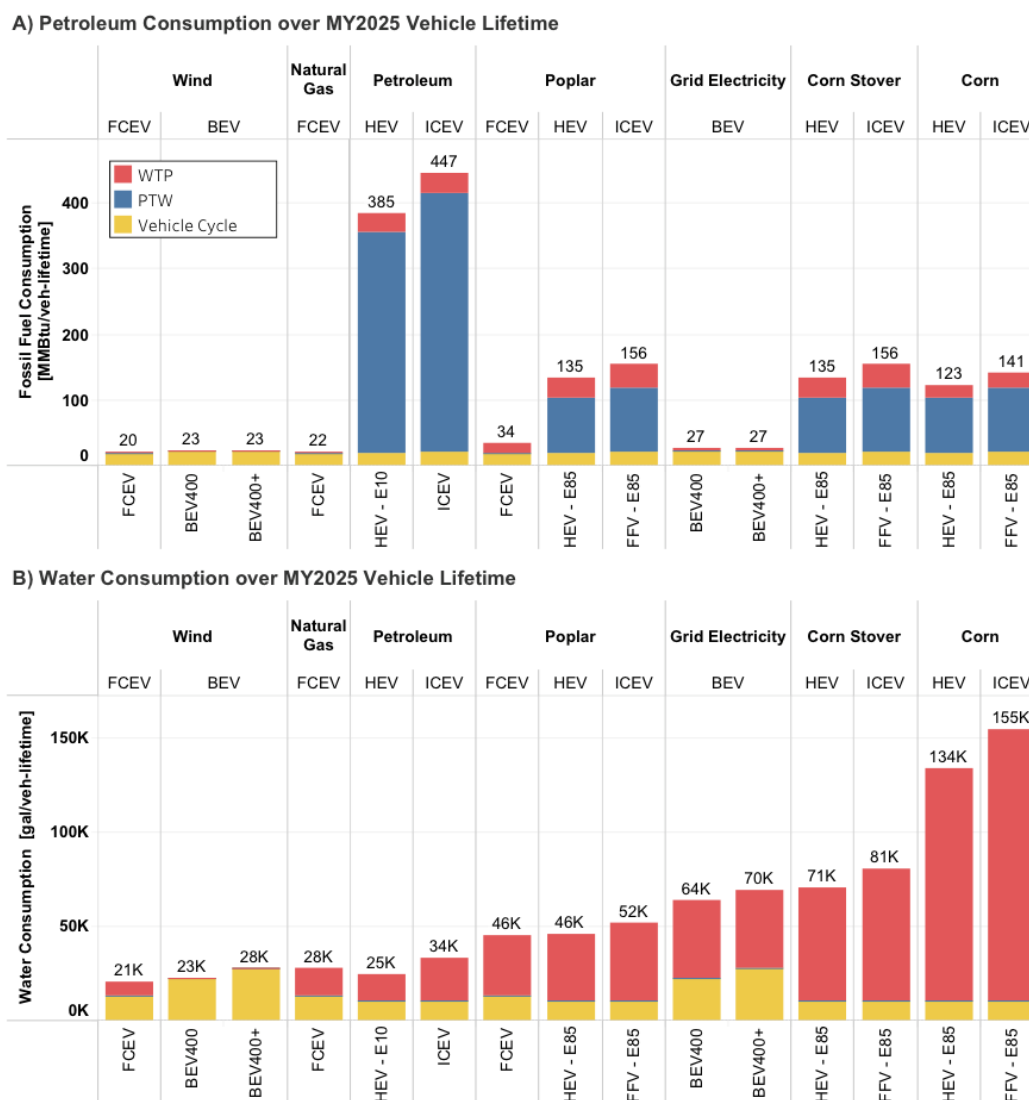


Figure 1. Life cycle (A) petroleum and (B) water consumption for MY 2025 vehicles modeled by FASTSim

The monetized health impacts of the three H2USA demand scenarios were calculated using the EASIUR model. Table 1 describes the cumulative (2016–2040) hydrogen demand for FCEVs in each scenario, along with the calculated emissions reductions and total monetized benefits. Figure 2 shows the geographical distribution of monetized benefits of displacing gasoline miles with hydrogen vehicle miles. Despite the National Expansion scenario displacing the most gasoline miles, the concentration of hydrogen-based miles in population centers in the State Success scenario results in the highest public health benefits.

Table 1. Air Pollution, Petroleum Reductions, and Water Consumption Results for the H2USA Demand Scenarios from 2016–2040

	Urban Markets	State Success	National Expansion
Hydrogen Consumption (kg)	5.0B	7.8B	12.4B
NO _x Reduction (tonnes)	37,000	67,000	105,000
PM _{2.5} Reduction (tonnes)	1,600	2,800	4,500
Monetized Public Health Benefit (\$)	\$1.23B	\$2.21B	\$1.70B
Net Petroleum Displacement (gallons)	13.2B	20.6B	33.7B
Net Water Consumption (gallons)	8.1B	3.8B	6.1B

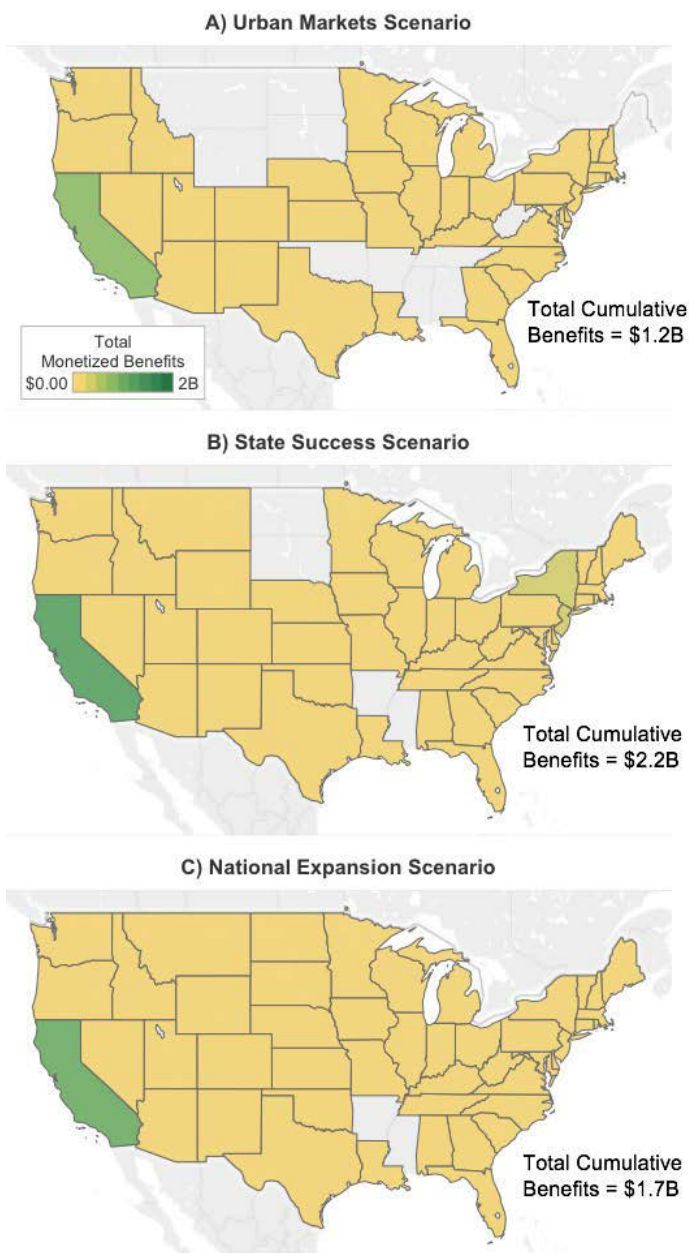


Figure 2. Map of the cumulative (2015–2040) monetized air quality benefits of the H2USA FCEV demand scenarios: (A) Urban Markets, (B) State Success, (C) National Expansion

Figure 3 compares the hydrogen infrastructure modeled for each H2USA scenario. Some combination of existing steam methane reforming (SMR) and new onsite SMR, and central SMR facilities is chosen as the least-cost option for hydrogen production in each of the H2USA scenarios. In each scenario, the most hydrogen is transported via gaseous hydrogen pipeline. However, the liquid truck delivery pathways are actually the longest in length.

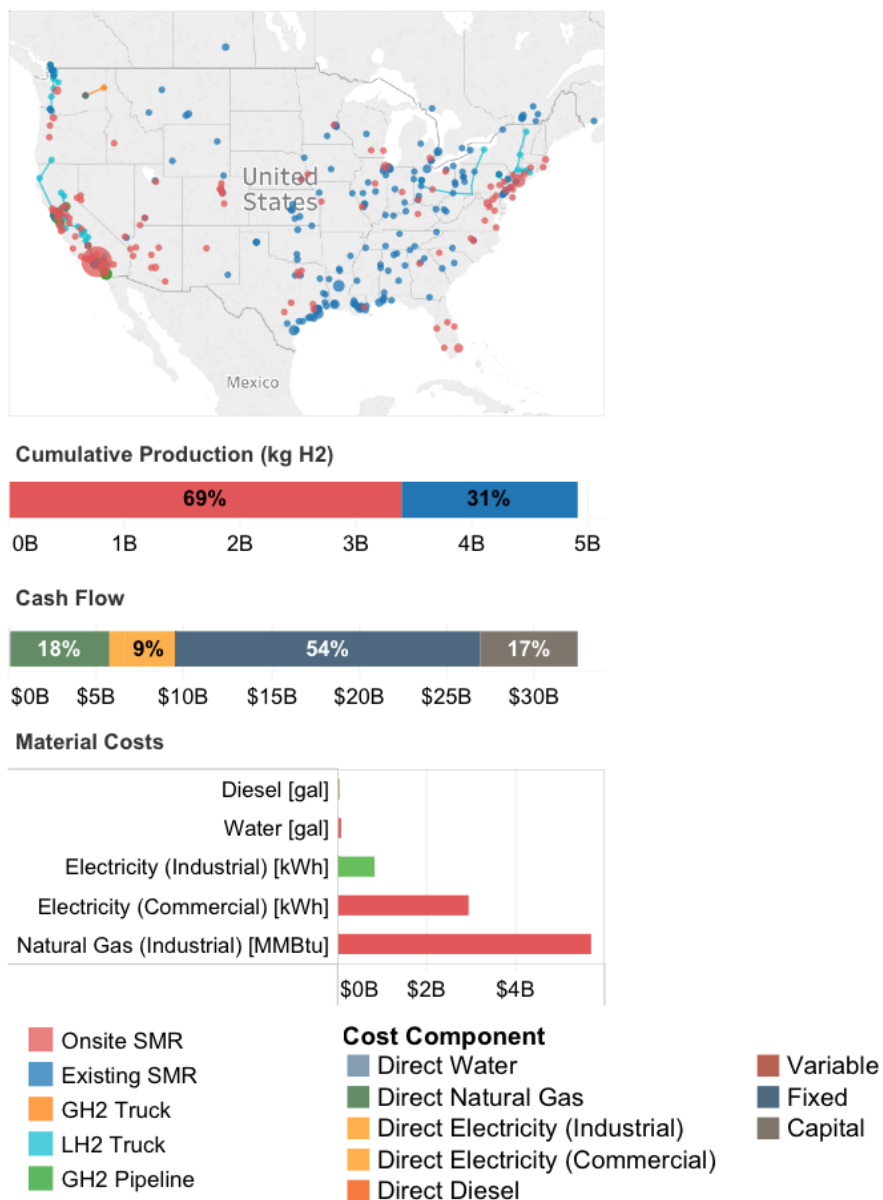


Figure 3. Network infrastructure for hydrogen production and transportation and energy consumption by technology (2016–2040) for the H2USA FCEV demand scenarios: (A) Urban Markets, (B) State Success, (C) National Expansion

Table 1 also describes the SERA model results of cumulative net petroleum displacement and net water consumption for the least-cost infrastructure buildout for each H2USA scenario. Despite the use of diesel for gaseous and liquid truck delivery, there is an increase in petroleum displacement in all of the scenarios. On the other hand, the upstream water consumption embodied in natural gas, electricity, and diesel in combination with direct water consumption for SMR results in a net water consumption in each of the scenarios. Figure 4 describes the net water consumption (upstream and direct consumption, as well as displacement based on the

water intensity of gasoline) and the locations of direct water consumption for each scenario. Interestingly, the net water consumption is the least in the State Success scenario. In all scenarios, there is an increase in direct water consumption in California. In the higher demand scenarios (State Success and National Expansion) there is also an increase in water consumption in the northeast, around New York City, as well as near the Gulf Coast in Texas and Louisiana.

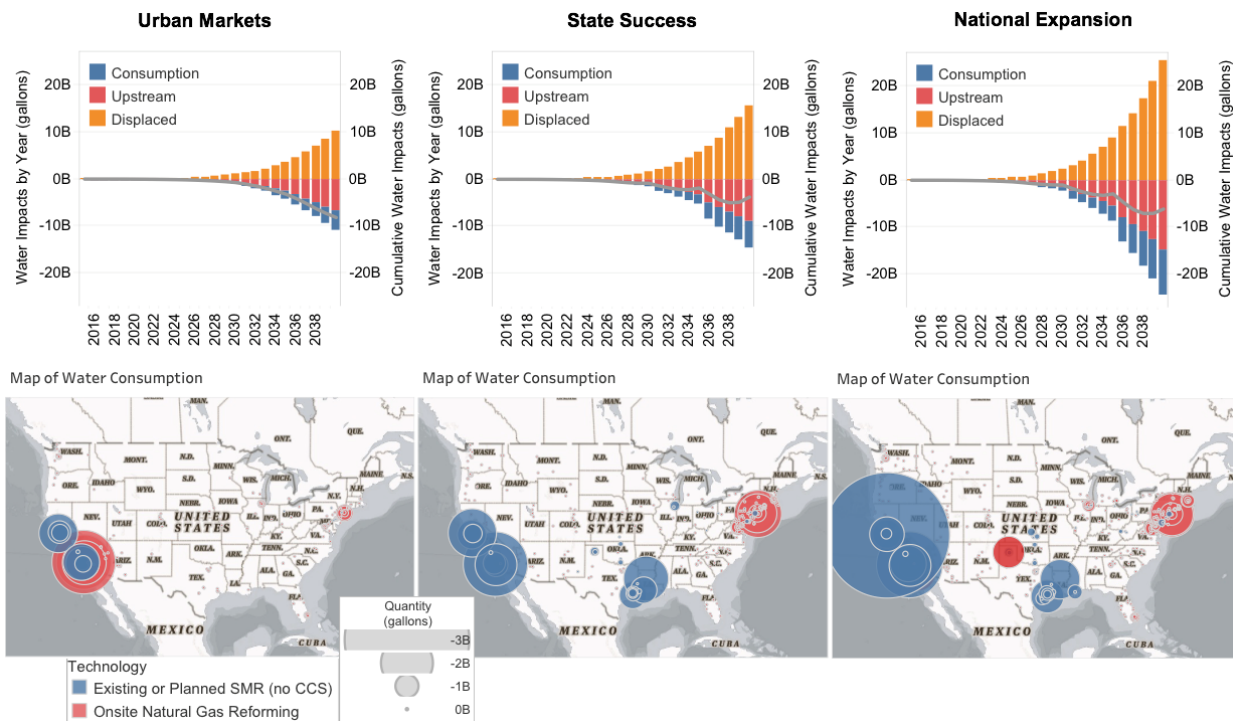


Figure 4. Net and direct water consumption for the H2USA FCEV demand scenarios: Urban Markets, State Success, National Expansion

CONCLUSIONS AND UPCOMING ACTIVITIES

Displacement of gasoline with hydrogen light-duty vehicles results in reductions in petroleum fuel consumption when considering the life cycle of FCEVs relative to ICEVs with comparable vehicle attributes as well as when considering the least-cost infrastructure needed to produce and deliver hydrogen to refueling stations. Water consumption over the life cycle of 400-mile range FCEVs is similar to gasoline ICEVs, and when the upstream and direct consumption for the least-cost infrastructure is considered, net consumption is predicted. Direct water consumption tends to be mostly located around demand centers (highly populated cities) such as Los Angeles, San Diego, New York, and San Francisco, where new and existing SMR facilities are expected to produce hydrogen.

In all three H2USA demand scenarios, air pollution reductions resulted and are estimated through the avoidance of exhaust emissions of gasoline light-duty vehicles. The monetized human health impacts of these reductions (from 2016–2040) are between \$1 billion and \$2 billion. Across all scenarios, over half of the cumulative monetized benefits are accrued in California, where there are a number of population-dense areas.

The air quality benefits of FCEVs are a major reason why applying the SASB framework to compare hydrogen and gasoline production as automotive fuels indicates that hydrogen companies will likely perform relatively better. When comparing across hydrogen production technologies, greenhouse gas emissions, water intensity, (fossil) energy intensity, and price/affordability also become differentiating factors. The HyReS framework can be used to address these and other factors to inform investment decisions on a spatio-temporal basis.

Future work using the SERA model will have HyReS capabilities to enable sustainability analysis for hydrogen production scenarios, including the H2@Scale analysis.

The figures of this report and others were created in Tableau and can be published online to inform stakeholders of the results of the H2@Scale scenario, H2USA scenarios (presented here), and sensitivity scenarios. Metrics addressed in the Tableau workbooks include detailed costs, energy consumption, water consumption, and emissions. Future work will include applying the HyReS framework to the next phases of H2@Scale analysis and other scenarios run with the SERA model. Future refinements could include vehicle emissions data to expand on the human health impacts.

FY 2018 PUBLICATIONS/PRESENTATIONS

1. Connelly, E. “Sustainability Analysis: Hydrogen Regional Sustainability (HyReS).” Presentation at the 2018 Annual Merit Review and Peer Evaluation Meeting, June 13, 2017, Washington, DC. https://www.hydrogen.energy.gov/pdfs/review18/sa059_connelly_2018_o.pdf.

REFERENCES

1. M. Melaina. “SERA Scenarios of Early Market Fuel Cell Electric Vehicle Introductions: Modeling Framework, Regional Markets, and Station Clustering.” NREL/PR-5400-64395. Presented at the 2015 ICEPAG Conference, Irvine, CA, March 23, 2015. <http://www.nrel.gov/docs/fy15osti/64395.pdf>.
2. B. Bush, M. Melaina, M. Penev, and W. Daniel. *SERA Scenarios of Early Market Fuel Cell Electric Vehicle Introductions*. NREL/TP-5400-56588 (Golden, CO: National Renewable Energy Laboratory, 2013). <http://www.nrel.gov/docs/fy13osti/56588.pdf>.
3. A. Elgowainy, D. Dieffenthaler, V. Sokolov, R. Sabbisetti, C. Cooney, and A. Anjum. *The Greenhouse gases, Regulated Emissions, and Energy use in Transportation (GREET) Model (v1.3.0.13081)*. [Software] (Argonne National Laboratory, 2013). <https://greet.es.anl.gov/>.
4. DOE. *2016 Billion-Ton Report: Advancing Domestic Resources for a Thriving Bioeconomy, Volume 1: Economic Availability of Feedstocks*. M.H. Langholtz, B. J. Stockes, and L. M. Eaton (Leads), ORNL/TM-2016/160 (Oak Ridge, TN: Oak Ridge National Laboratory, 2016). doi: 10.2172/1271651. <http://energy.gov/eere/bioenergy/2016-billion-ton-report>.
5. NREL. *Renewable Electricity Futures Study*. Hand, M.M., Baldwin, S., DeMeo, E., Reilly, J.M., Mai, T., Arent, D., Porro, G., Meshek, M., Sandor, D. eds. 4 vols. NREL/TP-6A20-52409. (Golden, CO: National Renewable Energy Laboratory, 2012). http://www.nrel.gov/analysis/re_futures/.
6. J. Heo, P.J. Adams, and H. Gao. “Reduced-form modeling of public health impacts of inorganic PM2.5 and precursor emissions.” *Atmospheric Environment* 137 (2016): 80–89. <https://doi.org/10.1016/j.atmosenv.2016.04.026>.
7. Sustainability Accounting Standards Board (SASB). SASB Conceptual Framework (February 2017). <https://www.sasb.org/wp-content/uploads/2017/02/SASB-Conceptual-Framework.pdf>.
8. M. Melaina, B. Bush, M. Muratori, J. Zuboy, and S. Ellis. *National Hydrogen Scenarios: How Many Stations, Where, and When?* Prepared by the National Renewable Energy Laboratory for the H2USA Locations Roadmap Working Group (2017). http://h2usa.org/sites/default/files/H2USA_LRWG_NationalScenarios2017.pdf.
9. M. Ruth. “H2@Scale Analysis.” Presentation at the 2018 Annual Merit Review and Peer Evaluation Meeting, June 13, 2017, Washington, DC.
10. A. Brooker, J. Gonder, L. Wang, E. Wood, et al. “FASTSim: A Model to Estimate Vehicle Efficiency, Cost and Performance.” SAE Technical Paper 2015-01-0973 (2015). doi:10.4271/2015-01-0973.
11. A. Brooker, J. Gonder, S. Lopp, and J. Ward. “ADOPT: A Historically Validated Light Duty Vehicle Consumer Choice Model.” SAE Technical Paper 2015-01-0974 (2015). doi:10.4271/2015-01-0974.

Regional Supply of Hydrogen

Chad Hunter, Michael Penev (Primary Contact),
Brian Bush, Elizabeth Connelly
National Renewable Energy Laboratory
15013 Denver West Parkway
Golden, CO 80401
Phone: (303) 275-3880
Email: michael.penev@nrel.gov

DOE Manager: Fred Joseck
Phone: (202) 586-7932
Email: Fred.Joseck@ee.doe.gov

Project Start Date: October 1, 2016
Project End Date: September 30, 2018

Overall Objectives

- Evaluate hydrogen supply chain scenarios for fuel cell electric vehicles (FCEVs) using the Scenario Evaluation and Regionalization Analysis (SERA) model.
- Leverage existing hydrogen production supply and determine lowest-cost supply chain growth options conforming to hydrogen demand growth through 2040.
- Evaluate novel high-pressure intra-city hydrogen supply (HyLine) economic competitiveness and practicality.

Fiscal Year (FY) 2018 Objectives

- Update the SERA model with the latest production, distribution, and dispensing capital and maintenance and operating specifications from the H2A (Hydrogen Analysis) and HDSAM (Hydrogen Delivery Scenario Analysis Model) model suites.
- Perform high-level technology cost estimation of high-pressure hydrogen pipelines.
- Produce an algorithm for estimating high-pressure pipeline build-out in urban areas.
- Update SERA with regional energy cost projections.
- Disaggregate U.S. hydrogen growth regionally using H2USA scenarios.

- Use SERA model to generate least-cost hydrogen supply chains.
- Prepare a final report.

Technical Barriers

This project addresses the following technical barriers from the Systems Analysis section of the Fuel Cell Technologies Office Multi-Year Research, Development, and Demonstration Plan¹:

Technical Approach: Infrastructure Analysis

- A. Future Market Behavior: Scenarios to understand vehicle-fuel interactions
- E. Unplanned Studies and Analysis: Response to H2USA public-private partnership and infrastructure deployment goals.

Contribution to Achievement of DOE Systems Analysis Milestones

This project addresses the following technical barriers from Systems Analysis section of the Fuel Cell Technologies Office Multi-Year Research, Development, and Demonstration Plan:

- Milestone 1.16: Complete analysis of program performance, cost status, and potential use of fuel cells for a portfolio of commercial applications. (4Q, 2018)
- Milestone 1.17: Complete analysis of program technology performance and cost status, and potential to enable use of fuel cells for a portfolio of commercial applications. (4Q, 2018)

FY 2018 Accomplishments

- Produced optimization framework for supply chain deployment for more than 3,000 cities in the United States in 5-year investment increments through the year 2040 with the use of the SERA model. The optimization included a new algorithm for intra-urban pipeline distribution to hydrogen stations from semi-central hydrogen production units.

¹ <https://energy.gov/eere/fuelcells/downloads/fuel-cell-technologies-office-multi-year-research-development-and-22>

- Exercised the model over disaggregated hydrogen demand growth scenarios from H2USA: National Expansion (high demand growth), State Success (medium growth), and Urban Markets (low growth).
- Produced regionalized cost of hydrogen based on regionally optimal supply chains.
- Showed substantial potential for retail adoption and economic and functional advantage of employment of high pressure pipeline intra-city hydrogen distribution (HyLine).

INTRODUCTION

This project evaluates a least-cost hydrogen supply chain to meet the growing hydrogen demand from light-duty FCEVs using the SERA model. Existing and new production technologies as well as various conventional transmission, delivery, and dispensing technologies are competed economically to determine the lowest-cost supply chain. A high-pressure (~1,000 bar) hydrogen transmission and delivery pipeline network (HyLine) is proposed to reduce distribution costs and improve network reliability. Three demand scenarios were evaluated as well as constraining different production technologies and varying existing hydrogen plant capacity utilization and selling price.

APPROACH

This work examines the existing U.S. hydrogen production capacity as well as potential nearby Canadian hydrogen production import availability. This work then combines three scenarios of estimated market demand for hydrogen from light-duty FCEVs [1] with the existing hydrogen supply to determine the highest probability locations for the development of new hydrogen generation capacity and quantify the investment costs required. Lastly, a least-cost, temporally and spatially resolved hydrogen production and distribution network is modeled using the SERA model to meet the growing hydrogen demand through 2050 under each FCEV demand scenario.

To reduce hydrogen distribution costs, this work introduces a scalable, semi-distributed high-pressure intraurban pipeline production and distribution network system (HyLine). Various semi-central production sites connecting stations via intraurban pipelines can reduce costs while delivering reliability and scalability improvements to the hydrogen distribution system. Pipeline distribution is the most cost-effective, industrial-scale distribution pathway for hydrogen today and has been implemented within as well as between major refinery and other hydrogen user and production facilities. Thus, a network of hydrogen refueling stations is also expected to ultimately make use of this lowest-cost delivery pathway. Prior work for examining pipelines has looked at the long-term cost potential [2], and this work adds transition analysis for market penetration and timing of the technology.

RESULTS

Results show that average U.S. dispensed hydrogen cost is \$16/kg (2016 real dollars) in 2018 and decreases to \$4.60/kg by 2040 (see Figure 1).

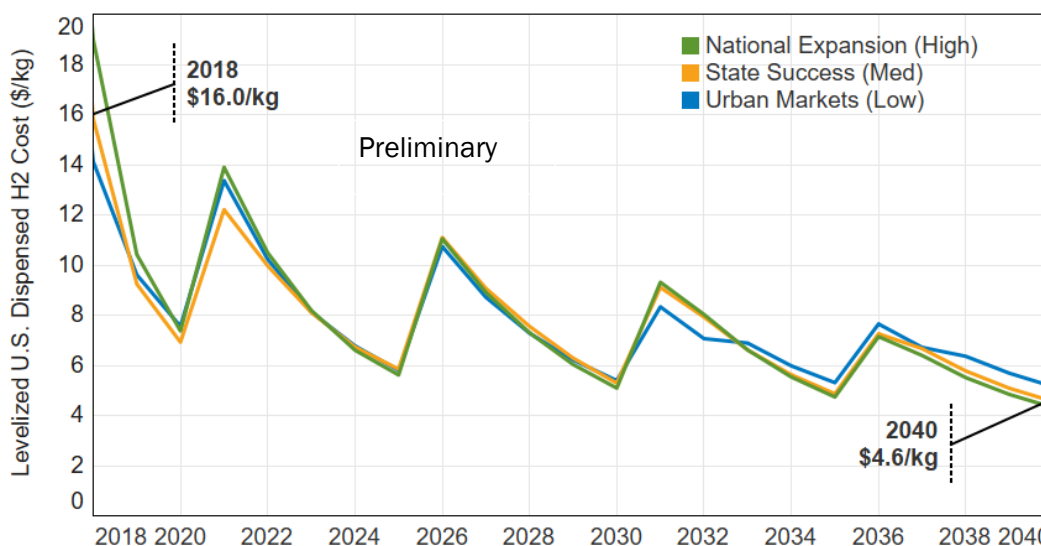


Figure 1. Average U.S. dispensed hydrogen cost for each light-duty vehicle demand scenario considered

SERA results, shown in Figure 2, indicate that existing hydrogen capacity in the Gulf Coast is used to meet demand in California while Northeast plants meet the large urban area demand around them. However, by 2030, new production plants are built both in the Northeast and in California to support the nearly 50 tonne/day hydrogen demand.

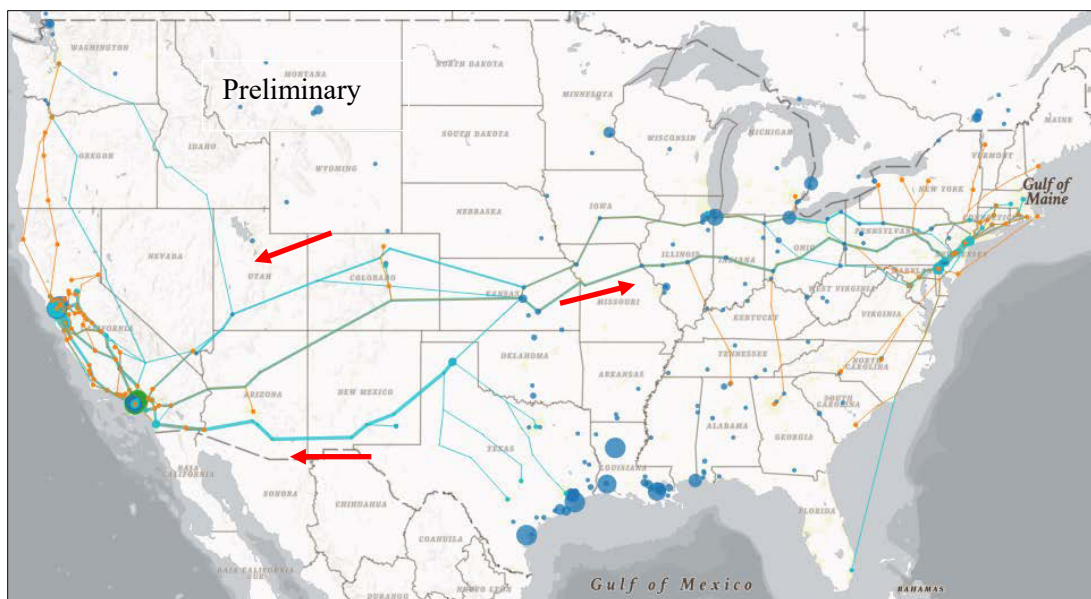


Figure 2. Hydrogen supply chain development over time for the State Success (Med) scenario. Infrastructure snapshot is of 2030.

Cumulative capital investment opportunity by 2040 is ~\$28 billion. Additionally, the growth of light-duty fuel cell electric vehicles results in the displacement of 4.0 billion gallons of gasoline each year. Lastly, the HyLine distribution pathway is shown to be economically competitive by 2030 with more than 50% of stations joining the pipeline network in eight urban areas by 2040 (see Figure 3).

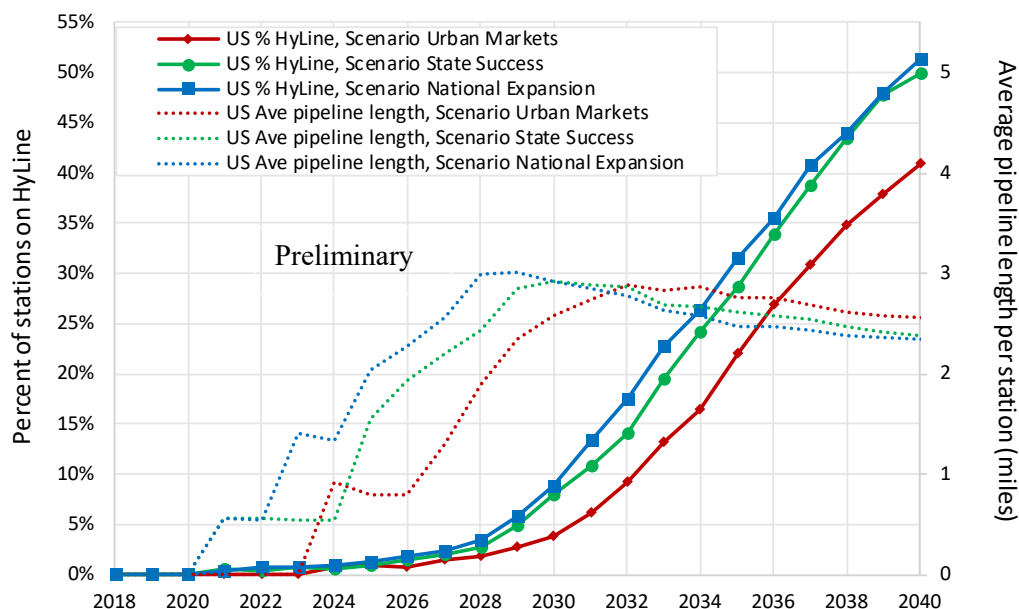


Figure 3. Estimated HyLine technology adoption over time for each demand scenario evaluated

CONCLUSIONS AND UPCOMING ACTIVITIES

The SERA model estimates that the average U.S. dispensed hydrogen cost is \$16/kg (2016 real dollars) in 2018 but drops to \$4.6/kg by 2040 driven by economies of scale. SERA results indicate that existing hydrogen capacity in the Gulf Coast is used to meet demand in California. However, by 2030, new production plants are built across the United States and concentrated in California and the Northeast to support the nearly 50 tonne/day hydrogen demand. Cumulative capital investment opportunity by 2040 is ~\$28 billion indicating a large market for new firms to enter the industry. Additionally, the growth of FCEVs results in the displacement of 4.0 billion gallons of gasoline each year. Finally, the HyLine distribution pathway is shown to be economically competitive by 2030 with more than 50% of stations joining the pipeline network in eight urban areas by 2040.

Future work seeks to further enhance modeling accuracy and realism and explicitly add renewable hydrogen production pathways. Items to consider would be identifying regionally specific land costs, incorporating existing pipeline infrastructure, adding non-vehicular hydrogen demand through the H2@Scale effort, which this modeling framework can readily implement, and evaluating the impact of renewable energy credits in regions that offer them.

FY 2018 PUBLICATIONS/PRESENTATIONS

1. M. Penev and C. Hunter, “Regional Supply of Hydrogen,” Project ID #SA063, U.S. Department of Energy Hydrogen and Fuel Cells Program 2018 Annual Merit Review and Peer Evaluation Meeting, Washington, DC, June 13–15, 2018.

REFERENCES

1. M. Melaina, B. Bush, M. Muratori, J. Zuboy and S. Ellis, *National Hydrogen Scenarios: How Many Stations, Where, and When?* Prepared by the National Renewable Energy Laboratory for the H2USA Locations Roadmap Working Group (2017), <https://www.nrel.gov/docs/fy18osti/71083.pdf>.
2. National Renewable Energy Laboratory, “SERA: Scenario Evaluation and Regionalization Analysis,” (2018), <http://nrel.github.io/sera/>.

Market Segmentation Analysis of Medium- and Heavy-Duty Trucks with a Fuel Cell Emphasis

Chad Hunter (Primary Contact), Michael Penev, and Brian Bush
National Renewable Energy Laboratory (NREL)
15013 Denver West Parkway
Golden, CO 80401
Phone: (303) 275-2925
Email: Chad.Hunter@nrel.gov

DOE Manager: Fred Joseck
Phone: (202) 586-7932
Email: Fred.Joseck@ee.doe.gov

Project Start Date: October 1, 2017
Project End Date: September 30, 2019

Overall Objectives

- Identify the most promising markets for medium-/heavy-duty vehicles using a systems analysis approach with established technology and cost targets.
- Assess technical barriers and opportunities for improvement in the medium-/heavy-duty fuel cell vehicle technology space to guide DOE investment in advanced technologies.

Fiscal Year (FY) 2018 Objectives

- Develop total cost of ownership (TCO) systems analysis framework to assess medium-/heavy-duty vehicles with advanced powertrain technology.
- Leverage existing systems analysis models including the Scenario Evaluation and Regionalization Analysis (SERA) model and the Future Automotive Systems Technology Simulation (FASTSim) model in the TCO analysis framework.
- Apply TCO analysis framework to Class 8 tractors and Class 4 parcel delivery trucks and draft report detailing key insights, areas of opportunity for fuel cell powertrain applications, and areas to focus research efforts and investments.

Technical Barriers

This project addresses the following technical barriers from the Systems Analysis section of the Fuel Cell Technologies Office Multi-Year Research, Development, and Demonstration Plan¹:

- Future Market Behavior
- Inconsistent Data, Assumptions and Guidelines
- Insufficient Suite of Models and Tools.

Contribution to Achievement of DOE Systems Analysis Milestones

This project will contribute to achievement of the following DOE milestones from the Systems Analysis section of the Fuel Cell Technologies Office Multi-Year Research, Development, and Demonstration Plan:

- Milestone 1.16: Complete analysis of program performance, cost status, and potential use of fuel cells for a portfolio of commercial applications. (4Q, 2018)
- Milestone 1.17: Complete analysis of program technology performance and cost status, and potential to enable use of fuel cells for a portfolio of commercial applications. (4Q, 2018)

FY 2018 Accomplishments

- Developed TCO systems analysis framework that includes both direct costs (purchase price, fuel, operating and maintenance) and indirect costs (dwell time costs due to refueling/recharging and payload opportunity costs from forgone revenue due to the truck being weight limited). By incorporating dwell time and payload opportunity costs, this analysis more accurately analyzes fuel cells for commercial applications (Milestones 1.16, 1.17) than previous studies.
- Completed comparative TCO evaluation of five different truck powertrain technologies (diesel,

¹ <https://www.energy.gov/eere/fuelcells/downloads/fuel-cell-technologies-office-multi-year-research-development-and-22>

diesel hybrid-electric, compressed natural gas, battery electric, and fuel cell electric) for three different truck applications (Class 8 long haul, Class 8 short haul, and Class 4 parcel delivery) and for different technology statuses (2018, 2020, 2040).

- Identified scenarios for fuel cell powertrain trucks to have the lowest TCO of all powertrains by 2020 if Fuel Cell Technologies Office program cost and performance targets are met. Analysis shows strong commercial application opportunities for fuel cell powertrains in Class 4 parcel delivery and Class 8 long haul trucking applications.

INTRODUCTION

The medium- and heavy-duty transportation sector is experiencing rapid changes in technology innovation. Alternative powertrains including fuel cell electric and battery electric have been announced within the last few years for truck applications across the medium- and heavy-duty spectrum [1–5]. Because trucks are primarily used for business applications, the value proposition associated with a truck is a key metric that helps determine if the truck technology will be adopted. The total cost of ownership (TCO) is a critical metric that firms use to assess the value proposition of a truck purchase. Although not the only metric a business will consider, the TCO provides a simple benchmark that allows for direct comparison across different truck options.

This project aims to provide a transparent, system analysis approach to medium- and heavy-duty vehicle TCO analysis to identify commercial vehicle applications that fuel cell powertrains may or may not be well suited for. By doing so, this analysis aims to provide insights and recommendations for stakeholders on which commercial vehicle applications could be pursued in the near term and potential barriers to adoption.

APPROACH

This project evaluates the TCO for three truck applications and five powertrains. The truck applications include Class 8 long haul (sleeper), Class 8 short haul (day cab), and Class 4 parcel delivery van. The powertrains analyzed are conventional (diesel), diesel hybrid-electric (HEV), compressed natural gas (CNG), fuel cell electric (FCEV), and battery electric (EV). The TCO includes all direct and indirect costs. Direct costs included in this analysis are the upfront purchase cost (segmented by powertrain component), taxes, regional fuel costs, and operating and maintenance costs. The indirect costs included in this analysis are dwell time costs due to refueling/recharging and payload opportunity costs (forgone revenue due to the truck being weight limited).

NREL's Future Automotive Systems Technology Simulator (FASTSim) model was used to build conventional vehicle models that match real-world performance and cost data including fuel economy, acceleration, and manufacturer's suggested retail price. FASTSim was then used to build cost-optimized powertrains for other powertrain technologies based on current costs and DOE future component performance and cost targets. Fuel costs were based on the 2018 Annual Energy Outlook and approximate hydrogen cost levels, operating and maintenance costs were based on an extensive literature survey, dwell time costs were based on stated carrier detention rates, and payload opportunity costs were based on typical less-than-truckload carrier rates observed today. All the cost data was input into the SERA model to compute the regional TCO for each truck application, powertrain, and model year.

RESULTS

Multiple scenarios were evaluated within this project. Under a scenario in which diesel and compressed natural gas prices are high while electricity and hydrogen prices are low (\$0.07/kWh and \$4/kg, respectively), the TCO for battery electric and fuel cell powertrains shows an advantage over diesel, HEV, and CNG by 2020. In this scenario, Class 8 long haul trucks (range requirement of 1,200 miles) with fuel cell powertrains could have a lower TCO than diesel by 2020 and may have the lowest TCO depending on the regional fuel prices that are considered. Figure 1 illustrates the TCO breakdown by powertrain technology for each model year analyzed across two U.S. census division regions. As seen in Figure 1, the Pacific region typically has higher fuel costs leading to higher TCO for diesel, diesel hybrid-electric, and CNG powertrains while electricity and hydrogen costs are assumed to be constant. This regional difference allows fuel cell powertrains to have the lowest TCO in the Pacific region while being slightly higher than CNG in the Middle Atlantic region.



Figure 1. Present value cost (\$/mile) for Class 8 long haul tractors traveling 100,000 mile/yr in the (top) Middle Atlantic and (bottom) Pacific region under the Low Electricity and Hydrogen Prices scenario

In the low electricity and hydrogen prices scenario, Class 8 short haul (range requirement of 500 miles) truck TCO follows a similar story as Class 8 long haul. By 2020, fuel cell electric powertrains are estimated to have the lowest TCO in certain high-fuel-cost regions such as the Pacific region. Figure 2 summarizes the Class 8 tractor TCO on a per-mile and per-ton-mile basis (where ton refers to the maximum tonnage of payload the truck can haul while remaining within the 80,000 lb gross vehicle weight rating) for the Pacific region as a function of vehicle range required.

As seen in Figure 2, by 2020 fuel cell and battery electric Class 8 tractors become very economically competitive with diesel powertrain technology. Additionally, under these conditions, fuel cell and battery powertrains dominate all Class 8 tractor ranges in 2040 with fuel cells being economically advantageous in the longer range requirement (>500 mile) regime and battery electric trucks being economically advantageous in the shorter range requirement (<500 mile) regime.

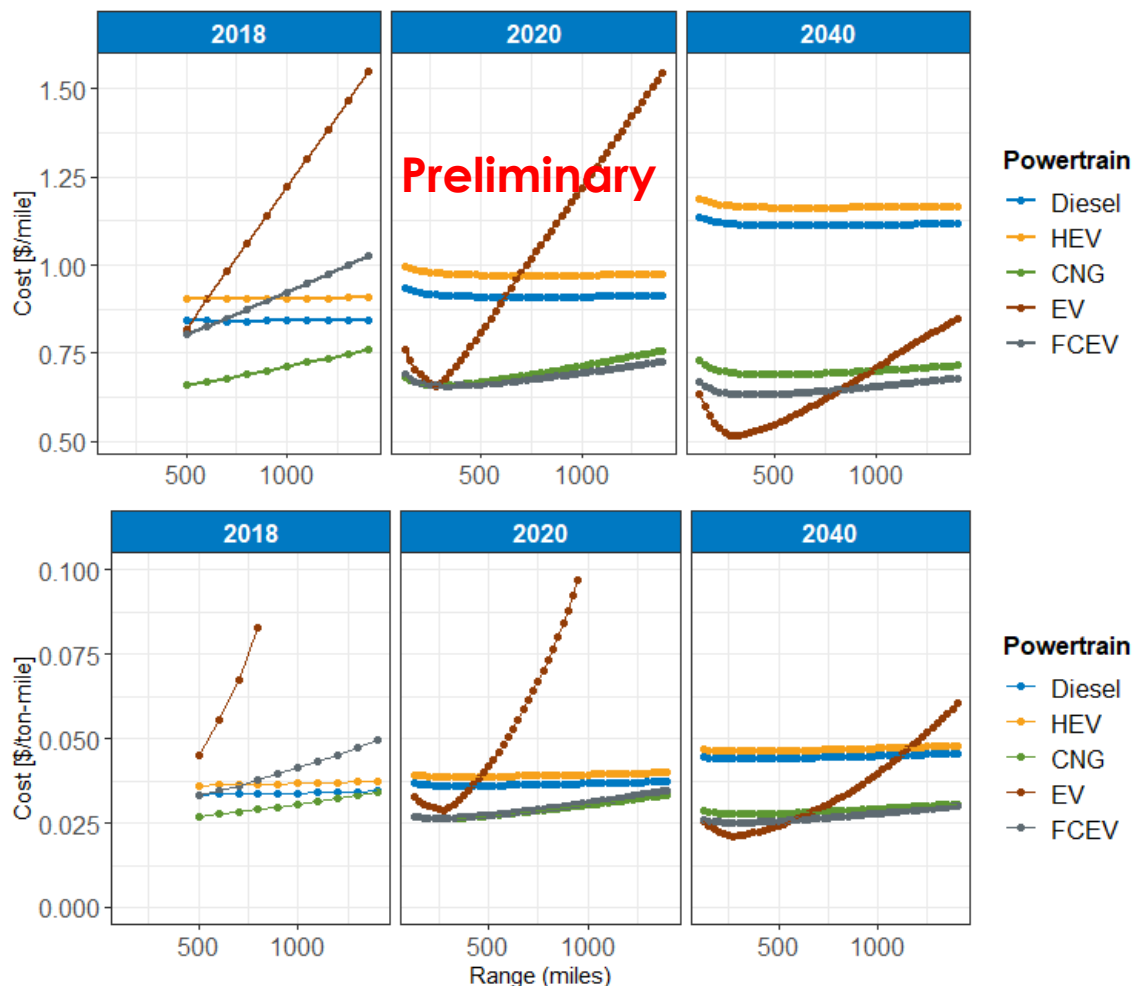


Figure 2. Present value cost (\$/mile and \$/ton-mile) for Class 8 tractors traveling 100,000 mile/yr in the Pacific region under the Low Electricity and Hydrogen Prices scenario

Class 4 parcel delivery (range requirement of 120 miles) TCO is more sensitive to upfront costs because the total miles driven is lower than the Class 8 trucks. Additionally, dwell time costs become significant because the vehicle range is low requiring more refueling events. In the scenario with low electricity and hydrogen fuel prices, the fuel cell electric powertrains show higher TCO with current technology (2018), but lower TCO by 2020 primarily by achieving reduction in fuel cell stack costs as seen in Figure 2. Battery electric powertrains do not have the lowest TCO primarily due to high battery costs in 2020 and relatively high dwell time costs from electric charging in 2040. In this scenario, battery electric charging occurred over 30 minutes but in other scenarios when trucks could be charged overnight, battery electric powertrains could have the lowest TCO by 2040.

These TCO results provide strong support that when accounting for all economic costs into a TCO analysis framework, fuel cell electric powertrains can result in a true cost advantage over conventional powertrains in these commercial applications if FCTO performance and cost targets are met (Milestone 1.16, 1.17).

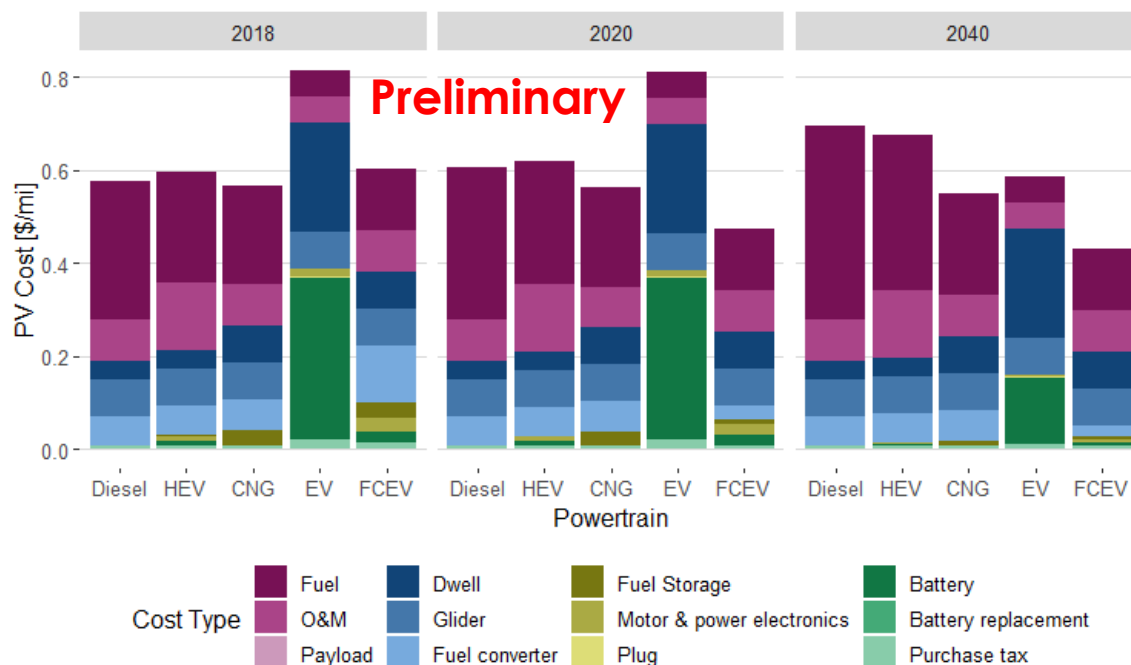


Figure 3. Present value cost (\$/mile) for 4 parcel delivery trucks traveling 30,000 mile/yr in the Middle Atlantic region

CONCLUSIONS AND UPCOMING ACTIVITIES

Overall, this project presents a transparent and consistent TCO systems analysis that includes both direct and indirect costs that influence the TCO of three types of commercial vehicles, five powertrains, and three technology statuses. Depending on the specific scenario evaluated, fuel cell and battery electric powertrains could provide a lower TCO than trucks with diesel, diesel hybrid-electric, and CNG powertrain technologies.

The funding for FY19 is expected to be used to complete the peer review process for an NREL report as well as document findings and make the data accessible for others to download and use. Additionally, a follow-on report is expected to be completed analyzing additional vehicles/vocations in the commercial vehicle space.

FY 2018 PUBLICATIONS/PRESENTATIONS

1. Chad A. Hunter. “Market Segmentation Analysis of Medium and Heavy Duty Trucks with a Fuel Cell Emphasis.” Presented at the DOE Hydrogen and Fuel Cells Program Annual Merit Review and Peer Evaluation Meeting, Washington, DC, June 13-15, 2018. NREL/PR-5400-71478.

REFERENCES

1. Bernd Heid, Russell Hensley, Stefan Knupfer, and Andreas Tschiesner. “What’s sparking electric-vehicle adoption in the truck industry?” McKinsey & Company website, Our Insights (September 2017). <https://www.mckinsey.com/industries/automotive-and-assembly/our-insights/whats-sparking-electric-vehicle-adoption-in-the-truck-industry>.
2. NACFE (North American Council for Freight Efficiency). “Medium-Duty Electric Trucks: Cost of Ownership.” (2018). <https://nacfe.org/future-technology/medium-duty-electric-trucks-cost-of-ownership/>.
3. Nikola. “Nikola One.” (2018). <https://nikolamotor.com/one>.
4. John O’Dell. “Here’s How Toyota Improved Project Portal, its Fuel Cell Truck.” Trucks.com News (July 30, 2018). <https://www.trucks.com/2018/07/30/toyota-fuel-cell-truck-improvements/>.
5. Tesla. “Tesla Semi.” (2018). <https://www.tesla.com/semi>.

Analysis of Cost Impacts of Integrating Advanced Onboard Storage Systems with Hydrogen Delivery

Amgad Elgowainy (Primary Contact), Ed Frank, Yusra Khalid, Krishna Reddi, and Jui-Kun Peng
Argonne National Laboratory
9700 South Cass Avenue
Lemont, IL 60439
Phone: (630) 252-3074
Email: aelgowainy@anl.gov

DOE Manager: Fred Joseck
Phone: (202) 586-7932
Email: Fred.Joseck@ee.doe.gov

Project Start Date: October 2017
Project End Date: Project continuation and direction determined annually by DOE

Overall Objectives

Evaluate the impacts of onboard storage technologies for light-duty fuel cell electric vehicles (FCEVs) on the cost of hydrogen delivery and refueling.

Fiscal Year (FY) 2018 Objectives

- Determine the impact of dispensing pressure (P) and temperature (T) on the levelized cost of hydrogen delivery and refueling.
- Compare the levelized cost of hydrogen delivery and refueling of alternative onboard storage technologies to the delivery and refueling cost of baseline 700 bar onboard storage.

Technical Barriers

This project directly addresses Technical Barriers A, B, C, E, and I in the Hydrogen Delivery section of the Fuel Cell Technologies Office Multi-Year Research, Development, and Demonstration Plan.¹ These barriers are:

- (A) Lack of Hydrogen/Carrier and Infrastructure Options Analysis
- (B) Reliability and Costs of Gaseous Hydrogen Compression

- (C) Reliability and Costs of Liquid Hydrogen Pumping
- (E) Gaseous Hydrogen Storage and Tube Trailer Delivery Costs
- (I) Other Fueling Site/Terminal Operations.

Contribution to Achievement of DOE Hydrogen Delivery Milestones

This project contributes to the following DOE milestones from the Hydrogen Delivery section of the Fuel Cell Technologies Office Multi-Year Research, Development, and Demonstration Plan:

- Task 1.5: Coordinating with the Hydrogen Production and Storage subprograms, identify optimized delivery pathways that meet a hydrogen delivery and dispensing cost of <\$2/gge for use in consumer vehicles. (4Q, 2020)
- Task 6.3: By 2020, reduce the cost of hydrogen delivery from the point of production to the point of use in consumer vehicles to <\$2/gge of hydrogen for the gaseous delivery pathway. (4Q, 2020).

FY 2018 Accomplishments

- Developed a techno-economic model for evaluating hydrogen delivery and refueling cost for various onboard storage options.
- Studied the impact of various dispensing pressures and temperatures on the cost of hydrogen delivery and refueling of fuel cell light duty vehicles.

¹ <https://www.energy.gov/eere/fuelcells/downloads/fuel-cell-technologies-office-multi-year-research-development-and-22>

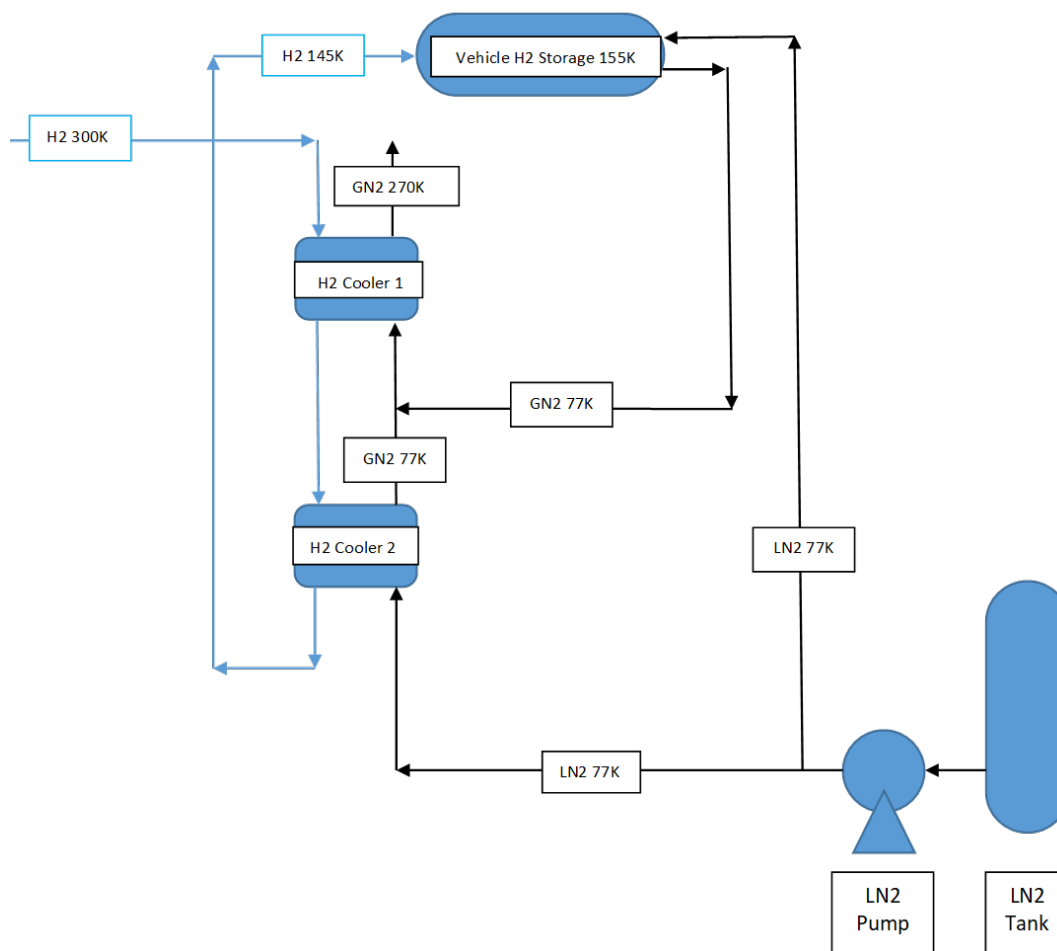


Figure 2. Cooling equipment configuration at hydrogen refueling station that requires LN2 temperature cooling of both hydrogen gas and onboard storage tank

For all evaluated dispensing options, we assume the following future scenario in an urban FCEV market:

- Market demand for 50,000 FCEVs (~30 metric tons per day)
- 37 hydrogen refueling stations (1,000 kg/day capacity, 80% capacity utilization)
- Cost reduction due to manufacturing volume/learning (20%–50% cost reduction depending on maturity of component technology)
- Truck delivery (500 bar tube trailers with 1 metric ton payload or LH2 tanker with 4 metric ton payload)
- Hydrogen production is located at 60 miles from city boundary.

APPROACH

- Define range of refueling conditions (e.g., P, T) for various onboard storage technologies
- Determine and size major items of refueling equipment (e.g., compressors, pumps, and heat exchangers)
- Acquire cost of delivery and refueling components for each onboard storage technology

- Implement refueling configuration and cost of components in the Hydrogen Delivery Scenario Analysis Model (HDSAM)
- Conduct techno-economic analysis and calculate the levelized refueling cost for baseline 700 bar onboard storage and the alternative storage options on a consistent basis (all costs are in 2016\$).

RESULTS

Figure 3 shows the impacts of various FCEV onboard storage P and T requirements on the levelized cost of hydrogen refueling, assuming gaseous tube trailer delivery. The first bar on the left of Figure 3 represents the refueling station capital and operation costs, by component, for the baseline 700 bar, -40°C dispensing case (e.g., for refueling FCEV type III or type IV carbon fiber composite overwrapped pressure tanks). The second bar from the left shows a dramatic decrease in compression, and thus refueling cost, compared to the baseline 700 bar dispensing case, due to the reduction in dispensing pressure from 700 to 100 bar (see Figure 1). The precooling cost associated with -40°C in the baseline 700 bar dispensing case is matched by the heat exchanger cost in the near ambient temperature dispensing case, mainly due to its much higher heat rejection load (~ 1 MW) compared to the refrigeration load of ~ 20 kW associated with the -40°C precooling. The third bar from the left in Figure 3 represents a case where the precooling of hydrogen and onboard storage, using LN2, is performed at the refueling station (see Figure 2). In this case, despite the low compression cost, the capital cost of LN2 precooling equipment, and the cost of delivering LN2 to the refueling station dominate the refueling cost, which exceeds the refueling cost of the baseline 700 bar, -40°C case. The last bar from the left in Figure 3 represents a case where the precooling of hydrogen to LN2 temperature is performed at an upstream central facility, with subsequent delivery of the cryogenic hydrogen in insulated tube trailers to the refueling station, thus saving the precooling investment at refueling station and reducing the overall refueling station cost. However, in such case, the cost of delivering cryogenic hydrogen to the refueling station is significantly higher compared to the case where hydrogen is cooled at the station using LN2. Thus, adding hydrogen delivery cost to the refueling cost provides a consistent system boundary for comparing the cost of different dispensing options, which is presented in Figure 4.

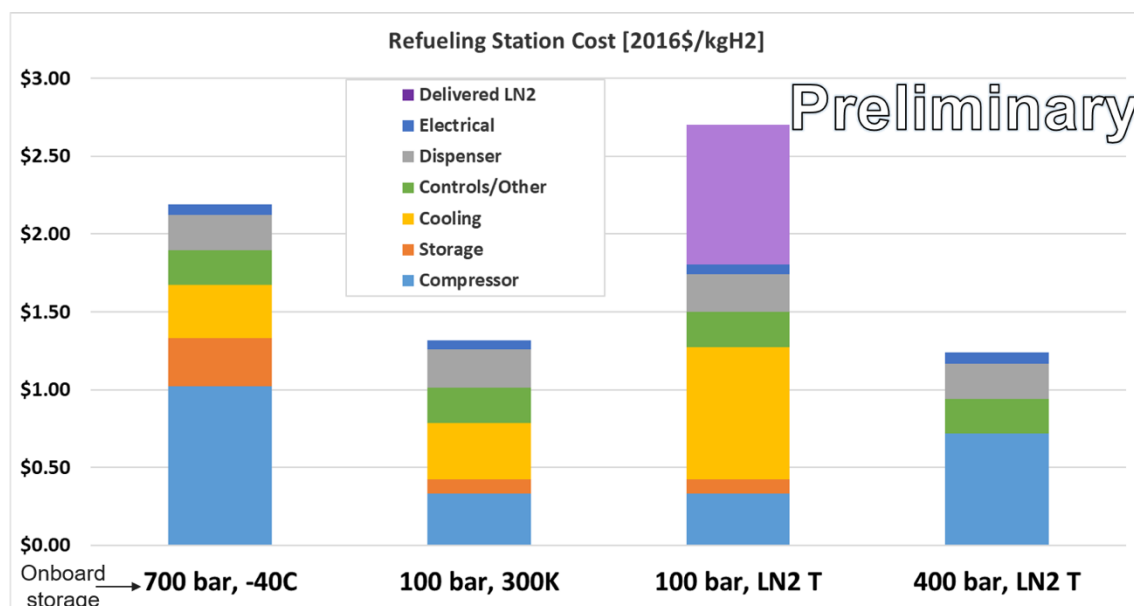


Figure 3. Impact of various FCEV onboard storage P and T requirements on the levelized cost of hydrogen refueling assuming gaseous tube trailer delivery

Figure 4 shows the impact of various FCEV onboard storage P and T requirements on the levelized cost of hydrogen delivery and refueling. For LH2 delivery in tankers, the delivery cost is more significant than refueling cost, mainly due to the liquefaction capital equipment and energy costs. For tube trailer deliveries, a trade-off between hydrogen delivery and refueling costs exists, depending on whether the precooling is achieved at a central facility before delivery to the refueling station, thus the precooling (or liquefaction) cost is implied in the delivery cost, or the precooling is performed at the refueling station, thus is explicit in the refueling cost. Figure 4 shows that FCEV onboard storage options requiring low pressure and near ambient temperature dispensing can significantly reduce the total hydrogen delivery and refueling cost. However, such onboard storage technology is yet to be discovered and requires significant research and development efforts before it can be realized.

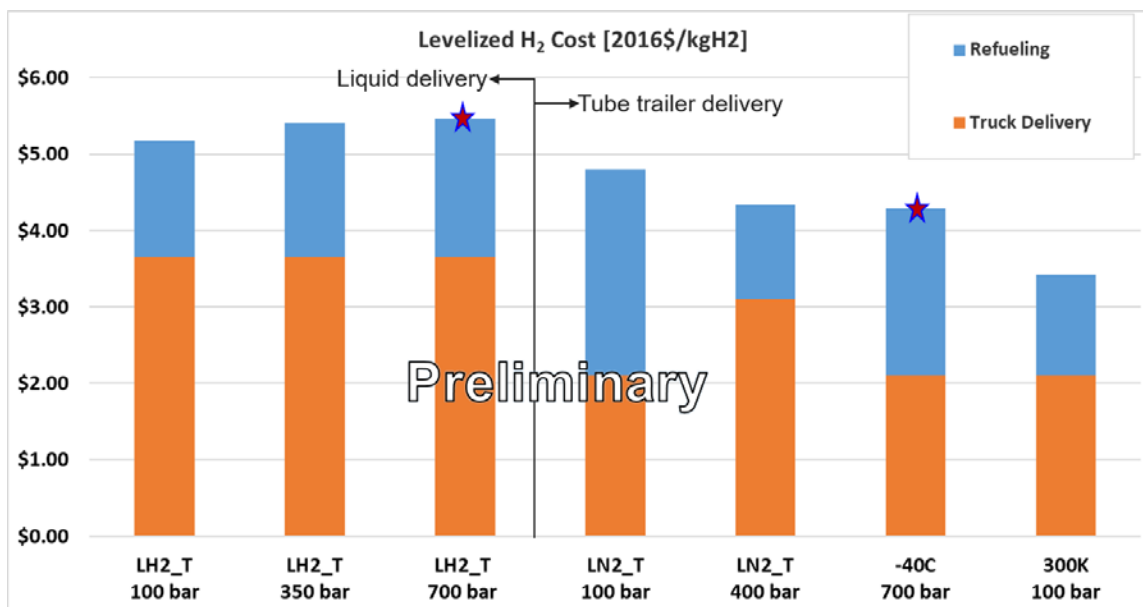


Figure 4. Impact of various FCEV onboard storage P and T requirements on the levelized cost of hydrogen delivery and refueling

CONCLUSIONS AND UPCOMING ACTIVITIES

The hydrogen delivery and refueling cost is strongly impacted by pressure and temperature requirements of FCEV onboard storage systems. Low pressure and near ambient temperature dispensing can significantly reduce hydrogen dispensing cost to FCEV customers. However, such an onboard storage system that can compete with the performance of the baseline 700 bar onboard storage system is yet to be developed. The conducted analysis can benefit from a detailed uncertainty analysis to capture the range of possible cost and performance of hydrogen delivery and refueling components.

REFERENCES

1. A. Elgowainy, K. Reddi, D.-Y. Lee, N. Rustagi and E. Gupta. "Techno-Economic and Thermodynamic Analysis of Pre-Cooling Systems at Gaseous Hydrogen Refueling Stations." *International Journal of Hydrogen Energy* 42, no. 49 (2017): 29067-29079.
2. K. Reddi, A. Elgowainy, N. Rustagi, and E. Gupta. "Impact of Hydrogen Refueling Configurations and Market Parameters on the Refueling Cost of Hydrogen." *International Journal of Hydrogen Energy* 42, no. 34 (2017): 21855-21865.

H2@Scale Analysis

Mark F. Ruth (Primary Contact), Paige Jadun, Amgad Elgowainy*, Nicholas Gilroy, Elizabeth Connelly, Josh Eichman, Max Wei†, Suzanne Singer§

National Renewable Energy Laboratory (NREL)
15013 Denver West Parkway
Golden, CO 80401-3305
Phone: (303) 384-6874

Email: mark.ruth@nrel.gov

* Argonne National Laboratory

† Lawrence Berkeley National Laboratory

§ Lawrence Livermore National Laboratory

DOE Manager: Neha Rustagi

Phone: (202) 586-8424

Email: Neha.Rustagi@ee.doe.gov

Project Start Date: January 2, 2017

Project End Date: March 31, 2019

Overall Objectives

- Improve fidelity of the value proposition of H2@Scale.
- Provide results that are supported by in-depth analysis of market potential and economics.
- Quantify potential impacts on economics, resource use, and emissions metrics.
- Identify regional opportunities and challenges.

Fiscal Year (FY) 2018 Objectives

- Incorporate feedback on the technical potential of hydrogen production in the United States via diverse approaches, and on the maximum market size for potential hydrogen demands.
- Develop national supply curves for hydrogen, assuming diverse methods of hydrogen production, and national demand curves for hydrogen consumption in current and potential future applications.
- Quantify the national economic potential of H2@Scale under several scenarios
- Complete a draft report summarizing the technical and economic potential of the H2@Scale concept.

Technical Barriers

This project addresses the following technical barriers from the Systems Analysis section of the Fuel Cell Technologies Office Multi-Year Research, Development, and Demonstration (MYRDD) Plan¹:

- (A) Future Market Behavior—Potential market for low-value energy and potential hydrogen markets beyond transportation
- (D) Insufficient Suite of Models and Tools—Tools integrating hydrogen as an energy carrier into the overall energy system and quantifying the value hydrogen provides
- (E) Unplanned Studies and Analysis—H2@Scale is a new concept and requires analysis of its potential impacts for input in prioritizing research and development.

It also addresses the following technical barriers from the Technology Validation section of the Fuel Cell Technologies Office Multi-Year Research, Development, and Demonstration Plan:

- (F) Centralized Hydrogen Production from Fossil Resources—Investigating potential value stacks for hydrogen production from various resources
- (G) Hydrogen Production from Renewable Resources—Investigating the potential for hydrogen to be produced from renewable electricity and support higher penetrations of renewable electricity generation.

Contribution to Achievement of DOE Milestones

This project will contribute to achievement of the following DOE milestone from the Systems Analysis section of the Fuel Cell Technologies Office Multi-Year Research, Development, and Demonstration Plan:

¹ <https://www.energy.gov/eere/fuelcells/downloads/fuel-cell-technologies-office-multi-year-research-development-and-22>

- Milestone 1.19: Complete analysis of the potential for hydrogen, stationary fuel cells, fuel cell vehicles, and other fuel cell applications such as material handling equipment including resources, infrastructure and system effects resulting from the growth in hydrogen market shares in various economic sectors (4Q, 2020).

In addition, this project will contribute to achievement of the following DOE milestone from the Technology Validation section of the Fuel Cell Technologies Office Multi-Year Research, Development, and Demonstration Plan:

- Milestone 3.9: Validate large-scale system for grid energy storage that integrates renewable hydrogen generation and storage with fuel cell power generation by operating for more than 10,000 hours with a round-trip efficiency of 40% (4Q, 2020).

FY 2018 Accomplishments

- Updated the estimate of the current maximum hydrogen demand market size to be 151 million metric tonnes (MMT) annually, including demands from refineries and the chemical processing industry, metals refining, ammonia

production, hydrogen use for biofuels refining, hydrogen use for synthetic fuels production, direct injection into the nation's natural gas system, light-duty fuel cell electric vehicles (FCEVs), other transportation including medium-duty and heavy-duty trucks, and seasonal energy storage for the electricity grid.

- Developed four national supply curves for hydrogen consisting of supplies from steam reforming of natural gas, high-temperature electrolysis using nuclear energy, and low-temperature electrolysis of otherwise curtailed electricity. The scenarios vary based on varying assumptions of natural gas prices, low-temperature electrolyzer prices, and electricity market structures.
- Developed three national demand curves for the hydrogen demands listed in a previous bullet. The curves vary depending upon assumptions regarding the evolution of the U.S. electricity system and the U.S. metals industry.
- Quantified the national economic potential for H₂@Scale ranging from 22 MMT/yr to 45 MMT/yr over five scenarios with various technology and market assumptions.

INTRODUCTION

H2@Scale is a U.S. Department of Energy (DOE) initiative that brings together stakeholders to advance affordable hydrogen production, transport, storage, and utilization to increase revenue opportunities in multiple energy sectors. The focus of this report is techno-economic modeling and analysis that was completed to characterize the overall potential of the H2@Scale vision, given evolutions in the U.S. energy system and future R&D advances. Figure 1 graphically represents H2@Scale by showing how hydrogen could fit into the overall energy system. It is based on utilizing hydrogen's unique ability to both support the electric grid and serve as a clean feedstock to a variety of demands. Hydrogen production can utilize intermittent electricity and heat, and therefore it can be used to stabilize the electricity grid and to enhance the financial viability of both baseload nuclear power and variable renewable generation. The hydrogen that is produced in that way can be stored for months without degradation and then used to provide electricity back to the grid or for a number of alternative purposes shown in Figure 1, including as fuel for FCEVs, as a chemical feedstock for refining and ammonia production, and as a clean energy supplement in the natural gas system.

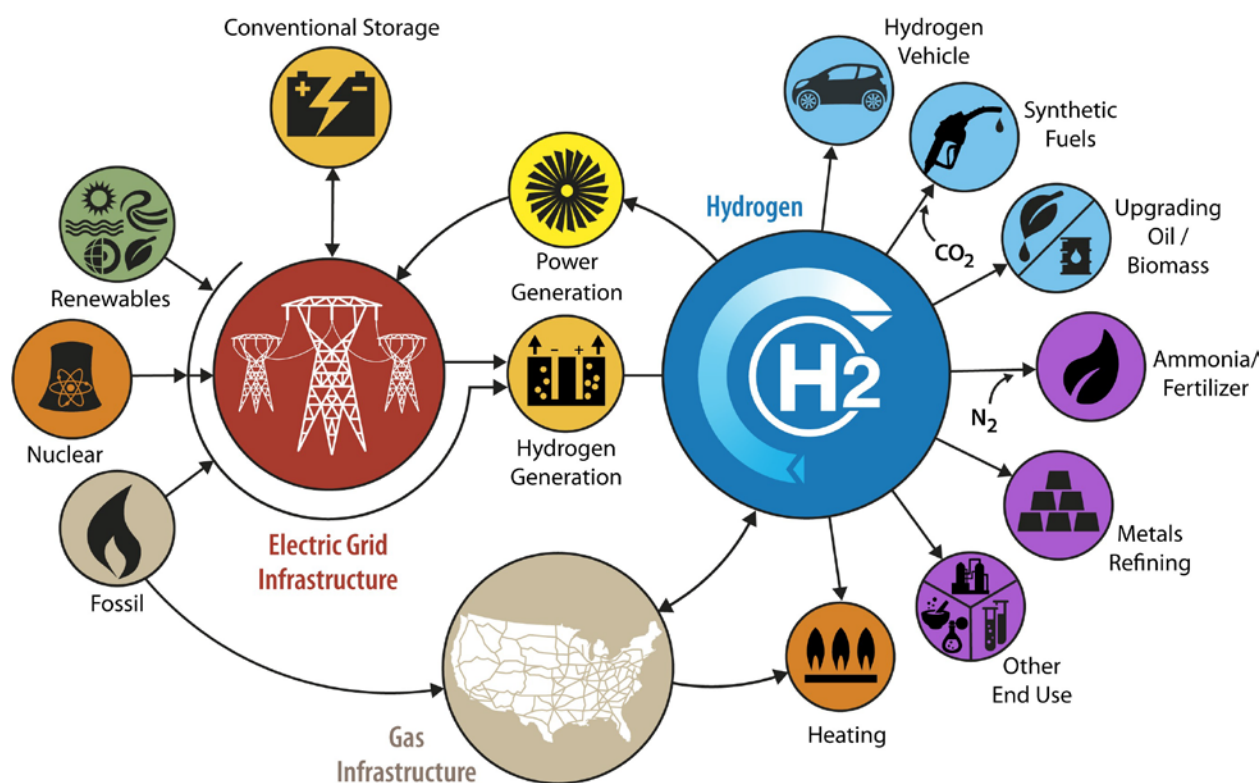


Figure 1. Graphical depiction of the H2@Scale concept, showing the use of otherwise curtailed electricity and other hydrogen generation resources and potential uses of hydrogen, including on-demand electricity, transportation, and industrial uses, in addition to injection into the natural gas infrastructure.

This project analyzes the economic potential of H2@Scale. It focuses on developing and communicating potential market size and impacts using techniques that can be justified and communicated to a broad range of audiences. Preliminary regional analyses and transition conceptualization are being performed in this project. Proposed work in future years extends the analysis to consider regional issues in depth, as well as storage and infrastructure development opportunities and challenges.

APPROACH

This project is composed of three stages. The first two are estimating (1) the maximum hydrogen market size under the H2@Scale concept and (2) the economic potential of the H2@Scale concept; these stages were initiated in FY 2017 and completed in FY 2018—excepting finalizing publications. The third stage, including additional analysis related to topics such as regional needs and constraints and storage and infrastructure development opportunities and challenges, has been initiated but will not be reported here.

The team estimated the economic potential as the market equilibrium between supply and demand using traditional micro-economic analysis techniques based on a theory of competitive markets, in which the price of a particular good will settle at a point where the quantity demanded at that price matches the quantity supplied at that price [1–2]. Demand curves were developed by estimating hydrogen price points based on users' willingness to pay for hydrogen (which is impacted by alternatives and elasticity), and potential locations for the following potential hydrogen demands: oil refining, metals refining, ammonia, biofuels, synthetic fuels and chemicals, supplementing natural gas, light-duty vehicles, other transportation, and seasonal energy storage for the electrical grid. Supply curves for hydrogen production via steam reforming of natural gas, low-temperature electrolysis of otherwise curtailed electricity, and high-temperature electrolysis using heat from nuclear energy were developed based on energy resource and technology cost assumptions including those from [3–5].

RESULTS

The maximum market sizes for hydrogen demand in the United States is estimated as 151 MMT/yr. This demand estimate comprises 74 MMT/yr for use in FCEVs, 28 MMT/yr for seasonal storage to ultimately be used in electricity generation, and 49 MMT/yr for industrial use (including oil refining and the chemical processing industry, metals, ammonia, biofuels, and synthetic fuels and chemicals) and blending into the natural gas system. Table 1 summarizes the maximum market sizes for hydrogen demands. The technical potential of U.S. resources is sufficient to supply the maximum potential hydrogen market.

Table 1. Maximum Market Size for Hydrogen Demands

Application	Maximum Market Size (MMT/yr)
Refineries and the chemical processing industry ^a	8
Metals	12
Ammonia	4
Biofuels	1
Synthetic fuels and chemicals	14
Natural gas supplementation	10
Light-duty FCEVs	57
Other transportation	17
Seasonal energy storage for the electricity grid	28
Total	151

^a Chemical processing industry not including metals, ammonia, methanol, or biofuels.

The team developed aggregated demand curves by combining demand quantities across the range of price points that the user is estimated to be willing to pay for hydrogen. The aggregated demand curves for each scenario are shown in Figure 2. The Business As Usual and Low NG (natural gas) Resource scenarios have the same demand curves above a hydrogen price of \$1.48/kg. Below this price point, deviations in these scenarios are due to differences in assumed natural gas prices, which influence hydrogen's viability in seasonal energy storage. The Increased Metals Refining, Improved Electrolysis, and Low Cost Electrolysis scenarios all assume the same demand curve, which is 4 MMT greater than in the Low NG Resource scenario at prices above \$1.70/kg and below \$2.50/kg; this additional demand is expected to come from the metals refining

sector. Competition between industries that use hydrogen (e.g., demand for hydrogen in gasoline production for use in internal combustion engine vehicles vs. demand for hydrogen for use in FCEVs) was assumed to have no significant effect on the cumulative market sizes. Such secondary effects were outside of the scope of this analysis. For example, the independent demand for refining is 7.5 MMT/yr, and the independent demand for light-duty vehicles is 23.7 MMT/yr. In scenarios with the hydrogen price low enough to include both demands, we estimate the quantity of hydrogen to be the sum of the refining and light-duty vehicle demands (31.2 MMT/yr) because excess refining products could be exported; that market analysis is outside the scope of this effort.

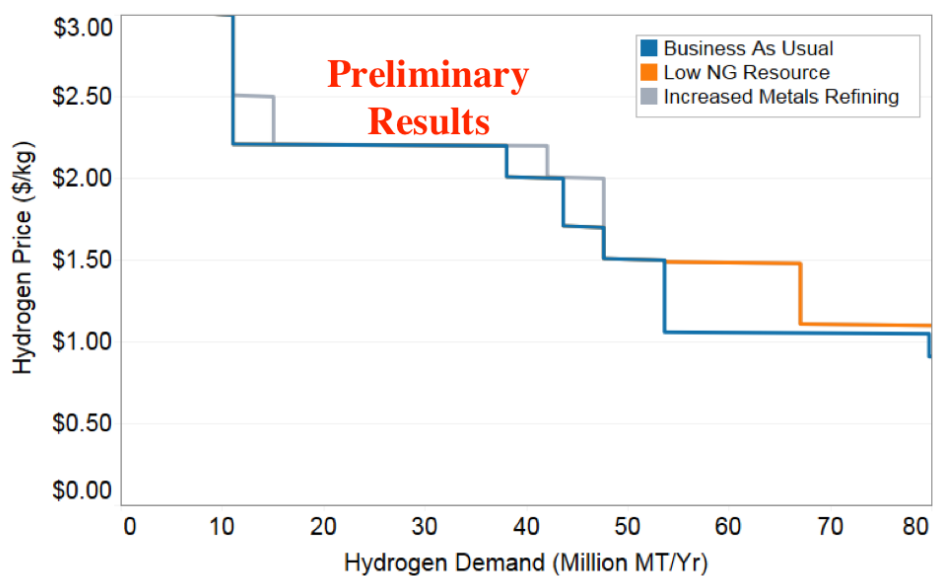


Figure 2. Aggregated demand curves for H2@Scale scenarios

The team estimated national supply curves based on production cost estimates for natural gas reforming, high-temperature electrolysis of nuclear energy, and low-temperature electrolysis of otherwise curtailed electricity, along with assumptions of the cost of delivery. The cost of hydrogen delivery can vary widely, given the proximity of production to demand. In the current work, simple assumptions of delivery cost have been made. The cost of infrastructure will be expanded in analysis in the coming years. Figure 3 shows the supply curves used in the analysis.

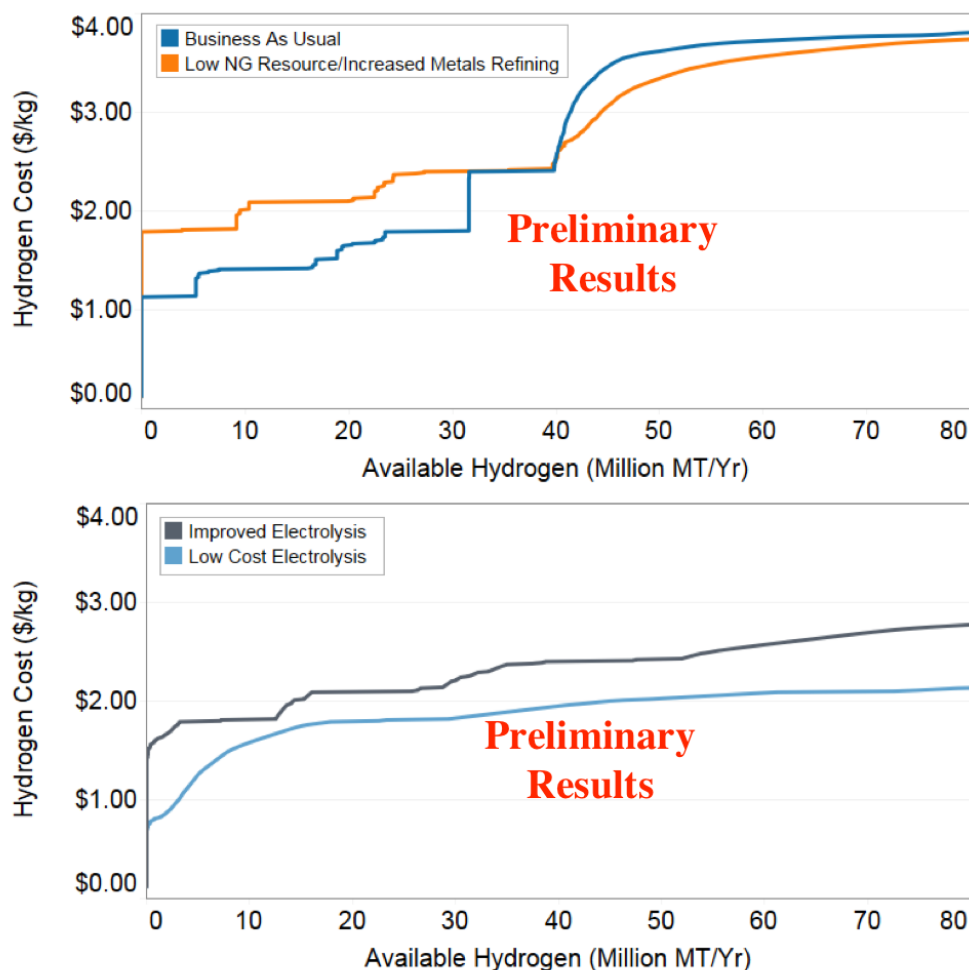


Figure 3. Aggregated supply curves for H2@Scale scenarios

The team estimated the economic potential of H2@Scale at the intersection between national supply and demand curves for five scenarios. The scenarios include varying assumptions about future conditions, including the performance of related markets (e.g., natural gas prices), the potential for market accessibility (e.g., the opportunity to purchase otherwise curtailed electricity at the selling price into the wholesale market), and other national decisions (e.g., whether a premium will be paid for domestically produced metals). Figure 4 shows the supply and demand curves of each scenario. The results range from 22 to 45 MMT/yr hydrogen market sizes. Across all the scenarios, hydrogen is demanded for refineries and the chemical processing industry, ammonia production, biofuels production, light-duty vehicles, and other transport; however, the quantities for light-duty vehicles and other transport vary. Some scenarios indicate a potential hydrogen demand for metals refining and methanol production.

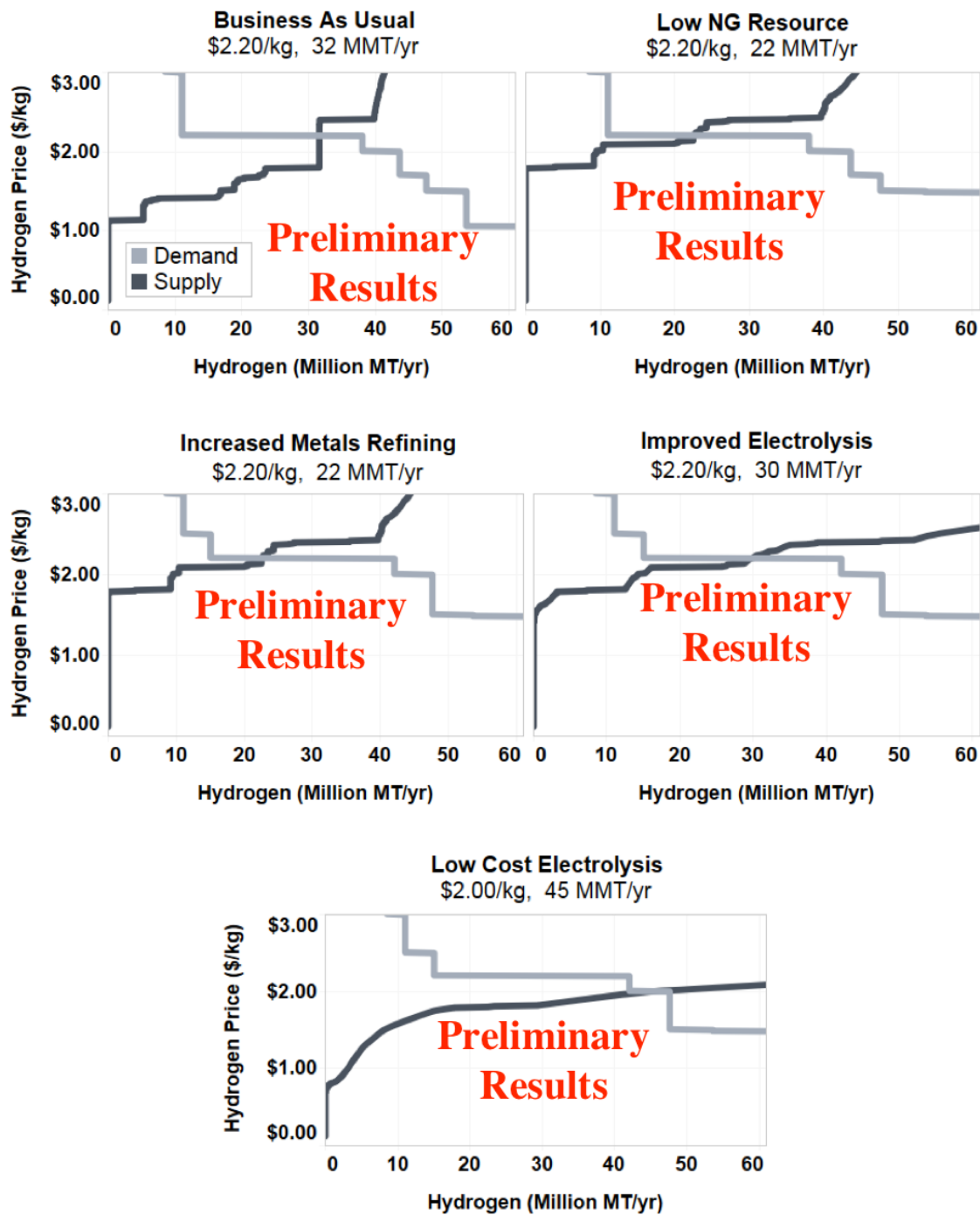


Figure 4. Supply and demand curves for the economic potential of five H2@Scale scenarios. Results are in the process of being finalized.

CONCLUSIONS AND UPCOMING ACTIVITIES

The team’s analysis indicates that the H2@Scale concept could have a large impact on the U.S. energy system. At 151 MMT/yr, the maximum potential hydrogen market is approximately 15 times larger than the current market. Most of that potential demand would be for applications that hydrogen is not currently supporting, and all of it is not likely to be achieved economically. The team estimated the economic potential of hydrogen in the United States to be 22–45 MMT/yr, depending on resource prices, hydrogen production technology R&D, and the price various users will pay for hydrogen, which depends in part on the cost of other technologies that provide the same services. These estimates are based on markets reaching equilibrium.

The team attempted to consider the full spectrum of hydrogen demands and most production options, but others should be considered as they are identified. Additional supply options including biomass and biogas conversion have not been included in the analysis to date. While these feedstocks already have other markets, an understanding of the competition between these markets would improve estimates of hydrogen supply potential. Delivery costs estimated in this analysis were simple assumptions. In-depth estimates of the necessary delivery and storage infrastructure would improve characterization of hydrogen supply potential. Finally, the estimates described here are based on markets achieving equilibrium. Market development and transition studies would improve understanding of challenges in achieving these penetrations.

FY 2018 PUBLICATIONS/PRESENTATIONS

1. Mark Ruth, Paige Jadun, and Amgad Elgowainy, “Potential Size of and Value Proposition for H2@Scale Concept” (presentation at the American Institute of Chemical Engineers Annual Meeting, November 1, 2017).
2. Mark Ruth, Paige Jadun, and Bryan Pivovar, “H2@Scale: Technical and Economic Potential of Hydrogen as an Energy Intermediate” (presentation at the Fuel Cell Seminar, November 9, 2017).
3. Mark Ruth and Paige Jadun, “H2@Scale Analysis and Project Developments” (presentation to the Hydrogen Technical Advisory Committee, February 13, 2018).
4. Mark Ruth, Paige Jadun, and Amgad Elgowainy, “H2@Scale Analysis” (presentation at the 2018 Fuel Cell Technologies Office Annual Merit Review, June 13, 2018).
5. Mark Ruth, “H2@Scale Value Proposition Considerations” (presentation at the H2@Scale R&D Consortium Kickoff Meeting, August 1, 2018).

REFERENCES

1. A.D. Brownlie and M.F. Lloyd Prichard, “Professor Fleeming Jenkin, 1833–1885 Pioneer in Engineering and Political Economy,” *Oxford Economic Papers* 15, no. 3 (1963): 204–216.
2. Robert A. Schwartz, *Micro Markets: A Market Structure Approach to Microeconomic Analysis* (Chichester: Wiley, 2010).
3. Energy Information Agency, “Annual Energy Outlook 2018” (Washington, DC: U.S. Energy Information Administration, 2018). <https://www.eia.gov/outlooks/aeo/>.
4. National Renewable Energy Laboratory, “NREL Annual Technology Baseline (ATB)” (2017). <https://atb.nrel.gov/>.
5. U.S. Department of Energy, “DOE H2A Analysis” (2012). https://www.hydrogen.energy.gov/h2a_analysis.html.

Small Business Innovation Research (SBIR) Projects

SBIR PHASE I (OFFICE OF SCIENCE, BASIC ENERGY SCIENCES)

General Techniques for Increasing Packing Density of Metal-Organic Frameworks for Enhanced Volumetric Storage of Hydrogen

NuMat Technologies
8025 Lamon Avenue, Skokie, IL 60077

Metal-organic frameworks are porous materials with great potential in several adsorption-based applications. For metal-organic frameworks to realize their potential in gas storage applications, including in fuel cell electric vehicles, these materials must be densified. This SBIR grant will focus on the densification and commercialization of metal-organic frameworks for onboard hydrogen storage in fuel cell electric vehicles.

High-Density Hydrogen Storage in Space-Filling Polyhedral Sorbents

NextGen Battery Technologies
1901 N. Moore St. Suite 1200, Arlington, VA 22209

NextGen will develop space-filling polyhedral adsorbent microliths that allow for high material packing densities in conventionally manufactured gas cylinders due to their small size (<0.5 cm), while retaining high porosities for rapid filling and discharge of the tank, and improved thermal conductivity. NextGen will demonstrate the hydrogen storage capabilities of this readily scalable technology on three classes of sorbent materials: activated carbons, metal-organic framework materials, and porous polymers, showing that it truly is a “materials-agnostic” solution.

Development of Novel Compaction Regimes for Hydrogen Storage Materials

E&G Associates, Inc.
100 Cherokee Blvd. Suite 332, Chattanooga, TN 37405

Current technology for hydrogen storage requires high-pressure systems that are too large and costly to be viable for transportation. This Phase I SBIR project’s objective is to develop a compact material-based solution, which allows high-volume hydrogen storage in a small footprint, making hydrogen-powered vehicles more feasible.

New Fluorinated Ionomers for Enhanced Oxygen Transport in Fuel Cell Cathodes

Compact Membrane Systems
335 Water Street, Newport, DE 19804

Compact Membrane Systems, Inc. has identified a family of ionomer materials that have very high oxygen permeability and are anticipated to have improved polymer electrolyte membrane fuel cell performance compared to industry standards. The Phase I program will focus on synthesizing and characterizing varied compositions (equivalent weights) of these ionomer materials and formulation into ionomer dispersions. Thin membranes will be fabricated from the dispersions and their oxygen permeances will be measured. Selected ionomers will be tested in membrane electrode assemblies and compared to industry standards.

Novel Fluorinated Ionomer for Polymer Electrolyte Membrane Fuel Cells

Giner, Inc.
89 Rumford Avenue, Newton, MA 02466-1311

Novel ionomers can lower catalyst layer transport resistances. This leads to improved fuel cell performance, especially under low-platinum and high-current-density operating conditions. The overall objective of this Phase I project is to design, synthesize, and characterize novel fluorinated ionomer for polymer electrolyte membrane fuel cell cathodes. The ionomers will demonstrate higher permeability to gases (oxygen and hydrogen) and low or no anion adsorption on platinum. Also, electrode morphology and structures will be correlated with fuel cell performance.

New Approaches to Improved Polymer Electrolyte Membrane Fuel Cell Catalyst Layers

Tetramer
657 South Mechanic Street, Pendleton, SC 29670

A viable solution to reduce the transport resistances in the catalyst layers is to create new ionomers that can provide good ion and oxygen transport needed to accomplish high-performing fuel cell catalysts. Characterization of transport properties of ionomers for various molecular architectures is the key step in the effort to create and identify the optimized polymer structure. Using this approach, we propose to develop, optimize, and demonstrate improved fuel cell catalyst ionomers based on new molecular architectures that will have dramatic improvements in performance and durability compared to current ionomers such as perfluorosulfonic acid materials.

Development of Innovative Gas Diffusion Layers for Polymer Electrolyte Membrane Fuel Cells

AvCarb Material Solutions, LLC
2 Industrial Avenue, Lowell, MA 01851

In this program AvCarb Material Solutions takes a multi-faceted approach to cost-effectively alter state-of-the-art fuel cell gas diffusion layer designs in a manner consistent with mass production, specifically focusing on improved water management and thermal/electrical properties.

High-Performance Gas Diffusion Layer

pH Matter, LLC
655 Singletree Drive, Columbus, OH 43229

In the proposed project, pH Matter, LLC will demonstrate a surface treatment approach that creates super-hydrophobic gas diffusion layers without compromising other important properties; the Phase I project will demonstrate gas diffusion layers with better hydrophobicity and gas transfer properties, acceptable corrosion resistance, and improved electrical conductivity that can be made cost effectively.

Gas Diffusion Layer Media Development for Improved Polymer Electrolyte Membrane Fuel Cell Performance

Techverse, Inc.
124 Goldenthal Court, Cary, NC 27519

In the proposed project, Techverse, Inc., collaborating with ElectroChem, Inc., will continue the development of a novel Teflon impregnation technique for hydrophobic treatment of fuel cell gas diffusion layers leading to its commercialization.

Advanced Manufacturing of Gas Diffusion Layers with Highly Engineered Porosity

Glacigen Materials, Inc.
288 Pronghorn Trail, Suite 2, Bozeman, MT 59718-7064

Glacigen Materials, in collaboration with Montana State University, proposes a Phase I SBIR project that will employ a proprietary embodiment of an advanced manufacturing technique to produce an exceptionally high-performance gas diffusion layer for polymer electrolyte membrane fuel cells. In the Phase I effort, Glacigen will create a gas diffusion layer with continuously graded and aligned porosity in a polytetrafluorethylene (Teflon)-treated titanium foam through scalable casting-based methods.

Controlled Porosity and Surface Coatings for Advanced Gas Diffusion Layers

Physical Sciences Inc.
20 New England Business Center, Andover, MA 01810-1077

This Phase I effort relies on two well-known ceramic processing technologies to produce novel gas diffusion layer structures. Physical Sciences Inc. will adapt the ice-templating and tape-casting method to produce gas diffusion layers with controlled, low tortuosity pores for enhanced water transport for better fuel cell performance. A pre-ceramic polymer approach will be used to deposit the SiC coatings on carbon surfaces for improved corrosion resistance and fuel cell durability.

Nanostructured Carbon-Based Gas Diffusion Layers for Enhanced Fuel Cell Performance

TDA Research, Inc.
12345 W. 52nd Avenue, Wheat Ridge, CO 80033-1916

Gas diffusion layers will be made from inexpensive precursors. We will optimize the physical properties (e.g., hydrophobicity/hydrophilicity and pore size distribution) of the new materials. They will be characterized ex situ (for corrosion, electrical and thermal conductivity, and surface morphology) and in situ by preparing membrane electrode assemblies from the most promising materials and testing their electrochemical performance under representative conditions. Based on the experimental results, we will carry out an engineering analysis to estimate cost of the new materials and compare their performance to that of current gas diffusion layers used in polymer electrolyte membrane fuel cells.

Innovative Bilayer Microporous Layer for Polymer Electrolyte Membrane Fuel Cells

Giner, Inc.
89 Rumford Avenue, Newton, MA 02466-1311

Giner proposes to create a new bilayer microporous layer-based design with combined pore size gradient and hydrophilic/hydrophobic gradient to control the water transport more effectively at both high and low humidity conditions. The introduction of a hydrophilic sublayer on top of a hydrophobic microporous layer will strengthen the driving force of water removal with minimized risk of dehydration in the catalyst layer and membrane.

Novel Membranes for Electrochemical Hydrogen Compression Enabling Increased Pressure Capability and Higher Pumping Efficiency

Xergy, Inc.
299 Cluckey Drive, Ste. A, Harrington, DE 19952

Xergy/Rochester Polytechnic Institute are developing membranes for high-pressure (875 bar) electrochemical hydrogen compression. Research and development efforts will include synthesis of novel ionomer and membrane chemistries followed by experimental evaluation to assess their mechanical strength under high pressure differentials.

Novel Sulfonated Block Copolymers for Efficient Electrochemical Hydrogen Compression

Sustainable Innovations
111 Roberts Street, Suite J, East Hartford, CT 06108

Sustainable Innovations Inc. and Rensselaer Polytechnic Institute are teaming to evaluate new ionic polymer membranes developed at Rensselaer Polytechnic Institute in Sustainable Innovations' electrochemical hydrogen separation and compression concepts. Gaia Energy Research Institute will provide techno-economic analysis of the new membrane manufacturing costs. The overall goal of this project is to enhance the reliability of electrochemical hydrogen compression by improving the durability of membranes.

SBIR PHASE II (OFFICE OF SCIENCE, BASIC ENERGY SCIENCES)

Multi-Functional Catalyst Support

PH Matter, LLC
6655 Singletree Dr., Columbus, OH 43229-1120

Hydrogen fuel cells are of interest for automotive applications because they produce zero emissions. However, fuel cells currently suffer from the high cost associated with precious metal electrode materials and long-term durability issues associated with voltage transients. In the proposed project, pH Matter will synthesize and demonstrate the performance of next-generation fuel cell electrode catalysts. The materials will outperform current precious metal catalysts in terms of cost, efficiency, and durability during operation. The unique properties of these materials allow them to be chemically resistant to degradation mechanisms suffered by traditional catalysts.

Novel Hydrocarbon Ionomers for Durable Proton Exchange Membranes

NanoSonic, Inc.
158 Wheatland Drive, Pembroke, VA 24136-3645

The objective of this project is to develop and demonstrate high-temperature hydrocarbon-based membranes that meet the chemical, thermal, and mechanical properties necessary for the demanding environments within a fuel cell vehicle. The approach involves the synthesis of novel, high-molecular-weight aromatic hydrocarbon membranes that possess polar moieties along the polymer backbone and pendant quaternary ammonium groups. During Phase I of this SBIR program, NanoSonic has manufactured a new class of durable, free-standing high-temperature hydrocarbon-based polymer electrolyte membranes as a low-cost alternative to expensive perfluorosulfonic acid ionomer-based membranes. The ionomers are mechanically tough and display high dimensional stability and low swelling. These innovative, structurally robust membranes exhibit fuel cell performance at 120°C with zero humidification. During the Phase II program, a series of novel phosphoric acid-imbibed poly (thioether benzonitrile) copolymers shall be evaluated per DOE's 2020 technical targets for membranes for transportation applications.

New Approaches to Improved Polymer Electrolyte Membrane Electrolyzer Ion Exchange Membranes

Tetramer Technologies, LLC
657 South Mechanic Street, Pendleton, SC 29670-1808

Electrolyzer systems produce high-value hydrogen on demand and on site via electrochemically splitting water. This Phase IIB project is directed at lowering electrolyzer cell costs while improving performance of the membrane. Tetramer Technologies, LLC has developed a new membrane molecular architecture, which during Phase II demonstrated equivalent or better performance to the current Nafion materials at 50% lower cost. These attributes directly address the DOE electrolyzer cost and performance targets. Key attributes of Tetramer's technology vs. the current Nafion electrolyzer membranes are improved physical performance properties, 50% lower hydrogen permeability, and equal or higher conductivity. This technology will provide thinner membranes that can lower costs and increase performance directly through decreased ionic resistance and indirectly through the reduction of the overall cell potential. The Phase IIB activities are focused on optimizing membrane performance, further lowering costs, scaling up manufacturing of the down-selected polymer membrane material, and initializing commercialization, culminating in the demonstration of the Tetramer membranes in stacks in prototype electrolyzer system units.

Flexible Barrier Coatings for Harsh Environments

GVD Corporation
45 Spinelli Place, Cambridge, MA 02138-1046

Many reliability problems stem from plastic and elastomer seals employed in hydrogen systems that leak and degrade because of the extreme-temperature, high-pressure, and high-wear hydrogen environments. There is a critical need for improved materials that can enable seals to operate reliably at both extreme temperatures ($-40^{\circ}\text{C} \leq T \leq 200^{\circ}\text{C}$) and high hydrogen pressures (>875 bar). Materials also need to withstand harsh environmental wear from repeated use. GVD Corporation proposes to utilize hydrogen gas barrier coatings deposited on such seals to shield them from hydrogen permeation and enable reliable, long-term operation. These barrier coatings are based on GVD's novel thin film vapor deposition technology. In GVD's process, an inorganic-organic multilayer barrier coating is fabricated from the vapor phase and grown directly on the surface of the elastomer seal. The coating deposits uniformly and conformally over three-dimensional seals and gaskets. Furthermore, these coatings are highly flexible and stable at 200°C. In Phase I and II, GVD demonstrated technical feasibility of the concept by depositing flexible, well-adhered barrier and lubricious

coating stacks on elastomeric and rigid substrates. These coatings survived temperatures up to 200°C while reducing permeability to helium by >60% (equivalent to a 70%–90% reduction in hydrogen permeability). During Phase IIA, GVD will optimize these materials for large-scale manufacturing and for use in hydrogen dispensers.

Diode Laser Sensor for Contaminants in Hydrogen Fuel

Southwest Sciences, Inc.,
1570 Pacheco St, Suite E-11, Santa Fe, NM 87505-3993

Low concentrations of contaminants in hydrogen fuel can foul or damage fuel cells in hydrogen fuel cell vehicles. Currently there is little monitoring of hydrogen quality at filling stations as there is no instrumentation available to continuously perform this function at the station. In this project, a portable diode laser sensor is being developed that will be able to perform these measurements at filling stations. The sensor will provide fast measurements so that each vehicle fill can be monitored. In the Phase I project, the feasibility of measuring hydrogen contaminants at desired levels and with a fast time response was demonstrated. Measurements were performed on low levels of carbon monoxide, carbon dioxide, and methane in hydrogen. In Phase II, the number of gases detected will be expanded to include ammonia, hydrogen sulfide, and water vapor, among others identified as critical by stakeholders. A prototype instrument will be developed and tested at a state quality assurance laboratory and a hydrogen fuel station. A contaminant detector for hydrogen fuel is needed to prevent fouling of hydrogen fuel cell vehicle engines. A laser instrument for the detection of hydrogen contaminants at fuel stations will be developed in this project.

SBIR PHASE I (OFFICE OF ENERGY EFFICIENCY AND RENEWABLE ENERGY)

Detection of Micron-Scale Flaws through Nonlinear Wave Mixing

Luna Innovations
301 1st Street, SW, Suite 200, Roanoke, VA 24011

Luna is developing an approach to detect micrometer-scale flaws in pressure vessels for hydrogen storage. Luna's approach will rely on nonlinear interactions between mixed acoustic waves to detect flaws. The approach focuses on electromagnetic acoustic transducer technology to allow non-contact inspections and rapid surface scanning. During Phase I, Luna focused on assessing the feasibility of identifying micrometer-scale flaws in steel alloys using non-collinear wave mixing through a breadboard system.

Highly Efficient Smart Tanks for Hydrogen Storage

TDA Research, Inc.
12345 W. 52nd Ave., Wheat Ridge, CO 80033

The commercial success of fuel cell electric vehicles requires significant reductions in the cost of hydrogen fueling. Current fueling stations require precooling equipment that chills the hydrogen to -40°C; this is needed to offset the temperature rise caused by compression during fueling to keep the compressed tank's operating temperature below its maximum operating temperature of 85°C. Reducing or eliminating the precooling requirement will reduce the cost of delivered hydrogen significantly. TDA Research proposes to develop a smart hydrogen storage tank that incorporates novel cooling schemes to quickly dissipate/absorb the heat of compression and keep the hydrogen gas temperature well below the hydrogen tank design temperature of 85°C with minimal impact on the cost, weight, volume, fill time, and well-to-powerplant efficiency. TDA's design maximizes the heat transfer area and the heat transfer coefficients to quickly dissipate the heat throughout the

refueling process. TDA will design and carry out sub-scale proof-of-concept tests of the smart tank design at the bench scale to demonstrate that we can carry out refueling from any charge state and ambient temperature conditions, eliminating the precooling requirements at the station. We will also complete a preliminary design of the smart hydrogen storage tank for fuel cell electric vehicles and compare it against the DOE baseline 700-bar system.

Phase Change Material Subsystem for Temperature Reduction during Fast Fill

Strategic Analysis, Inc.
4075 Wilson Blvd, Suite 200, Arlington, VA 22203

Growth in the fuel cell electric vehicle market beyond early adopters will require significant reductions in the cost of hydrogen fueling. During fueling, hydrogen is pre-cooled to -40°C to reduce the peak temperature rise in the tank to $<85^{\circ}\text{C}$. About 15% of the station cost is due to the precooling equipment. Precooling to these temperatures also increases performance requirements of the hydrogen dispensers, which account for 14% of station cost and increased maintenance frequency. A materials-based solution that takes advantage of the latent heat of changing phase from solid to liquid along with engineered high-surface-area heat transfer supports will be developed. Previous approaches to phase change material heat mitigation prevented the tank walls from exceeding 85°C but did not provide adequate surface area to prevent the gas temperature from exceeding 85°C . The current project will address this shortcoming by developing low-cost, high-surface-area, in-tank supports integrated with a phase change material to efficiently couple the excess gas thermal energy to the phase change material to limit the total gas temperature to $<85^{\circ}\text{C}$. The resulting product will be a tank insert that absorbs excess heat during refueling such that no precooling equipment at the station is required.

Thermally Conductive 700-bar Composite Tank for Hydrogen Storage

ADA Technologies, Inc.
11149 Bradford Road, Littleton, CO 80127

Precooling equipment accounts for about 15% of the cost of hydrogen fueling stations. Precooling is needed to maintain the tank's temperature under 85°C as heat is generated during the quick fill-up. ADA proposes to incorporate advanced materials into the design and fabrication of thermally conductive smart hydrogen tanks and reduce or eliminate the need for hydrogen precooling. In Phase I, the thermally conductive liner material will be manufactured and tested for strength, thermal conductivity, and hydrogen permeability at the coupon level. A thermally conductive overwrap will also be defined theoretically based on the existing carbon fiber-based products.

SBIR PHASE II (OFFICE OF ENERGY EFFICIENCY AND RENEWABLE ENERGY)

Emergency Hydrogen Refueler for Individual Consumer Fuel Cell Vehicles

Skyhaven Systems, LLC
2 Park Drive, Unit 4, Westford, MA 01886

Skyhaven Systems, LLC is developing an emergency hydrogen refueler that can be stored in the vehicle trunk and used by the consumer to refill the vehicle if they run out of hydrogen fuel away from a hydrogen fueling station. A chemical hydride and water conduit system was developed and demonstrated in a Phase I program to safely react producing hydrogen gas with the requisite purity for a fuel cell vehicle. Material and refueler

optimization focused on reacting 100% of the chemical hydride to hydrogen in a refueling period on the order of 15 minutes. Operational prototype hydrogen refuelers will be developed in the Phase II project that can produce 750 g of hydrogen gas to refill a fuel cell vehicle for a 50-mile driving range. The Phase II project will focus on material optimization, refueler design, codes and standards, hazardous materials and reliability assessment, manufacturing of the refueler, and prototype testing.

Cross-Polarized Near-Ultraviolet/Visible Detector for In-Line Quality Control of Polymer Electrolyte Membrane Materials

Mainstream Engineering Corporation
200 Yellow Place, Rockledge, FL 32955-5327

Mainstream is developing a commercializable, in-line quality control device with a single detector and two cross polarizers to identify defects and log defect location in membrane materials manufactured for polymer electrolyte membrane fuel cells. The experimental approach uses near-ultraviolet/visible light transmission techniques.

Ionomer Dispersion Impact on Advanced Fuel Cell and Electrolyzer Performance and Durability

Giner, Inc.
89 Rumford Avenue, Newton, MA 02466-1311

Previous work at Los Alamos National Laboratory has demonstrated improved fuel cell performance and durability using nonaqueous ionomer dispersions in the electrode. In this project Giner will translate this work to industrially relevant processes and materials, including new lower-equivalent-weight ionomers. Giner will develop low-cost roll-to-roll processes for membrane casting and electrode coating using these nonaqueous ionomer dispersions and validate these technologies for commercial applications in advanced fuel cell and electrolyzer systems.

Cryogenically Flexible, Low Permeability Thoreau's Rubber Hydrogen Dispenser Hose

NanoSonic, Inc.
158 Wheatland Drive, Pembroke, VA 24136-3645

Innovations in high-pressure (875-bar) hydrogen dispensing hoses are needed to improve reliability and reduce cost. Current dispensing hoses commonly fail multiple times a year and cost around \$2,000 each. Causes of premature failure include the stresses that they experience from pressure cycling, temperature cycling (ambient to -40°C), and hydrogen embrittlement. NanoSonic is engineering a new class D hydrogen dispensing hose to survive 51,240 fills (70 fills/day, 2 years). This metal-free state-of-the-art hose is based on a unique fiber-reinforced, high-performance, cryogenically flexible polymer to resist hydrogen embrittlement, survive thermal cycles, perform consistently at pressures greater than 875 bar (H70 service, 700 bar and safety overpressure), and endure mechanical wear and fatigue at the pump. During Phase I and II, a superior class of non-electrically conductive, low-glass-transition-temperature polymer hose cores were developed that exhibit ultra-low hydrogen permeation after 180° bending in a -50°C chamber and offer an innovative path to dissipate static electricity. A novel ceramer coupling agent was also developed to enhance the strength of adhesion between the fitting and hose, and it resulted in significantly enhanced hose burst strengths. During the Phase IIB program, a down-selected hose design will be joined with a new fitting, such that is ready for commercialization.

Low-Cost Alloys for Magnetocaloric Refrigeration

General Engineering & Research, LLC
10459 Roselle St. Ste. A, San Diego, CA 92121-1527

An emerging technology for hydrogen cooling and liquefaction is magnetic refrigeration due to its high efficiency. Magnetic refrigeration utilizes the magnetocaloric effect (MCE), which refers to the temperature change in magnetic materials after they are exposed to magnetic fields. A critical challenge of developing low-cost magnetic refrigerators is the cost and availability of materials that exhibit the MCE; such materials are typically rare-earth elements. During the Phase I effort, promising low-cost, high-performance MCE materials were discovered that function at temperatures below 50 K. For reference, the temperature for hydrogen liquefaction is 20 K. Phase II will involve a simultaneous effort of optimizing processing of the sub-50 K materials to reduce cost and continuing to identify promising MCE alloys for >50 K applications. The proposed research has the potential to contribute to a fundamental understanding of MCE within nanoscience and advance the state-of-the-art in refrigeration technologies. Ultimately, materials developed will be viable for a range of applications, including hydrogen liquefaction (20 K), nitrogen liquefaction (80 K), space applications (100–200 K), and room-temperature refrigeration and air conditioning.

Hydrogen Contaminations Detection

Sustainable Innovations, LLC
111 Roberts Street, Suite J, East Hartford, CT 06108-3653

The purity requirements outlined in SAE J7219, ISO 14687-2, and ISO 14687 standards establish a three-orders-of-magnitude accuracy for the instrumentation that is necessary to detect these extremely low levels of several critical contaminants. The design and verification of the conceptual approach of a cost-effective and reliable instrument that can sample the hydrogen at the nozzle of a delivery pump, and either certify acceptability or provide a signal to shut off the fuel distribution system, is critical for enabling this technology. In addition to the extremely low levels of contaminants that need to be measured, this instrument must be robust and stable over a very large range of temperatures and pressures. Sustainable Innovations, LLC has teamed with the University of Connecticut Center for Clean Energy Engineering to develop a unique and innovative multi-channel hydrogen fuel quality monitor to detect impurities in hydrogen. The proposed design will operate on stored hydrogen and will consist of an array of sensors, each tuned to respond to critical concentrations of a specific contaminant as defined in SAE J2719. These sensors will each be calibrated at selected impurity concentration values, and the real time measurements will be compared to the “fingerprint” of these responses. Models, using algorithms verified during this program, will complete an analysis of this data and provide a “go/no-go” signal to proceed with vehicular fueling. The technical objective of this program is to define, design, fabricate, and verify operation of a hydrogen contaminant detector for use as a “go/no go” sensor at the nozzle of a high-pressure hydrogen storage/dispensing system.

Phase I focused on alloy/composite catalyst selection for each contaminant; fabrication processes; selection and verification of cell electrolyte; generating a library of electrochemical data; and development and verification of the algorithms. Phase I efforts have shown that the concept will be able to detect the contaminants. Phase II efforts will focus on furthering the concept by testing with a larger list of contaminants, identifying and developing materials for improved selectivity and response times, and developing a fieldable prototype. The essential areas of development are selection of the catalyst material; design and fabrication of miniature electrodes; electrolyte selection; electrochemical data library for each contaminant; and algorithms to compare the measured current of the test samples to baseline. Successful development of a low-cost hydrogen contaminant sensor will prove critically important in expanding markets for hydrogen used in industrial and fueling applications.

H2@Scale CRADA Call Projects

An H2@Scale cooperative research and development agreement (CRADA) call was issued in August 2017 to seek qualified partners to participate in projects with the H2@Scale national laboratories consortium. The selected collaborative projects address key challenges associated with wide-scale production and use of hydrogen to address critical issues such as enabling grid resiliency, energy security, and domestic job creation and leadership in manufacturing. As of the end of fiscal year (FY) 2018, there were 24 selected CRADA call projects moving forward. Each project is receiving between \$25,000 and \$1,786,000 in Fuel Cell Technologies Office funding as a match of industry funding.

Table 1 lists the H2@Scale CRADA call projects, followed by brief descriptions of each project.

Table 1. H2@Scale CRADA Projects Active in FY 2018

Title	Industry Lead	Lab Lead
Development, Validation, and Benchmarking of Quantitative Risk Assessment Tools for Hydrogen Refueling Stations	Air Liquide	Sandia National Laboratories
Methane Pyrolysis for Base-Grown Carbon Nanotubes and CO ₂ -Free Hydrogen over Transition Metal Catalysts	C4-MCP, LLC	Pacific Northwest National Laboratory
California Hydrogen Infrastructure Research Consortium	California Governor's Office of Business and Economic Development	National Renewable Energy Laboratory
Hydrogen Safety Outreach by the Hydrogen Safety Panel to Expedite Hydrogen Fueling and Energy Project Deployment	Connecticut Center for Advanced Technology	Pacific Northwest National Laboratory
Hydrogen Safety Panel Evaluation of Hydrogen Facilities	California Energy Commission	Pacific Northwest National Laboratory
Valuation of Hydrogen Technology on the Electric Grid Using Production Cost Modeling	Electric Power Research Institute	National Renewable Energy Laboratory
Merchant Hydrogen at Scale: A Technical-Economic Case Study of the Potential for Nuclear Hydrogen Production	Exelon Corporation	Idaho National Laboratory
Holistic Fuel Cell Electric Vehicle / Hydrogen Station Optimization Model	Frontier Energy	National Renewable Energy Laboratory
Megawatt-Scale Proton Exchange Membrane-Based Electrolyzers for Renewable Energy Source Applications	Giner ELX, Inc.	National Renewable Energy Laboratory
Scalable Electrolytic Systems for Renewable Hydrogen Production	GTA, Inc.	National Renewable Energy Laboratory
Validating an Electrolysis System with High Output Pressure	Honda R&D Americas, Inc.	National Renewable Energy Laboratory
Turboexpander: Alternative Fueling Concept for Fuel Cell Electric Vehicle Fast Fill	Honda R&D Americas, Inc.	National Renewable Energy Laboratory
Membrane Electrode Assembly Manufacturing Automation Technology for the Electrochemical Compression of Hydrogen	HyET Hydrogen USA LLC	National Renewable Energy Laboratory
Membrane Technology for the Electrochemical Compression of Hydrogen	HyET Hydrogen USA LLC	Lawrence Berkley National Laboratory
Hydrogen Materials Compatibility of Low-Cost, High-Pressure, Polymer Hydrogen Dispensing Hoses	NanoSonic, Inc.	Pacific Northwest National Laboratory

Title	Industry Lead	Lab Lead
Develop a Tool to Estimate the Benefits of Tube-Trailer Consolidation Scheme for Station Builders	PDC Machines, Inc.	Argonne National Laboratory
Optimizing an Integrated Renewable-Electrolysis System	PG&E Corporation	National Renewable Energy Laboratory
Risk Analysis and Modeling to Improve Hydrogen Fuel Cell Vehicle Repair Garages Codes and Standards	Quong & Associates, Inc.	Sandia National Laboratories
Hydrogen Component Performance Diagnostic Testing	RIX Industries	National Renewable Energy Laboratory
Innovating High-Throughput Hydrogen Stations	Shell	National Renewable Energy Laboratory
Region-Specific Merchant Hydrogen Market Assessment and Techno-Economic Assessment of Electrolytic Hydrogen Generation	Southern Company	Idaho National Laboratory
Hybrid Electrical/Thermal Hydrogen Production Process Integrated with a Molten Salt Reactor Nuclear Power Plant	Southern Company	Idaho National Laboratory
Tatsuno Coriolis Flow Meter Development Testing in High-Pressure Hydrogen	Tatsuno	National Renewable Energy Laboratory
Evaluate High-Temperature Steam Electrolysis Coupled to PWR/MCFR/TWR for Hydrogen Production and Energy Storage	TerraPower, LLC Inc.	Idaho National Laboratory

H2@SCALE CRADA PROJECTS

Development, Validation, and Benchmarking of Quantitative Risk Assessment Tools for Hydrogen Refueling Stations

Air Liquide
9807 Katy Freeway
Houston, TX 77024

This project incorporates two tasks for a CRADA between Air Liquide and Sandia National Laboratories. The first task comprises a validation and benchmark comparison of risk and consequence software between Air Liquide and Sandia National Laboratories for the support of advancing quantitative risk assessment and improving the safety of hydrogen refueling stations. The second task involves developing a diagnostic tool for capturing three-dimensional data for large-scale hydrogen experiments to support code development for liquefied hydrogen refueling stations. Both of these tasks will utilize Sandia National Laboratories' core capabilities to advance the state-of-the-art knowledge about hydrogen behavior and quantitative risk assessment to defensibly revise safety codes and standards.

Methane Pyrolysis for Base-Grown Carbon Nanotubes and CO₂-Free Hydrogen over Transition Metal Catalysts

C4-MCP, LLC
2425 West Olympic Blvd., Ste. 4000
Santa Monica, CA 90404

This project aims to develop a new process for producing CO₂-free hydrogen and solid carbon from natural gas. The objective is to reduce the net production cost of hydrogen to <\$2/kg with the sale of valuable byproduct carbon. Recently researchers at West Virginia University reported a promising new catalyst innovation for non-oxidative thermochemical conversion of methane to CO₂-free hydrogen and solid carbon nanotubes. A catalyst was discovered that promotes “base growth” carbon nanotube formation rather than “tip growth”, which is the current technology. This enables catalyst regenerability while also generating a highly pure and crystalline carbon product. In partnership with West Virginia University, capability and expertise housed at Pacific Northwest National Laboratory is leveraged to build upon this prior research and improve catalyst design, develop the reactor engineering thus enabling a commercially viable process technology, understand the produced carbon characteristics and market potential, and evaluate the overall techno-economics. The envisioned outcome is the development of a transformational new process for producing CO₂-free hydrogen from inexpensive and domestically abundant natural gas while simultaneously offering the opportunity to reduce its net cost to <\$2/kg through sale of highly valuable crystalline solid carbon byproduct.

California Hydrogen Infrastructure Research Consortium

California Governor's Office of Business and Economic Development
1325 J Street, Suite 1800
Sacramento, CA 95814

A team of California agencies (California Air Resources Board, California Energy Commission, South Coast Air Quality Management District, and California Governor's Office of Business and Economic Development) and national laboratories has formed a research consortium focused on near-term hydrogen infrastructure development, deployment, and operation needs in California. Many of these partnerships have been in place for years through individual agreements and work scopes. This consortium intends to continue improving research coordination, impact, stakeholder participation, experiment quality, and information dissemination. Advances in hydrogen infrastructure target multiple nodes of the H2@Scale initiative. As demand increases,

improvements in station components and safety are essential to station deployment. Fully realizing the benefits of renewable hydrogen at the dispenser requires novel integration and economic options with renewables and the grid, as identified in H2@Scale. The consortium framework fits the H2@Scale cross-discipline and program collaborations, it has been under development for the last 3 months, and it will be finalized per the H2@Scale CRADA call schedule. The framework is intended to continue beyond this project for a long-lasting strategic partnership with the U.S. Department of Energy, agencies, and national laboratories.

Hydrogen Safety Outreach by the Hydrogen Safety Panel to Expedite Hydrogen Fueling and Energy Project Deployment

Connecticut Center for Advanced Technology, Inc.
222 Pitkin St, Suite 101
East Hartford, CT 06108

The Connecticut Center for Advanced Technology seeks to administer a “Hydrogen Safety Outreach” Program that would provide strategic outreach to building and code officials, project developers, maintenance and storage facility owners, and other interested stakeholders to facilitate the safe deployment and use of hydrogen technologies. Connecticut Center for Advanced Technology will seek to leverage the capabilities of the Hydrogen Safety Panel, administered by Pacific Northwest National Laboratory, as a resource to assist industry and other stakeholders in the Northeast United States.

Specific activities will include identification of hydrogen technology stakeholders, their roles, and challenges; publicizing Hydrogen Safety Panel training sessions to appropriate stakeholders; facilitating the exchange of information between stakeholders and the Hydrogen Safety Panel; and reviewing program reports and best practices. Benefits of the program include assurance that safety is adequately considered in early-market and highly visible projects, improved public confidence and acceptance of hydrogen technology, confirmation that safety features are appropriately designed, and acceleration of early-market deployment.

The outreach will begin in Connecticut, Rhode Island, New York, New Jersey, and Massachusetts, which are the core areas for hydrogen deployment in the Northeast United States, and will expand to other states as needed and appropriate.

Hydrogen Safety Panel Evaluation of Hydrogen Facilities

California Energy Commission
1516 9th Street, MS 6
Sacramento, CA 95814

Demonstrated safety in the production, distribution, dispensing, and use of hydrogen is critical to the successful implementation of a hydrogen refueling infrastructure and the widespread use of fuel cell technologies in transportation. Commercial hydrogen fuel technologies are starting to be deployed, which amplifies the attention paid to such new technologies because of public unfamiliarity. Loss of public confidence at an early stage of development could significantly delay or even preclude further progress in development and deployment of hydrogen and fuel cell technologies as zero-emission transportation solutions.

To ensure safety and minimize the probability of an incident, Pacific Northwest National Laboratory (PNNL) will lead the Hydrogen Safety Panel (HSP) to evaluate hydrogen safety plans in accordance with safety planning for hydrogen and fuel cells projects for proposed renewable hydrogen central production facilities and the light-duty hydrogen refueling infrastructure through the California Energy Commission’s future competitive solicitations. Applicants to California Energy Commission solicitations will have the opportunity to use the PNNL HSP resource while developing their renewable central hydrogen production facility or light-duty hydrogen refueling station applications. The PNNL HSP will evaluate the safety portion of the applications and will investigate incidents and safety practices and disseminate the findings and information

with authorities having jurisdiction and the public through h2tools.org. The completion of this project will enable the PNNL HSP to continue to promote the safety of hydrogen infrastructure in California and other parts of the United States.

The PNNL HSP is an essential resource to address the concerns about hydrogen as a safe and sustainable energy carrier, using more than 400 years of cumulative hydrogen safety experience, including committee members from National Fire Protection Association, SAE International, American Society of Mechanical Engineers, and the International Standards Organization. A key objective of the PNNL HSP is to integrate safety planning into funded hydrogen projects to ensure that all projects address related safety practices. This objective is crucial when siting, designing, and building renewable hydrogen facilities and light-duty hydrogen refueling stations.

Valuation of Hydrogen Technology on the Electric Grid Using Production Cost Modeling

Electric Power Research Institute
3420 Hillview Ave.
Palo Alto, CA 94304

This research project will estimate the value to the United States electric grid of deploying hydrogen technology (such as electrolyzers and hydrogen-fueled generation) under projected conditions of high renewable penetration. Large-scale grid simulation will be incorporated into a cost-benefit analysis to provide first-ever systems-level assessment of different hydrogen technology scenarios. Four utility companies will participate in scenario development and periodic review. This project will leverage the electric utility industry's working knowledge to develop relevant scenarios and the National Renewable Energy Laboratory's unique concentration of expertise in large-scale grid modeling, techno-economic modeling, and hydrogen technology.

Merchant Hydrogen at Scale: A Technical-Economic Case Study of the Potential for Nuclear Hydrogen Production

Exelon Corporation
10 S. Dearborn Street
Chicago, IL 60680

Existing nuclear plants are uniquely poised to produce hydrogen, providing low-cost power and/or steam for reliable, clean hydrogen generation. This study will determine the technical and economic feasibility of converting an existing nuclear plant (or several) for centralized or distributed hydrogen production. The study contemplates a deep economic analysis sufficient to provide a rationale for nuclear companies to make the investments required to convert their plants, stimulating the hydrogen economy and creating jobs. Exelon will work with a team that spans four national laboratories and additional industrial partners and anticipates that technical benefits to this project will include significant improvements and additions to national hydrogen and nuclear modeling and assessment resources.

Holistic Fuel Cell Electric Vehicle / Hydrogen Station Optimization Model

Frontier Energy, Inc.
1000 Broadway, Suite 410
Oakland, CA 94607

All current hydrogen vehicle fueling models focus on a limited portion of the hydrogen pathway from storage to pressure control, heat exchanger, dispenser, breakaway, hose, nozzle, vehicle receptacle, tubing, manifold(s), valve, and finally the compressed hydrogen storage system. Most hydrogen fueling models limit

their scope to the gas temperature behavior in the compressed hydrogen storage system. Some models have added the compressed hydrogen storage system, the breakaway, hose, nozzle, and vehicle components to account for pressure drop and heat transfer therefrom. The holistic fueling model being studied in this project will include all elements in the hydrogen pathway from the high-pressure storage tubes to the vehicle compressed hydrogen storage system.

There is no open-source, high-fidelity hydrogen fueling model available allowing automakers, hydrogen station operators, and other stakeholders to simulate the effects of out-of-bounds fueling conditions, novel tank geometries and materials, new fueling applications (e.g., motorcycles, medium/heavy-duty vehicles), and advanced fueling protocols all together. Proprietary models are available that encompass the entire vehicle-side and station-side fueling components, but they are closed-source and cost prohibitive. Further, these closed models are limited in scope (as described above) and do not provide simulation of the entire station.

Frontier Energy will partner with other industry stakeholders, including Honda R&D Americas, Ford, Hyundai, Linde, Air Liquide, NEL, Shell, Ivys, and others to leverage both the modeling and validation capabilities of the U.S. Department of Energy national labs to develop, validate, and disseminate an open-source fueling model that will, for the first time, address both the vehicle tank and the hydrogen station as a holistic system. The resulting model will help station providers, automakers, safety personnel, first responders, students, and others learn and model the behavior of hydrogen stations and the vehicles they serve.

As other open projects have shown (e.g., GREET, H2A, HDSAM, SERA, H2FAST), making this tool available for all to use and improve will lead to improved hydrogen systems, with a net gain to U.S. competitiveness.

Megawatt-Scale Proton Exchange Membrane-Based Electrolyzers for Renewable Energy Source Applications

Giner ELX, Inc.
89 Rumford Ave.
Newton, MA 02466

Proton-exchange membrane (PEM) electrolyzers have been well industrialized for pure hydrogen production in mobile refueling and energy storage applications when combined with renewable energy sources such as wind and solar. As the demand for these applications increases, electrolyzer stack manufacturers, including Giner ELX, are forced to scale up to stack sizes beyond their testing capabilities. Validation of new megawatt (MW)-scale electrolyzer stacks requires large electrolyzer test beds and electrical requirements that are available at the National Renewable Energy Laboratory's site.

Giner ELX recently developed a 'single stack' platform capable of operating up to 1 MW. In addition to scale-up of the cell active areas, Giner ELX focused on advancing the core key electrolyzer stack technology: increasing operating current density, improving efficiency, reducing cost, and extending lifetime.

The objective of this project is to validate Giner ELX's MW stack platform. The successful operation of the MW stack will be used to validate cell components, membrane, and catalyst under full operating conditions. Furthermore, the data will be used to develop future stack platforms capable of 5 MW and higher.

Scalable Electrolytic Systems for Renewable Hydrogen Production

GTA, Inc.
11403 Morgan Overlook Drive
Knoxville, TN 37931

The goal of GTA's work is development of scalable multi-megawatt water electrolysis systems that exclude platinum group metals, are constructed from readily available commodity materials, and are mass produced using advanced manufacturing and robotics. We fabricated and successfully tested a scalable technology readiness level (TRL) 4 laboratory prototype that demonstrated promising results for achieving the goal. We performed calculations and prepared scale drawings for an envisioned on-site TRL 8 electrolytic hydrogen production system at an offshore 8 MW wind turbine. The work plan of the CRADA project between the National Renewable Energy Laboratory and GTA focuses on validation of the current TRL 4 prototype with potential development and refinement for advancement to a TRL 5 system.

Validating an Electrolysis System with High Output Pressure

Honda R&D Americas, Inc.
1900 Harpers Way
Torrance, CA 90501

Hydrogen station designs are quickly evolving as more stations are installed and more end uses (e.g., light-duty, trucks, and buses) are coming online. Optimal station design depends heavily on the end use, location, and throughput demand of the station. There is no one-size-fits-all design in the hydrogen infrastructure space. Electrochemical compression has the potential to disrupt the hydrogen infrastructure industry, which currently relies on mechanical compression to reach high pressures.

In this project, Honda R&D Americas will partner with the National Renewable Energy Laboratory to perform baseline testing of their polymer electrolyte membrane-based electrochemical electrolysis stack capable of achieving pressures up to 70 MPa. The stack and system have been developed at Honda's R&D facility in Japan. Early studies of the stacks show promise in the technology with an approximate energy consumption reduction of 30% compared to mechanical compression. In theory, an electrochemical compression process should be more reliable than mechanical compression due to the reduction of moving parts.

Understanding new compression technologies and comparing them against the current state of the art will lead to innovations in station design and operation.

Turboexpander: Alternative Fueling Concept for Fuel Cell Electric Vehicle Fast Fill

Honda R&D Americas, Inc.
1900 Harpers Way
Torrance, CA 90501

In this project, Honda and the National Renewable Energy Laboratory are developing an alternative technology for achieving a fast fill at a hydrogen station. Hydrogen stations dispensing at 70 MPa struggle to achieve a 3–5 minute fill. Heating of the hydrogen during fueling occurs from two main effects: Joule Thomson heating across the control valve and compression heating in the tank. Joule Thomson heating is the result of the negative Joule Thomson coefficient that hydrogen exhibits at ambient temperatures when passed through an isenthalpic throttle (e.g., a valve or orifice). Current stations use a chiller and heat exchanger to precool and remove heat from the dispensed hydrogen thereby lowering the enthalpy of the dispensed gas to overcome the heating effects and avoid overheating of the gas in the tank. The alternative fueling concept will instead use a turboexpander to remove shaft power from the flowing hydrogen, lowering the enthalpy and

dropping the temperature, through a near isentropic expansion. The turboexpander concept has the advantage of providing a much smaller footprint and lower cost than existing chiller systems as well as reduced parasitic chiller losses by providing on-demand cooling. Turboexpander development will be conducted at the National Renewable Energy Laboratory utilizing the gravimetric test standard to measure parameters of flow, pressure, and temperature for characterizing turbine performance. Data will be used to compare turboexpander performance to the requirements of the existing SAE J2601 fueling protocol.

Membrane Electrode Assembly Manufacturing Automation Technology for the Electrochemical Compression of Hydrogen

HyET Hydrogen USA LLC
7801 Folsom Blvd 2020
Sacramento, CA 95826

Electrochemical compression has the possibility to outcompete mechanical compression for hydrogen end-use applications. While HyET has a compressor that can output 10 kg/day (fully scalable from home to industrial application) at up to 700 bar, the energy demand and reliability requires top-quality electrochemical hydrogen compressor (EHC) membrane electrode assemblies (MEAs) preferably prepared by cost-effective high-capacity manufacturing. High pressure requires a special MEA design, deviating from typical polymer electrolyte membrane fuel cell MEAs, with adapted catalyst layer substrates, asking for a modified coating process.

The National Renewable Energy Laboratory will help HyET by developing an automated catalyst-coating process fit for EHC MEA manufacturing. In addition, inline quality inspection methods will be developed or selected to improve the MEA quality as it is used for EHC stack assembly. In a joint effort, the National Renewable Energy Laboratory and HyET will eventually design an automated manufacturing process for the EHC MEA and approach potential U.S. suppliers of manufacturing equipment.

Membrane Technology for the Electrochemical Compression of Hydrogen

HyET Hydrogen USA LLC
7801 Folsom Blvd 2020
Sacramento, CA 95826

Electrochemical hydrogen compression has the potential to outcompete mechanical compression for hydrogen end-use applications. HyET has a compressor that can output 10 kg/day at up to 700 bar; the energy demand and reliability requires a thin membrane with high proton conductivity, low hydrogen crossover/back diffusion, and proper mechanical stability to withstand the mechanical stress during compression.

HyET has found a proton-conducting polymer with very high proton conductivity that is promising for application in electrochemical compressor cells. However, as a membrane the material lacks the mechanical stability for high-pressure use.

Therefore, Lawrence Berkeley National Laboratory will develop a cost-effective synthesis route ready for scale up, the proper chemistry for mechanical property improvement, and the membrane casting process. HyET will test the resulting membrane materials in electrochemical hydrogen compressor cells on conductivity and pressurization performance. In a joint effort, Lawrence Berkeley National Laboratory and HyET will assess the supply chain for the new polymer and membrane to find U.S. suppliers for polymer and thin films.

Hydrogen Materials Compatibility of Low-Cost, High-Pressure, Polymer Hydrogen Dispensing Hoses

NanoSonic, Inc.
158 Wheatland Drive
Pembroke, VA 24136

This project is focused on the durability of metal-free polymer-based hydrogen dispensing hoses with the hydrogen environment at the molecular level. NanoSonic is partnering with Pacific Northwest National Laboratory in this CRADA to utilize the lab's expertise in hydrogen polymer materials compatibility. The goal is to determine the lifetime of the hydrogen hose polymer and composite constituents via (1) time-temperature superposition studies via dynamic mechanical analysis under hydrogen, (2) friction and wear resistance under in situ hydrogen tribometry, and (3) multi-axis strain testing under cryogenic conditions. Pacific Northwest National Laboratory has the unique test equipment essential to gain this type of insight and lifetime prediction data. Importantly, the work conducted under the CRADA will increase the safety and reliability of NanoSonic's hydrogen hoses while expanding the market for use of our low-hydrogen-permeation polymers and durable cryogenic composites to realize the H2@Scale objectives to reduce the cost of hydrogen.

Develop a Tool to Estimate the Benefits of Tube-Trailer Consolidation Scheme for Station Builders

PDC Machines, Inc.
1875 Stout Drive
Warminster, PA 18974

The capital cost of hydrogen refueling stations is high, with the station currently contributing about half of the dispensed cost of hydrogen. The tube-trailer consolidation operation scheme patented by Argonne National Laboratory is expected to reduce the cost of the hydrogen refueling station by approximately 25%. The tube-trailer consolidation optimizes the operation of the refueling station by efficiently managing the compression and the low-pressure storage that supplies hydrogen to the station. Leveraging the refueling patented algorithm developed at Argonne National Laboratory, this project aims to develop a user-friendly tool that promotes and demonstrates the benefits of the tube-trailer consolidation for station developers. The tool would provide an estimate of various station cost and performance metrics, including the capital cost, tube-trailer payload utilization, the state of charge of vehicles filled for a given demand profile, and the refueling cost per unit of hydrogen dispensed, as a function of various design parameters. Most of the refueling stations in early markets will be supplied by gaseous hydrogen tube trailers, making the consolidation refueling algorithm and this project more relevant with respect to design and operation of refueling stations in these markets. PDC Machines will furnish Argonne National Laboratory, the developer of the consolidation operation algorithm, with performance curves of compressor models to incorporate in the tool. As the developer of the Hydrogen Delivery Scenario Analysis Model (HDSAM) and the Hydrogen Station Cost Optimization and Performance Evaluation (H2SCOPE) tool, Argonne National Laboratory is uniquely positioned to develop the tool, which will demonstrate the potential savings achievable with implementing the tube-trailer consolidation method for hydrogen refueling.

Optimizing an Integrated Renewable-Electrolysis System

PG&E Corporation
77 Beale Street
San Francisco, CA 94105

This study will holistically model the various value streams created by an integrated renewable power-electrolyzer system that produces hydrogen for use in the transportation sector. The model will be used to

design an optimized integrated renewable power–electrolyzer system (solar power plant, electrolyzer, and hydrogen storage). Knowledge of hydrogen systems gained during this project will contribute to PG&E’s future goal to build and test an integrated renewable power–electrolyzer system at one of PG&E’s existing solar facilities to demonstrate the interplay of these value streams in a real-world setting.

Risk Analysis and Modeling to Improve Hydrogen Fuel Cell Vehicle Repair Garages Codes and Standards

Quong & Associates, Inc.
1400 Geary Blvd., Suite 910
San Francisco, CA 94109

Existing codes and standards require repair garages that service hydrogen fuel cell vehicles to add costly equipment such as sensors, alarms, ventilation, and classified electrical equipment. This project will perform an application-specific risk analysis using software like the Hydrogen Risk Assessment Model to identify credible hazard scenarios resulting in unintentional indoor releases of hydrogen during maintenance operations. Results from the risk analysis will be used to identify key hydrogen release scenarios that may occur in the repair garages and require detailed modeling to characterize. Results from the modeling will be used to improve code requirements. Toyota and the team support this project because it can significantly reduce the cost of upgrading repair garages while maintaining the same levels of protection.

Hydrogen Component Performance Diagnostic Testing

RIX Industries
4900 Industrial Way
Benicia, CA 94510

H2@Scale is focused on the wide-scale adoption of hydrogen as a flexible energy storage medium. Due to the low volumetric energy density of gaseous hydrogen, compressors are an essential component of hydrogen storage. Hydrogen compressors that support a flexible grid and on-demand vehicle fueling undergo challenging operating conditions, such as a high number of start and stop cycles and wide input and discharge pressure ranges. Equally robust components are required for these conditions while still meeting the financial requirements of sustainable hydrogen compression.

This project seeks to investigate new seal materials and valves, both of which are responsible for many failures in today’s hydrogen compressors, with the goal of demonstrating improved performance and material compatibility.

Innovating High-Throughput Hydrogen Stations

Shell
281 Albany Street
Cambridge, MA 02139

Shell, Air Liquide, Toyota, Honda, and the National Renewable Energy Laboratory are partnering to address technical challenges to advance hydrogen infrastructure and support the expansion of existing and future markets. The collaboration is expected to provide station performance in high-mass-transfer and high-fill-frequency conditions to advance the design and operating strategies of high-throughput stations, supporting light-, medium-, and heavy-duty end-use applications. The information will support system and component solutions, along with optimization for storage, component integration, and renewable hydrogen sourcing. The work supports the broader H2@Scale target of increasing the penetration of variable renewable power and nuclear generation by providing technological advancements for hydrogen end uses in transportation.

Expected outcomes of the project include light-, medium-, and heavy-duty fueling data and specifications, station reliability research aimed at reducing maintenance costs, and advanced light-duty fueling components for control, pressure, and thermal management. In addition, the project will act as a hardware-in-the-loop incubator for new station technologies, integrating industry and researchers across market segments such as station owners, equipment suppliers, hydrogen suppliers, and national labs. New companies entering the market will be able to leverage the expanded infrastructure and capabilities at the National Renewable Energy Laboratory to reduce development costs and risks, resulting in more manufacturers and market competitiveness. The facility will be available to industry and researchers as part of the Energy Systems Integration Facility user facility model. To complete the work, existing National Renewable Energy Laboratory resources will be leveraged, including the Hydrogen Infrastructure Testing and Research Facility for existing and expanded infrastructure, as well as experimentation and analysis tools and personnel in the lab's Hydrogen and Fuel Cell Systems Engineering group.

Region-Specific Merchant Hydrogen Market Assessment and Techno-Economic Assessment of Electrolytic Hydrogen Generation

Southern Company Services, Inc.
600 18th Street North
Birmingham, AL 35203

Electrolyzers potentially bring value to both hydrogen generation and grid services, such as frequency regulation and firm capacity. Low-cost and otherwise curtailed nuclear, renewable, and hybrid steam/electricity generators could be used to generate hydrogen. This project analyzes the existing regional hydrogen markets (especially for low-CO₂ hydrogen), evaluates the value of grid services and firm capacity, explores the ability of electrolyzer technology to provide these services, and provides a techno-economic assessment of electrolytic hydrogen generation from otherwise curtailed resources.

Hybrid Electrical/Thermal Hydrogen Production Process Integrated with a Molten Salt Reactor Nuclear Power Plant

Southern Company Services, Inc.
600 18th Street North
Birmingham, AL 35203

This project buys down risk for the integration of molten salt reactors with hybrid thermal/electrical processes, including the production of hydrogen via a hybrid sulfur process. Molten salts have volumetric heat capacity similar to that of water (more than 200 times greater than that of helium). This makes them an excellent working fluid for high-temperature process heat applications. Previous work on the process, including detailed conceptual plant designs and cost estimates, was based on the use of high-temperature gas-cooled reactors with process heat delivered at 750°–950°C and 1.2–9 MPa for the decomposition step. This work focuses on the conceptual design of the integrated molten salt reactor–hybrid sulfur process (lower pressure and potentially lower temperature than previous work) and improving electrolysis performance.

Tatsuno Coriolis Flow Meter Development Testing in High-Pressure Hydrogen

Tatsuno North America, Inc.
7 Surrey Ln.
Rancho Palos Verdes, CA 90275

Hydrogen flow meter accuracy at 70 MPa dispensers has been identified as a technology challenge for deployment of hydrogen infrastructure. Current NIST Handbook 44 accuracy requirements for hydrogen use as

a motor vehicle fuel have been amended to a 5% acceptance tolerance with a 7% maintenance tolerance. This accuracy class is reduced from the 1.5% acceptance and 2.0% maintenance tolerance used for other motor vehicle fuels such as gasoline.

The reduced accuracy class was required by current accuracy limitations when measuring dispensed hydrogen. These limitations are based on additive contributions from flow meter accuracy and high-pressure hydrogen system effects. Flow meter development for improved accuracy will provide a direct benefit to the fuel cell vehicle customer interface and will help to prevent lost revenue by the station operator, thereby adding value to the business case for deploying hydrogen stations.

Flow meter characterization testing of the Tatsuno coriolis flow meter specifically designed for high-pressure hydrogen will utilize the gravimetric standard developed as part of the U.S. Department of Energy/National Renewable Energy Laboratory hydrogen flow meter benchmarking project.

Evaluate High-Temperature Steam Electrolysis Coupled to PWR/MCFR/TWR for Hydrogen Production and Energy Storage

TerraPower, LLC Inc.
330 120th Ave NE, Suite 100
Bellevue, WA 98005

Nuclear plants focused on hydrogen production can potentially generate increased revenues by optimizing between hydrogen generation, electricity production, and energy storage. This increase in revenue translates directly to new opportunities for nuclear power and the potential generation of new jobs. The project will evaluate the use of reversible high-temperature steam electrolysis (HTSE) for hydrogen production from TerraPower's traveling wave reactor (TWR) and molten chloride fast reactor (MCFR) designs, as well as from existing light-water reactors. This CRADA will leverage previous efforts at Idaho National Laboratory and Pacific Northwest National Laboratory related to testing and analysis of HTSE equipment, computational models, and techno-economic analysis. The objectives of this CRADA are:

1. Evaluate the methods and technology advantages of integrating TerraPower nuclear reactor designs and light-water reactor designs with reversible HTSE
2. Assess market opportunities for HTSE and identify industrial applications
3. Address the state of HTSE technology commercial readiness and nuclear reactor integration interface development and demonstration needs. This effort will help identify technology development and commercialization opportunities for Terra Power.

Acronyms, Abbreviations, and Definitions

ΔK	driving force	ATM-PP	benzyltrimethylammonium functionalized Diels-Alder poly(phenylene)
ΔS	entropy change	ATO	antimony-doped tin oxide
2-D	two-dimensional	AVT	A. V. Tchouvelev & Associates, Inc.
3-D	three-dimensional	AWARE-US	Available water remaining for the United States
A	ampere	AWSM	advanced water splitting materials
AB	acetylene black	B	magnetic induction
ABS	American Bureau of Shipping	BAPDA	Bay Area Planning Directors Association
AC	activated carbon	BaSce	Baseline Scenario analysis
ACI	ACI Services, Inc.	BCM	$BaCe_{0.25}Mn_{0.75}O_3$
(AD)Fe-N-C	atomically dispersed iron-nitrogen-carbon	BESS	battery energy storage system
AEM	anion exchange membrane	BET	Brunauer-Emmett-Teller
AEMEl	alkaline exchange membrane electrolyzer	BEV	battery electric vehicle
AEMFC	anion exchange membrane fuel cell	BMO	$BaMnO_3$
AEO	Annual Energy Outlook	BOC	best of class
AEP	amino ethyl piperazine	BOL	beginning of life
AFCB	American Fuel Cell Bus	BOP	balance of plant
AFDC	Alternative Fuels Data Center	BOS	balance of system
AFM	atomic force microscopy	BP	budget period
AHJ	authority having jurisdiction	BP-Ar(F _x)	perfluoroalkylsulfonate polymer(s)
AHMF	advanced hydrogen mobile fueler	BPN	alkyl ammonium functionalized poly(biphenylene); biphenylene
AIChE	American Institute of Chemical Engineers	BPN1	quaternary ammonium functionalized biphenyl-based polymer
ALD	atomic layer deposition	BPSH	biphenylsulfonic acid
AMFC	alkaline membrane fuel cell	BTMAOH	benzyltrimethylammonium hydroxide
AMM	Advanced Materials Manufacturing	BUT	butanediol
AMR	active magnetic regenerator; Annual Merit Review	BYZ	barium yttrium zirconate
ANL	Argonne National Laboratory	C&S	codes and standards
ANSI	American National Standards Institute	C5	five-carbon sugar (hemicellulose)
API	application program interface	C6	six-carbon sugar (cellulose)
APS	Advanced Photon Source	CaFCP	California Fuel Cell Partnership
APU	auxiliary power unit	CARB	California Air Resources Board
ASME	American Society of Mechanical Engineers	CBM	conduction band minimum
ASR	area specific resistance	CcH ₂	cryo-compressed hydrogen
AST	accelerated stability test; accelerated stress test	CCL	cathode catalyst layer
ASTM	ASTM International	CCM	catalyst-coated membrane
atmA	atmospheres pressure, absolute		

CCSI	continuous codes and standards improvement	dge	diesel gallon equivalent
CDO	code development organization	DGEBA	diglycidyl ether of bisphenol A
CDP	composite data product	DGEBF	diglycidyl ether of bisphenol F
CEC	California Energy Commission	DH	dehydrogenation
CF	carbon fiber; characterization factor	DIC	digital image correlation
CFD	computational fluid dynamics	DMA	dynamic mechanical analysis
CH	chemical hydrogen storage	DMAc	dimethylacetamide
cH ₂	compressed hydrogen	DME	dimethyl ether
CHS	Center for Hydrogen Safety	DMF	dimethylformamide
CL	catalyst layer	DMFC	direct methanol fuel cell
cm ²	square centimeters	DMIm	1,2-dimethylimidazole
CMU	Carnegie Mellon University	DMR	de-acetylated and mechanically refined
CNG	compressed natural gas	DMSO	dimethylsulfoxide
CO	carbon monoxide	DOE	U.S. Department of Energy
Co	cobalt	DOT	U.S. Department of Transportation
CO ₂	carbon dioxide	DR	demand response
COD	chemical oxygen demand	DRIFTS	diffuse reflectance infrared Fourier transform spectroscopy
CoF	coefficient of friction	DRTS	digital real-time simulator
COF	covalent organic framework	DSM	dimensionally stable membrane
Cold-cH ₂	cold-compressed hydrogen	DSM 1313	Deutsche Sammlung von Mikroorganismen 1313
COPV	composite overwrapped pressure vessel	DSRC	dedicated short-range communication
CPM	cycles per minute	EASIUR	Estimating Air pollution Social Impact Using Regression
CRC	cyclic redundancy check	ECSA	electrochemical surface area
CS	carbon steel	ED	electroless deposition
CSA	compact SOEC architecture	ED	Entner–Doudoroff pathway
CSA	Canadian Standards Association	EDC	Energy Dispatch Controller
CSM	Ce _x Sr _{2-x} MnO ₄	EDS	energy dispersive X-ray spectroscopy
CTE	coefficient of thermal expansion	EDXS	energy dispersive X-ray spectroscopy
CTE	Center for Transportation and the Environment	EERE	Office of Energy Efficiency and Renewable Energy
CY	calendar year	EG	ethylene glycol; expanded graphite
D-A	Dubinin-Astakhov	EHC	electrochemical hydrogen compressor/compression
DAPP	Diels-Alder poly(phenylene)	EIS	electrochemical impedance spectroscopy
DC	direct current	EMN	Energy Materials Network
DDCA	durability descriptor calculation automation	EMP	Embden-Meyerhof-Parnas pathway
DDS	dodecyl succinic anhydride	EMTA-NLA	Eshelby-Mori-Tanaka–Nonlinear Analysis
DETA	diethylene triamine		
DETAIL	Dynamic Energy Transport and Integration Laboratory		
DFMA	Design for Manufacture and Assembly		
DFT	density functional theory		

ENG	expanded natural graphite	FMEA	failure mode and effects analysis
EOD	electro-osmotic drag	F-MEC	fermentation and microbial electrolysis cell
EOL	end of life		
EOT	end of test	FMVSS	Federal Motor Vehicle Safety Standard
EPDM	ethylene propylenediamene		
ePTFE	expanded polytetrafluoroethylene	FNR	false-negative rate
eREV/EREV	extended range electric vehicle	FOA	funding opportunity announcement
ETFE	ethylene tetrafluoro ethylene polymer	FOM	figure of merit
		FPGA	field-programmable gate array
ETFECS	extended thin film electrocatalyst structures	FPR	false-positive rate
		FTA	Federal Transit Administration
EV	electric vehicle	FTIR	Fourier transform infrared spectroscopy
EW	equivalent weight		
F ⁻	fluoride ion	FTO	fluorine-doped tin oxide
FASTSim	Future Automotive Systems Technology Simulator	FY	fiscal year
		FZ	fusion zone
FC	fuel cell	g	grams
FCEB	fuel cell electric bus	g/s	grams per second
FCET	fuel cell electric truck	GCMS	gas chromatography-mass spectrometry
FCEV	fuel cell electric vehicle		
FCGR	fatigue crack growth rate	GDC	Gd _{0.1} Ce _{0.9} O _{1.95}
FCH JU	Fuel Cell and Hydrogen Joint Undertaking	GDE	gas diffusion electrode
		GDL	gas diffusion layer
FC-PAD	Fuel Cell Performance and Durability	Gen	generation
		GEN-II	second generation active magnetic regenerative refrigerator prototype
FCPP	fuel cell power plant	gge	gasoline gallon equivalent
FCS	fuel cell system	GH2	gaseous hydrogen
FCTO	Fuel Cell Technologies Office	GISAXS	grazing-incidence small-angle X-ray scattering
FCTT	Fuel Cell Tech Team		
FCV	fuel cell vehicles	GN2	gaseous nitrogen
FE	finite element; Office of Fossil Energy	GNG	go/no-go
		GPC	gel permeation chromatography
FEA	finite element analysis	GREET	Greenhouse gases, Regulated Emissions, and Energy use in Transportation model
FEC	front end controller		
FEMP	Federal Energy Management Program	GSE	ground support equipment
		GT	graphene tube
FeN ₄	iron atom coordinated to four nitrogen atoms	GTR	Global Technical Regulation
		GUI	graphical user interface
FeN _x	iron atom coordinated to “x” nitrogen atoms	GWE	Greenway Energy, LLC
		GWR	groundwater recharge
Fe _x N _y	iron-nitrogen species with “x” iron atoms coordinated to “y” nitrogen atoms	H	magnetic field induced by circulating current in a superconducting magnet
Fe-Zn-ZIF	zinc and iron zeolitic imidazolate framework	H ₂	hydrogen
FHWA	Federal Highway Administration		

H2A	Hydrogen Analysis model	HSC	high-surface-area carbon; high-surface carbon
H ₂ btdd	bis(1 <i>H</i> -1,2,3-triazolo[4,5- <i>b</i>],[4',5'- <i>i</i>])dibenzo[1,4]dioxin]	HSECoE	Hydrogen Storage Engineering Center of Excellence
H2FIRST	Hydrogen Fueling Infrastructure Research and Station Technology project	HSP	Hydrogen Safety Panel
H ₂ PhOHpydc	6-(4-carboxy-2-hydroxyphenyl)nicotinic acid	HT	high throughput
H ₂ S	hydrogen sulfide	HTAE	high-temperature alkaline electrolysis
H2VGI	hydrogen vehicle to grid integration	HTE	high-temperature electrolysis
H70	hydrogen service at 70 bar or 70 MPa	HTF	heat transfer fluid
HAADF	high angle annular dark field	HT-PEMFC	high-temperature polymer electrolyte membrane fuel cell
HA-FCG	hydrogen accelerated fatigue crack growth	HTT	hydrogen transport trailer
HAVO	Hawaii Volcanoes National Park	HX	heat exchanger
HAZ	heat affected zone	HyLine	high-pressure hydrogen pipeline for intra-urban distribution
HCD	hydrogen contaminant detector	HyMARC	Hydrogen Materials Advanced Research Consortium
HCD	high current density	HyRAM	Hydrogen Risk Assessment Models
HDPE	high-density polyethylene	HyReS	Hydrogen Regional Sustainability Framework
HDSAM	Hydrogen Delivery Scenario Analysis Model	HyS	hybrid sulfur
HDV	heavy-duty vehicle	HySCORE	Hydrogen Storage Characterization and Optimization Research Effort
HER	hydrogen evolution reaction	HyWAM	hydrogen wide area monitoring
HES	hydrogen energy system	Hz	Hertz
HEV	hybrid electric vehicle	I/C	ionomer-to-carbon ratio
HFC Nexus	Hydrogen Fuel Cell Nexus for the United States	I:C	ionomer-to-carbon ratio
HFR	high-frequency resistance	ICEV	internal combustion engine vehicle
HGV	hydrogen gas vehicle	ICHS	International Conference on Hydrogen Safety
HHC	Hawaii Hydrogen Carriers	ICP-MS	inductively coupled plasma mass spectrometry
Highway	EPA drive cycle representing highway type driving	IEC	ion exchange capacity
HIL	hardware-in-the-loop	IEEE	Institute of Electrical and Electronics Engineers
HiPoD	high power density cell	IFC	International Fire Code
HITRF	Hydrogen Infrastructure Testing and Research Facility	IJHE	International Journal of Hydrogen Energy
HNEI	Hawaii Natural Energy Institute	im	mass activity
HOR	hydrogen oxidation reaction	IMM	inverted metamorphic multijunction
HP	high pressure metal hydride candidate materials	INL	Idaho National Laboratory
HRS	hydrogen refueling station	IPA	isopropanol / 2-propanol
HR-TEM	high-resolution transmission electron microscopy	IR	infrared
HSAC	high-surface-area carbon		

<i>iR</i> -corrected	voltage/potential corrected for cell resistance	LSCF	(La,Sr)(Co,Fe)O ₃
<i>iR</i> -free	voltage/potential corrected for cell resistance	LTE	low-temperature electrolysis
IRIG	Inter-Laboratory Research Integration Group	mA	milliampere
IRS	ionomer-rich-surface	MA	mass activity
is	specific activity	MARAD	Maritime Administration
ISO	International Organization for Standardization	MarFC	maritime fuel cell
ITC	Investment Tax Credit	MAS NMR	magic angle spinning nuclear magnetic resonance
J-M	Johnson-Matthey	MASC	multi-acid side chain
JRC	(European) Joint Research Centre	MATI	modular adsorbent tank insert
K	Kelvin	MAWP	maximum allowable working pressure
KB	Ketjen black	max	maximum
kg	kilogram	MBE	molecular beam epitaxy
kMC	kinetic Monte Carlo	MBRC	miles between roadcall
kPaA	kiloPascals pressure, absolute	MCE	magnetocaloric effect
kW	kilowatt	m-CFDE	multi-electrode channel flow double electrode
kWh	kilowatt-hour	MCH	methyl cyclohexane
kW _{net}	net kilowatt electric	MCHL	magnetocaloric hydrogen liquefier
L	liter	MDHD	medium duty and heavy duty (vehicles)
L/D	length-to-diameter ratio	<i>m</i> -dobdc	4,6-dioxido-1,3-benzenedicarboxylate
LANL	Los Alamos National Laboratory	MDV	medium-duty vehicle
lbf	pound force	MEA	membrane electrode assembly
LBNL	Lawrence Berkeley National Laboratory	MEC	microbial electrolysis cell
lb	pounds mass	MeOH	methanol
LCD	low current density	MgB ₂ -THF	magnesium boride reacted with tetrahydrofuran
LDPE	low density polyethylene	MH	metal hydride
LDV	light-duty vehicle	MHC	metal hydride compressor
LH2	liquid hydrogen	Micro CT	micro computed tomography
LHC	liquid hydrogen carrier	MLVSI	multi-layer vacuum insulation
LHV	lower heating value	MMT	million metric tonnes
LI	laboratory instruction	MO	metal oxide
LLNL	Lawrence Livermore National Laboratory	MOCVD	metal organic chemical vapor deposition
LMRC	linear motor reciprocating compressor	MOF	metal organic framework
LN2	liquid nitrogen	MoP	molybdenum phosphide
LP	low pressure	MPa	megaPascal
LP@PF	low Pt@PGM-free	mph	miles per hour
LP@PFNF	low Pt@PGM-free nanofiber	MPL	microporous layer
LPHC	liquid phase hydrogen carrier	MSC	medium-surface-area carbon
LSAC	low-surface-area carbon		

MTA	County of Hawaii Mass Transit Agency	NTCNA	Nissan Technical Center North America
mV	millivolt	NTO	niobium-doped titanium oxide
MW	megawatt	NU	Northwestern University
MWh	megawatt-hour	O ₂	oxygen
MY	model year	OBU	onboard unit
MYRDD	Multi-Year Research, Development, and Demonstration	OCTA	Orange County Transportation Authority
NA	not applicable	OCV	open circuit voltage
NADH	nicotinamide adenine dinucleotide	OEM	original equipment manufacturer
NADPH	nicotinamide adenine dinucleotide phosphate	OER	oxygen evolution reaction
nano-CT	nanoscale X-ray computed tomography	OH	hydroxide
NaOH	sodium hydroxide	ORNL	Oak Ridge National Laboratory
NASA	National Aeronautics and Space Administration	ORR	oxygen reduction reaction
NBR	nitrile butyl rubber	OVC	ordered-vacancy compound
NC	nanocomposite	P	pressure
NDA	nondisclosure agreement	P&ID	pipng and instrumentation diagram
NE	Office of Nuclear Energy	PA	phosphoric acid
NELHA	Natural Energy Laboratory Hawaii Authority	PAA	poly(acrylic acid)
NFCTEC	National Fuel Cell Technology Evaluation Center	PAN	polyacrylonitrile
NFPA	National Fire Protection Association	PAP-TP-Me	poly(aryl piperidine) triphenyl methyl
NH ₃	ammonia	PAP-TP-MQN	poly(aryl piperidine) triphenyl mono quaternary ammonium
NHE	normal hydrogen electrode	PBI	polybenzimidazole
NHTSA	National Highway Traffic Safety Administration	PBI-PA	polybenzimidazole phosphoric acid
NIST	National Institute of Standards and Technology	PCE	proton conducting membrane
nm	nanometer	PCT	pressure, composition, temperature
NMP	N-methylpyrrolidone	Pd	palladium
NMR	nuclear magnetic resonance	PE	polyethylene
nPA	1-propanol l	PEC	photoelectrochemical
NPTF	nanoporous thin film	PEEK	polyetheretherketone
NPV	net present value	PEFC	polymer electrolyte fuel cell
NREL	National Renewable Energy Laboratory	PEM	polymer electrolyte membrane; proton exchange membrane
NSF DMREF	National Science Foundation Designing Materials to Revolutionize and Engineer our Future	PEMFC	polymer electrolyte membrane fuel cell; proton exchange membrane fuel cell
NSTF	nanostructured thin film	PEN	pentanediol
		PET	polyethylene terephthalate
		PF	perfluoro
		PFD	process flow diagram
		PFIA	perfluoro imide-acid
		PFSA	perfluorosulfonic acid
		PF-SFP	fluoride precursor

PG&E	Pacific Gas and Electric	QRA	quantitative risk assessment; quantitative risk analysis
PGM	platinum group metal		
PHA	preliminary hazard analysis; preliminary hazard assessment	R	load ratio
PI	principal investigator	R&D	research and development
Pip	piperidine	R2R	roll-to-roll
PL	photoluminescence	RCS	regulations, codes, and standards
PLL	potential loss of life	RD&D	research, development, and demonstration
PNNL	Pacific Northwest National Laboratory	RDE	rotating disk electrode
ppb	parts per billion	REF	Renewable Electricity Futures study
PPS	polyphenylene sulfide	RFP	request for proposals
PPS-40GF	polyphenylene sulfide with 40% glass fiber filler	RGA	residual gas analysis
PPSU	polyphenylsulfone	RH	rehydrogenation; relative humidity
PSD	particle size distribution	RHE	reversible hydrogen electrode
psi	pounds per square inch	RIF	infrared/reactive impinging flow
psig	pounds per square inch gage	RMSE	root mean square error
PSIS	powder sputter and implant system	RO ₂	local oxygen transport resistance
PSM	post-synthetic modification	ROI	record of invention
PSU	Pennsylvania State University	RPI	Rensselaer Polytechnic Institute
Pt	platinum	RPN	risk priority number
Pt/C	carbon-supported platinum	RRDE	rotating ring-disk electrode
PtCo	platinum-cobalt	RSDT	reactive spray deposition technology
PtCo/HSC	platinum and cobalt on high- surface-area carbon	RSU	roadside unit
PTFE	polytetrafluoroethylene	RT	room temperature
PTL	porous transport layer	RTO	ruthenium dioxide-titanium dioxide
PtNi	platinum-nickel	RTS	real-time simulation
PtNiNW	platinum-nickel nanowire	S&T	shell and tube (heat exchanger)
PtNW	platinum nanowire	SA	Strategic Analysis Inc.
PtRu	platinum-ruthenium	SAE	SAE International
Pt-TF	platinum-thin-film	SARTA	Stark Area Regional Transit Authority
PUD	pick-up and delivery (vehicles)	SASB	Sustainability Accounting Standards Board
PV	pressure volume	SBIR	Small Business Innovation Research
PVD	physical vapor deposition	SBV	Small Business Voucher
PWN	phosphonated poly(pentafluorosytrene)	SCAN	strongly constrained appropriately normed
PXRD	powder X-ray diffraction		
Pyr	pyridine	sccm	standard cubic centimeters per minute
Q	heat	SDE	SO ₂ depolarized electrolyzer
QA	quaternary ammonium	SDO	standards development organization
QAP	quaternary ammonium polymer		
QC	quality control		
QE	quantum efficiency		

SEBS	poly(styrene- <i>b</i> -(ethylene- <i>co</i> -butylene)- <i>b</i> -styrene)	TEM-EELS	transmission electron microscopy with electron energy loss spectroscopy
SED	strong electrostatic deposition	TETA	triethylene tetramine
SEM	scanning electron microscopy	Tg	glass transition temperature
SERA	Scenario Evaluation and Regionalization Analysis model	TGA	thermogravimetric analysis
SES	poly(styrene- <i>b</i> -ethylene- <i>b</i> -styrene)	THF	tetrahydrofuran
SFR	stagnation flow reactor	TIR	(SAE) Technical Information Report
SIO	Scripps Institution of Oceanography	TJ	tunnel junction
SISSO	sure independence screening and sparsifying operator	TKK	Tanaka Kikinzoku Kogyo K. K.
SLPM	standard liters per minute	TM	transition metal
SMR	steam methane reforming	TMA	trimethylamine
SMSI	strong metal support interaction	TMAC6PP	hexamethyl ammonium functionalized Diels-Alder poly(phenylene)
SMYS	specified minimum yield strength	TPD	thermally programmed desorption
SNL	Sandia National Laboratories	TPN	alkyl ammonium functionalized poly(terphenylene)
SOA	state of the art	TPRE	through-plane reactive excitation
SOEC	solid oxide electrolysis cell	tribo-	tribology
SOFC	solid oxide fuel cell	TRU	transport refrigeration unit
SPS	suspension plasma spray	TS	Technical Standard
SRNL	Savannah River National Laboratory	TTA	technology transfer agreement
SS	stainless steel	U.S.	United States
STC	solar thermochemical	UALR	University of Arkansas at Little Rock
STCH	solar thermochemical hydrogen	UCI	University of California, Irvine
STEM	scanning transmission electron microscopy	UConn	University of Connecticut
STF	$\text{Sr}(\text{Ti}_{0.3}\text{Fe}_{0.7})\text{O}_3$	UDDS	EPA drive cycle representing city type driving
STFC	$\text{Sr}(\text{Ti}_{0.3}\text{Fe}_{0.63}\text{Co}_{0.07})\text{O}_3$	UES	Unique Electric Solutions
STH	solar-to-hydrogen	UK CAER	University of Kentucky Center for Applied Energy Research
STWS	solar thermochemical water splitting	ULCL	ultra-low catalyst loading
SUNY	State University of New York	UN	United Nations
SWIFT	structured what-if analysis	UPS	United Parcel Service
SwRI	Southwest Research Institute	US06	EPA drive cycle with aggressive accelerations and some high-speed sections
sys/yr	systems per year	USAXS	ultra-small-angle X-ray scattering
T	temperature	USC	University of South Carolina
TBD	to be determined	USCAR	United States Council for Automotive Research
TC	technical committee	USCG	United States Coast Guard
Tc	Curie temperature	USGS	United States Geological Survey
TCO	total cost of ownership		
TEA	techno-economic analysis		
TEDS	thermal energy distribution system		
TEM	transmission electron microscopy		

UT-CEM	The University of Texas–Center for Electromechanics
UTF	ultrathin film
UTRC	United Technologies Research Center
UUV	unmanned underwater vehicle
UV	ultraviolet
V DC	voltage DC
VAC	volts alternating current
VACD	variable area control device
VBM	valence band maximum
VTIR	variable-temperature infrared
W/m ²	Watts per square meter
WaMM	water management membrane
WAVE	Wireless Access in Vehicular Environments
XAFS	X-ray absorption fine structure
XANES	X-ray absorption near-edge structure
XAS	X-ray absorption spectroscopy
XCT	X-ray computed tomography
XES	X-ray emission spectroscopy
XPS	X-ray photoelectron spectroscopy
XRD	X-ray diffraction
XRF	X-ray fluorescence
YSZ	(ZrO ₂) _{0.92} (Y ₂ O ₃) _{0.08}
ZANZEFF	Zero- and Near Zero-Emission Freight and Facilities
ZEBA	Zero Emission Bay Area
ZIF	zeolitic imidazolate framework
(Zn _{1-x} Fe _x)ZIF-F	zinc and iron zeolitic imidazolate framework fiber

Primary Contacts Index

Section Key

H2F	Hydrogen Fuel R&D
FC	Fuel Cell R&D
TAHI	Technology Acceleration and Hydrogen Infrastructure R&D
SCS	Safety, Codes and Standards
SA	Systems Analysis

A

Aceves, Salvador TAHI
Ahluwalia, Rajesh H2F, FC
Ahn, Channing H2F
Alia, Shaun TAHI
Allendorf, Mark H2F
Ayers, Katherine H2F (2)

B

Barilo, Nick SCS
Barnett, Scott H2F
Blanchard, Joe TAHI
Borup, Rod FC
Broerman, Eugene TAHI
Brooks, Kriston TAHI
Buttner, William SCS

C

Christensen, Steven H2F
Chung, Hoon H2F
Chung, Mike H2F
Connelly, Elizabeth SA
Corgnale, Claudio H2F

D

Dai, Sheng H2F
Daniel, Claus TAHI
De Castro, Emory FC
Denver, Jessie SCS
Dinh, Huyen H2F
Dismukes, Charles H2F

E

Ehrhart, Brian TAHI
Elgowainy, Amgad SA (2)

Eudy, Leslie TAHI
Ewan, Mitch TAHI

F

Fultz, Brent H2F

G

Gaillard, Nicolas H2F
Galbach, Phillip TAHI
Ganesan, Prabhu FC
Gennett, Thomas H2F
Ghezel-Ayagh, Hossein TAHI
Goodarzi, Abas TAHI
Greenway, Scott TAHI
Gu, Taoli TAHI

H

Hamdan, Monjid TAHI
Hanlin, Jason TAHI
Harned, Alleyn TAHI
Harrison, Kevin TAHI
Harrison, William FC
Haug, Andrew FC
Hecht, Ethan SCS
Holladay, Jamie TAHI
Hovsapian, Rob TAHI
Hunter, Chad SA

I

Ihnfeldt, Robin TAHI

J

James, Brian H2F (2), FC
Jaramillo, Thomas H2F
Johnson, Justin H2F
Johnson, Terry TAHI

K

Kim, Yu Seung H2F, FC (2)
 Kimball, Brett TAHI
 Kongkanand, Anusorn FC
 Kumaraguru, Swami FC

L

Lalli, Jennifer TAHI
 Litster, Shawn FC
 Liu, Di-Jia H2F (2), FC
 Liu, Hong H2F
 Lohse-Busch, Henning TAHI

M

Maness, Pin-Ching H2F
 Mann, Margaret TAHI
 Matter, Paul FC
 Mi, Zetian H2F
 Mukerjee, Sanjeev H2F
 Muna, Alice SCS
 Musgrave, Charles H2F
 Myers, Deborah FC

O

O'Brien, James TAHI
 Odom, Sara TAHI
 O'Hayre, Ryan H2F
 O'Shaughnessy, Shannan TAHI

P

Penev, Michael SA
 Perry, Mike FC
 Peters, Michael TAHI
 Pintauro, Peter FC
 Pivovar, Bryan FC (2)
 Pollica, Darryl TAHI

R

Ramani, Vijay FC
 Rivkin, Carl SCS
 Rockward, Tommy SCS
 Ronevich, Joseph TAHI
 Rousseau, Aymeric SA
 Ruth, Mark SA

S

San Marchi, Chris SCS
 Saur, Genevieve TAHI
 Saxena, Samveg TAHI
 Severa, Godwin H2F
 Shao, Yuyan FC
 Siegel, Donald H2F (2)
 Simmons, Kevin H2F, SCS
 Singh, Prabhakar H2F
 Spindelov, Jacob FC
 Sprik, Sam TAHI
 Stamenkovic, Vojislav FC
 Stechel, Ellen H2F
 Steinbach, Andrew FC

T

Thornton, Matthew H2F

U

Ulsh, Michael TAHI

V

Valente, Patrick TAHI

W

Wagener, Earl H2F
 Waldecker, James FC
 Wang, Jia FC
 Ward, Patrick H2F
 Weisenberger, Matthew H2F
 Wolverton, Chris H2F

X

Xu, Hui H2F, FC (3)

Y

Yaghi, Omar H2F
 Yelvington, Paul TAHI

Z

Zhu, Tianli H2F

Hydrogen and Fuel Cells Program Contacts

Sunita Satyapal

Director
Fuel Cell Technologies Office
Office of Energy Efficiency and Renewable Energy
U.S. Department of Energy
Phone: (202) 586-2336
Email: Sunita.Satyapal@ee.doe.gov

Priya Swamy

Operations Supervisor
Fuel Cell Technologies Office
Office of Energy Efficiency and Renewable Energy
U.S. Department of Energy
Phone: (202) 287-1875
Email: Priya.Swamy@ee.doe.gov

John Vetrano

Materials Sciences and Engineering Division
Basic Energy Sciences Program
Office of Science
U.S. Department of Energy
Phone: (301) 903-5976
Email: John.Vetrano@science.doe.gov

Regis Conrad

Office of Fossil Energy
U.S. Department of Energy
Phone: (301) 903-2827
Email: Regis.Conrad@hq.doe.gov

Melissa Bates

Office of Nuclear Energy
U.S. Department of Energy
Phone: (301) 903-0930
Email: Melissa.Bates@nuclear.energy.gov

HYDROGEN FUEL R&D

Eric Miller

Hydrogen Production Subprogram Manager
Fuel Cell Technologies Office
Office of Energy Efficiency and Renewable Energy
U.S. Department of Energy
Phone: (202) 287-5829
Email: Eric.Miller@ee.doe.gov

Ned Stetson

Hydrogen Storage Subprogram Manager
Fuel Cell Technologies Office
Office of Energy Efficiency and Renewable Energy
U.S. Department of Energy
Phone: (202) 586-9995
Email: Ned.Stetson@ee.doe.gov

Jesse Adams

Technology Manager
Fuel Cell Technologies Office
Office of Energy Efficiency and Renewable Energy
U.S. Department of Energy
Phone: (720) 356-1421
Email: Jesse.Adams@ee.doe.gov

Bahman Habibzadeh

Technology Manager
Fuel Cell Technologies Office
Office of Energy Efficiency and Renewable Energy
U.S. Department of Energy
Phone: (202) 287-1657
Email: Bahman.Habibzadeh@ee.doe.gov

David Peterson

Technology Manager
Fuel Cell Technologies Office
Office of Energy Efficiency and Renewable Energy
U.S. Department of Energy
Phone: (720) 356-1747
Email: David.Peterson@ee.doe.gov

Katie Randolph

Technology Manager
Fuel Cell Technologies Office
Office of Energy Efficiency and Renewable Energy
U.S. Department of Energy
Phone: (720) 356-1759
Email: Katie.Randolph@ee.doe.gov

FUEL CELL R&D

Dimitrios Papageorgopoulos

Fuel Cell R&D Subprogram Manager
Fuel Cell Technologies Office
Office of Energy Efficiency and Renewable Energy
U.S. Department of Energy
Phone: (202) 586-5463
Email: Dimitrios.Papageorgopoulos@ee.doe.gov

Donna Ho

Technology Manager
Fuel Cell Technologies Office
Office of Energy Efficiency and Renewable Energy
U.S. Department of Energy
Phone: (202) 586-8000
Email: Donna.Ho@ee.doe.gov

Greg Kleen

Technology Manager
Fuel Cell Technologies Office
Office of Energy Efficiency and Renewable Energy
U.S. Department of Energy
Phone: (720) 356-1672
Email: Gregory.Kleen@ee.doe.gov

TECHNOLOGY ACCELERATION AND HYDROGEN INFRASTRUCTURE R&D

Fred Joseck

Technology Acceleration and Hydrogen
Infrastructure R&D Manager
Fuel Cell Technologies Office
Office of Energy Efficiency and Renewable Energy
U.S. Department of Energy
Phone: (202) 586-7932
Email: Fred.Joseck@ee.doe.gov

Peter Devlin

Technology Acceleration Project Manager
Fuel Cell Technologies Office
Office of Energy Efficiency and Renewable Energy
U.S. Department of Energy
Phone: (202) 586-4905
Email: Peter.Devlin@ee.doe.gov

Nancy L. Garland

Technology Acceleration Project Manager
Fuel Cell Technologies Office
Office of Energy Efficiency and Renewable Energy
U.S. Department of Energy
Phone: (202) 586-5673
Email: Nancy.Garland@ee.doe.gov

Jason Marcinkoski

Technology Acceleration Project Manager
Fuel Cell Technologies Office
Office of Energy Efficiency and Renewable Energy
U.S. Department of Energy
Phone: (202) 586-7466
Email: Jason.Marcinkoski@ee.doe.gov

Neha Rustagi

Hydrogen Infrastructure R&D Project Manager
Fuel Cell Technologies Office
Office of Energy Efficiency and Renewable Energy
U.S. Department of Energy
Phone: (202) 586-8424
Email: Neha.Rustagi@ee.doe.gov

SAFETY, CODES AND STANDARDS

Laura Hill

Safety, Codes and Standards Project Manager
Fuel Cell Technologies Office
Office of Energy Efficiency and Renewable Energy
U.S. Department of Energy
Phone: (202) 586-8384
Email: Laura.Hill@ee.doe.gov

SYSTEMS ANALYSIS

Fred Joseck

Systems Analysis Subprogram Manager
Fuel Cell Technologies Office
Office of Energy Efficiency and Renewable Energy
U.S. Department of Energy
Phone: (202) 586-7932
Email: Fred.Joseck@ee.doe.gov

Shawna McQueen

Project Manager
Fuel Cell Technologies Office
Office of Energy Efficiency and Renewable Energy
U.S. Department of Energy
Phone: (202) 586-0833
Email: Shawna.McQueen@ee.doe.gov

Project Listings by State

Section Key

H2F	Hydrogen Fuel R&D
FC	Fuel Cell R&D
TAHI	Technology Acceleration and Hydrogen Infrastructure R&D
SCS	Safety, Codes and Standards
SA	Systems Analysis

Arizona

H2F Arizona State University: HydroGEN Seedling: Mixed Ionic Electronic Conducting Quaternary Perovskites: Materials by Design for Solar Thermochemical Hydrogen

California

H2F Stanford University: HydroGEN Seedling: Protective Catalyst Systems on III-V and Si-Based Semiconductors for Efficient, Durable Photoelectrochemical Water Splitting Devices

H2F California Institute of Technology: Design and Synthesis of Materials with High Capacities for Hydrogen Physisorption

H2F Sandia National Laboratories: HyMARC: A Consortium for Advancing Hydrogen Storage Materials

H2F Liox Power: HyMARC Seedling: Electrolyte-Assisted Hydrogen Storage Reactions

H2F University of California, Berkeley: HyMARC Seedling: Super Metalated Frameworks as Hydrogen Sponges

TAHI Sandia National Laboratories: Maritime Fuel Cell Generator Project

TAHI US Hybrid: Northeast Demonstration and Deployment of FCRx200

TAHI Lawrence Livermore National Laboratory: Performance and Durability Testing of Volumetrically Efficient Cryogenic Vessels and High-Pressure Liquid Hydrogen Pump

TAHI Electricore, Inc.: Innovative Advanced Hydrogen Mobile Fueler

TAHI Lawrence Berkeley National Laboratory: Integrated Systems Modeling of the Interactions between Stationary Hydrogen, Vehicles, and Grid Resources

TAHI Sandia National Laboratories: Fatigue Performance of High-Strength Pipeline Steels and Their Welds in Hydrogen Gas Service

TAHI Sandia National Laboratories: Metal Hydride Compression

TAHI General Engineering & Research: Low-Cost Magnetocaloric Materials Discovery

SCS Sandia National Laboratories: R&D for Safety, Codes and Standards: Materials and Components Compatibility

SCS Sandia National Laboratories: R&D for Safety, Codes and Standards: Hydrogen Behavior

SCS City and County of San Francisco: Advancing Fuel Cell Electric Vehicles in San Francisco and Beyond

Colorado

H2F National Renewable Energy Laboratory: Biomass to Hydrogen (B2H2)

H2F Huyen Dinh: HydroGEN Overview: A Consortium on Advanced Water-Splitting Materials

H2F Colorado School of Mines: HydroGEN Seedling: Accelerated Discovery of Solar Thermochemical Hydrogen Production Materials via High-Throughput Computational and Experimental Methods

- H2F University of Colorado Boulder: HydroGEN Seedling: Computationally Accelerated Discovery and Experimental Demonstration of High-Performance Materials for Advanced Solar Thermochemical Hydrogen Production
- H2F National Renewable Energy Laboratory: Hydrogen Storage System Modeling: Public Access, Maintenance, and Enhancements
- H2F National Renewable Energy Laboratory: HySCORE: Hydrogen Storage Characterization and Optimization Research Effort
- H2F National Renewable Energy Laboratory: HyMARC Seedling: Fluorinated Covalent Organic Frameworks: A Novel Pathway to Enhance Hydrogen Sorption and Control Isosteric Heats of Adsorption
- H2F National Renewable Energy Laboratory: HyMARC Seedling: Atomic Layer Deposition Synthesis of Novel Nanostructured Metal Borohydrides
- FC National Renewable Energy Laboratory: Extended Surface Electrocatalyst Development
- FC National Renewable Energy Laboratory: Advanced Ionomers and Membrane Electrode Assemblies for Alkaline Membrane Fuel Cells
- TAHI National Renewable Energy Laboratory: Fuel Cell Membrane Electrode Assembly Manufacturing R&D
- TAHI National Renewable Energy Laboratory: Manufacturing Competitiveness Analysis for Hydrogen Refueling Stations
- TAHI National Renewable Energy Laboratory: Technology Validation: Fuel Cell Bus Evaluations
- TAHI National Renewable Energy Laboratory: Hydrogen Station Data Collection and Analysis
- TAHI National Renewable Energy Laboratory: Optimal Stationary Fuel Cell Integration and Control (Energy Dispatch Controller)
- TAHI National Renewable Energy Laboratory: H2@Scale: Experimental Characterization of Durability of Advanced Electrolyzer Concepts in Dynamic Loading
- TAHI National Renewable Energy Laboratory: 700-bar Hydrogen Dispenser Hose Reliability Improvement
- TAHI National Renewable Energy Laboratory: Dispenser Reliability
- SCS National Renewable Energy Laboratory: National Codes and Standards Development and Outreach
- SCS National Renewable Energy Laboratory: NREL Hydrogen Sensor Testing Laboratory
- SA National Renewable Energy Laboratory: Sustainability Analysis: Hydrogen Regional Sustainability (HyReS)
- SA National Renewable Energy Laboratory: Regional Supply of Hydrogen
- SA National Renewable Energy Laboratory: Market Segmentation Analysis of Medium- and Heavy-Duty Trucks with a Fuel Cell Emphasis
- SA National Renewable Energy Laboratory: H2@Scale Analysis

Connecticut

- H2F Proton OnSite: Benchmarking Advanced Water Splitting Technologies: Best Practices in Materials Characterization
- H2F University of Connecticut: HydroGEN Seedling: Proton-Conducting Solid Oxide Electrolysis Cells for Large-Scale Hydrogen Production at Intermediate Temperatures
- H2F United Technologies Research Center: HydroGEN Seedling: Thin-Film, Metal-Supported, High-Performance, and Durable Proton-Solid Oxide Electrolyzer Cell

- H2F Proton OnSite: HydroGEN Seedling: High-Efficiency Proton Exchange Membrane Water Electrolysis Enabled by Advanced Catalysts, Membranes, and Processes
- FC United Technologies Research Center: High-Performance Polymer Electrolyte Membrane Fuel Cell Electrode Structures
- TAHI FuelCell Energy, Inc.: Modular Solid Oxide Electrolysis Cell System for Efficient Hydrogen Production at High Current Density

Delaware

- TAHI Xergy Inc.: Novel Membranes for Electrochemical Hydrogen Compression Enabling Increased Pressure Capability and Higher Pumping Efficiency

Florida

- TAHI Mainstream Engineering: In-Line Quality Control of Polymer Electrolyte Membrane Materials

Georgia

- TAHI Center for Transportation and the Environment: Fuel Cell Hybrid Electric Delivery Van

Hawaii

- H2F University of Hawaii: HydroGEN Seedling: Novel Chalcopyrites For Advanced Photoelectrochemical Water Splitting
- H2F University of Hawaii: HyMARC Seedling: Development of Magnesium Boride Etherates as Hydrogen Storage Materials
- TAHI Hawaii Natural Energy Institute: Hydrogen Energy Systems as a Grid Management Tool

Idaho

- TAHI Idaho National Laboratory: Grid Integration and Hydrogen Energy Generation: Modeling and Validation of Electrolyzers in Real-Time Grid Simulation
- TAHI Idaho National Laboratory: High-Temperature Electrolysis Test Stand

Illinois

- H2F Northwestern University: HydroGEN Seedling: Degradation Characterization and Modeling of a New Solid Oxide Electrolysis Cell Utilizing Accelerated Life Testing
- H2F Argonne National Laboratory: HydroGEN Seedling: Platinum-Group-Metal-Free Oxygen Evolution Reaction Catalysts for Proton Exchange Membrane Electrolyzers
- H2F Argonne National Laboratory: HydroGEN Seedling: Transformative Materials for High-Efficiency Thermochemical Production of Solar Fuels
- H2F Argonne National Laboratory: Systems Analysis of Physical and Materials-Based Hydrogen Storage
- H2F Argonne National Laboratory: HyMARC Seedling: "Graphene-Wrapped" Complex Hydrides as High-Capacity, Regenerable Hydrogen Storage Materials
- FC Argonne National Laboratory: Tailored High-Performance Low-Platinum-Group-Metal Alloy Cathode Catalysts
- FC Argonne National Laboratory: ElectroCat (Electrocatalysis Consortium)
- FC Argonne National Laboratory: Highly Efficient and Durable Cathode Catalyst with Ultralow Platinum Loading Through Synergetic Platinum/Platinum-Group-Metal-Free Catalytic Interaction
- FC Argonne National Laboratory: Performance of Advanced Automotive Fuel Cell Stacks and Systems with State-of-the-Art d-PtCo/C Cathode Catalyst in Membrane Electrode Assemblies

- TAHI Argonne National Laboratory: Toyota Mirai Testing
- SA Argonne National Laboratory: Regional Water Stress Analysis with Hydrogen Production at Scale
- SA Argonne National Laboratory: Analysis of Technology Improvement in Fuel Cell Vehicles
- SA Argonne National Laboratory: Analysis of Cost Impacts of Integrating Advanced Onboard Storage Systems with Hydrogen Delivery

Kentucky

- H2F University of Kentucky: Precursor Processing Development for Low-Cost, High-Strength Carbon Fiber for Composite Overwrapped Pressure Vessel Applications

Massachusetts

- H2F Giner, Inc.: High-Temperature Alkaline Water Electrolysis
- H2F Northeastern University: HydroGEN Seedling: Enabling Efficient Water Splitting with Advanced Materials Designed for High-pH Membrane Interface
- FC Giner, Inc.: ElectroCat: Durable Mn-Based Platinum-Group-Metal-Free Catalysts for Polymer Electrolyte Membrane Fuel Cells
- FC Giner, Inc.: FY15 SBIR II Release 2: Ionomer Dispersion Impact on Fuel Cell and Electrolyzer Performance and Durability
- FC Advent Technologies, Inc.: Facilitated Direct Liquid Fuel Cells with High-Temperature Membrane Electrode Assemblies
- FC Giner, Inc.: Advanced Catalysts and Membrane Electrode Assemblies for Reversible Alkaline Membrane Fuel Cells
- TAHI Giner ELX, Inc.: Electrochemical Compression
- TAHI Ivys Energy Solutions: Advancing Hydrogen Dispenser Technology by Using Innovative Intelligent Networks
- TAHI GVD Corporation: Advanced Barrier Coatings for Harsh Environments

Michigan

- H2F University of Michigan: HydroGEN Seedling: Monolithically Integrated Thin-Film/Silicon Tandem Photoelectrodes for High-Efficiency and Stable Photoelectrochemical Water Splitting
- H2F University of Michigan: Hydrogen Adsorbents with High Volumetric Density: New Materials and System Projections
- H2F University of Michigan: HyMARC Seedling: Optimized Hydrogen Adsorbents via Machine Learning and Crystal Engineering
- FC General Motors: Highly Accessible Catalysts for Durable High-Power Performance
- FC Ford Motor Company: Vapor Deposition Process for Engineering of Dispersed Polymer Electrolyte Membrane Fuel Cell Oxygen Reduction Reaction Pt/NbO_x/C Catalysts
- FC General Motors: Durable High-Power Membrane Electrode Assemblies with Low Platinum Loading

Minnesota

- FC 3M Company: Highly Active, Durable, and Ultra-Low-Platinum-Group-Metal Nanostructured Thin Film Oxygen Reduction Reaction Catalysts and Supports
- FC 3M Company: Novel Ionomers and Electrode Structures for Improved Polymer Electrolyte Membrane Fuel Cell Electrode Performance at Low Platinum-Group-Metal Loadings

Missouri

FC Washington University in St. Louis: Corrosion-Resistant Non-Carbon Electrocatalyst Supports for Proton Exchange Fuel Cells

New Jersey

H2F Rutgers University: HydroGEN Seedling: Best-in-Class Platinum-Group-Metal-Free Catalyst Integrated Tandem Junction Photoelectrochemical Water Splitting Devices

New Mexico

H2F Los Alamos National Laboratory: HydroGEN Seedling: High-Performance Ultralow-Cost Non-Precious-Metal Catalyst System for Anion Exchange Membrane Electrolyzer

H2F Los Alamos National Laboratory: HydroGEN Seedling: Scalable Elastomeric Membranes for Alkaline Water Electrolysis

FC Los Alamos National Laboratory: Advanced Electrocatalysts Through Crystallographic Enhancement

FC Los Alamos National Laboratory: Advanced Materials for Fully Integrated Membrane Electrode Assemblies in Anion Exchange Membrane Fuel Cells

FC Los Alamos National Laboratory: Polymer-Based Fuel Cells that Operate from 80°C to 220°C

FC Los Alamos National Laboratory: FC-PAD: Fuel Cell Performance and Durability Consortium

TAHI Sandia National Laboratories: Hydrogen Stations for Urban Sites

SCS Los Alamos National Laboratory: Fuel Quality Assurance Research and Development and Impurity Testing in Support of Codes and Standards

SCS Sandia National Laboratories: Hydrogen Quantitative Risk Assessment

New York

FC Brookhaven National Laboratory: Platinum Monolayer Electrocatalysts

TAHI Automated Dynamics: Continuous Fiber Composite Electrofusion Coupler

Ohio

FC pH Matter, LLC: FY16 SBIR II Release 1: Regenerative Fuel Cell System

TAHI Ohio Fuel Cell Coalition: Clean Energy Supply Chain and Manufacturing Competitiveness Analysis for Hydrogen and Fuel Cell Technologies

Oregon

H2F Oregon State University: Novel Hybrid Microbial Electrochemical System for Efficient Hydrogen Generation from Biomass

Pennsylvania

H2F Pennsylvania State University: Developing a New Polyolefin Precursor for Low-Cost, High-Strength Carbon Fiber

FC Carnegie Mellon University: ElectroCat: Advanced Platinum-Group-Metal-Free Cathode Engineering for High Power Density and Durability

South Carolina

H2F Tetramer Technologies, LLC: New Approaches to Improved Proton Exchange Membrane Electrolyzer Ion Exchange Membranes

- H2F Greenway Energy, LLC: HydroGEN Seedling: High-Temperature Reactor Catalyst Material Development for Low-Cost and Efficient Solar-Driven Sulfur-Based Processes
- H2F Savannah River National Laboratory: Investigation of Solid-State Hydrides for Autonomous Fuel Cell Vehicles
- FC Greenway Energy, LLC: ElectroCat: Platinum-Group-Metal-Free Engineered Framework Nano-Structure Catalyst
- TAHI Greenway Energy, LLC: Hybrid Electrochemical Hydrogen/Metal Hydride Compressor

Tennessee

- H2F Oak Ridge National Laboratory: Novel Plasticized Melt-Spinning Process of Polyacrylonitrile Fibers Based on Task-Specific Ionic Liquids
- FC Vanderbilt University: Fuel Cell Membrane Electrode Assemblies with Ultra-Low-Platinum Nanofiber Electrodes
- TAHI Oak Ridge National Laboratory: Roll-to-Roll Advanced Materials Manufacturing Lab Consortium
- TAHI Federal Express Corporation: FedEx Express Hydrogen Fuel Cell Extended-Range Battery Electric Vehicles

Texas

- TAHI Southwest Research Institute: Hydrogen Compression Application of the Linear Motor Reciprocating Compressor

Virginia

- H2F Strategic Analysis, Inc.: Analysis of Advanced Hydrogen Production Pathways
- H2F Strategic Analysis, Inc.: Hydrogen Storage Cost Analysis
- FC NanoSonic, Inc.: FY17 SBIR II Release 1: Novel Hydrocarbon Ionomers for Durable Polymer Electrolyte Membranes
- FC Strategic Analysis, Inc.: Fuel Cell Systems Analysis
- TAHI Virginia Clean Cities at James Madison University: Hydrogen Fuel Cell Nexus Business-to-Business Website
- TAHI NanoSonic, Inc.: Cryogenically Flexible, Low-Permeability Hydrogen Delivery Hose

Washington

- H2F Pacific Northwest National Laboratory: Material Challenges for Cryogenic Hydrogen Storage Technologies
- FC Pacific Northwest National Laboratory: ElectroCat: Highly Active and Durable Platinum-Group-Metal-Free Oxygen Reduction Reaction Electrocatalysts Through the Synergy of Active Sites
- TAHI Plug Power, Inc.: Fuel-Cell-Powered Airport Ground Support Equipment Deployment
- TAHI Pacific Northwest National Laboratory: Demonstration of Fuel Cell Auxiliary Power Unit to Power Truck Refrigeration Units in Refrigerated Trucks
- TAHI Pacific Northwest National Laboratory: Magnetocaloric Hydrogen Liquefaction
- SCS Pacific Northwest National Laboratory: Hydrogen Safety Panel, Safety Knowledge Tools, and First Responder Training Resources
- SCS Pacific Northwest National Laboratory: Compatibility of Polymeric Materials Used in the Hydrogen Infrastructure

Project Listings by Organization

Section Key

H2F	Hydrogen Fuel R&D
FC	Fuel Cell R&D
TAHI	Technology Acceleration and Hydrogen Infrastructure R&D
SCS	Safety, Codes and Standards
SA	Systems Analysis

3M Company

- FC Highly Active, Durable, and Ultra-Low-Platinum-Group-Metal Nanostructured Thin Film Oxygen Reduction Reaction Catalysts and Supports
- FC Novel Ionomers and Electrode Structures for Improved Polymer Electrolyte Membrane Fuel Cell Electrode Performance at Low Platinum-Group-Metal Loadings

Advent Technologies, Inc.

- FC Facilitated Direct Liquid Fuel Cells with High-Temperature Membrane Electrode Assemblies

Argonne National Laboratory

- H2F HydroGEN Seedling: Platinum-Group-Metal-Free Oxygen Evolution Reaction Catalysts for Proton Exchange Membrane Electrolyzers
- H2F Systems Analysis of Physical and Materials-Based Hydrogen Storage
- H2F HyMARC Seedling: “Graphene-Wrapped” Complex Hydrides as High-Capacity, Regenerable Hydrogen Storage Materials
- FC Tailored High-Performance Low-Platinum-Group-Metal Alloy Cathode Catalysts
- FC ElectroCat (Electrocatalysis Consortium)
- FC Highly Efficient and Durable Cathode Catalyst with Ultralow Platinum Loading Through Synergetic Platinum/Platinum-Group-Metal-Free Catalytic Interaction
- FC Performance of Advanced Automotive Fuel Cell Stacks and Systems with State-of-the-Art d-PtCo/C Cathode Catalyst in Membrane Electrode Assemblies
- TAHI Toyota Mirai Testing
- SA Regional Water Stress Analysis with Hydrogen Production at Scale
- SA Analysis of Technology Improvement in Fuel Cell Vehicles
- SA Analysis of Cost Impacts of Integrating Advanced Onboard Storage Systems with Hydrogen Delivery

Arizona State University

- H2F HydroGEN Seedling: Mixed Ionic Electronic Conducting Quaternary Perovskites: Materials by Design for Solar Thermochemical Hydrogen

Automated Dynamics

- TAHI Continuous Fiber Composite Electrofusion Coupler

Brookhaven National Laboratory

- FC Platinum Monolayer Electrocatalysts

California Institute of Technology

H2F Design and Synthesis of Materials with High Capacities for Hydrogen Physisorption

Carnegie Mellon University

FC ElectroCat: Advanced Platinum-Group-Metal-Free Cathode Engineering for High Power Density and Durability

Center for Transportation and the Environment

TAHI Fuel Cell Hybrid Electric Delivery Van

City and County of San Francisco

SCS Advancing Fuel Cell Electric Vehicles in San Francisco and Beyond

Colorado School of Mines

H2F HydroGEN Seedling: Accelerated Discovery of Solar Thermochemical Hydrogen Production Materials via High-Throughput Computational and Experimental Methods

Electricore, Inc.

TAHI Innovative Advanced Hydrogen Mobile Fueler

Federal Express Corporation

TAHI FedEx Express Hydrogen Fuel Cell Extended-Range Battery Electric Vehicles

Ford Motor Company

FC Vapor Deposition Process for Engineering of Dispersed Polymer Electrolyte Membrane Fuel Cell Oxygen Reduction Reaction Pt/NbO_x/C Catalysts

FuelCell Energy, Inc.

TAHI Modular Solid Oxide Electrolysis Cell System for Efficient Hydrogen Production at High Current Density

General Engineering & Research

TAHI Low-Cost Magnetocaloric Materials Discovery

General Motors

FC Highly Accessible Catalysts for Durable High-Power Performance

FC Durable High-Power Membrane Electrode Assemblies with Low Platinum Loading

Giner ELX, Inc.

TAHI Electrochemical Compression

Giner, Inc.

H2F High-Temperature Alkaline Water Electrolysis

FC ElectroCat: Durable Mn-Based Platinum-Group-Metal-Free Catalysts for Polymer Electrolyte Membrane Fuel Cells

FC FY15 SBIR II Release 2: Ionomer Dispersion Impact on Fuel Cell and Electrolyzer Performance and Durability

FC Advanced Catalysts and Membrane Electrode Assemblies for Reversible Alkaline Membrane Fuel Cells

Greenway Energy, LLC

H2F HydroGEN Seedling: High-Temperature Reactor Catalyst Material Development for Low-Cost and Efficient Solar-Driven Sulfur-Based Processes

TAHI Hybrid Electrochemical Hydrogen/Metal Hydride Compressor

FC ElectroCat: Platinum-Group-Metal-Free Engineered Framework Nano-Structure Catalyst

GVD Corporation

TAHI Advanced Barrier Coatings for Harsh Environments

Hawaii Natural Energy Institute

TAHI Hydrogen Energy Systems as a Grid Management Tool

Idaho National Laboratory

TAHI Grid Integration and Hydrogen Energy Generation: Modeling and Validation of Electrolyzers in Real-Time Grid Simulation

TAHI High-Temperature Electrolysis Test Stand

Ivys Energy Solutions

TAHI Advancing Hydrogen Dispenser Technology by Using Innovative Intelligent Networks

Lawrence Berkeley National Laboratory

TAHI Integrated Systems Modeling of the Interactions between Stationary Hydrogen, Vehicles, and Grid Resources

Lawrence Livermore National Laboratory

TAHI Performance and Durability Testing of Volumetrically Efficient Cryogenic Vessels and High-Pressure Liquid Hydrogen Pump

Liox Power

H2F HyMARC Seedling: Electrolyte-Assisted Hydrogen Storage Reactions

Los Alamos National Laboratory

H2F HydroGEN Seedling: High-Performance Ultralow-Cost Non-Precious-Metal Catalyst System for Anion Exchange Membrane Electrolyzer

H2F HydroGEN Seedling: Scalable Elastomeric Membranes for Alkaline Water Electrolysis

FC Advanced Electrocatalysts Through Crystallographic Enhancement

FC Advanced Materials for Fully Integrated Membrane Electrode Assemblies in Anion Exchange Membrane Fuel Cells

FC Polymer-Based Fuel Cells that Operate from 80°C to 220°C

FC FC-PAD: Fuel Cell Performance and Durability Consortium

SCS Fuel Quality Assurance Research and Development and Impurity Testing in Support of Codes and Standards

Mainstream Engineering

TAHI In-Line Quality Control of Polymer Electrolyte Membrane Materials

NanoSonic, Inc.

FC FY17 SBIR II Release 1: Novel Hydrocarbon Ionomers for Durable Polymer Electrolyte Membranes

TAHI Cryogenically Flexible, Low-Permeability Hydrogen Delivery Hose

National Renewable Energy Laboratory

H2F Biomass to Hydrogen (B2H2)

H2F HydroGEN Overview: A Consortium on Advanced Water-Splitting Materials

H2F Hydrogen Storage System Modeling: Public Access, Maintenance, and Enhancements

H2F HySCORE: Hydrogen Storage Characterization and Optimization Research Effort

H2F HyMARC Seedling: Fluorinated Covalent Organic Frameworks: A Novel Pathway to Enhance Hydrogen Sorption and Control Isosteric Heats of Adsorption

H2F HyMARC Seedling: Atomic Layer Deposition Synthesis of Novel Nanostructured Metal Borohydrides

FC Extended Surface Electrocatalyst Development

FC Advanced Ionomers and Membrane Electrode Assemblies for Alkaline Membrane Fuel Cells

TAHI Fuel Cell Membrane Electrode Assembly Manufacturing R&D

TAHI Manufacturing Competitiveness Analysis for Hydrogen Refueling Stations

TAHI Technology Validation: Fuel Cell Bus Evaluations

TAHI Hydrogen Station Data Collection and Analysis

TAHI Optimal Stationary Fuel Cell Integration and Control (Energy Dispatch Controller)

TAHI H2@Scale: Experimental Characterization of Durability of Advanced Electrolyzer Concepts in Dynamic Loading

TAHI 700-bar Hydrogen Dispenser Hose Reliability Improvement

TAHI Dispenser Reliability

SCS National Codes and Standards Development and Outreach

SCS NREL Hydrogen Sensor Testing Laboratory

SA Sustainability Analysis: Hydrogen Regional Sustainability (HyReS)

SA Regional Supply of Hydrogen

SA Market Segmentation Analysis of Medium- and Heavy-Duty Trucks with a Fuel Cell Emphasis

SA H2@Scale Analysis

Northeastern University

H2F HydroGEN Seedling: Enabling Efficient Water Splitting with Advanced Materials Designed for High-pH Membrane Interface

Northwestern University

H2F HydroGEN Seedling: Degradation Characterization and Modeling of a New Solid Oxide Electrolysis Cell Utilizing Accelerated Life Testing

H2F HydroGEN Seedling: Transformative Materials for High-Efficiency Thermochemical Production of Solar Fuels

Oak Ridge National Laboratory

H2F Novel Plasticized Melt-Spinning Process of Polyacrylonitrile Fibers Based on Task-Specific Ionic Liquids

TAHI Roll-to-Roll Advanced Materials Manufacturing Lab Consortium

Ohio Fuel Cell Coalition

TAHI Clean Energy Supply Chain and Manufacturing Competitiveness Analysis for Hydrogen and Fuel Cell Technologies

Oregon State University

H2F Novel Hybrid Microbial Electrochemical System for Efficient Hydrogen Generation from Biomass

Pacific Northwest National Laboratory

H2F Material Challenges for Cryogenic Hydrogen Storage Technologies

FC ElectroCat: Highly Active and Durable Platinum-Group-Metal-Free Oxygen Reduction Reaction Electrocatalysts Through the Synergy of Active Sites

TAHI Demonstration of Fuel Cell Auxiliary Power Unit to Power Truck Refrigeration Units in Refrigerated Trucks

TAHI Magnetocaloric Hydrogen Liquefaction

SCS Hydrogen Safety Panel, Safety Knowledge Tools, and First Responder Training Resources

SCS Compatibility of Polymeric Materials Used in the Hydrogen Infrastructure

Pennsylvania State University

H2F Developing a New Polyolefin Precursor for Low-Cost, High-Strength Carbon Fiber

pH Matter, LLC

FC FY16 SBIR II Release 1: Regenerative Fuel Cell System

Plug Power, Inc.

TAHI Fuel-Cell-Powered Airport Ground Support Equipment Deployment

Proton OnSite

H2F Benchmarking Advanced Water Splitting Technologies: Best Practices in Materials Characterization

H2F HydroGEN Seedling: High-Efficiency Proton Exchange Membrane Water Electrolysis Enabled by Advanced Catalysts, Membranes, and Processes

Rutgers University

H2F HydroGEN Seedling: Best-in-Class Platinum-Group-Metal-Free Catalyst Integrated Tandem Junction Photoelectrochemical Water Splitting Devices

Sandia National Laboratories

H2F HyMARC: A Consortium for Advancing Hydrogen Storage Materials

TAHI Maritime Fuel Cell Generator Project

- TAHI Hydrogen Stations for Urban Sites
TAHI Fatigue Performance of High-Strength Pipeline Steels and Their Welds in Hydrogen Gas Service
TAHI Metal Hydride Compression
SCS R&D for Safety, Codes and Standards: Materials and Components Compatibility
SCS R&D for Safety, Codes and Standards: Hydrogen Behavior
SCS Hydrogen Quantitative Risk Assessment

Savannah River National Laboratory

- H2F Investigation of Solid-State Hydrides for Autonomous Fuel Cell Vehicles

Southwest Research Institute

- TAHI Hydrogen Compression Application of the Linear Motor Reciprocating Compressor

Stanford University

- H2F HydroGEN Seedling: Protective Catalyst Systems on III-V and Si-Based Semiconductors for Efficient, Durable Photoelectrochemical Water Splitting Devices

Strategic Analysis, Inc.

- H2F Analysis of Advanced Hydrogen Production Pathways
H2F Hydrogen Storage Cost Analysis
FC Fuel Cell Systems Analysis

Tetramer Technologies, LLC

- H2F New Approaches to Improved Proton Exchange Membrane Electrolyzer Ion Exchange Membranes

United Technologies Research Center

- H2F HydroGEN Seedling: Thin-Film, Metal-Supported, High-Performance, and Durable Proton-Solid Oxide Electrolyzer Cell
FC High-Performance Polymer Electrolyte Membrane Fuel Cell Electrode Structures

University of California, Berkeley

- H2F HyMARC Seedling: Super Metalated Frameworks as Hydrogen Sponges

University of Colorado Boulder

- H2F HydroGEN Seedling: Computationally Accelerated Discovery and Experimental Demonstration of High-Performance Materials for Advanced Solar Thermochemical Hydrogen Production

University of Connecticut

- H2F HydroGEN Seedling: Proton-Conducting Solid Oxide Electrolysis Cells for Large-Scale Hydrogen Production at Intermediate Temperatures

University of Hawaii

- H2F HydroGEN Seedling: Novel Chalcopyrites For Advanced Photoelectrochemical Water Splitting
H2F HyMARC Seedling: Development of Magnesium Boride Etherates as Hydrogen Storage Materials

University of Kentucky

H2F Precursor Processing Development for Low-Cost, High-Strength Carbon Fiber for Composite Overwrapped Pressure Vessel Applications

University of Michigan

H2F HydroGEN Seedling: Monolithically Integrated Thin-Film/Silicon Tandem Photoelectrodes for High-Efficiency and Stable Photoelectrochemical Water Splitting

H2F Hydrogen Adsorbents with High Volumetric Density: New Materials and System Projections

H2F HyMARC Seedling: Optimized Hydrogen Adsorbents via Machine Learning and Crystal Engineering

US Hybrid

TAHI Northeast Demonstration and Deployment of FCRx200

Vanderbilt University

FC Fuel Cell Membrane Electrode Assemblies with Ultra-Low-Platinum Nanofiber Electrodes

Virginia Clean Cities at James Madison University

TAHI Hydrogen Fuel Cell Nexus Business-to-Business Website

Washington University in St. Louis

FC Corrosion-Resistant Non-Carbon Electrocatalyst Supports for Proton Exchange Fuel Cells

Xergy Inc.

TAHI Novel Membranes for Electrochemical Hydrogen Compression Enabling Increased Pressure Capability and Higher Pumping Efficiency